Optogenetic control of bio(techno)logical processes in bacteria at different cellular levels

Inaugural-Dissertation

zur Erlangung des Doktorgrades

der Mathematisch-Naturwissenschaftlichen Fakultät

der Heinrich-Heine-Universität Düsseldorf

vorgelegt von

Fabienne Hilgers

aus Langenfeld (Rhld.)

Düsseldorf, Juni 2021

Aus dem Institut für Molekulare Enzymtechnologie

der Heinrich-Heine-Universität Düsseldorf

Gedruckt mit der Genehmigung

der Mathematisch-Naturwissenschaftlichen Fakultät der

Heinrich-Heine-Universität Düsseldorf

Referent: Prof. Dr. Karl-Erich Jaeger

Korreferent: Prof. Dr. Jörg Pietruszka

Tag der mündlichen Prüfung: 02.12.2021

TABLE OF CONTENTS

A. CONFERENCE CONTRIBUTIONS

A.I. POSTER PRESENTATIONS

Hilgers F*, Binder D, Bier C, Hogenkamp F, Loeschcke A, Pietruszka J, Jaeger K-E and Drepper T (2017). Caged compounds as light sensitive switches for the production of valuable metabolites in biotechnology. Annual Conference 2017 of the Association for General and Applied Microbiology (VAAM), Würzburg/Germany, March 2017.

Hilgers F*, Hogenkamp F, Loeschcke A, Pietruszka J, Jaeger K-E and Drepper T (2017). Molecular and optogenetic tools for efficient biosynthesis of structurally diverse secondary metabolites. Annual congress “Biotechnologie 2020+”, Jülich/Germany, October 2017.

Hilgers F*, Hogenkamp F, Loeschcke A, Pietruszka J, Jaeger K-E and Drepper T (2017). Molecular and optogenetic tools for efficient biosynthesis of structurally diverse secondary metabolites. 2nd International BioSC Symposium, Cologne/Germany, November 2017.

Hogenkamp F*, Bier C, **Hilgers F**, Binder D, Drobietz D, Loeschcke A, Drepper T, Jaeger K-E, Pietruszka J (2018). Photocaged Carbohydrates: An Optogenetic Toolbox for Biotechnological Applications. Central European Conference on Photochemistry CECP, Bad Hofgastein/Austria, February 2018.

Hilgers F*, Hogenkamp F, Binder D, Loeschcke A, Pietruszka J, Jaeger K-E and Drepper T (2018). (Opto)genetic control of microbial cell factories for an efficient production of valuable secondary metabolites. 69. Mosbacher Kolloquium-"Synthetic Biology- from Understanding to Application", Mosbach/Germany, March 2018. ***Poster Award GBM***

Hilgers F*, Hogenkamp F, Binder D, Loeschcke A, Pietruszka J, Jaeger K-E and Drepper T (2018). Molecular and optogenetic tools for efficient biosynthesis of structurally diverse secondary metabolites. Annual Conference 2018 of the Association for General and Applied Microbiology (VAAM), Wolfsburg/Germany, April 2018. * **Poster Award ASM***

Hogenkamp F*, Bier C, **Hilgers F**, Binder D, Drobietz D, Loeschcke A, Drepper T, Jaeger K-E, Pietruszka J (2018). Synthesis of Photocaged Carbohydrates and their Biotechnological Applications. 27th PhotoIUPAC International Symposium on Photochemistry, Dublin/Ireland, July 2018.

Gerlach T*, **Hilgers F**, Bitzenhofer NL, Drepper T and Rother D (2018). Avoiding cross-reactivities in multi-step biocatalysis by light-induced enzyme deactivation. 9th International Congress on Biocatalysis, Hamburg/Germany, August 2018.

Gerlach T*, **Hilgers F**, Bitzenhofer NL, Drepper T and Rother D (2018). Avoiding cross-reactivities in multi-step biocatalysis by light-induced enzyme deactivation. ProcessNet-Jahrestagung und 33. DECHEMA-Jahrestagung der Biotechnologen 2018, Aachen/Germany, September 2018.

Hilgers F*, Hogenkamp F, Binder D, Loeschcke A, Pietruszka J, Jaeger K-E and Drepper T (2018). Optogenetics – light controlled biosynthesis of structurally diverse secondary metabolites. Aachen Protein Engineering Symposium (AcES) 2018, Aachen/Germany, October 2018.

Loeschcke A*, Weihmann R, **Hilgers F**, Drepper T *et al.* (2018). The CombiCom project: Combinatorial creation of structural diversity for novel high-value compounds. Aachen Protein Engineering Symposium (AcES) 2018, Aachen/Germany, October 2018.

Loeschcke A*, Weihmann R, **Hilgers F**, Drepper T *et al.* (2018). The CombiCom project: Combinatorial creation of structural diversity for novel high-value compounds. 3rd International BioSC Symposium, Bonn/Germany, November 2018.

Hilgers F*, Hogenkamp F, Binder D, Loeschcke A, Pietruszka J, Jaeger K-E and Drepper T (2018). (Opto)genetic control of microbial cell factories for an efficient biosynthesis of valuable secondary metabolites. 3rd International BioSC Symposium, Bonn/Germany, November 2018.

Hilgers F*, Hogenkamp F, Binder D, Loeschcke A, Pietruszka J, Jaeger K-E and Drepper T (2019). (Opto)genetic control of microbial cell factories for an efficient biosynthesis of valuable secondary metabolites. Annual Conference 2019 of the Association for General and Applied Microbiology (VAAM), Mainz/Germany, March 2019.

Klaus O*, Lappe A, **Hilgers F**, Hogenkamp F, Loeschcke A, Pietruszka J, Jaeger K-E and Drepper T (2019). Photocaged IPTG derivatives for light-controlled gene expression in *Rhodobacter capsulatus*. Annual Conference 2019 of the Association for General and Applied Microbiology (VAAM), Mainz/Germany, March 2019.

Bitzenhofer NL*, Ackermann YS, **Hilgers F**, Gensch T, Nonell S, Jaeger K-E and Drepper T (2019). Genetically encoded photosensitizers as a versatile tool to regulate bacterial processes by light. Annual Conference 2019 of the Association for General and Applied Microbiology (VAAM), Mainz/Germany, March 2019.

Hilgers F*, Bitzenhofer NL, Ackermann Y, Binder D, Burmeister A, Grünberger A, Loeschcke A, Pietruszka J, Jaeger K-E, Drepper T (2019). Lights on and action-programming microbial cell factories with light. 2nd Synthetic Biology for Natural Products Conference, Puerto Vallarta/Mexico, June 2019.

Hogenkamp F*, Bier C, **Hilgers F**, Binder D, Drobietz D, Loeschcke A, Drepper T, Jaeger K-E, Pietruszka J (2019). Synthesis of Photocaged Compounds. 21st ESOC European Symposium on Organic Chemistry, Vienna/Austria, July 2019.

Hilgers F*, Bitzenhofer NL, Ackermann Y, Binder D, Burmeister A, Grünberger A, Loeschcke A, Hogenkamp F, Pietruszka J, Jaeger K-E, Drepper T (2019). Lights on and action – optogenetic control of biosynthetic pathways. GCSB – German Conference on Synthetic Biology, Aachen/Germany September 2019.

Bitzenhofer NL*, **Hilgers F**, Ackermann YS, Burmeister A, Grünberger A, Jaeger K-E and Drepper T (2019). Genetically encoded PSs mediate photodynamic inactivation of pathogenic bacteria. GCSB – German Conference on Synthetic Biology, Aachen/Germany September 2019.

Hogenkamp F*, Bier C, **Hilgers F**, Binder D, Drobietz D, Loeschcke A, Drepper T, Jaeger K-E, Pietruszka J (2019). Heterocyclic Photocages for Carbohydrates. 27th ISHC International Society of Heterocyclic Chemistry Congress, Kyoto/Japan, September 2019.

Loeschcke A*, Weihmann R, **Hilgers F**, Drepper T, *et al.* (2019): CombiCom: combinatorial creation of structural diversity for novel high-value compounds. 4th International BioSC Symposium, Köln/Germany, November 2019.

Klaus O*, Loeschcke A, **Hilgers F**, Hage-Hülsmann J, Troost K, Jaeger K-E and Drepper T (2020). *Rhodobacter capsulatus* as a phototrophic platform organism for the synthesis of plant terpenes. Annual conference of the Association for General and Applied Microbiology (VAAM), Leipzig/Germany, March 2020.

* Presenting author.

A.II. ORAL PRESENTATIONS

Hilgers F*, Bitzenhofer NL, Hogenkamp F, Pietruszka J, Jaeger K-E and Drepper T (2019). Lights on and action – optogenetic control of microbial cell factories. BioSC PhD Retreat, Leverkusen/Germany, July 2019.

Hilgers F*, Bitzenhofer NL, Ackermann Y, Binder D, Burmeister A, Grünberger A, Loeschcke A, Pietruszka J, Jaeger KE and Drepper T (2019). Lights on and action – programming microbial cell factories with light. 17th International Congress on Photobiology and 18th Congress of the European Society for Photobiology, Barcelona/Spain, August 2019.

Hogenkamp F*, Bier C, **Hilgers F**, Binder D, Drobietz D, Loeschcke A, Drepper T, Jaeger K-E and Pietruszka J (2019). Heterocyclic Photocages for Carbohydrates. 27th ISHC International Society of Heterocyclic Chemistry Congress, Kyoto/Japan, September 2019.

Hilgers F*, Bitzenhofer NL, Ackermann Y, Hogenkamp F, Binder D, Burmeister A, Grünberger A, Loeschcke A, Pietruszka J, Jaeger K-E and Drepper T (2019). Lights on and action – programming microbial cell factories with light. B.R.A.I.N. Industry meeting, Zwingenbach/Germany, October 2019.

Bitzenhofer NL*, **Hilgers F**, Hogenkamp F, Binder D, Burmeister A, Grünberger A, Loeschcke A, Pietruszka J, Jaeger K-E and Drepper T (2019). Optogenetic switches in *P. putida* for a light-mediated control of cellular functions. *Pseudomonas* Grassroots Meeting, Leiden/Netherlands, November 2019.

Hilgers F*, Hogenkamp F, Loeschcke A, Pietruszka J, Jaeger K-E and Drepper T (2020). Lights on and action – New photobiotechnological approaches for the production of terpenes. CLIB Forum “Biotechnology appeals to all senses”, Germany, December 2020.

* Presenting author.

B. PUBLICATIONS

Hage-Hülsmann J, Grünberger A, Thies S, Santiago-Schübel B, Klein AS, Pietruszka J, Binder D, **Hilgers F**, Domröse A, Drepper T, Kohlheyer D, Jaeger K-E and Loeschcke A **(2018).** Natural biocide cocktails: Combinatorial antibiotic effects of prodigiosin and biosurfactants. *PLOS ONE,* 13(7):e0200940. doi: 10.1371/journal.pone.0200940

Endres S, Wingen M, Torra J, Ruiz-González R, Polen T, Bosio G, Bitzenhofer NL, **Hilgers F**, Gensch T, Nonell S, Jaeger K and Drepper T. **(2018)**. An optogenetic toolbox of LOV-based photosensitizers for light-driven killing of bacteria. *Scientific Reports,* 8(1):15021. doi: 10.1038/s41598-018-33291-4

Burmeister A, **Hilgers F**, Langner A, Westerwalbesloh C, Kerkhoff Y, Tenhaef N, Drepper T, Kohlheyer D, Von Lieres E, Noack S and Grünberger A **(2019)**. A microfluidic co-cultivation platform to investigate interactions in microbial communities on single-cell level. *Lab on a Chip,* 19(1):98-110. doi: 10.1039/c8lc00977e

Troost K, Loeschcke A, **Hilgers F**, Özgür AY, Weber TM, Santiago-Schübel B, Svensson V, Hage-Hülsmann J, Habash SS, Grundler FMW, Schleker ASS, Jaeger K-E and Drepper T. **(2019)**. Engineered *Rhodobacter capsulatus* as a phototrophic platform organism for the synthesis of plant sesquiterpenoids. *Frontiers in Microbiology*, 10:1998. doi: 10.3389/fmicb.2019.01998

Hilgers F*, Bitzenhofer NL*, Ackermann Y, Burmeister A, Grünberger A, Jaeger K-E and Drepper T **(2019)**. Genetically encoded photosensitizers as light-triggered antimicrobial agents. *International Journal of Molecular Sciences*, 20(18), 4608. doi: 10.3390/ijms20184608

Burmeister A, **Hilgers F** and Grünberger A **(2019)**. Mikrofluidische Einzelzell-Untersuchungen mikrobieller Interaktionen. *Biospektrum* 25: 515–519. doi: 10.1007/s12268-019-1088-9

Lee J, **Hilgers F**, Loeschke A, Jaeger K-E and Feldbrügge M **(2020)**. *Ustilago maydis* serves as a novel production host for the synthesis of plant and fungal sesquiterpenoids. *Frontiers in Microbiology,* 11:1655. doi: 10.3389/fmicb.2020.01655

Raber HF*, Heerde T*, El Din SN*, Flaig C, **Hilgers F**, Bitzenhofer NL, Jaeger K-E, Drepper T, Gottschalk K-E, Bodenberger NE, Weil T, Kubiczek DH and Rosenau F **(2020)**. Azulitox - a novel cancer-cell specific protein-photosensitizer. *Biomacromolecules*, 21, 12:5067–5076. doi: 10.1021/acs.biomac.0c01216

Hogenkamp F*, **Hilgers F***, Knapp A, Klaus O, Bier C, Binder D, Jaeger K-E, Drepper T and Pietruszka J. **(2021)**. Effect of photocaged isopropyl β-D-1-thiogalactopyranoside solubility on light-responsiveness of LacI-controlled expression systems in different bacteria. *ChemBioChem*, 2;22(3):539-547. doi: 10.1002/cbic.202000377

Hilgers F*, Habash SS*, Loeschcke A, Ackermann YS, Neumann S, Heck A, Klaus O, Hage-Hülsmann J, Grundler FMW, Jaeger K-E, Schleker ASS and Drepper T **(2021)**. β-caryophyllene production in the heterologous host *Rhodobacter capsulatus* and its biological activity. *Microorganisms*, 9(1), 168; doi: 10.3390/microorganisms9010168

Burmeister A, Akhtar Q, Hollmann L, Tenhaef N, Sokolowsky S, **Hilgers F**, Hogenkamp F, Marienhagen J, Noack S, Kohlheyer D and Grünberger A **(2021)**. (Optochemical) control of synthetic microbial co-culture interactions on microcolony level. *ACS Synthetic Biology*. doi: 10.1021/acssynbio.0c00382

Hage-Hülsmann J*, Klaus O*, Linke K, Troost K, Gora L, **Hilgers F**, Wirtz A, Santiago-Schübel B, Loeschcke A, Jaeger K-E and Drepper T **(2021)**. Production of C20, C30 and C40 terpenes in the engineered phototrophic bacterium *Rhodobacter capsulatus*. *Journal of Biotechnology*, 338:20-30. doi: 10.1016/j.jbiotec.2021.07.002

Hilgers F*, Hogenkamp F*, Klaus O, Kruse L, Lappe A, Loeschcke A, Bier C, Binder D, Jaeger K-E, Pietruszka J and Drepper T **(2021)**. Photocaged inducers for the non-invasive light control of production processes in the phototrophic bacterium *Rhodobacter capsulatus*. ***manuscript in preparation***

Hogenkamp F*, **Hilgers F***, Bitzenhofer NL, Ophoven V, Haase M, Bier C, Binder D, Jaeger K-E, Drepper T and Pietruszka J **(2021)**. Optochemical control of bacterial gene expression: novel photocaged compounds for different promoter systems *ChemBioChem*, doi: 10.1002/cbic.202100467

Lenz P, **Hilgers F**, Burmeister A, Zimmermann L, Volkenborn K, Grünberger A, Kohlheyer D, Drepper T, Jaeger K-E and Knapp A **(2021)**. The iSplit GFP assay detects intracellular recombinant proteins in *Bacillus subtilis*. *Microbial Cell Factories*, 20, 174, doi: 10.1186/s12934-021-01663-7

Hilgers F*, Hogenkamp F*, Bitzenhofer NL, Thies S, Jaeger K-E, Pietruszka J and Drepper T **(2021)**. Wavelength-selective control of mono- and di-rhamnolipid production in *P. putida*. *ACS Chemical Biology*, ***manuscript in preparation***

Burmeister A, **Hilgers F**, Brocke D, Drepper T, Kohlheyer D and Grünberger A **(2021).** Quantitative and dynamic online detection of bacterial conjugation events at the single cell level. *Frontiers in Microbiology*, ***manuscript in preparation***

*These authors contributed equally to this work.

C. ABBREVIATIONS

A	absorption
acetyl-CoA	acetyl-coenzyme A
ACP	acyl carrier protein
ANBP	nitrobiphenyl
aPDI/aPDT	antimicrobial photodynamic inactivation/therapy
ASOs	antisense oligonucleotides
BCMNB	4,5-bis(carboxymethoxy)-2-nitrobenzyl
BIST	bisstyrylthiophene
BLUF	blue-light sensors using flavin adenine dinucleotide receptors
BV	biliverdin
CALI	chromophore-assisted light inactivation
cAMP	cyclic AMP
CAP	catabolite activation protein
CAPCIB1	cryptochrome-interacting basic-helix-loop-helix protein
ConA	concanavalin A
CRY2	cryptochrome protein 2
DBTL cycle	Design-Build-Test-Learn cycle
DCC	dicyanocoumarin
DEAC	7-diethylaminocoumarin
DMAPP	dimethylallyl pyrophosphate
DMNB	1,2-dimethoxy-4-nitrobenzyl
DNA	deoxyribonucleic acid
DRL	di-rhamnolipid
DXP	1-deoxy-D-xylulose-5-phosphate pathway
eGFP	enhanced green fluorescent protein
EM(E)A	European Medicines (Evaluation) Agency
ε	extinction coefficient
F	fluorescence
FAD	flavin adenine dinucleotide
FALI	fluorophore-assisted light inactivation
FbFP	flavin-binding fluorescent protein
FDA	Food and Drug Administration
FKF1	flavin-binding, kelch domain, F-box protein
FMN	flavin mononucleotide
FPP	farnesyl pyrophosphate
GAP	glyceraldehyde-3-phosphate
GCPR	G protein-coupled receptor proteins
GFP	green fluorescent protein
GGPP	geranylgeranyl pyrophosphate
GPP	geranyl pyrophosphate
GRAS	generally recognized as safe
HAA	3-(3-hydroxyalkanoyloxy)alkanoate
HDAC	human histone deacetylase
ICM	intracytoplasmic membranes
IPP	isopentenyl pyrophosphate
IPTG	isopropyl-β-D-thiogalactopyranoside
IR	infrared
ISC	intersystem crossing
LacA	galactoside transacetylase
LacI	lac repressor of *lac* operon
LacY	β-galactoside/H^+-symporter
LacZ	β-galactosidase
LOV	Light-Oxygen-Voltage
LPS	lipopolysaccharides
MAP	2-methyl-3-pentyl-pyrrole
MBC	4-methoxy-2,2 bipyrrole-5-carboxyaldehyde
MEP	2-C-methyl-D-erythritol-4-phosphate pathway
MRL	mono-rhamnolipid
mRNA	messenger RNA
MVA	mevalonate pathway
NagR	transcriptional activator protein of *nag* operon
NahR	transcriptional activator protein of *nah* operon

NB	nitrobenzyl
NDBF	nitrodibenzofuran
NP	nitropiperonyl
NV	6-nitroveratryloxycarbonyl
P	phosphorescence
PCB	phycocyanobilin
PDT	photodynamic therapy
PhyB	phytochrome protein B
PIF3	phytochrome-interacting factor 3
PigC	prodigiosin ligase
PS	photosensitizer
RhlA	acyltransferase
RhlB	rhamnosyltransferase
RL	rhamnolipids
RNA	ribonucleic acid
ROS	reactive oxygen species
siRNAs	small interfering RNAs
TAT	transacting activator protein of transduction
TC	thiocoumarin
TCA cycle	tricarboxylic acid cycle
TCS	two-component system
TMG	thiomethyl-β-D-galactopyranoside
TOL plasmid	toluene degradation plasmid
TPU	two-photon uncaging
UV	ultraviolet
VVD	vivid light-sensitive protein
XylR	transcriptional activator protein of *xyl* operon
XylS	transcriptional activator protein of *xyl* operon
Φ_u	uncaging quantum yield

D. SUMMARY

In the field of synthetic biology, both a strict and straightforward orchestration, as well as a simple and robust visualization of biological processes are indispensable. The environmental factor light seems to be ideally suited for this task, as it represents a very precise, spatially, and temporally highly tunable and flexible stimulus. Thus, this thesis aimed to establish optogenetic strategies for controlling versatile biological processes on different cellular levels.

On the transcriptional level, novel variants of the light-responsive inducer molecule photocaged IPTG were successfully applied for light-inducible gene expression in several expression hosts, namely *E. coli*, *P. putida,* and *B. subtilis*. These photocaged inducer variants strongly differ either in their water-solubility or exhibit bathochromatically shifted absorption maxima. This optogenetic principle was further transferred to the phototrophic production host *R. capsulatus* by adapting the illumination conditions to allow for both phototrophic growth and optogenetic control. Additionally, photocaged benzoate derivatives and corresponding regulator/promoter systems, which had not yet been applied for light-mediated gene expression, were utilized for multichromatic orchestration of target gene expression in *P. putida*. To implement light control at the post-translational and cellular level, fluorescent proteins were characterized for their suitability as genetically encoded photosensitizers. It could be demonstrated that some fluorescent proteins generate high amounts of different reactive oxygen species thereby allowing to control enzyme activity as well as cell viability of various Gram-positive and Gram-negative bacteria as well as cancer cells. Further, metabolic pathways, such as the biosynthesis of plant terpenes, were established in *R. capsulatus* and optogenetic modulation of precursor accumulation could subsequently be demonstrated in case of carotenoid biosynthesis as a proof of concept. Finally, the new optogenetic toolbox was applied to control and/or visualize intercellular processes, such as the horizontal gene transfer, at the single-cell level.

Conclusively, versatile light-responsive tools for controlling biological functions on various cellular levels were established in *E. coli*, transferred to alternative expression hosts such as *P. putida*, *B. subtilis,* or *R. capsulatus* and finally applied in first biotechnological applications. These results thus clearly demonstrate a broad applicability of both the novel photocaged inducers and the genetically encoded photosensitizers as versatile optogenetic control systems for biotechnological and biomedical applications. Therefore, the established optogenetic on- and off-switches are

promising candidates for the light-dependent, dynamic control of metabolic, regulatory, and intercellular communication processes.

E. ZUSAMMENFASSUNG

Im Bereich der synthetischen Biologie ist die strikte Kontrolle und direkte Ansteuerung biologischer Prozesse sowie deren einfache und robuste Visualisierung von entscheidender Bedeutung. Der Umweltfaktor Licht ist als Stimulus hierfür hervorragend geeignet, da er sehr präzise und flexibel ist sowie mit einer hohen räumlichen und zeitlichen Auflösung eingesetzt werden kann. Daher hat die vorliegende Arbeit zum Ziel, geeignete optogenetischen Strategien zur Kontrolle von vielseitigen biologischen Prozessen auf unterschiedlichen Zellebenen zu etablieren.

Auf der Ebene der Gen-Transkription wurden neue Varianten des Licht-sensitiven Induktormoleküls *photocaged* IPTG eingesetzt. So konnte erfolgreich eine Licht-induzierbaren Genexpression in verschiedenen Wirtsorganismen, wie *E. coli*, *P. putida* und *B. subtilis*, implementiert werden. Diese *photocaged compound*-Varianten unterscheiden sich deutlich in ihrer Wasserlöslichkeit oder weisen rotverschobene Absorptionsmaxima auf. Um diese optogenetische Strategie auf den phototrophen Produktionsstamm *R. capsulatus* übertragen zu können, wurden dessen Beleuchtungsbedingungen so angepasst, dass sie sowohl phototrophes Wachstum mit infrarotem Licht, als auch optogenetische Kontrolle mit sichtbarem Licht ermöglichen. Zusätzlich konnten erstmals *photocaged* Benzoat-Derivate und entsprechende Regulator/Promotor-System zur Licht-gesteuerten Genexpression in *P. putida* eingesetzt werden.

Um eine Licht-basierten Kontrolle biologischer Prozesse auf post-translationaler Ebene und auf zellulärer ebene zu ermöglichen, wurden verschiedene Fluoreszenzproteine im Hinblick auf ihre Funktion als genetisch kodierte Photosensibilisatoren charakterisiert. Dabei konnte gezeigt werden, dass bestimmte Fluoreszenzproteine große Mengen unterschiedlicher reaktiver Sauerstoffspezien produzieren, welche zur Kontrolle von Enzymaktivitäten sowie zur Beeinflussung der Zellviabilität verschiedener Gram-positiver und Gram-negativer Bakterien und sogar von Tumorzellen genutzt werden konnten. Außerdem wurden verschiedene Stoffwechselwege wie etwa die Biosynthese von pflanzlichen Terpenen in *R. capsulatus* implementiert und am Beispiel der Carotenoid-Synthese gezeigt, dass die Akkumulierung von Vorstufenmolekülen optogenetisch moduliert werden kann. Zusätzlich konnte die Optogenetik auf Einzelzellebene zur Visualisierung und Kontrolle interzellulärer Prozesse wie dem horizontalen Gentransfer eingesetzt werden.

In der vorliegenden Arbeit wurden somit vielfältige Licht-sensitive Kontrollmechanismen biologischer Funktionen auf unterschiedlichen Zellebenen in *E. coli* etabliert, auf die

alternativen Expressionswirte *P. putida*, *B. subtilis* und *R. capsulatus* übertragen und anschließend in ersten biotechnologischen Anwendungen erprobt. Dabei zeigten die Ergebnisse eine breite Anwendbarkeit der neuen *photocaged inducers* und der genetisch kodierten Photosensibilisatoren als optogenetische Kontrollsysteme für die Biotechnologie und Biomedizin auf. Folglich stellen die hier etablierten optogenetischen An- und Aus-Schalter vielversprechende Kandidaten für den Einsatz zur Licht-abhängigen und dynamischen Kontrolle von Stoffwechselwegen, Regulationsmechanismen und interzellulären Kommunikationsprozessen dar.

I. INTRODUCTION

Biotechnology is a comprehensive area of biology harnessing living systems and biological components or processes, which gained increasing importance for applied research and industrial applications in the late 20th century and early 21st centuries. By providing sustainable, cleaner, and more efficient manufacturing processes, the vast field of biotechnology pursues to fight and prevent diseases, to obtain and preserve food as well as to reduce our environmental footprint, or in summary, to improve human purposes and meet society's most overriding challenges.

More recently, findings from synthetic biology have also been incorporated into the development of efficient biotechnological production processes, e.g., the engineering of microorganisms to create customized producers. Synthetic biology involves redesigning or developing biological systems such as cells, tissues, or organisms for useful purposes by providing them with new, defined properties [1–4]. To develop such artificial biological systems with predictable performance characteristics, the rational design and development of new biological parts and devices from naturally available components is an essential part of the strategy and will pave the way towards efficient and fully automated high-throughput optimization processes for metabolic and protein engineering, strain development or programming of signaling processes [5,6]. Synthetic biology researchers and companies around the world are harnessing the power of nature to treat diseases, manufacture chemicals, produce fuels, remediate contaminants, and for numerous other applications with benefits to humankind. To achieve these goals, bacteria are often used, which, depending on the specific aim, are engineered to achieve a high product yield or to optimize the intrinsic metabolism for the degradation/utilization of waste products (e.g., plastics) or renewable raw materials (e.g., lignin). These complex microbiological intra- and intercellular processes can be controlled or programmed at different levels (**Fig. I.1**): i) intracellular at both transcriptional and translation level to control the protein composition of a bacterial cell, which can be further expanded by expression of foreign genes and basically defines its biosynthetic capacity, ii) intracellular at the post-translational level (e.g., protein-protein interaction, interaction of proteins with other cell components) for the regulation/optimization of these catabolic and anabolic processes or the orchestration of complex metabolic pathways, iii) extracellular *via* cell-cell interaction such as the exchange of metabolites, signaling molecules, DNA or secreted proteins for share of labor communities or cell-to-cell communication, and finally, iv) extracellular by treating bacterial cells with toxic substances to control cell viability. In order to control the complex processes on all levels

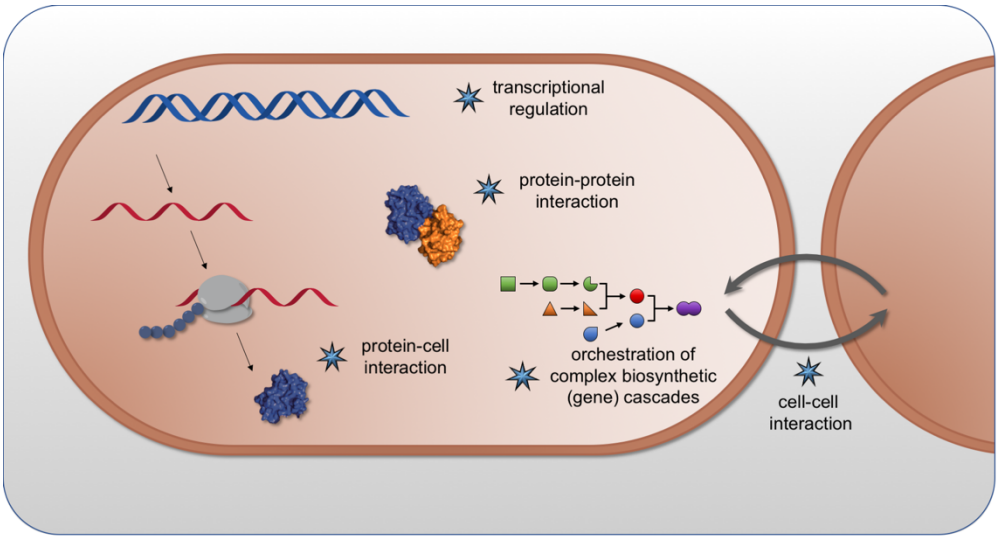

Figure I.1 Potential cellular targets to control bacterial processes at different levels and scales using tools from synthetic biology and optogenetics.
In synthetic biology, complex, engineered, or reprogrammed functions need to be controlled and orchestrated with high spatiotemporal resolution and at many different cellular levels. Transcriptional regulation can be modulated with a multitude of tools, such as promoter or terminator libraries, as well as positive or negative regulatory systems. At the post-translational level, enzyme levels or activities can be adapted using tools for inactivation such as protease tags, where the principal mechanism is based on protein-protein interaction. Another controlling tool is the use of proteins for interaction with or inactivation of further cellular components, such as DNA molecules or cell membranes, which can be assigned to the class of protein-cell interaction. Moreover, the aforementioned tools at both transcriptional and post-translational level proved valuable for a tight control of complex biosynthetic (gene) cascades in order to regulate or improve secondary metabolite production titers. Finally, regulation can be performed on a cell-to-cell level as applied for division of labor systems or the control of intercellular processes including horizontal gene transfer or the sharing of public goods within microbial communities.

in a concerted manner, special switches are needed that enable defined cellular functions to be switched on and off both in a controllable and predictable fashion. A promising approach to meet these requirements is the field of optogenetics, which uses the environmental factor light as an external trigger to regulate genetic or cellular elements [7–9]. This methodology offers various benefits, since light is, among others, tightly controllable, precisely targetable, and gradually adjustable. Thus, each regulatory level and the respective (optogenetic) application will be addressed in this introduction in further detail.

I.1. TRANSCRIPTIONAL REGULATION

I.1.1. BACTERIAL GENE REGULATION

Every microorganism on earth bears a multitude of different cellular processes that need to be controlled with high precision enabling it to take up nutrients, move, grow, reproduce, and finally adapt to continuously changing environmental conditions. Underlying these cellular processes is an incredibly large amount of genetic information, which encodes all physiological and morphological properties of an individual organism.

The genome of the bacterium *Escherichia coli*, for example, already encompasses over 4000 different genes [10]. The expression of genes must be precisely controlled to maintain life - which is not only an enormous challenge but also a compelling necessity, considering the resources and energy required for protein biosynthesis [11]. Obviously, this fact renders the constitutive and simultaneous expression of all genes entirely unfeasible and thus, bacteria have increased their efficiency by turning on a specific set of genes only when they are needed. Consequently, bacteria offer a high versatility and adaptability to their environment and are well-prepared for responding to external stimuli. On the molecular level, these responses are controlled by sophisticated regulatory networks, which orchestrate the expression of various genes clustered in transcriptional units and subjected to specific promoters. The promoter itself can be regulated by transcriptional activators and/or repressors responding to external stimuli such as oxygen availability or light intensity, pH or temperature changes, as well as the availability of a specific nutrient source or proximity to commensals or competitors [12–19]. In the following, regulatory systems relevant for this thesis will be presented in more detail. The most prominent example for those regulatory operons is the bacterial lactose utilization network, which was identified in *E. coli* in 1961 and encompasses a transcriptional unit tightly downregulated in the presence of glucose and exclusively transcribed upon lactose availability [20] (**Fig. I.2A**). This unit, which today is denoted as the ***lac* operon**, was found to be controlled by two proteins, the global catabolite activation protein (CAP) and the specific *lac* repressor (LacI), both binding in close proximity to the promoter of the tricistronic *lac* operon [21,22]. The here encoded genes *lacY*, *lacZ,* and *lacA* contribute to lactose metabolism: A membrane-integrated galactoside/H^+-symporter (LacY), also known as the *lac* permease, performs the uptake of lactose from the extracellular space, a β-galactosidase (LacZ) converts imported lactose molecules into their intermediates glucose, galactose, or 1,6-allolactose and finally a galactoside transacetylase (LacA) inactivates non-metabolizable thiogalactosides [23–25]. The first repressor protein LacI is encoded by the *lacI* gene upstream of the lac operon and is constitutively produced. In the absence of an inducer molecule, LacI forms a tetrameric structure which binds tightly to two of the three *lac* operator regions within the *lac* operon leading to a loop formation and thereby preventing transcription of the *lac* genes downstream of the P_{lac} promoter [22,24]. When the inducer allolactose is present in the environment, LacI binds it and undergoes a conformational change leading to its dissociation from the operator DNA and hence, to a derepression of *lac* gene expression. However, since *E. coli* preferentially utilizes glucose instead of

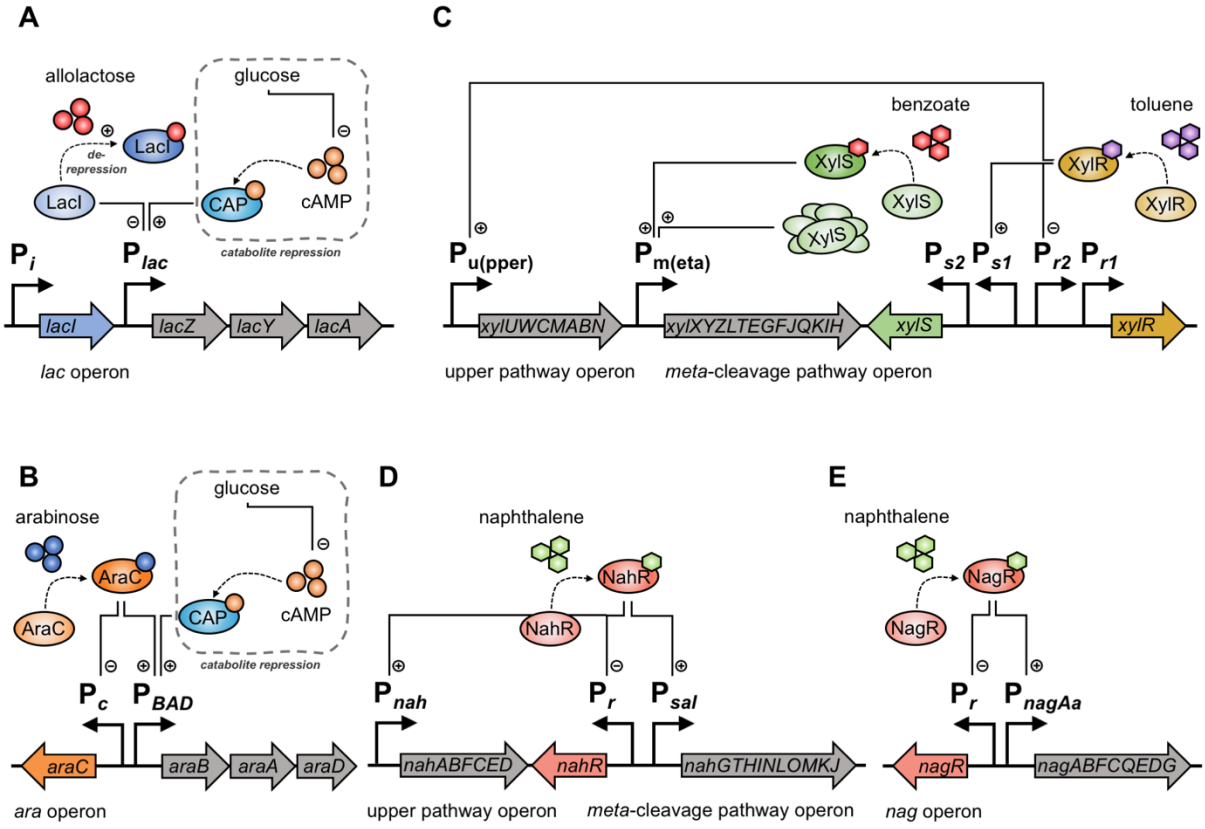

Figure I.2 Bacterial regulatory circuits for transcriptional control of selected carbon metabolization operons used in this thesis.
A) The *lac* operon, which encodes a β-galactoside/H+-symporter (LacY) for lactose uptake, a β-galactosidase (LacZ) for conversion of imported lactose, and a galactoside transacetylase (LacA) for inactivation of wrongly imported galactosides is negatively regulated by the repressor protein LacI. Upon binding of an inducer such as allolactose, LacI entails a conformational change and dissociates from the promoter region leading to the derepression of the P_{lac} promoter and thus, the start of *lac* gene transcription. In addition, this system is subject to catabolite repression in dependence of the cAMP level recognized by the catabolite activation protein (CAP). **B**) The *ara* operon encompasses the three genes *araB*, *araA,* and *araC*, which encode the enzymes responsible for the isomerization, phosphorylation, and epimerization of L-arabinose *via* L-ribulose and L-ribulose-5-phosphate to D-xylulose-5-phosphate. The operon is positively regulated by the activator protein AraC, which also represses its own expression *via* autoregulation and dimerizes upon arabinose binding to induce gene expression. The operon is also subject to catabolite repression depending on the cAMP levels or CAP activity. **C**) The gene cluster for toluene or benzoate derivatives metabolization is composed of two operons, the upper pathway operon, responsible for degradation of aromatic hydrocarbons to their aldehydes or carboxylic acids, and the *meta*-cleavage pathway operon for the degradation of those upper pathway intermediates to citric acid (TCA) cycle intermediates *via* catechol. Both operons are positively regulated by the activator proteins XylR, the master regulator, and XylS upon binding of a respective inducer molecule. While the expression of the *xylR* gene is autoregulated, the *xylS* gene is both constitutively expressed and additionally enhanced by XylR binding at its promoter P_{s1}. A hyperproduction of XylS leads to an inducer-independent induction of transcription from the *meta*-cleavage pathway operon. **D**) The *nah* regulatory system includes two operons, the upper pathway operon for the degradation of naphthalene to salicylate and the *meta*-cleavage pathway operon for the oxidation of salicylate to acetaldehyde and pyruvate *via* catechol. Both operons are subject to NahR-mediated activation of transcription upon binding of naphthalene, while NahR itself is expressed in an autoregulated manner. **E**) The *nag* operon encodes the genes for the degradation of naphthalene to fumarate and pyruvate *via* salicylate and gentisate. The transcription is positively regulated by the NagR protein, which activates the P_{nagAa} promoter upon binding of salicylate molecules.

lactose as a carbon source, a second mechanism is activated during glucose starvation that includes the production of cAMP molecules [20,26]. These molecules act as an allosteric effector for the CAP protein, which in turn initiates transcriptional activation of the *lac* promoter upon cAMP binding [15,21]. This repression system is frequently used by bacteria to control the nutrient hierarchy when exposed to two or more carbon sources of which one is clearly preferred [14]. In conclusion, a substantial *lac* gene expression requires both an allolactose-mediated derepression of the LacI repressor and the absence of glucose for further transcriptional activation by cAMP-bound CAP protein.

A further carbohydrate-responsive regulon is the ***ara* operon** (**Fig. I.2B**), which encompasses the three genes *araB,A,D* for the isomerization, phosphorylation, and epimerization of L-arabinose *via* L-ribulose and L-ribulose-5-phosphate to D-xylulose-5-phosphate [27,28]. Expression of *ara* genes is both positively and negatively regulated by the dimeric activator protein AraC, which, in the presence or absence of L-arabinose, is subject to a structural rearrangement and consequently binds or releases the related promoter $P_{BAD,}$ respectively [29]. Additionally, AraC negatively regulates its own expression by the constitutive P_c promoter *via* an autoregulatory mechanism. Similar to the *lac* operon, the *ara* operon is prone to catabolite repression in dependence of the cAMP level and respective CAP activity, since the utilization of D-xylulose-5-phosphate *via* the pentose-phosphate pathway is energetically more inefficient than glucose metabolism [30].

Besides carbohydrate-based regulatory operons, there is also a variety of aromatics-based regulation systems for the degradation of benzoate or naphthalene. One commonly described module originates from the TOL plasmid pWW0 of *Pseudomonas putida* for the **catabolism of benzoate or related hydrocarbons** [31–33] (**Fig. I.2C**). It contains two catabolic operons, the upper pathway operon, which encodes seven enzymes for the successive oxidation of hydrocarbons to their corresponding alcohol, aldehyde, or carboxylic acid and the *meta*-cleavage pathway operon encompassing 13 genes encoding enzymes for the conversion of those hydrocarbon intermediates to catechol, whose aromatic rings are then cleaved *via meta*-fission to produce the corresponding semialdehydes and finally citric acid (TCA) cycle intermediates [33]. Transcription of the upper operon is regulated by the master activator protein XylR, which activates its related promoter P_u upon binding of xylene or pathway intermediates in interaction with the sigma factor NtrA [34]. XylR itself is encoded by the *xylR* gene, which is expressed in high amounts and in a growth phase-independent manner by two tandem promoters, denoted as P_{r1} and P_{r2}. Besides its P_u-activating function, it further acts as a repressor of its own transcription [35,36]. The *meta*-cleavage pathway operon is positively regulated by the XylS protein, which belongs to the AraC

family of transcriptional regulators and activates its associated P_m promoter upon binding of a benzoate *meta*-pathway intermediate, preferably 3-metylbenzoate, and subsequent dimerization [37]. Since the P_s promoter is composed of two tandem promoters as well, XylS is not only expressed constitutively by its specific promoter P_{s2} on a low level but is also regulated by the activated form of the XylR regulator, which stimulates transcription from the additional promoter P_{s1} [35,38]. Consequently, XylS is hyperproduced leading to an inducer-independent activation of the P_m promoter [35,37]. In summary, particularly the *meta*-cleavage pathway operon is subject to a complex regulatory network of two activator proteins, the related regulator XylS and the master regulator XylR.

In addition to the aforementioned P_m/XylS system, other noteworthy examples for aromatics-responsive transcriptional circuits are the ***nah* operons** for naphthalene and phenanthrene degradation, which can be found in various pseudomonads including *Pseudomonas putida* or *Pseudomonas fluorescens* [39] (**Fig. I.2D**). This regulatory module consists of two operons, the upper pathway operon encompassing six genes for degradation of naphthalene to salicylate, and the *meta*-cleavage pathway operon including ten genes for oxidation of salicylate to acetaldehyde and pyruvate *via* catechol [39–41]. However, also other species, such as *Comamonas testosteroni, Ralstonia* sp. U2, or *Polaromonas naphthalenivorans* feature a closely related variant of this operon, namely the ***nag* operon** [42–44] (**Fig. I.2E**). Here, the *nag* genes encode the alternative gentisate pathway which, in contrast to the naphthalene catabolic pathway in pseudomonads, converts naphthalene to fumarate and pyruvate *via* salicylate and gentisate [44]. Additionally, the *nag* genes are organized in a single polycistronic operon [45]. Despite these differences, the transcriptional regulation of both systems is exceedingly similar, since both are controlled by the LysR-type regulator NahR or NagR, respectively [39,43,46]. These regulator proteins act as transcriptional activators for the two *nah* operons as well as the *nag* operon upon salicylate-binding [43,47,48] and are constitutively expressed [41,43,45,46]. In conclusion, both the two *nah* operons and the *nag* operon are only subject to an activator-mediated transcriptional control of NahR and NagR, respectively, in a straightforward manner.

Hence, the four presented regulatory networks provide a small insight into the complex but highly flexible process of transcriptional regulation in bacteria. Subsequently, it will be illustrated how these networks have been modified to create artificial, biotechnologically relevant regulation circuits.

I.1.2. SYNTHETIC TRANSCRIPTIONAL REGULATION CIRCUITS IN BIOTECHNOLOGY

Over the last decades, microorganisms have significantly contributed to the industrial production of bulk and fine chemicals as well as high-value compounds and agents [49–58]. Since the synthesis of mostly host foreign enzymes and the expression of the associated heterologous genes represents an enormous energy and metabolic burden, the precise control of target gene expression with high precision is of utmost importance for maximization of the production capacity [59–64]. In order to synchronize the production demand with the specific cellular capacity, the fine-tuning of enzyme expression *via* transcriptional regulation has proven to be the method of choice and is adapted in common synthetic biology systems, such as toggle switches or complex logic circuits [65–67]. Here, particular attention is paid to the timing of each cellular process, as the coordinated adjustment of the growth and production phase turned out to be essential for maximizing the overall production performance [8,68–70]. Hence, tools for controlling transcriptional processes are mandatory and therefore, various artificial systems have been designed based on the multitude of naturally occurring regulatory networks [12,65,66,71,72]. In the following, two groups of artificial transcriptional regulation systems will be presented in more detail. Finally, in addition to appropriate transcriptional regulators, the choice of the right expression host is of great importance for sufficient heterologous production processes and will be further elucidated in the second part of this chapter.

I.1.2.1. ARTIFICIAL EXPRESSION TOOLS

As aforementioned, the possibility to control and orchestrate the expression of heterologous genes is fundamental for maximized production yields of target proteins. A common approach is the use of transcriptional regulation circuits, which are derived from species-specific regulatory systems. Typically, those circuits include native or genetically engineered promoters or terminators as well as regulatory elements that activate, repress, or derepress target gene expression upon binding of a specific inducer molecule. In the following, three commonly used promoter systems, namely P_{lac}/LacI-derived systems, the P_{BAD}/AraC system, the P_m/XylS system, and finally the P_{nagAa}/NagR system will be described in more detail, since they were applied in this thesis.

As the *lac* operon (**chap. I.1.1**) is both the oldest known and the best studied transcriptional regulation system, it has been used to build a variety of artificial systems ever since. The native ***lac* promoter** was shown to be rather weak and thus was not

frequently used for overexpression of target genes [71,73,74] (**Fig. I.3A**). However, mutagenized promoter versions of P_{lac} were constructed with tremendously improved properties. Noteworthy variants are, for example, the *lacUV5* promoter [75], which exhibited a stronger expression level in combination with decreased catabolite repression but also a distinct basal expression [76–79]. Moreover, a combination of the −35 region of the *trp* promoter [80,81] and the −10 region of the *lacUV5* promoter resulted in the hybrid *tac* promoter [82], which was found to exert a ten-fold increased expression level in comparison to P_{lac} [83]. Additionally, a mutant version of *lacI* denoted as $lacI_q$ can be used, which features a mutation in the promoter region of the *lacI* gene resulting in a 10-fold enhanced *lacI* repressor expression and thus a decreased basal expression level [84]. However, all systems still exhibited a noticeable level of basal expression and were subject to catabolite repression. Thus, a second regulatory system, namely the T7 RNA polymerase system, was developed [85], which is based on a genomically integrated T7 bacteriophage RNA polymerase gene under control of the P_{lacUV5} and is most commonly used in combination with the strain *E. coli* BL21(DE3) [71,86,87] . This polymerase is not only faster than the *E. coli* RNA polymerase but can also be addressed orthogonally by using its unique promoter sequence. Owing to these features, the T7 system is characterized by a tremendously high yet robust expression performance and enabled the overexpression of thousands of homologous as well as heterologous proteins so far [71,86,88]. Further optimization of this system included the use of expression hosts bearing the T7 lysozyme, a natural inhibitor of T7 RNA polymerase, which drastically decreased the basal expression level [77,89,90]. LacI derepression and thus transcriptional activation can be initiated with increasing strength upon addition of natural inducers such as allolactose, a lactose intermediate, or galactose, as well as synthetic non-hydrolyzable inducers including thiomethyl-β-D-galactopyranoside (TMG) and isopropyl-β-D-thiogalactopyranoside (IPTG) [91–95].

In conclusion, the *lac*-based expression systems offer a robust, straightforward, and high-level gene expression with the possibility to sufficiently decrease basal activity. The natural P_{lac} system was adapted and optimized steadily to achieve good applicability in many different biotechnologically relevant organisms including *E. coli, B. subtilis C. glutamicum,* and *P. putida* [71,96–102]. However, the uptake of inducers is both performed *via* active transport processes by permeases and *via* diffusion, which could impede the transfer of this system to novel host organisms [103–105].

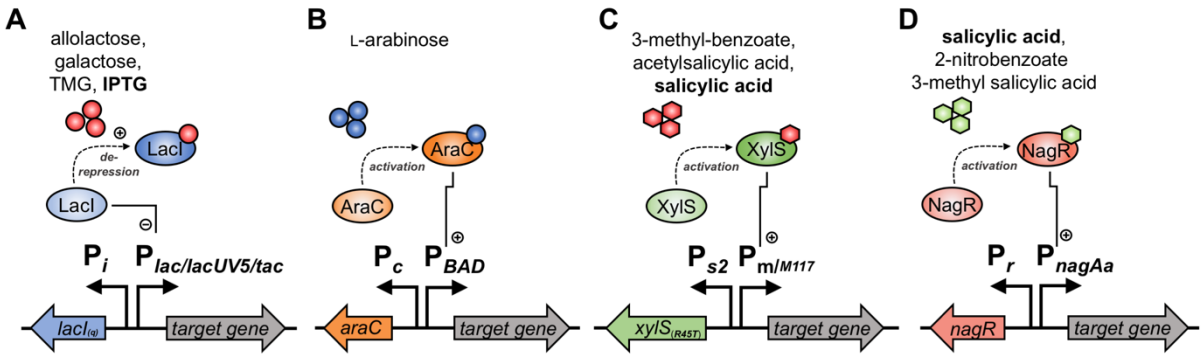

Figure I.3 Artificial tools for transcriptional regulation in bacteria.
A) As LacI activator-dependent systems, all *lac*-based regulons encompassing among others the P_{lac}, P_{lacUV5} or the P_{tac} promoters are subject to the same regulatory principle. Upon binding of a suited inducer such as β-D-1-thiogalactopyranoside (IPTG) or methyl-β-D-thiogalactopyranoside (TMG), LacI undergoes a conformational change leading to the dissociation from the operator region and thus, a derepression of transcription. For a tighter regulation, a mutant variant of *lacI*, denoted as $lacI_q$ can be used. **B**) The *ara* operon bears three enzymes for the isomerization, phosphorylation, and epimerization of L-arabinose to D-xylose-5-phosphate and is both positively and negatively regulated by the dimeric activator protein AraC in presence or in absence of L-arabinose, respectively. **C**) The P_m/XylS regulatory system is activated by XlyS association with the related operator region in the presence of a suitable inducer such as salicylic acid. For increased inducer promiscuity, a mutagenized variant of XylS, namely $XylS_{R45T}$ can be applied. Furthermore, an altered promoter variant, P_{M117}, can be used for an increased induction strength. **C**) Inducible gene expression *via* the P_{nagAa}/NagR regulon, which is activated by its activator protein NagR in the presence of salicylic acid.

Another commonly used carbohydrate-responsive promoter system is the **P_{BAD}/AraC system**, which has proven to be a valuable alternative for recombinant protein expression [27,71,106,107]. Besides its fast and strong expression response, the system is particularly characterized by a low basal activity upon addition of glucose, low inducer concentrations in *araBAD*-deletion strains, and a tight and gradually controllable expression due to AraC, which activates and represses transcription in the presence or absence of arabinose [103,106,108]. In its native form, the *ara* operon enables *E. coli* to take up and metabolize L-arabinose and thus, can only be activated by this specific aldopentose [107]. Additionally, the arabinose analog D-fucose acts as a competitive inhibitor, as it binds to AraC but does not activate transcription [109,110]. However, by mutation of AraC, the analog D-fucose, can be used for induction [33,111]. Another inhibitor of AraC was shown to be IPTG, as it exhibits a D-galactose moiety, which features a similar ring structure to L-arabinose [29]. By using a directed evolution approach, Keasling and co-workers could prove that the deletion of 12 amino acids at the C-terminus of AraC improved the expression system with respect to both arabinose sensitivity and IPTG-crosstalk [112]. Further, multiple-site saturation mutagenesis was used to broaden the inducer spectrum of AraC by D-arabinose and mevalonate [113,114]. Arabinose uptake is strictly dependent on the transport proteins AraE and AraFGH, which themselves are underlying a complex positive feedback loop, leading to

expression heterogeneity in intermediately induced cultures [107]. However, by expressing these proteins under the control of stronger and independent promoters, homogeneous expression was observed in dependence on increasing arabinose concentrations [115–117]. Although this system is most commonly applied for controlling gene expression in *E. coli*, it was also successfully used in alternative production hosts including *C. glutamicum*, *P. putida,* or *Gluconobacter oxydans* [118–121].

In addition to the two previous promoter systems, which can be induced with carbohydrates such as IPTG or L-arabinose, many aromatic-based promoter systems have also proved valuable for heterologous protein production [27,37,98,122–124]. One prominent example is the **P_m promoter** (**chap. I.1.1**) which is derived from the toluene or benzoate metabolization pathway of *P. putida* and is regulated by its specific activator protein XylS upon binding of benzoate derivatives (**Fig. I.3C**). To switch to this activated state, XylS preferentially binds 3-methylbenzoate, but a variety of other benzoate derivatives, such as acetylsalicylic acid and salicylic acid, both in the protonated and de-protonated state, are also accepted with lower affinities [32,37]. The introduction of point mutations in the *xylS* gene further broadened the inducer spectrum of the transcriptional activator and increased binding affinities for previously established benzoates, allowing for an enhanced transcription strength. For high-level protein production, the native promoter was randomly mutagenized resulting in a 14-fold increased production level for the ML1-17 variant, denoted as P_{M117}, but also in an increased basal activity [103,106,125].

So far, P_m/XylS derived expression systems could be used for controllable gene expression in various Gram-negative bacteria including *E. coli* or *Pseudomonas* sp. [106,119,126–128], but also in some Gram-positive organisms such as *Mycobacterium smegmatis* and *Mycobacterium tuberculosis* [129]. Considering the fact that the uptake of most aromatic inducers is performed passively *via* diffusion, this system seems to be easily adaptable to new bacterial hosts.

Besides the previously described P_m/XylS regulatory element, another aromatic-dependent expression tool based on the **P_{nagAa} promoter** (**chap. I.1.1**) is frequently used (**Fig. I.3D**). This promoter originates from the *nag* operons for degradation of naphthalene, which can be found, among others, in *C. testosteroni* or *Ralstonia* sp. and is regulated by its activator protein NagR in the presence of the inducer salicylic acid. Various other benzoates were tested for their ability to drive P_{nagAa}-mediated gene expression, but only a few compounds including 2-nitrobenzoate, 3-methyl salicylic acid, and acetylsalicylic acid were found to be marginally able to activate expression [43,130].

However, by random mutagenesis of the LysR-type regulator NagR, the inducer promiscuity could be increased [46,131].

Furthermore, randomized point mutations in the P_{nagAa} promoter region of the NagR activator-binding motif revealed a threefold increase in the effectiveness of salicylic acid induction [43]. Also, the combined use of both salicylic acid and 4-nitrobenzoate as inducers increased the expression strength [46]. During the last decades, the P_{nagAa}/NagR regulatory system was used for recombinant protein production mainly in pseudomonads such as *P. putida* [132–137] or *P. taiwanensis* [138,139], but there are also some studies performed in *E. coli* [130,140]. In addition, the related P_{sal}/NahR regulon was used in *P. putida* offering a tight and gradual regulation upon salicylic acid induction as well [119,141].

In summary, the P_{nagAa}/NagR system can be considered as a valuable tool for controlled gene expression, as inducer uptake is performed passively *via* diffusion and sufficient working concentrations are remarkably low [130,138,139].

I.1.2.2. SUITABLE MICROBIAL CELL FACTORIES

In addition to the choice of an appropriate expression tool, the selection of a suitable heterologous host is of great importance for successful protein or metabolite production. Relevant features that need to be provided by each organism are genetic accessibility and amenability to genetic engineering, the status as a non-pathogenic organism, robust growth up to high cell densities under process conditions, and finally an increased productivity in comparison to the native producer [51,142]. Since they meet these criteria, *E. coli*, *P. putida*, *B. subtilis,* and *C. glutamicum* are some of the most common representatives in biotechnological production processes [98,143,144]. In the following, these four microbes and further alternative production hosts are described in more detail, since they were extensively applied in this thesis.

The Gram-negative enterobacterium ***E. coli*** clearly enjoys the greatest popularity and is still recommended as a “what-to-try-first” approach because of its high productivity, its robust growth, its high versatility, and the existing deep knowledge of its physiology [56,144,145]. Since the Food and Drug Administration (FDA) approved the clinical use of human insulin, which was heterologously produced in *E. coli,* in the 80s [146], the share of recombinant pharmaceuticals produced in *E. coli* and licensed by the FDA and the European Medicines Agency (EMA) from 2004 to 2013 is 24% [144]. Further commonly produced natural products and recombinant proteins include the anti-malaria drug artemisinin [147,148], the antibiotic erythromycin A [149], growth hormones

[54,56,145], pneumococcal vaccines, and hepatitis B virus immunization [54,144,145]. Besides the aforementioned advantages, there are also some drawbacks when using *E. coli* as a platform for recombinant protein production. Firstly, it lacks post-translational modifications, which are necessary for the production of most eukaryotic proteins [55,108]. Secondly, it shows an affinity for the formation of inclusion bodies under high expression stress and the codon usage is not optimal for most mammalian genes [54,150–155]. And finally, the cell membrane of *E. coli* contains lipopolysaccharides (LPS), which are referred to as endotoxins and exhibit a strong fever-inducing effect in mammals [156]. Thus, the downstream processing and product purification for completely endotoxin-free end products is a laborious task [157].

Another highly relevant microbe is the Gram-positive bacterium ***B. subtilis***, which is widely used for recombinant protein production particularly in the fields of food production and food supplements [158]. It offers many advantageous features including its classification as a non-pathogenic production host, denoted as GRAS (*generally recognized as safe*) organism due to the absence of endotoxins, its genetic accessibility, and the availability of numerous genetic engineering tools as well as its outstanding secretory capacity [159–161]. Therefore, it is not surprising that about 60% of all commercially available enzymes are produced in *Bacillus* species, in particular, alkaline proteases for detergents or amylases for the starch-processing industry, but also food additives including vitamin B_{12} [71,159,162,163]. However, this species also bears some disadvantages such as the proteolytic degradation of heterologous target enzymes caused by the many inherent proteases, which nowadays can be addressed by specific protease-deficient strains [164–167].

A further key organism in industrial biotechnology is the Gram-positive actinobacterium ***C. glutamicum***, which is particularly exploited for the production of amino acids such as L-glutamate, L-lysine, and L-valine, or organic acids, including L-/D-lactate or succinate, and alcohols like ethanol [105,168]. Besides its characteristics as a non-endotoxic, non-sporulating, and genetically stable GRAS-certified organism, it offers valuable features like a low protease activity, a versatile primary and secondary metabolism, and finally, a broad acceptability of varying carbon sources [168–173]. Nonetheless, *C. glutamicum* exhibits some bottlenecks such as the low transformation efficiency in comparison to *E. coli* or relatively low production yields for some protein classes and thus, further effort should be made with respect to a more extensive use in biotechnological and pharmaceutical production processes [105,173].

Finally, a noteworthy organism for secondary metabolite production and natural products in general, is the rod-shaped Gram-negative soil bacterium ***P. putida***. Since it offers not

only a pronounced tolerance against organic solvent, xenobiotics, and redox stress, but also a highly versatile metabolism [132,174–178], it is rendered exceedingly suitable for biotechnological production of high-value natural products including rhamnolipids, terpenoids, polyketides, and amino acid-related metabolites [98,124,127,179–181]. However, to render the industrial use of engineered *P. putida* strains feasible for a broader product spectrum beyond high-value molecules, aspects such as an innovative strain design with excellent genomic stability as well as economically viable up-scaling and downstream processing strategies need to be addressed for optimization [98].

In addition to those well-established microbial cell factories, various alternative expression hosts emerged in recent years, which address more specific needs for recombinant protein or metabolite production. A promising example is the non-sulfur α-proteobacterium ***Rhodobacter capsulatus***, which is characterized by a versatile and highly flexible metabolism allowing for both anoxygenic, phototrophic growth or chemotrophic growth under (micro)aerobic conditions [182–184]. Under phototrophic conditions, most *Rhodobacter* species form large intracytoplasmic membranes (ICM), which are perfectly suited for storage of membrane proteins or hydrophobic metabolites, yet inherently designated for the incorporation of their photosystem apparatus [185,186]. Furthermore, the organism provides a multitude of redox cofactors as well as a naturally occurring carotenoid and terpene production capacity [185]. Thus, *R. capsulatus* combines the sustainable phototrophic lifestyle with unique physiological properties rendering it extremely valuable for the production of recombinant membrane proteins or high-value natural compounds, as demonstrated for the heterologous production of GPCR-like proteins or various plant-derived terpenes [186–189].

I.1.3. OPTOGENETIC CONTROL OF TRANSCRIPTION

The previous section presented a variety of prodigious regulatory systems and hosts as well as versatile approaches to overcome common problems in recombinant protein expression. Nevertheless, some tailbacks, such as induction heterogeneity, feedback loops, or non-gradual regulation, could still not be adequately solved. Moreover, those challenges occur repeatedly in many expression systems, thus making broad and more systematic approaches particularly suited to offer new perspectives [103,106,119]. Novel control systems for recombinant gene transcription, as well as the superordinate control of microbial gene expression should not only be tightly controllable, precisely targeted, and fast, but also homogeneous, and gradually triggerable. It turned out that one promising way to fulfill these requirements is the use of optogenetic approaches for

expression control. The field of optogenetics is commonly referred to as a methodology which uses light-responsive genetic or cellular elements for controlling biological functions [7–9]. Since light is a ubiquitous environmental factor, all forms of life on earth are in numerous different ways dependent on radiation energy for their survival and maintenance. The most prominent examples, which are widely distributed across the three kingdoms of life, include processes like photosynthesis performed by plants, algae, and certain bacteria, phototaxis, which is, for example, used by phototrophic bacteria for recognition of a sufficiently illuminated habitat or to escape strong UV radiation to avoid cell damage, and finally, the circadian rhythm. All these processes are controlled by light-responsive regulators such as photoreceptors including opsins (rhodopsins) in mammalian cells, *via* Light-Oxygen-Voltage (LOV)-photoreceptor in fungi and cyanobacteria or *via* phytochromes in plants [16,190–193]. Hence, these light-driven processes have also been extensively exploited for bioengineering. Starting with the first genetically encoded light-sensitive protein, a phytochrome/PIF3 fusion, for transcriptional control in yeast in 2002 [194] or the first light-driven ion channel, the channelrhodopsin-2, explored by Deisseroth and colleagues in 2006 [195], the use of optogenetics has spread to many different scientific areas and has become an integral part of current research in neuroscience as well as other bio(techno)logical disciplines for the control of diverse cellular functions including cell signaling, gene expression or protein activation/ deactivation [7,196]. The optogenetic tools for transcriptional control available to date can be broadly divided into two subgroups – the first group is composed of **genetically encoded light-sensitive proteins**, such as photoreceptors, and the second includes chemical-based photocaged small molecules such as photocaged inducers. In the first group, naturally occurring light-responsive proteins from plants, cyanobacteria, or algae are used for two different purposes. Firstly, they are harnessed for direct modulation of gene expression by using light-responsive transcription factors or repressors as well as enzymes such as light-sensitive polymerases [9] and secondly, they are combined with downstream effectors, such as a response regulator gaining a light-responsive two-component signaling system (TCS) [197]. The most prominent classes of photoreceptors certainly are the phytochromes, which are red and near-infrared (NIR) light-responsive [198,199], as well as the LOV-domain proteins and cryptochromes, which both are blue light-responsive [200–204]. Commonly photoreceptors can sense light because they have bound light-sensitive molecules called chromophores (**Fig. I.4C**). In the case of phytochromes, these are tetrapyrrole chromophores such as biliverdin IXα (BV) or phycocyanobilin (PCB), which absorb red and NIR light and subsequently induce reversible conformational changes in the protein structure. In mammalian cells and yeast, directly modulated two-hybrid or split protein

systems such as phytochrome protein B (PhyB) and the associated phytochrome-interacting factor 3 (PIF3) can be applied for controlled gene expression [194,205]. In bacteria, TCSs composed of inherent or engineered sensor histidine kinases and respective response regulators are used far more frequently (**Fig. I.4A**). A well-known example is the artificial photoreceptor Cph8, in which the osmosensory domain of a membrane-bound histidine kinase has been swapped with the cyanobacterial phytochrome Cph1 from *Synechocystis* sp. PCC6803. In the absence of light, the histidine kinase phosphorylates its corresponding response regulator OmpR and by this activates transcription, while red light illumination leads to an inactivation of both the histidine kinase and gene expression [206]. This TCS has an analogous structure to the cyanobacteriochrome system CcaS/CcaR, which regulates gene expression in response to red or green light, and both systems were successfully applied for an edge detection algorithm in *E. coli* [207], multicolored control of gene expression [208], domain swapping studies [197,209], and to tightly control cellular processes [210–213]. Additionally, NIR-responsive photoreceptors are available, which bind BV as a chromophore and can be applied in bacteria as well as yeast and mammalian cells [214–216].

The groups of flavin-dependent and blue light-sensitive photoreceptors includes the LOV proteins, which bind flavin mononucleotide (FMN) as a chromophore, the blue-light sensors using flavin adenine dinucleotide receptors (BLUF), which, as the name implies, bind flavin adenine dinucleotides (FAD), and the cryptochromes, which also employ FAD as its chromophore to initiate the light-induced conformational change (**Fig. I.4A**). The first blue light-dependent TCS to control transcription consists of the artificial kinase YF1, which was created by exchanging an oxygen-sensing domain of a natural sensor kinase FixL with the YvtA LOV domain from *B. subtilis* [217–220]. In analogy to the phytochrome TCS Cph8/OmpR, activation of transcription also occurs in the absence of light and *via* autophosphorylation of its respective response regulator FixJ, whereas the presence of blue light inactivates this process. Based on this system, extensions were implemented such as the inversion of light control using the λ phage repressor cI within the pDusk/ pDawn system from Möglich and co-workers [221], which was earlier also used to invert the multichromatic system of the red/far-red Cph8/OmpR system and the green/red CcaS/CcaR system [208] and could subsequently be used for the optogenetic control of LacI in an IPTG-independent manner [222].

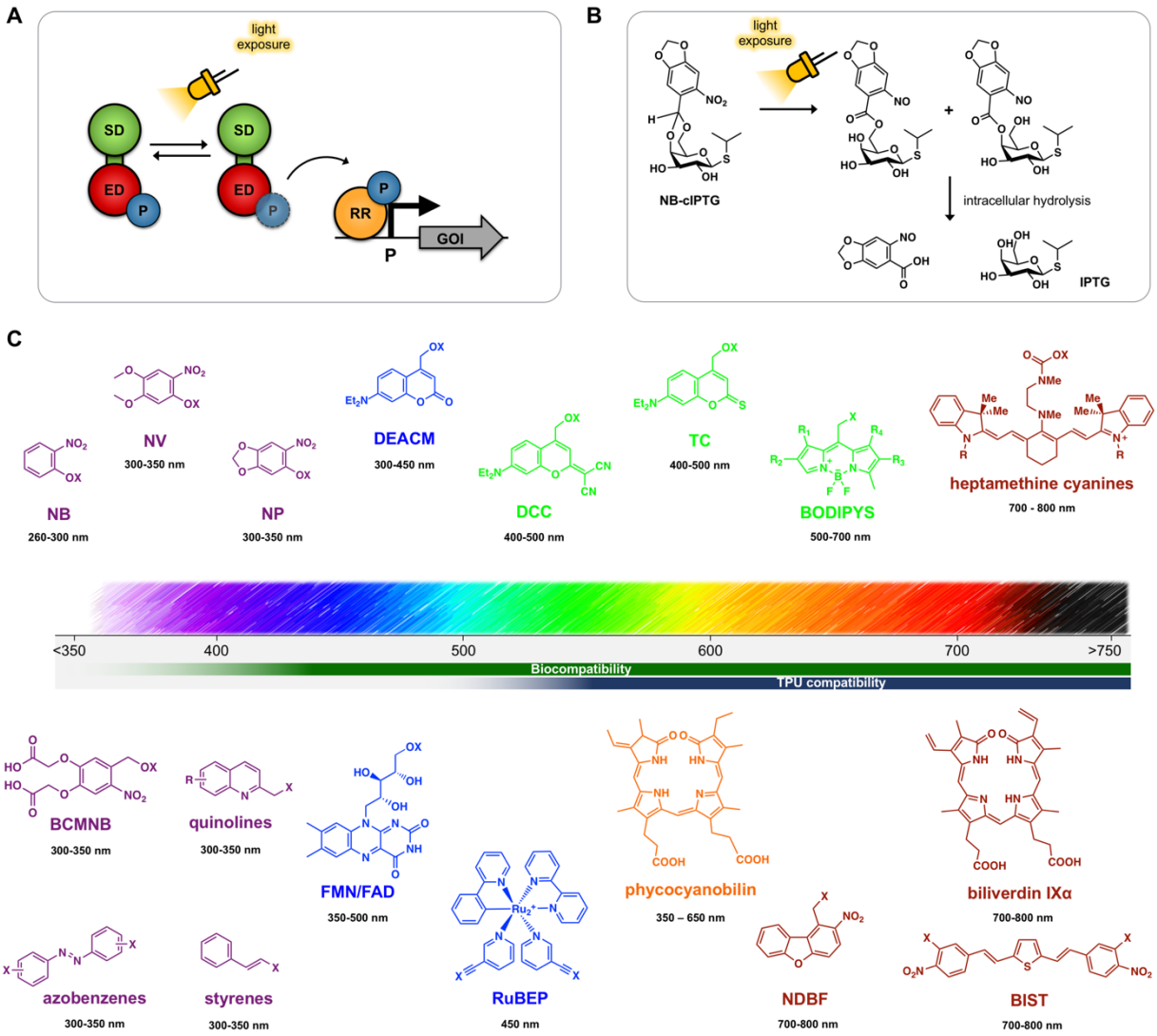

Figure I.4 Optogenetic switches for control of gene transcription and a selection of light-sensitive effector molecules that are harnessed by photocaged small molecules or photoreceptors.
A) Light-responsive photoreceptors are commonly two-component systems (TCS) that can be switched from a dark-adapted ground state to an excited state and vice versa by illumination with light of a specific wavelength. The receptor itself is composed of a sensor domain (SD) and an effector domain (ED), such as a histidine kinase domain. In the excited state, the effector domain phosphorylates (P) its response regulator (RR), which subsequently binds to a corresponding promoter and activates transcription of a gene of interest (GOI). **B**) The two-step photorelease of nitrobenzyl (NB)-photocaged IPTG starts with its cleavage into the two possible constitutional isomeric ester intermediates by exposure to UV-A light. Subsequently, intracellular hydrolysis by esterases releases the IPTG as well as the corresponding nitroso compound as a by-product. **C**) Light-sensitive effector molecules can on the one hand be photolabile protection groups, which are chemically bound to a target molecule or structure for inactivation and subsequent photorelease, and on the other hand, chromophores that undergo a structural or configurational change in response to a light stimulus, triggering conformational changes within the photoreceptor. The chromophores phycocyanobilin (PCB), biliverdin IXα (BV), or the flavin-based flavin mononucleotide (FMN) and flavin adenine dinucleotide (FAD) are predominantly found in photoreceptors. For chemical photoprotection, there is a whole range of molecules that can be used as light-sensitive photocages. These include not only well-established photolabile protection groups based on nitrobenzyl, quinolines, coumarin, cyanines or BODIPYS and RuBEPs, but also molecules that undergo *cis-trans* isomerization upon light irradiation such as azobenzenes or styrenes. X: variable moiety, NB: nitrobenzyl, NV: nitroveratryloxycarbonyl, NP: nitropiperonyl, BCMNB: bis(carboxymethoxy)-nitrobenzyl, DEACM: diethylaminocoumarin, DCC: dicyanocoumarin, TC: thiocoumarin, NDBF: dinitrobenzofuran, BIST: bisstyrylthiophene, TPU: two-photon uncaging, GOI: gene of interest.

In mammalian cells, gene expression is commonly controlled *via* photo-controllable transcription factors such as the flavin-binding, Kelch domain, F-box protein (FKF1), and its interaction partner GIGANTEA (GI) or the cryptochrome protein 2 (CRY2) with its Cryptochrome-Interacting Basic-helix-loop-helix protein (CIB1) [223–225]. In general, the advantage of flavin-dependent systems is the natural availability of FMN and FAD in common microbial hosts, whereas the chromophores of phytochromes, BV, and PCB, need to be added to the medium or produced heterologously in the targeted organism [9,205,206,226,227]. The use of genetically encoded photoreceptors offers some advantages, such as a very broad color spectrum with many available systems in the longer and thus less harmful wavelength range, commonly a good reversibility of the expression response, as well as few undesirable side reactions or cell toxicity in the target organism.

The second class of light-mediated transcriptional control systems are the **chemical-based photocaged small molecules** such as inducers, inhibitors and metal ions, proteins, or nucleic acids. By means of photolytic release of photosensitive groups or isomerization of chemicals, small molecules are made available for biological applications (**Fig. I.4B**). Since photocaged cAMP was successfully introduced as the first photocaged biomolecule in 1977 by Engels and Schlaeger [228], a variety of different effector molecules were made photo-sensitive by attaching photocages in order to gain spatiotemporal light-control over both chemical and biological processes, as nicely reviewed by Hughes *et al.*, Ankenbruck *et al.* and Hartmann *et al*. [7,196,229]. For light-mediated gene expression in particular, various small molecules have been used including photocaged IPTG, arabinose, and other carbohydrates in bacteria as well as abscisic acid or methionine in mammalian cells or yeast [230–235]. Furthermore, photocaged Cu^{2+} was successfully applied to gain control over gene expression in yeast [236] and finally, doxycycline was recently photocaged [237–239], but still not applied for light-controlled gene expression in bacteria. In addition, blue light-responsive human histone deacetylase (HDAC) inhibitors were recently applied in mammalian cells for the light control of epigenetically regulated transcription *via cis-trans* isomerization [240]. Further small molecule agonists of gene expression in mammalian cells have been photocaged, including nuclear hormones, β-ecdysone, and the CREB inhibitor [241–243]. For controlling expression in bacteria, a photocaged T7-RNA polymerase was constructed by incorporation of a photocaged tyrosine into the catalytic site, resulting in a photoactivation of gene expression in *E. coli* [244]. Moreover, photocaged small molecules for direct DNA or RNA interaction were constructed such as photocaged theophylline, which binds to an mRNA riboswitch and activates it upon illumination [245]. Finally, DNA or RNA can be directly modified to implement light control by attaching

photocages to various positions on the DNA/RNA strand. Thereby, gene expression can be activated by using small nucleotide fragments, as shown in various studies for mammalian cells or for cell-free approaches [246–254]. Genes can also be knocked down by the use of caged antisense oligonucleotides (ASOs) or small interfering RNAs (siRNAs), as nicely demonstrated for various mammalian cell lines [255–260]. However, most of these techniques seem to be preferably applied for mammalian cells, zebrafish models, mice, or cell-free approaches such as nanoparticles. Further *in vivo* applications in bacteria need to be elucidated in the near future.

One of the first and still most commonly used photolabile protection group is the nitrobenzyl (NB) group (**Fig I.4C**), since it is small and commercially available [7]. Its good accessibility by a straightforward synthesis together with the well-characterized photocleavage reaction still make its ongoing employment feasible [261,262]. However, since NB-photocaged compounds mainly absorb light in the UV-B/-C range, in which the radiation exerts toxic effects on cells and thus is less suitable for *in vivo* applications, the uncaging of NB is usually performed under UV-A irradiation (around 365 nm), in which the corresponding compounds only show a low absorption capacity. Thus, more advanced NB-derivatives have been developed that exhibit a bathochromic shift towards longer wavelength absorption and thus an improved biocompatibility [263–265]. Besides the UV-A light absorbing photocages 6-nitropiperonyl (NP), 1,2-dimethoxy-4- nitrobenzyl (DMNB), 6-nitroveratryloxycarbonyl (NV), and 4,5-bis(carboxymethoxy)-2-nitrobenzyl (BCMNB) [7,266], notable examples for derivatives with red-shifted absorption maxima are bisstyrylthiophene (BIST), nitrobiphenyl (ANBP), and nitrodibenzofuran (NDBF), which are partly suited for two-photon uncaging (TPU) [267–269]. During TPU, the excited singlet state of a chromophore is generated at about twice the conventional excitation wavelength by absorbing two photons from an ultra-fast laser almost simultaneously. Another frequently used protection group is based on coumarins and is UV-A light-responsive (365 nm – 400 nm) [270]. In contrast to NB and its derivatives, the absorption of coumarins can be red-shifted by chemical modification more easily and thus, various bathochromically shifted derivatives including thiocoumarin (TC), dicyanocoumarin (DCC) and 7-diethylaminocoumarin (DEAC) photocages were applied in mammalian cells and zebrafish so far [271–274]. Other possible photocages include quinolines (UV-A light), RuBEP (blue light) as well as BODIPYs and cyanines, which both can even be excited with NIR light [275–280], but especially cyanines are rarely used due to complex syntheses. In addition, the azobenzenes and styryl derivatives should be mentioned, which are not photocleavable but photoswitchable, as they undergo *cis-trans* isomerization upon irradiation with UV light or NIR light *via* TPU [281–283]. Although coumarin-based photocages are highly promising due to their chromatic

diversity, their synthesis has shown to be more complex in comparison to NB cages and is based on more expensive precursors [266]. Thus, NB-derived photocages are prevalently used in biology as particularly NP-photocages offer an outstanding *in vivo* applicability and a well-known and efficient photolysis.

In the context of the aforementioned biocompatibility, caged compounds must meet a number of requirements with respect to development, physicochemical properties and photo-release for a successful *in vivo* application. Firstly, the compound synthesis should be feasible and based on reasonably inexpensive and readily available precursors. In addition, the protecting group should be stable both *in vitro* and *in vivo*, and should offer the possibility of attaching effector moieties to allow flexible adjustment of both the absorption wavelength and the water solubility [266,270,284]. Beneficial physicochemical properties such as sufficient absorptivity, water-solubility, non-toxicity as well as *in vivo* and *in vitro* stability facilitate the employment of each photocaged compound and are crucial for the success of the respective application. Furthermore, an adequate extinction coefficient at the respective irradiation wavelength (ε; the fraction of incident light that is absorbed) and a high uncaging quantum yield (Φ_u; the proportion of photocaged molecules that undergoes photolysis upon absorption of a photon), seems beneficial, as uncaging upon illumination should be accomplished in a reasonable amount of time to prevent unwanted toxic effects or unwanted overheating of the cell culture. To achieve the complete biological induction response and thus make the use of photocaged inducers competitive with conventional inducers, complete photolysis should be ensured. Hence, when selecting existing photocages or synthesizing a new one, these requirements should be considered to guarantee a successful *in vivo* application.

Furthermore, the demand for protection groups suitable for multichromatic control of cellular processes is steadily increasing. Two- or even multicolor control circuits enable the orchestration of complex biological processes with high accuracy and high temporal resolution [229]. For this purpose, red-shifted protection groups are commonly combined with protection groups that absorb in the UV range to achieve a circuit with the greatest possible signal orthogonality [285–287]. So far, various protection group combinations have already been used for orthogonal substance release *in vitro* in hydrogels and nano materials or for (de)activation of protein functions as well as *in vivo* in mammalian cells [271,288–295]. Advantages of using photocaged small molecules include, for example, the necessity to express less associated proteins, such as the photoreceptor itself, as well as the enzymes for chromophore biosynthesis, and thus they can be used in almost any target organism without negatively influencing the metabolic and energy capacity.

However, a possible disadvantage is the lack of reversibility and potential cytotoxicity of the chemical protection groups [266,285,296].

In summary, there is a multitude of promising approaches for optogenetic control of biological processes, however, these often address mammalian cell systems. The optogenetic tools for controlling bacterial gene expression inevitably require extensive characterization and optimization to expand the toolbox of available systems and implement new promising properties, such as better solubility or red-shifted absorption. Moreover, the subsequent application of light control at flask to milliliter scale is another major challenge that would significantly improve the accessibility of optogenetics.

I.2. POST-TRANSLATIONAL REGULATION

Following a detailed description of the advantages and limitations of transcriptionally controlled biological processes in the previous chapter, various options for post-translational control of enzyme activity (**Fig. I.1**) that can be addressed *via* optogenetic strategies will be outlined in this section. These can, for example, be based on protein-protein interactions, such as the use of protein tags or chromophore-assisted light inactivation (CALI).

I.2.1. FUSION PROTEINS FOR CONTROLLING ENZYME ACTIVITY

Protein biosynthesis can not only be controlled at a transcriptional level, as discussed in the previous chapter, but also at a post-translational level. In bacteria, it is often based on post-translational modifications, such as phosphorylation, which results in structural changes within the protein, gylcosylation, which protects the protein against degradation by proteases [297,298], proteolysis for the truncation of individual proteins or peptides, for example the cleavage of signal peptides during secretion, and finally, protein degradation by proteases, which recognize a specific protein tag [299,300]. Particularly the peptide-based modifications are frequently adapted in biotechnological approaches for gaining control over enyzme activity or the localization of a specific target protein by using functional peptide tags or enzyme fusions [301–303].

In the following chapter, however, the focus will be on fusion enzymes or fusion tags and their application for light-mediated control of enzyme activity. Here, a distinction can be made between reversible and irreversible on- and off-switches [304,305]. Reversible switches are mostly generated by translational fusion with photo-responsive proteins and associated loop regions, such as the CRY2 domain from *Arabidopsis thaliana* or the LOV2 domain from *Avena sativa* [305–307]. The latter, for example, is composed of a FMN-binding core domain and a Jα-helical loop domain at the C-terminus [308]. Upon illumination with blue light, a cysteine in the LOV2 domain forms a covalent bond with the excited FMN molecule leading to a conformational change within the core domain followed by dissociation and unfolding of the Jα helix (**Fig. I.5A**). Additionally, the photo domains can be used for light-induced heterodimerization with their respective interaction partner (**Fig. I.5B**).

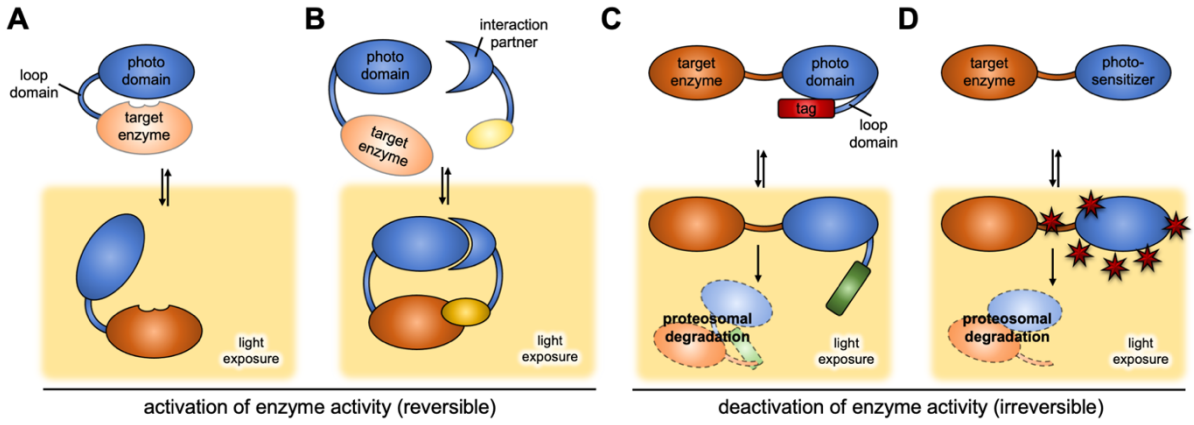

Figure I.5 Selected reversible and irreversible on- and off-switches based on fusion enzymes applicable for post-translational control of enzyme activities by light.
Recombinant fusions of catalytically active and light-responsive domains can be used to post-translationally control enzyme activity, as exemplarily shown for **A**) the reversible light-induced allosteric activation of a target enzyme using a photo domain or **B**) the reversible heterodimerization of a photo domain with its interaction partner, both fused to a respective target protein and its binding partner (yellow circle). **C**) Further, enzymes can also be deactivated using protein fusions as depicted for a light-controllable protein degron, which is based on a degeneration tag and a coupled photo domain, which itself is fused to the target enzyme. **D**) Finally, a deactivation can also be achieved by using a photosensitizer fused to the target enzyme. This photosensitizer produces reactive oxygen species (ROS; red asterisks) upon light exposure leading to the destruction of the fusion complex.

Prominent examples are the blue light-induced heterodimerization of the LOV domain bearing FKF1 protein from *A. thaliana* with the GIGANTEA (GI) protein, which again is triggered by the formation of a covalent bond between FMN and a cysteine of FKF1. This bond leads to a structural rearrangement allowing FKF1 to bind to GI [223]. Due to the size of GI and the low dark recovery of FKF1 [309], further heterodimerization systems based on LOV domains such as tunable, light-inducible dimerization tags (TULIPs) [310] or the improved light-inducible dimer (iLID) [311,312] were constructed. Irreversible methods for light-mediated control of enzyme activity mainly include off-switches, such

as protein-tag-mediated degradation of the target enzyme or the localized generation of reactive oxygen species (ROS). The first approach is likewise based on a photo domain fused to a target enzyme and the related loop domain, which in turn is fused to a degradation tag (**Fig. I.5C**) [313–316]. The latter uses chemical molecules or genetically encoded fluorescent proteins that produce ROS upon illumination (**Fig. I.5D**) and will be elucidated further in the following section, since it was applied in the framework of this thesis for controlling the activity of selected biosynthetic pathway enzymes.

I.2.2. PHOTOSENSITIZERS AS AN OPTOGENETIC TOOL FOR CONTROLLING ENZYME ACTIVITY

Photochromic chemical compounds that locally generate ROS when exposed to light of a certain wavelength are called photosensitizers (PS) [317,318]. Upon exposure, the photosensitizer is elevated from the electronic ground state (^{0}PS) to a singlet excited state (^{1}PS) *via* absorption (A) and subsequent internal conversion (IC) (**Fig. I.6A**). Afterwards, in addition to releasing energy *via* fluorescence (F), it can reach a long-living triplet state (^{3}PS) *via* intersystem crossing (ISC). From this point, various ROS can be created including superoxide radical anion ($O_2^{\bullet-}$), hydrogen peroxide (H_2O_2) and hydroxyl radical ($HO^{\bullet}$), which are generated by electron transfer of the photosensitizer's triplet state to molecular oxygen (type I mechanism), and singlet oxygen ($^1O_2$), which is formed by energy transfer of the triplet state to molecular triplet oxygen (type II mechanism) instead of returning to the ground state *via* phosphorescence (P) [319]. After this cycle, the PS returns to its electronic ground state and can re-enter the cycle by absorbing a new photon. Inactivation of target structures using ROS is most commonly referred to as chromophore-assisted light inactivation (CALI), but other names such as chromophore-assisted laser inactivation or fluorophore-assisted light inactivation (FALI) are likewise used. Due to a targeted delivery of the PS to a cellular structure using ligands or antibodies, or the fusion of a genetically encoded PS with the target enzyme, the ROS are produced in close proximity and the adjacent structure is irreversibly destroyed leading to a loss of function [320].

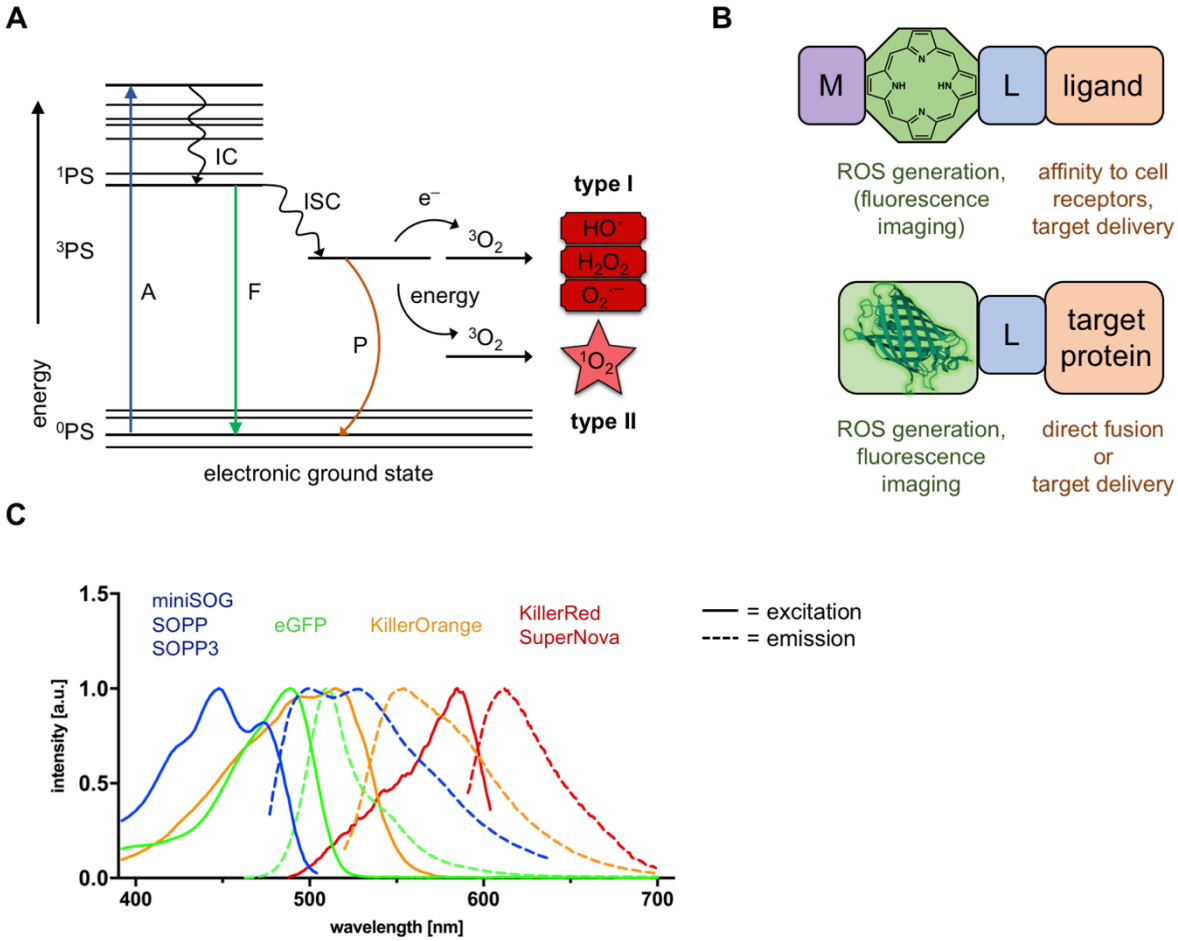

Figure I.6 Photosensitizer for light-mediated control of enzyme activity by formation of reactive oxygen species.
Photosensitizers (PS) are chromophores that produce reactive oxygen species (ROS) upon illumination with light of a certain wavelength. **A**) During exposure, the molecule is elevated from the electronic ground state (^{0}PS) to a singlet excited state (^{1}PS) *via* absorption (A) and internal conversion (IC). Subsequently, it can release energy *via* fluorescence (F) or reach a long-living triplet state (^{3}PS) *via* intersystem crossing (ISC). From this point, various ROS can be created including hydroxyl radicals (HO$^\bullet$), hydrogen peroxide (H_2O_2) and superoxide radical anions ($O_2^{\bullet-}$), which are generated by electron transfer of the photosensitizer's triplet state to molecular oxygen (type I mechanism), and singlet oxygen ($^1O_2$), which is formed by energy transfer of the triplet state to molecular oxygen (type II mechanism) instead of returning to the ground state *via* phosphorescence (P). **B**) Photosensitizers can be based on chemical compounds such as porphyrins (upper illustration) or on genetically encoded fluorescence proteins (bottom illustration). While an elaborate scaffold of hydrophilic moieties (M), linkers (L), and ligands or antibodies must be constructed to use chemicals *in vivo*, genetically encoded PSs can be fused to the target protein at DNA level and thus are expressed in an uncomplicated manner. (eGFP PDB ID: 6YLQ). **C**) Excitation (solid line) and emission (dashed line) spectra of selected genetically encoded photosensitizers. All LOV domain-derived proteins such as miniSOG, SOPP and SOPP3 bind flavin as a chromophore and thus exhibit an absorption maximum at around 450 nm and an emission maximum at 500 - 530 nm. Closely related GFP variants such as eGFP can be excited at around 490 nm and emit light at 510 nm. KillerOrange is a blue-shifted derivative of KillerRed, resulting in an absorption maximum in the green range at 500 nm and an emission maximum at 555 nm. KillerRed and its monomeric variant SuperNova absorb in the red spectrum at around 585 nm and emit light at 610 nm.

While singlet oxygen is highly reactive, resulting in a short lifetime of up to 2 µs and a diffusion range of around 150 nm [321,322], the other ROS and particularly H_2O_2 show a prolonged lifetime of 1 ms and thus can diffuse over longer distances or even between adjacent cells [323,324]. Hence, not only proteins or cellular components in close

proximity are damaged, but also the whole cellular environment, including cell walls, lipid membranes, or nucleic acids [325–327], which must be taken into account when choosing a suitable PS for the specific CALI application. Previously, the PSs malachite green and eosin proved valuable for light-mediated deactivation of an alkaline phosphatase, a β-galactosidase and an acetylcholine esterase [320,328]. Furthermore, dyes like ReAsH or fluorescein are frequently used [329–332]. Those chemical-based photosensitizers need to be combined with a targeting molecule, such as an antibody, a ligand, or a peptide tag and modified with various moieties for improved hydrophilicity to be applicable for intracellular targeting (**Fig. I.6.B**, upper illustration). However, due to the typically laborious design of the chemical-based PSs, there has been a constant search for novel or optimized photosensitizers. In this context, it has been observed that some modified fluorescent proteins based on the basic chromophore structure of the green fluorescent protein (GFP) such as eGFP can not only emit fluorescence when excited with light of a certain wavelength, but also produce ROS and thus can be utilized as a genetically encoded PS (**Fig. I.6B**, bottom illustration) [333]. Progressively, further genetically encoded PSs were found, such as the red fluorescent protein KillerRed derived from the hydrozoan chromoprotein anm2CP [334,335], which was successfully used for targeted inactivation of proteins in cell membranes, mitochondria, or nuclei [336–338]. In contrast to GFP, KillerRed is characterized as highly phototoxic and seems to produce ROS mainly *via* the type I mechanism under participation of molecular oxygen and upon illumination with green to orange light [339–342]. KillerRed was further optimized to obtain the monomeric derivative SuperNova, which shows similar photophysical and photosensitizing properties as KillerRed, but produces 10% less ROS *via* the type I and 5% more ROS *via* the type II mechanism and additionally allows for an uncomplicated fusion to target proteins [343]. In addition to SuperNova, a further derivative was developed, denoted as KillerOrange, which can be excited independently of KillerRed at a blue-shifted wavelength (**Fig. I.6C**) [344]. Besides these GFP-based PSs, there are also members of the group of flavin-binding fluorescent proteins (FbFPs), which are known to exhibit photosensitizing activity. The first known example is the mini singlet oxygen generator, short miniSOG, which is derived from the engineered, green-fluorescing LOV-domain 2 from *A. thaliana* phototropin 2 [345]. Unlike the GFP-related PSs, the LOV-based proteins bind an endogenous flavin chromophore such as FMN, which acts as a photosensitizer upon blue light illumination and results in the generation of $^1O_2$ *via* the type II reaction [345,346]. As the name suggests, miniSOG was proposed to be an efficient singlet oxygen producer, but this could not be proven in subsequent studies [347,348]. However, miniSOG was successfully used to perform CALI of synaptic release in neurons or of mitochondrial proteins in nematodes [349,350]. Two noteworthy

derivatives of miniSOG are SOPP and SOPP3, also known as singlet oxygen photosensitizing proteins, which were shown to offer strongly improved singlet oxygen quantum yields [346,351].

However, genetically encoded photosensitizers have not yet been used to control relevant pathway enzymes in microbial secondary metabolite biosynthesis (**Fig. I.1**, orchestration of complex biosynthetic pathways). Besides those LOV-derived variants, there are various other flavin-binding fluorescent proteins including iLOV and phiLOV [352,353], or proteins derived from bacterial photoreceptors such as DsFbFP and DsFbFP M49I (*Dinoroseobacter shibae*), CreiLOV (*Chlamydomonas reinhardtii*), EcFbFP (*B. subtilis*), or Pp1FbFP and Pp2FbFP (*P. putida*) [354–356], which all need to be characterized with respect to their photosensitizing properties in further detail.

In summary, chromophore-assisted light inactivation is a powerful tool that utilizes protein-protein interactions or protein fusions and light-sensitive chromophores to produce ROS and thereby selectively deactivating enzymes or other cellular molecules. The photosensitizing group can be a chemical molecule, which needs to be linked to a targeting structure such as ligands or antibodies, or a genetically encoded fluorescent protein that is able to produce ROS due to its encapsulated chromophore and can be genetically linked to the protein of interest. However, the number of fluorescent proteins used as fusion partners for CALI approaches is still quite low, although they offer valuable features including an easy linkage and a straightforward targeting to a specific cellular structure. Consequently, further fluorescent proteins known for ROS generation should be evaluated with respect to their suitability for light-mediated enzyme inactivation.

I.3. PROTEIN-CELL INTERACTIONS FOR OPTOGENETIC CONTROL OF CELLULAR PROCESSES

The use of fusion proteins consisting of an effector domain such as photosensitizers and a target domain represents a very valuable approach for the precise regulation/inactivation of desired proteins, as described in detail in the previous chapter. However, photosensitizers are well-established for the optogenetic control of cellular processes *via* protein-cell interactions (**Fig. I.1**). In this context, the following chapter focuses in particular on the use of those photosensitive proteins to control cell viability, as it is performed for bacterial populations in mono- or co-cultures, denoted as antimicrobial photodynamic inactivation (aPDI), or for tumor cells in photodynamic therapy (PDT) approaches [357,358]. Since both chemical and genetically encoded

photosensitizers produce not only short-lived singlet oxygen, but also longer-lived ROS, such as H_2O_2 upon illumination, they can also be used to target and destroy surrounding cellular organelles and membranes, finally triggering apoptosis of the respective cells. These cells can, for example, be multi-drug-resistant bacteria, which are addressed in aPDI approaches (**Fig. I.7A**) [319,327,358,359]. Here, particularly cationic photosensitizing chromophores or additional moieties are used to specifically target the negatively-charged cell membrane of bacteria, while avoiding damage to mammalian tissue [360,361]. Secondly, the potential of this method can be exploited for the treatment of tumor cells as it is frequently performed in biomedical applications, e.g., PDT (**Fig. I.7B**). Here, PSs are utilized for the treatment of various oncological and non-oncological diseases, as ROS lead to oxidative damage of tumor tissue, resulting in cell death and activation of the immune response [325,359,362].

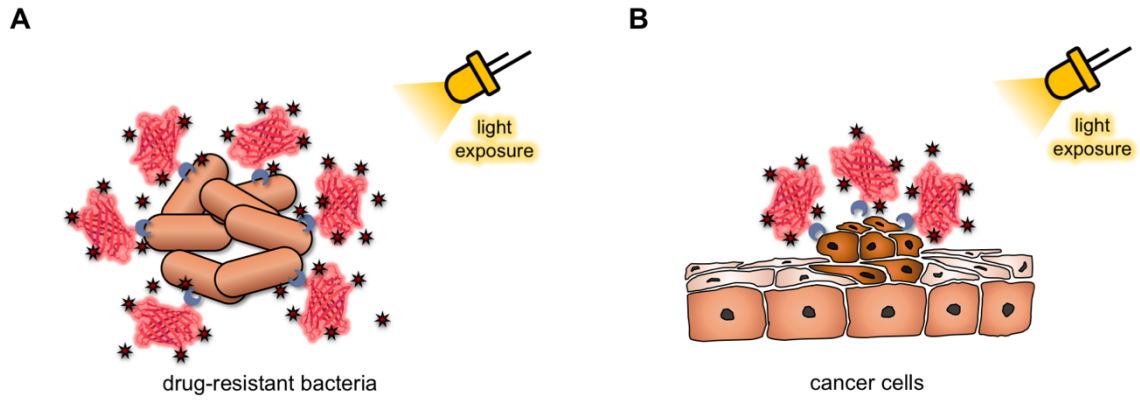

Figure I.7 Applications of genetically encoded photosensitizers for light-controlled modulation of cell viability.
A) The use of fluorescent proteins as photosensitizers (PS) proved valuable for various *in vivo* applications such as the field of antimicrobial photodynamic inactivation (aPDI). Here, multi-drug-resistant bacteria are damaged by reactive oxygen species (ROS) generated by genetically encoded PSs (red protein structure, KillerRed PDB ID: 2WIQ), which sometimes are additionally linked to a targeting structure (blue crescents), resulting in a significantly lower chance of resistance formation within a bacterial population. **B**) The use of photosensitizers could further be successfully applied for combating oncological diseases *via* photodynamic therapy (PDT), in which ROS produced by the PSs damage cancer cells and thereby lead to cell ablation and an increased immune response. For a targeted effect, delivery tags such as antibodies or ligand are used (blue crescents).

Chemical photosensitizers used in therapy are mainly based on tetrapyrroles, porphyrins, chlorines, phthalocyanines, phenothiazinium salts, methylene blue, or BODIPYS, which are combined with a targeting structure, such as an antibody or a ligand, or administered locally [318,319,357,358]. However, in addition to the aforementioned elaborate design of those PSs, there are further issues particularly in clinical application, including undesirable side effects such as prolonged skin and eye sensitivity to visible light and photoallergic reactions due to non-selective PS uptake [318,357,363]. Therefore, the demand for novel photosensitizers with reduced side effects was likewise growing in this

field, leading to the utilization of fluorescent proteins as genetically encoded PSs. In the recent years, mainly KillerRed was successfully applied for PDT treatments of mice and human cancer cell lines [336,364–367]. Additionally, miniSOG was employed for light-induced killing of cancer cells [368,369]. The initiation of cell ablation has so far been realized using red fluorescent proteins such as KillerRed or TagRFP for bacterial cells including *E. coli*, but also for mammalian cells [334,370,371]. In a study of Ruiz-Gonzales *et al.,* it could be shown that miniSOG outperforms TagRFP with respect to its toxicity towards bacterial cells [371].

In general, photosensitizers are a valuable tool for aPDI approaches, since ROS mostly trigger severe impairments with collateral damage, making it more difficult for resistance mechanisms to develop [372,373]. Furthermore, the generated ROS penetrate bacterial biofilms, which are of central importance for the infectivity of pathogenic bacteria such as *Pseudomonas aeruginosa* or *Staphylococcus aureus*, significantly better than conventional antibiotics, which need hours to days to achieve complete functionality [361,374,375]. Nonetheless, within the group of photosensitizers, genetically encoded fluorescent proteins are so far in the minority and thus should be further investigated regarding their applicability for killing cancer cells as well as multi-drug-resistant bacteria.

I.4. UTILIZATION OF LIGHT-RESPONSIVE TRANSCRIPTIONAL AND POST-TRANSLATIONAL CONTROL FOR BIOTECHNOLOGICAL APPLICATIONS

The detailed investigation of manifold biological processes is not only essential to gain a detailed insight into cellular functions and dynamics but also to successfully apply these findings in biotechnological bottom-up approaches. However, a profound understanding of important regulatory networks strongly requires the ability to both visualize and orchestrate dynamic *in vivo* processes in a straightforward and robust manner and with high spatiotemporal resolution. As described in the previous sections, light-mediated control over cellular functions can be gained besides others at the transcriptional and post-translational level (**chap. I.1.3 and I.2.2**). Considering a native, unmodified organism, which controls all its cellular processes with temporal perfection, exercising artificial control does not seem to be necessary. However, it gains importance when, for example, microbial production processes require the use of heterologous production hosts, or bacteria are not monitored within their usual environment but in artificial microbial consortia. In the following, both examples will be elucidated in more detail with respect to relevant high-value products and their production in alternative, heterologous

host organisms on the one hand and to possible application examples for controlling biological processes or even the composition of artificial microbial consortia on the other.

I.4.1. CONTROL OF NATURAL PRODUCT BIOSYNTHESIS

Natural products and their derivatives have taken a significant market share in the pharmaceutical industry over the last 40 years, accounting for over 60% of anticancer agents and nearly 50% of anti-infectives [376]. However, these compounds are usually laborious to synthesize chemically due to their complexity and sophisticated stereochemistry [143,377] and an extraction out of the native host, such as plants or fungi, is time-consuming and, in many cases, ecologically not feasible. Furthermore, some organisms might be human pathogenic microbes that are not culturable under lab conditions or suffer from insufficient growth or product titers [51,377–379]. Hence, the heterologous expression of one or even the entire biosynthetic gene cluster in a genetically accessible, non-toxic, and highly productive host is a promising alternative for the production and engineering of natural products. The increasing interest in bacteria as living cell factories arises from their diversified metabolism, which offers an impressive capacity for a multitude of biocatalytic transformations [380]. In addition to the primary metabolism, which provides metabolites needed for growth and maintenance of cellular functions, such as amino acids, fatty acids, and sugars, bacteria further produce so-called secondary metabolites. Those include antibiotics, siderophores, or signaling molecules [381–385] and are not essential for the central metabolism of the organism, but provide advantages for defense or for adaption under changing environmental conditions [386–388]. Due to those valuable features and their versatile biological effect on other organisms, secondary metabolites are utilized as natural antifungals and antibiotics, as well as anti-cancer and immunosuppressive compounds in the pharmaceutical industry [376,386,389]. However, the production of heterologous proteins in general, as well as the biosynthesis of heterologous secondary metabolites in particular, bears several challenges including (i) an effective transfer of the respective gene cluster to the preferred host, (ii) diverse bioactivities of heterologous secondary metabolite compounds leading to impaired strain stability, growth, or production yields, and (iii) an insufficiently coordinated gene expression or enzyme activity resulting in low production titers [51,390,391]. To address the first challenge, effective restriction-free cloning techniques have been developed in recent years, which are replacing conventional cloning methods based on the use of restriction endonucleases [51,392,393]. In addition to PCR- or recombinase-based methods, the transfer and

expression (TREX) system is particularly noteworthy in this context, as it enables the straightforward transfer, integration, and heterologous expression of complex gene clusters in different bacterial hosts, thus paving the way for the access to valuable natural products, as nicely demonstrated by the work of Domröse, Klein and Weihmann, who were able to heterologously produce prodiginines, phenazines and violacein derivatives in *P. putida* [390,391,394]. Once the integration of the heterologous genes has been successfully completed, it is important to ensure that the overproduction of the bioactive compound does not negatively affect the health and growth of the organism, which is often achieved by selecting a suitable and robust production host. While well-established platform organisms such as *E. coli* or *S. cerevisiae* are often used for the microbial production of non-toxic products or building blocks such as amino acids or isoprene scaffolds [51,143], specialized organisms are increasingly applied for the production of antimicrobial substances or more complex natural products (**chap. I.1.2.2**) [124,143,388,395]. In the following, three examples for complex natural product biosynthetic pathways, namely terpenes, prodiginines and rhamnolipids, will be elucidated in more detail and recent metabolic engineering strategies for an optimized metabolite production are briefly described. Those natural products classes were selected in the project context of the Bioeconomy Science Center (BioSC) project 'CombiCom', which focused on the exploitation of natural product biosynthetic pathways to deliver bioactive natural products and structurally derived compounds and thus, were likewise used as model biosynthetic pathways in this work.

Terpenes constitute one of the largest and most diverse secondary metabolite class encompassing over 80,000 compounds, which mainly are of plant-origin [396–399]. They all are characterized by an isoprenoid C_5 scaffold, which is repeatedly connected to form hemi- (C_5), mono- (C_{10}), sesqui- (C_{15}), di- (C_{20}), tri- (C_{30}), tetra- (C_{40}), and polyterpenes (>C_{40}) (**Fig. I.8**) [400,401].

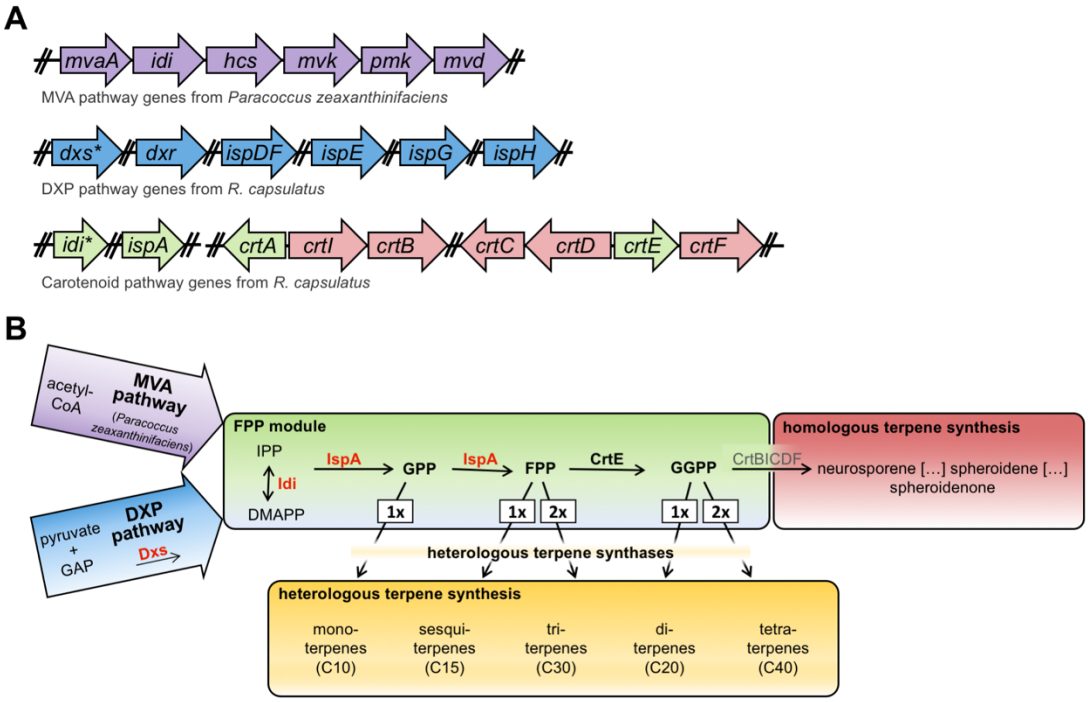

Figure I.8 Homologous and heterologous terpene biosynthesis pathway of *R. capsulatus* and a selection of metabolic engineering strategies for improved heterologous terpene titers.
A) The DXP pathway (blue arrows), which is composed of seven genes, is responsible for providing terpene precursor molecules, while the inherent carotenoid biosynthesis pathway (green and red arrows) encompasses nine genes located at several positions in the *R. capsulatus* genome and results in the production of various homologous terpenes. For a further increased terpene precursor supply, the heterologous MVA module from *Paracoccus zeaxanthinifaciens* (violet arrows) can be overexpressed. Genes indicated with an asterisk are available in two chromosomal copies. The gene *dxr* is also denoted as *ispC* and the gene *ispE* as *cmk*. **B**) Within the DXP pathway, pyruvate and GAP are used to build the terpene precursor molecules IPP and DMAPP. Additionally, acetyl-CoA can be used as a building block for such precursors, if the heterologous MVA module is co-expressed in the respective production strain. In the following, IPP and DMAPP are converted *via* the precursors GPP, FPP and GGPP to different homologous terpenes, such as the carotenoids spheroidene or neurosporene. If available, heterologous terpene synthase can be overexpressed for conversion of FPP and its derivatives to novel terpenes of varying complexity and isoprene chain length (yellow module). The enzyme names marked in red are common targets of metabolic engineering strategies for increased terpene titers. MVA: mevalonate, DXP: 1-deoxy-D-xylulose 5-phosphate, GAP: glyceraldehydes-3-phosphate, Dxs: 1-deoxy-D-xylulose 5-phosphate synthase, FPP: farnesyl pyrophosphate, IPP: isopentenyl pyrophosphate, DMAPP: dimethylallyl pyrophosphate, Idi: isopentenyl diphosphate isomerase, IspA: FPP synthase, GPP: geranyl pyrophosphate, CrtE: GGPP synthase, GGPP: geranylgeranyl pyrophosphate, CrtB: phytoene synthase, CrtC: hydroxyneurosporene synthase, CrtD: hydroxyneurosporene desaturase, CrtF: demethylspheroidene O-methyltransferase, CrtI: phytoene desaturase.

The terpenoid synthesis starts from the two isoprene intermediates isopentenyl pyrophosphate (IPP) and dimethylallyl pyrophosphate (DMAPP), which are produced from three acetyl-coenzyme A molecules (acetyl-CoA) *via* the mevalonate (MVA) pathway or from glyceraldehyde-3-phosphate (GAP) and pyruvate *via* the 1-deoxy-D-xylulose 5-phosphate (DXP) pathway, also denoted as the 2-C-methyl-D-erythritol 4-phosphate (MEP) pathway. Starting from IPP and DMAPP, the prenyltransferases catalyze the elongation of linear prenyl pyrophosphates *via* head-to-tail condensations resulting in the formation of the three terpene precursors C_{10}- geranyl pyrophosphate

(GPP), C_{15}- farnesyl pyrophosphate (FPP), and C_{20}- geranylgeranyl pyrophosphate (GGPP), which are subsequently used as precursor molecules for the biosynthesis of monoterpenoids, sesqui- and triterpenoids, or di- and tetraterpenoid, respectively. Afterwards, further rearrangements, cyclization reactions or decorating reactions may be performed *via* P450 monooxygenases, reductases, dehydrogenases, or transferases, further broadening the available terpene spectrum [402–407]. While the MVA pathway is predominantly found in eukaryotes (e.g., mammals, plants, and fungi), archaea, and a few bacteria [408,409], the DXP pathway mainly occurs in bacteria, cyanobacteria, and green algae [410]. Inherently, terpenes are employed for a variety of purposes in plant physiology and development, such as photoprotection or antioxidation (carotenoids), communication, and hormone signaling (e.g. pinene) or repellent activity against predators and parasites (e.g. verbenone, β-caryophyllene) [402,411–413]. Due to those versatile bioactivities, terpenes are also of commercial interest to the pharmaceutical sector for the treatment of pathogenic infections, inflammation or cancer [376,414,415]. Furthermore, they render terpenoids exceedingly interesting for the production of flavors and fragrances, biofuels or bio-based pesticides in agriculture [416–419]. As an industrial production host, mainly *E. coli* and *S. cerevisiae* are exploited, as documented by several heterologously produced and already marketed terpenes. Prominent examples are β-farnesene, which is produced in yeast by Amyris, valencene and nootkatone, both produced in yeast by Evolva, patchoulol and sclareol, which are produced in both yeast and *E. coli* by Firmenich or stevio glycosides, marketed under the name EverSweet® and produced in yeast by Cargill. Furthermore, alternative hosts such as *Rhodobacter sphaeroides* are increasingly applied, as illustrated by the marketed terpenes valencene and nootkatone by the biotech company Isobionics (now BASF) [419].

Currently, there are several approaches for engineering efficient terpenoid production strains, which can often be combined to increase effectiveness [396,420,421]. Here, modifications can be carried out at different levels, e.g., increasing endogenous precursor supply, modifying cofactor requirements, eliminating bottlenecks and competitive reactions, and mitigating the toxic effects of intermediates or products, as well as genetic and protein engineering [406,422–424]. Extensive research on the production of heterologous terpenes in the phototrophic bacterium *R. capsulatus* has been conducted, since it proved to be a promising host for the production of recombinant membrane proteins or valuable natural compounds (**chap. I.1.2.2**) [185–187]. It has been shown that engineering of isoprenoid precursor biosynthesis can lead to a strong increase in sesqui- and triterpenoid formation in *R. capsulatus* [187,425] and *R. sphaeroides* [426–430], and in particular, co-expression of a terpene synthase with

the FPP synthase IspA and/or enzymes of the heterologous MVA pathway led to significantly increased production of the corresponding plant terpenoids. However, as shown in various studies, overexpression of the isoprenoid intermediates in microbial hosts can lead to toxicity, metabolic stress and feedback inhibition [402,431–435], impairing the growth and production yield. This problem is often addressed by using controllable induction techniques with gradual promoters or expression systems that flexibly respond to product concentration or other environmental stimuli [417,436], as demonstrated for the dynamic regulation of FPP level in the terpene biosynthesis of *E. coli* [434]. Furthermore, increased yields can also be gained by reducing competitive reactions with dynamic promoters, but without impairments in cell survival, as shown for the yeast-based production of santalene [437] or the implementation of feedback loops for improving microbial biofuel production [438].

In summary, terpenes are valuable and versatile metabolites for both pharmaceutical and biotechnological applications. Thus, the heterologous production of novel terpene variants needs to be transferred to alternative expression hosts, such as the phototrophic bacterium *R. capsulatus*, as a natural terpene producer (**chap. I.1.2.2**), and their bioactivities should be elucidated with respect to further possible application fields such as antimicrobial treatments.

The bacterial secondary metabolites belonging to the group of **prodiginines** are red-pigmented, bioactive tripyrroles [439], which include compounds such as prodigiosin, undecylprodigiosin, norprodigiosin, cycloprodigiosin, or streptorubin B. They are naturally produced from amino acids and acetate building blocks by various proteobacterial species, including *Serratia*, *Hahella*, *Vibrio*, and *Streptomyces* [440–443]. In contrast to the great variety of terpenes, the diversity within prodiginines is rather limited as the compounds can be divided into only two main groups according to their structure: they either carry *n*-alkyl residues, such as prodigiosin, norprodigiosin, or undecylprodigiosin or are cyclized derivatives such as cycloprodigiosin and streptorubin B [441]. The biosynthesis genes of all prodiginines are encoded in a unidirectional gene cluster (**Fig. I.9A**) and proceeds *via* a bifurcated pathway, yielding the bipyrrole 2,2-bipyrrole-5-carboxyaldehyde (MBC), originated from proline and malonyl-coA, and a monopyrrole (e.g., 2-methyl-3-pentyl-pyrrole, MAP), produced from pyruvate and 2-octenal. MBC and the monopyrrole are finally condensed by a ligase, such as the prodigiosin ligase PigC, to form the tripyrrolic red-pigmented compound (**Fig. I.9B**). Afterwards, a cyclization reaction may be performed by non-heme iron oxidases [444]. While MBC synthesis is strictly conserved, the biosynthesis of monopyrrole

intermediates varies in terms of substitution patterns and functional proportions and is thus responsible for the natural diversity of prodiginines [394,441].

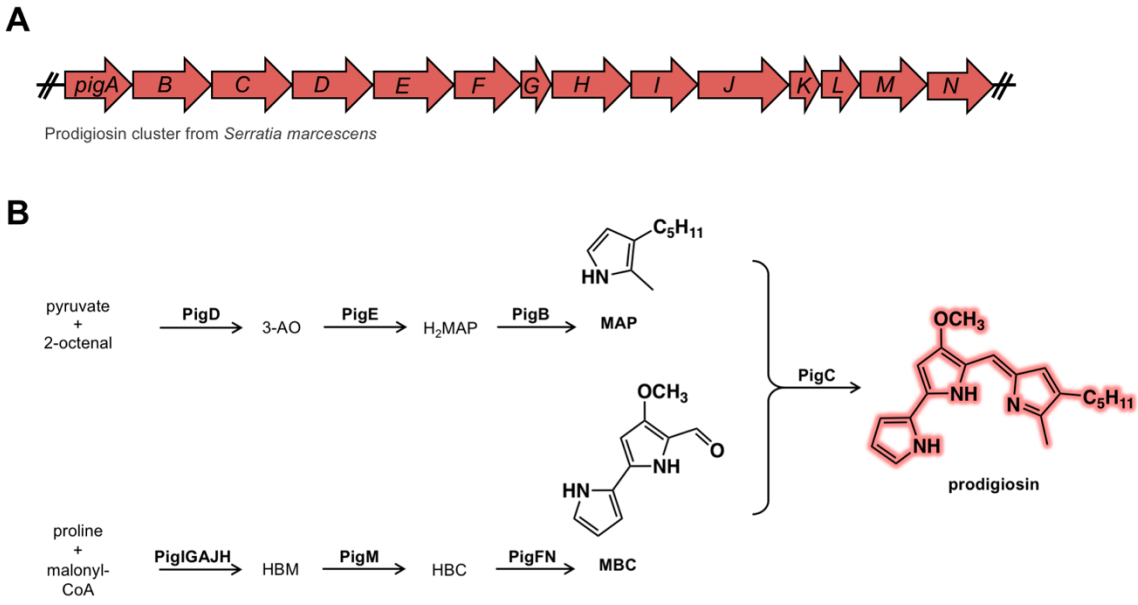

Figure I.9 Prodigiosin gene cluster and respective biosynthesis pathway.
A) The inherent prodigiosin biosynthesis cluster from *Serratia marcescens* encompasses 14 unidirectional genes with a total length of 21 kb. While the genes *pigB-pigE* encode enzymes responsible for the synthesis of MAP and the final condensation with MBC to form prodigiosin, the remaining genes *pigA* and *pigF-pigN* encode enzymes catalyzing the production of MBC. **B**) The prodigiosin biosynthesis is a bifurcated pathway starting on the one hand from pyruvate and 2-octenal, which are converted to the precursor molecule MAP by the enzymes PigD,E,B, and on the other hand from proline and malonyl-CoA, which are transformed to the precursor molecule MBC by the enzymes PigI,G,A,J,H,M,F,N. The two resulting molecules MAP and MBC are finally condensed to the red-colored prodigiosin by the enzyme PigC. MAP: 2-methyl-3-pentyl-pyrrole, MBC: 2,2-bipyrrole-5-carboxyaldehyde, 3-AO: 3-acetyloctanal, HBM: 4-hydroxy-2,2'-bipyrrole-5-methanol, HBC: 4-hydroxy-2,2'-bipyrrole-5-carbaldehyde, prodigiosin: 2-methyl-3-pentyl-6-methoxyprodiginine, PigD: 3-acetyloctanal synthase, PigE: 3-acetyloctanal aminotransferase, PigB: H_2MAP oxidase/ dehydrogenase, PigI: L-prolyl-AMP ligase, PigG: peptidyl carrier protein, PigA: L-prolyl-PCP dehydrogenase, PigJ: pyrrolyl-β-ketoacyl ACP synthase, PigH: HBM synthase/ aminotransferase, PigM: HBM oxidase/ dehydrogenase, PigF: 3-acetyloctanal aminotransferase, PigN: oxidoreductase.

Prodigiosin but also prodiginines, in general, offer a multitude of bioactivities, which make them promising candidate compounds for pharmaceutical and biotechnological industry. Firstly, they offer an antibiotic activity against various different species, including major human pathogens such as *Staphylococcus aureus* or *Streptococcus pyogenes* [445–449], with a particularly pronounced effect on Gram-positive bacteria [440]. Secondly, prodigiosin has been shown to exhibit promising activity against various cancer cell lines by induction of apoptosis, including hematopoietic cancer, breast cancer, oral cancer, and skin cancer [450–454], administered solely or in combination with other inhibitors [455]. A prominent example for a synthetic anti-cancer agent is the indole bipyrrole named Obatoclax, that is already being tested in phase II clinical trials for the treatment of various cancers such as mantle cell lymphoma, myelofibrosis or leukemia [456–458]. Additionally, prodiginines were

shown to exhibit antifungal and nematocidal activities, which is a valuable source for agricultural applications [459–461]. However, the availability of new-to-nature prodiginine derivatives is limited by their low diversity, rendering the use of semi- or mutasynthesis as well as *in silico* applications to broaden the product spectrum particularly attractive. Due to the bifurcated biosynthetic pathway and the natural promiscuity of PigC, mutasynthesis could be applied to specifically produce synthetic prodiginines by Pietruzska and coworkers [394,462]. Furthermore, PigC was subject to directed evolution approaches to enhance enzyme activity or broaden substrate promiscuity [463–465] or even replaced by homolog ligases from *Pseudoalteromonadaceae* strains [466]. Since those complex chemical and synthetic biological approaches require a strict and straightforward control of enzymatic activity, they might benefit from light-responsive regulatory tools on transcriptional or post-translational level.

Finally, an increasingly important group of secondary metabolites are **rhamnolipids (RL)**, which are bio-based surfactants that provide a more sustainable substitute for petrochemical-based tensides. In general, rhamnolipids belong to the group of glycolipids and thus, are amphiphilic compounds composed of one or two hydrophilic rhamnose molecules linked to one or two hydrophobic 3-hydroxy fatty acids of various chain lengths (C_x-C_y), such as 3-(3-hydroxyalkanoyloxy)alkanoate (HAA) (**Fig. I.10**) [467,468]. Depending on the number of sugar residues, they are referred to as mono-rhamnolipids (MRL) or di-rhamnolipids (DRL). In nature, rhamnolipids are mostly produced by bacteria of the genus *Pseudomonas*, with the opportunistic pathogen *P. aeruginosa* being one of the most prominent rhamnolipid producers, but they can also

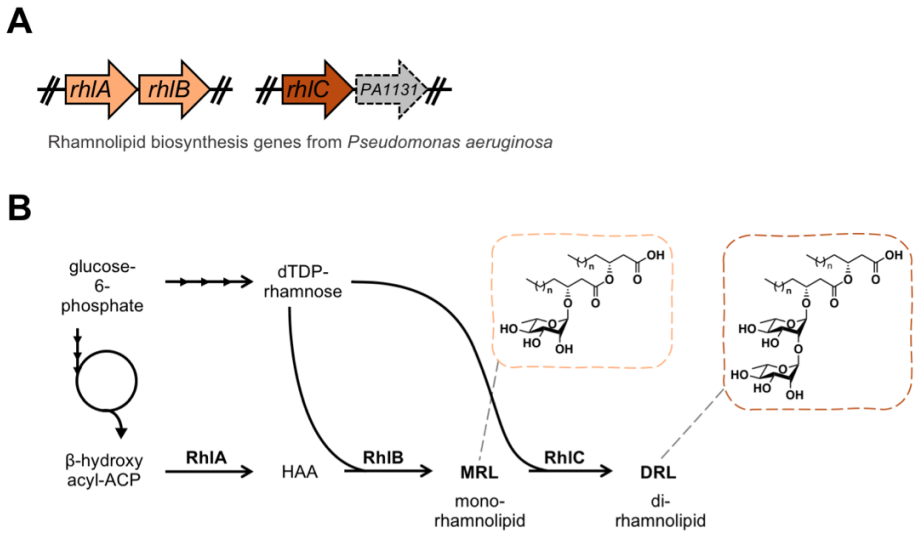

Figure I.10 Rhamnolipid biosynthesis genes and associated pathway in *Pseudomonas aeruginosa*. **A**) The biosynthesis of rhamnolipids is encoded by three genes and is organized in two bicistronic operons-*rhlA* together with *rhlB* and *rhlC* with *PA1131*, a gene of unknown function [472]. **B**) The acyltransferase

RhlA first assembles the 3-(3-hydroxyalkanoyloxy)alkanoic acid (HAA) from two activated β-hydroxy fatty acids and in a next step HAA is coupled with a molecule of activated dTDP-rhamnose by the rhamnosyltransferase RhlB *via* a β-glycosidic bond. The resulting mono-rhamnolipid (MRL) is converted to a di-rhamnolipid (DRL) by the rhamnosyltransferase RhlC, which catalyzes the addition of a further dTDP-rhamnose to the first rhamnose moiety. ACP: acyl carrier protein, dTDP: deoxythymidine diphosphate.

be found in *Burkholderia* spp. [468–470]. In *P. aeruginosa*, the length of fatty acid chains varies between C_8 and C_{14}, but most frequently C_{10}-C_{10} chains are found, whereas in *Burkholderia* species long-chain C_{14}-C_{14} fatty acids are mostly used [469,471].

The rhamnolipid biosynthesis encompasses three sequential enzymatic reactions (**Fig. I.10B**). In the first step, two 3-hydroxyacyl molecules bound to an acyl carrier protein (ACP) are esterized by the acyltransferase RhlA to form HAA [473]. The rhamnosyltransferase RhlB subsequently links an HAA molecule with activated dTDP-rhamnose to create MRLs [474,475]. In the last reaction, the rhamnosyltransferase RhlC catalyzes the addition of a second dTDP-rhamnose molecule to the MRLs, yielding DRLs [472]. While the genes encoding RhlA and RhlB are organized in a bicistronic operon, the gene encoding RhlC is part of a bicistronic operon with *PA1131*, a gene of unknown function (**Fig. I.10A**) [468,472]. Bacterial rhamnolipids fulfill important functions in their natural producer, such as enabling swarming motility and biofilm formation or act as virulence factors [476–479]. They also inhibit phagocytosis by host macrophages and enhance the uptake of hydrophobic substances [480,481]. However, since their amphiphilic character is valuable as a biosurfactant and they can be produced from renewable resources, which commonly exhibit a low ecotoxicological potential and offer an alternative to petrochemical-based surfactants, rhamnolipids have become a focus of interest in the biotechnology and pharmaceutical industry [482–486]. Besides their use for bioremediation and oil recovery, due to their emulsifying properties, they are also applied in the field of pharmaceuticals and cosmetics, as they show low toxicity, surface active properties and, antimicrobial activity [484,487–489]. Moreover, rhamnolipids are valuable bio-detergents and thus are increasingly added to detergent compositions, laundry products, shampoos and soaps [490,491]. Currently, *P. aeruginosa* is mostly used for the industrial production of rhamnolipids, but it features some disadvantages, such as a complex quorum-sensing-based regulatory mechanism of rhamnolipid biosynthesis or its general pathogenicity [492,493]. Therefore, there are increasing efforts to use heterologous hosts such as *E. coli*, *P. fluorescens,* and *P. putida* KT2440 [494–496] and to make them industrially competitive by means of metabolic engineering, adaptive laboratory evolution, and bioprocess optimization [137,482,497–499]. Additionally, attempts are being made to influence the composition of the rhamnolipid mixtures at the genetic level by means of metabolic engineering and the use of inducible promoters to finally be able to produce tailormade rhamnolipids [137,179,490]. In this

context, controlling the different rhamnolipid mixtures by means of light-responsive regulators could provide an advantage on the way to produce designer rhamnolipids [500].

In summary, the presented examples illustrate that versatile approaches are available to establish light control over different cellular processes. However, current tools necessarily require further characterization, optimization, and redesign to be adaptable to the requirements of these multifaceted biological processes.

I.5. OUTLINE OF THIS THESIS

The field of synthetic biology is based on the redesign or development of artificial, biological systems such as cells, tissues, or organisms with predictable performance characteristics. For this purpose, both the strict and straightforward orchestration as well as a simple and robust visualization of biological processes is indispensable. Light as environmental factor seems to be ideally suited for this task, as it represents a very precise, spatially, and temporally highly tunable and flexible stimulus. Thus, this thesis aimed to **establish optogenetic strategies for controlling versatile cellular processes on different cellular levels and at several experimental scales**.

The here addressed biological processes can be assigned to the following cellular level: (i) the transcriptional level and (ii) the post-translational level *via* protein-cell interactions. Furthermore, (iii) complex secondary metabolite pathways are established that could benefit from light control. Additionally, (iv) relevant visualization strategies on batch culture and single-cell level are utilized to online-monitor individual biological processes with high temporal resolution and under defined cultivation conditions.

First, photocaged IPTG variants with varied solubility were analyzed with respect to their usability for light-mediated transcriptional regulation in the expression hosts *E. coli*, *P. putida* and *B. subtills* (**chapter II.1.1**). Subsequently, the application of photocaged inducers for light-controlled gene expression was established for the alternative production host *R. capsulatus* under both phototrophic and non-phototrophic conditions (**chapter II.1.2**) Furthermore, challenges and solutions of photocaged inducer synthesis and their application in bacteria are illustrated by means of photocaged IPTG variants with red-shifted absorption characteristics and photocaged salicylic acid derivatives and corresponding promoter systems, which had not yet been applied for light-mediated gene expression (**chapter II.1.3**). Finally, photocaged inducers were utilized for wavelength-selective activation of gene expression in *P. putida* (**chapter II.1.4**). Additionally, fluorescent proteins were characterized with respect to both their spectroscopical and photosensitizing properties (**chapter II.2.1**) and subsequently, those proteins were analyzed for their suitability to control the cell viability of various Gram-positive and Gram-negative bacteria *via* light-mediated protein-cell interactions (**chapter II.2.2**). As an example of metabolic pathways that would benefit from light-mediated orchestration of enzyme activities or metabolite fluxes, the biosynthetic pathway of both homologous and heterologous terpenes was established in the alternative expression host *R. capsulatus* and optimized with respect to cultivation and illumination conditions to improve the terpene titers (**chapter II.3.1-3**).

II. RESULTS

This chapter is composed of nine manuscripts, which either have already been published or are about to be published in peer-reviewed journals. The presented work is based on joint publications resulting from a variety of fruitful collaborations with working groups in the context of the BioSC project CombiCom and beyond. In particular, I would like to mention the Institute of Bioorganic Chemistry of Prof. Jörg Pietruszka (University of Düsseldorf), the Multiscale Bioengineering group of Prof. Alexander Grünberger (University of Bielefeld) and the Molecular Phytomedicine group of Prof. Grundler (University of Bonn). The own contribution to the respective manuscript is commented on the first page of each document.

II.1. LIGHT-MEDIATED TOOLS FOR TRANSCRIPTIONAL REGULATION

II.1.1. NOVEL PHOTOCAGED IPTG VARIANTS FOR LIGHT-CONTROLLED GENE EXPRESSION IN *E. COLI*, *P. PUTIDA* AND *B. SUBTILIS*

Effect of photocaged isopropyl β-D-1-thiogalactopyranoside solubility on the light responsiveness of LacI-controlled expression systems in different bacteria

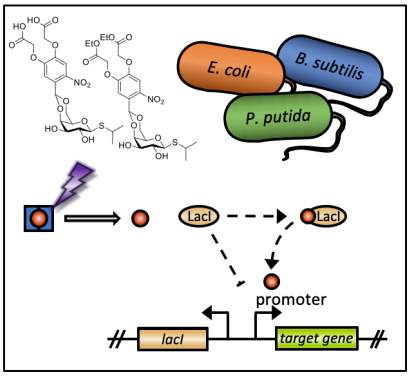

Fabian Hogenkamp*, **Fabienne Hilgers***, Andreas Knapp, Oliver Klaus, Claus Bier, Dennis Binder, Karl-Erich Jaeger, Thomas Drepper and Jörg Pietruszka

ChemBioChem, Feb 2;22(3):539-547 (2021). cbic.202000377

The online version may be found at: 10.1002/cbic.202000377

Status: published

For the Supporting Information see Appendix (**Chapter V.1., page 272**).

Own contribution:

Designing and performing biological experiments, plasmid constructions, analyzing *in vivo* data, writing parts of the manuscript.

ChemBioChem
Full Papers
doi.org/10.1002/cbic.202000377
Chemistry Europe
European Chemical Societies Publishing

Effect of Photocaged Isopropyl β-D-1-thiogalactopyranoside Solubility on the Light Responsiveness of LacI-controlled Expression Systems in Different Bacteria

Fabian Hogenkamp[+],[a] Fabienne Hilgers[+],[b] Andreas Knapp,[b] Oliver Klaus,[b] Claus Bier,[a] Dennis Binder,[b] Karl-Erich Jaeger,[b, c] Thomas Drepper,*[b] and Jörg Pietruszka*[a, c]

Photolabile protecting groups play a significant role in controlling biological functions and cellular processes in living cells and tissues, as light offers high spatiotemporal control, is non-invasive as well as easily tuneable. In the recent past, photoresponsive inducer molecules such as 6-nitropiperonyl-caged IPTG (NP-cIPTG) have been used as optochemical tools for Lac repressor-controlled microbial expression systems. To further expand the applicability of the versatile optochemical on-switch, we have investigated whether the modulation of cIPTG water solubility can improve the light responsiveness of appropriate expression systems in bacteria. To this end, we developed two new cIPTG derivatives with different hydrophobicity and demonstrated both an easy applicability for the light-mediated control of gene expression and a simple transferability of this optochemical toolbox to the biotechnologically relevant bacteria *Pseudomonas putida* and *Bacillus subtilis*. Notably, the more water-soluble cIPTG derivative proved to be particularly suitable for light-mediated gene expression in these alternative expression hosts.

Introduction

In general, optogenetics combines genetic and optical methods to allow fast control of cellular functions with high spatiotemporal resolution and in a non-invasive fashion.[1] The control over gene expression by light can basically be realised by employing genetically encoded photoreceptors or chemically photocaged (bio)molecules. Recombinant photoreceptors are typically based on light-responsive two- or one-component systems, are extensively studied and have been successfully employed as reversible photoswitches for light-mediated *in vivo* signal transduction in various biological applications.[2]

Besides the use of photoreceptors photolabile protecting groups were established as optochemical tools for a variety of diverse applications.[3] In recent years, many approaches were published, in which photocaged compounds have been used for controlling different cellular processes, ranging from cell signalling,[3b,4] over drug delivery[5] to gene expression.[6] In this context, especially 2-nitrobenzyl-photocaging groups (NB) and their derivatives such as 6-nitropiperonyl (NP) were commonly used to mediate an adequate and well-characterised UV-A light-triggered release of bioactive molecules.[3d,7] To implement caged compounds as versatile optochemical switches, a variety of photolabile protecting groups has been developed focusing on the i) redshifted absorption,[3b,8] ii) higher quantum yields[9] and iii) an improved solubility.[10] Especially for *in vivo* approaches an excellent stability towards enzymatic hydrolysis, good biocompatibility, and low overall toxicity of caged compounds (also including the photolysis products) are indispensable.[11] In addition, the extend of the caged compound's solubility could further modulate their ability to pass bacterial cell membranes either through passive processes including free diffusion and porin-based uptake or by active, membrane transporter-mediated processes.[12]

In the recent past, photoresponsive inducer molecules such as caged derivatives of doxycycline,[13] isopropyl β-D-thiogalactopyranoside (IPTG)[6a,b] or several other carbohydrates[6c,d] have been used as irreversible optochemical switches for appropriate microbial expression systems. Especially the applicability of 6-nitropiperonyl photocaged IPTG (NP-cIPTG, **1**) for bioengineering approaches using *Escherichia coli*[14] and *Corynebacterium glutamicum*[15] as production hosts could be demonstrated. However, a further expansion of the applicability in different expression hosts was for instance hindered by the low water-

[a] F. Hogenkamp,[+] Dr. C. Bier, Prof. Dr. J. Pietruszka
Institute of Bioorganic Chemistry
Heinrich Heine University Düsseldorf at Forschungszentrum Jülich
Stetternicher Forst, 52426 Jülich (Germany)
E-mail: j.pietruszka@fz-juelich.de
[b] F. Hilgers,[+] Dr. A. Knapp, O. Klaus, Dr. D. Binder, Prof. Dr. K.-E. Jaeger, Dr. T. Drepper
Institute of Molecular Enzyme Technology
Heinrich Heine University Düsseldorf at Forschungszentrum Jülich
Stetternicher Forst, 52426 Jülich (Germany)
E-mail: T.Drepper@fz-juelich.de
[c] Prof. Dr. K.-E. Jaeger, Prof. Dr. J. Pietruszka
Institute of Bio- and Geosciences (IBG-1: Biotechnology)
Forschungszentrum Jülich
Stetternicher Forst, 52426 Jülich (Germany)
[+] These authors contributed equally to this work.

Supporting information for this article is available on the WWW under https://doi.org/10.1002/cbic.202000377

ChemBioChem
Full Papers
doi.org/10.1002/cbic.202000377
Chemistry Europe
European Chemical Societies Publishing

solubility of NP-cIPTG (**1**; 0.7 mM), as appropriately high inducer concentrations were not soluble in the cultivation medium.

Derivatives of the 2-nitrobenzyl group with improved solubility in aqueous media have been applied before (Figure 1 A). Tsien and co-worker as well as Ni *et al.* conceived a 4,5-bis (carboxymethoxy)-2-nitrobenzyl protecting group (BC, **2**), which they stated to be highly water-soluble.

However, they masked the carboxylate **2** as acetoxymethyl ester **3** to facilitate diffusion across cell membranes.[12a,b] Russell *et al.* published a similar derivative **4**, but bearing an additional third carboxy group in the benzylic position, for the synthesis of photolabile tyrosine, whereby a solubility of at least 30 mM was reached.[10b] As the formation of a dioxolane is required for the protection of IPTG, previously reported α-carboxy-2-nitrobenzyl (α-CNB, **5**–**8**) photocages[10a,c,16] were not considered, because the α-carboxy-group increases solubility, but concurrently blocks the position where the dioxolane is later formed.

Based on these results the BC protecting group **2** was chosen in this work as a candidate for the synthesis of a charged, highly water-soluble photocaged IPTG derivative (Figure 1 B) and was further applied to determine the influence of the solubility and the charge on the inducer uptake through the cell membrane and the resulting expression response. In addition, the 4,5-bis(ethoxycarbonylmethoxy)-2-nitrobenzyl protecting group (BEC, **9**) harbouring lipophilic ester moieties, was selected as an alternative caging group, which might facilitate its passive diffusion across cell membranes. Afterwards, enzymatic hydrolysis of the ester moiety could lead to intracellular accumulation.[12c] To comparatively analyse the effect of caged inducer solubility on light dependent control of gene expression in bacteria, the two new cIPTG derivatives BEC-cIPTG (**10a**, derived from **9**) and BC-cIPTG (**10b**, derived from **2**) were synthesised and the maximum solubility was quantified. The photophysical properties as well as photolysis in aqueous media were characterised. Subsequently, the *in vivo* applicability of the newly synthesised compounds for light-inducible gene expression was analysed in comparison to the well-established NP-cIPTG (**1**) in *E. coli* in a time-resolved manner. Finally, we investigated whether optochemical control of gene expression can also be implemented in the alternative expression hosts *Pseudomonas putida* and *Bacillus subtilis*, which exhibit individual morphological and physiological properties. Therefore, we used the photocaged IPTG derivatives **1**, **10a**, and **10b** together with appropriate LacI repressor-controlled expression systems and comparatively evaluated their light-responsiveness.

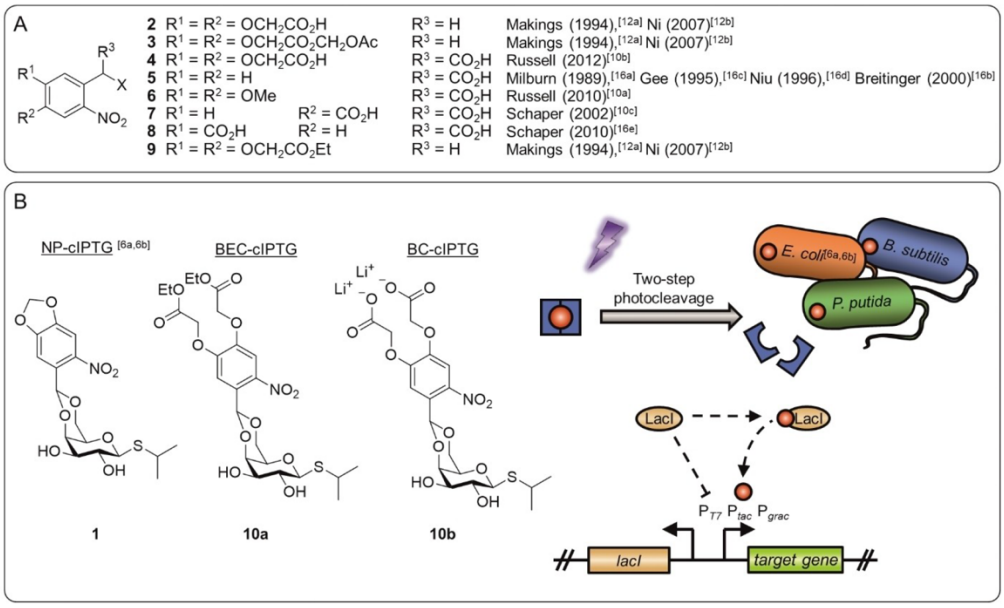

Figure 1. Photolabile protection groups and their application in this work. A) A variety of previously published photolabile protection groups with improved aqueous solubility or membrane permeability based on the NB photocaging group. B) Three photolabile protection groups were used in this work to construct the photocaged IPTG variants NP-cIPTG (**1**), BEC-cIPTG (**10a**) and BC-cIPTG (**10b**), strongly differing in their water solubility. These caged inducer molecules (red dot with blue frame) are biologically inactive; however, upon illumination with UV-A light, their activity can be restored by a two-step cleavage process. Subsequently, the IPTG binds the repressor protein LacI releasing LacI from the P_{T7}, P_{tac} or P_{grac} promoter and thus inducing gene expression. This principle was applied to analyse the effect of cIPTG solubility on the inducibility of LacI repressor-controlled target gene expression in *E. coli*, *P. putida*, and *B. subtilis*.

ChemBioChem
Full Papers
doi.org/10.1002/cbic.202000377
Chemistry Europe
European Chemical Societies Publishing

Results

Synthesis and photochemical properties of clPTGs

The BC-clPTG (**10b**) was synthesised in a three-step reaction (Scheme 1; yield over three steps: 24%) from 4,5-bis (ethoxycarbonylmethoxy)-2-nitrobenzaldehyde (**11**), which was obtained following the previously reported procedure by Ni *et al.* (see the Supporting Information).[12b] The 2-nitrobenzaldehyde derivative **11** was reacted with triethyl orthoformate to form the corresponding acetal **12** in 89% yield, which then was converted to BEC-clPTG (**10a**; 45%) in a transacetalisation, as the direct acetalization was not feasible. In this step the triethyl orthoformate was preferred to the trimethyl orthoformate due to the occurrence of transesterification during the acid-catalysed reaction, which was leading towards a mixture of products. After deprotection under basic conditions the BC-clPTG (**10b**) could be obtained in 59% yield as the corresponding lithium-salt, which promised advantageous solubility properties compared to the free-acid. NP-clPTG (**1**) was synthesised from 6-nitropiperonal (**13**) according to literature procedures.[6a,b] The purity of BEC-clPTG (**10a**), BC-clPTG (**10b**) and NP-clPTG (**1**) was determined by qNMR (Table S3 in the Supporting Information).

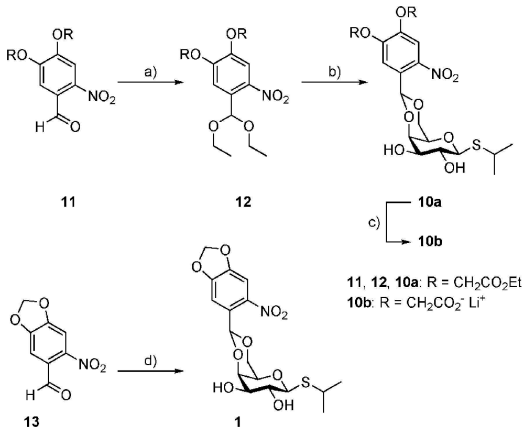

Scheme 1. Synthesis of BEC-, BC- and NP-photocaged IPTGs **10a**, **10b** and **1**: a) Triethyl orthoformate, pyridinium *p*-toluenesulfonate, ethanol, reflux, 19 h (89%); b) IPTG, *p*-toluenesulfonic acid, CH_2Cl_2, RT, 20 h (45%); c) 0.2 M LiOH (aq.), MeOH, 0 °C–RT, 1 h (59%); d) IPTG, sulfuric acid, DMSO, 0 °C–RT, 24 h (21%).

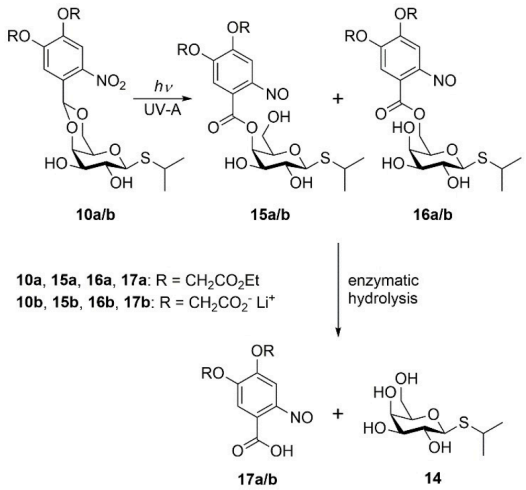

Scheme 2. Two-step release sequence after photolysis of BEC- and BC-photocaged IPTG **10a** and **10b** by irradiation with UV-A light and a subsequent enzymatic hydrolysis by a microbial esterase, as previously described.[6a,b]

Due to the structural similarity of the newly synthesised caged compounds **10a** and **10b** to the NP-clPTG (**1**), IPTG (**14**) should be released upon UV-A light exposure in a two-step photocleavage reaction as previously described.[6a,b] In the first step the irradiation with UV-A light leads to the formation of ester intermediates **15** and **16**, which might subsequently be cleaved by a microbial esterase. The corresponding nitroso compounds **17** are formed as the photo by-product (Scheme 2).

The *in vitro* characterisation (Tables 1 and S2, Figures S1–S3) of the new photocaged compounds **10a** and **10b** showed uncaging quantum yields (Φ_u) and molar extinction coefficients (ε) in the range of previously reported caged compounds.[6d,17] The resulting photolytic efficiencies ($\varepsilon\Phi_u$) are all in the same order of magnitude. However, more importantly the uncaging half-life time of the photolytic cleavage amounts to 2.2 min for BEC-clPTG (**10a**), 3.5 min for BC-clPTG (**10b**), and 3.4 min for NP-clPTG (**1**). This underlines the fast formation of the ester intermediates **15** and **16** (Figure S4, Table S2). Full photoconversion of the clPTG variants (1 mM) by irradiation with UV-A light (375 nm, 6.4 mW cm^{-2}) was achieved in less than 30 min for **10a** and **1**. For derivative **10b** about ~5% of the starting material remained after irradiation for 30 min (Figure S15).

The BC-clPTG (**10b**) showed a maximum solubility of 147 mM in deionised and degassed water, which is over 200 times higher than the maximum solubility of NP-clPTG (**1**),[6b] but only ~8% of the maximum solubility of IPTG (**14**) itself (Table 1). Other previously reported photocaged carbohydrates were in the range of 4–58 mM.[6d] In contrast, the BEC-

Table 1.

Compound	λ_{max} [nm]	ε[a] [M^{-1}cm^{-1}]	$t_{0.5}$[b] [min]	s[c] [mM]	Φ_u[d]	$\varepsilon\Phi_u$[a] [M^{-1}cm^{-1}]
1[e]	241 336	1690	3.4	0.7	0.50	845
10a[e]	298	1810	2.2	<0.1	0.68	1230
10b[f]	242 340	3543	3.5	147	0.46	1630
14	204	–	–	1941	–	–

[a] ε = molar extinction coefficient at λ = 375 nm. [b] $t_{0.5}$ = uncaging half-life time. [c] s = solubility in deionised and degassed water. [d] Φ_u = uncaging quantum yield upon 375 nm irradiation. [e] measured in MeOH. [f] measured in sodium phosphate buffer (0.1 mM, pH 7.5).

ChemBioChem | Full Papers doi.org/10.1002/cbic.202000377 | Chemistry Europe European Chemical Societies Publishing

cIPTG (**10a**) displayed a more than 7-times lower solubility of <0.1 mM, as expected due to the ester-protected carboxylic acids. Since the possible higher membrane permeability of BEC-cIPTG might result in an improved *in vivo* applicability, this cIPTG derivative was additionally used for further investigations.

Applicability of cIPTGs for light-controlled gene expression in bacteria

After the successful synthesis of BEC- and BC-cIPTG (**10a** and **10b**), we next analysed whether the different solubility of the cIPTG derivatives (solubility in aqueous solvents: **10b** ≫ **1** > **10a**, see Table 1) affect the inducibility of LacI repressor-controlled expression systems. The regulatory system, which originally controls the lactose consumption in *E. coli*, is one of the most often used regulation mechanisms for triggering heterologous gene expression in this host.[18] The development of different recombinant promoters (e.g., P_{tac}, P_{trc}, P_{T7}), whose activities can be tightly and gradually controlled by the concentration of the added inducer (e.g., the non-hydrolysable lactose analogue IPTG) led to its broad applicability in basic research and biotechnological production processes. Furthermore, the development of light-responsive NP-cIPTG (**1**) allowed for non-invasive light-mediated control of gene expression in *E. coli*.[6a–c] To further optimise light responsiveness of this promising optochemical on-switch in *E. coli* and to facilitate its transferability to other industrially relevant microbes, we used the following Gram-negative and -positive bacteria as appropriate model hosts offering individual morphological and physiological properties: i) *E. coli* Tuner(DE3) is a lactose permease-deficient strain and was shown to be well suited for NP-cIPTG-based light control of gene expression, because the uptake of appropriate inducers is solely dependent on passive diffusion processes. Previous studies using *E. coli* Tuner(DE3) revealed a very stringently controlled and homogeneous gene expression that gradually responded to changes of illumination time or light intensity.[6b,c,14] ii) *P. putida* KT2440 is a rod-shaped, Gram-negative soil bacterium, which offers a pronounced tolerance towards xenobiotics[19] as well as redox stress.[20] Besides its genetic accessibility and its FDA certification as a host-vector biosafety system,[21] *P. putida* exhibits an extraordinary versatile metabolism that makes it especially suited for a variety of biotechnological applications including the production of various high-value natural products and their derivatives.[22] iii) *Bacillus subtilis* DB430 is a Gram-positive bacterium commonly used as a "microbial cell factory" for high-level production and secretion of proteins for industrial applications.[23] In contrast to the Gram-negative bacteria used in this study, *B. subtilis* possesses a more rigid and thick cell wall which might act as an additional diffusion barrier for the photocaged IPTG molecules, but lacks an outer membrane. For all the here tested bacterial hosts, expression systems encompassing LacI-controlled, IPTG-inducible promoters have been successfully established in recent studies (Table S1).[6b,18, 22c, 24]

To exclude detrimental effects of the new caged inducers or UV-A light exposure on cell viability, we first analysed the growth of *E. coli*, *P. putida* and *B. subtilis* cells in the presence of the cIPTG derivatives **10a** and **10b** as well as their corresponding photoproducts in comparison to conventional IPTG (**14**). For these studies, we used inducer concentrations that were sufficient to fully induce reporter gene expression in the respective expression hosts (Figure S5). Comparative growth of all strains clearly demonstrated that UV-A light exposure (30 min, 365 nm, ~1 mW cm^{-2}) did not lead to considerable growth impairments in the presence (Figure S6) or absence (Figure S7) of IPTG (**14**) and its photocaged derivatives **1**, **10a** and **10b**. Furthermore, the stability of **1**, **10a** and **10b** were analysed by measuring the fluorescence intensity of cultures in the dark (Figure S6 A). The data clearly reveals a pronounced *in vivo* stability of the new cIPTG derivatives **10a** and **10b** over 20 h in LB medium at 30 °C.

Expression studies in E. coli: To further evaluate the applicability of the new cIPTG derivatives **10a** and **10b** in comparison to **1** in *E. coli*, we used the well-established strain *E. coli* Tuner (DE3) carrying the eYFP expression vector pRhotHi-2-lacI-EYFP.[6b,14] Initially, we could observe that, in contrast to the variants **1** and **10a** which form an emulsion-like structure at relevant concentrations in LB medium without considerable amounts of ethanol or DMSO, variant **10b** can be completely dissolved in the cultivation medium, superseding the use of additional solvents. To compare the UV-A light-induced gene expression mediated by differently soluble photocaged IPTG variants during *E. coli* cultivation, light exposure was carried out for 30 min in order to ensure sufficient photoconversion of **1**, **10a** and **10b** (Figure S4). First, the general applicability of cIPTG variants was evaluated by analysing eYFP expression in cultures that reached the stationary growth phase. As shown in Figure 2A, illumination of the already established NP-cIPTG resulted in comparable eYFP expression levels as in the control experiment, where conventional IPTG (**14**) was added. In contrast, the new water-soluble BC-cIPTG (**10b**) and the more hydrophobic BEC-cIPTG (**10a**) led to a slight decrease of reporter gene expression in this experimental setup.

To analyse the properties of the cIPTG variants in more detail, eYFP expression was subsequently online monitored during batch cultivation of *E. coli*. Illumination of BC-cIPTG (**10b**) resulted in the fastest induction response in the early logarithmic growth phase (~4–7 h after inoculation) as also indicated by a lower half-maximal responsiveness with $t_{0.5\ final} = 4.16$ h when compared to NP-cIPTG (**1**) and BEC-cIPTG (**10a**; $t_{0.5\ final} = 4.41$ and 4.51 h, respectively, Table S4 and Figure S8). Thus, these results give a first indication that NB caging group derivatives with improved water-solubility such as BC might slightly facilitate the overall uptake of cIPTG in *E. coli*. However, the lower final eYFP expression levels in the respective cultures point to a less efficient enzymatic release of IPTG from ester intermediates **15** and **16**, which is eventually caused by the increasing size of these photolabile protecting groups. All in all the differential solubility of tested cIPTG variants in aqueous solvents seems to play a minor role for optochemical *in vivo* applications in *E. coli*, since only marginal differences of light-controlled gene expression could be observed.

ChemBioChem
Full Papers
doi.org/10.1002/cbic.202000377
Chemistry Europe
European Chemical Societies Publishing

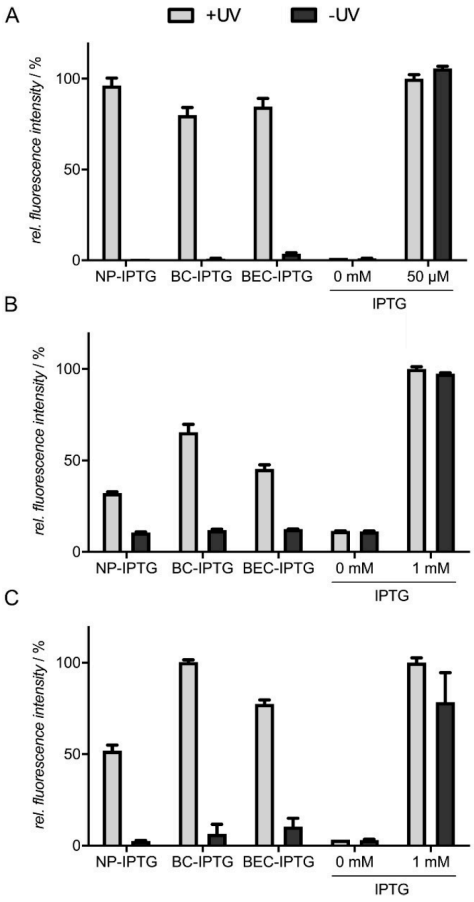

Figure 2. Light-controlled gene expression in A) *E. coli* Tuner(DE3)/pRhotHi-2-lacI-EYFP, B) *P. putida* KT2440/pVLT33-GFPmut3 and C) *B. subtilis* DB430/pHT01-sfGFP using NP-, BC-, and BEC-cIPTG. A) *In vivo* eYFP fluorescence (λ_{ex} = 508 nm, λ_{em} = 532 nm) of *E. coli* cultures supplemented with 50 µM of each cIPTG variant is shown in relation to a 50 µM IPTG (**14**) after 20 h (stationary growth phase). Induction was performed after 2.5 h by UV-A light exposure at 365 nm (~1 mW cm^{-2}) for 30 min or the addition of 50 µM **14**. B) *In vivo* GFPmut3 fluorescence (λ_{ex} = 508 nm, λ_{em} = 532 nm) of *P. putida* cultures supplemented with 1 mM of each cIPTG variant is shown in relation to a 1 mM IPTG (**14**) control after 20 h (stationary growth phase). Induction was performed after 3 h by UV-A light exposure at 365 nm (~1 mW cm^{-2}) for 30 min or the addition of 1 mM **14**. C) *In vivo* sfGFP fluorescence (λ_{ex} = 488 nm, λ_{em} = 520 nm) of cultures supplemented with 1 mM of each cIPTG variant is shown in relation to a 1 mM IPTG (**14**) control after 20 h. Induction was performed after 5 h by UV-A light exposure at 365 nm (~1 mW cm^{-2}) for 30 min or the addition of 1 mM **14**. *In vivo* fluorescence intensities were normalized to cell densities, and values are means of triplicate measurements. Error bars indicate the standard deviations.

Expression studies in P. putida: Next, we analysed whether the optochemical cIPTG/LacI system can be transferred to the Gram-negative bacterium *P. putida* KT2440 and if the solubility of the caged inducer has an effect on its *in vivo* applicability. In the following experiments, we used *P. putida* KT2440 carrying the expression vector pVLT33 harbouring a GFPmut3 gene, which is under control of the P_{tac} promoter (Table S1), and the same experimental setup as established for reference strain *E. coli* Tuner(DE3).

Because we could observe only basal induction of gene expression when 50 µM IPTG (**14**) was added to *P. putida* expression cultures (Figure S5), 1 mM of each IPTG derivative was used. As depicted in Figure 2B, the comparison of GFPmut3 fluorescence in *P. putida* cultures that reached the stationary growth phase demonstrates an induction of reporter gene expression of about 70% for BC-cIPTG (**10b**) when compared to conventional IPTG (**14**). In contrast, the use of NP- and BEC-cIPTG (**1** and **10a**) led to a lower induction response of ~50% or less. For BC-cIPTG (**10b**) the maximal responsiveness value $t_{0.5\ final}$ of 2.62 h is significantly slower than IPTG (**14**; $t_{0.5\ final}$ = 1.41 h; Figure S8 and Table S4). In summary, cIPTG constitutes an optochemical tool that can be used as an optogenetic switch for LacI-controlled expression systems in *P. putida*, but comparative expression studies revealed that modified IPTG variants **10a**, **10b** and **1** work less efficient than in *E. coli*. Remarkably, only the variant BC-cIPTG (**10b**) that offers an increased solubility in aqueous solution showed a satisfactory applicability for controlling gene expression by light. Similar to the *E. coli* Tuner(DE3), *P. putida* lacks a specific lactose permease.[30] Therefore, IPTG can only pass the cytoplasmic membrane *via* passive diffusion processes. Furthermore, in pseudomonads including *P. putida*, the outer membrane exhibits a reduced permeability as compared to *E. coli*. The uptake of small water-soluble molecules is mainly mediated by a defined set of specific porins such as OprF, which is characterised by a significantly slower diffusion rate compared to the more unspecific *E. coli* porins OmpF and OmpC.[25–26] As a consequence, the water-soluble compound **10b** could be transported over the outer membrane in a slower process.

Expression studies in B. subtilis: The Gram-positive bacterium *B. subtilis* was used as an expression host to determine the effect of inducer solubility on the uptake process, which is here solely influenced by the permeability of the cytoplasmic membrane and the surrounding cell wall. As this bacterium is not able to use lactose as a carbon source, and a lactose permease-encoding gene could not be identified in the genome,[27] the uptake of inducer molecules is most probably restricted to passive diffusion. To evaluate the cIPTG applicability, we used the *B. subtilis* DB430/pHT01-sfGFP strain, where fluorescence reporter expression is driven by the LacI-controlled P_{grac} promoter.[24b] Similar to *P. putida*, we added the respective inducer at a concentration of 1 mM to ensure full induction of recombinant gene expression (Figure S5). Remarkably, illumination of BC-cIPTG (**10b**) led to a strong and fast induction response comparable to the results obtained with IPTG (**14**; Figures 2C and S8, Table S4). In contrast, the induction with BEC-cIPTG (**10a**) led to a sfGFP expression level of around 75% in comparison to IPTG (**14**), while addition of NP-cIPTG (**1**) resulted in only 50% sfGFP fluorescence. Based on this observation, we cannot exclude that the cell wall of *B. subtilis*, which is much thicker (20–80 nm) than in Gram-negative organisms (5–10 nm),[28] is less permeable for the more hydro-

ChemBioChem
Full Papers
doi.org/10.1002/cbic.202000377
Chemistry Europe
European Chemical Societies Publishing

phobic cIPTG variants. In addition, the extremely fast responsiveness of BC-cIPTG (**10b**) in *B. subtilis* ($t_{0.5\,final}$ ~ 2.3 h), which also outperforms the respective induction response in *E. coli* ($t_{0.5\,final}$ ~ 4.3 h), might indicate an efficient catalytic cleavage of the ester intermediate after photoconversion. It should be noted that addition of BC- and BEC-cIPTG resulted in an increased basal target gene expression in non-illuminated cultures, which might be due to a slightly reduced stability of these cIPTG derivatives probably caused by a minimal catalytic release of the respective caging groups.

Analysis of expression heterogeneity: Finally, we elucidated, if the differential solubility of the applied cIPTG derivatives has an effect on the expression heterogeneity. For *E. coli* strain Tuner (DE3), we have previously proven a homogeneous induction response for both IPTG (**14**) and NP-cIPTG (**1**), which is primarily due to the absence of the permease and the resulting inducer uptake by diffusion.[6b] In contrast, for *Bacillus* species considerable expression heterogeneities are frequently described.[29] For the direct comparison of expression heterogeneity, fluorescence of the reporter proteins was determined at the single-cell level in light-exposed and non-illuminated cell cultures of *E. coli* and *B. subtilis* using flow cytometry. The results indicate that reporter gene expression was induced homogenously in *E. coli* cells irrespective of the added cIPTG variant (Figure S9 A) thereby corroborating observations from microfluidic investigations with NP-cIPTG (**1**).[6b] Similarly, the differential solubility of cIPTG variants did not affect the rate of expression heterogeneity in *B. subtilis* although it is generally more pronounced than in *E. coli* (Figure S9 B). Thus, expression heterogeneity is not provoked by a varying efficiency of inducer uptake.

Discussion

We developed the two new cIPTG derivatives **10a** and **10b** with varying hydrophobicity and aimed to analyse whether the change of cIPTG solubility affects the inducibility of LacI repressor-controlled target gene expression in *E. coli, P. putida* and *B. subtilis*. In the here presented *in vivo* studies, the derivatives are stable against spontaneous hydrolysis and did not induce elevated basal expression of target genes in the dark. In *E. coli*, only marginal differences of light-controlled gene expression could be observed for the new cIPTG variants in comparison to the well-established NP-cIPTG (**1**). Nevertheless, the increased water-solubility of derivative **10b** and its homogeneous dispersion without addition of an organic cosolvent, noticeably improves the applicability of this cIPTG derivative. The transfer to *P. putida* and *B. subtilis* clearly demonstrated that the solubility of photocaged inducer molecules is an important aspect that has to be considered for the establishment of a light-controlled expression system. Here, BC-cIPTG (**10b**), the variant that offers an increased solubility in aqueous solution, resulted in high expression levels together with a comparable or even increased induction factor in comparison to IPTG (for direct comparison of cIPTG derivatives' induction factors see Table S5). In this context it should be noted that, besides the improved solubility in microbial cultivation media, the diverging hydrophobicity of the cIPTG variants as well as the negative charge in case of BC-IPTG might additionally affect the complex processes that are involved in light-induced gene expression. These processes include i) the efficiency of photoconversion under the applied cultivation and illumination conditions, ii) the enzymatic hydrolysis of cIPTG ester intermediates by cytoplasmic, periplasmic or extracellular esterases, and iii) the individual permeability of cell membranes for cIPTG, the ester intermediates or released inducer. Thus, the individual physiological and morphological properties of the chosen microbial expression host might exhibit relevant differences such as the respective membrane composition or the ability for active inducer uptake *via* appropriate transporters. In Gram-negative bacteria, for example, the inducer has to pass two membranes, a process that occurs through i) free diffusion (both membranes), ii) passive transport processes involving unspecific or specific porins (outer membrane), and iii) active transport mechanisms that are facilitated by suitable permeases (cytoplasmic membrane). In Gram-positive bacteria, even though only one membrane needs to be passed, the surrounding cell wall is much thicker than in Gram-negative hosts and thus a distinct interaction with the differently soluble cIPTG variants might additionally influence their uptake. However, to unravel the role of individual properties of respective bacterial strains for cIPTG uptake and IPTG release, further experiments have to be performed in future studies.

In conclusion, we have constructed two new caged IPTG variants, characterised their (photo)chemical properties and demonstrated an easy applicability for the light-mediated control of gene expression in Gram-negative and Gram-positive bacteria. Because of their differential solubility, BC-, NP- and BEC-cIPTG constitute a valuable "starter set" which enables an easy access to a robust, light-responsive expression system in a broad variety of different hosts. Due to the non-invasive nature, the here presented optochemical on-switches additionally allow the external triggering of gene expression in closed biological systems thereby making, for example, anaerobic expression hosts more accessible in the near future.

Experimental Section

General remarks: All chemicals for synthesis were obtained from commercial suppliers and used without further purification unless stated otherwise. Solvents were reagent grade and were dried as well as purified by common methods. Thin-layer chromatography (TLC) was performed using pre-coated silica gel plates (Polygram® SIL G/UV, Macherey-Nagel) and components were visualised by oxidative staining or UV light. Flash chromatography was performed on silica gel (Merck silica gel 60 (0.063–0.200 μm) and solvents for flash chromatography (petroleum ether/ethyl acetate) were distilled prior to use. Optical rotation was determined at 20 °C on a Perkin Elmer Polarimeter 241 MC against sodium D-line and melting points were recorded using a Büchi melting point B-545 apparatus. The NMR spectra (^{1}H and ^{13}C) were measured at 20 °C on a Bruker Avance/DRX 600 spectrometer in deuterated solvents ($CDCl_3$, $[D_6]$DMSO, D_2O). The chemical shifts are given in ppm relative to the solvent (^{1}H: $CDCl_3$ = 7.26 ppm, ^{1}H: $[D_6]$DMSO = 3.31 ppm or ^{1}H: D_2O = 4.79 ppm/^{13}C: $CDCl_3$ = 77.16 ppm or ^{13}C: $[D_6]$

ChemBioChem | Full Papers doi.org/10.1002/cbic.202000377 | Chemistry Europe European Chemical Societies Publishing

DMSO = 39.52 ppm). Signals were assigned by means of H COSY, HSQC and HMBC experiments. The IR spectra were recorded with a Perkin Elmer SpectrumOne IR-spectrometer ATR (Waltham, USA). HRMS (ESI) spectra were recorded by the centrum of analytics of the Heinrich Heine University. UV/Vis absorption spectra were recorded on a Genesys 10S UV/VIS Spectrophotometer (Thermo Scientific) and uncaging experiments were performed in a quartz cuvette with the LUMOS 43® from Atlas Photonics at 375 nm. Light intensity was quantified using a Thermal Power Sensor (S302 C, Thorlabs Inc, USA) and the decay was detected by a Jasco HPLC system [column: Hyperclone 5 µ ODS (C18) 120 (Phenomenex)] combined with an UV/Vis-detector.

Synthesis of 4,5-Bis(ethoxycarbonylmethoxy)-2-nitrobenzylaldehyde diethyl acetal (12): To a solution of 4,5-bis (ethoxycarbonylmethoxy)-2-nitrobenzaldehyde (**11**) (3.00 g, 8.44 mmol) in ethanol (50 mL) triethyl orthoformate (1.88 g, 12.6 mmol, 1.50 equiv.) and pyridinium *p*-toluenesulfonate (424 mg, 1.69 mmol, 0.20 equiv.) were added and heated under reflux for 19 h. A dean-stark trap filled with molecular sieve (3 Å) was utilised for the constant removal of water. After the reaction was completed as indicated by TLC, it was washed with saturated $NaHCO_3$ solution. The aqueous phase was then extracted with CH_2Cl_2 and the combined organic phase was dried with anhydrous Na_2SO_4 and concentrated under reduced pressure. The residue was purified by flash column chromatography on SiO_2 (petroleum ether/ethyl acetate 85:15) to yield a yellow solid (3.22 g, 7.51 mmol, 89%). R_f = 0.25 (petroleum ether/ethyl acetate 80:20) m.p. 62.1 °C; ^{1}H NMR (600 MHz, [D$_6$]DMSO): δ = 1.12 (t, $^3J_{2',1'}$ = 7.1 Hz, 6 H, 2′-*H*), 1.22 (t, $^3J_{11,10\text{ and }11',10'}$ = 7.1 Hz, 6 H, 11-*H* and 11′-*H*), 3.50 (dq, $^2J_{1'a,1'b}$ = 9.3 Hz, $^3J_{1'a,2'}$ = 7.1 Hz, 2 H, 1′$_a$-*H*), 3.62 (dq, $^2J_{1'b,1'a}$ = 9.3 Hz, $^3J_{1'b,2'}$ = 7.1 Hz, 2 H, 1′$_b$-*H*), 4.18 (q, $^3J_{10,11\text{ or }10',11'}$ = 7.1 Hz, 2 H, 10-*H* or 10′-*H*), 4.19 (q, $^3J_{10,11\text{ or }10',11'}$ = 7.1 Hz, 2 H, 10-*H* or 10′-*H*), 4.96 (s, 2 H, 8′-*H*), 4.99 (s, 2 H, 8-*H*), 5.88 (s, 1 H, 7-*H*), 7.09 (s, 1 H, 6-*H*), 7.57 ppm (s, 1 H, 3-*H*); ^{13}C NMR (151 MHz, [D$_6$]DMSO): δ = 14.0 (*C*-11 and *C*-11′), 14.9 (*C*-2′), 60.8 (*C*-10 or *C*-10′), 60.9 (*C*-10 or *C*-10′), 65.5 (*C*-8 or *C*-8′), 65.6 (*C*-8 or *C*-8′), 97.7 (*C*-7), 110.6 (*C*-3), 111.5 (*C*-6), 127.9 (*C*-1), 141.4 (*C*-2), 146.5 (*C*-4), 150.2 (*C*-5), 168.1 (*C*-9 or *C*-9′), 168.1 ppm (*C*-9 or *C*-9′); IR (ATR-film): $\tilde{\nu}$ = 2981, 1755, 1692, 1581, 1526, 1446, 1346, 1291, 1196, 1176, 1080, 878, 796 cm^{-1}; HRMS (ESI): *m/z* calcd for $C_{19}H_{27}NO_{10}^+$: 447.1973 $[M+NH_4]^+$; found: 447.1972.

Synthesis of BEC-cIPTG (10a): To a solution of 4,5-bis (ethoxycarbonylmethoxy)-2-nitrobenzylaldehyde diethyl acetal (**12**) (1.00 g, 2.33 mmol, 1.50 equiv.) in dry CH_2Cl_2 (6 mL) IPTG (370 mg, 1.55 mmol) was added. After 5 min p-TSA (11.8 mg, 0.06 mmol, 4 mol%) was added to the suspension and it was stirred at room temperature for 20 h. After the reaction was completed as indicated by TLC, a small amount of triethylamine was added and the reaction was concentrated under reduced pressure. The residue was purified by flash column chromatography on SiO_2 (petroleum ether/ethyl acetate 50:50 to 20:80) to yield a white solid (403 mg, 0.70 mmol, 45%). R_f = 0.35 (petroleum ether/ethyl acetate 20:80); m.p. 104.5 °C; $[\alpha]$ = −68 (c = 1.0 in $CHCl_3$); ^{1}H NMR (600 MHz, $CDCl_3$): δ = 1.31 (t, $^3J_{11,10\text{ or }11',10'}$ = 7.2 Hz, 6 H, 11-*H* and 11′-*H*), 1.35 (d, $^3J_{CH3\text{-}a/b,SCH}$ = 6.8 Hz, 3 H, *CH*$_3$-a or *CH*$_3$-b), 1.36 (d, $^3J_{CH3\text{-}a/b,SCH}$ = 6.8 Hz, 3 H, *CH*$_3$-a or *CH*$_3$-b), 2.56 (brs, 2 H, 2″-*OH* and 3″-*OH*), 3.25 (septet, $^3J_{SCH,CH3\text{-}a/b}$ = 6.8 Hz, 1 H, S*CH*), 3.52 (dt, $^3J_{5'',6''}$ = 1.7 Hz, $^3J_{5'',4''}$ = 1.2 Hz, 1 H, 5″-*H*), 3.64–3.70 (m, 2 H, 2″-*H* and 3″-*H*), 4.08 (dd, $^2J_{6''b,6''a}$ = 12.5 Hz, $^3J_{6''b,5''}$ = 1.7 Hz, 1 H, 6″-*H*$_b$), 4.24–4.31 (m, 6 H, 10-*H* / 10′-*H* / 4″-*H* / 6″-*H*$_a$), 4.41 (d, $^3J_{1'',2''}$ = 8.7 Hz, 1 H, 1″-*H*), 4.77 (s, 2 H, 8-*H*), 4.82 (s, 2 H, 8′-*H*), 6.21 (s, 1 H, 7-*H*), 7.35 (s, 1 H, 6-*H*), 7.54 ppm (s, 1 H, 3-*H*); ^{13}C NMR (151 MHz, $CDCl_3$): δ = 14.3 (*C*-11 or *C*-11′), 14.3 (*C*-11 or *C*-11′), 24.1 (*CH*$_3$-a or *CH*$_3$-b), 24.3 (*CH*$_3$-a or *CH*$_3$-b), 35.5 (SCH), 61.8 (*C*-10 or *C*-10′), 61.9 (*C*-10 or *C*-10′), 66.4 (*C*-8 or *C*-8′), 66.6 (*C*-8 or *C*-8′), 69.8 (*C*-6″), 70.1 (*C*-5″), 70.3 (*C*-3″), 73.9 (*C*-2″), 76.2 (*C*-4″), 85.7 (*C*-1″), 96.6 (*C*-7), 111.5 (*C*-3), 112.8 (*C*-6), 127.7 (*C*-1), 141.3 (*C*-2), 147.6 (*C*-4), 151.7 (*C*-5), 167.9 (*C*-9 or *C*-9′), 167.9 ppm (*C*-9 or *C*-9′); IR (ATR-film): $\tilde{\nu}$ = 3478, 2967, 2916, 2866, 1747, 1520, 1287, 1176, 1097, 1077, 1027, 989 cm^{-1}; UV/Vis (MeOH): λ_{max} (ε) = 298 nm (8006 dm^3 mol^{-1} cm^{-1}); HRMS (ESI): *m/z* calcd for $C_{24}H_{37}N_2O_{13}S$: 593.2011 $[M+NH_4]^+$; found: 593.2011.

Synthesis of BC-cIPTG (10b): A solution of BEC-cIPTG (**10a**) (200 mg, 0.35 mmol) in MeOH (3.5 mL) was cooled to 0 °C and a 0.2 M solution of LiOH (3.5 mL) was added. The reaction mixture was stirred for 1 h at room temperature. After the reaction was completed as indicated by TLC, the MeOH was evaporated under reduced pressure and the remaining solution was lyophilised overnight. The residue was suspended in THF, sonicated for 15 min and filtrated. After washing with small amounts of cold THF a white solid (107 mg, 0.21 mmol, 59%) was obtained. m.p. 190 °C (decay); $[\alpha]$ = −92 (c = 1.0 in H_2O); ^{1}H NMR (600 MHz, D_2O): δ = 1.29 (d, $^3J_{CH3\text{-}a,SCH}$ = 6.8 Hz, 3 H, *CH*$_3$-a), 1.31 (d, $^3J_{CH3\text{-}b,SCH}$ = 6.8 Hz, 3 H, *CH*$_3$-b), 3.26 (septet, $^3J_{SCH,CH3\text{-}a/b}$ = 6.8 Hz, 1 H, S*CH*), 3.66 (t, $^3J_{5'',6''}$ = 9.8 Hz, 1 H, 2″-*H*), 3.71–3.82 (m, 2 H, 3″-*H*, 5″-*H*), 4.18 (m, 2 H, 6″-*H*), 4.37 (d, $^3J_{4'',3''}$ = 3.6 Hz, 1 H, 4″-*H*), 4.60 (s, 2 H, 8′-*H*), 4.62 (d, $^3J_{1'',2''}$ = 9.8 Hz, 1 H, 1″-*H*), 4.67 (d, J = 2.6 Hz, 2 H, 8-*H*), 6.20 (s, 1 H, 7-*H*), 7.32 (s, 1 H, 6-*H*), 7.55 ppm (s, 1 H, 3-*H*); ^{13}C NMR (151 MHz, D_2O): δ = 22.9 (*CH*$_3$-a), 23.3 (*CH*$_3$-b), 35.0 (SCH), 67.3(C-8′), 67.4 (C-8), 69.1 (C-2″), 69.3 (C-6″), 69.6 (C-5″), 72.8 (C-3″), 76.5 (C-4″), 84.8 (C-1″), 96.4 (C-7), 109.2 (C-3), 110.8 (C-6), 126.3 (C-1), 140.0 (C-2), 147.2 (C-4), 151.5 (C-5), 175.1 (C-9), 175.4 ppm (C-9′); IR (ATR-film): $\tilde{\nu}$ = 3124, 3043, 1605, 1522, 1398, 1335, 1277, 1077, 1047, 1024, 824 cm^{-1}; UV/Vis (H_2O): λ_{max} (ε) = 245 (5008), 342 nm (3191 dm^3 mol^{-1} cm^{-1}); HRMS (ESI): *m/z* calcd for $C_{20}H_{29}N_2O_{13}S^+$: 537.1385 $[M+NH_4]^+$; found: 537.1382.

Determination of purity by qNMR: The purity of the photocaged IPTG derivatives **10a**, **10b** and **1** was determined via quantitative NMR. 3,5-bis(trifluoromethyl)bromobenzene was utilised as internal standard for **10a** as well as **1** and (methanesulfonyl)methane for **10b**. The spectra were measured at 20 °C on a Bruker Avance/DRX 600 spectrometer with 64 scans each and 30 µs relaxation time between each scan. The results in Table S3 are means of triplicate measurements.

Solubility analysis: The solubility of **10a**, **10b** and **14** was determined photometrically at 25 °C using a spectrophotometer Shimadzu UV-1800 (CPS-240A). The absorbance of a serial dilution in degassed and deionised water was measured at the absorption maximum of the respective compound. A saturated solution was measured under the same conditions. The solubility was calculated using the Beer-Lambert law.[13b]

Hydrolytic stability: For the determination of the hydrolytic stability, a 1 mM solution of the respective compound in methanol or sodium phosphate buffer (0.1 M, pH 7.5) was stored in the dark at room temperature. Samples were removed after 0 and 24 h and analysed by reversed-phase HPLC.

Quantification of uncaging half-life times: A 1 mM solution of each photocaged compound in methanol or sodium phosphate buffer (0.1 M, pH 7.5) was prepared. In a cuvette 1 mL of this solution was irradiated at room temperature using the LUMOS 43 (375 nm) for a certain time period. The sample was then analysed by reverse phase HPLC Jasco HPLC system [column: Hyperclone 5 µ ODS (C_{18}) 120 (Phenomenex)]. For each photocaged compound, the procedure was repeated for different irradiation times. The decrease of concentration was measured by an UV detector.[6d]

Determination of uncaging quantum yields: The quantum yields of **1**, **10a** and **10b** were determined by a relative method in comparison to the quantum yield of 2-nitropiperonylacetate (NPA-Ac), as this substrate shows a sufficient similarity to **1**, **10a** and **10b**. The procedure was followed as previously described in literature (Figure S4 and Table S2).[6c,30]

ChemBioChem | Full Papers doi.org/10.1002/cbic.202000377 | Chemistry Europe European Chemical Societies Publishing

Bacterial strains and plasmids: The *E. coli* strain DH5α[31] was used for all cloning procedures, while the *E. coli* strain S17-1[32] and Tuner (DE3) (Novagen) were applied for conjugation and expression studies, respectively. All *E. coli* strains, the *P. putida* strain KT2440[33] and the *B. subtilis* strain DB430[34] were grown on LB agar plates or in liquid LB medium (Luria/Miller, Carl Roth®), at 37 °C (*E. coli*) or 30 °C (*P. putida, B. subtilis*). Media were supplemented either with kanamycin (50 μg mL^{-1}), gentamicin (25 μg mL^{-1}), irgasan (25 μg mL^{-1}) or chloramphenicol (5 μg mL^{-1}), when appropriate.

All bacterial strains and plasmids used in this study are listed in Table S1, Supporting Information.

Plasmid construction: All recombinant DNA techniques were carried out as described by Sambrook *et al.*[35] For the construction of the *B. subtilis* expression vector pHT01-sfGFP, the sfGFP-encoding gene was synthesised with flanking NdeI and HindIII restriction sites (Eurofins Genomics, Germany) and subsequently cloned into pET-22(b) (Novagen, Merck). The resulting vector pET-22(b)-sfGFP was used as template for SLIC cloning[36] of a DNA fragment encompassing the *sfgfp* gene into the *B. subtilis* expression vector pHT01 (MoBiTec, Germany) using oligos 3–6 (Table S1, Supporting Information). The *P. putida* expression vector pVLT33-GFPmut3 was constructed by restriction and ligation. To this end, the *gfpmut3* gene was amplified with flanking *Eco*RI and *Xba*I restriction sites *via* PCR using oligos 1–2 (Table S1). Afterwards, the *Eco*RI/*Xba*I hydrolysed fragment was ligated into the likewise hydrolysed vector backbone pVLT33, resulting in the final expression vector pVLT33-GFPmut3. Correct nucleotide sequences of all constructs were confirmed by Sanger sequencing (Eurofins Genomics).

Cultivation conditions: All *E. coli*, *P. putida* and *B. subtilis* expression cultures were grown in 48-well Flowerplates® in a BioLector microbioreactor system (m2p labs, Germany) (800 μL LB medium, 1200 rpm, 30 °C), inoculated with an optical density at 580 nm of 0.05. During cultivation, the cell density was measured online through the scattered light intensity at 620 nm. In addition, fluorescence of eYFP and GFP variants (GFPmut3 and sfGFP) were continuously determined using a 508/532 nm and 488/520 nm filter, respectively. cIPTG variants **10a**, **10b** or NP-cIPTG (**1**) were added prior inoculation (final concentration: 50 μM for *E. coli*, 1 mM for *P. putida* and *B. subtilis;* purities of cIPTG variant after synthesis were taken into account accordingly) and expression of reporter genes was induced during the early logarithmic growth phase (after approx. 2.5 h for *E. coli*, 3 h for *P. putida* and 5 h for *B. subtilis*) *via* UV-A light exposure (VL-315.BL lamp, Vilber Lourmat, France; ~1 mW cm^{-2}, 30 min exposure) or by addition of equal amounts of conventional IPTG (**14**) after illumination.

Determination of expression heterogeneity: For measurement of the expression heterogeneity, *E. coli* and *B. subtilis* cultures were analysed on the single-cell level by flow cytometry regarding their fluorescence intensity and distribution. Expression cultures were grown as described above and were subsequently sampled as soon as they reached the late logarithmic growth phase (after 8 h for *E. coli* and after 10 h for *B. subtilis*). For this purpose, 40 μL was taken out of the Flowerplate® cultures and added to 600 μL PBS buffer (pH 7.4). Subsequently, the cells were harvested by centrifugation (2 min, 15000 rpm – 21130×g, RT), adjusted to an optical density of 0.5 (OD_{580}) in 100 μL PBS buffer and then transferred into a 96-well microtiter plate (Greiner Bio-One GmbH, Frickenhausen, Germany). Finally, these samples were analysed with a flow cytometer (Amnis® CellStreamTM System, Luminex Corporation, Austin, USA). The individual cellular fluorescence brightness was measured using a 488-nm laser (15% intensity for *E. coli* and 5% for *B. subtilis*) for excitation and a 528/46 nm bandpass filter for detection. To exclude cell debris and cell aggregates, the cells were also analysed regarding their size (forward scatter, FSC) and granularity (side scatter, SSC). FSC was measured using an FSC laser (nm) with 80% of the laser power for *E. coli* and 50% for *B. subtilis* and a 456/51 nm bandpass filter for detection. For determination of SSC a nm-light laser with 80% of the laser power for *E. coli* and 50% for *B. subtilis* (773/56 nm bandpass filter) was used. Based on the scatter plots, bacterial cells were gated from irrelevant counts for fluorescence analysis. Flow cytometric data were evaluated with the CellStream™ Analysis Software (Merck, now Luminex Corporation).

Acknowledgements

The work was supported by grants from German Federal Ministry of Education and Research (BMBF, FKZ: 031A167A), the Bioeconomy Science Center, and the European Regional Development Fund (ERDF: 34.EFRE-0300096 and 34.EFRE-0300097) within the project CLIB-Kompetenzzentrum Biotechnologie CKB). The scientific activities of the Bioeconomy Science Center were financially supported by the Ministry of Innovation, Science and Research of the German federal state of North Rhine-Westphalia MIWF within the framework of the NRW Strategieprojekt BioSC (no. 313/323-400-00213). The authors thank Dr. Anita Loeschcke for the helpful discussion, Sonja Kubicki for the construction of the plasmid pVLT33-GFPmut3, Vera Ophoven for synthetic, and Birgit Henßen for analytical support. Open access funding enabled and organized by Projekt DEAL.

Conflict of Interest

The authors declare no conflict of interest.

Keywords: caged compounds · gene expression · optogenetics · photochemistry · synthetic biology

[1] K. Deisseroth, *Nat. Methods* **2011**, *8*, 26–29.
[2] a) R. M. Hughes, *Crit. Rev. Biochem. Mol. Biol.* **2018**, *53*, 453–474; b) Z. Liu, J. Zhang, J. Jin, Z. Geng, Q. Qi, Q. Liang, *Front. Microbiol.* **2018**, *9*, 2692; c) E. M. Zhao, Y. Zhang, J. Mehl, H. Park, M. A. Lalwani, J. E. Toettcher, J. L. Avalos, *Nature* **2018**, *555*, 683–687; d) S. R. Schmidl, F. Ekness, K. Sofjan, K. N. M. Daeffler, K. R. Brink, B. P. Landry, K. P. Gerhardt, N. Dyulgyarov, R. U. Sheth, J. J. Tabor, *Nat. Chem. Biol.* **2019**, *15*, 690–698.
[3] a) C. Brieke, F. Rohrbach, A. Gottschalk, G. Mayer, A. Heckel, *Angew. Chem. Int. Ed.* **2012**, *51*, 8446–8476; *Angew. Chem.* **2012**, *124*, 8572–8604; b) A. Bardhan, A. Deiters, *Curr. Opin. Struct. Biol.* **2019**, *57*, 164–175; c) L. Gardner, A. Deiters, *Curr. Opin. Chem. Biol.* **2012**, *16*, 292–299; d) A. Deiters, *Curr. Opin. Chem. Biol.* **2009**, *13*, 678–686; e) T. Drepper, U. Krauss, S. Meyer zu Berstenhorst, J. Pietruszka, K.-E. Jaeger, *Appl. Microbiol. Biotechnol.* **2011**, *90*, 23–40.
[4] a) J. Liu, J. Hemphill, S. Samanta, M. Tsang, A. Deiters, *J. Am. Chem. Soc.* **2017**, *139*, 9100–9103; b) D. Kolarski, A. Sugiyama, G. Breton, C. Rakers, D. Ono, A. Schulte, F. Tama, K. Itami, W. Szymanski, T. Hirota, B. L. Feringa, *J. Am. Chem. Soc.* **2019**, *141*, 15784–15791.
[5] J. M. Silva, E. Silva, R. L. Reis, *J. Control. Release* **2019**, *298*, 154–176.
[6] a) D. D. Young, A. Deiters, *Angew. Chem. Int. Ed.* **2007**, *46*, 4290–4292; *Angew. Chem.* **2007**, *119*, 4368–4370; b) D. Binder, A. Grünberger, A. Loeschcke, C. Probst, C. Bier, J. Pietruszka, W. Wiechert, D. Kohlheyer, K.-E. Jaeger, T. Drepper, *Integr. Biol.* **2014**, *6*, 755–765; c) D. Binder, C. Bier, A. Grünberger, D. Drobietz, J. Hage-Hülsmann, G. Wandrey, J. Büchs, D. Kohlheyer, A. Loeschcke, W. Wiechert, K.-E. Jaeger, J. Pietruszka, T. Drepper, *ChemBioChem* **2016**, *17*, 296–299; d) C. Bier, D. Binder, D.

ChemBioChem | Full Papers doi.org/10.1002/cbic.202000377 | Chemistry Europe European Chemical Societies Publishing

Drobietz, A. Loeschcke, T. Drepper, K.-E. Jaeger, J. Pietruszka, *Synthesis* **2017**, *49*, 42–52; e) P. M. Kusen, G. Wandrey, V. Krewald, M. Holz, S. Meyer zu Berstenhorst, J. Büchs, J. Pietruszka, *J. Biotechnol.* **2017**, *258*, 117–125; f) P. M. Kusen, G. Wandrey, C. Probst, A. Grünberger, M. Holz, S. Meyer zu Berstenhorst, D. Kohlheyer, J. Büchs, J. Pietruszka, *ACS Chem. Biol.* **2016**, *11*, 2915–2922.

[7] J. E. T. Corrie in *Dynamic Studies in Biology: Phototriggers, Photoswitches and Caged Biomolecules*, (Eds.: M. Goeldner, R. Givens), Wiley-VCH, Weinheim, **2005**, pp. 1–94.

[8] a) A. Y. Vorobev, A. E. Moskalensky, *Comput. Struct. Biotechnol. J.* **2019**, *18*, 27–34; b) I. Aujard, C. Benbrahim, M. Gouget, O. Ruel, J.-B. Baudin, P. Neveu, L. Jullien, *Chem. Eur. J.* **2006**, *12*, 6865–6879.

[9] A. Specht, M. Goeldner, *Angew. Chem. Int. Ed.* **2004**, *43*, 2008–2012; *Angew. Chem.* **2004**, *116*, 2042–2046.

[10] a) A. G. Russell, M.-E. Ragoussi, R. Ramalho, C. W. Wharton, D. Carteau, D. M. Bassani, J. S. Snaith, *J. Org. Chem.* **2010**, *75*, 4648–4651; b) A. G. Russell, M. J. Sadler, H. J. Laidlaw, A. Gutierrez-Loriente, C. W. Wharton, D. Carteau, D. M. Bassani, J. S. Snaith, *Photochem. Photobiol. Sci.* **2012**, *11*, 556–563; c) K. Schaper, S. Mobarekeh, C. Grewer, *Eur. J. Org. Chem.* **2002**, *2002*, 1037–1046; d) M. Noguchi, M. Skwarczynski, H. Prakash, S. Hirota, T. Kimura, Y. Hayashi, Y. Kiso, *Bioorg. Med. Chem.* **2008**, *16*, 5389–5397.

[11] A. P. Pelliccioli, J. Wirz, *Photochem. Photobiol. Sci.* **2002**, *1*, 441–458.

[12] a) L. R. Makings, R. Y. Tsien, *J. Biol. Chem.* **1994**, *269*, 6282–6285; b) J. Ni, D. A. Auston, D. A. Freilich, S. Muralidharan, E. A. Sobie, J. P. Y. Kao, *J. Am. Chem. Soc.* **2007**, *129*, 5316–5317; c) K. M. Schelkle, C. Schmid, K. Yserentant, M. Bender, I. Wacker, M. Petzoldt, M. Hamburger, D.-P. Herten, R. Wombacher, R. R. Schröder, U. H. F. Bunz, *Angew. Chem. Int. Ed.* **2017**, *56*, 4724–4728; *Angew. Chem.* **2017**, *129*, 4802–4806.

[13] a) S. B. Cambridge, D. Geissler, S. Keller, B. Cürten, *Angew. Chem. Int. Ed.* **2006**, *45*, 2229–2231; *Angew. Chem.* **2006**, *118*, 2287–2289; b) S. B. Cambridge, D. Geissler, F. Calegari, K. Anastassiadis, M. T. Hasan, A. F. Stewart, W. B. Huttner, V. Hagen, T. Bonhoeffer, *Nat. Methods* **2009**, *6*, 527–531.

[14] G. Wandrey, C. Bier, D. Binder, K. Hoffmann, K.-E. Jaeger, J. Pietruszka, T. Drepper, J. Büchs, *Microb. Cell Fact.* **2016**, *15*, 1–16.

[15] D. Binder, J. Frohwitter, R. Mahr, C. Bier, A. Grünberger, A. Loeschcke, P. Peters-Wendisch, D. Kohlheyer, J. Pietruszka, J. Frunzke, K.-E. Jaeger, V. F. Wendisch, T. Drepper, *Appl. Environ. Microbiol.* **2016**, *82*, 6141–6149.

[16] a) T. Milburn, N. Matsubara, A. P. Billington, J. B. Udgaonkar, J. W. Walker, B. K. Carpenter, W. W. Webb, J. Marque, W. Denk, *Biochemistry* **1989**, *28*, 49–55; b) H.-G. A. Breitinger, R. Wieboldt, D. Ramesh, B. K. Carpenter, G. P. Hess, *Biochemistry* **2000**, *39*, 5500–5508; c) K. R. Gee, L. Niu, K. Schaper, G. P. Hess, *J. Org. Chem.* **1995**, *60*, 4260–4263; d) L. Niu, K. R. Gee, K. Schaper, G. P. Hess, *Biochemistry* **1996**, *35*, 2030–2036; e) K. Schaper, S. A. Madani Mobarekeh, P. Doro, D. Maydt, *Photochem. Photobiol.* **2010**, *86*, 1247–1254.

[17] J. E. T. Corrie, *J. Chem. Soc. Perkin Trans. 1* **1993**, 2161–2166.

[18] K. Terpe, *Appl. Microbiol. Biotechnol.* **2006**, *72*, 211–222.

[19] a) O. Simon, I. Klaiber, A. Huber, J. Pfannstiel, *J. Proteomics* **2014**, *109*, 212–227; b) Ö. Akkaya, D. R. Pérez-Pantoja, B. Calles, P. I. Nikel, V. de Lorenzo, *MBio* **2018**, *9*, e01512–18.

[20] a) M. Fernández, S. Conde, J. de la Torre, C. Molina-Santiago, J.-L. Ramos, E. Duque, *Antimicrob. Agents Chemother.* **2012**, *56*, 1001–1009; b) M. Chavarría, P. I. Nikel, D. Pérez-Pantoja, V. de Lorenzo, *Environ. Microbiol.* **2013**, *15*, 1772–1785.

[21] L. F. Kampers, R. J. Volkers, V. A. Martins dos Santos, *Microb. Biotechnol.* **2019**, *12*, 845–848.

[22] a) P. I. Nikel, V. de Lorenzo, *New Biotechnol.* **2014**, *31*, 562–571; b) T. Tiso, R. Zauter, H. Tulke, B. Leuchtle, W.-J. Li, B. Behrens, A. Wittgens, F. Rosenau, H. Hayen, L. M. Blank, *Microb. Cell Fact.* **2017**, *16*, 225; c) P. I. Nikel, V. de Lorenzo, *Metab. Eng.* **2018**, *50*, 142–155; d) E. Martínez-García, V. de Lorenzo, *Curr. Opin. Biotechnol.* **2019**, *59*, 111–121; e) A. Loeschcke, S. Thies, *Curr. Opin. Biotechnol.* **2020**, *65*, 213–224; f) M. R. Incha, M. G. Thompson, J. M. Blake-Hedges, Y. Liu, A. N. Pearson, M. Schmidt, J. W. Gin, C. J. Petzold, A. M. Deutschbauer, J. D. Keasling, *Metab. Eng. Commun.* **2020**, *10*, e00119.

[23] J. van Dijl, M. Hecker, *Microb. Cell Fact.* **2013**, *12*, 3.

[24] a) S. C. Troeschel, S. Thies, O. Link, C. I. Real, K. Knops, S. Wilhelm, F. Rosenau, K.-E. Jaeger, *J. Biotechnol.* **2012**, *161*, 71–79; b) H. D. Nguyen, T. T. P. Phan, W. Schumann, *Curr. Microbiol.* **2007**, *55*, 89–93; c) M. M. Bagdasarian, E. Amann, R. Lurz, B. Rückert, M. Bagdasarian, *Gene* **1983**, *26*, 273–282.

[25] H. Löwe, P. Sinner, A. Kremling, K. Pflüger-Grau, *Microb. Biotechnol.* **2020**, *13*, 97–106.

[26] E. Eren, J. Vijayaraghavan, J. Liu, B. R. Cheneke, D. S. Touw, B. W. Lepore, M. Indic, L. Movileanu, B. van den Berg, *PLoS Biol.* **2012**, *10*, e1001242.

[27] a) O. Krispin, R. Allmansberger, *J. Bacteriol.* **1998**, *180*, 2265–2270; b) M. Steinmetz, in *Bacillus subtilis and Other Gram-Positive Bacteria: Biochemistry, Physiology* and Molecular Genetics (Eds.: A. L. Sonenshein, J. A. Hoch, R. Losick), American Society of Microbiology, Washington, **1993**, pp. 157–170.

[28] M. R. J. Salton, K. S. Kim, in *Medical Microbiology*, 4th ed. (Ed.: S. Baron), University of Texas Medical Branch at Galveston, Galveston, **1996**, Chapter 2.

[29] a) K. M. Münch, J. Müller, S. Wienecke, S. Bergmann, S. Heyber, R. Biedendieck, R. Münch, D. Jahn, *Appl. Environ. Microbiol.* **2015**, *81*, 5976–5986; b) T. N. Ploss, E. Reilman, C. G. Monteferrante, E. L. Denham, S. Piersma, A. Lingner, J. Vehmaanperä, P. Lorenz, J. M. van Dijl, *Microb. Cell Fact.* **2016**, *15*, 57; c) D. B. Kearns, R. Losick, *Genes Dev.* **2005**, *19*, 3083–3094; d) D. Dubnau, R. Losick, *Mol. Microbiol.* **2006**, *61*, 564–572.

[30] a) F. Bley, K. Schaper, H. Görner, *Photochem. Photobiol.* **2008**, *84*, 162–171; b) B. A. M. Bier, *PhD thesis*, Heinrich Heine University Düsseldorf (Germany), **2011**.

[31] D. Hanahan, *J. Mol. Biol.* **1983**, *166*, 557–580.

[32] R. Simon, U. Priefer, A. Pühler, *Bio/Technology* **1983**, *1*, 784–791.

[33] M. Bagdasarian, R. Lurz, B. Rückert, F. C. H. Franklin, M. M. Bagdasarian, J. Frey, K. N. Timmis, *Gene* **1981**, *16*, 237–247.

[34] R. H. Doi, S.-L. Wong, F. Kawamura, *Trends Biotechnol.* **1986**, *4*, 232–235.

[35] J. Sambrook, E. F. Fritsch, T. Maniatis, *Molecular Cloning: A Laboratory Manual*, Cold Spring Harbor Laboratory Press, Cold Spring Harbor, **1989**, p. 1546.

[36] J.-Y. Jeong, H.-S. Yim, J.-Y. Ryu, H. S. Lee, J.-H. Lee, D.-S. Seen, S. G. Kang, *Appl. Environ. Microbiol.* **2012**, *78*, 5440–5443.

Manuscript received: June 12, 2020
Revised manuscript received: August 31, 2020
Accepted manuscript online: September 11, 2020
Version of record online: October 23, 2020

II.1.2. APPLICATION OF PHOTOCAGED INDUCERS FOR IMPLEMENTATION OF LIGHT CONTROL IN *R. CAPSULATUS*

Photocaged inducers for the non-invasive light control of production processes in the phototrophic bacterium *Rhodobacter capsulatus*

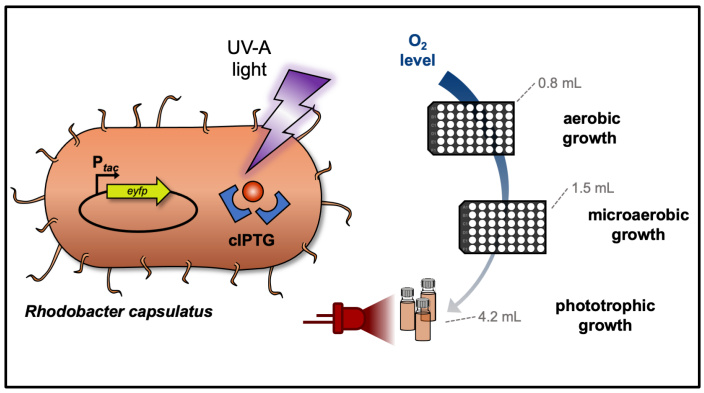

Fabienne Hilgers*, Fabian Hogenkamp*, Oliver Klaus, Luzie Kruse, Alessa Lappe, Anita Loeschcke, Claus Bier, Dennis Binder, Karl-Erich Jaeger, Jörg Pietruszka and Thomas Drepper

Target journal: PLoS One

Status: manuscript in preparation

For the Supporting Information see Appendix (**Chapter V.2.**, **page 295**).

Own contribution:

Designing and performing biological experiments, plasmid constructions, analyzing *in vivo* data, writing the manuscript.

Photocaged inducers for the non-invasive light control of production processes in the phototrophic bacterium *Rhodobacter capsulatus*

Fabienne Hilgers[1¶], Fabian Hogenkamp[2¶] Oliver Klaus[1], Luzie Kruse[1], Alessa Lappe[1], Anita Loeschcke[1], Claus Bier[2], Dennis Binder[1], Karl-Erich Jaeger[1,3], Jörg Pietruszka[2,3*] and Thomas Drepper[1*]

[1] Institute of Molecular Enzyme Technology, Heinrich Heine University Düsseldorf at Forschungszentrum Jülich, Jülich, Germany

[2] Institute of Bioorganic Chemistry, Heinrich Heine University Düsseldorf at Forschungszentrum Jülich, Jülich, Germany

[3] Institute of Bio- and Geosciences: Biotechnology (IBG-1), Forschungszentrum Jülich, Jülich, Germany

* Corresponding author

Email: t.drepper@fz-juelich.de

¶ These authors contributed equally to this work.

Abstract

Photocaged inducer molecules, especially photocaged isopropyl-β-D-1-thiogalactopyranoside (cIPTG), are well-established optochemical tools for light-regulated gene expression and have been extensively applied in *Escherichia coli* and alternative bacterial hosts like *Corynebacterium glutamicum, Pseudomonas putida* or *Bacillus subtilis*. In this study, we aimed to implement a light-mediated on-switch for target gene expression in the facultative anoxygenic phototroph *Rhodobacter capsulatus* by using cIPTG under both phototrophic and non-phototrophic cultivation conditions. We could demonstrate that especially nitropiperonyl- (NP)-cIPTG can be applied for light-mediated control of target gene expression in this alternative host. Furthermore, we successfully applied the optochemical approach to control the intrinsic carotenoid biosynthesis to showcase engineering of a cellular function. Photocaged IPTG thus represents a light-responsive tool which offers various promising properties suitable for future biotechnological applications including automated multi-factorial engineering of target gene expression as well as optimization of production processes for high-value products.

Introduction

In the field of optogenetics, the application of light offers various advantageous properties such as non-invasive control with high spatiotemporal resolution [1–5]. In this context, photolabile protecting groups are a well-established tool for controlling a multitude of cellular processes including cell signaling [1,6,7] or gene expression [8–12]. For light-regulated gene expression, especially photocaged isopropyl-β-D-1-thiogalactopyranoside (cIPTG) was e.g. applied for automated optimization of heterologous gene expression in *Escherichia coli* using a high-throughput screening system [13]. The growth medium can be supplemented with photocaged IPTG, which remains non-functional, until a light-pulse releases the inducer from its cage so that it can induce expression of target genes under control of a *lac* (or *lac*-type) promoter by specific interaction with the LacI repressor. Caged IPTG has further been utilized to control gene expression in alternative expression hosts like *Corynebacterium glutamicum, Pseudomonas putida* or *Bacillus subtilis* [14,15]. Recently, we expanded the applicability of caged IPTG by introducing two novel cIPTG derivatives with varying compound solubilities in aqueous solution [15]. While the well-established 6-nitropiperonyl photocaged IPTG (NP-cIPTG) is almost insoluble in the

cultivation medium, 4,5-bis(carboxymethoxy)-2-nitrobenzyl photocaged IPTG (BC-cIPTG) offers a significantly higher water-solubility. 4,5-bis(ethoxycarbonylmethoxy)-2-nitrobenzyl photocaged IPTG (BEC-cIPTG), in contrast, shows also low solubility, but might exhibit an improved membrane-permeability due to its hydrophobic side chains.

When conventionally inducible expression systems are applied in anaerobic bacteria, the induction process (i.e. the addition of the corresponding inducer molecule) is more challenging due to the tightly closed cultivation vessels. In this case, the induction of gene expression in a log phase culture requires an invasive process such as the opening of cultivation vessels, which might conflict with the maintenance of strictly anaerobic conditions. In contrast, inoculation of cell cultures in media that were directly supplemented with the inducer often results in reduced cell growth and/or product yields, since the synthesis of heterologous proteins or metabolites competes with biomass formation [16–22]. In addition, the engineering of complex biosynthetic pathways often requires the possibility to specifically control the expression of defined pathway genes with both a high temporal resolution and flexibility. In this study, we thus aimed at implementing non-invasive light-control for target gene expression in the facultative anaerobic bacterium *Rhodobacter capsulatus* by using photocaged IPTG.

R. capsulatus is a metabolically versatile bacterium that is able to grow either under phototrophic conditions (i.e. in the absence of oxygen and presence of light) by performing anoxygenic photosynthesis or under chemotrophic conditions (in the presence molecular oxygen) [23–25]. Upon reduction of oxygen tension, *R. capsulatus* starts to form an extracellular capsule composed of exopolysaccharides (EPS) and an intracytoplasmic membrane (ICM) system, which harbors the photosynthesis apparatus [26–29]. Since the intracellular membrane system can function as a naturally enlarged storage compartment for membrane-embedded enzymes and metabolites, the phototrophic lifestyle renders novel approaches possible where *R. capsulatus* is applied as an alternative host for the production of otherwise difficult-to-express membrane proteins as well as hydrophobic secondary metabolites such as plant-derived terpenes [30–33]. However, the EPS capsule as well as the ICM might function as natural diffusion barriers making the uptake of (caged) inducers less efficient.

In the laboratory, non-phototrophic cultivation of *Rhodobacter* is usually performed in the dark using shaking flasks to ensure aerobic or microaerobic conditions. For phototrophic growth, tightly sealed hungate tubes (with culture volumes of up to 15 mL), sealable bottles (volume ≤ 2 L) or bioreactors (volume ≥ 1 L) are used and illumination is mostly conducted by applying conventional light bulbs [30,34–39]. Phototrophic growth is particularly well established [31,32,36,37,40,41] and offers robust

and fast cell division for a variety of different applications, as the broad emission spectrum of bulb light is suitable for the excitation of all photopigments of *R. capsulatus*, namely the carotenoids spheroidene (λ^{abs}_{max} = 454, 478, 509 nm) and spheroidenone (λ^{abs}_{max} = 500 nm) as well as bacteriochlorophyll *a* (Bchl *a*, λ^{abs}_{max} = 800 and 860 nm) [33]. In this work, we established the (micro)aerobic cultivation in the BioLector microbioreactor system, allowing online-monitoring of growth and (optochemical) induction of gene expression in small cultivation volumes. For anaerobic, phototrophic cultivation, we analyzed whether optogenetic induction of gene expression by using UV-A light-responsive caged inducers can be implemented in *R. capsulatus* cultures solely illuminated with IR light (λ_{max} = 800 nm) (Figure 1 A). We additionally evaluated the usability of the three cIPTG variants NP-cIPTG, BEC-cIPTG and BC-cIPTG for this optochemical approach (Figure 1 B) [15].

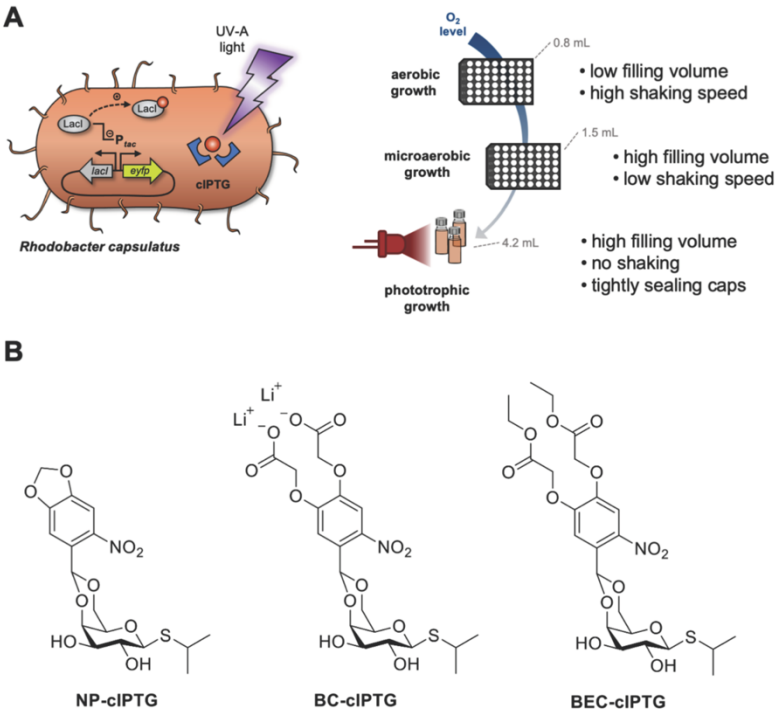

Figure 1: Experimental strategy for establishment of optochemical control over gene expression in *R. capsulatus* under non-phototrophic and phototrophic growth conditions. **A**) Light-controlled expression of the reporter gene *eyfp* in *R. capsulatus* using photocaged IPTG (cIPTG; red circle with blue frames). Upon illumination with UV-A light (purple flash symbol), the protection group is cleaved off, the previously inactive IPTG molecule is released and induces LacI/P_{tac}-mediated eYFP expression. **B**) Photocaged IPTG variants NP-cIPTG, BC-cIPTG and BEC-cIPTG used in this study.

As those photocaged molecules strongly differ in hydrophobicity and water-solubility, we wanted to compare their general usability for light-controlled gene expression in *R. capsulatus* under phototrophic (high level of EPS and ICM formation) and non-phototrophic (moderate to low EPS and ICM formation) conditions. For these studies, we chose *R. capsulatus* SB1003, as it is particularly suited for various biotechnological applications including the production of terpenes, as illustrated in our recent studies [30–32,42]. In summary, we could demonstrate that photocaged inducer molecules and especially NP-cIPTG can be applied for light-mediated control over gene expression in this alternative host under all tested growth conditions. Furthermore, we successfully applied this optogenetic approach to control the intrinsic carotenoid pathway to showcase engineering of secondary metabolite biosynthesis. This light-responsive on-switch thus offers various promising properties suitable for biotechnological applications.

Results and Discussion

cIPTG-mediated light control of gene expression in *Rhodobacter capsulatus* under non-phototrophic conditions

In order to establish a cIPTG-based optogenetic control of gene expression in the facultative phototrophic organism *R. capsulatus*, we first constructed the expression plasmid pRholHi-2-eYFP containing the repressor gene *lacI*, the LacI-controlled P_{tac} promoter (Table S1; Supporting Information) and the downstream located *eyfp* reporter gene, whose expression was first analyzed in *R. capsulatus* under aerobic and microaerobic conditions in the absence of light. Since we implemented small scale cultivation of *R. capsulatus* in the BioLector for the first time, the filling volume of the Round Well plates as well as the shaking frequencies were appropriately adapted to control the aeration of cultures during non-phototrophic growth (Fig. 1 B; Figure S 1; Supporting Information). To this end, the *R. capsulatus* strain carrying the corresponding eYFP expression vector pRholHi-2-eYFP was cultivated without addition of IPTG but with varying filling volumes and shaking frequencies for 48 h. In these cultures, bacterial growth (Figure S1 A) and the dissolved oxygen tension (DOT; Figure S1 B) were online-monitored using the scattered light intensity and DO optodes (m2p-labs, Germany), respectively. Sufficient conditions for aerobic or microaerobic growth were found to be 800 µL filling volume and 800 rpm shaking frequency or 1500 µL and 400 rpm, respectively. To evaluate the functionality and inducibility of the LacI/P_{tac} promoter system in *R. capsulatus* under non-phototrophic growth conditions,

IPTG was added at increasing concentrations (0 – 10 mM) to the medium after 9 h of cultivation (early logarithmic growth phase) and reporter gene expression was analyzed by detecting the specific eYFP fluorescence (Figure S2 A and B; Supporting Information). The results show a comparatively high eYFP expression for IPTG concentrations of 1 mM and above; thus, 1 mM was chosen as sufficient inducer concentration in all further experiments. To evaluate, whether cIPTG derivatives can be applied for light-controlled gene expression in *R. capsulatus* under non-phototrophic conditions, we analyzed the induction response of NP-cIPTG, BC-cIPTG and BEC-cIPTG in comparison to IPTG for the strain *R. capsulatus* SB1003/ pRholHi-2-eYFP in the presence and absence of UV-A light. Both experiments revealed considerable induction levels of at least 70% and up to nearly 150% for all three cIPTG derivatives leading to induction levels of at least 70% and up to nearly 150% in comparison to IPTG (Figure 2 A and B).

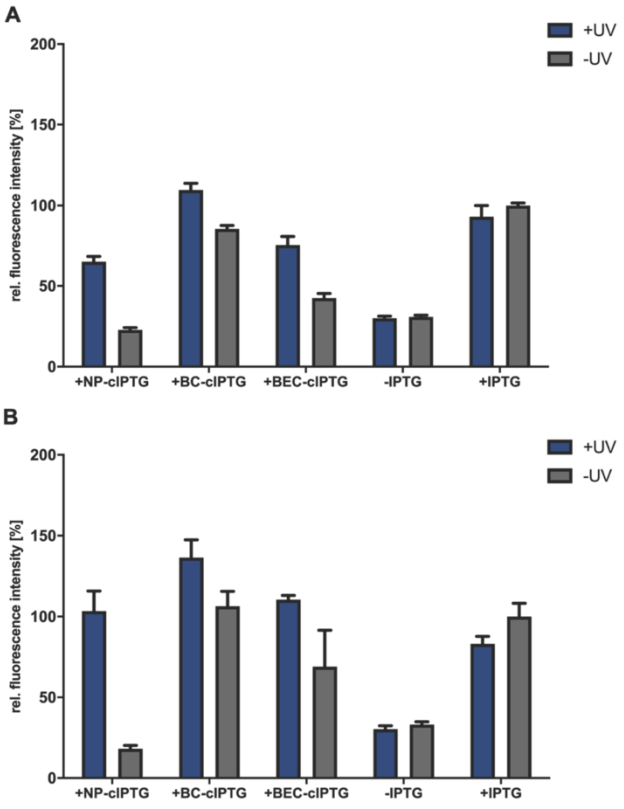

Figure 2. Application of cIPTG derivatives for light-mediated control of gene expression in *R. capsulatus* under non-phototrophic conditions. **A-B**) Light-controlled eYFP reporter gene expression in aerobically (**A**) and microaerobically (**B**) grown *R. capsulatus* SB1003 cultures carrying pRholHi-2-eYFP using the

three cIPTG derivatives NP-, BC- and BEC-cIPTG. Biomass-normalized eYFP *in vivo* fluorescence (λ_{ex}= 508 nm, λ_{em}= 532 nm) of cultures supplemented with 1 mM of each cIPTG variant is shown in relation to a 1 mM IPTG control after 48 h of cultivation (RVC medium, 30°C; for aerobic cultures 800 rpm and 800 µL filling volume and for microaerobic cultures 400 rpm and 1500 µL filling volume). Induction was performed after 9 h *via* UV-A light exposure at 365 nm (~1 mW/cm^2) for 30 min or the addition of 1 mM IPTG. Values are means of individual biological triplicates. Error bars indicate the respective standard deviations.

However, only NP-cIPTG showed a reasonably low induction level under light exclusion for aerobic and microaerobic cultivation conditions over 48 h in RCV medium at 30°C, whereas the use of BC-cIPTG and BEC-cIPTG led to high illumination-independent fluorescence signals. In order to identify factors that might be responsible for the observed instability effect, the light-independent cleavage of IPTG was analyzed in a control experiment using the well-established strain *E. coli* Tuner(DE3). To this end, we measured the induction of *eyfp* reporter gene expression upon addition of cIPTG variants, which were previously incubated either in LB or RCV medium (negative control) or in *R. capsulatus* culture supernatant (Figure S3 C; Supporting Information). These data show that no auto-hydrolysis was observed for any cIPTG derivative in sole LB or RCV medium, whereas BC- and BEC-cIPTG elicited an increased fluorescence signal when pre-treated with *R. capsulatus* supernatant. This could give a first hint that host specific enzymes or metabolites might be involved in the light-independent hydrolysis of BC- and BEC-cIPTG. We also tested the toxicity of each compound and the corresponding photoproducts to exclude further unfavorable side effects on both aerobically and microaerobically grown *R. capsulatus* cells. By comparing the growth behavior of accordingly supplemented cultures with cultures where IPTG was added to the cultivation medium (Figure S3 A and B; Supporting Information), no toxic effects could be observed for the caged inducer variants as indicated by similar growth rates in the logarithmic phases. We therefore identified the non-toxic and functional NP-cIPTG as the most promising candidate for light-controlled induction of gene expression in *R. capsulatus* under aerobic and microaerobic conditions. Additionally, to further exclude a negative effect of UV-A light exposure on the *R. capsulatus* eYFP expression strain, growth behavior of UV-A light-exposed and non-exposed cultures was comparatively analyzed in the presence and absence of IPTG (Figure S4; Supporting Information), showing no considerable effect of this treatment on the growth of respective strains.

In summary, we successfully established an optogenetic strategy allowing light control of gene expression in *R. capsulatus* under non-phototrophic conditions. In a next step, we evaluated the applicability of this system under phototrophic conditions, where additional bottlenecks may arise such as permanent illumination necessary for photosynthesis and the formation of EPS and ICM that might function as additional cellular diffusion barriers.

Light-mediated induction of gene expression in *Rhodobacter capsulatus* under anaerobic, phototrophic growth conditions

In the laboratory, phototrophic *R. capsulatus* cultures are typically grown in sealed hungate tubes under constant illumination with bulb light to ensure both a strict oxygen exclusion and optimal light conditions. First, we analyzed whether illumination of cultures, which is essential for phototrophic growth, already leads to unwanted uncaging effects. For this purpose, we used 1,2-dimethoxy-4-nitrobenzene (DMNB) as a molecular UV-A light detector suitable for the quantitative analysis of nitrobenzyl-based photouncaging processes [2,43,44]. Under UV-A light exposure, the DMNB molecule undergoes a full conversion into 2-methoxy-5-nitrophenolate (MNP) accompanied by a sensitively detectable increase of absorption at λ_{max} = 422 nm (Figure S5; Supporting Information) [45,46]. To detect undesired uncaging processes induced by different light sources applicable for phototrophic cultivation of *R. capsulatus* cells [33,42,47], the DMNB solution was exposed for 48 h either to bulb light (broad emission spectrum with high IR light and low UV light components) or IR light (monochromatic, λ_{max}= 850 nm). Additionally, a dark control and samples with increasing UV-A light exposure times from 30 min to 90 min were performed (Figure 3).

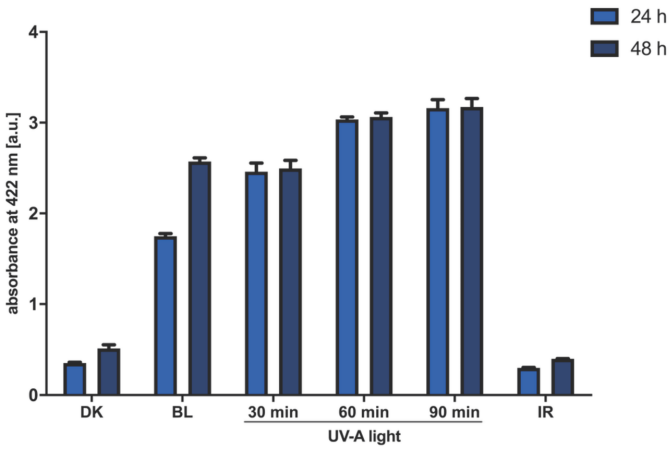

Figure 3. Photochemical detection of UV-A light exposure under various illumination conditions using DMNB. Light-mediated formation of 2-methoxy-5-nitrophenolate (MNP) from a 1.25 mM DMNB solution in aqueous potassium hydroxide was determined spectrophotometrically *via* the increase of absorbance at 422 nm after illumination with bulb light (BL, 2500 lx) and IR light (IR, λ_{max}= 850 nm; 1.23 mW/cm^2) for 24 h or 48 h. DMNB photoconversion was compared to samples that have been exposed to UV-A light for 30–90 min (λ_{max}= 365 nm; 5.4 mW/cm^2) or kept unexposed (dark control, DK). Values are means of triplicate measurements. Error bars indicate the respective standard deviations.

Interestingly, analysis of photochemical MNP formation at 422 nm after 24 h and 48 h revealed that exposure to bulb light leads to absorption values comparable to samples that were irradiated by UV-A light for 30 min. Thus, bulb light is not applicable as a light source for the phototrophic cultivation of *R. capsulatus* if cIPTG is intended to be used as an optogenetic on-switch. In contrast, IR light seems to be a promising alternative light source, as even after 48 h no photoconversion of DMNB could be detected, since the IR exposure wavelength is beyond the absorption wavelength of DMNB. To determine, which IR light intensities are needed for efficient phototrophic growth of *R. capsulatus,* cells were cultivated with IR light of increasing intensities ranging from 0.5 mW/cm^2 up to 5.1 mW/cm^2 using a custom-made IR light LED panel [33] and analyzed the growth behavior (Figure S6; Supporting Information). The data revealed that both too high and too low IR light intensities have a negative effect on phototrophic growth due to insufficient energy supply or adverse cultivation temperatures. However, illumination properties of IR LED panels at 850 nm (i.e. the absorption maximum of the photopigment BChl *a*) could be appropriately adjusted for phototrophic growth of *R. capsulatus*: An IR-light intensity of 1.7 mW/cm^2 led to similar cell densities as compared to bulb light irradiation without exceeding the optimal growth temperature.

Finally, we analyzed whether photocleavable cIPTG derivatives can be used for non-invasive control of gene expression in phototrophically growing *R. capsulatus* cells by UV-A light exposure. To this end, the strain *R. capsulatus* SB1003 carrying the plasmid pRholHi-2-eYFP was cultivated under constant IR light illumination and reporter gene expression in cIPTG-supplemented cultures was induced after 6 h (early logarithmic growth phase) with 30 min of UV-A light. Resulting eYFP fluorescence was analyzed when cells reached the stationary growth phase (48 h). As shown in Figure 4, UV-A light-induced uncaging of the cIPTG derivatives NP- and BC-cIPTG resulted in even higher eYFP expression levels as in the control experiment, where IPTG was added to UV-A exposed cultures, while the expression strength of BEC-cIPTG was slightly inferior to this control culture. Remarkably, changing the water solubility of cIPTG did not result in improved eYFP expression levels under phototrophic growth conditions. Based on the approximately similar output observed after IPTG and NP-cIPTG induction under aerobic, microaerobic, and phototrophic conditions, it can be concluded that putative IPTG diffusion barriers formed by ICM and EPS do not exert a significant influence on NP-cIPTG uptake. In addition, as previously observed in cultures that have been grown under aerobic and microaerobic conditions, BC-cIPTG and BEC-cIPTG were not stable during phototrophic cultivation, resulting in

almost equally high induction levels in the dark control as compared to the UV-A light exposed cultures. In contrast, NP-cIPTG also showed sufficient stability under phototrophic growth conditions.

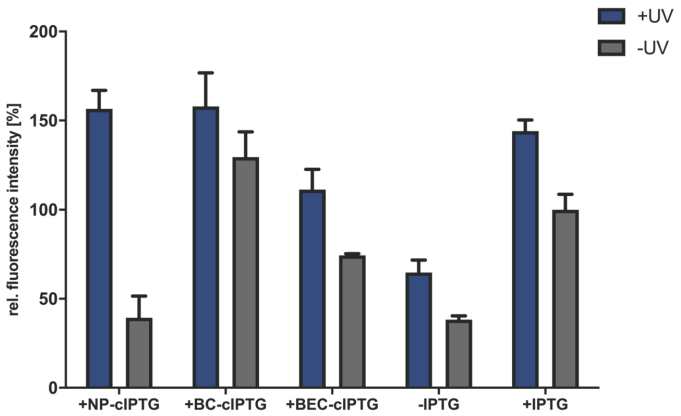

Figure 4. Light-controlled induction of gene expression in phototrophically grown *R. capsulatus* cells. The strain *R. capsulatus* SB1003 carrying pRholHi-2-eYFP was cultivated in RCV medium supplemented with 1 mM IPTG (Figure S2; Supporting Information) or with one of the three cIPTG derivatives NP-, BC- and BEC-cIPTG before inoculation (30°C, screw neck vials, IR light (λ_{max} = 850 nm, 1.7 mW/cm^2)). Biomass-normalized eYFP *in vivo* fluorescence (λ_{ex}: 508 nm, λ_{em}: 532 nm) is shown in relation to the non-illuminated control culture supplemented with 1 mM IPTG (-UV) after 48 h of cultivation. Induction was performed after 6 h *via* UV-A light exposure (365 nm; ~2 mW/cm^2) for 30 min. Values are means of individual biological triplicates. Error bars indicate the respective standard deviations.

Further it should be noted that the cell density-normalized eYFP expression strength under phototrophic conditions is significantly higher (2.2 a.u.) than under aerobic (0.42 a.u.) or microaerobic conditions (0.67 a.u.), as also documented in the study of Katzke and co-workers, where the expression strength of the T7-promoter system was superior under phototrophic growth conditions in the *R. capsulatus* strain B10S [40]. Additionally, phototrophically grown cultures without supplemented IPTG exhibited a high basal eYFP expression level (Figures 2 and 4; Figure S2; Supporting Information). Since wild-type control cultures without an expression plasmid did not show significantly increased fluorescence levels (Figure S2), the promoter system appears to be affected by high basal expression, possibly caused by an insufficient amount of the LacI repressor. As noted in previous studies, increasing the level of LacI has been shown to be extremely valuable for reducing basal expression and thereby increasing the tightness of an expression system [48,49].

The data presented so far can be summarized as follows: (i) the eYFP expression experiments clearly demonstrated that NP-cIPTG can in principle be used as an optogenetic on-switch for the non-invasive control of heterologous gene expression in *R. capsulatus*. (ii) Neither constant illumination with IR light, which is required for photosynthesis, nor morphological changes (formation of ICM and EPS) negatively

affected the function of the light-responsive inducer molecule. Hence, the optogenetic switch can be used for the facultative phototrophic bacterium under both non-phototrophic and phototrophic growth conditions.

In the following, we applied the light switch to modulate an intrinsic biosynthetic secondary metabolite pathway of *R. capsulatus*. We chose an early enzymatic step of the carotenoid pathway, which is responsible for the production of essential precursor molecules such as farnesyl pyrophosphate (FPP) for both homologous terpenes (e.g. the photopigments spheroidene and spheroidenone) and heterologous sesqui- and triterpenes (Figure 5 A) [31,33,50].

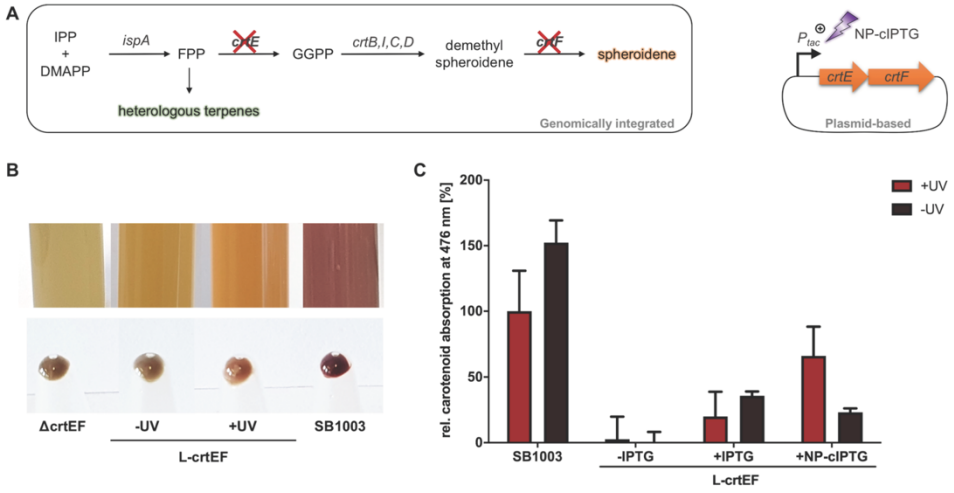

Figure 5. Light-controlled induction of carotenoid production in phototrophically grown *R. capsulatus* SB1003 *ΔcrtEF* cells carrying pRholHi-2-crtE-crtF. **A**) Intrinsic carotenoid synthesis of *R. capsulatus* starting from the terpene C_5 building blocks IPP and DMAPP. Deletion of genes encoding the relevant carotenoid pathway enzymes CrtE and CrtF results in a carotenoid-deficient strain [31]. The genes *crtE* and *crtF* were cloned in a plasmid and placed under control of the P_{tac} promoter to facilitate IPTG-based control. Light-mediated induction of *crt* gene expression was achieved by using NP-cIPTG. IPP: isopentenyl pyrophosphate; DMAPP: dimethylallyl pyrophosphate; IspA: FPP synthase; FPP: farnesyl pyrophosphate; CrtE: GGPP synthase; GGPP: geranylgeranyl pyrophosphate; CrtB: phytoene synthase; CrtI: phytoene desaturase; CrtC: hydroxyneurosporene synthase; CrtD: hydroxyneurosporene desaturase; CrtF: demethylspheroidene O-methyltransferase. **B**) Pigmentation of phototrophically grown *R. capsulatus* strains SB1003 *ΔcrtEF* (ΔcrtEF), SB1003 *ΔcrtEF*/ pRholHi-2-crtE-crtF supplemented with 1 mM NP-cIPTG under non-illuminated (-UV, L-crtEF) or UV-A illuminated conditions (+UV, L-crtEF) and SB1003 wildtype strain (SB1003). Besides liquid cultures, a cell pellet corresponding to an optical density at 660 nm of 2.5 are shown. **C**) Carotenoid absorption at 476 nm of culture extracts of *R. capsulatus* SB1003 *ΔcrtEF*/ pRholHi-2-crtE-crtF (L-crtEF) supplemented with 1 mM of NP-cIPTG (+NP-cIPTG) is shown in relation to the respective absorption of extracts from *R. capsulatus* SB1003 wildtype (SB1003) cells. In addition, cell cultures supplemented with 1 mM IPTG (positive control, +IPTG) or without IPTG (negative control, -IPTG) likewise analyzed after 96 h of phototrophic cultivation (RVC medium, 30°C, screw neck vials, IR light (λ_{max} = 850 nm, 1.7 mW/cm^2)). *R. capsulatus* SB1003 *ΔcrtEF* extracts were used to determine the background absorption of *R. capsulatus* cells at 476 nm and thus corresponding values were subtracted from all other values. Induction was performed after a cultivation time of 24 h *via* UV-A light exposure at 365 nm (~2 mW/cm^2)

for 30 min. Values are means of individual biological triplicates. Error bars indicate the respective standard deviations.

In a mutant strain lacking the relevant carotenoid biosynthesis genes *crtE* and *crtF*, intrinsic carotenoid biosynthesis cannot be performed, which results in a distinct greenish-colored phenotype [31]. We used this strain for light-controlled complementation of the observed mutant phenotype, by placing *crtEF* expression under light control.

For this purpose, the plasmid pRholHi-2-crtE-crtF was transferred to the deletion strain *R. capsulatus* SB1003 *ΔcrtEF* and cells were grown phototrophically for four days under IR light (λ_{max} = 850 nm, 1.7 mW/cm^2). Induction of the plasmid-encoded genes *crtE* and *crtF* was performed after 24 h (because of the slower growth of this mutant) *via* appropriate UV-A light exposure (30 min, λ_{max} = 365 nm, 2 mW/cm^2) or by adding IPTG prior to culture inoculation. For quantification of the carotenoid accumulation, photopigments were extracted from cell cultures with ethanol. Subsequently, the absorption of extracted carotenoids was analyzed in comparison to cultures containing IPTG as well as *R. capsulatus* SB1003 wildtype and SB1003 *ΔcrtEF* cultures as corresponding positive and negative controls using a Tecan Microplate reader (Figure 5 C). While *R. capsulatus* SB1003 *ΔcrtEF* cultures without induction of *crtEF* expression exhibited a similar pigmentation as observed in the control strain (ΔcrtEF) (Figure 5 B), addition of IPTG resulted in a clearly visible change of the cell coloration indicating a partial complementation of the phenotype that is caused by the *crt* gene deletion. This observation could be verified by quantitative analysis of the corresponding carotenoid absorption (Figure 5 C). In addition, optogenetic induction of *crtEF* gene expression using NP-cIPTG could almost completely restore the carotenoid-deficient phenotype resulting in a pronounced carotenoid absorption level thereby underpinning the importance of non-invasive, optogenetic control of these biosynthesis processes under anaerobic conditions. This can open up new strategies for the dynamic modulation of substrate fluxes in complex secondary metabolite pathways such as the terpene pathway in phototrophic bacteria, which were recently shown to be promising alternative production hosts for the sustainable production of plant terpenes [31–33].

Discussion

For the establishment of photocaged inducers as an alternative optogenetic switch allowing non-invasive induction of gene expression in the phototroph *R. capsulatus*, two parameters needed to be addressed: (i) the general functionality of photocaged inducers with respect to their stability in host-

specific cultivation medium, their non-toxicity, and their induction efficiency and (ii) the implementation of an optogenetic control tool that is compatible with specific growth conditions of this host, such as varying oxygenation and constant illumination necessary for phototrophic cultivation.

Firstly, we could show that all photocaged IPTG variants exhibit minimal interference with the biological system, which is a prerequisite for a control tool, since all three cIPTG variants were non-toxic and functional in the host organism. However, only NP-cIPTG showed a pronounced stability in cultures that were grown in the absence of UV-A light. By using NP-cIPTG derivative, we were finally able to control gene expression with an induction strength comparable to IPTG.

Subsequently, the photocaged inducer molecule was evaluated with respect to its non-invasive applicability, since it should function robustly under diverse host-specific growth conditions. We could prove the applicability of NP-cIPTG under aerobic, microaerobic, and phototrophic conditions and applied it successfully for light-mediated expression of FPP converting enzymes involved in the host-specific carotenoid biosynthesis.

For the establishment of light-mediated control of biotechnological processes in the phototrophic bacterium *R. capsulatus*, we applied IR light-emitting LED panels as alternative light sources suitable for irradiation of BChl *a*, which is essential for photosynthesis, while omitting emission of light in the visible range. Consequently, the spectral range of 300-800 nm can be utilized for additional optogenetic approaches such as the use of photocaged inducers, as shown here, or a variety of photoreceptors including well-known blue light-responsive photoreceptors of the LOV-, BLUF- or cryptochrome families [5,51–54] or green light-responsive photoreceptors (e.g. CcaS cyanobacteriochrome receptor and CarH cobalamine-dependent receptor [55–58]). The CarH photoreceptor would be especially well-suited for optogenetic control in *R. capsulatus*, as its chromophore 5'-deoxyadenosylcobalamin, a form of vitamin B_{12}, is naturally provided by this organism [59].

Originally, energy acquisition in *R. capsulatus* during anaerobic growth is preferably performed *via* anoxygenic photosynthesis using both carotenoids and BChl *a* as photopigments [60,61]. By narrowing the light emission spectrum to the IR range, only BChl *a* absorbs light for energy acquisition and principally, most of the isoprenoid precursors can be redirected to recombinant secondary metabolite pathways to produce high-value compounds such as plant sesquiterpenes. In this context, the optogenetic control of the carotenoid production might offer the possibility to precisely adjust the carotenoid level in *R. capsulatus* cultures allowing to balance the FPP level for obtaining high titers of heterologous terpenes. This approach seems to be promising as an accumulation of FPP can exert toxic

effects on the host organism [62–64] and the production of heterologous terpenes in *R. capsulatus* is most commonly performed in carotenoid-producing strains in which resources for endogenous carotenoid production are drained from the heterologous terpene pathway [30,32,33]. Recently, the production titers of the triterpene cycloartenol in *R. capsulatus* cultures were shown to be increased 3-fold in a carotenoid-deficient *R. capsulatus* strain [31]. However, cultivation of the terpene producing strain was performed microaerobically in this case and could therefore not benefit from ICM formation and elevated isoprene metabolism associated with anaerobic phototrophic growth [32]. In the future, heterologous production of terpenes could thus be improved by performing phototrophic growth with optogenetically adjusted carotenoid levels to ensure an optimal utilization of the toxic FPP intermediate. Consequently, the established phototrophic cultivation process in combination with light-mediated regulation using photocaged inducers opens up the possibility to address more complex controlled metabolic pathways in the future. By means of combining different optogenetic stimuli, this on-switch offers a light-driven regulation approach for dynamically controlling metabolic pathways in a rapid, tunable and user-controlled manner. In future studies, this tool could furthermore prove valuable for automated control processes, where an optogenetic stimulus controls cellular processes such as growth or target gene expression in response to a specific biosensor signal in a closed-loop setup [65–68].

In conclusion, we successfully established NP-cIPTG as a suitable on-switch for light-controlled gene expression in *R. capsulatus*. Neither constant illumination with IR light, which is required for photosynthesis, nor morphological changes such as the formation of ICM and EPS, resulted in limited applicability of the light-responsive inducer molecule. The presented toolset can contribute to non-invasive, light-mediated bioprocess optimization, induction profiling or strain development for an improved microbial synthesis of bioproducts [18,20,69,70].

Material and Methods

Bacterial strains and plasmids: The *Escherichia coli* strain DH5α [71] was used for cloning and the strain S17-1 [72] for the conjugational transfer of expression plasmids. All *E. coli* strains were grown at 37°C on LB agar plates or in liquid LB medium (Luria/Miller, Carl Roth®), supplemented with kanamycin (50 µg mL^{-1}) when necessary. The *Rhodobacter capsulatus* strain SB1003 [25] was grown on PY agar plates containing 2% Select Agar (Thermo Fisher Scientific) or in RCV liquid medium containing 15 mM ammonium and supplemented with kanamycin (25 µg mL^{-1}) at 30°C. For cultivation of strain SB1003, rifampicin (25 µg mL^{-1}) was used additionally. If not stated otherwise, cultivation was conducted under anaerobic, photoheterotrophic conditions and permanent illumination with bulb light (2500 lx), as described previously [32].

All bacterial strains as well as the construction and genetic properties of plasmids used in this study are listed in Table S1 (Supporting Information).

Cultivation of *R. capsulatus* for target gene expression: The aerobic and microaerobic expression cultures were grown in RCV + ammonium medium at 30°C using 48-well Round Well Plates® in a BioLector microbioreactor system (m2p labs, Germany) applying variable filling volumes and shaking frequencies to control dissolved oxygen tension (800, 1000 and 1500 µL; 800 rpm or 400 rpm, respectively). Cultures were inoculated with an optical density of 0.1 determined at 660 nm. The cell density was measured during cultivation *via* scattered light intensity at 620 nm and the eYFP fluorescence intensities were online monitored using a 508/532 nm filter. Heterologous and homologous gene expression was induced during early logarithmic phase (after approx. 9 h) *via* UV-A light exposure (VL-315.BL lamp, Vilber Lourmat, France; ~1 mW/cm^2, 30 min exposure) in RCV medium that was supplemented with BC-, BEC- or NP-cIPTG (1 mM) or by adding IPTG (1 mM) directly after light exposure in corresponding control cultures. The phototrophic expression cultures were inoculated with a starting OD_{660nm} of 0.5 in completely filled 4.2 mL screw neck vials (N13; Macherey-Nagel, Düren, Germany) using tight screw caps with a bonded septum (Macherey-Nagel, Düren, Germany) in RCV + ammonium medium at 30°C. Those were shown to be appropriate cultivation vessels for phototrophic growth in a previous study [33]. To establish adequate environmental conditions for anoxygenic photosynthesis, cells were permanently illuminated with IR light (850 nm, 1.7 mW/cm^2). The expression was induced after 6 h by UV-A light irradiation (365 nm, 2 mW/cm^2, 30 min exposure) using NP-, BC-,

or BEC-cIPTG (1 mM) added prior to cultivation. The same concentration of IPTG was used for corresponding control experiments. After 48 h of cultivation, *R. capsulatus* biomass and eYFP fluorescence were determined. For comparable measurements, 800 µL of each vial were transferred to one well of a Round Well Plate and further incubated at 30°C for 1.5 h in a BioLector microbioreactor system (m2p labs, Germany) (800 µL, 800 rpm) to ensure O_2-dependent YFP chromophore maturation. After eYFP maturation was completed, the cell density was measured *via* scattered light intensity at 620 nm and the eYFP fluorescence was determined by using a 508/532 nm filter.

DMNB-actinometry: For the DMNB assay, 1.25 mM DMNB was dissolved in aqueous KOH solution (0.5 M) with 10%(v/v) DMSO. The alkaline DMNB solution was subsequently incubated under the same conditions applied for phototrophic growth of *R. capsulatus*. DMNB photoconversion to MNP was monitored by the increase of absorption at a wavelength of 422 nm (100 µL, Tecan Infinite M1000 Pro microplate reader). The UV-A exposure was carried out using a UV-A hand lamp (VL-315.BL 45 W, Vilber Lourmat, France; 5.4 mW/cm^2 at 365 nm for 1.5 cm distance to light source), the other light sources were used as described above.

Carotenoid production and extraction: The carotenoid complementation assay was performed using 4.2 mL screw neck vials (N13; Macherey-Nagel, Düren, Germany) for cultivation in NP-cIPTG supplemented RCV + ammonium medium (starting OD660nm = 0.1, 30°C, anaerobic conditions, permanent illumination with IR light (850 -nm, 1.7 mW/cm^2)). The expression of the *crtEF* genes was induced after 24 h *via* UV-A light exposure (365 nm, 2 mW/cm^2, 30 min exposure). IPTG was also added prior to the cultivation. After further 72 h of cultivation, cells corresponding to an optical density at 660 nm of 2.5 were pelleted and resuspended in 10 µl RCV medium. For carotenoid extraction, 500 µL ethanol (100% p.a.) was added and suspensions were thoroughly vortexed at room temperature before the pigment extracts were cleared by centrifugation. For carotenoid absorption, 100 µL of those extracts were analyzed for their respective absorption at 476 nm using an Infinite M1000 Pro microplate reader (Tecan Group LTD., Maennedorf, Switzerland).

For all illumination experiments, intensities of different light sources were quantified at relevant wavelengths (i.e. 365 and 850 nm) by using a Thermal Power Sensor (S302C, Thorlabs Inc, USA).

Synthesis of photocaged compounds: NP-cIPTG [8,9], BEC-cIPTG and BC-cIPTG [15] were synthesized as published previously.

Determination of compound purity by qNMR: The purity of the NP-cIPTG, BEC-cIPTG and BC-cIPTG was determined *via* quantitative NMR. (Methanesulfonyl)methane was utilized as internal standard for BC-cIPTG and 3,5-bis(trifluoromethyl)bromobenzene for NP-cIPTG as well as BEC-cIPTG. The spectra were measured at 20°C on a Bruker Avance/DRX 600 spectrometer with 64 scans each and 30 µs relaxation time between each scan. The results in Table S2 are means of triplicate measurements.

Keywords: caged compounds • light-controlled gene expression • optogenetic • purple non-sulfur photosynthetic bacteria • *Rhodobacter capsulatus*

References

1. Bardhan A, Deiters A. Development of photolabile protecting groups and their application to the optochemical control of cell signaling. Curr Opin Struct Biol. 2019;57: 164–175. doi:10.1016/j.sbi.2019.03.028

2. Brieke C, Rohrbach F, Gottschalk A, Mayer G, Heckel A. Light-controlled tools. Angew Chem Int Ed. 2012;51: 8446–8476. doi:10.1002/anie.201202134

3. Gardner L, Deiters A. Light-controlled synthetic gene circuits. Curr Opin Chem Biol. 2012;16: 292–299. doi:10.1016/j.cbpa.2012.04.010

4. Deiters A. Light activation as a method of regulating and studying gene expression. Curr Opin Chem Biol. 2009. 13: 678-686. doi:10.1016/j.cbpa.2009.09.026

5. Drepper T, Krauss U, Meyer zu Berstenhorst S, Pietruszka J, Jaeger K-E. Lights on and action! Controlling microbial gene expression by light. Appl Microbiol Biotechnol. 2011;90: 23–40. doi:10.1007/s00253-011-3141-6

6. Liu J, Hemphill J, Samanta S, Tsang M, Deiters A. Genetic code expansion in zebrafish embryos and its application to optical control of cell signaling. J Am Chem Soc. 2017;139: 9100–9103. doi:10.1021/jacs.7b02145

7. Kolarski D, Sugiyama A, Breton G, Rakers C, Ono D, Schulte A, et al. Controlling the circadian clock with high temporal resolution through photodosing. J Am Chem Soc. 2019. doi:10.1021/jacs.9b05445

8. Young DD, Deiters A. Photochemical activation of protein expression in bacterial cells. Angew Chem Int Ed. 2007;46: 4290–4292. doi:10.1002/anie.200700057

9. Binder D, Grünberger A, Loeschcke A, Probst C, Bier C, Pietruszka J, et al. Light-responsive control of bacterial gene expression: precise triggering of the *lac* promoter activity using photocaged IPTG. Integr Biol. 2014;6: 755–765. doi:10.1039/C4IB00027G

10. Gardner L, Zou Y, Mara A, Cropp TA, Deiters A. Photochemical control of bacterial signal processing using a light-activated erythromycin. Mol Biosyst. 2011; 7: 2554-2557. doi:10.1039/c1mb05166k

11. Bier C, Binder D, Drobietz D, Loeschcke A, Drepper T, Jaeger K-E, et al. Photocaged carbohydrates: versatile tools for controlling gene expression by light. Synthesis (Stuttg). 2016;49: 42–52. doi:10.1055/s-0035-1562617

12. Kusen PM, Wandrey G, Krewald V, Holz M, Berstenhorst SM zu, Büchs J, et al. Light-controlled gene expression in yeast using photocaged Cu^{2+}. J Biotechnol. 2017;258: 117–125. doi:10.1016/j.jbiotec.2017.04.032

13. Wandrey G, Bier C, Binder D, Hoffmann K, Jaeger K-E, Pietruszka J, et al. Light-induced gene expression with photocaged IPTG for induction profiling in a high-throughput screening system. Microb Cell Fact. 2016;15: 63. doi:10.1186/s12934-016-0461-3

14. Binder D, Frohwitter J, Mahr R, Bier C, Grünberger A, Loeschcke A, et al. Light-controlled cell factories: employing photocaged isopropyl-β-D-thiogalactopyranoside for light-mediated optimization of *lac* promoter-based gene expression and (+)-valencene biosynthesis in *Corynebacterium glutamicum*. Appl Environ Microbiol. 2016;82: 6141–6149. doi:10.1128/AEM.01457-16

15. Hogenkamp F, Hilgers F, Knapp A, Klaus O, Bier C, Binder D, et al. Effect of photocaged isopropyl β-D-1-thiogalactopyranoside solubility on the light responsiveness of LacI-controlled expression systems in different bacteria. ChemBioChem. 2021;22: 539–547. doi:10.1002/cbic.202000377

16. Rodolfi L, Zittelli GC, Bassi N, Padovani G, Biondi N, Bonini G, et al. Microalgae for oil: Strain selection, induction of lipid synthesis and outdoor mass cultivation in a low-cost photobioreactor. Biotechnol Bioeng. 2009;102: 100–112. doi:10.1002/bit.22033

17. Malik S, Hossein Mirjalili M, Fett-Neto AG, Mazzafera P, Bonfill M. Living between two worlds:

498 Two-phase culture systems for producing plant secondary metabolites. Crit Rev Biotechnol.
499 2013;33: 1–22. doi:10.3109/07388551.2012.659173

500 18. Monshupanee T, Nimdach P, Incharoensakdi A. Two-stage (photoautotrophy and heterotrophy)
501 cultivation enables efficient production of bioplastic poly-3-hydroxybutyrate in auto-sedimenting
502 cyanobacterium. Sci Rep. 2016;6: 37121. doi:10.1038/srep37121

503 19. Narala RR, Garg S, Sharma KK, Thomas-Hall SR, Deme M, Li Y, et al. Comparison of microalgae
504 cultivation in photobioreactor, open raceway pond, and a two-stage hybrid system. Front Energy
505 Res. 2016;4: 1–10. doi:10.3389/fenrg.2016.00029

506 20. Nagappan S, Devendran S, Tsai P-C, Dahms H-U, Ponnusamy VK. Potential of two-stage
507 cultivation in microalgae biofuel production. Fuel. 2019;252: 339–349.
508 doi:10.1016/j.fuel.2019.04.138

509 21. Aziz MMA, Kassim KA, Shokravi Z, Jakarni FM, Liu HY, Zaini N, et al. Two-stage cultivation
510 strategy for simultaneous increases in growth rate and lipid content of microalgae: A review.
511 Renew Sustain Energy Rev. 2020;119: 109621. doi:10.1016/j.rser.2019.109621

512 22. Pagels F, Lopes G, Vasconcelos V, Guedes AC. White and red LEDs as two-phase batch for
513 cyanobacterial pigments production. Bioresour Technol. 2020;307: 123105.
514 doi:10.1016/j.biortech.2020.123105

515 23. Stoppani AO, Fuller RC, Calvin M. Carbon dioxide fixation by *Rhodopseudomonas capsulatus*.
516 J Bacteriol. 1955;69: 491–501. doi:10.1128/jb.69.5.491-501.1955

517 24. Tabita FR. The biochemistry and metabolic regulation of carbon metabolism and CO_2 fixation in
518 purple bacteria. Anoxygenic Photosynthetic Bacteria Advances in Photosynthesis and
519 Respiration, vol 2. Springer, Dordrecht; 1995. pp. 885–914. doi:10.1007/0-306-47954-0_41

520 25. Strnad H, Lapidus A, Paces J, Ulbrich P, Vlcek C, Paces V, et al. Complete genome sequence
521 of the photosynthetic purple nonsulfur bacterium *Rhodobacter capsulatus* SB1003. J Bacteriol.
522 2010;192: 3545–6. doi:10.1128/JB.00366-10

523 26. Bräutigam E, Fiedler F, Woitzik D, Flammann HT, Weckesser J. Capsule polysaccharide-protein-
524 peptidoglycan complex in the cell envelope of *Rhodobacter capsulatus*. Arch Microbiol. 1988;150:
525 567–573. doi:10.1007/BF00408251

526 27. Drews G, Oelze J. Organization and differentiation of membranes of phototrophic bacteria. Adv
527 Microb Physiol. 1981. 22: 1–92. doi:10.1016/S0065-2911(08)60325-2

528 28. Drews G. The intracytoplasmic membranes of purple bacteria--assembly of energy-transducing
529 complexes. J Mol Microbiol Biotechnol. 2013;23: 35–47. doi:10.1159/000346518

530 29. Tucker JD, Siebert CA, Escalante M, Adams PG, Olsen JD, Otto C, et al. Membrane invagination
531 in *Rhodobacter sphaeroides* is initiated at curved regions of the cytoplasmic membrane, then
532 forms both budded and fully detached spherical vesicles. Mol Microbiol. 2010;76: 833–47.
533 doi:10.1111/j.1365-2958.2010.07153.x

534 30. Loeschcke A, Dienst D, Wewer V, Hage-Hülsmann J, Dietsch M, Kranz-Finger S, et al. The
535 photosynthetic bacteria *Rhodobacter capsulatus* and *Synechocystis sp.* PCC 6803 as new hosts
536 for cyclic plant triterpene biosynthesis. PLoS One. 2017;12: e0189816.
537 doi:10.1371/journal.pone.0189816

538 31. Hage-Hülsmann J, Metzger S, Wewer V, Buechel F, Troost K, Thies S, et al. Biosynthesis of
539 cycloartenol by expression of plant and bacterial oxidosqualene cyclases in engineered
540 *Rhodobacter capsulatus*. J Biotechnol 2019; 4: 100014. doi:10.1016/j.btecx.2020.100014

541 32. Troost K, Loeschcke A, Hilgers F, Özgür AY, Weber TM, Santiago-Schübel B, et al. Engineered
542 *Rhodobacter capsulatus* as a phototrophic platform organism for the synthesis of plant
543 sesquiterpenoids. Front Microbiol. 2019;10: 1998. doi:10.3389/fmicb.2019.01998

544 33. Hilgers F, Habash SS, Loeschcke A, Ackermann YS, Neumann S, Heck A, et al. Heterologous
545 production of β-caryophyllene and evaluation of its activity against plant pathogenic fungi.
546 Microorganisms. 2021; 9: 168. doi:10.3390/microorganisms9010168

547 34. Katzke N, Bergmann R, Jaeger K-E, Drepper T. Heterologous high-level gene expression in the
548 photosynthetic bacterium *Rhodobacter capsulatus*. Meth Mol Biol. 2012. 824: 251–269.

549 doi:10.1007/978-1-61779-433-9_13

550 35. Khan NE, Nybo SE, Chappell J, Curtis WR. Triterpene hydrocarbon production engineered into
551 a metabolically versatile host- *Rhodobacter capsulatus*. Biotechnol Bioeng. 2015;112: 1523–32.
552 doi:10.1002/bit.25573

553 36. Obeid J, Magnin JP, Flaus JM, Adrot O, Willison JC, Zlatev R. Modelling of hydrogen production
554 in batch cultures of the photosynthetic bacterium *Rhodobacter capsulatus*. Int J Hydrogen
555 Energy. 2009;34: 180–185. doi:10.1016/j.ijhydene.2008.09.081

556 37. Boran E, Özgür E, van der Burg J, Yücel M, Gündüz U, Eroglu I. Biological hydrogen production
557 by *Rhodobacter capsulatus* in solar tubular photo bioreactor. J Clean Prod. 2010;18: S29–S35.
558 doi:10.1016/j.jclepro.2010.03.018

559 38. Uyar B. Bioreactor design for photofermentative hydrogen production. Bioprocess Biosyst Eng.
560 2016;39: 1331–1340. doi:10.1007/s00449-016-1614-9

561 39. Gebicki J, Modigell M, Schumacher M, van der Burg J, Roebroeck E. Comparison of two reactor
562 concepts for anoxygenic H_2 production by *Rhodobacter capsulatus*. J Clean Prod. 2010;18: S36–
563 S42. doi:10.1016/j.jclepro.2010.05.023

564 40. Katzke N, Arvani S, Bergmann R, Circolone F, Markert A, Svensson V, et al. A novel T7 RNA
565 polymerase dependent expression system for high-level protein production in the phototrophic
566 bacterium *Rhodobacter capsulatus*. Protein Expr Purif. 2010; 69: 137-146.
567 doi:10.1016/j.pep.2009.08.008

568 41. Elkahlout K, Sagir E, Alipour S, Koku H, Gunduz U, Eroglu I, et al. Long-term stable hydrogen
569 production from acetate using immobilized *Rhodobacter capsulatus* in a panel photobioreactor.
570 Int J Hydrogen Energy. 2019;44: 18801–18810. doi:10.1016/j.ijhydene.2018.10.133

571 42. Peters L, Weidenfeld I, Klemm U, Loeschcke A, Weihmann R, Jaeger K-E, et al. Phototrophic
572 purple bacteria as optoacoustic *in vivo* reporters of macrophage activity. Nat Commun. 2019;10:
573 1191. doi:10.1038/s41467-019-09081-5

574 43. Pelliccioli AP, Wirz J. Photoremovable protecting groups: Reaction mechanisms and applications.
575 Photochem Photobiol Sci. 2002; 1:441-458. doi:10.1039/b200777k

576 44. Nakayama K, Heise I, Görner H, Gärtner W. Peptide release upon photoconversion of 2-
577 nitrobenzyl compounds into nitroso derivatives. Photochem Photobiol. 2011; 87: 1031-1035.
578 doi:10.1111/j.1751-1097.2011.00957.x

579 45. van Riel HCHA, Lodder G, Havinga E. Photochemical Methoxide Exchange in Some
580 Nitromethoxybenzenes. The Role of the Nitro Group in Sn2 Ar* Reactions. J Am Chem Soc.
581 1981; 103: 7257-7262. doi:10.1021/ja00414a036

582 46. Zhang JY, Esrom H, Boyd IW. UV intensity measurement of 308 nm excimer lamp using
583 chemical actinometer. Appl Surf Sci. 1999; 138-139: 315-319. doi:10.1016/S0169-
584 4332(98)00412-7

585 47. Kaschner M, Loeschcke A, Krause J, Minh BQ, Heck A, Endres S, et al. Discovery of the first
586 light-dependent protochlorophyllide oxidoreductase in anoxygenic phototrophic bacteria. Mol
587 Microbiol. 2014;93: 1066–1078. doi:10.1111/mmi.12719

588 48. Dubendorf JW, Studier FW. Controlling basal expression in an inducible T7 expression system
589 by blocking the target T7 promoter with *lac* repressor. J Mol Biol. 1991;219: 45–59.
590 doi:10.1016/0022-2836(91)90856-2

591 49. Studier FW. Use of bacteriophage T7 lysozyme to improve an inducible T7 expression system.
592 J Mol Biol. 1991;219: 37–44. doi:10.1016/0022-2836(91)90855-Z

593 50. Troost K, Loeschcke A, Hilgers F, Özgür AY, Weber TM, Santiago-Schübel B, et al. Engineered
594 *Rhodobacter capsulatus* as a phototrophic platform organism for the synthesis of plant
595 sesquiterpenoids. Front Microbiol. 2019;10: 1998. doi:10.3389/fmicb.2019.01998

596 51. Briggs WR, Christie JM. Phototropins 1 and 2: versatile plant blue-light receptors. Trends Plant
597 Sci. 2002;7: 204–210. doi:10.1016/S1360-1385(02)02245-8

598 52. Losi A, Gärtner W. Bacterial bilin- and flavin-binding photoreceptors. Photochem Photobiol Sci.
599 2008;7l: 1168–78. doi:10.1039/b802472c

53. Gomelsky M, Klug G. BLUF: A novel FAD-binding domain involved in sensory transduction in microorganisms. Trends Biochem Sci. 2002;27: 497–500. doi:10.1016/S0968-0004(02)02181-3

54. Lin C, Todo T. The cryptochromes. Genome Biol. 2005;6: 220-220.9. doi:10.1186/gb-2005-6-5-220

55. Hirose Y, Shimada T, Narikawa R, Katayama M, Ikeuchi M. Cyanobacteriochrome CcaS is the green light receptor that induces the expression of phycobilisome linker protein. Proc Natl Acad Sci U S A. 2008; 105: 9528-9533. doi:10.1073/pnas.0801826105

56. Tabor JJ, Levskaya A, Voigt C a. Multichromatic control of gene expression in *Escherichia coli*. J Mol Biol. 2011;405: 315–324. doi:10.1016/j.jmb.2010.10.038

57. Padmanabhan S, Jost M, Drennan CL, Elías-Arnanz M. A new facet of vitamin B12 : gene regulation by cobalamin-based photoreceptors. Annu Rev Biochem. 2017;86: 485–514. doi:10.1146/annurev-biochem-061516-044500

58. Chatelle C, Ochoa-Fernandez R, Engesser R, Schneider N, Beyer HM, Jones AR, et al. A Green-light-responsive system for the control of transgene expression in mammalian and plant cells. ACS Synth Biol. 2018;7: 1349–1358. doi:10.1021/acssynbio.7b00450

59. Cheng Z, Li K, Hammad LA, Karty JA, Bauer CE. Vitamin B12 regulates photosystem gene expression *via* the CrtJ antirepressor AerR in *Rhodobacter capsulatus*. Mol Microbiol. 2014;91: 649–664. doi:10.1111/mmi.12491

60. Gregor J. Regulation of bacterial photosynthesis genes by oxygen and light. FEMS Microbiol Lett. 1999;179: 1–9. doi:10.1016/S0378-1097(99)00374-2

61. Bauer C, Elsen S, Swem LR, Swem DL, Masuda S. Redox and light regulation of gene expression in photosynthetic prokaryotes. Allen JF, Raven JA, editors. Philos Trans R Soc Lond Ser B Biol Sci. 2003;358: 147–154. doi:10.1098/rstb.2002.1189

62. Martin VJJ, Pitera DJ, Withers ST, Newman JD, Keasling JD. Engineering a mevalonate pathway in *Escherichia coli* for production of terpenoids. Nat Biotechnol. 2003;21: 796–802. doi:10.1038/nbt833

63. Pitera DJ, Paddon CJ, Newman JD, Keasling JD. Balancing a heterologous mevalonate pathway for improved isoprenoid production in *Escherichia coli*. Metab Eng. 2007;9: 193–207. doi:10.1016/j.ymben.2006.11.002

64. Dahl RH, Zhang F, Alonso-Gutierrez J, Baidoo E, Batth TS, Redding-Johanson AM, et al. Engineering dynamic pathway regulation using stress-response promoters. Nat Biotechnol. 2013;31: 1039–1046. doi:10.1038/nbt.2689

65. Lalwani MA, Zhao EM, Avalos JL. Current and future modalities of dynamic control in metabolic engineering. Curr Opin Biotechnol. 2018;52: 56–65. doi:10.1016/j.copbio.2018.02.007

66. Boada Y, Vignoni A, Picó J, Carbonell P. Extended metabolic biosensor design for dynamic pathway regulation of cell factories. iScience. 2020;23: 101305. doi:10.1016/j.isci.2020.101305

67. Toettcher JE, Gong D, Lim WA, Weiner OD. Light-based feedback for controlling intracellular signaling dynamics. Nat Methods. 2011;8: 837–839. doi:10.1038/nmeth.1700

68. Milias-Argeitis A, Rullan M, Aoki SK, Buchmann P, Khammash M. Automated optogenetic feedback control for precise and robust regulation of gene expression and cell growth. Nat Commun. 2016;7: 12546. doi:10.1038/ncomms12546

69. Zhang D, Wan M, del Rio-Chanona EA, Huang J, Wang W, Li Y, et al. Dynamic modelling of *Haematococcus pluvialis* photoinduction for astaxanthin production in both attached and suspended photobioreactors. Algal Res. 2016;13: 69–78. doi:10.1016/j.algal.2015.11.019

70. Lindberg P, Park S, Melis A. Engineering a platform for photosynthetic isoprene production in cyanobacteria, using *Synechocystis* as the model organism. Metab Eng. 2010;12: 70–79. doi:10.1016/j.ymben.2009.10.001

71. Hanahan D. Studies on transformation of *Escherichia coli* with plasmids. J Mol Biol. 1983;166: 557–580. doi:10.1016/S0022-2836(83)80284-8

72. Simon R, Priefer U, Pühler A. A Broad host range mobilization system for *in vivo* genetic

650 engineering: transposon mutagenesis in gram-negative bacteria. Bio/Technology. 1983;1: 784–
651 791. doi:10.1038/nbt1183-784

652

II.1.3. CHALLENGES AND SOLUTIONS IN CAGED COMPOUND SYNTHESIS AND *IN VIVO* APPLICATION

Optochemical Control of Bacterial Gene Expression:

Novel Photocaged Compounds for Different Promoter Systems

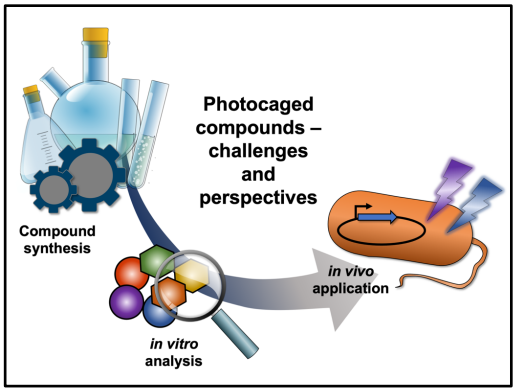

Fabian Hogenkamp*, **Fabienne Hilgers***, Nora Lisa Bitzenhofer, Vera Ophoven, Mona Haase, Claus Bier, Dennis Binder, Karl-Erich Jaeger, Thomas Drepper and Jörg Pietruszka

ChemBioChem, 22, 2021. cbic.202000467

The online version may be found at: 10.1002/cbic.202100467

Status: published

For the Supporting Information see Appendix (**Chapter V.3., page 307**).

Own contribution:

Designing and performing biological experiments, plasmid constructions, analyzing *in vivo* data, writing parts of the manuscript.

ChemBioChem

Full Papers
doi.org/10.1002/cbic.202100467

Chemistry Europe
European Chemical Societies Publishing

Optochemical Control of Bacterial Gene Expression: Novel Photocaged Compounds for Different Promoter Systems

Fabian Hogenkamp[+],[a] Fabienne Hilgers[+],[b] Nora Lisa Bitzenhofer,[b] Vera Ophoven,[a] Mona Haase,[a] Claus Bier,[a] Dennis Binder,[b] Karl-Erich Jaeger,[b, c] Thomas Drepper,*[b] and Jörg Pietruszka*[a, c]

Photocaged compounds are applied for implementing precise, optochemical control of gene expression in bacteria. To broaden the scope of UV-light-responsive inducer molecules, six photocaged carbohydrates were synthesized and photochemically characterized, with the absorption exhibiting a red-shift. Their differing linkage through ether, carbonate, and carbamate bonds revealed that carbonate and carbamate bonds are convenient. Subsequently, those compounds were successfully applied *in vivo* for controlling gene expression in *E. coli via* blue light illumination. Furthermore, benzoate-based expression systems were subjected to light control by establishing a novel photocaged salicylic acid derivative. Besides its synthesis and *in vitro* characterization, we demonstrate the challenging choice of a suitable promoter system for light-controlled gene expression in *E. coli*. We illustrate various bottlenecks during both photocaged inducer synthesis and *in vivo* application and possibilities to overcome them. These findings pave the way towards novel caged inducer-dependent systems for wavelength-selective gene expression.

Introduction

Gene expression is a fundamental biological process which needs to be tightly controlled both *in vivo* and for biotechnological applications. Light provides an orthogonal, external, easily tuneable stimulus with high spatiotemporal resolution and thus constitutes an ideal signal for this purpose.[1] In the recent past, light-controlled gene expression has been established in form of two concepts either by employing light-sensitive proteins or light-activatable (bio)molecules.[2] Mostly, genetically encoded light-sensitive photoreceptors, which have their natural origin in plants or fungi (e.g. LOV domains, phytochromes or other photosensory proteins), are used to construct recombinant control elements applicable for activating or repressing transcription.[1b,3] In contrast, light-activatable molecules consist of a bioactive component and a photoremovable protecting group, retaining it in an inactive state until irradiation with a certain wavelength restores its bioactivity by photochemically initiated covalent bond cleavage.[4] Different types of biomolecules as nucleic acids, peptides or small inducer molecules can be targeted with this method to achieve light-regulated gene expression.[1b,5] However, there is still a limited number of small molecule-inducible gene expression systems available, which have been addressed by light-regulation. Most of them were targeted in eukaryotic cells by ecdysone,[6] doxycycline,[7] tamoxifen,[8] cyclofen-OH,[9] methionine,[10] and copper.[11] Isopropyl β-D-1-thiogalactopyranoside (IPTG, **1a**),[12] erythromycin[13] and a variety of carbohydrates (arabinose (**2a**),[14] glucose, galactose, rhamnose, lactose)[15] were employed in bacteria, viz. *Escherichia coli*. Among them, only photocaged IPTG derivatives were recently applied to alternative production hosts, namely *Corynebacterium glutamicum*,[16] *Pseudomonas putida*,[17] and *Bacillus subtilis*.[17]

A photocaged compound has to fulfil different requirements: It should offer strong absorption (ε) at the desired wavelength, a high quantum yield (ϕ) and efficiency ($\varepsilon\phi$) of the corresponding photoreaction, as well as a low background activity prior to irradiation. Furthermore, it must be non-toxic and stable as well as soluble in the targeted media.[18] The application of photocaged small inducer molecules in bacteria is challenging: Cultivation of bacteria usually occurs at elevated temperatures (30–37 °C), requires long cultivation conditions (≥ 24 h), and, most notably, a variety of different degrading

[a] F. Hogenkamp,[+] V. Ophoven, M. Haase, Dr. C. Bier, Prof. Dr. J. Pietruszka
Institute of Bioorganic Chemistry
Heinrich Heine University Düsseldorf at Forschungszentrum Jülich Stetternicher Forst, 52426 Jülich (Germany)
and
Bioeconomy Science Center (BioSC)
E-mail: J.Pietruszka@fz-juelich.de

[b] F. Hilgers,[+] N. L. Bitzenhofer, Dr. D. Binder, Prof. Dr. K.-E. Jaeger, Dr. T. Drepper
Institute of Molecular Enzyme Technology Heinrich Heine University Düsseldorf at Forschungszentrum Jülich, Stetternicher Forst
52426 Jülich (Germany)
and
Bioeconomy Science Center (BioSC)
E-mail: T.Drepper@fz-juelich.de

[c] Prof. Dr. K.-E. Jaeger, Prof. Dr. J. Pietruszka
Institute of Bio- and Geosciences (IBG-1: Biotechnology)
Forschungszentrum Jülich GmbH, 52426 Jülich (Germany)

[+] These authors contributed equally to this work.

Supporting information for this article is available on the WWW under https://doi.org/10.1002/cbic.202100467

This article is part of a Special Collection dedicated to the Biotrans 2021 conference. Please see our homepage for more articles in the collection.

ChemBioChem
Full Papers
doi.org/10.1002/cbic.202100467
Chemistry Europe
European Chemical Societies Publishing

enzymes are present, which are unique for each cultivation host. Therefore, even marginal instability of photocaged inducer molecules can lead to a significant expression level even in an unirradiated sample. An effective light-controllable expression system thus requires a low basal expression, a broad dynamic range, and gradual controllability of the expression rate.[19] As not every photocaged inducer is suitable for every application, it is worthwhile to examine the pitfalls in the design of these light-responsive compounds. In this study, we describe the synthesis of new representatives of the well-established class of photocaged carbohydrates featuring redshifted absorption, and the exploration of non-carbohydrate responsive promoter systems for light-mediated control of gene expression in *E. coli*.

A bathochromic absorption shift of a photocaged compound should provide enhanced bio-applicability as the irradiation is less likely to be absorbed by cellular components and thus avoids cell damage or even death.[20] This also leads to improved flexibility regarding the irradiation period and intensity. Contrary to eukaryotes,[8a,9a,c,21] photocaged small molecule inducers cleavable with light of >400 nm wavelength and at short irradiation time have not been used for bacteria. As many well-established bacterial promoter systems such as the P_{T7}/LacI-, $P_{lac/tac}$/LacI or P_{BAD}/AraC regulatory systems are inducible by the addition of carbohydrates (Figure 1A, B),[22] a photocaged carbohydrate with redshifted absorption appears as a promising target for synthesis and *in vivo* evaluation as an optochemical inducer in *E. coli*. In addition, we tested different types of linkages in photocaged inducers.

Beside the above-mentioned IPTG- or arabinose-inducible expression systems, benzoate-based systems find increasing applications for controlling heterologous gene expression.[23] Thus, in a second part, a novel photocaged salicylic acid derivative was used to demonstrate the challenging choice of a suitable promoter system. Besides the photocaged compound synthesis and *in vitro* characterization, we evaluated both the P_m/XylS and the P_{nagAa}/NagR expression systems (Figure 1C, D) for their usability for light-mediated control of gene expression in *E. coli* and proved the applicability of the latter in combination with photocaged salicylic acid. In conclusion, we illustrate several drawbacks in the synthesis of functional photocaged inducers and their applications and show possibilities to overcome them.

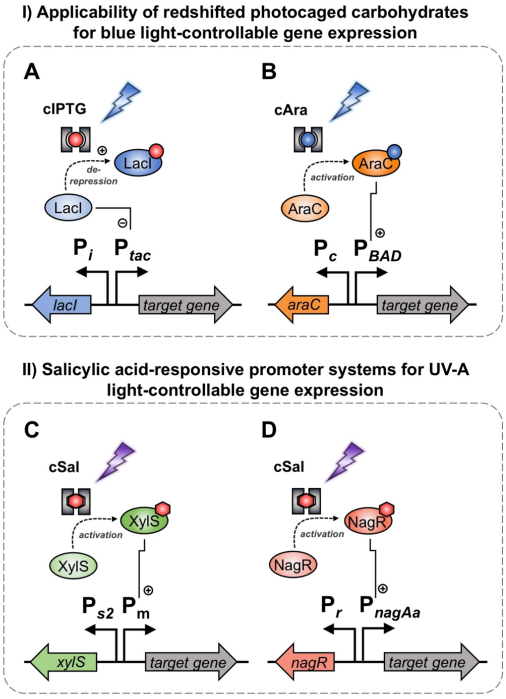

Figure 1. Promoter systems for optogenetic control of target gene expression used in this study. Firstly, the applicability of photocaged carbohydrates for controlling gene expression with blue light (flash symbol) was evaluated. For induction with photocaged IPTG (cIPTG, red dot with grey frame), the well-established P_{tac}/LacI promoter system (A) was chosen, in which the P_{tac} promoter is subject to regulation by the LacI activator protein. Upon binding of a suited inducer such as IPTG (red dot), LacI undergoes a conformational change leading to the dissociation from the operator region and thus, derepression of transcription. For induction with photocaged arabinose (cAra, blue dot with grey frame), the P_{BAD}/AraC promoter system (B) was applied, which is positively regulated by the activator protein AraC upon L-arabinose (blue dot) binding. As a second step, salicylic acid-responsive promoter systems were for the first time evaluated for photo-controllable gene expression using photocaged salicylic acid derivatives (cSal, red hexagon with grey frame). For this purpose, the P_m/XylS regulatory system was applied, which is positively controlled by the activator protein XylS in the presence of salicylic acid (red hexagon). Furthermore, the P_{nagAa}/NagR regulon was evaluated, which is also positively regulated by its activator protein NagR in the presence of salicylic acid (red hexagon).

Results and Discussion

Photocaged carbohydrates with redshifted absorption

Selection and design of target structures: So far, only *ortho*-nitrobenzyl derived protected carbohydrates have been reported as inducer molecules and tested for controlling gene expression. Besides this photolabile protecting group (PPG), coumarin derivatives offer similar advantages such as a high biocompatibility, a comparatively fast and easy chemical synthesis, but in contrast, their maximum absorption wavelength can be modified by small structural changes.[18,24] Therefore, we chose the 7-diethylaminocoumarin **3** regarding wavelength-selective applications and the dicyanocoumarin **4** with the hope of orthogonal applications, as this modification grants an even more pronounced bathochromic shift (Figure 2).[25]

Different strategies exist for the introduction of photolabile protecting groups onto reactive groups of the effector molecules, which have been reviewed before.[24] They are always dependent on the functional groups provided by the effector molecules and whether a modification of this moiety is blocking its biological function.[26] We choose a pair of carbohydrates [IPTG (**1a**) and arabinose (**2a**)] which only provide hydroxy groups. Therefore, one is limited towards utilising acetals, ethers, carbonates, or carbamates (when combined with a self-

ChemBioChem
Full Papers
doi.org/10.1002/cbic.202100467
Chemistry Europe
European Chemical Societies Publishing

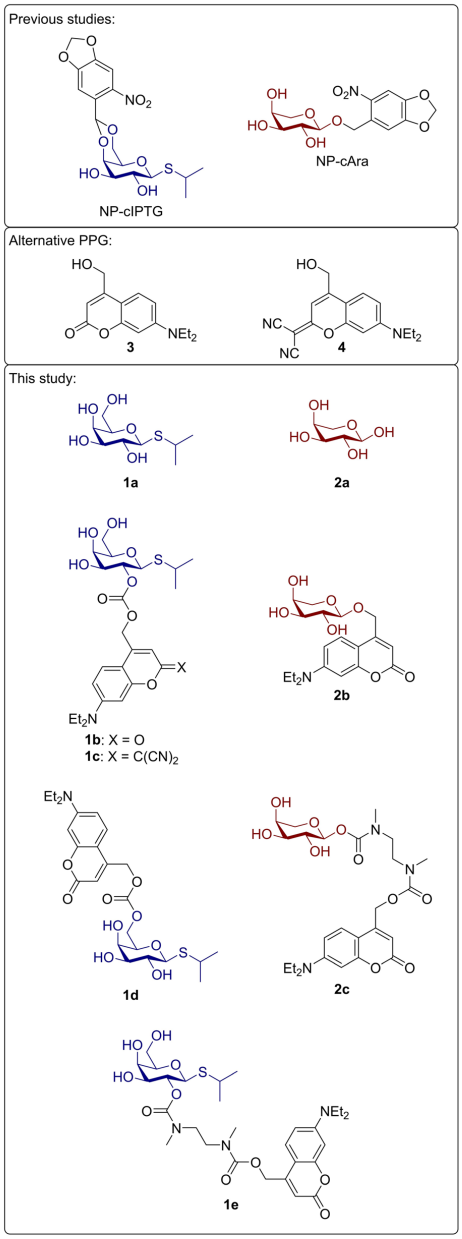

Figure 2. Photocaged carbohydrates deployed in previous publications,[12c,14] alternative photolabile protecting groups **3** and **4** serving as starting point and targeted photocaged inducer molecules **1b–e** and **2b–c** based on the effector molecules **1a** and **2a** potentially suitable for bathochromically shifted irradiation.

immolative spacer) as linkage. IPTG (**1a**) and arabinose (**2a**) were chosen as targets, since for both molecules, light-controlled gene expression systems have already been established. Furthermore, they provide three different types of hydroxy groups, which differ in their reactivity, namely a primary, a secondary and an anomeric hydroxy group. Based on the results of previous publications, acetals were excluded as linkage. For coumarins, a six-membered-ring acetal, which represents the leading motive in nitrobenzyl derivatives of IPTG, would most likely not be photolysable due to a particularly high stability, which was reported by Lin and Lawrence.[27] Photolysis could be achieved exclusively through the reduction of electron-density in the six-membered ring acetal by addition of an ester moiety.[28]

Synthesis of target structures. Overall, six photocaged carbohydrates bearing different photolabile protecting groups (**1b–e**, **2b–c**) were synthesized. They all originated from the well-established coumarin motive tethered *via* ether, carbonate, or carbamate moieties. Synthesis procedures for all starting materials are described in the Supporting Information. These include the synthesis routes towards coumarins **3** as well as **5–7**, which were obtained following previously published procedures, and synthesis routes towards the protected carbohydrates **8–12**.

The first synthesis was performed in analogy to previously published photocaged carbohydrates.[14–15] Therefore, ether **13** was prepared *via* a Koenigs-Knorr-type reaction of coumarin **3** and 2,3,4-tri-*O*-acetyl-β-L-arabinopyranosyl bromide (**8**) (59% yield). In the following deprotection the acetate-protecting groups were removed under basic conditions by addition of ammonia in methanol to give photocaged arabinose **2b** (Scheme 1) in a quantitative yield.

The carbonates **14** and **15** were prepared with the protected carbohydrate **9** by reaction with the activated coumarin carbonates **5** and **6**, respectively, with yields ranging from 77% to 96%. The activated carbonate **5** was analogously converted with the protected carbohydrate **10** into carbonate **16** (66% yield) (Scheme 2). To access the photocaged carbohydrates **1b**, **1c** and **1d**, the carbonates **14**, **15**, and **16** were deprotected with trifluoroacetic acid (TFA) (78–96% yield). Finally, the carbamates **17** and **18** were synthesized by addition of the coumarin amine **7** to the activated carbohydrate derivatives **11** as well as **12** in the presence of *N*,*N*-diisopropylethylamine (DIPEA) and 4-dimethylaminopyridine (DMAP) with yields ranging from 85% to 97% (Scheme 3). After deprotection with TFA or else ammonia in methanol, the

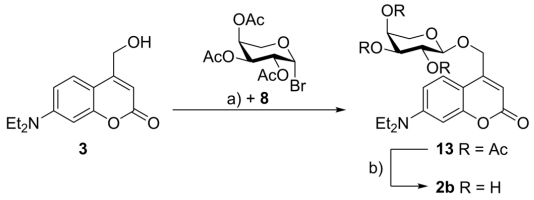

Scheme 1. Synthetic scheme for preparation of photocaged arabinose **2b**. Reagents and conditions: a) AgOTf, CH_2Cl_2, RT, 22 h, 59%; b) NH_3 in MeOH (7 M), MeOH, RT, quant.

ChemBioChem
Full Papers
doi.org/10.1002/cbic.202100467
Chemistry Europe
European Chemical Societies Publishing

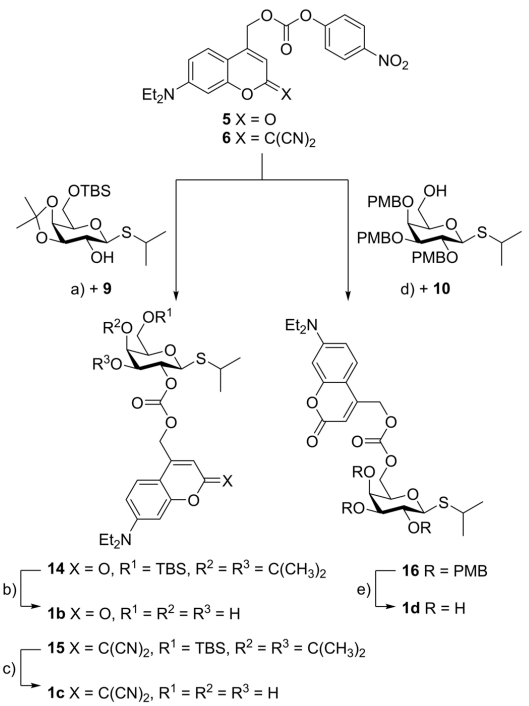

Scheme 2. Synthetic scheme for preparation of photocaged IPTG **1 b**, **1 c** and **1 d**. Reagents and conditions: a) DMAP, CH_2Cl_2, RT, 20 h, 77–96 %; b) TFA, H_2O, CH_2Cl_2, 0 °C, 10 min, 96 %; c) TFA, H_2O, CH_2Cl_2, 0 °C, 10 min, 92 %; d) DMAP, CH_2Cl_2, RT, 20 h, 66 %; e) TFA, H_2O, CH_2Cl_2, 0 °C→RT, 1 h, 78 %.

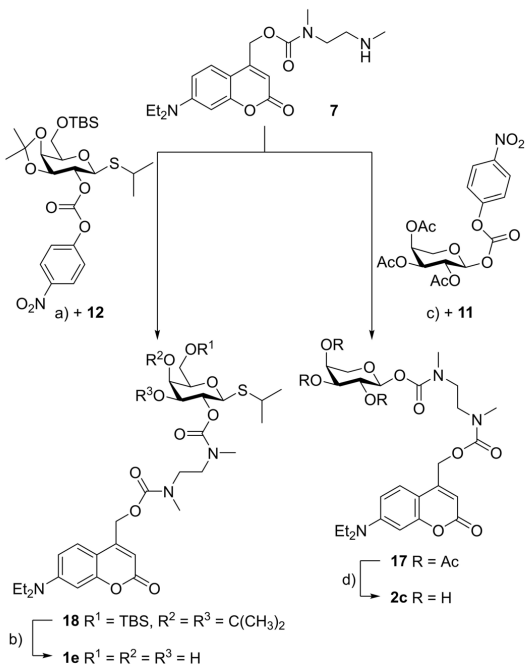

Scheme 3. Synthetic scheme for preparation of photocaged arabinose **2 c** and photocaged IPTG **1 e**. Reagents and conditions: a) DIPEA, DMAP, CH_2Cl_2, RT, 24 h, 97 %; b) TFA, H_2O, 0 °C, 10 min, quant.; c) DIPEA, DMAP, CH_2Cl_2, RT, 24 h, 85 %; d) NH_3 in MeOH (7 M), MeOH, RT, 86 %.

products **2 c** and **1 e** were obtained in high (86 %) to quantitative yields. The purity of all synthesized photocaged carbohydrates was confirmed by ^{1}H-, ^{13}C-NMR, HRMS and HPLC (for detailed synthesis procedures see Supporting Information).

***In vitro* characterization of target structures**: Initially the photochemical and photophysical properties of the photocaged carbohydrates were determined *in vitro* (Table 1). Previously published photocaged carbohydrates showed absorption maxima in the range of 336–358 nm.[14–15,17] In contrast, the absorption maxima (λ_{max}) of compounds **1 b**+**d** and **2 b**–**c** are redshifted by at least 28–50 nm and show peak at ~386 nm (Figure 3A). An exception is the photocaged IPTG **1 c**, which showed an additional strong bathochromic shift of ~100 nm to an absorption maximum at 488 nm, due to the introduction of the dicyanomethylene group (Figures S1–6). Additionally, the molar extinction coefficients (ε) of the novel photocaged carbohydrates **1 b**–**d** and **2 b**–**c** proved to be adequately high for efficient photolysis even upon irradiation with wavelengths up to 430 nm (Table 1). Especially carbonate **1 c** shows interesting parameters for orthogonal uncaging due to its strongly redshifted absorption maximum and its comparatively low molar extinction coefficient at 375 nm ($\varepsilon = 1300\ M^{-1}cm^{-1}$). Uncaging quantum yields (φ_u) and the resulting photolytic efficiency ($\varepsilon\varphi_u$) were in the range of previously reported coumarins.[29]

A look at the decay curves of compounds **2 b**, **1 b** und **1 e** after irradiation at 405 nm (determined by HPLC) as well as hydrolysis in the dark allows to compare the applicability of the different linkages (Figure 3C). The ether **2 b** was resilient against hydrolysis in the dark but showed only tenuous photolysis after irradiation. Thus, about 90 % of the photocaged compound **2 b** remained unreacted after irradiation for 30 min. This can be explained by the low pK_b value of the released anion, since the stabilization of the released anion is crucial for the heterolytic bond cleavage mechanism and the prevention of non-productive ion-recombination.[30] For a thorough evaluation, it was nonetheless included in the *in vivo* experiments. The carbonate **1 b** showed the fastest decay after irradiation with complete release of the inducer in under 2 min. A stability comparison of photocaged IPTG **1 b** and **1 d** displayed that even though they only differ in their linkage position (2-OH vs. 6-OH), compound **1 d** shows almost no hydrolysis, whereas compound **1 b** is not entirely stable (Table 1). The carbonate **1 c**, bearing the dicyano group, demonstrated the highest hydrolysis rate in the dark with only 70 % of starting material remaining after 24 h without irradiation. This can be explained by a reduced electron density at the carbonate moiety, which should facilitate hydrolysis. Differences in carbonate stability have been reported before.[31]

ChemBioChem
Full Papers
doi.org/10.1002/cbic.202100467
Chemistry Europe
European Chemical Societies Publishing

Table 1. Spectral and (photo-)chemical properties of photocaged carbohydrates **1b–e** and **2b–c**.

Compound	λ_{max}[a] [nm]	ε(375)[b] [$M^{-1}cm^{-1}$]	ε(405)[b] [$M^{-1}cm^{-1}$]	ε(430)[b] [$M^{-1}cm^{-1}$]	S[c] [%]	$\varphi_u(\lambda_{irr})$[d]	$\varepsilon\varphi_u(\lambda_{irr})$ [$M^{-1}cm^{-1}$]
2b[e]	388	8100	7100	2600	94	4.51×10^{-4} (405)	4 (405)
1b[f]	386	22900	18000	4000	88	3.20×10^{-2} (375)	687 (375)
							120 (430)
1c[f]	488	1700	2900	7900	70	2.35×10^{-2} (430)	34 (375)
							158 (430)
1d[f]	386	11000	8700	1900	100	3.46×10^{-2} (375)	330 (375)
1e[f]	386	15900	12000	2300	95	1.01×10^{-2} (430)	159 (375)
							23 (430)
2c[f]	385	13100	9500	1700	100	1.33×10^{-2} (430)	17 (430)

[a] Long-wavelength absorption maxima. [b] $\varepsilon(\lambda_{irr})$ = Molar extinction coefficient at irradiation wavelength λ_{irr}. [c] S = Stability against hydrolysis in the dark after 24 h (in % of remaining compound). [d] $\varphi_u(\lambda_{irr})$ = Uncaging quantum yield determined at irradiation wavelength λ_{irr}. [e] Measured in H_2O/DMSO 99:1. [f] Measured in Tris buffer (20 mM, pH = 7.5)/MeCN 1:1.

Considering the diverging stabilities *in vitro*, carbonate **1d** appears to exhibit the best properties for the *in vivo* experiments.

The carbamate **1e** was stable against hydrolysis in the dark as well and released the self-immolative spacer nearly completely after irradiation for 15 min. Overall, carbamate **2c** displayed similar properties and its exemplary uncaging cascade is shown in Scheme 4. After irradiation, the heterolytic cleavage leads to decarboxylation subsequently exposing the amine group of the spacer. The intermediate **19** should undergo intramolecular 5-*exo*-trig cyclization to form the five-membered cyclic urea-derivative **20** (self-immolation) and release the inducer **2a**.[32] In literature the release of a carbohydrate by the *N,N'*-dimethylethylenediamine linker has been reported with a release efficiency of up to 60% after 2 h.[33] HPLC analysis of the carbamates **1e** and **2c** could only confirm the successful uncaging and therefore the release of an ethylenediamine-inducer intermediate, but not the following self-immolation step. Accordingly, this step was monitored *via* ESI-MS (Figures S24–25) confirming that after irradiation the corresponding intermediate was formed. For compound **1e** the intermediate refused to under-go self-immolation, whereas for compound **2c** a decrease of intermediate **19** was monitored.

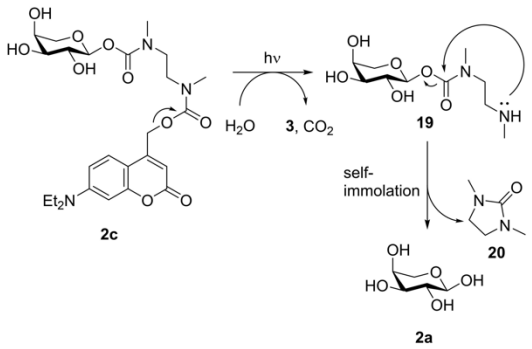

Scheme 4. Representative release cascade after irradiation of compound **2c** in aqueous media.

Nonetheless, both carbamates were tested *in vivo* as well to confirm the *in vitro* results. The detailed uncaging kinetics (Figures S8–13; Table S3) and stability measurements (Figure S22) of all synthesized photocaged carbohydrates are shown in the Supporting Information.

Photocaged carbohydrates for light-controlled gene expression: Next, the synthesized photocaged carbohydrates were tested for their applicability for light-mediated induction of gene expression in the well-established expression host *E. coli*. In the following experiments, we firstly used the strain *E. coli* Tuner (DE3), as this strain offers a passive IPTG uptake due to a deletion of the *lacY* gene encoding the lactose permease and thus a homogeneous and precisely controllable reporter gene expression.[12c,34] Furthermore, the expression plasmid pRhotHi-lacI-eYFP harbouring the *eyfp* reporter gene under the control of the well-established P_{T7}/LacI promoter system was used, as this regulatory system was proven to provide both tightly regulated and gradually controllable target gene expression.[12a,17,34] Secondly, for arabinose-inducible gene expression, the previously published strain *E. coli* LMG194 was chosen, since it bears the Δ*ara714* deletion, which encompasses most of the *araBAD* operon, and thus is not able to metabolise arabinose.[35] This allows for using lower inducer concentrations in comparison to the strain *E. coli* Tuner (DE3).[34] Additionally, the expression plasmid pBTBX-2-mCherry harbouring the mCherry gene under the control of the well-known P_{BAD} promoter was used, since this system was repeatedly applied for tight and gradually controllable gene expression in *E. coli*.[14,34,36]

As a first step, all relevant photocaged inducers were evaluated with respect to their biotoxicity. For this purpose, the biomass of cultures supplemented with a respective compound were compared to uninduced cultures, as well as to cultures induced with the conventional inducer (Figure S26 A–D). The measurements did not reveal any negative effect of photocaged derivatives on the growth of the cultures, so that a biotoxicity can be precluded. Subsequently, the usability and induction strength of photocaged IPTG **1b** was compared with photocaged IPTG **1d** (Figure 4A, B) under illumination with visible light. Here, both caged IPTG variants led to eYFP fluorescence intensities between 60 and 90% in comparison to

ChemBioChem
Full Papers
doi.org/10.1002/cbic.202100467
Chemistry Europe
European Chemical Societies Publishing

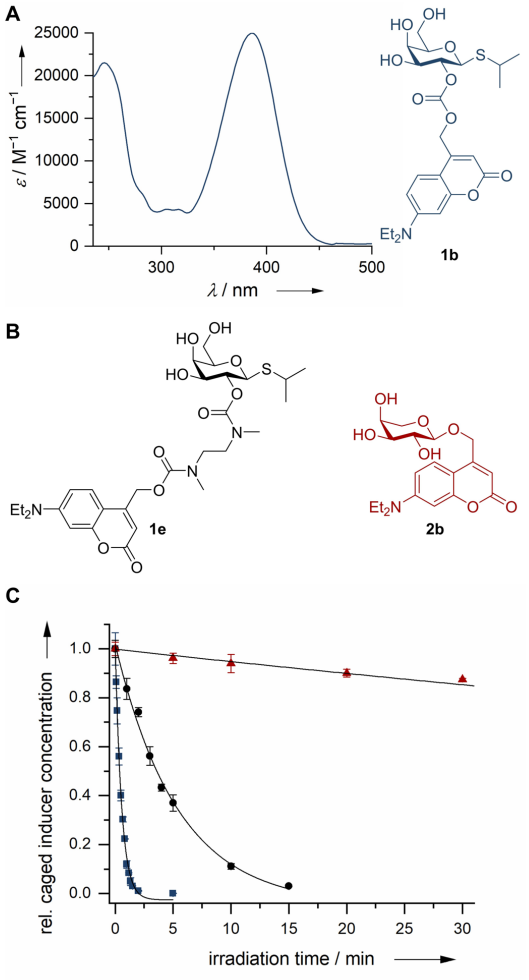

Figure 3. A) Exemplary absorption spectrum of photocaged inducer molecule **1 b**. B) Molecular structures of photocaged inducer molecules **1 b**, **1 e** and **2 b**. C) Comparison of decay of photocaged inducer molecules **1 b**, **1 e** and **2 b** after irradiation at 405 nm. Ether **2 b** (red triangles), Carbonate **1 b** (blue squares), Carbamate **1 e** (black circle).

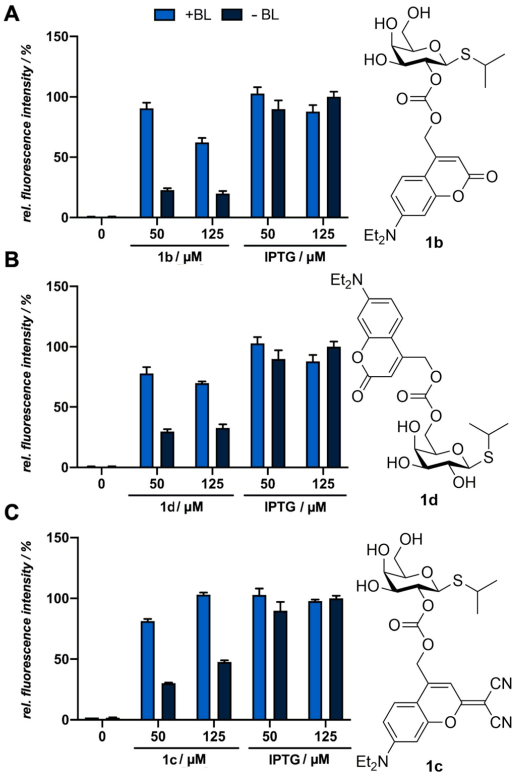

Figure 4. Normalized *in vivo* eYFP fluorescence intensity of *E. coli* Tuner (DE3)/pRhotHi-2-lacI-eYFP expression cultures supplemented with 50 µM and 125 µM of the photocaged compounds **1 b** (A), **1 d** (B) or **1 c** (C). All cultures were incubated in the dark for 20 h in LB medium at 30 °C. Induction of reporter gene expression was performed after 2.5 h by blue light exposure at 447 nm (+BL; ~10 mW cm^{-2}) for 10 min [**1 b**, **1 c**, **1 d** or by the addition of respective amounts of conventional IPTG (**1 a**)]. *In vivo* fluorescence intensities were determined by using a Tecan Microplate Reader (eYFP: λ_{ex} = 488 nm, λ_{em} = 527 nm), normalized to cell densities and are shown in relation to the respective fluorescence intensities of a culture kept in the dark (-BL). Values are means of triplicate measurements. Error bars indicate the respective standard deviations.

cultures, which were equimolarly induced with conventional IPTG (**1 a**). Furthermore, it can be seen that 50 µM caged IPTG is sufficient for a pronounced target gene expression in both cases since an increased compound concentration led to a decreased induction strength with comparable or even higher signals in the dark controls. Contrary to expectations resulting from the *in vitro* stability data, photocaged IPTG **1 b** is more stable under *in vivo* conditions compared to photocaged IPTG **1 d**. This could be explained by an improved stability towards esterases, since the linkage is tethered at a secondary alcohol whereby it could be sterically more difficult to access. Subsequently, we evaluated the photocaged IPTG **1 c** regarding its applicability for light-controlled gene expression (Figure 4C). The *in vivo* experiments revealed that photocaged IPTG **1 c** showed between 80% and 100% induction strength in comparison to cultures induced with equimolar concentrations of conventional IPTG (**1 a**). Although the use of 125 µM led to higher induction levels, the dark control cultures showed increased fluorescence signals in comparison to the cultures induced with 50 µM, which probably is caused by instability effects in the cultivation medium or hydrolysis by host-specific enzymes. Hence, the use of lower caged IPTG concentrations again seems to be favourable as it leads to a sufficiently high induction strength, but lower induction levels in the unexposed cultures.

ChemBioChem
Full Papers
doi.org/10.1002/cbic.202100467
Chemistry Europe
European Chemical Societies Publishing

Since carbonates are known to be more susceptible to hydrolysis than carbamates we also tested the compounds **1e** and **2c** as an alternative.[37] However, as previously implied by the *in vitro* measurements, no light-mediated induction could be observed for compound **1e** due to the insufficient release of the inducer by the self-immolative spacer (Figure S27). The experiment was performed under suitable conditions for the release such as elevated temperatures (37 °C), a polar solvent and a slightly basic pH-value (pH = 7.4) as it is known that the self-immolation is affected by these external parameters.[32] Compound **2c**, in contrast, demonstrated a superior applicability as it led to mCherry fluorescence intensities of ~50% in comparison to cultures which were equimolarly induced with conventional arabinose (**2a**) (Figure 5A). This difference in reactivity can be explained by the higher acidity of the anomeric hemiacetal OH group[38] and the subsequently improved stabilization of the resulting anion. This underlines that the self-immolation proceeds when the released carbohydrate anion possesses a sufficiently high pK_b value. The low fluorescence intensities of cultures in the dark reveal a pronounced *in vivo* stability of the carbamates **1e** and **2c**. The *in vivo* applicability of compound **2b** was investigated as well, but it caused only a marginal increase in fluorescence (Figure 5B).

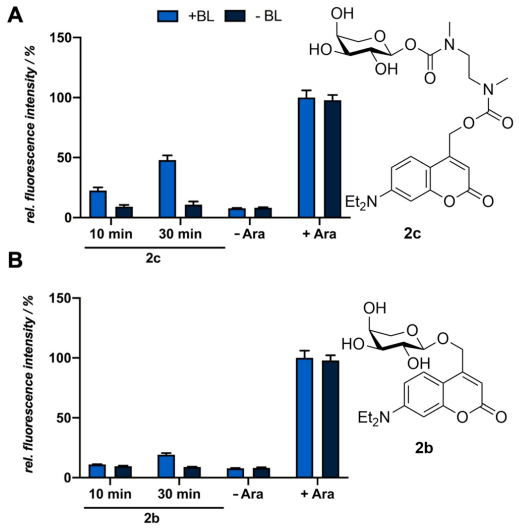

Figure 5. Normalized *in vivo* mCherry fluorescence intensity of *E. coli* LMG194/pBTBX-2-mCherry expression cultures supplemented with 50 μM of the photocaged arabinose variants **2c** (A) and **2b** (B). All cultures were incubated in the dark for 20 h in LB medium at 37 °C and light-mediated induction of reporter gene expression was performed after 2.5 h by blue light exposure at 447 nm (+BL; ~10 mW cm^{-2}) for 10 or 30 min or the addition of respective amounts of conventional arabinose (**2a**). *In vivo* fluorescence intensities were determined by using a Tecan Microplate Reader (mCherry: λ_{ex} = 580 nm, λ_{em} = 610 nm), normalized to cell densities and are shown in relation to the respective fluorescence intensities of a culture induced with conventional arabinose (**2a**) and exposed to blue light for 30 min. Values are means of triplicate measurements. Error bars indicate the respective standard deviations.

In summary, novel photocaged IPTG and arabinose variants with bathochromically shifted absorption maxima could be synthesized. The *in vivo* application in *E. coli* demonstrated that these compounds, and particularly the photocaged IPTG variants **1b** and **1c**, are sufficiently stable and lead to a pronounced induction response upon illumination.

Salicylic acid-responsive promoter systems for light-controlled gene expression: After extending the repertoire of photocaged carbohydrates towards compounds possessing bathochromically shifted absorption maxima, we attempted to expand the photocaged inducer toolbox by using photocaged aromatic compounds instead of carbohydrates for light-mediated control of gene expression. Several well-established and suitable promoter systems can be induced with aromatic compounds such as toluene, anthranilic acid or benzene, proved valuable for transcriptional control in various bacterial hosts.[23a,39] We therefore choose salicylic acid (**21**) as an inducer molecule and evaluated two promoter systems for their suitability for light-mediated gene expression in *E. coli* Tuner (DE3). Notably, like all enterobacteria, *E. coli* typically favours simple carbon sources like sugars over complex carbohydrates or aromatic compounds and therefore does not possess specific transporters for salicylic acid (**21**). Uptake solely occurs *via* passive diffusion processes.[40] We used the P_m/XylS expression system (Figure 1C), which originates from the *P. putida* TOL *meta* operon for the degradation of benzoates. In a first step, an inducer, e.g., *m*-toluic or salicylic acid,[41] interacts with the XylS regulatory protein, which subsequently initiates gene transcription from its associated promotor P_m. Applicability of this regulatory system for transcriptional regulation of gene expression was demonstrated in well-established bacteria such as *E. coli* or *P. putida*.[34,42] Thus, we used the expression strain *E. coli* Tuner (DE3) carrying the plasmids pM117-R45T-GFPmut3 or pM-R45T-GFPmut3 harbouring the gene *gfpmut3* under the control of the $P_{m\ M1\text{-}17}$ or the native P_m promoter, respectively (Table S1). The promoter $P_{m\ M1\text{-}17}$ is a high-level expression variant of the native P_m promoter.[23b,36] To enable a promiscuous induction with diverse benzoate derivatives, in particular salicylic acid (**21**) and *m*-toluic acid, a XylS regulator protein carrying the mutation R45T was used.[41,43] As a second alternative, we evaluated the P_{nagAa}/NagR regulatory system from *Comamonas testosteroni* GZ42 (Figure 1D).[44] This system originally belongs to the *nag* operon allowing for naphthalene utilization and is based on the LysR-type transcriptional regulator NagR, which activates its associated promoter P_{nagAa} upon addition of the inducer salicylic acid (**21**).[45] In recent years, this system was frequently used for target gene expression in different bacterial hosts such as *E. coli*, *P. putida* or *Pseudomonas taiwanensis*.[46] The expression system of choice in our study was the strain *E. coli* Tuner (DE3) carrying the plasmid pBNTmcs-mCherry-Km, which harbours the mCherry-encoding reporter gene under the control of the P_{nagAa}/NagR system (Table S1).

Selection and design of target structure: Since the P_m/XylS as well as the P_{nagAa}/NagR promoter systems can both be activated by salicylic acid (**21**), we focused on the synthesis of a photocaged salicylic acid (cSal). For the initial setup of this new

ChemBioChem
Full Papers
doi.org/10.1002/cbic.202100467
Chemistry Europe
European Chemical Societies Publishing

photocaged inducer class and to fulfil the previously stated properties for application in cell cultivation media, a reliable and established photocage was chosen and for simplicity no additional modifications were made for release at wavelengths above 400 nm. Therefore, the 4,5-bis(carboxymethoxy)-2-nitrobenzyl protecting group (BC) was selected, which is photoactivatable at around 375 nm and readily soluble in aqueous buffer. To ensure the required high stability, an ether bond was chosen as linkage rendering it resistant against esterases and hydrolysis. Hence, the BC-cSal (**22a**) and its corresponding sodium salt **22b** were synthesized (Figure 6).

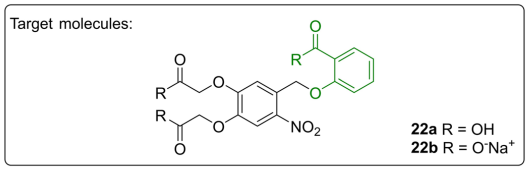

Figure 6. Targeted photocaged salicylic acids **22a** and **22b**.

Synthesis of target structure: Starting from 4,5-bis-(ethoxycarbonylmethoxy)-2-nitrobenzaldehyde (**23**), which was obtained following a previously reported procedure,[17,47] 2-*O*-[4,5-bis(carboxymethoxy)-2-nitrobenzyl]salicylic acid (BC-cSal, **21**) was synthesized in a four-step reaction (Scheme 5, yield over four steps: 59%). The aldehyde **23** was reduced with sodium borohydride to give the 2-nitrobenzylalcohol derivative **24**, which was converted into the corresponding bromide **25** *via* the Appel reaction.[48] *O*-Alkylation of ethyl salicylate with the bromide **25** resulted in formation of the photocaged ethyl salicylate **26**. The subsequent deprotection under basic conditions and elevated temperature yielded the target structure BC-cSal (**22a**), which could be further converted to the corresponding sodium salt **22b**.

***In vitro* characterization of target structure**: The absorption spectrum of BC-cSal (**22a**) shows a maximum (λ_{max}) at 346 nm in sodium phosphate buffer (0.1 M, pH = 7.4) with a molar extinction coefficient (ε) of 5900 $M^{-1}cm^{-1}$ (Scheme 5B; Figure S7). Upon irradiation for 15 min with UV-A light (375 nm) salicylic acid (**21**) was completely released from BC-cSal (**22a**) with a quantum yield (φ_u) of 7.68×10^{-3} in sodium phosphate buffer (0.1 M, pH = 7.4) (Figure S14; Table S3). The solubility was sufficient (~3 mM) for the intended application and could be further improved when converted to its sodium salt form **22b** (>100 mM). HPLC monitoring of a 0.5 mM solution in sodium phosphate buffer (0.1 M, pH = 7.4) over 24 h showed no significant decrease in concentration of BC-cSal (**22a**), indicating an adequate *in vitro* stability (Figure S23).

In vivo* application of novel photocaged salicylic acid derivatives in *E. coli: We analyzed whether the novel caged salicylate derivative BC-cSal (**22a**) in its acid form is suitable for light-controlled induction of gene expression in the common expression host *E. coli*. For this purpose, first both the P_m and the $P_{m\ M1\text{-}17}$-based expression systems were tested for sufficient GFPmut3 reporter gene expression upon addition of increasing salicylic acid (**21**) concentrations in complex but undefined LB medium as well as in synthetic and defined M9CA-Gly minimal medium. As shown in Figure 7A, the salicylic acid-mediated induction of GFPmut3 production worked well in M9CA-Gly medium. However, the induction response is drastically decreased in LB medium, presumably caused by changing pH values during cultivation and the resulting dissociation state of the inducer.[23a] Furthermore, it could be seen that nearly no increase in induction response could be obtained with Sal concentrations over 250 μM, which was also shown by Binder *et al.*[34] and that, contrary to past studies,[36] both promoter variants showed almost identical fluorescence levels. As a second step, the *in vivo* toxicity of the novel photocaged salicylic acid variants were evaluated by comparing the biomass of cultures supplemented with caged Sal with both uninduced cultures and cultures induced with conventional salicylic acid (Figure S26E). It could be seen that none of the derivatives had

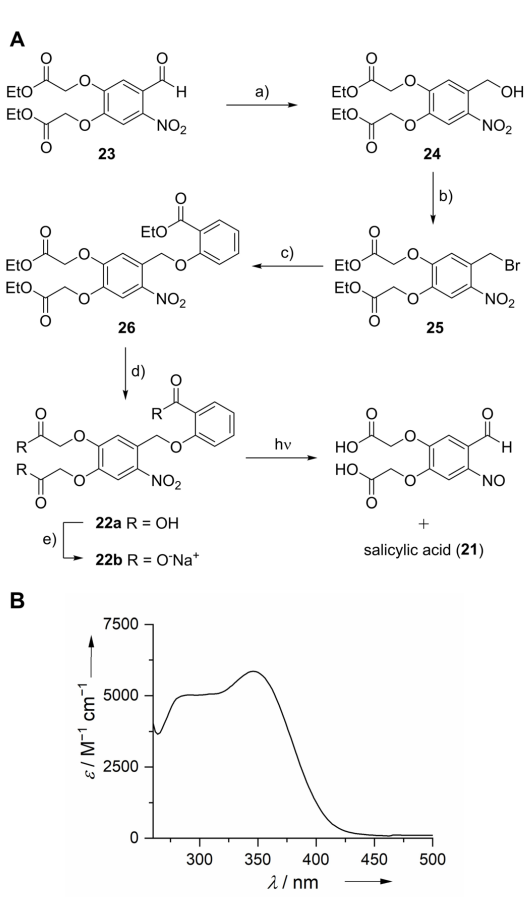

Scheme 5. A) Synthetic scheme for preparation of BC-cSal (**22a**) and BC-cSal*Na (**22b**). Reagents and conditions: a) $NaBH_4$, CH_2Cl_2, EtOH, AcOH, 0 °C, 3 h, 73%; b) CBr_4, PPh_3, CH_2Cl_2, 0 °C→RT, 6 h, 96%; c) ethyl salicylate, K_2CO_3, acetone, RT, 2 d, 92%; d) KOH (0.2 M), MeOH, 60 °C, 4 h, 92%; e) NaOH (0.2 M), MeOH, RT, 5 min, quant. B) Absorption spectrum of compound **22a**.

ChemBioChem
Full Papers
doi.org/10.1002/cbic.202100467
Chemistry Europe
European Chemical Societies Publishing

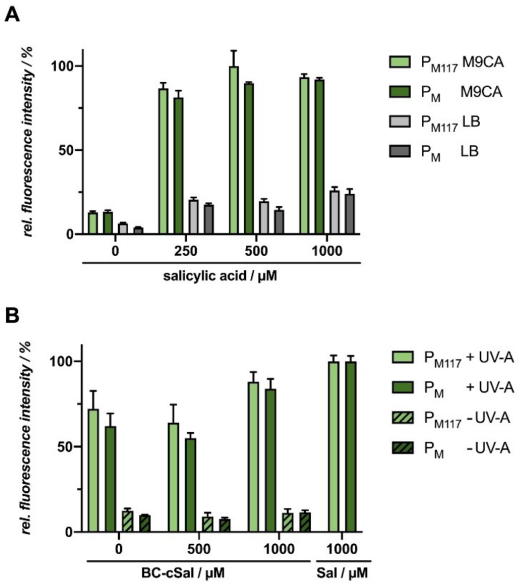

Figure 7. Light-controlled gene expression in *E. coli* Tuner (DE3)/pM117(pM)-R45T-GFPmut3 using BC-cSal (**22a**). A) *In vivo* GFPmut3 fluorescence (λ_{ex} = 508 nm, λ_{em} = 532 nm) of *E. coli* cultures grown in LB medium (grey) or M9CA minimal medium (green) at 30 °C after 20 h (stationary growth phase). Induction was performed after 6 h with salicylic acid (**21**) concentrations ranging from 0 to 1000 µM. B) *In vivo* GFPmut3 fluorescence (λ_{ex} = 508 nm, λ_{em} = 532 nm) of *E. coli* cultures grown in M9CA minimal medium at 30 °C and supplemented with 500 µM or 1000 µM of BC-cSal (**22a**) is shown in relation to a 0 and 1000 µM salicylic acid (Sal) control after 20 h (stationary growth phase). Induction was performed after 6 h *via* UV-A light exposure at 365 nm (~1 mW cm^{-2}) for 30 min or the addition of 1000 µM salicylic acid (Sal). *In vivo* fluorescence intensities were normalized to cell densities and values are means of individual biological triplicates. Error bars indicate the respective standard deviations.

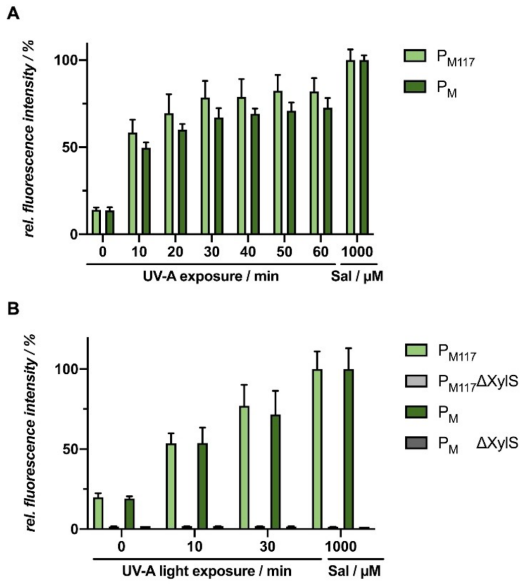

Figure 8. Light-controlled gene expression in *E. coli* Tuner(DE3)/pM117-R45T-GFPmut3 or pM-R45T-GFPmut3 using UV-A light. A) *In vivo* GFPmut3 fluorescence (λ_{ex} = 508 nm, λ_{em} = 532 nm) of *E. coli* cultures illuminated with UV-A light for different exposure time is shown in relation to a salicylic acid control (Sal). Induction was performed after 6 h *via* UV-A light exposure at 365 nm (~1 mW cm^{-2}) or the addition of 1000 µM Sal. B) *In vivo* GFPmut3 fluorescence of *E. coli* cultures harbouring plasmid with both XylS gene and, as a negative control, a *xylS* gene deletion (ΔXylS) plasmid variant and illuminated with UV-A light for 10–30 min is shown in relation to a 1000 µM salicylic acid control (Sal). Induction was performed after 6 h *via* UV-A light exposure at 365 nm (~1 mW cm^{-2}) or the addition of 1000 µM Sal. *In vivo* fluorescence intensities were normalized to cell densities and values are means of individual biological triplicates. Error bars indicate the respective standard deviations.

a negative influence on bacterial growth, thus no toxicity effect could be detected. For induction with the caged Sal variant BC-cSal (**22a**), the induction response at both caged inducer concentrations was comparable with conventional salicylate (Figure 7B). Without UV-A light exposure, no fluorescence increase could be detected, which illustrates the *in vivo* stability of this variant. However, the fluorescence level of the control without inducer was significantly increased in comparison to the control in the dark.

As the UV-A light exposure was the only modified parameter, we analyzed the influence of UV-A light on this expression system without addition of an inducer (Figure 8A). Surprisingly, upon increasing exposure time, the GFP expression levels for both promoter variants increased likewise nearly reaching the fluorescence level of the control culture, where 1000 µM salicylate was added for induction of reporter gene expression. This unexpected effect could be elucidated further in order to achieve a more precisely tuneable, gradual induction process mandatory for the potential use of this system as a stand-alone regulator element. To check whether this effect is associated with the transcriptional regulator XylS or can also be observed independently, we performed the same experiment with ΔXylS plasmid variants for both promoters (Figure 8B).

After illumination with UV-A light for 10 to 30 min, GFPmut3 production could only be observed when XylS is present, while cultures harbouring the expression plasmid with ΔXylS variant exhibited almost no fluorescence. These findings indicate that there might be a connection between the UV-A light as an environmental factor and the XylS-dependent signal transduction. The expression of the XylS protein, which belongs to the XylS/AraC regulator family,[49] is naturally stimulated by two different promoters, the Ps2 and the Ps1. The Ps2 promoter induces low constitutive expression of *xylS*[50] and is σ^{32}-dependent during exponential growth phase and σ^{S} (or σ^{38})-dependent in early stationary phase and thereafter.[51] Beyond that, *xylS* expression is also induced by the master regulator XylR from the σ^{54}-dependent promoter Ps1,[50] which, in contrast to Ps2, is controlled by catabolite repression.[52] Under the influence of UV-A light, the heat shock sigma factor RpoH (σ^{32}) as well as the common stress sigma factor RpoS (σ^{38}) might be

ChemBioChem
Full Papers
doi.org/10.1002/cbic.202100467
Chemistry Europe
European Chemical Societies Publishing

upregulated in *E. coli*, even though σ^{38} is generally known to be active during stationary phase.[53] Those two sigma factors might stimulate the Ps2 promoter resulting in a hyperproduction of XylS, which in turn would lead to the induction of the P_m promoter even in absence of the effector molecule.[54] Hence, the observed results indicate that this promoter system is unsuitable for the application of photocaged inducer molecules, as the use of UV-light is indispensable for the uncaging process. However, the P_m/XylS system allows for gradually controlling gene expression by light that does not require a chemical inducer, even though it still needs to be characterized in more detail prior to its actual application.

As the above used P_m/XylS-based expression system led to an induction of gene expression upon illumination with UV-A light in *E. coli*, we tested the P_{nagAa}/NagR system, which can similarly be induced with salicylic acid, and thus might be alternatively applicable for BC-cSal-mediated light control of gene expression in *E. coli*. Firstly, the P_{nagAa}-based expression system was tested for sufficient mCherry reporter gene expression in the strain *E. coli* Tuner (DE3)/pBNTmcs-mCherry-Km upon addition of increasing salicylic acid (**21**) concentrations (0–1000 μM) in complex LB medium as well as in synthetic M9CA-Gly minimal medium (Figure 9A). Interestingly, a sufficient induction strength could only be observed in LB medium, while M9CA medium led to minor fluorescent levels. Hence, further experiments were performed with LB medium. Secondly, the usability of the novel photocaged salicylic acid derivative BC-cSal (**22a**) as well as its respective sodium salt form **22b** was analyzed. The sodium salt form **22b** allows for an increased solubility in the cultivation medium and eliminates the need to dissolve the substance in organic solvents such as ethanol or DMSO before use. The sodium salt variant **22b** indeed exhibited an improved solubility in comparison to the conventional acid form, which had to be pre-solved in DMSO, and was nearly equally stable under dark/non-induced conditions (Figure 9B). Furthermore, both BC-cSal variants led to comparably high fluorescence levels as the culture induced with conventional salicylic acid (**21**). However, to increase the responsiveness of the system, the basal activity and the overall expression level need to be optimized. This could be done, for example, by directed promoter mutagenesis or by the supplementary addition of 4-nitrobenzoate to the cultivation medium, as described previously.[45a,55]

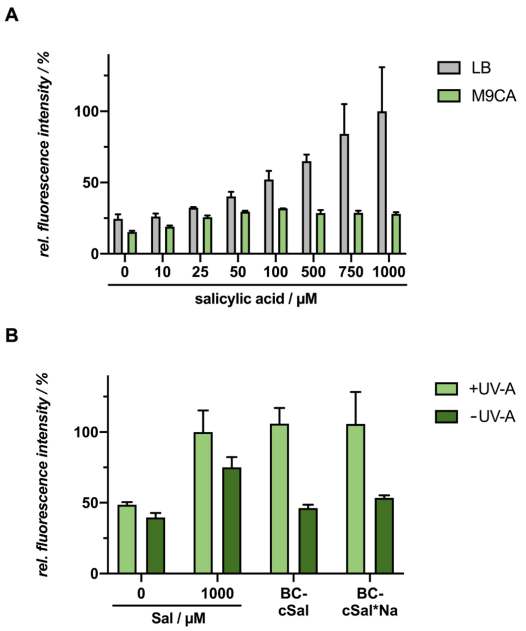

Figure 9. Light-controlled gene expression in *E. coli* Tuner (DE3)/pBNTmcs-mCherry-Km using novel caged salicylic acid derivatives. A) *In vivo* mCherry fluorescence (λ_{ex} = 580 nm, λ_{em} = 610 nm) of *E. coli* cultures grown in LB medium (light green) or M9CA-Gly minimal medium (dark green) at 30 °C after 20 h (stationary growth phase). Induction was performed after 2 h with salicylic acid (**19**) concentrations ranging from 0 to 1000 μM. B) *In vivo* mCherry fluorescence (λ_{ex} = 580 nm, λ_{em} = 610 nm) of *E. coli* cultures grown in LB medium at 30 °C and supplemented with 1000 μM of BC-cSal (**22a**) and BC-cSal sodium salt (BC-cSal*Na, **22b**) is shown in relation to control cultures, where reporter gene expression was not induced (0 μM) or induced by adding 1000 μM salicylic acid (Sal) after 20 h (stationary growth phase). Induction was performed after 2 h *via* UV-A light exposure at 365 nm (~1 mW cm^{-2}) for 30 min or the addition conventional inducer (Sal). *In vivo* fluorescence intensities were normalized to cell densities and values are means of triplicate measurements. Error bars indicate the respective standard deviations.

Conclusions

We have synthesized a variety of coumarin-caged carbohydrates and evaluated their photochemical and photophysical properties with respect to their applicability for light-controlled gene expression in bacteria. Of the various types of linkages tested, only the carbonates **1b** and **1c** as well as the carbamate **2c** proved to be suitable with some restrictions. For carbonates, concentrations must be low to reduce the influence of hydrolysis in the dark and esterase cleavage. Despite these limitations photocaged IPTG **1b** and **1c** are decent aspirants for optochemical applications requiring bathochromically shifted excitation. We demonstrated that even though the photolysis of the hydrolysis-stable carbamates **1e** and **2c** proceeds in a suitable timeframe, the released spacer tethered to the investigated carbohydrates refused to undergo self-immolation for compound **1e** where it was linked to the 2-OH group of IPTG. When tethered to the anomeric OH group of arabinose **2a** as in compound **2c** the self-immolation was successful.

Secondly, we evaluated the newly synthesized salicylic acid-based caged compound BC-cSal (**22a**) as well as its sodium salt derivative **22b** for their use as optochemical on-switch. Two salicylic acid-inducible promoter systems were chosen that should enable light-mediated induction of gene expression in *E. coli*. The P_m/XylS system, which was tested first, exhibited auto-induction effects caused by UV-A light exposure even without BC-cSal (**22a**). Although this fact renders the use of this system unfeasible in combination with photocaged inducers, it represents a promising regulatory system that might be

ChemBioChem
Full Papers
doi.org/10.1002/cbic.202100467
Chemistry Europe
European Chemical Societies Publishing

gradually addressable exclusively with UV-A light and will be further investigated in future studies. The second P_{nagAa}/NagR system proved suitable for the use of photocaged salicylic acid **22a**, although the responsiveness of the system needs to be improved by reducing the basal activity and by increasing the induction strength. Hence, these results indicate that the applicability of each host and system has to be evaluated with respect to potential side effects caused by UV-A light exposure itself and its interplay with additional factors such as media composition.

In summary, these results highlight the importance of a photocaged compound toolbox that can be used to address the different demands of varying organisms and expression systems. Moreover, the redshifted variants and the expansion of the available promoter systems addressable by light-activatable inducer molecules pave the way towards a combination of multiple optochemical inducers with diverging absorption maxima for control of complex biosynthetic pathways in a multi-chromatic fashion.

Experimental Section

Synthesis of photocaged compounds: Details on the synthesis and characterization of the photocaged compounds **1b**–**e**, **2b**–**c** and **22a**–**b** are provided in the Supporting Information.

Determination of photon flux density: The photon flux density ($q_{n,p}$) of each light source of the LUMOS 43 (375 nm, 405 nm, 430 nm) was measured by ferrioxalate actinometry following a standard protocol.[56] The obtained values are summarized in Table S3.

Irradiation experiments: For the photocaged compound **1b**–**e** and **2c** a 0.5 mM solution in Tris buffer (20 mM, pH = 7.5)/MeCN 1:1 was prepared. For the photocaged compounds **2b** respectively **21** a 0.5 mM solution in H_2O or else sodium phosphate buffer (100 mM, pH = 7.4) was prepared. In a cuvette 1 mL of this solution was irradiated at room temperature using the LUMOS 43 (375 nm, 405 nm, or 430 nm) for a definite time. The sample was then analyzed by reversed-phase HPLC Jasco HPLC system [column: Hyperclone 5 µ ODS (C18) 120 (Phenomenex)]. For each photocaged compound, the procedure was repeated for different irradiation times. The decrease of concentration was measured by an UV detector.[15]

Determination of uncaging quantum yields: The uncaging quantum yield (ϕ_u) for the release of the inducer molecules is defined by Equation 1.

$$\phi_u = \frac{\text{number of consumed reactant}}{\text{number of absorbed photons}} \quad (1)$$

Values for the photocaged compounds **1b**–**e**, **2b**–**c** and **21** were calculated in accordance with a standard method using Equation 2.[57]

$$\phi_u = \frac{\left(\frac{dn}{dt}\right)}{q_{n,p}[1-10^{-A}]} \quad (2)$$

The term (*dn/dt*) refers to the decay rate of the photocaged compound (mol s^{-1}), $q_{n,p}$ to the photon flux density (mol s^{-1}) and A is the absorbance at the excitation wavelength λ.

Hydrolytic stability: For the determination of the hydrolytic stability, a freshly prepared 0.5 mM solution of the photocaged compounds **1b**–**e** and **2c** in Tris buffer (20 mM, pH = 7.5)/MeCN 1:1 as well as **2b** respectively **21** in H_2O or sodium phosphate buffer (100 mM, pH = 7.4) were stored in the dark at room temperature. Samples were removed after 0 and 24 h and analyzed by reversed-phase HPLC.

Bacterial strains and plasmids: For all cloning procedures, the *E. coli* strain DH5α[58] was used, while the *E. coli* strain Tuner (DE3) (Novagen) was applied for the expression studies. All *E. coli* strains were grown on LB agar plates or in liquid LB medium (Luria/Miller, Carl Roth®) or M9CA-Gly minimal medium[34] at 37 °C if not stated otherwise and all media were supplemented with kanamycin (50 µg mL^{-1}) for strain maintenance if appropriate.

All bacterial strains and plasmids used in this study are listed in Table S1, Supporting Information.

Plasmid construction: All recombinant DNA techniques were conducted as described by Sambrook *et al.*[59] For construction of the expression vector pM-R45T-GFPmut3, which offers a benzoate induction with a broader inducer spectrum, the previously described R45T mutation[41,43] was introduced to the XylS activator protein *via* overlap extension PCR[60] using oligos 1–4 (Table S1, Supporting Information). The resulting PCR product was *SalI*/ *Sac*I digested and inserted into the likewise hydrolyzed target plasmid pSB-M-2-g[36] *via* ligation, yielding the final plasmid pM-R45T-GFPmut3. For construction of the expression plasmid pBNTmcs-mCherry-Km, the *mcherry* reporter gene was extracted out of the plasmid pJT'Tmcs-mCherry[61] *via EcoRI*/ *Xba*I digestion and inserted into the likewise hydrolyzed target plasmid pBNTmcs(t)-Km.[46b] The plasmid pBTBX-2-mCherry was constructed using the In-Fusion® HD Cloning Plus kit (Takara Bio Europe, St Germain en Laye, France). For this purpose, the plasmid backbone of pBTBX-2 was amplified by PCR using oligos 5 and 6 (pBTBX-2 was a gift from Ryan Gill, Addgene plasmid # 26068). The *mcherry* reporter gene was extracted out of the plasmid pJT'Tmcs-mCherry[61] using oligos 7 and 8 (containing homologous sequences suitable for integration into the amplified pBTBX-2 plasmid backbone) and the plasmid pJT'Tmcs-mCherry as template. Finally, both fragments were assembled using the In-Fusion® cloning reaction mix as indicated by the supplier. Correct nucleotide sequences of all constructs were confirmed by Sanger sequencing (Eurofins Genomics, Germany).

Expression cultures for novel photocaged IPTG and arabinose variants: All *E. coli* cultures were grown in 48-well Flowerplates® in a ThermoMixer C (Eppendorf, Germany) (800 µL LB medium, 1200 rpm, 30 or 37 °C) in the dark for 20 h and previously inoculated with a cell density corresponding to an optical density of 0.05 at 580 nm if not stated otherwise. Induction was performed after 2.5 h by blue light exposure at 447 nm (~10 mW cm^{-2}) for 10 min or the addition of respective amounts of conventional IPTG (**1a**) or arabinose (**2a**). The LED diodes exhibit an emission range of 410–500 nm and an emission maximum at 447 nm (LUXEON Z Color Line (LXZ1-PR01) Royal Blue, Lumileds, USA; for an emission spectrum see data sheet available at the manufactures website https://lumileds.com/products/color-leds/luxeon-z-colors/). *In vivo* eYFP or mCherry fluorescence intensities were determined using a Tecan Microplate Reader (λ_{ex} = 488 nm, λ_{em} = 527 nm or λ_{ex} = 580 nm, λ_{em} = 610 nm, respectively), normalized to cell densities and are shown in relation to the respective fluorescence intensities of a culture induced with conventional IPTG (**1a**) or arabinose (**2a**).

ChemBioChem
Full Papers
doi.org/10.1002/cbic.202100467
Chemistry Europe
European Chemical Societies Publishing

Expression cultures for novel cSal variants: All *E. coli* cultures were grown in 48-well Flowerplates® in a ThermoMixer C (Eppendorf, Germany) (800 μL LB medium or M9CA-Gly minimal medium, 1200 rpm, 30 °C) in the dark for 20 h. Previously, expression cultures were inoculated with a cell density corresponding to an optical density of 0.01 (P_m and $P_{M1\text{-}17}$ promoter system) or 0.05 (P_{nagAa} promoter system) at 580 nm if not stated otherwise. Induction was performed after 6 or 2 h by UV-A light exposure at 365 nm (~1 mW cm^{-2}) for 30 min or the addition of respective amounts of conventional salicylic acid. The UV-A lamp exhibits an emission range of 320–400 nm and an emission maximum at 365 nm (VL-315.BL 45-W lamp, Vilber Lourmat, Germany). *In vivo* GFPmut3 or mCherry fluorescence intensities were determined using a Tecan Microplate Reader (λ_{ex} = 488 nm, λ_{em} = 527 nm or λ_{ex} = 580 nm, λ_{em} = 610 nm, respectively), normalized to cell densities and are shown in relation to the respective fluorescence intensities of a culture induced with conventional salicylic acid.

Acknowledgements

The work was supported by grants from the Bioeconomy Science Center, the scientific activities of the Bioeconomy Science Center were financially supported by the Ministry of Culture and Science of the German federal state of North Rhine-Westphalia MKW within the framework of the NRW Strategieprojekt BioSC (no. 313/323-400-00213). Open Access funding enabled and organized by Projekt DEAL.

Conflict of Interest

The authors declare no conflict of interest.

Keywords: caged compounds · gene expression · optogenetics · photochemistry · synthetic biology

[1] a) T. Drepper, U. Krauss, S. Meyer zu Berstenhorst, J. Pietruszka, K.-E. Jaeger, *Appl. Microbiol. Biotechnol.* **2011**, *90*, 23–40; b) D. Hartmann, J. M. Smith, G. Mazzotti, R. Chowdhry, M. J. Booth, *Biochem. Soc. Trans.* **2020**, *48*, 1645–1659.
[2] F. Hamouri, W. Zhang, I. Aujard, T. Le Saux, B. Ducos, S. Vriz, L. Jullien, D. Bensimon, in *Methods Enzymol., Vol. 624* (Ed.: A. Deiters), Academic Press, **2019**, pp. 1–23.
[3] a) T. Ziegler, A. Möglich, *Front. Mol. Biosci.* **2015**, *2*, 30; b) Z. Liu, J. Zhang, J. Jin, Z. Geng, Q. Qi, Q. Liang, *Front. Microbiol.* **2018**, *9*; c) R. M. Hughes, *Crit. Rev. Biochem. Mol. Biol.* **2018**, *53*, 453–474.
[4] S. R. Adams, R. Y. Tsien, *Annu. Rev. Physiol.* **1993**, *55*, 755–784.
[5] A. Deiters, *Curr. Opin. Chem. Biol.* **2009**, *13*, 678–686.
[6] W. Lin, C. Albanese, R. G. Pestell, D. S. Lawrence, *Chem. Biol.* **2002**, *9*, 1347–1353.
[7] a) D. J. Sauers, M. K. Temburni, J. B. Biggins, L. M. Ceo, D. S. Galileo, J. T. Koh, *ACS Chem. Biol.* **2010**, *5*, 313–320; b) S. B. Cambridge, D. Geissler, F. Calegari, K. Anastassiadis, M. T. Hasan, A. F. Stewart, W. B. Huttner, V. Hagen, T. Bonhoeffer, *Nat. Methods* **2009**, *6*, 527–531; c) S. B. Cambridge, D. Geissler, S. Keller, B. Cürten, *Angew. Chem. Int. Ed.* **2006**, *45*, 2229–2231; *Angew. Chem.* **2006**, *45*, 2287–2289.
[8] a) P. T. Wong, E. W. Roberts, S. Tang, J. Mukherjee, J. Cannon, A. J. Nip, K. Corbin, M. F. Krummel, S. K. Choi, *ACS Chem. Biol.* **2017**, *12*, 1001–1010; b) T. Faal, P. T. Wong, S. Tang, A. Coulter, Y. Chen, C. H. Tu, J. R. Baker, S. K. Choi, M. A. Inlay, *Mol. BioSyst.* **2015**, *11*, 783–790; c) M. A. Inlay, V. Choe, S. Bharathi, N. B. Fernhoff, J. R. Baker, I. L. Weissman, S. K. Choi, *Chem. Commun.* **2013**, *49*, 4971–4973; d) K. H. Link, Y. Shi, J. T. Koh, *J. Am. Chem. Soc.* **2005**, *127*, 13088–13089; e) Y. Shi, J. T. Koh, *ChemBioChem* **2004**, *5*, 788–796.
[9] a) A. P. Gorka, T. Yamamoto, J. Zhu, M. J. Schnermann, *ChemBioChem* **2018**, *19*, 1239–1243; b) D. K. Sinha, P. Neveu, N. Gagey, I. Aujard, C. Benbrahim-Bouzidi, T. Le Saux, C. Rampon, C. Gauron, B. Goetz, S. Dubruille, M. Baaden, M. Volovitch, D. Bensimon, S. Vriz, L. Jullien, *ChemBioChem* **2010**, *11*, 653–663; c) L. Fournier, C. Gauron, L. Xu, I. Aujard, T. Le Saux, N. Gagey-Eilstein, S. Maurin, S. Dubruille, J.-B. Baudin, D. Bensimon, M. Volovitch, S. Vriz, L. Jullien, *ACS Chem. Biol.* **2013**, *8*, 1528–1536.
[10] P. M. Kusen, G. Wandrey, C. Probst, A. Grünberger, M. Holz, S. Meyer zu Berstenhorst, D. Kohlheyer, J. Büchs, J. Pietruszka, *ACS Chem. Biol.* **2016**, *11*, 2915–2922.
[11] P. M. Kusen, G. Wandrey, V. Krewald, M. Holz, S. M. zu Berstenhorst, J. Büchs, J. Pietruszka, *J. Biotechnol.* **2017**, *258*, 117–125.
[12] a) G. Wandrey, C. Bier, D. Binder, K. Hoffmann, K.-E. Jaeger, J. Pietruszka, T. Drepper, J. Büchs, *Microb. Cell Fact.* **2016**, *15*, 1–16; b) D. Binder, C. Probst, C. Bier, A. Loeschcke, A. Grünberger, *BIOspektrum* **2015**, *21*, 612–615; c) D. Binder, A. Grünberger, A. Loeschcke, C. Probst, C. Bier, J. Pietruszka, W. Wiechert, D. Kohlheyer, K.-E. Jaeger, T. Drepper, *Integr. Biol.* **2014**, *6*, 755–765; d) D. D. Young, A. Deiters, *Angew. Chem. Int. Ed.* **2007**, *46*, 4290–4292; *Angew. Chem.* **2007**, *119*, 4368–4370.
[13] L. Gardner, Y. Zou, A. Mara, T. A. Cropp, A. Deiters, *Mol. BioSyst.* **2011**, *7*, 2554–2557.
[14] D. Binder, C. Bier, A. Grünberger, D. Drobietz, J. Hage-Hülsmann, G. Wandrey, J. Büchs, D. Kohlheyer, A. Loeschcke, W. Wiechert, K.-E. Jaeger, J. Pietruszka, T. Drepper, *ChemBioChem* **2016**, *17*, 296–299.
[15] C. Bier, D. Binder, D. Drobietz, A. Loeschcke, T. Drepper, K.-E. Jaeger, J. Pietruszka, *Synthesis* **2017**, *49*, 42–52.
[16] a) D. Binder, J. Frohwitter, R. Mahr, C. Bier, A. Grünberger, A. Loeschcke, P. Peters-Wendisch, D. Kohlheyer, J. Pietruszka, J. Frunzke, K.-E. Jaeger, V. F. Wendisch, T. Drepper, *Appl. Environ. Microbiol.* **2016**, *82*, 6141–6149; b) A. Burmeister, Q. Akhtar, L. Hollmann, N. Tenhaef, F. Hilgers, F. Hogenkamp, S. Sokolowsky, J. Marienhagen, S. Noack, D. Kohlheyer, A. Grünberger, *ACS Synth. Biol.* **2021**, *10*, 1308–1319.
[17] F. Hogenkamp, F. Hilgers, A. Knapp, O. Klaus, C. Bier, D. Binder, K.-E. Jaeger, T. Drepper, J. Pietruszka, *ChemBioChem* **2021**, *22*, 539–547.
[18] P. Klán, T. Šolomek, C. G. Bochet, A. Blanc, R. Givens, M. Rubina, V. Popik, A. Kostikov, J. Wirz, *Chem. Rev.* **2013**, *113*, 119–191.
[19] R. Kent, N. Dixon, *Trends Biotechnol.* **2020**, *38*, 316–333.
[20] J. Olejniczak, C.-J. Carling, A. Almutairi, *J. Controlled Release* **2015**, *219*, 18–30.
[21] B. Goegan, F. Terzi, F. Bolze, S. Cambridge, A. Specht, *ChemBioChem* **2018**, *19*, 1341–1348.
[22] a) K. Terpe, *Appl. Microbiol. Biotechnol.* **2006**, *72*, 211–222; b) S. Gräslund, P. Nordlund, J. Weigelt, B. M. Hallberg, J. Bray, O. Gileadi, S. Knapp, U. Oppermann, C. Arrowsmith, R. Hui, J. Ming, S. dhe-Paganon, H.-w. Park, A. Savchenko, A. Yee, A. Edwards, R. Vincentelli, C. Cambillau, R. Kim, S.-H. Kim, Z. Rao, Y. Shi, T. C. Terwilliger, C.-Y. Kim, L.-W. Hung, G. S. Waldo, Y. Peleg, S. Albeck, T. Unger, O. Dym, J. Prilusky, J. L. Sussman, R. C. Stevens, S. A. Lesley, I. A. Wilson, A. Joachimiak, F. Collart, I. Dementieva, M. I. Donnelly, W. H. Eschenfeldt, Y. Kim, L. Stols, R. Wu, M. Zhou, S. K. Burley, J. S. Emtage, J. M. Sauder, D. Thompson, K. Bain, J. Luz, T. Gheyi, F. Zhang, S. Atwell, S. C. Almo, J. B. Bonanno, A. Fiser, S. Swaminathan, F. W. Studier, M. R. Chance, A. Sali, T. B. Acton, R. Xiao, L. Zhao, L. C. Ma, J. F. Hunt, L. Tong, K. Cunningham, M. Inouye, S. Anderson, H. Janjua, R. Shastry, C. K. Ho, D. Wang, H. Wang, M. Jiang, G. T. Montelione, D. I. Stuart, R. J. Owens, S. Daenke, A. Schütz, U. Heinemann, S. Yokoyama, K. Büssow, K. C. Gunsalus, *Nat. Methods* **2008**, *5*, 135–146; c) J. C. Samuelson, in *Heterologous Gene Expression in E. coli: Methods in Molecular Biology (Methods and Protocols), Vol. 705* (Eds.: J. T. Evans, M. Q. Xu), Humana, **2011**.
[23] a) T. Brautaset, R. Lale, S. Valla, *Microb. Biotechnol.* **2009**, *2*, 15–30; b) I. Bakke, L. Berg, T. E. V. Aune, T. Brautaset, H. Sletta, A. Tøndervik, S. Valla, *Appl. Environ. Microbiol.* **2009**, *75*, 2002–2011.
[24] M. J. Hansen, W. A. Velema, M. M. Lerch, W. Szymanski, B. L. Feringa, *Chem. Soc. Rev.* **2015**, *44*, 3358–3377.
[25] L. Fournier, I. Aujard, T. Le Saux, S. Maurin, S. Beaupierre, J. B. Baudin, L. Jullien, *Chem. Eur. J.* **2013**, *19*, 17494–17507.
[26] A. Deiters, *ChemBioChem* **2010**, *11*, 47–53.
[27] W. Lin, D. S. Lawrence, *J. Org. Chem.* **2002**, *67*, 2723–2726.
[28] A. Laguerre, S. Hauke, J. Qiu, M. J. Kelly, C. Schultz, *J. Am. Chem. Soc.* **2019**, *141*, 16544–16547.
[29] R. Weinstain, T. Slanina, D. Kand, P. Klán, *Chem. Rev.* **2020**, *120*, 13135–13272.

ChemBioChem
Full Papers
doi.org/10.1002/cbic.202100467
Chemistry Europe
European Chemical Societies Publishing

[30] R. Schmidt, D. Geissler, V. Hagen, J. Bendig, *J. Phys. Chem. A* **2007**, *111*, 5768–5774.
[31] A. Z. Suzuki, T. Watanabe, M. Kawamoto, K. Nishiyama, H. Yamashita, M. Ishii, M. Iwamura, T. Furuta, *Org. Lett.* **2003**, *5*, 4867–4870.
[32] A. Alouane, R. Labruère, T. Le Saux, F. Schmidt, L. Jullien, *Angew. Chem. Int. Ed.* **2015**, *54*, 7492–7509; *Angew. Chem.* **2015**, *127*, 7600–7619.
[33] R. Wang, K. Cai, H. Wang, C. Yin, J. Cheng, *Chem. Commun.* **2018**, *54*, 4878–4881.
[34] D. Binder, C. Probst, A. Grünberger, F. Hilgers, A. Loeschcke, K.-E. Jaeger, D. Kohlheyer, T. Drepper, *PLoS One* **2016**, *11*, e0160711.
[35] L. M. Guzman, D. Belin, M. J. Carson, J. Beckwith, *J. Bacteriol.* **1995**, *177*, 4121–4130.
[36] S. Balzer, V. Kucharova, J. Megerle, R. Lale, T. Brautaset, S. Valla, *Microb. Cell Fact.* **2013**, *12*, 26.
[37] M. Noguchi, M. Skwarczynski, H. Prakash, S. Hirota, T. Kimura, Y. Hayashi, Y. Kiso, *Bioorg. Med. Chem.* **2008**, *16*, 5389–5397.
[38] a) S. Feng, C. Bagia, G. Mpourmpakis, *J. Phys. Chem. A* **2013**, *117*, 5211–5219; b) V. Dimakos, M. S. Taylor, *Chem. Rev.* **2018**, *118*, 11457–11517.
[39] P. I. Nikel, V. de Lorenzo, *Metab. Eng.* **2018**, *50*, 142–155.
[40] a) A. Basu, R. Shrivastava, B. Basu, S. K. Apte, P. S. Phale, *J. Bacteriol.* **2007**, *189*, 7556; b) J. L. Ramos, S. Marqués, K. N. Timmis, *Annu. Rev. Microbiol.* **1997**, *51*, 341–373.
[41] J. L. Ramos, A. Stolz, W. Reineke, K. N. Timmis, *Proc. Natl. Acad. Sci. USA* **1986**, *83*, 8467–8471.
[42] a) A. Gawin, S. Valla, T. Brautaset, *Microb. Biotechnol.* **2017**, *10*, 702–718; b) P. Calero, S. I. Jensen, A. T. Nielsen, *ACS Synth. Biol.* **2016**, *5*, 741–753; c) P. I. Nikel, V. de Lorenzo, *Metab. Eng.* **2013**, *15*, 98–112.
[43] J. L. Ramos, C. Michan, F. Rojo, D. Dwyer, K. Timmis, *J. Mol. Biol.* **1990**, *211*, 373–382.
[44] L. Hüsken, R. Beeftink, J. de Bont, J. Wery, *Appl. Microbiol. Biotechnol.* **2001**, *55*, 571–577.
[45] a) R. M. Jones, B. Britt-Compton, P. A. Williams, *J. Bacteriol.* **2003**, *185*, 5847–5853; b) S. L. Fuenmayor, M. Wild, A. L. Boyes, P. A. Williams, *J. Bacteriol.* **1998**, *180*, 2522 S. L. Fuenmayor, M. Wild, A. L. Boyes, P. A. Williams, *J. Bacteriol.* **1998**, *180*, 2522–2530.
[46] a) J.-P. Meijnen, J. H. de Winde, H. J. Ruijssenaars, *Appl. Environ. Microbiol.* **2008**, *74*, 5031; b) S. Verhoef, H. Ballerstedt, R. J. M. Volkers, J. H. de Winde, H. J. Ruijssenaars, *Appl. Microbiol. Biotechnol.* **2010**, *87*, 679–690; c) J.-P. Meijnen, S. Verhoef, A. A. Briedjlal, J. H. de Winde, H. J. Ruijssenaars, *Appl. Microbiol. Biotechnol.* **2011**, *90*, 885–893; d) N. J. P. Wierckx, H. Ballerstedt, J. A. M. de Bont, J. Wery, *Appl. Environ. Microbiol.* **2005**, *71*, 8221–8227; e) J. H. Lee, R. J. Mitchell, M. B. Gu, *J. Biotechnol.* **2007**, *131*, 330–334; f) C. Lenzen, B. Wynands, M. Otto, J. Bolzenius, P. Mennicken, L. M. Blank, N. Wierckx, *Front. Bioeng. Biotechnol.* **2019**, *7*, 130.
[47] J. Ni, D. A. Auston, D. A. Freilich, S. Muralidharan, E. A. Sobie, J. P. Y. Kao, *J. Am. Chem. Soc.* **2007**, *129*, 5316–5317.
[48] R. Appel, *Angew. Chem. Int. Ed.* **1975**, *14*, 801–811; *Angew. Chem.* **1975**, *87*, 863–874.
[49] a) M.-T. Gallegos, C. Michán, J. L. Ramos, *Nucleic Acids Res.* **1993**, *21*, 807–810; b) J. L. Ramos, F. Rojo, L. Zhou, K. N. Timmis, *Nucleic Acids Res.* **1990**, *18*, 2149–2152.
[50] M.-T. Gallegos, S. Marqués, J. L. Ramos, *J. Bacteriol.* **1996**, *178*, 2356–2361.
[51] a) S. Marqués, M.-T. Gallegos, J. L. Ramos, *Mol. Microbiol.* **1995**, *18*, 851–857; b) K. Tanaka, Y. Takayanagi, N. Fujita, A. Ishihama, H. Takahashi, *Proc. Natl. Acad. Sci. USA* **1993**, *90*, 3511–3515; c) S. Marqués, M. Manzanera, M.-M. González-Pérez, M.-T. Gallegos, J. L. Ramos, *Mol. Microbiol.* **1999**, *31*, 1105–1113.
[52] W. A. Duetz, S. Marqués, C. de Jong, J. L. Ramos, J. G. van Andel, *J. Bacteriol.* **1994**, *176*, 2354–2361.
[53] a) A. D. Grossman, D. B. Straus, W. A. Walter, C. A. Gross, *Genes Dev.* **1987**, *1*, 179–184; b) P. C. Loewen, B. Hu, J. Strutinsky, R. Sparling, *Can. J. Microbiol.* **1998**, *44*, 707–717; c) R. Hengge-Aronis, *Microbiol. Mol. Biol. Rev.* **2002**, *66*, 373–395.
[54] a) S. Inouye, A. Nakazawa, T. Nakazawa, *J. Bacteriol.* **1987**, *169*, 3587–3592; b) N. Mermod, J. L. Ramos, A. Bairoch, K. N. Timmis, *Mol. Gen. Genet.* **1987**, *207*, 349–354; c) R. A. Spooner, K. Lindsay, F. C. H. Franklin, *J. Gen. Microbiol.* **1986**, *132*, 1347–1358.
[55] R. Lönneborg, P. Brzezinski, *BMC Biochem.* **2011**, *12*, 49.
[56] a) C. A. Parker, E. J. Bowen, *Proc. R. Soc. London Ser. A* **1953**, *220*, 104–116; b) C. G. Hatchard, C. A. Parker, E. J. Bowen, *Proc. R. Soc. London Ser. A* **1956**, *235*, 518–536; c) H. J. Kuhn, S. E. Braslavsky, R. Schmidt, *Pure Appl. Chem.* **2004**, *76*, 2105–2146.
[57] S. E. Braslavsky, *Pure Appl. Chem.* **2007**, *79*, 293–465.
[58] D. Hanahan, *J. Mol. Biol.* **1983**, *166*, 557–580.
[59] J. Sambrook, E. F. Fritsch, T. Maniatis, *Molecular Cloning: A Laboratory Manual*, Cold Spring Harbor Laboratory Press, Cold Spring Harbor, NY, **1989**.
[60] A. Urban, S. Neukirchen, K.-E. Jaeger, *Nucleic Acids Res.* **1997**, *25*, 2227–2228.
[61] A. Burmeister, F. Hilgers, A. Langner, C. Westerwalbesloh, Y. Kerkhoff, N. Tenhaef, T. Drepper, D. Kohlheyer, E. von Lieres, S. Noack, A. Grünberger, *Lab Chip* **2019**, *19*, 98–110.

Manuscript received: September 1, 2021
Revised manuscript received: November 2, 2021
Accepted manuscript online: November 8, 2021
Version of record online: ■■, ■■

II.1.4. WAVELENGTH-SELECTIVE CONTROL OF GENE EXPRESSION IN *P. PUTIDA*

Wavelength-selective control of mono- and di-rhamnolipid synthesis in *Pseudomonas putida* using photocaged compounds

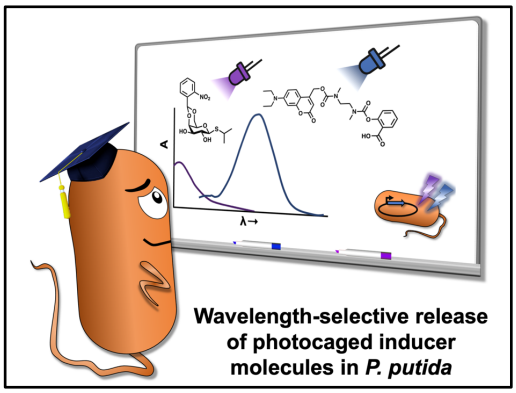

Fabienne Hilgers*, Fabian Hogenkamp*, Nora Lisa Bitzenhofer, Stephan Thies, Karl-Erich Jaeger, Jörg Pietruszka and Thomas Drepper

Target journal: *ACS Synthetic Biology*

Status: manuscript in preparation

For the Supporting Information see Appendix (**Chapter V.4.**, **page 412**).

Own contribution:

Designing and performing biological experiments, plasmid constructions, analyzing *in vivo* data, writing parts of the manuscript.

Wavelength-selective control of mono- and di-rhamnolipid synthesis in *Pseudomonas putida* using photocaged compounds

Fabienne Hilgers[+][a], Fabian Hogenkamp[+][b], Nora Lisa Bitzenhofer[a], Stephan Thies[a], Karl-Erich Jaeger[a, c], Jörg Pietruszka*[b, c] and Thomas Drepper*[a]

[a] F. Hilgers, N.L. Bitzenhofer, Dr. S. Thies, Prof. Dr. K.-E. Jaeger, Dr. T. Drepper
Institute of Molecular Enzyme Technology Heinrich Heine University Düsseldorf at Forschungszentrum Jülich
Stetternicher Forst, 52426 Jülich (Germany)
E-mail: T.Drepper@fz-juelich.de

[b] F. Hogenkamp, Prof. Dr. J. Pietruszka
Institute of Bioorganic Chemistry, Heinrich Heine University Düsseldorf at Forschungszentrum Jülich
Stetternicher Forst, 52426 Jülich (Germany)
E-mail: J.Pietruszka@fz-juelich.de

[c] Prof. Dr. K.-E. Jaeger, Prof. Dr. J. Pietruszka
Institute of Bio- and Geosciences (IBG-1: Biotechnology), Forschungszentrum Jülich
Stetternicher Forst, 52426 Jülich (Germany)

[+] These authors contributed equally to this work.

Abstract

The control of bacterial gene expression using chemical inducers is well-established in a variety of different organisms and is frequently applied in both biotechnological and industrial applications. Since the manual addition of inducer molecules offers a limited applicability, various optogenetic tools emerged during the last few decades, which all use the environmental factor light as an external stimulus. A prominent example are photocaged molecules, which were successfully applied for controlling gene expression in bacteria. However, the engineered light-regulated gene expression systems are mostly monochromatic as transcription from a given promoter is reversibly or irreversibly activated by one light color. Hence, we describe the wavelength-selective photocontrol of bacterial gene expression using two photocaged inducer molecules, namely caged IPTG and caged salicylic acid, in the versatile expression host *Pseudomonas putida* KT2440. Finally, we evaluated the applicability of our system for the multichromatic orchestration of the complex biosynthetic rhamnolipid pathway in *P. putida*.

Keywords

Optogenetics, photocaged inducers, multichromatic control, gene expression, *Pseudomonas putida*

Introduction

As the precise control of bacterial gene expression is an essential tool for understanding and manipulating biological systems, the use of chemical inducers for transcriptional control has a long history in a variety of different organisms and for both biotechnological and industrial applications [1–5]. The efficient control of gene expression helps to achieve maximal production of the desired products by circumventing the problem of metabolic burden in biological systems [6–10]. Common inducible promoters used for gene expression are based on the addition of chemicals such as isopropyl β-D-1-thiogalactopyranoside (IPTG), arabinose or anhydrotetracycline [11,12]. However, a manual addition of inducer molecules during the cultivation process bears some disadvantages including the disruption of well-defined cultivation parameters or the limited applicability for high throughput applications [13]. Hence, various tools emerged during the last few decades which all use the environmental factor light as an external stimulus for controlling gene expression. Beside the application of genetically encoded photoreceptors [14–18], photocaged molecules gained more and more interest and were successfully applied for a wide range of different applications [13,19–24]. However, the engineered light-regulated gene expression systems are mostly monochromatic as transcription from a given promoter is reversibly or irreversibly activated by one light color [25–27]. The development of multichromatic gene regulation systems, in which different light wavelengths regulate the expression of different genes, allows a more sophisticated control of

synthetic and natural gene regulatory networks and could help balancing complex metabolic pathways [28–31]. In recent years, several examples for multichromatic control of gene expression have been established [32–35], however, all of those control circuits rely on the use of photoreceptors for transcriptional regulation. The use of multichromatic photocaged molecules was so far mainly limited to photoresponsive surfaces [36,37], neurology [38,39], drug delivery [40], gene silencing [41], the control of signaling pathways [42] and bacterial growth [43] as well as development of zebrafish embryos [44]. Very recently, a first example of multichromatic regulation of gene expression has been reported in mammalian cells by photoactivation of mRNA [45]. In this context, the terms wavelength-orthogonal and -selective control should be defined accurately. A wavelength-orthogonal arrangement includes two or more processes, which are completely spectral independent, whereas a wavelength-specific process may include components with a certain spectral crosstalk between each other, but without affecting the desired functionality [46–48]. Thus, for a minimal spectral overlap of the two photocaged compounds, the light colors can be regulated in any order, thereby achieving the greatest possible flexibility. Here we describe the wavelength-selective photocontrol of bacterial transcription using two photocaged inducer molecules, namely caged IPTG (cIPTG) and caged salicylic acid (cSal), in the versatile expression host *Pseudomonas putida* KT2440. This organism is a rod-shaped, Gram-negative soil bacterium with a highly versatile metabolism and an extraordinary tolerance to xenobiotics, organic solvents and other environmental stresses [49–53] making *P. putida* strains especially interesting for biocatalysis and industrial applications [54–57] as well as the production of various high-value natural products [58–61]. To achieve a multichromatic control over gene expression, we evaluated the applicability of the well-known LacI/P_{tac} promoter system in combination with the NagR/P_{nagAa} system. While the first has already been successfully applied for light control in various organisms including *Escherichia coli*, *P. putida* or *Rhodobacter capsulatus* using photocaged IPTG [22,62], the latter has not been subjected to light control using photocaged inducers in *P. putida* so far. Originally, the NagR/P_{nagAa} promotor system is based on the *nag* operon from *Comamonas testosteroni* GZ42 allowing the utilization of naphthalene and phenanthrene as carbon sources and is composed of the LysR-type regulator NagR and the associated promoter P_{nagAa} [63]. Over the last few decades this system was used for the control of benzoate-mediated heterologous gene expression in different bacterial hosts such as *P. putida*, *Pseudomonas taiwanensis* or *E. coli* [64–69]. However, in terms of light controlled gene expression, the development of light-responsive transcriptional inducer molecules has been largely limited to photocaged carbohydrates including caged IPTG [19,22,70], caged arabinose [71], or caged glucose [72], leaving the benzoate-inducible promoter systems rather aside. Hence, the establishment of novel photocaged salicylate variants addressing the NagR/P_{nagAa} system in *P. putida* presented in this study should close this gap. Finally, we evaluated the

applicability of our system for the multichromatic orchestration of the complex biosynthetic rhamnolipid pathway in *P. putida*.

Results

Photocaged inducer design.

For the following investigations two cIPTG-derivatives as well as four cSal-derivatives were employed. The syntheses and characterization of 6-Nitropiperonyl cIPTG (NP-cIPTG, **1**) and 4,5-bis(carboxymethoxy)-2-nitrobenzyl cSal (BC-cSal, **2**) as well as its corresponding sodium salt **3** (BC-cSal*Na) were previously published elsewhere [22,70,73]. The synthetic route to the novel photocaged inducer molecules, namely 2-nitrobenzyl cIPTG (NB-cIPTG, **4**) and the coumarin-based cSal **5** (DC-cSal) as well as its corresponding sodium salt **6** (DC-cSal*Na) are described in detail in the supporting information (Scheme S1–3). The *in vitro* photochemical properties of the new compounds were characterized (Figure S4–8). The absorption spectra of the potentially combinable photocaged compounds are shown in combination with the emission spectra of the LED diodes applied in this study (Figure 1).

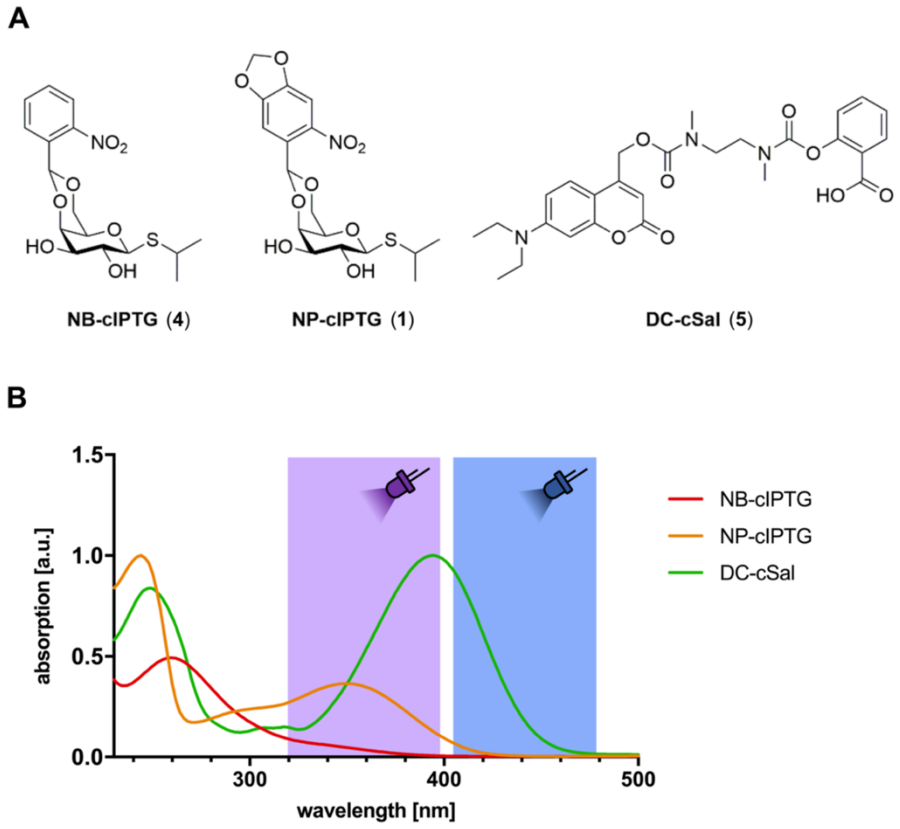

Figure 1. Experimental setup of wavelength-selective uncaging experiment. **A**) Photocaged inducer variants NB-cIPTG (**4**), NP-cIPTG (**1**) and DC-cSal (**5**) investigated in this study. **B**) The UV-Vis absorption spectra of NB-cIPTG

(**4**, red), NP-cIPTG (**1**, orange) and DC-cSal (**5**, green) underlaid with the wavelength ranges of the UV-A (violet zone) and the blue light sources (blue zone).

Establishment of the NagR/P_{nagAa} expression system in *P. putida*.

Initially, the NagR/P_{nagAa}-based expression system was evaluated in *P. putida* KT2440 to gain information about suitable inducer concentrations, expression strength of the fluorescence reporter mCherry and the applicability of different cSal variants. For this purpose, we comparably analyzed the induction response of several cSal derivatives in expression cultures of *P. putida* KT2440 carrying the mCherry expression vector pBNTmcs-mCherry. The cSal derivatives included two BC-cSal variants (**2**, **3**), which were recently applied for light-mediated gene expression in *E. coli* [73], and two DC-Sal variants (**5**, **6**). Within each subgroup, the compounds were tested in their common acidic form as well as in their sodium salt form (*Na) offering an enhanced water solubility. The observed efficiency of reporter gene expression represents the integrated response of the cells to all processes involved in caged inducer uptake and salicylic acid release. These include the passage of cSal derivatives across the two membranes, the efficiency of their photoconversion as well as the enzymatic cleavage of the photoproduct by intra- and/or extracellular esterases. As shown in Figure 2A, illumination of all cSal variants resulted in even higher mCherry expression levels as in the control experiment, where salicylic acid (Sal) was added.

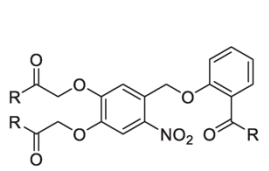

BC-cSal (2): R = OH
BC-cSal*Na (3): R = O^-Na^+

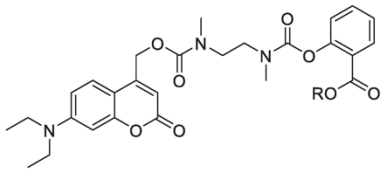

DC-cSal (5): R = OH
DC-cSal*Na (6): R = O^-Na^+

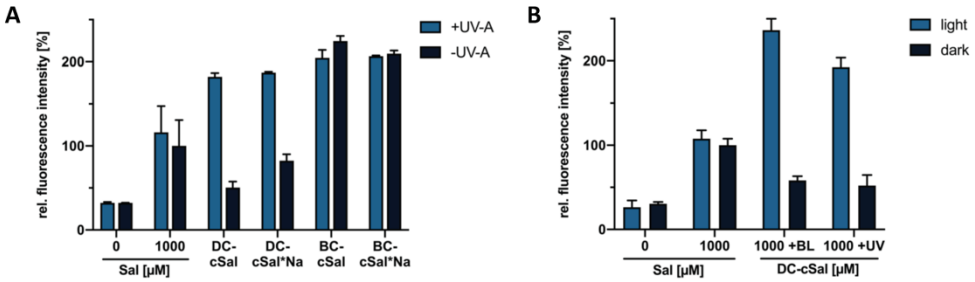

Figure 2. Light-controlled gene expression in *P. putida* KT2440/pBNTmcs-mCherry using cSal variants.
A) *In vivo* mCherry fluorescence (λ_{ex} = 580 nm, λ_{em} = 610 nm) of *P. putida* cultures supplemented with 1000 µM of DC-cSal (**5**), it's sodium form DC-cSal*Na (**6**), BC-cSal (**2**) and its sodium form BC-cSal*Na (**3**) is shown in relation to a 1000 µM salicylic acid (Sal) control after 20 h (stationary growth phase). Induction was performed after 3 h *via*

to a 1000 µM salicylic acid (Sal) control after 20 h (stationary growth phase). Induction was performed after 3 h *via* UV-A light exposure (365 nm, ~1 mW cm^{-2}) for 30 min or by the addition of 1000 µM Sal. **B**) *In vivo* mCherry fluorescence (λ_{ex} = 580 nm, λ_{em} = 610 nm) of *P. putida* cultures supplemented with 1000 µM of DC-cSal (**5**) is shown in relation to a 1000 µM salicylic acid (Sal) control after 20 h (stationary growth phase). Induction was performed after 3 h *via* blue light exposure (447 nm, ~10 mW cm^{-2}), UV-A light exposure (365 nm, ~1 mW cm^{-2}) for 30 min or by the addition of 1000 µM Sal. *In vivo* fluorescence intensities were normalised to cell densities and values are means of triplicate measurements. Error bars indicate the respective standard deviations.

Since the exposure time should guarantee a full photo-conversion of all tested cSal variants, this observation could be explained by either an optimized uptake or enzymatic conversion of the caged inducers. Interestingly, there is no significant difference between the DC-cSal (**5**) or its corresponding sodium salt form **6** with respect to the induction strength but a noticeable decrease in compound stability could be seen for the highly water-soluble salt form **6**, exhibiting an mCherry fluorescence of nearly 50 % in comparison to the UV-A exposed culture. Interestingly, the BC-cSal variants **2** and **3** both showed a sufficient induction strength, but a drastically decreased stability after a cultivation period of 20 h, resulting in a complete induction without any UV-A light. This result is in strong contrast to the recently published application in *E. coli* [73], where BC-cIPTG could successfully be applied without severe instability effects. This result could possibly be explained by the individual set of intra- and extracellular enzymes each organism produces, especially in varying cultivation media and has recently also been observed for selected photocaged IPTG variants in *R. capsulatus* [62]. However, the acid form of DC-cSal (**5**) showed a particularly good applicability, as it offers a higher induction response in comparison to salicylic acid as well as a sufficient *in vivo* stability. In order to further evaluate the applicability of caged salicylic acid for non-invasive control of heterologous gene expression, the photorelease of the best performing cSal variant, the acidic form of DC-cSal (**5**), was analyzed after UV-A light illumination in comparison to blue light illumination, as this variant exhibits an absorption maximum at around 390 nm and thus, should be addressable by both excitation wavelengths (Figure 1). For this purpose, *P. putida* cells carrying the expression plasmid pBNTmcs-mCherry were cultivated and induction was performed using both salicylic acid and DC-cSal (**5**) (Fig. 2B). For uncaging, both UV-A light (365 nm, ~1 mW cm^{-2}) and blue light (447 nm, ~10 mW cm^{-2}) were applied. Fluorescence measurements after 20 h of cultivation revealed that the expression cultures supplemented with DC-cSal (**5**) again showed higher induction levels in comparison to salicylic acid and exhibited only a moderate instability in the absence of light. Furthermore, blue light showed to be well suited for the photorelease of DC-cSal (**5**) thus paving the way to a multichromatic induction system in combination with an additional UV-A light responsive photocage.

Multichromatic control of gene expression.

To enable a two-colored induction of gene expression in *P. putida*, the salicylic acid-responsive promoter system NagR/P_{nagAa} should be combined with a second promoter system. To this end, we chose a well-established IPTG-controlled expression system based on a LacI/P_{tac}-mediated reporter gene expression. Since we observed that uncaging of DC-cSal (**5**) was possible with both UV-A light and blue light (Figure 2B), it was of great importance to find a caging group with a hypsochromically shifted absorption maximum that can be uncaged with UV-A light exclusively to ensure a wavelength-selective uncaging process. The 2-nitrobenzyl (NB) caging group offers this feature, as it is characterized by an absorption maximum of around 260 nm (Figure 1). To combine both promoter systems, *P. putida* KT2440 cells were transformed with two expression plasmids, the pBNTmcs-mCherry plasmid allowing for NagR/P_{nagAa}-mediated expression of mCherry and the pVLT33-GFPmut3 plasmid enabling LacI/P_{tac}-mediated expression of GFPmut3 (in the following denoted as strain *P. putida*/ combi). Thus, this strain offers a two-colored expression readout when both cSal and cIPTG is added (Fig. S1, Supporting Information). Furthermore, the expression level of mCherry and GFPmut3 are comparable to strains producing only one fluorescence reporter and the chronological order of induction does not influence the fluorescence intensity. As a first step, the strain *P. putida*/ combi was characterized with respect to suitable inducer concentrations (Figure 3). For salicylic acid, concentrations between 10 µM and 1000 µM were used, while concentrations of 25 µM up to 4000 µM were tested for IPTG, since working concentrations of salicylic acid for the NagR/P_{nagAa} system are described to be lower than those of IPTG for the LacI/P_{tac} system in *Pseudomonas* sp. [22,65,68].

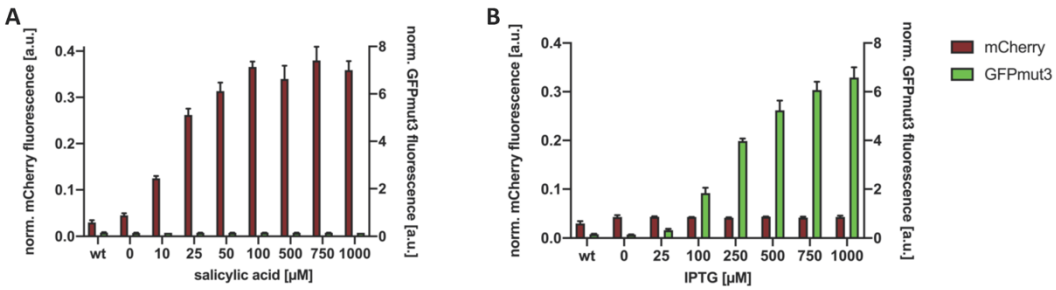

Figure 3. Induction profile of the *P. putida* strain KT2440/ combi carrying the plasmids pBNTmcs-mCherry and pVLT33-GFPmut3 for determination of sufficient inducer concentrations. **A**) *In vivo* mCherry fluorescence (λ_{ex} = 580 nm, λ_{em} = 610 nm) and GFPmut3 fluorescence (λ_{ex} = 508 nm, λ_{em} = 523 nm of *P. putida* cultures supplemented with increasing amounts of salicylic acid (Sal) is shown after 20 h of cultivation (stationary growth phase) compared to a wildtype control (wt). Induction was performed after 3 h *via* addition of 10–1000 µm Sal. **B**) *In vivo* mCherry fluorescence (λ_{ex} = 580 nm, λ_{em} = 610 nm) and GFPmut3 fluorescence (λ_{ex} = 508 nm, λ_{em} = 523 nm of *P. putida* cultures supplemented with increasing amounts of IPTG is shown after 20 h of cultivation (stationary growth phase) compared to a wildtype control (wt). Induction was performed after 3 h *via* addition of 25–4000 µm IPTG. *In vivo* fluorescence intensities were normalised to cell densities and values are means of triplicate measurements. Error bars indicate the respective standard deviations.

The comparison of resulting reporter gene fluorescence for induction with salicylic acid showed that 100 µM already leads to a complete induction of mCherry fluorescence (Figure 3A), while the induction response of GFPmut3 fluorescence increased steadily in dependence of the IPTG concentration (Figure 3B). As the use of caged inducer molecules is desired in further experiments, working concentrations should be kept as low as possible to avoid wasting elaborately synthetized compounds. Therefore, 50 µM Sal and 500 µM IPTG were used for all further experiments ensuring a sufficient induction response with simultaneous cost-effective handling of the substances. In the following, the induction strength using cSal and cIPTG derivatives under increasing exposure times was analyzed to determine the shortest possible but still sufficient exposure time. Exposure times between 1 min and 30 min and between 20 and 60 min were tested for DC-cSal (**5**) and NB-cIPTG (**4**), respectively (Figure 4).

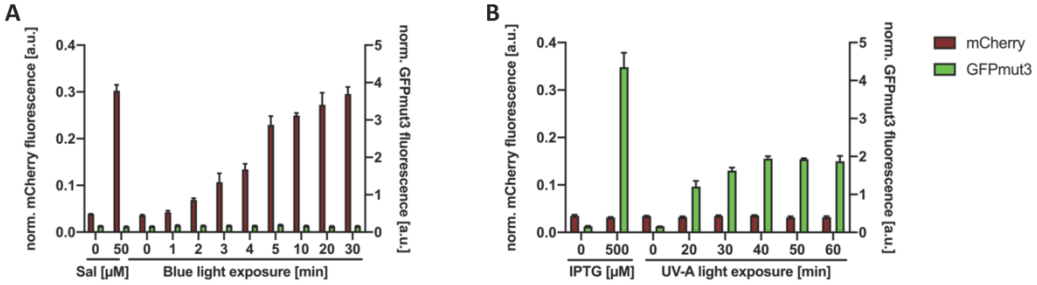

Figure 4. Determination of sufficient blue light and UV-A light exposure times for *P. putida* strain KT2440/ combi carrying the plasmids pBNTmcs-mCherry and pVLT33-GFPmut3. **A**) *In vivo* mCherry fluorescence (λ_{ex} = 580 nm, λ_{em} = 610 nm) and GFPmut3 fluorescence (λ_{ex} = 508 nm, λ_{em} = 523 nm of *P. putida* cultures containing 50 µM DC-cSal (**5**) and exposed for increasing durations with blue light (447 nm; 10 mW cm^{-2}) is shown in relation to a 50 µM salicylic acid (Sal) control after 20 h of cultivation (stationary growth phase). Induction was performed after 3 h *via* blue light exposure for 5–60 min or the addition of 50 µM conventional Sal. **B**) *In vivo* mCherry fluorescence (λ_{ex} = 580 nm, λ_{em} = 610 nm) and GFPmut3 fluorescence (λ_{ex} = 508 nm, λ_{em} = 523 nm of *P. putida* cultures containing 500 µM NB-cIPTG (**4**) and exposed for increasing durations with UV-A light (365 nm; 1 mW cm^{-2}) is shown in relation to a 500 µm IPTG control after 20 h of cultivation (stationary growth phase). Induction was performed after 3 h *via* blue light exposure for 20–60 min or the addition of 50 µM conventional Sal. *In vivo* fluorescence intensities were normalised to cell densities and values are means of triplicate measurements. Error bars indicate the respective standard deviations.

Interestingly, for DC-cSal (**5**) an exposure time of only 5 or 10 min resulted in 78% reporter gene expression in relation to an induction with 50 µM conventional Sal (Figure 4A). The UV-A light-mediated uncaging of NB-cIPTG (**4**) was completed after 40 min, but as the long-time exposure of cultures with UV-A light might have disadvantageous effects on the cells, a shortened duration of 30 min will be used instead for sufficient uncaging of over 80% (Figure 4B). The respective second fluorescence reporter signal always stayed on a constant, non-significant level, demonstrating that no crosstalk between the two systems occurred. In contrast to DC-cSal (**5**), the use of NB-cIPTG (**4**) did not lead to induction levels comparable to the positive control with conventional IPTG, which is in good agreement with our previous work using NP-cIPTG (**1**) for light-controlled induction of gene expression in *P. putida*, where this cIPTG variant only resulted in an induction response of around 40% in comparison to

conventional IPTG [22]. To exclude disadvantageous effects of the new caged inducers on cell viability, the growth of *P. putida* cells was analyzed in the presence of DC-cSal (**5**) and NB-cIPTG (**4**), as well as their corresponding photoproducts in comparison to conventional inducers. Comparative growth of all strains clearly demonstrated that neither the conventional inducer nor the caged inducer or their photoproducts lead to considerable growth impairments (Figure S2A, Supporting Information). However, when light exposed cultures were compared to cultures that were kept in the dark, a prolonged lag-phase and thus, a delayed production of the fluorescence reporters could be detected (Figure S3, Supporting Information), which might be due to an increased stress level upon exposure with two light sources. Finally, the stability of the photocaged compounds was analyzed by measuring the fluorescence intensity of cultures in the dark (Figure S2B, Supporting Information). The data clearly demonstrates a high *in vivo* stability of DC-cSal (**5**) and NB-cIPTG (**4**) over 20 h in LB medium at 30 °C.

Wavelength-selective control of gene expression.

After characterization of both caged inducer variants, their applicability for two-colored light control of gene expression was evaluated. For this purpose, the strain *P. putida*I combi was cultivated with both caged inducers and induction was performed after 3 h and 6 h using blue light (447 nm; ~10 mW cm^{-2}) and UV-A light (365 nm; ~1 mW cm^{-2}), respectively. As positive and negative controls, cultures were illuminated with only one light color each or in complete absence of light. The induction strength was analyzed by measuring the fluorescence intensity of each culture in a BioLector system in comparison to cultures supplemented with 50 µM Sal and 500 µM IPTG. As depicted in Figure 5A, both 5 and 10 min of blue light exposure led to mCherry fluorescence levels comparable to cultures supplemented with 50 µM Sal, while the following exposure with UV-A light resulted in only around 40% GFPmut3 fluorescence intensity compared to the 500 µM IPTG control.

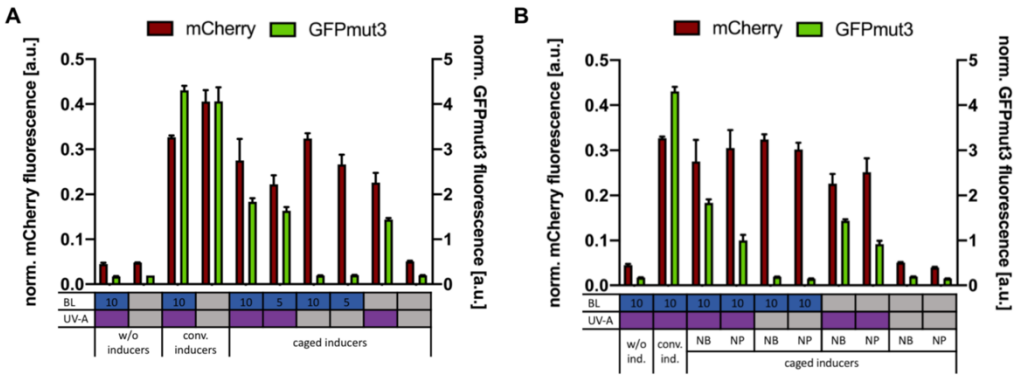

Figure 5. Two-colored induction of gene expression in the strain *P. putida*I combi carrying the plasmids pBNTmcs-mCherry and pVLT33-GFPmut3. **A**) *In vivo* mCherry fluorescence (λ_{ex} = 580 nm, λ_{em} = 610 nm) and GFPmut3 fluorescence (λ_{ex} = 508 nm, λ_{em} = 523 nm of *P. putida* cultures containing 50 µM DC-cSal (**5**) and 500 µM NB-cIPTG (**4**) is shown in relation to a 50 µM salicylic acid and 500 µM IPTG control after 25 h of cultivation (stationary

growth phase). Induction was performed after 3 h and 6 h *via* blue light (**BL**; blue box; 447 nm; 10 mW cm^{-2}) exposure for 5 or 10 min and UV-A light (**UV-A**; violet box; 365 nm; 1 mW cm^{-2}) exposure for 30 min, respectively, or the addition of 50 µM Sal and 500 µM IPTG (**conv. inducers**). **B**) *In vivo* mCherry fluorescence (λ_{ex} = 580 nm, λ_{em} = 610 nm) and GFPmut3 fluorescence (λ_{ex} = 508 nm, λ_{em} = 523 nm) of *P. putida* cultures containing 50 µM DC-cSal (**5**) and 500 µM NB-cIPTG (**4**, **NB**) or NP-cIPTG (**1**, **NP**) is shown in relation to a 50 µM salicylic acid (Sal) and 500 µM IPTG control after 25 h of cultivation (stationary growth phase). Induction was performed after 3 h and 6 h *via* blue light (**BL**; blue box; 447 nm; 10 mW cm^{-2}) exposure for 10 min and UV-A light (**UV-A**; violet box; 365 nm; 1 mW cm^{-2}) exposure for 30 min, respectively, or the addition of 50 µM Sal and 50 µM IPTG (**conv. ind.**). Light exposure is indicated by a colored box, while the absence of exposure is illustrated by a grey box. The exposure times for blue light are represented by the respective number of minutes annotated in each box. *In vivo* fluorescence intensities were normalized to cell densities and values are means of triplicate measurements. Error bars indicate the respective standard deviations.

Furthermore, exclusive blue light exposure for 5 or 10 min did not lead to a substantial GFPmut3 signal, which shows that NB-cIPTG (**4**) is not addressed by blue light. In contrast, an exclusive UV-A light exposure for 30 min resulted in a distinct mCherry fluorescence signal of around 70% compared to an induction with salicylic acid. These results underline that a two-colored control of reporter gene expression is possible using DC-cSal (**5**) and NB-cIPTG (**4**). However, it is of great relevance to use a defined illumination order, as DC-cIPTG (**5**) is also addressable by UV-A light. As an alternative to NB-cIPTG (**4**), we also tested the well-established NP-cIPTG (**1**), which offers a higher extinction coefficient and a bathochromatically shifted absorption maximum of around 336 nm [22]. Analysis of GFPmut3 reporter fluorescence after illumination revealed a decreased induction level for NP-cIPTG (**1**) in comparison to NB-cIPTG (**4**) of around 50%, even though a good stability under blue light could also be detected for NP-cIPTG (**1**) (Figure 5B). Thus, NB-cIPTG (**4**) proved to be a sufficient inducer in combination with DC-cSal (**5**), exhibiting a substantial inducibility upon UV-A light exposure, while sufficient compound stability could be detected under blue light illumination as well as in unexposed culture.

Multichromatic gene expression for rhamnolipid production.

As a proof of concept, the multichromatic control of gene expression was transferred to the biosynthesis of rhamnolipids. These compounds are microbial biosurfactants naturally produced by *Pseudomonas aeruginosa* or *Burkholderia* species [74–77], which aim to replace synthetical surfactants in fields of biotechnology and industrial applications [78,79]. The production of bio-based, recombinant rhamnolipids has several advantages, including the use of biosafety-certified production strains, the use of raw or waste materials as feedstock or their bio-degradability [80,81]. Rhamnolipids are commonly composed of one (mono-rhamnolipids; mRL) or two (di-rhamnolipids; dRL) rhamnose molecules linked through a β-glycosidic bond to up to three 3-hydroxyfatty acids with various chain lengths [58,82]. The heterologous production of rhamnolipids in biosafety organisms such as *P. putida* is realized by transferring the biosynthesis operon *rhlABC* from a native rhamnolipid producer to the desired production strain and results in the biosynthesis of complex rhamnolipid mixtures with considerable yields [82–84]. The rhamnolipid biosynthesis is composed of three sequential reactions, starting with

the formation of 3-(hydroxyalkanoyloxy)alkanoic acid (HAA) from two activated 3-hydroxyacyl molecules (HFA) and its subsequent conversion to mRL performed by two enzymes encoded by the genes *rhlAB*. In the last reaction, an enzyme encoded by *rhlC* performs the conversion of mRL to dRL [85,86]. However, as each mixture features different physico-chemical characteristics, the production of tailor-made biosurfactants composed of purposely adjusted congener compositions is of great interest for various industrial applications [58]. Thus, we here applied the multichromatic optogenetic system to specifically address relevant steps within the mono- and di-rhamnolipid biosynthesis offering the possibility to individually adjust both product levels. For this purpose, the previously constructed mono-rhamnolipid-producing *P. putida* strain SK40 was used [84]. This strain harbors the relevant biosynthesis genes for mono-rhamnolipid production from *P. aeruginosa* PAO1, namely *rhlAB*, as well as the fluorescence reporter gene *eyfp* under the control of the salicylic acid-responsive NagR/P_{nagAa} promoter system, integrated into its chromosome. Additionally, the strain carries the plasmid pVLT33-rhlC harboring the *rhlC* gene from *P. aeruginosa* PAO1 for conversion of mono- to di-rhamnolipids under control of a IPTG-responsive LacI/P_{tac} promoter system [82], in the following denoted as SK40/ *rhlC* (Figure 6A).

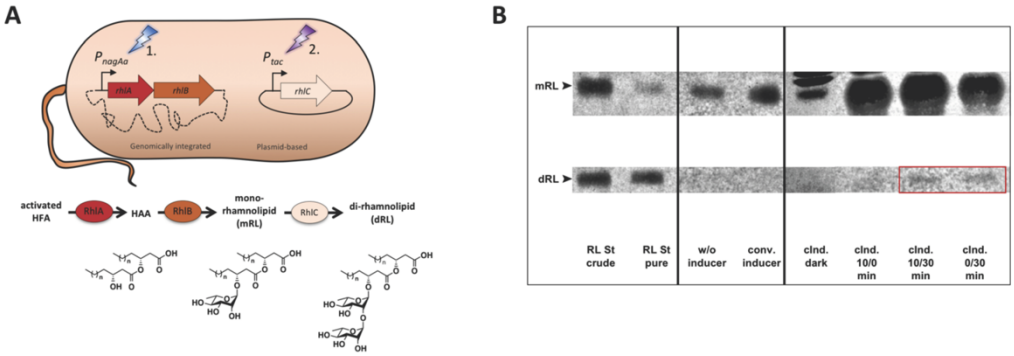

Figure 6. Wavelength-selective induction of rhamnolipid production in *P. putida*. **A**) The *P. putida* strain SK40/ *rhlC* carries the genes *rhlAB* responsible for mono-rhamnolipid (mRL) production under the control the NagR/P_{nagAa} promoter system on its chromosome and the plasmid pVLT33-rhlC harboring the gene *rhlC* under control of the LacI/P_{tac} promoter system responsible for conversion of mRL to di-rhamnolipids (dRL). **B**) α-naphthol stained TLC plate of ethanol extracts obtained from culture supernatants from *P. putida* SK40/ *rhlC* in comparison to a crude and a purified rhamnolipid standard (RL St crude/ pure) and to an uninduced culture (w/o inducer). Cultures were supplemented with 50 µM salicylic acid and 500 µM IPTG (conv. inducer) or 50 µM DC-cSal (**5**) and 500 µM NB-cIPTG (**4**) (cInd.) and grown over 48 h in LB medium +10% glucose (w/v) at 30°C and 1200 rpm. Induction of mRL production was performed after 3.5 h using blue light exposure at 447 nm (~10 mW cm^{-2}) for 10 min or addition of 50 µM conventional salicylic acid and dRL production was induced after 18 h using UV-A light exposure at 365 nm (~1 mW cm^{-2}) for 30 min or the addition of 500 µM conventional IPTG. HFA: hydroxy fatty acids; HAA: 3-(hydroxyalkanoyloxy)alkanoic acid; mRL: mono-rhamnolipids; dRL: di-rhamnolipids.

The *P. putida* strain SK40/ *rhlC* was cultivated in LB-medium with 10% glucose over 48 h in a BioLector system and induction of mRL production was performed after 3.5 h using blue light exposure at 447 nm (~10 mW cm^{-2}) for 10 min or addition of salicylic acid. After 18 h, dRL production was induced using UV-A light exposure at 365 nm (~1 mW cm^{-2}) for 30 min or

addition of IPTG. Rhamnolipid mixtures were analyzed after 48 h of cultivation (late stationary growth phase) with respect to their congener composition using TLC (Figure 6B). Interestingly, strong mRL bands could be detected for cultures supplemented with cSal, indicating even higher mRL production titers in comparison to an induction with salicylic acid. In samples of cultures that were illuminated with blue and UV-A light, both mRL and dRL production could be detected. However, the dRL bands were relatively weak, so that further measurements for quantification, such as TLC with coupled ESI-MS measurements, need to be performed as a final step.

Chapters not yet included in this manuscript: final quantification of rhamnose titers using TLC-ESI-MS, and the conclusion.

Methods

Bacterial strains and plasmids: The *E. coli* strain DH5α [87] was used for cloning procedures and the strain *P. putida* KT2440 was used for expression studies. All bacterial strains were grown on LB agar plates or in liquid LB medium (Luria/Miller, Carl Roth®) at 37°C for *E. coli* and at 30°C for *P. putida* if not stated otherwise. All media were supplemented with kanamycin (50 µg mL^{-1} for *E. coli* and 25 µg mL^{-1} for *P. putida)* or gentamicin (25 µg mL^{-1} for *P. putida)* for strain maintenance if appropriate.
All bacterial strains and plasmids used in this study are listed in Table S1, Supporting Information.
Plasmid construction: All recombinant DNA techniques were conducted in accordance with Sambrook *et al*. [88]. For construction of the expression vector pBNTmcs-mCherry-Gm, which offers a salicylic acid-mediated expression of the *mcherry* reporter gene under the control of the P_{nagAa} promoter, the In-Fusion® HD Cloning Plus kit (Takara Bio Europe, St Germain en Laye, France) was applied. The previously described plasmid pBNTmcs-mCherry-Km [73] was amplified using oligos 1 and 2 (Table S1, Supporting Information). Additionally, the *mcherry* reporter gene was amplified *via* PCR using oligos 3 and 4 (containing homologous sequences suitable for integration into the amplified pBNTmcs-mCherry plasmid backbone) and the plasmid pJT'Tmcs-mCherry [89]. Finally, both fragments were assembled using the In-Fusion® cloning reaction mix as indicated by the supplier gaining the plasmid pBNTmcs-mCherry-Gm. Correct nucleotide sequences of all constructs were confirmed by Sanger sequencing (Eurofins Genomics, Germany).

Expression cultures for novel cSal variants: All *P. putida* cultures were grown in 48-well Flowerplates® in a ThermoMixer C (Eppendorf, Germany) (800 µL LB medium, 1200 rpm,

30°C) in the dark for 20 h and were previously inoculated with a cell density corresponding to an optical density of 0.05 at 600 nm. If not stated otherwise, induction was performed after 3 h by blue light exposure at 447 nm (~10 mW cm^{-2}) for 10 min, UV-A light exposure at 365 nm (~1 mW cm^{-2}) for 30 min or the addition of respective amounts of salicylic acid. *In vivo* mCherry fluorescence intensities were determined using a Tecan Microplate Reader (λ_{ex} = 580 nm, λ_{em} = 610 nm), normalized to cell densities and are shown in relation to the respective fluorescence intensities of a culture induced with salicylic acid.

Expression cultures for multichromatic light control: All *P. putida* cultures were grown in 48-well Flowerplates® in a ThermoMixer C (Eppendorf, Germany) (800 µL LB medium, 1200 rpm, 30°C) in the dark for 25 h and were previously inoculated with a cell density corresponding to an optical density of 0.05 at 600 nm. If not stated otherwise, induction was performed after 3 h by blue light exposure at 447 nm (~10 mW cm^{-2}) for 5 or 10 min and after 6 h by UV-A light exposure at 365 nm (~1 mW cm^{-2}) for 30 min or the addition of respective amounts of salicylic acid and IPTG. *In vivo* GFPmut3 *and* mCherry fluorescence intensities were determined using a Tecan Microplate Reader (λ_{ex} = 508 nm, λ_{em} = 523 nm ,λ_{ex} = 580 nm, λ_{em} = 610 nm, respectively), normalized to cell densities and are shown in relation to the respective fluorescence intensities of a culture induced with salicylic acid and IPTG.

Expression cultures for rhamnolipid production: All *P. putida* cultures were grown in 48-well Flowerplates® in a BioLector microbioreactor system (m2p-labs, Baesweiler, Germany) (800 µL LB medium+10% glucose (w/v), 1200 rpm, 30°C) in the dark for 25 h and were previously inoculated with a cell density corresponding to an optical density of 0.05 at 600 nm. Induction was performed after 3.5 h by blue light exposure at 447 nm (~10 mW cm^{-2}) for 10 min or the addition of 50 µM salicylic acid. After 18 h, the second induction was performed by UV-A light exposure at 365 nm (~1 mW cm^{-2}) for 30 min or the addition of 500 µM IPTG.

Extraction and TLC analysis of rhamnolipids (according to [80]): After cultivation, the cell suspension of each well was centrifuged and 500 µL supernatant was collected. It was extracted with 500 µL ethyl acetate for three times and the solvent phases were combined and evaporated at 60°C under reduced pressure. Subsequently, extracts were solved in 10 µL ethanol and stored at 4°C until analysis. For TLC analysis, ethanol extracts were spot several times on ALUGRAM® SIL G/UV254 plates (Macherey-Nagel, Düren, Germany) and developed in chloroform: methanol: acetic acid (65:15:2 (v/v/v)). After the plate was dried, it was homogeneously covered with a detection solution (0.15 g orcinol, 42 mL deionized water, 8.4 mL H_2SO_4 (60%, v/v)) using a TLC sprayer (CAMAG AG & Co. GmbH, Muttenz, Switzerland) and heated up to 110°C until the spots were visible. The TLC plate was analyzed using a CAMAG TLC® Visualizer 2 (CAMAG AG & Co. GmbH, Muttenz, Switzerland).

Determination of uncaging half-life times: A 1 mM solution of NB-cIPTG (**4**) in MeOH/H_2O 30:70 and of DC-cSal (**5**) in sodium phosphate buffer (100 mM, pH = 7.4) was prepared. Each solution (1 mL) was filled in a cuvette and was irradiated at room temperature using the LUMOS 43 (375 nm or 430 nm) for a definite time. Following this, the sample was analysed by reversed-phase HPLC Jasco HPLC system [column: Hyperclone 5 µ ODS (C18) 120 (Phenomenex)]. The procedure was repeated for different irradiation times and the decrease of concentration was measured by an UV detector [72].

References

1. Zhou, S.; Du, G.; Kang, Z.; Li, J.; Chen, J.; Li, H.; Zhou, J. The application of powerful promoters to enhance gene expression in industrial microorganisms. *World J. Microbiol. Biotechnol.* **2017**, *33*, 23, doi:10.1007/s11274-016-2184-3.
2. Lee, J.-Y.; Na, Y.-A.; Kim, E.; Lee, H.-S.; Kim, P. The Actinobacterium *Corynebacterium glutamicum*, an industrial workhorse. *J. Microbiol. Biotechnol.* **2016**, *26*, 807–822, doi:10.4014/jmb.1601.01053.
3. Song, A.A.-L.; In, L.L.A.; Lim, S.H.E.; Rahim, R.A. A review on *Lactococcus lactis*: from food to factory. *Microb. Cell Fact.* **2017**, *16*, 55, doi:10.1186/s12934-017-0669-x.
4. Vickers, C.E.; Williams, T.C.; Peng, B.; Cherry, J. Recent advances in synthetic biology for engineering isoprenoid production in yeast. *Curr. Opin. Chem. Biol.* **2017**, *40*, 47–56, doi:10.1016/j.cbpa.2017.05.017.
5. Johnson, T.J.; Gibbons, J.L.; Gu, L.; Zhou, R.; Gibbons, W.R. Molecular genetic improvements of cyanobacteria to enhance the industrial potential of the microbe: A review. *Biotechnol. Prog.* **2016**, *32*, 1357–1371, doi:10.1002/btpr.2358.
6. Lynch, M.; Marinov, G.K. The bioenergetic costs of a gene. *Proc. Natl. Acad. Sci. U. S. A.* **2015**, doi:10.1073/pnas.1514974112.
7. Qian, Y.; Huang, H.H.; Jiménez, J.I.; Del Vecchio, D. Resource competition shapes the response of genetic circuits. *ACS Synth. Biol.* **2017**, doi:10.1021/acssynbio.6b00361.
8. Weiße, A.Y.; Oyarzún, D.A.; Danos, V.; Swain, P.S. Mechanistic links between cellular trade-offs, gene expression, and growth. *Proc. Natl. Acad. Sci. U. S. A.* **2015**, doi:10.1073/pnas.1416533112.
9. Kurland, C.G.; Dong, H. Bacterial growth inhibition by overproduction of protein. *Mol. Microbiol.* 1996.
10. Cardinale, S.; Arkin, A.P. Contextualizing context for synthetic biology - identifying causes of failure of synthetic biological systems. *Biotechnol. J.* 2012.
11. Terpe, K. Overview of bacterial expression systems for heterologous protein production: from molecular and biochemical fundamentals to commercial systems. *Appl. Microbiol. Biotechnol.* **2006**, *72*, 211–222, doi:10.1007/s00253-006-0465-8.
12. Balzer, S.; Kucharova, V.; Megerle, J.; Lale, R.; Brautaset, T.; Valla, S. A comparative analysis of the properties of regulated promoter systems commonly used for recombinant gene expression in *Escherichia coli*. *Microb. Cell Fact.* **2013**, *12*, 1–14, doi:10.1186/1475-2859-12-26.
13. Wandrey, G.; Bier, C.; Binder, D.; Hoffmann, K.; Jaeger, K.-E.; Pietruszka, J.; Drepper, T.; Büchs, J. Light-induced gene expression with photocaged IPTG for induction profiling in a high-throughput screening system. *Microb. Cell Fact.* **2016**, *15*, 63, doi:10.1186/s12934-016-0461-3.
14. Liu, Z.; Zhang, J.; Jin, J.; Geng, Z.; Qi, Q.; Liang, Q. Programming bacteria with light—sensors and applications in synthetic biology. *Front. Microbiol.* **2018**, *9*, doi:10.3389/fmicb.2018.02692.
15. Lalwani, M.A.; Ip, S.S.; Carrasco-López, C.; Day, C.; Zhao, E.M.; Kawabe, H.; Avalos, J.L. Optogenetic control of the *lac* operon for bacterial chemical and protein production. *Nat. Chem.*

Biol. **2020**, doi:10.1038/s41589-020-0639-1.

16. Castillo-Hair, S.M.; Baerman, E.A.; Fujita, M.; Igoshin, O.A.; Tabor, J.J. Optogenetic control of *Bacillus subtilis* gene expression. *Nat. Commun.* **2019**, *10*, 3099, doi:10.1038/s41467-019-10906-6.

17. Liu, Q.; Tucker, C.L. Engineering genetically-encoded tools for optogenetic control of protein activity. *Curr. Opin. Chem. Biol.* **2017**, *40*, 17–23, doi:10.1016/j.cbpa.2017.05.001.

18. Hartmann, D.; Smith, J.M.; Mazzotti, G.; Chowdhry, R.; Booth, M.J. Controlling gene expression with light: a multidisciplinary endeavour. *Biochem. Soc. Trans.* **2020**, *48*, 1645–1659, doi:10.1042/BST20200014.

19. Binder, D.; Frohwitter, J.; Mahr, R.; Bier, C.; Grünberger, A.; Loeschcke, A.; Peters-Wendisch, P.; Kohlheyer, D.; Pietruszka, J.; Frunzke, J.; et al. Light-controlled cell factories: Employing photocaged isopropyl-β-D-thiogalactopyranoside for light-mediated optimization of *lac*-based gene expression and (+)-valencene biosynthesis in *Corynebacterium glutamicum*. *Appl. Environ. Microbiol.* **2016**, doi:10.1128/AEM.01457-16.

20. Kusen, P.M.; Wandrey, G.; Probst, C.; Grünberger, A.; Holz, M.; Meyer zu Berstenhorst, S.; Kohlheyer, D.; Büchs, J.; Pietruszka, J. Optogenetic regulation of tunable gene expression in yeast using photo-labile caged methionine. *ACS Chem. Biol.* **2016**, *11*, 2915–2922, doi:10.1021/acschembio.6b00462.

21. Kusen, P.M.; Wandrey, G.; Krewald, V.; Holz, M.; Berstenhorst, S.M. zu; Büchs, J.; Pietruszka, J. Light-controlled gene expression in yeast using photocaged Cu^{2+}. *J. Biotechnol.* **2017**, *258*, 117–125, doi:10.1016/j.jbiotec.2017.04.032.

22. Hogenkamp, F.; Hilgers, F.; Knapp, A.; Klaus, O.; Bier, C.; Binder, D.; Jaeger, K.-E.; Drepper, T.; Pietruszka, J. Effect of photocaged isopropyl β-D-1-thiogalactopyranoside solubility on the light responsiveness of LacI-controlled expression systems in different bacteria. *ChemBioChem* **2021**, *22*, 539–547, doi:10.1002/cbic.202000377.

23. Gorka, A.P.; Yamamoto, T.; Zhu, J.; Schnermann, M.J. Cyanine photocages enable spatial control of inducible Cre-mediated recombination. *ChemBioChem* **2018**, *19*, 1239–1243, doi:10.1002/cbic.201800061.

24. Zhang, W.; Hamouri, F.; Feng, Z.; Aujard, I.; Ducos, B.; Ye, S.; Weiss, S.; Volovitch, M.; Vriz, S.; Jullien, L.; et al. Control of protein activity and gene expression by cyclofen-OH uncaging. *ChemBioChem* **2018**, *19*, 1232–1238, doi:10.1002/cbic.201700630.

25. Levskaya, A.; Chevalier, A.A.; Tabor, J.J.; Simpson, Z.B.; Lavery, L.A.; Levy, M.; Davidson, E.A.; Scouras, A.; Ellington, A.D.; Marcotte, E.M.; et al. Synthetic biology: engineering *Escherichia coli* to see light. *Nature* **2005**, *438*, 441–2, doi:10.1038/nature04405.

26. Möglich, A.; Ayers, R.A.; Moffat, K. Design and signaling mechanism of light-regulated histidine kinases. *J. Mol. Biol.* **2009**, *385*, 1433–44, doi:10.1016/j.jmb.2008.12.017.

27. Shimizu-Sato, S.; Huq, E.; Tepperman, J.M.; Quail, P.H. A light-switchable gene promoter system. *Nat. Biotechnol.* **2002**, doi:10.1038/nbt734.

28. Brieke, C.; Rohrbach, F.; Gottschalk, A.; Mayer, G.; Heckel, A. Light-controlled tools. *Angew. Chemie - Int. Ed.* **2012**, *51*, 8446–76, doi:10.1002/anie.201202134.

29. Hansen, M.J.; Velema, W.A.; Lerch, M.M.; Szymanski, W.; Feringa, B.L. Wavelength-selective cleavage of photoprotecting groups: strategies and applications in dynamic systems. *Chem. Soc. Rev.* **2015**, *44*, 3358–3377, doi:10.1039/C5CS00118H.

30. Klán, P.; Šolomek, T.; Bochet, C.G.; Blanc, A.; Givens, R.; Rubina, M.; Popik, V.; Kostikov, A.; Wirz, J. Photoremovable protecting groups in chemistry and biology: reaction mechanisms and efficacy. *Chem. Rev.* **2013**, *113*, 119–191, doi:10.1021/cr300177k.

31. Ajikumar, P.K.; Xiao, W.-H.; Tyo, K.E.J.; Wang, Y.; Simeon, F.; Leonard, E.; Mucha, O.; Phon, T.H.; Pfeifer, B.; Stephanopoulos, G. Isoprenoid pathway optimization for taxol precursor overproduction in *Escherichia coli*. *Science.* **2010**, *330*, 70–74, doi:10.1126/science.1191652.

32. Tabor, J.J.; Levskaya, A.; Voigt, C. a Multichromatic control of gene expression in *Escherichia coli*. *J Mol Biol* **2011**, *405*, 315–324, doi:10.1016/j.jmb.2010.10.038.

33. Schmidl, S.R.; Sheth, R.U.; Wu, A.; Tabor, J.J. Refactoring and optimization of light-switchable *Escherichia coli* two-component systems. *ACS Synth. Biol.* **2014**, *3*, 820–831, doi:10.1021/sb500273n.

34. Olson, E.J.; Hartsough, L.A.; Landry, B.P.; Shroff, R.; Tabor, J.J. Characterizing bacterial gene circuit dynamics with optically programmed gene expression signals. *Nat. Methods* **2014**, *11*, 449–55, doi:10.1038/nmeth.2884.

35. Fernandez-Rodriguez, J.; Moser, F.; Song, M.; Voigt, C.A. Engineering RGB color vision into *Escherichia coli*. *Nat. Chem. Biol.* **2017**, *13*, 706–708, doi:10.1038/nchembio.2390.

36. Stegmaier, P.; Alonso, J.M.; Del Campo, A. Photoresponsive surfaces with two independent wavelength-selective functional levels. *Langmuir* **2008**, *24*, 11872–11879, doi:10.1021/la802052u.

37. San Miguel, V.; Bochet, C.G.; Del Campo, A. Wavelength-selective caged surfaces: How many functional levels are possible? *J. Am. Chem. Soc.* **2011**, *133*, 5380–5388, doi:10.1021/ja110572j.

38. Amatrudo, J.M.; Olson, J.P.; Agarwal, H.K.; Ellis-Davies, G.C.R. Caged compounds for multichromic optical interrogation of neural systems. *Eur. J. Neurosci.* 2015, *41*, 5–16.

39. Stanton-Humphreys, M.N.; Taylor, R.D.T.; Mc Dougall, C.; Hart, M.L.; Brown, C.T.A.; Emptage, N.J.; Conway, S.J. Wavelength-orthogonal photolysis of neurotransmitters *in vitro*. *Chem. Commun.* **2012**, *48*, 657–659, doi:10.1039/c1cc15135e.

40. Wu, M.; Lin, X.; Tan, X.; Li, J.; Wei, Z.; Zhang, D.; Zheng, Y.; Zheng, A.; Zhao, B.; Zeng, Y.; et al. Photoresponsive nanovehicle for two ondependent wavelength light-triggered sequential release of P-gp shRNA and doxorubicin to optimize and enhance synergistic therapy of multidrug-resistant cancer. *ACS Appl. Mater. Interfaces* **2018**, *10*, 19416–19427, doi:10.1021/acsami.8b03823.

41. Yamazoe, S.; Liu, Q.; McQuade, L.E.; Deiters, A.; Chen, J.K. Sequential gene silencing using wavelength-selective caged morpholino oligonucleotides. *Angew. Chemie Int. Ed.* **2014**, *53*, 10114–10118, doi:10.1002/anie.201405355.

42. Priestman, M.A.; Sun, L.; Lawrence, D.S. Dual wavelength photoactivation of cAMP-and cGMP-dependent protein kinase signaling pathways. *ACS Chem. Biol* **2011**, *6*, 377–384, doi:10.1021/cb100398e.

43. Velema, W.A.; van der Berg, J.P.; Szymanski, W.; Driessen, A.J.M.; Feringa, B.L. Orthogonal control of antibacterial activity with light. *ACS Chem. Biol.* **2014**, *9*, 1969–1974, doi:10.1021/cb500313f.

44. Fournier, L.; Gauron, C.; Xu, L.; Aujard, I.; Le Saux, T.; Gagey-Eilstein, N.; Maurin, S.; Dubruille, S.; Baudin, J.B.; Bensimon, D.; et al. A blue-absorbing photolabile protecting group for *in vivo* chromatically orthogonal photoactivation. *ACS Chem. Biol.* **2013**, *8*, 1528–1536, doi:10.1021/cb400178m.

45. Zhang, D.; Jin, S.; Piao, X.; Devaraj, N.K. Multiplexed photoactivation of mRNA with single-cell resolution. *ACS Chem. Biol.* **2020**, *15*, 1773–1779, doi:10.1021/acschembio.0c00205.

46. Bochet, C.G. Orthogonale Photolyse von Schutzgruppen. *Angew. Chemie* **2001**, *113*, 2140–2142, doi:10.1002/1521-3757(20010601)113:11<2140::AID-ANGE2140>3.0.CO;2-R.

47. Blanc, A.; Bochet, C.G. Wavelength-controlled orthogonal photolysis of protecting groups. *J. Org. Chem.* **2002**, *67*, 5567–5577, doi:10.1021/jo025837m.

48. Olson, J.P.; Banghart, M.R.; Sabatini, B.L.; Ellis-Davies, G.C.R. Spectral evolution of a photochemical protecting group for orthogonal two-color uncaging with visible light. *J. Am. Chem. Soc.* **2013**, *135*, 15948–15954, doi:10.1021/ja408225k.

49. Ramos, J.L.; Duque, E.; Huertas, M.J.; Haidour, A. Isolation and expansion of the catabolic potential of a *Pseudomonas putida* strain able to grow in the presence of high concentrations of aromatic hydrocarbons. *J. Bacteriol.* **1995**, doi:10.1128/jb.177.14.3911-3916.1995.

50. Simon, O.; Klaiber, I.; Huber, A.; Pfannstiel, J. Comprehensive proteome analysis of the response of *Pseudomonas putida* KT2440 to the flavor compound vanillin. *J. Proteomics* **2014**, *109*, 212–227, doi:10.1016/j.jprot.2014.07.006.

588 51. Akkaya, Ö.; Pérez-Pantoja, D.R.; Calles, B.; Nikel, P.I.; de Lorenzo, V. The metabolic redox
589 regime of *Pseudomonas putida* tunes its evolvability toward novel xenobiotic substrates. *MBio*
590 **2018**, doi:10.1128/mBio.01512-18.

591 52. Fernández, M.; Conde, S.; de la Torre, J.; Molina-Santiago, C.; Ramos, J.-L.; Duque, E.
592 Mechanisms of resistance to chloramphenicol in *Pseudomonas putida* KT2440. *Antimicrob.*
593 *Agents Chemother.* **2012**, *56*, 1001–1009, doi:10.1128/AAC.05398-11.

594 53. Chavarría, M.; Nikel, P.I.; Pérez-Pantoja, D.; de Lorenzo, V. The Entner-Doudoroff pathway
595 empowers *Pseudomonas putida* KT2440 with a high tolerance to oxidative stress. *Environ.*
596 *Microbiol.* **2013**, *15*, 1772–1785, doi:10.1111/1462-2920.12069.

597 54. Tiso, T.; Wierckx, N.; Blank, L.M. Non-Pathogenic *Pseudomonas* as platform for industrial
598 biocatalysis. In *Industrial Biocatalysis*; 2014 ISBN 9789814463898.

599 55. Nikel, P.I.; de Lorenzo, V. *Pseudomonas putida* as a functional chassis for industrial biocatalysis:
600 From native biochemistry to trans-metabolism. *Metab. Eng.* 2018.

601 56. Franden, M.A.; Jayakody, L.N.; Li, W.-J.; Wagner, N.J.; Cleveland, N.S.; Michener, W.E.; Hauer,
602 B.; Blank, L.M.; Wierckx, N.; Klebensberger, J.; et al. Engineering *Pseudomonas putida* KT2440
603 for efficient ethylene glycol utilization. *Metab. Eng.* **2018**, *48*, 197–207,
604 doi:10.1016/j.ymben.2018.06.003.

605 57. Kohlstedt, M.; Starck, S.; Barton, N.; Stolzenberger, J.; Selzer, M.; Mehlmann, K.; Schneider, R.;
606 Pleissner, D.; Rinkel, J.; Dickschat, J.S.; et al. From lignin to nylon: Cascaded chemical and
607 biochemical conversion using metabolically engineered *Pseudomonas putida*. *Metab. Eng.* **2018**,
608 *47*, 279–293, doi:10.1016/j.ymben.2018.03.003.

609 58. Tiso, T.; Zauter, R.; Tulke, H.; Leuchtle, B.; Li, W.-J.; Behrens, B.; Wittgens, A.; Rosenau, F.;
610 Hayen, H.; Blank, L.M. Designer rhamnolipids by reduction of congener diversity: production and
611 characterization. *Microb. Cell Fact.* **2017**, *16*, 225, doi:10.1186/s12934-017-0838-y.

612 59. Martínez-García, E.; de Lorenzo, V. *Pseudomonas putida* in the quest of programmable
613 chemistry. *Curr. Opin. Biotechnol.* **2019**, *59*, 111–121, doi:10.1016/j.copbio.2019.03.012.

614 60. Loeschcke, A.; Thies, S. Engineering of natural product biosynthesis in *Pseudomonas putida*.
615 *Curr. Opin. Biotechnol.* 2020.

616 61. Incha, M.R.; Thompson, M.G.; Blake-Hedges, J.M.; Liu, Y.; Pearson, A.N.; Schmidt, M.; Gin,
617 J.W.; Petzold, C.J.; Deutschbauer, A.M.; Keasling, J.D. Leveraging host metabolism for
618 bisdemethoxycurcumin production in *Pseudomonas putida*. *Metab. Eng. Commun.* **2020**, *10*,
619 e00119, doi:10.1016/j.mec.2019.e00119.

620 62. Hilgers, F.; Hogenkamp, F.; Klaus, O.; Kruse, L.; Lappe, A.; Loeschcke, A.; Bier, C.; Binder, D.;
621 Jaeger, K.-E.; Pietruszka, J.; et al. Photocaged inducers for the non-invasive light control of
622 production processes in the phototrophic bacterium *Rhodobacter capsulatus*. *PLOS One* **2021**
623 ***under revision***.

624 63. Hüsken, L.E.; Beeftink, R.; de Bont, J.A.M.; Wery, J. High-rate 3-methylcatechol production in
625 *Pseudomonas putida* strains by means of a novel expression system. *Appl. Microbiol. Biotechnol.*
626 **2001**, *55*, 571–577, doi:10.1007/s002530000566.

627 64. Meijnen, J.-P.; de Winde, J.H.; Ruijssenaars, H.J. Engineering *Pseudomonas putida* S12 for
628 efficient utilization of D-xylose and L-arabinose. *Appl. Environ. Microbiol.* **2008**, *74*, 5031–5037,
629 doi:10.1128/AEM.00924-08.

630 65. Verhoef, S.; Ballerstedt, H.; Volkers, R.J.M.; de Winde, J.H.; Ruijssenaars, H.J. Comparative
631 transcriptomics and proteomics of p-hydroxybenzoate producing *Pseudomonas putida* S12:
632 novel responses and implications for strain improvement. *Appl. Microbiol. Biotechnol.* **2010**, *87*,
633 679–690, doi:10.1007/s00253-010-2626-z.

634 66. Meijnen, J.-P.; Verhoef, S.; Briedjlal, A.A.; de Winde, J.H.; Ruijssenaars, H.J. Improved p-
635 hydroxybenzoate production by engineered *Pseudomonas putida* S12 by using a mixed-
636 substrate feeding strategy. *Appl. Microbiol. Biotechnol.* **2011**, *90*, 885–893, doi:10.1007/s00253-
637 011-3089-6.

638 67. Wierckx, N.J.P.; Ballerstedt, H.; de Bont, J.A.M.; Wery, J. Engineering of solvent-tolerant
639 *Pseudomonas putida* S12 for bioproduction of phenol from glucose. *Appl. Environ. Microbiol.*

2005, *71*, 8221–8227, doi:10.1128/AEM.71.12.8221-8227.2005.

68. Lenzen, C.; Wynands, B.; Otto, M.; Bolzenius, J.; Mennicken, P.; Blank, L.M.; Wierckx, N. High-yield production of 4-hydroxybenzoate from glucose or glycerol by an engineered *Pseudomonas taiwanensis* VLB120. *Front. Bioeng. Biotechnol.* **2019**, *7*, doi:10.3389/fbioe.2019.00130.

69. Lee, J.H.; Mitchell, R.J.; Gu, M.B. Chemical-specific continuous biomonitoring using a recombinant bioluminescent bacterium DNT5 (*nagR-nagAa::luxCDABE*). *J. Biotechnol.* **2007**, doi:10.1016/j.jbiotec.2007.06.020.

70. Binder, D.; Grünberger, A.; Loeschcke, A.; Probst, C.; Bier, C.; Pietruszka, J.; Wiechert, W.; Kohlheyer, D.; Jaeger, K.-E.; Drepper, T. Light-responsive control of bacterial gene expression: Precise triggering of the *lac* promoter activity using photocaged IPTG. *Integr. Biol.* **2014**, *6*, 755–765, doi:10.1039/c4ib00027g.

71. Binder D, Bier C, Grünberger A, Drobietz D, Hage-Hülsmann J, Wandrey G, et al. Photocaged arabinose: A novel optogenetic switch for rapid and gradual control of microbial gene expression. *ChemBioChem*. **2016**;*17*: 296–299. doi:10.1002/cbic.201500609

72. Bier, C.; Binder, D.; Drobietz, D.; Loeschcke, A.; Drepper, T.; Jaeger, K.-E.; Pietruszka, J. Photocaged carbohydrates: versatile tools for controlling gene expression by light. *Synthesis (Stuttg).* **2016**, *49*, 42–52, doi:10.1055/s-0035-1562617.

73. Hogenkamp, F.; Hilgers, F.; Bitzenhofer, N.L.; Ophoven, V.; Haase, M.; Bier, C.; Binder, D.; Jaeger, K.-E.; Drepper, T.; Pietruszka, J. Photocaged compounds for controlling bacterial gene expression – challenges, solutions, and surprising observations. *ChemBioChem* **2021 *ready for submission***.

74. Müller, M.M.; Hörmann, B.; Kugel, M.; Syldatk, C.; Hausmann, R. Evaluation of rhamnolipid production capacity of *Pseudomonas aeruginosa* PAO1 in comparison to the rhamnolipid over-producer strains DSM 7108 and DSM 2874. *Appl. Microbiol. Biotechnol.* **2011**, *89*, 585–592, doi:10.1007/s00253-010-2901-z.

75. Tavares, L.F.D.; Silva, P.M.; Junqueira, M.; Mariano, D.C.O.; Nogueira, F.C.S.; Domont, G.B.; Freire, D.M.G.; Neves, B.C. Characterization of rhamnolipids produced by wild-type and engineered *Burkholderia kururiensis*. *Appl. Microbiol. Biotechnol.* **2013**, *97*, 1909–1921, doi:10.1007/s00253-012-4454-9.

76. Costa, S.G.V.A.O.; Déziel, E.; Lépine, F. Characterization of rhamnolipid production by *Burkholderia glumae*. *Lett. Appl. Microbiol.* **2011**, *53*, 620–627, doi:10.1111/j.1472-765X.2011.03154.x.

77. Häußler, S.; Rohde, M.; von Neuhoff, N.; Nimtz, M.; Steinmetz, I. Structural and functional cellular changes induced by *Burkholderia pseudomallei* rhamnolipid. *Infect. Immun.* **2003**, *71*, 2970–2975, doi:10.1128/IAI.71.5.2970-2975.2003.

78. Sekhon Randhawa, K.K.; Rahman, P.K.S.M. Rhamnolipid biosurfactants-past, present, and future scenario of global market. *Front. Microbiol.* **2014**, *5*, 454, doi:10.3389/fmicb.2014.00454.

79. Abdel-Mawgoud, A.M.; Hausmann, R.; Lépine, F.; Müller, M.M.; Déziel, E. *Biosurfactants*; 2011; Vol. 20; ISBN 978-3-642-14489-9.

80. Wittgens, A.; Santiago-Schuebel, B.; Henkel, M.; Tiso, T.; Blank, L.M.; Hausmann, R.; Hofmann, D.; Wilhelm, S.; Jaeger, K.-E.; Rosenau, F. Heterologous production of long-chain rhamnolipids from *Burkholderia glumae* in *Pseudomonas putida*—a step forward to tailor-made rhamnolipids. *Appl. Microbiol. Biotechnol.* **2018**, *102*, doi:10.1007/s00253-017-8702-x.

81. Henkel, M.; Müller, M.M.; Kügler, J.H.; Lovaglio, R.B.; Contiero, J.; Syldatk, C.; Hausmann, R. Rhamnolipids as biosurfactants from renewable resources: Concepts for next-generation rhamnolipid production. *Process Biochem.* **2012**, *47*, 1207–1219, doi:https://doi.org/10.1016/j.procbio.2012.04.018.

82. Wittgens, A.; Kovacic, F.; Müller, M.M.; Gerlitzki, M.; Santiago-Schübel, B.; Hofmann, D.; Tiso, T.; Blank, L.M.; Henkel, M.; Hausmann, R.; et al. Novel insights into biosynthesis and uptake of rhamnolipids and their precursors. *Appl. Microbiol. Biotechnol.* **2017**, *101*, 2865–2878, doi:10.1007/s00253-016-8041-3.

83. Tiso, T.; Sabelhaus, P.; Behrens, B.; Wittgens, A.; Rosenau, F.; Hayen, H.; Blank, L.M. Creating

metabolic demand as an engineering strategy in *Pseudomonas putida* – rhamnolipid synthesis as an example. *Metab. Eng. Commun.* **2016**, *3*, 234–244, doi:10.1016/j.meteno.2016.08.002.

84. Tiso, T.; Ihling, N.; Kubicki, S.; Biselli, A.; Schonhoff, A.; Bator, I.; Thies, S.; Karmainski, T.; Kruth, S.; Willenbrink, A.-L.; et al. Integration of genetic and process engineering for optimized rhamnolipid production using *Pseudomonas putida*. *Front. Bioeng. Biotechnol.* **2020**, *8*, 1–24, doi:10.3389/fbioe.2020.00976.

85. Ochsner, U.A.; Fiechter, A.; Reiser, J. Isolation, characterization, and expression in *Escherichia coli* of the *Pseudomonas aeruginosa rhlAB* genes encoding a rhamnosyltransferase involved in rhamnolipid biosurfactant synthesis. *J. Biol. Chem.* **1994**, *269*, 19787–19795, doi:10.1016/s0021-9258(17)32089-6.

86. Rahim, R.; Ochsner, U.A.; Olvera, C.; Graninger, M.; Messner, P.; Lam, J.S.; Soberón-Chávez, G. Cloning and functional characterization of the *Pseudomonas aeruginosa rhlC* gene that encodes rhamnosyltransferase 2, an enzyme responsible for di-rhamnolipid biosynthesis. *Mol. Microbiol.* **2001**, *40*, 708–718, doi:10.1046/j.1365-2958.2001.02420.x.

87. Hanahan, D. Studies on transformation of *Escherichia coli* with plasmids. *J. Mol. Biol.* **1983**, *166*, 557–580, doi:10.1016/S0022-2836(83)80284-8.

88. Sambrook, J.; Fritsch, E.F.; T. Maniatis *Molecular cloning : a laboratory manual.*; Cold Spring Habor Laboratory Press, New York., 1989;

89. Burmeister, A.; Hilgers, F.; Langner, A.; Westerwalbesloh, C.; Kerkhoff, Y.; Tenhaef, N.; Drepper, T.; Kohlheyer, D.; von Lieres, E.; Noack, S.; et al. A microfluidic co-cultivation platform to investigate microbial interactions at defined microenvironments. *Lab Chip* **2019**, *19*, 98–110, doi:10.1039/C8LC00977E.

II.2. LIGHT-RESPONSIVE TOOLS FOR CONTROLLING PROCESSES ON THE POST-TRANSLATIONAL LEVEL

II.2.1. FLUORESCENT PROTEINS AS GENETICALLY ENCODED PHOTOSENSITIZERS

An optogenetic toolbox of LOV-based photosensitizers for light-driven killing of bacteria

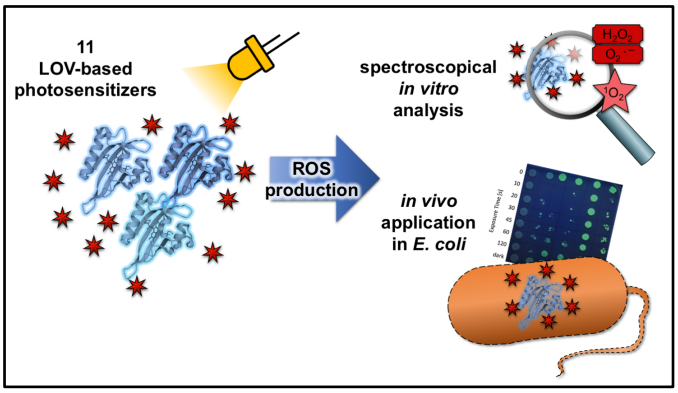

Stephan Endres, Marcus Wingen, Joaquim Torra, Rubén Ruiz-González, Tino Polen, Gabriela Bosio, Nora Lisa Bitzenhofer, **Fabienne Hilgers**, Thomas Gensch, Santi Nonell, Karl-Erich Jaeger, Thomas Drepper

Scientific Reports 8(1):15021. (2018). s41598-018-33291-4

The online version may be found at: 10.1038/s41598-018-33291-4

Status: published

For the Supporting Information see Appendix (**Chapter V.5.**, **page 436**).

Own contribution:

Planning and performing *in vivo* toxicity experiments, analyzing data, editing manuscript.

www.nature.com/scientificreports

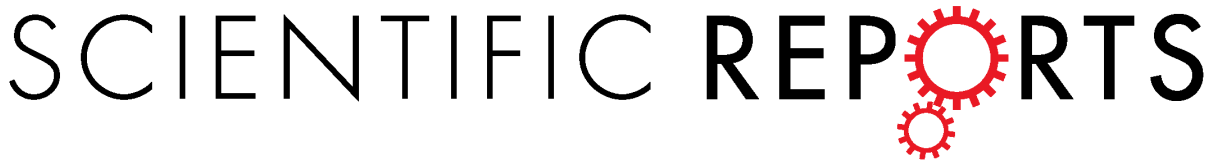

OPEN

An optogenetic toolbox of LOV-based photosensitizers for light-driven killing of bacteria

Received: 29 December 2017
Accepted: 26 September 2018
Published online: 09 October 2018

Stephan Endres[1,2], Marcus Wingen[1], Joaquim Torra[3], Rubén Ruiz-González[3], Tino Polen[4], Gabriela Bosio[5,6], Nora Lisa Bitzenhofer[1], Fabienne Hilgers[1], Thomas Gensch[6], Santi Nonell[3], Karl-Erich Jaeger[1,4] & Thomas Drepper[1]

Flavin-binding fluorescent proteins (FPs) are genetically encoded *in vivo* reporters, which are derived from microbial and plant LOV photoreceptors. In this study, we comparatively analyzed ROS formation and light-driven antimicrobial efficacy of eleven LOV-based FPs. In particular, we determined singlet oxygen ($^1O_2$) quantum yields and superoxide photosensitization activities via spectroscopic assays and performed cell toxicity experiments in *E. coli*. Besides miniSOG and SOPP, which have been engineered to generate $^1O_2$, all of the other tested flavoproteins were able to produce singlet oxygen and/or hydrogen peroxide but exhibited remarkable differences in ROS selectivity and yield. Accordingly, most LOV-FPs are potent photosensitizers, which can be used for light-controlled killing of bacteria. Furthermore, the two variants Pp2FbFP and DsFbFP M49I, exhibiting preferential photosensitization of singlet oxygen or singlet oxygen and superoxide, respectively, were shown to be new tools for studying specific ROS-induced cell signaling processes. The tested LOV-FPs thus further expand the toolbox of optogenetic sensitizers usable for a broad spectrum of microbiological and biomedical applications.

Antimicrobial photodynamic inactivation (aPDI) and photodynamic therapy (PDT) have been developed and applied for treating localized microbial infections and solid tumors (for example see references[1–3]). Both therapies are principally based on the local and light-driven formation of cytotoxic reactive oxygen species (ROS), which immediately induce cell damage during illumination. Here, ROS formation specifically relies on the combination of (i) a phototoxic, light-absorbing compound referred to as photosensitizer (PS), (ii) an excitation source, emitting light of the appropriate wavelength that can be absorbed by the PS and finally (iii) molecular oxygen (O_2). After light absorption, the PS undergoes a transition from the electronic ground state to a singlet excited state and, via intersystem crossing, further to its triplet excited state. The long lifetime of the PS triplet state allows it to produce ROS through either energy transfer to O_2 yielding singlet oxygen ($^1O_2$; type-II mechanism) or through electron transfer from a neighborhood donor to produce a radical anion that further reacts with O_2 to generate primarily the superoxide radical anion ($O_2^{\bullet-}$) and, through a cascade of redox reactions, other ROS such as hydrogen peroxide (H_2O_2) and hydroxyl radicals ($HO^{\bullet}$). This pathway is referred to as the type-I mechanism. Most PSs are capable of undergoing both type-I and -II reactions whereby the outcome of the competition being strongly conditioned by the PS micro-environment. Intracellular ROS production, in turn, results in rapid photo-oxidation of different macromolecules, including proteins, membrane lipids, as well as DNA and RNA, which can finally lead to cell death[4,5]. In particular, $^1O_2$ is highly reactive and has a lifetime of about 3 µs and a limited diffusion range of approximately 270 nm[6,7] in a cell, making it a potent toxic agent for aPDI and PDT[8].

Exogenously applied dyes have several limitations as PS, including their poor selectivity and limited pharmacokinetics. Therefore, alternative PS with better selectivity towards bacteria and tumor tissue and higher cell-killing efficiency need to be developed. Genetically encoded photosensitizers (i.e. proteins that bind - covalently or non-covalently - a chromophore capable of ROS photosensitization) are a new class of PS that exhibits

[1]Institute of Molecular Enzyme Technology, Heinrich-Heine-University Düsseldorf, Forschungszentrum Jülich GmbH, Jülich, Germany. [2]m2p-labs GmbH, Baesweiler, Germany. [3]Institut Químic de Sarrià, Universitat Ramon Llull, Barcelona, Spain. [4]Institute of Bio- and Geosciences, IBG-1: Biotechnology, Forschungszentrum Jülich GmbH, Jülich, Germany. [5]Instituto de Investigaciones Teóricas y Aplicadas, Universidad Nacional de La Plata, La Plata, Argentina. [6]Institute of Complex Systems, ICS-4: Cellular Biophysics, Forschungszentrum Jülich GmbH, Jülich, Germany. Stephan Endres, Marcus Wingen and Joaquim Torra contributed equally. Correspondence and requests for materials should be addressed to S.N. (email: santi.nonell@iqs.url.edu) or T.D. (email: t.drepper@fz-juelich.de)

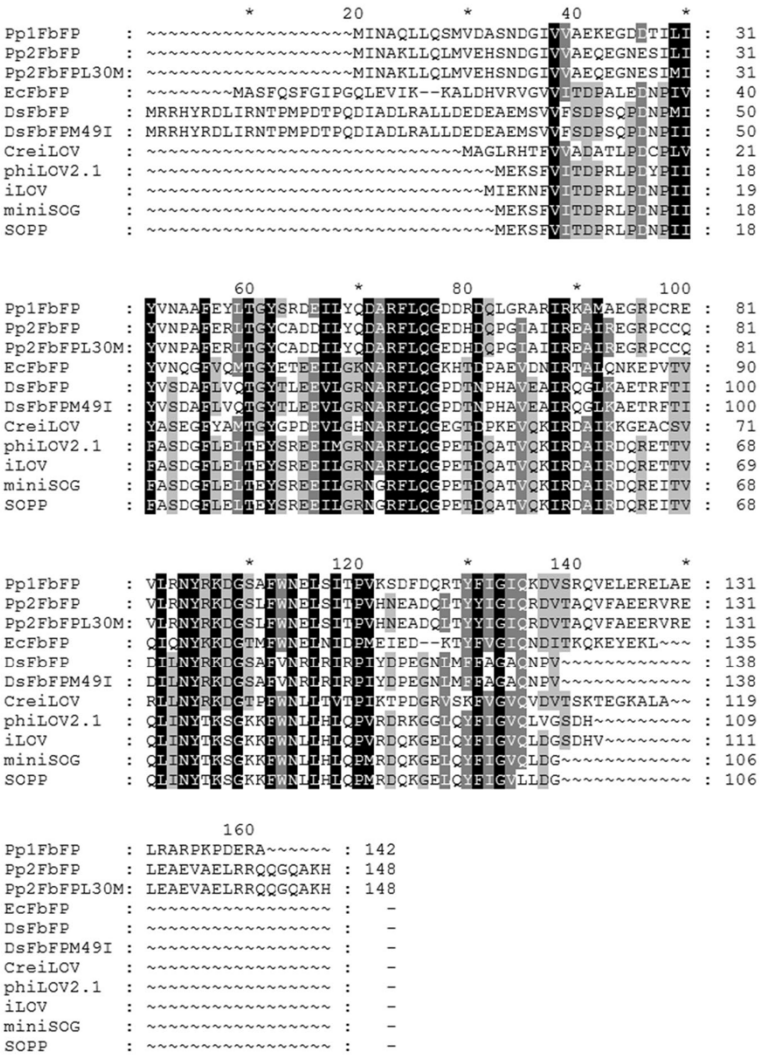

Figure 1. Multiple amino acid sequence alignment of the tested LOV-based fluorescent proteins. Homologous and similar residues are marked in black and grey.

many advantages for different biological and medical applications: intracellular synthesis and accumulation can be controlled and adapted by using inducible expression systems[9]. In addition, the PS can be fused to specific targeting sequences (e.g. leader peptides or antibodies) to selectively direct the recombinant protein to particular cellular structures, compartments or cell types of interest.

In the last decade, two different classes of optogenetic sensitizers have been developed. The first class encompasses fluorescent proteins of the green fluorescent protein (GFP) family[10,11], whereas the second class harbors flavin-binding fluorescent proteins that are derived from light-oxygen-voltage (LOV) photoreceptor domains[12–14].

Photosensitizers of the GFP family: First studies demonstrated that GFP is a rather ineffective photosensitizer, whose ROS-production efficiency is influenced by the chromophore's accessibility to molecular oxygen[11,15,16]. In contrast, KillerRed, a dimeric GFP-homolog derived from the non-fluorescent hydrozoan chromoprotein anm2CP, was shown to be an efficient photosensitizer that primarily generates $O_2^{\bullet-}$ via type-I reaction[10,17,18]. This photosensitizer was successfully applied for photo-inducible killing of targeted cell populations[10,19–22], directed inactivation of proteins via chromophore assisted light inactivation (CALI)[23–26] and ROS-signaling[27,28]. Recently, the monomeric KillerRed derivatives such as SuperNova and KillerOrange have been developed, which exhibit phototoxicity in bacteria and mammalian cells and further allow fusion to target proteins for CALI without affecting the quaternary structure[29–31]. Structural analyses revealed that a water-filled channel connecting the chromophore with the protein surface might lead to an increased photosensitizing activity via facilitated O_2 and ROS transport[31,32]. In contrast to the above mentioned GFP-based PS, the red monomeric protein TagRFP, derived

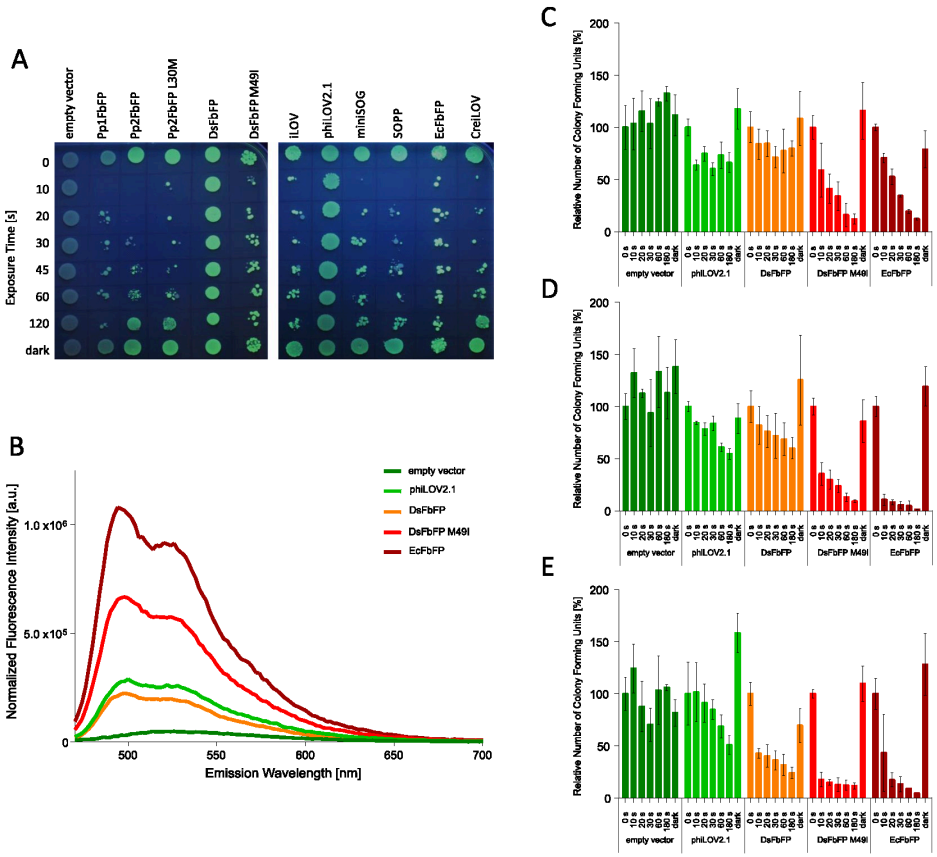

Figure 2. *In vivo* phototoxicity assay of LOV-based fluorescent proteins. (**A**) Plate spot assay. Samples of *E. coli* cultures expressing the respective FP, were illuminated with blue light ($\lambda = 448$ nm; 130 mW cm^{-2}) for a defined period of time and subsequently placed on agar plates. Colony growth in dependence of the illumination time served as a first indicator for individual LOV-FP phototoxicities. The empty vector and samples of each culture that were kept in the dark were used as controls. Green colonies represent fluorescing cells while colonies of non-fluorescing cells appear blueish due to UV-A-light illumination. (**B**–**E**) Analysis of colony forming units (CFU). The colony forming capacity of FbFP-expressing *E. coli* BL21 (DE3) cells was investigated after 0, 10, 20, 30, 60 and 180 s of blue light irradiation. Samples of *E. coli* cells harboring the respective FbFP expression plasmids were incubated for three hours after induction and fluorescence emission spectra of the respective cell extracts were measured in PBS buffer (**B**). Fluorescence spectra of the five bacterial cultures were normalized to their cell density characterized by the absorbance at 580 nm (OD_{580}). For CFU determination, cell cultures were diluted to a final cell density of $OD_{580} = 0.1$ in PBS buffer (pH 7.4). Subsequently, cells were illuminated using different intensities of blue light (10 mW cm^{-2} (**C**); 90 mW cm^{-2} (**D**) and 130 mW cm^{-2} (**E**)). At given time points, aliquots of the irradiated cells were transferred to LB agar plates and incubated overnight at 37 °C in the dark. The data represents the mean values of three independent experiments and standard deviations are indicated by error bars.

from the *Entacmaea quadricolor* fluorescent protein TurboRFP[33] generates $^1O_2$[16] and was shown to kill *E. coli* by endogenously generated $^1O_2$ upon green light irradiation[34].

Photosensitizers of the LOV-FP family: Recently, efforts to produce genetically encoded fluorescent proteins that efficiently generate intracellular $^1O_2$ for correlative light electron microscopy (CLEM) have turned to the generation of miniSOG (mini Singlet Oxygen Generator) engineered from the *Arabidopsis thaliana* phototropin 2 LOV2 domain (*At* LOV2 phot2)[35]. Photophysical properties of miniSOG were extensively characterized[35–37] and the photosensitizer has been successfully applied as tag for CLEM[35,38–45], cell ablation in *Caenorhabditis elegans* and *Drosophila melanogaster*[46–49] as well as for light-induced killing of targeted cancer cells[50,51]. Since then a large number of miniSOG derivatives has been developed, including SOPP (singlet oxygen photosensitizing protein)[52], miniSOG Q103V[45], miniSOG2[49], and SOPP3[53]. While previous works have focused on characterizing and improving miniSOG's properties, comparatively less effort has been devoted to explore other LOV-FPs from different origins. In this work, we therefore comparatively analyzed eleven LOV-FPs derived from microbes and plants with a focus on the antimicrobial phototoxicity and their ability to produce ROS via type-I and type-II reactions.

LOV-FPs have been originally designed as alternative FPs that can be used for *in vivo* analysis of cellular functions in the absence of molecular oxygen[54,55]. The first variants of this new class of *in vivo* reporter proteins were either derived from (i) bacterial photoreceptors, including proteins from *Pseudomonas putida*, *Dinoroseobacter shibae* and *Bacillus subtilis*, termed as FMN-binding fluorescent proteins (FbFPs) or (ii) *Arabidopsis thaliana* phototropin2 LOV2 domain, designated as iLOV[56] and its more photostable variant phiLOV[57]. In addition, new LOV-based FPs have recently been developed by engineering photoreceptors from *Chlamydomonas reinhardtii* (CreiLOV)[58] and thermophilic microbes[59]. Many of the LOV-FPs have been successfully applied as intracellular reporters in different pro- and eukaryotic cells under hypoxic and anoxic conditions[54,60–64]. Moreover, a detailed overview of the photophysical characteristics of several LOV-FPs was recently published[65].

In this study, we now could show that most of the tested LOV-FPs are potent photosensitizers that can be used for efficient killing of microbial cells and for studying ROS-induced stress responses in a light-dependent manner.

Results

In vivo assessment of LOV-FP-mediated phototoxicity in _E. coli_. Within the last ten years, many different flavin-binding fluorescent proteins that are based on LOV photoreceptor proteins from plant, algae and bacteria have been successfully established and applied[55,66]. Among them, the two LOV-FP derivatives miniSOG and SOPP were initially engineered as potent, genetically encoded photosensitizers that are capable of producing sufficient amounts of ROS (predominantly $^1O_2$) for targeted cell killing[35–37,48,50–52]. All of the phototoxicity studies, however, have been carried out in nematodes or cancer cells but not in bacteria, the primary target in aPDI. To this end, we first comparatively analyzed the light-induced antimicrobial activities of eleven LOV-FPs, exhibiting moderate to high sequence identities but different fluorescence quantum yields (Φ_F) ranging from 0.20 (phiLOV2.1) to 0.44 (EcFbFP) (Fig. 1 and Table 1). Besides miniSOG and SOPP, the LOV-FPs iLOV and phiLOV2.1 are derived from the *A. thaliana* Phot2 LOV2 domain[35,52,56,57]. In contrast, the other seven representatives of the LOV-FP family are based on microbial LOV photoreceptors from *P. putida* (Pp1FbFP, Pp2FbFP, Pp2FbFP L30M[54,65,67]), *D. shibae* (DsFbFP, DsFbFP M49I[65],), *B. subtilis* (EcFbFP[54]) and *C. rheinhardtii* (CreiLOV[58]) of which Pp2FbFP L30M was recently reported to efficiently produce $^1O_2$ upon blue light irradiation[67]. To get a first impression of the potential for aPDI, we initially compared the phototoxicity of LOV-FPs in *E. coli* BL21 (DE3) cells during illumination with intense blue light ($\lambda_{max} = 448$ nm, 130 mW cm^{-2}) using a simple plate spot assay (Fig. 2A). Approximately half of the tested LOV-FPs exhibited strong light-triggered antimicrobial activities, resulting in a pronounced growth impairment, already after only 10 seconds of blue-light irradiation. Among the other, Pp2FbFP, Pp2FbFP L30M or CreiLOV required longer illumination, whereas *E. coli* cells expressing phiLOV2.1 or DsFbFP were almost unaffected even after prolonged exposure to blue-light.

To further characterize LOV-FP mediated phototoxicity, we quantitatively determined the cell viability by counting colony forming units, which is more sensitive due to sample dilution before spreading light-treated cells onto agar plates. The viability of *E. coli* cells expressing representative FbFPs that exhibited either low (phiLOV2.1 and DsFbFP) or high (DsFbFPM49I and EcFbFP) activity in the plate spot assay was measured in dependence on exposure time and applied light intensity. As shown in Fig. 2C–E, increasing the illumination time (10–180 seconds), as well as the light intensity (10, 90 and 130 mW cm^{-2}), gradually decreased the number of viable bacteria for all FbFPs, although for phiLOV2.1 and DsFbFP cell death was more modest (Fig. 2E). In contrast, in the case of DsFbFP M49I and EcFbFP (these variants already showed pronounced phototoxicities in the plate spot assay) almost all cells were killed under these illumination conditions. Analysis of LOV-FP-mediated fluorescence emission in corresponding cell extracts revealed that fluorescence intensities (and thus protein accumulation levels) differed strongly for the tested *E. coli* strains (Fig. 2B). Thus, a better comparison of LOV-FPs should take into account such differences in protein levels. To this end, we comparatively analyzed individual LOV-FP phototoxicities using the propidium iodide cell-death assay[68] and normalized it to the respective *in vivo* fluorescence (see materials and methods for details). To precisely determine differences in phototoxic activities, we applied low light intensities (10 mW cm^{-2}) in this assay. The results presented in Fig. 3 show the increase in PI fluorescence in dependence of illumination time (0 to 60 minutes).

Based on the normalized PI fluorescence, *in vivo* phototoxicity of the tested LOV-FP-based photosensitizers can be classified into three different groups: The first encompasses SOPP, DsFbFP M49I, Pp1FbFP and iLOV, where blue-light illumination of *E. coli* cells resulted in a fast and strong increase of PI fluorescence. Thus this group of LOV-FPs exhibits a high, light-triggered antimicrobial activity in our assay. The second group contains the medium-toxic variants Pp2FbFP, EcFbFP, miniSOG and CreiLOV, whose PI fluorescence signals developed slower during blue-light illumination and exhibited a lower intensity compared to those of the first group. The third LOV-FP group contains the less-toxic proteins phiLOV2.1, DsFbFP and Pp2FbFP L30M. Samples of *E. coli* cells expressing these three variants did not show a significant increase in PI fluorescence upon the applied low-light conditions. In a control experiment, where aliquots of the same *E. coli* LOV-FP expression cultures were kept in the dark for 60 minutes, no significant changes in the PI fluorescence could be detected (Supplemental Fig. S2), thereby confirming that the observed increase in PI fluorescence is specifically induced by the phototoxic activity of the tested LOV-FPs.

While the PI-based experiment presented in Fig. 3 indicates that most LOV-FPs can damage the cell envelope of *E. coli* via light-induced ROS formation, it is not clear whether this is – at the level of single cells – an antimicrobial effect that occurs homogeneously within the culture. To demonstrate that the increase of PI fluorescence directly correlates to the growing number of killed cells under continuous blue-light illumination (in contrast to the possibility, that just a subset of susceptible bacteria is responsible for the PI fluorescence signal due to an individually increasing level of mRNA under the tested conditions), development of the PI signal was analyzed in single cells using a fluorescence microscope. As shown in Supplemental Fig. S3, *E. coli* cells expressing either DsFbFP (Supplemental Fig. S3A) or DsFbFP M49I (Supplemental Fig. S3B) exhibited a detectable FbFP-mediated green fluorescence (consider images I and II) as well as a homogeneous development of a strong PI fluorescence

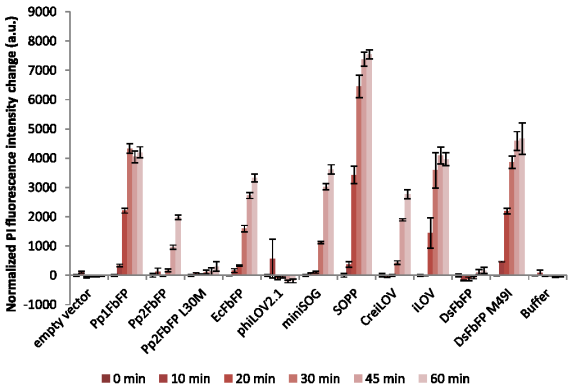

Figure 3. Analysis of LOV-FP phototoxicity using propidium iodide as quantitative marker for dead *E. coli* cells. The bars show the change in PI fluorescence intensity ($\lambda_{ex} = 535$ nm, $\lambda_{em} = 617$ nm) over 60 minutes of blue-light illumination (~10 mW cm^{-2}). The data was normalized to the amount of functional protein per cell. The corresponding raw data can be found in Supplemental Fig. S1. To ascribe the observed effects to blue-light exposure, a control experiment in the dark was conducted, which showed no significant changes for all tested LOV-PS (Supplemental Fig. S2). The data represent the mean values of three independent experiments, the error bars indicate the calculated standard deviations.

Name	Source organism	Excitation λ_{max} (nm)	Emission λ_{max} (nm)	ε (M^{-1} cm^{-1})	Φ_F	Brightness (M^{-1} cm^{-1})	Φ_Δ
Pp1FbFP	*P. putida*	450[65]	496[65]	13,900 ± 500[65]	0.27 ± 0.01[65]	3,750[65]	0.23
Pp2FbFP	*P. putida*	449[65]	495[65]	14,200 ± 50[65]	0.22 ± 0.01[65]	3,120[65]	0.11
Pp2FbFP L30M	*P. putida*	449	495	14,800 ± 100	0.25 ± 0.01	3,700	0.10
DsFbFP	*D. shibae*	449[65]	498[65]	14,300 ± 50[65]	0.35 ± 0.01[65]	5,000[65]	0.33
DsFbFP M49I	*D. shibae*	450	498	13,700 ± 500	0.36 ± 0.01	4,930	0.42
EcFbFP	*B. subtilis*	448[65]	496[65]	14,500 ± 200[65]	0.44 ± 0.01[65]	6,380[65]	0.07
iLOV	*A. thaliana*	450[94]	497[94]	14,800 ± 300[94]	0.33 ± 0.01[94]	4,850	0.05
phiLOV2.1	*A. thaliana*	450[65]	497[65]	n.d. [65]	0.20 ± 0.01[65]	2,840	0.01
miniSOG	*A. thaliana*	447[65]	497[65]	14,200 ± 700[65]	0.41 ± 0.01[65]	5,820[65]	0.03[36,37] 0.04[this study]
SOPP	*A. thaliana*	440	490	n.d.	0.33 ± 0.01	4,690	0.25
CreiLOV	*C. reinhardtii*	449	497	14,200 ± 400	0.32 ± 0.01	4,540	0.04
miniSOG Q130V	*A. thaliana*	n.p.	n.p.	n.p.	n.p.	n.d.	0.39[45]
SOPP3	*A. thaliana*	439[53]	490[53]	15,000[53]	0.41[53]	6,150	0.60[53]
TagRFP	*E. quadricolor*	555[33]	584[33]	100,000[33]	0.48[33]	48,000	0.004[16]
FMN		444[65]	531[65]	12,200[95]	0.25 ± 0.01	3,050	0.57

Table 1. Singlet oxygen quantum yields (Φ_Δ) and photophysical properties of LOV- and GFP-based photosensitizers. Extinction coefficient (ε) and fluorescence quantum yield (Φ_F) of LOV-based PS that were analyzed in this study (highlighted in bold) are given as mean values with standard deviations determined from three independent measurements. The fluorescence brightness is the product of individual ε and Φ_F values. The extinction coefficient as well as the brightness of phiLOV2.1 and SOPP could not be determined directly (n.d.), as both proteins aggregated at 95 °C. Therefore, for further calculations, an average extinction coefficient of 14,200 M^{-1}cm^{-1} was assumed for these variants. For a better comparability, values of miniSOG Q103V, SOPP3 and TagRFP (marked in bold and italic) that have been obtained from indicated publications were also listed; n.p.: not published.

as a function of time (consider images III-VIII) after illumination (102 mW; 460–490 nm). The corresponding control (*E. coli* cells carrying the corresponding empty expression vector) did not show a detectable PI signal even after prolonged blue-light exposure times (Supplemental Fig. S3C). Furthermore, as expected from *in vivo* phototoxicity assays, the two investigated LOV-FPs exhibit rather different phototoxicities: While expression of DsFbFP M49I resulted in maximal, saturating PI fluorescence signal after 105 s, the PI fluorescence signal of DsFbFP accumulating cells was significantly lower even after longer blue light illumination. The microscopic analysis thus clearly demonstrates that (i) illumination of LOV-FPs accumulating *E. coli* cells results in a homogeneous increase of PI influx (and thus increase of PI fluorescence), which shows (ii) a clear dependency on illumination time and (iii) most probably on individual properties of tested LOV-FPs.

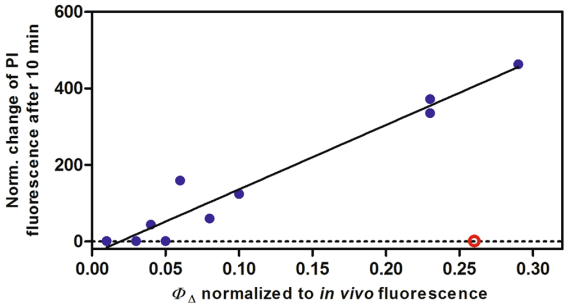

Figure 4. Protein phototoxicity in *E. coli* cells in relation to singlet oxygen production. Correlation between the extent of cell death, measured by propidium iodide (PI) fluorescence, and the amount of singlet oxygen produced during the first 10-min irradiation period. This was calculated based on multiplying the singlet oxygen quantum yield by the percentage of protein fluorescence remaining after 10-min irradiation. The underlying reason for this correction is that the proteins photobleach to different extent over time (see Supplemental Fig. S4, Fig. 3 and ref.[65]), hence the rate of singlet oxygen production during the irradiation period considered has decreased concomitantly. The protein fluorescence is a measure of the amount of protein still intact after the irradiation period. The data point indicated by the red circle represents the determined values of the outlier DsFbFP.

In summary, our *in vivo* data clearly demonstrate that many of the tested LOV-FPs can be used as photosensitizers suitable for efficient light-controlled killing of *E. coli* cells. These properties thus render them potentially suitable for antimicrobial photodynamic inactivation (aPDI). In comparison to conventional treatment of bacterial infections with antibiotics, aPDI exhibits several advantages, including a ROS-based broad spectrum of activities against a multitude of different microbes together with a high efficacy towards resting cells and pathogenic strains that exhibit multiple antibiotic resistances (e.g. reviewed in refs[69,70]). Furthermore, because of the high reactivity and short lifetime of ROS and the resulting damage of very different essential biomolecules in the targeted microbe, formation of resistances to aPDI in bacteria must be considered highly unlikely even when cells are treated repetitively with sublethal doses of light[71–73]. In addition to that, the possibility of controlling the expression of FbFPs in the pathogenic bacteria offers an added attractive to this new class of biological photosensitizers.

***In vitro* measurements of LOV-FP-dependent singlet oxygen production.** In order to analyze, if the observed difference in *in vivo* phototoxicities is caused by distinct $^1O_2$ production levels, we next determined individual singlet oxygen quantum yields of the purified fluorescent proteins by measuring the $^1O_2$ phosphorescence at $\lambda = 1275$ nm in deuterated PBS buffer as described in Torra *et al.*[67]. The results of these experiments are summarized in Table 1 and show a broad variability of $^1O_2$ photosensitization yields. DsFbFP M49I exhibited the highest $^1O_2$ Φ_Δ with 0.42. Furthermore, the value for SOPP ($\Phi_\Delta = 0.25$) matches the published value from Westberg *et al.*, who generated this protein by means of site-directed protein engineering based on miniSOG[52]. These two values also correlate well with the high phototoxicity *in vivo*. The Φ_Δ values of the other LOV-FPs are significantly smaller, ranging from 0.01 (phiLOV2.1) to 0.33 (DsFbFP). The lowest singlet oxygen quantum yield of phiLOV2.1 is also in good agreement with the observed absence of *in vivo* toxicity. In addition, some of the LOV-FPs with intermediate singlet oxygen production rates (e.g. EcFbFP with a Φ_Δ of 0.07) were also classified as moderately toxic *in vivo* photosensitizers. However, considerable deviations of *in vivo* phototoxicity and $^1O_2$ quantum yield were also observed for some of the tested LOV-FPs. For example, iLOV illumination resulted in a very strong PI signal in the *in vivo* toxicity assay, but spectroscopic analysis revealed a low Φ_Δ value (0.05). On the other hand, the high Φ_Δ value of DsFbFP (0.33) did not correspond to its weak *in vivo* phototoxicity. The discrepancies observed for some of the LOV-based PS were to be expected. Regarding the Φ_Δ measurements, it is arguable whether in all cases the values derived from solution measurements are representative of the Φ_Δ values inside the cells. Specifically, the microenvironment of the protein inside a living cell may affect its ability to produce $^1O_2$ e.g., because of different protein conformations and/or interactions with other cellular components. For example, Westberg *et al.* recently observed that the increase of temperature has a remarkable effect on O_2-dependent quenching of FMN triplet state – a phenomenon that can also be differently affected by the individual properties of the surrounding protein as described for miniSOG and SOPP[53]. In addition, it must be kept in mind that the Φ_Δ values are assumed to be proportional to the intensity of $^1O_2$ phosphorescence, whereas the biological effects are due to $^1O_2$ molecules being released from the protein. Thus, our measured Φ_Δ values describe the total amount of $^1O_2$ molecules produced by the individual photosensitizer, but may not reflect the number of $^1O_2$ molecules being actually released. This is particularly the case for LOV-FPs with triplet lifetimes of hundreds of microseconds in air-saturated solutions, such as DsFbFP and DsFbFP M49I ($\tau_T > 500$ µs), which clearly reflects a very low accessibility of molecular oxygen to the chromophore. It is thus reasonable to expect that the generated $^1O_2$ will only partially escape from the protein. To address this question, indirect $^1O_2$ detection measurements for the two DsFbFP variants were performed using the chemical trap uric acid (UA), which specifically and irreversibly reacts with $^1O_2$[74]. The Φ_Δ values determined in dPBS solution were 0.28 and 0.36 for DsFbFP and DsFbFP M49I, respectively, in good agreement with the values obtained by the direct $^1O_2$ luminescence detection method. These results

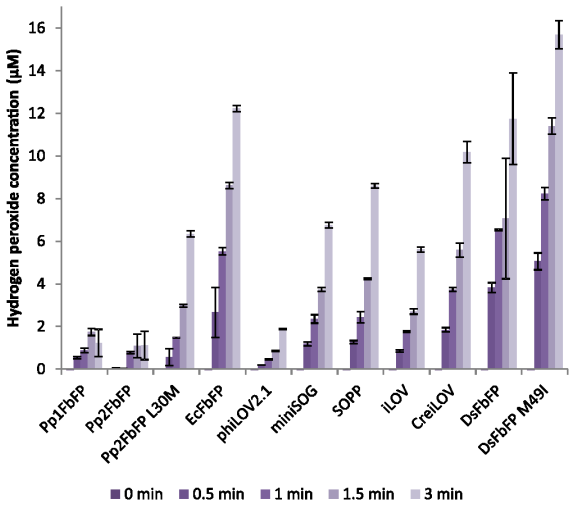

Figure 5. Quantification of LOV-PS-catalyzed hydrogen peroxide formation. The determination of hydrogen peroxide, produced by the LOV-PS as a reaction of blue-light exposure ($\lambda_{max} = 447$ nm, ~10 mW cm^{-2}), was performed with purified proteins (final concentration $OD_{450} = 0.05$) by applying the Amplex® Red Hydrogen Peroxide/Peroxidase Assay Kit. The bars show the time-dependent increase of hydrogen peroxide formation for all tested photosensitizes. The control experiment in the dark did not lead to detectable H_2O_2 production for all tested proteins (Supplemental Fig. S2). The data represent the mean values of three independent experiments, the error bars the calculated standard deviations.

thus confirm that $^1O_2$ molecules indeed escape from the protein matrix and reach the bulk solvent. Therefore, the discrepancies observed between $^1O_2$ production and photokilling experiments should arise from processes other than protein deactivation of $^1O_2$ molecules.

Returning to the PI results presented in Fig. 3, it is highly revealing that the time evolution of the PI fluorescence leveled off at different upper-limit values for each protein, resulting in a clear sigmoidal shape. This observation is particularly relevant since it implies that photobleaching of the proteins is a critical factor that limits their phototoxic properties. In fact, if the extent of cell death is plotted against the actual *amount* of singlet oxygen produced by each protein during the first 10-min irradiation period, a clear correlation is obtained (Fig. 4), indicating that singlet oxygen is the major cytotoxic species for most LOV-FPs studied and confirming the importance of photobleaching.

***In vitro* analysis of LOV-FP-catalyzed hydrogen peroxide production.** We further investigated the LOV-FP-dependent production of $O_2^{\bullet-}$ and H_2O_2 that has already been demonstrated for miniSOG and SOPP[37,52]. To this end, we illuminated samples of the purified photosensitizer proteins (final $OD_{450} = 0.05$) with blue light and analyzed the resorufin-specific fluorescence - the product of the Amplex Red reaction with H_2O_2 as described in the material and methods section. The results of this experiment indicate large differences in the H_2O_2 production rates of the studied LOV-FPs (Fig. 5). In particular, phiLOV2.1, Pp1- and Pp2FbFP produce low H_2O_2 concentrations ($\leq$2 µM), whereas all other tested proteins reached values between ~6µM and ~16µM. Especially the two DsFbFP variants as well as EcFbFP and CreiLOV showed notably high hydrogen peroxide production during illumination. The correlation of light treatment and H_2O_2 production was evidenced by the dark control which resulted in no significant H_2O_2 accumulation in all tested samples (Supplemental Fig. S2). In summary, our data confirmed considerable type-I-driven ROS formation of LOV-FPs, whereas the efficiencies strongly differ between the tested proteins. In this context it is worth mentioning that some of the tested LOV-FPs seem to preferentially produce ROS either via the type-I or type-II photosensitization process, as observed for Pp1- and Pp2FbFP (intermediate $^1O_2$ and low H_2O_2 production rates) and DsFbFP M49I (high H_2O_2 and $^1O_2$ production rates), which make them promising candidates for studying cell signaling processes that are induced by different reactive oxygen species with high spatiotemporal resolution.

Using Pp2FbFP and DsFbFP M49I as optogenetic tools for analyzing ROS-induced stress responses in *E. coli*. In our previous experiments we could demonstrate considerable production of ROS for almost all of the tested LOV-FPs. However, selectivity and efficiency of light-driven ROS formation strongly vary between those proteins. This observation led us to the question if some of the variants can be utilized as selective and non-invasive intracellular ROS generators, to analyze specific responses to oxidative stress in bacteria. Using a DNA-microarray approach, we comparatively analyzed H_2O_2 and $^1O_2$ induced changes in the transcriptome of *E. coli* cells, applying either DsFbFP M49I or Pp2FbFP. As expected, a number of *E. coli* genes could be identified whose expression rates were significantly upregulated after illumination (Table 2). Remarkably, 25 genes showed higher expression levels in blue-light exposed *E. coli* cells accumulating the singlet oxygen and hydrogen

Gene	Increased expression (x-fold)	*p*-value	Assigned function
DsFbFP M49I			
*dps**	27.6	0.002	nucleoid-associated protein[80,81]
azoR	13.0	0.002	FMN- and NADH-dependent azoreductase[96,97]
*sufB**	12.0	0.008	alternative iron-sulfur cluster assembly system[78,84]
lacI	11.2	0.048	transcription repressor[98]
*ahpC**	7.5	0.005	NADH peroxidase[79]
*sufC**	6.8	0.012	alternative iron-sulfur cluster assembly system[78,84]
*sufS**	6.7	0.014	alternative iron-sulfur cluster assembly system[78,84]
*sufD**	5.5	0.017	alternative iron-sulfur cluster assembly system[78,84]
yhaK	5.4	0.014	bicupin-related protein[86]
pspA	5.1	0.004	phage shock protein[99]
ybiJ	5.1	0.012	Unknown
glpE	4.8	0.003	Sulfurtransferase[100]
mokB	4.8	0.031	Predicted regulatory peptide
*mntH**	4.7	0.021	Divalent metal ion transporter[101]
*ahpF**	4.6	0.014	NADH peroxidase[79]
*katG**	4.2	0.015	catalase[79]
*grxA**	4.2	0.017	glutaredoxin I[102]
*hemH**	4.1	0.020	ferrochelatase[78]
*trxC**	4.0	0.009	thioredoxin II[103]
pspD	3.8	0.003	phage shock protein[99]
clpS	3.8	0.002	Part of ClpAP-protease complex[104]
pspB	3.7	0.029	phage shock protein[99]
pspC	3.3	0.008	phage shock protein[99]
*yaaA**	3.1	0.021	Unknown
*sufE**	2.9	0.008	alternative iron-sulfur cluster assembly system[78,84]
Pp2FbFP			
azoR	7.7	0.023	FMN- and NADH-dependent azoreductase[96,97]
ybiJ	6.6	0.034	Unknown
yhaK	5.6	0.055	bicupin-related protein[86]
gntK	4.0	0.046	gluconokinase[105]

Table 2. DNA microarray-based, genome-wide analysis of ROS-induced stress response mediated by light-exposed LOV-PS in *E. coli*. LOV-PS Pp2FbFP and DsFbFP M49I were expressed in *E. coli* BL21(DE3) cells and illuminated with blue light (Pp2FbFP: 5 min, DsFbFP: 15 min). Transcriptome profiles were compiled from illuminated samples and compared to non-illuminated controls. In this way, genes were identified that showed a significant increase in their expression level ($\geq$3-fold, p-value ≤ 0.05), as a reaction to light exposure. Genes that are induced by OxyR are marked with an asterisk. The data represents the mean values of three independent experiments.

peroxide-producing variant DsFbFP M49I. In bacteria, H_2O_2 generally serves as signal molecule that can be recognized by the transcriptional regulator OxyR, which in turn specifically activates genes of the OxyR regulon[75–78]. Accordingly, 14 blue-light induced genes belong to the OxyR regulon (Table 2; marked by an asterisk), including the genes *ahpCF* and *katG* encoding the NADH peroxidase and catalase. Both enzymes are known to predominantly scavenge H_2O_2 in bacteria, as for example reviewed in[79]. However, the strongest induction was observed for the *dps* gene (~28-fold), which codes for the "DNA-binding protein from starved cells" (Dps) that is known to protect DNA against ROS-mediated damage in *E. coli* and other bacteria[80–83]. Furthermore, most of the *suf* genes are induced via DsFbFP M49I-dependent ROS formation. The SufABCDSE complex functions as an alternative iron-sulfur cluster assembly system which can substitute the housekeeping Isc (FeS cluster assembly) system after its hydrogen peroxide-mediated inactivation[78,84]. In addition, some of the blue-light induced genes not belonging to the OxyR regulon code for enzymes that are known to play a role in redox stress response. For example, AzoR, an FMN-dependent NADH-azoreductase, was shown to be essential for growth of *E. coli* in the presence of quinones that facilitate accumulation of ROS via deleterious redox cycling[85].

In contrast, only four genes were strongly upregulated in *E. coli* cells expressing the singlet oxygen forming Pp2FbFP (Table 2), although this LOV-FP variant exerted clear phototoxicity in our *in vivo* experiments (Figs 2 and 3). Two of these genes, namely the above mentioned *azoR* as well as *yhaK*, were also induced in cells expressing DsFbFP M49I and the respective gene products seem either to be potentially involved in sensing (YhaK)[86] or compensating (AzoR) oxidative stress in *E. coli*.

In photosynthetic bacteria, regulatory processes and mechanisms of $^1O_2$ defense have been extensively analyzed (e.g. reviewed in[7]). In contrast, specific responses of non-phototrophic bacteria towards singlet oxygen is

still poorly understood. Kim and coworkers presented first evidences that OxyR might also (directly or indirectly) be involved in singlet oxygen signaling in *E. coli*[87]. Our results, however, indicate that intracellularly generated $^1O_2$ does not result in the activation of the OxyR regulon. The observed differences in the *E. coli* expression pattern thus give a first indication that the two tested LOV-FPs represent new blue-light responsive ROS-generators that can be used for studying specific hydrogen peroxide- or singlet oxygen-mediated stress responses in bacteria.

Discussion

In this study, we investigated the phototoxicity of eleven LOV-FPs in *E. coli* and analyzed differences in efficiency and selectivity of ROS formation. We could demonstrate that most of the flavin-binding fluorescent proteins are capable of producing singlet oxygen and hydrogen peroxide to a certain extent. Consequently, the tested LOV-FPs exhibit low to high phototoxicity when applied for light-driven killing of bacterial cells. Basically, the encapsulation of the photosensitizing flavin chromophore by the LOV domain should guarantee that the individual photoinitiated processes are independent of the PS's surrounding. However, it is clearly not the case, since the specific amino acid sequence of each protein dramatically modulates the properties of the chromophore. In addition, photostability is a key factor in the outcome of aPDT applications. In this regard, the alleged lack of consistency of the photokilling experiments with the $^1O_2$ production capacity has been rationalized by the photobleaching of the photosensitizing proteins, and a clear correlation between the amount of $^1O_2$ and the antimicrobial activity is observed when applying low light-doses.

The data presented here demonstrate that the characterized LOV-FPs clearly expand the toolbox of optogenetic sensitizers. Especially, (i) differences in singlet oxygen quantum yields, (ii) selective formation of $^1O_2$ and H_2O_2 as well as (iii) gradual differences in photodynamic inactivation of *E. coli* cells render them suitable photosensitizers for a broad range of *in vivo* applications.

For example, since increasing and multiple antibiotic resistances of different Gram-positive and Gram-negative pathogens represent one of the most important therapeutical challenges, alternative agents are urgently needed. Here, genetically encoded PS with high phototoxicities can help to selectively fight against human pathogens, without producing resistances by using them, for instance, as recombinant immunophotosensitizer. The applicability of immonophotosensitizers was already demonstrated for targeted tumor therapy. For example, KillerRed and miniSOG could genetically be fused to the single-chain variable fragment antibody 4D5scFv, which specifically binds to HER2/neu tyrosine kinase receptors. In that way, both immunophotosensitizers exhibited light-mediated cytotoxic effects on HER2/neu-hyperexpressing tumor cells (see[14] and references therein) - a therapeutic strategy that could easily be transferred to selective aPDI approaches. Alternatively, LOV-based PS can be intracellularly targeted to different compartments where $^1O_2$- and H_2O_2-induced stress can be triggered by light with a high spatio-temporal resolution. This may facilitate the development of new aPDI strategies as well as foster studies regarding ROS-stress thereby amending current methods and therapies with chemical photosensitizers. In future, bacteria that are able to selectively target and proliferate in tumors can be further used for local delivery of tailor-made photosensitizer proteins and subsequent photodynamic treatment as recently demonstrated with KillerRed[88]. Because of the low penetration depth of blue light into mammalian tissues, both aPDI and PDT might be limited to surface exposed pathogens and tumors. However, new surgery techniques nowadays allow delivering light to almost any region of the human body via endoscopes and fiber optics, as for example discussed in[70].

In contrast, low to moderately phototoxic LOV-PS could be utilized as new optogenetic tools for light-triggered control of bacterial cell growth. This application could be of particular importance e.g. for studying natural microbial communities, which often rely on symbiotic relationships of organisms with unknown biological functions. Here, genetically encoded PS can be used to specifically tag an individual species residing within a community or biofilm thereby opening up new optogenetic strategies to analyze its *in vivo* function.

Finally, we would like to point out that genetically encoded PSs such as miniSOG are shown to be useful tags for analyzing the function of target proteins inside living cells and tissues via light-controlled inhibition (CALI)[14]. This strategy is universally applicable for living cells and tissues, although ROS formation has to be carefully adjusted to avoid off-target effects or even cell death due to high amounts of freely diffusing ROS. Here, the LOV-based optogenetic sensitizers presented in our study exhibiting different ROS formation capabilities again can directly help to find suitable conditions for efficient CALI without harming the surrounding cellular molecules.

Consequently, the alternative LOV-photosensitizers can be applied as a versatile light-responsive biobrick system with adjustable phototoxicities which will be highly beneficial for future optogenetic and biomedical applications.

Methods

Construction of LOV-FPs expression vectors. Genes encoding SOPP, CreiLOV and iLOV harboring an *Nde*I and *Xho*I restriction site at the respective 5′- and 3′- end were obtained by commercial gene synthesis (Eurofins Genomics, Ebersberg, Germany). Subsequently, the synthetic DNA fragments were cloned into the *Nde*I and *Xho*I sites of the pET28a vector (Novagen, distributed by Merck KGaA, Darmstadt, Germany). DsFbFP M49I was generated by overlap extension PCR using the pET28a DsFbFP vector DNA[65] as template and the oligonucleotide primers DsFbFP-up: 5′-CAGCCATATGCGCAGAC-3′, DsFbFP-dn: 5′- GTGCTCGAGTCAGACCGGG-3′, DsFbFP 49I-up: 5′-CAACCCGATTATCTATGTC-3′ and DsFbFP 49I-dn: 5′-GACATAGATAATCGGGTTG-3′. The resulting final PCR fragments were hydrolyzed with *Nde*I and *Xho*I and ligated into the respective sites of the pET28a vector. DNA cloning was conducted using the *Escherichia coli* strain DH5α[89] and DNA plasmid isolations from bacterial cells were performed using the commercial innuPREP Plasmid Mini Kit (Analytik Jena, Jena, Germany), as described by the manufacturer. All final vector constructs were verified by DNA-sequencing (Eurofins Genomics, Ebersberg, Germany).

***Escherichia coli*-based *in vivo* phototoxicity assays.** Time-resolved, qualitative comparison of phototoxic effect caused by eleven FbFPs (Table 1) on *E. coli* BL21(DE3) (Novagen, distributed by Merck KGaA, Darmstadt, Germany) was carried out by plate spot assay. *E. coli* cells harboring the respective LOV-FP expression vectors were cultivated in 100 ml flasks at 37 °C. Three hours after induction of LOV-FP expression (addition of 0.4 mM IPTG), samples were taken out of the expression cultures and diluted to a final cell density ($OD_{580} = 0.025$) in PBS-Buffer (140 mM NaCl; 12.5 mM Na_2HPO_4; 2.7 mM KCl; 1.8 mM KH_2PO_4, pH 7.4). The cell suspension was transferred into a macro cuvette and placed directly on top of a blue-light emitting LED (LUXEON Rebel XLML PR01 0425; $\lambda = 448$ nm; 130 mW cm^{-2}). At given time points (0 to 120 sec) 3 µl-aliquots were taken out of the illuminated cell solutions and dropped on an LB agar plate, containing 0.2% lactose. A culture of *E. coli* cells carrying the empty vector pET28a as well as non-irradiated samples of each LOV-FP expression culture were used for appropriate control experiments. Subsequently, agar plates were incubated at 37 °C overnight. To distinguish between fluorescing and non-fluorescing colonies, agar plates were finally photographed under UV-light ($\lambda = 365$ nm) illumination. Phototoxicity of LOV-FPs is indicated by an impaired cell growth and only fluorescent colonies were taken into account, as non- fluorescent colonies represent cells that did not express the protein at the time of illumination due to population heterogeneity.

To quantitatively determine the cell viability rate of *E. coli* expressing different phototoxic LOV-FPs the colony forming capacity was measured in dependence of exposure time light intensity. *E. coli* BL21 (DE3) cells harboring the respective expression vectors pET28a-phiLOV2.1, pET28a-DsFbFP, pET28a-DsFbFP M49I and pET28a-EcFbFP, respectively, were cultivated in 100 mL flasks at 37 °C. Three hours after induction with 0.4 mM IPTG, the fluorescence spectra of the LOV-based FbFPs were measured in whole cell extracts that have been resuspended in PBS buffer (pH 7.4). To minimize the influence of different growth rates in the expression cultures, all spectra were normalized to $OD_{580} = 1$. The fluorescence emission spectra were measured using a microplate reader (Infinite M1000 Pro, Tecan Group LTD., Maennedorf, Switzerland). For determination of colony forming units (CFU) before and after illumination, the cultures were diluted to a final OD_{580} of 0.1 in PBS buffer (pH 7.4). The cell suspension was transferred into a macro cuvette and illuminated with different intensities (90 mW cm^{-2} and 130 mW cm^{-2}) of a blue light emitting LED (LUXEON Rebel XLML PR01 0425; $\lambda_{max} = 448$ nm). To reach an illumination intensity of 10 mW cm^{-2} the samples were transferred into a 48-well microtiter plate (FlowerPlate; m2p-laps GmbH,Aachen,Germany) and illuminated with blue light ($\lambda_{max} = 447$ nm, ~10 mW cm^{-2}) in a microbioreactor (BioLector; m2p-laps GmbH, Aachen, Germany). At given time points (0 to 180 s), 100 µL of the irradiated cell solutions were taken out of the respective illumination setup and diluted to predefined cell densities in LB-media (here, an appropriate dilution was chosen which finally results in approximately 100–200 colonies on agar plates). From these samples, 100 µL were plated on LB agar plates and incubated at 37 °C overnight in the dark. Additionally, a non-irradiated dark-treated sample of each FbFP expression culture was used as a control.

Quantitative analysis of light-induced cell-death was conducted using propidium iodide (PI), a fluorescent dye that selectively enters dead cells and develops a specific fluorescence signal with λ_{max} at 617 nm when excited with yellow light (535 nm) after intercalation into DNA[68]. To comparatively characterize phototoxicities of cytoplasmic LOV-FPs in *E. coli*, chemo-competent *E. coli* BL21(DE3) cells were transformed with recombinant pET28a vectors allowing the expression of the respective fluorescent reporter genes. Therefore, *E. coli* expression cultures were inoculated with an optical density (OD_{580}) of 0.1 in Terrific Broth (Carl Roth, Karlsruhe, Germany) auto-induction media, supplemented with 0.2% lactose, 0.03% glucose and 50 µg ml^{-1} Kanamycin. Cell cultivations (culture volume: 800 µl) were performed in microtiter plate (FlowerPlate) using the BioLector (m2p-labs GmbH, Baesweiler, Germany), for six hours at 37 °C under continuous shaking (1500 rpm). Subsequently, cultures were harvested via centrifugation, washed with PBS (pH 7.4) and finally resuspended in 1300 µL assay buffer (PBS pH 7.4, 100 µM EDTA, 5 µM PI, Sigma Aldrich) with a final cell density of $OD_{580} = 0.5$. These samples were subsequently transferred to a fresh FlowerPlate and placed into the BioLector with a LED blue light source for homogeneous illumination of the entire flower plate. To ensure optimal oxygen supply for photosensitizing, *E. coli* cells were illuminated with blue light ($\lambda_{max} = 447$ nm, ~10 mW cm^{-2}) under continuous shaking (1100 rpm, 30 °C). At several time points, 100 µl samples were taken and analyzed regarding their LOV-FP-mediated fluorescence intensity (excitation at 450 nm, emission at 495 nm) and PI fluorescence (excitation at 535 nm, emission at 617 nm) using a microplate reader (Infinite M1000 Pro, Tecan Group LTD., Maennedorf, Switzerland). To be able to evaluate LOV-FP-mediated phototoxicity regardless of its respective expression efficiency in *E. coli*, the data was normalized using equation 1, where I_n is the normalized PI fluorescence intensity, I_{raw} the raw PI fluorescence, I_{FP} the LOV-FP-fluorescence intensity of the cell culture before blue-light illumination, Φ_F the fluorescence quantum yield and ε the molar extinction coefficient of the respective LOV-FP (see Table 1):

$$I_n = \frac{I_{raw}}{\left(\frac{I_{FP}}{\Phi_F \times \varepsilon}\right)} \quad (1)$$

Heterologous expression, purification and spectral characterization of LOV-based FPs. Expression and purification of all tested LOV-based fluorescent proteins (Table 1) was performed as described before[65], except that the isolated proteins were stored in phosphate buffered saline (PBS), pH 7.4. Furthermore, spectroscopic and photophysical analysis of CreiLOV, DsFbFP M49I, iLOV and SOPP, including the determination of fluorescence quantum yields and extinction coefficient followed the descriptions in the above mentioned publication.

Spectroscopic determination of singlet oxygen quantum yields of isolated LOV-FPs. Direct detection of $^1O_2$ phosphorescence at 1275 nm was carried out using a customized PicoQuant Fluotime 200 lifetime system and an AO-Z-473 solid state AOM Q-switched laser (Changchun New Industries Optoelectronics

Technology Co., China), used for excitation at 473 nm (<1.5 mW average power) and working at 1.5 kHz repetition rate. Further details on the instrumentation and methods used for $^1O_2$ detection are described elsewhere[45,90]. The time-resolved emission decays were analyzed by fitting *Eq. 2* to the data using GraphPad Prism 5.

$$S_{(t)} = S_{(0)}\frac{\tau_\Delta}{\tau_\Delta - \tau_T}\left(e^{\frac{-t}{\tau_\Delta}} - e^{\frac{-t}{\tau_T}}\right) \quad (2)$$

τ_T and τ_Δ are the lifetimes of the photosensitizer triplet state and of $^1O_2$, respectively and $S_{(0)}$ is a quantity proportional to Φ_Δ.

Φ_Δ was determined by comparing the $S_{(0)}$ values of optically-matched solutions of the corresponding flavoproteins and flavin mononucleotide (FMN) at 473 nm (Eq. 3)[91].

$$\phi_{\Delta,flavoprotein} = \frac{S_{(0)flavoprotein}}{S_{(0)FMN}}\phi_{\Delta,FMN} \quad (3)$$

FMN was taken as reference photosensitizer with $\Phi_\Delta = 0.51$ in PBS[92] and 0.57 in dPBS[45].

Determination of superoxide-anion and hydrogen peroxide formation of purified LOV-FPs. For the determination of LOV-FP-mediated O_2^-/H_2O_2 production the commercial Amplex® Red Hydrogen Peroxide/Peroxidase Assay Kit (Molecular Probes, Invitrogen) was used. The analysis was performed according to the manufacturer's manual with purified LOV-FPs adjusted to a final absorbance of 0.05 at $\lambda = 450$ nm. To determine entire type I-dependent ROS formation, 4 U ml^{-1} superoxide dismutase (Sigma Aldrich) was supplemented to the reaction buffer to catalyze the conversion of superoxide anions to H_2O_2. Sample irradiation was conducted in microtiter plates (FlowerPlates) within a microbioreactor (BioLector, m2p-labs GmbH, Baesweiler, Germany) at 1100 rpm and 30 °C with a LED blue light source emitting light with λ_{max} at 447 nm and an intensity of ~10 mW cm^{-2}. Fluorescence intensities of resorufin (the product of the Amplex Red reaction) were determined in a microplate reader (Infinite® M1000 Pro, Tecan Group LTD., Maennedorf, Switzerland) with an excitation wavelength of $\lambda = 571$ nm and an emission at $\lambda =$ at 585 nm. To determine final H_2O_2 concentrations after LOV-FP illumination, the measured resorufin fluorescence intensities were subsequently compared with an H_2O_2 calibration curve (0 to 20 µM H_2O_2).

Analysis of LOV-FP-mediated stress response in *E. coli*. To analyze differences in global oxidative stress response in *E. coli* that were induced by Pp2FbFP and DsFbFP M49I, a DNA microarray-based analysis was conducted. *E. coli* cells expressing the respective photosensitizers were cultivated in LB-media, supplemented with 50 µg ml^{-1} kanamycin (25 ml culture volume in 500 ml Erlenmeyer flasks, start $OD_{580} = 0.05$). The cultures were incubated at 37 °C and under continuous shaking (130 rpm) in the dark. LOV-FP expression was induced by addition of 0.4 mM IPTG during the logarithmic growth phase (~$OD_{580} = 0.7$). Three hours after induction, cultures were divided into two test cultures with a volume of 25 ml in 500 ml Erlenmeyer flasks and an OD_{580} of 0.5. For light treatment one of these cultures was placed between two blue-light emitting LED-panels ($\lambda = 462$ nm, 100 mW cm^{-2}, Insta Elektro, Lüdenscheid, Germany, panel distance: 30 cm), whereas the second culture was kept in the dark. To ensure optimal oxygen supply of cells during irradiation process, cultures were supplemented with stirring bars and placed on magnetic stirrers. Since the selectivity and efficiency of light-driven ROS formation strongly vary between those proteins, we first evaluated different exposure times (5, 10, 15 and 30 minutes) for full induction of LOV-FP-mediated stress-response in *E. coli*. To this end, samples containing an OD_{580} of 3 were harvested after light treatment by centrifugation and the cell pellets were shock frozen in liquid nitrogen and subsequently stored at −80 °C. RNA isolation, cDNA synthesis, microarray hybridization and data analysis were performed as described before[93] except the utilization of DNA-microarrays carrying probes for the genes of *E. coli* MG1655 strain. Detailed transcriptome analyses of light-induced stress-response based on independent biological triplicates were finally carried out under best illumination conditions (i.e. Pp2FbFP: 5 min, DsFbFP M49I: 15 min) as described above.

Data Availability

The datasets generated during and/or analyzed during the current study are available from the corresponding authors on reasonable request. The microarray data generated and analyzed in this study are accessible in NCBI's Gene Expression Omnibus through accession number GSE110168.

References

1. Agostinis, P. *et al.* Photodynamic therapy of cancer: an update. *CA Cancer J Clin* **61**, 250–281, https://doi.org/10.3322/caac.20114 (2011).
2. St Denis, T. G. *et al.* All you need is light: antimicrobial photoinactivation as an evolving and emerging discovery strategy against infectious disease. *Virulence* **2**, 509–520, https://doi.org/10.4161/viru.2.6.17889 (2011).
3. Wainwright, M. *et al.* Photoantimicrobials-are we afraid of the light? *Lancet Infect Dis* **17**, e49–e55, https://doi.org/10.1016/S1473-3099(16)30268-7 (2017).
4. Halliwell, B. & Gutteridge, J. M. C. *Free radical in biology and medicine*. 5th Edition edn, Oxford University Press (2015).
5. Robertson, C. A., Evans, D. H. & Abrahamse, H. Photodynamic therapy (PDT): a short review on cellular mechanisms and cancer research applications for PDT. *J Photochem Photobiol B* **96**, 1–8, https://doi.org/10.1016/j.jphotobiol.2009.04.001 (2009).
6. Skovsen, E., Snyder, J. W., Lambert, J. D. & Ogilby, P. R. Lifetime and diffusion of singlet oxygen in a cell. *J Phys Chem B* **109**, 8570–8573, https://doi.org/10.1021/jp051163i (2005).
7. Glaeser, J., Nuss, A. M., Berghoff, B. A. & Klug, G. Singlet oxygen stress in microorganisms. *Adv Microb Physiol* **58**, 141–173, https://doi.org/10.1016/B978-0-12-381043-4.00004-0 (2011).

8. Nonell, S. & Flors, C. *Singlet Oxygen: Applications in Biosciences and Nanosciences*. Vol. 1&2 (The Royal Society of Chemistry, 2016).
9. Flors, C. & Nonell, S. In *Handbook of Photomedicine* (eds M. R. Hamblin & Y. Huang) 275–280 (CRC Press, 2013).
10. Bulina, M. E. *et al.* A genetically encoded photosensitizer. *Nat Biotechnol* **24**, 95–99, https://doi.org/10.1038/nbt1175 (2006).
11. Jiménez-Banzo, A. *et al.* Singlet oxygen photosensitisation by GFP mutants: oxygen accessibility to the chromophore. *Photochem Photobiol Sci* **9**, 1336–1341, https://doi.org/10.1039/c0pp00125b (2010).
12. Shcherbakova, D. M., Shemetov, A. A., Kaberniuk, A. A. & Verkhusha, V. V. Natural photoreceptors as a source of fluorescent proteins, biosensors, and optogenetic tools. *Annu Rev Biochem* **84**, 519–550, https://doi.org/10.1146/annurev-biochem-060614-034411 (2015).
13. Wojtovich, A. P. & Foster, T. H. Optogenetic control of ROS production. *Redox Biol* **2**, 368–376, https://doi.org/10.1016/j.redox.2014.01.019 (2014).
14. Souslova, E. A., Mironova, K. E. & Deyev, S. M. Applications of genetically encoded photosensitizer miniSOG: from correlative light electron microscopy to immunophotosensitizing. *J Biophotonics* **10**, 338–352, https://doi.org/10.1002/jbio.201600120 (2017).
15. Jiménez-Banzo, A., Nonell, S., Hofkens, J. & Flors, C. Singlet oxygen photosensitization by EGFP and its chromophore HBDI. *Biophys J* **94**, 168–172, https://doi.org/10.1529/biophysj.107.107128 (2008).
16. Ragàs, X., Cooper, L. P., White, J. H., Nonell, S. & Flors, C. Quantification of photosensitized singlet oxygen production by a fluorescent protein. *Chemphyschem* **12**, 161–165, https://doi.org/10.1002/cphc.201000919 (2011).
17. Vegh, R. B. *et al.* Reactive oxygen species in photochemistry of the red fluorescent protein "Killer Red". *Chem Commun (Camb)* **47**, 4887–4889, https://doi.org/10.1039/c0cc05713d (2011).
18. Wang, Y., Nartiss, Y., Steipe, B., McQuibban, G. A. & Kim, P. K. ROS-induced mitochondrial depolarization initiates PARK2/PARKIN-dependent mitochondrial degradation by autophagy. *Autophagy* **8**, 1462–1476, https://doi.org/10.4161/auto.21211 (2012).
19. Liao, Z. X., Li, Y. C., Lu, H. M. & Sung, H. W. A genetically-encoded KillerRed protein as an intrinsically generated photosensitizer for photodynamic therapy. *Biomaterials* **35**, 500–508, https://doi.org/10.1016/j.biomaterials.2013.09.075 (2014).
20. Serebrovskaya, E. O. *et al.* Targeting cancer cells by using an antireceptor antibody-photosensitizer fusion protein. *Proc Natl Acad Sci USA* **106**, 9221–9225, https://doi.org/10.1073/pnas.0904140106 (2009).
21. Serebrovskaya, E. O. *et al.* Phototoxic effects of lysosome-associated genetically encoded photosensitizer KillerRed. *J Biomed Opt* **19**, 071403, https://doi.org/10.1117/1.JBO.19.7.071403 (2014).
22. Shirmanova, M. V. *et al.* Phototoxic effects of fluorescent protein KillerRed on tumor cells in mice. *J Biophotonics* **6**, 283–290, https://doi.org/10.1002/jbio.201200056 (2013).
23. Bulina, M. E. *et al.* Chromophore-assisted light inactivation (CALI) using the phototoxic fluorescent protein KillerRed. *Nat Protoc* **1**, 947–953, https://doi.org/10.1038/nprot.2006.89 (2006).
24. Destaing, O. *et al.* β1A integrin is a master regulator of invadosome organization and function. *Mol Biol Cell* **21**, 4108–4119, https://doi.org/10.1091/mbc.E10-07-0580 (2010).
25. Lan, L. *et al.* Novel method for site-specific induction of oxidative DNA damage reveals differences in recruitment of repair proteins to heterochromatin and euchromatin. *Nucleic Acids Res* **42**, 2330–2345, https://doi.org/10.1093/nar/gkt1233 (2014).
26. Serebrovskaya, E. O. *et al.* Light-induced blockage of cell division with a chromatin-targeted phototoxic fluorescent protein. *Biochem J* **435**, 65–71, https://doi.org/10.1042/BJ20101217 (2011).
27. Shibuya, T. & Tsujimoto, Y. Deleterious effects of mitochondrial ROS generated by KillerRed photodynamic action in human cell lines and *C. elegans*. *J Photochem Photobiol B* **117**, 1–12, https://doi.org/10.1016/j.jphotobiol.2012.08.005 (2012).
28. Wang, B. *et al.* Mitochondria are targets for peroxisome-derived oxidative stress in cultured mammalian cells. *Free Radic Biol Med* **65**, 882–894, https://doi.org/10.1016/j.freeradbiomed.2013.08.173 (2013).
29. Takemoto, K. *et al.* SuperNova, a monomeric photosensitizing fluorescent protein for chromophore-assisted light inactivation. *Sci Rep* **3**, 2629, https://doi.org/10.1038/srep02629 (2013).
30. Sarkisyan, K. S. *et al.* KillerOrange, a Genetically Encoded Photosensitizer Activated by Blue and Green Light. *PLoS One* **10**, e0145287, https://doi.org/10.1371/journal.pone.0145287 (2015).
31. Pletneva, N. V. *et al.* Crystal Structure of Phototoxic Orange Fluorescent Proteins with a Tryptophan-Based Chromophore. *PLoS One* **10**, e0145740, https://doi.org/10.1371/journal.pone.0145740 (2015).
32. Roy, A., Carpentier, P., Bourgeois, D. & Field, M. Diffusion pathways of oxygen species in the phototoxic fluorescent protein KillerRed. *Photochem Photobiol Sci* **9**, 1342–1350, https://doi.org/10.1039/c0pp00141d (2010).
33. Merzlyak, E. M. *et al.* Bright monomeric red fluorescent protein with an extended fluorescence lifetime. *Nat Methods* **4**, 555–557, https://doi.org/10.1038/nmeth1062 (2007).
34. Ruiz-González, R., White, J. H., Agut, M., Nonell, S. & Flors, C. A genetically-encoded photosensitiser demonstrates killing of bacteria by purely endogenous singlet oxygen. *Photochem Photobiol Sci* **11**, 1411–1413, https://doi.org/10.1039/c2pp25126d (2012).
35. Shu, X. *et al.* A genetically encoded tag for correlated light and electron microscopy of intact cells, tissues, and organisms. *PLoS Biol* **9**, e1001041, https://doi.org/10.1371/journal.pbio.1001041 (2011).
36. Ruiz-González, R. *et al.* Singlet oxygen generation by the genetically encoded tag miniSOG. *J Am Chem Soc* **135**, 9564–9567, https://doi.org/10.1021/ja4020524 (2013).
37. Pimenta, F. M., Jensen, R. L., Breitenbach, T., Etzerodt, M. & Ogilby, P. R. Oxygen-dependent photochemistry and photophysics of "miniSOG," a protein-encased flavin. *Photochem Photobiol* **89**, 1116–1126, https://doi.org/10.1111/php.12111 (2013).
38. Burgers, P. P. *et al.* A small novel A-kinase anchoring protein (AKAP) that localizes specifically protein kinase A-regulatory subunit I (PKA-RI) to the plasma membrane. *J Biol Chem* **287**, 43789–43797, https://doi.org/10.1074/jbc.M112.395970 (2012).
39. Boassa, D. *et al.* Mapping the subcellular distribution of alpha-synuclein in neurons using genetically encoded probes for correlated light and electron microscopy: implications for Parkinson's disease pathogenesis. *J Neurosci* **33**, 2605–2615, https://doi.org/10.1523/JNEUROSCI.2898-12.2013 (2013).
40. Boassa, D., Nguyen, P., Hu, J., Ellisman, M. H. & Sosinsky, G. E. Pannexin2 oligomers localize in the membranes of endosomal vesicles in mammalian cells while Pannexin1 channels traffic to the plasma membrane. *Front Cell Neurosci* **8**, 468, https://doi.org/10.3389/fncel.2014.00468 (2014).
41. Ludwig, A. *et al.* Molecular composition and ultrastructure of the caveolar coat complex. *PLoS Biol* **11**, e1001640, https://doi.org/10.1371/journal.pbio.1001640 (2013).
42. Cleyrat, C. *et al.* Mpl traffics to the cell surface through conventional and unconventional routes. *Traffic* **15**, 961–982, https://doi.org/10.1111/tra.12185 (2014).
43. Ou, H. D., Deerinck, T. J., Bushong, E., Ellisman, M. H. & O'Shea, C. C. Visualizing viral protein structures in cells using genetic probes for correlated light and electron microscopy. *Methods* **90**, 39–48, https://doi.org/10.1016/j.ymeth.2015.06.002 (2015).
44. Strickfaden, H., Xu, Z. Z. & Hendzel, M. J. Visualization of miniSOG Tagged DNA Repair Proteins in Combination with Electron Spectroscopic Imaging (ESI). *J Vis Exp*. https://doi.org/10.3791/52893 (2015).
45. Rodriguez-Pulido, A. *et al.* Assessing the potential of photosensitizing flavoproteins as tags for correlative microscopy. *Chem Commun (Camb)* **52**, 8405–8408, https://doi.org/10.1039/c6cc03119f (2016).
46. Lin, J. Y. *et al.* Optogenetic inhibition of synaptic release with chromophore-assisted light inactivation (CALI). *Neuron* **79**, 241–253, https://doi.org/10.1016/j.neuron.2013.05.022 (2013).

47. Qi, Y. B., Garren, E. J., Shu, X., Tsien, R. Y. & Jin, Y. Photo-inducible cell ablation in *Caenorhabditis elegans* using the genetically encoded singlet oxygen generating protein miniSOG. *Proc Natl Acad Sci USA* **109**, 7499–7504, https://doi.org/10.1073/pnas.1204096109 (2012).
48. Xu, S. & Chisholm, A. D. Highly efficient optogenetic cell ablation in *C. elegans* using membrane-targeted miniSOG. *Sci Rep* **6**, 21271, https://doi.org/10.1038/srep21271 (2016).
49. Makhijani, K. *et al.* Precision Optogenetic Tool for Selective Single- and Multiple-Cell Ablation in a Live Animal Model System. *Cell Chem Biol* **24**, 110–119, https://doi.org/10.1016/j.chembiol.2016.12.010 (2017).
50. Mironova, K. E. *et al.* Genetically encoded immunophotosensitizer 4D5scFv-miniSOG is a highly selective agent for targeted photokilling of tumor cells *in vitro*. *Theranostics* **3**, 831–840, https://doi.org/10.7150/thno.6715 (2013).
51. Ryumina, A. P. *et al.* Flavoprotein miniSOG as a genetically encoded photosensitizer for cancer cells. *Biochim Biophys Acta* **1830**, 5059–5067, https://doi.org/10.1016/j.bbagen.2013.07.015 (2013).
52. Westberg, M., Holmegaard, L., Pimenta, F. M., Etzerodt, M. & Ogilby, P. R. Rational design of an efficient, genetically encodable, protein-encased singlet oxygen photosensitizer. *J Am Chem Soc* **137**, 1632–1642, https://doi.org/10.1021/ja511940j (2015).
53. Westberg, M., Bregnhøj, M., Etzerodt, M. & Ogilby, P. R. No Photon Wasted: An Efficient and Selective Singlet Oxygen Photosensitizing Protein. *J Phys Chem B* **121**, 9366–9371, https://doi.org/10.1021/acs.jpcb.7b07831 (2017).
54. Drepper, T. *et al.* Reporter proteins for *in vivo* fluorescence without oxygen. *Nat Biotechnol* **25**, 443–445, https://doi.org/10.1038/nbt1293 (2007).
55. Drepper, T., Gensch, T. & Pohl, M. Advanced *in vivo* applications of blue light photoreceptors as alternative fluorescent proteins. *Photochem Photobiol Sci* **12**, 1125–1134, https://doi.org/10.1039/c3pp50040c (2013).
56. Chapman, S. *et al.* The photoreversible fluorescent protein iLOV outperforms GFP as a reporter of plant virus infection. *Proc Natl Acad Sci USA* **105**, 20038–20043, https://doi.org/10.1073/pnas.0807551105 (2008).
57. Christie, J. M. *et al.* Structural tuning of the fluorescent protein iLOV for improved photostability. *J Biol Chem* **287**, 22295–22304, https://doi.org/10.1074/jbc.M111.318881 (2012).
58. Mukherjee, A. *et al.* Engineering and characterization of new LOV-based fluorescent proteins from *Chlamydomonas reinhardtii* and *Vaucheria frigida*. *ACS Synth Biol* **4**, 371–377, https://doi.org/10.1021/sb500237x (2015).
59. Wingen, M., Jaeger, K. E., Gensch, T. & Drepper, T. Novel Thermostable Flavin-binding Fluorescent Proteins from Thermophilic Organisms. *Photochem Photobiol* **93**, 849–856, https://doi.org/10.1111/php.12740 (2017).
60. Cui, G. Z. *et al.* Targeted gene engineering in *Clostridium cellulolyticum* H10 without methylation. *J Microbiol Methods* **89**, 201–208, https://doi.org/10.1016/j.mimet.2012.02.015 (2012).
61. Król, J. E., Rogers, L. M., Krone, S. M. & Top, E. M. Dual reporter system for *in situ* detection of plasmid transfer under aerobic and anaerobic conditions. *Appl Environ Microbiol* **76**, 4553–4556, https://doi.org/10.1128/AEM.00226-10 (2010).
62. Landete, J. M. *et al.* Use of anaerobic green fluorescent protein versus green fluorescent protein as reporter in lactic acid bacteria. *Appl Microbiol Biotechnol* **99**, 6865–6877, https://doi.org/10.1007/s00253-015-6770-3 (2015).
63. Lobo, L. A., Smith, C. J. & Rocha, E. R. Flavin mononucleotide (FMN)-based fluorescent protein (FbFP) as reporter for gene expression in the anaerobe *Bacteroides fragilis*. *FEMS Microbiol Lett* **317**, 67–74, https://doi.org/10.1111/j.1574-6968.2011.02212.x (2011).
64. Walter, J. *et al.* Flavin mononucleotide-based fluorescent proteins function in mammalian cells without oxygen requirement. *PLoS One* **7**, e43921, https://doi.org/10.1371/journal.pone.0043921 (2012).
65. Wingen, M. *et al.* The photophysics of LOV-based fluorescent proteins-new tools for cell biology. *Photochem Photobiol Sci* **13**, 875–883, https://doi.org/10.1039/c3pp50414j (2014).
66. Christie, J. M., Gawthorne, J., Young, G., Fraser, N. J. & Roe, A. J. LOV to BLUF: flavoprotein contributions to the optogenetic toolkit. *Mol Plant* **5**, 533–544, https://doi.org/10.1093/mp/sss020 (2012).
67. Torra, J. *et al.* Singlet oxygen photosensitisation by the fluorescent protein Pp2FbFP L30M, a novel derivative of *Pseudomonas putida* flavin-binding Pp2FbFP. *Photochem Photobiol Sci* **14**, 280–287, https://doi.org/10.1039/c4pp00338a (2015).
68. Crowley, L. C. *et al.* Measuring Cell Death by Propidium Iodide Uptake and FlowCytometry. *Cold Spring Harb Protoc* **2016**, pdb rot087163, https://doi.org/10.1101/pdb.prot087163 (2016).
69. Tim, M. Strategies to optimize photosensitizers for photodynamic inactivation of bacteria. *J Photochem Photobiol B* **150**, 2–10, https://doi.org/10.1016/j.jphotobiol.2015.05.010 (2015).
70. Hamblin, M. R. Antimicrobial photodynamic inactivation: a bright new technique to kill resistant microbes. *Curr Opin Microbiol* **33**, 67–73, https://doi.org/10.1016/j.mib.2016.06.008 (2016).
71. Giuliani, F. *et al. In vitro* resistance selection studies of RLP068/Cl, a new Zn(II) phthalocyanine suitable for antimicrobial photodynamic therapy. *Antimicrob Agents Chemother* **54**, 637–642, https://doi.org/10.1128/AAC.00603-09 (2010).
72. Maisch, T. Resistance in antimicrobial photodynamic inactivation of bacteria. *Photochem Photobiol Sci* **14**, 1518–1526, https://doi.org/10.1039/c5pp00037h (2015).
73. Kashef, N. & Hamblin, M. R. Can microbial cells develop resistance to oxidative stress in antimicrobial photodynamic inactivation? *Drug Resist Updat* **31**, 31–42, https://doi.org/10.1016/j.drup.2017.07.003 (2017).
74. Rabello, B. R. *et al.* Singlet oxygen dosimetry using uric acid as a chemical probe: Systematic evaluation. *J Photochem Photobiol A Chem* **238**, 53–62, https://doi.org/10.1016/j.jphotochem.2012.04.012 (2012).
75. Åslund, F., Zheng, M., Beckwith, J. & Storz, G. Regulation of the OxyR transcription factor by hydrogen peroxide and the cellular thiol-disulfide status. *Proc Natl Acad Sci USA* **96**, 6161–6165 (1999).
76. Chiang, S. M. & Schellhorn, H. E. Regulators of oxidative stress response genes in *Escherichia coli* and their functional conservation in bacteria. *Arch Biochem Biophys* **525**, 161–169, https://doi.org/10.1016/j.abb.2012.02.007 (2012).
77. Marinho, H. S., Real, C., Cyrne, L., Soares, H. & Antunes, F. Hydrogen peroxide sensing, signaling and regulation of transcription factors. *Redox Biol* **2**, 535–562, https://doi.org/10.1016/j.redox.2014.02.006 (2014).
78. Zheng, M. *et al.* DNA microarray-mediated transcriptional profiling of the *Escherichia coli* response to hydrogen peroxide. *J Bacteriol* **183**, 4562–4570, https://doi.org/10.1128/JB.183.15.4562-4570.2001 (2001).
79. Mishra, S. & Imlay, J. Why do bacteria use so many enzymes to scavenge hydrogen peroxide? *Arch Biochem Biophys* **525**, 145–160, https://doi.org/10.1016/j.abb.2012.04.014 (2012).
80. Altuvia, S., Almirón, M., Huisman, G., Kolter, R. & Storz, G. The *dps* promoter is activated by OxyR during growth and by IHF and sigma S in stationary phase. *Mol Microbiol* **13**, 265–272 (1994).
81. Moore, J. M. *et al.* Roles of Nucleoid-Associated Proteins in Stress-Induced Mutagenic Break Repair in Starving *Escherichia coli*. *Genetics* **201**, 1349–1362, https://doi.org/10.1534/genetics.115.178970 (2015).
82. Xia, X. *et al.* OxyR-activated expression of Dps is important for *Vibrio cholerae* oxidative stress resistance and pathogenesis. *PLoS One* **12**, e0171201, https://doi.org/10.1371/journal.pone.0171201 (2017).
83. Moparthi, V. K. *et al.* The two Dps proteins, NpDps2 and NpDps5, are involved in light-induced oxidative stress tolerance in the N_2-fixing cyanobacterium *Nostoc punctiforme*. *Biochim Biophys Acta* **1857**, 1766–1776, https://doi.org/10.1016/j.bbabio.2016.08.003 (2016).
84. Jang, S. & Imlay, J. A. Hydrogen peroxide inactivates the *Escherichia coli* Isc iron-sulphur assembly system, and OxyR induces the Suf system to compensate. *Mol Microbiol* **78**, 1448–1467, https://doi.org/10.1111/j.1365-2958.2010.07418.x (2010).
85. Liu, G., Zhou, J., Fu, Q. S. & Wang, J. The *Escherichia coli* azoreductase AzoR Is involved in resistance to thiol-specific stress caused by electrophilic quinones. *J Bacteriol* **191**, 6394–6400, https://doi.org/10.1128/JB.00552-09 (2009).

86. Gurmu, D. *et al*. The crystal structure of the protein YhaK from *Escherichia coli* reveals a new subclass of redox sensitive enterobacterial bicupins. *Proteins* **74**, 18–31, https://doi.org/10.1002/prot.22128 (2009).
87. Kim, S. Y., Kim, E. J. & Park, J. W. Control of singlet oxygen-induced oxidative damage in *Escherichia coli*. *J Biochem Mol Biol* **35**, 353–357 (2002).
88. Yan, L., Kanada, M., Zhang, J., Okazaki, S. & Terakawa, S. Photodynamic Treatment of Tumor with Bacteria Expressing KillerRed. *PLoS One* **10**, e0131518, https://doi.org/10.1371/journal.pone.0131518 (2015).
89. Hanahan, D. Studies on transformation of *Escherichia coli* with plasmids. *J Mol Biol* **166**, 557–580 (1983).
90. Jiménez-Banzo, A., Ragàs, X., Kapusta, P. & Nonell, S. Time-resolved methods in biophysics. 7. Photon counting vs. *analog time-resolved singlet oxygen phosphorescence detection. Photochem Photobiol Sci* **7**, 1003–1010, https://doi.org/10.1039/b804333g (2008).
91. Nonell, S. & Braslavsky, S. E. Time-resolved singlet oxygen detection. *Methods Enzymol* **319**, 37–49 (2000).
92. Baier, J. *et al*. Singlet oxygen generation by UVA light exposure of endogenous photosensitizers. *Biophys J* **91**, 1452–1459, https://doi.org/10.1529/biophysj.106.082388 (2006).
93. Pelzer, A. *et al*. Subtilase SprP exerts pleiotropic effects in *Pseudomonas aeruginosa*. *Microbiologyopen* **3**, 89–103, https://doi.org/10.1002/mbo3.150 (2014).
94. Davari, M. D. *et al*. Photophysics of the LOV-Based Fluorescent Protein Variant iLOV-Q489K Determined by Simulation and Experiment. *J Phys Chem B* **120**, 3344–3352, https://doi.org/10.1021/acs.jpcb.6b01512 (2016).
95. Whitby, L. G. A new method for preparing flavin-adenine dinucleotide. *Biochem J* **54**, 437–442 (1953).
96. Ito, K. *et al*. Crystallization and preliminary X-ray analysis of AzoR (azoreductase) from *Escherichia coli*. *Acta Crystallogr Sect F Struct Biol Cryst Commun* **61**, 399–402, https://doi.org/10.1107/S1744309105007918 (2005).
97. Ito, K. *et al*. Three-dimensional structure of AzoR from *Escherichia coli*. An oxidereductase conserved in microorganisms. *J Biol Chem* **281**, 20567–20576, https://doi.org/10.1074/jbc.M513345200 (2006).
98. Matthews, K. S. & Nichols, J. C. Lactose repressor protein: functional properties and structure. *Prog Nucleic Acid Res Mol Biol* **58**, 127–164 (1998).
99. Darwin, A. J. The phage-shock-protein response. *Mol Microbiol* **57**, 621–628, https://doi.org/10.1111/j.1365-2958.2005.04694.x (2005).
100. Ray, W. K., Zeng, G., Potters, M. B., Mansuri, A. M. & Larson, T. J. Characterization of a 12-kilodalton rhodanese encoded by *glpE* of *Escherichia coli* and its interaction with thioredoxin. *J Bacteriol* **182**, 2277–2284 (2000).
101. Makui, H. *et al*. Identification of the *Escherichia coli* K-12 Nramp orthologue (MntH) as a selective divalent metal ion transporter. *Mol Microbiol* **35**, 1065–1078 (2000).
102. Tao, K. *oxyR*-dependent induction of *Escherichia coli grx* gene expression by peroxide stress. *J Bacteriol* **179**, 5967–5970 (1997).
103. Ritz, D. *et al*. Thioredoxin 2 is involved in the oxidative stress response in *Escherichia coli*. *J Biol Chem* **275**, 2505–2512 (2000).
104. Hou, J. Y., Sauer, R. T. & Baker, T. A. Distinct structural elements of the adaptor ClpS are required for regulating degradation by ClpAP. *Nat Struct Mol Biol* **15**, 288–294, https://doi.org/10.1038/nsmb.1392 (2008).
105. Izu, H., Adachi, O. & Yamada, M. Purification and characterization of the *Escherichia coli* thermoresistant glucokinase encoded by the *gntK* gene. *FEBS Lett* **394**, 14–16 (1996).

Acknowledgements
This work was supported by grants from the Federal Ministry of Education and Research (OptoSys, FKZ 031A16), from the Spanish Ministerio de Economía y Competitividad (CTQ2016-78454-C2-1-R) and from Fundació la Marató de TV3 (grant No. 20133133). JT thanks the Boehringer Ingelheim Foundation for a Travel Grant.

Author Contributions
S.E., M.W., T.P., T.G., S.N. and T.D. conceived and designed the experiments. S.E., M.W., J.T., G.B., T.G., R.R.G., N.L.B. and F.H. performed the experiments. S.E., M.W., J.T., G.B., R.R.G., T.P., T.G., S.N. and T.D. analyzed the data. M.W., S.N., K.E.J. and T.D. wrote the manuscript. All authors read and approved the final manuscript.

Additional Information
Supplementary information accompanies this paper at https://doi.org/10.1038/s41598-018-33291-4.

Competing Interests: The authors declare no competing interests.

Publisher's note: Springer Nature remains neutral with regard to jurisdictional claims in published maps and institutional affiliations.

II.2.2. PHOTOSENSITIZERS FOR ANTIMICROBIAL PHOTODYNAMIC INACTIVATION

Genetically encoded photosensitizers as light-triggered antimicrobial agents

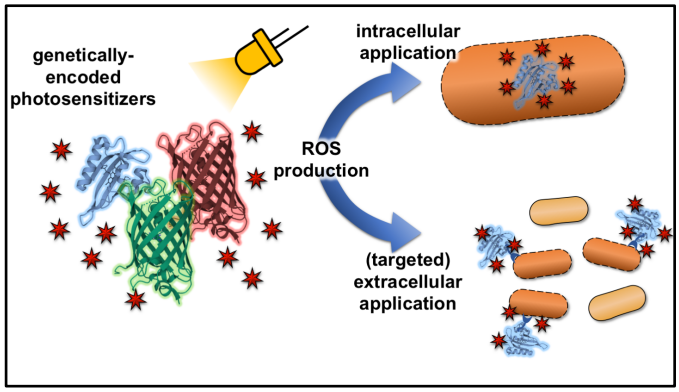

Fabienne Hilgers*, Nora Lisa Bitzenhofer*, Yannic Ackermann, Alina Burmeister, Alexander Grünberger, Karl-Erich Jaeger, Thomas Drepper

Int. J. Mol. Sci., *20(18), 4608.* (2019). ijms20184608

The online version may be found at: 10.3390/ijms20184608

Status: published

For the Supporting Information see Appendix (**Chapter V.6.**, **page 445**).

Own contribution:

Designing and performing experiments, analyzing data, writing parts of the manuscript.

International Journal of
Molecular Sciences

MDPI

Article

Genetically Encoded Photosensitizers as Light-Triggered Antimicrobial Agents

Fabienne Hilgers [1,†], Nora Lisa Bitzenhofer [1,†], Yannic Ackermann [1], Alina Burmeister [2,3], Alexander Grünberger [2,3], Karl-Erich Jaeger [1,3] and Thomas Drepper [1,*]

1 Institute of Molecular Enzyme Technology, Heinrich-Heine-University Düsseldorf, Forschungszentrum Jülich GmbH, D-52428 Jülich, Germany; f.hilgers@fz-juelich.de (F.H.); n.bitzenhofer@fz-juelich.de (N.L.B.); yannic.ackermann@uni-duesseldorf.de (Y.A.); k.-e.jaeger@fz-juelich.de (K.-E.J.)
2 Multiscale Bioengineering, Bielefeld University, D-33501 Bielefeld, Germany; a.burmeister@fz-juelich.de (A.B.); alexander.gruenberger@uni-bielefeld.de (A.G.)
3 Institute of Bio- and Geosciences, IBG-1: Biotechnology, Forschungszentrum Jülich GmbH, D-52428 Jülich, Germany
* Correspondence: t.drepper@fz-juelich.de
† These authors contributed equally to this work.

Received: 2 August 2019; Accepted: 13 September 2019; Published: 17 September 2019

check for updates

Abstract: Diseases caused by multi-drug resistant pathogens have become a global concern. Therefore, new approaches suitable for treating these bacteria are urgently needed. In this study, we analyzed genetically encoded photosensitizers (PS) related to the green fluorescent protein (GFP) or light-oxygen-voltage (LOV) photoreceptors for their exogenous applicability as light-triggered antimicrobial agents. Depending on their specific photophysical properties and photochemistry, these PSs can produce different toxic ROS (reactive oxygen species) such as $O_2^{\bullet-}$ and H_2O_2 via type-I, as well as $^1O_2$ via type-II reaction in response to light. By using cell viability assays and microfluidics, we could demonstrate differences in the intracellular and extracellular phototoxicity of the applied PS. While intracellular expression and exogenous supply of GFP-related PSs resulted in a slow inactivation of *E. coli* and pathogenic Gram-negative and Gram-positive bacteria, illumination of LOV-based PSs such as the singlet oxygen photosensitizing protein SOPP3 resulted in a fast and homogeneous killing of these microbes. Furthermore, our data indicate that the ROS type and yield as well as the localization of the applied PS protein can strongly influence the antibacterial spectrum and efficacy. These findings open up new opportunities for photodynamic inactivation of pathogenic bacteria.

Keywords: photosensitizer (PS); light-oxygen-voltage (LOV) proteins; antimicrobial photodynamic inactivation (aPDI); green fluorescent protein (GFP); flavin-binding fluorescent protein (FbFP); optogenetics; extracellular phototoxicity; antibiotics

1. Introduction

Since the rapid worldwide emergence of multi-drug resistant bacteria, in conjunction with a decline in the development and production of new antimicrobial agents, the efficient treatment of various life-threatening pathogens has become increasingly endangered. For this reason, major research efforts aim to develop alternative antimicrobial therapies to prevent, treat, and finally eliminate multidrug resistance [1–3]. Antimicrobial photodynamic inactivation (aPDI) evolved in the last years as a method to treat microbial infections after realizing the potential of photodynamic therapy (PDT), which is increasingly used in cancer therapy [4,5]. PDT and aPDI combine the use of visible light with a light-sensitive dye—referred to as photosensitizer (PS)—and are based on the local formation of toxic reactive oxygen species (ROS).

The produced ROS react fast with molecules of the PS microenvironment and thus can immediately induce damages of lipid membranes, cell walls, proteins, and nucleic acids [6–8]. Because of the broad spectrum of ROS-sensitive targets, aPDI does not induce resistances in microorganisms and further allows efficient inactivation of multi-drug resistant pathogens [9–11].

Upon light absorption, the PS undergoes a transition from the electronic ground state to a singlet excited state and further to a longer-lived triplet state via intersystem crossing (ISC). Here, the generation of ROS can follow two alternative pathways: the triplet state-PS can interact with molecular oxygen by transferring an electron to O_2 yielding a superoxide radical anion ($O_2^{\bullet -}$) that can further be converted into other ROS, including hydrogen peroxide (H_2O_2) and the hydroxyl radical ($HO^{\bullet}$). This pathway is referred to as a type-I mechanism. Alternatively, the type-II pathway involves an energy transfer from the excited PS to molecular oxygen, thereby generating singlet oxygen ($^1O_2$). Due to its unstable electron configuration, this form is extremely transient and highly reactive, resulting in a lifetime of up to 2 µs and a diffusion range of ~150 nm, depending on the dynamics of the photosensitizing protein [12,13]. In contrast, hydrogen peroxide shows a lifetime of about 1 ms and thus can diffuse over longer distances or even between microbial cells [14,15].

Because of the short ROS lifetimes, the localization of the applied PSs and their close proximity to microbial target molecules can play an important role for efficient aPDI. Therefore, cationic photosensitizing chromophores are frequently used to predominantly bind negatively charged surfaces of Gram-positive and Gram-negative bacteria, thereby avoiding excessive damage to mammalian cells and tissues [16,17]. Most widely used cationic PSs, whose antibacterial activities against multi-drug resistant pathogenic bacteria could already successfully be demonstrated, include porphyrinoids like porphyrins, chlorins, and phthalocyanines, as well as fullerenes and phenothiazinium dyes (e.g., toluidine blue O and methylene blue) [18–22]. However, the application of chemical PSs as light-triggered anti-infectives face some major drawbacks, including (i) a limited selectivity for bacteria and pathogens, (ii) an inefficient uptake by microbial cells, (iii) their subsequent secretion by microbial multidrug efflux pumps, and (iv) their heterogeneous distribution within a microbial population or biofilm. In addition, the local environment can strongly influence the photophysics of a PS, which might result in a divergent phototoxicity in dependence on its localization and the targeted pathogen. These limitations provoked the development of more effective PSs including genetically encoded PSs. In contrast to chemical PSs, genetic engineering approaches enable the fusion of tailored targeting sequences (e.g., leader peptides or antibodies) to photosensitizing proteins thereby facilitating their accumulation at particular cellular structures, compartments, or pathogens of interest. In addition, genetically encoded PSs can be seen as protein encased phototoxic chromophores where the protein envelope ensures a constant local environment and robust ROS formation irrespective of the PS localization [23].

Two major classes of genetically encoded PSs have been established. The first class includes fluorescent proteins (FPs), which exhibit a green fluorescent protein (GFP)-like structure; the second class encompasses flavin-binding fluorescent proteins derived from the light-oxygen-voltage (LOV) photoreceptor domain of plants, algae, and bacteria (LOV-PSs) [24–27]. KillerRed and the Singlet Oxygen Generator (miniSOG) were the first members of the GFP and LOV families that have been described as genetically encoded PSs [28,29]. So far, these photosensitizing proteins could successfully be applied, for example, (i) in the analysis of ROS signaling [30,31], (ii) for killing cancer cells in different PDT approaches [32–36], and (iii) for light-mediated control of protein activity via chromophore-assisted light inactivation (CALI) [37–40]. Recently, the KillerRed-derivatives SuperNova and KillerOrange as well as the miniSOG variant SOPP3 were engineered, showing improved photosensitizer properties [25,26,41]. While SuperNova has similar spectral characteristics as described for the original KillerRed protein with an absorption maximum at 579 nm, the spectrally tuned derivative KillerOrange exhibits a blue-shifted spectrum with absorption maxima at 455 and 514 nm [25,26]. In contrast, as a typical member of the LOV family, SOPP3 can be excited with blue light (λ_{max} = 440 nm, [41]). Besides their spectral characteristics, the three PSs differ significantly in their ability to form ROS when irradiated [23,42]. In comparison to all of the so far characterized LOV-based PSs, SOPP3 exhibits the highest singlet oxygen quantum yield (Φ_Δ) of about 0.6 and spectroscopic in vitro characterization

revealed that this photosensitizer protein selectively produces singlet oxygen via type-II reaction [41]. On the other hand, KillerRed—and presumably also its derivatives—primarily generate the superoxide anion and downstream oxidants, such as hydrogen peroxide through type-I photochemistry [42–44].

In a recent study, we demonstrated that most LOV-based fluorescent proteins, which were originally designed as alternative reporters for the in vivo analysis of oxygen-limited systems [45,46], were potent photosensitizers that could be applied for a light-controlled killing of *E. coli* when expressed intracellularly [47]. Here, we have evaluated the intracellular phototoxicity of three further GFP- and LOV-related PSs using *E. coli* as a model organism. In addition, we analyzed the antimicrobial efficacy and spectrum of exogenously applied GFP- and LOV-PSs with different photosensitizing activities towards Gram-positive and Gram-negative pathogens. Finally, we show data indicating that the cell envelope of the human pathogen *Pseudomonas aeruginosa* can be targeted by using the lectin LecB fused to the recombinant photosensitizing protein DsFbFP M49I, which resulted in an increased phototoxicity.

2. Results and Discussion

2.1. Phototoxicity of SOPP3, SuperNova, and KillerOrange in the Cytoplasm of E. coli

To compare the applicability of SOPP3, SuperNova, and KillerOrange for aPDI, we initially analyzed their intracellular phototoxicity. To this end, we determined the viability of PS-producing *E. coli* cells after illumination with blue light (LED with λ_{max} = 448 nm for SOPP3 and KillerOrange) or orange light (λ_{max} = 600 nm for SuperNova) by counting the colony forming units (CFU). The phototoxic effects of the endogenous PSs towards *E. coli* cells were measured in dependence on different light intensities (130–1 mW cm^{-2}) as well as illumination times (0–30 min). As a reference, we additionally analyzed *E. coli* cells expressing EcFbFP, a LOV-based PS that was shown to perform moderate type-I and -II-mediated ROS formation resulting in an intermediate phototoxicity [47]. As shown in Figure 1, the increase of light intensity or illumination time resulted in a clear decrease of the number of viable bacterial cells for all of the tested LOV- and GFP-PSs, although the phototoxic efficacy differs strongly between the variants.

Remarkably, upon illumination with light intensities of 130 to 10 mW cm^{-2}, SOPP3 showed a very high phototoxicity as reflected by an almost complete cell death within the first 10 s of blue light illumination (Figure 1a–c). In comparison, for EcFbFP a more pronounced dependency on illumination time and light intensity could be observed. Surprisingly, the GFP-like PSs KillerOrange and SuperNova exhibited comparatively low light-induced toxicities. Consequently, high light intensities and prolonged illumination times up to 30 min were necessary to induce detectable cell death whereas low light intensities or short illumination times resulted in only minor or even no phototoxic effects (Figure 1). In contrast, for none of the applied illumination conditions significantly reduced cell viabilities could be observed when *E. coli* cells were used that harbor the empty expression vector. Furthermore, a very low light intensity of 1 mW cm^{-2} was not sufficient to induce an observable phototoxic effect for each of the tested PS proteins (Figure 1d). These control experiments clearly demonstrate that *E. coli* viability is only affected by appropriately illuminated PSs. Accordingly, the wavelength that has been used for the excitation of SOPP3 and KillerOrange did not activate phototoxicity of SuperNova and vice versa (Supplementary Figure S1a). Thus, the combination of blue light activated PSs with SuperNova allows a simultaneous application in one experimental setup, e.g., for studying the function of defined species within microbial consortia.

Since accumulation levels of PS proteins can strongly differ as demonstrated recently [47], we analyzed the intracellular phototoxicity of the chosen PS proteins in more detail by correlating cell death with the amount of functional photosensitizing protein per cell. To this end, we used the propidium iodide (PI) assay. The increase in PI fluorescence indicates the ability of the tested PS to damage *E. coli* cells through light-induced ROS generation. The obtained PI fluorescence can subsequently be normalized to the individual PS-dependent fluorescence intensity of cell culture as well as the specific fluorescence brightness of the respective PS and changes of PI fluorescence during the first 10-min irradiation period were used for comparing individual intracellular phototoxicities as

Int. J. Mol. Sci. **2019**, *20*, 4608

described recently [47]. Due to the high phototoxicity of the LOV-based photosensitizers, these studies were performed at a lower light intensity (10 mW cm^{-2}) to precisely determine illumination-dependent changes of *E. coli* cell viability in dependence on the corresponding PS activities. The results of the quantitative phototoxicity assay are presented in Figure 2a. As already indicated by the cell viability assay (Figure 1), SOPP3 exhibits by far the highest light-triggered antimicrobial activity of all tested LOV-based PSs as indicated by the almost maximally achievable change of PI fluorescence already after ten minutes of illumination (for comparison see also the results published by Endres and coworkers [47]). In contrast, the GFP-like proteins, KillerOrange and SuperNova are less-toxic photosensitizing proteins exhibiting no significant changes in PI fluorescence and only a slow and marginal increase of PI fluorescence, even after prolonged irradiation (Figure 2a) or increased light intensities (Supplementary Figure S1b).

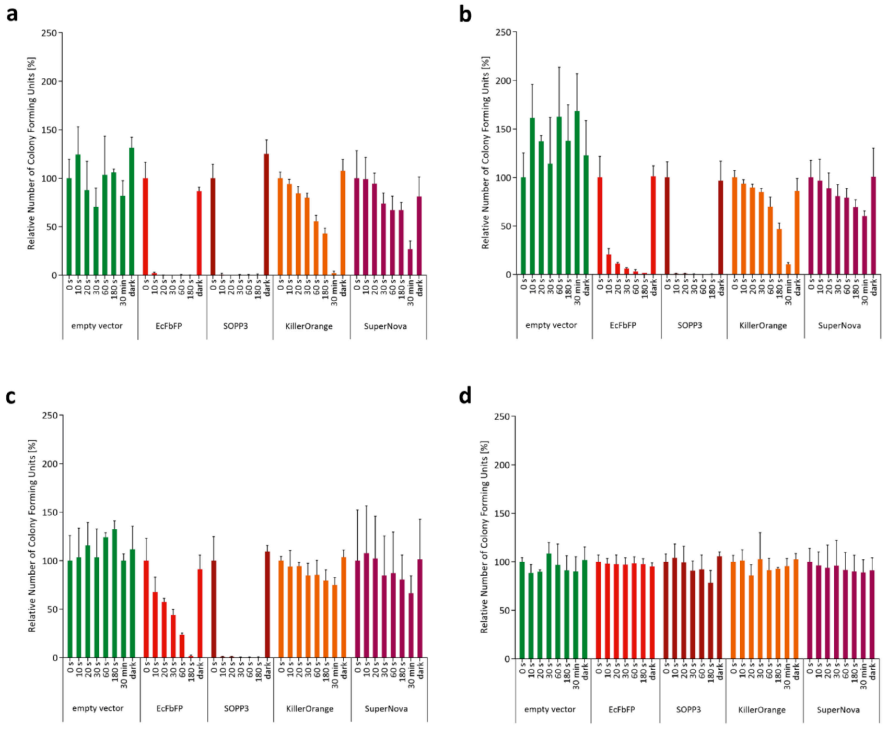

Figure 1. Analysis of colony forming units (CFU) for comparative analysis of in vivo phototoxicity of genetically encoded photosensitizers (PSs). The colony forming capacity of PS-producing *E. coli* cells was measured in dependence on illumination time and light intensity ((**a**) ~130 mW cm^{-2}; (**b**) ~90 mW cm^{-2}; (**c**) ~10 mW cm^{-2}; and (**d**) ~1 mW cm^{-2}). For this, cultures of *E. coli* BL21(DE3) cells harboring the respective expression vectors were diluted to a finale $OD_{580\ nm}$ of 0.1 in 1x PBS buffer (pH 7.4) and then illuminated with blue light (λ_{max} = 450 nm) and, in the case of SuperNova, with orange light (λ_{max} = 600 nm). As a control experiment, *E. coli* cells harboring an empty vector were also illuminated with blue light using the four light intensities. After given time points (0 to 30 min), aliquots of the irradiated cells were transferred to Lysogeny Broth (LB) agar plates and incubated overnight at 37 °C in the dark. Decrease of CFUs represents the time-dependent efficacy of the genetically encoded PSs. Data represent mean values of three independent experiments and their corresponding standard deviations indicated by error bars.

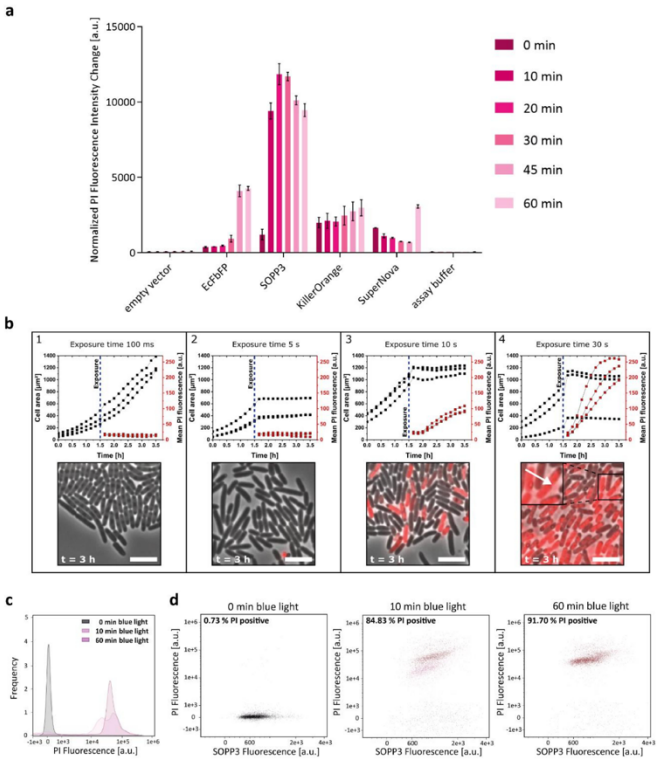

Figure 2. Quantitative in vivo phototoxicity studies of genetically encoded PSs using the propidium iodide (PI) cell death assay. (**a**) For the PI-based cell death assay, *E. coli* cells carrying the respective pET28a(+) derivatives were adjusted to an $OD_{580\ nm}$ of 0.5 in 1x PI assay buffer (pH 7.4) and illuminated with low light intensities (~10 mW cm^{-2}) of blue (λ_{max} = 447 nm) or orange light (λ_{max} = 600 nm). The bars indicate the change in PI fluorescence intensity (λ_{ex} = 535 nm; λ_{em} = 617 nm) in dependence on exposure time. The data were normalized to the amount of functional protein per cell to exclude an influence of different protein accumulation levels. The data represent the mean values of three independent experiments and the error bars indicate the calculated standard deviations. (**b**) Intracellular phototoxicity of SOPP3 in *E. coli*. Growth and PI fluorescence data of single cells were monitored over time in microfluidic experiments using *E. coli* pET28a-SOPP3. (1) 100 ms blue light exposure (λ_{max} = 445 nm) after 1.5 h cultivation time. (2) 5 s blue light exposure after 1.5 h cultivation time. (3) 10 s blue light exposure after 1.5 h cultivation time (4) 30 s blue light exposure after 1.5 h cultivation time. The arrow indicates a position where a cell lysis event resulted in the release of red fluorescent nucleic acids. In each graph, data from three representative microfluidic chambers are shown. Scale bar = 5 µm. (**c**) Measurement of cell death by PI uptake via flow cytometry (FCM). *E. coli* cells harboring the expression vector pET28a-SOPP3 were analyzed for fluorescence and gated based on forward scatter (FSC) and side scatter (SSC) to exclude cell debris and accumulation of cells. Samples for FCM were prepared as described for the PI-based cell death assay. The propidium iodide fluorescence intensity of each cell was measured using a 561 nm-laser (and a 611/31 nm (red) bandpass filter) and plotted using a log scale. The data shown in the histogram represent the frequency of cellular PI signal intensities for SOPP3 producing *E. coli* cells before (0 min) and after 10 and 60 min of blue light illumination. (**d**) For quantitative analysis of ROS-mediated cell death, the SOPP3 fluorescence of *E. coli* cells was analyzed with a 488 nm-laser, detected by a 528/46 nm bandpass filter and plotted against the PI fluorescence before and after blue light illumination. Dead *E. coli* cells (presented as red populations) are shifted to higher PI fluorescence values and the percentage of dead cells is displayed in the upper left corner. Living cells are represented as black populations. An empty vector control was also analyzed to exclude a toxic blue light effect on the cells (Supplementary Figure S2c).

Local variations in the cellular microenvironment including the uneven distribution of oxygen or nutrients, e.g., within a bacterial colony, can result in variations of cellular physiology and replication. Consequently, such inhomogeneities could affect the efficacy of PS-mediated phototoxicity that might, in turn, result in a delayed or heterogeneous killing of individual cells within a population. In a next step, we therefore analyzed if the light-induced antimicrobial effect occurs homogenously for every single cell on the microcolony level. For this purpose, *E. coli* cells expressing SOPP3, which showed the highest phototoxicity in previous experiments, were cultivated in microfluidic monolayer cultivation chambers. The growth chambers are designed to follow (i) cell growth, as well as (ii) distribution of intracellular protein accumulation (SOPP3 fluorescence), and (iii) cell death (PI fluorescence) before and after blue light exposure within a developing single-layered microcolony (Figure 2b and Supplementary Figure S2a).

The results of the representative microfluidic cultivation experiments are plotted as cell growth (chamber area that is occupied by growing cells) and mean PI fluorescence within a chamber during cultivation for four different exposure times (100 ms, 5 s, 10 s, and 30 s). Exemplary images of the cultivations at different exposure times are shown after 3 h cultivation. Interestingly, a strong impact of the exposure time on both the cell growth and the PI fluorescence intensity could be seen, leading to three different phenotypes. After an exposure time of 100 ms, cell viability is almost unaffected as indicated by the rapid increase of the cell area, while the respective PI fluorescence remained low. After an exposure of 5 s, the cell area stayed constant and therefore cell growth seemed to be impaired. However, no PI fluorescence signal was detectable; apparently, the cell membranes were not harmed yet by the produced ROS. Finally, after an exposure time of 10 s and 30 s, cell growth was completely inhibited and additionally, the PI fluorescence increased rapidly indicating a high ROS production and thereby an extensive damage of the cells and their membranes. Remarkably, although SOPP3 fluorescence was almost uniformly distributed in all cells as expected for the chosen *E. coli* expression system [48], a heterogeneous development of PI fluorescence could be observed after 10 s of blue light exposure which is independent of the respective position of the cells within the microcolony (Figure 2b and Supplementary Figure S2a). However, an illumination of 30 s resulted in an equally distributed PI fluorescence with comparable fluorescence signal intensities in all cells of the chamber, confirming a homogeneous and position-independent ROS response within the entire culture after prolonged illumination.

To further analyze the distribution of PS toxicity within a larger population (10,000 cells), ROS-mediated cell damage was quantified via flow cytometry (FCM) (Figure 2c,d). Bacterial events were gated by size and granularity (FSC and SSC) (Supplementary Figure S2b) and then the bacterial population was analyzed regarding the PI and SOPP3 fluorescence. The PI fluorescence was plotted against the respective PS fluorescence before and after blue light illumination (exposure time: 10 and 60 min). As expected, no significant PI signal could be measured in cells that were kept in the dark as well as in *E. coli* cells harboring the empty vector (Supplementary Figure 2c). After 10 min of blue light exposure, roughly 85% of the analyzed cells are dead, as indicated by the positive PI signal (shown in red). Interestingly, two subpopulations with slightly differing PI fluorescence intensities could be observed after 10 min of blue light exposure (Figure 2d). However, longer blue light illumination resulted in comparably strong PI fluorescence in 92% of the analyzed cells (Figure 2d, 60 min). These results are in good accordance with the microfluidic data, as PS-mediated toxicity resulted in a "two step" induction of PI fluorescence in dependence on the applied illumination time. At this point, however, it is worth mentioning that even a low PI fluorescence signal of a single cell already indicates large lesions of the cell membrane allowing influx of PI and thus its death. Therefore, the increase of the PI fluorescence signal at the single-cell level most probably reflects the time-delayed influx of PI and its subsequent intercalation into the DNA. Interestingly, we could also observe cell lysis events that resulted in the release of red fluorescent nucleic acids (Figure 2b, (4)) which might also lead to subsequent decrease of cellular PI fluorescence signal intensities. Taken together, single-cell analysis of SOPP3-mediated phototoxicity clearly demonstrates a high, light-triggered antimicrobial efficacy against *E. coli* cells that is almost independent of the local environment at least in the used experimental setup. These properties make SOPP3 and the other

genetically encoded photosensitizers suitable candidates for an application as light-driven antimicrobial agents in aPDI to fight human pathogens. However, for therapeutic applications PSs are usually added exogenously to the pathogenic organism instead of being synthetized intracellularly. For this reason, we next analyzed the extracellular phototoxicity of selected LOV-based and GFP-related PSs.

2.2. Extracellular Phototoxicity of Different LOV- and GFP-Photosensitizer Proteins

To study the applicability of genetically encoded photosensitizers as light-activated antimicrobial agents, the phototoxicity of exogenous GFP-related and LOV-based PSs was further analyzed. In addition to SOPP3, SuperNova, and KillerOrange, different LOV-based PSs were used in this study exhibiting divergent ratios of type-I and -II photosensitizing activities and, hence, intracellular phototoxicities: besides EcFbFP and DsFbFP M49I, two LOV variants showing both type-I and type-II photosensitizing activities accompanied by comparatively high intracellular phototoxicities, Pp1FbFP and Pp2FbFP were chosen as PS derivatives with a moderate antimicrobial efficacy but selective singlet oxygen formation [47]. The extracellular killing efficiency of purified photosensitizing proteins has first been investigated in a plate spot assay using *E. coli* cells as a proof of concept. As shown in Figure 3a, exogenous addition of all tested PSs, except SuperNova, clearly affected the cell viability of *E. coli* cells after high intensity light irradiation (130 mW cm^{-2}). However, in contrast to intracellularly located PSs, the exogenous approach required a longer exposure time of 8 (EcFbFP) to 15 min (Pp1-, Pp2FbFP, KillerOrange). In a control experiment, where *E. coli* cells were illuminated with possibly toxic blue light without adding purified PSs, no changes in growth behavior could be observed (Supplementary Figure S3a).

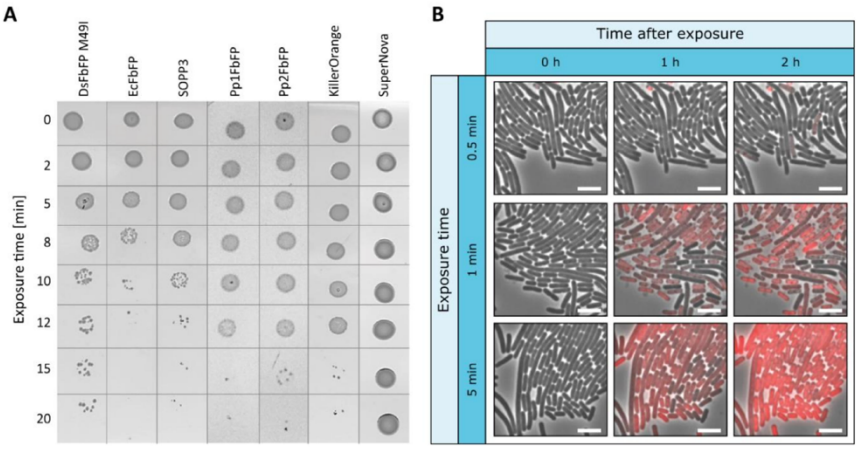

Figure 3. Extracellular antimicrobial activity of genetically encoded PSs on *E. coli* cells. (**a**) To investigate the effect of extracellularly added PSs, purified proteins have been analyzed by a plate spot assay. For this, *E. coli* cells were supplemented with the respective PS variants adjusted to an $OD_{450\ nm}$ (or $OD_{580\ nm}$ in the case of SuperNova) of 0.2 and then illuminated for different time periods with intense (~130 mW cm^{-2}) blue (λ_{max} = 448 nm) or orange light (λ_{max} = 600 nm). Subsequently, 3 µL of the irradiated cells were dropped on agar plates and incubated at 37 °C overnight. To exclude blue light toxicity, a plate spot assay without the addition of a photosensitizer was performed as a control experiment (Supplementary Figure S3a). (**b**) Extracellular phototoxicity of SOPP3 on *E. coli* cells. Representative images from microfluidic experiments with extracellular SOPP3 ($OD_{450\ nm}$ = 0.3) addition and blue light exposure (λ_{max} = 445 nm). Images are shown for selected exposure times (0.5 min, 1 min, 5 min) and times after exposure (0 h, 1 h, 2 h). Scale bar = 5 µm.

To further analyze the accessibility of single *E. coli* cells to PS proteins that are assembled within a microcolony, the bacteria were cultivated in a microfluidic monolayer chip while adding purified SOPP3 to the growth medium (Figure 3b). As expected, illumination of extracellular PSs also resulted in almost complete cell death as indicated by increasing PI fluorescence in single cells. Remarkably, a similar heterogeneous PI pattern could be observed at an intermediate exposure time of 1 min, which is again independent of the relative position of bacterial cells within the microcolony. An irradiation of five minutes, however, also resulted in a strong PI signal that occurs homogenously within the whole *E. coli* population. Again, compared to the above described microfluidic observation with intracellularly expressed PSs, approximately 10-fold longer illumination times are necessary to reach a comparable phototoxic effect. Consequently, we could demonstrate that *E. coli* can efficiently and homogenously be killed using exogenously applied PS proteins.

Next, we tested the extracellular PS against the facultative pathogenic Gram-positive bacteria *Staphylococcus epidermidis* and *Staphylococcus aureus* [49,50] as well as *Corynebacterium glutamicum*, which is related to clinically concerning *Corynebacterium diphtheria* and *Mycobacterium tuberculosis* [51,52]. In addition, the Gram-negative non-pathogenic bacterium *Pseudomonas putida* and the opportunistic human pathogen *Pseudomonas aeruginosa*, whose carbapenem-resistant strains where grouped by the World Health Organization (WHO) into the "Priority 1: CRITICAL" class of pathogens [53], were included in the phototoxicity assay. All results of the plate spot assays are shown in Supplementary Figure S3b–f. Based on this data set and experimental setup, the phototoxic effect depended on the used photosensitizer, as well as the tested microorganisms, and light-induces growth impairment could roughly be classified into five categories as summarized in Figure 4. For example, *P. putida* is rather sensitive to extracellularly added photosensitizers, as illumination resulted in a pronounced growth impairment irrespective of the tested PS variants. Similar results were observed with *C. glutamicum* and *E. coli* where only SuperNova did not show a phototoxic effect. Remarkably, the pathogenic species exhibited an increased tolerance towards photodynamic inactivation. For instance, cell growth of *P. aeruginosa* was only significantly affected by DsFbFP M49I, EcFbFP, and SOPP3 (Figure 4 and Supplementary Figure S3f). In contrast, the Gram-positive pathogens *S. epidermidis* and *S. aureus* could only be killed by the variants Pp1- and Pp2FbFP that are known to be less-toxic while exclusively forming $^1O_2$ via type-II reaction (Figure 4 and Supplementary Figure S3b,c [47]). This observation is in good agreement with previous reports describing that Gram-negative bacteria are more susceptible to $O_2^{\bullet-}$, H_2O_2, and $HO^{\bullet}$ whereas Gram-positive bacteria show higher sensitivities towards $^1O_2$ [54,55]. These differences might be explained by the divergent morphology: while Gram-negative bacteria possess an outer membrane that acts as an additional permeability barrier for extracellularly generated singlet oxygen, Gram-positive bacteria allow a direct translocation of the PS through the more permeable cell wall thereby facilitating a direct accessibility of the cytoplasmic membrane to this highly toxic ROS [56,57].

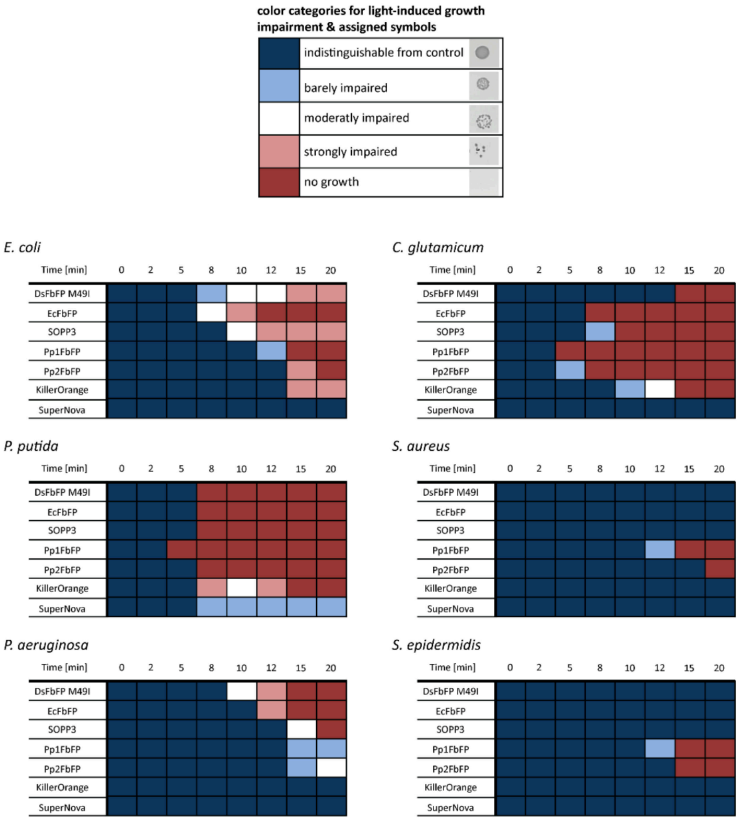

Figure 4. Extracellular antimicrobial activity of seven genetically encoded PSs against different bacterial strains. The growth responses of *E. coli*, *P. putida*, *P. aeruginosa*, *C. glutamicum*, *S. aureus*, and *S. epidermidis* were analyzed after addition of PSs by a plate spot assay. The detected colony formations were classified into five categories according to their cell survival: no growth impairment (dark blue), barely impaired growth (light blue), moderately impaired growth (white), strongly impaired growth (light red), and completely killed cells (dark red). For a better understanding of the data, the observed colony appearances, which correspond to the respective color categories, are shown in the upper panel.

In this context, it should be noted that Westberg and coworkers could demonstrate by spectroscopic characterization that SOPP3 produces singlet oxygen with a quantum yield which fits to the quantum yield of FMN triplet state formation thereby implicating elimination of a competing type-I reaction in this engineered PS [41]. In addition, SOPP3 exhibits a very high singlet oxygen quantum yield (Φ_Δ) of about 0.6 [41], as compared to Pp1- und Pp2-FbFP (Φ_Δ = 0.23 and 0.11) [47]. Therefore, we expected comparable antibiotic spectra of SOPP3, Pp1FbFP and Pp2FbFP for the tested bacteria but with differential phototoxicities (SOPP3 > Pp1FbFP > Pp2FbFP). However, the results presented here surprisingly indicate that the antimicrobial spectrum of SOPP3 rather resembles that of EcFbFP and DsFbFP M49I although these PSs are capable of efficiently producing $O_2^{\bullet-}$ and H_2O_2 via type-I in addition to $^1O_2$ producing type-II reaction [47]. To analyze, if differences in the antimicrobial spectra could be explained by the PS's individual capabilities to perform type-I photosensitizing reactions under the tested exogenous conditions, we subsequently quantified $O_2^{\bullet-}$ and H_2O_2 formation in vitro as described recently [47]. Therefore, the Amplex®Red reagent was used, which is converted to the red-colored product resorufin in the presence of H_2O_2. The reaction is catalyzed by a horseradish peroxidase (HRP) in a 1:1 stoichiometry, thus allowing a direct correlation between the detected

absorption of resorufin and the generated hydrogen peroxide. Since the Amplex®Red assay detects hydrogen peroxide, a superoxide dismutase (SOD) was added to the reaction mixture in order to enzymatically convert $O_2^{\bullet-}$ generated by the purified PS proteins upon illumination into H_2O_2. As expected, light exposure of EcFbFP and DsFbFP M49I resulted in considerable amounts of H_2O_2 formation after an illumination time of 5 min, whereas barely increased resorufin absorption could be detected in the samples containing Pp1- and Pp2FbFP thereby corroborating our previously published results (Supplementary Figure S4). Unexpectedly, KillerOrange and SuperNova showed a comparatively low type-I photosensitizing activity. In accordance with this observation, the two GFP-like PSs needed a much longer illumination time of up to 30 min to produce detectable amounts of H_2O_2, which could also explain the weak phototoxicities that were observed in the in vivo experiments. Surprisingly, SOPP3 exhibited the by far highest H_2O_2 production level, which is almost four times higher than EcFbFP and DsFbFP M49I. These results give thus a first indication that the specificity and efficiency of type-I and –II ROS formation seem to shape the efficacy and antimicrobial spectrum of the tested genetically encoded photosensitizers. However, especially the selectivity of ROS formation, inside and outside of living cells, clearly requires further examination by using appropriate detection methods under conditions relevant for the specific application.

Our data illustrated, as expected, that the localization of the applied PSs in either the intra- or extracellular space of bacterial cells plays an important role for the phototoxicity. Presumably, this is caused by variations of the PS concentration within the respective compartment, which, in turn, can directly influence the frequency of interactions between ROS and the ROS-sensitive cellular structures. To evaluate, if the extracellular phototoxicity of a protein-encased PS can be enhanced by specifically directing it to the bacterial cell envelope, we fused DsFbFP M49I, which exhibits the highest extracellular phototoxicity for the human pathogen *P. aeruginosa*, to the lectin LecB (Figure 5a). LecB is a multivalent sugar-binding protein derived from *P. aeruginosa* that is naturally formed by the bacterium for biofilm formation and initiation of human infections [58–60]. This lectin can bind to various sugar moieties located on the surface of *P. aeruginosa* cells [61,62] and it was recently published that LecB immobilized on the surface of hydrogels can be used to efficiently capture *P. aeruginosa* cells for their treatment with antimicrobial peptides [63]. Based on these findings, we analyzed if LecB can be used to facilitate the extracellular attachment of C-terminally fused DsFbFP M49I to *P. aeruginosa* for their efficient photodynamic inactivation. To analyze, if extracellular DsFbFP M49I-LecB shows improved cellular binding and phototoxicity, PS and PI fluorescence signals of washed cells were monitored in comparison to free DsFbFP M49I in the absence and presence of LecB-inhibiting D-mannose. The results shown in Figure 5b indicate that fusion with LecB enables DsFbFP M49I to bind over four times more efficiently to *P. aeruginosa* cells in the absence of D-mannose. More importantly, the extracellular antimicrobial phototoxicity of DsFbFP M49I-LecB increased 3.8-fold in comparison to the unmodified PS (Figure 5c). Consequently, the DsFbFP M49I-LecB fusion protein allowed an improved targeting and photodynamic inactivation of *P. aeruginosa*, presumably because more of the PS proteins are positioned close to the cell surface and ROS thus have to overcome shorter distances in order to damage cellular components.

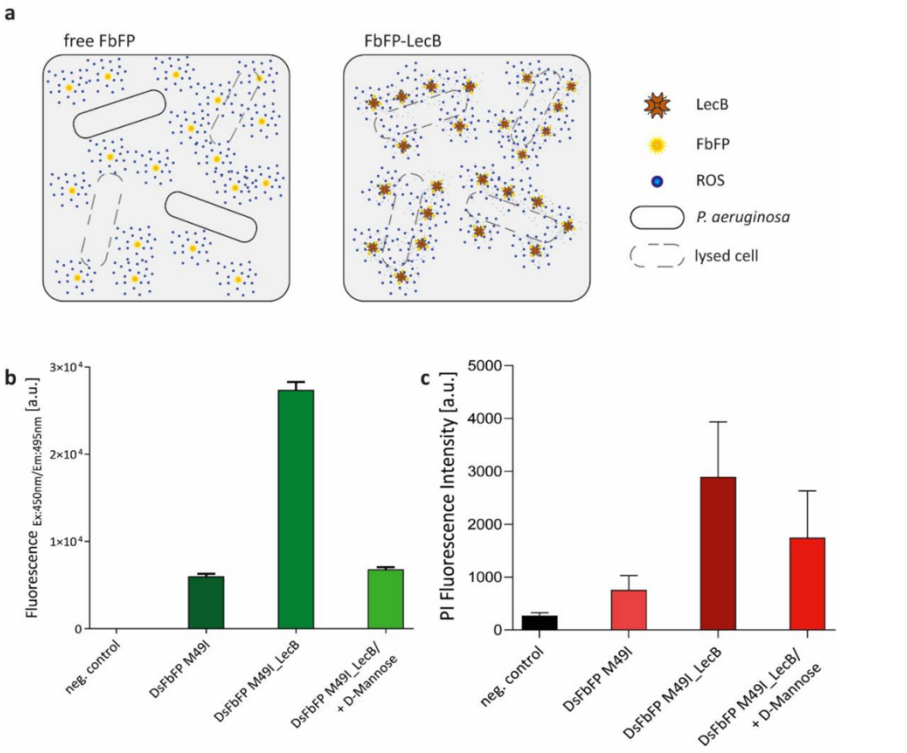

Figure 5. Phototoxicity towards *Pseudomonas aeruginosa* of a genetically encoded photosensitizer fused to the lectin LecB. (**a**) General strategy for improving extracellular phototoxicity of genetically encoded PSs by directing them to specific cellular structures. In this case, fusion with the lectin LecB can help to direct the PS to the *P. aeruginosa* cell envelope thereby allowing efficient killing of the pathogenic bacterium by light-driven ROS formation. (**b**) In order to test improved binding of DsFbFP M49I_LecB to *P. aeruginosa* cells, planktonic cells were mixed with DsFbFP or DsFbFP M49I-LecB (adjusted to a final $OD_{450\,nm}$ of 0.2), washed and subsequently investigated for FbFP fluorescence. In addition, the fusion protein DsFbFP M49I-LecB was incubated with D-mannose (final concentration 200 mg mL^{-1}), which reduces fluorescence by targeted detachment from the cell surface. As a control experiment, *P. aeruginosa* cells without the addition of photosensitizers were measured. The data represent the mean values of three independent experiments and the error bars indicate the calculated standard deviations. (**c**) In vivo phototoxicity analysis was performed to evaluate the effect of DsFbFP M49I-LecB. To avoid that direct contact of PI and ROS, produced by extracellular PS upon illumination, leads to a decrease of PI fluorescence (see supplementary Figure S5 for details), the PI assay for monitoring cell viability was adapted by incubating the PSs with the *P. aeruginosa* cells first and then adding PI after a washing step. Both free and fused photosensitizers were used for comparison. As a control experiment, cells without the addition of DsFbFP M49I or DsFbFP M49I-LecB were used. The data represent the mean values of three independent experiments and the calculated standard deviations are shown.

3. Materials and Methods

3.1. Construction of Expression Vectors

The genes of SOPP3, KillerOrange, and SuperNova were codon optimized for expression in *Escherichia coli*, *Rhodobacter capsulatus*, and *Pseudomonas putida* and obtained by commercial gene synthesis (Eurofins Genomics, Ebersberg, Germany; Geneart Gene Synthesis, distributed by Thermo Fisher Scientific, Regensburg, Germany) (Supplementary Figure S6). The genes were hydrolyzed

with *Nde*I and *Xho*I whose restriction sites were placed during synthesis at 5′ and 3′ ends of each gene, respectively, and they were subsequently cloned into the *Nde*I and *Xho*I sites of the commercially available pET28a(+) vector (Novagen, distributed by Merck KGaA, Darmstadt, Germany). For generating the PS-LecB fusion protein, cloning was performed via the InFusion® HD Cloning Plus kit (Takara Bio Europe, St Germain en Laye, France) as indicated by the supplier. Therefore, the DsFbFP M49I gene was amplified by PCR using primer pair 1/2 (Supplementary Table S1) (containing homologous sequences suitable for integration into the *Nho*I/*Xho*I hydrolyzed plasmid pURE [62], which in turn contains the *lecB* gene), and the plasmid pET28a-DsFbFP M49I as a template [47]. For the following purification a 6x-Histidine-tag was added to the previously constructed plasmid by mutagenesis primer pair 3/4 (Supplementary Table S1) (containing a His_6-tag) and using the InFusion® HD Cloning Plus kit (Takara Bio, Mountain View, CA, USA). All cloning experiments were conducted using *Escherichia coli* DH5α [64]. For isolation and purification of plasmid DNA from bacterial cells, the "innuPREP Plasmid Mini Kit" (Analytik Jena, Jena, Germany) was used. All newly constructed expression vectors were verified by DNA-sequencing (Eurofins Genomics, Ebersberg, Germany) (Supplementary Table S1).

3.2. Heterologous Expression and Purification

Expression of the genetically encoded PSs as well as the fusion constructs was performed in *E. coli* strain BL21(DE3) (Novagen #69450, distributed by Merck KGaA, Darmstadt, Germany). Cells were grown in 1 L auto-induction (AI) medium containing 47.6 g L^{-1} terrific broth (TB) (ready-to-use-mixture; Carl Roth, Karlsruhe, Germany), 0.05% glucose and 0.2% lactose in 5 L shake flasks at 37 °C for 24 h. For stable plasmid replication, media were supplemented with 50 µg mL^{-1} kanamycin or 100 µg mL^{-1} ampicillin, respectively. After harvesting, bacterial cells were resuspended in lysis buffer (50 mM NaH_2PO_4, 300 mM NaCl, pH 8.0) and disrupted using a French Press Cell Disrupter (Thermo Electron Corporation, Waltham, MA, USA). Supernatant of cell lysates was clarified by centrifugation (30 min, 4000 rpm, 4 °C) and subsequently applied to a 5 mL Ni^{2+}-NTA metal-ion-exchange-chromatography-superflow-column (Qiagen, Hilden, Germany) with a flowrate of 2 mL min^{-1} and washed with eight column volumes of wash buffer (50 mM NaH_2PO_4, 300 mM NaCl, 50 mM imidazole, pH 8.0). Finally, the target proteins were eluted with the same buffer containing 250 mM imidazole. After purification, buffer exchange was performed in 10 kDa molecular-weight cutoff concentration units (Pall Corporation, New York, NY, USA). The sugar binding function and fluorescence activity of the DsFbFP M49I-LecB fusion partners were proven using a hemolysis assay and fluorescence spectrometry (Ackermann et al.). The purified proteins were stored in protein storage buffer (10 mM NaH_2PO_4, 10 mM NaCl, pH 8.0) at 4 °C in the dark.

3.3. Phototoxicity Analysis in Escherichia coli

To quantitatively determine the intracellular phototoxic effect of the photosensitizers, the colony forming capacity was measured in dependence on exposure time and light intensity. The experiment was performed as described before using light intensities of ~130 to 1 mW cm^{-2} and different illumination times (0 to 3 min) [47]. However, the illumination time was extended up to 30 min for the GFP-like photosensitizers as well as the empty vector control. Furthermore, for SuperNova, a light intensity of 85 mW cm^{-2} and 8 mW cm^{-2} at 580 nm was achieved by using a high-power LED (Nichia NCSA219B-V1 SMD-LED, amber, λ_{max} = 600 nm, 1 W; maximal light intensity at 600 nm = 138 mW cm^{-2}, emission spectra are shown in supplementary Figure S7) placed at the top of a macro cuvette or upon 5.5 cm long spacers, respectively. The intensity was determined with the help of an optical power and energy meter (PM100D, Thorlabs, Newton, NJ, USA). Emission spectra of the used high-power LEDs were measured with a fluorescence spectrometer (Varian Cary Eclipse, Agilent Technologies, Ratingen, Germany). Additionally, the influence of a fourth light intensity (1 mW cm^{-2}) was investigated. To reach the intensity of 1 mW cm^{-2} a programmable matrix of light-emitting diodes has been assembled with the assistance of Prof. Dr. Andreas Möglich as previously described [65].

For this approach, 1000 µL of the *E. coli* cells, which have been adjusted to a final $OD_{580\,nm}$ of 0.1 were transferred into a black colored 96-deepwell plate (Riplate® RW, 43001-0216, black, Ritter GmbH, Schwabmünchen, Germany) and illuminated with the programmable LED matrix which has been directly placed on top of the deepwell plate.

Light-induced cell death was furthermore analyzed using propidium iodide (PI) which is a fluorescent dye that selectively enters dead cells and shows a significant fluorescence at λ = 617 nm after intercalation into DNA [66]. The experiment was performed with *E. coli* BL21(DE3) cells (Novagen, distributed by Merck KGaA, Darmstadt, Germany) transformed with recombinant pET28a(+) expression vectors (Supplementary Table S1) which allows the expression of the respective photosensitizers. The expression culture was inoculated to an $OD_{580\,nm}$ of 0.05 in Lysogeny Broth (LB) medium (Carl Roth, Karlsruhe, Germany) supplemented with 50 µg mL^{-1} kanamycin. Cultivation was performed in a 48-well microtiter plate (FlowerPlate, m2p-labs GmbH, Baesweiler, Germany) with a final volume of 1 mL at 37 °C and 1200 rpm. After induction with 0.4 mM IPTG at an $OD_{580\,nm}$ of 0.6 to 0.8, the cells were incubated for 3 h under continuous shaking. Subsequently, the cells were adjusted to an $OD_{580\,nm}$ of 0.5, washed with PBS buffer (pH 7.4) and finally resuspended in 1 mL PI assay buffer (100 µM EDTA, 5 µM PI in PBS, pH 7.4). The samples were transferred into another FlowerPlate and illuminated with blue light (λ = 447 nm, 10 mW cm^{-2}) in a microbioreactor (BioLector, m2p-labs GmbH, Baesweiler, Germany). In the case of SuperNova, spacers of 5.5 cm were positioned between the sample and the high-power LED (Nichia NCSA219B-V1 SMD-LED, amber, λ = 600 nm, 1 W, resulting in a light intensity of 8 mW cm^{-2} at 580 nm) as described above. At several time points, 100 µL of the irradiated cell solution were transferred into a 96-well microtiter plate (Greiner Bio-One GmbH, Frickenhausen, Germany) and analyzed regarding the respective PS fluorescence (LOV-based PS: λ_{ex} = 450 nm, λ_{em} = 495 nm; KillerOrange: λ_{ex} = 450 nm, λ_{em} = 555 nm; SuperNova: λ_{ex} = 580 nm, λ_{em} = 610 nm) as wells as PI fluorescence (λ_{ex} = 535 nm, λ_{em} = 617 nm) using a microplate reader (Infinite® M1000 Pro, Tecan Group LTD., Maennedorf, Switzerland). For evaluation, the PI fluorescence was normalized to the expression coefficient (ExCo) to determine PS-mediated phototoxicity regardless of its expression efficiency in *E. coli* [47]. The normalized PI intensity (I_n) was determined using equation 1, where I_{raw} is the raw PI fluorescence, I_{PS} the LOV-FP-fluorescence intensity of the cell culture before blue light illumination, Φ_F the fluorescence quantum yield and ε the molar extinction coefficient of the respective LOV-FP (equation 1):

$$I_n = \frac{I_{raw}}{\left(\frac{I_{PS}}{\Phi_F \; x \; \varepsilon}\right)} \quad (1)$$

The following values were used for calculation of the normalized PI intensity (I_n): EcFbFP (ε = 14,500 M^{-1} cm^{-1}; Φ_F = 0.44) [46], SOPP3 (ε = 15,000 M^{-1} cm^{-1}; Φ_F = 0.41) [41], KillerOrange (ε = 22,600 M^{-1} cm^{-1}; Φ_F = 0.42) [26], SuperNova (ε = 33,600 M^{-1} cm^{-1}; Φ_F = 0.30) [25].

3.4. Single-Cell Cultivation and Analysis

To address the question whether the PI signal and with that the light-induced damage of cells via ROS generation occurs homogenously within in the culture, single-cell analysis has been carried out using flow cytometry and microfluidic analysis.

3.4.1. Flow Cytometry (FCM)

Flow cytometry that allows multiparametric analysis of cellular characteristic, has been used to analyze bacterial cells regarding their intrinsic fluorescence and cell viability using PI. Based on the PI assay, *E. coli* BL21(DE3) cells (Novagen, distributed by Merck KGaA, Darmstadt, Germany) harboring the expression vector pET28a-SOPP3 has been cultivated in LB medium (Carl Roth, Karlsruhe, Germany) supplemented with 50 µg mL^{-1} kanamycin and inoculated with an $OD_{580\,nm}$ of 0.05 in 100 mL shake flasks at 37 °C and 120 rpm. *E. coli* cells carrying the empty vector were used as an appropriate control experiment. When cultures reached an optical density of 0.6 to 0.8 (approximately after

an incubation time of 2 h) gene expression was induced by adding 0.4 mM IPTG and cultivation was continued at the same conditions for 3 h. Then, the cells were harvested by centrifugation (2 min, 15,000 rpm, RT), washed in PBS buffer (pH 7.4) and finally adjusted to an $OD_{580\ nm}$ of 0.5 in 1 mL PI assay buffer containing PBS, 100 µM EDTA and 5 µM PI and then transferred into a 48-well microtiter plate (Round Well Plate, m2p-labs GmbH, Baesweiler, Germany). Illumination was performed using a BioLector (λ = 447 nm, 10 mW cm^{-2}, m2p-labs GmbH, Baesweiler, Germany). After 0, 10 and 60 min, aliquots (100 µL) of the irradiated cultures were taken and analyzed with a flow cytometer (Amnis® CellStreamTM System, Merck, now Luminex Corporation, Austin, USA). Samples were analyzed using a 561 nm-laser with a maximum power of 150 mW and fluorescence was detected by a 611/31 nm (red) bandpass filter. Furthermore, the intrinsic SOPP3 fluorescence was measured with a 488 nm-laser (maximal laser power of 200 mW) and detected by a 528/46 nm bandpass filter. To exclude cell debris and cell accumulations, the cells were also analyzed regarding their size (forward scatter, FSC) and granularity (side scatter, SSC). FSC was measured using a FSC laser with 30% of the laser power (456/51 nm bandpass filter) and for the SSC a dedicated laser with 100% of the laser power (773/56 nm bandpass filter) was used. Based on the scatter plots, bacterial cells were gated from irrelevant counts for fluorescence analysis. Flow cytometric data were evaluated with the CellStreamTM Analysis Software (Merck, now Luminex Corporation, Austin, TX, USA).

3.4.2. Microfluidic Chip Design and Fabrication

Disposable polydimethylsiloxane (PDMS) chips for single-cell analysis were fabricated as previously described [67,68]. In short, photolithography was used for the production of a structured silicon wafer, which was used as a master mold for PDMS softlithography. The microfluidic chips consist of three arrays of cultivation chambers with 50 cultivation chambers each (dimensions of one cultivation chamber: 1 µm × 60 µm × 70 µm). The chamber height of 1 µm restricts cell growth to a monolayer, allowing the analysis of cell growth with full spatio-temporal resolution [69]. The chamber arrays are interconnected by parallel-arranged 10 µm deep supply channels.

3.4.3. Microfluidic Single-Cell Cultivation

Prior chip inoculation cells were pre-cultured in 100 mL (filling volume: 10 mL) shake flasks until the $OD_{580\ nm}$ reached a value of 0.5. The chip was inoculated with cell suspension until a few cells got randomly trapped in the cultivation chambers [70]. Afterwards, the cells were continuously perfused with fresh medium using a flow rate of 200 nL min^{-1}. During cultivation the chip was kept at 37 °C. All microfluidic experiments for the analysis of intracellular phototoxicity were performed with *E. coli* Tuner(DE3) harboring pET28a-SOPP3. After chip inoculation, cells were cultivated for 1.5 h with a continuous supply of LB medium containing additionally 0.1 mM IPTG, 0.1 mM EDTA, and 0.1 µM PI. Subsequently, single chambers were exposed to blue light (fluorescence filter λ_{max} = 445 nm) with exposure times ranging from 100 ms to 10 s. Extracellular phototoxicity of SOPP3 was tested with *E. coli* Tuner(DE3) wild-type cells that were grown in the microfluidic chip for 1.5 h with continuous LB medium supply. Then the medium was exchanged with LB medium containing SOPP3 ($OD_{450\ nm}$ = 0.3) and 0.1 µM PI. A higher medium flow (900 nL min^{-1}) was applied to exchange the medium rapidly. After 20 min the flow was stopped to induce batch-like conditions [48] and single chambers were exposed to blue light with times ranging from 30 s to 5 min.

3.4.4. Live-Cell Imaging and Image Analysis

Microfluidic experiments were performed on an inverted automated microscope (Nikon Eclipse Ti, Nikon, Tokyo, Japan), equipped with a laser assisted focus system for optimal imaging. A benchtop incubation chamber (PECON, Germany) ensured optimal temperature conditions. The inlets of the microfluidic systems were connected to a syringe pump system (neMESYS, CETONI, Korbussen, Germany) for continuous medium supply. Nikon software NIS Elements AR 4.30.02 was used for automated time-lapse imaging. The microfluidic chip was placed in an in-house fabricated

chip-holder and phase contrast and fluorescence images were taken every 10 min using a 100x oil immersion objective (CFI Plan Apo Lambda DM 100×-magnification, NA 1.45).

The PI fluorescence was captured with a mCherry filter (λ_{ex} = 562 nm, λ_{em} = 641 nm, DM= 593 nm) and blue light was applied with a blue light filter (λ_{ex} = 445 nm, λ_{em} = 494 nm, DM = 470 nm). Fluorescence light intensity was set to 10% of maximum intensity (max. 3.5 W white light output).

Segmentation was performed using the neural network-based segmentation tool JUNN (Sachs et al.), which is based upon the U-Net [71] neural network structure. Segmented images were further processed with the open source software Fiji [72]. Phototoxicity was quantified by an increase in PI fluorescence inside the cells. The cell area for each image was calculated and mean fluorescence intensities of each chamber was determined by measuring the fluorescence value and subtracting the background fluorescence.

3.5. Extracellular Phototoxicity Analysis

Analysis of the extracellular phototoxicity was performed with six different bacterial strains, including Gram-negative and -positive organisms. Cultivation was performed in LB medium (Carl Roth, Karlsruhe, Germany) in 100 mL (filling volume: 10 mL) shake flasks inoculated with an $OD_{580\,nm}$ of 0.05 of the respective bacterial strain. Cultures containing cells of *E. coli* BL21(DE3), *Pseudomonas aeruginosa* PAO1 (ATCC: 27853), *Staphylococcus aureus* (ATCC: 25923) or *S. epidermidis* (ATCC: 12228) were incubated at 37 °C for 5 h. For cultivating *P. putida* KT2440 (ATCC: 47054) or *Corynebacterium glutamicum* (ATCC: 13032) cells, a cultivation temperature of 30 °C was set. After incubation, the cells were diluted to a cell density corresponding to an $OD_{580\,nm}$ of 0.25 in PBS buffer (pH 7.4). Subsequently, 15 µL of the cells were transferred into a macro cuvette, purified photosensitizer was added with a final absorption of 0.2 at its absorption maximum (450 nm or 580 nm) and the suspension was then adjusted to a final volume of 150 µL with 1x PBS buffer (pH 7.4). The macro cuvette was directly placed on top of a blue (Nichia NCSB219B-V1 SMD-LED, royal blue, λ_{max} = 448 nm, 130 mW cm^{-2}) or an orange light-emitting LED (Nichia NCSA219B-V1 SMD-LED, amber, λ_{max} = 600 nm, 138 mW cm^{-2}). In order to ensure a constant room temperature during exposure, cooling units were installed on both sides of the cuvette. At given time points (0 to 20 min), 3 µL aliquots were taken out of the irradiated cell solutions and dropped on LB agar plates. Additionally, light-induced effects in the absence of extracellularly supplied photosensitizers were analyzed for cultures of all bacterial strains. The agar plates were incubated at 37 °C or in case of *P. putida* KT2440 and *C. glutamicum* at 30 °C overnight. Phototoxicity of extracellularly added PSs is indicated by growth impairment.

To adapt the PI assay to the requirements of extracellular PS addition, some preliminary experiments with pure DNA were performed. 10 µL salmon sperm (1 mg mL^{-1}) (Sigma-Aldrich Chemie GmbH, Hamburg, Germany) was used and EcFbFP was added according to an $OD_{450\,nm}$ of 0.2. The solution was then filled up to 90 µL with 1x PBS buffer. Depending on the test conditions, 10 µL PI buffer was added before or after exposure. The whole suspension was transferred into a 96-well microtiter plate (Greiner Bio-One GmbH, Frickenhausen, Germany), which was directly placed on top of a blue light-emitting LED (λ_{max} = 448 nm; 130 mW cm^{-2}). The PI fluorescence signal (λ_{Em} = 535 nm; λ_{Ex} = 617 nm) was measured after an illumination time of 20 min with the microplate reader (Infinite® M1000 Pro, Tecan Group LTD., Maennedorf, Switzerland).

For the DsFbFP M49I-LecB fusion protein, a modified PI assay was performed. After incubation, *P. aeruginosa* PAO1 cells were diluted to a cell density corresponding to an $OD_{580\,nm}$ of 0.25 in 1x PBS buffer (pH 7.4). Subsequently, 10 µL of culture suspension were transferred into a reaction tube and the purified fusion protein was added resulting in a final absorption ($OD_{450\,nm}$) of 0.2. As a control, 20 µL of a 1 g mL^{-1} stock solution D-Mannose was additionally added. The suspension was then adjusted to a final volume of 90 µL with 1x PBS buffer (pH 7.4). After an incubation time of 1 h, the whole suspension was transferred into a 96-well microtiter plate (Greiner Bio-One GmbH, Frickenhausen, Germany), which was directly placed on top of a blue light-emitting LED (λ_{max} = 448 nm; 130 mW cm^{-2}). After an illumination time of 20 min, 10 µL PI buffer (10×) was added.

The PI signal (λ_{ex} = 535 nm, λ_{em} = 617 nm) was then measured with a microplate reader (Infinite® M1000 Pro, Tecan Group LTD., Maennedorf, Switzerland).

3.6. Statistical Analysis

Data management and analysis were carried out using Microsoft Excel 2010 (Microsoft Corporation, Redmond, WA, USA) and GraphPad Prism 8.0.2 (GraphPad Software, San Diego, CA, USA). The datasets generated during this work are available from the corresponding author on reasonable request.

4. Conclusions

Current approaches to improve photodynamic therapies include the development and application of genetically encoded photosensitizers. This relatively new class of PSs exhibits a robust photochemistry of the photosensitizing chromophore, which is less prone to influences of the surrounding environment. In addition, linked protein domains with defined binding specificities principally allow directing the phototoxic agent to ROS-sensitive cellular structures. Thus, topically or locally delivered PSs with genetically engineered binding specificity could help to selectively and non-invasively treat multi-drug resistant pathogens proliferating in wounds, burns, or soft tissues in the near future. In this context, our data give a first indication that the ROS type and yield as well as the localization of the applied PS protein can strongly influence the antibacterial spectrum and efficacy. To this end, specificity of PS-mediated ROS formation by type-I and -II reactions, as well as the contribution of different ROS to the antimicrobial efficacy against Gram-positive and -negative pathogens, opens up new opportunities for efficient treatment of various life-threatening pathogens. Clearly, however, there is a need for further investigation.

Supplementary Materials: Supplementary materials can be found at http://www.mdpi.com/1422-0067/20/18/4608/s1.

Author Contributions: N.L.B., F.H., A.G., and T.D. conceived and designed the experiments. N.L.B., F.H., Y.A., and A.B. performed the experiments. N.L.B., F.H., A.G., A.B. and T.D. analyzed the data. N.L.B., F.H., K.-E.J. and T.D. wrote the manuscript. All authors read and approved the final manuscript.

Funding: This work was supported by grants from the Bioeconomy Science Center. The scientific activities of the Bioeconomy Science Center were financially supported by the Ministry of Innovation, Science and Research of the German federal state of North Rhine-Westphalia MIWF within the framework of the NRW Strategieprojekt BioSC (No. 313/323-400-00213). A.G. and A.B. were supported by the Helmholtz Association (PD-311).

Acknowledgments: The authors gratefully acknowledge Sebastian Thalmann from Luminex for his help with the flow cytometer experiments and very fruitful discussions and remarks on data processing and evaluation. In addition, the authors would like to thank Thomas Gensch (Forschungszentrum Jülich, Germany) as well as Filip Kovačić (Heinrich-Heine-University Düsseldorf, Germany) for the helpful discussion and Achim Heck (Forschungszentrum Jülich, Germany) for proofreading. Furthermore, the authors would like to thank Dietrich Kohlheyer for access and support in microfluidic chip fabrication and live-cell imaging microscopy and Christian Sachs for support in images-based analysis.

Conflicts of Interest: The authors declare no conflict of interest.

Abbreviations

aPDI	Antimicrobial photodynamic inactivation
PDT	Photodynamic therapy
PS	Photosensitizer
ROS	Reactive oxygen species
ISC	Intersystem crossing
FP	Fluorescent protein
GFP	Green fluorescent protein
FbFP	Flavin-binding protein
LOV	Light-oxygen-voltage
SOG	Singlet Oxygen Generator
CALI	Chromophore-assisted light inactivation

SOPP	Singlet oxygen photosensitizing protein
LED	Light-emitting diode
CFU	Colony forming units
PI	Propidium iodide
FCM	Flow cytometry
FSC	Forward scatter
SSC	Side scatter
WHO	World Health Organization
HRP	Horseradish peroxidase
SOD	Superoxide dismutase
AI	Auto-induction medium
TB	Terrific Broth medium
LB	Lysogeny Broth medium
NTA	Nitrilotriacetic acid
OD	Optical density
LB	Lysogeny Broth medium
PBS	Phosphate buffer saline
ExCo	Extinction coefficient
PDMS	Polydimethylsiloxane
DM	Dichroic mirror
IPTG	Isopropyl-β-D-1-thiogalactopyranoside

References

1. Denis, T.G.; Dai, T.; Izikson, L.; Astrakas, C.; Anderson, R.R.; Hamblin, M.R.; Tegos, G.P. All you need is light. *Virulence* **2011**, *2*, 509–520. [CrossRef] [PubMed]
2. Li, X.-Z.; Plésiat, P.; Nikaido, H. The Challenge of Efflux-Mediated Antibiotic Resistance in Gram-Negative Bacteria. *Clin. Microbiol. Rev.* **2015**, *28*, 337–418. [CrossRef] [PubMed]
3. Jackson, N.; Czaplewski, L.; Piddock, L.J.V. Discovery and development of new antibacterial drugs: Learning from experience? *J. Antimicrob. Chemother.* **2018**, *73*, 1452–1459. [CrossRef] [PubMed]
4. Moan, J.; Peng, Q. An outline of the hundred-year history of PDT. *Anticancer. Res.* **2003**, *23*, 3591–3600. [PubMed]
5. Vatansever, F.; de Melo, W.C.M.A.; Avci, P.; Vecchio, D.; Sadasivam, M.; Gupta, A.; Chandran, R.; Karimi, M.; Parizotto, N.A.; Yin, R.; et al. Antimicrobial strategies centered around reactive oxygen species—Bactericidal antibiotics, photodynamic therapy, and beyond. *FEMS Microbiol. Rev.* **2013**, *37*, 955–989. [CrossRef] [PubMed]
6. Robertson, C.A.; Evans, D.H.; Abrahamse, H. Photodynamic therapy (PDT): A short review on cellular mechanisms and cancer research applications for PDT. *J. Photochem. Photobiol. B* **2009**, *96*, 1–8. [CrossRef] [PubMed]
7. Halliwell, B.; Gutteridge, J.M.C. *Free Radicals in Biology and Medicine*, 5th ed.; Oxford University Press: New York, NY, USA, 2015; ISBN 0198717482.
8. Hamblin, M.R.; Abrahamse, H. Can light-based approaches overcome antimicrobial resistance? *Drug Dev. Res.* **2019**, *80*, 48–67. [CrossRef]
9. Grinholc, M.; Szramka, B.; Olender, K.; Graczyk, A. Bactericidal effect of photodynamic therapy against methicillin-resistant *Staphylococcus aureus* strain with the use of various porphyrin photosensitizers. *Acta Biochim. Pol.* **2007**, *54*, 665–670. [PubMed]
10. Maisch, T.; Spannberger, F.; Regensburger, J.; Felgenträger, A.; Bäumler, W. Fast and effective: Intense pulse light photodynamic inactivation of bacteria. *J. Ind. Microbiol. Biotechnol.* **2012**, *39*, 1013–1021. [CrossRef]
11. Maisch, T. Resistance in antimicrobial photodynamic inactivation of bacteria. *Photochem. Photobiol. Sci.* **2015**, *14*, 1518–1526. [CrossRef]
12. Jensen, R.L.; Arnbjerg, J.; Birkedal, H.; Ogilby, P.R. Singlet Oxygen's Response to Protein Dynamics. *J. Am. Chem. Soc.* **2011**, *133*, 7166–7173. [CrossRef] [PubMed]
13. Ogilby, P.R. Singlet oxygen: There is indeed something new under the sun. *Chem. Soc. Rev.* **2010**, *39*, 3181. [CrossRef] [PubMed]

14. Mishina, N.M.; Tyurin-Kuzmin, P.A.; Markvicheva, K.N.; Vorotnikov, A.V.; Tkachuk, V.A.; Laketa, V.; Schultz, C.; Lukyanov, S.; Belousov, V.V. Does Cellular Hydrogen Peroxide Diffuse or Act Locally? *Antioxid. Redox Signal.* **2011**, *14*, 1–7. [CrossRef] [PubMed]
15. Reth, M. Hydrogen peroxide as second messenger in lymphocyte activation. *Nat. Immunol.* **2002**, *3*, 1129–1134. [CrossRef] [PubMed]
16. Sharma, S.K.; Mroz, P.; Dai, T.; Huang, Y.; St Denis, T.G.; Hamblin, M.R. Photodynamic Therapy for Cancer and for Infections: What Is the Difference? *Isr. J. Chem.* **2012**, *52*, 691–705. [CrossRef] [PubMed]
17. Hamblin, M.R. Antimicrobial photodynamic inactivation: A bright new technique to kill resistant microbes. *Curr. Opin. Microbiol.* **2016**, *33*, 67–73. [CrossRef] [PubMed]
18. Wainwright, M.; Maisch, T.; Nonell, S.; Plaetzer, K.; Almeida, A.; Tegos, G.P.; Hamblin, M.R. Photoantimicrobials—Are we afraid of the light? *Lancet Infect. Dis.* **2017**, *17*, e49–e55. [CrossRef]
19. Sobotta, L.; Skupin-Mrugalska, P.; Piskorz, J.; Mielcarek, J. Porphyrinoid photosensitizers mediated photodynamic inactivation against bacteria. *Eur. J. Med. Chem.* **2019**, *175*, 72–106. [CrossRef]
20. Huang, L.; Huang, Y.-Y.; Mroz, P.; Tegos, G.P.; Zhiyentayev, T.; Sharma, S.K.; Lu, Z.; Balasubramanian, T.; Krayer, M.; Ruzie, C.; et al. Stable Synthetic Cationic Bacteriochlorins as Selective Antimicrobial Photosensitizers. *Antimicrob. Agents Chemother.* **2010**, *54*, 3834–3841. [CrossRef]
21. Tegos, G.P.; Demidova, T.N.; Arcila-Lopez, D.; Lee, H.; Wharton, T.; Gali, H.; Hamblin, M.R. Cationic Fullerenes Are Effective and Selective Antimicrobial Photosensitizers. *Chem. Biol.* **2005**, *12*, 1127–1135. [CrossRef]
22. Wainwright, M. The development of phenothiazinium photosensitisers. *Photodiagn. Photodyn. Ther.* **2005**, *2*, 263–272. [CrossRef]
23. Westberg, M.; Etzerodt, M.; Ogilby, P.R. Rational design of genetically encoded singlet oxygen photosensitizing proteins. *Curr. Opin. Struct. Biol.* **2019**, *57*, 56–62. [CrossRef] [PubMed]
24. Vegh, R.B.; Solntsev, K.M.; Kuimova, M.K.; Cho, S.; Liang, Y.; Loo, B.L.W.; Tolbert, L.M.; Bommarius, A.S. Reactive oxygen species in photochemistry of the red fluorescent protein "Killer Red". *Chem. Commun.* **2011**, *47*, 4887–4889. [CrossRef] [PubMed]
25. Takemoto, K.; Matsuda, T.; Sakai, N.; Fu, D.; Noda, M.; Uchiyama, S.; Kotera, I.; Arai, Y.; Horiuchi, M.; Fukui, K.; et al. SuperNova, a monomeric photosensitizing fluorescent protein for chromophore-assisted light inactivation. *Sci. Rep.* **2013**, *3*, 2629. [CrossRef] [PubMed]
26. Sarkisyan, K.S.; Zlobovskaya, O.A.; Gorbachev, D.A.; Bozhanova, N.G.; Sharonov, G.V.; Staroverov, D.B.; Egorov, E.S.; Ryabova, A.V.; Solntsev, K.M.; Mishin, A.S.; et al. KillerOrange, a Genetically Encoded Photosensitizer Activated by Blue and Green Light. *PLoS ONE* **2015**, *10*, e0145287. [CrossRef]
27. Souslova, E.A.; Mironova, K.E.; Deyev, S.M. Applications of genetically encoded photosensitizer miniSOG: From correlative light electron microscopy to immunophotosensitizing. *J. Biophotonics* **2017**, *10*, 338–352. [CrossRef] [PubMed]
28. Bulina, M.E.; Chudakov, D.M.; Britanova, O.V.; Yanushevich, Y.G.; Staroverov, D.B.; Chepurnykh, T.V.; Merzlyak, E.M.; Shkrob, M.A.; Lukyanov, S.; Lukyanov, K.A. A genetically encoded photosensitizer. *Nat. Biotechnol.* **2006**, *24*, 95–99. [CrossRef]
29. Shu, X.; Lev-Ram, V.; Deerinck, T.J.; Qi, Y.; Ramko, E.B.; Davidson, M.W.; Jin, Y.; Ellisman, M.H.; Tsien, R.Y. A Genetically Encoded Tag for Correlated Light and Electron Microscopy of Intact Cells, Tissues, and Organisms. *PLoS Biol.* **2011**, *9*, e1001041. [CrossRef]
30. Shibuya, T.; Tsujimoto, Y. Deleterious effects of mitochondrial ROS generated by KillerRed photodynamic action in human cell lines and *C. elegans*. *J. Photochem. Photobiol. B Biol.* **2012**, *117*, 1–12. [CrossRef]
31. Wang, B.; Van Veldhoven, P.P.; Brees, C.; Rubio, N.; Nordgren, M.; Apanasets, O.; Kunze, M.; Baes, M.; Agostinis, P.; Fransen, M. Mitochondria are targets for peroxisome-derived oxidative stress in cultured mammalian cells. *Free Radic. Biol. Med.* **2013**, *65*, 882–894. [CrossRef]
32. Serebrovskaya, E.O.; Edelweiss, E.F.; Stremovskiy, O.A.; Lukyanov, K.A.; Chudakov, D.M.; Deyev, S.M. Targeting cancer cells by using an antireceptor antibody-photosensitizer fusion protein. *Proc. Natl. Acad. Sci. USA* **2009**, *106*, 9221–9225. [CrossRef]
33. Shirmanova, M.V.; Serebrovskaya, E.O.; Lukyanov, K.A.; Snopova, L.B.; Sirotkina, M.A.; Prodanetz, N.N.; Bugrova, M.L.; Minakova, E.A.; Turchin, I.V.; Kamensky, V.A.; et al. Phototoxic effects of fluorescent protein KillerRed on tumor cells in mice. *J. Biophotonics* **2013**, *6*, 283–290. [CrossRef]
34. Liao, Z.-X.; Li, Y.-C.; Lu, H.-M.; Sung, H.-W. A genetically encoded KillerRed protein as an intrinsically generated photosensitizer for photodynamic therapy. *Biomaterials* **2014**, *35*, 500–508. [CrossRef]

35. Mironova, K.E.; Proshkina, G.M.; Ryabova, A.V.; Stremovskiy, O.A.; Lukyanov, S.A.; Petrov, R.V.; Deyev, S.M. Genetically Encoded Immunophotosensitizer 4D5scFv-miniSOG is a Highly Selective Agent for Targeted Photokilling of Tumor Cells in vitro. *Theranostics* **2013**, *3*, 831–840. [CrossRef]
36. Ryumina, A.P.; Serebrovskaya, E.O.; Shirmanova, M.V.; Snopova, L.B.; Kuznetsova, M.M.; Turchin, I.V.; Ignatova, N.I.; Klementieva, N.V.; Fradkov, A.F.; Shakhov, B.E.; et al. Flavoprotein miniSOG as a genetically encoded photosensitizer for cancer cells. *Biochim. Biophys. Acta Gen. Subj.* **2013**, *1830*, 5059–5067. [CrossRef]
37. Bulina, M.E.; Lukyanov, K.A.; Britanova, O.V.; Onichtchouk, D.; Lukyanov, S.; Chudakov, D.M. Chromophore-assisted light inactivation (CALI) using the phototoxic fluorescent protein KillerRed. *Nat. Protoc.* **2006**, *1*, 947–953. [CrossRef]
38. Destaing, O.; Planus, E.; Bouvard, D.; Oddou, C.; Badowski, C.; Bossy, V.; Raducanu, A.; Fourcade, B.; Albiges-Rizo, C.; Block, M.R. β1A Integrin Is a Master Regulator of Invadosome Organization and Function. *Mol. Biol. Cell* **2010**, *21*, 4108–4119. [CrossRef]
39. Serebrovskaya, E.O.; Gorodnicheva, T.V.; Ermakova, G.V.; Solovieva, E.A.; Sharonov, G.V.; Zagaynova, E.V.; Chudakov, D.M.; Lukyanov, S.; Zaraisky, A.G.; Lukyanov, K.A. Light-induced blockage of cell division with a chromatin-targeted phototoxic fluorescent protein. *Biochem. J.* **2011**, *435*, 65–71. [CrossRef]
40. Lan, L.; Nakajima, S.; Wei, L.; Sun, L.; Hsieh, C.-L.; Sobol, R.W.; Bruchez, M.; Van Houten, B.; Yasui, A.; Levine, A.S. Novel method for site-specific induction of oxidative DNA damage reveals differences in recruitment of repair proteins to heterochromatin and euchromatin. *Nucleic Acids Res.* **2014**, *42*, 2330–2345. [CrossRef]
41. Westberg, M.; Bregnhøj, M.; Etzerodt, M.; Ogilby, P.R. No Photon Wasted: An Efficient and Selective Singlet Oxygen Photosensitizing Protein. *J. Phys. Chem. B* **2017**, *121*, 9366–9371. [CrossRef]
42. Trewin, A.J.; Berry, B.J.; Wei, A.Y.; Bahr, L.L.; Foster, T.H.; Wojtovich, A.P. Light-induced oxidant production by fluorescent proteins. *Free Radic. Biol. Med.* **2018**, *128*, 157–164. [CrossRef]
43. Pletnev, S.; Gurskaya, N.G.; Pletneva, N.V.; Lukyanov, K.A.; Chudakov, D.M.; Martynov, V.I.; Popov, V.O.; Kovalchuk, M.V.; Wlodawer, A.; Dauter, Z.; et al. Structural Basis for Phototoxicity of the Genetically Encoded Photosensitizer KillerRed. *J. Biol. Chem.* **2009**, *284*, 32028–32039. [CrossRef]
44. Lee, W.; Kim, I.; Rhee, Y.M. A proton transfer network that generates deprotonated tyrosine is a key to producing reactive oxygen species in phototoxic KillerRed protein. *Phys. Chem. Chem. Phys.* **2018**, *20*, 22342–22350. [CrossRef]
45. Drepper, T.; Eggert, T.; Circolone, F.; Heck, A.; Krauß, U.; Guterl, J.-K.; Wendorff, M.; Losi, A.; Gärtner, W.; Jaeger, K.-E. Reporter proteins for in vivo fluorescence without oxygen. *Nat. Biotechnol.* **2007**, *25*, 443–445. [CrossRef]
46. Wingen, M.; Potzkei, J.; Endres, S.; Casini, G.; Rupprecht, C.; Fahlke, C.; Krauss, U.; Jaeger, K.-E.; Drepper, T.; Gensch, T. The photophysics of LOV-based fluorescent proteins—New tools for cell biology. *Photochem. Photobiol. Sci.* **2014**, *13*, 875–883. [CrossRef]
47. Endres, S.; Wingen, M.; Torra, J.; Ruiz-González, R.; Polen, T.; Bosio, G.; Bitzenhofer, N.L.; Hilgers, F.; Gensch, T.; Nonell, S.; et al. An optogenetic toolbox of LOV-based photosensitizers for light-driven killing of bacteria. *Sci. Rep.* **2018**, *8*, 15021. [CrossRef]
48. Binder, D.; Grünberger, A.; Loeschcke, A.; Probst, C.; Bier, C.; Pietruszka, J.; Wiechert, W.; Kohlheyer, D.; Jaeger, K.-E.; Drepper, T. Light-responsive control of bacterial gene expression: Precise triggering of the *lac* promoter activity using photocaged IPTG. *Integr. Biol.* **2014**, *6*, 755–765. [CrossRef]
49. Otto, M. *Staphylococcus Epidermidis*—The "Accidental" Pathogen. *Nat. Rev. Microbiol.* **2009**, *7*, 555–567. [CrossRef]
50. Van Wamel, W.J.B. *Staphylococcus aureus* infections, some second thoughts. *Curr. Opin. Infect. Dis.* **2017**, *30*, 303–308. [CrossRef]
51. Barraud, O.; Badell, E.; Denis, F.; Guiso, N.; Ploy, M.-C. Antimicrobial Drug Resistance in *Corynebacterium diphtheriae mitis*. *Emerg. Infect. Dis.* **2011**, *17*, 2078–2080. [CrossRef]
52. Miotto, P.; Cirillo, D.M.; Migliori, G.B. Drug Resistance in *Mycobacterium tuberculosis*: Molecular Mechanisms Challenging Fluoroquinolones and Pyrazinamide Effectiveness. *Chest* **2015**, *147*, 1135–1143. [CrossRef]
53. Tacconelli, E.; Magrini, N.; Kahlmeter, G.; Singh, N. *Global Priority List of Antibiotic-Resistant Bacteria to Guide Research, Discovery, and Development of New Antibiotics*; World Health Organization: Geneva, Switzerland, 2017; Volume 27, p. 7.

54. Wang, D.; Li, Q.; Qiu, J.; Zhang, X.; Ge, N.; Liu, X. Corrosion Motivated ROS Generation Helps Endow Titanium with Broad-Spectrum Antibacterial Abilities. *Adv. Mater. Interfaces* **2019**, *6*, 1900514. [CrossRef]
55. Huang, L.; Xuan, Y.; Koide, Y.; Zhiyentayev, T.; Tanaka, M.; Hamblin, M.R. Type I and Type II mechanisms of antimicrobial photodynamic therapy: An in vitro study on gram-negative and gram-positive bacteria. *Lasers Surg. Med.* **2012**, *44*, 490–499. [CrossRef]
56. Mai-Prochnow, A.; Clauson, M.; Hong, J.; Murphy, A.B. Gram positive and Gram negative bacteria differ in their sensitivity to cold plasma. *Sci. Rep.* **2016**, *6*, 38610. [CrossRef]
57. Dahl, T.A.; Midden, W.R.; Hartman, P.E. Comparison of killing of gram-negative and gram-positive bacteria by pure singlet oxygen. *J. Bacteriol.* **1989**, *171*, 2188–2194. [CrossRef]
58. Passos da Silva, D.; Matwichuk, M.L.; Townsend, D.O.; Reichhardt, C.; Lamba, D.; Wozniak, D.J.; Parsek, M.R. The *Pseudomonas aeruginosa* lectin LecB binds to the exopolysaccharide Psl and stabilizes the biofilm matrix. *Nat. Commun.* **2019**, *10*, 2183. [CrossRef]
59. Bücher, K.S.; Babic, N.; Freichel, T.; Kovacic, F.; Hartmann, L. Monodisperse Sequence-Controlled α-L-Fucosylated Glycooligomers and Their Multivalent Inhibitory Effects on LecB. *Macromol. Biosci.* **2018**, *18*, 1800337. [CrossRef]
60. Cott, C.; Thuenauer, R.; Landi, A.; Kühn, K.; Juillot, S.; Imberty, A.; Madl, J.; Eierhoff, T.; Römer, W. *Pseudomonas aeruginosa* lectin LecB inhibits tissue repair processes by triggering β-catenin degradation. *Biochim. Biophys. Acta Mol. Cell Res.* **2016**, *1863*, 1106–1118. [CrossRef]
61. Imberty, A.; Wimmerová, M.; Mitchell, E.P.; Gilboa-Garber, N. Structures of the lectins from *Pseudomonas aeruginosa*: Insights into the molecular basis for host glycan recognition. *Microbes Infect.* **2004**, *6*, 221–228. [CrossRef]
62. Tielker, D.; Rosenau, F.; Bartels, K.-M.; Rosenbaum, T.; Jaeger, K.-E. Lectin-based affinity tag for one-step protein purification. *Biotechniques* **2006**, *41*, 327–332. [CrossRef]
63. Bodenberger, N.; Kubiczek, D.; Halbgebauer, D.; Rimola, V.; Wiese, S.; Mayer, D.; Rodriguez Alfonso, A.A.; Ständker, L.; Stenger, S.; Rosenau, F. Lectin-Functionalized Composite Hydrogels for "Capture-and-Killing" of Carbapenem-Resistant *Pseudomonas aeruginosa*. *Biomacromolecules* **2018**, *19*, 2472–2482. [CrossRef]
64. Hanahan, D. Studies on transformation of *Escherichia coli* with plasmids. *J. Mol. Biol.* **1983**, *166*, 557–580. [CrossRef]
65. Hennemann, J.; Iwasaki, R.S.; Grund, T.N.; Diensthuber, R.P.; Richter, F.; Möglich, A. Optogenetic Control by Pulsed Illumination. *ChemBioChem* **2018**, *19*, 1296–1304. [CrossRef]
66. Crowley, L.C.; Scott, A.P.; Marfell, B.J.; Boughaba, J.A.; Chojnowski, G.; Waterhouse, N.J. Measuring Cell Death by Propidium Iodide Uptake and Flow Cytometry. *Cold Spring Harb. Protoc.* **2016**, *2016*. [CrossRef]
67. Gruenberger, A.; Probst, C.; Heyer, A.; Wiechert, W.; Frunzke, J.; Kohlheyer, D. Microfluidic Picoliter Bioreactor for Microbial Single-Cell Analysis: Fabrication, System Setup, and Operation. *J. Vis. Exp.* **2013**. [CrossRef]
68. Grünberger, A.; Probst, C.; Helfrich, S.; Nanda, A.; Stute, B.; Wiechert, W.; von Lieres, E.; Nöh, K.; Frunzke, J.; Kohlheyer, D. Spatiotemporal microbial single-cell analysis using a high-throughput microfluidics cultivation platform. *Cytom. Part A* **2015**, *87*, 1101–1115. [CrossRef]
69. Burmeister, A.; Hilgers, F.; Langner, A.; Westerwalbesloh, C.; Kerkhoff, Y.; Tenhaef, N.; Drepper, T.; Kohlheyer, D.; von Lieres, E.; Noack, S.; et al. A microfluidic co-cultivation platform to investigate microbial interactions at defined microenvironments. *Lab Chip* **2019**, *19*, 98–110. [CrossRef]
70. Probst, C.; Grünberger, A.; Braun, N.; Helfrich, S.; Nöh, K.; Wiechert, W.; Kohlheyer, D. Rapid inoculation of single bacteria into parallel picoliter fermentation chambers. *Anal. Methods* **2015**, *7*, 91–98. [CrossRef]
71. Ronneberger, O.; Fischer, P.; Brox, T. U-Net: Convolutional Networks for Biomedical Image Segmentation. In Proceedings of the Medical Image Computing and Computer-Assisted Intervention-MICCAI 2015, Munich, Germany, 5–9 October 2015; Navab, N., Hornegger, J., Wells, W.M., Frangi, A.F., Eds.; Springer International Publishing: Cham, Switzerland, 2015; pp. 234–241.
72. Schindelin, J.; Arganda-Carreras, I.; Frise, E.; Kaynig, V.; Longair, M.; Pietzsch, T.; Preibisch, S.; Rueden, C.; Saalfeld, S.; Schmid, B.; et al. Fiji: An open-source platform for biological-image analysis. *Nat. Methods* **2012**, *9*, 676–682. [CrossRef]

II.3. ESTABLISHMENT OF SECONDARY METABOLITE PATHWAYS IN VERSATILE HETEROLOGOUS HOSTS

II.3.1. HETEROLOGOUS SYNTHESIS OF PLANT TERPENES IN *R. CAPSULATUS*

Engineered *Rhodobacter capsulatus* as a phototrophic platform organism for the synthesis of plant sesquiterpenoids

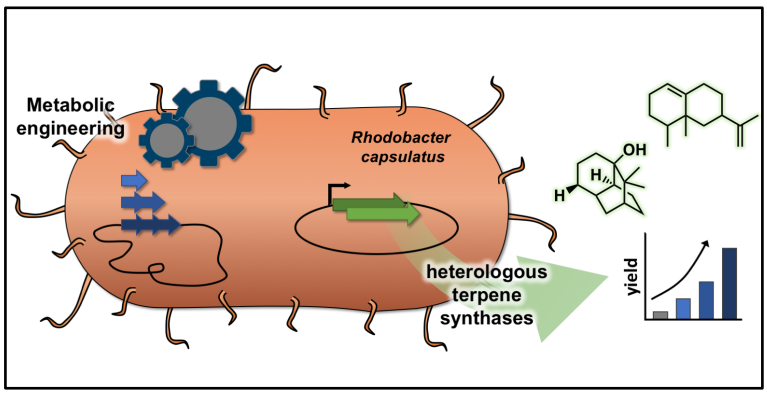

Katrin Troost, Anita Loeschcke, **Fabienne Hilgers**, Armagan Yakup Özgür, Tim Moritz Weber, Beatrix Santiago-Schübel, Vera Svensson, Jennifer Hage-Hülsmann, Samer S. Habash, Florian M.W. Grundler, A. Sylvia S. Schleker, Karl-Erich Jaeger and Thomas Drepper

Front. Microbiol. 10:1998. (2019). fmicb.2019.01998

The online version may be found at: *10.3389/fmicb.2019.01998*

Status: published

For the Supporting Information see Appendix (**Chapter V.7.**, **page 457**).

Own contribution: Establishment of compound quantification method for final determination of product titers, writing parts of the manuscript.

frontiers in Microbiology

ORIGINAL RESEARCH
published: 06 September 2019
doi: 10.3389/fmicb.2019.01998

Engineered *Rhodobacter capsulatus* as a Phototrophic Platform Organism for the Synthesis of Plant Sesquiterpenoids

Katrin Troost[1], Anita Loeschcke[1], Fabienne Hilgers[1], Armagan Yakup Özgür[1], Tim Moritz Weber[1], Beatrix Santiago-Schübel[2], Vera Svensson[1], Jennifer Hage-Hülsmann[1], Samer S. Habash[3], Florian M. W. Grundler[3], A. Sylvia S. Schleker[3], Karl-Erich Jaeger[1,4] and Thomas Drepper[1]**

[1] Institute of Molecular Enzyme Technology, Heinrich Heine University Düsseldorf, Düsseldorf, Germany, Forschungszentrum Jülich GmbH, Jülich, Germany, [2] Central Institute for Engineering, Electronics and Analytics ZEA-3, Analytics, Forschungszentrum Jülich GmbH, Jülich, Germany, [3] INRES-Molecular Phytomedicine, Rhenish Friedrich–Wilhelm University of Bonn, Bonn, Germany, [4] Institute of Bio- and Geosciences IBG-1, Biotechnology, Forschungszentrum Jülich GmbH, Jülich, Germany

OPEN ACCESS

Edited by:
Lei Chen,
Tianjin University, China

Reviewed by:
Guodong Luan,
Qingdao Institute of Bioenergy and Bioprocess Technology (CAS), China
Huan Lin,
Hainan University, China

***Correspondence:**
Anita Loeschcke
a.loeschcke@fz-juelich.de
Thomas Drepper
t.drepper@fz-juelich.de

Specialty section:
This article was submitted to Microbiotechnology, Ecotoxicology and Bioremediation, a section of the journal Frontiers in Microbiology

Received: 25 June 2019
Accepted: 15 August 2019
Published: 06 September 2019

Citation:
Troost K, Loeschcke A, Hilgers F, Özgür AY, Weber TM, Santiago-Schübel B, Svensson V, Hage-Hülsmann J, Habash SS, Grundler FMW, Schleker ASS, Jaeger KE and Drepper T (2019) Engineered Rhodobacter capsulatus as a Phototrophic Platform Organism for the Synthesis of Plant Sesquiterpenoids. Front. Microbiol. 10:1998. doi: 10.3389/fmicb.2019.01998

Sesquiterpenoids are a large class of natural compounds offering manifold properties valuable for food, cosmetics, agriculture, and pharma industry. Production in microorganisms is a sustainable approach to provide sesquiterpenoids for research and industrial use independent of their natural sources. This requires the functional transfer of the respective biocatalytic pathways in an adequate host microorganism offering a sufficient supply of precursors that is ideally adjusted to the individual demand of the recombinant biosynthesis route. The phototrophic purple bacterium *Rhodobacter capsulatus* offers unique physiological properties that are favorable for biosynthesis of hydrophobic terpenes. Under phototrophic conditions, it develops a large intracytoplasmic membrane suitable for hosting membrane-bound enzymes and metabolites of respective biosynthetic pathways. In addition, *Rhodobacter* harbors an intrinsic carotenoid biosynthesis that can be engineered toward the production of foreign terpenes. Here, we evaluate *R. capsulatus* as host for the production of plant sesquiterpenoids under phototrophic conditions using patchoulol and valencene as a proof of concept. The heterologous expression of patchoulol synthase PcPS from *Pogostemon cablin* as well as the valencene synthases CsVS from *Citrus sinensis* and CnVS from *Callitropsis nootkatensis* led to the production of the respective sesquiterpenoids in *R. capsulatus*. To analyze, if gradually adjustable formation of the key precursor farnesylpyrophosphate (FPP) is beneficial for sesquiterpene synthesis under phototrophic conditions, the intrinsic 1-deoxy-D-xylulose 5-phosphate (DXP) pathway genes as well as the heterologous mevalonate pathway genes were modularly expressed in various combinations. To this end, different plasmids and chromosomally integrated expression tools were developed harboring the strong and tightly controlled P_{nif} promoter for heterologous gene expression. Notably, comparative studies identified a distinct combination of precursor biosynthetic genes as best-performing setup for each of the tested sesquiterpene synthases. In summary, we could demonstrate

that *R. capsulatus* is a promising alternative platform organism that is suited for sustainable sesquiterpenoid formation under phototrophic cultivation conditions. A modular engineering of *R. capsulatus* strains via tailored co-expression of FPP biosynthetic genes further allowed adaptation of sesquiterpene precursor formation to its catalytic conversion by different plant terpene synthases.

Keywords: terpenoid, natural product, valencene, patchoulol, *Rhodobacter capsulatus*, metabolic engineering

INTRODUCTION

The class of terpenoid secondary metabolites comprises over 80,000 structurally diverse compounds, a majority of which was isolated from plants (Bian et al., 2017; Christianson, 2017; Pemberton et al., 2017). In fact, terpenoids represent one of the main groups of secondary metabolites with diverse biological functions and valuable properties for various industrial applications (Kallscheuer et al., 2018). Terpenoids are basically divided into different terpene classes based on the number of carbon atoms: hemi- (C5), mono- (C10), sesqui- (C15), di- (C20), tri- (C30), tetra- (C40), and polyterpenes (>C40) (Ruzicka, 1953; Croteau et al., 2000). All terpenoids are biosynthesized from the isoprene C5 scaffolds isopentenyl pyrophosphate (IPP) and dimethylallyl pyrophosphate (DMAPP), which are built via the mevalonate (MVA) pathway or the 1-deoxy-D-xylulose 5-phosphate (DXP) pathway, also called 2-*C*-methyl-D-erythritol 4-phosphate (MEP) pathway. The MVA pathway, which uses acetyl-CoA as substrate, is mainly present in eukaryotes (mammals, plants and fungi), but also archaea and a few bacteria (Boucher and Doolittle, 2000); the DXP pathway, which starts from glyceraldehylde-3-phosphate (GAP) and pyruvate, is particularly used by bacteria, cyanobacteria, and green algae (Frank and Groll, 2017). The latter also occurs in plants where it is located in the plastids while the MVA pathway is cytosolic (Dewick, 2002). IPP and DMAPP represent the starting molecules for the biosynthesis of elongated linear prenyl pyrophosphates in subsequent head-to-tail condensations catalyzed by prenyltransferases, yielding C10 geranyl pyrophosphate (GPP), C15 farnesyl pyrophosphate (FPP), and C20 geranylgeranyl pyrophosphate (GGPP). GPP serves as precursor for monoterpenoids, FPP for sesqui- and triterpenoids and GGPP for di- and tetraterpenoids.

The structurally highly diverse terpenoids naturally fulfill manifold functions, including photoprotection (carotenoids), repellant activity against predators and parasites (e.g., verbenone), communication (e.g., pinene), regulation of the membrane fluidity (bacterial hopanoids, eukaryotic sterols), electron transfer in the respiratory chain and photosynthesis (ubiquinone and plastoquinone), or hormone activity (e.g., gibberellins) (Langenheim, 1994; Gershenzon and Dudareva, 2007; Pichersky and Raguso, 2016). Due to their bioactive properties, some terpenoids can be utilized as agents that are effective against pathogens, inflammations, or cancer (Efferth, 2017; Schempp et al., 2018). Moreover, many are applicable as flavors and fragrances in the food and cosmetics industry such as the sesquiterpenoids patchoulol and valencene. Due to its characteristic earthy and woody scent, patchoulol is one of the most prominent fragrances for the perfume and cosmetic industry (Bauer et al., 2001). Valencene is commercially used to add its citrus flavor to beverages (Schempp et al., 2018). In the past, these compounds were exclusively obtained from natural plant sources. Patchoulol was extracted from the Indian patchouli *Pogostemon cablin* and valencene from different citrus species like *Citrus sinensis*. However, the biotechnological production in microbial hosts can represent an ecologically favorable, cost-effective and sustainable alternative production route (Marienhagen and Bott, 2013; Kallscheuer et al., 2018; Schempp et al., 2018). In fact, large-scale biotechnological production has been demonstrated for some prominent terpenoids, for example artemisinic acid, which is the precursor of the antimalaria agent artemisinin (Paddon et al., 2013). Furthermore, different industrial terpenoid flavor and fragrance compounds produced by engineered microorganisms, including β-farnesene, valencene, nootkatone and patchoulol, are nowadays marketed by the companies Amyris, Evolva, Isobionics, and Firmenich, respectively (Schempp et al., 2018).

Since appropriately high product titers are essential for the development of a bioeconomically feasible production process, one research focus is the engineering of microbial host metabolism and target pathways (Kirby and Keasling, 2008; Mitchell, 2011; Chen et al., 2015; Bian et al., 2017). The most

Abbreviations: CDP-ME, 4-diphosphocytidyl-2-*C*-methylerythritol; CDP-MEP, 4-diphosphocytidyl-2-*C*-methyl-D-erythritol 2-phosphate; CnVS, *Callitropsis nootkatensis* valencene synthase; CrtA, spheroidene monooxygenase; CrtB, phytoene synthase; CrtC, hydroxyneurosporene synthase; CrtD, hydroxyneurosporene desaturase; CrtE, GGPP synthase; CrtF, demethylspheroidene O-methyltransferase; CrtI, phytoene desaturase; CsVS, *Citrus sinensis* valencene synthase; DMAPP, dimethylallyl pyrophosphate; DXP, 1-deoxy-D-xylulose 5-phosphate; DxR, 1-deoxy-D-xylulose 5-phosphate reductoisomerase; DxS, 1-deoxy-D-xylulose 5-phosphate synthase; FPP, farnesyl pyrophosphate; GAP, glyceraldehydes-3-phosphate; GGPP, geranylgeranyl pyrophosphate; GPP, geranyl pyrophosphate; HMB-PP, (*E*)-4-Hydroxy-3-methyl-but-2-enyl pyrophosphate; HMG-CoA, 3-hydroxy-3-methylglutaryl-CoA; HMGR, 3-hydroxy-3-methyl-glutaryl-CoA reductase; HMGS, 3-hydroxy-3-methyl-glutaryl-CoA synthase; Idi, isopentenyl diphosphate isomerase; IPP, isopentenyl pyrophosphate; IspA, FPP synthase; IspD, 2-*C*-methyl-D-erythritol 4-phosphate cytidylyltransferase; IspE, 4-diphosphocytidyl-2-*C*-methyl-D-erythritol kinase; IspF, 2-*C*-methyl-D-erythritol 2,4-cyclodiphosphate synthase; IspG, (*E*)-4-hydroxy-3-methyl-but-2-enyl diphosphate synthase; IspH, (*E*)-4-hydroxy-3-methyl-but-2-enyl diphosphate reductase; MEcPP, 2-*C*-methyl-D-erythritol 2,4-cyclodiphosphate; MEP, 2-*C*-methyl-D-erythritol 4-phosphate; MK, mevalonate-5-kinase; MP, mevalonate-5-phosphate; MPP, mevalonate-5-pyrophosphate; MVA, mevalonate; PcPS, *Pogostemon cablin* patchoulol synthase; PMD, mevalonate-5-diphosphate decarboxylase; PMK, phosphomevalonate kinase.

commonly used microorganisms for the heterologous terpenoid production are *Escherichia coli* and *Saccharomyces cerevisiae*, but also others including phototrophic bacteria are gaining interest, as documented by the *Rhodobacter sphaeroides*-based production of valencene and nootkatone, marketed by Isobionics. The phototrophic non-sulfur purple α-proteobacteria of the genus *Rhodobacter* feature some physiological characteristics which are especially advantageous for terpenoid production: (i) the cell membrane is commonly considered to be a critical determinant in terpenoid production, since it can function as storage compartment for pathway enzymes and hydrophobic compounds (Das et al., 2007; Arendt et al., 2017). In contrast to non-phototrophic microbes, species of the genus *Rhodobacter* can form a highly enlarged intracytoplasmic membrane system (ICM) where the components of the photosynthetic apparatus are naturally housed (Tucker et al., 2010; Drews, 2013). The ICM thus constitutes a naturally enlarged reservoir for membrane-embedded enzymes and metabolites. (ii) Relying on the DXP pathway for precursor supply, these phototrophic bacteria synthesize the carotenoids (i.e., tetraterpenoids) spheroidene and spheroidenone (Armstrong et al., 1989; Armstrong, 1997), thereby offering a robust and effective isoprenoid metabolism as basis for engineering the host's metabolism toward recombinant terpenoid production. (iii) *Rhodobacter* species are capable of growing photo(hetero)trophically in inexpensive minimal media at relatively high growth rates, allowing to use sunlight as energy source within sustainable cultivation processes.

Previous studies showing the production of triterpenoids in *R. capsulatus* (Khan et al., 2015), and the sesquiterpenoid valencene in *R. sphaeroides* (Beekwilder et al., 2014) have indicated that heterologous terpenoid production can be optimized by engineering the isoprenoid precursor biosynthesis. Here, co-expression of an FPP synthase (IspA) and rate-limiting enzymes of the DXP pathway DxS synthase and IPP isomerase (Idi) (Khan et al., 2015) as well as the introduction of the MVA pathway (Beekwilder et al., 2014), which does not naturally occur in *Rhodobacter*, were initially demonstrated to enhance recombinant terpenoid production.

In this study, we therefore aimed to investigate if modular co-expression of DXP/MVA genes by the strictly controlled P_{nif} promoter can help to reconstitute plant sesquiterpenoid pathways in *R. capsulatus*. To analyze terpenoid formation under phototrophic growth conditions, patchoulol and valencene synthases from different plants were used as an example.

MATERIALS AND METHODS

Bacterial Strains and Cultivation Conditions

Escherichia coli strain DH5α (Hanahan, 1983) was used for cloning and strain S17-1 (Simon et al., 1983) for conjugation. *E. coli* was cultivated at 37°C on LB agar plates or in liquid LB medium (Luria/Miller, Carl Roth®), supplemented with 50 μg/mL kanamycin, 10 μg/mL gentamicin or 10 μg/mL tetracycline when appropriate. *R. capsulatus* SB1003 (Strnad et al., 2010) was used for heterologous terpene production. The wildtype strain and derivatives thereof were cultivated on PY agar plates (Klipp et al., 1988) containing 2% (*w*/*v*) Select Agar (Thermo Fisher Scientific) or in RCV liquid medium (Weaver et al., 1975) at 30°C, both supplemented with 25 μg/mL rifampicin. For strain SB1003-MVA, additional 4 μg/mL gentamicin were used. Cultivation was conducted under anaerobic photoheterotrophic conditions and permanent illumination with bulb light (2500 lx).

Construction of Strain SB1003-MVA

For construction of strain *R. capsulatus* SB1003-MVA, a vector carrying the MVA gene cluster as interposon cassette was constructed. To this end, chromosomal sequences upstream (*Nde*I-*crp'-fdxD-nifH'-Xba*I, 1.5 kb) and downstream (*Kpn*I-"*nifK-nifU1-rpoN*"-*Xho*I-*Eco*RI, 1.5 kb) of the *nifHDK* operon of *R. capsulatus* SB1003 were PCR-amplified and cloned into vector pUC18 to create vector pUC18-nifupdown. The MVA pathway encoding gene cluster from *Paracoccus zeaxanthinifaciens* ATCC 21588 (*Xba*I-*mvaA-idi-hsc-mvk-pmk-mvd-Nhe*I/*Kpn*I, 6.4 kb) was amplified by PCR using genomic DNA as template. A gentamicin resistance gene with the respective promoter (*Nhe*I-*aacC1-Kpn*I, 0.8 kb) and a mob-Tc cassette (*Xho*I-*oriT-tetR-Xho*I, 2.6 kb) were PCR-amplified using vector pIC20H-RL (Loeschcke et al., 2013) as template. The MVA pathway genes and *aacC1* were cloned successively into pUC18-nifupdown between the chromosomal up- and downstream sequences of the *nifHDK* operon, and the mob-Tet cassette was added aside that to construct vector pMVA-int-Pnif. This construct was transferred to *R. capsulatus* by conjugation. Among exconjugants, clones carrying the MVA gene cluster in the chromosome were identified by use of gentamicin-supplemented medium. Replica-plating on tetracycline and gentamicin-supplemented medium showed that the strain was exclusively obtained with single-cross-over integration. Therefore, the strain was cultivated on gentamicin-containing medium to ensure stability of the integration cassette.

Construction of Expression Vectors

The expression vector pRhon5Hi-2 was cloned using pRhotHi-2 (Katzke et al., 2010) as respective backbone. For the construction, genomic DNA of *R. capsulatus* was isolated as a template for PCR. For the amplification of the 401-bp P_{nif} DNA fragment (NCBI Genbank Accession MG208548 deposited by Özgür and coworkers), primers Pnif-fw and Pnif-rv were used harboring an *Nhe*I and *Xba*I site, respectively. After hydrolyzation, the P_{nif} fragment was cloned into the *Nhe*I and *Xba*I sites of vector pRhotHi-2, thereby substituting the original T7 promoter. The sequences of patchoulol synthase PcPS from *P. cablin* (UniProt: Q49SP3.1), the valencene synthases CnVS from *Callitropsis nootkatensis* (GenBank: AFN21429.1) and CsVS from *Citrus sinensis* (Uniprot: Q71MJ3) were used to generate DNA sequences with suitable codon-usage for expression in *R. capsulatus* with the help of the Codon Optimization Tool by IDT Integrated DNA Technologies and the Graphical Codon Usage Analyzer tool (Fuhrmann et al., 2004). Genes were obtained as synthetic DNA by Eurofins Genomics (*PcPS*, 1.7 kb;

CsVS, 1.6 kb; and *CnVS*, 1.8 kb) flanked by appropriate restriction endonuclease recognition sequences (*Nde*I/*Hin*dIII). The genes encoding IspA from *R. capsulatus* SB1003 (*ispA*, 0.9 kb), 1-deoxy-D-xylulose-5-phosphate synthase and IPP isomerase from *Rhodobacter sphaeroides* 2.4.1 (*dxs*, 1.9 kb; *idi*, 0.5 kb) and the gene cluster encoding the MVA biosynthesis pathway from *Paracoccus zeaxanthinifaciens* ATCC 21588 (*mvaA-idi-hsc-mvk-pmk-mvd*, 6.3 kb) were amplified using the respective genomic DNA as template. Suitable restriction endonuclease recognition sequences were added via the oligonucleotide primers for the following procedures: all genes were cloned into expression vector pRhon5Hi-2, enabling an induction of target gene expression via the provided nitrogen source. Terpenoid synthase (TPS) encoding genes, namely *PcPS*, *CsVS*, *CnVS*, were cloned into the vector as *Nde*I/*Hin*dIII fragments, creating pRhon5Hi-2-PcPS/CsVS/CnVS, respectively. The TPS genes are thereby placed immediately downstream of the P_{nif} promoter and RBS of the vector. To generate vectors carrying one additional isoprenoid biosynthetic gene or the MVA gene cluster, i.e., with the architecture pRhon5Hi-2-TPS-ispA/dxs/idi/MVA, the different PCR products were cloned into the three variants of pRhon5Hi-2-TPS as *Hin*dIII/*Xho*I fragments. For the construction of the expression cassettes carrying combinations of increasing length downstream of the TPS genes with the structure *TPS-ispA-dxs*/*TPS-ispA-dxs-idi*/*TPS-ispA-dxs-idi-MVA*, the PCR products of *ispA*, *dxs*, *idi* and the *MVA* cluster were cloned successively into the vector pRhon5Hi-TPS as *Hin*dIII/*Xho*I, *Mlu*I/*Xho*I, *Spe*I/*Xho*I, *Kpn*I/*Xho*I fragments, respectively. A scheme of the described strategies for cloning of expression vectors, nucleotide sequences of expressed sesquiterpenoid synthases and used primers are summarized in **Supplementary Figure S1** and **Supplementary Tables S1, S2**.

Heterologous Production of Plant Sesquiterpenoids Valencene and Patchoulol in *R. capsulatus*

For the expression of the heterologous genes in *R. capsulatus*, respective pRhon5Hi-2-based plasmids were transferred to the host via conjunctional transfer employing *E. coli* S17-1 as donor as previously described (Klipp et al., 1988). Thereafter, exconjugants were selected and further cultivated on PY agar, containing 25 μg/mL kanamycin and 25 μg/mL rifampicin. Subsequently, photoheterotrophic cultivation was conducted in liquid RCV medium containing 25 μg/mL kanamycin and 25 μg/mL rifampicin in airtight Hungate tubes (Hungate, 1969): pre-cultures of 15 mL RCV medium containing 0.1% $(NH_4)_2SO_4$ were inoculated with cells from agar plates and incubated for 48 h. Expression cultures were inoculated from pre-cultures to an initial OD_{660nm} of 0.05 in 14 mL RCV medium containing 0.1% serine as exclusive nitrogen source. The absence of ammonium together with photoheterotrophic conditions (the absence of oxygen) led to the induction of the P_{nif}-dependent target gene expression. The cultures were overlaid with 500 μL *n*-dodecane for extraction of the heterologously produced terpenoids, and incubated for 5 days without agitation.

GC-Analysis and Quantification of Sesquiterpenoids

After cultivation of expression cultures, Hungate tubes were incubated for further 24 h under permanent shaking at 130 rpm in a Multitron Standard incubation shaker (Infors HT) in the dark in a horizontal position to facilitate product extraction into the organic phase before sampling of 100 μL *n*-dodecane. The *n*-dodecane samples were subjected to gas chromatographic (GC) analysis employing the Agilent *6890N* gas chromatograph equipped with a (5%-phenyl)-methylpolysiloxane *HP-5* column (length, 30 m; inside diameter, 0.32 mm; film thickness, 0.25 μm; Agilent Technologies) and a flame ionization detector (FID). The injector and FID temperatures were set to 240 and 250°C, respectively. Volumes of 4 μL (patchoulol) or 2 μL (valencene) of a sample were injected splitless, with helium as carrier gas. The column temperature was maintained at 100°C for 5 min, increased at 10°C/min to 180°C, and then at 20°C/min to 300°C. The signals of heterologously produced terpenoids were assigned to products by comparison of retention times to commercial references of (−)-patchoulol from Carbosynth (product code: FP09677, retention time: 13.47 min) and (+)-valencene obtained from Sigma Aldrich (product number: 75056, retention time: 11.22 min). In order to determine product titers in cultures, the effective transfer from producing cells into the organic phase was assessed as described in Supplementary Method section "Analysis of *n*-Dodecane-Mediated Sesquiterpenoid Extraction From Phototrophically Grown *R. capsulatus*." Essentially, cells were disrupted, extracted with *n*-dodecane and products were quantified using calibration curves of the reference compounds, taking into account the specific transfer efficiencies of the sesquiterpenoids into the organic phase in this process.

RESULTS

Modular Concept for Engineering Sesquiterpenoid Synthesis in *R. capsulatus*

To establish stringently controlled recombinant expression in *R. capsulatus* under phototrophic growth conditions, we first constructed vector pRhon5Hi-2 (**Supplementary Figure S1**). The new expression vector carries the P_{nif} promoter of the *R. capsulatus nifHDK* operon encompassing the structural genes of the molybdenum-dependent-nitrogenase enzyme complex (Haselkorn, 1986) as an *Nhe*I/*Xba*I fragment (NCBI Genbank Accession MG208548 deposited by Özgür and coworkers). This promoter is considered to be strong and is known to be strictly repressed by NH_4^+ and oxygen (Kranz and Haselkorn, 1985; Masepohl et al., 2002), thereby enabling the induction of target gene expression under phototrophic conditions (due to the absence of molecular oxygen) and ammonium depletion. Like all other pRho-vectors (Katzke et al., 2010, 2012), pRhon5Hi-2 is further characterized by a broad-host range replicon, a MOB site for conjugational transfer, two antibiotic resistance genes for plasmid maintenance, a hexahistidine-tag encoding region and

a multiple cloning site for directed insertion of target genes as described previously.

Since the availability of molecular oxygen is one of the major environmental factors for controlling intrinsic ICM formation, carotenoid biosynthesis and nitrogen fixation in *R. capsulatus*, we first analyzed co-induction of P_{nif}-dependent EYFP reporter gene expression (**Supplementary Figure S2**) and spheroidene/spheroidenone formation (**Supplementary Figure S3**) in dependence on O_2. To this end, the EYFP gene was cloned in the expression vector pRhon5Hi-2 and subsequently transferred to *R. capsulatus* wildtype strain SB1003. The resulting clones were cultivated either under standard photoheterotrophic (i.e., anaerobic condition and constant illumination) or various microaerobic conditions (i.e., heterotrophic growth in the dark). To gradually restrict the oxygen concentration of the cultivation medium under non-phototrophic conditions, increasing filling volumes (20–70 ml) were applied in 100 mL shake flasks. Samples of all cultures were subjected to fluorescence and western blot analyses. The results of the EYFP expression studies clearly demonstrated that pRhon5Hi-2-mediated gene expression is fully induced under phototrophic conditions (-O_2) whereas increasing oxygen concentrations in the medium resulted in a step-wise reduction of P_{nif} activity. In contrast, high oxygen concentrations (**Supplementary Figure S2**, 20 mL) or addition of 15 mM ammonium (**Supplementary Figure S2**) led to a complete repression of P_{nif}-controlled gene expression. As expected, carotenoid accumulation accompanied by ICM formation can analogously be induced in *R. capsulatus* by applying oxygen-limited and phototrophic cultivation conditions (**Supplementary Figure S3**). In summary, phototrophic cultivation leads to a concerted and strong co-induction of intrinsic terpene biosynthesis and P_{nif}-controlled gene expression and was thus used for the following experiments.

In order to test the applicability of the P_{nif} system for installing pathways of plant sesquiterpenoids (−)-patchoulol and (+)-valencene in *R. capsulatus*, the patchoulol synthase from *P. cablin* (PcPS) and the valencene synthase from *C. nootkatensis* (CnVS) were used. Both enzymes were previously described as highly active when expressed in the bacteria *Corynebacterium glutamicum* and *Rhodobacter sphaeroides* (Beekwilder et al., 2014; Binder et al., 2016; Henke et al., 2018). We also included the valencene synthase from *Citrus sinensis* (CsVS) which was previously reported to be less effective in this context (Beekwilder et al., 2014; Frohwitter et al., 2014) to comparatively evaluate the role of differential co-expression of precursor biosynthetic genes on variable sesquiterpenoid synthase-dependent FPP conversion. Based on engineering strategies that were previously identified as effective (Beekwilder et al., 2014; Khan et al., 2015), we aimed to establish an integrated concept of engineering modules that can be applied for recombinant sesquiterpenoid production in *R. capsulatus* (**Figure 1**).

FPP is the direct precursor for the production of heterologous sesquiterpenoids. Therefore, the strategies to increase the sesquiterpenoid production are primarily focused on an increased FPP supply, which can be achieved by enhancing the biosynthesis of FPP via overexpression of upstream pathway genes of the DXP, MVA, and prenyl phosphate modules.

To increase FPP biosynthesis in *R. capsulatus*, three enzymes of the intrinsic DXP pathway that are generally known to be rate-limiting were overexpressed: (i) the DxS-synthase and isopentenyl pyrophosphate isomerase (Idi) of *R. sphaeroides* (DXP module) and (ii) the IspA from *R. capsulatus* (prenyl phosphate module). In each case, expression of additional gene copies should provide an enhanced respective enzymatic activity in addition to the intrinsic capacities of the host. Moreover, we employed the alternative MVA pathway to establish a second route from central metabolism to isoprenoid biosynthesis. To this end (iii) the MVA gene cluster from *Paracoccus zeaxanthinifaciens* encompassing the genes *mvaA, idi, hsc, mvk, pmk,* and *mvd* (MVA module) was co-expressed. The genes encode all necessary enzymes for the conversion of acetoacetyl-CoA, which is provided by *R. capsulatus*, to IPP/DMAPP (Hümbelin et al., 2002).

For the construction of pRhon5Hi-2-based expression plasmids, the plant terpene synthase (TPS) genes, whose sequences were adapted to the *R. capsulatus* codon usage, were first inserted into the vector pRhon5Hi-2 thereby building the backbone for subsequent modular cloning steps. To evaluate individual effects of IspA, DxS, and Idi as well as the MVA enzymes, the respective genes were cloned downstream of the TPS genes in the vector (**Figure 1B** and **Supplementary Figure S1**). Moreover, to evaluate cumulative effects, the synthetic operons were stepwise extended by incremental combinations of the DXP and/or prenyl phosphate module genes together with the genes of the MVA module. Since the size of the synthetic operons grows with each module gene, which can lead to an increased instability of recombinant plasmids, we additionally integrated the 6.3-kb MVA gene cluster in place of the chromosomally located *nifHDK* operon of *R. capsulatus* SB1003 thereby placing it under control of P_{nif} promoter (**Figure 1C**).

Details about plasmid cloning and strain generation including an overview about the plasmid cloning strategy, nucleotide sequences of codon-adapted terpenoid synthase genes and a primer table are summarized in **Supplementary Figure S1** and **Supplementary Tables S1, S2**.

Engineering of PcPS-Mediated Patchoulol Production in *R. capsulatus* via Modular Co-expression of Precursor Pathway Genes

To initially evaluate the applicability of *R. capsulatus* for the production of sesquiterpenoids, the expression plasmids pRhon5Hi-2-PcPS solely carrying the patchoulol synthase gene from *Pogostemon cablin* was first transferred into *R. capsulatus* wildtype strain SB1003. To analyze, if modular co-expression of different precursor genes (**Figure 1**) can help to increase patchoulol formation in the phototrophic host, plasmids pRhon5Hi-2-PcPS-ispA, pRhon5Hi-2-PcPS-dxs, pRhon5Hi-2-PcPS-idi and pRhon5Hi-2-PcPS-MVA (plasmids allowing co-expression of the patchoulol synthase together with a single precursor module) as well as pRhon5Hi-2-PcPS-ispA-dxs,

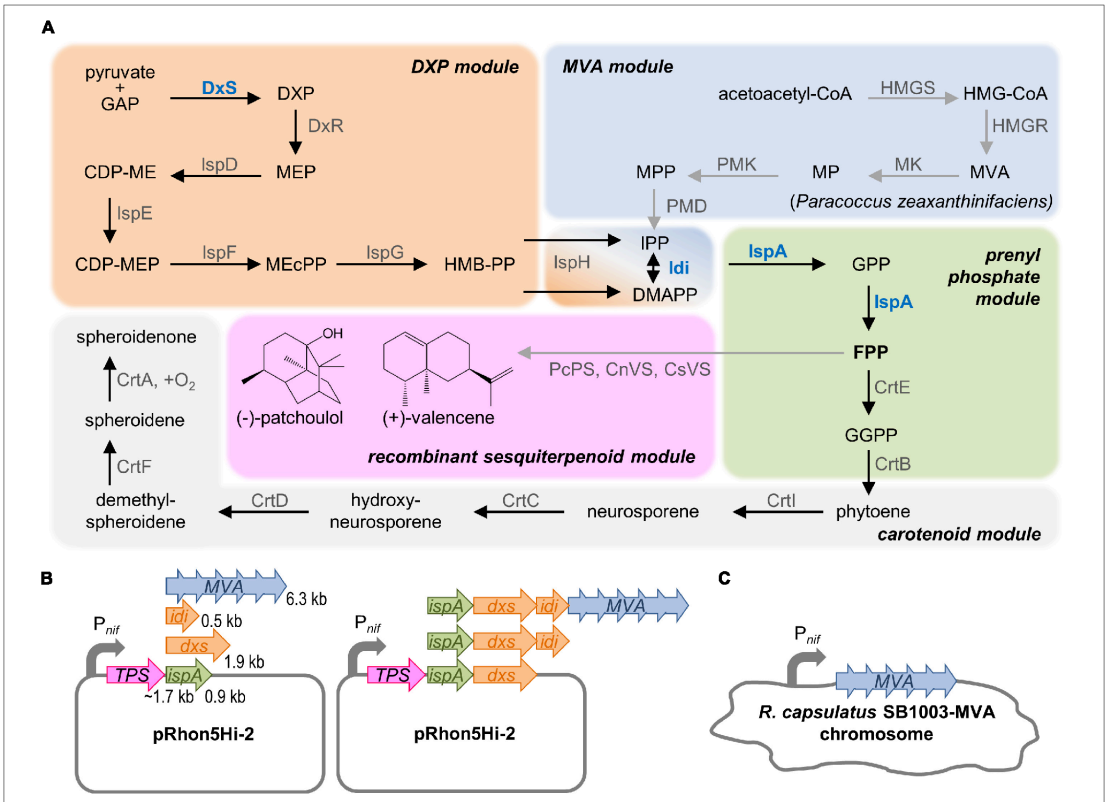

FIGURE 1 | Strategy for modular engineering of sesquiterpenoid production in *R. capsulatus*. **(A)** The intrinsic terpene biosynthesis of *R. capsulatus* (black arrows) and implementation of recombinant terpene biosynthetic steps (gray arrows) is shown, schematically grouped in modules: The native DXP module, including the formation of name-giving DXP, synthesizes C5 building blocks IPP, and DMAPP from pyruvate and GAP. IPP and DMAPP are further naturally converted to elongated prenyl phosphates yielding GPP, FPP, and GGPP, and the latter represents the substrate for the formation of specific C40 carotenoid scaffolds of *R. capsulatus*. Recombinant sesquiterpenoid biosynthesis can be installed by conversion of FPP via respective terpene synthases (TPS) such as the patchoulol or valencene synthase. To increase the synthesis of plant sesquiterpenoids, the MVA pathway, including the formation of name-giving MVA, can be recruited as additional C5 building module. Here, *R. capsulatus* intrinsically uses acetyl-CoA to provide acetoacetyl-CoA, which can be converted to IPP/DMAPP by heterologous enzymes (of *Paracoccus zeaxanthinifaciens*). In addition, the DXP as well as the prenyl phosphate modules can be tuned by overexpression of typical bottleneck enzymes DxS, Idi and IspA (highlighted in blue). **(B)** Schematic representation of the plasmid system for the modular P_{nif}-based co-expression of *ispA*, *dxs*, *idi* and/or the MVA gene cluster along with the TPS genes. Length of genes is indicated in kilo base pairs (kb). **(C)** Engineering of the *R. capsulatus* chromosome by integration of the MVA gene cluster in place of the *nifHDK* operon under control of P_{nif}. See list of abbreviations.

pRhon5Hi-2-PcPS-ispA-dxs-idi and pRhon5Hi-2-PcPS-ispA-dxs-idi-MVA (i.e., plasmids with combined precursor module genes) were transferred into the same strain. To comparatively analyze patchoulol formation in all generated strains under phototrophic conditions, cells were cultivated anaerobically in an ammonium-depleted medium under constant illumination and product formation was determined in the late stationary growth phase by analyzing *n*-dodecane samples by use of gas chromatography (**Figure 2**).

Photoheterotrophic cultivation of *R. capsulatus* wildtype solely expressing *PcPS* led to a minor patchoulol signal (**Figure 2A**, see **Supplementary Figure S4** for GC-MS analysis) which was absent in controls without the terpene synthase. In contrast, co-expression of IspA encoding *ispA* or DXP pathway genes *dxs* or *idi* resulted in an enhanced signal with a relative increase of factor 9–15. Co-expression of *PcPS* and the MVA gene cluster even increased the patchoulol accumulation 26-fold compared to the reference strain *R. capsulatus* SB1003 with pRhon5Hi-2-PcPS.

Next, we analyzed if patchoulol synthesis can be further enhanced in *R. capsulatus* when *PcPS* is co-expressed together with incremental combinations of respective precursor module genes. Surprisingly, none of the tested strains exhibited a significant increase of product formation. Remarkably, no patchoulol accumulation was detectable in the strain carrying

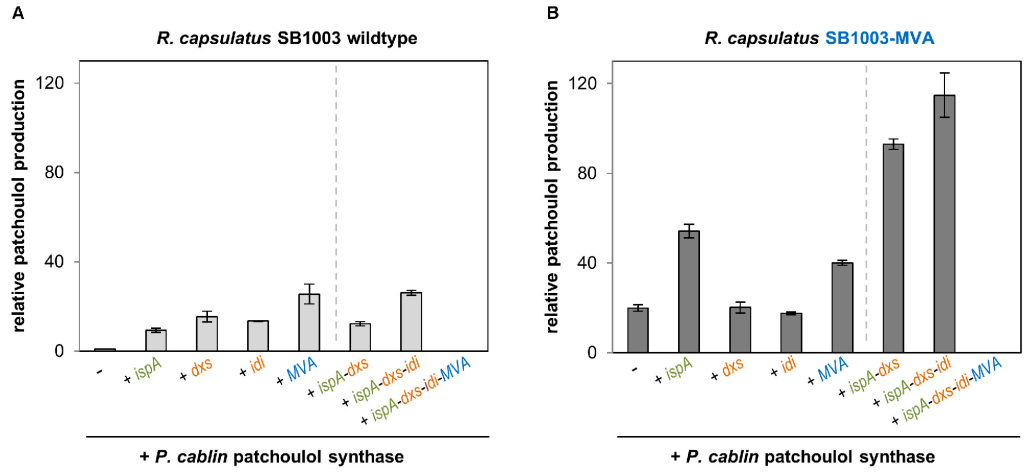

FIGURE 2 | Patchoulol production in the *R. capsulatus* wildtype and modularly engineered strains. Patchoulol synthase PcPS from *Pogostemon cablin* was expressed in *R. capsulatus* SB1003 wildtype **(A)** and SB1003-MVA **(B)** harboring different sets of plasmid-encoded precursor module genes. Product formation was determined in cell cultures after 5 days of photoheterotrophic cultivation (late stationary growth phase). The sesquiterpene was sampled in an overlaid *n*-dodecane phase for GC-FID analysis. Increase of patchoulol production in engineered strains is shown as relative units using *R. capsulatus* SB1003 carrying the plasmid-encoded PcPS gene as reference strain. Data represent mean values and respective standard deviations from three independent cultivations. Plasmid-based co-expression of *ispA*, *dxs*, *idi*, and MVA genes is indicated below the bars. Strains with constructs for co-expression of the patchoulol synthase and single precursor module genes are grouped on the left side of the dashed line whereas strains with combined precursor module genes are shown on the right side.

the combination of all precursor module genes (*ispA-dxs-idi-MVA*) for plasmid-based expression. However, loss of the plasmid (18 kb) can be excluded as a reason for this finding due to positive selection conditions implemented with kanamycin in the medium. Further, instabilities of the promoter sequences or coding regions of isoprenoid converting enzymes appear unlikely since the same results could be observed in several independent experiments. Therefore, the results hint to feed-forward inhibition effects as further detailed in the discussion of this manuscript. In addition, we alternatively installed the MVA gene cluster of *P. zeaxanthinifaciens* in the *R. capsulatus* chromosome (**Figure 1C**).

To comparatively analyze sesquiterpenoid production in the recombinant strain *R. capsulatus* SB1003-MVA, the same pRhon5Hi-2-PcPS variants, that were previously evaluated in the wildtype strain SB1003, were used (**Figure 2B**). The expression of *PcPS* in *R. capsulatus* SB1003-MVA already led to a 20-fold increased patchoulol accumulation in comparison to the reference strain *R. capsulatus* SB1003 with plasmid pRhon5Hi-2-PcPS. Thus, in this strain patchoulol accumulates at comparable amounts that were gained in the respective wildtype strain harboring the plasmid-encoded MVA module. While co-expression of *PcPS* together with plasmid-encoded IspA, DxS or MVA module genes had moderate effects on product formation or did not lead to a further improved patchoulol production in *R. capsulatus* SB1003-MVA, the combined co-expression of *ispA-dxs* and *ispA-dxs-idi* resulted in remarkably higher product accumulation (93- and 115-fold in comparison to the reference strain). Again, no patchoulol accumulation was detectable with the plasmid carrying the assembly *ispA-dxs-idi-MVA*. In summary, we could show that in the *R. capsulatus* wildtype, the FPP precursor supply provided by the enzymes of the DXP, prenyl phosphate and MVA modules, represents a critical bottleneck for patchoulol production. Hence, a 126-fold increased patchoulol accumulation could be established in the phototrophic host upon concerted expression of chromosomally located MVA and plasmid-encoded *ispA, dxs,* and *idi* genes.

CsVS- and CnVS-Mediated Valencene Production in *R. capsulatus* SB1003 and SB1003-MVA

By using the patchoulol synthase PcPS from *P. cablin*, we could demonstrate that the phototrophic bacterium *R. capsulatus* is basically suitable for the production of plant-derived sesquiterpenoids. In addition, our results clearly show that modular co-expression of homologous or heterologous enzymes involved in the supply of the central sesquiterpenoid precursor FPP can help to considerably increase product formation.

After these findings, we next investigated if the combination of precursor modules, which was identified as best for patchoulol production, can also be used for the synthesis of other plant sesquiterpenoids. To consider different activities of sesquiterpenoid synthases in this context, two valencene synthases from orange *Citrus sinensis* and Nootka cypress *Callitropsis nootkatensis* that were shown to perform differently in an *R. sphaeroides in vivo* assay (Beekwilder et al., 2014) were used

for comparative studies in the modularly engineered *R. capsulatus* strains. To this end, the two codon-optimized valencene synthase genes were cloned into a set of pRhon5Hi-2 vectors carrying representative combinations of precursor module genes that had resulted in different patchoulol yields. The resulting plasmids were subsequently transferred into *R. capsulatus* wildtype strain SB1003 as well as the engineered strain SB1003-MVA. Cells were subsequently cultivated under photoheterotrophic conditions and valencene accumulation was comparatively analyzed in the late stationary phase (**Figure 3**).

As expected, expression of the CsVS gene in *R. capsulatus* SB1003 already resulted in accumulation of low but detectable

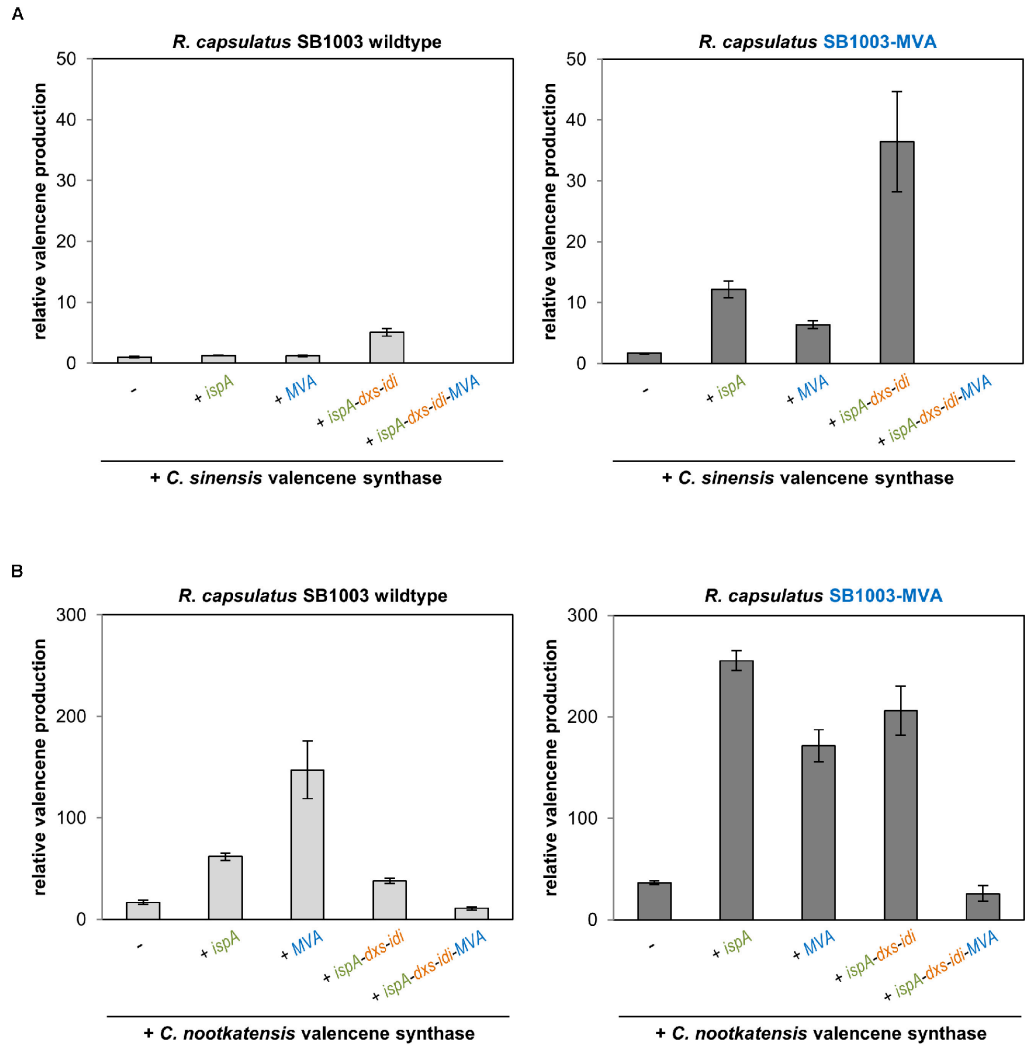

FIGURE 3 | Valencene production in the *R. capsulatus* wildtype and engineered strains. Valencene synthases CsVS from *Citrus sinensis* **(A)** and CnVS from *Callitropsis nootkatensis* **(B)** were expressed using pRhon5Hi-2-derivatives harboring different sets of precursor module genes in *R. capsulatus* SB1003 wildtype and the engineered SB1003-MVA strain. Valencene was sampled after 5 days of photoheterotrophic cultivation in an overlaid *n*-dodecane phase for GC-FID analysis. Increase of valencene production in engineered strains is normalized to the peak area of the valencene signal of the respective reference strain (*R. capsulatus* wildtype strain SB1003 carrying the plasmid-encoded CsVS). Data represent mean values and respective standard deviations from three independent cultivations. Plasmid-based co-expression of *ispA*, *dxs*, *idi*, and MVA genes is indicated below the bars.

amounts of valencene (**Figure 3A** and **Supplementary Figure S4** for GC-MS analysis). In contrast to *PcPS*-mediated patchoulol production, co-expression of *CsVS* together with *ispA* or MVA genes only resulted in a marginal increase of product formation whereas concerted co-expression of *ispA*, *dxs* and *idi* led to a fivefold higher valencene amount. Expression of CsVS in *R. capsulatus* SB1003-MVA also resulted in a comparatively low valencene production (∼1.6 fold increase in comparison to the wildtype strain), while co-expression of IspA or the plasmid-encoded MVA module increased the sesquiterpenoid production by a factor of 12 and 6, respectively. However, combined co-expression of the *CsVS* gene together with *ispA*, *dxs* and *idi* in *R. capsulatus* SB1003-MVA provided remarkably higher product formation resulting in a 36-fold increase in relation to the reference strain SB1003 harboring pRhon5Hi-2-CsVS. The combination of all module genes (*ispA-dxs-idi-MVA*) for plasmid-based *CsVS* expression could not establish detectable valencene accumulation in the *R. capsulatus* wildtype and SB1003-MVA strain as previously found for patchoulol.

C. nootkatensis valencene synthase-dependent valencene synthesis was analogously tested in *R. capsulatus*. Here, expression of the alternative synthase gene in the *R. capsulatus* SB1003 wildtype already resulted in a 16-fold increased valencene accumulation (**Figure 3B**), thus corroborating previous studies reporting higher activity of CnVS compared to CsVS (Beekwilder et al., 2014; Frohwitter et al., 2014). Co-expression of *ispA* and plasmid-encoded MVA module further enhanced valencene accumulation levels up to 147-fold. Surprisingly, co-expression of *ispA* together with DXP module genes led to reduced valencene accumulation. The co-expression of all module genes (*ispA-dxs-idi-MVA*) further reduced product levels but notably yielded for the first time detectable product levels. Expression of *CnVS* in *R. capsulatus* SB1003-MVA already resulted in a 37-fold higher valencene accumulation compared to the reference strain. Remarkably, product formation could be further increased up to 255-fold by co-expression of *ispA*. In contrast to the results that were gained using the sesquiterpene synthases PcPS and CsVS, neither the implementation of the plasmid-encoded MVA pathway nor the co-expression of the DXP module genes resulted in a further increased product accumulation. These results clearly indicate that the implementation of new sesquiterpenoid synthases in the photosynthetic production host *R. capsulatus* requires, in any case, the evaluation of upstream pathway modules for gaining best results.

Time-Dependent Patchoulol and Valencene Accumulation in Engineered *R. capsulatus* Strains

Using patchoulol and valencene as showcase, we could demonstrate that *R. capsulatus* can be used as production host that accumulates plant-derived sesquiterpenoids during phototrophic growth. However, since we analyzed sesquiterpenoid formation so far only at the late-stationary growth phase, we subsequently performed an initial characterization of patchoulol and valencene production over time in strains that were determined to enable maximal product accumulation. Therefore, sesquiterpenoid production of *R. capsulatus* SB1003-MVA carrying vector pRhon5Hi-2-PcPS-ispA-dxs-idi and pRhon5Hi-2-CnVS-ispA, respectively, were monitored for 5 days (**Figure 4**).

In the logarithmic growth phase (24 h), patchoulol titers were comparatively low but steadily increased over incubation time until a maximum was reached after 96 h (**Figure 4A**). Low accumulation levels could initially also be observed for valencene production. However, in that case highest accumulation levels could already be detected after 48 h (**Figure 4B**). At this time-point, cells have typically reached the end of the exponential growth phase. After this, the valencene titer remained rather constant over time. To finally estimate product yields as accurately as possible, we analyzed (i) the individual transfer efficiencies of patchoulol and valencene from cell culture into the *n*-dodecane phase, (ii) the effect of the intracytoplasmic membrane that is predominantly formed by *R. capsulatus* under phototrophic conditions on *n*-dodecane-based product extraction, (iii) the differences in sesquiterpenoid transfer efficiencies after single compared to repeated *n*-dodecane extraction as well as, (iv) the effect of the *n*-dodecane layer on the final product titers (see Supplementary Method section "Analysis of *n*-Dodecane-Mediated Sesquiterpenoid Extraction From Phototrophically Grown *R. capsulatus*"). By taking the different factors into account, we were able to determine product titers of 24 ± 2 mg/L patchoulol (*R. capsulatus* SB1003-MVA with pRhon5Hi-2-PcPS-ispA-dxs-idi after 120 h of cultivation) and 18 ± 3 mg/L valencene (*R. capsulatus* SB1003-MVA harboring pRhon5Hi-2-CnVS-ispA after 48 h of cultivation), respectively. Corresponding productivities were calculated based on these values and the reached cell densities (**Supplementary Table S3**).

In summary, the results of *Rhodobacter*-based patchoulol and valencene production demonstrate that this bacterium can basically serve as an alternative sesquiterpenoid production chassis. In addition, the here presented P_{nif}-based expression tools allow modular adaptation of precursor gene expression under phototrophic growth conditions and thereby tuning of sesquiterpenoid formation.

DISCUSSION

In this study we demonstrated the biosynthesis of plant sesquiterpenoids patchoulol and valencene in *R. capsulatus* under phototrophic conditions and the modular improvement of production by engineering of precursor biosynthesis. In particular, P_{nif}-based co-expression of IspA, selected enzymes of the DXP pathway and the MVA pathway resulted in a substantial improvement of sesquiterpenoid production. The results are thus in agreement with previous studies, where engineering of isoprenoid precursor biosynthesis was shown to be a powerful means to boost terpenoid production in microbial hosts as recently reviewed by Schrader and colleagues for the production of terpenoid flavor and fragrance compounds (Schempp et al., 2018).

For example, the DXP synthase DxS in the intrinsic DXP pathway as well as the IPP isomerase Idi have previously been

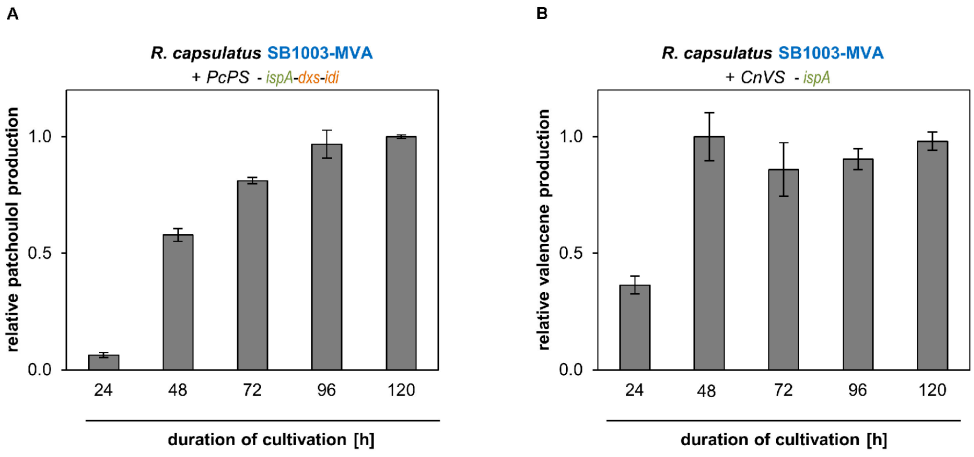

FIGURE 4 | Patchoulol and valencene accumulation of best performing *R. capsulatus* strains over time. Patchoulol synthase PcPS from *P. cablin* **(A)** and valencene synthases CnVS from *C. nootkatensis* **(B)** were expressed in engineered *R. capsulatus* strains (as specified above panels). Relative product formation was determined during photoheterotrophic cultivation via GC-FID analysis of an overlaid *n*-dodecane phase. Data is normalized to highest peak area values, accordingly, and represents mean values and respective standard deviations from three independent cultivations.

identified as central bottlenecks and their overexpression has been proven to be beneficial for bacterial isoprenoid production, e.g., in *E. coli* (Lv et al., 2013), *C. glutamicum* (Henke et al., 2018), and *R. capsulatus* (Khan et al., 2015). Increased DxS enzymatic capacity enhances the provision of the precursors IPP and DMAPP, which in turn can only be efficiently elongated if their ratio is adapted appropriately by IPP isomerase. While DMAPP and IPP are both required in the initial condensation of the two C5 units to C10 GPP, the further steps of elongation to C15 FPP and C20 GGPP specifically require additional IPP.

Although the DXP pathway is more prevalent in bacteria, a number of species additionally or exclusively possess the MVA pathway (Boucher and Doolittle, 2000). This route can be additionally implemented in bacterial producers, which are naturally equipped with only the DXP pathway, thereby further improving terpenoid precursor supply (e.g., Zurbriggen et al., 2012; Beekwilder et al., 2014). Here, we used MVA pathway genes from *P. zeaxanthinifaciens* for engineering *R. capsulatus,* as previous studies using the closely related bacterium *R. sphaeroides* indicated that these genes are suitable to boost terpenoid production in phototrophic α-proteobacteria (Beekwilder et al., 2014). *P. zeaxanthinifaciens* exclusively uses the MVA pathway (Eisenreich et al., 2002) which thus covers the entire cellular isoprenoid demand, e.g., for quinone and carotenoid formation (Boronat and Rodríguez-Concepción, 2015). The MVA genes from *P. zeaxanthinifaciens* are particularly suitable for the expression in *R. capsulatus* since both organisms exhibit an identical GC content (67%) which facilitates functional expression.

Besides the precursor pathways which provide the C5 units for isoprenoid synthesis, IspA activity is also of central importance for the production of sesquiterpenoids as this determines the available substrate pool for a given synthase enzyme. In line with this, multiple studies have previously described increased terpenoid production by co-expression of IspA in different hosts including *E. coli* for α-farnesene production (Wang et al., 2011) and *R. capsulatus* for squalene production (Khan et al., 2015).

Considering our findings of improved patchoulol and valencene titers upon P_{nif} promoter-based co-expression of the mentioned genes, we corroborate here the usefulness of all three strategies, i.e., engineering of the DXP pathway, transfer of the MVA pathway, and reinforcing IspA activity, as well as synergies of their combination (Yang et al., 2016; Schempp et al., 2018). However, we could also observe negative effects of co-expressing precursor biosynthesis genes for sesquiterpenoid production. Such effects may be assigned to the fact that both, the DXP and the MVA pathway are strictly regulated to avoid accumulation of isoprenoid intermediates in the cell. Multiple regulatory circuits have been described to control the DXP pathway (Banerjee and Sharkey, 2014; Frank and Groll, 2017), including the feedback inhibition of DxS by IPP, and DMAPP (Banerjee et al., 2013), and feedback modulation of IspF activity by FPP (Bitok and Meyers, 2012). Similarly, the MVA pathway comprises known feedback loops. For example, HMG-CoA reductase and the MVA kinase are feedback inhibited by FPP (Miziorko, 2011; Scalcinati et al., 2012). Notably, accumulation of MVA pathway intermediates HMG-CoA and MVA, and likewise IPP and FPP were shown to exert toxic effects on *E. coli* and inhibit cellular growth (Martin et al., 2003; Pitera et al., 2007; Dahl et al., 2013). This effect can be alleviated by expression of heterologous terpene synthase enzymes. Prenyl phosphate elongation seems likewise controlled. IspA is inhibited by high concentrations of its substrate IPP and its product FPP, as it has been demonstrated for the human enzyme (Barnard and Popják, 1981; Park et al., 2017).

These phenomena indicate the central importance of the activity of an introduced sesquiterpenoid synthase. The enzyme's capability to consume FPP most likely significantly determines which measures in the precursor biosynthetic pathways are beneficial, and which evoke adverse effects. In the present study, we therefore established a set of different expression vectors and an *R. capsulatus* expression strain SB1003-MVA equipped with the MVA pathway, so that different engineering strategies may be pursued and thereby, the metabolite flux can be adapted to different terpenoid synthases.

Scientific studies on the biotechnological production of patchoulol have largely focused on the yeast *S. cerevisiae* as host. There, engineering strategies have included expression of *P. cablin* patchoulol synthase together with IspA as fused protein and co-expression of HMG-CoA reductase of the MVA pathway, reaching 41.6 mg/L patchoulol (Gruchattka and Kayser, 2015). Yeast-derived patchoulol is already marketed by the company Firmenich. Recently, patchoulol production was installed in *C. glutamicum*, reaching a titer of 60 mg/L upon co-expression of *ispA*, *dxs* and *idi* in a fed-batch fermentation (Henke et al., 2018). We report here on 24 mg/L patchoulol production in photoheterotrophic cultivation of *R. capsulatus* carrying the MVA pathway genes in the chromosome and a plasmid for expression of *PcPS* along with *ispA*, *dxs* and *idi*. Valencene production has been established in diverse host systems, including *S. cerevisiae* (Beekwilder et al., 2014) and *Schizophyllum commune* (Scholtmeijer et al., 2014). A valencene titer of 41 mg/L could be achieved in *C. glutamicum* through strain optimization in combination with light-controlling gene expression (Binder et al., 2016). However, the highest titers of 352 mg/L were so far reached in an optimized *R. sphaeroides* strain (Beekwilder et al., 2014). Biotechnological valencene produced in yeast and *R. sphaeroides* is marketed by the companies Evolva and Isobionics, respectively. However, although modular engineering of the closely related *R. capsulatus* resulted in a 255-fold increased accumulation of valencene, the here reported titer is much lower (18 mg/L). Differences in product titers and accumulation over time clearly indicate that sesquiterpenoid production in *R. capsulatus* requires further investigation. Recently, it was demonstrated that yields of the sesquiterpene amorphadiene in chemoheterotrophically grown *R. sphaeroides* cells can be strongly increased by optimizing the cultivation conditions (Orsi et al., 2019). In this study, it could be shown that the C/N ratio, which can be altered by changing the supplemented carbon and nitrogen sources, as well as the oxygen availability, have an important impact on substrate-to-product conversion. Orsi et al. further speculated that poly-β-hydroxybutyrate (PHB), a storage compound which is formed in *Rhodobacter* under nitrogen-limiting conditions, can be utilized in the stationary growth phase thereby facilitating sesquiterpene production during growth limitation. Therefore, understanding the complex metabolic networks will be important to further improve the production of sesquiterpenes in phototrophic α-proteobacteria.

However, besides using *Rhodobacter* as a biotechnological production host, the specific physiological properties together with the here described modular adaptability of terpenoid formation make this bacterium an attractive candidate for future agricultural and therapeutic applications: (i) Secondary metabolites including sesquiterpenoids, which are produced by plants upon biotic stresses, are involved in direct and indirect plant defense mechanisms against herbivores and plant pathogens (Pichersky and Gershenzon, 2002; Wang et al., 2018; Block et al., 2019). While the role of terpenes in defense against aboveground plant pathogens and herbivores is well described, examples for belowground interspecies communication mechanisms are rare but indicate a crucial function of terpenes in plant defense against various pathogens including insects, fungi, bacteria and nematodes (Ohri and Pannu, 2009; Huang and Osbourn, 2019). In a preliminary study, we could now demonstrate that valencene is active against the plant pathogenic nematode *Heterodera schachtii* (Schleker et al. manuscript in preparation) – an observation that further corroborates this assumption. Since *R. capsulatus* was identified as a plant growth promoting bacterium naturally occurring in root microbiomes of various plants including *Brassica rapa*, rice, sugar beet, and barley (Çakmakçi et al., 2006, 2007; Gamal-Eldin and Elbanna, 2011; Hussein et al., 2014), appropriately engineered *Rhodobacter* strains delivering selected terpenes may constitute a possible future means for plant protection and reduction of fertilizer application in agricultural crop production. (ii) In addition, we could recently demonstrate that *R. capsulatus* can be used as an *in vivo* marker for multispectral optoacoustic tomography-based analysis of macrophage presence and activity inside of solid tumors (Peters et al., 2019). Therefore, production and reporter properties of *R. capsulatus* could also be combined to develop a new theranostic platform allowing selective *in situ* delivery of anti-cancer terpenoids together with visualization of the drug release process.

In summary, *R. capsulatus* poses a promising phototrophic host for the production of sesquiterpenoids. Besides these terpenoid targets, recombinant biosynthesis of carotenoids (tetraterpenoids) like β-carotene (Loeschcke et al., 2013) and the triterpenoids squalene, botryococcene, cycloartenol and lupeol in this bacterium has already been described (Khan et al., 2015; Loeschcke et al., 2017). However, the P_{nif}-based expression tools together with the modular engineering approaches developed in this study can further help to characterize new terpenoids whose biosynthetic genes are identified via genome mining. In addition, it will facilitate the development of new sustainable production processes and chassis suitable for selective delivery of bioactive molecules. Indeed, ongoing studies in our group already indicate a broader applicability of this terpenoid production toolbox. Further refinement and dynamic control of precursor biosynthesis enabling plugging in different terpenoid pathways with individual precursor demands, and engineering of terpenoid secretion may contribute to improve sustainable terpenoid production.

DATA AVAILABILITY

All data generated or analyzed during this study are included in the manuscript and/or the **Supplementary Files**.

AUTHOR CONTRIBUTIONS

TD and K-EJ conceived the research concept. KT, AL, and TD designed the experiments. KT, AÖ, VS, FH, SH, and TW performed the experimental work. BS-S performed the GC-MS analytics. KT, AL, JH-H, FG, SS, and TD analyzed the data and wrote the manuscript. All authors read and approved the final manuscript.

FUNDING

This research was funded by the Ministry of Culture and Science of the German State of North Rhine-Westphalia MKW (NRW Strategieprojekt BioSC No.313/323-400-00213), the German Federal Ministry of Education and Research BMBF (HT-ENZ), and the German Research Foundation DFG (Cluster of Excellence on Plant Sciences CEPLAS, EXC1028). The funding bodies had no role in the design of the study and collection, analysis, and interpretation of data or in writing the manuscript.

ACKNOWLEDGMENTS

The authors gratefully acknowledge the funding by the organizations mentioned in the Funding section. Additionally, the authors thankfully acknowledge Dr. Nadine Katzke for valuable advice on GC-FID analysis and Dr. Achim Heck for revising the manuscript.

SUPPLEMENTARY MATERIAL

The Supplementary Material for this article can be found online at: https://www.frontiersin.org/articles/10.3389/fmicb.2019.01998/full#supplementary-material

REFERENCES

Arendt, P., Miettinen, K., Pollier, J., De Rycke, R., Callewaert, N., and Goossens, A. (2017). An endoplasmic reticulum-engineered yeast platform for overproduction of triterpenoids. *Metab. Eng.* 40, 165–175. doi: 10.1016/j.ymben.2017.02.007

Armstrong, G. A. (1997). Genetics of eubacterial carotenoid biosynthesis: a colorful tale. *Annu. Rev. Microbiol.* 51, 629–659. doi: 10.1146/annurev.micro.51.1.629

Armstrong, G. A., Alberti, M., Leach, F., and Hearst, J. E. (1989). Nucleotide sequence, organization, and nature of the protein products of the carotenoid biosynthesis gene cluster of *Rhodobacter capsulatus*. *Mol. Gen. Genet.* 216, 254–268. doi: 10.1007/bf00334364

Banerjee, A., and Sharkey, T. D. (2014). Methylerythritol 4-phosphate (MEP) pathway metabolic regulation. *Nat. Prod. Rep.* 31, 1043–1055. doi: 10.1039/c3np70124g

Banerjee, A., Wu, Y., Banerjee, R., Li, Y., Yan, H., and Sharkey, T. D. (2013). Feedback inhibition of deoxy-D-xylulose-5-phosphate synthase regulates the methylerythritol 4-phosphate pathway. *J. Biol. Chem.* 288, 16926–16936. doi: 10.1074/jbc.M113.464636

Barnard, G. F., and Popják, G. (1981). Human liver prenyltransferase and its characterization. *Biochim. Biophys. Acta* 661, 87–99. doi: 10.1016/0005-2744(81)90086-3

Bauer, K., Garbe, D., and Surburg, H. (2001). *Common Fragrance and Flovor Materials*. Weinheim: Wiley-VCH.

Beekwilder, J., van Houwelingen, A., Cankar, K., van Dijk, A. D. J., de Jong, R. M., Stoopen, G., et al. (2014). Valencene synthase from the heartwood of Nootka cypress (*Callitropsis nootkatensis*) for biotechnological production of valencene. *Plant Biotechnol. J.* 12, 174–182. doi: 10.1111/pbi.12124

Bian, G., Deng, Z., and Liu, T. (2017). Strategies for terpenoid overproduction and new terpenoid discovery. *Curr. Opin. Biotechnol.* 48, 234–241. doi: 10.1016/j.copbio.2017.07.002

Binder, D., Frohwitter, J., Mahr, R., Bier, C., Grünberger, A., Loeschcke, A., et al. (2016). Light-controlled cell factories: employing photocaged isopropyl-β-D-thiogalactopyranoside for light-mediated optimization of lac promoter-based gene expression and (+)-valencene biosynthesis in *Corynebacterium glutamicum*. *Appl. Environ. Microbiol.* 82, 6141–6149. doi: 10.1128/AEM.01457-1416

Bitok, J. K., and Meyers, C. F. (2012). 2C-Methyl-D-erythritol 4-phosphate enhances and sustains cyclodiphosphate synthase IspF activity. *ACS Chem. Biol.* 7, 1702–1710. doi: 10.1021/cb300243w

Block, A. K., Vaughan, M. M., Schmelz, E. A., and Christensen, S. A. (2019). Biosynthesis and function of terpenoid defense compounds in maize (*Zea mays*). *Planta* 249, 21–30. doi: 10.1007/s00425-018-2999-92

Boronat, A., and Rodríguez-Concepción, M. (2015). "Terpenoid biosynthesis in prokaryotes," in *Biotechnology of Isoprenoids*, eds J. Schrader, and J. Bohlmann, (Berlin: Springer), 3–18. doi: 10.1007/10_2014_285

Boucher, Y., and Doolittle, W. F. (2000). The role of lateral gene transfer in the evolution of isoprenoid biosynthesis pathways. *Mol. Microbiol.* 37, 703–716. doi: 10.1046/j.1365-2958.2000.02004.x

Çakmakçi, R., Dönmez, F., Aydın, A., and Şahin, F. (2006). Growth promotion of plants by plant growth-promoting rhizobacteria under greenhouse and two different field soil conditions. *Soil Biol. Biochem.* 38, 1482–1487. doi: 10.1016/j.soilbio.2005.09.019

Çakmakçi, R., Dönmez, M. F., and Erdoğan, Ü. (2007). The effect of plant growth promoting rhizobacteria on barley seedling growth, nutrient uptake, some soil properties, and bacterial counts. *Turk* 31, 189–199.

Chen, Y., Zhou, Y. J., Siewers, V., and Nielsen, J. (2015). "Enabling technologies to advance microbial isoprenoid production," in *Biotechnology of Isoprenoids*, eds J. Schrader, and J. Bohlmann, (Berlin: Springer), 143–160. doi: 10.1007/10_2014_284

Christianson, D. W. (2017). Structural and chemical biology of terpenoid cyclases. *Chem. Rev.* 117, 11570–11648. doi: 10.1021/acs.chemrev.7b00287

Croteau, R., Kutchan, T. M., and Lewis, N. G. (2000). "Natural products (secondary metabolites)," in *Biochemistry and Molecular Biology of Plants*, eds B. Buchanan, W. Gruissem, and R. Jones, (Rock Ville: American Society of Plant Physiologists), 1250–1318.

Dahl, R. H., Zhang, F., Alonso-Gutierrez, J., Baidoo, E., Batth, T. S., Redding-Johanson, A. M., et al. (2013). Engineering dynamic pathway regulation using stress-response promoters. *Nat. Biotechnol.* 31, 1039–1046. doi: 10.1038/nbt.2689

Das, A., Yoon, S.-H., Lee, S.-H., Kim, J.-Y., Oh, D.-K., and Kim, S.-W. (2007). An update on microbial carotenoid production: application of recent metabolic engineering tools. *Appl. Microbiol. Biotechnol.* 77, 505–512. doi: 10.1007/s00253-007-1206-1203

Dewick, P. M. (2002). The biosynthesis of C5-C25 terpenoid compounds. *Nat. Prod. Rep.* 19, 181–222. doi: 10.1039/b002685i

Drews, G. (2013). The intracytoplasmic membranes of purple bacteria - assembly of energy-transducing complexes. *J. Mol. Microbiol. Biotechnol.* 23, 35–47. doi: 10.1159/000346518

Efferth, T. (2017). From ancient herb to modern drug: *Artemisia annua* and artemisinin for cancer therapy. *Semin. Cancer Biol.* 46, 65–83. doi: 10.1016/j.semcancer.2017.02.009

Eisenreich, W., Bacher, A., Berry, A., Bretzel, W., Hümbelin, M., Lopez-Ulibarri, R., et al. (2002). Biosynthesis of zeaxanthin *via* mevalonate in *Paracoccus* species strain PTA-3335. A product-based retrobiosynthetic study. *J. Org. Chem.* 67, 871–875. doi: 10.1021/jo016084r

Frank, A., and Groll, M. (2017). The methylerythritol phosphate pathway to isoprenoids. *Chem. Rev.* 117, 5675–5703. doi: 10.1021/acs.chemrev.6b00537

Frohwitter, J., Heider, S. A. E., Peters-Wendisch, P., Beekwilder, J., and Wendisch, V. F. (2014). Production of the sesquiterpene (+)-valencene by metabolically engineered *Corynebacterium glutamicum*. *J. Biotechnol.* 191, 205–213. doi: 10.1016/j.jbiotec.2014.05.032

Fuhrmann, M., Hausherr, A., Ferbitz, L., Schödl, T., Heitzer, M., and Hegemann, P. (2004). Monitoring dynamic expression of nuclear genes in *Chlamydomonas reinhardtii* by using a synthetic luciferase reporter gene. *Plant Mol. Biol.* 55, 869–881. doi: 10.1007/s11103-004-2150-2156

Gamal-Eldin, H., and Elbanna, K. (2011). Field evidence for the potential of *Rhodobacter capsulatus* as biofertilizer for flooded rice. *Curr. Microbiol.* 62, 391–395. doi: 10.1007/s00284-010-9719-x

Gershenzon, J., and Dudareva, N. (2007). The function of terpene natural products in the natural world. *Nat. Chem. Biol.* 3, 408–414. doi: 10.1038/nchembio.2007.5

Gruchattka, E., and Kayser, O. (2015). *In vivo* validation of in silico predicted metabolic engineering strategies in yeast: disruption of α-ketoglutarate dehydrogenase and expression of ATP-citrate lyase for terpenoid production. *PLoS One* 10:e0144981. doi: 10.1371/journal.pone.0144981

Hanahan, D. (1983). Studies on transformation of *Escherichia coli* with plasmids. *J. Mol. Biol.* 166, 557–580. doi: 10.1016/s0022-2836(83)80284-8

Haselkorn, R. (1986). Organization of the genes for nitrogen fixation in photosynthetic bacteria and cyanobacteria. *Annu. Rev. Microbiol.* 40, 525–547. doi: 10.1146/annurev.mi.40.100186.002521

Henke, N. A., Wichmann, J., Baier, T., Frohwitter, J., Lauersen, K. J., Risse, J. M., et al. (2018). Patchoulol production with metabolically engineered *Corynebacterium glutamicum*. *Genes* 9:219. doi: 10.3390/genes9040219

Huang, A. C., and Osbourn, A. (2019). Plant terpenes that mediate below-ground interactions: prospects for bioengineering terpenoids for plant protection. *Pest Manag. Sci.* 75, 2368–2377. doi: 10.1002/ps.5410

Hümbelin, M., Thomas, A., Lin, J., Li, J., Jore, J., and Berry, A. (2002). Genetics of isoprenoid biosynthesis in *Paracoccus zeaxanthinifaciens*. *Gene* 297, 129–139. doi: 10.1016/s0378-1119(02)00877-6

Hungate, R. E. (1969). A roll tube method for cultivation of strict anaerobes. *Meth. Microbiol.* 3, 117–132. doi: 10.1016/s0580-9517(08)70503-8

Hussein, K. A., Jung, Y. S., and Joo, J. H. (2014). Plant growth promoting activities of some rhizosphere bacteria and their effect on *Brassica rapa* growth. *Korean J. Soil Sci. Fert.* 47, 141–146. doi: 10.7745/KJSSF.2014.47.3.141

Kallscheuer, N., Classen, T., Drepper, T., and Marienhagen, J. (2018). Production of plant metabolites with applications in the food industry using engineered microorganisms. *Curr Opin. Biotechnol.* 56, 7–17. doi: 10.1016/j.copbio.2018.07.008

Katzke, N., Arvani, S., Bergmann, R., Circolone, F., Markert, A., Svensson, V., et al. (2010). A novel T7 RNA polymerase dependent expression system for high-level protein production in the phototrophic bacterium *Rhodobacter capsulatus*. *Protein Expr. Purif.* 69, 137–146. doi: 10.1016/j.pep.2009.08.008

Katzke, N., Bergmann, R., Jaeger, K.-E., and Drepper, T. (2012). Heterologous high-level gene expression in the photosynthetic bacterium *Rhodobacter capsulatus*. *Methods Mol. Biol.* 824, 251–269. doi: 10.1007/978-1-61779-433-9-13

Khan, N. E., Nybo, S. E., Chappell, J., and Curtis, W. R. (2015). Triterpene hydrocarbon production engineered into a metabolically versatile host - *Rhodobacter capsulatus*. *Biotechnol. Bioeng.* 112, 1523–1532. doi: 10.1002/bit.25573

Kirby, J., and Keasling, J. D. (2008). Metabolic engineering of microorganisms for isoprenoid production. *Nat. Prod. Rep.* 25, 656–661. doi: 10.1039/b802939c

Klipp, W., Masepohl, B., and Pühler, A. (1988). Identification and mapping of nitrogen fixation genes of *Rhodobacter capsulatus*: duplication of a nifA-nifB region. *J. Bacteriol.* 170, 693–699. doi: 10.1128/jb.170.2.693-699.1988

Kranz, R. G., and Haselkorn, R. (1985). Characterization of nif regulatory genes in *Rhodopseudomonas capsulata* using lac gene fusions. *Gene* 40, 203–215. doi: 10.1016/0378-1119(85)90043-5

Langenheim, J. H. (1994). Higher plant terpenoids: a phytocentric overview of their ecological roles. *J. Chem. Ecol.* 20, 1223–1280. doi: 10.1007/BF02059809

Loeschcke, A., Dienst, D., Wewer, V., Hage-Hülsmann, J., Dietsch, M., Kranz-Finger, S., et al. (2017). The photosynthetic bacteria *Rhodobacter capsulatus* and *Synechocystis* sp. PCC 6803 as new hosts for cyclic plant triterpene biosynthesis. *PLoS One* 12:e0189816. doi: 10.1371/journal.pone.0189816

Loeschcke, A., Markert, A., Wilhelm, S., Wirtz, A., Rosenau, F., Jaeger, K.-E., et al. (2013). TREX: a universal tool for the transfer and expression of biosynthetic pathways in bacteria. *ACS Synth. Biol.* 2, 22–33. doi: 10.1021/sb3000657

Lv, X., Xu, H., and Yu, H. (2013). Significantly enhanced production of isoprene by ordered coexpression of genes dxs, dxr, and idi in *Escherichia coli*. *Appl. Microbiol. Biotechnol.* 97, 2357–2365. doi: 10.1007/s00253-012-4485-4482

Marienhagen, J., and Bott, M. (2013). Metabolic engineering of microorganisms for the synthesis of plant natural products. *J. Biotechnol.* 163, 166–178. doi: 10.1016/j.jbiotec.2012.06.001

Martin, V. J., Pitera, D. J., Withers, S. T., Newman, J. D., and Keasling, J. D. (2003). Engineering a mevalonate pathway in *Escherichia coli* for production of terpenoids. *Nat. Biotechnol.* 21, 796–802. doi: 10.1038/nbt833

Masepohl, B., Drepper, T., Paschen, A., Gross, S., Pawlowski, A., Raabe, K., et al. (2002). Regulation of nitrogen fixation in the phototrophic purple bacterium *Rhodobacter capsulatus*. *J. Mol. Microbiol. Biotechnol.* 4, 243–248.

Mitchell, W. (2011). Natural products from synthetic biology. *Curr. Opin. Chem. Biol.* 15, 505–515. doi: 10.1016/j.cbpa.2011.05.017

Miziorko, H. M. (2011). Enzymes of the mevalonate pathway of isoprenoid biosynthesis. *Arch. Biochem. Biophys.* 505, 131–143. doi: 10.1016/j.abb.2010.09.028

Ohri, P., and Pannu, S. K. (2009). Effect of terpenoids on nematodes: a review. *J. Environ. Res. Dev.* 4, 171–177.

Orsi, E., Folch, P. L., Monje-López, V. T., Fernhout, B. M., Turcato, A., Kengen, S. W. M., et al. (2019). Characterization of heterotrophic growth and sesquiterpene production by *Rhodobacter sphaeroides* on a defined medium. *J. Ind. Microbiol. Biotechnol.* doi: 10.1007/s10295-019-02201-6 [Epub ahead of print].

Paddon, C. J., Westfall, P. J., Pitera, D. J., Benjamin, K., Fisher, K., McPhee, D., et al. (2013). High-level semi-synthetic production of the potent antimalarial artemisinin. *Nature* 496, 528–532. doi: 10.1038/nature12051

Park, J., Zielinski, M., Magder, A., Tsantrizos, Y. S., and Berghuis, A. M. (2017). Human farnesyl pyrophosphate synthase is allosterically inhibited by its own product. *Nat. Commun.* 8:14132. doi: 10.1038/ncomms14132

Pemberton, T. A., Chen, M., Harris, G. G., Chou, W. K. W., Duan, L., Köksal, M., et al. (2017). Exploring the influence of domain architecture on the catalytic function of diterpene synthases. *Biochemistry* 56, 2010–2023. doi: 10.1021/acs.biochem.7b00137

Peters, L., Weidenfeld, I., Klemm, U., Loeschcke, A., Weihmann, R., Jaeger, K.-E., et al. (2019). Phototrophic purple bacteria as optoacoustic *in vivo* reporters of macrophage activity. *Nat. Commun.* 10:1191. doi: 10.1038/s41467-019-09081-5

Pichersky, E., and Gershenzon, J. (2002). The formation and function of plant volatiles: perfumes for pollinator attraction and defense. *Curr. Opin. Plant Biol.* 5, 237–243. doi: 10.1016/S1369-5266(02)00251-250

Pichersky, E., and Raguso, R. A. (2016). Why do plants produce so many terpenoid compounds? *New Phytol.* 220, 692–702. doi: 10.1111/nph.14178

Pitera, D. J., Paddon, C. J., Newman, J. D., and Keasling, J. D. (2007). Balancing a heterologous mevalonate pathway for improved isoprenoid production in *Escherichia coli*. *Metab. Eng.* 9, 193–207. doi: 10.1016/j.ymben.2006.11.002

Ruzicka, L. (1953). The isoprene rule and the biogenesis of terpenic compounds. *Experientia* 9, 357–367. doi: 10.1007/BF02167631

Scalcinati, G., Knuf, C., Partow, S., Chen, Y., Maury, J., Schalk, M., et al. (2012). Dynamic control of gene expression in *Saccharomyces cerevisiae* engineered for the production of plant sesquitepene α-santalene in a fed-batch mode. *Metab. Eng.* 14, 91–103. doi: 10.1016/j.ymben.2012.01.007

Schempp, F. M., Drummond, L., Buchhaupt, M., and Schrader, J. (2018). Microbial cell factories for the production of terpenoid flavor and fragrance compounds. *J. Agric. Food Chem.* 66, 2247–2258. doi: 10.1021/acs.jafc.7b00473

Scholtmeijer, K., Cankar, K., Beekwilder, J., Wösten, H. A., Lugones, L. G., and Bosch, D. (2014). Production of (+)-valencene in the mushroom-forming fungus S. commune. *Appl. Microbiol. Biotechnol.* 98, 5059–5068. doi: 10.1007/s00253-014-5581-5582

Simon, R., Priefer, U., and Pühler, A. (1983). A broad host range mobilization system for *in vivo* genetic engineering. *Nat. Biotechnol.* 1, 784–791. doi: 10.1038/nbt1183-784

Strnad, H., Lapidus, A., Paces, J., Ulbrich, P., Vlcek, C., Paces, V., et al. (2010). Complete genome sequence of the photosynthetic purple nonsulfur bacterium *Rhodobacter capsulatus* SB 1003. *J. Bacteriol* 192, 3545–3546. doi: 10.1128/JB.00366-310

Tucker, J. D., Siebert, C. A., Escalante, M., Adams, P. G., Olsen, J. D., Otto, C., et al. (2010). Membrane invagination in *Rhodobacter sphaeroides* is initiated at curved regions of the cytoplasmic membrane, then forms both budded and fully detached spherical vesicles. *Mol. Microbiol.* 76, 833–847. doi: 10.1111/j.1365-2958.2010.07153.x

Wang, C., Yoon, S.-H., Jang, H.-J., Chung, Y.-R., Kim, J.-Y., Choi, E.-S., et al. (2011). Metabolic engineering of *Escherichia coli* for α-farnesene production. *Metab. Eng.* 13, 648–655. doi: 10.1016/j.ymben.2011.08.001

Wang, W., Li, Y., Dang, P., Zhao, S., Lai, D., and Zhou, L. (2018). Rice secondary metabolites: structures, roles, biosynthesis, and metabolic regulation. *Molecules* 23:3098. doi: 10.3390/molecules23123098

Weaver, P. F., Wall, J. D., and Gest, H. (1975). Characterization of *Rhodopseudomonas capsulata*. *Arch. Microbiol.* 105, 207–216. doi: 10.1007/bf00447139

Yang, C., Gao, X., Jiang, Y., Sun, B., Gao, F., and Yang, S. (2016). Synergy between methylerythritol phosphate pathway and mevalonate pathway for isoprene production in *Escherichia coli*. *Metab. Eng.* 37, 79–91. doi: 10.1016/j.ymben.2016.05.003

Zurbriggen, A., Kirst, H., and Melis, A. (2012). Isoprene production via the mevalonic acid pathway in *Escherichia coli* (bacteria). *Bioenerg. Res.* 5, 814–828. doi: 10.1007/s12155-012-9192-4

Conflict of Interest Statement: The authors declare that the research was conducted in the absence of any commercial or financial relationships that could be construed as a potential conflict of interest.

II.3.2. *R. CAPSULATUS* AS HETEROLOGOUS HOST FOR THE PRODUCTION OF BIOACTIVE TERPENES

Heterologous production of β-caryophyllene and evaluation of its activity against plant pathogenic fungi

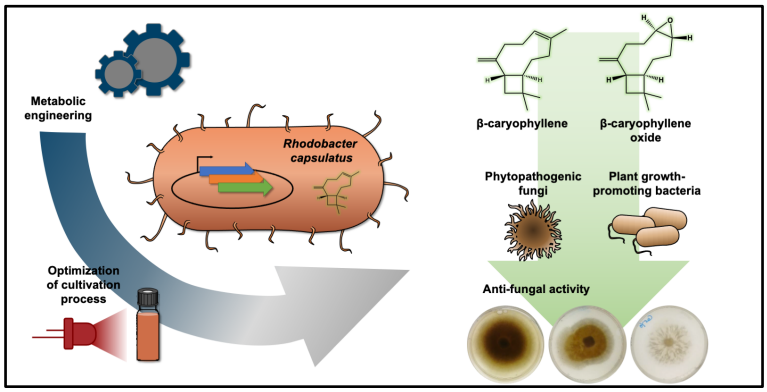

Fabienne Hilgers*, Samer S. Habash*, Anita Loeschcke, Yannic Sebastian Ackermann, Stefan Neumann, Florian M. W. Grundler, Karl-Erich Jaeger, A. Sylvia S. Schleker and Thomas Drepper

Microorganisms. 9(1), 168. (2021). microorganisms9010168

The online version may be found at: 10.3390/microorganisms9010168

Status: published

For the Supporting Information see Appendix (**Chapter V.8.**, **page 472**).

Own contribution: Designing and performing experiments concerning terpene production in *Rhodobacter* and analysis of antibacterial activities, plasmid constructions, analyzing data, writing the manuscript.

microorganisms

MDPI

Article

Heterologous Production of β-Caryophyllene and Evaluation of Its Activity against Plant Pathogenic Fungi

Fabienne Hilgers [1,†], Samer S. Habash [2,†], Anita Loeschcke [1], Yannic Sebastian Ackermann [1], Stefan Neumann [2], Achim Heck [3], Oliver Klaus [1], Jennifer Hage-Hülsmann [1], Florian M. W. Grundler [2], Karl-Erich Jaeger [1,3], A. Sylvia S. Schleker [2,*] and Thomas Drepper [1,*]

[1] Institute of Molecular Enzyme Technology, Heinrich-Heine-University Düsseldorf, Forschungszentrum Jülich, Wilhelm-Johnen-Straße, 52428 Jülich, Germany; f.hilgers@fz-juelich.de (F.H.); a.loeschcke@fz-juelich.de (A.L.); y.ackermann@fz-juelich.de (Y.S.A.); o.klaus@fz-juelich.de (O.K.); j.hage-huelsmann@fz-juelich.de (J.H.-H.); karl-erich.jaeger@fz-juelich.de (K.-E.J.)

[2] INRES—Molecular Phytomedicine, University of Bonn, Karlrobert-Kreiten-Str. 13, 53115 Bonn, Germany; samer@uni-bonn.de (S.S.H.); sneuman1@uni-bonn.de (S.N.); grundler@uni-bonn.de (F.M.W.G.)

[3] Institute of Bio- and Geosciences (IBG-1: Biotechnology) Forschungszentrum Jülich, Wilhelm-Johnen-Straße, 52428 Jülich, Germany; a.heck@fz-juelich.de

* Correspondence: sylvia.schleker@uni-bonn.de (A.S.S.S.); t.drepper@fz-juelich.de (T.D.)

† These authors contributed equally to this work.

Abstract: Terpenoids constitute one of the largest and most diverse groups within the class of secondary metabolites, comprising over 80,000 compounds. They not only exhibit important functions in plant physiology but also have commercial potential in the biotechnological, pharmaceutical, and agricultural sectors due to their promising properties, including various bioactivities against pathogens, inflammations, and cancer. In this work, we therefore aimed to implement the plant sesquiterpenoid pathway leading to β-caryophyllene in the heterologous host *Rhodobacter capsulatus* and achieved a maximum production of 139 ± 31 mg L^{-1} culture. As this sesquiterpene offers various beneficial anti-phytopathogenic activities, we evaluated the bioactivity of β-caryophyllene and its oxygenated derivative β-caryophyllene oxide against different phytopathogenic fungi. Here, both compounds significantly inhibited the growth of *Sclerotinia sclerotiorum* and *Fusarium oxysporum* by up to 40%, while growth of *Alternaria brassicicola* was only slightly affected, and *Phoma lingam* and *Rhizoctonia solani* were unaffected. At the same time, the compounds showed a promising low inhibitory profile for a variety of plant growth-promoting bacteria at suitable compound concentrations. Our observations thus give a first indication that β-caryophyllene and β-caryophyllene oxide are promising natural agents, which might be applicable for the management of certain plant pathogenic fungi in agricultural crop production.

Keywords: terpenoids; sesquiterpene production; *Rhodobacter capsulatus*; β-caryophyllene; bioactivity; phytopathogens; plant pathogenic fungi; plant growth-promoting bacteria

Citation: Hilgers, F.; Habash, S.S.; Loeschcke, A.; Ackermann, Y.S.; Neumann, S.; Heck, A.; Klaus, O.; Hage-Hülsmann, J.; Grundler, F.M.W.; Jaeger, K.-E.; et al. Heterologous Production of β-Caryophyllene and Evaluation of Its Activity against Plant Pathogenic Fungi. *Microorganisms* **2021**, *9*, 168. https://doi.org/10.3390/microorganisms9010168

Received: 10 December 2020
Accepted: 10 January 2021
Published: 14 January 2021

1. Introduction

Among secondary metabolites, terpenoids including the class of sesquiterpenoids represent one of the largest and most diverse groups with over 80,000 known compounds, mostly isolated from plants [1–4]. Based on their number of carbon atoms, they can be divided into the subclasses of hemi- (C_5), mono- (C_{10}), sesqui- (C_{15}), di- (C_{20}), tri- (C_{30}), tetra- (C_{40}) and polyterpenes (>C_{40}) [5,6]. In general, the terpenoid synthesis starts from the two isoprene intermediates isopentenyl pyrophosphate (IPP) and dimethylallyl pyrophosphate (DMAPP), which are provided either by the mevalonate (MVA) pathway or by the 1-deoxy-D-xylulose 5-phosphate (DXP) pathway, also known as the 2-C-methyl-D-erythritol 4-phosphate (MEP) pathway. While the MVA pathway uses acetyl-Coenzyme A (acetyl-CoA) as a substrate and is predominantly found in eukaryotes (e.g., mammals, plants,

and fungi), archaea and a few bacteria [7], the DXP pathway starts from glyceraldehyde-3-phosphate (GAP) and pyruvate and primarily occurs in bacteria, cyanobacteria, and green algae [8]. Starting from IPP and DMAPP, the elongation of linear prenyl pyrophosphates is catalyzed by prenyltransferases via head-to-tail condensations and results in C_{10} geranyl pyrophosphate (GPP), C_{15} farnesyl pyrophosphate (FPP), and C_{20} geranylgeranyl pyrophosphate (GGPP). Finally, GPP is used as a precursor molecule for the synthesis of monoterpenoids, FPP for sesqui- and triterpenoid production, and GGPP for di- and tetraterpenoid biosynthesis. Terpenes exhibit manifold functions in plant physiology and development, including photoprotection (carotenoids), communication (e.g., pinene), or repellant activity against predators and parasites (e.g., verbenone, β-caryophyllene) [9–11]. Furthermore, terpenes are of commercial interest for the pharmaceutical sector due to their various bioactivities suitable for the treatment of pathogen infections, inflammation, or cancer [12,13]. For example, the sesquiterpene farnesol shows inhibitory effects against antibiotic-resistant *Staphylococci*, not only inhibiting the growth of planktonic cells in free suspension but also suppressing biofilm formation of *Staphylococcus aureus*, *Staphylococcus epidermidis*, and *Burkholderia pseudomallei* [14–17]. In the past, these compounds were exclusively obtained from essential oils of natural plant sources, requiring complex and time-consuming downstream processing. β-caryophyllene, for example, was extracted from *Cannabis sativa* [18], clove basil, *Ocimum gratissimum* [19], or representatives of the plant genus *Cordia*, such as *Cordia verbenaceae* [20]. However, the application of microorganisms as heterologous hosts allows the establishment of alternative, cost-effective, and sustainable biotechnological production processes [21–26]. As the efficiency of such processes strongly depends on the achieved production titers, metabolic engineering of the applied hosts together with the optimization of the respective secondary metabolite pathways has gained more attention in the recent past [1,27–31]. So far, terpenoids were mostly produced in the heterologous hosts *Escherichia coli* and *Saccharomyces cerevisiae* [32–36]. However, in recent studies, the terpene production in less common microbes such as phototrophs has also been established and optimized, as for example documented by the *Rhodobacter*-based production of β-farnesene, nootkatone, valencene, and amorphadiene [23,37–40], or the production of various terpenes in cyanobacteria [41].

The phototrophic non-sulfur α-proteobacteria of the genus *Rhodobacter* feature some unique physiological properties, making them interesting microbial hosts for heterologous terpene production: (i) the cell membrane is commonly considered to be a critical determinant in terpenoid production since it can function as a storage compartment for the involved enzymes and metabolites [42,43]. In this context, *Rhodobacter* seems to be particularly suited for terpene production since the bacterium can form an extended intracytoplasmic membrane system (ICM), thereby providing a naturally enlarged reservoir for membrane-bound enzymes and terpenes [44,45]. (ii) As these phototrophic bacteria produce the carotenoids spheroidene and spheroidenone using the DXP pathway [46,47], they further offer a robust and effective isoprenoid metabolism that can be engineered for efficient terpenoid production. (iii) *Rhodobacter* species enable photo(hetero)tropic growth in low-cost minimal media at relatively high growth rates, allowing the utilization of sunlight as an energy source for sustainable cultivation and production processes. Recent studies could demonstrate that engineering the isoprenoid precursor biosynthesis can lead to a strong increase of sesqui- and triterpenoid formation in *R. capsulatus* [39,48,49] and *R. sphaeroides* [38,40,50–52]. In particular, the co-expression of a terpene synthase with the FPP synthase IspA, and/or enzymes constituting the heterologous MVA pathway, resulted in enhanced production of the corresponding plant terpenoids.

A major problem in agricultural crop production is the large number of plant-damaging animals such as insects, mites, and nematodes or pathogens including viruses, bacteria, and fungi, some of which lead to high economic losses of around 60% globally [53]. One of the most widely distributed and destructive pathogens of plants causing white mold disease in more than 400 host plants all over the world is the fungus *Sclerotinia sclerotiorum* (Lib.) de Bary [54]. Another devastating example of fungal diseases is the plant vascular wilt

caused by the *Fusarium* species [55]. Other fungal pathogens such as *Phoma lingam* [56,57], *Alternaria brassicicola* [58], and *Rhizoctonia solani* [59,60] also cause major yield reduction in important crops. To control these pathogens and due to the rapidly growing world population and the resulting increase of food consumption, farmers are using synthetic and biological substances as fertilizers, pesticides, or growth regulators side by side with the cultivation of resistant or tolerant plant varieties [61–64]. Each of these methods has its limitations, but so far, the use of pesticides is the most convenient and commonly used method. Nevertheless, these can have numerous severe side effects on the environment, including the soil [65]. The soil is inhabited by an enormous diversity of organisms that are important players in maintaining a functional ecosystem and that comprise microorganisms with beneficial properties for plant development and health. For that reason, effective and sustainable alternatives are needed. Firstly, plants, as a part of a complex ecosystem, can produce enormous amounts of secondary metabolites for their survival and maintenance. Phenolics and terpenes are examples of metabolites that are produced by plants and act as antimicrobial agents and feeding deterrents [66–72]. The presence of a wide range of terpenes encouraged their use as nature-inspired plant protection agents in agriculture or their use for drug development. One of the commonly stress-associated terpenes is the sesquiterpene β-caryophyllene [73–75]. As mentioned in the previous section, various studies showed that β-caryophyllene exhibits diverse biological activities against many organisms. From a plant protection perspective β-caryophyllene was reported to promote plant growth, to induce plant defense genes, to attract entomopathogenic nematodes, and to be active against certain plant pathogenic bacteria and fungi [76–80].

In this study, we therefore aimed to use the modular co-expression of DXP/MVA genes in combination with the strictly controlled P_{nif} promoter to reconstitute the pathway of the plant sesquiterpene β-caryophyllene in *R. capsulatus* and to optimize the production under phototrophic growth conditions. For heterologous sesquiterpene production, the β-caryophyllene synthase QHS1 from *Artemisia annua* was used. Since this terpene offers a variety of beneficial bioactivities, we further evaluated the potential use of β-caryophyllene and its oxygenated derivative β-caryophyllene oxide as nature-derived fungicides. To this end, the bioactivity of β-caryophyllene/oxide against both representative plant growth-promoting bacteria and phytopathogenic fungi was investigated.

2. Materials and Methods

2.1. Bacterial Strains and Cultivation Conditions

The *Escherichia coli* strain DH5α and strain S17-1 were used for cloning and conjugation of plasmid DNA [81,82]. *E. coli* cells were cultivated at 37 °C using LB agar plates or liquid medium (Luria/Miller, Carl Roth®, Karlsruhe, Germany), containing kanamycin (25 μg mL^{-1}) when appropriate. *R. capsulatus* SB1003 [83] and SB1003-MVA [39], encompassing the chromosomally located genes *mvaA*, *idi*, *hsc*, *mvk*, *pmk* and *mvd* (also designated as MVA gene cluster) from *Paracoccus zeaxanthinifaciens*, were used for plant terpene production. All *R. capsulatus* strains used in this study were either cultivated on PY agar plates [84] containing 2% (*w*/*v*) Select Agar (Thermo Fisher Scientific, Waltham, MA, USA) or in RCV liquid medium [85] at 30 °C. Both media were supplemented with rifampicin (25 μg mL^{-1}). For cultivation of the recombinant *Rhodobacter* strain SB1003-MVA, gentamicin (4 μg mL^{-1}) was further added to the medium. If not stated otherwise, photoheterotrophic cultivation was conducted under anaerobic conditions and permanent illumination with bulb light (2500 lx), as described previously [39]. All bacterial strains and plasmids used in this study are listed in Table S1 (Supplementary Materials). All strains for bioactivity and minimum inhibitory concentration (MIC) evaluation are listed in the respective results section.

2.2. Construction of Expression Vectors

The expression vectors used in this study are based on the pRhon5Hi-2 vector carrying the promoter of the *nifH* gene for heterologous gene expression [39]. The sequence of β-caryophyllene synthase QHS1 from *A. annua* (UniProt: Q8SA63) was used to generate

an appropriate synthetic gene whose DNA sequence is suitable for the codon-usage of *R. capsulatus*. For DNA sequence adaptation, the Codon Optimization Tool by IDT Integrated DNA Technologies and the Graphical Codon Usage Analyzer tool were used [86]. The 1.7-kb *QHS1* gene was obtained from Eurofins Genomics. The synthetic DNA fragment was flanked by appropriate restriction endonuclease recognition sequences (*Xba*I/*Hin*dIII). The final sequence of the synthetic DNA fragment is shown in the Supplementary Materials. For the construction, the *Xba*I/*Hin*dIII hydrolyzed *QHS1* fragment was inserted into likewise hydrolyzed pRhon5Hi-2 as well as a variant, providing the additional isoprenoid biosynthetic gene *ispA*. Thereby, the expression vectors pRhon5Hi-2-QHS1 and pRhon5Hi-2-QHS1-ispA were constructed, carrying the terpene synthase gene immediately downstream of the P_{nif} promoter of the vector. Correct nucleotide sequences of all constructs were confirmed by Sanger sequencing (Eurofins Genomics, Ebersberg, Germany). The *QHS1* expression vectors are summarized in Table S1 (Supplementary Materials).

2.3. Cultivation of R. capsulatus for Heterologous Terpene Production

For the expression of the heterologous terpene biosynthetic genes, respective pRhon5Hi-2-based plasmids were transferred to cells of different *R. capsulatus* strains via conjugational transfer employing *E. coli* S17-1 as donor [84]. Thereafter, transconjugants were selected and further cultivated on PY agar containing kanamycin (25 μg mL^{-1}) and rifampicin (25 μg mL^{-1}). Subsequently, *Rhodobacter* cells were cultivated in airtight 4.5 mL screw neck vials (Macherey-Nagel, Düren, Germany) or airtight 15 mL hungate tubes [87] in liquid RCV medium containing kanamycin (25 μg mL^{-1}) and rifampicin (25 μg mL^{-1}). Precultures were cultivated in 15 mL RCV medium containing 0.1% $(NH_4)_2SO_4$ inoculated with cells from a freshly grown PY agar plate and incubated for 48 h at 30 °C and with bulb light illumination. Expression cultures were inoculated from precultures to an optical density at 660 nm of 0.05 in 4.5 mL or 15 mL RCV medium containing 0.1% serine as an exclusive nitrogen source. Subsequently, cells were incubated at 30 °C under permanent illumination with bulb light (3.6 mW cm^{-2} at 850 nm) or IR light (5.6 mW cm^{-2} at 850 nm) for 3–5 days. For microaerobic expression cultures, cells were cultivated in 20–60 mL RCV medium containing 0.1% serine in 100 mL flasks at 30 °C and 130 rpm in the dark. The absence of ammonium and the cultivation under oxygen-limited conditions led to the induction of the P_{nif}-dependent target gene expression. For the extraction of the produced sesquiterpenes, the cultures were overlaid with 150 μL or 500 μL *n*-dodecane, respectively, during inoculation [88].

2.4. Extraction, GC Analysis and Quantification of Sesquiterpenes

Basically, analysis of produced sesquiterpenes was conducted as described in Troost et al., 2019 [39]. In the following, the procedure is briefly described. To facilitate terpene extraction into the organic phase (*n*-dodecane) after cultivation, screw neck vials or hungate tubes were incubated in a horizontal position under permanent shaking (130 rpm, 30 °C, 24 h, in the dark) using a Multitron Standard incubation shaker (Infors HT). The *n*-dodecane samples were analyzed by gas chromatography (GC) using the Agilent *6890N* gas chromatograph equipped with a (5%-phenyl)-methylpolysiloxane *HP-5* column (length, 30 m; inside diameter, 0.32 mm; film thickness, 0.25 μm; Agilent Technologies) and a flame ionization detector (FID). The temperatures of the injector and FID were set to 240 and 300 °C, respectively. The GC was loaded with a 4-μL sample of each *n*-dodecane layer using a split ratio of 100:1 with helium as carrier gas. The following column temperatures were used during analysis: (i) 100 °C for 5 min, (ii) increased of temperature with a heating rate of 10 °C per min up to 180 °C, (iii) increased of temperature with a heating rate of 20 °C per min up to 300 °C. The signal of β-caryophyllene produced in *R. capsulatus* was verified by comparison of its retention times to a corresponding reference (β-caryophyllene from Sigma Aldrich, product number: 22075, retention time: 10.13 min). In order to determine the final product titers, the transfer efficiency from producing cells into the *n*-dodecane phase was determined as described in Supplementary Method section "Analysis of *n*-dodecane-

mediated β-caryophyllene extraction from phototrophically grown *R. capsulatus*". In brief, accumulated terpenes were extracted from cell lysates using *n*-dodecane. Subsequently, products were quantified using calibration curves of the reference compound, taking into account the specific transfer efficiencies of β-caryophyllene.

2.5. Effect of β-Caryophyllene and β-Caryophyllene Oxide on Plant Pathogenic Fungi

Isolates of the plant pathogenic fungi *P. lingam*, *S. sclerotiorum* and *A. brassicicola* were obtained from the Leibniz-Institut DSMZ (Deutsche Sammlung von Mikroorganismen und Zellkulturen GmbH, Braunschweig, Germany), while isolates of *F. oxysporum*, *R. solani* were obtained from the INRES, Plant Diseases and Plant Protection, University of Bonn. All isolates were sub-cultured on potato dextrose agar (PDA) at 24 °C and were used in this study to evaluate the bioactivity of the compounds on hyphal growth.

To test the bioactivities of β-caryophyllene and β-caryophyllene oxide, compounds were dissolved in a mixture of DMSO and Tween 20 (ratio of 1:2) to prepare differently concentrated stock solutions. These were mixed with PDA to gain the final concentrations 62.5, 125, and 250 μg mL^{-1} and to prepare PDA agar plates with terpenoids. The final DMSO and Tween 20 concentrations were always 1% (v/v) and 0.5% (v/v), respectively. Fungal discs with a diameter of 0.5 cm were cut from the culture media of freshly grown agar plates without terpenoids and placed upside down in the middle of PDA plates containing the chemicals. PDA plates with 0.5% (v/v) DMSO and 1% (v/v) Tween 20 alone were used as control. All plates were incubated for 7 days at 24 °C. Subsequently, the diameter of the fungal colony was measured, and the percentage of growth inhibition compared to the solvent control was calculated. Differences between the treatments were statistically analyzed using SigmaPlot software by one-way analysis of variance (ANOVA) and multiple comparisons for significance were performed at ($p < 0.05$) using the Holm-Sidak method.

2.6. Determination of the Minimum Inhibitory Concentration (MIC) of β-Caryophyllene and β-Caryophyllene Oxide in Liquid Cultures of Bacteria

The minimum inhibitory concentration of β-caryophyllene and β-caryophyllene was determined according to reference [89]. For the precultures, 10 mL Müller Hinton (MH) medium (Merck, Germany) was first inoculated in 100 mL flasks with four single bacterial colonies. For *R. capsulatus*, RCV was used. The liquid cultures were incubated for 18 h at 130 rpm and 37 °C (*R. capsulatus* at 30 °C). For the main cultures, MH or RCV medium was supplemented with differently concentrated stock solutions of β-caryophyllene and β-caryophyllene oxide in a mixture of DMSO and Tween 20 (ratio 1:2) to gain final concentrations of 62.5, 125, and 250 μg mL^{-1}. All bacterial cultures were adjusted to a cell density corresponding to an optical density at 625 nm of 0.1 and then diluted 50-fold with medium for *B. subtilis*, *P. putida*, *P. fluorescens*, *R. rhizogenes* and *P. polymyxa* and 2-fold for *R. capsulatus*. For the inoculation of 96-well microtiter plates (Greiner Bio-One GmbH, Frickenhausen, Germany), 50 μL MH medium with the corresponding concentration of the substance to be tested and the solvent controls were mixed with 50 μL of previously diluted bacterial culture, resulting in an end optical density at 625 nm of 0.001 and 0.025, respectively. The solvent control contained 1% (v/v) Tween 20 and 0.5% (v/v) DMSO. After inoculation, the microtiter plates (MTPs) were first shaken in a SpectraMax i3x (Molecular Devices, San Jose, CA, USA) plate photometer for 20 s to mix the solution and then incubated for 20 h at 37 °C. *R. capsulatus* was incubated at 30 °C and 300 rpm. For subsequent determination of the MICs, the optical density of cell cultures was determined at 625 nm in a plate photometer. The MIC was defined based on the European Committee on Antimicrobial Susceptibility Testing (EUCAST) guidelines as the compound concentration at which an optical density at 625 nm minus the background absorbance equals 0 [90].

3. Results

In the past, terpenoids were exclusively obtained from natural plant sources, e.g., by extracting them from essential oils, requiring a complex and time-consuming downstream

processing. The heterologous production of sesquiterpenes in a suitable microbial host, however, bears many benefits. For example, it offers the possibility to solely produce a desired compound so that it can be rather easily purified without the need of removing closely related constituents [21,34]. Thus, we here aimed to reconstitute the plant sesquiterpene pathway of β-caryophyllene in *R. capsulatus* and optimize the production under phototrophic growth conditions. Since many sesquiterpenoids exhibit promising antimicrobial activities, the antifungal efficacy of β-caryophyllene and its oxidized form against phytopathogenic fungi were evaluated.

3.1. Establishment of β-Caryophyllene Production in R. capsulatus via Overexpression of Isoprenoid Precursor Genes

Recently, we described the heterologous synthesis of the plant sesquiterpenoids valencene and patchoulol in the phototrophic bacterium *R. capsulatus* and its modular improvement by engineering the biosynthesis of the central precursor FPP [39]. To evaluate if *R. capsulatus* and the modular engineering principle can analogously be applied for the synthesis of the plant-derived sesquiterpene β-caryophyllene, we expressed the gene encoding β-caryophyllene synthase QHS1 from *A. annua* in the bacterial host. To this end, the expression vectors pRhon5Hi-2-QHS1 and pRhon5Hi-2-QHS1-ispA, carrying an additional copy of the intrinsic FPP synthase gene *ispA*, were transferred to the *R. capsulatus* wild type strain SB1003 and strain SB1003-MVA. The latter strain additionally contains the chromosomally integrated MVA pathway genes derived from *Paracoccus zeaxanthinifaciens* and thus offers a second isoprenoid biosynthesis pathway. To compare the β-caryophyllene production in all *Rhodobacter* strains grown under phototrophic conditions, cells were incubated in the absence of molecular oxygen and ammonium under constant bulb light illumination. Terpene accumulation was determined in the late stationary growth phase by analyzing *n*-dodecane samples via GC-FID measurements. The increase of β-caryophyllene production in tested *R. capsulatus* strains is shown in Figure 1 as relative values using *R. capsulatus* SB1003 solely carrying the plasmid-encoded *QHS1* gene as reference strain.

As shown in Figure 1, the expression of the β-caryophyllene synthase gene *QHS1* in *R. capsulatus* strain SB1003 led to a measurable production of β-caryophyllene. Remarkably, the co-expression of *QHS1* and *ispA* in the *R. capsulatus* strain SB1003 as well as *QHS1* expression in the engineered SB1003-MVA strain did not result in increased β-caryophyllene synthesis. However, concerted expression of *QHS1* and *ispA* in *R. capsulatus* SB1003-MVA led to a considerable increase of sesquiterpenoid production of about 300% in comparison to the reference strain.

3.2. Optimization of β-Caryophyllene Production in R. capsulatus via Modification of Cultivation Conditions

In the above-described experiments, we could demonstrate that modular engineering of the isoprenoid biosynthesis can also be applied to improve β-caryophyllene production in *R. capsulatus*. Next, we analyzed whether the modification of cultivation conditions including a prolonged cultivation time or the change of illumination parameters can further improve the product yield in the better-performing strain SB1003-MVA. First, β-caryophyllene accumulation was comparatively analyzed over five days in photoheterotrophically-grown cultures of *R. capsulatus* strain SB1003-MVA carrying pRhon5Hi-2-QHS1 or pRhon5Hi-2-QHS1-ispA. Product formation was determined by analyzing the overlaid *n*-dodecane samples via GC-FID measurements (Figure 2, blue bars).

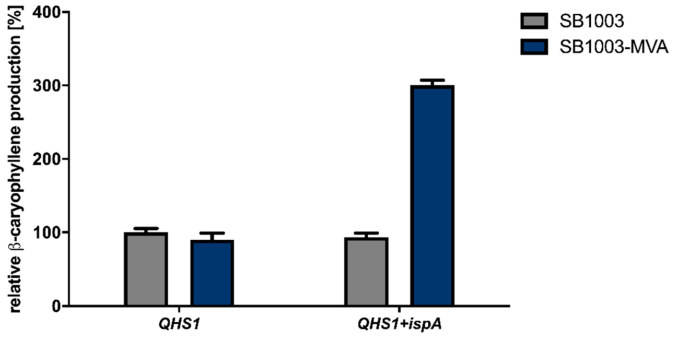

Figure 1. Heterologous β-caryophyllene production in the *R. capsulatus* strains SB1003 and SB1003-MVA. The β-caryophyllene synthase gene *QHS1* from *A. annua* was expressed in *R. capsulatus* SB1003 wild type (grey bars) and SB1003-MVA (blue bars), which additionally carries the MVA gene cluster from *P. zeaxanthinifaciens* to enable a second isoprenoid biosynthesis route. Moreover, the *ispA* gene encoding the *R. capsulatus* FPP synthase was co-expressed on the same plasmid to further enhance sesquiterpene production titers. Product formation was determined in cell cultures after three days of photoheterotrophic cultivation (gas-tight hungate tubes, 30 °C) under ammonium depletion and constant illumination with bulb light (3.6 mW cm^{-2} at 850 nm). The produced β-caryophyllene was sampled in overlaid *n*-dodecane phases for GC-FID analysis. The increase of β-caryophyllene production in engineered *R. capsulatus* strains is shown as relative values. To this end, the *R. capsulatus* SB1003 carrying the plasmid-encoded *QHS1* gene was used as a reference strain. Values are means of three independent biological replicates (n = 3) and error bars indicate the respective standard deviations.

The highest product levels could be detected after three days of cultivation, where cells have typically reached the beginning of the stationary growth phase. The elongation of the cultivation time did not show increased product accumulation so that all further production experiments were carried out for three days. Under standard phototrophic conditions, conventional light bulbs are used for the illumination of *R. capsulatus* cells [39,49]. This conventional light source offers a broad emission spectrum with a relatively high proportion in the infrared (IR) light range (>750 nm; 3.6 mW cm^{-2} at 850 nm) suitable for excitation of bacteriochlorophyll *a* (BChl *a*) exhibiting excitation maxima at 800 and 860 nm (Figure S6, Supplementary Materials, Reference [91]). To improve the illumination conditions for sesquiterpene production under phototrophic conditions, we subsequently analyzed if the use of (i) alternative cultivation vessels offering a better light penetration of cell cultures by a more favorable surface-area-to-volume ratio (Table S2, Supplementary Materials) or (ii) a customized IR-LED array (5.6 mW cm^{-2} at 850 nm) suitable for specific excitation of the photopigment BChl *a* with high light intensities can help to increase product formation.

To investigate the influence of illumination conditions on the heterologous production of β-caryophyllene, the strain SB1003-MVA carrying the expression vector pRhon5Hi-2-QHS1-ispA was cultivated over three days under photoheterotrophic conditions and constant illumination with bulb light or IR light in an ammonium-depleted medium in screw neck vials. As shown in Figure 2, the change of cultivation vessel geometry resulted only in a slight increase of β-caryophyllene production of *R. capsulatus* SB1003-MVA (pRhon5Hi-2-QHS1-ispA), whereas high irradiation with IR light led to a 1.9-fold increase of the final product accumulation. These results indicate that the applied illumination conditions should be taken into account to reach high product yields when *R. capsulatus* is used as an alternative terpene production host. This assumption is further supported by the observation that product levels were much lower in *R. capsulatus* SB1003-MVA (pRhon5Hi-2-QHS1-ispA) cultures that have been grown under non-phototrophic, i.e., microaerobic conditions (Figure 2, green bars). For non-phototrophic cultivation, *R. capsulatus* SB1003-MVA (pRhon5Hi-2-QHS1-ispA) was grown in 100 mL, unbaffled shake flasks containing different volumes of medium in the dark to implement different aeration conditions

(green bars). Those conditions could lead to the formation of β-caryophyllene oxide, the oxygenated derivative of β-caryophyllene. As previously described, a filling volume of 60 mL is most suitable for the induction of intrinsic terpene formation and P_{nif}-mediated target gene expression in *R. capsulatus* [39], which is corroborated by the observed β-caryophyllene production levels. Nevertheless, only a quarter of the product yield could be achieved under microaerobic, non-phototrophic growth conditions when compared to the corresponding values of phototrophically grown cells (*R. capsulatus* SB1003-MVA, pRhon5Hi-2-QHS1-ispA, 3 days, bulb light), and only traces of the oxygenated derivative were detectable (data not shown). However, to fully understand the effects of varying cultivation conditions on β-caryophyllene production, further experiments have to be performed in future studies.

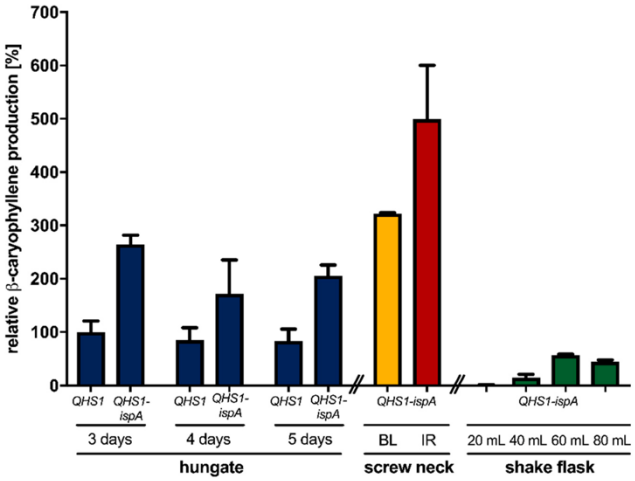

Figure 2. Heterologous β-caryophyllene production in the *R. capsulatus* strain SB1003-MVA with dependence on the cultivation time and illumination conditions. The β-caryophyllene accumulation was determined in *R. capsulatus QHS1* expression strains SB1003-MVA (pRhon5Hi-2-QHS1) and SB1003-MVA (pRhon5Hi-2-QHS1-ispA). First, product formation was determined in cell cultures after three, four, and five days of photoheterotrophic cultivation in 15 mL hungate tubes using standard illumination conditions (bulb lights, 3.6 mW cm^{-2} at 850 nm) and RCV medium supplemented with 0.1% serine. Blue bars represent the results of this experiment. Second, illumination conditions were changed by cultivating *R. capsulatus* strain SB1003-MVA (pRhon5Hi-2-QHS1-ispA) for three days under photoheterotrophic conditions using either constant illumination with bulb lights (BL; 3.6 mW cm^{-2} at 850 nm, yellow bar) or IR-emitting diodes (IR; 5.6 mW cm^{-2} at 850 nm, red bar). Here, 4.5-mL screw neck vials were used to improve light penetration due to a more favorable surface-area-to-volume ratio of this cultivation vessel. For non-phototrophic cultivation, the same strain was grown in 100-mL, unbaffled shake flasks containing different volumes of serine-supplemented RCV medium (shake flask, green bars). In all cultures, the produced β-caryophyllene was sampled in overlaid *n*-dodecane phases for GC-FID analysis. The increase of β-caryophyllene production is shown as relative values using *R. capsulatus* SB1003-MVA carrying the QHS1 expression plasmid pRhon5Hi-2-QHS1 as a reference strain. Values are the means of three independent biological replicates ($n = 3$) and the error bars indicate the respective standard deviations.

To accurately determine the final product titers, we analyzed (i) the individual transfer efficiency of β-caryophyllene from intact cells into the *n*-dodecane phase, (ii) the effect of the ICM, which is formed by *R. capsulatus* cells under phototrophic conditions, on sesquiterpenoid extraction, (iii) the differences in terpene transfer efficiencies when comparing single and repeated *n*-dodecane extraction, and finally (iv) the effect of the presence and absence

of organic solvent on the final product titers (Supplementary Method section "Analysis of *n*-dodecane-mediated β-caryophyllene extraction from phototrophically grown *R. capsulatus*"). Finally, we were able to determine a product titer of 90 ± 19 mg L^{-1} β-caryophyllene for *R. capsulatus* SB1003-MVA with pRhon5Hi-2-QHS1-ispA after 3 days of cultivation in hungate tubes under bulb light. This titer could be further increased by using IR light and screw neck vials for cultivation, reaching a final product titer of 139 ± 31 mg L^{-1}. Based on these values and the reached cell densities, the respective productivities were further calculated (Table S3, Supplementary Materials).

In summary, we showed that *R. capsulatus* can efficiently synthesize the sesquiterpene β-caryophyllene. Furthermore, the modular adaptation of precursor gene expression under phototrophic growth conditions as well as the adjustment of cultivation conditions resulted in an increased sesquiterpenoid formation.

3.3. Evaluation of Bioactivities of β-Caryophyllene and β-Caryophyllene Oxide against Different Phytopathogenic Organisms

The agricultural industry is affected by a dwindling number of effective antimicrobial substances. On the other hand, farmers have to control plant pathogenic organisms without damaging non-target organisms. As β-caryophyllene and β-caryophyllene oxide offer a variety of beneficial bioactivities [70,79,92–95], we evaluated the potential use of those two sesquiterpenes as a nature-derived fungicide. To this end, we analyzed the activity against different phytopathogenic fungi, as well as various plant growth-promoting bacteria (PGPB).

3.3.1. Bioactivities of β-Caryophyllene and β-Caryophyllene Oxide against Phytopathogenic Fungi

We investigated the bioactivity of β-caryophyllene and β-caryophyllene oxide, which can be formed spontaneously by uncatalyzed processes [96,97], against the plant pathogenic fungi *S. sclerotiorum*, *F. oxysporum*, *A. brassicicola*, *P. lingam*, and *R. solani*. This analysis would additionally reveal whether the compound's oxygenation influences potential antifungal properties. Therefore, PDA agar plates were supplemented with increasing concentrations of both compounds, fungal discs were transferred onto these plates and fungal growth was determined. Evaluation revealed that the degree of growth inhibition due to direct terpene exposure varied depending on the compound and the fungus (Figure 3).

Both compounds inhibited the hyphal growth of *S. sclerotiorum* when compared to the solvent control. The inhibition reached up to 30% when the fungus was exposed to β-caryophyllene, while it was up to 40% when the fungus was cultivated on medium containing β-caryophyllene oxide. The effect against *F. oxysporum* was less pronounced. Around 20% inhibition was observed when the fungus was cultivated on the β-caryophyllene-supplemented medium, while it was around 30% in the case of β-caryophyllene oxide. Finally, the presence of β-caryophyllene in the growth medium slightly inhibited the growth of *A. brassicicola* while inhibition was higher and reached a maximum of 10% when β-caryophyllene oxide was used. No significant effect of both compounds was observed against *P. lingam* and *R. solani* (Figure S7, Supplementary Materials). Our results thus reveal that β-caryophyllene and its oxidized form possess antifungal activity against certain phytopathogenic fungi and that β-caryophyllene oxide tends to be more effective in inhibiting fungal growth.

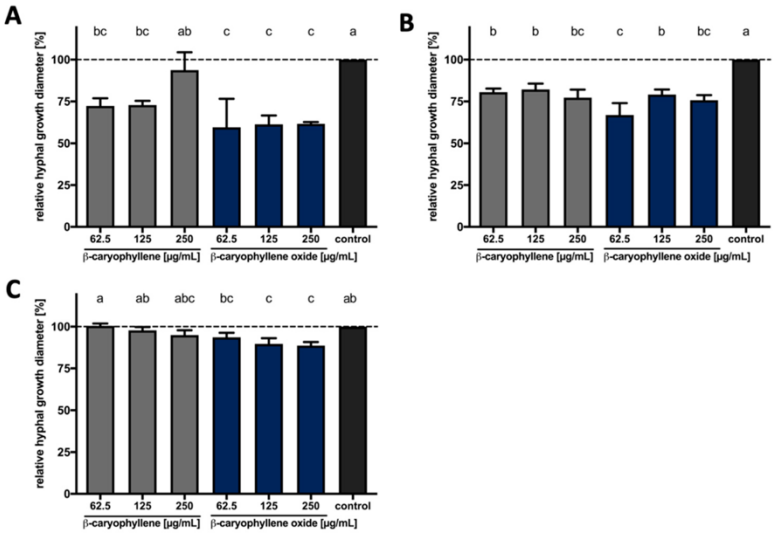

Figure 3. The effect of β-caryophyllene and β-caryophyllene oxide on the hyphal growth of plant pathogenic fungi. The effect of β-caryophyllene and β-caryophyllene oxide against *S. sclerotiorum* (**A**), *F. oxysporum* (**B**) and *A. brassicicola* (**C**). Final concentrations of 62.5 µg mL^{-1}, 125 µg mL^{-1}, and 250 µg mL^{-1} of β-caryophyllene (grey bars) and β-caryophyllene oxide (blue bars) in PDA growth medium were used. Medium mixed with the solvents DMSO and Tween 20 (final concentrations, 0.5% and 1% *v*/*v*, respectively) was used as the control (black bars). An equally sized disk with fungal mycelium was placed in the center of each plate and incubated for seven days at 24 °C. Subsequently, the diameter of each fungal colony was measured, and the relative growth compared to the solvent control was calculated. Each bar represents the mean ± standard deviation of three independent biological measurements with three technical replicates each ($n = 9$). Different letters on the top of the bars indicate significant differences between the treatments based on ANOVA and Holm-Sidak post-hoc method ($p < 0.05$), while the same letters represent no significant differences.

3.3.2. Antimicrobial Activities against Plant Growth-Promoting Bacteria

As the previous investigations showed antifungal properties against several phytopathogenic fungi, the use of the sesquiterpenoids as natural compound-based plant protection products could be considered. To investigate potential toxic off-target effects on bacteria that promote plant growth, we next examined whether the addition of β-caryophyllene/oxide affects the growth of bacteria at concentrations used in the hyphal growth assay. For this purpose, the growth of representatives of the plant growth-promoting bacteria (PGPB) group [98–100], including the two diazotrophic bacteria *Rhizobium rhizogenes* and *Rhodobacter capsulatus* [101,102], the two bacilli *Bacillus subtilis* [103,104] and *Paenibacillus polymyxa* [105], as well as the pseudomonads *Pseudomonas fluorescens* [104] and *Pseudomonas putida* [106] was analyzed in presence of β-caryophyllene and β-caryophyllene oxide. Both compounds were added to diluted bacterial cultures in increasing concentrations. After overnight incubation, the MICs were determined according to the respective optical density of the cell cultures (Figure 4).

The bacteria *R. rhizogenes*, *R. capsulatus*, *B. subtilis*, and *P. polymyxa* did not show reduced cell growth in comparison to the solvent control upon the addition of the two terpenes β-caryophyllene and β-caryophyllene oxide (Figure 4A–D). These bacteria showed an increase in growth, which could be explained by the metabolization of the terpenes. For *P. putida*, no effect of β-caryophyllene oxide was detected compared to the solvent control (Figure 4F). β-caryophyllene showed an influence on *P. putida*, which was concentration independent since all tested concentrations led to comparable cell growth. The cell densi-

ties were about 40% lower compared to the solvent control. This effect was also observed for *P. fluorescens*, where the two terpenes reduced growth by up to 40% (Figure 4E).

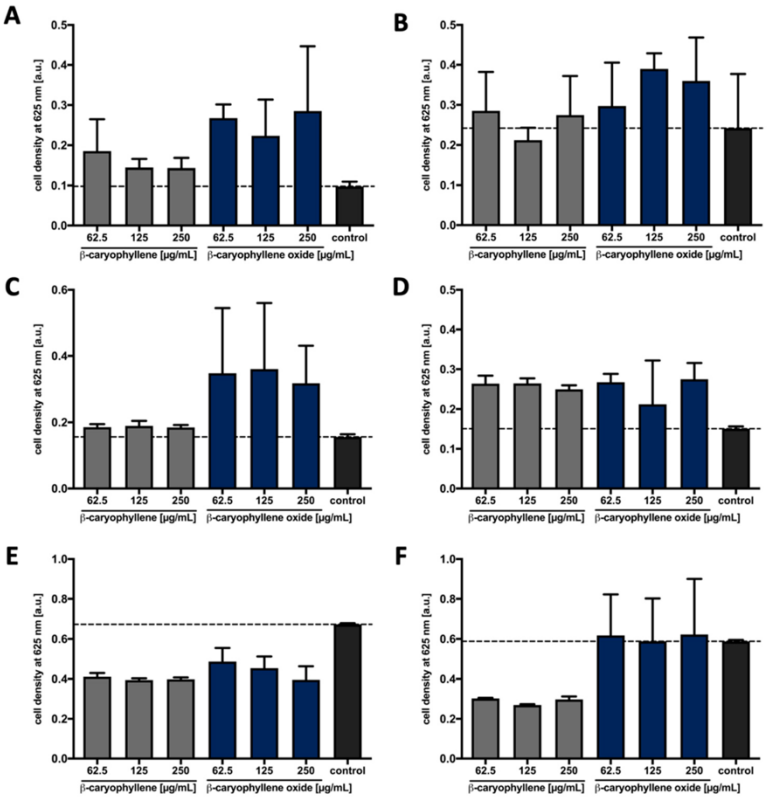

Figure 4. The influence of β-caryophyllene and β-caryophyllene oxide on the growth of plant growth-promoting bacteria. Final concentrations of 62.5 µg mL^{-1}, 125 µg mL^{-1} and 250 µg mL^{-1} of β-caryophyllene (grey bars) and β-caryophyllene oxide (blue bars) were added to cultures of *R. rhizogenes* (**A**), *R. capsulatus* (**B**), *B. subtilis* (**C**), *P. polymyxa* (**D**), *P. fluorescens* (**E**) and *P. putida* (**F**) in 100 µL MH medium (*R. capsulatus* in RCV medium) in MTPs. The final solvent concentration was 1% (*v*/*v*) Tween 20 and 0.5% (*v*/*v*) DMSO. To determine the influence of the terpenes on the growth of the bacteria, the cells were incubated stationary for 20 h at 37 °C (*R. capsulatus* at 30 °C) and the cell density was measured at 625 nm using a plate photometer. The solvent control (control, black bars) was MH or RCV medium containing 1% (*v*/*v*) Tween 20 and 0.5% (*v*/*v*) DMSO. Values are means of three independent biological replicates (n = 3) and error bars indicate the respective standard deviations.

In summary, for β-caryophyllene and β-caryophyllene oxide, no MIC could be determined for any of the tested PGPB, but a reduction of cell growth could be observed for both Pseudomonads. As a diverse group of different representative soil bacteria was tested, the results nevertheless indicate that β-caryophyllene and β-caryophyllene oxide do not exhibit strong broad-spectrum antibacterial activities at concentrations which considerably inhibit the hyphal growth of *S. sclerotiorum* and *F. oxysporum* (63 µg mL^{-1}).

4. Discussion

The management of plant pathogens in the process of crop production is crucial, no matter whether organic, integrated, or conventional farming practices are applied.

For many decades, synthetic pesticides were considered the fastest and most effective pest and pathogen control method. Recently, due to the rise of public health concerns about pesticide toxicity and harm to the environment, many of these effective chemicals were banned, thereby markedly limiting the options for plant protection. Therefore, it is important to find environmentally safe and sustainable natural products to control pathogens and thus ensure yield and food quality. In this context, plant metabolites are a rich source of bioactive compounds explorable for the use of preventing and controlling plant pathogenic microbes. In the last decade, several studies investigated terpenoids as potential antiphytopathogenic compounds [67,71,76,77,107,108]. β-caryophyllene is a natural bicyclic sesquiterpene that is a constituent of many essential oils. Many studies showed that these essential oils, which are containing β-caryophyllene as one of the main ingredients, are active against plant pathogens [109–111]. For example, methanol extracts from *Artemisia annua* leaves, one of the common β-caryophyllene producers, strongly inhibit the growth of the plant pathogenic fungi *F. oxysporum* and *Fusarium solani* [79]. In another study, the essential oil from *Murraya paniculata* leaves showed inhibitory activities on the mycelial growth of *S. sclerotiorum*, a fungus that poses a high risk to several crops. The gas chromatography analysis of the essential oil composition introduced β-caryophyllene as one of the main constituents (23.8%) [109]. Furthermore, essential oils from *Piper aduncum*, which also has β-caryophyllene as one of its main constituents (7.2%), inhibited the mycelial growth of the fungus *S. sclerotiorum* [110]. As a second alternative or complementary means for plant protection, there is also a multitude of important and useful microorganisms that support plant growth, which are called plant growth-promoting bacteria and plant growth-promoting fungi (PGPF). To offset the negative effects of chemical substances or make their use superfluous, more and more PGPB are now being used in agriculture [112]. Microorganisms can fulfill different functions in this process. *Bacillus subtilis*, for example, accumulates at the root system during the germination of various plants and prevents competing harmful fungi from spreading [103]. Diazotrophic organisms can supply plants with biologically available nitrogen by fixing atmospheric dinitrogen, thus making it available to the plants [113]. When fighting phytopathogens, it is important to consider and ideally avoid negative off-target effects on the above-mentioned beneficial microorganisms. Corresponding tests are therefore now frequently included in the first evaluation of antimicrobial activities.

So far, no studies were investigating the effect of pure β-caryophyllene and β-caryophyllene oxide against a selection of phytopathogenic fungi aiming to determine and compare the potential antifungal properties of the two compounds and species-specific differences in sensitivity. In our current study, we show the potential of sustainable production of β-caryophyllene in the heterologous host *Rhodobacter capsulatus* and the species-specific promoting or inhibitory effects for selected plant growth-promoting bacteria for both of the tested sesquiterpenoids at appropriate compound concentrations. Furthermore, we tested the bioactivities of both β-caryophyllene and β-caryophyllene oxide against several plant pathogenic fungi and showed that both substances were active against certain fungi. Interestingly, the oxidized form tended to be even more effective, and additionally has a more beneficial activity profile concerning the PGPB. These results are supported by previous reports which are introducing β-caryophyllene as a bioactive compound in its purified form [79] and as a component of several essential oils [109,110]. The purified β-caryophyllene showed a MIC of 130 μg mL^{-1} for *F. oxysporum* [79], which is below the maximal concentration tested in this study. However, our plate-based approach is not completely comparable with the method used for MIC determination in liquid medium. According to our results, the inhibitory effect of the hyphal growth was different depending on the tested fungus. Such a difference is dependent on the fungal species and frequently described by previous studies showing that the novel fungicide 3-[5-(4-chlorophenyl)-2,3-dimethyl-3-isoxazolidinyl] pyridine (SYP-Z048) affected several pathogenic fungi in different ways [114]. Overall, our current results demonstrate that both β-caryophyllene and β-caryophyllene oxide exhibit bioactivity against plant pathogenic fungi and therefore

could be suitable as potential fungicides in agriculture as, in contrast to many broad-spectrum pesticides, they do not harm many species of plant growth-promoting bacteria. However, despite the sesquiterpenes being natural compounds, which are often associated with non-harmful ecotoxicological profiles, effects against *Pseudomonas* species were corroborated and will need to be taken into account. So far, there is only limited information about the individual activities of terpenes against plant pathogens and the underlying molecular mechanisms. To be able to explain the differences we observed in the activity of the two terpenes against the different organisms and to get more data on the activity spectrum, our investigations need to be extended by including more target and non-target organisms. In addition, the respective modes of action on the molecular level have to be determined. Besides additional plant pathogens, this not only includes analyzing further plant growth-promoting bacteria, but it must be tested if plant growth-promoting fungi react sensitively to the terpenes, as indicated by a previous promising study [80]. In particular, fungi of the genus *Trichoderma*, which are said to have many advantageous properties for plants, could be investigated more closely [115,116].

To be able to provide appropriate quantities of an active antifungal substance, the heterologous production of promising sesquiterpenes in a suitable microbial host bears various benefits, such as the possibility to solely produce the desired compound without complex downstream processing and in high amounts. Therefore, we established the biosynthesis of the plant sesquiterpene β-caryophyllene in the heterologous production host *R. capsulatus* under phototrophic and non-phototrophic conditions. For this purpose, the intrinsic isoprenoid biosynthesis pathway was optimized in terms of its precursor supply. In particular, the P_{nif}-based co-expression of *ispA* and the genetically integrated MVA pathway resulted in a substantial increase in sesquiterpenoid production of around 300%. These results are in agreement with previous studies, where engineering of isoprenoid precursor supply was a valuable tool to increase the terpenoid production in *Rhodobacter* [38,40,48] and other bacterial hosts [23,117–125]. Also, we were able to increase the terpene production level further by changing the cultivation conditions from bulb light in a 14 mL hungate tube to IR light in a 4.5 mL screw neck vial, achieving a final β-caryophyllene titer of 139.29 ± 31.35 mg L^{-1} and a specific productivity of 1.30 ± 0.32 mg g^{-1} dry cells h^{-1}. In recent studies, production titers around 220 mg L^{-1} [126] and specific productivities of 1.15 mg g^{-1} dry cells h^{-1} [127] were achieved in *E. coli*. Thus, we attained yields comparable to the current literature and successfully established *R. capsulatus* as a heterologous host for the production of β-caryophyllene. Furthermore, the β-caryophyllene yields achieved in *R. capsulatus* could be sufficient to use this host as a microbial system for in situ agent delivery. In the future, sesquiterpenoid producing *R. capsulatus* might thus be applicable as cell extracts with biocontrol activities for plant protection or as engineered antiphytopathogenic PGPB that can be added as live cultures to soils contained in vertical farming.

Supplementary Materials: The following are available online at https://www.mdpi.com/2076-2607/9/1/168/s1. Figure S1: Transfer efficiency of the β-caryophyllene reference compound from cultivation medium into the *n*-dodecane phase in the presence of intact *R. capsulatus* cells in hungate and screw neck vials, Figure S2: Transfer efficiency of the β-caryophyllene reference compound from cultivation medium into the *n*-dodecane phase in the presence of intact and disrupted *R. capsulatus* cells, Figure S3: Extraction efficiency of the β-caryophyllene reference compound from cultivation medium in the presence of disrupted and intact *R. capsulatus* cells by repeatedly using *n*-dodecane as organic solvent over four days, Figure S4: Comparison of relative β-caryophyllene formation in *R. capsulatus* production strains cultivated with and without an *n*-dodecane layer, Figure S5: Quantification of extracted β-caryophyllene via a calibration curve of β-caryophyllene reference signals in GC-FID analyses, Figure S6: Emission range of different light sources and the absorption spectrum of phototrophically cultivated *R. capsulatus* cells [128], Figure S7: Effect of β-caryophyllene and β-caryophyllene oxide on the hyphal growth of plant pathogenic fungi, Table S1: Bacterial strains and plasmids used in this study, Table S2: Cultivation vessel specifications, Table S3: Productivities of β-caryophyllene in *R. capsulatus* SB1003 cultures.

Author Contributions: Conceptualization, T.D., A.L., K.-E.J., A.S.S.S., F.M.W.G.; methodology, F.H., Y.S.A., J.H.-H., A.H., S.S.H.; validation, F.H., S.S.H.; formal analysis, S.S.H., F.H.; investigation, F.H., S.S.H., Y.S.A., S.N., O.K.; writing—original draft preparation, F.H., S.S.H.; writing—review and editing, T.D., A.S.S.S., A.L., K.-E.J., F.M.W.G.; visualization, F.H.; supervision, T.D., A.L., A.S.S.S.; project administration, A.L., T.D., A.S.S.S., K.-E.J., F.M.W.G.; funding acquisition, A.L., T.D., A.S.S.S., K.-E.J., F.M.W.G. All authors have read and agreed to the published version of the manuscript.

Funding: The work was supported by grants from the Bioeconomy Science Center, and the European Regional Development Fund (ERDF: 34.EFRE-0300096) within the project CLIB-Kompetenzzentrum Biotechnologie CKB). The scientific activities of the Bioeconomy Science Center were financially supported by the Ministry of Innovation, Science and Research of the German federal state of North Rhine-Westphalia MIWF within the framework of the NRW Strategieprojekt BioSC (No. 313/323-400-00213).

Institutional Review Board Statement: Not applicable.

Informed Consent Statement: Not applicable.

Data Availability Statement: The datasets generated and/or analyzed during the current study are available from the corresponding authors on reasonable request.

Acknowledgments: The authors would like to thank Olaf Cladders, Edwin Thiemann, Volker Neu, and Helmut Guenther from Vossloh-Schwabe Lighting Solutions GmbH & Co. KG (Kamp-Lintfort, Germany) for their time, efforts and tremendous expertise in the LED array development thereby making the "illumination project" possible.

Conflicts of Interest: The authors declare no conflict of interest. The funders had no role in the design of the study, in the collection, analyzes, or interpretation of data, in the writing of the manuscript, or in the decision to publish the results.

References

1. Bian, G.; Deng, Z.; Liu, T. Strategies for terpenoid overproduction and new terpenoid discovery. *Curr. Opin. Biotechnol.* **2017**, *48*, 234–241. [CrossRef] [PubMed]
2. Christianson, D.W. Structural and Chemical Biology of Terpenoid Cyclases. *Chem. Rev.* **2017**, *117*, 11570–11648. [CrossRef] [PubMed]
3. Pemberton, T.A.; Chen, M.; Harris, G.G.; Chou, W.K.W.; Duan, L.; Köksal, M.; Genshaft, A.S.; Cane, D.E.; Christianson, D.W. Exploring the Influence of Domain Architecture on the Catalytic Function of Diterpene Synthases. *Biochemistry* **2017**, *56*, 2010–2023. [CrossRef] [PubMed]
4. Wink, M. Modes of Action of Herbal Medicines and Plant Secondary Metabolites. *Medicines* **2015**, *2*, 251–286. [CrossRef]
5. Ruzicka, L. The isoprene rule and the biogenesis of terpenic compounds. *Experientia* **1953**, *9*, 357–367. [CrossRef]
6. Croteau, R.; Kutchan, T.M.; Lewis, N.G. Secondary Metabolites. *Biochem. Mol. Biol. Plants* **2000**, *7*, 1250–1318.
7. Boucher, Y.; Doolittle, W.F. The role of lateral gene transfer in the evolution of isoprenoid biosynthesis pathways. *Mol. Microbiol.* **2000**, *37*, 703–716. [CrossRef]
8. Frank, A.; Groll, M. The Methylerythritol Phosphate Pathway to Isoprenoids. *Chem. Rev.* **2017**, *117*, 5675–5703. [CrossRef]
9. Langenheim, J.H. Higher plant terpenoids: A phytocentric overview of their ecological roles. *J. Chem. Ecol.* **1994**, *20*, 1223–1280. [CrossRef]
10. Gershenzon, J.; Dudareva, N. The function of terpene natural products in the natural world. *Nat. Chem. Biol.* **2007**, *3*, 408–414. [CrossRef]
11. Pichersky, E.; Raguso, R.A. Why do plants produce so many terpenoid compounds? *New Phytol.* **2018**, *220*, 692–702. [CrossRef] [PubMed]
12. Efferth, T. From ancient herb to modern drug: *Artemisia annua* and artemisinin for cancer therapy. *Semin. Cancer Biol.* **2017**, *46*, 65–83. [CrossRef] [PubMed]
13. Mahizan, N.A.; Yang, S.-K.; Moo, C.-L.; Song, A.A.-L.; Chong, C.-M.; Chong, C.-W.; Abushelaibi, A.; Lim, S.-H.E.; Lai, K.-S. Terpene Derivatives as a Potential Agent against Antimicrobial Resistance (AMR) Pathogens. *Molecules* **2019**, *24*, 2631. [CrossRef] [PubMed]
14. Walencka, E.; Rozalska, S.; Wysokinska, H.; Rozalski, M.; Kuzma, L.; Rozalska, B. Salvipisone and aethiopinone from *Salvia sclarea* hairy roots modulate staphylococcal antibiotic resistance and express anti-biofilm activity. *Planta Med.* **2007**, *73*, 545–551. [CrossRef] [PubMed]
15. Jabra-Rizk, M.A.; Meiller, T.F.; James, C.E.; Shirtliff, M.E. Effect of farnesol on *Staphylococcus aureus* biofilm formation and antimicrobial susceptibility. *Antimicrob. Agents Chemother.* **2006**, *50*, 1463–1469. [CrossRef] [PubMed]
16. Gomes, F.I.A.; Teixeira, P.; Azeredo, J.; Oliveira, R. Effect of farnesol on planktonic and biofilm cells of *Staphylococcus epidermidis*. *Curr. Microbiol.* **2009**, *59*, 118–122. [CrossRef] [PubMed]

17. Castelo-Branco, D.S.C.M.; Riello, G.B.; Vasconcelos, D.C.; Guedes, G.M.M.; Serpa, R.; Bandeira, T.J.P.G.; Monteiro, A.J.; Cordeiro, R.A.; Rocha, M.F.G.; Sidrim, J.J.C.; et al. Farnesol increases the susceptibility of *Burkholderia pseudomallei* biofilm to antimicrobials used to treat melioidosis. *J. Appl. Microbiol.* **2016**, *120*, 600–606. [CrossRef]
18. Malingre, T.; Hendriks, H.; Batterman, S.; Bos, R.; Visser, J. The Essential Oil of *Cannabis sativa*. *Planta Med.* **1975**, *28*, 56–61. [CrossRef]
19. De Vasconcelos Silva, M.; Craveiro, A.; Abreu Matos, F.; Machado, M.I.; Alencar, J. Chemical variation during daytime of constituents of the essential oil of *Ocimum gratissimum* leaves. *Fitoterapia* **1999**, *70*, 32–34. [CrossRef]
20. Matias, E.F.F.; Alves, E.F.; Silva, M.K.N.; Carvalho, V.R.A.; Figueredo, F.G.; Ferreira, J.V.A.; Coutinho, H.D.M.; Silva, J.M.F.L.; Ribeiro-Filho, J.; Costa, J.G.M. Seasonal variation, chemical composition and biological activity of the essential oil of *Cordia verbenacea* DC (*Boraginaceae*) and the sabinene. *Ind. Crops Prod.* **2016**, *87*, 45–53. [CrossRef]
21. Marienhagen, J.; Bott, M. Metabolic engineering of microorganisms for the synthesis of plant natural products. *J. Biotechnol.* **2013**, *163*, 166–178. [CrossRef]
22. Kallscheuer, N.; Classen, T.; Drepper, T.; Marienhagen, J. Production of plant metabolites with applications in the food industry using engineered microorganisms. *Curr. Opin. Biotechnol.* **2019**, *56*, 7–17. [CrossRef]
23. Schempp, F.M.; Drummond, L.; Buchhaupt, M.; Schrader, J. Microbial Cell Factories for the Production of Terpenoid Flavor and Fragrance Compounds. *J. Agric. Food Chem.* **2018**, *66*, 2247–2258. [CrossRef] [PubMed]
24. Pham, J.V.; Yilma, M.A.; Feliz, A.; Majid, M.T.; Maffetone, N.; Walker, J.R.; Kim, E.; Cho, H.J.; Reynolds, J.M.; Song, M.C.; et al. A Review of the Microbial Production of Bioactive Natural Products and Biologics. *Front. Microbiol.* **2019**, *10*, 1–27.
25. Cravens, A.; Payne, J.; Smolke, C.D. Synthetic biology strategies for microbial biosynthesis of plant natural products. *Nat. Commun.* **2019**, *10*, 2142.
26. Sgobba, E.; Wendisch, V.F. Synthetic microbial consortia for small molecule production. *Curr. Opin. Biotechnol.* **2020**, *62*, 72–79. [CrossRef] [PubMed]
27. Kirby, J.; Keasling, J.D. Metabolic engineering of microorganisms for isoprenoid production. *Nat. Prod. Rep.* **2008**, *25*, 656–661. [PubMed]
28. Mitchell, W. Natural products from synthetic biology. *Curr. Opin. Chem. Biol.* **2011**, *15*, 505–515. [CrossRef] [PubMed]
29. Chen, Y.; Zhou, Y.J.; Siewers, V.; Nielsen, J. Enabling technologies to advance microbial isoprenoid production. *Adv. Biochem. Eng. Biotechnol.* **2015**, *148*, 143–160.
30. Wong, J.; Rios-Solis, L.; Keasling, J.D. Microbial Production of Isoprenoids. In *Consequences of Microbial Interactions with Hydrocarbons, Oils, and Lipids: Production of Fuels and Chemicals*; Lee, S.Y., Ed.; Springer International Publishing: Cham, Switzerland, 2016; pp. 1–24. ISBN 978-3-319-31421-1.
31. Helfrich, E.J.N.; Lin, G.-M.; Voigt, C.A.; Clardy, J. Bacterial terpene biosynthesis: Challenges and opportunities for pathway engineering. *Beilstein J. Org. Chem.* **2019**, *15*, 2889–2906.
32. Chemler, J.A.; Koffas, M.A.G. Metabolic engineering for plant natural product biosynthesis in microbes. *Curr. Opin. Biotechnol.* **2008**, *19*, 597–605. [CrossRef] [PubMed]
33. Paddon, C.J.; Westfall, P.J.; Pitera, D.J.; Benjamin, K.; Fisher, K.; McPhee, D.; Leavell, M.D.; Tai, A.; Main, A.; Eng, D.; et al. High-level semi-synthetic production of the potent antimalarial artemisinin. *Nature* **2013**, *496*, 528–532. [CrossRef] [PubMed]
34. Atanasov, A.G.; Waltenberger, B.; Pferschy-Wenzig, E.-M.M.; Linder, T.; Wawrosch, C.; Uhrin, P.; Temml, V.; Wang, L.; Schwaiger, S.; Heiss, E.H.; et al. Discovery and resupply of pharmacologically active plant-derived natural products: A review. *Biotechnol. Adv.* **2015**, *33*, 1582–1614. [CrossRef]
35. Zhang, C.; Hong, K. Production of Terpenoids by Synthetic Biology Approaches. *Front. Bioeng. Biotechnol.* **2020**, *8*, 347. [CrossRef] [PubMed]
36. Yu, Y.; Rasool, A.; Liu, H.; Lv, B.; Chang, P.; Song, H.; Wang, Y.; Li, C. Engineering *Saccharomyces cerevisiae* for high yield production of α-amyrin via synergistic remodeling of α-amyrin synthase and expanding the storage pool. *Metab. Eng.* **2020**, *62*, 72–83. [CrossRef]
37. Bauer, K.; Garbe, D.; Surburg, H. *Common Fragrance and Flavor Materials*; Wiley-VCH: Weinheim, Germany, 2001.
38. Beekwilder, J.; van Houwelingen, A.; Cankar, K.; van Dijk, A.D.J.; de Jong, R.M.; Stoopen, G.; Bouwmeester, H.; Achkar, J.; Sonke, T.; Bosch, D. Valencene synthase from the heartwood of Nootka cypress (*Callitropsis nootkatensis*) for biotechnological production of valencene. *Plant Biotechnol. J.* **2014**, *12*, 174–182. [CrossRef]
39. Troost, K.; Loeschcke, A.; Hilgers, F.; Özgür, A.Y.; Weber, T.M.; Santiago-Schübel, B.; Svensson, V.; Hage-Hülsmann, J.; Habash, S.S.; Grundler, F.M.W.; et al. Engineered *Rhodobacter capsulatus* as a Phototrophic Platform Organism for the Synthesis of Plant Sesquiterpenoids. *Front. Microbiol.* **2019**, *10*, 1998. [CrossRef]
40. Orsi, E.; Folch, P.L.; Monje-López, V.T.; Fernhout, B.M.; Turcato, A.; Kengen, S.W.M.; Eggink, G.; Weusthuis, R.A. Characterization of heterotrophic growth and sesquiterpene production by *Rhodobacter sphaeroides* on a defined medium. *J. Ind. Microbiol. Biotechnol.* **2019**, *46*, 1179–1190. [CrossRef]
41. Lin, P.-C.; Pakrasi, H.B. Engineering cyanobacteria for production of terpenoids. *Planta* **2019**, *249*, 145–154. [CrossRef]
42. Das, A.; Yoon, S.-H.; Lee, S.-H.; Kim, J.-Y.; Oh, D.-K.; Kim, S.-W. An update on microbial carotenoid production: Application of recent metabolic engineering tools. *Appl. Microbiol. Biotechnol.* **2007**, *77*, 505–512. [CrossRef]
43. Arendt, P.; Miettinen, K.; Pollier, J.; De Rycke, R.; Callewaert, N.; Goossens, A. An endoplasmic reticulum-engineered yeast platform for overproduction of triterpenoids. *Metab. Eng.* **2017**, *40*, 165–175. [CrossRef] [PubMed]

44. Tucker, J.D.; Siebert, C.A.; Escalante, M.; Adams, P.G.; Olsen, J.D.; Otto, C.; Stokes, D.L.; Hunter, C.N. Membrane invagination in *Rhodobacter sphaeroides* is initiated at curved regions of the cytoplasmic membrane, then forms both budded and fully detached spherical vesicles. *Mol. Microbiol.* **2010**, *76*, 833–847. [CrossRef] [PubMed]
45. Drews, G. The intracytoplasmic membranes of purple bacteria—Assembly of energy-transducing complexes. *J. Mol. Microbiol. Biotechnol.* **2013**, *23*, 35–47. [CrossRef] [PubMed]
46. Armstrong, G.A.; Alberti, M.; Leach, F.; Hearst, J.E. Nucleotide sequence, organization, and nature of the protein products of the carotenoid biosynthesis gene cluster of *Rhodobacter capsulatus*. *Mol. Gen. Genet. MGG* **1989**, *216*, 254–268. [CrossRef]
47. Armstrong, G.A. Genetics of eubacterial carotenoid biosynthesis: A colorful tale. *Annu. Rev. Microbiol.* **1997**, *51*, 629–659. [CrossRef]
48. Khan, N.E.; Nybo, S.E.; Chappell, J.; Curtis, W.R. Triterpene hydrocarbon production engineered into a metabolically versatile host—*Rhodobacter capsulatus*. *Biotechnol. Bioeng.* **2015**, *112*, 1523–1532. [CrossRef]
49. Loeschcke, A.; Dienst, D.; Wewer, V.; Hage-Hülsmann, J.; Dietsch, M.; Kranz-Finger, S.; Hüren, V.; Metzger, S.; Urlacher, V.B.; Gigolashvili, T.; et al. The photosynthetic bacteria *Rhodobacter capsulatus* and *Synechocystis* sp. PCC 6803 as new hosts for cyclic plant triterpene biosynthesis. *PLoS ONE* **2017**, *12*, e0189816. [CrossRef]
50. Orsi, E.; Beekwilder, J.; Peek, S.; Eggink, G.; Kengen, S.W.M.; Weusthuis, R.A. Metabolic flux ratio analysis by parallel 13C labeling of isoprenoid biosynthesis in *Rhodobacter sphaeroides*. *Metab. Eng.* **2020**, *57*, 228–238. [CrossRef]
51. Orsi, E.; Mougiakos, I.; Post, W.; Beekwilder, J.; Dompè, M.; Eggink, G.; Van Der Oost, J.; Kengen, S.W.M.; Weusthuis, R.A. Growth-uncoupled isoprenoid synthesis in *Rhodobacter sphaeroides*. *Biotechnol. Biofuels* **2020**, *13*. [CrossRef]
52. Orsi, E.; Beekwilder, J.; van Gelder, D.; van Houwelingen, A.; Eggink, G.; Kengen, S.W.M.; Weusthuis, R.A. Functional replacement of isoprenoid pathways in *Rhodobacter sphaeroides*. *Microb. Biotechnol.* **2020**, *13*, 1082–1093. [CrossRef]
53. Oerke, E.-C. Crop losses to pests. *J. Agric. Sci.* **2006**, *144*, 31–43. [CrossRef]
54. Bolton, M.D.; Thomma, B.P.H.J.; Nelson, B.D. *Sclerotinia sclerotiorum* (Lib.) de Bary: Biology and molecular traits of a cosmopolitan pathogen. *Mol. Plant Pathol.* **2006**, *7*, 1–16. [CrossRef] [PubMed]
55. Okungbowa, F.I.; Shittu, H.O. *Fusarium* wilts: An overview. *Environ. Res. J.* **2012**, *6*, 83–102.
56. West, J.S.; Kharbanda, P.D.; Barbetti, M.J.; Fitt, B.D.L. Epidemiology and management of *Leptosphaeria maculans* (phoma stem canker) on oilseed rape in Australia, Canada and Europe. *Plant Pathol.* **2001**, *50*, 10–27. [CrossRef]
57. Fitt, B.D.L.; Brun, H.; Barbetti, M.J.; Rimmer, S.R. World-Wide Importance of Phoma Stem Canker (*Leptosphaeria maculans* and *L. biglobosa*) on Oilseed Rape (*Brassica napus*). *Eur. J. Plant Pathol.* **2006**, *114*, 3–15. [CrossRef]
58. Singh, H.K.; Singh, R.B.; Kumar, P.; Singh, M.; Yadav, J.K.; Singh, P.K.; Chauhan, M.P.; Shakywar, R.C.; Maurya, K.N.; Priyanka, B.S.; et al. *Alternaria* blight of rapeseed mustard–A Review. *J. Environ. Biol.* **2017**, *38*, 1405–1420. [CrossRef]
59. Verma, P.R. Biology and control of *Rhizoctonia solani* on rapeseed: A Review. *Phytoprotection* **2005**, *77*, 99–111. [CrossRef]
60. Paulitz, T.C.; Okubara, P.A.; Schillinger, W.F. First Report of Damping-Off of Canola Caused by *Rhizoctonia solani* AG 2-1 in Washington State. *Plant Dis.* **2006**, *90*, 829. [CrossRef]
61. Bridge, J. Nematode management in sustainable and subsistence agriculture. *Annu. Rev. Phytopathol.* **1996**, *34*, 201–225. [CrossRef]
62. Heydari, A.; Pessarakli, M. A Review on Biological Control of Fungal Plant Pathogens Using Microbial Antagonists. *J. Biol. Sci.* **2010**, *10*, 273–290. [CrossRef]
63. Habash, S.; Al-Banna, L. Phosphonate fertilizers suppressed root knot nematodes *Meloidogyne javanica* and *M. incognita*. *J. Nematol.* **2011**, *43*, 95–100. [PubMed]
64. Timper, P. Conserving and enhancing biological control of nematodes. *J. Nematol.* **2014**, *46*, 75–89. [PubMed]
65. Lu, C.; Tian, H. Global nitrogen and phosphorus fertilizer use for agriculture production in the past half century: Shifted hot spots and nutrient imbalance. *Earth Syst. Sci. Data* **2017**, *9*, 181–192. [CrossRef]
66. Cheng, A.-X.; Xiang, C.-Y.; Li, J.-X.; Yang, C.-Q.; Hu, W.-L.; Wang, L.-J.; Lou, Y.-G.; Chen, X.-Y. The rice (E)-β-caryophyllene synthase (OsTPS3) accounts for the major inducible volatile sesquiterpenes. *Phytochemistry* **2007**, *68*, 1632–1641. [CrossRef] [PubMed]
67. Echeverrigaray, S.; Zacaria, J.; Beltrão, R. Nematicidal Activity of Monoterpenoids against the Root-Knot Nematode *Meloidogyne incognita*. *Phytopathology* **2010**, *100*, 199–203. [CrossRef]
68. Zengin, H.; Baysal, A.H. Antibacterial and antioxidant activity of essential oil terpenes against pathogenic and spoilage-forming bacteria and cell structure-activity relationships evaluated by SEM microscopy. *Molecules* **2014**, *19*, 17773–17798. [CrossRef]
69. Dambolena, J.S.; Zunino, M.P.; Herrera, J.M.; Pizzolitto, R.P.; Areco, V.A.; Zygadlo, J.A. Terpenes: Natural Products for Controlling Insects of Importance to Human Health—A Structure-Activity Relationship Study. *Psyche A J. Entomol.* **2016**, *2016*, 1–17. [CrossRef]
70. Araniti, F.; Sánchez-Moreiras, A.M.; Graña, E.; Reigosa, M.J.; Abenavoli, M.R. Terpenoid trans -caryophyllene inhibits weed germination and induces plant water status alteration and oxidative damage in adult *Arabidopsis*. *Plant Biol.* **2017**, *19*, 79–89. [CrossRef]
71. Pungartnik, C. Antifungal Potential of Terpenes from *Spondias Purpurea* L. Leaf Extract against *Moniliophthora perniciosa* that causes Witches Broom Disease of *Theobroma cacao*. *Int. J. Complement. Altern. Med.* **2017**, *7*. [CrossRef]
72. Habash, S.S.; Könen, P.P.; Loeschcke, A.; Wüst, M.; Jaeger, K.-E.; Drepper, T.; Grundler, F.M.W.; Schleker, A.S.S. The Plant Sesquiterpene Nootkatone Efficiently Reduces *Heterodera schachtii* Parasitism by Activating Plant Defense. *Int. J. Mol. Sci.* **2020**, *21*, 9627. [CrossRef]

73. Kigathi, R.N.; Unsicker, S.B.; Reichelt, M.; Kesselmeier, J.; Gershenzon, J.; Weisser, W.W. Emission of Volatile Organic Compounds After Herbivory from *Trifolium pratense* (L.) Under Laboratory and Field Conditions. *J. Chem. Ecol.* **2009**, *35*, 1335–1348. [CrossRef] [PubMed]
74. Pazouki, L.; Kanagendran, A.; Li, S.; Kännaste, A.; Rajabi Memari, H.; Bichele, R.; Niinemets, Ü. Mono- and sesquiterpene release from tomato (*Solanum lycopersicum*) leaves upon mild and severe heat stress and through recovery: From gene expression to emission responses. *Environ. Exp. Bot.* **2016**, *132*, 1–15. [CrossRef] [PubMed]
75. Muchlinski, A.; Chen, X.; Lovell, J.T.; Köllner, T.G.; Pelot, K.A.; Zerbe, P.; Ruggiero, M.; Callaway, L.; Laliberte, S.; Chen, F.; et al. Biosynthesis and Emission of Stress-Induced Volatile Terpenes in Roots and Leaves of Switchgrass (*Panicum virgatum* L.). *Front. Plant Sci.* **2019**, *10*, 1144. [CrossRef] [PubMed]
76. Huang, M.; Sanchez-Moreiras, A.M.; Abel, C.; Sohrabi, R.; Lee, S.; Gershenzon, J.; Tholl, D. The major volatile organic compound emitted from *Arabidopsis thaliana* flowers, the sesquiterpene (E)-β-caryophyllene, is a defense against a bacterial pathogen. *New Phytol.* **2012**, *193*, 997–1008. [CrossRef] [PubMed]
77. Rasmann, S.; Köllner, T.G.; Degenhardt, J.; Hiltpold, I.; Toepfer, S.; Kuhlmann, U.; Gershenzon, J.; Turlings, T.C.J. Recruitment of entomopathogenic nematodes by insect-damaged maize roots. *Nature* **2005**, *434*, 732–737. [CrossRef]
78. Degenhardt, J.; Hiltpold, I.; Kollner, T.G.; Frey, M.; Gierl, A.; Gershenzon, J.; Hibbard, B.E.; Ellersieck, M.R.; Turlings, T.C.J. Restoring a maize root signal that attracts insect-killing nematodes to control a major pest. *Proc. Natl. Acad. Sci. USA* **2009**, *106*, 13213–13218. [CrossRef]
79. Ma, Y.-N.; Chen, C.-J.; Li, Q.-Q.; Xu, F.-R.; Cheng, Y.-X.; Dong, X. Monitoring Antifungal Agents of *Artemisia annua* against *Fusarium oxysporum* and *Fusarium solani*, Associated with *Panax notoginseng* Root-Rot Disease. *Molecules* **2019**, *24*, 213. [CrossRef]
80. Yamagiwa, Y.; Inagaki, Y.; Ichinose, Y.; Toyoda, K.; Hyakumachi, M.; Shiraishi, T. *Talaromyces wortmannii* FS2 emits β-caryophyllene, which promotes plant growth and induces resistance. *J. Gen. Plant. Pathol.* **2011**, *77*, 336–341. [CrossRef]
81. Hanahan, D. Studies on transformation of *Escherichia coli* with plasmids. *J. Mol. Biol.* **1983**, *166*, 557–580. [CrossRef]
82. Simon, R.; Priefer, U.; Pühler, A. A Broad Host Range Mobilization System for In Vivo Genetic Engineering: Transposon Mutagenesis in Gram Negative Bacteria. *Bio/Technology* **1983**, *1*, 784–791. [CrossRef]
83. Strnad, H.; Lapidus, A.; Paces, J.; Ulbrich, P.; Vlcek, C.; Paces, V.; Haselkorn, R. Complete genome sequence of the photosynthetic purple nonsulfur bacterium *Rhodobacter capsulatus* SB1003. *J. Bacteriol.* **2010**, *192*, 3545–3546. [CrossRef] [PubMed]
84. Klipp, W.; Masepohl, B.; Pühler, A. Identification and mapping of nitrogen fixation genes of *Rhodobacter capsulatus*: Duplication of a nifA-nifB region. *J. Bacteriol.* **1988**, *170*, 693–699. [CrossRef] [PubMed]
85. Weaver, P.F.; Wall, J.D.; Gest, H. Characterization of *Rhodopseudomonas capsulata*. *Arch. Microbiol.* **1975**, *105*, 207–216. [CrossRef] [PubMed]
86. Fuhrmann, M.; Hausherr, A.; Ferbitz, L.; Schödl, T.; Heitzer, M.; Hegemann, P. Monitoring dynamic expression of nuclear genes in *Chlamydomonas reinhardtii* by using a synthetic luciferase reporter gene. *Plant Mol. Biol.* **2004**, *55*, 869–881. [CrossRef] [PubMed]
87. Hungate, R.E. *Chapter IV A Roll Tube Method for Cultivation of Strict Anaerobes*; Norris, J.R., Ribbons, D.W.B.T.-M., Eds.; Academic Press: Cambridge, MA, USA, 1969; Volume 3, pp. 117–132.
88. Rodriguez, S.; Kirby, J.; Denby, C.M.; Keasling, J.D. Production and quantification of sesquiterpenes in *Saccharomyces cerevisiae*, including extraction, detection and quantification of terpene products and key related metabolites. *Nat. Protoc.* **2014**, *9*, 1980–1996. [CrossRef]
89. Wiegand, I.; Hilpert, K.; Hancock, R.E.W. Agar and broth dilution methods to determine the minimal inhibitory concentration (MIC) of antimicrobial substances. *Nat. Protoc.* **2008**, *3*, 163–175. [CrossRef]
90. European Committee for Antimicrobial Susceptibility Testing (EUCAST) of the European Society of Clinical Microbiology and Infectious Diseases (ESCMID). Determination of minimum inhibitory concentrations (MICs) of antibacterial agents by broth dilution. *Clin. Microbiol. Infect.* **2003**, *9*, ix–xv. [CrossRef]
91. Kim, S.; Jahandar, M.; Jeong, J.H.; Lim, D.C. Recent Progress in Solar Cell Technology for Low-Light Indoor Applications. *Curr. Altern. Energy* **2019**, *3*, 3–17. [CrossRef]
92. Ruberto, G.; Baratta, M.T. Antioxidant activity of selected essential oil components in two lipid model systems. *Food Chem.* **2000**, *69*, 167–174. [CrossRef]
93. Medeiros, R.; Passos, G.F.; Vitor, C.E.; Koepp, J.; Mazzuco, T.L.; Pianowski, L.F.; Campos, M.M.; Calixto, J.B. Effect of two active compounds obtained from the essential oil of *Cordia verbenacea* on the acute inflammatory responses elicited by LPS in the rat paw. *Br. J. Pharmacol.* **2007**, *151*, 618–627. [CrossRef]
94. Fidyt, K.; Fiedorowicz, A.; Strządała, L.; Szumny, A. β-caryophyllene and β-caryophyllene oxide-natural compounds of anticancer and analgesic properties. *Cancer Med.* **2016**, *5*, 3007–3017. [CrossRef] [PubMed]
95. Paula-Freire, L.I.G.; Andersen, M.L.; Gama, V.S.; Molska, G.R.; Carlini, E.L.A. The oral administration of trans-caryophyllene attenuates acute and chronic pain in mice. *Phytomedicine* **2014**, *21*, 356–362. [CrossRef] [PubMed]
96. Sköld, M.; Karlberg, A.-T.; Matura, M.; Börje, A. The fragrance chemical β-caryophyllene—Air oxidation and skin sensitization. *Food Chem. Toxicol.* **2006**, *44*, 538–545. [CrossRef] [PubMed]
97. Steenackers, B.; Neirinckx, A.; De Cooman, L.; Hermans, I.; De Vos, D. The strained sesquiterpene β-caryophyllene as a probe for the solvent-assisted epoxidation mechanism. *ChemPhysChem* **2014**, *15*, 966–973. [CrossRef]
98. De Souza, R.; Ambrosini, A.; Passaglia, L.M.P. Plant growth-promoting bacteria as inoculants in agricultural soils. *Genet. Mol. Biol.* **2015**, *38*, 1678–4685. [CrossRef]

99. Nath Yadav, A. Plant Growth Promoting Bacteria: Biodiversity and Multifunctional Attributes for Sustainable Agriculture. *Adv. Biotechnol. Microbiol.* **2017**, *5*. [CrossRef]
100. Singh, V.K.; Singh, A.K.; Singh, P.P.; Kumar, A. Interaction of plant growth promoting bacteria with tomato under abiotic stress: A review. *Agric. Ecosyst. Environ.* **2018**, *267*, 129–140. [CrossRef]
101. Çakmakçi, R.; Dönmez, F.; Aydin, A.; Şahin, F. Growth promotion of plants by plant growth-promoting rhizobacteria under greenhouse and two different field soil conditions. *Soil Biol. Biochem.* **2006**, *38*, 1482–1487. [CrossRef]
102. Çakmakçi, R.; Dönmez, M.F.; Erdoğan, Ü. The effect of plant growth promoting rhizobacteria on Barley seedling growth, nutrient uptake, some soil properties, and bacterial counts. *Turk. J. Agric. For.* **2007**, *31*, 189–199.
103. Lahlali, R.; Peng, G.; Gossen, B.D.; McGregor, L.; Yu, F.Q.; Hynes, R.K.; Hwang, S.F.; McDonald, M.R.; Boyetchko, S.M. Evidence that the Biofungicide Serenade (*Bacillus subtilis*) Suppresses Clubroot on Canola via Antibiosis and Induced Host Resistance. *Phytopathology* **2012**, *103*, 245–254. [CrossRef]
104. Berg, G. Plant-microbe interactions promoting plant growth and health: Perspectives for controlled use of microorganisms in agriculture. *Appl. Microbiol. Biotechnol.* **2009**, *84*, 11–18. [CrossRef] [PubMed]
105. El-Howeity, M.A.; Asfour, M.M. Response of some varieties of canola plant (*Brassica napus* L.) cultivated in a newly reclaimed desert to plant growth promoting rhizobacteria and mineral nitrogen fertilizer. *Ann. Agric. Sci.* **2012**, *57*, 129–136. [CrossRef]
106. Bertrand, H.; Nalin, R.; Bally, R.; Cleyet-Marel, J.-C. Isolation and identification of the most efficient plant growth-promoting bacteria associated with canola (*Brassica napus*). *Biol. Fertil. Soils* **2001**, *33*, 152–156. [CrossRef]
107. Ntalli, N.; Ferrari, F.; Giannakou, I.O.; Menkissoglu-Spiroudi, U. Synergistic and antagonistic interactions of terpenes against *Meloidogyne incognita* and the nematicidal activity of essential oils from seven plants indigenous to Greece. *Pest. Manag. Sci.* **2011**, *67*, 341–351. [CrossRef] [PubMed]
108. Jiménez-Reyes, M.F.; Carrasco, H.; Olea, A.F.; Silva-Moreno, E. Natural Compounds: A Sustainable Alternative to the Phytopathogens Control. *J. Chil. Chem. Soc.* **2019**, *64*, 4459–4465. [CrossRef]
109. Da Silva, F.; Alves, C.; Oliveira Filho, J.; Vieira, T.; Crotti, A.E.; Miranda, M. Chemical constituents of essential oil from *Murraya paniculata* leaves and its application to in vitro biological control of the fungus *Sclerotinia sclerotiorum*. *Food Sci. Technol.* **2019**, *39*. [CrossRef]
110. Valadares, A.C.F.; Alves, C.C.F.; Alves, J.M.; de Deus, I.P.B.; de Oliveira Fi, J.G.; Dos Santos, T.C.L.; Dias, H.J.; Crotti, A.E.M.; Miranda, M.L.D. Essential oils from *Piper aduncum* inflorescences and leaves: Chemical composition and antifungal activity against *Sclerotinia sclerotiorum*. *An. Acad. Bras. Cienc.* **2018**, *90*, 2691–2699. [CrossRef]
111. Yang, C.; Yang, C.; Gao, X.; Jiang, Y.; Sun, B.; Gao, F.; Yang, S. Synergy between methylerythritol phosphate pathway and mevalonate pathway for isoprene production in *Escherichia coli* Synergy between methylerythritol phosphate pathway and mevalonate pathway for isoprene production in *Escherichia coli*. *Metab. Eng.* **2016**, *37*, 79–91. [CrossRef]
112. Syed, S.; Prasad Tollamadugu, N.V.K.V. Chapter 16—Role of Plant Growth-Promoting Microorganisms as a Tool for Environmental Sustainability. In *Recent Developments in Applied Microbiology and Biochemistry*; Buddolla, V., Ed.; Academic Press: Cambridge, MA, USA, 2019; pp. 209–222. ISBN 978-0-12-816328-3.
113. Dobbelaere, S.; Vanderleyden, J.; Okon, Y. Plant Growth-Promoting Effects of Diazotrophs in the Rhizosphere. *CRC Crit. Rev. Plant Sci.* **2003**, *22*, 107–149. [CrossRef]
114. Chen, F.; Han, P.; Liu, P.; Si, N.; Liu, J.; Liu, X. Activity of the novel fungicide SYP-Z048 against plant pathogens. *Sci. Rep.* **2014**, *4*, 6473. [CrossRef]
115. Guzmán-Guzmán, P.; Porras-Troncoso, M.D.; Olmedo-Monfil, V.; Herrera-Estrella, A. *Trichoderma* Species: Versatile Plant Symbionts. *Phytopathology* **2018**, *109*, 6–16. [CrossRef] [PubMed]
116. Finkel, O.M.; Castrillo, G.; Herrera Paredes, S.; Salas González, I.; Dangl, J.L. Understanding and exploiting plant beneficial microbes. *Curr. Opin. Plant. Biol.* **2017**, *38*, 155–163. [CrossRef] [PubMed]
117. Anthony, J.R.; Anthony, L.C.; Nowroozi, F.; Kwon, G.; Newman, J.D.; Keasling, J.D. Optimization of the mevalonate-based isoprenoid biosynthetic pathway in *Escherichia coli* for production of the anti-malarial drug precursor amorpha-4,11-diene. *Metab. Eng.* **2009**, *11*, 13–19. [CrossRef] [PubMed]
118. Ajikumar, P.K.; Xiao, W.-H.; Tyo, K.E.J.; Wang, Y.; Simeon, F.; Leonard, E.; Mucha, O.; Phon, T.H.; Pfeifer, B.; Stephanopoulos, G. Isoprenoid Pathway Optimization for Taxol Precursor Overproduction in *Escherichia coli*. *Science (80-)* **2010**, *330*, 70–74. [CrossRef]
119. Henke, N.; Wichmann, J.; Baier, T.; Frohwitter, J.; Lauersen, K.; Risse, J.; Peters-Wendisch, P.; Kruse, O.; Wendisch, V. Patchoulol Production with Metabolically Engineered *Corynebacterium glutamicum*. *Genes* **2018**, *9*, 219. [CrossRef]
120. Frohwitter, J.; Heider, S.A.E.; Peters-Wendisch, P.; Beekwilder, J.; Wendisch, V.F. Production of the sesquiterpene (+)-valencene by metabolically engineered *Corynebacterium glutamicum*. *J. Biotechnol.* **2014**, *191*, 205–213. [CrossRef]
121. Chen, H.; Zhu, C.; Zhu, M.; Xiong, J.; Ma, H.; Zhuo, M.; Li, S. High production of valencene in *Saccharomyces cerevisiae* through metabolic engineering. *Microb. Cell Fact.* **2019**, *18*, 195.
122. Westfall, P.J.; Pitera, D.J.; Lenihan, J.R.; Eng, D.; Woolard, F.X.; Regentin, R.; Horning, T.; Tsuruta, H.; Melis, D.J.; Owens, A.; et al. Production of amorphadiene in yeast, and its conversion to dihydroartemisinic acid, precursor to the antimalarial agent artemisinin. *Proc. Natl. Acad. Sci. USA* **2012**, *109*, E111–E118.
123. Englund, E.; Shabestary, K.; Hudson, E.P.; Lindberg, P. Systematic overexpression study to find target enzymes enhancing production of terpenes in *Synechocystis* PCC 6803, using isoprene as a model compound. *Metab. Eng.* **2018**, *49*, 164–177. [CrossRef]

124. Bentley, F.K.; Zurbriggen, A.; Melis, A. Heterologous expression of the mevalonic acid pathway in cyanobacteria enhances endogenous carbon partitioning to isoprene. *Mol. Plant.* **2014**, *7*, 71–86. [CrossRef]
125. Krieg, T.; Sydow, A.; Faust, S.; Huth, I.; Holtmann, D. CO_2 to Terpenes: Autotrophic and Electroautotrophic α-Humulene Production with *Cupriavidus necator*. *Angew. Chem. Int. Ed.* **2018**, *57*, 1879–1882. [CrossRef] [PubMed]
126. Yang, J.; Li, Z.; Guo, L.; Du, J.; Bae, H.-J. Biosynthesis of β-caryophyllene, a novel terpene-based high-density biofuel precursor, using engineered *Escherichia coli*. *Renew. Energy* **2016**, *99*, 216–223. [CrossRef]
127. Yang, J.; Nie, Q. Engineering *Escherichia coli* to convert acetic acid to β-caryophyllene. *Microb. Cell Fact.* **2016**, *15*, 74. [CrossRef] [PubMed]
128. Hogenkamp, F.; Hilgers, F.; Knapp, A.; Klaus, O.; Bier, C.; Binder, D.; Jaeger, K.-E.; Drepper, T.; Pietruszka, J. Effect of Photocaged Isopropyl β-D-1-Thiogalactopyranoside Solubility on Light-Responsiveness of LacI-controlled Expression Systems in Different Bacteria. *ChemBioChem* **2020**. [CrossRef] [PubMed]

II.3.3. HETEROLOGOUS PRODUCTION OF VERSATILE TERPENES IN *R. CAPSULATUS*

Production of C_{20}, C_{30} and C_{40} terpenes in the engineered phototrophic bacterium *Rhodobacter capsulatus*

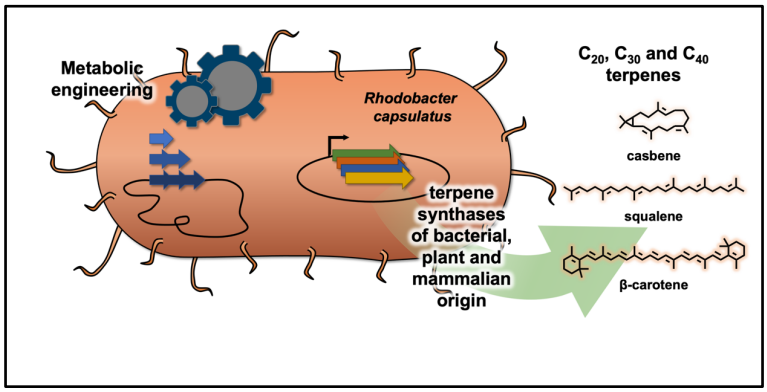

Jennifer Hage-Hülsmann*, Oliver Klaus*, Karl Linke, Katrin Troost, Lukas Gora, **Fabienne Hilgers**, Astrid Wirtz, Beatrix Santiago-Schübel, Anita Loeschcke, Karl-Erich Jaeger and Thomas Drepper

Journal of Biotechnology, 338, 20-30. (2021). j.jbiotec.2021.07.002

The online version may be found at: 10.1016/j.jbiotec.2021.07.002

Status: published

For the Supporting Information see Appendix (**Chapter V.9.**, **page 483**).

Own contribution: Terpene analytics, editing manuscript.

Journal of Biotechnology 338 (2021) 20–30

Contents lists available at ScienceDirect

Journal of Biotechnology

journal homepage: www.elsevier.com/locate/jbiotec

Production of C20, C30 and C40 terpenes in the engineered phototrophic bacterium *Rhodobacter capsulatus*

Jennifer Hage-Hülsmann [a,d,1], Oliver Klaus [a,1], Karl Linke [a], Katrin Troost [a], Lukas Gora [a], Fabienne Hilgers [a,e], Astrid Wirtz [b], Beatrix Santiago-Schübel [c], Anita Loeschcke [a,d,e,*], Karl-Erich Jaeger [a,b,d,e], Thomas Drepper [a,d,e,*]

[a] Institute of Molecular Enzyme Technology, Heinrich Heine University Düsseldorf, Forschungszentrum Jülich, Jülich, Germany
[b] Institute of Bio- and Geosciences IBG-1, Forschungszentrum Jülich, Jülich, Germany
[c] Central Division of Analytical Chemistry ZEA-3: Analytik/Biospec, Forschungszentrum Jülich, Jülich, Germany
[d] Cluster of Excellence on Plant Sciences (CEPLAS), Germany
[e] Bioeconomy Science Center (BioSC), Forschungszentrum Jülich, Jülich, Germany

ARTICLE INFO

Keywords:
Rhodobacter capsulatus
Engineering biosynthesis of terpenes
Diterpene casbene
Triterpene squalene
Squalene synthases
Tetraterpene β-carotene

ABSTRACT

Terpenes constitute one of the largest groups of secondary metabolites that are used, for example, as food-additives, fragrances or pharmaceuticals. Due to the formation of an intracytoplasmic membrane system and an efficient intrinsic tetraterpene pathway, the phototrophic α-proteobacterium *Rhodobacter capsulatus* offers favorable properties for the production of hydrophobic terpenes. However, research efforts have largely focused on sesquiterpene production. Recently, we have developed modular tools allowing to engineer the biosynthesis of terpene precursors. These tools were now applied to boost the biosynthesis of the diterpene casbene, the triterpene squalene and the tetraterpene β-carotene in *R. capsulatus* SB1003. Selected enzymes of the intrinsic isoprenoid pathway and the heterologous mevalonate (MVA) pathway were co-expressed together with the respective terpene synthases in various combinations. Remarkably, co-expression of genes *ispA*, *idi* and *dxs* enhanced the synthesis of casbene and β-carotene. In contrast, co-expression of precursor biosynthetic genes with the squalene synthase from *Arabidopsis thaliana* reduced squalene titers. Therefore, we further employed four alternative pro- and eukaryotic squalene synthases. Here, the synthase from *Methylococcus capsulatus* enabled highest product levels of 90 mg/L squalene upon co-expression with *ispA*. In summary, we demonstrate the applicability of *R. capsulatus* for the heterologous production of diverse terpene classes and provide relevant insights for further development of such platforms.

1. Introduction

Terpenes are one of the largest groups of secondary metabolites that are ubiquitously present in organisms of all kingdoms of life (Chen et al., 2011; Dickschat, 2016; Schmidt-Dannert, 2014). A multitude of plant terpenes are applicable as ingredients in drugs, cosmetics or food products because they exhibit diverse relevant properties including antibiotic and antioxidant activities, a pleasant color, fragrance or flavor (Efferth, 2017; Mahizan et al., 2019; Schempp et al., 2018; Wołosik et al., 2013). Since the chemical synthesis of many terpenes is economically unfeasible and the extraction from their natural sources cannot be realized in a sustainable way, biotechnological approaches represent a promising strategy for accessing these compounds (Marienhagen and Bott, 2013; Schempp et al., 2018).

Terpenes are biosynthesized from the C5 isoprene building blocks isopentenyl pyrophosphate (IPP) and dimethylallyl pyrophosphate (DMAPP), and classified as hemi- (C5), mono- (C10), sesqui- (C15), di- (C20), tri-(C30) and tetraterpenes (C40). The isoprene precursor scaffolds IPP and DMAPP are generated *via* the mevalonate (MVA) pathway, which uses acetyl-CoA as substrate, or the 2-*C*-methyl-D-erythritol 4-

* Corresponding authors at: Institute of Molecular Enzyme Technology, Heinrich Heine University Düsseldorf, Forschungszentrum Jülich, Jülich, Germany.
E-mail addresses: j.hage-huelsmann@fz-juelich.de (J. Hage-Hülsmann), o.klaus@fz-juelich.de (O. Klaus), karllinke89@gmail.com (K. Linke), katrin.troost@gmx.de (K. Troost), LukasFJ@web.de (L. Gora), f.hilgers@fz-juelich.de (F. Hilgers), a.wirtz@fz-juelich.de (A. Wirtz), b.santiago-schuebel@fz-juelich.de (B. Santiago-Schübel), a.loeschcke@fz-juelich.de (A. Loeschcke), karl-erich.jaeger@fz-juelich.de (K.-E. Jaeger), t.drepper@fz-juelich.de (T. Drepper).
[1] Equally contributed.

https://doi.org/10.1016/j.jbiotec.2021.07.002
Received 3 December 2020; Received in revised form 28 June 2021; Accepted 1 July 2021
Available online 5 July 2021

phosphate (MEP) pathway (also referred to as DXP pathway), which uses glyceraldehyde-3-phosphate (GAP) and pyruvate. While the MVA pathway occurs in all eukaryotes and is less abundant in prokaryotes, the MEP pathway is predominant in bacteria as well as in plastids of green algae and plants (Frank and Groll, 2017; Lombard and Moreira, 2011). IPP and DMAPP are used as substrates for a series of condensation steps to yield geranyl pyrophosphate GPP (C10), farnesyl pyrophosphate FPP (C15) and geranylgeranyl pyrophosphate GGPP (C20). GPP can be converted to monoterpenoids, FPP to sesqui- and triterpenoids, and GGPP to di- and tetraterpenoids by respective terpene synthase enzymes.

Key factors for successful heterologous production of terpenes in bacteria are a suitable host organism and the employed terpene synthase enzyme. Specifically, the bacterial host should provide a sufficient precursor supply and an appropriate storage capacity for potentially toxic compounds (Cravens et al., 2019; Das et al., 2007; Schempp et al., 2018). To further optimize terpene production *via* metabolic engineering, molecular genetic tools need to be established for the applied host system. In addition, terpene synthase enzymes from diverse origin were reported to often differ significantly in their performance for a recombinant biosynthesis approach and thus represent a critical determinant of success (Beekwilder et al., 2014; Qiao et al., 2019; Troost et al., 2019). Efforts in microbial terpene production have long focused on the use of established workhorses such as *E. coli* and yeast, but more recently, also alternative host organisms of the class of phototrophic bacteria are receiving increased attention (Moser and Pichler, 2019; Schempp et al., 2018). An established representative of this group is the Gram-negative facultative phototrophic non-sulfur purple α-proteobacterium *Rhodobacter capsulatus*. This bacterium possesses the MEP pathway to yield IPP and DMAPP, which are converted into each other by the IPP isomerase Idi. The FPP synthase IspA catalyzes the elongation *via* GPP to FPP, which is then further elongated by GGPP synthase CrtE, providing the C20 scaffold GGPP as substrate for the phytoene synthase and the following biosynthetic steps to form the *Rhodobacter*-specific carotenoids spheroidene and spheroidenone (see Fig. 1). Under phototrophic growth conditions, *R. capsulatus* generates an intracytoplasmic membrane system (ICM) from invaginations of the cytoplasmic membrane (Chory et al., 1984). Besides its function of housing the photosynthesis apparatus including the photopigments bacteriochlorophyll *a* and the carotenoids, the ICM offers a storage space for heterologously produced enzymes and compounds, thus possibly enabling the bacterium to sustain increased accumulation of hydrophobic products. The applicability of *Rhodobacter* species for heterologous terpene production has been shown for several examples including sesqui-, tri- and tetraterpenes (Beekwilder et al., 2014; Hage-Hülsmann et al., 2019; Khan et al., 2015; Loeschcke et al., 2017, 2013; Orsi et al., 2019; Troost et al., 2019).

For sesquiterpenes, it was shown that the production capacity of *Rhodobacter* can be increased by strengthening the elongation of prenyl phosphates by co-expression of FPP synthase along with a sesquiterpene synthase. Further, terpene production can be enhanced by increased synthesis of isoprene units *via* the intrinsic MEP pathway by co-expression of DxS (1-deoxy-D-xylulose 5-phosphate synthase) and Idi.

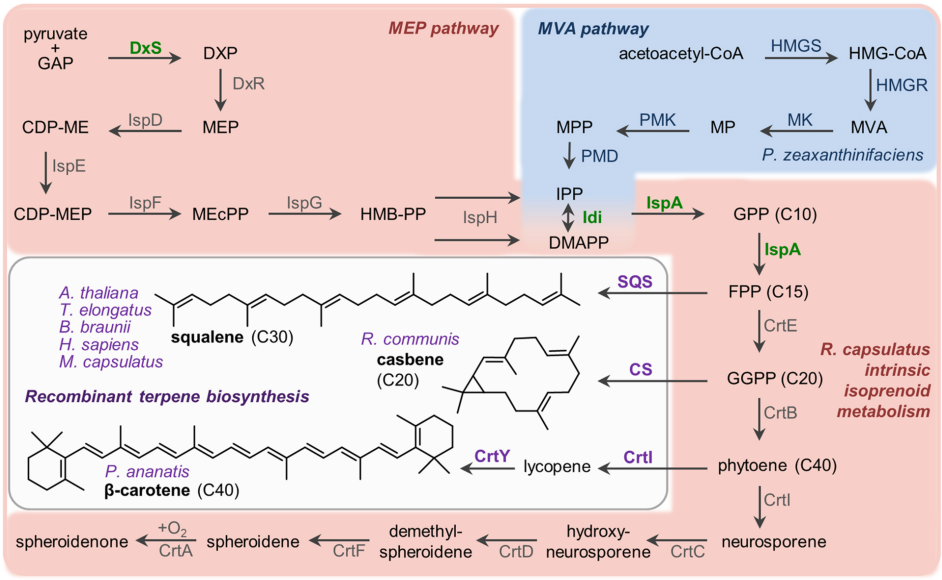

Fig. 1. Engineering concept for production of different terpenes in *R. capsulatus*. In the *R. capsulatus* intrinsic isoprenoid metabolism (red), the MEP pathway provides C5 isoprene building blocks IPP and DMAPP, which are elongated and converted to C40 carotenoids. Recombinant terpene biosynthesis (gray box) is implemented by expression of heterologous enzymes (purple): SQS: squalene synthase (originating from different organisms) for conversion of FPP to squalene; CS: casbene synthase from *R. communis* for conversion of GGPP to casbene; CrtI and CrtY: phytoene desaturase and lycopene cyclase from *P. ananatis* for the conversion of phytoene to β-carotene. To enhance terpene production, the DXP synthase and IPP isomerase (DxS and Idi from *R. sphaeroides*), as well as FPP synthase (IspA from *R. capsulatus*) of the intrinsic isoprenoid metabolism were additionally co-expressed (highlighted in green). Furthermore, an alternative route to build isoprene precursors from central metabolism *via* mevalonate was installed (blue) by expression of the MVA pathway genes from *P. zeaxanthinifaciens*. **Metabolites**: GAP, glyceraldehyde-3-phosphate; DXP, 1-deoxy-D-xylulose 5-phosphate; CDP-ME, 4-diphosphocytidyl-2-*C*-methyl-D-erythritol; CDP-MEP, CDP-ME 2-phosphate; MEcPP, 2-*C*-methyl-D-erythritol-2,4-cyclodiphosphate; HMBPP, 1-hydroxy-2-methyl-2-(*E*)-butenyl 4-diphosphate; HMG-CoA, (*S*)-3-hydroxy-3-methylglutaryl-CoA; MP, phosphomevalonate; MPP, diphosphomevalonate. **Further enzymes**: DxR, DXP reductoisomerase; IspD, MEP cytidylyltransferase; IspE, CDP-ME kinase; IspF, MEcPP synthase; IspG, HMBPP synthase; IspH, HMBPP reductase; HMGS, HMG-CoA synthase; HMGR, HMG-CoA reductase; MK, mevalonate-5-kinase; PMK, MP kinase; PMD, MPP decarboxylase; CrtB, phytoene synthase; CrtI, phytoene desaturase; CrtC, hydroxyneurosporene synthase; CrtD, hydroxyneurosporene desaturase; CrtF, demethylspheroidene *O*-methyltransferase; CrtA, spheroidene monooxygenase.

Moreover, the introduction of the MVA pathway, which does not naturally occur in this host, was demonstrated to enhance terpene production. Such measures have enabled successful sesquiterpene production in *Rhodobacter* (Beekwilder et al., 2014; Orsi et al., 2019; Troost et al., 2019). Two *Rhodobacter* species, namely *R. capsulatus* and *R. sphaeroides* have raised particular interest as microbial cell factories (Heck and Drepper, 2017; Orsi et al., 2021) and the latter is industrially applied for the production of the sesquiterpenes valencene and nootkatone marketed by Isobionics (now BASF). The heterologous biosynthesis of other classes of terpenes in *Rhodobacter* species is, however, less explored.

In the present study, we thus aimed to focus on the production of representatives of C20, C30 and C40 terpenes, namely casbene, squalene and β-carotene, in *R. capsulatus* SB1003. Hence, we employed the casbene synthase *Rc*CS from the castor bean shrub *Ricinus communis* (Mau and West, 1994), the squalene synthase SQS1 from the small flowering plant thale cress *Arabidopsis thaliana* (Busquets et al., 2008), and the phytoene desaturase CrtI together with lycopene cyclase CrtY of the proteobacterium *Pantoea ananatis* (Misawa et al., 1990). We further evaluated metabolic engineering strategies, which were recently established for sesquiterpene production in *R. capsulatus* by implementing co-expression of precursor biosynthetic genes *ispA*, *dxs*, and *idi* of the intrinsic isoprenoid metabolism and all genes of the MVA pathway (Troost et al., 2019), for optimizing the production of di-, tri- and tetraterpenes. The here presented data demonstrate that the metabolic engineering approach could successfully be transferred resulting in an enhanced production of casbene and β-carotene. Surprisingly, squalene production could not be improved when the *A. thaliana* synthase was employed. We therefore tested four alternative squalene synthases from the thermophilic cyanobacterium *Thermosynechococcus elongatus*, the green colonial microalga *Botryococcus braunii*, the Gram-negative methanotroph *Methylococcus capsulatus*, and *Homo sapiens*, finding highest production by the latter two in an engineered background. Therefore, the modular metabolic engineering approaches applied in this study enabled us to identify genetic setups that resulted in improved product titers of the target terpenes and demonstrate applicability of *R. capsulatus* as a platform organism for di-, tri-, and tetraterpene production.

2. Materials and methods

2.1. Bacterial strains and cultivation conditions

Escherichia coli strains DH5α (Hanahan, 1983) and S17-1 (Simon et al., 1983) were used for cloning and conjugational transfer (Klipp et al., 1988) of DNA into *Rhodobacter capsulatus*. *E. coli* cells were cultivated in LB medium (Luria/ Miller, Carl Roth: 10 g/L tryptone, 5 g/L yeast extract, 10 g/L sodium chloride) under constant shaking or on LB agar plates containing 1.5 % agar (*w/v*, Bacto agar, Difco) at 37 °C. Kanamycin was added to a final concentration of 50 µg/mL. *R.capsulatus* strains SB1003 (Strnad et al., 2010) and SB1003-MVA (Troost et al., 2019), which carries the MVA gene cluster (*mvaA-idi-hsc-mvk-pmk-mvd*) of *P. zeaxanthinifaciens*, were cultivated phototrophically on PY (peptone-yeast) agar plates (10 g/L Bacto peptone, 0.5 g/L Bacto yeast extract and 20 g/L Select Agar) or in liquid RCV minimal medium (1 mL/L 20 % $MgSO_4$ (*w/v*), 1 mL/L 7.5 % $CaCl_2$ (*w/v*), 2 mL/L 1% EDTA (*w/v*), 2.4 mL/L 0.5 % $FeSO_4$ (*w/v*) supplemented with 2 mL/L 37 % HCl, 1 mL/L 0.1 % thiamine (*w/v*), 1 mL/L trace element solution [0.4 g/L $MnSO_4$(x1 H_2O), 0.7 g/L H_3BO_3, 0.01 g/L $Cu(NO_3)_2$(x3 H_2O), 0.06 g/L $ZnSO_4$(x7 H_2O), 0.02 g/L $NaMoO_4$(x2 H_2O)]; pH 6.8) at 30 °C under anaerobic phototrophic conditions (bulb light, 2500 lx). For incubation of agar plates, anaerobic conditions were implemented by using airtight cultivation containers and gas packs to deplete atmospheric oxygen (Microbiology Anaerocult A system, Merck KgaA, Darmstadt, Germany). Liquid cultivations were performed in Hungate glass tubes, which can be capped airtight with a septum and a screw cap.

2.2. Construction of expression vectors

The di-, tri- and tetraterpene biosynthetic genes were obtained by gene synthesis (Eurofins Genomics, Ebersberg, Germany) with optimized codon-usage for expression in *R. capsulatus* (Supplementary Table S1) and were designated as follows. We used casbene synthase (encoded by *RcCS*) from *Ricinus communis* (NCBI Protein XP_002513340.1) (Mau and West, 1994) for casbene biosynthesis. Phytoene desaturase was used together with lycopene cyclase, encoded by *crtY-crtI* from *Pantoea ananatis* (NCBI Protein P21687.1 and P21685.1) (Misawa et al., 1990) for β-carotene synthesis. Different squalene synthases were selected for biosynthesis of the triterpene. We used the squalene synthase 1 (SQS1) from *Arabidopsis thaliana* (At4g34640; NCBI Protein NP_195190.1) (Busquets et al., 2008), as in our previous studies (Loeschcke et al., 2017). For *Bb*SQS, we used a version of the squalene synthase from *Botryococcus braunii* (GenBank Protein AAF20201.1), which was employed to install squalene synthesis in *R. capsulatus* before (Khan et al., 2015) with a truncation of 26 amino acids at the C-terminus, which was previously shown to facilitate enhanced expression in *E. coli* (Okada et al., 2000). We used *Te*SQS from *Thermosynechococcus elongates* BP1 (NCBI Reference Sequence: NP_681887.1), which has shown high *in vitro* activity and was functionally expressed in *E. coli* (Katabami et al., 2015; Lee and Poulter, 2008). A truncated version of the human squalene synthase (NCBI Reference AAH09251.1) was employed as *Hs*SQS, with deletion of the N-terminal 30 amino acids and the C-terminal 47 amino acids, based on previous reports (Katabami et al., 2015; Thompson et al., 1998). The squalene synthase *Mc*SQS from *Methylococcus capsulatus* str. Bath (NCBI Protein CAA71097.1) was used because it was reported to be expressed as a soluble protein (Ohtake et al., 2014). During gene synthesis, restriction endonuclease recognition sites, and homologous vector sequences were added at the 5′ or 3′ ends, as appropriate for cloning.

All terpene biosynthetic genes were cloned into the expression vector pRhon5Hi-2 (Troost et al., 2019) carrying the host-specific P_{nif} promotor (NCBI Genbank Accession MG208548). Vectors pRhon5Hi-2-RcCS and pRhon5Hi-2-crtY-crtI were constructed by cloning the synthetic gene *RcCS* or the *crtY-crtI* cassette as *Nde*I/*Hind*III fragments into vector pRhon5Hi-2. To this end, *crtY-crtI* was amplified *via* PCR, adding the restriction sites to the ends by use of appropriate primers, while *RcCS* was obtained with *Nde*I/*Hind*III sites *via* gene synthesis. The gene *ispA* (*R. capsulatus* SB1003) was amplified *via* PCR using genomic DNA as template, introducing *Hind*III and *Xho*I sites with the primers. The cassette *ispA-dxs-idi* (*dxs* and *idi* from *R. sphaeroides* 2.4.1) was obtained as *Hind*III/*Xho*I-fragment by hydrolysis of vector pRhon5Hi-2-CnVS-ispA-dxs-idi (Troost et al., 2019). These genes and gene cassettes were used to construct vectors pRhon5Hi-2-RcCS-ispA and pRhon5Hi-2-RcCS-ispA-dxs-idi, as well as pRhon5Hi-2-crtY-crtI-ispA and pRhon5Hi-2-crtY-crtI-ispA-dxs-idi. Construction of pRhon5Hi-2- SQS1 was previously described (Loeschcke et al., 2017). It was used as template to amplify SQS1 with appropriate primers adding the necessary restriction sites to clone the gene as an *Xba*I/*Hind*III fragment in vectors pRhon5Hi-2-CnVS-ispA and pRhon5Hi-2-CnVS-ispA-dxs-idi (Troost et al., 2019), thereby replacing the gene *CnVS* with SQS1 to generate expression vectors pRhon5Hi-2-SQS1-ispA and pRhon5Hi2-SQS1-ispA-dxs-idi. The analogous constructs carrying the squalene synthase genes of other organisms were likewise constructed, with the difference that the 5′ end and 3′ end extensions were added during gene synthesis, so that the appropriate sequences could be readily excised without additional PCR. Relevant gene sequences on each construct were verified by sequencing performed by Eurofins Genomics (Ebersberg, Germany). All oligonucleotide primers, plasmids and strains used in this study are listed in Supplementary Table S2.

2.3. Heterologous expression of terpene biosynthesis genes in *R. capsulatus*

For introduction of terpene biosynthesis genes in *R. capsulatus*, respective pRhon5Hi-2-based vectors were transferred to the host *via* conjugation as previously described (Klipp et al., 1988). Exconjugants were subsequently selected and further cultivated on PY agar, containing 25 µg/mL kanamycin and 25 µg/mL rifampicin. For heterologous expression of terpene biosynthesis genes, cultivation was conducted in liquid RCV medium with 4 g/L malate containing 25 µg/mL kanamycin under anaerobic phototrophic conditions (bulb light, 2500 lx) in 15 mL Hungate tubes at 30 °C. Pre-cultures of 15 mL RCV medium containing 0.1 % $(NH_4)_2SO_4$ were inoculated and incubated for 72 h. Expression cultures were inoculated from pre-cultures to an initial OD_{660nm} of 0.05 in RCV medium containing 0.1 % serine as sole nitrogen source. The omission of ammonium together with implementation of anaerobic conditions ensured derepression of the P_{nif} promoter and target protein expression (Troost et al., 2019). A culture volume of 15 mL medium was used for squalene and β-carotene production cultures. For analysis of casbene production, 14 mL cultures were overlayed with 0.5 mL *n*-dodecane. Cultures were incubated for 2 days (48 h), until an OD_{660nm} of ~2-3 was reached before sampling and product analysis. For analysis of squalene and β-carotene, samples of cells corresponding to OD_{660nm} = 7.5 in 1 mL (i.e. approximately 3 mL of the cultures, depending on the specific cell density) were harvested by centrifugation (10 min, 1800 g, 4 °C), the medium was discarded, and pellets stored at -20 °C. All cultivations were conducted at least as triplicates and, for verification, repeated in independent experimental runs.

2.4. Sampling and GC analysis of casbene

After 48 h of cultivation, expression cultures in Hungate tubes with *n*-dodecane were incubated in a Multitron Standard incubation shaker (Infors HT) for additional 24 h at 30 °C in horizontal position under constant shaking at 130 rpm for further extraction of casbene from expression cultures. Thereafter, 100 µL of the *n*-dodecane layer were harvested for GC analysis. Casbene amounts could not be determined quantitatively because an authentic reference was missing. Instead, relative production levels were estimated in GC-FID analyses from areas of peaks which exclusively occurred in samples from *Rc*CS expression cultures and were absent in those of the *R. capsulatus* wildtype SB1003 or SB1003-MVA. The gas chromatograph *6890 N* (Agilent) equipped with an Agilent (5%-Phenyl)-methylsiloxane *HP*-5 column (30 m length, 0.32 mm inside diameter, 0.25 µm film thickness) was used for splitless injection of 2 µL sample volumes, using helium as carrier gas. The injector temperature was set to 240 °C and the FID to 250 °C. The oven temperature was held at 100 °C for 5 min, then ramped to 180 °C at 10 °C/min, finally to 300 °C at 20 °C/min. Signals were detected using a flame ionization detector (FID), and peak areas obtained at a retention time of 15.91 min were evaluated. GC-MS analysis was employed for corroboration of casbene (272 g/mol) accumulation in the *n*-dodecane layer. To this end, 1 µL was injected directly into a Trace GC Ultra gas chromatograph coupled to an ITQ 900 mass spectrometer (Thermo Scientific). Separation was achieved in a capillary (30 m length, 0.25 mm diameter) with a 0.25 µm film of FS-5 supreme (CS Chromatographie Service). Split mode with a split ratio of 10 was used for the injector with the inlet temperature set to 250 °C. The oven was programmed to start at 100 °C and a 1 min hold, after which temperature increased to 300 °C at a rate of 5 °C/min. Helium was used as carrier gas at a flow rate of 1 mL/min. MS data were collected from 50 to 650 *m/z* during the temperature ramp. The MS spectrum of a peak, which occurred at 29-30 min in the extracted ion chromatogram (EIC) of 272 *m/z*, was found to match previously published casbene spectra (King et al., 2014; Luo et al., 2016).

2.5. Preparation of whole cell extracts for analysis of squalene and β-carotene

Extraction of squalene from pelleted cells from *R. capsulatus* expression cultures was performed by addition of 2 mL acetone. The samples were vortexed, incubated at 50 °C and 600 rpm for 15 min and cell debris was finally separated from acetone by centrifugation (3 min, 2900 *g*, 22 °C). The acetone supernatants were transferred into fresh tubes and supplemented with 1.5 mL of 1 M NaCl solution and mixed. Afterwards, 1.8 mL *n*-hexane was added and samples were extracted for 30 s by mixing with a test tube shaker. Phase separation was reached by centrifugation (1 min, 2900 *g*, 22 °C). Finally, the *n*-hexane organic phases were transferred into fresh reaction tubes and dried using a vacuum centrifugation (20 min, 30 °C).

2.6. HPLC analysis of squalene

Dried *R. capsulatus* cell extracts were solved in 150 µL methanol-acetonitrile mixture (1:1) and used for analysis of produced squalene *via* HPLC-UV/Vis with an LC-2010 HT system (Shimadzu). Reversed phase chromatography was performed with a Kinetex C18 column (75 mm x 4.6 mm, 2.6 µm, Phenomenex) and a respective guard column. Chromatograms were recorded at 202 nm. Sample volumes of 10 µL were injected and the separation occurred with a flow rate of 1 mL/min and at an oven temperature of 35 °C. The mobile phase consisted of acetonitrile (A), methanol (B) and 2-propanol (C). Starting conditions of 14 min analyses were 80/20 (%A/B), followed by a gradient to solvent compositions of 76/19/5 (%A/B/C), then to 72/18/10 (%A/B/C), and to 56/14/30 (%A/B/C), that were reached after 2.5 min, 4.25 min and 6.00 min, respectively. The last was held for 3 min, before returning to starting conditions within 0.5 min. Those were maintained for 4.5 min for re-equilibration. Squalene amounts were quantified by calibration with a commercial authentic reference (Sigma-Aldrich). To account for extraction losses, titers in the cultures were determined *via* calibration curves generated by addition of defined amounts of authentic squalene to cell pellets of the *R. capsulatus* wildtype, and analysis of squalene signals after the same extraction procedure as applied for samples from expression cultures.

2.7. HPLC analysis of β-carotene

Dried *R. capsulatus* cell extracts were solved in 150 µL pure ethanol (p.a.) and analyzed by HPLC-PDA using an LC10Ai system (Shimadzu) equipped with the SPD-M10Avp photodiode array detector (PDA). A C30 reversed phase HPLC column (250 × 4.6 mm, 5 µm, YMC-Europe GmbH, Dinslaken, Germany) with a guard column filled with the same material (20 mm × 4.0 mm) was used for chromatography at 30 °C column oven temperature and 1 mL/min solvent flow rate. The mobile phase consisted of methanol (A), ethyl acetate (B) and acetonitrile containing 0.1 % formic acid (C). Starting conditions of 39 min analysis runs were 15/15/70 (%A/B/C) for 4 min, followed by a gradient to 10/70/20 (%A/B/C) in 15 min. This proportion was maintained for 14 min, before returning to starting conditions within 1 min which was maintained for re-equilibration for 5 min. Chromatograms were recorded at 450 nm, and absorbance spectra (from 350−550 nm) of peaks were extracted from PDA-data. Detected signals were analyzed in comparison with authentic references of carotenoids that were expected to result from heterologous gene expression, i.e. neurosporene (Standard from CaroteNature, Münsingen, Switzerland; 24.6 min), lycopene (Standard from DHI, Hørsholm, Denmark; 32 min) and β-carotene (Sigma-Aldrich; 18.5 min). Titers of β-carotene in cell cultures were estimated based on a calibration curve generated by addition of defined amounts of authentic β-carotene to cell pellets of the *R. capsulatus* wildtype, and analysis of β-carotene signals after the same extraction procedure as applied for samples from expression cultures. The signal attributed to all-*trans* β-carotene (18.5 min) was used for integration and additional signals

putatively assigned to geometrical *cis* isomers (Bononi et al., 2002; Schierle et al., 2004) were ignored for quantification as the ratio of all-*trans* to *cis* isomers was similar in all samples. Intrinsic spheroidene was identified based on the relative retention time (26.8 min) and known absorbance properties (Britton, 1995).

2.8. Analysis of Rhodobacter capsulatus pigmentation and dry cell weight

R. capsulatus pigmentation was determined by UV-Vis spectrophotometry. To this end, cell material equivalent to 1 mL with an optical density of 1 at a wavelength of 660 nm was harvested. Cell pellets were dispersed in 50 µL H_2O and cells were disrupted by adding 1 mL ethanol (p.a.). For a better cell disruption, samples were incubated for 5 min at 40 °C shaking (800 rpm). Afterwards, cell debris was pelleted by centrifugation (2 min, max. speed, 22 °C). Absorption of the ethanol samples at 455 nm was determined in a UV-Vis spectrophotometer (Thermo Scientific) as a measure of spheroidene levels.

The correlation of dry cell weight (DCW) of photoheterotrophically grown *R. capsulatus* in RCV medium to measured optical cell density at 660 nm, was determined by harvesting differently concentrated 1 mL samples of liquid cultures of the wildtype strain *R. capsulatus* SB1003 with optical densities at 660 nm of 0.5, 1.0, 1.5, 2.0 and 2.5. After centrifugation (10 min, 1100 g, 22 °C), supernatants were discarded and cell pellets were stored overnight at -20 °C before pellets were dried for 24 h in a freeze dryer (Lyovac GT2, Steris). The sample tubes were weighed before and after collection of cells to measure cell weight, enabling determination of a correlation of 1 mL OD_{660nm} = 1 with 0.6 mgDCW.

3. Results

3.1. Engineering concepts for the production of C20, C30 and C40 terpenes in R. capsulatus

In order to analyze if the recently developed tools for modular engineering of sesquiterpenoid synthesis in *R. capsulatus* (Troost et al., 2019) can be transferred to the phototrophic production of C20, C30 and C40 terpenes, we used the diterpene casbene, the triterpene squalene and the tetraterpene β-carotene as showcase targets (Fig. 1). The C20 diterpene casbene is produced in *Euphorbiaceae* (Dueber et al., 1978). The compound is known to exhibit antifungal activity (Moesta and West, 1985) and represents the precursor of further pharmacologically active diterpenes (Le et al., 2009) which accumulate in the plants (Liao et al., 2009). The casbene synthase *Rc*CS from castor bean *Ricinus communis* was chosen for expression in *R. capsulatus* to catalyze the cyclization of GGPP to casbene, since it could be functionally expressed in microorganisms before (Reiling et al., 2004). The C40 tetraterpene β-carotene is likewise derived from GGPP and occurs in microorganisms, fungi and plants (Avalos and Limón, 2015; Sandmann, 1994). This pigment is of interest for its antioxidant properties and provitamin A function (Britton et al., 2008), and is utilized as food colorant in livestock industry to enhance the color of e.g. salmon or egg yolk (Bauernfeind, 1981; Mortensen, 2006). We have previously identified the phytoene desaturase CrtI and lycopene cyclase CrtY of the bacterium *Pantoea ananatis* (Misawa et al., 1990) as suitable for the heterologous carotenoid biosynthesis in *Rhodobacter* (Loeschcke et al., 2013), where they can implement conversion of the intrinsic GGPP condensation product phytoene to β-carotene. Squalene belongs to the group of C30 triterpenes and occurs as biosynthetic product in various microorganisms including fungi, all plants and animals (Xu et al., 2016). The compound is applied e.g. in cosmetics (Huang et al., 2009), and is discussed for applications in the pharmaceutical and biofuel sector (Fox, 2009; Reddy and Couvreur, 2009; Yoshida et al., 2012). In addition, squalene is the central precursor of valuable cyclic triterpenes as, for example, cycloartenol and lupeol (Thimmappa et al., 2014). We selected the squalene synthase SQS1 of *Arabidopsis thaliana* (Busquets et al., 2008), which we employed in our previous studies (Hage-Hülsmann et al., 2019; Loeschcke et al., 2017) for successful conversion of FPP to squalene in *R. capsulatus*. The squalene titers we previously obtained under microaerobic (i.e. non-phototrophic) conditions in the wildtype strain SB1003 were relatively low (~8 mg/L) (Loeschcke et al., 2017). We thus aimed to analyze the transferability of the engineering strategies which prove successful for sesquiterpene synthesis in our previous study (Troost et al., 2019).

Accordingly, the FPP synthase IspA from *R. capsulatus* was co-expressed to enhance the prenyl phosphate elongation. Furthermore, the enzymes DxS and Idi (from *R. sphaeroides*) of the MEP pathway were co-expressed in addition to the intrinsic enzymes in order to increase the abundance of IPP and DMAPP. Finally, the isoprenoid biosynthesis pathway *via* mevalonate of *Paracoccus zeaxanthinifaciens* (Hümbelin et al., 2002) was installed as an alternative route to C5 precursors of terpenoid biosynthesis. For gene expression in *R. capsulatus*, we used the host-specific P_{nif} promoter, which enables strong induction under anaerobic conditions with serine as sole nitrogen source in the medium (Troost et al., 2019). Codon usage adapted terpene biosynthesis genes were thus cloned in the vector pRhon5Hi-2 together with *ispA* or the cassette *ispA-dxs-idi* (Supplementary Table S1). These constructs were used for expression in the wildtype strain SB1003 as well as the recombinant strain SB1003-MVA, which carries the MVA gene cluster in the chromosome under control of P_{nif} (Troost et al., 2019).

3.2. Heterologous biosynthesis of GGPP-derived casbene and β-carotene

In order to evaluate the applicability of the modular *R. capsulatus* engineering approach for production of the diterpene casbene, the expression vectors pRhon5Hi-2-RcCS, pRhon5Hi-2-RcCS-ispA and pRhon5Hi-2-RcCS-ispA-dxs-idi harboring the casbene synthase from *R. communis* and MEP pathway genes were transferred into the strains *R. capsulatus* SB1003 (wildtype) and SB1003-MVA (strain with recombinant MVA pathway). After photoheterotrophic cultivation in the presence of *n*-dodecane for two days, samples of the solvent were prepared for analyses by gas chromatography and flame ionization detection (GC-FID). Since casbene is not commercially available as a reference substance, we first compared obtained chromatograms of the wildtype strain SB1003 and SB1003-MVA with samples of respective *Rc*CS expression strains, which exhibited a distinct additional signal. Relative quantification of the putative casbene signal was conducted on the basis of measured peak areas (Fig. 2A, left panel). GC coupled with mass spectrometric detection was employed to corroborate accumulation of a compound with a mass spectrum corresponding to previously reported analyses of casbene (King et al., 2014; Luo et al., 2016) (Fig. 2A, right panel). Co-expression of *ispA* as well as *ispA-dxs-idi* in strain SB1003 resulted in a 1.7- and 2.3-fold increased casbene titer, demonstrating the applicability of our previously established engineering tools (Troost et al., 2019) also for diterpene production in *R. capsulatus*. The presence of the MVA pathway showed no effect on casbene levels (SB1003-MVA + *RcCS*), or even a drastic decrease of the casbene levels when *ispA* or *ispA-dxs-idi* were additionally co-expressed. In these strains, enhanced stress levels may increase the risk of plasmid instability, but since the result was confirmed in independent experimental runs, plasmid rearrangement effects appear rather unlikely. Therefore, we speculate metabolic effects to be the reason for the low product levels in SB1003-MVA under co-expression of the FPP synthase and MEP pathway genes.

To evaluate the engineering concepts for tetraterpene production, vectors pRhon5Hi-2-crtY-crtI, pRhon5Hi-2-crtY-crtI-ispA and pRhon5Hi-2-crtY-crtI-ispA-dxs-idi were employed for β-carotene synthesis in *R. capsulatus* strains SB1003 and SB1003-MVA. After 2 days of photoheterotrophic cultivation, carotenoids were extracted from cells and subsequently analyzed (Fig. 2B, left panel). Using HPLC coupled with a photo diode array detector, produced β-carotene was quantified with an authentic reference for calibration. The expression of the carotenoid biosynthesis genes from *P. ananatis* alone and in combination with *ispA* in

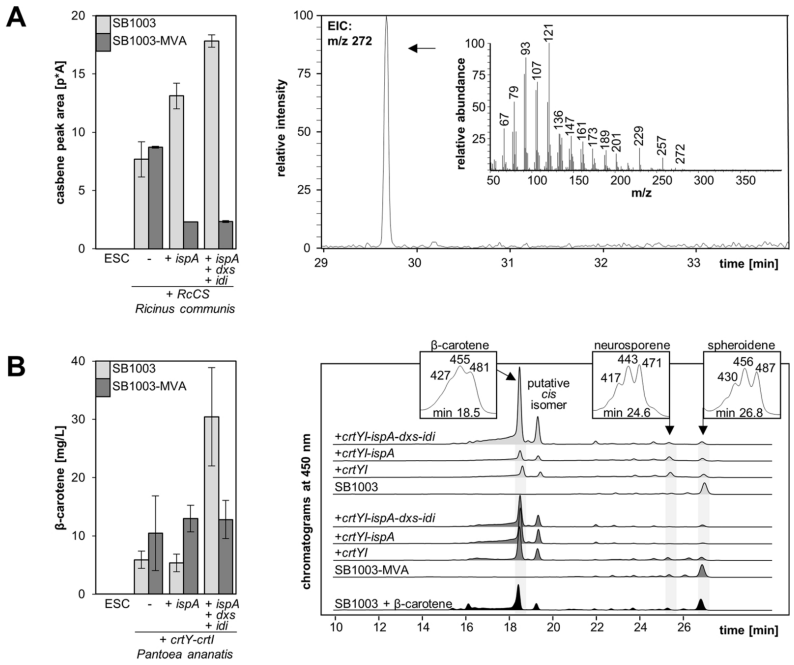

Fig. 2. Production of casbene and β-carotene in *R. capsulatus*. Production of the non-native di- and tetraterpenes was implemented by pRhon5Hi-2-based expression of casbene synthase (*Rc*CS) from *R. communis* or phytoene desaturase (CrtI) and lycopene cyclase (CrtY) from *P. ananatis* in *R. capsulatus* SB1003 (light gray) under photoheterotrophic cultivation conditions. The co-expressed genes *ispA* (from *R. capsulatus*), *dxs* and *idi* (from *R. sphaeroides*) are localized on the respective expression vectors in synthetic operons. The MVA gene cluster from *P. zeaxanthinifaciens* was co-expressed by use of strain SB1003-MVA (dark gray). **(A)** Casbene accumulation in an overlaid *n*-dodecane phase was quantified as relative peak areas by GC-FID (left) and verified by GC–MS analysis (right). **(B)** β-carotene production was analyzed by HPLC-PDA using an authentic reference for calibration and calculation of product titers based on the signal attributed to all-*trans* β-carotene. Putative *cis* isomers were ignored for quantification. HPLC chromatograms (recorded at 450 nm) are representative of replicate experiments (min. triplicate), with specific absorption spectra extracted from PDA data at the indicated retention times of β-carotene, neurosporene and spheroidene. Results in the bar diagrams represent means of independent replicate cultivations (min. triplicate) with the respective standard deviations. ESC, empty strain control.

strain SB1003 resulted in similar titers of about 5 mg/L β-carotene. In this strain, the co-expression of *ispA-dxs-idi*, however, led to a significant increase to 30 mg/L. Co-expression of the MVA pathway genes had a positive effect, with mean titers roughly doubled yielding ~10 mg/L compared to the wildtype strain expressing CrtI and CrtY. This level remained basically unchanged when *ispA* or *ispA-dxs-idi* were additionally co-expressed in SB1003-MVA. In none of the strains, the intermediate lycopene was detected. Specific yields of β-carotene are summarized in the Supplementary Table S3.

HPLC-traces moreover revealed that in the engineered strains, the intrinsic carotenoid biosynthesis was significantly altered by implementation of β-carotene production (Fig. 2B, right panel). The amounts of spheroidene, which accumulates as main carotenoid in the bacterium under anaerobic conditions, were reduced upon expression of CrtI and CrtY from *P. ananatis*. Interestingly, this effect did not seem to be compensated when precursor biosynthetic genes were co-expressed. We further observed that especially cells expressing only CrtI and CrtY produced traces of neurosporene, an intermediate in spheroidene biosynthesis. Nevertheless, heterologous terpene biosynthesis did not affect phototrophic growth of *R. capsulatus* for any of the terpene production setups, as cell densities were all in the same range at the time of sampling (see Fig. S1). In summary, we could demonstrate the biosynthesis of casbene and moderate production of β-carotene as proof of concept. For both, co-expression of the recombinant biosynthetic genes with *ispA-dxs-idi* led to best results in the wildtype background, while use of strain SB1003-MVA yielded rather inconclusive results.

3.3. Heterologous biosynthesis of the FPP-derived triterpene squalene

To test if squalene production could be likewise optimized in *R. capsulatus* by the modular engineering approach, squalene synthase 1 (SQS1) from *A. thaliana*, here referred to as *At*SQS, was introduced into strains SB1003 and SB1003-MVA *via* the vectors pRhon5Hi-2-SQS1, pRhon5Hi-2-SQS1-ispA and pRhon5Hi-2-SQS1-ispA-dxs-idi. Cells were harvested after two days of photoheterotrophic cultivation for extraction and analysis by HPLC-UV, using an authentic reference for calibration and determination of squalene titers (Fig. 3, top panel). Squalene titers of around 65 mg/L were reached by expressing the synthase alone in *R. capsulatus* SB1003. Surprisingly, each metabolic engineering approach – co-expression of *ispA*, *ispA-dxs-idi*, the MVA cluster, or their combination – reduced titers to a minimum of around 12 mg/L (*R. capsulatus* SB1003-MVA harboring pRhon5Hi-2-SQS1-ispA-dxs-idi).

To test, if product levels could be enhanced by applying our engineering tools when squalene synthases from other organisms are employed, we chose respective enzymes from four different organisms, namely the thermophilic cyanobacterium *Thermosynechococcus elongatus* (*Te*SQS), the green colonial microalga *Botryococcus braunii* (*Bb*SQS), the Gram-negative methanotroph *Methylococcus capsulatus* (*Mc*SQS), and *Homo sapiens* (*Hs*SQS). These were selected as promising candidates for having been functionally expressed in prokaryotes previously, or exhibiting high *in vitro* activities (Katabami et al., 2015; Khan et al., 2015; Lee and Poulter, 2008; Ohtake et al., 2014; Okada et al., 2000; Thompson et al., 1998). Based on previous reports, full length sequences or truncated versions were employed as detailed in the Methods Section and in Supplementary Table S1. The genes were cloned in the pRhon5Hi-2-based expression vectors for co-expression of precursor biosynthetic genes and squalene analysis according to the above described experiments.

In comparison to the initially tested *At*SQS, expression of *Te*SQS and *Bb*SQS in *R. capsulatus* SB1003 led to much lower titers (around 20 mg/L), while *Hs*SQS and *Mc*SQS enabled titers in a similar range with 43 and 71 mg/L. This observation indicates that the analyzed synthases might exhibit differences regarding their functional expression, stability, or activity. Remarkably, very different patterns of product titers were observed upon co-expression of precursor biosynthetic genes for every synthase, again demonstrating a benefit of the modular engineering toolset. While product titers could not be enhanced by co-expression of precursor biosynthetic genes in the case of *Bb*SQS, the low product levels obtained with *TeSQS*

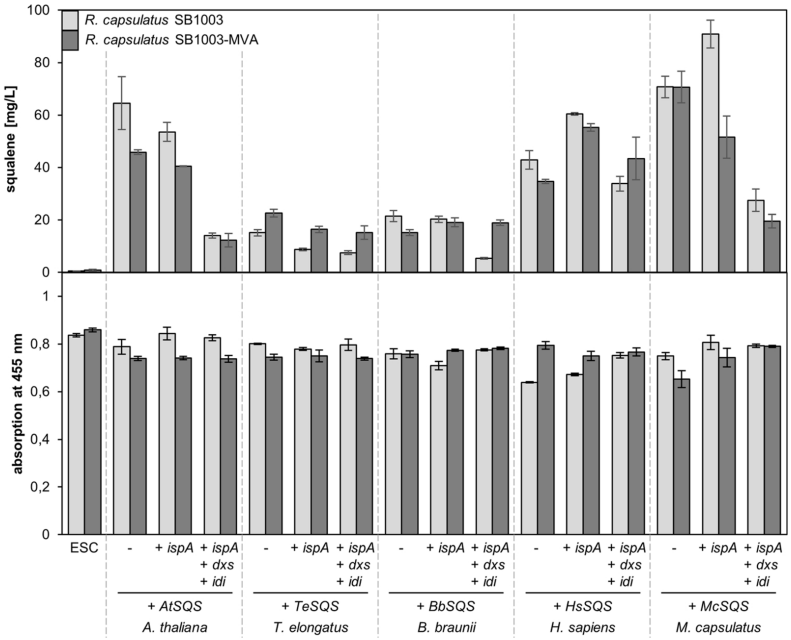

Fig. 3. Production of squalene in *R. capsulatus*. Production was implemented by pRhon5Hi-2-based expression of squalene synthases from *A. thaliana* (*At*), *T. elongatus* (*Te*), *B. braunii* (*Bb*), *H. sapiens* (*Hs*) and *M. capsulatus* (*Mc*) in *R. capsulatus* SB1003. The genes *ispA* (from *R. capsulatus*), *dxs* and *idi* (from *R. sphaeroides*) were co-expressed on the vector in synthetic operons. The MVA gene cluster from *P. zeaxanthinifaciens* was co-expressed by use of strain SB1003-MVA. After photoheterotrophic cultivation, squalene production was analyzed by HPLC-UV analysis using an authentic reference for calibration and calculation of product titers (mg/L, upper panel). Absorption at 455 nm in whole cell EtOH extracts (lower panel) is shown as a measure of spheroidene production. Results represent means of independent triplicate cultivations with the respective standard deviations. ESC, empty strain control.

could be increased by use of the strain SB1003-MVA (providing 23 mg/L). Squalene accumulation obtained with *Hs*SQS or *Mc*SQS was increased by co-expression of *ispA* in strain SB1003, yielding 61 mg/L and the overall highest squalene titer of 90 mg/L, respectively, within this comparative experiment. Specific yields of squalene are summarized in the Supplementary Table S3. Taken together, our studies thus showed that with *R. capsulatus* (i) casbene biosynthesis is generally possible, (ii) moderate β-carotene titers can be reached, and (iii) very different squalene levels - from moderate to substantial maximal titers - were obtained with five different synthases in diverse engineering setups. We therefore chose the latter case to investigate if intrinsic carotenoid levels differed in the set of squalene production strains during phototrophic growth. We first compared the strains SB1003 and SB1003-MVA and, remarkably, did not observe an increase in the signal of the intrinsic carotenoids upon introduction of the MVA pathway. Interestingly, carotenoid-specific absorption of ethanol extracts was also largely unaffected by squalene production in comparison to the empty strain controls (Fig. 3, bottom panel). Hence, our results indicate that squalene production did not consume significant amounts of cellular isoprenoids at the expense of intrinsic carotenoid biosynthesis, but the intrinsic metabolism was capable of compensating for additional FPP consumption to some extent. Moreover, we did not observe strong effects on cell growth (Fig. S2). In summary, our toolkits previously established for the heterologous biosynthesis of sesquiterpenoids (Troost et al., 2019) proved suitable to implement the biosynthesis of di-, tri- and tetraterpenes. The different effects of individual combinations of engineering modules (Table 1) highlight the value of easy-to-apply genetic setups allowing to identify optimal production conditions.

4. Discussion

This study clearly demonstrates the applicability of *R. capsulatus* as an alternative phototrophic production host for di-, tri-, and tetraterpenes using casbene, squalene and β-carotene as model compounds. In addition, we show the effects of metabolic engineering and use of different terpene biosynthetic enzymes on terpene production .

Table 1
Genetic setups for the highest terpene levels in *R. capsulatus* within our studies.

	Test case (synthase / product)	Setup resulting in highest product level (strain / co-expressed genes on pRhon5Hi-2)	Reference
	*Pc*PS / patchoulol	SB1003-MVA / *ispA-dxs-idi*	(Troost et al., 2019)
C15	*Cs*VS / valencene	SB1003-MVA / *ispA-dxs-idi*	(Troost et al., 2019)
	*Cn*VS / valencene	SB1003-MVA / *ispA*	(Troost et al., 2019)
C20	*Rc*CS / casbene	SB1003 / *ispA-dxs-idi*	This study
	*At*SQS / squalene	SB1003 / -	This study
	*Te*SQS / squalene	SB1003-MVA / -	This study
C30	*Bb*SQS / squalene	SB1003 / -	This study
	*Hs*SQS / squalene	SB1003 / *ispA*	This study
	*Mc*SQS / squalene	SB1003 / *ispA*	This study
C40	CrtYI / β-carotene	SB1003 / *ispA-dxs-idi*	This study

The beneficial effects of enhancing the precursor synthesis in the isoprenoid anabolic pathway for terpenoid production are well-known (Moser and Pichler, 2019). Likewise, the necessity of fine-tuning due to feedback and feedforward inhibitory effects within the biosynthetic pathway has been discussed (Dahl et al., 2013; Hage-Hülsmann et al., 2019; Park et al., 2017; Troost et al., 2019). For casbene and β-carotene production, co-expression of terpene biosynthetic enzymes from *R. communis* and *P. ananatis*, respectively, with IspA, DxS and Idi was most successful in our study. The same biosynthetic module also led to best results in our previous study on heterologous sesquiterpene biosynthesis in the host (Troost et al., 2019), when combined with the additional expression of the MVA pathway (Table 1). However, in the present study, strengthening the intrinsic isoprenoid metabolism of *R. capsulatus* at the steps of DXP synthase, IPP isomerase and FPP synthase was more effective than the implementation of the MVA pathway or combinations of both. This might indicate an interaction between the

MEP and MVA pathway, as recently discussed for *R. sphaeroides* (Orsi et al., 2020), but the exact mechanisms and factors influencing it remain to be elucidated.

For squalene production, we used five different synthase genes from all kingdoms, whose expression resulted in diverse initial product titers and further produced differential results upon co-expression of precursor biosynthetic genes. While co-expression of the MVA pathway genes was not beneficial for product titers in most cases, and the *ispA-dxs-idi* cassette either had no effect or reduced the production level in every case, co-expression of *ispA* enhanced squalene levels when squalene synthases from *H. sapiens* or *M. capsulatus* were used. These enzymes also showed relatively high initial product titers when expressed alone. Therefore, accumulation of IPP or FPP, which has been reported to exert inhibitory effects on human FPP synthase (Barnard and Popják, 1981; Park et al., 2017), may be avoided due to more efficient conversion to squalene. However, the *A. thaliana* synthase likewise produced a high initial titer, but all engineering approaches led to reduced product levels. This may indicate that further enzyme properties affecting substrate inhibition, which is known for the squalene synthase from yeast (Zhang et al., 1993), are likely additionally relevant. In this context, it is worth underlining that application of the same engineering toolkit for the production of the sesquiterpenes patchoulol and valencene in *R. capsulatus* revealed that strain SB1003-MVA (Table 1), which facilitates the co-expression of the MVA pathway genes, was the best production strain (Troost et al., 2019). This observation thus underpins the value of the modular engineering concept which can help to further develop *Rhodobacter* as a versatile platform organism for the production of diverse terpene classes, allowing individual adaptation in order to meet the requirements of the respective recombinant terpene pathway.

In general, terpene compounds are of high commercial interest. Thus, diverse microbial production systems have been established for their biosynthesis (Kallscheuer et al., 2018; Moser and Pichler, 2019). *Rhodobacter* species have been identified as suitable hosts for sesquiterpene production (Beekwilder et al., 2014; Orsi et al., 2019; Troost et al., 2019) and are applied in industrial processes by Isobionics (now BASF) (Schempp et al., 2018). Since the biosynthesis of other classes of terpenes in these bacteria is less established, we aimed to explore di-, tri-, and tetraterpene synthesis, choosing the above mentioned compounds casbene, squalene and β-carotene as examples. Generally, the heterologous microbial biosynthesis of the plant diterpene casbene and derivatives thereof, which exhibit promising therapeutic effects, has been established in the context of academic and industrial research (e.g. by the company Evolva). Here, maximal production above 100 mg/L was reached in *S. cerevisiae*, aided by metabolic engineering (Callari et al., 2018; Kirby et al., 2010; Wong et al., 2018). Recombinant casbene biosynthesis with titers of ~ 30 µg/L (normalized to a cell density of 1) has also been shown in *E. coli* (Reiling et al., 2004). Due to the absence of a commercial reference, accurate quantification of the product is thus far not possible *via* a straightforward calibration curve, and estimations have relied on the use of other terpenes like α-gurjunene, cembrene or in-house produced extracts. We demonstrate here for the first time applicability of the α-proteobacterium *R. capsulatus* as phototrophic production platform for this plant natural product. Further studies including accurate product quantification are still necessary for assessment of the prokaryotic host in comparison to the well-performing yeast systems, regarding casbene production.

In contrast to casbene, the tetraterpene β-carotene is an established component of various commercial products, marketed by diverse companies including BASF and DSM (Saini and Keum, 2019). While large parts of the required demand are manufactured by chemical synthesis, microbial production of natural β-carotene is gaining importance. Aside from the use of microalgae and other microbes (Dufossé, 2017; Qiang et al., 2019; Wichuk et al., 2014; Yuan and Alper, 2019), both, *S. cerevisiae* and *E. coli*–based host systems have been established, reaching titers at gram scale with the prokaryote after engineering precursor biosynthesis and optimizing fermentation conditions (López et al., 2019; Yang and Guo, 2014). We have now demonstrated that *R. capsulatus* can accumulate 30 mg/L (15 mg/g DCW) β-carotene, which is identical to the recently described yield that could be gained in the closely related *R. sphaeroides* (Qiang et al., 2019), but notably without bioprocess optimization.

Like β-carotene, the triterpene squalene is used in diverse commercial products, for which deep-sea shark liver oil has represented the major source (Gohil et al., 2019). Obtaining the compound from wild-type or engineered microorganisms in economically attractive processes can offer a paradigm change and refrainment from this practice. Very promising studies showed high-level squalene accumulation in natural producers like marine eukaryotic Thraustochytrids (Aasen et al., 2016). In addition, squalene biosynthesis has been engineered in established microbial workhorses, which offer advantages in e.g., growth rates, high-density fermentation and amenability to genetic modifications. Here, squalene titers over 2 g/L have been demonstrated for metabolically engineered *S. cerevisiae* under optimized conditions (Han et al., 2018). *E. coli*-based production reached 230 mg/L squalene upon co-expression of precursor biosynthetic genes (Katabami et al., 2015). In this study, human SQS produced higher titers than the *T. elongatus* enzyme. In contrast, *T. elongatus* SQS was superior to the human synthase for triterpene biosynthesis in *S. cerevisiae* (Qiao et al., 2019). Squalene production has also been established in *R. capsulatus* before, using SQS enzymes from *B. braunii* (Khan et al., 2015). Here, engineering of the MEP pathway led to ca. 14 mg/g DCW with glucose supplementation. In our previous study, expression of *A. thaliana* SQS1 and cultivation under non-phototrophic, microaerobic conditions led to titers of 8 mg/L squalene (Loeschcke et al., 2017). Compared to that, cultivation under photoheterotrophic conditions in the present study enhanced the titer by an order of magnitude. Generally, comparability of product levels obtained in different studies is limited due to variation of multiple parameters, e.g. in the expression system or cultivation regime. By the direct comparison in this study, we identified the SQS from *M. capsulatus*, which was previously only characterized *in vitro*, as most suitable for high-level triterpene production in *R. capsulatus* (maximal titer 90 mg/L, maximal specific yield 58 mg/g DCW), along with the enzymes from *A. thaliana*, and *H. sapiens*, while *B. braunii* and *T. elongatus* SQS enabled only minor product titers. Altogether, here demonstrated product titers are promising but potential industrial applicability remains to be elucidated in further research to assess e.g., bioprocess optimization.

Heterologous production of the named amounts of β-carotene and squalene had different effects on the intrinsic carotenoid production of *R. capsulatus*. Expression of CrtI and CrtY from *P. ananatis* effectively redirected isoprenoid biosynthesis to β-carotene and led to a drastic decrease in the intrinsic carotenoid spheroidene. This indicates that the desaturase CrtI of *P. ananatis* (Misawa et al., 1990) exhibits higher catalytic activity than the intrinsic CrtI of *R. capsulatus* (Armstrong et al., 1989), or has higher affinity to the substrate phytoene. Furthermore, *P. ananatis* CrtI can use neurosporene as substrate for conversion to lycopene by one further desaturation (Hunter et al., 1994), competing with the intrinsic neurosporene hydroxylase CrtC. In addition, substrate inhibition or feedback inhibition loops by products might not apply for the recombinant enzymes. In this context, it remains to be elucidated why low amounts of neurosporene and not lycopene were found to accumulate in strains expressing β-carotene biosynthetic enzymes. Interestingly, no obvious impairment of photoheterotrophic growth was observed for *crtY-crtI* expressing strains, suggesting that β-carotene was functionally incorporated in photosynthetic complexes, as previously shown for closely related *R. sphaeroides* (Hunter et al., 1994). Biosynthesis of squalene, which led to significantly higher product levels, only had a minor impact on *R. capsulatus* carotenoid production, showing that the intrinsic metabolism was capable of compensating for the associated enhanced consumption of isoprene units. On the other hand, it was interesting to note that co-expression of the MVA pathway did not raise spheroidene levels strongly. Since the implementation of this

pathway can lead to significant elevation of heterologous terpene product levels (Beekwilder et al., 2014; Troost et al., 2019), this may indicate a strict regulation system governing the accumulation of intrinsic tetraterpenes.

In the light of urgently required ecologically friendly technologies for building a sustainable bio-based economy, a paradigm change in the chemical industries is aspired. Since phototrophic hosts can utilize CO_2 for the synthesis of valuable compounds and – in contrast to plants – do not compete for arable land or drinking water, their use as alternative hosts promises sustainable terpene production processes (Frigaard, 2016; Heck and Drepper, 2017; Schempp et al., 2018), and has already been adopted by industry in some cases (Dufossé, 2017). For the here addressed compounds, the research interest in phototrophic host systems is documented by e.g., green alga *Chlamydomonas*-based biosynthesis of casbene (Lauersen et al., 2018), microalga *Dunaliella*- and proteobacterium *R. sphaeroides*-based production of β-carotene (Bonnefond et al., 2017; Qiang et al., 2019), and cyanobacteria- or proteobacterium *R. capsulatus*-based synthesis of squalene (Khan et al., 2015; Loeschcke et al., 2017). Our study contributes to this portfolio, demonstrating the biosynthesis of these C20, C30 and C40 terpenes in *R. capsulatus*, and moreover provides insightful case studies using metabolic engineering and recombinant enzymes.

CRediT authorship contribution statement

Jennifer Hage-Hülsmann: Data curation, Writing - original draft. **Oliver Klaus:** Investigation, Methodology, Data curation. **Karl Linke:** Methodology. **Katrin Troost:** Methodology. **Lukas Gora:** Methodology. **Fabienne Hilgers:** Methodology. **Astrid Wirtz:** Methodology. **Beatrix Santiago-Schübel:** Methodology. **Anita Loeschcke:** Data curation, Writing - review & editing, Visualization, Supervision. **Karl-Erich Jaeger:** Conceptualization, Writing - review & editing. **Thomas Drepper:** Conceptualization, Writing - review & editing, Supervision.

Declaration of Competing Interest

The authors report no declarations of interest.

Acknowledgements

JHH was funded by the Deutsche Forschungsgemeinschaft *via*CEPLAS - Cluster of Excellence on Plant Science (EXC1028). The work of OK was funded by the state of North Rhine Westphalia (NRW) and the European Regional Development Fund (EFRE), Project "CLIB-Kompetenzzentrum Biotechnologie (CKB)"34.EFRE-0300096. KT, FH and AL were funded by the Ministry of Culture and Science of the German State of North Rhine-Westphalia through NRW Strategieprojekt BioSC (No. 313/323-400-00213). The authors thankfully acknowledge Dr. Nadine Katzke and Esther Knieps-Grünhagen for valuable discussions on terpene biosynthesis in *R. capsulatus*, GC and HPLC analysis.

Appendix A. Supplementary data

Supplementary material related to this article can be found, in the online version, at doi:https://doi.org/10.1016/j.jbiotec.2021.07.002.

References

Aasen, I.M., Ertesvåg, H., Heggeset, T.M.B., Liu, B., Brautaset, T., Vadstein, O., Ellingsen, T.E., 2016. Thraustochytrids as production organisms for docosahexaenoic acid (DHA), squalene, and carotenoids. Appl. Microbiol. Biotechnol. 100, 4309–4321. https://doi.org/10.1007/s00253-016-7498-4.

Armstrong, G.A., Alberti, M., Leach, F., Hearst, J.E., 1989. Nucleotide sequence, organization, and nature of the protein products of the carotenoid biosynthesis gene cluster of *Rhodobacter capsulatus*. Mol. Gen. Genet. 216, 254–268. https://doi.org/10.1007/BF00334364.

Avalos, J., Limón, M.C., 2015. Biological roles of fungal carotenoids. Curr. Genet. 61, 309–324. https://doi.org/10.1007/s00294-014-0454-x.

Barnard, G.F., Popják, G., 1981. Human liver prenyltransferase and its characterization. Biochim. Biophys. Acta 661, 87–99. https://doi.org/10.1016/0005-2744(81)90086-3.

Bauernfeind, J.C., 1981. Carotenoids as Colorants and Vitamin A Precursors, Technological and Nutritional Applications (Ed.). Academic Press.

Beekwilder, J., van Houwelingen, A., Cankar, K., van Dijk, A.D.J., de Jong, R.M., Stoopen, G., Bouwmeester, H., Achkar, J., Sonke, T., Bosch, D., 2014. Valencene synthase from the heartwood of Nootka cypress (*Callitropsis nootkatensis*) for biotechnological production of valencene. Plant Biotechnol. J. 12, 174–182. https://doi.org/10.1111/pbi.12124.

Bonnefond, H., Moelants, N., Talec, A., Mayzaud, P., Bernard, O., Sciandra, A., 2017. Coupling and uncoupling of triglyceride and beta-carotene production by *Dunaliella salina* under nitrogen limitation and starvation. Biotechnol. Biofuels 10, 25. https://doi.org/10.1186/s13068-017-0713-4.

Bononi, M., Commissati, I., Lubian, E., Fossati, A., Tateo, F., 2002. A simplified method for the HPLC resolution of α-carotene and β-carotene (*trans* and *cis*) isomers. Anal. Bioanal. Chem. 372, 401–403. https://doi.org/10.1007/s00216-001-1144-3.

Britton, G., 1995. UV/VIS spectroscopy. In: Britton, G., Liaaen-Jensen, S., Pfander, H. (Eds.), Carotenoids. Birkhäuser, Basel, pp. 13–62.

Britton, G., Liaaen-Jensen, S., Pfander, H., 2008. Carotenoids Volume 4: Natural Functions (Eds.). Birkhäuser, Basel.

Busquets, A., Keim, V., Closa, M., del Arco, A., Boronat, A., Arró, M., Ferrer, A., 2008. *Arabidopsis thaliana* contains a single gene encoding squalene synthase. Plant Mol. Biol. 67, 25–36. https://doi.org/10.1007/s11103-008-9299-3.

Callari, R., Meier, Y., Ravasio, D., Heider, H., 2018. Dynamic control of *ERG20* and *ERG9* expression for improved casbene production in *Saccharomyces cerevisiae*. Front. Bioeng. Biotechnol. 6, 160. https://doi.org/10.3389/fbioe.2018.00160.

Chen, F., Tholl, D., Bohlmann, J., Pichersky, E., 2011. The family of terpene synthases in plants: a mid-size family of genes for specialized metabolism that is highly diversified throughout the kingdom. Plant J. 66, 212–229. https://doi.org/10.1111/j.1365-313X.2011.04520.x.

Chory, J., Donohue, T.J., Varga, A.R., Staehelin, L.A., Kaplan, S., 1984. Induction of the photosynthetic membranes of *Rhodopseudomonas sphaeroides*: biochemical and morphological studies. J. Bacteriol. 159, 540–554.

Cravens, A., Payne, J., Smolke, C.D., 2019. Synthetic biology strategies for microbial biosynthesis of plant natural products. Nat. Commun. 10, 2142. https://doi.org/10.1038/s41467-019-09848-w.

Dahl, R.H., Zhang, F., Alonso-Gutierrez, J., Baidoo, E., Batth, T.S., Redding-Johanson, A. M., Petzold, C.J., Mukhopadhyay, A., Lee, T.S., Adams, P.D., Keasling, J.D., 2013. Engineering dynamic pathway regulation using stress-response promoters. Nat. Biotechnol. 31, 1039–1046. https://doi.org/10.1038/nbt.2689.

Das, A., Yoon, S.-H., Lee, S.-H., Kim, J.-Y., Oh, D.-K., Kim, S.-W., 2007. An update on microbial carotenoid production: application of recent metabolic engineering tools. Appl. Microbiol. Biotechnol. 77, 505–512. https://doi.org/10.1007/s00253-007-1206-3.

Dickschat, J.S., 2016. Bacterial terpene cyclases. Nat. Prod. Res. 33, 87–110. https://doi.org/10.1039/c5np00102a.

Dueber, M.T., Adolf, W., West, C.A., 1978. Biosynthesis of the diterpene phytoalexin casbene: partial purification and characterization of casbene synthetase from *Ricinis communis*. Plant Physiol. 62, 598–603. https://doi.org/10.1104/pp.62.4.598.

Dufossé, L., 2017. Current carotenoid production using microorganisms. In: Singh, O. (Ed.), Bio-Pigmentation and Biotechnological Implementations. Wiley & Sons, pp. 87–106. https://doi.org/10.1002/9781119166191.ch4.

Efferth, T., 2017. From ancient herb to modern drug: *Artemisia annua* and artemisinin for cancer therapy. Semin. Cancer Biol. 46, 65–83. https://doi.org/10.1016/j.semcancer.2017.02.009.

Fox, C.B., 2009. Squalene emulsions for parenteral vaccine and drug delivery. Molecules 14, 3286–3312. https://doi.org/10.3390/molecules14093286.

Frank, A., Groll, M., 2017. The methylerythritol phosphate pathway to isoprenoids. Chem. Rev. 117, 5675–5703. https://doi.org/10.1021/acs.chemrev.6b00537.

Frigaard, N.U., 2016. Biotechnology of anoxygenic phototrophic bacteria. Adv. Biochem. Eng. Biotechnol. 156, 139–154. https://doi.org/10.1007/10_2015_5006.

Gohil, N., Bhattacharjee, G., Khambhati, K., Braddick, D., Singh, V., 2019. Engineering strategies in microorganisms for the enhanced production of squalene: advances, challenges and opportunities. Front. Bioeng. Biotechnol. 7, 50. https://doi.org/10.3389/fbioe.2019.00050.

Hage-Hülsmann, J., Metzger, S., Wewer, V., Buechel, F., Troost, K., Thies, S., Loeschcke, A., Jaeger, K.-E., Drepper, T., 2019. Biosynthesis of cycloartenol by expression of plant and bacterial oxidosqualene cyclases in engineered *Rhodobacter capsulatus*. J. Biotechnol. X 4, 100014. https://doi.org/10.1016/j.btecx.2020.100014.

Han, J.Y., Seo, S.H., Song, J.M., Lee, H., Choi, E.-S., 2018. High-level recombinant production of squalene using selected *Saccharomyces cerevisiae* strains. J. Ind. Microbiol. Biotechnol. 45, 239–251. https://doi.org/10.1007/s10295-018-2018-4.

Hanahan, D., 1983. Studies on transformation of *Escherichia coli* with plasmids. J. Mol. Biol. 166, 557–580. https://doi.org/10.1016/S0022-2836(83)80284-8.

Heck, A., Drepper, T., 2017. Engineering photosynthetic α-proteobacteria for the production of recombinant proteins and terpenoids. In: Hallenbeck, P.C., Cham, S.I. P. (Eds.), Modern Topics in the Phototrophic Prokaryotes: Environmental and Applied Aspects. Springer International Publishing, pp. 395–425, 395–425.

Huang, Z.-R., Lin, Y.-K., Fang, J.-Y., 2009. Biological and pharmacological activities of squalene and related compounds: potential uses in cosmetic dermatology. Molecules 14, 540–554. https://doi.org/10.3390/molecules14010540.

Hümbelin, M., Thomas, A., Lin, J., Li, J., Jore, J., Berry, A., 2002. Genetics of isoprenoid biosynthesis in *Paracoccus zeaxanthinifaciens*. Gene 297, 129–139. https://doi.org/10.1016/S0378-1119(02)00877-6.

Hunter, C.N., Hundle, B.S., Hearst, J.E., Lang, H.P., Gardiner, A.T., Takaichi, S., Cogdell, R.J., 1994. Introduction of new carotenoids into the bacterial photosynthetic apparatus by combining the carotenoid biosynthetic pathways of *Erwinia herbicola* and *Rhodobacter sphaeroides*. J. Bacteriol. 176, 3692–3697. https://doi.org/10.1128/jb.176.12.3692-3697.1994.

Kallscheuer, N., Classen, T., Drepper, T., Marienhagen, J., 2018. Production of plant metabolites with applications in the food industry using engineered microorganisms. Curr. Opin. Biotechnol. 56, 7–17. https://doi.org/10.1016/j.copbio.2018.07.008.

Katabami, A., Li, L., Iwasaki, M., Furubayashi, M., Saito, K., Umeno, D., 2015. Production of squalene by squalene synthases and their truncated mutants in *Escherichia coli*. J. Biosci. Bioeng. 119, 165–171. https://doi.org/10.1016/j.jbiosc.2014.07.013.

Khan, N.E., Nybo, S.E., Chappell, J., Curtis, W.R., 2015. Triterpene hydrocarbon production engineered into a metabolically versatile host - *Rhodobacter capsulatus*. Biotechnol. Bioeng. 112, 1523–1532. https://doi.org/10.1002/bit.25573.

King, A.J., Brown, G.D., Gilday, A.D., Larson, T.R., Graham, I.A., 2014. Production of bioactive diterpenoids in the *Euphorbiaceae* depends on evolutionarily conserved gene clusters. Plant Cell 26, 3286–3298. https://doi.org/10.1105/tpc.114.129668.

Kirby, J., Nishimoto, M., Park, J.G., Withers, S.T., Nowroozi, F., Behrendt, D., Rutledge, E.J.G., Fortman, J.L., Johnson, H.E., Anderson, J.V., Keasling, J.D., 2010. Cloning of casbene and neocembrene synthases from Euphorbiaceae plants and expression in *Saccharomyces cerevisiae*. Phytochemistry 71, 1466–1473. https://doi.org/10.1016/j.phytochem.2010.06.001.

Klipp, W., Masepohl, B., Pühler, A., 1988. Identification and mapping of nitrogen fixation genes of *Rhodobacter capsulatus*: duplication of a *nifA-nifB* region. J. Bacteriol. 170, 693–699. https://doi.org/10.1128/jb.170.2.693-699.1988.

Lauersen, K.J., Wichmann, J., Baier, T., Kampranis, S.C., Pateraki, I., Møller, B.L., Kruse, O., 2018. Phototrophic production of heterologous diterpenoids and a hydroxy-functionalized derivative from *Chlamydomonas reinhardtii*. Metab. Eng. 49, 116–127. https://doi.org/10.1016/j.ymben.2018.07.005.

Le, T.T.T., Gardner, J., Hoang-Le, D., Schmidt, C.W., MacDonald, K.P., Lambley, E., Schroder, W.A., Ogbourne, S.M., Suhrbier, A., 2009. Immunostimulatory cancer chemotherapy using local ingenol-3-angelate and synergy with immunotherapies. Vaccine 27, 3053–3062. https://doi.org/10.1016/j.vaccine.2009.03.025.

Lee, S., Poulter, C.D., 2008. Cloning, solubilization, and characterization of squalene synthase from *Thermosynechococcus elongatus* BP-1. J. Bacteriol. 190, 3808–3816. https://doi.org/10.1128/JB.01939-07.

Liao, S.-G., Chen, H.-D., Yue, J.-M., 2009. Plant orthoesters. Chem. Rev. 109, 1092–1140. https://doi.org/10.1021/cr0782832.

Loeschcke, A., Markert, A., Wilhelm, S., Wirtz, A., Rosenau, F., Jaeger, K.-E., Drepper, T., 2013. TREX: a universal tool for the transfer and expression of biosynthetic pathways in bacteria. ACS Synth. Biol. 2, 22–33. https://doi.org/10.1021/sb3000657.

Loeschcke, A., Dienst, D., Wewer, V., Hage-Hülsmann, J., Dietsch, M., Kranz-Finger, S., Hüren, V., Metzger, S., Urlacher, V.B., Gigolashvili, T., Kopriva, S., Axmann, I.M., Drepper, T., Jaeger, K.-E., 2017. The photosynthetic bacteria *Rhodobacter capsulatus* and *Synechocystis* sp. PCC 6803 as new hosts for cyclic plant triterpene biosynthesis. PLoS One 12, e0189816. https://doi.org/10.1371/journal.pone.0189816.

Lombard, J., Moreira, D., 2011. Origins and early evolution of the mevalonate pathway of isoprenoid biosynthesis in the three domains of life. Mol. Biol. Evol. 28, 87–99. https://doi.org/10.1093/molbev/msq177.

López, J., Cataldo, V.F., Peña, M., Saa, P.A., Saitua, F., Ibaceta, M., Agosin, E., 2019. Build your bioprocess on a solid strain—β-carotene production in recombinant *Saccharomyces cerevisiae*. Front. Bioeng. Biotechnol. 7, 171. https://doi.org/10.3389/fbioe.2019.00171.

Luo, D., Callari, R., Hamberger, B., Wubshet, S.G., Nielsen, M.T., Andersen-Ranberg, J., Hallström, B.M., Cozzi, F., Heider, H., Møller, B.L., Staerk, D., Hamberger, B., 2016. Oxidation and cyclization of casbene in the biosynthesis of *Euphorbia* factors from mature seeds of *Euphorbia lathyris* L. Proc. Natl. Acad. Sci. U.S.A. 113, E5082–E5089. https://doi.org/10.1073/pnas.1607504113.

Mahizan, N.A., Yang, S.-K., Moo, C.-L., Song, A.A.-L., Chong, C.-M., Chong, C.-W., Abushelaibi, A., Lim, S.-H.E., Lai, K.-S., 2019. Terpene derivatives as a potential agent against antimicrobial resistance (AMR) pathogens. Molecules 24, 2631. https://doi.org/10.3390/molecules24142631.

Marienhagen, J., Bott, M., 2013. Metabolic engineering of microorganisms for the synthesis of plant natural products. J. Biotechnol. 163, 166–178. https://doi.org/10.1016/j.jbiotec.2012.06.001.

Mau, C.J.D., West, C.A., 1994. Cloning of casbene synthase cDNA: evidence for conserved structural features among terpenoid cyclases in plants. Proc. Natl. Acad. Sci. U.S.A. 91, 8497–8501. https://doi.org/10.1073/pnas.91.18.8497.

Misawa, N., Nakagawa, M., Kobayashi, K., Yamano, S., Izawa, Y., Nakamura, K., Harashima, K., 1990. Elucidation of the *Erwinia uredovora* carotenoid biosynthetic pathway by functional analysis of gene products expressed in *Escherichia coli*. J. Bacteriol. 172, 6704–6712. https://doi.org/10.1128/jb.172.12.6704-6712.1990.

Moesta, P., West, C., 1985. Casbene synthetase: regulation of phytoalexin biosynthesis in *Ricinus communis* L. seedlings. Purification of casbene synthetase and regulation of its biosynthesis during elicitation. Arch. Biochem. Biophys. 238, 325–333. https://doi.org/10.1016/0003-9861(85)90171-7.

Mortensen, A., 2006. Carotenoids and other pigments as natural colorants. Pure Appl. Chem. 78, 1477–1491. https://doi.org/10.1351/pac200678081477.

Moser, S., Pichler, H., 2019. Identifying and engineering the ideal microbial terpenoid production host. Appl. Microbiol. Biotechnol. 103, 5501–5516. https://doi.org/10.1007/s00253-019-09892-y.

Ohtake, K., Saito, N., Shibuya, S., Kobayashi, W., Amano, R., Hirai, T., Sasaki, S., Nakano, C., Hoshino, T., 2014. Biochemical characterization of the water-soluble squalene synthase from *Methylococcus capsulatus* and the functional analyses of its two DXXD(E)D motifs and the highly conserved aromatic amino acid residues. FEBS J. 281, 5479–5497. https://doi.org/10.1111/febs.13090.

Okada, S., Devarenne, T.P., Chappell, J., 2000. Molecular characterization of squalene synthase from the green microalga *Botryococcus braunii*. Race B. Arch. Biochem. Biophys. 373, 307–317. https://doi.org/10.1006/abbi.1999.1568.

Orsi, E., Folch, P.L., Monje-López, V.T., Fernhout, B.M., Turcato, A., Kengen, S.W.M., Eggink, G., Weusthuis, R.A., 2019. Characterization of heterotrophic growth and sesquiterpene production by *Rhodobacter sphaeroides* on a defined medium. J. Ind. Microbiol. Biotechnol. 46, 1179–1190. https://doi.org/10.1007/s10295-019-02201-6.

Orsi, E., Beekwilder, J., van Gelder, D., van Houwelingen, A., Eggink, G., Kengen, S.W. M., Weusthuis, R.A., 2020. Functional replacement of isoprenoid pathways in *Rhodobacter sphaeroides*. Microb. Biotechnol. 13, 1082–1093. https://doi.org/10.1111/1751-7915.13562.

Orsi, E., Beekwilder, J., Eggink, G., Kengen, S.W.M., Weusthuis, R.A., 2021. The transition of *Rhodobacter sphaeroides* into a microbial cell factory. Biotechnol. Bioeng. 118, 531–541. https://doi.org/10.1002/bit.27593.

Park, J., Zielinski, M., Magder, A., Tsantrizos, Y.S., Berghuis, A.M., 2017. Human farnesyl pyrophosphate synthase is allosterically inhibited by its own product. Nat. Commun. 8, 14132. https://doi.org/10.1038/ncomms14132.

Qiang, S., Su, A.P., Li, Y., Chen, Z., Hu, C.Y., Meng, Y.H., 2019. Elevated *β*-carotene synthesis by the engineered *Rhodobacter sphaeroides* with enhanced CrtY expression. J. Agric. Food Chem. 67, 9560–9568. https://doi.org/10.1021/acs.jafc.9b02597.

Qiao, W., Zhou, Z., Liang, Q., Mosongo, I., Li, C., Zhang, Y., 2019. Improving lupeol production in yeast by recruiting pathway genes from different organisms. Sci. Rep. 9, 2992. https://doi.org/10.1038/s41598-019-39497-4.

Reddy, L.H., Couvreur, P., 2009. Squalene: a natural triterpene for use in disease management and therapy. Adv. Drug Deliv. Rev. 61, 1412–1426. https://doi.org/10.1016/j.addr.2009.09.005.

Reiling, K.K., Yoshikuni, Y., Martin, V.J.J., Newman, J., Bohlmann, J., Keasling, J.D., 2004. Mono and diterpene production in *Escherichia coli*. Biotechnol. Bioeng. 87, 200–212. https://doi.org/10.1002/bit.20128.

Saini, R.K., Keum, Y.-S., 2019. Microbial platforms to produce commercially vital carotenoids at industrial scale: an updated review of critical issues. J. Ind. Microbiol. Biotechnol. 46, 657–674. https://doi.org/10.1007/s10295-018-2104-7.

Sandmann, G., 1994. Carotenoid biosynthesis in microorganisms and plants. Eur. J. Biochem. 223, 7–24. https://doi.org/10.1111/j.1432-1033.1994.tb18961.x.

Schempp, F.M., Drummond, L., Buchhaupt, M., Schrader, J., 2018. Microbial cell factories for the production of terpenoid flavor and fragrance compounds. J. Agric. Food Chem. 66, 2247–2258. https://doi.org/10.1021/acs.jafc.7b00473.

Schierle, J., Pietsch, B., Ceresa, A., Fizet, C., Waysek, E.H., 2004. Method for the determination of β-carotene in supplements and raw materials by reversed-phase liquid chromatography: single laboratory validation. J. AOAC Int. 87, 1070–1082.

Schmidt-Dannert, C., 2014. Biosynthesis of terpenoid natural products in fungi. In: Schrader, J., Bohlmann, J. (Eds.), Biotechnology of Isoprenoids. Advances in Biochemical Engineering/Biotechnology. Springer, Cham, pp. 19–61. https://doi.org/10.1007/10_2014_283.

Simon, R., Priefer, U., Pühler, A., 1983. A broad host range mobilization system for *in vivo* genetic engineering: transposon mutagenesis in Gram negative bacteria. Nat. Biotechnol. 1, 784–791. https://doi.org/10.1038/nbt1183-784.

Strnad, H., Lapidus, A., Paces, J., Ulbrich, P., Vlcek, C., Paces, V., Haselkorn, R., 2010. Complete genome sequence of the photosynthetic purple nonsulfur bacterium *Rhodobacter capsulatus* SB 1003. J. Bacteriol. 192, 3545–3546. https://doi.org/10.1128/JB.00366-10.

Thimmappa, R., Geisler, K., Louveau, T., O'Maille, P., Osbourn, A., 2014. Triterpene biosynthesis in plants. Annu. Rev. Plant Biol. 65, 225–257. https://doi.org/10.1146/annurev-arplant-050312-120229.

Thompson, J.F., Danley, D.E., Mazzalupo, S., Milos, P.M., Lira, M.E., Harwood Jr, H.J., 1998. Truncation of human squalene synthase yields active, crystallizable protein. Arch. Biochem. Biophys. 350, 283–290. https://doi.org/10.1006/abbi.1997.0502.

Troost, K., Loeschcke, A., Hilgers, F., Özgür, A.Y., Weber, T.M., Santiago-Schübel, B., Svensson, V., Hage-Hülsmann, J., Habash, S.S., Grundler, F.M.W., Schleker, A.S.S., Jaeger, K.-E., Drepper, T., 2019. Engineered *Rhodobacter capsulatus* as a phototrophic platform organism for the synthesis of plant sesquiterpenoids. Front. Microbiol. 10, 1998. https://doi.org/10.3389/fmicb.2019.01998.

Wichuk, K., Brynjólfsson, S., Fu, W., 2014. Biotechnological production of value-added carotenoids from microalgae: emerging technology and prospects. Bioengineered 5, 204–208. https://doi.org/10.4161/bioe.28720.

Wołosik, K., Knaś, M., Zalewska, A., Niczyporuk, M., Przystupa, A.W., 2013. The importance and perspective of plant-based squalene in cosmetology. J. Cosmet. Sci. 64, 59–66.

Wong, J., de Rond, T., D'Espaux, L., van der Horst, C., Dev, I., Rios-Solis, L., Kirby, J., Scheller, H., Keasling, J., 2018. High-titer production of lathyrane diterpenoids from sugar by engineered *Saccharomyces cerevisiae*. Metab. Eng. 45, 142–148. https://doi.org/10.1016/j.ymben.2017.12.007.

Xu, W., Ma, X., Wang, Y., 2016. Production of squalene by microbes: an update. World J. Microbiol. Biotechnol. 32, 195. https://doi.org/10.1007/s11274-016-2155-8.

Yang, J., Guo, L., 2014. Biosynthesis of β-carotene in engineered *E. coli* using the MEP and MVA pathways. Microb. Cell Fact. 13, 160. https://doi.org/10.1186/s12934-014-0160-x.

Yoshida, M., Tanabe, Y., Yonezawa, N., Watanabe, M.M., 2012. Energy innovation potential of oleaginous microalgae. Biofules 3, 761–781. https://doi.org/10.4155/bfs.12.63.

Yuan, S.-F., Alper, H.S., 2019. Metabolic engineering of microbial cell factories for production of nutraceuticals. Microb. Cell Fact. 18, 46. https://doi.org/10.1186/s12934-019-1096-y.

Zhang, D., Jennings, S.M., Robinson, G.W., Poulter, C.D., 1993. Yeast squalene synthase: expression, purification, and characterization of soluble recombinant enzyme. Arch. Biochem. Biophys. 304, 133–143. https://doi.org/10.1006/abbi.1993.1331.

III. GENERAL DISCUSSION

Within this thesis, versatile light-responsive tools for controlling biological functions on various cellular levels were established in *E. coli*, transferred to alternative expression hosts such as *P. putida* or *R. capsulatus* and finally applied in first biotechnological applications. First, existing tools for light-mediated control of transcription were extended by additional variants including both yet unestablished promoter systems and photocaged inducer molecules, as well as more advanced protecting groups to modulate factors such as compound solubility or absorption wavelength (**chap. II.1**). Second, fluorescent proteins were characterized with respect to their photophysical and photosensitizing properties *in vitro* and were subsequently applied for the killing of several Gram-positive and Gram-negative bacteria (**chap. II.2**). Finally, biosynthetic pathways of natural products such as various terpenes were established in the alternative production hosts *R. capsulatus* (**chap. II.3**). Additionally, associated publications of several cooperation partners are listed and discussed, offering either tools for online-monitoring of intra- and intercellular processes or first application possibilities of the previously established light-responsive tools (**Fig. III.1**).

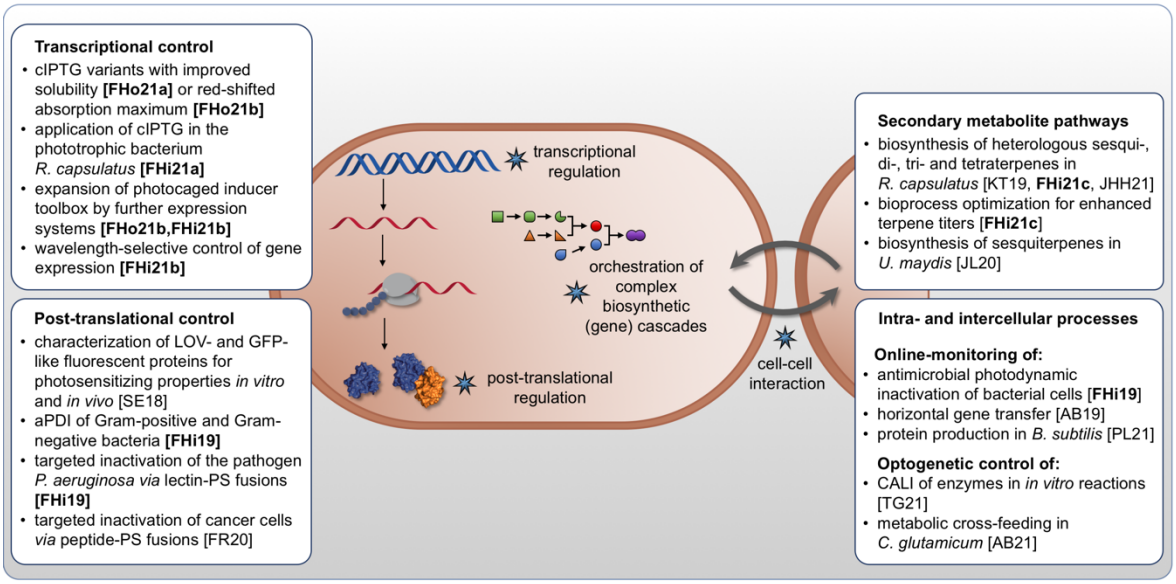

Figure III.1 Optogentic systems developed and co-developed within this work and in associated publications of cooperation partners.
The established regulatory systems adressed various levels including the transcriptional, post-translational and cellular level. Furthermore, implemented biosynthetic pathways and cellular processes that could be online-monitored or optogenetically controlled are listed. To simplify the assignment, the manuscripts have been given abbreviations in brackets. These consist of the initials of the main author and the year of publication. Multiple publications in the same year are further indicated by an additional letter. Publications as main author are marked in bold letters. References: **FHo21a** [501], **FHo21b** [502], **FHi21a** [503], **FHi21b** [504], SE18 [505], **FHi19** [506], FR20 [507], KT19 [188], **FHi21c** [189], JHH21 [508], JL20 [509], AB19 [510], PL21 [511], TG21 [512], AB21 [513].

In the following section, the optogenetic tools, secondary metabolite pathways and online-monitoring concepts for intracellular processes developed and described in **chapters II.1 - II.3** will be summarized (**chap. III.1**). Further, the optogenetic tools, namely the photocaged inducers and photosensitizers, are discussed in the context of possible optimization strategies (**chap. III.2**). Finally, selected application fields of the established optogenetic tools, such as the orchestration of secondary metabolite pathways or the regulation of cell-cell interactions to engineer artificial microbial consortia, will be elucidated to underline the broad applicability of optogenetic control systems and to guide future studies (**chap. III.3**). To simplify the assignment, the manuscripts have been given abbreviations in brackets. These consist of the initials of the main author and the year of publication. Multiple publications in the same year are further indicated by an additional letter. Publications as main author are marked in bold letters.

III.1. Optogenetic tools, secondary metabolite production chassis and visualization strategies of cellular processes

III.1.1. Tools for light-mediated transcriptional control

The possibility to precisely control and orchestrate the expression of heterologous genes or complete gene clusters is fundamental for efficient protein production and successful implementation of foreign secondary metabolite pathways in bacterial hosts, since it guarantees both a balanced energy and metabolic burden. For this purpose, various light-responsive switches suitable for transcriptional control based on photocaged inducer molecules were established and evaluated not only in *E. coli*, but also in alternative production hosts such as *B. subtilis*, *R. capsulatus*, or *P. putida* (**chap. II.1** [501–504]). In the following, the results are briefly summarized, considering the individual features and findings of each system and the most important aspects are concluded in **Table III.1**. Initially, the previously established NP-photocaged IPTG [231,514], which exhibits a limited solubility in water-based systems, was complemented by two further cIPTG variants with differing hydrophobicity [**FHo21a**, 501]. BC-cIPTG bears hydrophilic carboxylic side chains, while BEC-cIPTG additionally harbors lipophilic ester moieties, which could facilitate an improved passive membrane uptake. In *E. coli*, the differential solubility of tested photocaged IPTG variants seems to play a minor role for optochemical *in vivo* applications, since NP-cIPTG remains the best suited variant followed by BC-cIPTG. For *P. putida* and *B. subtilis*, however, BC-cIPTG proved to be a well-suited alternative, as it exhibits an induction level of around 70% and up to 100% in comparison

to IPTG, respectively. In further studies, all three derivatives were applied for the light-mediated control of gene expression in the alternative host *R. capsulatus* under phototrophic and non-phototrophic conditions [**FHi21a**, 503]. Here, especially NP-cIPTG proved valuable under all three growth conditions, as it offers a sufficient responsiveness and even exceeds the induction level of IPTG under microaerobic and phototrophic conditions. In contrast, BC- and BEC-cIPTG, although they also reached the induction level of IPTG, were subject to a severe instability effect *in vivo* and thus, are not applicable for light-mediated control of transcription in this host.

Table III.1 Comparison of established tools for light-responsive on-switches for transcriptional control in bacteria. For each expression system, the highest expression levels are highlighted in green, underlining the suitability of the respective caged inducers. Specific numeral designation of each photocaged compound within the respective primary publication: NP-cIPTG **1**, BC-cIPTG **10b**, BEC-cIPTG **10a**, DC-2-cIPTG **1b**, DC-6-cIPTG **1d**, DCC-cIPTG **1c**, DC-cAra **2b**, DC-NN-cAra **2c**, BC-cSal **21**, BC-cSal*Na **25**, DC-cSal **5**, DC-cSal*Na **6**, NB-cIPTG **4**.

Compound		Expression system	Expression level [x-fold] [a]	Expression level [%] [b]	Advantages	Applicability [c] (challenges)	Ref.
Photo-caged IPTG	NP-cIPTG	*E. coli* Tuner(DE3) LacI/P_{T7}	115	96	Low working concentrations (50 µM), strong and tight induction	+++ (low solubility of NP-cIPTG, two-step photorelease)	**FHo21a** [501]
	BC-cIPTG		84	80			
	BEC-cIPTG		24	85			
Photo-caged IPTG	NP-cIPTG	*P. putida* KT2440 LacI/P_{tac}	3	32	BC-cIPTG reaches 65% of IPTG induction	++ (high working concentrations (1 mM), low induction level)	
	BC-cIPTG		5	65			
	BEC-cIPTG		3	45			
Photo-caged IPTG	NP-cIPTG	*B. subtilis* DB430 LacI/P_{grac}	20	52	Strong and fast induction, BC-cIPTG comparable to IPTG induction	+++ (high working concentrations (1 mM))	
	BC-cIPTG		15	100			
	BEC-cIPTG		7	77			
Photo-caged IPTG	NP-cIPTG	*R. capsulatus* SB1003 (high/low/no O_2) LacI/P_{tac}	(3/6/4)	(65/103/157)	NP-cIPTG exceeds IPTG under low/ no O_2 conditions	++ (high working concentrations (1 mM), high basal expression[d], BC- & BEC-cIPTG not stable *in vivo*)	**FHi21a** [503]
	BC-cIPTG		(1.3/1.3/1.2)	(109/136/158)			
	BEC-cIPTG		(2/2/2)	(75/110/111)			

Table III.1 continued.

Compound		Expression system	Expression level [x-fold] [a]	Expression level [%] [b]	Advantages	Applicability [c] (challenges)	Ref.
Photo-caged IPTG	DC-2-cIPTG [e]	*E. coli* Tuner(DE3) LacI/P_{T7}	4	90	Blue-light responsive, low working concentrations (50 µM)	++ (reduced compound stability in dark controls)	**FHo21b** [502]
	DC-6-cIPTG [e]		3	77			
	DCC-cIPTG		3	81			
Photo-caged arabi-nose	DC-cAra	*E. coli* LMG194 AraC/P_{BAD}	3	20	Blue-light responsive, low working concentrations	+ (low induction level) [g]	
	DC-NN-cAra [f]		4	48			
Photo-caged salicylic acid	BC-cSal	*E. coli* Tuner(DE3) NagR/P_{nagAa}	3	106	BC-cIPTG induction level comparable to Sal	+ (high working concentrations (1 mM), low compound stability in dark controls	
	BC-cSal *Na		2	106			
Photo-caged salicylic acid	BC-cSal	*P. putida* KT2440 NagR/P_{nagAa}	0.9	204	Blue-light responsive, low working concentrations, DC-NN-cSal significantly exceeds Sal induction level	+++ (BC-cSal variants are not stable *in vivo*)	**FHi21b** [504]
	BC-cSal *Na		1.0	206			
	DC-NN-cSal [f]		4	182			
	DC-NN-cSal*Na [f]		2	187			
Photo-caged IPTG	NB-cIPTG	*P. putida* KT2440 LacI/P_{tac}	9	43	Compatible for multichromatic system, Good compound stability, low basal expression	++ (only ~40% induction in comparison to IPTG)	

[a] expression level of induced cultures in comparison to the expression level under non-induced conditions
[b] expression level of caged compound in comparison to conventional inducer in equimolar concentration
[c] suitability of the system indicated by the number of pluses, where one + means limited suitability and +++ means excellent suitability.
[d] high basal expression of this system could be abolished *via* overexpression of *lac* repressor
[e] the respective number indicates the linkage position (2-OH vs. 6-OH) of the caging group at IPTG
[f] NN= abbreviation for photocaged compound variant with carbamate linker between protection group and inducer molecule
[g] photolysis could be improved by an alternative linker

Additionally, intrinsic carotenoid production of *R. capsulatus* was light controlled by using photocaged IPTG. The induction with NP-cIPTG led to an elevated induction response in comparison to cultures induced with IPTG and thus underlines the broad applicability of photocaged inducers for controlling metabolic pathways (see **chap. III.3.2**). In addition to photocaged IPTG variants with altered water solubility, further variants with red-shifted absorption maxima were constructed and applied *in vivo* to avoid the need for UV-A light exposure and to allow additional applications as part of an optogenetic multi-wavelength control system [**FHo21b** 502]. For this purpose, coumarin-based protection groups, such as diethylaminocoumarin (DC) or dicyanocoumarin (DCC), were exploited and linked to the respective inducer molecule through carbonate, carbamate, or ether bonds. In comparison to NB-based photocages, they offer a bathochromatically-shifted absorption maximum and thus can be addressed with blue light (**Fig. III.2**). In *E. coli*, the three carbonate variants DC-2-cIPTG, DC-6-cIPTG and DCC-cIPTG exhibited a high induction level, which for the former was comparable to cultures induced with IPTG. However, all blue light-responsive variants suffered from elevated induction levels in the unexposed cultures, possibly due to reduced compound stability under *in vivo* conditions [**FHo21b** 502]. Besides photocaged IPTG, also photocaged arabinose was tested with a coumarin-based protection group fused either *via* an ether bond (DC-cAra) or *via* an additional linker and a carbamate bond (DC-NN-cAra) to allow for a reliable and precise photorelease upon illumination [**FHo21b** 502].

A

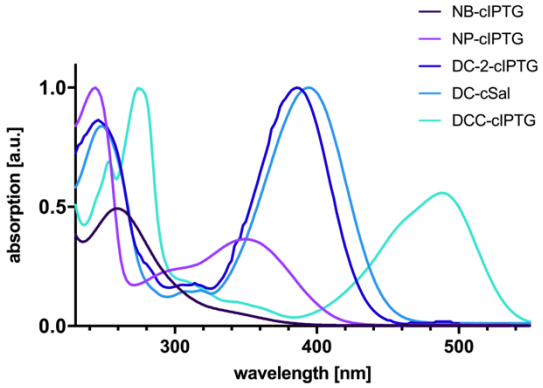

B

Compound	Designation in manuscript	Absorption maxima [nm]	Reference
NB-cIPTG	4	260	**FHi21b** [504]
NP-cIPTG BC-cIPTG BEC-cIPTG	1 10b 10a	336 340 298	**FHo21a** [501]
BC-cSal	21	346	**FHo21b** [502]
DC-2-cIPTG DC-6-cIPTG	1b 1d	386 386	**FHo21b** [502]
DC-cAra DC-NN-cAra	2b 2c	388 385	**FHo21b** [502]
DC-cSal	5	394	**FHi21b** [504]
DCC-cIPTG	1c	488	**FHo21b** [502]

Figure III.2 Photophysical properties of photocaged compounds established within several manuscripts in the framework of this thesis.
A) UV-Vis spectra of selected photocaged compounds are exemplarily shown demonstrating the obtained red-shift of the newly synthesized variants in comparison to the well-established NB and NP protection groups, which are UV light-responsive. **B)** Absorption maxima of each photocaged inducer applied in this work. Additionally, the specific numeral designation of each compound within the respective publication is indicated to facilitate the assignment. NB: nitrobenzyl, NP: nitropiperonyl, DC: diethylaminocoumarin, DCC: dicyanocoumarin, Sal: salicylic acid, Ara: arabinose, NN: carbamate linker.

In this case, only the DC-NN-cAra variant showed a sufficient induction response of about 50% in comparison to arabinose, while the other cAra derivative exhibited an

insufficient photolysis as also underlined by *in vitro* measurements. Finally, the group of photocaged inducer molecules was extended by four new derivatives based on salicylic acid [**FHo21b** 502], which, in comparison to most of the established photocages, addresses toluate or benzoate-based expression systems that are especially well known for transcriptional regulation in pseudomonads [98,124]. BC-cSal and its sodium salt form BC-cSal*Na were successfully applied in *E. coli* and the former exhibited an induction level comparable to salicylic acid. However, elevated hydrolysis in unexposed cultures could be observed for both variants. In *P. putida*, BC-cSal and the blue light-responsive, coumarin-based DC-cSal were applied in their acidic and sodium salt form and while both BC-cSal derivatives exhibited an insufficient stability under unexposed conditions, DC-cSal in its acidic form could be successfully applied for light-mediated control of gene expression with remarkably low working concentrations of 50 µM [**FHi21b** 504]. Further, DC-cSal could be combined with the UV-absorbing NB-cIPTG to form a novel two-wavelength induction system in *P. putida*. Although NB-cIPTG only exhibited an induction level of around 40% in comparison to IPTG, the system did not show high basal expression and the compound stability was sufficient, so that the expression of two genes could be individually controlled *via* UV-A and blue light exposure, respectively.

In summary, photocaged inducer molecules have proven to be a valuable tool for the light-mediated control of transcription. Not only various inducer molecules belonging to the group of carbohydrates and benzoates, but also versatile protection groups with altered properties such as solubility or a bathochromic shift were successfully utilized for photocaged compound synthesis and *in vivo* application in *E. coli*. Furthermore, selected photocaged inducers were transferred to promising alternative expression hosts such as *B. subtilis*, *P. putida* or *R. capsulatus*.

III.1.2. Light-mediated post-translational control of cell viability

Cellular processes can be regulated not only by protein-protein interactions, but also by protein-cell interactions. In this context, the use of proteins to control cell viability is a particularly valuable approach, which is applied for the control of bacterial populations in mono- or co-cultures, such as in antimicrobial photodynamic inactivation (aPDI) or for the inactivation of tumor cells in photodynamic therapy (PDT). A well-established method for inactivation of target cells is the use of photosensitizers, which produce both short-lived and longer-lived ROS species upon illumination. Besides chemical-based photosensitizers, fluorescent proteins are frequently used as genetically encoded photosensitizers, since they offer several benefits including their good biocompatibility

and their straightforward and flexible application based on a targeted localization and the possibility for genetic fusion with the target protein [368,369]. Hence, various LOV- and GFP-based fluorescent proteins were analyzed in this work with respect to their photophysical and photosensitizing properties and subsequently applied for killing of different Gram-positive and Gram-negative bacteria. The evaluated genetically encoded photosensitizers and their photosensitizing *in vitro* and *in vivo* properties are listed in **Table III.2**.

Table III.2 Photophysical and photosensitizing properties of LOV- and GFP-like photosensitizers. Red boxes indicate the most toxic PS variants with either mostly type I ROS production (upper box) or the production of both ROS types (lower box). The respective publication is indicated by a reference, whereby the associated publications can be assigned to the following abbreviation: [505] SE18, [506] **FHi19**. The H_2O_2 formation and toxicity of each PS is indicated by the number of pluses, where – means barely any H_2O_2 production/ phototoxicity and + to ++++ means low to high H_2O_2 production/ phototoxicity. n.d.: not determined.

Name	Excitation/ Emission λ_{max} [nm]	Singlet oxygen quantum yield Φ_Δ [505]	H_2O_2/ $O_2^{\bullet-}$ formation [505,506]	*In vivo* phototoxicity [505,506]		Extracellular phototoxicity [506]	
				CFU	PI	Gram –	Gram +
Pp1FbFP	450/496	0.23	–	n.d.	++	+	++
Pp2FbFP	449/495	0.11	–	n.d.	+	+	++
EcFbFP	448/496	0.07	++	++	++	++	+
iLOV	450/497	0.05	+	n.d.	++	n.d.	n.d.
phiLOV2.1	450/497	0.01	–	+	–	n.d.	n.d.
DsFbFP	449/495	0.33	++	++	–	n.d.	n.d.
DsFbFP M49I	450/498	0.42	+++	+++	+++	+++	+
SOPP	440/490	0.25	++	n.d.	+++	n.d.	n.d.
SOPP3	439/490	0.60 [346]	++++	++++	++++	+	+
KillerOrange	455/514	n.d.	+	+	+	+	–
SuperNova	579/610	0.02 [515]	+	–	+	–	–

As aforementioned (**chap. I.2.2**), photosensitizers can produce ROS *via* the type I or the type II mechanism, resulting either in the production of superoxide radical anion ($O_2^{\bullet-}$), hydrogen peroxide (H_2O_2), and hydroxyl radical ($HO^{\bullet}$) or in the formation of singlet oxygen ($^1O_2$). Interestingly, the evaluated PSs can be assigned to two subgroups – PSs that mainly produce $^1O_2$, such as Pp1FbFP and Pp2FbFP, and PSs that produce both $^1O_2$ and ROS of the type I pathway (e.g., $O_2^{\bullet-}$ and H_2O_2), such as EcFbFP, DsFbFP, DsFbFP M49I, SOPP and SOPP3 [**SE18** 505, **FHi19** 506]. In general, the LOV-like PSs produced ROS in significantly higher quantities in comparison to GFP-like variants, which can among others be explained by a good oxygen accessibility of the chromophore

[516,517]. For an *in vivo* evaluation of selected PSs, both an intracellular production in *E. coli* and an extracellular addition to various Gram-negative and Gram-positive bacteria was performed [**FHi19** 506]. The intracellular production of ROS in *E. coli* resulted in differential toxicities with DsFbFP M49I, SOPP and SOPP3 being the strongest photosensitizers, which is in good correlation with the $^1O_2$ and H_2O_2 *in vitro* data (**Tab. III.2**). For an extracellular application, DsFbFP M49I and EcFbFP, which both produce type I and type II ROS, proved to be particularly valuable for the killing of Gram-negative bacteria including the pathogen *P. aeruginosa*, while Pp1FbFP and Pp2FbFP were most effective against Gram-positive bacteria, such as *Staphylococcus aureus* and *Staphylococcus epidermis*. Interestingly, SOPP3, which originally was constructed for the exclusive production of singlet oxygen and exhibits a singlet oxygen quantum yield of 0.6 [346], showed an antimicrobial spectrum similar to DsFbFP M49I and EcFbFP rather than Pp1FbFP and Pp2FbFP. This finding is in good agreement with the *in vitro* data on H_2O_2 production thereby underpinning the conclusion that SOPP3 can produce not only type I but also type II ROS.

The pathogenic species exhibited an increased resistance against all the applied PSs. While *P. aeruginosa* was severely affected only by DsFbFP M49I, EcFbFP and SOPP3, the *Staphylococcus* strains were exclusively sensitive to Pp1FbFP and Pp2FbFP, which is in good agreement with previous reports [518,519] and might be explained by the divergent membrane and cell wall morphology in terms of composition and thickness [520,521]. To further increase the toxicity for pathogenic bacteria, a PS was specifically directed to the bacterial cell envelope. For this purpose, DsFbFP M49I was genetically fused to the *P. aeruginosa*-specific lectin LecB, which binds to various sugar moieties located on the surface of *P. aeruginosa* cells. By doing so, the binding efficiency of DsFbFP M49I to the target cell could be increased over 4-fold and the extracellular antimicrobial toxicity by 3.8-fold. Within the associated master thesis of Yannic Ackermann it was further shown that SOPP3 was not well applicable as targeted photosensitizer, since an increased binding affinity upon LecB fusion could not be detected [522].

In summary, various LOV- and GFP-type fluorescent proteins were evaluated with respect to their photophysical, and photosensitizing properties and selected variants were used as genetically encoded photosensitizers for versatile applications including antimicrobial photodynamic inactivation of Gram-positive and Gram-negative bacteria.

III.1.3. ESTABLISHMENT OF SECONDARY METABOLITE PATHWAYS AS A POTENTIAL TARGET FOR OPTOGENETIC REGULATORY TOOLS

Many microbial production processes for both bulk and high-value natural products require the use of heterologous hosts, which guarantee a stable and highly productive bioprocess. However, both the production of heterologous proteins and the biosynthesis of heterologous secondary metabolites in particular pose several challenges including toxicity of heterologous secondary metabolite compounds leading to impaired growth or low production yields. Furthermore, insufficiently coordinated gene expression or enzyme activity often results in low production titers. To circumvent these disadvantages, alternative hosts are increasingly being employed for the production of bioactive compounds. In this context, metabolic engineering strategies or the application of suitable regulatory circuits are generally used to steadily increase production yields or even expand the substance spectrum by new-to-nature variants. Hence, the production of relevant high-value natural products, such as plant terpenes, in the alternative, heterologous host *R. capsulatus* was established and metabolic engineering as well as bioprocess optimization strategies were applied to improve the final product yields as summarized in **Table III.3**.

Table III.3 Successfully produced terpenoids in *R. capsulatus* and applied engineering strategies. Notably high terpene titers are highlighted in green. *R.s.*: *R. sphaeroides, S.c.: S. cerevisiae, C.g.: C. glutamicum, E.c.: E. coli.*

Terpene	Host organism/ strain	Heterologous synthase	Over-expressed genes	Product yield [mg L^{-1}]	Reference	Literature yields [mg L^{-1}]
valencene	*R. capsulatus* SB1003-MVA	CsVS (*Citrus sinensis*)	*MVA, ispA*	3	KT19 [188]	352 *R. s.* [426] 539 *S. c.* [523]
		CnVS (*Callitropsis nootkatensis*)	*MVA, ispA, dxs, idi*	18		
patchoulol		PcPS (*Pogostemon cablin*)	*MVA, ispA, dxs, idi*	24		60 *C. g.* [524]
β-caryo-phyllene		QHS1 (*Artemisia annua*)	*MVA, ispA*	139	**FHi21c** [189]	220 *E. c.* [525]
casbene	*R. capsulatus* SB1003	RcCS (*Ricinius communis*)	*ispA, dxs, idi,*	17	JHH21 [508]	>100 *S. c.* [526–528]
squalene		McSQS (*Methylococcus capsulatus*)	*ispA*	90		2000 *S. c.* [529]
β-carotene		CrtYI (*Pantoea ananatis*)	*ispA, dxs, idi,*	30		>2000 *E. c.* [530,531] >1000 *S. c.* [532]

Since *R. capsulatus* offers unique physiological properties, such as the development of an extensive intracytoplasmic membrane under phototrophic conditions for the storage of membrane-associated enzymes or hydrophobic metabolites as well as an intrinsic carotenoid biosynthesis, it is particularly well suited for biosynthesis of hydrophobic terpenoids. Therefore, *R. capsulatus* was chosen for the production of various heterologous sesqui-, di-, tri-, and tetraterpenes from both plant and bacterial origin [KT19 188, **FHi21c** 189, JHH21 508]. In any cases, the exclusive overexpression of the terpene synthase did not lead to high product titers, so that metabolic engineering was performed as one possibility for increasing terpene yields. It could be shown that the production capacity of *R. capsulatus* can be enhanced by the co-production of enzymes responsible for the precursor supply of the terpene pathway such as the FPP synthase IspA, the 1-deoxy-D-xylulose 5-phosphate synthase DxS or the isopentenyl diphosphate isomerase Idi [KT19 188, **FHi21c** 189, JHH21 508]. Furthermore, an introduction of the heterologous MVA pathway into the hosts' chromosome, which also contributes positively to the precursor synthesis, resulted in additionally increased sesquiterpene titers. Interestingly, as depicted in **Table III.3**, this metabolic engineering concept cannot simply be applied to every new target terpene, following the slogan "the more, the better", but must rather be tailored individually to each novel terpene by selecting appropriate gene combinations for co-expression to meet the requirements of the respective terpene synthase. Additionally, for sesqui- and triterpenes it could be shown that the choice of a suitable heterologous synthase is highly relevant for an optimal production process [KT19 188, JHH21 508]. Further, bioprocess optimization could positively affect the terpene yields by increasing the light or energy input during phototrophic cultivation in general as well as by adjusting the illumination spectrum from broad-spectrum bulb light to narrow-spectrum IR light [**FHi21c** 189].

In conclusion, *R. capsulatus* proved as valuable heterologous host for the biosynthesis of several classes of terpenoids of bacterial, plant or mammalian origin. By applying individually tailored metabolic engineering strategies to increase selected precursor fluxes or by bioprocess engineering, terpene titers could be increased, making this secondary metabolite pathway a promising target for precisely and straightforward light control.

III.1.4. ONLINE-MONITORING TOOLS FOR VISUALIZATION AND CONTROL OF CELLULAR PROCESSES

As described in detail in the previous sections, tools have been developed that allow for a precise regulation of biological processes on different cellular levels. However, the visualization of these intra- and particularly intercellular processes within mono- or co-cultures still represents a major challenge. Thus, visualization concepts were successfully established from milliliter to microliter scale, which allow monitoring with high spatiotemporal resolution and offer first application possibilities of the previously established light-responsive tools.

Firstly, online-monitoring of bacterial cultures during *in vivo* analysis of novel photocaged inducers was applied using a parallelized Bioreactor system on milliliter scale. Since this method offers an online-monitoring not only of growth processes and the production of various fluorescent target proteins, but also of other cultivation parameters such as the dissolved oxygen tension in the cultivation medium in real-time, it was possible to determine the induction kinetics for the afore described cIPTG derivatives in three hosts *E. coli*, *P. putida* and *B. subtilis* [**FHo21a** 501]. Further, non-phototrophic growth of *R. capsulatus* was adapted to this cultivation method in order to gain insights into the respective growth behavior and protein production level of each culture under varying growth conditions. In addition, the dissolved oxygen tension was measured during cultivation and allowed the determination of aeration conditions sufficient for aerobic or microaerobic growth [**FHi21a** 503]. Disadvantages of this online-monitored batch cultivation, however, include the lack of information on population heterogeneity related to growth, cell morphology, or individual cellular expression levels. Thus, flow cytometric analyses are commonly applied for the investigation of population heterogeneity, allowing for the analysis of millions of single cells in a short period of time. The gained data set reveals a quantitative snapshot of a microbial culture, which can be assembled into a semi-continuous measurement by adding further data sets. By this purpose, flow cytometry measurements were used to analyze the homogeneity of the light-induced antimicrobial effect of intracellularly produced photosensitizers on cells in a population [**FHi19** 506]. It could be shown that ROS-mediated cell death occurred in two phases depending on the respective illumination time. While short illumination times led to two subpopulations of PI-positive cells, after a prolonged illumination time a nearly homogeneous PI fluorescence in over 90% of the analyzed cells was observed. Additionally, control over the growth of a sub-population within an artificial consortium was partly obtained in the master thesis of Nora Bitzenhofer by intracellularly expressed photosensitizers, which led to exposure time-dependent cell death of the target cells

[533]. However, a prolonged exposure time also resulted in the inactivation of the non-expressing cell population. Thus, the phototoxicity of the PS, but even more the analysis method should be adapted to gain more insights about the spatial distribution of the ROS. Hence, this semi-continuous approach offers quantitative heterogeneity data of specific time points but is not able to perform an actual dynamic analysis of phenotypic heterogeneity including single-cell linage or the distinction between environmental or intrinsic phenotypic heterogeneity.

As an alternative method, microfluidic cultivation can be performed, which offers not only in-depth knowledge about bacterial growth, morphology, and target gene expression, but also about phenotypic heterogeneity of populations at the single-cell level under defined environmental conditions. Since the microfluidic cultivation chambers are interconnected by supply channels, this method allows for both batch and continuous flow cultivations, the latter particularly enabling long-term studies. Furthermore, a simple medium exchange for adaption of nutrient composition or inducer concentrations as well as a straightforward tracking of cell lineage is possible, in contrast to flow cytometry [534]. In this work, microfluidic single-cell analysis proved to be a valuable tool for several approaches. Firstly, this method was chosen to analyze the heterogeneity of ROS-mediated cell damage by intracellularly produced PS and the accessibility of single *E. coli* cells to extracellularly added PS proteins [**FHi19** 506]. In both cases, the cell damage was strongly dependent on the illumination time. While initially ROS only led to growth impairments without affecting cell viability, prolonged illumination led to variable damage within each cell, until further illumination finally led to a homogenization of cell damage and thus to cell death within the whole microcolony. This effect was independent of the position of the respective cell within the microcolony and could be observed although the PS fluorescence was homogeneously distributed over the whole cell population.

In conclusion, online-monitoring approaches on milliliter and microliter scale as well as on single-cell level were successfully established to investigate specific protein-cell or cell-cell interactions such as targeted cell ablation. While the microbioreactor system only offers insights into the whole batch culture, flow cytometry offers a semi-continuous and quantitative analysis of hundred thousand of cells on single-cell level. The use of microfluidics further allows for continuous monitoring of selected cells within two-dimensional microcolonies under well-defined environmental conditions and with high spatiotemporal resolution.

III.2. COMPARISON TO OPTOGENETIC SWITCHES AND OPTIMIZATION STRATEGIES FOR FUTURE STUDIES

In this section, the two established optogenetic tools, namely photocaged inducers and genetically encoded photosensitizers, are discussed in the context of alternative light-mediated control systems published recently and possible optimization approaches are elucidated to guide future studies.

III.2.1. OPTOGENETIC TOOLS FOR TRANSCRIPTIONAL CONTROL

The control of bacterial gene expression using photocaged inducer molecules was first performed in 2007 by Young and Deiters, who used NP-cIPTG for light-mediated and P_{lac}-derived expression of *lacZ* in *E. coli* BL21(DE3) [230]. Based on this approach, photocaged IPTG and further caged carbohydrates were optimized and applied for light control of various expression systems in *E. coli* [231–233]. Within this thesis, the preexisting toolbox was complemented in close collaboration with the Institute of Bioorganic Chemistry (IBOC) by more advanced photocaged compounds to address the following categories: i) the compound solubility, ii) novel microbial hosts, iii) the absorption wavelength and iv) yet unestablished promoter systems and photocaged inducer molecules. When comparing protection groups with altered hydrophobicity, such as the BC- or BEC-group (**Tab. III.1**), it could be seen that especially the more water-soluble BC-cIPTG led to an 2-fold increase of the induction response in *P. putida* and *B. subtilis* in comparison to NP-cIPTG and a comparable induction strength to IPTG [**FHo21a** 501]. Furthermore, by using BC-cIPTG, the induction process could be accelerated by up to 40% in *P. putida and E. coli*, while it prolonged the induction response in *B. subtilis* by around 30%. So far, only the more hydrophobic NP-cIPTG was applied for transcriptional light control in *B. subtilis* and *P. putida* but led to drastically decreased induction responses in comparison to the IPTG control [535,536]. Hence, particularly the application of the novel BC-cIPTG variant in *P. putida* and *B. subtilis* is a promising alternative for the well-established NP-cIPTG. However, the induction level of BC-cIPTG in *P. putida* could be further elevated by guaranteeing an efficient uptake of photocaged IPTG intermediates *via* overexpression of suitable permeases, which however, must be capable of importing molecules with large and expansive protecting groups. Furthermore, a complete enzymatic hydrolysis of the photocaged molecule needs to be ensured to gain the highest possible induction level, since BC-cIPTG, equally to its predecessor NP-cIPTG, requires a two-step uncaging mechanism [231]. This mechanism includes the hydrolysis of one ester bond *via* illumination with UV-A light and the second ester bond *via* enzymatic hydrolysis, which could be facilitated *via*

overexpression of unspecific esterases or other hydrolases or even by supplementation of the cultivation medium with natural oils to induce production of intrinsic esterases or lipases [536]. As an alternative to IPTG-responsive systems, benzoate-inducible systems, such as the NagR/P_{nagAa} system, may be considered. Here, DC-cSal showed a significantly increased induction level of nearly 2-fold in comparison to an induction with salicylic acid under extremely low inducer concentrations of 50 µM [**FHi21b** 504]. Furthermore, the three cIPTG variants with altered solubility were applied for light-mediated transcriptional control in the phototrophic host *R. capsulatus*. NP-cIPTG proved to be well applicable exhibiting an induction level between 80% and 160% in comparison to the IPTG control (**Tab. III.1**) and with acceptably low fluorescence signals in the unexposed control cultures. Remarkably, BC- and BEC-cIPTG showed to be not suitable, since they are prone to a severe instability effect in the unilluminated cultures nearly reaching the induction level of the exposed cultures [**FHi21a** 503]. This effect could not be attributed to the influence of the cultivation media but could possibly be due to host-specific enzymes that facilitate the hydrolysis of both photocaged inducer molecule linkages without the need of UV-A light illumination.

Since all currently available photocages for transcriptional control of bacterial gene expression are UV-A light-responsive, the inducer toolbox was further complemented by variants with a bathochromatically shifted absorption maximum, which consequently can be addressed with blue light illumination [**FHo21b** 502]. For this purpose, coumarin-based cages, such as diethylaminocoumarin (DC) or dicyanocoumarin (DCC), linked through carbonate, carbamate or ether bonds were constructed and evaluated for their applicability *in vivo*. While photocaged small molecule inducers with absorption maxima over 400 nm are frequently applied in eukaryotes [271,537–539], the here established photocaged IPTG variants were the first inducers for controlling bacterial gene expression with light of a wavelength longer than 400 nm. Alternatively, only genetically encoded photoreceptor-based systems are available for transcriptional control in bacteria using blue light [221,540–542]. Particularly, the novel carbonate-linked DC-2-cIPTG and the carbamate-linked DC-NN-cAra proved to be suitable with some restrictions regarding their stability resulting in either an elevated expression of target genes in the dark controls or a slow photolysis of the linker, respectively. The carbonate DC-6-cIPTG, in contrast, proved to be more hydrolysis sensitive, probably due to the linkage position at the 6-OH group, which might be sterically more accessible by esterases. In general, it can be concluded that for the *in vivo* application of carbonate-linked cages, the concentrations should be reasonable low to reduce the influence of hydrolysis in the dark putatively mediated by esterase cleavage. Additionally, the hydrolysis-stable carbamate-linked DC-NN-cAra could be subjected to a longer

illumination time and the pH value of the cultivation medium during illumination should not fall below pH 7 to favor the release mechanism of the linker. Furthermore, an alternative linker with optimized self-immolation characteristics could be used for a faster photorelease [543]. The ether-linked DC-cAra was characterized by a slow *in vitro* photorelease and an insufficient induction of target gene expression in *in vivo* measurements. This can be explained by an insufficient photoheterolysis due to the poor leaving group properties of arabinose, rendering it unsuitable in combination with an ether linkage [270,544]. Nevertheless, novel photocaged inducers were established, which can be addressed by illumination with blue light and thus pave the way towards a multi-chromatic transcriptional control of several genes or even complex biosynthetic pathways by combining different photocaged inducers with diverging absorption maxima. Furthermore, the toolbox could be expanded by a blue light-responsive photocaged arabinose variant, which can be applied for the transcriptional control of the well-established P_{BAD}/AraC promoter system.

Besides the application of carbohydrate-based photocaged inducer variants, BC-cSal as well as its sodium salt derivative were evaluated for their usability to control transcription of two salicylic acid-responsive promoter systems in *E. coli*, namely the P_m/XylS and the P_{nagAa}/NagR system [**FHo21b** 502]. The first proved to be not suitable for light-controlled regulation using photocages, since transcription was initiated by sole illumination with UV-A light but without the addition of salicylic acid as inducer molecule. This effect was probably due to a light-mediated induction of stress-related sigma factors leading to the hyperproduction of the positive LysR-type regulator XylS upon illumination, which in the following can activate gene expression in an inducer-independent manner [35,37]. This mechanism, however, also bears the possibility to use the P_m/XylS system as inducer-independent method for gradually controlling transcription in dependence on the illumination time with UV-A light. An alternative approach was recently published by Romano *et al.*, where they adapted the positive regulator AraC to be light-inducible without the need of arabinose supplementation by domain-swapping with photosensitive receptor domains [545]. In the case of the P_m/XylS system, however, no genetic modifications need to be performed, since the native promoter system turned out to be UV-A light responsive under minimal medium conditions. The second salicylic acid-responsive promoter system P_{nagAa}/NagR was suitable for light-mediated control of transcription, particularly by using BC-cSal in its acidic form, which led to induction level comparable to the IPTG control and a decreased fluorescence in the unilluminated controls when compared to its sodium salt derivative. However, the responsiveness of the system needs to be further improved by reducing the basal activity or by increasing the overall induction strength, which could be performed, for example, by directed

promoter mutagenesis or by supplementation of 4-nitrobenzoate during cultivation [43,46]. Notably, the BC-cSal variants were constructed using ether bonds for linkage, which previously proved to be unsuitable for DC-cAra [**FHo21b** 502]. In this case, however, the tethering *via* an ether bond showed to be applicable, since the photorelease of NB-based photocages follows a different reaction mechanism, which is not determined by the strength of the inducer molecules' leaving group properties, but rather on the stability of the resulting radical within the protection group upon photolysis [270,546].

In addition to the application of salicylic acid-responsive promoter systems in *E. coli*, the photocaged ether BC-cSal and its sodium salt derivative as well as a coumarin-based carbamate variant DC-NN-cSal both in its acid and in its sodium salt form were used to control gene expression in *P. putida* [**FHi21b** 504]. Interestingly, both BC-cSal derivatives showed a major instability in unexposed cultures, which possibly is due to host-specific enzyme hydrolysis, as both compounds worked well in the same cultivation medium in *E. coli.* The DC-NN-cSal derivatives, by contrast, proved to be well suited for blue light-mediated transcriptional control, exceeding the salicylic acid control by up to 180% (**Tab. III.1**). Additionally, the more water-soluble sodium salt form again exhibited a higher induction level in the dark controls, so that their use, similar to the BC-cIPTG derivatives in *E. coli*, is only recommended if the preliminary dissolution of the compound in organic solvents such as DMSO or ethanol should pose a problem for the biological system. The DC-NN-cSal variant was further evaluated for its applicability in a multi-chromatic induction system in combination with NB-cIPTG and showed a good induction level at inducer concentrations of only 50 µM and a rapid photorelease upon blue light illumination for 5 minutes. Thus, the carbamate linkage of DC-NN-cSal offered a fast and more sufficient photorelease in comparison to the previously described DC-NN-cAra, since salicylic acid offers a stronger leaving group in comparison to arabinose, determining the efficacy of the photoheterolysis [**FHo21b** 504, 270]. Conclusively, a wavelength-selective induction system addressable with UV-A and blue light could be established by combining cIPTG and cSal derivatives. So far, this is the first multi-chromatic system for light-mediated transcriptional control in bacteria based on photocaged inducers molecules. All alternative multi-chromatic systems found in literature are either based on artificial photoreceptors [9,547], such as Cph8, CcaS, YF1 or AraC applied in bacteria [208,210,545] as well as PhyB or VVD applied in mammalian cells [548,549] or on photoprotective groups [285,296], which so far were only applied *in vivo* in mammalian cells or zebrafish [271,288,294,295]. However, as the established system only offers a wavelength selective control of transcription, further investigation should be made regarding photocaging groups with absorption maxima in the blue or green light, but without a substantial absorption in the UV-A range, such as

dicyanocoumarins, thiocoumarines or BODIPYS [272,273,277,279]. Moreover, the stability of those compounds under unexposed conditions as well as under the very specific *in vivo* conditions imposed by the selected expression host and the experimental design of the cultivation process need to be ensured. Furthermore, the combination of photocaged inducers with photoreceptors for controlling transcription in a multi-chromatic fashion seems to be a promising possibility to enable light control with red-shifted absorption. Particularly for *R. capsulatus*, the cobalamine-dependent photoreceptor CarH [550,551] is especially well-suited since its chromophore 5'-deoxyadenosylcobalamin, a form of vitamin B_{12}, is naturally provided by this organism [552].

In conclusion, novel photocaged inducers for the light-mediated regulation of bacterial gene expression could be successfully established, which expand the toolbox by utilization of novel inducer molecules such as salicylic acid, novel photocaging groups with altered solubility or bathochromatically shifted absorption and finally alternative expression hosts including *P. putida*, *B. subtilis* and *R. capsulatus*. Hence, the improvements pave the way towards a more universal applicability of this optogenetic system.

III.2.2. PHOTOSENSITIZERS FOR CONTROLLING CELL VIABILITY

The use of genetically encoded photosensitizers (PS) to control cell viability *via* protein-cell interactions is a particularly valuable approach, which can be applied for the control of bacterial populations, such as in antimicrobial photodynamic inactivation (aPDI). Here, inactivation of target cells is performed by the production of both short-lived and longer-lived ROS species upon illumination. Within the framework of this thesis, several LOV- and GFP-like fluorescent proteins were characterized with respect to their photophysical and photosensitizing properties *in vitro* and *in vivo* [SE18 505, **FHi19** 506]. The *in vitro* analysis revealed that the PSs can be assigned to one of two subgroups: the first one includes PSs that produce ROS using mainly the type I reaction, such as Pp1FbFP and Pp2FbFP, and the PSs in the second group produce ROS by means of both the type I and type II reaction, such as DsFbFP M49I and SOPP3, which in turn represent the strongest producer in this subgroup. The *in vivo* application of selected PSs for killing of *E. coli* cells showed a good correlation between the *in vitro* and *in vivo* data. Additionally, a pattern in the activity spectrum could be observed, as PSs producing type I ROS were more potent against Gram-positive bacteria, while the PSs that produce both types of ROS are most effective against Gram-negative bacteria [**FHi19** 506]. Additionally, by

fusing the PS SOPP3 to a specific lectin it could be targeted to *P. aeruginosa* cells and increased the cell toxicity by nearly 4-fold.

For an improved functionality of the PS-mediated control of cell viability, different approaches should be pursued. Firstly, additional fluorescent proteins should be analyzed with respect to their photosensitizing properties including their ROS selectivity and yield. Recently, two novel variants of the LOV-like protein Mr4511 from *M. radiotolerans* were constructed *via* single site mutation of a reactive cysteine, which exhibited strongly increased singlet oxygen quantum yields of around 0.2 to 0.5 [553]. Furthermore, the well-known photosensitizers SuperNova, KillerRed and miniSOG were subjected to directed evolution, which increased their phototoxicity against bacteria and/or mammalian cells [554,555]. Obviously, further rational mutation approaches are required to expand the portfolio of genetically encoded photosensitizers by variants with more selective or stronger ROS production, which would be even more suited for therapeutic applications [556]. In addition to this methodology, proteins with an alternative photosensitizing chromophore, such as malachite green or its derivatives, could be constructed, as recently shown by Bruchez and coworkers and analyzed in detail by Dichmann *et al*. [557,558]. Furthermore, SuperNova Green was recently developed to expand the color palette and to achieve multi-chromatic control over ablation of selective cancer cells [559]. A similar approach was conducted earlier by Williams *et al.*, who combined miniSOG and KillerRed for multi-chromatic ablation of cholinergic motor neurons in *Caenorhabditis elegans* [337]. A second possibility to improve the toxicity of PS is the utilization of targeting tags, such as antibodies or peptides, as recently shown by cooperation partners [FR20 507]. Here, the photosensitizer EcFbFP was successfully applied for photodynamic therapy of tumor cells by fusion to a cell-penetrating peptide derived from azurin. Thus, this fusion protein is cell wall permeable, specifically addresses tumor cells and causes cell death of around 90% in comparison to an external application of the PS. For targeted delivery of PSs to relevant, pathogenic bacteria, similar approaches were established. Zhou *et al.* used a hepta-arginine peptide functionalized at the C-terminus with a chemically-based PS, which selectively bound to Gram-positive bacteria and led to complete cell death upon illumination [560]. Additionally, Niu and coworkers constructed a PS conjugate with the transacting activator protein of transduction peptide, which drives internalization of the construct into the membrane of Gram-negative bacteria [561]. Further targeting structures include antimicrobial peptide conjugates [562], which bind and disrupt the cell membrane, proteins that are naturally exposed on the outer cell membrane, such as protein A in *S. aureus* [563], or proteins that specifically bind components of the bacterial outer cell membrane, such as the lipopolysaccharide-binding homo-tetrameric lectin

ConA [564] for Gram-negative bacteria. Thus, to specifically address further cell types, including cancer cells or pathogenic bacterial species, research must be conducted with respect to novel targeting structures [565–567].

III.3. APPLICATIONS THAT COULD BENEFIT FROM OPTOGENETIC CONTROL

In the framework of this thesis, different optogenetic and optochemical systems were established, which allow for the control of diverse cellular processes, including transcriptional control as well as the control of protein-cell interactions. Since these regulatory tools are characterized by various advantageous properties, such as rapid, gradually controllable and non-invasive activation, they offer a promising possibility for the orchestration of more complex inter- and intracellular processes. In the following, this approach will be explained in more detail using various biotechnologically relevant examples, such as the inactivation of proteins by means of protein-protein interactions *via* chromophore-assisted light inactivation, the regulation of complex biosynthetic gene clusters, and finally the control and online-monitoring of cell-cell interactions within mono- and co-cultures to engineer artificial consortia.

III.3.1. PROTEIN INACTIVATION BY PROTEIN-PROTEIN INTERACTIONS USING CALI

As described in **chapter II.2.2**, several fluorescent proteins were exploited as genetically encoded photosensitizers, which locally generate several reactive oxygen species (ROS) species upon exposure to light of a certain wavelength [SE18 505]. In the framework of this thesis, genetically encoded PS were mainly applied for the inactivation of target cells, such as several Gram-positive and Gram-negative bacteria or cancer cells [SE18 505,**FHi19** 506, FR20 507]. It could be shown that the choice of an appropriate PS seems to be important, since both the ROS species and the amount of ROS produced by each PS varies significantly. However, not only the control of cell viability within a population, but also the targeted destruction of cellular structures, such as proteins or lipids, bears manifold applications and is commonly denoted as chromophore-assisted light inactivation (CALI). In case of genetically encoded photosensitizers, the targeting of the protein of interest is performed by generation of a translational fusion between the chosen protein and a respective photosensitizer. By this, ROS are produced in close proximity and the adjacent structure is irreversibly destroyed leading to a loss of protein activity. This technique can both be applied for controlling the enzyme activity in *in vitro* reactions or *in vivo* for the orchestration of biosynthetic pathways. Gerlach *et al*. recently

tested the PSs SOPP3, SOPP, EcFbFP, Pp2FbFP and SuperNova for their suitability for CALI of a carboligase and could successfully show that SOPP3 and SOPP fusion constructs sufficiently inactivate the target protein by up to 90% upon blue light illumination, but without affecting the enzyme activity in unexposed controls [TG21 512]. Interestingly, the fusion to EcFbFP and Pp2FbFP lead to aggregation of the fusion proteins, which were partly active, but challenging to handle. This effect only appeared for dimeric PSs in combination with the tetrameric structure of the carboligase, while the monomeric variants SOPP, SOPP3 and SuperNova formed soluble fusion proteins. In a next step, the best-performing PS candidate, SOPP3, was applied in a multi-step enzyme cascade producing the pharmaceutical precursor tetrahydroisoquinoline [568]. Here, fusion of SOPP3 to relevant pathway enzymes and subsequent blue light-mediated inactivation at a certain time point avoided cross-reactivity and led to a substantial product increase of 65%. For further applications of PSs in multi-step enzyme cascades, the combination of SOPP3 with a bathochromatically shifted PS variant, such as the novel variants KillerRed 2 or SuperNova 2 [554] would be promising to enable a multi-chromatic inactivation of two enzymes in an independent manner. Notably, SuperNova 2 should be preferred due to its monomeric structure in order to avoid aggregation of the fusion proteins. Furthermore, it shows an enhanced toxicity in comparison to its predecessor SuperNova, which showed to be not applicable for CALI applications due to its low ROS formation [TG21 512]. In an additional approach, the two PSs EcFbFP and SOPP were successfully used for CALI of the transferase PigC belonging to the prodigiosin biosynthetic pathway within an associated master thesis of Nora Bitzenhofer [533]. Here, the bifurcated pathway served as a valuable proof-of-concept application, since only the last step, the condensation of MAP and MBC by PigC, results in the formation of a colored product, the tripyrrole prodigiosin, which can be easily quantified (**Fig. III.3A**). Upon blue light illumination, the PS fusion reduced the product formation and thus the enzyme activity of PigC by up to 50% in an *in vitro* reaction. By adding the respective non-fused PS to a control reaction, it was further shown that SOPP led to a reduced product formation upon illumination, while EcFbFP showed no reduction, thus underlining that the ROS production capacity is an important factor, which must be considered when selecting a PS for a respective CALI application. In a second step, the CALI approach was transferred to PigD, an enzyme within the prodigiosin pathway responsible for the formation of MAP, in an *in vivo* approach by Jana Ehlers during her bachelor's thesis in our working group [569].

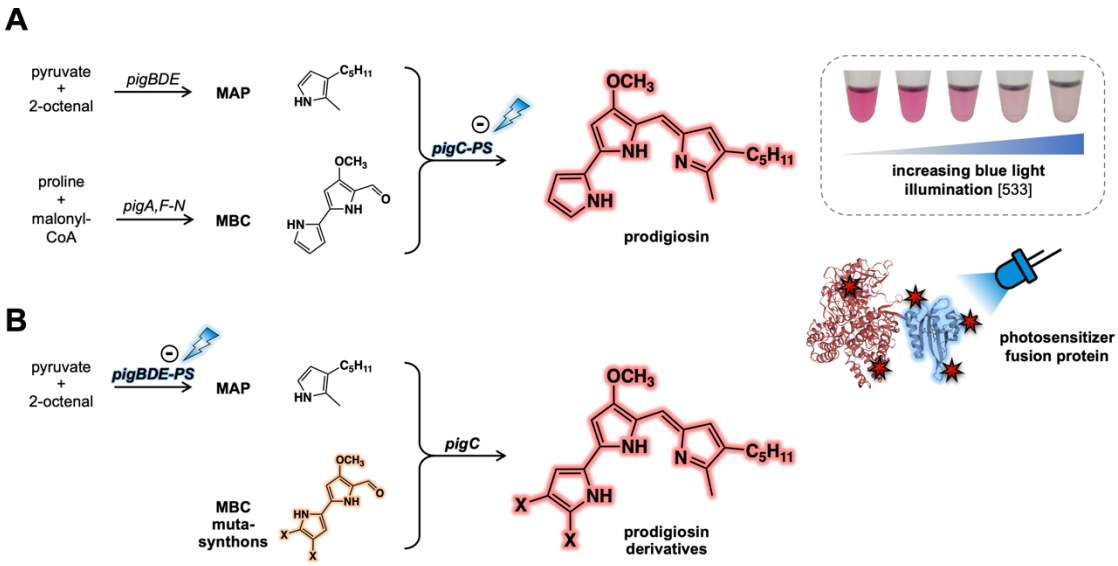

Figure III.3 Several target enzymes for chromophore-assisted light inactivation in the prodigiosin biosynthetic pathway (adapted from Bitzenhofer 2018 [533] **and Ehlers 2019** [569]**).**
The bifurcated prodigiosin biosynthetic pathway is a valuable target for a proof-of-concept CALI application, since only the last step of the synthesis, the condensation of MAP and MBC, leads to the formation of the red-colored prodigiosin, which can be easily quantified. **A**) The fusion of the final condensing enzyme PigC with a photosensitizer (PS) and subsequent blue light illumination leads to the inactivation of PigC, which can be measured *via* prodigiosin formation. **B**) In addition to PigC, additional relevant pathway enzymes can be inactivated, such as PigD, which is responsible for the synthesis of MAP, resulting in a light-dependent regulation of MAP levels. In combination with a respective *pigA,F-N* deletion strain, artificial MBC mutasynthons could be supplemented to gain new-to-nature prodigiosin derivatives. MAP: 2-methyl-3-pentyl-pyrrole, MBC: 2,2-bipyrrole-5-carboxyaldehyde, prodigiosin: 2-methyl-3-pentyl-6-methoyprodiginine, PigC: prodigiosin synthase, PigD: 3-acetyloctanal synthase.

It could be shown that the prodigiosin formation could be reduced by nearly 40% upon illumination using a EcFbFP-PigD fusion protein in a *P. putida pigD* deletion strain. This first *in vivo* application shows that CALI is a promising way to gradually control PigD in this biosynthetic pathway, resulting in a light-dependent regulation of MAP levels. In combination with a respective *pigA,F-N* deletion strain, artificial MBC mutasynthons could be supplemented to gain new-to-nature prodigiosin derivatives in a mutasynthesis approach (**Fig. III.3B**), as performed for MAP mutasynthons by Klein *et al*. [394,462].

In summary, chromophore-assisted light inactivation is a powerful tool that utilizes protein fusions and light-sensitive chromophores to selectively produce ROS and by this inactivate targeted pathway enzymes. In the following chapter, further application possibilities of optogenetic regulators, such as CALI, for the orchestration of secondary metabolite pathways are discussed.

III.3.2. Optogenetic regulation of complex biosynthetic gene clusters

As aforementioned, the production or engineering of natural compounds by expression of a heterologous gene or even an entire biosynthetic gene cluster in a well-established, genetically accessible, and highly productive host poses a promising possibility that is increasingly being integrated into biotechnological and industrial processes. Besides all advantages a heterologous host can offer, there are some challenges to be tackled for a successful production of complex secondary metabolites including possible bioactivities of intermediate or end products as well as an insufficiently coordinated gene expression or enzyme activity, both leading to impaired growth or production yields [51]. For this purpose, specialized organisms are increasingly applied for the production of antimicrobial substances or more complex secondary metabolite products [143,388,395]. A good example for this strategy is the production of heterologous terpenes in the phototrophic host *R. capsulatus*. Since the broad class of terpenes offers various promising bioactivities, it is of commercial interest to various industrial sectors for the production of pharmaceuticals, flavors and fragrances, biofuels or bio-based pesticides [416–419]. For an optimized production of those isoprene-derived compounds, extensive efforts were made with respect to metabolic engineering and bioprocess optimization addressing, among others, the following issues: increasing endogenous precursor supply, modifying cofactor requirements, eliminating bottlenecks and competitive reactions, mitigating the toxic effects of intermediates or products, as well as genetic and protein engineering [406,422–424]. For *R. capsulatus* [187,425] and *R. sphaeroides* [426–430] in particular, it was demonstrated that engineering of the isoprenoid precursor synthesis results in a strongly increased sesqui- and triterpenoid production, which could also be shown within this thesis. In detail, the co-expression of a terpene synthase with the FPP synthase IspA and/or enzymes of the heterologous MVA pathway led to significantly increased production of the corresponding plant terpenoids (**Tab. III.2**) [KT19 188, **FHi21c** 189, JHH21 508]. Nonetheless, various studies revealed that overproduction of isoprenoid intermediates in the heterologous host can be toxic for the producer cell or leads to metabolic stress and feedback inhibition and in turn, to decreased growth and production titers [402,431–435]. Besides recently published approaches, where production yields were improved by either using dynamic promoter systems for regulation of the precursor supply [434], by reduction of competitive side reactions [437] or by the implementation of feedback loops [438], the application of photocaged inducer molecules pose another promising way to regulate the precursor levels for optimized production titers (**Fig. III.4A**).

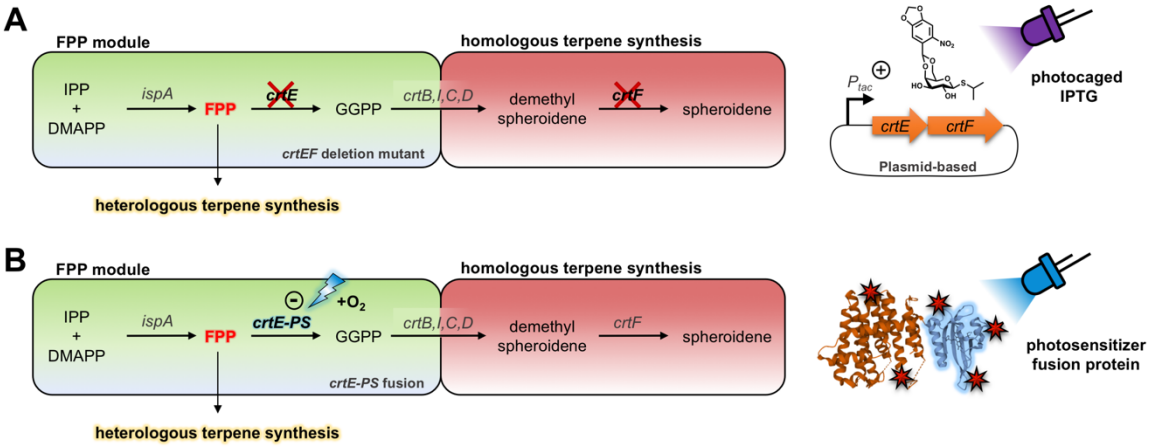

Figure III.4 Optogenetic strategies for balancing the FPP levels for an optimized heterologous terpene production. For optimized terpene production titers in *R. capsulatus*, the level of the precursor molecule FPP needs to be balanced between the homologous carotenoid biosynthesis pathway and the heterologous terpene pathway, since FPP is known to exert metabolic stress or even cell toxicity in several bacterial hosts. Thus, two optogenetic strategies are proposed using either photocaged inducer molecules or genetically encoded photosensitizers. **A**) The intrinsic carotenoid synthesis of *R. capsulatus* starts from the C_5 building blocks IPP and DMAPP. In a carotenoid-deficient strain, deletion of genes encoding the relevant carotenoid pathway enzymes CrtE and CrtF can be complemented by IPTG-mediated expression of the crtE and crtF genes on a plasmid. Light-mediated induction of *crt* gene expression using NP-cIPTG can be utilized to balance the FPP flux and thus, avoiding unwanted metabolic stress. **B**) Alternatively, a translational fusion of *crtE* with a photosensitizer-encoding gene leads to the production of a CrtE-PS fusion protein, which may be gradually inactivated upon blue light illumination and by this should similarly allow the balance of FPP utilization. IPP: isopentenyl pyrophosphate; DMAPP: dimethylallyl pyrophosphate; IspA: FPP synthase; FPP: farnesyl pyrophosphate; CrtE: GGPP synthase; GGPP: geranylgeranyl pyrophosphate; CrtB: phytoene synthase; CrtI: phytoene desaturase; CrtC: hydroxyneurosporene synthase; CrtD: hydroxyneurosporene desaturase; CrtF: demethylspheroidene O-methyltransferase; PS: photosensitizer; (CrtE PDB structure: 6SXL, PS PDB structure: 6GPU).

As demonstrated in this thesis, the expression of FPP converting enzymes within the host-specific carotenoid biosynthesis of *R. capsulatus* could be fine-tuned applying cIPTG under phototrophic conditions [**FHi21a** 503]. Along with the adapted illumination wavelength in the IR range, this approach could be transferred to the production of heterologous terpenes under phototrophic growth conditions in future studies. Here, the use of a carotenoid-deficient strain, which was recently shown to produce triterpenoids with increased yields [570], could be engineered by implementing the expression of genomically deleted *crt* genes under cIPTG control for adjustable carotenoid levels. Hence, light could be employed for balancing the FPP level between the production of homologous carotenoids or heterologous terpenes and thus preventing negative effects of elevated FPP levels, which might lower the production titers.

Alternatively, photosensitizers could be applied for inactivation of relevant carotenoid pathway enzymes, such as CrtE (**Fig. III.4B**). An inactivation can be facilitated by a C- or N-terminal translational fusion of the *crtE* gene with a photosensitizer-encoding gene. By this means, the CrtE activity could be optogenetically regulated to ensure a balanced FPP pool, which may avoid metabolic stress and thus leads to an increased production

of heterologous terpenoids. However, since the photosensitizing process is dependent on molecular oxygen, the critical oxygen concentration needs to be determined and the cultivation process needs to be adapted with respect to a temporarily elevated oxygen input if necessary. Certainly, those optogenetic on- and off-switches could be transferred to further promising organisms, such as the fungus *U. maydis*, which was recently exploited as heterologous host of the plant-derived sesquiterpene valencene and the fungal sesquiterpene α-cuprenene by Lee *et al.* [JL20 509]. Here, metabolic engineering was applied by implementing the carotenoid biosynthesis to produce lycopene as readout of intracellular FPP titers. By overexpression of the heterologous valencene synthase CnVS or the α-cuprenene synthase Cop6, terpene titers in the mg L^{-1} scale could be produced, rendering *U. maydis* particularly valuable for the production of fungal terpenes.

In a similar way to the above-described modifications, both optogenetic tools offer the possibility to control further secondary metabolite pathways, such as the rhamnolipid biosynthesis in *P. putida*. As mentioned in **chapter I.4.I**, rhamnolipids are commonly produced in a predefined mixture of mono- and di-rhamnolipids (MRL and DRL) in *P. putida*. However, the possibility of producing tailored rhamnolipid mixtures is very promising, since the physico-chemical properties of each rhamnolipid blend varies greatly depending on its composition. Recently, the production of MRL and DRL could be controlled by applying photocaged inducers addressable with two different light colors [**FHi21b** 504]. For this purpose, the genes responsible for the production of MRL, namely *rhlA* and *rhlB*, where subjected to cSal control by placing them behind a salicylic acid-responsive promoter [504]. Upon blue light illumination, MRL were produced in even higher amounts compared to the salicylic acid control cultures. Upon UV-A light illumination, the expression of the *rhlC* gene was activated, which encodes an enzyme responsible for the conversion of MRL to DRL. This wavelength-selective system thus enables the independent control of both biosynthetic processes with a high temporal resolution (**Fig. III.5A**). The approach could be used in future studies for an induction profiling to generate tailored rhamnolipid mixtures depending on the starting point of illumination, the duration of illumination or the illumination intensity. However, the system so far only offers a wavelength-selective, but not an orthogonal process, since the blue light-responsive cSal variant can also be addressed with UV-A light [**FHi21b** 504].

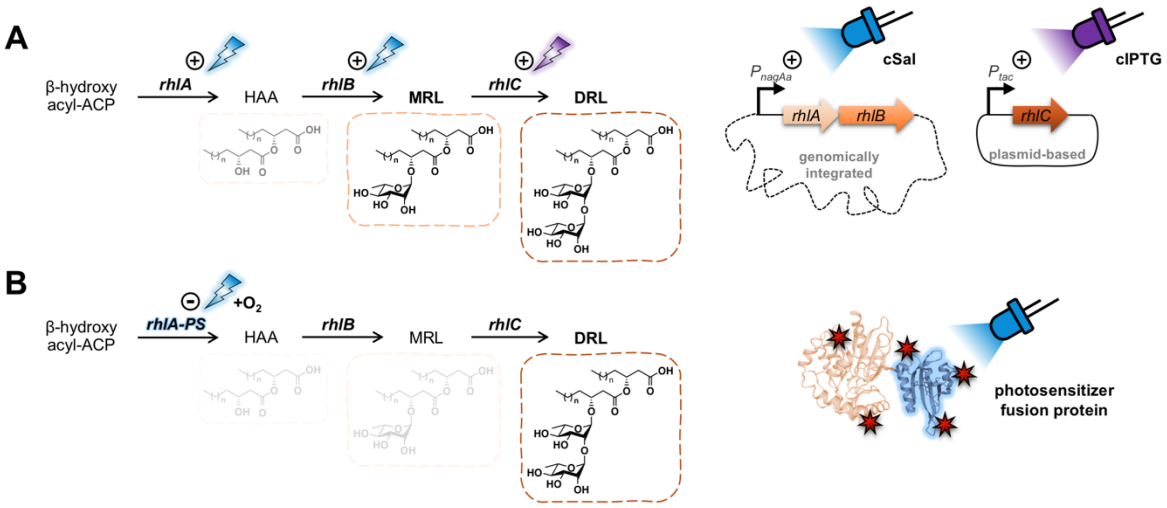

Figure III.5 Optogenetic strategies to orchestrate the rhamnolipid biosynthesis in *P. putida* for the production of tailormade rhamnolipid mixtures.
Since the physico-chemical properties of rhamnolipid blends vary greatly depending on their composition, the possibility of producing tailored mixtures is very promising. This could be achieved by targeted optogenetic control of the production volume of each individual component using photocaged inducer molecules or genetically encoded photosensitizers. **A**) Rhamnolipid biosynthesis is encoded by the three genes *rhlA*, *rhlB* and *rhlC* and starts with the conversion of activated β-hydroxy fatty acids to HAA by RhlA. Subsequently, HAA is transformed to a MRL by RhlB upon addition of an activated rhamnose molecule and further to DRL by RhlC *via* linkage of another activated rhamnose moiety. Modification of the rhamnolipid mixture and thus orchestration of MRL and DRL production can be implemented by bringing *rhlAB* and *rhlC* under the control of two different promoters. Light-responsive control of those two processes can be gained by using the corresponding photocaged inducer molecules, namely cSal and cIPTG and by variation of parameters such as the start of illumination, the duration of exposure or the illumination intensity. **B**) Alternatively, photosensitizers can be used to produce rhamnolipid mixtures with varying MRL amounts. For this purpose, a translational fusion of *rhlA* with a photosensitizer-encoding gene is constructed that leads to the production of a RhlA-PS fusion protein. This fusion protein can be gradually inactivated upon blue light illumination after a certain time point, so that MRL are predominantly converted to DRL by RhlC leading to an individually adjustable DRL purity in dependence on the level of RhlA inactivation. HAA: 3-(3-hydroxyalkanoyloxy)alkanoic acid; MRL: mono-rhamnolipid; DRL: di- rhamnolipid; ACP: acyl carrier protein; (RhlA SMR structure: Q51559; PS PDB structure: 6GPU).

Novel photocaged salicylic acid variants with minimized absorption in the 300 – 400 nm range would allow the activation of both uncaging processes in a sequentially-independent manner. Additionally, photosensitizers can be applied for the adaption of the rhamnolipid mixture by gradually inactivating the enzyme RhlA, which mediates the conversion of activated hydroxy fatty acids to HAA (**Fig. III.5B**). For this purpose, the RhlA-encoding gene needs to be translationally fused to the gene of a selected photosensitizer, so that a fusion protein is generated. At a desired time point, the enzyme is inactivated *via* blue light illumination and the existing intermediates are gradually converted to DRL without new ones being reproduced, leading to a individually adjustable DRL purity in dependence on the level of RhlA inactivation.

In summary, both optogenetic systems, the use of photocaged inducer molecules and the application of photosensitizers, represent a powerful and highly versatile method for

precisely orchestrate complex metabolic pathways with high temporal resolution, e.g., to increase the final production yield or to adjust the composition of the end product.

III.3.3. Control of Intra- and Intercellular Processes in bacterial communities by light

In nature, microorganisms live in communities, which commonly are composed of a multitude of different species living together for their mutual benefit [571,572]. The stability of these consortia is not only based on cellular interactions, such as aggregation, biofilm formation or horizontal gene transfer, but also on small molecule- or protein-based interactions including protein secretion or metabolite transfer, e.g., for quorum-sensing. The metabolites originate from substrate conversion processes, which are mostly catalyzed in a concerted manner following the division of labor principle and are shared as a public good, referred to as commensalistic and mutualistic interactions, or released to negatively affect a member of the own community or an external, opposing organism in a predatory or competing interaction [573]. Although natural microbial communities have been used for centuries in production processes, e.g., for cheese, wine or beer, little is known about the specific interactions between species, as the study of microbial communities still remains challenging [572,573]. To overcome these difficulties, synthetic microbial consortia are being created that allow for the generation of defined microbial systems with reduced complexity, while still retaining the key features of their natural counterparts [571,572,574]. This way, a synthetic community can be (i) used as a model system for the study of the performance and stability of microbial communities in detail as a top-down approach or (ii) utilized for analyzing the optimal conditions necessary to generate specific interactions like symbiosis or competition and how a complex community structure can emerge from these in a bottom-up approach. Besides serving as model systems to better understand such microbial communities, artificial consortia also represent a promising new frontier of biotechnology. The synthetic design offers the possibility to balance the weaknesses of a respective production host by skillfully assembling the consortium [575] or the use of an auxiliary population to outsource the production of a particular carbon source or the secretion of an enzyme that in turn degrades the available carbon source into smaller and more accessible molecules [576,577]. Additionally, a spatial distribution of a biosynthetic pathway of complex or toxic secondary metabolites among several organisms [578], or a parallel optimization of different parts of the biosynthetic pathway within a division of labor concept [575,579] can be performed. By means of systems biology and rational design, artificial microbial consortia could be successfully used, e.g., for the production

of natural products [580,581], high-value compounds [574] and small molecules [582], but also for the production of biofuels or pollution control of waste water [574,583,584]. To ensure proper co-cultivation, the individual division rates of each population and thus the composition of the synthetic consortium must be strictly regulated. This is often realized by using special selective media or by adjusting the cell titers [575], but non-invasive regulation using light-sensitive antibiotics or engineered mutualistic interactions between each individual population has also been established [585–587]. However, the implementation of alternative regulatory mechanisms, such as the control of horizontal gene transfer, is also conceivable as it should provide a precise and straightforward control of communication processes with high spatiotemporal resolution. A major challenge in this context is the regulation and online-monitoring of those intra- and intercellular processes, the cellular compositions of a mixed consortium or their biological output signals over a long cultivation period. To analyze the individual populations, as well as changes and heterogeneity within the co-culture, flow cytometry approaches proved valuable in various applications. However, also microfluidic single-cell analysis offers promising possibilities for time-resolved tracking of cell division and monitoring of individual biological responses at the single-cell level under defined cultivation conditions. To visualize secretion of recombinant proteins, the split GFP assay was developed and applied for the gradual quantification of several secreted protein in *B. subtilis* [588,589]. Based on this system, Lenz *et al.* recently developed the iSplit GFP assay for the straightforward quantification of intracellularly produced recombinant proteins in *B. subtilis* [PL21 511], which can be applied for online monitoring in a BioLector system in batch cultures as well as on single-cell level, as nicely shown for an analysis in a microfluidic chip. With this system, insights into both the intracellular localization and the production heterogeneity of the recombinant β-glucuronidase GUS from *E. coli* could be achieved as a proof-of-concept approach. In the currently prepared doctoral thesis of Patrick Lenz, both the extracellular and the intracellular split GFP system will be combined using two engineered split protein versions sufficiently differing in their excitation and emission wavelength [590]. Furthermore, this system includes a measure for secretion stress by means of a third orthogonal fluorescent output. Thus, the three assay parameters will allow for a combined analysis of intracellularly and secreted recombinant protein as well as the associated secretion stress in a bacterial culture. Additionally, Burmeister *et al*. developed a specific microfluidic chip design to enable cultivation of two populations in close proximity, but without direct cell contact, which was utilized for investigation of both intra- and interspecies, microbial interactions such as microbial cross-feeding of two *C. glutamicum* strains or horizontal gene transfer between *E. coli* and *P. putida* strains, respectively [AB19 510]. While metabolite cross-

feeding could be observed in co-cultures using the divided chip design, bacterial conjugation only took place after direct cell-cell contact in an unsegmented microfluidic chip. In addition to this research, different media compositions and growth conditions were analyzed with respect to the frequency of successful horizontal gene transfer events in the master thesis of Daniela Brocke [591]. In a follow-up publication, the established co-cultivation platform was recently used to develop and characterize an optochemically controllable bacterial consortium on microcolony level consisting of two C. *glutamicum* strains [AB21 513]. Here, an L-lysine auxotrophic strain is combined with a variant that is able to produce L-lysine in dependence of photocaged IPTG. Upon illumination, the growth rate of the auxotrophic strain could be increased by up to 70% in comparison to uninduced cultures, which underlines the suitability of photocaged inducer for light control of an intercellular interaction in a microbial community. The co-cultivation chip design was furthermore used to study inter-species interactions and the use of public goods within an artificial consortium of *R. capsulatus* and *P. putida* cells during the associated master studies of Luzie Kruse [592]. In this work, *P. putida* was designed to offer an iron-independent biosynthesis of the siderophore pyoverdine. Instead of the natural mechanism sensing iron depletion, pyoverdine production was induced by the addition of IPTG or the photocaged variant BC-cIPTG. Subsequent co-cultivation experiments using microfluidics revealed that *R. capsulatus*, which did not show growth under iron limitation in monocultures, was able to grow in the presence of *P. putida* cells. Hereby it could be proved that the siderophore pyoverdine acts as a common good in this consortium and further that cell growth of one community member can be selectively controlled by a commensalistic interaction.

This thesis underlines that both photocaged inducers and photosensitizers are valuable and well applicable tools for the control of intra- and intercellular processes or interactions in a non-invasive fashion and with high spatiotemporal control (**Fig. III.6**).

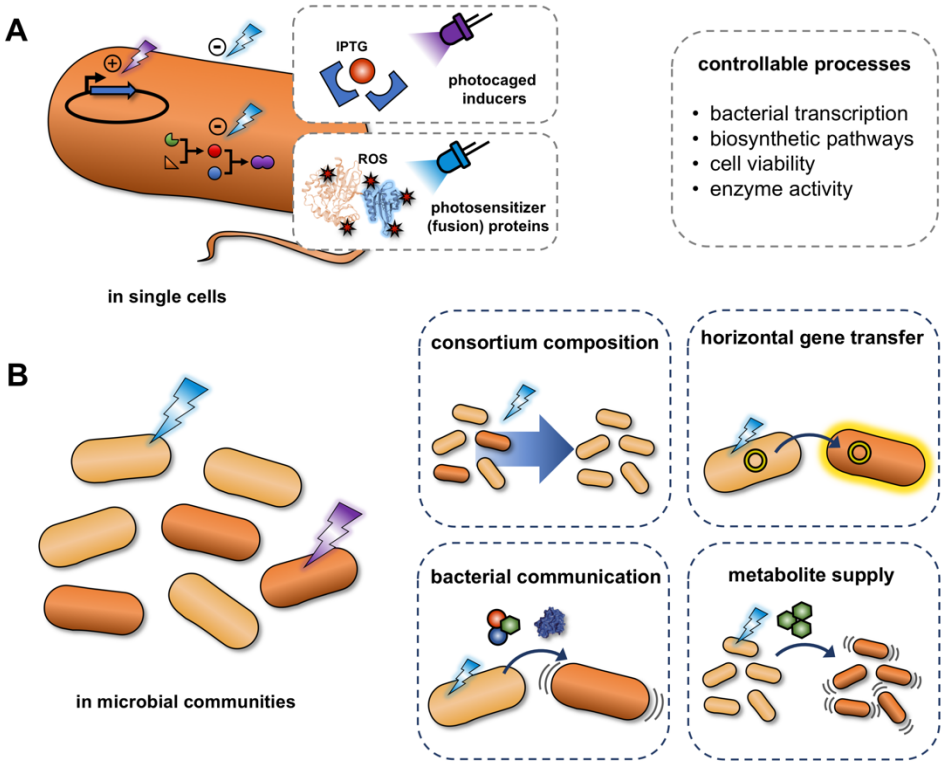

Figure III.6 Optogenetic strategies to orchestrate cellular functions established in this thesis and possibilities for their application to control processes in microbial communities.
A) Within this thesis, two optogenetic tools, namely photocaged compounds and photosensitizers, were developed and successfully applied *in vivo* for the control of various processes on different cellular levels. **B**) In addition, those optogenetic tools are extremely valuable for the control of processes within microbial consortia. Hereby, not only the composition of the co-culture, but also bacterial communication, horizontal gene transfer or the sharing of metabolite could be subjected to light control and subsequently online-monitored on single-cell level to gain a deeper understanding of the respective process or even the whole bacterial community.

Besides the highly flexible, ready-to-use control over bacterial gene expression, an additional regulatory off-switch could be implemented post-translationally to orchestrate cell viability or enzyme activity in a straightforward and sophisticated manner. In future studies, both photocaged inducer molecules and genetically encoded photosensitizers could be used for controlling the composition of other relevant microbial consortia or regulating processes such as horizontal gene transfer, plasmid replication, predation, metabolite exchange and consumption or protein secretion.

IV. REFERENCES

1. Benner SA, Sismour AM. Synthetic biology. Nature Reviews Genetics. 2005. doi:10.1038/nrg1637

2. Endy D. Foundations for engineering biology. Nature. 2005. doi:10.1038/nature04342

3. Dhar PK, Weiss R. Enabling the new biology of the 21st century. Systems and Synthetic Biology. 2007. doi:10.1007/s11693-006-9000-6

4. Voigt CA. Synthetic biology. ACS Synthetic Biology. 2012. doi:10.1021/sb300001c

5. Carbonell P, Jervis AJ, Robinson CJ, Yan C, Dunstan M, Swainston N, Vinaixa M, Hollywood KA, Currin A, Rattray NJW, Taylor S, Spiess R, Sung R, Williams AR, Fellows D, Stanford NJ, Mulherin P, Le Feuvre R, Barran P, Goodacre R, Turner NJ, Goble C, Chen GG, Kell DB, Micklefield J, Breitling R, Takano E, Faulon JL, Scrutton NS. An automated Design-Build-Test-Learn pipeline for enhanced microbial production of fine chemicals. Commun Biol. 2018;1: 1–10. doi:10.1038/s42003-018-0076-9

6. Orsi E, Beekwilder J, Eggink G, Kengen SWM, Weusthuis RA. The transition of *Rhodobacter sphaeroides* into a microbial cell factory. Biotechnol Bioeng. 2021;118: 531–541. doi:10.1002/bit.27593

7. Hartmann D, Smith JM, Mazzotti G, Chowdhry R, Booth MJ. Controlling gene expression with light: a multidisciplinary endeavour. Biochem Soc Trans. 2020;48: 1645–1659. doi:10.1042/BST20200014

8. Lalwani MA, Zhao EM, Avalos JL. Current and future modalities of dynamic control in metabolic engineering. Curr Opin Biotechnol. 2018;52: 56–65. doi:10.1016/j.copbio.2018.02.007

9. Baumschlager A, Khammash M. Synthetic biological approaches for optogenetics and tools for transcriptional light-control in bacteria. Adv Biol. 2021; 2000256. doi:10.1002/adbi.202000256

10. Blattner FR. The complete genome sequence of *Escherichia coli* K-12. Science (80-). 1997;277: 1453–1462. doi:10.1126/science.277.5331.1453

11. Saier MH. Microcompartments and protein machines in prokaryotes. J Mol Microbiol Biotechnol. 2013;23: 243–269. doi:10.1159/000351625

12. Browning DF, Busby SJW. Local and global regulation of transcription initiation in bacteria. Nat Rev Microbiol. 2016;14: 638–650. doi:10.1038/nrmicro.2016.103

13. Beales N. Adaptation of microorganisms to cold temperatures, weak acid preservatives, low pH, and osmotic stress: a review. Compr Rev Food Sci Food Saf. 2004. doi:10.1111/j.1541-4337.2004.tb00057.x

14. Deutscher J. The mechanisms of carbon catabolite repression in bacteria. Curr Opin Microbiol. 2008;11: 87–93. doi:10.1016/j.mib.2008.02.007

15. Görke B, Stülke J. Carbon catabolite repression in bacteria: many ways to make the most out of nutrients. Nat Rev Microbiol. 2008;6: 613–624.

doi:10.1038/nrmicro1932

16. Gomelsky M, Hoff WD. Light helps bacteria make important lifestyle decisions. Trends Microbiol. 2011;19: 441–8. doi:10.1016/j.tim.2011.05.002

17. Elías-Arnanz M, Padmanabhan S, Murillo FJ. Light-dependent gene regulation in nonphototrophic bacteria. Curr Opin Microbiol. 2011;14: 128–135. doi:10.1016/j.mib.2010.12.009

18. Ponomarova O, Patil KR. Metabolic interactions in microbial communities: untangling the Gordian knot. Curr Opin Microbiol. 2015;27: 37–44. doi:10.1016/j.mib.2015.06.014

19. Miller MB, Bassler BL. Quorum Sensing in Bacteria. Annu Rev Microbiol. 2001;55: 165–199. doi:10.1146/annurev.micro.55.1.165

20. Jacob F, Monod J. Genetic regulatory mechanisms in the synthesis of proteins. J Mol Biol. 1961;3: 318–356. doi:10.1016/S0022-2836(61)80072-7

21. Busby S, Ebright RH. Transcription activation by catabolite activator protein (CAP). J Mol Biol. 1999;293: 199–213. doi:10.1006/jmbi.1999.3161

22. Lewis M. The *lac* repressor. C R Biol. 2005;328: 521–548. doi:10.1016/j.crvi.2005.04.004

23. Guan L, Kaback HR. Lessons from lactose permease. Annu Rev Biophys Biomol Struct. 2006;35: 67–91. doi:10.1146/annurev.biophys.35.040405.102005

24. Jobe A, Bourgeois S. The *lac* repressor-operator interaction. J Mol Biol. 1972;72: 139–152. doi:10.1016/0022-2836(72)90075-7

25. Andrews KJ, Lin ECC. Thiogalactoside transacetylase of the lactose operon as an enzyme for detoxification. J Bacteriol. 1976. doi:10.1128/jb.128.1.510-513.1976

26. Wilson CJ, Zhan H, Swint-Kruse L, Matthews KS. The lactose repressor system: paradigms for regulation, allosteric behavior and protein folding. Cell Mol Life Sci. 2007;64: 3–16. doi:10.1007/s00018-006-6296-z

27. Brautaset T, Lale R, Valla S. Positively regulated bacterial expression systems. Microb Biotechnol. 2009;2: 15–30. doi:10.1111/j.1751-7915.2008.00048.x

28. Guzman L-M, Belin D, Carson MJ, Beckwith J. Tight regulation, modulation, and high-level expression by vectors containing the arabinose P_{BAD} promoter. J Bacteriol. 1995;177: 4121–4130. doi: 10.1128/jb.177.14.4121-4130.1995

29. Schleif R. AraC protein, regulation of the L-arabinose operon in *Escherichia coli* , and the light switch mechanism of AraC action. FEMS Microbiol Rev. 2010;34: 779–796. doi:10.1111/j.1574-6976.2010.00226.x

30. Miyada CG, Stoltzfus L, Wilcox G. Regulation of the araC of *Escherichia coli*: catabolite repression, autoregulation, and effect on *araBAD* expression. Proc Natl Acad Sci U S A. 1984;81: 4120–4124. doi:10.1073/pnas.81.13.4120

31. Worsey MJ, Williams AP. Metablism of toluene and xylenes by *Pseudomonas putida* (*arvilla*) mt2: evidence for a new function of the TOL plasmid. J Bacteriol. 1975. doi:10.1128/jb.124.1.7-13.1975

32. Ramos JL, Stolz A, Reineke W, Timmis KN. Altered effector specificities in regulators of gene expression: TOL plasmid xylS mutants and their use to engineer expansion of the range of aromatics degraded by bacteria. Proc Natl Acad Sci. 1986;83: 8467–8471. doi:10.1073/pnas.83.22.8467

33. Marqués S, Ramos JL. Transcriptional control of the *Pseudomonas putida* TOL plasmid catabolic pathways. Mol Microbiol. 1993;9: 923–929. doi:10.1111/j.1365-2958.1993.tb01222.x

34. Mermod N, Ramos JL, Bairoch A, Timmis KN. The *xylS* gene positive regulator of TOL plasmid pWWO: Identification, sequence analysis and overproduction leading to constitutive expression of meta cleavage operon. MGG Mol Gen Genet. 1987. doi:10.1007/BF00331600

35. Ramos JL, Marqués S, Timmis KN. Transcriptional control of the *Pseudomonas* TOL plasmid catabolic operons is achieved through an interplay of host factors and plasmid-encoded regulators. Annu Rev Microbiol. 1997;51: 341–73. doi:10.1146/annurev.micro.51.1.341

36. de las Heras A, Fraile S, de Lorenzo V. Increasing signal specificity of the TOL network of *Pseudomonas putida* mt-2 by rewiring the connectivity of the master regulator XylR. PLoS Genet. 2012;8: e1002963. doi:10.1371/journal.pgen.1002963

37. Gawin A, Valla S, Brautaset T. The XylS/ Pm regulator/promoter system and its use in fundamental studies of bacterial gene expression, recombinant protein production and metabolic engineering. Microb Biotechnol. 2017;10: 702–718. doi:10.1111/1751-7915.12701

38. Gallegos MT, Marqués S, Ramos JL. Expression of the TOL plasmid *xylS* gene in *Pseudomonas putida* occurs from a σ70-dependent promoter or from σ70- and σ54-dependent tandem promoters according to the compound used for growth. J Bacteriol. 1996. doi:10.1128/jb.178.8.2356-2361.1996

39. Yen K-M, Serdar CM, Gunsalus IC. Genetics of naphthalene catabolism in Pseudomonads. CRC Crit Rev Microbiol. 1988;15: 247–268. doi:10.3109/10408418809104459

40. Schell MA. Homology between nucleotide sequences of promoter regions of *nah* and *sal* operons of NAH7 plasmid of *Pseudomonas putida*. Proc Natl Acad Sci U S A. 1986;83: 369–373. doi:10.1073/pnas.83.2.369

41. Puntus IF, Ryazanova LP, Zvonarev AN, Funtikova T V., Kulakovskaya T V. The role of mineral phosphorus compounds in naphthalene biodegradation by *Pseudomonas putida*. Appl Biochem Microbiol. 2015;51: 202–208. doi:10.1134/S0003683815020143

42. Goyal AK, Zylstra GJ. Genetics of naphthalene and phenanthrene degradation by *Comamonas testosteroni*. J Ind Microbiol Biotechnol. 1997;19: 401–407. doi:10.1038/sj.jim.2900476

43. Jones RM, Britt-Compton B, Williams PA. The naphthalene catabolic (*nag*) genes of *Ralstonia* sp. strain U2 are an operon that is regulated by NagR, a LysR-type transcriptional regulator. J Bacteriol. 2003;185: 5847–5853. doi:10.1128/JB.185.19.5847-5853.2003

44. Jeon CO, Park M, Ro H-SS, Park W, Madsen EL. The naphthalene catabolic (*nag*)

genes of *Polaromonas naphthalenivorans* CJ2: evolutionary implications for two gene clusters and novel regulatory control. Appl Environ Microbiol. 2006;72: 1086–1095. doi:10.1128/AEM.72.2.1086-1095.2006

45. Zhou N-Y, Fuenmayor SL, Williams PA. *Nag* genes of *Ralstonia* (formerly *Pseudomonas*) sp. strain U2 encoding enzymes for gentisate catabolism. J Bacteriol. 2001;183: 700–708. doi:10.1128/JB.183.2.700-708.2001

46. Lönneborg R, Brzezinski P. Factors that influence the response of the LysR-type transcriptional regulators to aromatic compounds. BMC Biochem. 2011;12: 49. doi:10.1186/1471-2091-12-49

47. Schell MA, Wender PE. Identification of the *nahR* gene product and nucleotide sequences required for its activation of the *sal* operon. J Bacteriol. 1986;166: 9–14. doi:10.1128/JB.166.1.9-14.1986

48. Schell MA. Molecular biology of the LysR family of transcriptional regulators. Annu Rev Microbiol. 1993;47: 597–626. doi:10.1146/annurev.mi.47.100193.003121

49. Jullesson D, David F, Pfleger B, Nielsen J. Impact of synthetic biology and metabolic engineering on industrial production of fine chemicals. Biotechnol Adv. 2015;33: 1395–1402. doi:10.1016/j.biotechadv.2015.02.011

50. Lee SY, Kim HU. Systems strategies for developing industrial microbial strains. Nat Biotechnol. 2015;33: 1061–1072. doi:10.1038/nbt.3365

51. Zhang MM, Wang Y, Ang EL, Zhao H. Engineering microbial hosts for production of bacterial natural products. Nat Prod Rep. 2016;33: 963–987. doi:10.1039/C6NP00017G

52. Medema MH, Breitling R, Bovenberg R, Takano E. Exploiting plug-and-play synthetic biology for drug discovery and production in microorganisms. Nat Rev Microbiol. 2011;9: 131–137. doi:10.1038/nrmicro2478

53. Heux S, Meynial-Salles I, O'Donohue MJ, Dumon C. White biotechnology: State of the art strategies for the development of biocatalysts for biorefining. Biotechnol Adv. 2015;33: 1653–1670. doi:10.1016/j.biotechadv.2015.08.004

54. Baeshen MN, Al-Hejin AM, Bora RS, Ahmed MMM, Ramadan HAI, Saini KS, Baeshen NA, Redwan EM. Production of biopharmaceuticals in *E. coli*: current scenario and future perspectives. J Microbiol Biotechnol. 2015;25: 953–962. doi:10.4014/jmb.1412.12079

55. Berlec A, Štrukelj B. Current state and recent advances in biopharmaceutical production in *Escherichia coli*, yeasts and mammalian cells. J Ind Microbiol Biotechnol. 2013;40: 257–274. doi:10.1007/s10295-013-1235-0

56. Ferrer-Miralles N, Domingo-Espín J, Corchero J, Vázquez E, Villaverde A. Microbial factories for recombinant pharmaceuticals. Microb Cell Fact. 2009;8: 17. doi:10.1186/1475-2859-8-17

57. Huang C-J, Lin H, Yang X. Industrial production of recombinant therapeutics in *Escherichia coli* and its recent advancements. J Ind Microbiol Biotechnol. 2012;39: 383–399. doi:10.1007/s10295-011-1082-9

58. Schmidt FR. Recombinant expression systems in the pharmaceutical industry. Appl Microbiol Biotechnol. 2004;65: 363–372. doi:10.1007/s00253-004-1656-9

59. Borkowski O, Bricio C, Murgiano M, Rothschild-Mancinelli B, Stan G-B, Ellis T. Cell-free prediction of protein expression costs for growing cells. Nat Commun. 2018;9: 1457. doi:10.1038/s41467-018-03970-x

60. Liu Q, Schumacher J, Wan X, Lou C, Wang B. Orthogonality and burdens of heterologous and gate gene circuits in *E. coli*. ACS Synth Biol. 2018;7: 553–564. doi:10.1021/acssynbio.7b00328

61. Gorochowski TE, Chelysheva I, Eriksen M, Nair P, Pedersen S, Ignatova Z. Absolute quantification of translational regulation and burden using combined sequencing approaches. Mol Syst Biol. 2019;15. doi:10.15252/msb.20188719

62. Ceroni F, Algar R, Stan GB, Ellis T. Quantifying cellular capacity identifies gene expression designs with reduced burden. Nat Methods. 2015;12: 415–418. doi:10.1038/nmeth.3339

63. Sabi R, Tuller T. Modelling and measuring intracellular competition for finite resources during gene expression. Journal of the Royal Society Interface. Royal Society Publishing; 2019. doi:10.1098/rsif.2018.0887

64. Frumkin I, Schirman D, Rotman A, Li F, Zahavi L, Mordret E, Asraf O, Wu S, Levy SF, Pilpel Y. Gene Architectures that Minimize Cost of Gene Expression. Mol Cell. 2017;65: 142–153. doi:10.1016/j.molcel.2016.11.007

65. Bradley RW, Buck M, Wang B. Tools and Principles for Microbial Gene Circuit Engineering. J Mol Biol. 2016;428: 862–888. doi:10.1016/j.jmb.2015.10.004

66. Engstrom MD, Pfleger BF. Transcription control engineering and applications in synthetic biology. Synth Syst Biotechnol. 2017;2: 176–191. doi:10.1016/j.synbio.2017.09.003

67. Kent R, Dixon N. Contemporary Tools for Regulating Gene Expression in Bacteria. Trends Biotechnol. 2020;38: 316–333. doi:10.1016/j.tibtech.2019.09.007

68. Kurland CG, Dong H. Bacterial growth inhibition by overproduction of protein. Mol Microbiol. 1996;21: 1–4. doi:10.1046/j.1365-2958.1996.5901313.x

69. Burg JM, Cooper CB, Ye Z, Reed BR, Moreb EA, Lynch MD. Large-scale bioprocess competitiveness: the potential of dynamic metabolic control in two-stage fermentations. Current Opinion in Chemical Engineering. Elsevier Ltd; 2016. pp. 121–136. doi:10.1016/j.coche.2016.09.008

70. Woodley JM. Towards the sustainable production of bulk-chemicals using biotechnology. N Biotechnol. 2020;59: 59–64. doi:10.1016/j.nbt.2020.07.002

71. Terpe K. Overview of bacterial expression systems for heterologous protein production: from molecular and biochemical fundamentals to commercial systems. Appl Microbiol Biotechnol. 2006;72: 211–222. doi:10.1007/s00253-006-0465-8

72. Zhou S, Du G, Kang Z, Li J, Chen J, Li H, Zhou J. The application of powerful promoters to enhance gene expression in industrial microorganisms. World J Microbiol Biotechnol. 2017;33: 23. doi:10.1007/s11274-016-2184-3

73. Polisky B, Bishop RJ, Gelfand DH. A plasmid cloning vehicle allowing regulated expression of eukaryotic DNA in bacteria. Proc Natl Acad Sci U S A. 1976;73: 3900–3904. doi:10.1073/pnas.73.11.3900

74. Gronenborn B. Overproduction of phage Lambda repressor under control of the *lac* promotor of *Escherichia coli*. MGG Mol Gen Genet. 1976;148: 243–250. doi:10.1007/BF00332898

75. Wanner BL, Kodaira R, Neidhardt FC. Physiological regulation of a decontrolled *lac* operon. J Bacteriol. 1977;130: 212–222. doi:10.1128/jb.130.1.212-222.1977

76. Grossman TH, Kawasaki ES, Punreddy SR, Osburne MS. Spontaneous cAMP-dependent derepression of gene expression in stationary phase plays a role in recombinant expression instability. Gene. 1998;209: 95–103. doi:10.1016/S0378-1119(98)00020-1

77. Dubendorf JW, Studier FWW. Controlling basal expression in an inducible T7 expression system by blocking the target T7 promoter with *lac* repressor. J Mol Biol. 1991;219: 45–59. doi:10.1016/0022-2836(91)90856-2

78. Studier FW. Use of bacteriophage T7 lysozyme to improve an inducible T7 expression system. J Mol Biol. 1991;219: 37–44. doi:10.1016/0022-2836(91)90855-Z

79. Pan SH, Malcolm BA. Reduced background expression and improved plasmid stability with pET vectors in BL21 (DE3). Biotechniques. 2000;29: 1234–1238. doi:10.2144/00296st03

80. Siebenlist U. *E. coli* RNA polymerase interacts homologously with two different promoters. Cell. 1980;20: 269–281. doi:10.1016/0092-8674(80)90613-3

81. Rosenberg M, Court D. Regulatory Sequences involved in the promotion and termination of RNA transcription. Annu Rev Genet. 1979;13: 319–353. doi:10.1146/annurev.ge.13.120179.001535

82. De Boer HA, Comstock LJ, Vassert M. The *tac* promoter: A functional hybrid derived from the *trp* and *lac* promoters. Proc NatL Acad Sci USA. 1983;80: 21–25. doi:10.1073/pnas.80.1.21

83. Amann E, Brosius J, Ptashne M. Vectors bearing a hybrid *trp-lac* promoter useful for regulated expression of cloned genes in *Escherichia coli*. Gene. 1983;25: 167–178. doi:10.1016/0378-1119(83)90222-6

84. Calos MP. DNA sequence for a low-level promoter of the *lac* repressor gene and an “up” promoter mutation. Nature. 1978;274: 762–765. doi:10.1038/274762a0

85. Studier FW, Moffatt BA. Use of bacteriophage T7 RNA polymerase to direct selective high-level expression of cloned genes. J Mol Biol. 1986;189: 113–130. doi:10.1016/0022-2836(86)90385-2

86. Samuelson JC. Recent developments in difficult protein expression: A guide to *E. coli* strains, promoters, and relevant host mutations. Methods Mol Biol. 2011. doi:10.1007/978-1-61737-967-3_11

87. Tegel H, Ottosson J, Hober S. Enhancing the protein production levels in *Escherichia coli* with a strong promoter. FEBS J. 2011;278: 729–739. doi:10.1111/j.1742-4658.2010.07991.x

88. Gräslund S, Nordlund P, Weigelt J, Hallberg BM, Bray J, Gileadi O, Knapp S, Oppermann U, Arrowsmith C, Hui R, Ming J, dhe-Paganon S, Park HW, Savchenko A, Yee A, Edwards A, Vincentelli R, Cambillau C, Kim R, Kim SH, Rao Z, Shi Y, Terwilliger TC, Kim CY, Hung LW, Waldo GS, Peleg Y, Albeck S, Unger

T, Dym O, Prilusky J, Sussman JL, Stevens RC, Lesley SA, Wilson IA, Joachimiak A, Collart F, Dementieva I, Donnelly MI, Eschenfeldt WH, Kim Y, Stols L, Wu R, Zhou M, Burley SK, Emtage JS, Sauder JM, Thompson D, Bain K, Luz J, Gheyi T, Zhang F, Atwell S, Almo SC, Bonanno JB, Fiser A, Swaminathan S, Studier FW, Chance MR, Sali A, Acton TB, Xiao R, Zhao L, Ma LC, Hunt JF, Tong L, Cunningham K, Inouye M, Anderson S, Janjua H, Shastry R, Ho CK, Wang D, Wang H, Jiang M, Montelione GT, Stuart DI, Owens RJ, Daenke S, Schütz A, Heinemann U, Yokoyama S, Büssow K, Gunsalus KC. Protein production and purification. Nature Methods. 2008. doi:10.1038/nmeth.f.202

89. Moffatt BA, Studier FW. T7 lysozyme inhibits transcription by T7 RNA polymerase. Cell. 1987;49: 221–227. doi:10.1016/0092-8674(87)90563-0

90. Wagner S, Klepsch MM, Schlegel S, Appel A, Draheim R, Tarry M, Hogbom M, van Wijk KJ, Slotboom DJ, Persson JO, de Gier J-W. Tuning *Escherichia coli* for membrane protein overexpression. Proc Natl Acad Sci. 2008;105: 14371–14376. doi:10.1073/pnas.0804090105

91. Monod J, Cohen-Bazire G, Cohn M. [The biosynthesis of beta-galactosidase (lactase) in Escherichia coli; the specificity of induction]. Biochim Biophys Acta. 1951;7: 585–599. doi:10.1016/0006-3002(51)90072-8

92. Monod J. [Specific inductors and inhibitors in the biosynthesis of an enzyme; beta-galactosidase of *Escherichia coli*]. Bull World Health Organ. 1952;6: 59–64. PMID: 14954411

93. Boezi JA, Cowie DB. Kinetic studies of β-galactosidase induction. Biophys J. 1961;1: 639–647. doi:10.1016/S0006-3495(61)86913-0

94. Cohn M. Contributions of studies on the beta-galactosidase of *Escherichia coli* to our understanding of enzyme synthesis. Bacteriol Rev. 1957;21: 140–168. doi:10.1128/MMBR.21.3.140-168.1957

95. Gilbert W, Muller-Hill B. Isolation of the *lac* repressor. Proc Natl Acad Sci. 1966;56: 1891–1898. doi:10.1073/pnas.56.6.1891

96. Troeschel SC, Thies S, Link O, Real CI, Knops K, Wilhelm S, Rosenau F, Jaeger K-E. Novel broad host range shuttle vectors for expression in *Escherichia coli*, *Bacillus subtilis* and *Pseudomonas putida*. J Biotechnol. 2012;161: 71–79. doi:10.1016/j.jbiotec.2012.02.020

97. de Lorenzo V, Eltis L, Kessler B, Timmis KN. Analysis of *Pseudomonas* gene products using *lacIq/Ptrp-lac* plasmids and transposons that confer conditional phenotypes. Gene. 1993;123: 17–24.

98. Nikel PI, de Lorenzo V. *Pseudomonas putida* as a functional chassis for industrial biocatalysis: From native biochemistry to *trans*-metabolism. Metab Eng. 2018;50: 142–155. doi:10.1016/j.ymben.2018.05.005

99. Eikmanns BJ, Kleinertz E, Liebl W, Sahm H. A family of *Corynebacterium glutamicum*/*Escherichia coli* shuttle vectors for cloning, controlled gene expression, and promoter probing. Gene. 1991;102: 93–98. doi:10.1016/0378-1119(91)90545-M

100. Kortmann M, Kuhl V, Klaffl S, Bott M. A chromosomally encoded T7 RNA polymerase-dependent gene expression system for *Corynebacterium glutamicum*: Construction and comparative evaluation at the single-cell level.

Microb Biotechnol. 2015;8: 253–265. doi:10.1111/1751-7915.12236

101. Bagdasarian MM, Amann E, Lurz R, Rückert B, Bagdasarian M. Activity of the hybrid *trp-lac (tac)* promoter of *Escherichia coli* in *Pseudomonas putida*. Construction of broad-host-range, controlled-expression vectors. Gene. 1983;26: 273–282. doi:10.1016/0378-1119(83)90197-X

102. Nguyen HD, Phan TTP, Schumann W. Expression vectors for the rapid purification of recombinant proteins in *Bacillus subtilis*. Curr Microbiol. 2007;55: 89–93. doi:10.1007/s00284-006-0419-5

103. Binder D, Probst C, Grünberger A, Hilgers F, Loeschcke A, Jaeger K-E, Kohlheyer D, Drepper T. Comparative single-cell analysis of different *E. coli* dxpression systems during microfluidic cultivation. PLoS One. 2016;11: 1–19. doi:10.1371/journal.pone.0160711

104. Hansen LH, Knudsen S, Sørensen SJ. The effect of the lacY gene on the induction of IPTG inducible promoters, studied in *Escherichia coli* and *Pseudomonas fluorescens*. Curr Microbiol. 1998;36: 341–347. doi:10.1007/s002849900320

105. Lee MJ, Kim P. Recombinant protein expression system in *Corynebacterium glutamicum* and its application. Front. Microbiol. 2018. p. 2523. doi:10.3389/fmicb.2018.02523

106. Balzer S, Kucharova V, Megerle J, Lale R, Brautaset T, Valla S. A comparative analysis of the properties of regulated promoter systems commonly used for recombinant gene expression in *Escherichia coli*. Microb Cell Fact. 2013;12: 1–14. doi:10.1186/1475-2859-12-26

107. Marschall L, Sagmeister P, Herwig C. Tunable recombinant protein expression in *E. coli*: promoter systems and genetic constraints. Appl. Microbiol. Biotechnol. 2017. pp. 501–512. doi:10.1007/s00253-016-8045-z

108. Rosano GL, Ceccarelli EA. Recombinant protein expression in *Escherichia coli*: advances and challenges. Front. Microbiol. 2014. p. 172. doi:10.3389/fmicb.2014.00172

109. Greenblatt J, Schleif R. Arabinose C protein: regulation of the arabinose operon *in vitro*. Nat New Biol. 1971;233: 166–170. doi:10.1038/newbio233166a0

110. Wilcox G. The Interaction of L-Arabinose and D-Fucose with AraC Protein. J Biol Chem. 1974;249: 6892–6894. doi:10.1016/S0021-9258(19)42141-8

111. Beverin S, Sheppard DE, Park SS. D-Fucose as a gratuitous inducer of the L-arabinose operon in strains of *Escherichia coli* B-r mutant in gene *araC*. J Bacteriol. 1971;107: 79–86. doi:10.1128/jb.107.1.79-86.1971

112. Lee SK, Chou HH, Pfleger BF, Newman JD, Yoshikuni Y, Keasling JD. Directed evolution of AraC for improved compatibility of arabinose- and lactose-inducible promoters. Appl Environ Microbiol. 2007;73: 5711–5715. doi:10.1128/AEM.00791-07

113. Tang SY, Fazelinia H, Cirino PC. AraC regulatory protein mutants with altered effector specificity. J Am Chem Soc. 2008;130: 5267–5271. doi:10.1021/ja7109053

114. Tang S-Y, Cirino PC. Design and application of a mevalonate-responsive regulatory protein. Angew Chemie Int Ed. 2011;50: 1084–1086.

doi:10.1002/anie.201006083

115. Khlebnikov A, Risa Ø, Skaug T, Carrier TA, Keasling JD. Regulatable arabinose-inducible gene expression system with consistent control in all cells of a culture. J Bacteriol. 2000;182: 7029–7034. doi:10.1128/JB.182.24.7029-7034.2000

116. Fritz G, Megerle JA, Westermayer SA, Brick D, Heermann R, Jung K, Rädler JO, Gerland U. Single cell kinetics of phenotypic switching in the arabinose utilization system of *E. coli*. PLoS One. 2014;9: e89532. doi:10.1371/journal.pone.0089532

117. Afroz T, Biliouris K, Kaznessis Y, Beisel CL. Bacterial sugar utilization gives rise to distinct single-cell behaviours. Mol Microbiol. 2014;93: 1093–1103. doi:10.1111/mmi.12695

118. Zhang Y, Shang X, Lai S, Zhang G, Liang Y, Wen T. Development and application of an arabinose-inducible expression system by facilitating inducer uptake in *Corynebacterium glutamicum*. Appl Environ Microbiol. 2012;78: 5831–5838. doi:10.1128/AEM.01147-12

119. Calero P, Jensen SI, Nielsen AT. Broad-host-range ProUSER vectors enable fast characterization of inducible promoters and optimization of p-coumaric acid production in *Pseudomonas putida* KT2440. ACS Synth Biol. 2016. doi:10.1021/acssynbio.6b00081

120. Thompson MG, Valencia LE, Blake-Hedges JM, Cruz-Morales P, Velasquez AE, Pearson AN, Sermeno LN, Sharpless WA, Benites VT, Chen Y, Baidoo EEK, Petzold CJ, Deutschbauer AM, Keasling JD. Omics-driven identification and elimination of valerolactam catabolism in *Pseudomonas putida* KT2440 for increased product titer. Metab Eng Commun. 2019;9: e00098. doi:10.1016/j.mec.2019.e00098

121. Fricke PM, Link T, Gätgens J, Sonntag C, Otto M, Bott M, Polen T. A tunable l-arabinose-inducible expression plasmid for the acetic acid bacterium *Gluconobacter oxydans*. Appl Microbiol Biotechnol. 2020;104: 9267–9282. doi:10.1007/s00253-020-10905-4

122. Ramos JL, Gonzalez-Carrero M, Timmis KN. Broad-host range expression vectors containing manipulated *meta*-cleavage pathway regulatory elements of the TOL plasmid. FEBS Lett. 1988;226: 241–246. doi:10.1016/0014-5793(88)81431-5

123. Blatny JM, Brautaset T, Winther-Larsen HC, Karunakaran P, Valla S. Improved broad-host-range RK2 vectors useful for high and low regulated gene expression levels in gram-negative bacteria. Plasmid. 1997;38: 35–51. doi:10.1006/plas.1997.1294

124. Loeschcke A, Thies S. Engineering of natural product biosynthesis in *Pseudomonas putida*. Curr Opin Biotechnol. 2020;65: 213–224. doi:10.1016/j.copbio.2020.03.007

125. Bakke I, Berg L, Aune TEV, Brautaset T, Sletta H, Tøndervik A, Valla S. Random mutagenesis of the Pm promoter as a powerful strategy for improvement of recombinant-gene expression. Appl Environ Microbiol. 2009;75: 2002–2011. doi:10.1128/AEM.02315-08

126. Lale R, Berg L, Stüttgen F, Netzer R, Stafsnes M, Brautaset T, Aune TEV, Valla S. Continuous control of the flow in biochemical pathways through 5’ untranslated

region sequence modifications in mRNA expressed from the broad-host-range promoter Pm. Appl Environ Microbiol. 2011;77: 2648–2655. doi:10.1128/AEM.02091-10

127. Nikel PI, de Lorenzo V. Robustness of *Pseudomonas putida* KT2440 as a host for ethanol biosynthesis. N Biotechnol. 2014. doi:10.1016/j.nbt.2014.02.006

128. de Lorenzo V, Fernández S, Herrero M, Jakubzik U, Timmis KN. Engineering of alkyl- and haloaromatic-responsive gene expression with mini-transposons containing regulated promoters of biodegradative pathways of *Pseudomonas*. Gene. 1993;130: 41–46. doi:10.1016/0378-1119(93)90344-3

129. Dragset MS, Barczak AK, Kannan N, Mærk M, Flo TH, Valla S, Rubin EJ, Steigedal M. Benzoic acid-inducible gene expression in Mycobacteria. PLoS One. 2015;10: e0134544. doi:10.1371/journal.pone.0134544

130. Mitchell RJ, Gu MB. Construction and evaluation of *nagR-nagAa::lux* fusion strains in biosensing for salicylic acid derivatives. Appl Biochem Biotechnol - Part A Enzym Eng Biotechnol. 2005;120: 183–197. doi:10.1385/ABAB:120:3:183

131. Ju K-S, Parales J V., Parales RE. Reconstructing the evolutionary history of nitrotoluene detection in the transcriptional regulator NtdR. Mol Microbiol. 2009;74: 826–843. doi:10.1111/j.1365-2958.2009.06904.x

132. Wierckx NJP, Ballerstedt H, de Bont JAM, Wery J. Engineering of solvent-tolerant *Pseudomonas putida* S12 for bioproduction of phenol from glucose. Appl Environ Microbiol. 2005;71: 8221–8227. doi:10.1128/AEM.71.12.8221-8227.2005

133. Meijnen JP, Verhoef S, Briedjlal AA, De Winde JH, Ruijssenaars HJ. Improved p-hydroxybenzoate production by engineered *Pseudomonas putida* S12 by using a mixed-substrate feeding strategy. Appl Microbiol Biotechnol. 2011. doi:10.1007/s00253-011-3089-6

134. Verhoef S, Ballerstedt H, Volkers RJM, de Winde JH, Ruijssenaars HJ. Comparative transcriptomics and proteomics of p-hydroxybenzoate producing *Pseudomonas putida* S12: novel responses and implications for strain improvement. Appl Microbiol Biotechnol. 2010;87: 679–690. doi:10.1007/s00253-010-2626-z

135. Foti M, Médici R, Ruijssenaars HJ. Biological production of monoethanolamine by engineered *Pseudomonas putida* S12. J Biotechnol. 2013;167: 344–349. doi:10.1016/j.jbiotec.2013.07.013

136. Schmitz S, Nies S, Wierckx N, Blank LM, Rosenbaum MA. Engineering mediator-based electroactivity in the obligate aerobic bacterium *Pseudomonas putida* KT2440. Front Microbiol. 2015;6: 1–13. doi:10.3389/fmicb.2015.00284

137. Tiso T, Ihling N, Kubicki S, Biselli A, Schonhoff A, Bator I, Thies S, Karmainski T, Kruth S, Willenbrink A-L, Loeschcke A, Zapp P, Jupke A, Jaeger K-E, Büchs J, Blank LM. Integration of genetic and process engineering for optimized rhamnolipid production using *Pseudomonas putida*. Front Bioeng Biotechnol. 2020;8: 1–24. doi:10.3389/fbioe.2020.00976

138. Lenzen C, Wynands B, Otto M, Bolzenius J, Mennicken P, Blank LM, Wierckx N. High-yield production of 4-hydroxybenzoate from glucose or glycerol by an engineered *Pseudomonas taiwanensis* VLB120. Front Bioeng Biotechnol. 2019;7. doi:10.3389/fbioe.2019.00130

139. Neves D, Vos S, Blank LM, Ebert BE. *Pseudomonas* mRNA 2.0: boosting gene expression through enhanced mRNA stability and translational efficiency. Front Bioeng Biotechnol. 2020;7: 458. doi:10.3389/fbioe.2019.00458

140. Lee JH, Mitchell RJ, Gu MB. Chemical-specific continuous biomonitoring using a recombinant bioluminescent bacterium DNT5 (*nagR-nagAa::luxCDABE*). J Biotechnol. 2007;131: 330–334. doi:10.1016/j.jbiotec.2007.06.020

141. Becker PD, Royo JL, Guzman CA. Exploitation of prokaryotic expression systems based on the salicylate-dependent control circuit encompassing *nahR*/*Psal*. Bioeng Bugs. 2010;1: 246–253. doi:10.4161/bbug.1.4.11247

142. Moses T, Mehrshahi P, Smith AG, Goossens A. Synthetic biology approaches for the production of plant metabolites in unicellular organisms. J Exp Bot. 2017;68: 4057–4074. doi:10.1093/jxb/erx119

143. Cravens A, Payne J, Smolke CD. Synthetic biology strategies for microbial biosynthesis of plant natural products. Nat Commun. 2019;10: 2142. doi:10.1038/s41467-019-09848-w

144. Pham J V., Yilma MA, Feliz A, Majid MT, Maffetone N, Walker JR, Kim E, Cho HJ, Reynolds JM, Song MC, Park SR, Yoon YJ. A review of the microbial production of bioactive natural products and biologics. Front Microbiol. 2019;10: 1–27. doi:10.3389/fmicb.2019.01404

145. Sanchez-Garcia L, Martín L, Mangues R, Ferrer-Miralles N, Vázquez E, Villaverde A. Recombinant pharmaceuticals from microbial cells: A 2015 update. Microb. Cell Fact. BioMed Central Ltd.; 2016. p. 33. doi:10.1186/s12934-016-0437-3

146. Human insulin receives FDA approval. FDA Drug Bulletin; Dec, 1982 pp. 18–19. PMID: 6762312. Available: https://pubmed.ncbi.nlm.nih.gov/6762312/

147. Abdin MZ, Israr M, Rehman RU, Jain SK. Artemisinin, a novel antimalarial drug: Biochemical and molecular approaches for enhanced production. Planta Medica. © Georg Thieme Verlag Stuttgart · New York; 2003. pp. 289–299. doi:10.1055/s-2003-38871

148. Chang MCY, Eachus RA, Trieu W, Ro DK, Keasling JD. Engineering *Escherichia coli* for production of functionalized terpenoids using plant P450s. Nat Chem Biol. 2007;3: 274–277. doi:10.1038/nchembio875

149. Zhang H, Wang Y, Wu J, Skalina K, Pfeifer BA. Complete biosynthesis of erythromycin A and designed analogs using *E. coli* as a heterologous host. Chem Biol. 2010;17: 1232–1240. doi:10.1016/j.chembiol.2010.09.013

150. Prouty WF, Karnovsky MJ, Goldberg AL. Degradation of abnormal proteins in *Escherichia coli*. Formation of protein inclusions in cells exposed to amino acid analogs. J Biol Chem. 1975;250: 1112–1122. doi:10.1016/s0021-9258(19)41897-8

151. Marston FA. The purification of eukaryotic polypeptides synthesized in *Escherichia coli.* Biochem J; 1986. pp. 1–12. doi:10.1042/bj2400001

152. Martínez-Alonso M, González-Montalbán N, García-Fruitós E, Villaverde A. Learning about protein solubility from bacterial inclusion bodies. Microb Cell Fact. 2009;8: 4. doi:10.1186/1475-2859-8-4

153. Villaverde A, Carrió MM. Protein aggregation in recombinant bacteria: Biological

role of inclusion bodies. Biotechnol Lett; 2003. pp. 1385–1395. doi:10.1023/A:1025024104862

154. Makrides SC. Strategies for achieving high-level expression of genes in *Escherichia coli*. Microbiol. Revs. American Society for Microbiology; 1996. pp. 512–538. doi:10.1128/mmbr.60.3.512-538.1996

155. McNulty DE, Claffee BA, Huddleston MJ, Kane JF. Mistranslational errors associated with the rare arginine codon CGG in *Escherichia coli*. Protein Expr Purif. 2003;27: 365–374. doi:10.1016/S1046-5928(02)00610-1

156. Wassenaar TM, Zimmermann K. Lipopolysaccharides in food, food supplements, and probiotics: should we be worried? Eur J Microbiol Immunol. 2018;8: 63–69. doi:10.1556/1886.2018.00017

157. Petsch D. Endotoxin removal from protein solutions. J Biotechnol. 2000;76: 97–119. doi:10.1016/S0168-1656(99)00185-6

158. Zhang K, Su L, Wu J. Recent advances in recombinant protein production by *Bacillus subtilis*. Annu Rev Food Sci Technol. 2020;11: 295–318. doi:10.1146/annurev-food-032519-051750

159. Westers L, Westers H, Quax WJ. *Bacillus subtilis* as cell factory for pharmaceutical proteins: a biotechnological approach to optimize the host organism. Biochim Biophys Acta - Mol Cell Res. 2004;1694: 299–310. doi:10.1016/j.bbamcr.2004.02.011

160. Harwood CR, Cranenburgh R. *Bacillus* protein secretion: an unfolding story. Trends Microbiol. 2008;16: 73–79. doi:10.1016/j.tim.2007.12.001

161. Simonen M, Palva I. Protein secretion in *Bacillus* species. Microbiol Rev. 1993;57: 109–37. doi: 10.1128/mr.57.1.109-137.1993

162. Palva I. Molecular cloning of α-amylase gene from *Bacillus amyloliquefaciens* and its expression in *B. subtilis*. Gene. 1982;19: 81–87. doi:10.1016/0378-1119(82)90191-3

163. Mohammed Y, Lee B, Kang Z, Du G. Development of a two-step cultivation strategy for the production of vitamin B12 by *Bacillus megaterium*. Microb Cell Fact. 2014;13: 102. doi:10.1186/s12934-014-0102-7

164. Ferrari E, Jarnagin AS, Schmidt BF. Commercial production of extracellular enzymes. *Bacillus subtilis* and other Gram-positive bacteria. Washington, DC, USA: ASM Press; 2014. pp. 917–937. doi:10.1128/9781555818388.ch62

165. Li W, Zhou X, Lu P. Bottlenecks in the expression and secretion of heterologous proteins in *Bacillus subtilis*. Res Microbiol. 2004;155: 605–610. doi:10.1016/j.resmic.2004.05.002

166. Ye R, Kim J-H, Kim B-G, Szarka S, Sihota E, Wong S-L. High-level secretory production of intact, biologically active staphylokinase from *Bacillus subtilis*. Biotechnol Bioeng. 1999;62: 87–96. doi:10.1002/(SICI)1097-0290(19990105)62:1<87::AID-BIT10>3.0.CO;2-I

167. Wu XC, Lee W, Tran L, Wong SL. Engineering a *Bacillus subtilis* expression-secretion system with a strain deficient in six extracellular proteases. J Bacteriol. 1991;173: 4952–4958. doi:10.1128/JB.173.16.4952-4958.1991

168. Lee J-Y, Na Y-A, Kim E, Lee H-S, Kim P. The actinobacterium *Corynebacterium glutamicum*, an industrial workhorse. J Microbiol Biotechnol. 2016;26: 807–822. doi:10.4014/jmb.1601.01053

169. Nakamura Y, Nishio Y, Ikeo K, Gojobori T. The genome stability in *Corynebacterium* species due to lack of the recombinational repair system. Gene. 2003;317: 149–155. doi:10.1016/S0378-1119(03)00653-X

170. Kawaguchi H, Vertès AA, Okino S, Inui M, Yukawa H. Engineering of a xylose metabolic pathway in *Corynebacterium glutamicum*. Appl Environ Microbiol. 2006;72: 3418–28. doi:10.1128/AEM.72.5.3418-3428.2006

171. Wendisch VF, Bott M, Eikmanns BJ. Metabolic engineering of *Escherichia coli* and *Corynebacterium glutamicum* for biotechnological production of organic acids and amino acids. Curr Opin Microbiol. 2006;9: 268–274. doi:10.1016/j.mib.2006.03.001

172. Sasaki M, Jojima T, Inui M, Yukawa H. Simultaneous utilization of D-cellobiose, D-glucose, and D-xylose by recombinant *Corynebacterium glutamicum* under oxygen-deprived conditions. Appl Microbiol Biotechnol. 2008;81: 691–699. doi:10.1007/s00253-008-1703-z

173. Liu X, Yang Y, Zhang W, Sun Y, Peng F, Jeffrey L, Harvey L, McNeil B, Bai Z. Expression of recombinant protein using *Corynebacterium glutamicum*: progress, challenges and applications. Crit Rev Biotechnol. 2016;36: 652–664. doi:10.3109/07388551.2015.1004519

174. Simon O, Klaiber I, Huber A, Pfannstiel J. Comprehensive proteome analysis of the response of *Pseudomonas putida* KT2440 to the flavor compound vanillin. J Proteomics. 2014;109: 212–227. doi:10.1016/j.jprot.2014.07.006

175. Akkaya Ö, Pérez-Pantoja DR, Calles B, Nikel PI, de Lorenzo V. The metabolic redox regime of *Pseudomonas putida* tunes its evolvability toward novel xenobiotic substrates. MBio. 2018;9. doi:10.1128/mBio.01512-18

176. Kieboom J, Dennis JJ, de Bont JAM, Zylstra GJ. Identification and molecular characterization of an efflux pump involved in *Pseudomonas putida* S12 solvent tolerance. J Biol Chem. 1998;273: 85–91. doi:10.1074/jbc.273.1.85

177. Fernández M, Conde S, de la Torre J, Molina-Santiago C, Ramos J-L, Duque E. Mechanisms of resistance to chloramphenicol in *Pseudomonas putida* KT2440. Antimicrob Agents Chemother. 2012;56: 1001–1009. doi:10.1128/AAC.05398-11

178. Chavarría M, Nikel PI, Pérez-Pantoja D, De Lorenzo V. The Entner-Doudoroff pathway empowers *Pseudomonas putida* KT2440 with a high tolerance to oxidative stress. Environ Microbiol. 2013;15: 1772–1785. doi:10.1111/1462-2920.12069

179. Tiso T, Zauter R, Tulke H, Leuchtle B, Li W-J, Behrens B, Wittgens A, Rosenau F, Hayen H, Blank LM. Designer rhamnolipids by reduction of congener diversity: production and characterization. Microb Cell Fact. 2017;16: 225. doi:10.1186/s12934-017-0838-y

180. Martínez-García E, de Lorenzo V. *Pseudomonas putida* in the quest of programmable chemistry. Current Opinion in Biotechnology. 2019. doi:10.1016/j.copbio.2019.03.012

181. Incha MR, Thompson MG, Blake-Hedges JM, Liu Y, Pearson AN, Schmidt M, Gin

JW, Petzold CJ, Deutschbauer AM, Keasling JD. Leveraging host metabolism for bisdemethoxycurcumin production in *Pseudomonas putida*. Metab Eng Commun. 2020. doi:10.1016/j.mec.2019.e00119

182. Stoppani AO, Fuller RC, Calvin M. Carbon dioxide fixation by *Rhodopseudomonas capsulatus*. J Bacteriol. 1955;69: 491–501. doi:10.1128/jb.69.5.491-501.1955

183. Tabita FR. The biochemistry and metabolic regulation of carbon metabolism and CO_2 fixation in purple bacteria. Anoxygenic Photosynthetic Bacteria: Advances in Photosynthesis and Respiration, vol 2. Springer, Dordrecht; 1995. pp. 885–914. doi:10.1007/0-306-47954-0_41

184. Strnad H, Lapidus A, Paces J, Ulbrich P, Vlcek C, Paces V, Haselkorn R. Complete genome sequence of the photosynthetic purple nonsulfur bacterium *Rhodobacter capsulatus* SB1003. J Bacteriol. 2010;192: 3545–6. doi:10.1128/JB.00366-10

185. Heck A, Drepper T. Engineering photosynthetic α-proteobacteria for the production of recombinant proteins and terpenoids. Modern Topics in the Phototrophic Prokaryotes: Environmental and Applied Aspects. Springer International Publishing; 2017. pp. 395–425. doi:10.1007/978-3-319-46261-5_12

186. Özgür AY. Evaluation of a *Rhodobacter capsulatus nif* promoter-based system for the heterologous expression of therapeutically relevant membrane proteins. Heinrich Heine University Düsseldorf. 2015. Dissertation.

187. Loeschcke A, Dienst D, Wewer V, Hage-Hülsmann J, Dietsch M, Kranz-Finger S, Hüren V, Metzger S, Urlacher VB, Gigolashvili T, Kopriva S, Axmann IM, Drepper T, Jaeger K-E. The photosynthetic bacteria *Rhodobacter capsulatus* and *Synechocystis sp.* PCC 6803 as new hosts for cyclic plant triterpene biosynthesis. PLoS One. 2017;12: e0189816. doi:10.1371/journal.pone.0189816

188. Troost K, Loeschcke A, Hilgers F, Özgür AY, Weber TM, Santiago-Schübel B, Svensson V, Hage-Hülsmann J, Habash SS, Grundler FMW, Schleker ASS, Jaeger K-E, Drepper T. Engineered *Rhodobacter capsulatus* as a phototrophic platform organism for the synthesis of plant sesquiterpenoids. Front Microbiol. 2019;10: 1998. doi:10.3389/fmicb.2019.01998

189. Hilgers F, Habash SS, Loeschcke A, Ackermann YS, Neumann S, Heck A, Klaus O, Hage-Hülsmann J, Grundler FMW, Jaeger K-E, Schleker ASS, Drepper T. Heterologous production of β-caryophyllene and evaluation of its activity against plant pathogenic fungi. Microorganisms. 2021;9. doi:10.3390/microorganisms9010168

190. Bhaya D. Light matters: phototaxis and signal transduction in unicellular cyanobacteria. Mol Microbiol. 2004;53: 745–754. doi:10.1111/j.1365-2958.2004.04160.x

191. Losi A, Gärtner W. Bacterial bilin- and flavin-binding photoreceptors. Photochem Photobiol Sci. 2008;7: 1168–78. doi:10.1039/b802472c

192. Montgomery BL. Sensing the light: photoreceptive systems and signal transduction in cyanobacteria. Mol Microbiol. 2007;64: 16–27. doi:10.1111/j.1365-2958.2007.05622.x

193. Berson DM, Dunn FA, Takao M. Phototransduction by retinal ganglion cells that

set the circadian clock. Science. 2002;295: 1070–1073. doi:10.1126/science.1067262

194. Shimizu-Sato S, Huq E, Tepperman JM, Quail PH. A light-switchable gene promoter system. Nat Biotechnol. 2002;20: 1041–1044. doi:10.1038/nbt734

195. Deisseroth K, Feng G, Majewska AK, Miesenböck G, Ting A, Schnitzer MJ. Next-generation optical technologies for illuminating genetically targeted brain circuits. J. Neurosci. 2006. pp. 10380–10386. doi:10.1523/JNEUROSCI.3863-06.2006

196. Hughes RM. A compendium of chemical and genetic approaches to light-regulated gene transcription. Crit Rev Biochem Mol Biol. 2018;53: 453–474. doi:10.1080/10409238.2018.1487382

197. Schmidl SR, Sheth RU, Wu A, Tabor JJ. Refactoring and optimization of light-switchable *Escherichia coli* two-component systems. ACS Synth Biol. 2014;3: 820–831. doi:10.1021/sb500273n

198. Nagatani A. Phytochrome: structural basis for its functions. Curr Opin Plant Biol. 2010;13: 565–70. doi:10.1016/j.pbi.2010.07.002

199. Rockwell NC, Su Y-S, Lagarias JC. Phytochrome structure and signaling mechanisms. Annu Rev Plant Biol. 2006;57: 837–58. doi:10.1146/annurev.arplant.56.032604.144208

200. Briggs WR, Christie JM. Phototropins 1 and 2: versatile plant blue-light receptors. Trends Plant Sci. 2002;7: 204–210. doi:10.1016/S1360-1385(02)02245-8

201. Losi A. The bacterial counterparts of plant phototropins. Photochem Photobiol Sci. 2004;3: 566–574. doi:10.1039/b400728j

202. Krauss U, Minh BQ, Losi A, Gärtner W, Eggert T, von Haeseler A, Jaeger K-E. Distribution and phylogeny of light-oxygen-voltage-blue-light-signaling proteins in the three kingdoms of life. J Bacteriol. 2009;191: 7234–7242. doi:10.1128/JB.00923-09

203. Losi A, Gärtner W. Old chromophores, new photoactivation paradigms, trendy applications: flavins in blue light-sensing photoreceptors. Photochem Photobiol. 2011;87: 491–510. doi:10.1111/j.1751-1097.2011.00913.x

204. Lin C, Todo T. The cryptochromes. Genome Biol. 2005;6: 220-220.9. doi:10.1186/gb-2005-6-5-220

205. Müller K, Engesser R, Metzger S, Schulz S, Kämpf MM, Busacker M, Steinberg T, Tomakidi P, Ehrbar M, Nagy F, Timmer J, Zubriggen MD, Weber W. A red/far-red light-responsive bi-stable toggle switch to control gene expression in mammalian cells. Nucleic Acids Res. 2013;41: e77–e77. doi:10.1093/nar/gkt002

206. Levskaya A, Chevalier AA, Tabor JJ, Simpson ZB, Lavery LA, Levy M, Davidson EA, Scouras A, Ellington AD, Marcotte EM, Voigt CA. Synthetic biology: engineering *Escherichia coli* to see light. Nature. 2005;438: 441–2. doi:10.1038/nature04405

207. Tabor JJ, Salis HM, Simpson ZB, Chevalier AA, Levskaya A, Marcotte EM, Voigt CA, Ellington AD. A Synthetic genetic edge detection program. Cell. 2009;137: 1272–1281. doi:10.1016/j.cell.2009.04.048

208. Tabor JJ, Levskaya A, Voigt C a. Multichromatic control of gene expression in

Escherichia coli. J Mol Biol. 2011;405: 315–324. doi:10.1016/j.jmb.2010.10.038

209. Schmidl SR, Ekness F, Sofjan K, Daeffler KNM, Brink KR, Landry BP, Gerhardt KP, Dyulgyarov N, Sheth RU, Tabor JJ. Rewiring bacterial two-component systems by modular DNA-binding domain swapping. Nat Chem Biol. 2019;15: 690–698. doi:10.1038/s41589-019-0286-6

210. Fernandez-Rodriguez J, Moser F, Song M, Voigt CA. Engineering RGB color vision into *Escherichia coli*. Nat Chem Biol. 2017;13: 706–708. doi:10.1038/nchembio.2390

211. Mushnikov N V., Fomicheva A, Gomelsky M, Bowman GR. Inducible asymmetric cell division and cell differentiation in a bacterium. Nat Chem Biol. 2019;15: 925–931. doi:10.1038/s41589-019-0340-4

212. Milias-Argeitis A, Rullan M, Aoki SK, Buchmann P, Khammash M. Automated optogenetic feedback control for precise and robust regulation of gene expression and cell growth. Nat Commun. 2016;7: 12546. doi:10.1038/ncomms12546

213. Olson EJ, Hartsough LA, Landry BP, Shroff R, Tabor JJ. Characterizing bacterial gene circuit dynamics with optically programmed gene expression signals. Nat Methods. 2014;11: 449–55. doi:10.1038/nmeth.2884

214. Ong NT, Olson EJ, Tabor JJ. Engineering an *E. coli* near-infrared light sensor. ACS Synth Biol. 2018;7: 240–248. doi:10.1021/acssynbio.7b00289

215. Kaberniuk A, Shemetov AA, Verkhusha V V. A bacterial phytochrome-based optogenetic system controllable with near-infrared light. Nat Methods. 2016;13: 591–597. doi:10.1038/nmeth.3864

216. Redchuk TA, Omelina ES, Chernov KG, Verkhusha V V. Near-infrared optogenetic pair for protein regulation and spectral multiplexing. Nat Chem Biol. 2017;13: 633–639. doi:10.1038/nchembio.2343

217. Möglich A, Moffat K. Structural basis for light-dependent signaling in the dimeric LOV domain of the photosensor YtvA. J Mol Biol. 2007;373: 112–126. doi:10.1016/j.jmb.2007.07.039

218. Möglich A, Ayers RA, Moffat K. Design and signaling mechanism of light-regulated histidine kinases. J Mol Biol. 2009;385: 1433–1444. doi:10.1016/j.jmb.2008.12.017

219. Drepper T, Krauss U, Meyer zu Berstenhorst S, Pietruszka J, Jaeger K-E. Lights on and action! Controlling microbial gene expression by light. Appl Microbiol Biotechnol. 2011;90: 23–40. doi:10.1007/s00253-011-3141-6

220. Christie JM, Gawthorne J, Young G, Fraser NJ, Roe AJ. LOV to BLUF: flavoprotein contributions to the optogenetic toolkit. Mol Plant. 2012;5: 533–44. doi:10.1093/mp/sss020

221. Ohlendorf R, Vidavski RR, Eldar A, Moffat K, Möglich A. From dusk till dawn: one-plasmid systems for light-regulated gene expression. J Mol Biol. 2012;416: 534–42. doi:10.1016/j.jmb.2012.01.001

222. Lalwani MA, Ip SS, Carrasco-López C, Day C, Zhao EM, Kawabe H, Avalos JL. Optogenetic control of the *lac* operon for bacterial chemical and protein production. Nat Chem Biol. 2020. doi:10.1038/s41589-020-0639-1

223. Yazawa M, Sadaghiani AM, Hsueh B, Dolmetsch RE. Induction of protein-protein interactions in live cells using light. Nat Biotechnol. 2009;27: 941–945. doi:10.1038/nbt.1569

224. Wang X, Chen X, Yang Y. Spatiotemporal control of gene expression by a light-switchable transgene system. Nat Methods. 2012;9: 266–269. doi:10.1038/nmeth.1892

225. Taslimi A, Zoltowski B, Miranda JG, Pathak GP, Hughes RM, Tucker CL. Optimized second-generation CRY2-CIB dimerizers and photoactivatable Cre recombinase. Nat Chem Biol. 2016;12: 425–430. doi:10.1038/nchembio.2063

226. Uda Y, Goto Y, Oda S, Kohchi T, Matsuda M, Aoki K. Efficient synthesis of phycocyanobilin in mammalian cells for optogenetic control of cell signaling. Proc Natl Acad Sci U S A. 2017;114: 11962–11967. doi:10.1073/pnas.1707190114

227. Kyriakakis P, Catanho M, Hoffner N, Thavarajah W, Hu VJ, Chao SS, Hsu A, Pham V, Naghavian L, Dozier LE, Patrick GN, Coleman TP. Biosynthesis of orthogonal molecules using ferredoxin and ferredoxin-NADP+ reductase systems enables genetically encoded PhyB optogenetics. ACS Synth Biol. 2018;7: 706–717. doi:10.1021/acssynbio.7b00413

228. Engels J, Schlaeger EJ. Synthesis, structure, and reactivity of adenosine cyclic 3',5'-phosphate benzyl triesters. J Med Chem. 1977;20: 907–911.

229. Ankenbruck N, Courtney T, Naro Y, Deiters A. Optochemical control of biological processes in cells and animals. Angew Chemie Int Ed. 2018;57: 2768–2798. doi:10.1002/anie.201700171

230. Young DD, Deiters A. Photochemical activation of protein expression in bacterial cells. Angew Chemie Int Ed. 2007;46: 4290–4292. doi:10.1002/anie.200700057

231. Binder D, Grünberger A, Loeschcke A, Probst C, Bier C, Pietruszka J, Wiechert W, Kohlheyer D, Jaeger K-E, Drepper T. Light-responsive control of bacterial gene expression: precise triggering of the *lac* promoter activity using photocaged IPTG. Integr Biol. 2014;6: 755–765. doi:10.1039/C4IB00027G

232. Bier C, Binder D, Drobietz D, Loeschcke A, Drepper T, Jaeger K-E, Pietruszka J. Photocaged carbohydrates: versatile tools for controlling gene expression by light. Synthesis (Stuttg). 2016;49: 42–52. doi:10.1055/s-0035-1562617

233. Binder D, Bier C, Grünberger A, Drobietz D, Hage-Hülsmann J, Wandrey G, Büchs J, Kohlheyer D, Loeschcke A, Wiechert W, Jaeger K-E, Pietruszka J, Drepper T. Photocaged Arabinose: A Novel Optogenetic Switch for Rapid and Gradual Control of Microbial Gene Expression. ChemBioChem. 2016;17: 296–299. doi:10.1002/cbic.201500609

234. Wright CW, Guo ZF, Liang F Sen. Light control of cellular processes by using photocaged abscisic acid. ChemBioChem. 2015;16: 254–261. doi:10.1002/cbic.201402576

235. Kusen PM, Wandrey G, Probst C, Grünberger A, Holz M, Meyer zu Berstenhorst S, Kohlheyer D, Büchs J, Pietruszka J. Optogenetic regulation of tunable gene expression in yeast using photo-labile caged methionine. ACS Chem Biol. 2016;11: 2915–2922. doi:10.1021/acschembio.6b00462

236. Kusen PM, Wandrey G, Krewald V, Holz M, Berstenhorst SM zu, Büchs J, Pietruszka J. Light-controlled gene expression in yeast using photocaged Cu^{2+}. J

Biotechnol. 2017;258: 117–125. doi:10.1016/j.jbiotec.2017.04.032

237. Cambridge SB, Geissler D, Calegari F, Anastassiadis K, Hasan MT, Stewart AF, Huttner WB, Hagen V, Bonhoeffer T. Doxycycline-dependent photoactivated gene expression in eukaryotic systems. Nat Methods. 2009;6: 527–531. doi:10.1038/nmeth.1340

238. Sauers DJ, Temburni MK, Biggins JB, Ceo LM, Galileo DS, Koh JT. Light-Activated Gene Expression Directs Segregation of Co-cultured Cells in Vitro. ACS Chem Biol. 2010;5: 313–320. doi:10.1021/cb9002305

239. Cambridge SB, Geissler D, Keller S, Cürten B. A caged doxycycline analogue for photoactivated gene expression. Angew Chem Int Ed Engl. 2006;45: 2229–31. doi:10.1002/anie.200503339

240. Reis SA, Ghosh B, Hendricks JA, Szantai-Kis DM, Törk L, Ross KN, Lamb J, Read-Button W, Zheng B, Wang H, Salthouse C, Haggarty SJ, Mazitschek R. Light-controlled modulation of gene expression by chemical optoepigenetic probes. Nat Chem Biol. 2016;12: 317–323. doi:10.1038/nchembio.2042

241. Link KH, Cruz FG, Ye HF, O'Reilly KE, Dowdell S, Koh JT. Photo-caged agonists of the nuclear receptors RARγ and TRβ provide unique time-dependent gene expression profiles for light-activated gene patterning. Bioorganic Med Chem. 2004;12: 5949–5959. doi:10.1016/j.bmc.2004.08.022

242. Lin W, Albanese C, Pestell RG, Lawrence DS. Spatially discrete, light-driven protein expression. Chem Biol. 2002;9: 1347–1353. doi:10.1016/S1074-5521(02)00288-0

243. Imoto T, Kawase A, Minoshima M, Yokoyama T, Bito H, Kikuchi K. Photolytic release of a caged inhibitor of an endogenous transcription factor enables optochemical control of CREB-mediated gene expression. Org Lett. 2020;22: 22–25. doi:10.1021/acs.orglett.9b03568

244. Chou C, Young DD, Deiters A. Photocaged T7 RNA polymerase for the light activation of transcription and gene function in pro- and eukaryotic cells. ChemBioChem. 2010;11: 972–977. doi:10.1002/cbic.201000041

245. Walsh S, Gardner L, Deiters A, Williams GJ. Intracellular light-activation of riboswitch activity. ChemBioChem. 2014; 1–7. doi:10.1002/cbic.201400024

246. Zhang D, Jin S, Piao X, Devaraj NK. Multiplexed photoactivation of mRNA with single-cell resolution. ACS Chem Biol. 2020;15: 1773–1779. doi:10.1021/acschembio.0c00205

247. Zhang D, Zhou CY, Busby KN, Alexander SC, Devaraj NK. Light-activated control of translation by enzymatic covalent mRNA labeling. Angew Chemie Int Ed. 2018;57: 2822–2826. doi:10.1002/anie.201710917

248. Yamaguchi S, Chen Y, Nakajima S, Furuta T, Nagamune T. Light-activated gene expression from site-specific caged DNA with a biotinylated photolabile protection group. Chem Commun. 2010;46: 2244–2246. doi:10.1039/b922502a

249. Ogasawara S. Control of cellular function by reversible photoregulation of translation. ChemBioChem. 2014;15: 2652–2655. doi:10.1002/cbic.201402495

250. Monroe WT, McQuain MM, Chang MS, Alexander JS, Haselton FR. Targeting expression with light using caged DNA. J Biol Chem. 1999;274: 20895–20900.

doi:10.1074/jbc.274.30.20895

251. Kröck L, Hechel A. Photoinduced transcription by using temporarily mismatched caged oligonucleotides. Angew Chemie - Int Ed. 2005;44: 471–473. doi:10.1002/anie.200461779

252. Stafforst T, Stadler JM. Photoactivation of a psoralen-blocked luciferase gene by blue light. Angew Chemie Int Ed. 2013;52: 12448–12451. doi:10.1002/anie.201306150

253. Heimes M, Kolmar L, Brieke C. Efficient cosubstrate enzyme pairs for sequence-specific methyltransferase-directed photolabile caging of DNA. Chem Commun. 2018;54: 12718–12721. doi:10.1039/c8cc05913f

254. Liang X, Wakuda R, Fujioka K, Asanuma H. Photoregulation of DNA transcription by using photoresponsive T7 promoters and clarification of its mechanism. FEBS J. 2010;277: 1551–1561. doi:10.1111/j.1742-4658.2010.07583.x

255. Govan JM, Young DD, Lusic H, Liu Q, Lively MO, Deiters A. Optochemical control of RNA interference in mammalian cells. Nucleic Acids Res. 2013;41: 10518–10528. doi:10.1093/nar/gkt806

256. Govan JM, Uprety R, Thomas M, Lusic H, Lively MO, Deiters A. Cellular delivery and photochemical activation of antisense agents through a nucleobase caging strategy. ACS Chem Biol. 2013;8: 2272–2282. doi:10.1021/cb400293e

257. Sakamoto T, Shigeno A, Ohtaki Y, Fujimoto K. Photo-regulation of constitutive gene expression in living cells by using ultrafast photo-cross-linking oligonucleotides. Biomater Sci. 2014;2: 1154–1157. doi:10.1039/c4bm00117f

258. Zhang L, Chen C, Fan X, Tang X. Photomodulating gene expression by using caged siRNAs with single-aptamer modification. ChemBioChem. 2018;19: 1259–1263. doi:10.1002/cbic.201700623

259. Yang L, Kim HB, Sul J-Y, Yeldell SB, Eberwine JH, Dmochowski IJ. Efficient synthesis of light-triggered circular antisense oligonucleotides targeting cellular protein expression. ChemBioChem. 2018;19: 1250–1254. doi:10.1002/cbic.201800012

260. Mikat V, Heckel A. Light-dependent RNA interference with nucleobase-caged siRNAs. RNA. 2007;13: 2341–2347. doi:10.1261/rna.753407

261. Deiters A. Principles and applications of the photochemical control of cellular processes. ChemBioChem. 2010;11: 47–53. doi:10.1002/cbic.200900529

262. Young DD, Deiters A. Photochemical control of biological processes. Org Biomol Chem. 2007;5: 999–1005. doi:10.1039/b616410m

263. Görner H. Effects of 4,5-dimethoxy groups on the time-resolved photoconversion of 2-nitrobenzyl alcohols and 2-nitrobenzaldehyde into nitroso derivatives. Photochem Photobiol Sci. 2005;4: 822–828. doi:10.1039/b506393k

264. Schaper K, Madani Mobarekeh SA, Doro P, Maydt D. The α,5-dicarboxy-2-nitrobenzyl caging group, a tool for biophysical applications with improved hydrophilicity: synthesis, photochemical properties and biological characterization. Photochem Photobiol. 2010;86: 1247–1254. doi:10.1111/j.1751-1097.2010.00803.x

265. Jayakumar MKG, Idris NM, Zhang Y. Remote activation of biomolecules in deep tissues using near-infrared-to-UV upconversion nanotransducers. Proc Natl Acad Sci U S A. 2012;109: 8483–8488. doi:10.1073/pnas.1114551109

266. Goeldner M, Givens RS. Dynamic Studies in Biology: Phototriggers, Photoswitches and Caged Biomolecules. Wiley-VCH; 2005. doi:10.1002/3527605592

267. Agarwal HK, Janicek R, Chi SH, Perry JW, Niggli E, Ellis-Davies GCR. Calcium uncaging with visible light. J Am Chem Soc. 2016;138: 3687–3693. doi:10.1021/jacs.5b11606

268. Fichte MAH, Weyel XMM, Junek S, Schäfer F, Herbivo C, Goeldner M, Specht A, Wachtveitl J, Heckel A. Three-dimensional control of DNA hybridization by orthogonal two- color two-photon uncaging. Angew Chemie. 2016;128: 9094–9098. doi:10.1002/ange.201603281

269. Momotake A, Lindegger N, Niggli E, Barsotti RJ, Ellis-Davies GCR. The nitrodibenzofuran chromophore: A new caging group for ultra-efficient photolysis in living cells. Nat Methods. 2006;3: 35–40. doi:10.1038/nmeth821

270. Klán P, Šolomek T, Bochet CG, Blanc A, Givens R, Rubina M, Popik V, Kostikov A, Wirz J. Photoremovable protecting groups in chemistry and biology: reaction mechanisms and efficacy. Chem Rev. 2013;113: 119–191. doi:10.1021/cr300177k

271. Fournier L, Gauron C, Xu L, Aujard I, Le Saux T, Gagey-Eilstein N, Maurin S, Dubruille S, Baudin JB, Bensimon D, Volovitch M, Vriz S, Jullien L. A blue-absorbing photolabile protecting group for *in vivo* chromatically orthogonal photoactivation. ACS Chem Biol. 2013;8: 1528–1536. doi:10.1021/cb400178m

272. Fournier L, Aujard I, Le Saux T, Maurin S, Beaupierre S, Baudin J, Jullien L. Coumarinylmethyl caging groups with redshifted absorption. Chem – A Eur J. 2013;19: 17494–17507. doi:10.1002/chem.201302630

273. Bojtár M, Kormos A, Kis-Petik K, Kellermayer M, Kele P. Green-light activatable, water-soluble red-shifted coumarin photocages. Org Lett. 2019;21: 9410–9414. doi:10.1021/acs.orglett.9b03624

274. Olson JP, Kwon H-B, Takasaki KT, Chiu CQ, Higley MJ, Sabatini BL, Ellis-Davies GCR. Optically selective two-photon uncaging of glutamate at 900 nm. J Am Chem Soc. 2013;135: 5954–7. doi:10.1021/ja4019379

275. O'Connor MJ, Beebe LL, Deodato D, Ball RE, Page AT, Vanleuven AJ, Harris KT, Park S, Hariharan V, Lauderdale JD, Dore TM. Bypassing glutamic acid decarboxylase 1 (Gad1) induced craniofacial defects with a photoactivatable translation blocker morpholino. ACS Chem Neurosci. 2019;10: 266–278. doi:10.1021/acschemneuro.8b00231

276. Griepenburg JC, Rapp TL, Carroll PJ, Eberwine J, Dmochowski IJ. Ruthenium-caged antisense morpholinos for regulating gene expression in zebrafish embryos. Chem Sci. 2015;6: 2342–2346. doi:10.1039/c4sc03990d

277. Goswami PP, Syed A, Beck CL, Albright TR, Mahoney KM, Unash R, Smith EA, Winter AH. BODIPY-derived photoremovable protecting groups unmasked with green light. J Am Chem Soc. 2015;137: 3783–3786. doi:10.1021/jacs.5b01297

278. Rubinstein N, Liu P, Miller EW, Weinstain R. Meso-Methylhydroxy BODIPY: A

scaffold for photo-labile protecting groups. Chem Commun. 2015;51: 6369–6372. doi:10.1039/c5cc00550g

279. Peterson JA, Wijesooriya C, Gehrmann EJ, Mahoney KM, Goswami PP, Albright TR, Syed A, Dutton AS, Smith EA, Winter AH. Family of BODIPY photocages cleaved by single photons of visible/near-infrared light. J Am Chem Soc. 2018;140: 7343–7346. doi:10.1021/jacs.8b04040

280. Gorka AP, Nani RR, Zhu J, Mackem S, Schnermann MJ. A near-IR uncaging strategy based on cyanine photochemistry. J Am Chem Soc. 2014;136: 14153–14159. doi:10.1021/ja5065203

281. Beharry AA, Woolley GA. Azobenzene photoswitches for biomolecules. Chem Soc Rev. 2011;40: 4422–4437. doi:10.1039/c1cs15023e

282. Görner H, Kuhn HJ. Cis-trans photoisomerization of stilbenes and stilbene-like molecules . John Wiley & Sons, Ltd; 2007. pp. 1–117. doi:10.1002/9780470133507.ch1

283. Dong M, Babalhavaeji A, Collins C V., Jarrah K, Sadovski O, Dai Q, Woolley GA. Near-infrared photoswitching of azobenzenes under physiological conditions. J Am Chem Soc. 2017;139: 13483–13486. doi:10.1021/jacs.7b06471

284. Brieke C, Rohrbach F, Gottschalk A, Mayer G, Heckel A. Light-controlled tools. Angew Chemie - Int Ed. 2012;51: 8446–76. doi:10.1002/anie.201202134

285. Hansen MJ, Velema WA, Lerch MM, Szymanski W, Feringa BL. Wavelength-selective cleavage of photoprotecting groups: strategies and applications in dynamic systems. Chem Soc Rev. 2015;44: 3358–3377. doi:10.1039/C5CS00118H

286. Bochet CG. Wavelength-selective cleavage of photolabile protecting groups. Tetrahedron Lett. 2000;41: 6341–6346. doi:10.1016/S0040-4039(00)01050-9

287. Blanc A, Bochet CG. Wavelength-controlled orthogonal photolysis of protecting groups. J Org Chem. 2002;67: 5567–5577. doi:10.1021/jo025837m

288. Olson JP, Banghart MR, Sabatini BL, Ellis-Davies GCR. Spectral evolution of a photochemical protecting group for orthogonal two-color uncaging with visible light. J Am Chem Soc. 2013;135: 15948–15954. doi:10.1021/ja408225k

289. Ellis-Davies GCR. Caged compounds: Photorelease technology for control of cellular chemistry and physiology. Nat. Methods. Nature Publishing Group; 2007. pp. 619–628. doi:10.1038/nmeth1072

290. San Miguel V, Bochet CG, Del Campo A. Wavelength-selective caged surfaces: How many functional levels are possible? J Am Chem Soc. 2011;133: 5380–5388. doi:10.1021/ja110572j

291. Rodrigues-Correia A, Weyel XMM, Heckel A. Four levels of wavelength-selective uncaging for oligonucleotides. Org Lett. 2013;15: 5500–5503. doi:10.1021/ol402657j

292. Stanton-Humphreys MN, Taylor RDT, Mc Dougall C, Hart ML, Brown CTA, Emptage NJ, Conway SJ. Wavelength-orthogonal photolysis of neurotransmitters *in vitro*. Chem Commun. 2012;48: 657–659. doi:10.1039/c1cc15135e

293. Goguen BN, Aemissegger A, Imperiali B. Sequential activation and deactivation

of protein function using spectrally differentiated caged phosphoamino acids. J Am Chem Soc. 2011;133: 11038–11041. doi:10.1021/ja2028074

294. Kantevari S, Matsuzaki M, Kanemoto Y, Kasai H, Ellis-Davies GCR. Two-color, two-photon uncaging of glutamate and GABA. Nat Methods. 2010;7: 123–125. doi:10.1038/nmeth.1413

295. Priestman MA, Sun L, Lawrence DS. Dual wavelength photoactivation of cAMP- and cGMP-dependent protein kinase signaling pathways. ACS Chem Biol. 2011;6: 377–384. doi:10.1021/cb100398e

296. Weinstain R, Slanina T, Kand D, Klán P. Visible-to-NIR-light activated release: from small molecules to nanomaterials. Chem Rev. 2020; acs.chemrev.0c00663. doi:10.1021/acs.chemrev.0c00663

297. Cain JA, Solis N, Cordwell SJ. Beyond gene expression: The impact of protein post-translational modifications in bacteria. J Proteomics. 2014;97: 265–286. doi:10.1016/j.jprot.2013.08.012

298. Forrest S, Welch M. Arming the troops: Post-translational modification of extracellular bacterial proteins. Sci. Prog. 2020. pp. 1–22. doi:10.1177/0036850420964317

299. Freudl R. Signal peptides for recombinant protein secretion in bacterial expression systems. Microb. Cell Fact. BioMed Central Ltd.; 2018. pp. 1–10. doi:10.1186/s12934-018-0901-3

300. Varshavsky A. N-degron and C-degron pathways of protein degradation. Proc Natl Acad Sci USA. 2019. pp. 358–366. doi:10.1073/pnas.1816596116

301. Hemmerich J, Rohe P, Kleine B, Jurischka S, Wiechert W, Freudl R, Oldiges M. Use of a Sec signal peptide library from *Bacillus subtilis* for the optimization of cutinase secretion in *Corynebacterium glutamicum*. Microb. Cell Fact. 2016;15. doi:10.1186/s12934-016-0604-6

302. Bosslet K, Czech J, Lorenz P, Sedlacek HH, Schuermann M, Seemann G. Molecular and functional characterisation of a fusion protein suited for tumour specific prodrug activation. Br J Cancer. 1992;65: 234–238. doi:10.1038/bjc.1992.47

303. Aalbers FS, Fraaije MW. Enzyme fusions in biocatalysis: coupling reactions by pairing enzymes. ChemBioChem. 2019;20: 20–28. doi:10.1002/cbic.201800394

304. Claaßen C, Gerlach T, Rother D. Stimulus-responsive regulation of enzyme activity for one-step and multi-step syntheses. Adv Synth Catal. 2019; adsc.201900169. doi:10.1002/adsc.201900169

305. Tischer D, Weiner OD. Illuminating cell signalling with optogenetic tools. Nat. Rev. Mol. Cell Biol. Nature Publishing Group; 2014. pp. 551–558. doi:10.1038/nrm3837

306. Weitzman M, Hahn KM. Optogenetic approaches to cell migration and beyond. Curr. Opin. Cell Biol. Elsevier Ltd; 2014. pp. 112–120. doi:10.1016/j.ceb.2014.08.004

307. Zhang K, Cui B. Optogenetic control of intracellular signaling pathways. Trends Biotechnol. 2015;33: 92–100. doi:10.1016/j.tibtech.2014.11.007

308. Harper SM, Neil LC, Gardner KH. Structural basis of a phototropin light switch.

Science. 2003;301: 1541–1544. doi:10.1126/science.1086810

309. Ziegler T, Möglich A. Photoreceptor engineering. Front Mol Biosci. 2015;2: 30. doi:10.3389/fmolb.2015.00030

310. Strickland D, Lin Y, Wagner E, Hope CM, Zayner J, Antoniou C, Sosnick TR, Weiss EL, Glotzer M. TULIPs: Tunable, light-controlled interacting protein tags for cell biology. Nat Methods. 2012;9: 379–384. doi:10.1038/nmeth.1904

311. Lungu OI, Hallett RA, Choi EJ, Aiken MJ, Hahn KM, Kuhlman B. Designing photoswitchable peptides using the AsLOV2 domain. Chem Biol. 2012;19: 507–517. doi:10.1016/j.chembiol.2012.02.006

312. Guntas G, Hallett RA, Zimmerman SP, Williams T, Yumerefendi H, Bear JE, Kuhlman B. Engineering an improved light-induced dimer (iLID) for controlling the localization and activity of signaling proteins. Proc Natl Acad Sci USA. 2015;112: 112–117. doi:10.1073/pnas.1417910112

313. Jungbluth M, Renicke C, Taxis C. Targeted protein depletion in *Saccharomyces cerevisiae* by activation of a bidirectional degron. BMC Syst Biol. 2010;4: 176. doi:10.1186/1752-0509-4-176

314. Renicke C, Schuster D, Usherenko S, Essen LO, Taxis C. A LOV2 domain-based optogenetic tool to control protein degradation and cellular function. Chem Biol. 2013;20: 619–626. doi:10.1016/j.chembiol.2013.03.005

315. Lutz AP, Renicke C, Taxis C. Controlling protein activity and degradation using blue light. Methods Mol. Biol. Humana Press Inc.; 2016. pp. 67–78. doi:10.1007/978-1-4939-3512-3_5

316. Taxis C. Development of a synthetic switch to control protein stability in eukaryotic cells with light. Methods Mol Biol. 1596;596: 241-255. doi:10.1007/978-1-4939-6940-1_15

317. Liao JC, Roidert J, Jay DG. Chromophore-assisted laser inactivation of proteins is mediated by the photogeneration of free radicals. Proc Nati Acad Sci USA. 1994.

318. Abrahamse H, Hamblin MR. New photosensitizers for photodynamic therapy. Biochem. J. Portland Press Ltd; 2016; 473(4): 347–364. doi:10.1042/BJ20150942

319. Wainwright M, Maisch T, Nonell S, Plaetzer K, Almeida A, Tegos GP, Hamblin MR. Photoantimicrobials—are we afraid of the light? Lancet Infect Dis. 2017;17: e49–e55. doi:10.1016/S1473-3099(16)30268-7

320. Jay DG. Selective destruction of protein function by chromophore-assisted laser inactivation. Proc Natl Acad Sci USA. 1988;85: 5454–5458. doi:10.1073/pnas.85.15.5454

321. Jensen RL, Arnbjerg J, Birkedal H, Ogilby PR. Singlet oxygen's response to protein dynamics. J Am Chem Soc. 2011;133: 7166–7173. doi:10.1021/ja2010708

322. Ogilby PR. Singlet oxygen: there is indeed something new under the sun. Chem Soc Rev. 2010;39: 3181. doi:10.1039/b926014p

323. Reth M. Hydrogen peroxide as second messenger in lymphocyte activation. Nat Immunol. 2002;3: 1129–1134. doi:10.1038/ni1202-1129

324. Mishina NM, Tyurin-Kuzmin PA, Markvicheva KN, Vorotnikov A V., Tkachuk VA, Laketa V, Schultz C, Lukyanov S, Belousov V V. Does cellular hydrogen peroxide diffuse or act locally? Antioxid Redox Signal. 2010;14: 1–7. doi:10.1089/ars.2010.3539

325. Robertson CA, Evans DH, Abrahamse H. Photodynamic therapy (PDT): a short review on cellular mechanisms and cancer research applications for PDT. J Photochem Photobiol B. 2009;96: 1–8. doi:10.1016/j.jphotobiol.2009.04.001

326. Halliwell B, Gutteridge JMC. Free Radicals in Biology and Medicine. 5. Oxford University Press; 2015. doi:10.1093/acprof:oso/9780198717478.001.0001

327. Hamblin MR, Abrahamse H. Can light-based approaches overcome antimicrobial resistance? Drug Dev Res. 2019;80: 48–67. doi:10.1002/ddr.21453

328. Takemoto K, Matsuda T, McDougall M, Klaubert DH, Hasegawa A, Los G V., Wood K V., Miyawaki A, Nagai T. Chromophore-assisted light inactivation of halotag fusion proteins labeled with eosin in living cells. ACS Chem Biol. 2011;6: 401–406. doi:10.1021/cb100431e

329. Tour O, Meijer RM, Zacharias DA, Adams SR, Tsien RY. Genetically targeted chromophore-assisted light inactivation. Nat Biotechnol. 2003;21: 1505–1508. doi:10.1038/nbt914

330. Beck S, Sakurai T, Eustace BK, Beste G, Schier R, Rudert F, Jay DG. Fluorophore-assisted light inactivation: A high-throughput tool for direct target validation of proteins. Proteomics. 2002;2: 247. doi:10.1002/1615-9861(200203)2:3<247::AID-PROT247>3.0.CO;2-K

331. Marek KW, Davis GW. Transgenically encoded protein photoinactivation (FlAsH-FALI): Acute inactivation of synaptotagmin I. Neuron. 2002;36: 805–813. doi:10.1016/S0896-6273(02)01068-1

332. Jay DG. Chromophore-assisted light inactivation: A twenty-year retrospective. Laser Imaging and Manipulation in Cell Biology. Weinheim, Germany: Wiley-VCH Verlag GmbH & Co. KGaA; 2010. pp. 71–81. doi:10.1002/9783527632053.ch4

333. Rajfur Z, Roy P, Otey C, Romer L, Jacobson K. Dissecting the link between stress fibres and focal adhesions by CALI wit EGFP fusion proteins. Nat Cell Biol. 2002;4: 286–293. doi:10.1038/ncb772

334. Bulina ME, Chudakov DM, Britanova O V., Yanushevich YG, Staroverov DB, Chepurnykh T V., Merzlyak EM, Shkrob MA, Lukyanov S, Lukyanov KA. A genetically encoded photosensitizer. Nat Biotechnol. 2006;24: 95–99. doi:10.1038/nbt1175

335. Bulina ME, Lukyanov KA, Britanova O V., Onichtchouk D, Lukyanov S, Chudakov DM. Chromophore-assisted light inactivation (CALI) using the phototoxic fluorescent protein KillerRed. Nat Protoc. 2006;1: 947–953. doi:10.1038/nprot.2006.89

336. Liao Z-X, Li Y-C, Lu H-M, Sung H-W. A genetically-encoded KillerRed protein as an intrinsically generated photosensitizer for photodynamic therapy. Biomaterials. 2014;35: 500–508. doi:10.1016/j.biomaterials.2013.09.075

337. Williams DC, ElBejjani R, Ramirez PM, Coakley S, Kim SA, Lee H, Wen Q, Samuel A, Lu H, Hilliard MA, Hammarlund M. Rapid and permanent neuronal inactivation *in vivo via* subcellular generation of reactive oxygen with the use of

KillerRed. Cell Rep. 2013;5: 553–563. doi:10.1016/j.celrep.2013.09.023

338. Serebrovskaya EO, Gorodnicheva T V., Ermakova G V., Solovieva EA, Sharonov G V., Zagaynova E V., Chudakov DM, Lukyanov S, Zaraisky AG, Lukyanov KA. Light-induced blockage of cell division with a chromatin-targeted phototoxic fluorescent protein. Biochem J. 2011;435: 65–71. doi:10.1042/BJ20101217

339. Vegh RB, Solntsev KM, Kuimova MK, Cho S, Liang Y, Loo BLW, Tolbert LM, Bommarius AS. Reactive oxygen species in photochemistry of the red fluorescent protein "Killer Red." Chem Commun. 2011;47: 4887. doi:10.1039/c0cc05713d

340. Pletnev S, Gurskaya NG, Pletneva N V., Lukyanov KA, Chudakov DM, Martynov VI, Popov VO, Kovalchuk M V., Wlodawer A, Dauter Z, Pletnev V. Structural basis for phototoxicity of the genetically encoded photosensitizer KillerRed. J Biol Chem. 2009;284: 32028–32039. doi:10.1074/jbc.M109.054973

341. Lee W, Kim I, Rhee YM. A proton transfer network that generates deprotonated tyrosine is a key to producing reactive oxygen species in phototoxic KillerRed protein. Phys Chem Chem Phys. 2018;20: 22342–22350. doi:10.1039/C8CP02939C

342. Trewin AJ, Berry BJ, Wei AY, Bahr LL, Foster TH, Wojtovich AP. Light-induced oxidant production by fluorescent proteins. Free Radic Biol Med. 2018;128: 157–164. doi:10.1016/j.freeradbiomed.2018.02.002

343. Takemoto K, Matsuda T, Sakai N, Fu D, Noda M, Uchiyama S, Kotera I, Arai Y, Horiuchi M, Fukui K, Ayabe T, Inagaki F, Suzuki H, Nagai T. SuperNova, a monomeric photosensitizing fluorescent protein for chromophore-assisted light inactivation. Sci Rep. 2013;3: 2629. doi:10.1038/srep02629

344. Sarkisyan KS, Zlobovskaya OA, Gorbachev DA, Bozhanova NG, Sharonov G V., Staroverov DB, Egorov ES, Ryabova A V., Solntsev KM, Mishin AS, Lukyanov KA. KillerOrange, a genetically encoded photosensitizer activated by blue and green light. PLoS One. 2015;10: e0145287. doi:10.1371/journal.pone.0145287

345. Shu X, Lev-Ram V, Deerinck TJ, Qi Y, Ramko EB, Davidson MW, Jin Y, Ellisman MH, Tsien RY. A genetically encoded tag for correlated light and electron microscopy of intact cells, tissues, and organisms. PLoS Biol. 2011;9: e1001041. doi:10.1371/journal.pbio.1001041

346. Westberg M, Bregnhøj M, Etzerodt M, Ogilby PR. No Photon Wasted: An efficient and selective singlet oxygen photosensitizing protein. J Phys Chem B. 2017;121: 9366–9371. doi:10.1021/acs.jpcb.7b07831

347. Pimenta FM, Jensen RL, Breitenbach T, Etzerodt M, Ogilby PR. Oxygen-dependent photochemistry and photophysics of "MiniSOG," a protein-encased flavin. Photochem Photobiol. 2013;89: 1116–1126. doi:10.1111/php.12111

348. Ruiz-González R, Cortajarena AL, Mejias SH, Agut M, Nonell S, Flors C. Singlet oxygen generation by the genetically encoded tag minisog. J Am Chem Soc. 2013;135: 9564–9567. doi:10.1021/ja4020524

349. Lin JY, Sann SB, Zhou K, Nabavi S, Proulx CD, Malinow R, Jin Y, Tsien RY. Optogenetic inhibition of synaptic release with chromophore-assisted light inactivation (CALI). Neuron. 2013;79: 241–253. doi:10.1016/j.neuron.2013.05.022

350. Wojtovich AP, Wei AY, Sherman TA, Foster TH, Nehrke K. Chromophore-assisted

light inactivation of mitochondrial electron transport chain complex II in *Caenorhabditis elegans*. Sci Rep. 2016;6: 1–13. doi:10.1038/srep29695

351. Westberg M, Holmegaard L, Pimenta FM, Etzerodt M, Ogilby PR. Rational design of an efficient, genetically encodable, protein-encased singlet oxygen photosensitizer. J Am Chem Soc. 2015;137: 1632–1642. doi:10.1021/ja511940j

352. Chapman S, Faulkner C, Kaiserli E, Garcia-Mata C, Savenkov EI, Roberts AG, Oparka KJ, Christie JM. The photoreversible fluorescent protein iLOV outperforms GFP as a reporter of plant virus infection. Proc Natl Acad Sci. 2008;105: 20038–20043. doi:10.1073/pnas.0807551105

353. Christie JM, Hitomi K, Arvai AS, Hartfield KA, Mettlen M, Pratt AJ, Tainer JA, Getzoff ED. Structural tuning of the fluorescent protein iLOV for improved photostability. J Biol Chem. 2012;287: 22295–22304. doi:10.1074/jbc.M111.318881

354. Drepper T, Eggert T, Circolone F, Heck A, Krauß U, Guterl J-K, Wendorff M, Losi A, Gärtner W, Jaeger K-E. Reporter proteins for *in vivo* fluorescence without oxygen. Nat Biotechnol. 2007;25: 443–445. doi:10.1038/nbt1293

355. Wingen M, Potzkei J, Endres S, Casini G, Rupprecht C, Fahlke C, Krauss U, Jaeger K-E, Drepper T, Gensch T. The photophysics of LOV-based fluorescent proteins – new tools for cell biology. Photochem Photobiol Sci. 2014;13: 875–883. doi:10.1039/C3PP50414J

356. Mukherjee A, Weyant KB, Agrawal U, Walker J, Cann IKO, Schroeder CM. Engineering and characterization of new LOV-based fluorescent proteins from *Chlamydomonas reinhardtii* and *Vaucheria frigida.* ACS Synth Biol. 2015;4: 371–377. doi:10.1021/sb500237x

357. Agostinis P, Berg K, Cengel KA, Foster TH, Girotti AW, Gollnick SO, Hahn SM, Hamblin MR, Juzeniene A, Kessel D, Korbelik ; Mladen, Moan J, Pawel Mroz ;, Nowis D, Piette J, Wilson BC, Golab ; Jakub. Photodynamic therapy of cancer: an update. CA Cancer J Clin. 2011;61: 250–281. doi:10.3322/caac.20114

358. St. Denis TG, Dai T, Izikson L, Astrakas C, Anderson RR, Hamblin MR, Tegos GP. All you need is light, antimicrobial photoinactivation as an evolving and emerging discovery strategy against infectious disease. Virulence. Taylor and Francis Inc.; 2011. pp. 509–520. doi:10.4161/viru.2.6.17889

359. Moan J, Peng Q. An outline of the history of PDT. Photodynamic therapy. Cambridge: Royal Society of Chemistry; 2003. pp. 1–18. doi:10.1039/9781847551658-00001

360. Yin R, Hamblin M. Antimicrobial Photosensitizers: Drug discovery under the spotlight. Curr Med Chem. 2015;22: 2159–2185. doi:10.2174/0929867322666150319120134

361. Hamblin MR. Antimicrobial photodynamic inactivation: a bright new technique to kill resistant microbes. Curr Opin Microbiol. 2016;33: 67–73. doi:10.1016/j.mib.2016.06.008

362. Sharma SK, Mroz P, Dai T, Huang Y, St Denis TG, Hamblin MR. Photodynamic therapy for cancer and for infections: what is the difference? Isr J Chem. 2012;52: 691–705. doi:10.1002/ijch.201100062

363. Otvagin VF, Kuzmina NS, Krylova L V, Volovetsky AB, Nyuchev A V, Gavryushin

AE, Meshkov IN, Gorbunova YG, Romanenko Y V, Koifman OI, Balalaeva I V, Fedorov AY. Water-soluble chlorin/arylaminoquinazoline conjugate for photodynamic and targeted therapy. J Med Chem. 2019;62(24): 11182-11193. doi:10.1021/acs.jmedchem.9b01294

364. Shirmanova M V., Serebrovskaya EO, Lukyanov KA, Snopova LB, Sirotkina MA, Prodanetz NN, Bugrova ML, Minakova EA, Turchin I V., Kamensky VA, Lukyanov SA, Zagaynova E V. Phototoxic effects of fluorescent protein KillerRed on tumor cells in mice. J Biophotonics. 2013;6: 283–290. doi:10.1002/jbio.201200056

365. Shirmanova M, Yuzhakova D, Snopova L, Perelman G, Serebrovskaya E, Lukyanov K, Turchin I, Subochev P, Lukyanov S, Kamensky V, Zagaynova E. Towards PDT with Genetically Encoded Photosensitizer KillerRed: A Comparison of Continuous and Pulsed Laser Regimens in an Animal Tumor Model. PLoS One. 2015;10: e0144617. doi:10.1371/journal.pone.0144617

366. Takehara K, Tazawa H, Okada N, Hashimoto Y, Kikuchi S, Kuroda S, Kishimoto H, Shirakawa Y, Narii N, Mizuguchi H, Urata Y, Kagawa S, Fujiwara T. Targeted photodynamic virotherapy armed with a genetically encoded photosensitizer. Mol Cancer Ther. 2016;15: 199–208. doi:10.1158/1535-7163.MCT-15-0344

367. Yuan M, Liu C, Li J, Ma W, Yu X, Zhang P, Ji Y. The effects of photodynamic therapy on leukemia cells mediated by KillerRed, a genetically encoded fluorescent protein photosensitizer. BMC Cancer. 2019;19: 934. doi:10.1186/s12885-019-6124-0

368. Ryumina AP, Serebrovskaya EO, Shirmanova M V., Snopova LB, Kuznetsova MM, Turchin I V., Ignatova NI, Klementieva N V., Fradkov AF, Shakhov BE, Zagaynova E V., Lukyanov KA, Lukyanov SA. Flavoprotein miniSOG as a genetically encoded photosensitizer for cancer cells. Biochim Biophys Acta - Gen Subj. 2013;1830: 5059–5067. doi:10.1016/j.bbagen.2013.07.015

369. Souslova EA, Mironova KE, Deyev SM. Applications of genetically encoded photosensitizer miniSOG: from correlative light electron microscopy to immunophotosensitizing. J Biophotonics. 2017;10: 338–352. doi:10.1002/jbio.201600120

370. Waldeck W, Heidenreich E, Mueller G, Wiessler M, Tóth K, Braun K. ROS-mediated killing efficiency with visible light of bacteria carrying different red fluorochrome proteins. J Photochem Photobiol B Biol. 2012;109: 28–33. doi:10.1016/j.jphotobiol.2012.01.002

371. Ruiz-González R, White JH, Agut M, Nonell S, Flors C. A genetically-encoded photosensitiser demonstrates killing of bacteria by purely endogenous singlet oxygen. Photochem Photobiol Sci. 2012;11: 1411–1413. doi:10.1039/c2pp25126d

372. Giuliani F, Martinelli M, Cocchi A, Arbia D, Fantetti L, Roncucci G. *In vitro* resistance selection studies of RLP068/Cl, a new Zn(II) phthalocyanine suitable for antimicrobial photodynamic therapy. Antimicrob Agents Chemother. 2010;54: 637–642. doi:10.1128/AAC.00603-09

373. Maisch T. Resistance in antimicrobial photodynamic inactivation of bacteria. Photochem Photobiol Sci. 2015;14: 1518–26. doi:10.1039/c5pp00037h

374. De Melo WCMA, Avci P, De Oliveira MN, Gupta A, Vecchio D, Sadasivam M, Chandran R, Huang Y-Y, Yin R, Perussi LR. Photodynamic inactivation of biofilm:

taking a lightly colored approach to stubborn infection. Expert Rev Anti Infect Ther. 2013;11: 669–693.

375. Van Dyck K, Pinto RM, Pully D, Van Dijck P. Microbial interkingdom biofilms and the quest for novel therapeutic strategies. Microorganisms. MDPI AG; 2021;9(2): 412 doi:10.3390/microorganisms9020412

376. Newman DJ, Cragg GM. Natural products as sources of new drugs over the nearly four decades from 01/1981 to 09/2019. J. Nat. Prod. American Chemical Society; 2020;83,3: 770–803. doi:10.1021/acs.jnatprod.9b01285

377. Luo Y, Li B-Z, Liu D, Zhang L, Chen Y, Jia B, Zeng B-X, Zhao H, Yuan Y-J. Engineered biosynthesis of natural products in heterologous hosts. Chem Soc Rev. 2015;44: 5265–5290. doi:10.1039/C5CS00025D

378. Chemler JA, Koffas MAG. Metabolic engineering for plant natural product biosynthesis in microbes. Curr Opin Biotechnol. 2008;19: 597–605. doi:https://doi.org/10.1016/j.copbio.2008.10.011

379. Marienhagen J, Bott M. Metabolic engineering of microorganisms for the synthesis of plant natural products. J Biotechnol. 2013;163: 166–78. doi:10.1016/j.jbiotec.2012.06.001

380. Schmidt EW. Trading molecules and tracking targets in symbiotic interactions. Nat. Chem. Biol. 2008;4: 466–473. doi:10.1038/nchembio.101

381. Hibbing ME, Fuqua C, Parsek MR, Peterson SB. Bacterial competition: Surviving and thriving in the microbial jungle. Nat. Rev. Microbiol. 2010;8: 15–25. doi:10.1038/nrmicro2259

382. Miethke M, Marahiel MA. Siderophore-based iron acquisition and pathogen control. Microbiol Mol Biol Rev. 2007;71: 413–451. doi:10.1128/mmbr.00012-07

383. Keller L, Surette MG. Communication in bacteria: An ecological and evolutionary perspective. Nat. Rev. Microbiol. 2006;4: 249–258. doi:10.1038/nrmicro1383

384. Vaishnav P, Demain AL. Unexpected applications of secondary metabolites. Biotechnol. Adv. Elsevier; 2011;29,2: 223–229. doi:10.1016/j.biotechadv.2010.11.006

385. Wallenstein MD, Weintraub MN. Emerging tools for measuring and modeling the *in situ* activity of soil extracellular enzymes. Soil Biol Biochem. 2008;40: 2098–2106. doi:10.1016/j.soilbio.2008.01.024

386. Hanson JR. Natural Products. A Cambridge: Royal Society of Chemistry; 2007. doi:10.1039/9781847551535

387. Guttenberger N, Blankenfeldt W, Breinbauer R. Recent developments in the isolation, biological function, biosynthesis, and synthesis of phenazine natural products. Bioorg Med Chem. 2017;25: 6149–6166. doi:10.1016/j.bmc.2017.01.002

388. Hug JJ, Krug D, Müller R. Bacteria as genetically programmable producers of bioactive natural products. Nat Rev Chem. 2020. doi:10.1038/s41570-020-0176-1

389. Cragg GM, Newman DJ. Natural products: A continuing source of novel drug leads. Biochim Biophys Acta - Gen Subj. 2013;1830: 3670–3695.

doi:10.1016/j.bbagen.2013.02.008

390. Domröse A, Klein AS, Hage-Hülsmann J, Thies S, Svensson V, Classen T, Pietruszka J, Jaeger K-E, Drepper T, Loeschcke A. Efficient recombinant production of prodigiosin in *Pseudomonas putida*. Front Microbiol. 2015;6: 972. doi:10.3389/fmicb.2015.00972

391. Weihmann R, Domröse A, Drepper T, Jaeger K-E, Loeschcke A. Protocols for yTREX /Tn5-based gene cluster expression in *Pseudomonas putida*. Microb Biotechnol. 2020;13: 250–262. doi:10.1111/1751-7915.13402

392. Cobb RE, Ning JC, Zhao H. DNA assembly techniques for next-generation combinatorial biosynthesis of natural products. J Ind Microbiol Biotechnol. 2014;41: 469–477. doi:10.1007/s10295-013-1358-3

393. Luo Y, Enghiad B, Zhao H. New tools for reconstruction and heterologous expression of natural product biosynthetic gene clusters. Nat Prod Rep. 2016;33: 174–182. doi:10.1039/c5np00085h

394. Klein AS, Domröse A, Bongen P, Brass HUC, Classen T, Loeschcke A, Drepper T, Laraia L, Sievers S, Jaeger K-E, Pietruszka J. New podigiosin derivatives obtained by mutasynthesis in *Pseudomonas putida*. ACS Synth Biol. 2017;6: 1757–1765. doi:10.1021/acssynbio.7b00099

395. Park D, Swayambhu G, Pfeifer BA. Heterologous biosynthesis as a platform for producing new generation natural products. Curr. Opin. Biotechnol. Elsevier Ltd; 2020;66: 123–130. doi:10.1016/j.copbio.2020.06.014

396. Bian G, Deng Z, Liu T. Strategies for terpenoid overproduction and new terpenoid discovery. Curr Opin Biotechnol. 2017;48: 234–241. doi:10.1016/j.copbio.2017.07.002

397. Christianson DW. Structural and chemical biology of terpenoid cyclases. Chem Rev. 2017;117: 11570–11648. doi:10.1021/acs.chemrev.7b00287

398. Pemberton TA, Chen M, Harris GG, Chou WKW, Duan L, Köksal M, Genshaft AS, Cane DE, Christianson DW. Exploring the influence of domain architecture on the catalytic function of diterpene synthases. Biochemistry. 2017;56: 2010–2023. doi:10.1021/acs.biochem.7b00137

399. Wink M. Modes of action of herbal medicines and plant secondary metabolites. Medicines. 2015;2: 251–286. doi:10.3390/medicines2030251

400. Ruzicka L. The isoprene rule and the biogenesis of terpenic compounds. Experientia. 1953;9: 357–367. doi:10.1007/BF02167631

401. Croteau R, Kutchan TM, Lewis NG. Secondary metabolites. Biochem Mol Biol Plants. 2000;7: 1250–1318. doi:10.1016/j.phytochem.2011.10.011

402. Tholl D. Biosynthesis and biological functions of terpenoids in plants. Adv Biochem Eng Biotechnol. 2015;148. doi:10.1007/10_2014_295

403. Janocha S, Schmitz D, Bernhardt R. Terpene hydroxylation with microbial cytochrome p450 monooxygenases. Adv Biochem Eng Biotechnol. 2015;148: 215–250. doi:10.1007/10_2014_296

404. Pateraki I, Heskes AM, Hamberger B. Cytochromes P450 for terpene functionalisation and metabolic engineering. Adv Biochem Eng Biotechnol.

2015;148: 107–139. doi:10.1007/10_2014_301

405. Karunanithi PS, Zerbe P. Terpene synthases as metabolic gatekeepers in the evolution of plant terpenoid chemical diversity. Front. Plant Sci. Frontiers Media S.A.; 2019;10: 1166. doi:10.3389/fpls.2019.01166

406. Kampranis SC, Makris AM. Developing a yeast cell factory for the production of terpenoids. Comput. Struct. Biotechnol. J. 2012. p. e201210006. doi:10.5936/csbj.201210006

407. Chang MCY, Keasling JD. Production of isoprenoid pharmaceuticals by engineered microbes. Nat Chem. Biol. 2006. pp. 674–681. doi:10.1038/nchembio836

408. Boucher Y, Doolittle WF. The role of lateral gene transfer in the evolution of isoprenoid biosynthesis pathways. Mol Microbiol. 2000;37: 703–16. doi:10.1046/j.1365-2958.2000.02004.x

409. Miziorko HM. Enzymes of the mevalonate pathway of isoprenoid biosynthesis. Archives of biochemistry and biophysics. Academic Press; 2011. pp. 131–143. doi:10.1016/j.abb.2010.09.028

410. Frank A, Groll M. The methylerythritol phosphate pathway to isoprenoids. Chem Rev. 2017;117: 5675–5703. doi:10.1021/acs.chemrev.6b00537

411. Langenheim JH. Higher plant terpenoids: A phytocentric overview of their ecological roles. J Chem Ecol. 1994;20: 1223–80. doi:10.1007/BF02059809

412. Gershenzon J, Dudareva N. The function of terpene natural products in the natural world. Nat Chem Biol. 2007;3: 408–14. doi:10.1038/nchembio.2007.5

413. Pichersky E, Raguso RA. Why do plants produce so many terpenoid compounds? New Phytol. 2018;220: 692–702. doi:10.1111/nph.14178

414. Wang G, Tang W, Bidigare RR. Terpenoids as therapeutic drugs and pharmaceutical agents. Natural. Products. Humana Press; 2005. pp. 197–227. doi:10.1007/978-1-59259-976-9_9

415. Mahizan NA, Yang S-K, Moo C-L, Song AA-L, Chong C-WC-M, Chong C-WC-M, Abushelaibi A, Lim S-HE, Lai K-S. Terpene derivatives as a potential agent against antimicrobial resistance (AMR) pathogens. Molecules. 2019;24: 2631. doi:10.3390/molecules24142631

416. Bohlmann J, Keeling CI. Terpenoid biomaterials. Plant J. 2008;54: 656–669. doi:10.1111/j.1365-313X.2008.03449.x

417. George KW, Alonso-Gutierrez J, Keasling JD, Lee TS. Isoprenoid drugs, biofuels, and chemicals—artemisinin, farnesene, and beyond. Adv Biochem Eng Biotechnol. 2015;148: 355–389. doi:10.1007/10_2014_288

418. Moser S, Pichler H. Identifying and engineering the ideal microbial terpenoid production host. Appl Microbiol Biotechnol. 2019;103: 5501–5516. doi:10.1007/s00253-019-09892-y

419. Schempp FM, Drummond L, Buchhaupt M, Schrader J. Microbial Cell Factories for the Production of Terpenoid Flavor and Fragrance Compounds. J Agric Food Chem. 2018;66: 2247–2258. doi:10.1021/acs.jafc.7b00473

420. Mitchell W. Natural products from synthetic biology. Curr Opin Chem Biol. 2011;15: 505–15. doi:10.1016/j.cbpa.2011.05.017

421. Chen Y, Zhou YJ, Siewers V, Nielsen J. Enabling technologies to advance microbial isoprenoid production. Adv Biochem Eng Biotechnol. 2015;148: 143–60. doi:10.1007/10_2014_284

422. Kirby J, Keasling JD. Metabolic engineering of microorganisms for isoprenoid production. Nat Prod Rep. 2008;25: 656–61. doi:10.1039/b802939c

423. Lee JW, Na D, Park JM, Lee J, Choi S, Lee SY. Systems metabolic engineering of microorganisms for natural and non-natural chemicals. Nat Chem Biol. 2012. pp. 536–546. doi:10.1038/nchembio.970

424. Liu Y, Shin H dong, Li J, Liu L. Toward metabolic engineering in the context of system biology and synthetic biology: advances and prospects. Applied Microbiology and Biotechnology. Springer Verlag; 2015. pp. 1109–1118. doi:10.1007/s00253-014-6298-y

425. Khan NE, Nybo SE, Chappell J, Curtis WR. Triterpene hydrocarbon production engineered into a metabolically versatile host- *Rhodobacter capsulatus*. Biotechnol Bioeng. 2015;112: 1523–32. doi:10.1002/bit.25573

426. Beekwilder J, van Houwelingen A, Cankar K, van Dijk ADJ, de Jong RM, Stoopen G, Bouwmeester H, Achkar J, Sonke T, Bosch D. Valencene synthase from the heartwood of Nootka cypress (*Callitropsis nootkatensis*) for biotechnological production of valencene. Plant Biotechnol J. 2014;12: 174–82. doi:10.1111/pbi.12124

427. Orsi E, Folch PL, Monje-López VT, Fernhout BM, Turcato A, Kengen SWM, Eggink G, Weusthuis RA. Characterization of heterotrophic growth and sesquiterpene production by *Rhodobacter sphaeroides* on a defined medium. J Ind Microbiol Biotechnol. 2019. doi:10.1007/s10295-019-02201-6

428. Orsi E, Beekwilder J, Peek S, Eggink G, Kengen SWM, Weusthuis RA. Metabolic flux ratio analysis by parallel ^{13}C labeling of isoprenoid biosynthesis in *Rhodobacter sphaeroides*. Metab Eng. 2020;57: 228–238. doi:10.1016/j.ymben.2019.12.004

429. Orsi E, Mougiakos I, Post W, Beekwilder J, Dompè M, Eggink G, Van Der Oost J, Kengen SWM, Weusthuis RA. Growth-uncoupled isoprenoid synthesis in *Rhodobacter sphaeroides*. Biotechnol Biofuels. 2020;13: 123. doi:10.1186/s13068-020-01765-1

430. Orsi E, Beekwilder J, van Gelder D, van Houwelingen A, Eggink G, Kengen SWM, Weusthuis RA. Functional replacement of isoprenoid pathways in *Rhodobacter sphaeroides*. Microb Biotechnol. 2020;13,4: 1082-1093. doi:10.1111/1751-7915.13562

431. Martin VJJ, Pitera DJ, Withers ST, Newman JD, Keasling JD. Engineering a mevalonate pathway in *Escherichia coli* for production of terpenoids. Nat Biotechnol. 2003;21: 796–802. doi:10.1038/nbt833

432. Pitera DJ, Paddon CJ, Newman JD, Keasling JD. Balancing a heterologous mevalonate pathway for improved isoprenoid production in *Escherichia coli*. Metab Eng. 2007;9: 193–207. doi:10.1016/j.ymben.2006.11.002

433. Sivy TL, Fall R, Rosenstiel TN. Evidence of isoprenoid precursor toxicity in

Bacillus subtilis. Biosci Biotechnol Biochem. 2011;75: 2376–2383. doi:10.1271/bbb.110572

434. Dahl RH, Zhang F, Alonso-Gutierrez J, Baidoo E, Batth TS, Redding-Johanson AM, Petzold CJ, Mukhopadhyay A, Lee TS, Adams PD, Keasling JD. Engineering dynamic pathway regulation using stress-response promoters. Nat Biotechnol. 2013;31: 1039–1046. doi:10.1038/nbt.2689

435. Banerjee A, Sharkey TD. Methylerythritol 4-phosphate (MEP) pathway metabolic regulation. Nat Prod Rep. 2014;31: 1043–1055. doi:10.1039/C3NP70124G

436. Woolston BM, Edgar S, Stephanopoulos G. Metabolic engineering: past and future. Annu Rev Chem Biomol Eng. 2013;4: 259–288. doi:10.1146/annurev-chembioeng-061312-103312

437. Scalcinati G, Knuf C, Partow S, Chen Y, Maury J, Schalk M, Daviet L, Nielsen J, Siewers V. Dynamic control of gene expression in *Saccharomyces cerevisiae* engineered for the production of plant sesquiterpene α-santalene in a fed-batch mode. Metab Eng. 2012;14: 91–103. doi:10.1016/j.ymben.2012.01.007

438. Dunlop MJ, Keasling JD, Mukhopadhyay A. A model for improving microbial biofuel production using a synthetic feedback loop. Syst Synth Biol. 2010;4: 95–104. doi:10.1007/s11693-010-9052-5

439. Wasserman HH, Mckeon JE, Smith L, Forgione P. Prodigiosin. Structure and partial synthesis. J Am Chem Soc. 1960;82: 506–507. doi:10.1021/ja01487a075

440. Darshan N, Manonmani HK. Prodigiosin and its potential applications. J. Food Sci. Technol. Springer India; 2015;52,9: 5393–5407. doi:10.1007/s13197-015-1740-4

441. Williamson NR, Fineran PC, Leeper FJ, Salmond GPC. The biosynthesis and regulation of bacterial prodiginines. Nat Rev Microbiol. 2006;4: 887–899. doi:10.1038/nrmicro1531

442. Fürstner A. Chemie und Biologie des Roseophilins und der Prodigiosin-Alkaloide: 2500 Jahre im Überblick. Angew Chemie. 2003;115: 3706–3728. doi:10.1002/ange.200300582

443. Hu DX, Withall DM, Challis GL, Thomson RJ. Structure, chemical synthesis, and biosynthesis of prodiginine natural products. Chem. Rev. American Chemical Society; 2016. pp. 7818–7853. doi:10.1021/acs.chemrev.6b00024

444. Bruner SD. Enzyme catalysis: C-H activation is a Reiske business. Nat Chem. 2011;3: 342–343. doi:10.1038/nchem.1038

445. Darshan N, Manonmani HK. Prodigiosin inhibits motility and activates bacterial cell death revealing molecular biomarkers of programmed cell death. AMB Express. 2016;6: 50. doi:10.1186/s13568-016-0222-z

446. Lapenda JC, Silva PA, Vicalvi MC, Sena KXFR, Nascimento SC. Antimicrobial activity of prodigiosin isolated from *Serratia marcescens* UFPEDA 398. World J Microbiol Biotechnol. 2015;31: 399–406. doi:10.1007/s11274-014-1793-y

447. Priya KA, Satheesh S, Ashokkumar B, Varalakshmi P, Selvakumar G, Sivakumar N. Antifouling activity of prodigiosin from estuarine isolate of *Serratia marcescens* CMST 07. Microbiological Research In Agroecosystem Management. Springer India; 2013. pp. 11–21. doi:10.1007/978-81-322-1087-0_2

448. Stankovic N, Senerovic L, Ilic-Tomic T, Vasiljevic B, Nikodinovic-Runic J. Properties and applications of undecylprodigiosin and other bacterial prodigiosins. Applied Microbiology and Biotechnology. Springer Verlag; 2014. pp. 3841–3858. doi:10.1007/s00253-014-5590-1

449. Suryawanshi RK, Patil CD, Borase HP, Salunke BK, Patil S V. Studies on production and biological potential of prodigiosin by *Serratia marcescens*. Appl Biochem Biotechnol. 2014;173: 1209–1221. doi:10.1007/s12010-014-0921-3

450. Hassankhani R, Sam MR, Esmaeilou M, Ahangar P. Prodigiosin isolated from cell wall of Serratia marcescens alters expression of apoptosis-related genes and increases apoptosis in colorectal cancer cells. Med Oncol. 2015;32: 1–8. doi:10.1007/s12032-014-0366-0

451. Khanafari A, Assadi MM, Fakhr FA. Review of prodigiosin, pigmentation in *Serratia marcescens.* Online J Biol Sci. 2006;6: 1–13. doi:10.3844/ojbsci.2006.1.13

452. Williamson NR, Fineran PC, Gristwood T, Chawrai SR, Leeper FJ, Salmond GPC. Anticancer and immunosuppressive properties of bacterial prodiginines. Future Microbiol. Future Medicine Ltd.; 2007. pp. 605–618. doi:10.2217/17460913.2.6.605

453. Montaner B, Navarro S, Piqué M, Vilaseca M, Martinell M, Giralt E, Gil J, Pérez-Tomás R. Prodigiosin from the supernatant of *Serratia marcescens* induces apoptosis in haematopoietic cancer cell lines. Br J Pharmacol. 2000;131: 585–593. doi:10.1038/sj.bjp.0703614

454. Lin SR, Chen YH, Tseng FJ, Weng CF. The production and bioactivity of prodigiosin: quo vadis? Drug Discov. Today. Elsevier Ltd; 2020;25,5: 828–836. doi:10.1016/j.drudis.2020.03.017

455. Anwar MM, Shalaby M, Embaby AM, Saeed H, Agwa MM, Hussein A. Prodigiosin/PU-H71 as a novel potential combined therapy for triple negative breast cancer (TNBC): preclinical insights. Sci Rep. 2020;10. doi:10.1038/s41598-020-71157-w

456. Basit F, Cristofanon S, Fulda S. Obatoclax (GX15-070) triggers necroptosis by promoting the assembly of the necrosome on autophagosomal membranes. Cell Death Differ. 2013;20: 1161–1173. doi:10.1038/cdd.2013.45

457. Parikh SA, Kantarjian H, Schimmer A, Walsh W, Asatiani E, El-Shami K, Winton E, Verstovsek S. Phase II study of obatoclax mesylate (GX15-070), a small-molecule BCL-2 family antagonist, for patients with myelofibrosis. Clin Lymphoma, Myeloma Leuk. 2010;10: 285–289. doi:10.3816/CLML.2010.n.059

458. Schimmer AD, Raza A, Carter TH, Claxton D, Erba H, DeAngelo DJ, Tallman MS, Goard C, Borthakur G. A multicenter phase I/II study of obatoclax mesylate administered as a 3- Or 24-hour infusion in older patients with previously untreated acute myeloid leukemia. PLoS One. 2014;9. doi:10.1371/journal.pone.0108694

459. Roberts DP, McKenna LF, Lakshman DK, Meyer SLF, Kong H, de Souza JT, Lydon J, Baker CJ, Buyer JS, Chung S. Suppression of damping-off of cucumber caused by Pythium ultimum with live cells and extracts of *Serratia marcescens* N4-5. Soil Biol Biochem. 2007;39: 2275–2288. doi:10.1016/j.soilbio.2007.03.029

460. Rahul S, Chandrashekhar P, Hemant B, Chandrakant N, Laxmikant S, Satish P. Nematicidal activity of microbial pigment from *Serratia marcescens*. Nat Prod Res. 2014;28: 1399–1404. doi:10.1080/14786419.2014.904310

461. Habash SS, Brass HUC, Klein AS, Klebl DP, Weber TM, Classen T, Pietruszka J, Grundler FMW, Schleker ASS. Novel prodiginine derivatives demonstrate bioactivities on plants, nematodes, and fungi. Front Plant Sci. 2020;11: 1545. doi:10.3389/fpls.2020.579807

462. Klein AS, Brass HUC, Klebl DP, Classen T, Loeschcke A, Drepper T, Sievers S, Jaeger K-E, Pietruszka J. Preparation of cyclic prodiginines by mutasynthesis in *Pseudomonas putida* KT2440. ChemBioChem. 2018;19: 1545–1552. doi:10.1002/cbic.201800154

463. Brands S, Brass HUC, Klein AS, Pietruszka J, Ruff AJ, Schwaneberg U. A colourimetric high-throughput screening system for directed evolution of prodigiosin ligase PigC. Chem Commun. 2020;56: 8631–8634. doi:10.1039/d0cc02181d

464. Brands S, Sikkens JG, Davari MD, Brass HUC, Klein AS, Pietruszka J, Ruff AJ, Schwaneberg U. Understanding substrate binding and the role of gatekeeping residues in PigC access tunnels. Chem. Commun. Royal Society of Chemistry; 2021;57,21: 2681–2684. doi:10.1039/d0cc08226k

465. Brands S, Brass HUC, Klein AS, Sikkens JG, Davari MD, Pietruszka J, Ruff AJ, Schwaneberg U. KnowVolution of prodigiosin ligase PigC towards condensation of short-chain prodiginines. Catal Sci Technol. 2021;11: doi:10.1039/d0cy02297g

466. Brass HUC, Klein AS, Nyholt S, Classen T, Pietruszka J. Condensing enzymes from *Pseudoalteromonadaceae* for prodiginine synthesis. Adv Synth Catal. 2019;361: adsc.201900183. doi:10.1002/adsc.201900183

467. Jarvis FG, Johnson MJ. A Glyco-lipide produced by *Pseudomonas aeruginosa*. J Am Chem Soc. 1949;71: 4124–4126. doi:10.1021/ja01180a073

468. Wittgens A, Kovacic F, Müller MM, Gerlitzki M, Santiago-Schübel B, Hofmann D, Tiso T, Blank LM, Henkel M, Hausmann R, Syldatk C, Wilhelm S, Rosenau F. Novel insights into biosynthesis and uptake of rhamnolipids and their precursors. Appl Microbiol Biotechnol. 2017;101: 2865–2878. doi:10.1007/s00253-016-8041-3

469. Abdel-Mawgoud AM, Hausmann R, Lépine F, Müller MM, Déziel E. Biosurfactants. 2011. doi:10.1007/978-3-642-14490-5

470. Costa SGVAO, Déziel E, Lépine F. Characterization of rhamnolipid production by *Burkholderia glumae*. Lett Appl Microbiol. 2011;53: 620–627. doi:10.1111/j.1472-765X.2011.03154.x

471. Dubeau D, Déziel E, Woods DE, Lépine F. *Burkholderia thailandensis* harbors two identical rhl gene clusters responsible for the biosynthesis of rhamnolipids. BMC Microbiol. 2009;9: 263. doi:10.1186/1471-2180-9-263

472. Rahim R, Ochsner UA, Olvera C, Graninger M, Messner P, Lam JS, Soberón-Chávez G. Cloning and functional characterization of the *Pseudomonas aeruginosa rhlC* gene that encodes rhamnosyltransferase 2, an enzyme responsible for di-rhamnolipid biosynthesis. Mol Microbiol. 2001;40: 708–718. doi:10.1046/j.1365-2958.2001.02420.x

473. Rehm BHA, Mitsky TA, Steinbüchel A. Role of fatty acid *de novo* biosynthesis in polyhydroxyalkanoic acid (PHA) and rhamnolipid synthesis by *Pseudomonads*: Establishment of the transacylase (PhaG)-mediated pathway for PHA biosynthesis in *Escherichia coli*. Appl Environ Microbiol. 2001;67: 3102–3109. doi:10.1128/AEM.67.7.3102-3109.2001

474. Rahim R, Burrows LL, Monteiro MA, Perry MB, Lam JS. Involvement of the *rml* locus in core oligosaccharide and O-polysaccharide assembly in *Pseudomonas aeruginosa*. Microbiology. 2000;146: 2803–2814. doi:10.1099/00221287-146-11-2803

475. Ochsner UA, Fiechter A, Reiser J. Isolation, characterization, and expression in *Escherichia coli* of the *Pseudomonas aeruginosa rhlAB* genes encoding a rhamnosyltransferase involved in rhamnolipid biosurfactant synthesis. J Biol Chem. 1994;269: 19787–19795. doi:10.1016/s0021-9258(17)32089-6

476. Kohler T, Curty LK, Barja F, Van Delden C, Pechere JC. Swarming of *Pseudomonas aeruginosa* is dependent on cell-to-cell signaling and requires flagella and pili. J Bacteriol. 2000;182: 5990–5996. doi:10.1128/JB.182.21.5990-5996.2000

477. Davey ME, Caiazza NC, O'Toole GA. Rhamnolipid surfactant production affects biofilm architecture in *Pseudomonas aeruginosa* PAO1. J Bacteriol. 2003;185: 1027–1036. doi:10.1128/JB.185.3.1027-1036.2003

478. Tremblay J, Richardson A-P, Lépine F, Déziel E. Self-produced extracellular stimuli modulate the *Pseudomonas aeruginosa* swarming motility behaviour. Environ Microbiol. 2007;9: 2622–2630. doi:10.1111/j.1462-2920.2007.01396.x

479. Kownatzki R, Tümmler B, Döring G. Rhamnolipids of *Pseudomonas aeruginosa* in sputum of cystic fibrosis patients. Lancet. 1987;329: 1026–1027. doi:10.1016/S0140-6736(87)92286-0

480. McClure CD, Schiller NL. Inhibition of macrophage phagocytosis by *Pseudomonas aeruginosa* rhamnolipids *in vitro* and *in vivo*. Curr Microbiol. 1996;33: 109–117. doi:10.1007/s002849900084

481. Zhang Y, Miller RM. Effect of a *Pseudomonas* rhamnolipid biosurfactant on cell hydrophobicity and biodegradation of octadecane. Appl Environ Microbiol. 1994;60: 2101–2106. doi:10.1128/aem.60.6.2101-2106.1994

482. Henkel M, Müller MM, Kügler JH, Lovaglio RB, Contiero J, Syldatk C, Hausmann R. Rhamnolipids as biosurfactants from renewable resources: Concepts for next-generation rhamnolipid production. Process Biochem. 2012;47: 1207–1219. doi:https://doi.org/10.1016/j.procbio.2012.04.018

483. Johann S, Seiler TB, Tiso T, Bluhm K, Blank LM, Hollert H. Mechanism-specific and whole-organism ecotoxicity of mono-rhamnolipids. Sci Total Environ. 2016;548–549: 155–163. doi:10.1016/j.scitotenv.2016.01.066

484. Sekhon Randhawa KK, Rahman PKSM. Rhamnolipid biosurfactants-past, present, and future scenario of global market. Front Microbiol. 2014;5: 454. doi:10.3389/fmicb.2014.00454

485. Brandt KD, Hartung C. Cosmetics containing rhamnolipids. EP2786742A1, 2013. Available: https://patents.google.com/patent/EP2786742A1/en?q=(rhamnolipids)&before=p

riority:20131230&after=priority:20130101&oq=(rhamnolipids)+before:priority:20131230+after:priority:20130101

486. Singh A, Van Hamme JD, Ward OP. Surfactants in microbiology and biotechnology: Part 2. Application aspects. Biotechnol Adv. 2007;25: 99–121. doi:10.1016/j.biotechadv.2006.10.004

487. Rahman KSM, Rahman TJ, Kourkoutas Y, Petsas I, Marchant R, Banat IM. Enhanced bioremediation of n-alkane in petroleum sludge using bacterial consortium amended with rhamnolipid and micronutrients. Bioresour Technol. 2003;90: 159–168. doi:10.1016/S0960-8524(03)00114-7

488. Magalhães L, Nitschke M. Antimicrobial activity of rhamnolipids against *Listeria monocytogenes* and their synergistic interaction with nisin. Food Control. 2013;29: 138–142. doi:10.1016/j.foodcont.2012.06.009

489. Vecino X, Cruz JM, Moldes AB, Rodrigues LR. Biosurfactants in cosmetic formulations: trends and challenges. Critical Reviews in Biotechnology. Taylor and Francis Ltd; 2017. pp. 911–923. doi:10.1080/07388551.2016.1269053

490. Wittgens A, Rosenau F. On the road towards tailor-made rhamnolipids: current state and perspectives. Appl. Microbiol. Biotechnol. Springer Verlag; 2018. pp. 8175–8185. doi:10.1007/s00253-018-9240-x

491. Parry AJ, Parry NJ, Peilow AC, Stevenson PS. Combinations of rhamnolipids and enzymes for improved cleaning. EP2596087A1, 2013. Available: https://patents.google.com/patent/EP2596087A1/en?oq=EP+2596087A1

492. Toribio J, Escalante AE, Soberón-Chávez G. Rhamnolipids: Production in bacteria other than *Pseudomonas aeruginosa*. Eur J Lipid Sci Technol. 2010;112: 1082–1087. doi:10.1002/ejlt.200900256

493. Wittgens A, Santiago-Schuebel B, Henkel M, Tiso T, Blank LM, Hausmann R, Hofmann D, Wilhelm S, Jaeger K-E, Rosenau F. Heterologous production of long-chain rhamnolipids from *Burkholderia glumae* in *Pseudomonas putida*—a step forward to tailor-made rhamnolipids. Appl Microbiol Biotechnol. 2018;102: 1229–1239. doi:10.1007/s00253-017-8702-x

494. Ochsner UA, Reiser J, Fiechter A, Witholt B. Production of *Pseudomonas aeruginosa* rhamnolipid biosurfactants in heterologous hosts. Appl Environ Microbiol. 1995;61.

495. Wang Q, Fang X, Bai B, Liang X, Shuler PJ, Goddard WA, Tang Y. Engineering bacteria for production of rhamnolipid as an agent for enhanced oil recovery. Biotechnol Bioeng. 2007;98: 842–853. doi:10.1002/bit.21462

496. Wittgens A, Tiso T, Arndt TT, Wenk P, Hemmerich J, Müller C, Wichmann R, Küpper B, Zwick M, Wilhelm S, Hausmann R, Syldatk C, Rosenau F, Blank LM. Growth independent rhamnolipid production from glucose using the non-pathogenic *Pseudomonas putida* KT2440. Microb Cell Fact. 2011;10: 80. doi:10.1186/1475-2859-10-80

497. Bator I, Wittgens A, Rosenau F, Tiso T, Blank LM. Comparison of three xylose pathways in *Pseudomonas putida* KT2440 for the synthesis of valuable products. Front Bioeng Biotechnol. 2020;7: 1–18. doi:10.3389/fbioe.2019.00480

498. Askitosari TD, Berger C, Tiso T, Harnisch F, Blank LM, Rosenbaum MA. Coupling an electroactive *Pseudomonas putida* KT2440 with bioelectrochemical

rhamnolipid production. Microorganisms. 2020;8: 1959. doi:10.3390/microorganisms8121959

499. Bator I, Karmainski T, Tiso T, Blank LM. Killing two birds with one stone – strain engineering facilitates the development of a unique rhamnolipid production process. Front Bioeng Biotechnol. 2020;8: 1–16. doi:10.3389/fbioe.2020.00899

500. Tiso T, Sabelhaus P, Behrens B, Wittgens A, Rosenau F, Hayen H, Blank LM. Creating metabolic demand as an engineering strategy in *Pseudomonas putida* – Rhamnolipid synthesis as an example. Metab Eng Commun. 2016;3: 234–244. doi:10.1016/j.meteno.2016.08.002

501. Hogenkamp F, Hilgers F, Knapp A, Klaus O, Bier C, Binder D, Jaeger K-E, Drepper T, Pietruszka J. Effect of photocaged isopropyl β-D-1-thiogalactopyranoside solubility on the light responsiveness of LacI-controlled expression systems in different bacteria. ChemBioChem. 2021;22: 539–547. doi:10.1002/cbic.202000377

502. Hogenkamp F, Hilgers F, Bitzenhofer NL, Ophoven V, Haase M, Bier C, Binder D, Jaeger K-E, Drepper T, Pietruszka J. Optochemical Control of Bacterial Gene Expression: Novel Photocaged Compounds for Different Promoter Systems ChemBioChem. 2021;21. doi: 10.1002/cbic.202100467

503. Hilgers F, Hogenkamp F, Klaus O, Kruse L, Lappe A, Loeschcke A, Bier C, Binder D, Jaeger K-E, Pietruszka J, Drepper T. Photocaged inducers for the non-invasive light control of production processes in the phototrophic bacterium *Rhodobacter capsulatus*. 2021.*manuscript in preparation*

504. Hilgers F, Hogenkamp F, Bitzenhofer NL, Thies S, Jaeger K-E, Pietruszka J, Drepper T. Wavelength-selective control of mono- and dirhamnoplipid production in *Pseudomonas putida*. 2021.*manuscript in preparation*

505. Endres S, Wingen M, Torra J, Ruiz-González R, Polen T, Bosio G, Bitzenhofer NL, Hilgers F, Gensch T, Nonell S, Jaeger K-E, Drepper T. An optogenetic toolbox of LOV-based photosensitizers for light-driven killing of bacteria. Sci Rep. 2018;8: 15021. doi:10.1038/s41598-018-33291-4

506. Hilgers F, Bitzenhofer NL, Ackermann Y, Burmeister A, Grünberger A, Jaeger K-E, Drepper T. Genetically encoded photosensitizers as light-triggered antimicrobial agents. Int J Mol Sci. 2019;20: 4608. doi:10.3390/ijms20184608

507. Raber HF, Heerde T, El Din SN, Flaig C, Hilgers F, Bitzenhofer N, Jäger K-E, Drepper T, Gottschalk K, Bodenberger NE, Weil T, Kubiczek DH, Rosenau F. Azulitox- A *Pseudomonas aeruginosa* P28-derived cancer-cell-specific protein photosensitizer. Biomacromolecules. 2020; acs.biomac.0c01216. doi:10.1021/acs.biomac.0c01216

508. Hage-Hülsmann J, Klaus O, Linke K, Troost K, Gora L, Hilgers F, Wirtz A, Santiago-Schübel B, Loeschcke A, Jaeger K-E, Drepper T. Production of C20, C30 and C40 terpenes in the engineered phototrophic bacterium *Rhodobacter capsulatus.* J Biotechnol. 2021;338:20-30. doi: 10.1016/j.jbiotec.2021.07.002

509. Lee J, Hilgers F, Loeschke A, Jaeger K-E, Feldbrügge M. *Ustilago maydis* serves as a novel production host for the synthesis of plant and fungal sesquiterpenoids. Front Microbiol. 2020;11. doi:10.3389/fmicb.2020.01655

510. Burmeister A, Hilgers F, Langner A, Westerwalbesloh C, Kerkhoff Y, Tenhaef N,

Drepper T, Kohlheyer D, Von Lieres E, Noack S, Grünberger A. A microfluidic co-cultivation platform to investigate microbial interactions at defined microenvironments. Lab Chip. 2019;19: 98–110. doi:10.1039/C8LC00977E

511. Lenz P, Hilgers F, Burmeister A, Zimmermann L, Volkenborn K, Grünberger A, Kohlheyer D, Drepper T, Jaeger K-E, Knapp A. The iSplit GFP assay detects intracellular recombinant proteins in *Bacillus subtilis*. Microb Cell Fact. 2021; 20, 174. doi: 10.1186/s12934-021-01663-7

512. Gerlach T, Schain J, Ampomah Nsiah B, van Schie MMCH, Drepper T, Rother D. Photo-regulation of enzyme activity: the inactivation of a carboligase with genetically encoded photosensitizer fusion tags. 2021.*ready for submission*

513. Burmeister A, Akhtar Q, Hollmann L, Tenhaef N, Hilgers F, Hogenkamp F, Sokolowsky S, Marienhagen J, Noack S, Kohlheyer D, Grünberger A. (Optochemical) control of synthetic microbial coculture interactions on a microcolony level. ACS Synth Biol. 2021; acssynbio.0c00382. doi:10.1021/acssynbio.0c00382

514. Wandrey G, Bier C, Binder D, Hoffmann K, Jaeger K-E, Pietruszka J, Drepper T, Büchs J. Light-induced gene expression with photocaged IPTG for induction profiling in a high-throughput screening system. Microb Cell Fact. 2016;15: 63. doi:10.1186/s12934-016-0461-3

515. Onukwufor JO, Trewin AJ, Baran TM, Almast A, Foster TH, Wojtovich AP. Quantification of reactive oxygen species production by the red fluorescent proteins KillerRed, SuperNova and mCherry. Free Radic Biol Med. 2020;147: 1–7. doi:10.1016/j.freeradbiomed.2019.12.008

516. Ragàs X, Cooper LP, White JH, Nonell S, Flors C. Quantification of photosensitized singlet oxygen production by a fluorescent protein. ChemPhysChem. 2011;12: 161–165. doi:10.1002/cphc.201000919

517. Jiménez-Banzo A, Ragàs X, Abbruzzetti S, Viappiani C, Campanini B, Flors C, Nonell S. Singlet oxygen photosensitisation by GFP mutants: Oxygen accessibility to the chromophore. Photochem Photobiol Sci. 2010;9: 1336–1341. doi:10.1039/c0pp00125b

518. Wang D, Li Q, Qiu J, Zhang X, Ge N, Liu X. Corrosion motivated ROS generation helps endow titanium with broad-spectrum antibacterial abilities. Adv Mater Interfaces. 2019;6: 1900514. doi:10.1002/admi.201900514

519. Huang L, Xuan Y, Koide Y, Zhiyentayev T, Tanaka M, Hamblin MR. Type I and Type II mechanisms of antimicrobial photodynamic therapy: an *in vitro* study on Gram-negative and Gram-positive bacteria. Lasers Surg Med. 2012;44: 490–9. doi:10.1002/lsm.22045

520. Mai-Prochnow A, Clauson M, Hong J, Murphy AB. Gram-positive and Gram-negative bacteria differ in their sensitivity to cold plasma. Sci Rep. 2016;6: 38610. doi:10.1038/srep38610

521. Dahl TA, Midden WR, Hartman PE. Comparison of killing of Gram-negative and Gram-positive bacteria by pure singlet oxygen. J Bacteriol. 1989;171: 2188–2194. doi:10.1128/jb.171.4.2188-2194.1989

522. Ackermann YS. Antimikrobielle Effekte von genetisch kodierten Photosensibilisatoren und Terpenen. Heinrich Heine University Düsseldorf. 2019.

Master thesis.

523. Chen H, Zhu C, Zhu M, Xiong J, Ma H, Zhuo M, Li S. High production of valencene in *Saccharomyces cerevisiae* through metabolic engineering. Microb Cell Fact. 2019;18: 195. doi:10.1186/s12934-019-1246-2

524. Henke N, Wichmann J, Baier T, Frohwitter J, Lauersen K, Risse J, Peters-Wendisch P, Kruse O, Wendisch V. Patchoulol Production with metabolically engineered *Corynebacterium glutamicum*. Genes (Basel). 2018;9: 219. doi:10.3390/genes9040219

525. Yang J, Li Z, Guo L, Du J, Bae H. Biosynthesis of β-caryophyllene, a novel terpene-based high-density biofuel precursor, using engineered *Escherichia coli*. Renew Energy. 2016;99: 216–223. doi:10.1016/j.renene.2016.06.061

526. Callari R, Meier Y, Ravasio D, Heider H. Dynamic control of ERG20 and ERG9 expression for improved casbene production in *Saccharomyces cerevisiae*. Front Bioeng Biotechnol. 2018;6. doi:10.3389/fbioe.2018.00160

527. Kirby J, Nishimoto M, Park JG, Withers ST, Nowroozi F, Behrendt D, Rutledge EJG, Fortman JL, Johnson HE, Anderson J V. Cloning of casbene and neocembrene synthases from *Euphorbiaceae* plants and expression in *Saccharomyces cerevisiae*. Phytochemistry. 2010;71: 1466–1473. doi:10.1016/j.phytochem.2010.06.001

528. Wong J, de Rond T, D'Espaux L, van der Horst C, Dev I, Rios-Solis L, Kirby J, Scheller H, Keasling J. High-titer production of lathyrane diterpenoids from sugar by engineered *Saccharomyces cerevisiae*. Metab Eng. 2018;45: 142–148. doi:10.1016/j.ymben.2017.12.007

529. Han JY, Seo SH, Song JM, Lee H, Choi ES. High-level recombinant production of squalene using selected *Saccharomyces cerevisiae* strains. J Ind Microbiol Biotechnol. 2018;45: 239–251. doi:10.1007/s10295-018-2018-4

530. Wu Y, Yan P, Li Y, Liu X, Wang Z, Chen T, Zhao X. Enhancing β-carotene production in *Escherichia coli* by perturbing central carbon metabolism and improving the NADPH Supply. Front Bioeng Biotechnol. 2020;8: 585. doi:10.3389/fbioe.2020.00585

531. Yang J, Guo L. Biosynthesis of β-carotene in engineered *E. coli* using the MEP and MVA pathways. Microb Cell Fact. 2014;13: 1–11. doi:10.1186/s12934-014-0160-x

532. López J, Cataldo VF, Peña M, Saa PA, Saitua F, Ibaceta M, Agosin E. Build your bioprocess on a solid strain—β-carotene production in recombinant *Saccharomyces cerevisiae*. Front Bioeng Biotechnol. 2019;7: 171. doi:10.3389/fbioe.2019.00171

533. Bitzenhofer NL. Light-driven control of bacterial processes by genetically encoded photosensitizers. Heinrich Heine University Düsseldorf. 2018. Master thesis.

534. Grünberger A, Probst C, Helfrich S, Nanda A, Stute B, Wiechert W, von Lieres E, Nöh K, Frunzke J, Kohlheyer D. Spatiotemporal microbial single-cell analysis using a high-throughput microfluidics cultivation platform. Cytom Part A. 2015;87: 1101–1115. doi:10.1002/cyto.a.22779

535. Bitzenhofer NL. Verwendung von photocaged compounds zur Licht-gesteuerten Expression in *Bacillus*. Heinrich Heine University Düsseldorf. 2016. Bachelor

thesis.

536. Kubicki S. Licht-gesteuerte Genexpression in industriell relevanten Bakterien. Heinrich Heine University Düsseldorf. 2015. Bachelor thesis.

537. Wong PT, Roberts EW, Tang S, Mukherjee J, Cannon J, Nip AJ, Corbin K, Krummel MF, Choi SK. Control of an unusual photo-claisen rearrangement in coumarin caged tamoxifen through an extended spacer. ACS Chem Biol. 2017;12: 1001–1010. doi:10.1021/acschembio.6b00999

538. Gorka AP, Yamamoto T, Zhu J, Schnermann MJ. Cyanine Photocages enable spatial control of inducible Cre-mediated recombination. ChemBioChem. 2018;19: 1239–1243. doi:10.1002/cbic.201800061

539. Goegan B, Terzi F, Bolze F, Cambridge S, Specht A. Synthesis and characterization of photoactivatable doxycycline analogues bearing two-photon-sensitive photoremovable groups suitable for light-induced gene expression. ChemBioChem. 2018;19: 1341–1348. doi:10.1002/cbic.201700628

540. Baumschlager A, Aoki SK, Khammash M. Dynamic blue light-inducible T7 RNA polymerases (Opto-T7RNAPs) for precise spatiotemporal gene expression control. ACS Synth Biol. 2017;6: 2157–2167. doi:10.1021/acssynbio.7b00169

541. Li X, Zhang C, Xu X, Miao J, Yao J, Liu R, Zhao Y, Chen X, Yang Y. A single-component light sensor system allows highly tunable and direct activation of gene expression in bacterial cells. Nucleic Acids Res. 2020;48: E33. doi:10.1093/nar/gkaa044

542. Jayaraman P, Devarajan K, Chua TK, Zhang H, Gunawan E, Poh CL. Blue light-mediated transcriptional activation and repression of gene expression in bacteria. Nucleic Acids Res. 2016;44: 6994–7005. doi:10.1093/nar/gkw548

543. Chen EKY, McBride RA, Gillies ER. Self-immolative polymers containing rapidly cyclizing spacers: Toward rapid depolymerization rates. Macromolecules. 2012;45: 7364–7374. doi:10.1021/ma301667c

544. Schade B, Hagen V, Schmidt R, Herbrich R, Krause E, Eckardt T, Bendig J. Deactivation behavior and excited-state properties of (coumarin-4-yl)methyl derivatives. 1. Photocleavage of (7-methoxycoumarin-4-yl)methyl-caged acids with fluorescence enhancement. J Org Chem. 1999;64: 9109–9117. doi:10.1021/jo9910233

545. Romano E, Baumschlager A, Akmeriç EB, Palanisamy N, Houmani M, Schmidt G, Öztürk MA, Ernst L, Khammash M, Di Ventura B. Engineering AraC to make it responsive to light instead of arabinose. Nat Chem Biol. 2021; 1–11. doi:10.1038/s41589-021-00787-6

546. Schaper K, Etinski M, Fleig T. Theoretical investigation of the excited states of 2-nitrobenzyl and 4,5-methylendioxy-2-nitrobenzyl caging groups. Photochem Photobiol. 2009;85: 1075–1081. doi:10.1111/j.1751-1097.2009.00560.x

547. Liu Z, Zhang J, Jin J, Geng Z, Qi Q, Liang Q. Programming bacteria with light-sensors and applications in synthetic biology. Front Microbiol. 2018;9. doi:10.3389/fmicb.2018.02692

548. Müller K, Engesser R, Schulz S, Steinberg T, Tomakidi P, Weber CC, Ulm R, Timmer J, Zurbriggen MD, Weber W. Multi-chromatic control of mammalian gene expression and signaling. Nucleic Acids Res. 2013;41. doi:10.1093/nar/gkt340

549. Redchuk TA, Kaberniuk AA, Verkhusha V V. Near-infrared light-controlled systems for gene transcription regulation, protein targeting and spectral multiplexing. Nat Protoc. 2018;13: 1121–1136. doi:10.1038/nprot.2018.022

550. Padmanabhan S, Pérez-Castaño R, Elías-Arnanz M. B_{12}-based photoreceptors: from structure and function to applications in optogenetics and synthetic biology. Curr Opin Struct Biol. 2019;57: 47–55. doi:10.1016/j.sbi.2019.01.020

551. Chatelle C, Ochoa-Fernandez R, Engesser R, Schneider N, Beyer HM, Jones AR, Timmer J, Zurbriggen MD, Weber W. A Green-light-responsive system for the control of transgene expression in mammalian and plant cells. ACS Synth Biol. 2018;7: 1349–1358. doi:10.1021/acssynbio.7b00450

552. Cheng Z, Li K, Hammad LA, Karty JA, Bauer CE. Vitamin B_{12} regulates photosystem gene expression *via* the CrtJ antirepressor AerR in *Rhodobacter capsulatus*. Mol Microbiol. 2014;91: 649–664. doi:10.1111/mmi.12491

553. Consiglieri E, Xu Q, Bregnhøj M, Westberg M, Ogilby PR, Losi A. Single mutation in a novel bacterial LOV protein yields a singlet oxygen generator. Photochem Photobiol Sci. 2019;18: 2657–2660. doi:10.1039/C9PP00328B

554. Gorbachev DA, Staroverov DB, Lukyanov KA, Sarkisyan KS. Genetically encoded red photosensitizers with enhanced phototoxicity. Int J Mol Sci. 2020;21: 8800. doi:10.3390/ijms21228800

555. Makhijani K, To T-L, Ruiz-González R, Lafaye C, Royant A, Shu X. Precision optogenetic tool for selective single- and multiple-cell ablation in a live animal model system. Cell Chem Biol. 2017;24: 110–119. doi:10.1016/j.chembiol.2016.12.010

556. Westberg M, Etzerodt M, Ogilby PR. Rational design of genetically encoded singlet oxygen photosensitizing proteins. Curr Opin Struct Biol. 2019;57: 56–62. doi:10.1016/j.sbi.2019.01.025

557. He J, Wang Y, Missinato MA, Onuoha E, Perkins LA, Watkins SC, St Croix CM, Tsang M, Bruchez MP. A genetically targetable near-infrared photosensitizer. Nat Methods. 2016;13: 263–268. doi:10.1038/nmeth.3735

558. Dichmann L, Bregnhøj M, Liu H, Westberg M, Poulsen TB, Etzerodt M, Ogilby PR. Photophysics of a protein-bound derivative of malachite green that sensitizes the production of singlet oxygen. Photochem Photobiol Sci. 2021. doi:10.1007/s43630-021-00032-y

559. Riani YD, Matsuda T, Takemoto K, Nagai T. Green monomeric photosensitizing fluorescent protein for photo-inducible protein inactivation and cell ablation. BMC Biol. 2018;16: 1–12. doi:10.1186/s12915-018-0514-7

560. Zhou J, Qi G Bin, Wang H. A purpurin-peptide derivative for selective killing of Gram-positive bacteria *via* insertion into cell membrane. J Mater Chem B. 2016;4: 4855–4861. doi:10.1039/c6tb00406g

561. Gao S, Yan X, Xie G, Zhu M, Ju X, Stang PJ, Tian Y, Niu Z. Membrane intercalation-enhanced photodynamic inactivation of bacteria by a metallacycle and TAT-decorated virus coat protein. Proc Natl Acad Sci USA. 2019;116: 23437–23443. doi:10.1073/pnas.1911869116

562. Ucuncu M, Mills B, Duncan S, Staderini M, Dhaliwal K, Bradley M. Polymyxin-based photosensitizer for the potent and selective killing of Gram-negative

bacteria. Chem Commun. 2020;56: 3757–3760. doi:10.1039/d0cc00155d

563. Gross S, Brandis A, Chen L, Rosenbach-Belkin V, Roehrs S, Scherz A, Salomon Y. Protein-A-mediated targeting of bacteriochlorophyll-IgG to *Staphylococcus aureus:* A model for enhanced site-specific photocytotoxicity. Photochem Photobiol. 1997;66: 872–878. doi:10.1111/j.1751-1097.1997.tb03240.x

564. Cantelli A, Piro F, Pecchini P, Di Giosia M, Danielli A, Calvaresi M. Concanavalin. A Rose Bengal bioconjugate for targeted Gram-negative antimicrobial photodynamic therapy. J Photochem Photobiol B Biol. 2020;206: 111852. doi:10.1016/j.jphotobiol.2020.111852

565. Sai DL, Lee J, Nguyen DL, Kim Y-P. Tailoring photosensitive ROS for advanced photodynamic therapy. Exp Mol Med. 2021;53: 495–504. doi:10.1038/s12276-021-00599-7

566. Shilova O, Shramova E, Proshkina G, Deyev S. Natural and designed toxins for precise therapy: modern approaches in experimental oncology. Int J Mol Sci. 2021;22: 4975. doi:10.3390/ijms22094975

567. Klausen M, Ucuncu M, Bradley M. Design of photosensitizing agents for targeted antimicrobial photodynamic therapy. Molecules. 2020;25: 5239. doi:10.3390/molecules25225239

568. Gerlach T, M.C.H. van Schie M, Ampomah Nsiah B, Drepper T, Rother D. On-demand enzyme inactivation: Avoiding cross-reactivity in multi-step biocatalysis by genetically encoded photosensitizer fusion tags. 2021.*ready for submission*

569. Ehlers J. Chromophore-assisted light inactivation (CALI) für die Licht-gesteuerte Kontrolle des Prodigiosin-Biosyntheseweges. Heinrich Heine University Düsseldorf. 2019.Bachelor thesis.

570. Hage-Hülsmann J, Metzger S, Wewer V, Buechel F, Troost K, Thies S, Loeschcke A, Jaeger K-E, Drepper T. Biosynthesis of cycloartenol by expression of plant and bacterial oxidosqualene cyclases in engineered *Rhodobacter capsulatus*. J Biotechnol X. 2019;4: 100014. doi:10.1016/j.btecx.2020.100014

571. Ghosh S, Chowdhury R, Bhattacharya P. Mixed consortia in bioprocesses: role of microbial interactions. Appl. Microbiol. Biotechnol. 2016. pp. 4283–4295. doi:10.1007/s00253-016-7448-1

572. Jagmann N, Philipp B. Design of synthetic microbial communities for biotechnological production processes. J Biotechnol. 2014;184: 209–218. doi:10.1016/j.jbiotec.2014.05.019

573. Großkopf T, Soyer OS. Synthetic microbial communities. Curr Opin Microbiol. 2014. pp. 72–77. doi:10.1016/j.mib.2014.02.002

574. Rosero-Chasoy G, Rodríguez-Jasso RM, Aguilar CN, Buitrón G, Chairez I, Ruiz HA. Microbial co-culturing strategies for the production high value compounds, a reliable framework towards sustainable biorefinery implementation – an overview. Bioresource Technology. 2021. p. 124458. doi:10.1016/j.biortech.2020.124458

575. Zhou K, Qiao K, Edgar S, Stephanopoulos G. Distributing a metabolic pathway among a microbial consortium enhances production of natural products. Nat Biotechnol. 2015;33: 377–383. doi:10.1038/nbt.3095

576. Minty JJ, Singer ME, Scholz SA, Bae CH, Ahn JH, Foster CE, Liao JC, Lin XN.

Design and characterization of synthetic fungal-bacterial consortia for direct production of isobutanol from cellulosic biomass. Proc Natl Acad Sci USA. 2013;110: 14592–14597. doi:10.1073/pnas.1218447110

577. Gagic D, Ciric M, Wen WX, Ng F, Rakonjac J. Exploring the secretomes of microbes and microbial communities using filamentous phage display. Front. Microbiol. 2016. doi:10.3389/fmicb.2016.00429

578. Agapakis CM, Boyle PM, Silver PA. Natural strategies for the spatial optimization of metabolism in synthetic biology. Nat Chem Biol. 2012. pp. 527–535. doi:10.1038/nchembio.975

579. Hays SG, Patrick WG, Ziesack M, Oxman N, Silver PA. Better together: Engineering and application of microbial symbioses. Curr Opin Biotechnol. 2015. pp. 40–49. doi:10.1016/j.copbio.2015.08.008

580. Zhuang L, Zhang H. Utilizing cross-species co-cultures for discovery of novel natural products. Curr Opin Biotechnol. 2021. pp. 252–262. doi:10.1016/j.copbio.2021.01.023

581. Wang R, Zhao S, Wang Z, Koffas MA. Recent advances in modular co-culture engineering for synthesis of natural products. Curr Opin Biotechnol. 2020. pp. 65–71. doi:10.1016/j.copbio.2019.09.004

582. Sgobba E, Wendisch VF. Synthetic microbial consortia for small molecule production. Curr Opin Biotechnol. 2020;62: 72–79. doi:https://doi.org/10.1016/j.copbio.2019.09.011

583. Song H, Ding M-Z, Jia X-Q, Ma Q, Yuan Y-J. Synthetic microbial consortia: from systematic analysis to construction and applications. Chem Soc Rev. 2014;43: 6954–81. doi:10.1039/c4cs00114a

584. Migahed F, Abdelrazak A, Fawzy G. Batch and continuous removal of heavy metals from industrial effluents using microbial consortia. Int J Environ Sci Technol. 2017;14: 1169–1180. doi:10.1007/s13762-016-1229-3

585. Velema WA, van der Berg JP, Szymanski W, Driessen AJM, Feringa BL. Orthogonal control of antibacterial activity with light. ACS Chem Biol. 2014;9: 1969–1974. doi:10.1021/cb500313f

586. Shou W, Ram S, Vilar JMG. Synthetic cooperation in engineered yeast populations. Proc Natl Acad Sci USA. 2007;104: 1877–1882. doi:10.1073/pnas.0610575104

587. Kerner A, Park J, Williams A, Lin XN. A Programmable *Escherichia coli* consortium *via* tunable symbiosis. PLoS One. 2012;7: e34032. doi:10.1371/journal.pone.0034032

588. Knapp A, Ripphahn M, Volkenborn K, Skoczinski P, Jaeger K-E. Activity-independent screening of secreted proteins using split GFP. J Biotechnol. 2017;258: 110–116. doi:10.1016/j.jbiotec.2017.05.024

589. Volkenborn K, Kuschmierz L, Benz N, Lenz P, Knapp A, Jaeger K-E. The length of ribosomal binding site spacer sequence controls the production yield for intracellular and secreted proteins by *Bacillus subtilis*. Microb Cell Fact. 2020;19: 154. doi:10.1186/s12934-020-01404-2

590. Lenz P. Optimierung bakterieller Sekretionswege und kombinierte

Nachweissysteme für eine holistische Detektion rekombinanter Proteine. Heinrich Heine University Düsseldorf. Dissertation in preparation.

591. Brocke D. Spatio-temporal analysis of bacterial conjugation in microfluidic cultivation chips at the single-cell level. RWTH Aachen University. 2020. Master thesis.

592. Kruse L. Pyoverdine-mediated iron acquisition in co-culture of *Rhodobacter capsulatus* and *Pseudomonas putida*. Heinrich Heine University Düsseldorf. 2020. Master thesis.

V. APPENDIX

V.1. SUPPORTING INFORMATION FOR CHAPTER II.1.1 – NOVEL PHOTOCAGED IPTG VARIANTS FOR LIGHT-MEDIATED TARGET GENE EXPRESSION IN *E. COLI*, *P. PUTIDA* AND *B. SUBTILIS*

ChemBioChem

Supporting Information

Effect of Photocaged Isopropyl β-D-1-thiogalactopyranoside Solubility on the Light Responsiveness of LacI-controlled Expression Systems in Different Bacteria

Fabian Hogenkamp[+], Fabienne Hilgers[+], Andreas Knapp, Oliver Klaus, Claus Bier, Dennis Binder, Karl-Erich Jaeger, Thomas Drepper,* and Jörg Pietruszka*

The online version may be found at: cbic202000377-sup-0001-misc_information.pdf

Table of Contents

S1 Supporting methods

S1.1 Synthesis of 3,4-bis(ethoxycarbonylmethoxy)benzaldehyde (18)

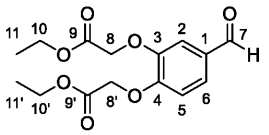

To a solution of 3,4-dihydroxybenzaldehyde (3.00 g, 21.7 mmol) in DMF (42 mL) K_2CO_3 (12.2 g, 86.9 mmol, 4.00 equiv.) was added and it was stirred for 30 min at room temperature. The reaction mixture was cooled to 0 °C and ethyl bromoacetate was added dropwise. The reaction mixture was stirred for additional 30 min at 0 °C, before it was stirred at room temperature for 16 h. The reaction was quenched by addition of water (60 mL). The aqueous phase was extracted with ethyl acetate. The organic phase was washed with saturated NaCl solution, dried with anhydrous $MgSO_4$ and concentrated under reduced pressure. The residue was purified by flash-column chromatography on SiO_2 (petroleum ether/ethyl acetate 7:3) to yield a white solid (5.88 g, 19.0 mmol, 87%). The spectroscopic data are in agreement with previously reported literature values.[1] R_f = 0.27 (petroleum ether/ethyl acetate 7:3); m.p. 55 °C, Lit.[2]: 55 - 56 °C; ^{1}H-NMR (600 MHz, $CDCl_3$): δ = 1.28 (t, $^3J_{11,10 \text{ or } 11',10'}$ = 7.2 Hz, 3 H, 11-*H* or 11′-*H*), 1.29 (t, $^3J_{11,10 \text{ or } 11',10'}$ = 7.2 Hz, 3 H, 11-*H* or 11′-*H*), 4.26 (q, $^3J_{10,11 \text{ or } 10',11'}$ = 7.2 Hz, 4 H, 10-*H* and 10′-*H*), 4.76 (s, 2 H, 8-*H*), 4.80 (s, 2 H, 8′-*H*), 6.92 (d, $^3J_{5,6}$ = 8.3 Hz, 1 H, 5-*H*), 7.37 (d, $^4J_{2,6}$ = 1.9 Hz, 1 H, 2-*H*), 7.47 (dd, $^3J_{6,5}$ = 8.3 Hz, $^4J_{6,2}$ = 1.9 Hz, 1 H, 6-*H*), 9.83 ppm (s, 1 H, 7-*H*); ^{13}C-NMR (151 MHz, $CDCl_3$): δ = 14.27 (*C*-11 and *C*-11′), 61.63 (*C*-10 or *C*-10′), 61.74 (*C*-10 or *C*-10′), 66.25 (*C*-8), 66.28 (*C*-8′), 113.05 (*C*-2), 113.66 (*C*-5), 127.00 (*C*-6), 131.14 (*C*-1), 148.39 (*C*-3), 153.17 (*C*-4), 168.16 (*C*-9′), 168.39 (*C*-9), 190.59 ppm (*C*-7); IR (ATR-film): $\tilde{\nu}$ = 2977, 1755, 1724, 1687, 1585, 1510, 1429, 1207, 1138, 1054, 1024, 671 cm^{-1}; MS (ESI, positive-ion): m/z (%): 333.2 (100) $[M+Na]^+$, 349.1 (40) $[M+K]^+$.

S1.2 Synthesis of 4,5-bis(ethoxycarbonylmethoxy)-2-nitrobenzaldehyde (11)

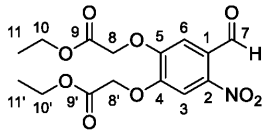

A solution of KNO_3 (2.31 g, 22.8 mmol, 1.25 equiv.) in trifluoroacetic acid (30 mL) was cooled to 0 °C and a solution of 3,4-bis(ethoxycarbonylmethoxy)benzaldehyde (**18**) (5.66 g, 18.2 mmol, 0.9 M) in trifluoroacetic acid was added dropwise. The reaction mixture was stirred for 1 h at 0 °C and for 16 h at room temperature. Then it was concentrated under reduced pressure, the residue was dissolved in ethyl acetate and washed with saturated $NaHCO_3$ and saturated NaCl solution. The organic phase was dried with anhydrous $MgSO_4$ and concentrated under reduced pressure. The residue was purified by flash-column chromatography on SiO_2 (petroleum ether/ethyl acetate 6:4) to yield a yellow solid (4.44 g, 12.5 mmol, 69%). The spectroscopic data are in agreement with previously reported literature values.[1] R_f = 0.44 (toluene/ethyl acetate 85:15); m.p. 94 °C; ^{1}H-NMR (600 MHz, $CDCl_3$): δ = 1.30 (t, $^3J_{11,10 \text{ or } 11',10'}$ = 7.2 Hz, 3 H, 11-*H* or 11′-*H*), 1.32 (t, $^3J_{11,10 \text{ or } 11',10'}$ = 7.2 Hz, 3 H, 11-*H* or 11′-*H*), 4.28 (q, $^3J_{10,11 \text{ or } 10',11'}$ = 7.2 Hz, 2 H, 10-*H* or 10′-*H*), 4.29 (q, $^3J_{10,11 \text{ or } 10',11'}$ = 7.2 Hz, 2 H, 10-*H* or 10′-*H*), 4.85 (s, 2 H, 8-*H* or 8′-*H*), 4.86 (s, 2 H, 8-*H* or 8′-*H*), 7.34 (s, 1 H, 3-*H*), 7.58 (s, 1 H, 6-*H*), 10.41 ppm (s, 1 H, 7-*H*); ^{13}C-NMR (151 MHz, $CDCl_3$): δ = 14.2 (*C*-11 or *C*-11′), 14.3 (*C*-11 or *C*-11′), 62.0 (*C*-10 or *C*-10′), 62.1 (*C*-10 or *C*-10′), 66.1 (*C*-8 or *C*-8′), 66.4 (*C*-8 or *C*-8′), 110.4 (*C*-6), 112.5 (*C*-3), 126.3 (*C*-1 or *C*-2), 144.2 (*C*-1 or *C*-2), 150.9 (*C*-4 or *C*-5), 151.9 (*C*-4 or *C*-5), 167.3 (*C*-9 or *C*-9′), 167.4 (*C*-9 or *C*-9′), 187.3 ppm (*C*-7); IR (ATR-film): $\tilde{\nu}$ = 2987, 1740, 1687, 1570, 1507, 1283, 1196, 1168, 1070, 1022, 792 cm^{-1}; MS (ESI, positive-ion): m/z (%): 378.2 (50) $[M+Na]^+$.

S1.3 Bacterial strains and plasmids

All bacterial strains, plasmids and oligonucleotides used in this study are listed in Table S1.

Table S1: Bacterial strains, plasmids and oligonucleotides used in this study.

Strains, plasmids, oligonucleotides	Relevant features, description or sequences[a]	References
	Strains	
***E. coli* DH5α**	*F⁻ Φ80lacZΔM15 Δ(lacZYA-argF) U169 recA1 endA1 hsdR17 phoA supE44 thi-1 gyrA96 relA1 deoR*	[3]
***E. coli* S17-1**	Ec294::[RP4-2 (Tc^R::Mu)(Km^R::Tn7)] *recA, thi, pro, hsdR⁻ hsdM⁺* Tp^R Sm^R	[4]
***E. coli* Tuner(DE3)**	*F⁻ompT hsdS*$_B$ *(*r_B^- m_B^-*) gal dcm lacY1(DE3)*	Novagen, Merck KGaA
***P. putida* KT2440**	Wild-type	[5]
***B. subtilis* DB430**	*trpC2 his nprE aprE bpf ispI*	[6]
	Plasmids	
pRhotHi-2-lacI-EYFP	pBBR1-MCS-derivative, Km^R, Cm^R, pBBR22b-*lacI*, P_{T7}-lacO-MCS with *Nde*I *Xho*I inserted *eyfp*	[7]
pVLT33	R6K, RSF1010 *lacI*^{q}, Kan^R, P_{tac}	[8]
pVLT33-GFPmut3	R6K, RSF1010 *lacI*^{q}, Kan^R, P_{tac} with *EcoR*I *Xba*I inserted *gfpmut3*	This work
pET-22(b)-sfGFP	Ap^R, *lacI*, P_{T7}-lacO-MCS with *Nde*I *Hin*dIII inserted *sfgfp*	This work
pHT01	Pgrac-lacO-MCS, *lacI*, Cm^R	MoBiTec, Germany
pHT01-sfGFP	Pgrac-lacO-MCS, *lacI*, Cm^R, *sfgfp*	This work
	Oligonucleotides	
1) EcoRI_GFP_fw	Binds at the 5' end of the *gfpmut3* gene, inserts *EcoR*I site 5'-ATATGAATTCATGGTACCAAGTAAAGGAG-3'	This work
2) XbaI_GFP_rev	Binds at the 3' end of the *gfpmut3* gene, inserts *Hind*III site 5'-ATATTCTACATTATTTGTATAGTTCATC CATGC-3'	This work
3) pHT01_fw	Amplification of pHT01 plasmid for SLIC cloning 5'- GAAGGGAATTCATATTACTTAGAGGAT ACT-3′	This work
4) pHT01_rev	Amplification of pHT01 plasmid for SLIC cloning 5'- CCTCCTTTAATTGGGAATTGTTATCCG-3'	This work
5) sfgfp_fw	Binds at the 5'end of the *sfgfp* gene for SLIC cloning 5'- GGATAACAATTCCCAATTAAAGGAGGA GATATACATATGAGCAAAGGAGAAGA-3'	This work
6) sfgfp_rev	Binds at the 3' end of the *sfgfp* gene for SLIC cloning 5'- GTATCCTCTAAGTAATATGAATTCCCTTC CAGCCGGATCTCAGTGGT-3'	This work

S2 Supporting data

S2.1 UV-Vis spectra of compounds

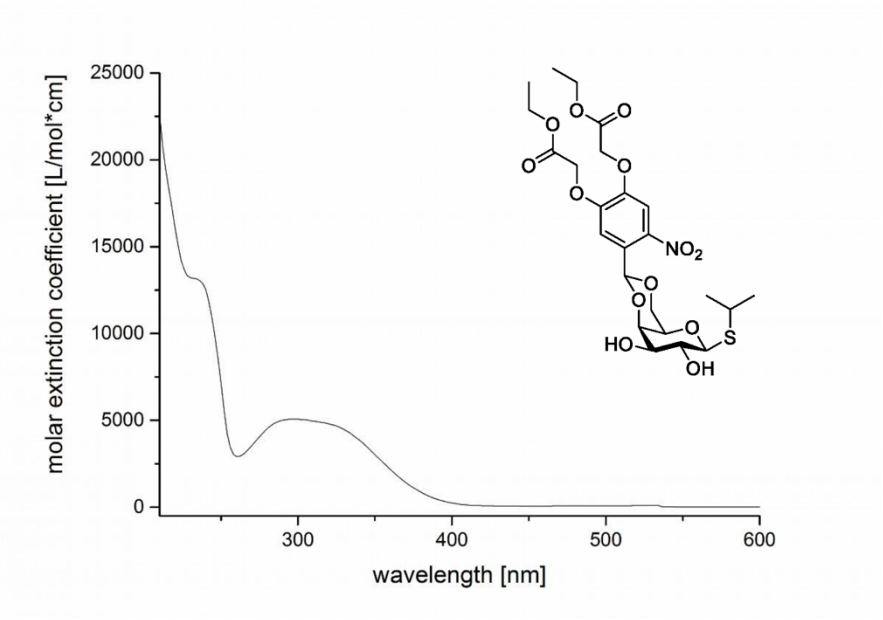

Figure S1: UV-Vis spectrum of compound **10a** (0.125 mM in MeOH, 25 °C).

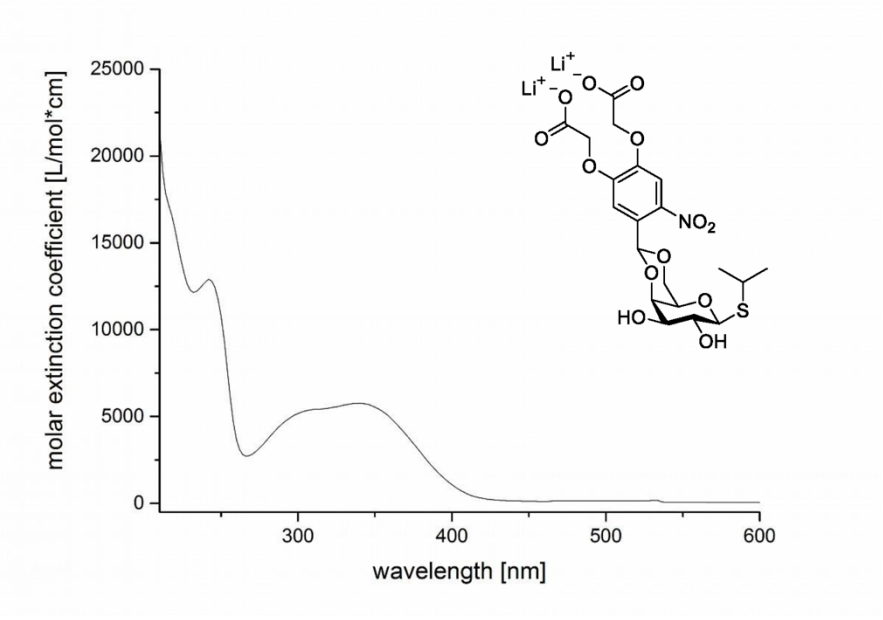

Figure S2: UV-Vis spectrum of compound **10b** [0.125 mM in sodium phosphate buffer (0.1 mM, pH 7.5), 25 °C].

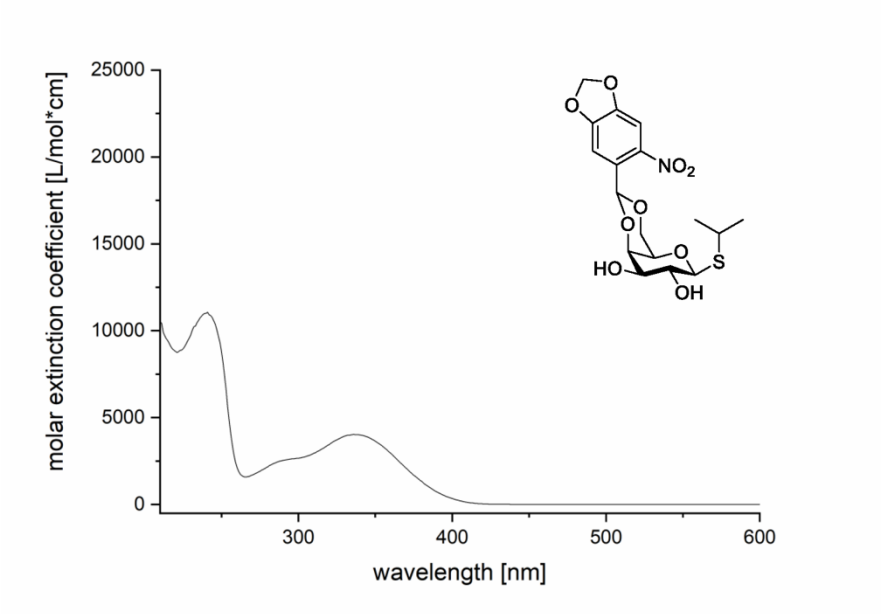

Figure S3: UV-Vis spectrum of compound **1** (0.200 mM in MeOH, 25 °C).

S2.2 Determination of uncaging half-life times

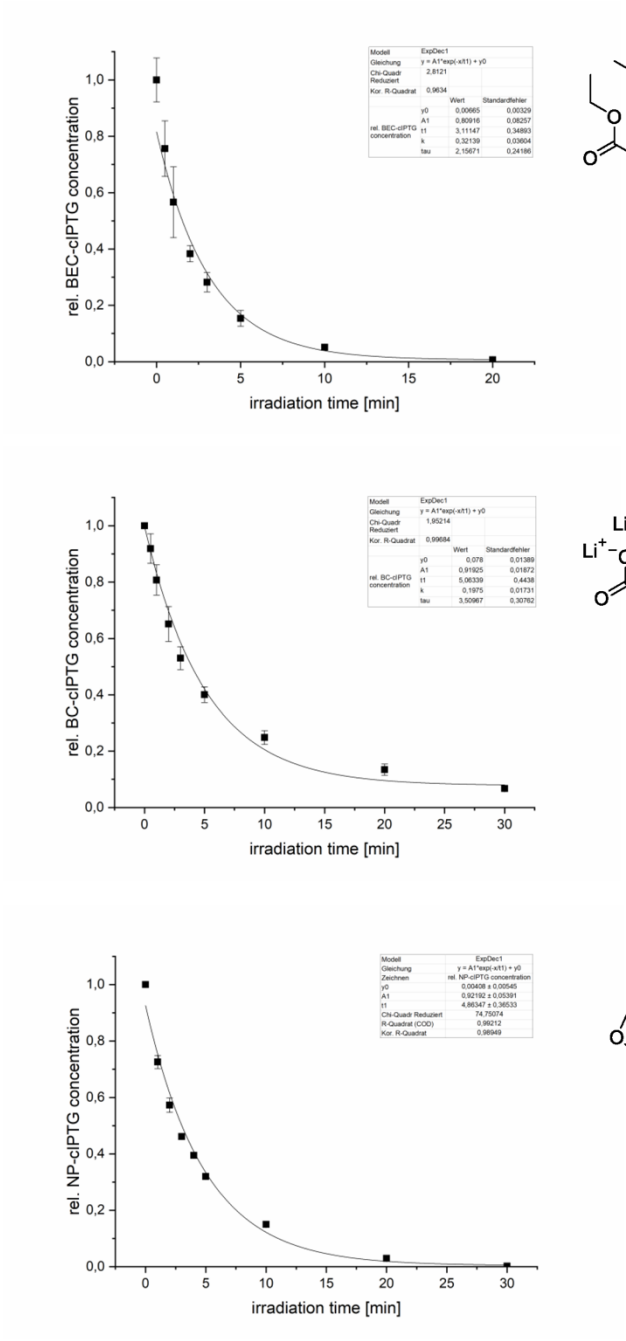

Figure S4: *In vitro* decay of caged IPTG controlled via reverse phase HPLC of compounds **10a**, **1** (1 mM in MeOH) and **10b** [1 mM in sodium phosphate buffer (0.1 mM, pH 7.5)]; 375 nm, 6.4 mW cm^{-2}, room temperature.

Table S2: Fitting parameters and uncaging half-life times $t_{0.5}$ for caged IPTG derivatives.

Inducer	y_0	A_1	t_1	k	$t_{0.5}$ **[min]**
BEC-cIPTG (**10a**)	0.00665	0.80916	3.11147	0.32139	2.15671
BC-cIPTG (**10b**)	0.078	0.91925	5.06339	0.1975	3.50967
NP-cIPTG (**1**)	0.00408	0.92192	4.86347	0.20561	3.3711

S2.3 Determination of purity by qNMR

Table S3: Compound purities determined by qNMR

Compound	Purity [%]
BEC-cIPTG (**10a**)	90.7 ± 1.3
BC-cIPTG (**10b**)	74.0 ± 2.5
NP-cIPTG (**1**)	80.4 ± 2.3

S2.4 Determination of IPTG concentrations sufficient for the induction of gene expression in *E. coli*, *P. putida* and *B. subtilis*

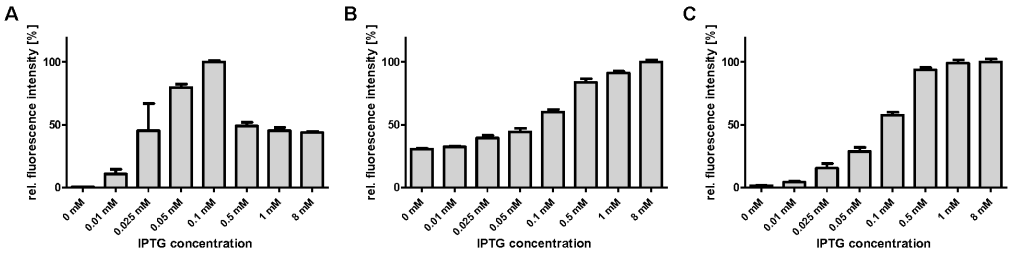

Figure S5: Relative fluorescence intensities of *E. coli* Tuner(DE3)/pRhotHi-2-lacI-eYFP (**A**), *P. putida* KT2440/pVLT33-GFPmut3 (**B**) and *B. subtilis* DB430/pHT01-sfGFP (**C**) expression cultures supplemented with increasing amounts of IPTG (**14**). Cultures were incubated in LB medium for 20 h in the dark at 30 °C. Induction of gene expression was performed after 2.5 h for *E. coli*, after 3 h for *P. putida* and after 5 h for *B. subtilis* by adding IPTG (**14**) concentrations ranging from 0 to 8 mM. *In vivo* fluorescence intensities were determined by using a BioLector system (eYFP: λex = 508 nm, λem = 532 nm, GFPmut3: λex = 508 nm, λem = 532 nm, sfGFP: λex = 488 nm, λem = 520 nm) and normalised to cell densities. Values are means of triplicate measurements. Error bars indicate the respective standard deviations.

S2.5 Stability and toxicity of novel photocaged IPTG variants

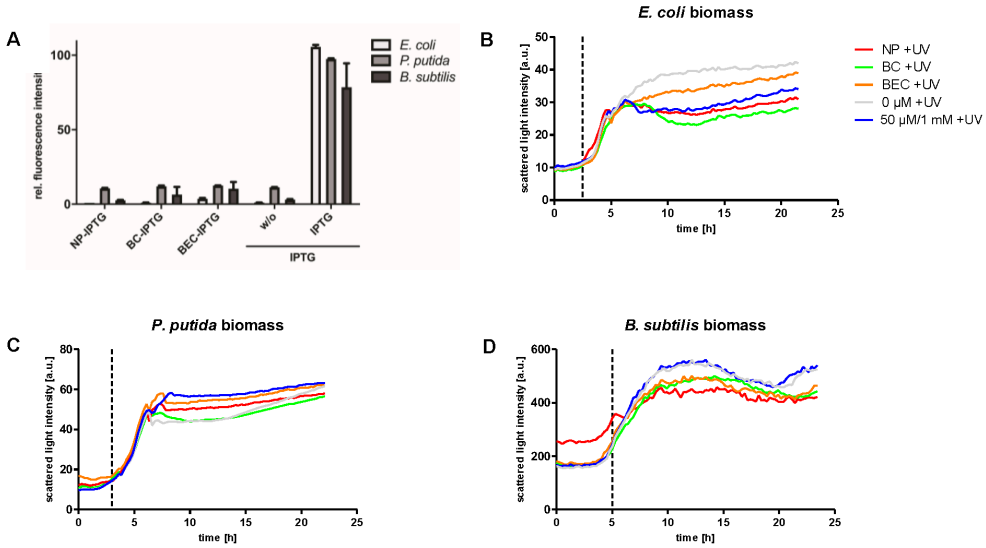

Figure S6: A) Normalised fluorescence intensity of *E. coli* Tuner(DE3)/pRhotHi-2-lacI-eYFP, *P. putida* KT2440/pVLT33-GFPmut3 and *B. subtilis* DB430/pHT01-sfGFP expression cultures (supplemented with 50 µM of each compound for *E. coli* and 1 mM for *P. putida* and *B. subtilis*). All cultures were incubated in the dark for 20 h in LB medium at 30 °C. *In vivo* stability of new photocaged IPTG variants **10a** (BEC) and **10b** (BC) is reflected by the low induction of reporter gene expression and was compared to NP-cIPTG (**1**, NP) as well as to cultures with and without IPTG (**14**). *In vivo* fluorescence intensities were determined by using a BioLector system (eYFP: λex = 508 nm, λem = 532 nm, GFPmut3: λex = 508 nm, λem = 532 nm, sfGFP: λex = 488 nm, λem = 520 nm) normalised to cell densities and are shown in relation to the respective fluorescence intensities of IPTG (**14**). Values are means of triplicate measurements. Error bars indicate the respective standard deviations. **B-D)** Growth curves of *E. coli* Tuner(DE3)/pRhotHi-2-lacI-eYFP, *P. putida* KT2440/pVLT33-GFPmut3 and *B. subtilis* DB430/pHT01-sfGFP expression cultures in the presence of novel photocaged IPTG variants **10a** (BEC) and **10b** (BC) compared to **1** (NP) as well as uninduced (0 mM) and induced (50 µM/1 mM of **14**). Cells were grown over 20 h using a BioLector system (LB medium supplemented with 50 µM of each caged compound for *E. coli* and 1 mM for *P. putida* and *B. subtilis*, 30 °C, 1200 rpm). Cell growth was analysed by determining the scattered light intensity. After 2.5, 3, and 5 h, formation of photoproducts was induced in cultures of *E. coli, P. putida* and *B. subtilis via* light exposure at 365 nm (~1 mW cm^{-2}, indicated by dashed lines) for 30 min or by the addition of conventional IPTG (**14**). Values are means of triplicate measurements.

S2.6 Effect of UV-A light illumination on cell growth and fluorescence of *E. coli*, *P. putida* and *B. subtilis* expression cultures

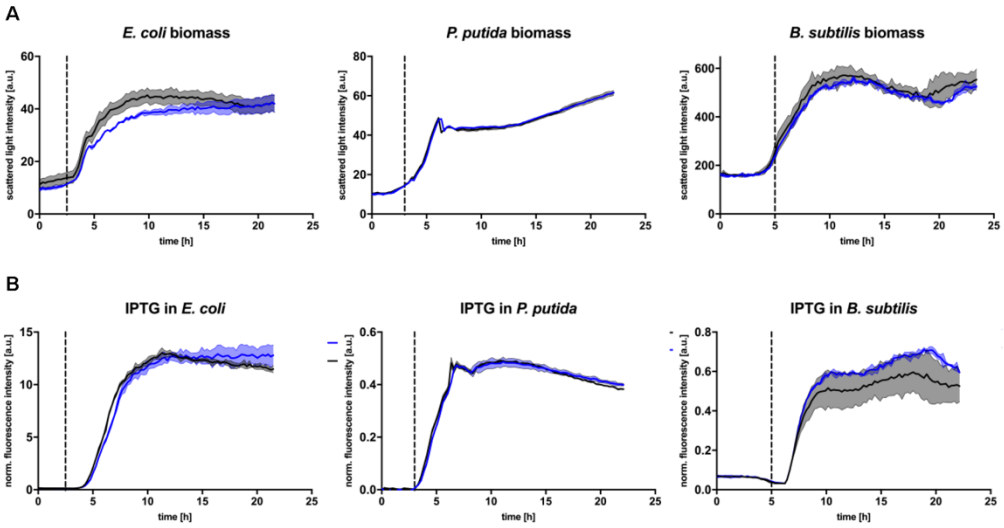

Figure S7: A) Growth curves of *E. coli* Tuner(DE3)/pRhotHi-2-lacI-eYFP, *P. putida* KT2440/pVLT33-GFPmut3 and *B. subtilis* DB430/pHT01-sfGFP expression cultures in the presence (blue line) and absence (black line) of UV-A light. Cells were grown over 20 h using a BioLector system (LB medium without inducer, 30 °C, 1200 rpm). Cell growth was analyzed by determining the scattered light intensity. After 2.5h (*E. coli*), 3 (*P. putida*), and 5 h (*B. subtilis*), cultures were exposed to UV-A light at 365 nm (~1 mW cm^{-2}, indicated by dashed lines) for 30 min. Values are means of triplicate measurements. Error bars indicate the respective standard deviations. **B)** Increase of fluorescent reporter-mediated signals during cultivation of *E. coli* Tuner(DE3)/pRhotHi-2-lacI-eYFP, *P. putida* KT2440/pVLT33-GFPmut3 and *B. subtilis* DB430/pHT01-sfGFP expression cultures with (blue line) and without (black line) UV-A exposure at 365 nm (~1 mW cm^{-2}) for 30 min; cells were grown over 20 h in LB medium at 30 °C and 1200 rpm using a BioLector system. Induction was performed using 50 µM of IPTG (**7**) for *E. coli* and 1 mM IPTG for *P. putida* and *B. subtilis*. The individual time point of induction is indicated by the dashed lines (*E. coli* 2.5 h, *P. putida* 3 h, *B. subtilis* 5 h). *In vivo* fluorescence intensities were determined by using a BioLector system (eYFP: λex = 508 nm, λem = 532 nm, GFPmut3: λex = 508 nm, λem = 532 nm, sfGFP: λex = 488 nm, λem = 520 nm) and normalised to cell densities. Values are means of triplicate measurements.

S2.7 Comparative analysis of light-responsiveness of cIPTG variants in different bacterial expression systems

In order to analyse the light-responsiveness of BC-, BEC-, and NP-cIPTG in different bacterial expression hosts, fluorescent protein expression was online monitored during batch cultivation in LB medium at 30 °C and 1200 rpm using a BioLector system (eYFP: λex = 508 nm, λem = 532 nm, GFPmut3: λex = 508 nm, λem = 532 nm, sfGFP: λex = 488 nm, λem = 520 nm). To analyse time-resolved fluorescent protein signals of *E. coli* Tuner(DE3)/pRhotHi-2-lacI-eYFP, *P. putida* KT2440/pVLT33-GFPmut3 and *B. subtilis* DB430/pHT01-sfGFP expression strains, cultures were supplemented with IPTG (**7**), BEC-cIPTG (**10a**), BC-cIPTG (**10b**), and NP-cIPTG (**1**). Induction of gene expression was performed after 2.5 h, 3 h or 5 h for *E. coli, P. putida* and *B. subtilis*, respectively, *via* UV-A light exposure at 365 nm (~1 mW cm^{-2}) for 30 min or the addition of **14**. Cell density-normalised fluorescence signal curves (Fig. S8) were plotted and fitted to a sigmoidal Boltzmann fit using GraphPad Prism 5.03 ®. The half-maximal responsiveness of each cIPTG variant was calculated from fitting parameters (Table S4) using the following standard equation for sigmoidal Boltzmann fitting:

$$y = \frac{A_1 - A_2}{1 + e^{(x - x_0)idx}} + A_2$$

Table S4: Calculation of half-maximal responsiveness $t_{0.5}$ for the lacI/P_{tac}/P_{T7}/P_{grac}-regulated systems using fitting parameters from sigmoidal Boltzmann fits. Final half-maximal responsiveness $t_{0.5}$ final was calculated as the difference of $t_{0.5}$ calc. and the induction time point t_0. ($y_{0.5}$ = fluorescence intensity at half-maximal time value, A1 = initial value, A2 = final value, x_0 = center value, dx = time constant)

Inducer	$y_{0.5}$	A1	A2	x_0	dx	$t_{0.5}$ [h] calc.	t_0 [h]	$t_{0.5}$ [h] final
***E. coli* Tuner(DE3)/pRhotHi-2-lacI-eYFP**								
NP-IPTG (1)	6.36	-0.12	12.36	6.87	1.21	6.91	2.5	4.41
BC-IPTG (10b)	5.52	-0.16	10.55	6.59	1.41	6.66	2.5	4.16
BEC-IPTG (10a)	4.36	-0.01	8.68	7.01	0.91	7.01	2.5	4.51
IPTG (14)	6.49	-0.13	12.61	6.71	0.99	6.75	3.0	3.75
***P. putida* KT2440/pVLT33-GFPmut3**								
NP-IPTG (1)	0.06	-0.01	0.10	6.37	0.78	6.58	3.0	3.58
BC-IPTG (10b)	0.15	-0.01	0.28	5.55	0.67	5.62	3.0	2.62
BEC-IPTG (10a)	0.09	0.00	0.17	5.87	0.82	5.94	3.0	2.94
IPTG (14)	0.23	0.00	0.45	4.89	0.61	4.91	3.5	1.41
***B. subtilis* DB430/pHT01-sfGFP**								
NP-IPTG (1)	0.11	0.04	0.34	7.25	0.60	6.96	5.0	1.96
BC-IPTG (10b)	0.25	0.06	0.68	7.52	0.61	7.31	5.0	2.31
BEC-IPTG (10a)	0.17	0.06	0.51	7.30	0.68	6.97	5.0	1.97
IPTG (14)	0.24	0.05	0.64	7.80	0.68	7.57	5.5	2.07

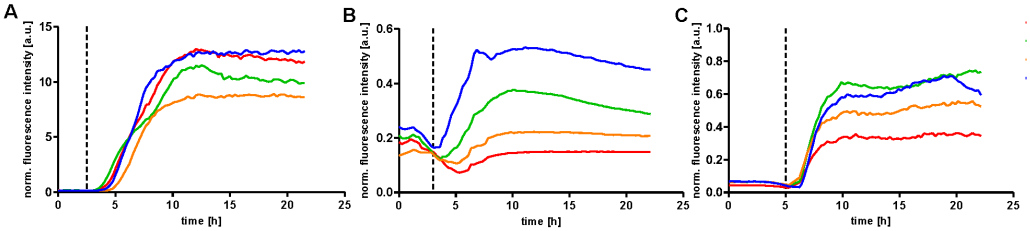

Figure S8: Normalised fluorescence protein expression profiles of *E. coli* Tuner(DE3)/pRhotHi-2-lacI-eYFP (**A**), *P. putida* KT2440/pVLT33-GFPmut3 (**B**) and *B. subtilis* DB430/pHT01-sfGFP (**C**) cultures supplemented with IPTG (**7**; blue line), BEC-cIPTG (**10a**; orange line), BC-cIPTG (**10b**; green line), and NP-cIPTG (**1**; red line) (50 µM of each compound were used for *E. coli* and 1 mM for *P. putida* and *B. subtilis*). Cells were grown over 20 h in LB medium at 30 °C and 1200 rpm using a BioLector system. Induction was performed using UV-A exposure at 365 nm (~1 mW cm^{-2}) for 30 min or respective amount of IPTG (**14**). Time of induction is indicated by dashed lines (*E. coli* 2.5 h, *P. putida* 3 h, *B. subtilis* 5 h). *In vivo* fluorescence intensities were online-monitored during cultivation (eYFP: λex = 508 nm, λem = 532 nm, GFPmut3: λex = 508 nm, λem = 532 nm, sfGFP: λex = 488 nm, λem = 520 nm) and normalised to cell densities. Values are means of triplicate measurements.

Table S5: Calculation of induction factors for IPTG and light-responsive cIPTG in *E. coli* Tuner(DE3)/pRhotHi-2-lacI-eYFP, *P. putida* KT2440/pVLT33-GFPmut3 and *B. subtilis* DB430/pHT01-sfGFP. Cultures were supplemented with IPTG (**14**), BEC-cIPTG (**10a**), BC-cIPTG (**10b**), and NP-cIPTG (**1**) in concentrations of 50 µM of each compound for *E. coli* and 1 mM for *P. putida* and *B. subtilis*. These values correspond to Figure 2 shown in the result section.

Inducer	**Induction factor**		
	E. coli	***P. putida***	***B. subtilis***
NP-cIPTG **(1)**	114.93±3.47	3.03±0.10	20.14±1.22
BC-cIPTG **(10b)**	87.57±21.15	5.47±0.12	21.80±11.94
BEC-cIPTG **(10a)**	23.45±2.36	3.62±0.20	8.20±2.67
IPTG (-UV-A)	96.80±2.56	8.65±0.14	25.62±2.21

S2.8 Heterogeneity of light-induced reporter gene expression in *E. coli* and *B. subtilis* using different cIPTG variants

Caged inducer variants **10a** (BEC), **10b** (BC) and **1** (NP) were used in comparison to conventional IPTG (**14**) to analyse the heterogeneity of reporter gene expression in *E. coli* Tuner(DE3)/pRhotHi-2-lacI-eYFP (**A, C**) and *B. subtilis* DB430/pHT01-sfGFP (**B, D**) cultures. To this end, fluorescence intensity and fluorescence distribution of 10,000 cells of a population were determined using flow cytometry when cultures reached the late logarithmic growth phase (8 h for *E. coli* and 10 h for *B. subtilis*).

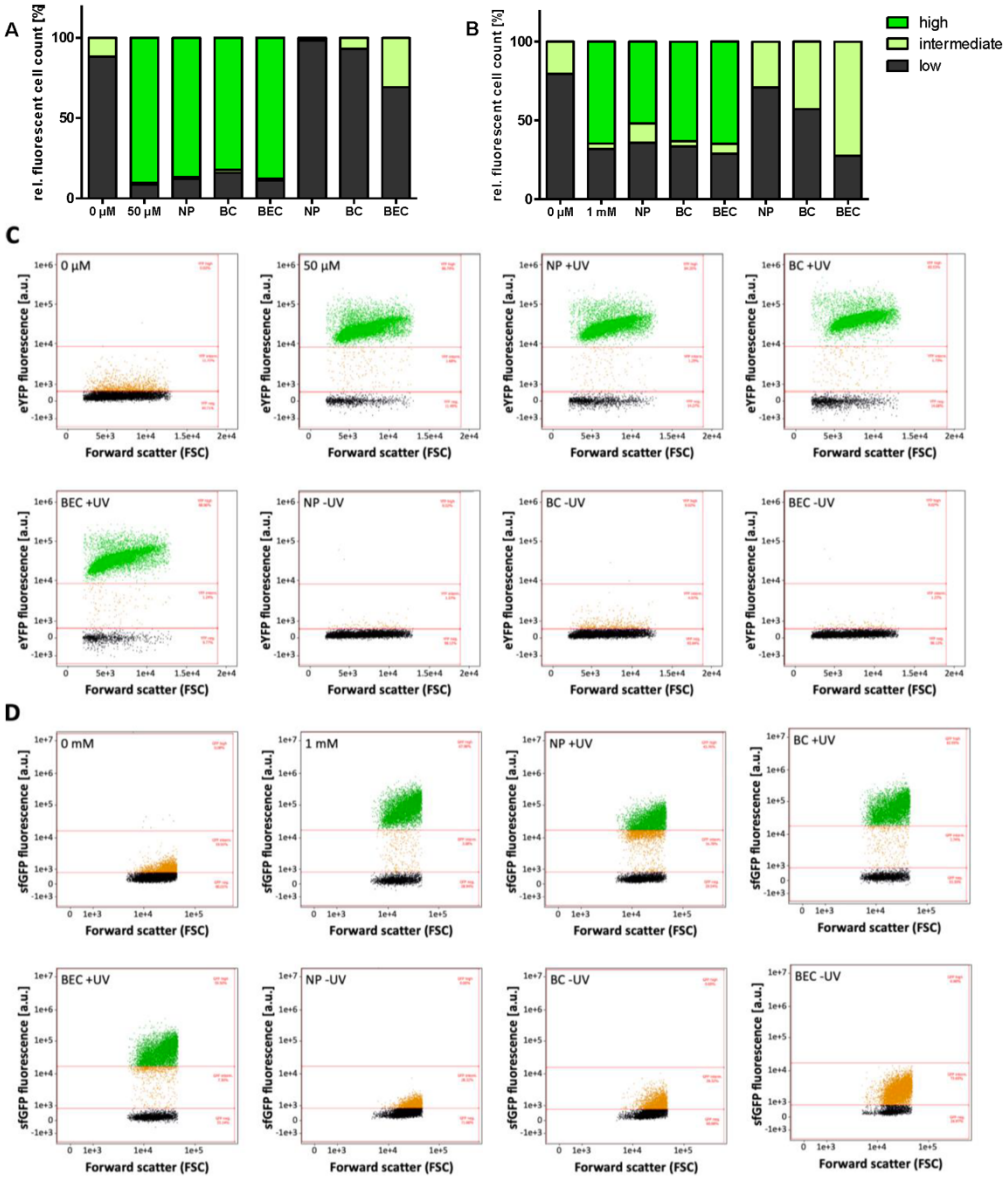

Figure S9: Single cell analysis of *E. coli* Tuner(DE3)/pRhotHi-2-lacI-eYFP (**A**) and *B. subtilis* DB430/pHT01-sfGFP (**B**) expression cultures supplemented with 50 µM of each caged compound for *E. coli* and 1 mM for *B. subtilis*. Induction was

performed after 2.5 h for *E. coli* and after 5 h for *B. subtilis* using UV-A light (30 min, ~1 mW cm^{-2}) or common IPTG (**14**). As a negative control, cells of both species were identically cultivated but kept in the dark. Culture samples were collected after late logarithmic growth phase (8 h for *E. coli* and 10 h for *B. subtilis*) and analysed using flow cytometry. The cells were gated based on FSC and SSC to exclude cell debris and accumulation of cells. The fluorescence intensities of eYFP or sfGFP were measured using a 488 nm-laser and a 528/46 nm bandpass filter and intensity values were classified into the three categories "high", "intermediate" and "low". All values are means of triplicate measurements. Raw data of the diagrams depicted in (**A**) and (**B**) are shown for *E. coli* Tuner(DE3)/pRhotHi-2-lacI-eYFP (**C**) and *B. subtilis* DB430/pHT01-sfGFP (**D**). Initially, the cells were gated based on their respective FSC and SSC signals to exclude cell debris and accumulation of cells. Afterwards, they were analysed regarding both their eYFP or sfGFP fluorescence intensity and their forward scatter signal (FSC). All graphs are representative examples of triplicate measurements.

S2.9 NMR spectra of compounds

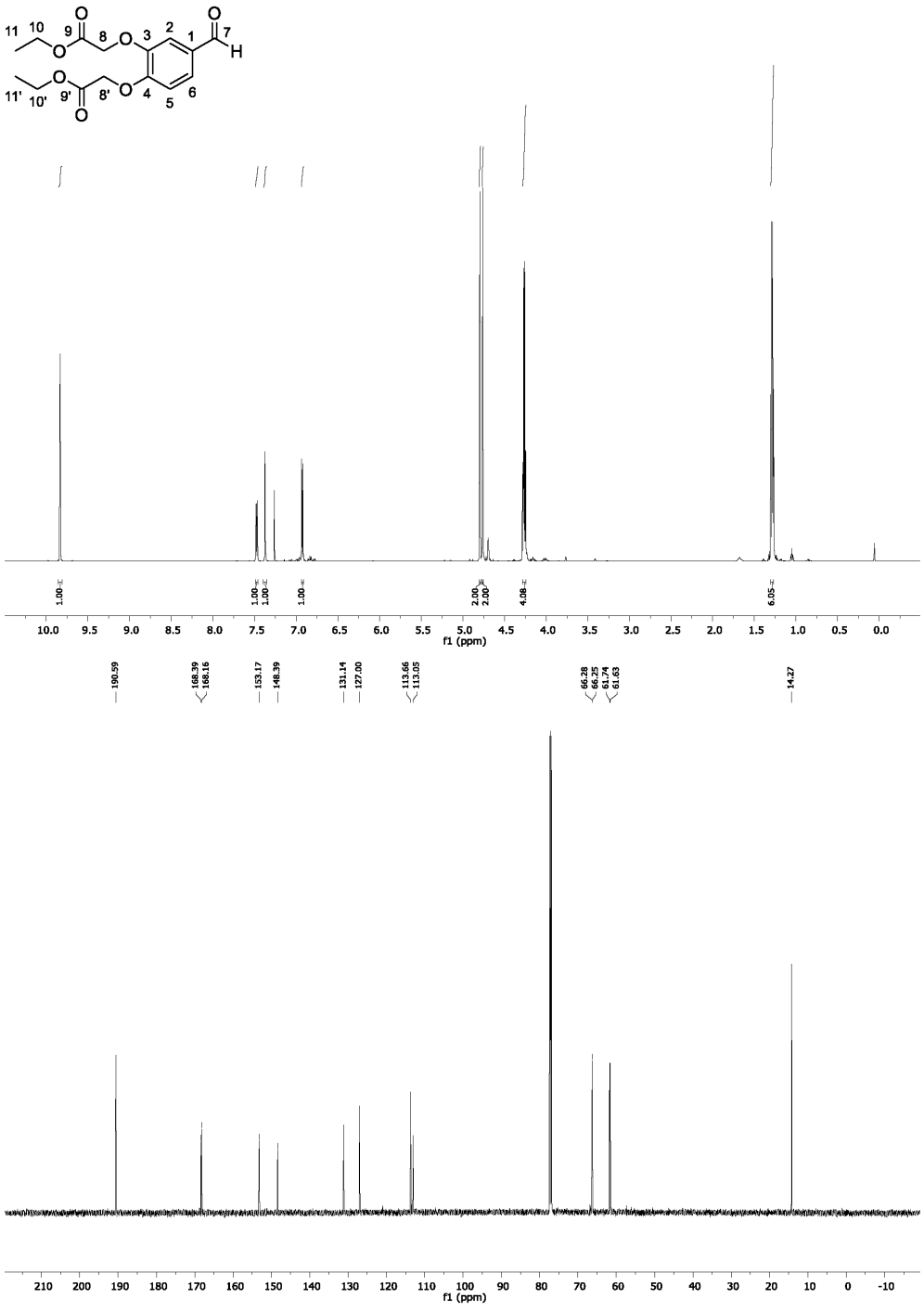

Figure S10: ^{1}H- and ^{13}C-NMR spectra of **18** in $CDCl_3$ (600 MHz/151 MHz).

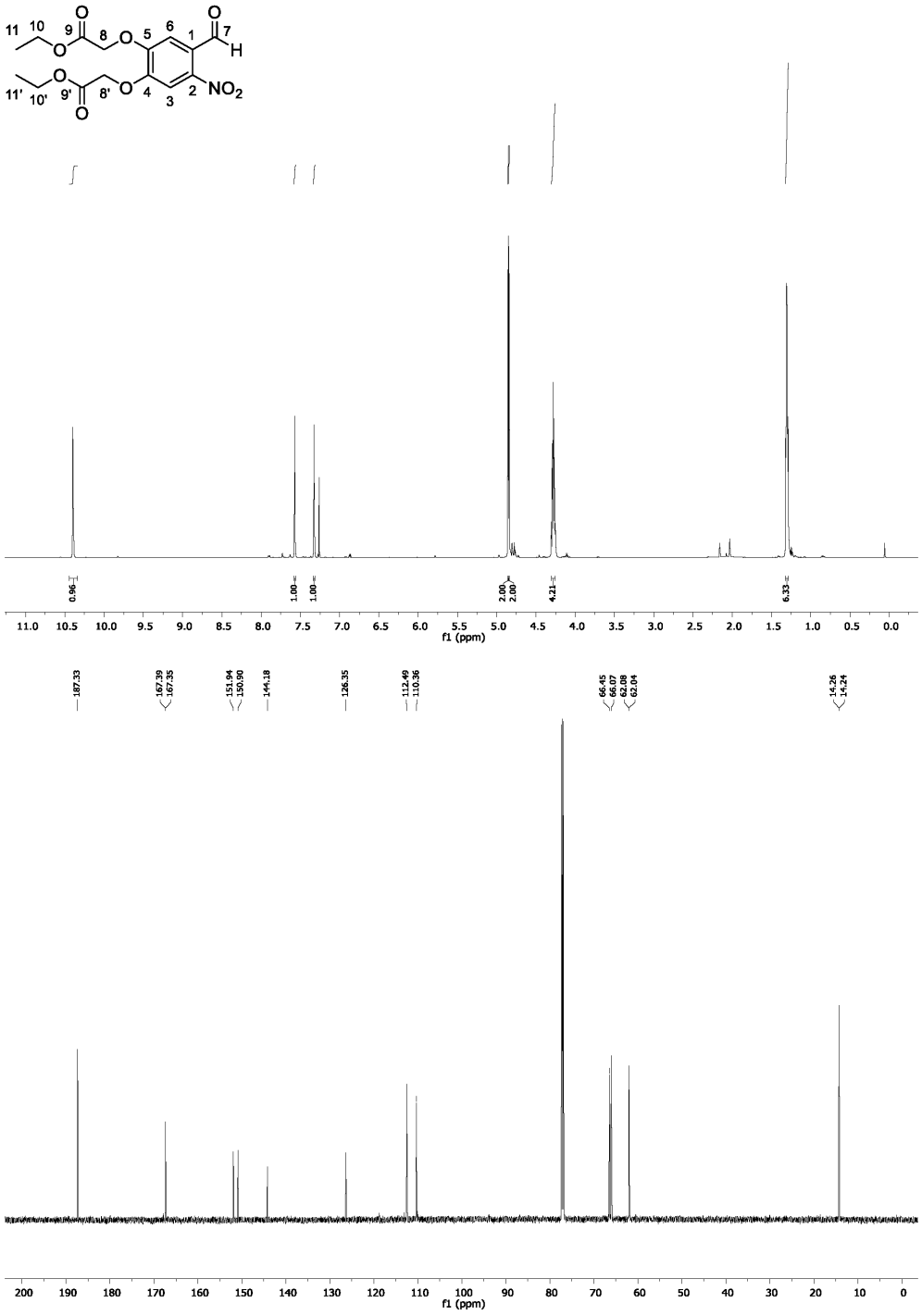

Figure S11: ^{1}H- and ^{13}C-NMR spectra of **11** in $CDCl_3$ (600 MHz/151 MHz).

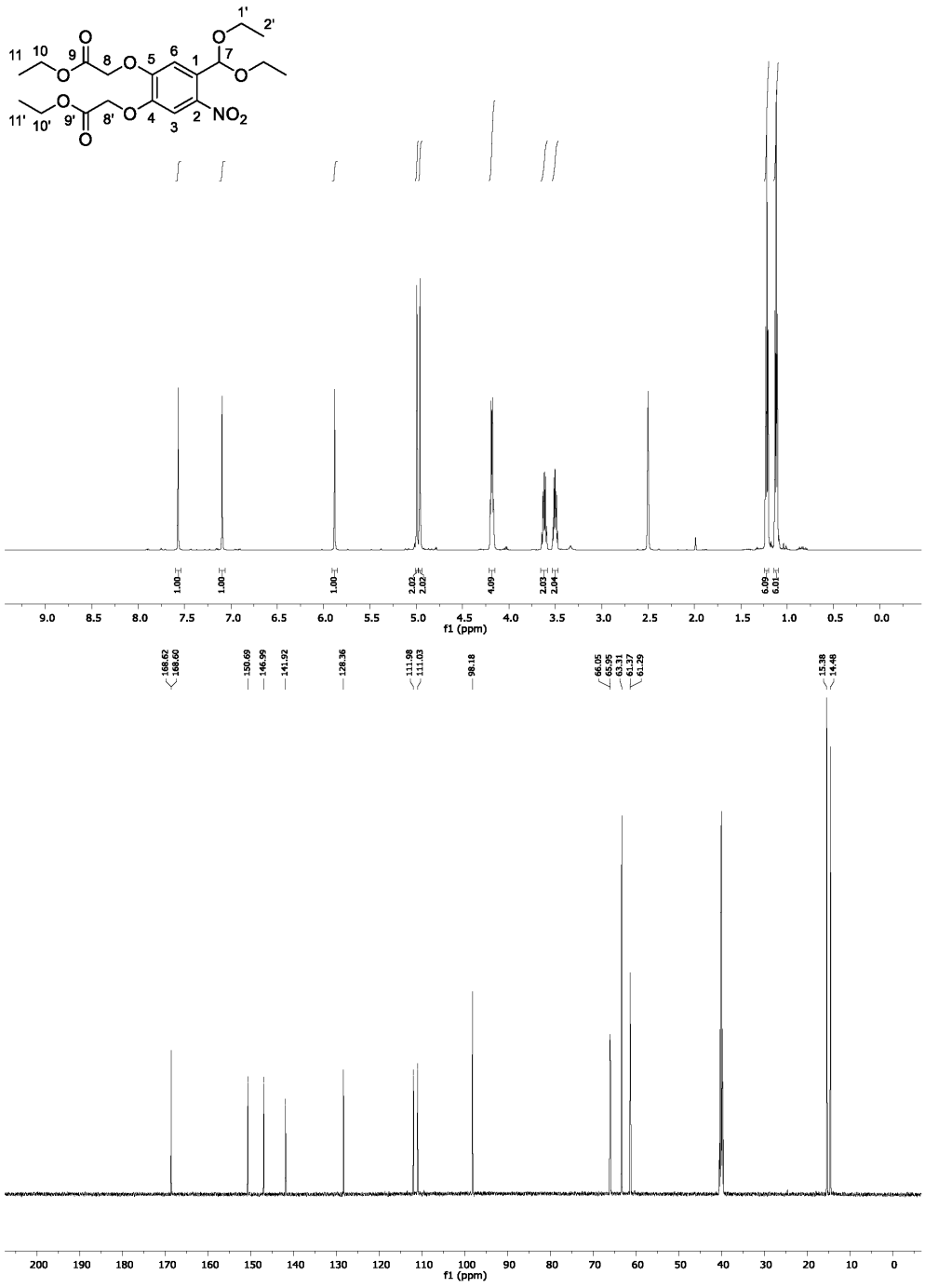

Figure S12: ^{1}H- and ^{13}C-NMR spectra of **12** in DMSO (600 MHz/151 MHz).

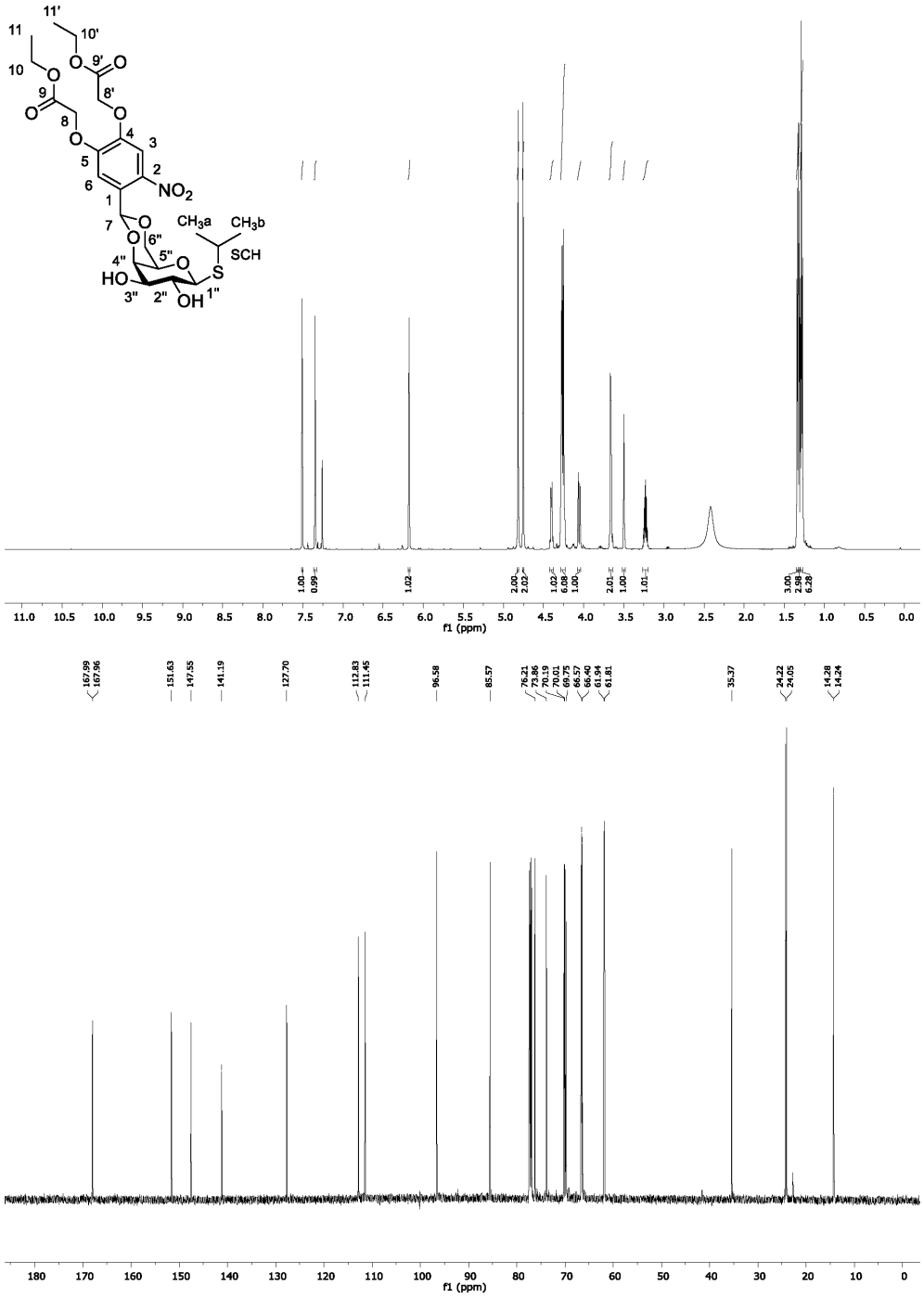

Figure S13: ^{1}H- and ^{13}C-NMR spectra of **10a** in $CDCl_3$ (600 MHz/151 MHz).

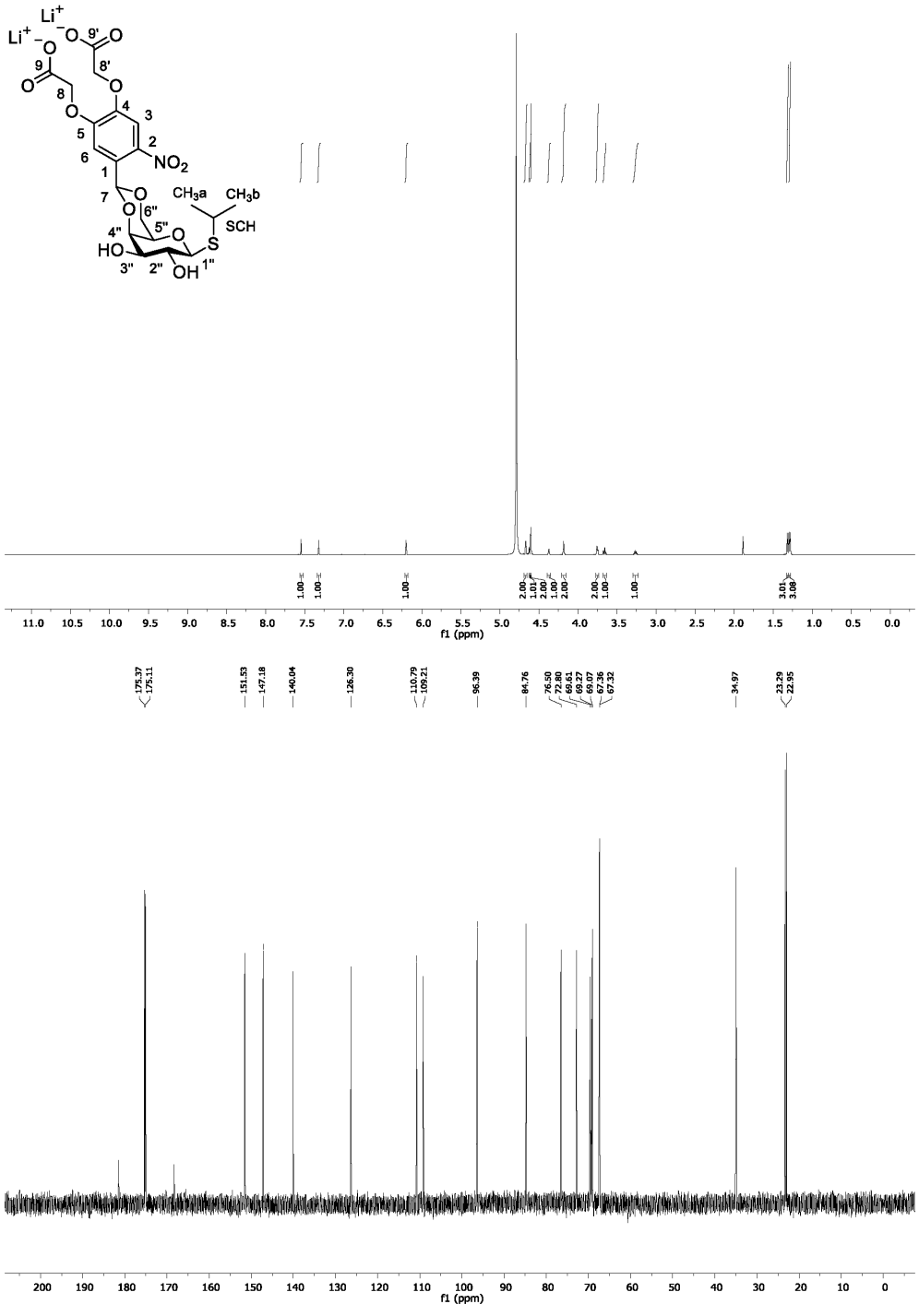

Figure S14: ^{1}H- and ^{13}C-NMR spectra of **10b** in D_2O (600 MHz/151 MHz).

S2.10 HPLC-Traces

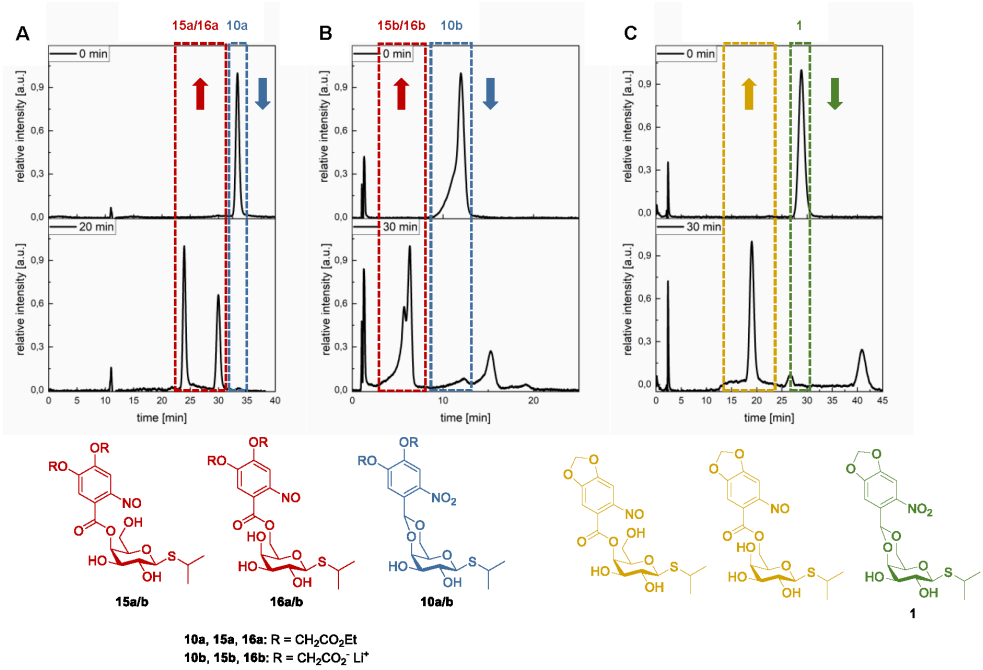

Figure S15: **A**) UV trace at 298 nm of the reverse phase HPLC analysis of BEC-cIPTG (**10a**) (1 mM in MeOH) before irradiation and after 20 min of irradiation (375 nm, 6.4 mW cm^{-2}, room temperature). **B**) UV trace at 340 nm of the reverse phase HPLC analysis of BC-cIPTG (**10b**) [1 mM in sodium phosphate buffer (0.1 mM, pH 7.5)] before irradiation and after 30 min of irradiation (375 nm, 6.4 mW cm^{-2}, room temperature). **C**) UV trace at 336 nm of the reverse phase HPLC analysis of NP-cIPTG (**1**) (1 mM in MeOH) before irradiation and after 30 min of irradiation (375 nm, 6.4 mW cm^{-2}, room temperature). Assignment of photoproducts for **A**), **B**) and **C**) was performed by observation of shifts in the UV-spectrum, which were in accordance to previously investigated derivatives.[9]

[1] J. Ni, D. A. Auston, D. A. Freilich, S. Muralidharan, E. A. Sobie, J. P. Y. Kao, *J. Am. Chem. Soc.* **2007**, *129*, 5316-5317.

[2] E. Brunet, M. a. T. Alonso, O. Juanes, O. Velasco, J. C. Rodríguez-Ubis, *Tetrahedron* **2001**, *57*, 3105-3116.

[3] D. Hanahan, *J. Mol. Biol.* **1983**, *166*, 557-580.

[4] R. Simon, U. Priefer, A. Pühler, *Bio/Technology* **1983**, *1*, 784-791.

[5] M. Bagdasarian, R. Lurz, B. Rückert, F. C. H. Franklin, M. M. Bagdasarian, J. Frey, K. N. Timmis, *Gene* **1981**, *16*, 237-247.

[6] R. H. Doi, S.-L. Wong, F. Kawamura, *Trends Biotechnol.* **1986**, *4*, 232-235.

[7] D. Binder, A. Grunberger, A. Loeschcke, C. Probst, C. Bier, J. Pietruszka, W. Wiechert, D. Kohlheyer, K.-E. Jaeger, T. Drepper, *Integr. Biol.* **2014**, *6*, 755-765.

[8] V. de Lorenzo, L. Eltis, B. Kessler, K. N. Timmis, *Gene* **1993**, *123*, 17-24.

[9] a) F. Bley, K. Schaper, H. Görner, *Photochem. Photobiol.* **2008**, *84*, 162-171; b) C. Bier, Heinrich Heine University Düsseldorf (Düsseldorf, Germany), **2017**.

V.2. SUPPORTING INFORMATION FOR CHAPTER II.1.2 – PHOTOCAGED INDUCERS FOR OPTOGENETIC CONTROL OF GENE EXPRESSION IN *R. CAPSULATUS*

Photocaged inducers for the non-invasive light control of production processes in the phototrophic bacterium *Rhodobacter capsulatus*

Fabienne Hilgers[1¶], Fabian Hogenkamp[2¶] Oliver Klaus[1], Luzie Kruse[1], Alessa Lappe[1], Anita Loeschcke[1], Claus Bier[2], Dennis Binder[1], Karl-Erich Jaeger[1,3], Jörg Pietruszka[2,3] and Thomas Drepper[1*]

[1] Institute of Molecular Enzyme Technology, Heinrich Heine University Düsseldorf at Forschungszentrum Jülich, Jülich, Germany

[2] Institute of Bioorganic Chemistry, Heinrich Heine University Düsseldorf at Forschungszentrum Jülich, Jülich, Germany

[3] Institute of Bio- and Geosciences: Biotechnology (IBG-1), Forschungszentrum Jülich, Jülich, Germany

Supporting Information

Table of contents

1 Supporting methods

Bacterial strains and plasmids

All bacterial strains, plasmids and oligonucleotides used in this study are listed in Table S1.

Table S1: Bacterial strains, plasmids and oligonucleotides used in this study.

Strains, plasmids, oligonucleotides	Relevant features, description or sequences	References
	Strains	
***E. coli* DH5α**	*F⁻ Φ80lacZΔM15 Δ(lacZYA-argF) U169 recA1 endA1 hsdR17 phoA supE44 thi-1 gyrA96 relA1 deoR*	[1]
***E. coli* S17-1**	Ec294::[RP4-2 (Tc^R::Mu)(Km^R::Tn7)] *recA, thi, pro, hsdR⁻ hsdM⁺* Tp^R, Sm^R	[2]
***E. coli* Tuner(DE3)**	*F⁻ ompT hsdS*$_B$ (r_{B^-} m_{B^-}) *gal dcm lacY1*(DE3)	Novagen, Merck KGaA
***R. capsulatus* SB1003**	Wild-type, Rif^R	[3]
R. capsulatus* SB1003 *ΔcrtEF	*ΔcrtE*, *ΔcrtF*, Rif^R,Sm^R	[4]
	Plasmids	
pRholHi-2-eYFP	pBBR1-MCS-derivative, Km^R, Cm^R, with *SmaI*/*Xho*I inserted *lacI*^{q}-P_{tac}-lacO, *eyfp*	This work
pRholHi-2-crtE-crtF	pBBR1-MCS-derivative, Km^R, Cm^R, with *Xba*I/*Xho*I inserted *crtE* and *Xho*I inserted *crtF*	This work
pRhofHi-2-eYFP	pBBR1-MCS-derivative, Km^R, Cm^R, P_{fru} with *SmaI*/*Xho*I inserted *eyfp*	Troost, unpublished
pRhokHi-2-eYFP	pBBR1-MCS-derivative, Km^R, Cm^R, P_{aphII} with *NdeI*/*BamH*I inserted *eyfp*	[5]
pRhotHi-2-lacI-eYFP	pBBR1-MCS-derivative, Km^R, Cm^R, pBBR22b-*lacI*, P_{T7}-lacO-MCS with *Nde*I *Xho*I inserted *eyfp*	[6]
	Oligonucleotides	
1) SmaI_Ptac_eYFP_fw	Binds at the 5' end of the *lacI*$_q$ gene on pEKEX-2-eYFP plasmid, contains *Sma*I site. 5'-ATATCCCGGGCAAACATGGCCTGTCGC TTG-3'	This work
2) XhoI_Ptac_eYFP_rev	Binds at the 3' end of the *eyfp* gene on pEKEX-e-eYFP plasmid, contains *Xho*I site. 5'-ATATCTCGAGCACACTACCATCGGCGC TAC-3'	This work
3) CrtE_XbaI_for	Binds at the 5' end of the *crtE* gene in the *R. capsulatus* SB1003 genome, contains *Xba*I site. 5'- ATATAGCTCTAGAGCTCGTGACGCAGC GGAGGGCTCGGG -3'	This work
4) CrtE_XhoI_rev	Binds at the 3' end of the *crtE* gene in the *R. capsulatus* SB1003 genome, contains *Xho*I site. 5'-GGTGGTGGTGCTCGATCAGCCGCGTTCG GCCTC-3'	This work
5) CrtF_XhoI_for	Binds at the 5' end of the *crtF* gene in the *R. capsulatus* SB1003 genome, inserts homologous regions for InFusion® cloning. 5′-GGGCTGACCGCTCGAGTGCCGAAGGACGAC CACAC-3′	This work
6) CrtF_XhoI_rev	Binds at the 3' end of the *crtF* gene in the *R. capsulatus* SB1003 genome, inserts homologous regions for InFusion® cloning. 5'-GGTGGTGGTGCTCGATCAGCCGCG TTCGGCCTC-3'	This work

All recombinant DNA techniques were carried out using *E. coli* DH5α as described by Sambrook *et al*.[7]. Construction of expression vectors were carried out using restriction and ligation cloning. The PCR fragment containing the gene for $lacI^q$ and the P_{tac} promoter was amplified from a synthetic gene construct on the shuttle vector pEKEX-2 (Eurofins Genomics, Ebersberg, Germany) with oligos 1 and 2 generating appropriate *Sma*I/*Xho*I restriction sites at its 5'- and 3'-ends. This fragment was inserted into the likewise hydrolyzed plasmid pRhofHi-2-eYFP to build the plasmid pRholHi-2-eYFP. For the plasmid pRholHi-2-crtE-crtF, the gene *crtE* was amplified from the genome of *R. capsulatus* SB1003 with oligos 3 and 4 generating appropriate *Xba*I/*Xho*I restriction sites at its 5'- and 3'-ends. The PCR fragment was inserted into the likewise hydrolyzed plasmid pRholHi-2-eYFP to build the plasmid pRholHi-2-crtE. Finally, the *crtF* gene was PCR amplified from the genome of *R. capsulatus* SB1003 with oligos 5 and 6 generating appropriate homologous sequences at its 5'- and 3'-ends suitable for integration into the *Xho*I hydrolyzed plasmid pRholHi-2-crtE. Integration was performed *via* InFusion® Cloning (Takara Bio Europe, St Germain en Laye, France) to build the final plasmid pRholHi-2-crtE-crtF.

2 Supporting data

Determination of suitable cultivation parameters for aerobic and microaerobic growth of *R. capsulatus*

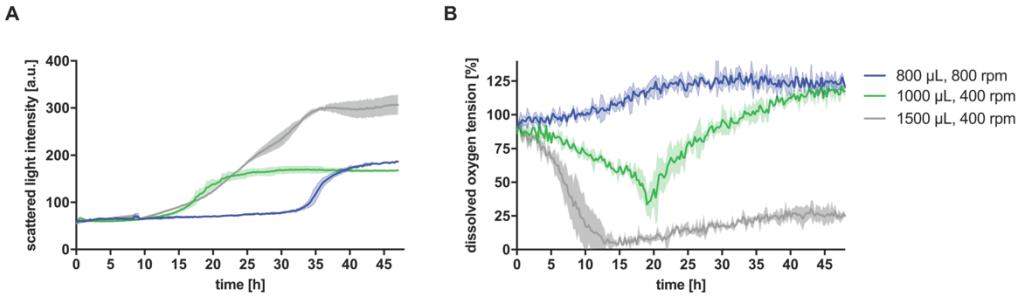

Figure S1: (A) Cell growth of *R. capsulatus* SB1003/pRholHi-2-eYFP expression cultures under varying filling volumes and shaking frequencies. The bacteria were grown in RCV medium for 48 h in Round Well Plates in the dark at 30°C. To identify filling volumes and shaking frequencies that are appropriate for aerobic and microaerobic growth, the following cultivation conditions were applied: (i) 800 rpm and with 800 µL RCV medium (blue), (ii) 400 rpm and 1000 µL RCV medium (green) and (iii) 400 rpm and 1500 µL RCV medium (grey). Cell growth was analyzed by determining the scattered light intensity using a BioLector system. Values are means of individual biological triplicates. Error bars indicate the respective standard deviations. **(B)** Dissolved oxygen tension (DOT) of the same *R. capsulatus* cultures as described in A). The DOT was determined in plates with oxygen sensitive optodes during cultivation of *Rhodobacter* in the BioLector system (λ_{ex} = 520 nm, λ_{em} = 600 nm). Values are means of individual biological triplicates. Error bars indicate the respective standard deviations.

To control the oxygen level during non-phototrophic growth, the filling volume of the Round Well plate as well as the shaking frequencies were appropriately adapted so that a maximal aeration (around 100%) and a minimal aeration (< 25%) were maintained throughout the cultivation. For this purpose, bacterial growth (Figure S1A) and the dissolved oxygen tension (DOT; Figure S1B) were online-monitored using the scattered light intensity and DO optodes (m2p-labs, Germany), respectively. A filling volume of 800 µL and a shaking frequency of 800 rpm resulted in a constant oxygen tension of 100% (Figure S1, blue line). To reduce the DOT during *R. capsulatus* cultivation, a filling volume of 1000 µL and a shaking frequency of 400 rpm were applied. However, these conditions were not sufficient for constant microaerobic growth, as the oxygen tension increased up to 100% during stationary growth phase (Figure S1, green line). Therefore, a lager filling volume (1500 µL) at the same shaking frequency were used, which led to a strongly decreased oxygen tension of under 25% during both logarithmic and stationary growth phase (Figure S1, grey line). Notably, the different aeration regimes led to strong differences in growth dynamics and maximal cell densities.

Determination of IPTG concentrations sufficient for the induction of *eyfp* reporter gene expression in *R. capsulatus* under aerobic, microaerobic and phototrophic conditions

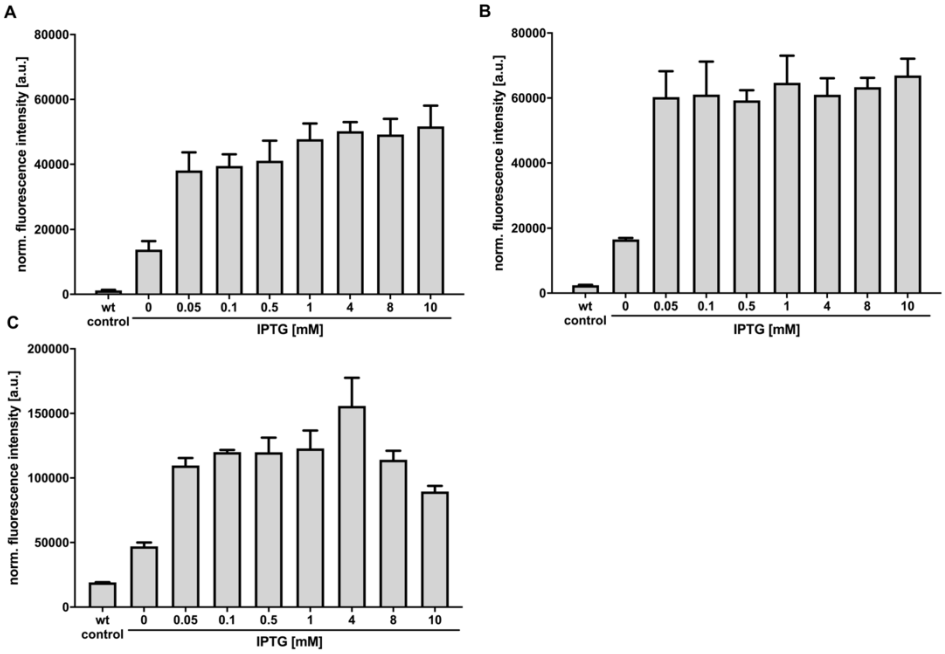

Figure S2: Relative eYFP fluorescence intensities of *R. capsulatus* SB1003/pRholHi-2-eYFP cultures grown aerobically **(A)**, microaerobically **(B)** or anaerobically **(C)** and supplemented with increasing amounts of IPTG. Aerobic and microaerobic cultures were incubated in 800 µL or 1500 µL RCV medium and a shaking frequency of 800 rpm or 400 rpm for 48 h in the dark at 30°C. Induction of gene expression was performed after 9 h by adding IPTG at concentrations ranging from 0 to 10 mM. Phototrophic cultures were incubated in 4.2 mL RCV medium for 48 h at 30°C under constant illumination with bulb light (2000 lx) and IPTG was added prior to culture inoculation. *In vivo* fluorescence intensities of all cultures were determined by using a BioLector system (eYFP: λ_{ex} = 508 nm, λ_{em} = 532 nm) and values were normalized to cell densities. Values are means of individual biological triplicates. Error bars indicate the respective standard deviations.

Considerably high eYFP expression levels could be seen for IPTG concentrations of 1 mM and above, thus 1 mM was chosen as a sufficient inducer concentration in all further experiments.

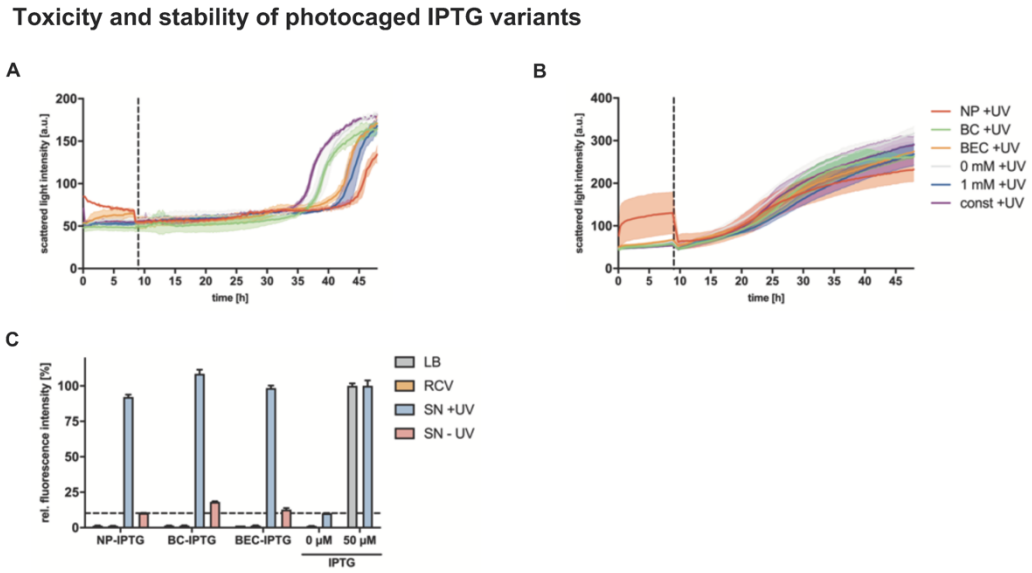

Figure S3: (**A-B)** Growth curves of *R. capsulatus* SB1003/pRholHi-2-eYFP expression cultures in the presence of the photocaged IPTG variants compared to an uninduced (0 mM), induced (1 mM IPTG) and constitutive expression culture (*R. capsulatus* SB1003/pRhokHi-2-eYFP). Cells were grown over 48 h using a BioLector system (RCV medium supplemented with 1 mM of each caged compound, 30°C, 800 rpm and 800 µL filling volume for aerobic cultures **(A)**, 400 rpm and 1500 µL for microaerobic cultures **(B)**). Cell growth was analyzed by determining the scattered light intensity. After 9 h, formation of photoproducts was induced in cultures of *R. capsulatus via* light exposure at 365 nm (~1 mW/cm^2, indicated by dashed lines) for 30 min. The addition of IPTG to comparatively grown cell cultures was used as a control. Values are means of individual biological triplicates. Error bars indicate the respective standard deviations. **(C)** EYFP *in vivo* fluorescence intensity of E. *coli* Tuner (DE3)/pRhotHi-2-lacI-eYFP expression cultures supplemented with 50 µM of the photocaged inducers which were previously incubated under different conditions. Firstly, the three caged inducers (1 mM) were incubated in LB (grey bars) or RCV (orange bars) medium for 48 h at 30°C and added to the *E. coli* cultures afterwards in appropriate concentrations resulting in an end concentration of 50 µM. Secondly, culture supernatants (SN) of aerobically grown *R. capsulatus* SB1003 cultures supplemented with all three photocaged compounds and treated with (blue bars) or without (red bars) UV-A light were harvested after 48 h. Subsequently, they were sterile filtrated and added to the *E. coli* cultures in appropriate concentrations (50 µM). The *E. coli* cultures were incubated in the dark for 20 h in LB medium at 30°C. The addition of inducer-containing supernatants was performed after 2 h. *In vivo* stability of the photocaged IPTG variants is reflected by a low induction of reporter gene expression. As positive control, *E. coli* Tuner (DE3)/ pRhotHi-2-lacI-eYFP cultures supplemented with and without IPTG were used. *In vivo* fluorescence intensities were determined by using a BioLector system (eYFP: λ_{ex} = 508 nm, λ_{em} = 532 nm) and are shown in relation to the respective fluorescence intensities gained by *R. capsulatus* expression cultures that have been induced with IPTG. All values are normalized to cell-densities and are means of individual biological triplicates. Error bars indicate the respective standard deviations.

The high scattered light values at the beginning of the cultivation (Figure S3 A and B) can be attributed to the poorer water solubility of BEC- and NP-cIPTG at concentrations of 1 mM, as a certain amount of these compounds initially form emulsions in the cultivation medium. Consequently, they contribute significantly more to the scattered light value than the bacterial cells that are initially still present in low numbers. However, exposure to UV-A light dissolves these emulsions, which is reflected by the rapid decrease in the scattered light intensity after 9 h.

In addition to analyzing the light-independent release of IPTG *via* eYFP reporter gene expression, a control experiment with the well-established expression strain *E. coli* Tuner(DE3) indicated that cIPTG instability was not detectable in sole LB or RCV medium, but only in supernatant of *R. capsulatus* expression cultures (Figure S3 C; Supporting Information). This indicates that the instability of BC-cIPTG and BEC-cIPTG is caused by using *R. capsulatus* as expression host, probably due to host specific enzymes or metabolism products.

Effect of UV-A light illumination on growth and *eyfp* reporter gene expression of *R. capsulatus* SB1003/pRholHi-2-eYFP cultures under aerobic and microaerobic conditions

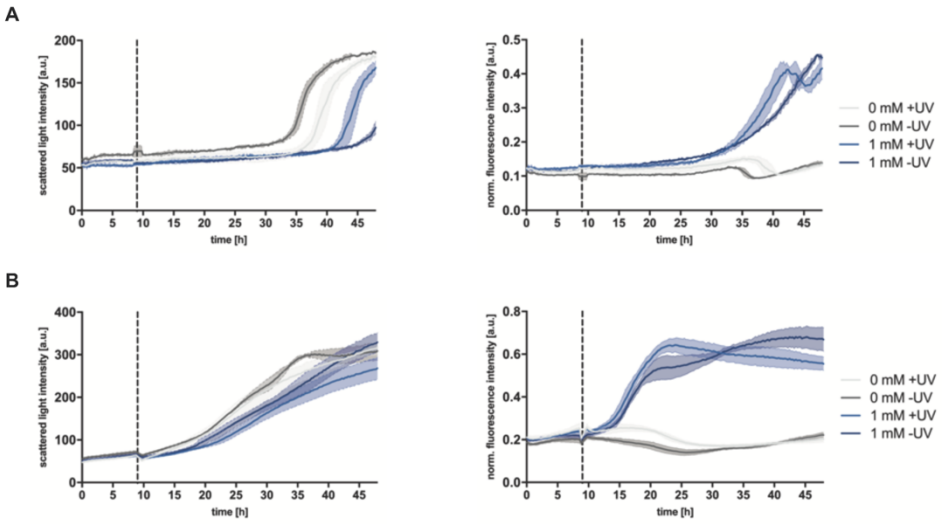

Figure S4: Cell growth and eYFP fluorescence during cultivation of *R. capsulatus* SB1003/pRholHi-2-eYFP. Cells were grown over 48 h in RCV medium at 30°C, 800 rpm and with 800 µL filling volume for aerobic conditions **(A)** and 400 rpm and 1500 µL for microaerobic conditions **(B)** using a BioLector system. Induction of eYFP gene expression was performed using 1 mM of IPTG (blue lines; uninduced grey lines). Simultaneously, cultures were incubated with (light lines) and without (dark line) UV-A light exposure at 365 nm (~1 mW/cm^2) for 30 min. The time point of induction is indicated by the dashed lines (9 h). Cell growth was analyzed by determining the scattered light intensity and the *in vivo* eYFP fluorescence intensities were measured at λ_{ex} = 508 nm, λ_{em} = 532 nm and normalized to cell densities. Values are means of individual biological triplicates. Error bars indicate the respective standard deviations.

DMNB-actinometry for photochemical monitoring of UV-A light exposure

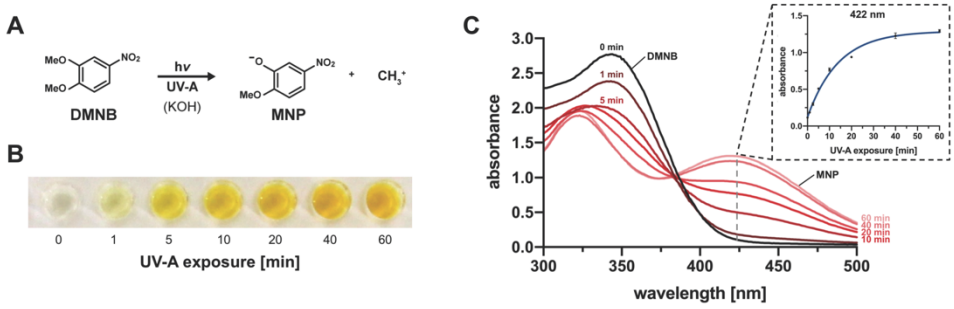

Figure S5: Photochemical monitoring of UV-A light exposure using DMNB actinometry. **(A)** Photochemical formation of 2-methoxy-5-nitrophenolate (MNP) from 1,2-dimethoxy-4-nitrobenzene (DMNB) using UV-A light in aqueous potassium hydroxide solution. **(B)** Colorimetric changes of DMNB solution upon increased UV-A exposure. **(C)** Light-mediated conversion of DMNB (1.25 mM) after 0, 1, 5, 10, 20, 40 and 60 min of mid-power UV-A light exposure (5.4 mW/cm^2). Grey dashed lines indicate respective maximal absorption differences of ΔA_{max}=351 and 422 nm in the UV-A to blue range; the insert shows the relation between absorbance at 422 nm and the duration of UV-A exposure. Values are means of triplicate measurements. Error bars indicate the respective standard deviations.

Evaluation of IR-light intensities for optimal phototrophic growth of *R. capsulatus* SB1003 expression cultures

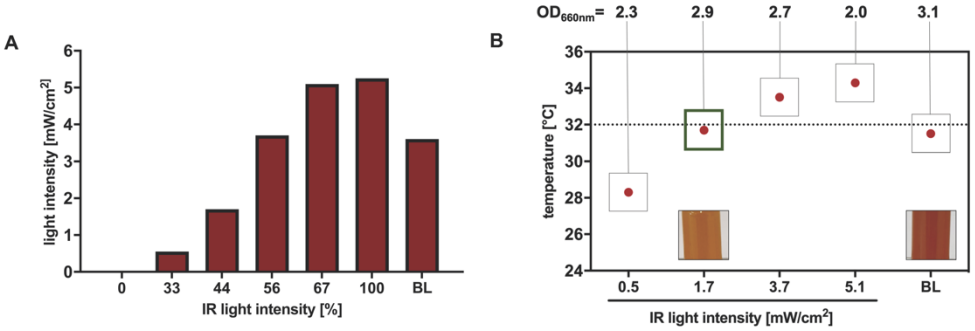

Figure S6: (**A**) Detected IR light intensities [mW/cm^2] at λ_{max}= 850 nm of IR panels from Vossloh-Schwabe [8] for increasing intensity settings, which can be set *via* a rotary knob with a continuous adjustment are shown in comparison to the IR light amount of bulb light (BL) at λ_{max}= 850 nm. Light intensity quantifications were conducted using a Thermal Power Sensor (S302C, Thorlabs Inc, USA). (**B**) Medium temperature at suitable IR light intensities after 48 h of cultivation and two pictures of corresponding *R. capsulatus* SB1003 cultures as well as the respective optical density at 660 nm. The cultivation temperature of 33°C should not be exceeded to avoid adverse effects on cell growth. The culture without any growth impairment and with the highest cell density is marked with a green frame and can be compared to cultures exposed with bulb light (BL).

For the determination of suitable IR light intensities for efficient phototrophic growth of *R. capsulatus,* cells were cultivated with IR light of increasing intensities ranging from 0.5 mW/cm^2 up to 5.1 mW/cm^2 (Figure S6 A) and analyzed with respect to their growth behavior (Figure S6 B). Screw neck vials, which were used as cultivation vessels, were placed in a distance of approx. 10 cm from each IR panel. Interestingly, all IR light cultures showed a reduced red/brownish coloring in comparison to a culture grown under blub light. Adequately grown cultures without any sunken cells could only be detected for IR light intensities of 1.7 mW/cm^2 and 3.1 mW/cm^2 represented by cell numbers corresponding to an optical density at 660 nm of 2.9 and 2.7, which are comparable to the optical density of cultures grown in bulb light (OD_{660nm}= 3.1). Lower or higher IR light intensities led to decreased cell densities and unequally distributed cultures with sunken cells indicating a hampered cell viability. Presumably, this was on the one hand due to the insufficient exposure intensity and on the other hand due to the excessively high temperature of over 33°C in the cultivation medium for the highest IR light intensity. For all following experiments, an IR light intensity of 1.7 mW/cm^2 was chosen as this condition offers an appropriate medium temperature and the highest cell density after 48 h.

DNA sequence of CrtE and CrtF from *R. capsulatus* SB1003 for cIPTG-mediated expression in *R. capsulatus* cultures.

The shown sequence encompasses the *crtE* (red bases) and *crtF* gene (blue bases) referring to the mRNA sequence published in GenBank: CP001312.1, encoding the GGPP synthase CrtE and the demethylspheroidene O-methyltransferase CrtF (UniProtKB: P17060 and P17061, respectively). At the 5'- and 3'-end, the *crtE* DNA fragment carries appropriate *Xba*I/*Xho*I restriction sites for cloning.

*Xba*I **RBS** **Start** *crtE*

TCTAGAGCTCGTGACGCAGC**GGAGGG**CTCTGTC**ATG**TCTCTGGATAAACGTATC
GAGTCGGCGCTGGTCAAGGCGCTGTCACCCGAGGCTTTGGGTGAATCTCCGCCGT
TGCTTGCCGCCGCGCTGCCTTACGGGGTGTTTCCCGGCGGCGCGCGGATCCGGCC
GACGATCCTTGTCTCGGTCGCGCTCGCCTGTGGCGACGATTGCCCGGCGGTCACC
GATGCCGCGGCCGTGGCGCTGGAGCTGATGCATTGCGCGAGCCTCGTGCATGACG
ATCTGCCCGCCTTCGACAATGCCGACATCCGGCGCGGCAAGCCGAGCCTTCACAA
GGCCTATAATGAACCGCTTGCGGTTCTGGCGGGCGACAGCCTGCTGATCCGCGGC
TTCGAAGTGCTGGCCGATGTCGGCGCCGTCAACCCGGACCGGGCGCTGAAGCTGA
TCTCGAAACTGGGTCAGCTGTCGGGGGCGCGCGGCGGGATCTGCGCCGGTCAGG
CCTGGGAAAGCGAATCCAAGGTCGATCTGGCCGCCTATCATCAGGCGAAGACCG
GGGCGCTGTTCATTGCCGCGACCCAGATGGGGGCGATTGCGGCGGGCTACGAGG
CCGAACCCTGGTTCGATCTGGGCATGCGGATCGGCTCGGCCTTCCAGATCGCCGA
CGACCTGAAAGACGCGCTGATGTCGGCCGAGGCAATGGGCAAGCCCGCCGGGCA
GGACATCGCGAACGAACGCCCGAATGCGGTCAAGACGATGGGCATCGAGGGCGC
GCGCAAACATCTGCAAGATGTGCTGGCGGGGGCGATCGCCTCGATCCCGTCCTGC
CCCGGTGAGGCGAAGCTGGCCCAGATGGTGCAGCTTTACGCCCACAAGATCATG

Stop *Xho*I/ **Start** *crtF*

GACATCCCGGCCAGCGCCGAGAGGGGC**TGA**CCGCTCGA**GTG**CCGAAGGACGACC
ACACGGGCGCGACGGCCGACCGGACCGCGCAGCCGACAGGAACGGGAAAGCAG
CCGCTGGTTCCGGGCCAGCCCGGGGCGGCGCCGGTGCAGCCGGGGCGGGTGAAT
TTCTTCACCCGGATCGCGCTGTCGCAACGGCTGCATGAAATCTTCGAACGCCTGC
CGCTGATGAACCGCGTCACCCGGCGCGAGGGCGAGGCGCTCTTCGACATCGTTTC
GGGCTTCGTGCAAAGCCAGGTTCTCTTGGCGATCGTCGAATTCCGGGTGCTGCAT
ATTCTGGCCGGGGCCTCTTGGCCCTTGCCGCAACTGGCCGAACGCACCGGCCTGG
CCGAGGACCGGCTGGCGGTGCTGATGCAGGCCGCCGCCGCCTTGAAGCTGGTGA
AATTCCGCCGCGGTCTGTGGCAGCTTGCCCCGCGTGGCGCCGCCTTCATCACCGT
GCCAGGGCTCGAGGCGATGGTGCGCCATCACCCCGTCCTTTACCGCGATCTGGCC
GATCCGGTGGCTTTTCTGAAAGGCGACATCGAACCCGAGCTGGCGGGCTTCTGGC
CCTATGTCTTCGGGCCGCTGGCGCAGGAAGATGCGGGGCTCGCCGAGCGCTATTC
GCAGCTGATGGCCGACAGCCAGCGCGTCGTGGCCGATGACACCTTGCGGCTTGTC
GATCTGCGCGATGCCAAGCGGGTGATGGATGTGGGCGGCGGCACCGGGGCCTTC
CTGCGCGTCGTGGCCAAGCTTTACCCCGAGCTGCCCTTGACGCTGTTCGACCTGCC
GCATGTGCTGTCGGTGGCGGACCGCTTCAGCCCGAAGCTCGATTTCGCGCCGGGC
AGCTTCCGCGACGATCCGATCCCGCAGGGCGCCGATGTCATCACTTTGGTGCGCG
TGCTGTATGACCATCCTGACAGCGTCGTCGAACCGCTTCTGGCCAAGGTGCATGC
CGCCTTGCCGCCGGGCGGGCGTCTGATCATCTCGGAGGCGATGGCGGGGGGCGC
AAAACCCGACCGTGCCTGCGATGTCTATTTCGCCTTCTACACGATGGCGATGAGT
TCGGGGCGCACGCGTTCCCCCGAAGAGATCAAGCAAATGCTTGAAAAAGCTGGG
TTCACCAAGGTGTCGAAACCGCGGACCCTGCGCCCCTTCATCACCTCGGTGATCG
AGGCCGAACGCGGC**TGA**

Stop

Determination of photocaged compound purity by qNMR

Table S2: Compound purities determined by qNMR.

Compound	Purity [%]
NP-cIPTG	88.9 ± 3.4
BEC-cIPTG	90.7 ± 1.3
BC-cIPTG	79.6 ± 1.8

The spectral and (photo-)chemical properties (solubility, absorption maximum, molar extinction coefficient, uncaging quantum yield, uncaging half-life time) of the photocaged compounds NP-cIPTG, BEC-cIPTG and BC-cIPTG have been reported previously [9].

References

1. Hanahan, D. Studies on transformation of *Escherichia coli* with plasmids. *J. Mol. Biol.* **1983**, *166*, 557–580, doi:10.1016/S0022-2836(83)80284-8.

2. Simon, R.; Priefer, U.; Pühler, A. A Broad host range mobilization system for *in vivo* genetic engineering: transposon mutagenesis in gram-negative bacteria. *Bio/Technology* **1983**, *1*, 784–791, doi:10.1038/nbt1183-784.

3. Strnad, H.; Lapidus, A.; Paces, J.; Ulbrich, P.; Vlcek, C.; Paces, V.; Haselkorn, R. Complete genome sequence of the photosynthetic purple nonsulfur bacterium *Rhodobacter capsulatus* SB1003. *J. Bacteriol.* **2010**, *192*, 3545–6, doi:10.1128/JB.00366-10.

4. Hage-Hülsmann, J.; Metzger, S.; Wewer, V.; Buechel, F.; Troost, K.; Thies, S.; Loeschcke, A.; Jaeger, K.-E.; Drepper, T. Biosynthesis of cycloartenol by expression of plant and bacterial oxidosqualene cyclases in engineered *Rhodobacter capsulatus*. *J. Biotechnol.* **2019**, *4*, 100014, doi:10.1016/j.btecx.2020.100014.

5. Katzke, N.; Bergmann, R.; Jaeger, K.-E.; Drepper, T. Heterologous high-level gene expression in the photosynthetic bacterium *Rhodobacter capsulatus*. In *Methods in Molecular Biology*; 2012; pp. 251–269 ISBN 9781617794322.

6. Binder, D.; Grünberger, A.; Loeschcke, A.; Probst, C.; Bier, C.; Pietruszka, J.; Wiechert, W.; Kohlheyer, D.; Jaeger, K.-E.; Drepper, T. Light-responsive control of bacterial gene expression: precise triggering of the *lac* promoter activity using photocaged IPTG. *Integr. Biol.* **2014**, *6*, 755–765, doi:10.1039/C4IB00027G.

7. Sambrook, J.; Fritsch, E.F.; T. Maniatis *Molecular cloning : a laboratory manual.*; Cold Spring Habor Laboratory Press, New York., **1989**.

8. Hilgers, F.; Habash, S.S.; Loeschcke, A.; Ackermann, Y.S.; Neumann, S.; Heck, A.; Klaus, O.; Hage-Hülsmann, J.; Grundler, F.M.W.; Jaeger, K.-E.; Schleker, A.S.S.; Drepper, T. Heterologous production of β-caryophyllene and evaluation of its activity against plant pathogenic fungi. *Microorganisms*. **2021**;9. doi:10.3390/microorganisms9010168

9. Hogenkamp, F.; Hilgers, F.; Knapp, A.; Klaus, O.; Bier, C.; Binder, D.; Jaeger, K. E.; Drepper, T. & Pietruszka, J. Effect of photocaged isopropyl β-D-1-thiogalactopyranoside solubility on the light responsiveness of LacI-controlled expression systems in different bacteria. *ChemBioChem*. **2021**;22: 539–547. doi:10.1002/cbic.202000377

V.3. SUPPORTING INFORMATION FOR CHAPTER II.1.3 – CHALLENGES AND SOLUTIONS IN CAGED COMPOUND SYNTHESIS AND *IN VIVO* APPLICATION

ChemBioChem

Supporting Information

Optochemical Control of Bacterial Gene Expression: Novel Photocaged Compounds for Different Promoter Systems

Fabian Hogenkamp[+], Fabienne Hilgers[+], Nora Lisa Bitzenhofer, Vera Ophoven, Mona Haase, Claus Bier, Dennis Binder, Karl-Erich Jaeger, Thomas Drepper,* and Jörg Pietruszka*

Table of Contents

S1 Bacterial strains and plasmids

All bacterial strains, plasmids and oligonucleotides used in this study are listed in Table S1.

Table S1: Bacterial strains, plasmids and oligonucleotides used in this study.

Strains, plasmids, oligonucleotides	Relevant features, description or sequences [a,b]	References
	Strains	
***E. coli* DH5α**	*F⁻ Φ80lacZΔM15 Δ(lacZYA-argF) U169 recA1 endA1 hsdR17 phoA supE44 thi-1 gyrA96 relA1 deoR*	[1]
***E. coli* Tuner (DE3)**	*F⁻ ompT hsdS*$_B$ ($r_B^- m_B^-$) *gal dcm lacY1(DE3)*	Novagen, Merck KGaA
***E. coli* LMG194**	*F– ΔlacX74 galE galK thi rpsL ΔphoA Δara714 leu::Tn10*	[2]
	Plasmids	
pRhotHi-2-lacI-eYFP	pBBR1-MCS-derivative, Km^R, Cm^R, pBBR22b-*lacI*, P_{T7}-lacO-MCS with *Nde*I *Xho*I inserted *eyfp*	[3]
pM117-R45T-GFPmut3	pMB1 replicon, *xylS* with R45T mutation, $P_{m\ M1\text{-}17}$ with inserted *gfpmut3*	[4]
pM-R45T-GFPmut3	pMB1 replicon, *xylS* with R45T mutation, P_m with inserted *gfpmut3*	[5] and this work
pBNTmcs(t)-Km	Km^R, *nagR*, vector for *PnagAa* and *tac* RBS controlled expression	[6]
pBNTmcs-mCherry-Km	pBNTmcs(t)-Km derivative with *EcoR*I/*Xba*I inserted *mcherry*	This work
pBTBX-2	pBBR1 replicon, Km^R, *araC*, araBAD promoter	[7]
pBTBX-2-mCherry	pBBR1 replicon, Km^R, *araC*, araBAD promoter with *tac* RBS and inserted *mcherry*	This work
	Oligonucleotides	
1) XylS_SalI_fw	Binds upstream of *Sal*I-site after *xylS*. Sequence: 5'-GAGACACAACGTGGCTTTCC-3'	[4]
2) XylS_SacI_rev	Binds upstream of *Sac*I-site in front of *xylS*. Sequence: 5'- ATCGACTTGGCGCCTTTCTAC-3'	[4]
3) XylS_R45T_rev	Binds within *xylS* and inserts R45T point mutation. Sequence: 5'- CAGGCA<u>C</u>GCTGCACCACAGAATC-3'	[4]
4) XlyS_R45T_fw	Binds within *xylS* and inserts R45T point mutation. Sequence: 5'- GATTCTGTGGTGCAGC<u>G</u>TGCCTG-3'	[4]
5) pBTBX_for	Binds at the 3' end of the pBTBX-2 plasmid. 5'- GTTCTAGAAAATTCGTCAACG -3'	This work
6) pBTBX_rev	Binds at the 5' end of the araBAD promoter on the pBTBX-2 plasmid. 5'- CATACCCGTTTTTTTGGGCTAG -3'	This work
7) mCherry_for	Binds at the 5' end of the *mcherry* gene, inserts overhangs for In-Fusion® cloning. Sequence: 5'- **GTTTTTTTGGGCTAG**CAGGAA ACAGGAGGTACC-3'	This work
8) mCherry_rev	Binds at the 3' end of *mcherry* gene, inserts overhangs for In-Fusion® cloning. Sequence: 5'-**GTTGACGAATTTTCTAGAAC**T TACTTGTACAGCTCG-3'	This work

[a] Underlined nucleotides indicate the point mutation used for XylS mutagenesis (AGG → ACG).

[b] Bold nucleotides indicate the inserted overhangs for In-Fusion® cloning.

S2 General methods for chemical synthesis procedures

All chemicals for synthesis were obtained from commercial suppliers and used without further purification unless stated otherwise. Solvents were reagent grade and were dried as well as purified by common methods. Thin-layer chromatography (TLC) was performed using pre-coated silica gel plates (Polygram® SIL G/UV, Macherey-Nagel) and components were visualized via oxidative staining or UV-light. Flash chromatography was performed on silica gel (Merck silica gel 60 (0.063−0.200 μm) and solvents for flash chromatography (petroleum ether/ethyl acetate/dichloromethane/*n*-pentane) were distilled prior to use. Optical rotation was determined at 20 °C on a Perkin Elmer Polarimeter 241 MC against sodium D-line and melting points were recorded using a Büchi melting point B-545 apparatus. The NMR spectra (^{1}H and ^{13}C) were measured at 20 °C on a Bruker Avance/DRX 600 spectrometer in deuterated solvents ($CDCl_3$, DMSO-d_6, acetone-d_6, D_2O). The chemical shifts are given in ppm relative to the solvent (^{1}H: $CDCl_3$ = 7.26 ppm, ^{1}H: DMSO-d_6 = 3.31 ppm, ^{1}H: acetone-d_6 = 2.05 ppm, ^{1}H: D_2O = 4.79 ppm / ^{13}C: $CDCl_3$ = 77.16 ppm, ^{13}C: DMSO-d_6 = 39.52 ppm, ^{13}C: acetone-d_6 = 29.84 ppm). Signals were assigned by means of H-COSY-, HSQC- and HMBC-experiments and splitting patterns are reported as singlet (s), doublet (d), triplet (t), multiplet (m), and broad singlet (brs). The IR spectra were recorded with a Perkin Elmer SpectrumOne IR-spectrometer ATR (Waltham, USA). HRMS (ESI) spectra were recorded by the centrum of analytics of the Heinrich Heine University. UV-Vis absorption spectra were recorded on a Genesys 10S UV/VIS Spectrophotometer (Thermo Scientific) and uncaging experiments were performed in a quartz cuvette with the LUMOS 43® from Atlas Photonics at 375 nm, 405 nm and 430 nm. Light intensity was quantified using a Thermal Power Sensor (S302C, Thorlabs Inc, USA) and the decay was detected by a Jasco HPLC system [column: Hyperclone 5 μ ODS (C18) 120 (Phenomenex)] combined with an UV/Vis-detector.

S3 Experimental procedures for the preparation of compounds

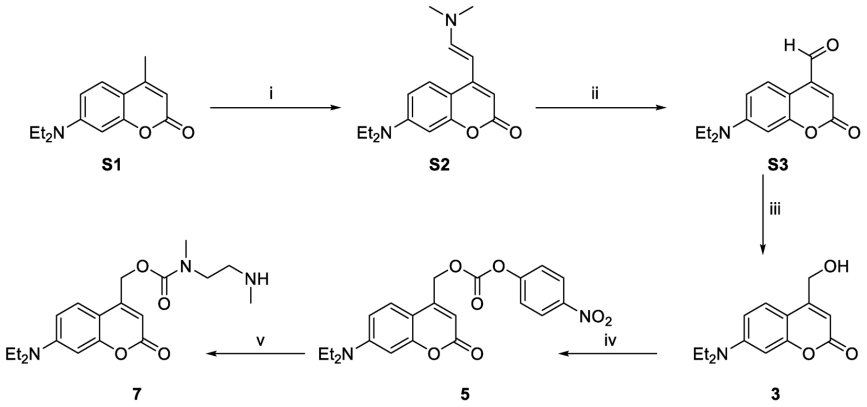

Scheme S1: Synthetic scheme for preparation of coumarin **7**. Reagents and conditions: i) DMF-DMA, DMF, reflux, 23 h; ii) $NaIO_4$, THF/H_2O (1:1), rt, 2 h; iii) $NaBH_4$, EtOH, 0 °C → rt, 4 h; iv) 4-nitrophenyl chloroformate, DIPEA, CH_2Cl_2, rt, 19 h; v) *N*,*N*′-dimethylethylenediamine, CH_2Cl_2, 0 °C, 30 min.

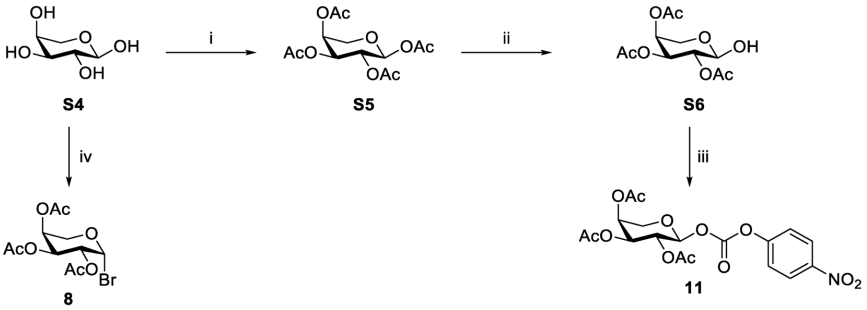

Scheme S2: Synthetic scheme for preparation of carbohydrates **8** and **11**. Reagents and conditions: i) Ac_2O, DMAP, pyridine, 0 °C → rt, 18 h; ii) AcOH, ethylenediamine, THF, rt, 24 h; iii) 4-nitrophenyl chloroformate, 2,6-lutidine, MeCN, rt, 18 h; iv) Ac_2O, HBr (33 wt%) in AcOH, rt, 3 h.

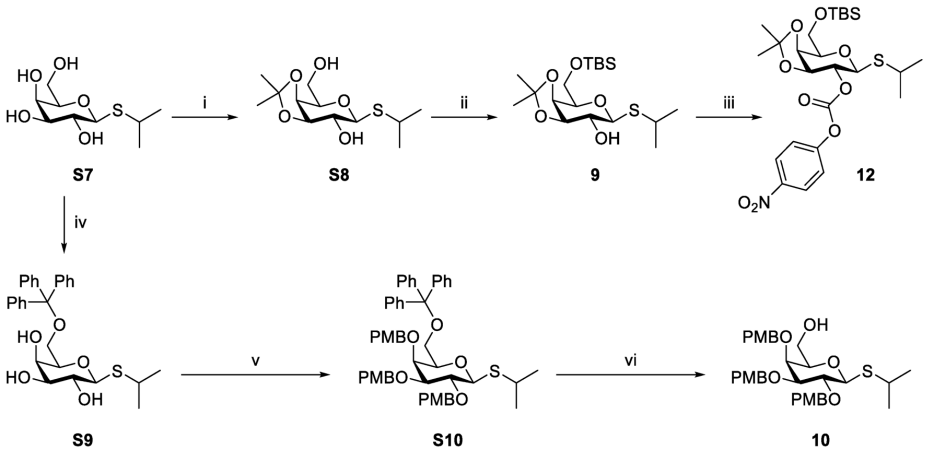

Scheme S3: Synthetic scheme for preparation of carbohydrates **10** and **12**. Reagents and conditions: i) 2,2-dimethoxypropane, CSA, acetone, rt, 8 h; ii) TBS-Cl, pyridine, rt, 20 h; iii) 4-nitrophenyl chloroformate, pyridine, rt, 20 h; iv) TrCl, DMAP, pyridine, rt, 18 h; v) PMB-Cl, NaH, DMF, rt, 18 h; vi) CSA, MeOH, CH_2Cl_2, 0 °C → rt, 48 h.

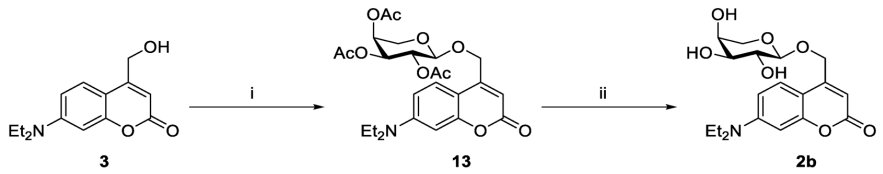

Scheme S4: Synthetic scheme for preparation of photocaged arabinose **2b**. Reagents and conditions: i) **8**, AgOTf, CH_2Cl_2, rt, 22 h; ii) NH_3 in MeOH (7 M), MeOH, rt.

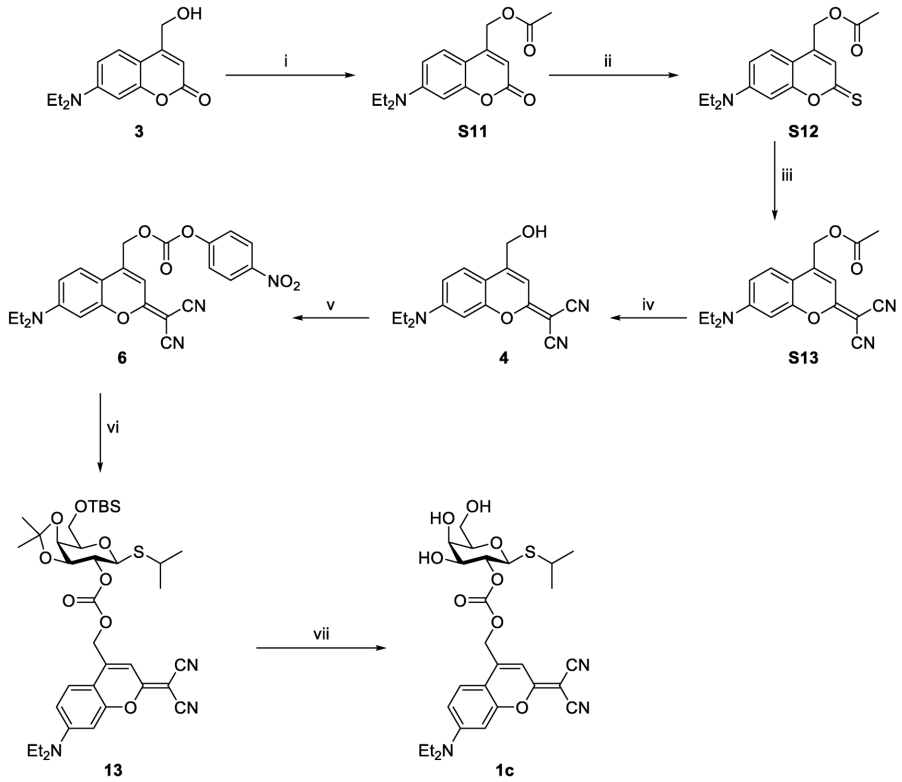

Scheme S5: Synthetic scheme for preparation of photocaged IPTG **1c**. Reagents and conditions: i) AcOH, DCC, DMAP, 0 °C → rt, 20 h; ii) Lawesson's reagent, toluene, reflux, 12 h; iii) malononitrile, NEt_3, $AgNO_3$, rt, 4 h; iv) HCl in EtOH (1.25 M), EtOH, reflux, 15 h; v) 4-nitrophenyl chloroformate, DIPEA, CH_2Cl_2, 22 h; vi) **9**, DMAP, CH_2Cl_2, rt, 20 h; vii) TFA, H_2O, CH_2Cl_2, 0 °C, 10 min.

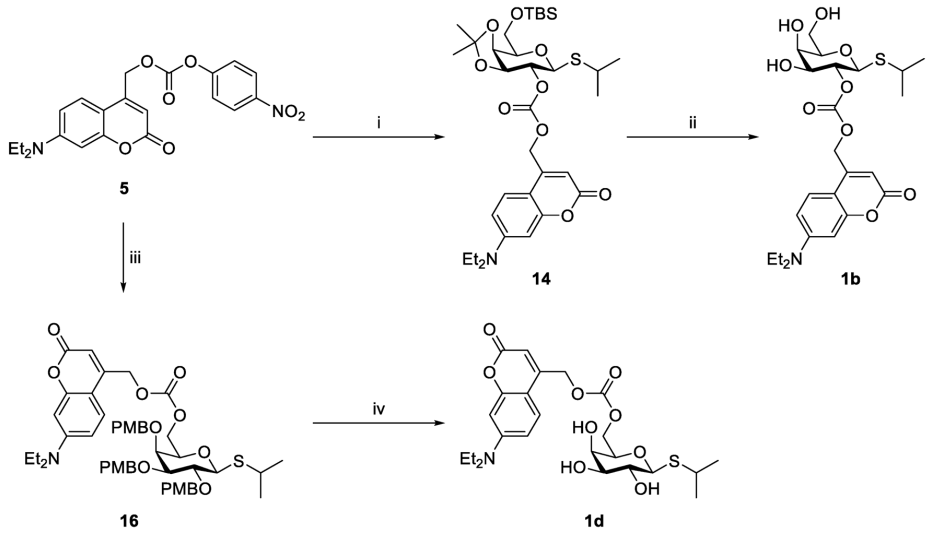

Scheme S6: Synthetic scheme for preparation of photocaged IPTG **1b** and **1d**. Reagents and conditions: i) **9**, DMAP, CH_2Cl_2, rt, 20 h; ii) TFA, H_2O, CH_2Cl_2, 0 °C, 10 min; iii) **10**, DMAP, CH_2Cl_2, rt, 20 h; iv) TFA, H_2O, CH_2Cl_2, 0 °C → rt, 1 h.

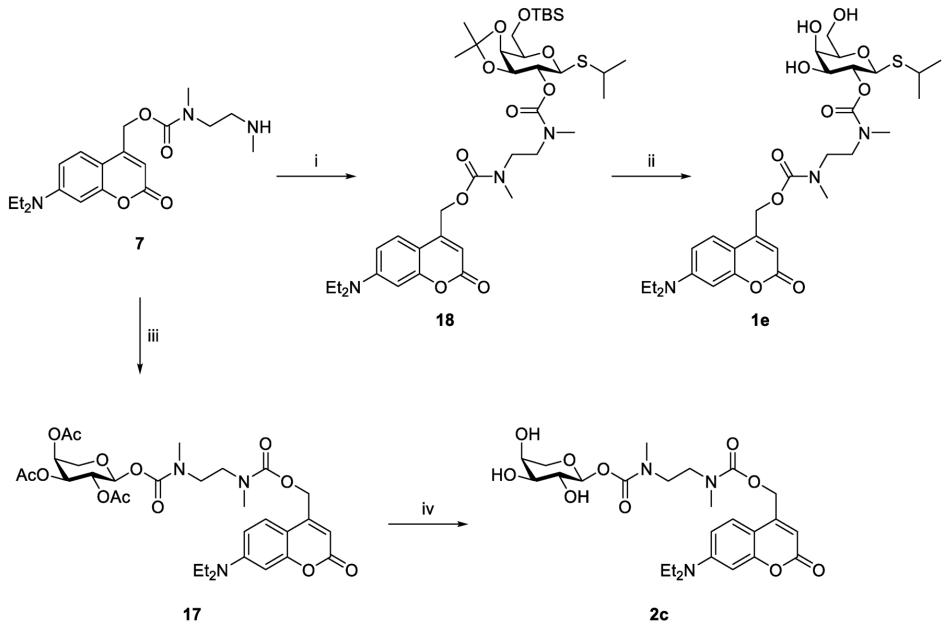

Scheme S7: Synthetic scheme for preparation of photocaged IPTG **1e** and photocaged arabinose **2c**. Reagents and conditions: i) **12**, DIPEA, DMAP, CH_2Cl_2, rt, 24 h; ii) TFA, H_2O, 0 °C, 10 min; iii) **11**, DIPEA, DMAP, CH_2Cl_2, rt, 24 h; iv) NH_3 in MeOH (7 M), MeOH, rt.

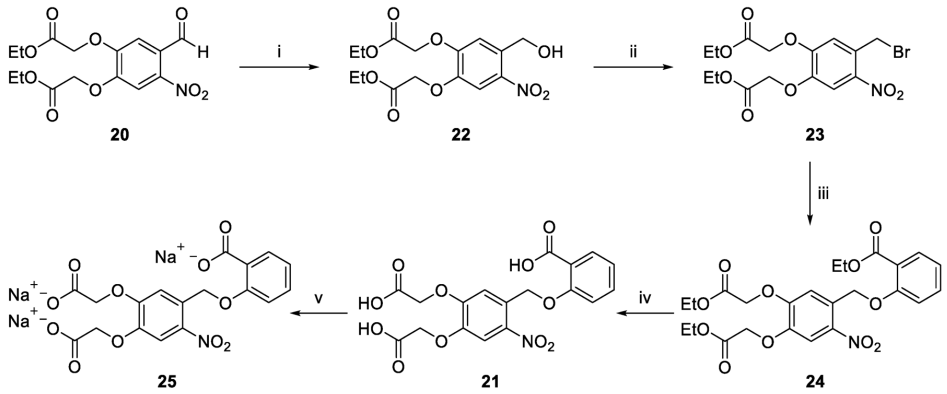

Scheme S8: Synthetic scheme for preparation of photocaged salicylic acid **21** and the corresponding sodium form **25**. Reagents and conditions: i) $NaBH_4$, CH_2Cl_2, EtOH, AcOH, 0 °C, 3 h; ii) CBr_4, PPh_3, CH_2Cl_2, 0 °C → rt, 6 h; iii) ethyl salicylate, K_2CO_3, acetone, rt, 2 d; iv) KOH (0.2 M), MeOH, 60 °C, 4 h; v) NaOH (0.2 M), MeOH, rt, 5 min.

S3.1 Synthesis of (*E*)-7-(Diethylamino)-4-[2-(dimethylamino)vinyl]-2*H*-chromen-2-one (S2)

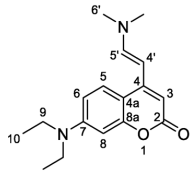

Coumarin **S2** was synthesized using a procedure of Weinrich *et al.*[8] Coumarin **S1** (15.0 g, 64.9 mmol) was dissolved in DMF (150 mL). After the addition of DMF-DMA (17.2 mL, 130 mmol) the reaction mixture was heated to reflux for 23 h. The reaction mixture was cooled to room temperature, diluted with CH_2Cl_2 and saturated $NaHCO_3$ solution was added. The organic phase was separated, and the aqueous phase was extracted with CH_2Cl_2. The combined organic phase was dried with anhydrous $MgSO_4$ and concentrated under reduced pressure to yield a brown solid (18.4 g, 64.3 mmol, 99%). The compound **S2** was used in the following reactions without further purification. The spectroscopic data are consistent with previously reported literature values.[8] ^{1}H-NMR (600 MHz, $CDCl_3$): δ [ppm] = 1.18 (t, $^3J_{10,9}$ = 7.2 Hz, 6 H, 10-H), 2.98 (s, 6 H, 6′-H), 3.38 (q, $^3J_{9,10}$ = 7.2 Hz, 4 H, 9-H), 5.21 (d, $^3J_{4',5'}$ = 13 Hz, 1 H, 4′-H), 5.84 (s, 1 H, 3-H), 6.47 (d, $^4J_{8,6}$ = 2.6 Hz, 1 H, 8-H), 6.54 (dd, $^3J_{6,5}$ = 9.0 Hz, $^4J_{6,8}$ = 2.6 Hz, 1 H, 6-H), 7.20 (d, $^3J_{5',4'}$ = 13.0 Hz, 1 H, 5′-H), 7.51 (d, $^3J_{5,6}$ = 9.0 Hz, 1 H, 5-H); ^{13}C-NMR (151 MHz, $CDCl_3$): δ [ppm] = 12.6 (C-10), 41.0 (C-6′), 44.7 (C-9), 87.5 (C-4′), 93.5 (C-3), 98.2 (C-8), 108.0 (C-6), 108.2 (C-4a), 124.9 (C-5), 146.7 (C-5′), 150.2 (C-7), 152.4 (C-4), 156.5 (C-8a), 163.5 (C-2); R_f = 0.33 (CH_2Cl_2/EtOAc 70:30); IR (atr-film): $\tilde{\nu}$ [cm^{-1}] = 1676, 1606, 1566, 1375, 1234, 1114, 1054, 974, 772, 625; MS (ESI, positive ion): m/z (%) = 287.3 (100) $[M+H]^+$; m.p.: 183 °C.

S3.2 Synthesis of 7-(Diethylamino)-2-oxo-2*H*-chromene-4-carbaldehyde (S3)

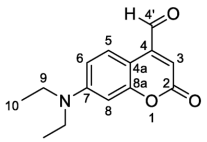

Coumarin **S3** was synthesized using a procedure of Weinrich *et al.*[8] Coumarin **S2** (18.4 g, 64.3 mmol) was dissolved in THF/H_2O (1:1, 110 mL). After the addition of $NaIO_4$ (41.3 g, 193 mmol) the reaction mixture was stirred for 2 h at room temperature. The precipitate was filtered off, washed with ethyl acetate and volatile solvents were removed under reduced pressure and washed with saturated $NaHCO_3$ solution. The organic phase was separated and the aqueous layer was extracted with CH_2Cl_2. The combined organic phase was dried with anhydrous $MgSO_4$ and concentrated under reduced pressure to yield a brown solid (15.7 g, 64.1 mmol, quant.). The compound **S3** was used in the following reactions without further purification. The spectroscopic data are consistent with previously reported literature values.[8] ^{1}H-NMR (600 MHz, $CDCl_3$): δ [ppm] = 1.22 (t, $^3J_{10,9}$ = 7.1 Hz, 6 H, 10-H), 3.43 (q, $^3J_{9,10}$ = 7.1 Hz, 4 H, 9-H), 6.45 (s, 1 H, 3-H), 6.53 (d, $^4J_{8,6}$ = 2.6 Hz, 1 H, 8-H), 6.63 (dd, $^3J_{6,5}$ = 9.2 Hz, $^4J_{6,8}$ = 2.6 Hz, 1 H, 6-H), 8.31 (d, $^3J_{5,6}$ = 9.2 Hz, 1 H, 5-H), 10.03 (s, 1 H, 4′-H); ^{13}C-NMR (151 MHz, $CDCl_3$): δ [ppm] = 12.5 (C-10), 45.0 (C-9), 97.9 (C-8), 104.0 (C-4a), 109.8 (C-6), 117.6 (C-3), 127.2 (C-5), 144.0 (C-8a), 151.0 (C-7), 157.5 (C-4), 162.0 (C-2), 192.6 (C-4′); R_f = 0.29 (PE/EtOAc 50:50); IR (atr-film): $\tilde{\nu}$ [cm^{-1}] = 2972, 1703, 1607, 1582, 1518, 1424, 1376, 1354, 1267, 1228, 1196, 1142, 1111, 1077, 1053, 901, 822, 780, 732, 640, 475; MS (ESI, positive ion): m/z (%) = 278.3 (100) $[M+CH_3OH+H]^+$; m.p.: 77.7 °C.

S3.3 Synthesis of 7-(Diethylamino)-4-(hydroxymethyl)-2*H*-chromen-2-one (3)

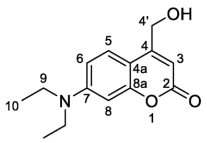

Coumarin **3** was synthesized using a modified procedure of Weinrich *et al.*[8] Coumarin **S3** (5.00 g, 20.4 mmol) was dissolved in ethanol (405 mL) and cooled to 0 °C. After the addition of $NaBH_4$ at 0 °C the reaction mixture was stirred at room temperature for 4 h. The reaction was quenched by addition of 1 M HCl (150 mL) and diluted with H_2O (90.0 mL). The solution was extracted with CH_2Cl_2 (3×100 mL) and the combined organic phase was washed with H_2O (90 mL). Subsequently it was dried with anhydrous $MgSO_4$ and concentrated under reduced pressure. The residue was purified by flash-column chromatography on SiO_2 (petroleum ether/ethyl acetate 50:50) to yield a yellow solid (2.07 g, 8.37 mmol, 41%). The spectroscopic data are consistent with previously reported literature values.[8] ^{1}H-NMR (600 MHz, $CDCl_3$): δ [ppm] = 1.20 (t, $^3J_{10,9}$ = 7.1 Hz, 6 H, 10-H), 1.93 (t, $^3J_{OH,4'}$ = 5.8 Hz, 1 H, 4′-OH), 3.41 (q, $^3J_{9,10}$ = 7.1 Hz, 4 H, 9-H), 4.83 (dd, $^3J_{4',OH}$ = 5.8 Hz, $^4J_{4',3}$ = 1.3 Hz, 2 H, 4′-H), 6.25 (t, $^4J_{3,4'}$ = 1.3 Hz, 1 H, 3-H), 6.51 (d, $^4J_{8,6}$ = 2.6 Hz, 1 H, 8-H), 6.56 (dd, $^3J_{6,5}$ = 9.0 Hz, $^4J_{6,8}$ = 2.6 Hz, 1 H, 6-H), 7.32 (d, $^3J_{5,6}$ = 9.0 Hz, 1 H, 5-H); ^{13}C-NMR (151 MHz, $CDCl_3$): δ [ppm] = 12.5 (C-10), 44.8 (C-9), 60.8 (C-4′), 97.7 (C-8), 105.2 (C-3), 106.4 (C-4a), 108.7 (C-6), 124.5 (C-5), 150.6 (C-7), 155.6 (C-4), 156.1 (C-8a), 163.2 (C-2); R_f = 0.36 (PE/EtOAc 50:50); IR (atr-film): $\tilde{\nu}$ [cm^{-1}] = 2013, 2001, 1000; MS (ESI, positive ion): m/z (%) = 254.3 (100) $[M+Li]^+$; m.p.: 139.9 °C.

S3.4 Synthesis of [7-(Diethylamino)-2-oxo-2*H*-chromen-4-yl]methyl (4-nitrophenyl) carbonate (5)

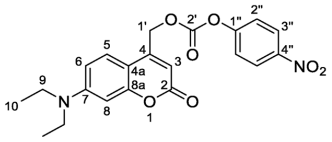

Coumarin **5** was synthesized using modified procedures of Gao *et al.*[9] and Fomina *et al.*[10] Coumarin **3** (2.00 g, 8.09 mmol) was dissolved in dry CH_2Cl_2 (10.0 mL) under nitrogen atmosphere. *N*,*N*-Diisopropylethylamine (DIPEA) (2.82 mL, 16.2 mmol) was added and the reaction mixture was stirred for 15 min before 4-nitrophenyl chloroformate (3.26 g, 16.2 mmol) dissolved in dry CH_2Cl_2 (10 mL) was added over 2 h via a syringe pump. The reaction mixture was stirred for 19 h and diluted with CH_2Cl_2. It was washed with 1 M HCl (20 mL) and saturated $NaHCO_3$ solution (3×20 mL). The organic phase was dried with anhydrous $MgSO_4$ and concentrated under reduced pressure. The residue was purified by flash-column chromatography on SiO_2 (CH_2Cl_2/*n*-pentane 98:2) to yield a yellow solid (1.48 g, 3.60 mmol, 44%). The spectroscopic data are consistent with previously reported literature values.[9] ^{1}H-NMR (600 MHz, $CDCl_3$): δ [ppm] = 1.22 (t, $^3J_{10,9}$ = 7.1 Hz, 6 H, 10-H), 3.43 (q, $^3J_{9,10}$ = 7.1 Hz, 4 H, 9-H), 5.40 (s, 2 H, 1′-H) 6.22 (s, 1 H, 3-H), 6.54 (d, $^4J_{8,6}$ = 2.6 Hz, 1 H, 8-H), 6.61 (dd, $^3J_{6,5}$ = 9.0 Hz, $^4J_{6,8}$ = 2.6 Hz, 1 H, 6-H), 7.31 (d, $^3J_{5,6}$ = 9.0 Hz, 1 H, 5-H), 7.42 (d, $^3J_{2'',3''}$ = 8.6 Hz, 2 H, 2″-H), 8.30 (d, $^3J_{3'',2''}$ = 8.6 Hz, 2 H, 3″-H); ^{13}C-NMR (151 MHz, $CDCl_3$): δ [ppm] = 12.5 (C-10), 44.9 (C-9), 65.9 (C-1′), 98.0 (C-8), 105.7 (C-4a), 107.0 (C-3), 108.9 (C-6), 121.8 (C-2″), 124.4 (C-5), 125.5 (C-3″), 145.7 (C-4″), 147.9 (C-4), 151.0 (C-7), 152.3 (C-2′), 155.3 (C-1″), 156.5 (C-8a), 161.7 (C-2); R_f = 0.10 (CH_2Cl_2/*n*-pentane 98:2); IR (atr-film): $\tilde{\nu}$ [cm^{-1}] = 2968, 1772, 1708, 1591, 1520, 1489, 1446, 1423, 1335, 1268, 1218, 1194, 1142, 1109, 1090, 1040, 986, 956, 856, 838, 816, 792, 750, 704, 679, 567, 528, 493, 467; HRMS (ESI): m/z calculated for $C_{21}H_{21}N_2O_7^+$ $[M+H]^+$: 413.1343; found: 413.1340; m.p.: 159.9 °C.

S3.5 Synthesis of [7-(Diethylamino)-2-oxo-2*H*-chromen-4-yl]methyl methyl[2-(methylamino)ethyl]carbamate (7)

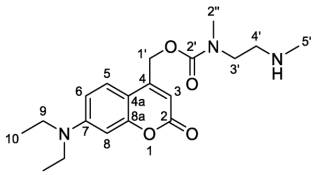

Coumarin **7** was synthesized using a modified procedure of Fomina *et al.*[10] Coumarin **5** (50.0 mg, 0.12 mmol) was dissolved in CH_2Cl_2 (1.30 mL). It was added dropwise over 30 min to a solution of *N*,*N*′-dimethylethylenediamine (0.14 mL, 1.21 mmol) in CH_2Cl_2 (2.6 mL) at 0 °C. The reaction mixture was stirred for 30 min at 0 °C. The solvent was removed under reduced pressure, the residue was

dissolved in ethyl acetate and washed subsequently with saturated $NaHCO_3$ and saturated NaCl solution. The organic phase was dried with anhydrous $MgSO_4$ and concentrated under reduced pressure. The residue was purified by flash-column chromatography on SiO_2 (ethyl acetate/methanol/triethylamine 87:10:3) to yield a viscous dark yellow oil (27.0 mg, 74.7 µmol, 62%). ^{1}H-NMR (600 MHz, $CDCl_3$): δ [ppm] = 1.19 (t, $^3J_{10,9}$ = 7.1 Hz, 6 H, 10-H), 2.42–2.51 (m, 4 H, 5′-H, NH), 2.80 (m_c, 2 H, 4′-H), 2.95–3.04 (m, 3 H, 2″-H), 3.39 (q, $^3J_{9,10}$ = 7.1 Hz, 4 H, 9-H), 3.44–3.49 (m, 2 H, 3′-H), 5.23 (s, 2 H, 1′-H), 6.10 (s, 1 H, 3-H), 6.49 (d, $^4J_{8,6}$ = 2.6 Hz, 1 H, 8-H), 6.55 (dd, $^3J_{6,5}$ = 9.0 Hz, $^4J_{6,8}$ = 2.6 Hz, 1 H, 6-H), 7.27–7.31 (m, 1 H, 5-H); ^{13}C-NMR (151 MHz, $CDCl_3$): δ [ppm] = 12.5 (C-10), 34.8, 35.5 (C-2″), 36.1, 36.4 (C-5′), 44.8 (C-9), 48.6, 48.9 (C-3′), 49.3, 49.7 (C-4′), 62.5, 62.6 (C-1′), 97.9 (C-8), 105.8 (C-4a), 106.1, 106.2 (C-3), 108.7 (C-6), 124.4, 124.5 (C-5), 150.6, 150.7 (C-4, C-7), 155.6, 155.9 (C-2′), 156.3 (C-8a), 162.2 (C-2); R_f = 0.15 (EtOAc/MeOH/NEt_3 87:10:3); IR (atr-film): $\tilde{\nu}$ [cm^{-1}] = 2960, 2926, 2859, 1709, 1605, 1526, 1422, 1358, 1275, 1197, 1143, 1078, 821, 767; HRMS (ESI): m/z calculated for $C_{19}H_{28}N_3O_4^+$ $[M+H]^+$: 362.2074; found: 362.2077.

S3.6 Synthesis of L-Arabinopyranose tetraacetate (S4)

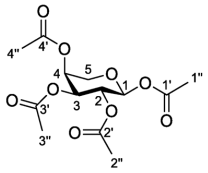

α-L-Arabinopyranose tetraacetate (**S4**) was synthesized using a procedure of Wahler *et al.*[11] α-L-Arabinopyranose (**2a**) (1.00 g, 6.66 mmol) was dissolved in dry pyridine (5.00 mL) and cooled to 0 °C. After the addition of acetic anhydride (5.04 mL, 53.3 mmol) and 4-dimethylaminopyridine (DMAP) (325 mg, 2.66 mmol) the reaction mixture was stirred for 18 h with the temperature slowly rising to room temperature. The reaction was quenched and diluted by addition of water and ethyl acetate. The organic phase was separated and washed with water as well as saturated NaCl solution. Subsequently it was dried with anhydrous $MgSO_4$ and concentrated under reduced pressure. Repeated coevaporation with toluene under reduced pressure yielded a colourless solid (1.77 g, 5.58 mmol, 84%). The spectroscopic data are consistent with previously reported literature values.[11] ^{1}H-NMR (600 MHz, $CDCl_3$): δ [ppm] = 2.01, 2.01, 2.13, 2.14 (s, 12 H, 1″-H, 2″-H, 3″-H, 4″-H), 3.81 (dd, $^2J_{5a,5b}$ = 13.2 Hz, $^3J_{5a,4}$ = 2.0 Hz, 1 H, 5-H_a), 4.05 (dd, $^2J_{5b,5a}$ = 13.2 Hz, $^3J_{5a,4}$ = 1.5 Hz, 1 H, 5-H_b), 5.28–5.39 (m, 3 H, 2-H, 3-H, 4-H), 6.33 (d, $^3J_{1,2}$ = 3.1 Hz, 1 H, 1-H); ^{13}C-NMR (151 MHz, $CDCl_3$): δ [ppm] = 20.7, 20.8, 21.0, 21.0 (C-1″, C-2″, C-3″, C-4″), 62.9 (C-5), 66.8 (C-3 or C-4), 67.1 (C-2), 68.5 (C-3 or C-4), 90.3 (C-1), 169.2 (C-1′), 170.0, 170.2, 170.4 (C-2′, C-3′, C-4′); R_f = 0.63 (PE/EtOAc 1:1); IR (atr-film): $\tilde{\nu}$ [cm^{-1}] = 1736, 1372, 1212, 1137, 1113, 1065, 1010, 942, 894, 755, 602, 552, 471; MS (ESI, positive ion): m/z (%) = 341.0 (100) $[M+Na]^+$, 357.0 (15) $[M+K]^+$; m.p.: 94.4 °C; $[\alpha]_D^{20}$ = 151.8 (c = 0.5, $CHCl_3$).

S3.7 Synthesis of (2,3,4-Tri-*O*-acetyl)-α/β-L-arabinopyranose (S5)

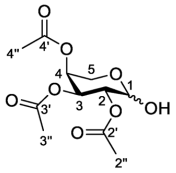

(2,3,4-tri-*O*-acetyl)-α/β-L-arabinopyranose (**S5**) was synthesized using a procedure of Duléry *et al*.[12] Glacial acetic acid (1.01 mL, 17.6 mmol) was added dropwise to a solution of ethylenediamine (1.01 mL, 15.1 mmol) in THF (250 mL), which immediately lead to the formation of a precipitate. L-arabinopyranose tetraacetate (**S4**) (4.00 g, 12.6 mmol) was added and the reaction mixture was stirred at room temperature for 24 h. After the addition of water, the reaction mixture was extracted with CH_2Cl_2. The organic phase was subsequently washed with 1 M HCl, saturated $NaHCO_3$ solution and water. Following this, the organic phase was dried with anhydrous $MgSO_4$ and concentrated under reduced pressure. The residue was purified by flash-column chromatography on SiO_2 (petroleum ether/ethyl acetate 55:45) to yield (2,3,4-tri-*O*-acetyl)-α/β-L-arabinopyranose (**S5**) as a colorless oil (2.28 g, 8.26 mmol, 66%) in α:β ratio of 1:3. The spectroscopic data are consistent with previously reported literature values.[13] α/β-Anomers: R_f = 0.18 (PE/EtOAc 1:1); IR (atr-film): $\tilde{\nu}$ [cm^{-1}] = 3455, 1739, 1371, 1216, 1139, 1057, 1007, 936, 889, 765, 736, 603, 465; MS (ESI, positive ion): m/z (%) = 299.0 (100) $[M+Na]^+$; α-Anomer: ^{1}H-NMR (600 MHz, $CDCl_3$): δ [ppm] = 2.00 (s, 3 H, CH_3), 2.08 (s, 3 H, CH_3), 2.13 (s, 3 H, CH_3), 3.66 (dd, $^2J_{5a,5b}$ = 13.4 Hz, $^3J_{5a,4}$ = 1.1 Hz, 1 H, 5-H_a), 4.01 (dd, $^2J_{5b,5a}$ = 13.4 Hz, $^3J_{5a,4}$ = 2.5 Hz, 1 H, 5-H_b), 4.60 (d, $^3J_{1,2}$ = 6.7 Hz, 1 H, 1-H), 5.03–5.09 (m, 2 H, 2-H and 3-H), 5.24–5.27 (m, 1 H, 4-H); ^{13}C-NMR (151 MHz, $CDCl_3$): δ [ppm] = 20.7, 20.9, 21.0 (C-2″, C-3″, C-4″), 64.2 (C-5), 68.1 (C-4), 70.2 (C-2), 71.3 (C-3), 96.2 (C-1), 170.2, 170.5, 171.2 (C-2′, C-3′, C-4′); β-Anomer: ^{1}H-NMR (600 MHz, $CDCl_3$): δ [ppm] = 2.00 (s, 3 H, 4″-H), 2.08 (s, 3 H, 2″-H or 3″-H), 2.12 (s, 3 H, 2″-H or 3″-H), 3.59 (brs, 1 H, 1-OH), 3.68 (dd, $^2J_{5a,5b}$ = 13.1 Hz, $^3J_{5a,4}$ = 2.3 Hz, 1 H, 5-H_a), 4.18 (dd, $^2J_{5b,5a}$ = 13.1 Hz, $^3J_{5a,4}$ = 1.5 Hz, 1 H, 5-H_b), 5.16 (dd, $^3J_{3,2}$ = 10.5 Hz, $^3J_{3,4}$ = 3.4 Hz, 1 H, 3-H), 5.33–5.36 (m, 1 H, 4-H), 5.38 (dd, $^3J_{2,3}$ = 10.5 Hz, $^3J_{2,1}$ = 3.5 Hz, 1 H, 2-H), 5.45 (d, $^3J_{1,2}$ = 3.5 Hz, 1 H, 1-H); ^{13}C-NMR (151 MHz, $CDCl_3$): δ [ppm] = 20.8 (C-4″), 20.9 (C-2″ or C-3″), 21.0 (C-2″ or C-3″), 60.4 (C-5), 67.0 (C-2), 68.8 (C-3), 69.2 (C-4), 91.0 (C-1), 170.3 (C-4′), 170.6 (C-2′), 170.6 (C-3′).

S3.8 Synthesis of 4-Nitrophenyl-(2,3,4-tri-*O*-acetyl)-α-L-arabinopyranosyl carbonate (11)

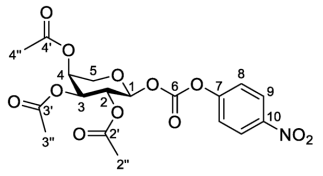

Carbohydrate **11** was synthesized using a modified procedure of André *et al*.[14] The anomeric mixture of carbohydrate **S5** (408 mg, 1.48 mmol) was dissolved in MeCN (49.0 mL) and cooled to 0 °C. After the addition of 4-nitrophenyl chloroformate (316 mg, 1.57 mmol) and 2,6-lutidine (0.18 mL, 1.57 mmol) the reaction mixture was stirred for 18 h at room temperature. The reaction mixture was quenched by addition of water and diluted with CH_2Cl_2. The organic phase was washed with water and saturated NaCl solution. Following this, the organic phase was dried with anhydrous $MgSO_4$ and concentrated under reduced pressure. The residue was purified by flash-column chromatography on SiO_2 (petroleum ether/ethyl acetate 60:40) to mainly yield the α-anomer as a colorless solid (133 mg, 302 µmol, 20%). Unreacted substrate was reisolated as an anomeric mixture with α:β ratio of 1:1.8. ^{1}H-NMR (600 MHz, $CDCl_3$): δ [ppm] = 2.10 (s, 3 H, 3″-H), 2.14 (s, 3 H, 4″-H), 2.14 (s, 3 H, 2″-H), 3.83 (dd, $^2J_{5a,5b}$ = 12.5 Hz, $^3J_{5a,4}$ = 2.8 Hz, 1 H, 5-H$_a$), 4.18 (dd, $^2J_{5b,5a}$ = 12.5 Hz, $^3J_{5a,4}$ = 5.1 Hz, 1 H, 5-H$_b$), 5.19 (dd, $^3J_{3,2}$ = 7.8 Hz, $^3J_{3,4}$ = 3.4 Hz, 1 H, 3-H), 5.31–5.36 (m, 2 H, 2-H, 4-H), 5.69 (d, $^3J_{1,2}$ = 5.6 Hz, 1 H, 1-H), 7.41 (d, $^3J_{8,9}$ = 9.1 Hz, 2 H, 8-H), 8.29 (d, $^3J_{9,8}$ = 9.1 Hz, 2 H, 9-H); ^{13}C-NMR (151 MHz, $CDCl_3$): δ [ppm] = 20.8, 20.9, 21.0 (C-2″, C-3″, C-4″), 62.8 (C-5), 66.3 (C-4), 67.9 (C-2), 69.0 (C-3), 96.1 (C-1), 121.8 (C-8), 125.5 (C-9), 145.8 (C-10), 151.1 (C-6), 155.1 (C-7), 169.3 (C-2′), 170.0 (C-3′), 170.1 (C-4′); R_f = 0.28 (PE/EtOAc 70:30); IR (atr-film): $\tilde{\nu}$ [cm^{-1}] = 1746, 1594, 1527, 1492, 1370, 1346, 1217, 1173, 1087, 1055, 965, 913, 860, 729, 599, 504; HRMS (ESI): m/z calculated for $C_{18}H_{23}N_2O_{12}^+$ $[M+NH_4]^+$: 459.1246; found: 459.1247; m.p.: 52–58 °C; $[\alpha]_D^{20}$ = -3 (c = 1.0, $CHCl_3$).

S3.9 Synthesis of 2,3,4-tri-*O*-acetyl-β-L-arabinopyranosyl bromide (8)

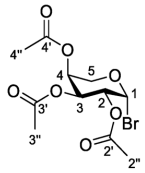

The carbohydrate **8** was synthesized using a procedure of Kartha *et al*.[15] α-L-Arabinopyranose (**2a**) (1.00 g, 6.66 mmol) was dissolved in acetic anhydride (5.04 mL, 53.3 mmol) and stirred at room temperature. HBr solution 33 wt% in AcOH (1.50 mL, 8.57 mmol) was added to the suspension. After the solid was completely dissolved (1 h) additional HBr solution 33 wt% in AcOH (7.5 mL, 42.9 mmol) was added and the reaction mixture was stirred for additional 2 h. Subsequently the reaction mixture was concentrated under reduced pressure. Toluene (3×20 ml) was added and removed under reduced pressure. The crude product was recrystallized from Et_2O to yield a colorless solid (926 mg, 2.73 mmol, 41%). The spectroscopic data are consistent with previously reported literature values.[16] ^{1}H-NMR (600 MHz, $CDCl_3$): δ [ppm] = 2.03 (s, 3 H, CH_3), 2.11 (s, 3 H, CH_3), 2.15 (s, 3 H, CH_3), 3.93 (dd, $^2J_{5a,5b}$ = 13.3 Hz, $^3J_{5a,4}$ = 1.7 Hz, 1 H, 5-H$_a$), 4.21 (d, $^2J_{5b,5a}$ = 13.3 Hz, 1 H, 5-H$_b$), 5.09 (ddd, $^3J_{2,3}$ = 11.8 Hz, $^3J_{2,1}$ = 3.9 Hz, $^3J_{2,4}$ = 1.6 Hz, 1 H, 2-H), 5.37–5.43 (m, 2 H, 3-H, 4-H), 6.70 (d, $^3J_{1,2}$ = 3.9 Hz, 1 H, 1-H); ^{13}C-NMR (151 MHz, $CDCl_3$): δ [ppm] = 20.8, 20.9, 21.0 (C-2″, C-3″, C-4″), 64.9 (C-5), 67.8, 68.0 (C-3, C-4), 68.1 (C-2), 89.8 (C-1), 169.9, 170.2, 170.2 (C-2′, C-3′, C-4′).; R_f = 0.70 (PE/EtOAc 1:1); IR (atr-film): $\tilde{\nu}$ [cm^{-1}] = 1734, 1375, 1211, 1098, 1069, 1043, 992, 929, 891, 685, 577, 601, 539, 473; m.p.: 115.6 °C; $[\alpha]_D^{20}$ = 153.3 (c = 1.0, $CHCl_3$)

S3.10 Synthesis of Isopropyl 3,4-*O*-(1-methylethylidene)-1-thio-β-D-galactopyranoside (S6)

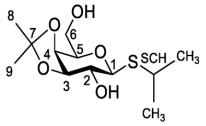

Carbohydrate **S6** was synthesized using a modified procedure of Du *et al.*[17] Isopropyl β-D-1-thiogalactopyranoside (**1a**) (5.00 g, 19.9 mmol) was dissolved in acetone (147 mL). After the addition of camphorsulfonic acid (CSA) (945 mg, 3.99 mmol) and 2,2-dimethoxypropane (3.66 mL, 29.9 mmol) the reaction mixture was stirred for 8 h at room temperature. The reaction mixture was quenched by addition of $NaHCO_3$ and the solvent was removed under reduced pressure. The residue was dissolved in CH_2Cl_2 and subsequently washed with $NaHCO_3$ solution. The aqueous phase was extracted with CH_2Cl_2 (3×) and the combined organic phases were washed with saturated NaCl solution. Following this, the organic phase was dried with anhydrous $MgSO_4$ and concentrated under reduced pressure. The residue was purified by flash-column chromatography on SiO_2 (petroleum ether/ethyl acetate 50:50) to yield a white solid (3.90 g, 14.0 mmol, 70%). ^{1}H-NMR (600 MHz, DMSO-d_6): δ [ppm] = 1.22 (d, $^3J_{CH3,SCH}$ = 6.9 Hz, 3 H, CH_3), 1.23 (d, $^3J_{CH3,SCH}$ = 6.9 Hz, 3 H, CH_3), 1.25 (s, 3 H, 7-H or 8-H), 1.38 (s, 3 H, 7-H or 8-H), 3.14 (septet, $^3J_{SCH,CH3}$ = 6.9 Hz, 1 H, SCH), 3.23 (ddd, $^3J_{2,1}$ = 9.9 Hz, $^3J_{2,3}$ = 6.6 Hz, $^3J_{2,2\text{-OH}}$ = 6.1 Hz, 1 H, 2-H), 3.51 (m, 2 H, 6-H), 3.73 (td, $^3J_{5,6}$ = 6.3 Hz, $^3J_{5,4}$ = 2.0 Hz, 1 H, 5-H), 3.92 (dd, $^3J_{3,2}$ = 6.6 Hz, $^3J_{3,4}$ = 5.6 Hz, 1 H, 3-H), 4.14 (dd, $^3J_{4,3}$ = 5.6 Hz, $^3J_{4,5}$ = 2.0 Hz, 1 H, 4-H), 4.35 (d, $^3J_{1,2}$ = 9.9 Hz, 1 H, 1-H), 4.73 (t, $^3J_{6\text{-OH},6}$ = 5.6 Hz, 1 H, 6-OH), 5.29 (d, $^3J_{2\text{-OH},2}$ = 6.1 Hz, 1 H, 2-OH); ^{13}C-NMR (151 MHz, DMSO-d_6): δ [ppm] = 23.7 (CH_3), 23.8 (CH_3), 26.4, 28.2 (C-7, C-8), 33.4 (SCH), 60.6 (C-6), 71.8 (C-2), 73.4 (C-4), 76.5 (C-5), 79.5 (C-3), 83.9 (C-1), 108.4 (C-7); R_f = 0.23 (PE/EtOAc 50:50); IR (atr-film): $\tilde{\nu}$ [cm^{-1}] = 3301, 2990, 2924, 2864, 1460, 1369, 1239, 1215, 1141, 1073, 1020, 962, 872, 840, 725, 641, 570, 536, 504; HRMS (ESI): m/z calculated for $C_{12}H_{26}NO_5S^+$ $[M+NH_4]^+$: 296.1526; found: 296.1527; m.p.: 89.8 °C; $[\alpha]_D^{20}$ = 3.4 (c = 1.0, $CHCl_3$)

S3.11 Synthesis of Isopropyl 3,4-*O*-(1-methylethylidene)-6-*O*-(*tert*-butyldimethylsilyl)-1-thio-β-D-galactopyranoside (9)

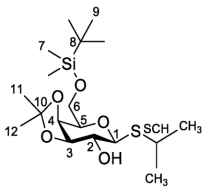

Carbohydrate **9** was synthesized using a modified procedure of Du *et al.*[17] Carbohydrate **S6** (1.00 g, 3.59 mmol) was dissolved in dry pyridine (20.0 mL) under nitrogen atmosphere. *Tert*-butyldimethylsilyl chloride (TBS-Cl) (1.14 g, 7.54 mmol) was added portion wise and the reaction mixture was stirred for 20 h at room temperature. After completion, the solvent was removed under reduced pressure. The residue was dissolved in CH_2Cl_2 and subsequently washed with water. The organic phase was dried with anhydrous $MgSO_4$ and concentrated under reduced pressure. The residue was purified by flash-column chromatography on SiO_2 (petroleum ether/ethyl acetate 85:15) to yield a white solid (1.05 g, 2.67 mmol, 74%). ^{1}H-NMR (600 MHz, DMSO-d_6): δ [ppm] = 0.04 (s, 3 H, 7-H), 0.05 (s, 3 H, 7-H), 0.86 (s, 9 H, 9-H), 1.22 (d, $^3J_{CH3,SCH}$ = 6.8 Hz, 3 H, CH_3), 1.23 (d, $^3J_{CH3,SCH}$ = 6.8 Hz, 3 H, CH_3), 1.24 (s, 3 H, 11-H or 12-H), 1.38 (s, 3 H, 11-H or 12-H), 3.13 (septet, $^3J_{SCH,CH3}$ = 6.8 Hz, 1 H, SCH), 3.23 (dd, $^3J_{2,1}$ = 9.9 Hz, $^3J_{2,3}$ = 7.0 Hz, 1 H, 2-H), 3.66 (dd, $^2J_{6a,6b}$ = 10.4 Hz, $^3J_{6a,5}$ = 7.2 Hz, 1 H, 6-H_a), 3.71 (dd, $^2J_{6b,6a}$ = 10.4 Hz, $^3J_{6b,5}$ = 5.4 Hz, 1 H, 6-H_b), 3.81 (ddd, $^3J_{5,6a}$ = 7.2 Hz, $^3J_{5,6b}$ = 5.4 Hz, $^3J_{5,4}$ = 2.0 Hz, 1 H, 5-H), 3.93 (dd, $^3J_{3,2}$ = 7.0 Hz, $^3J_{3,4}$ = 5.4 Hz, 1 H, 3-H), 4.14 (dd, $^3J_{4,3}$ = 5.4 Hz, $^3J_{4,5}$ = 2.0 Hz, 1 H, 4-H), 4.37 (d, $^3J_{1,2}$ = 9.9 Hz, 1 H, 1-H), 5.28 (brs, 1 H, 2-OH); ^{13}C-NMR (151 MHz, DMSO-d_6): δ [ppm] = –5.6 (C-7), –5.4 (C-7), 17.9 (C-8), 23.7 (CH_3), 23.8 (CH_3), 25.6 (C-9), 26.3, 28.1 (C-11, C-12), 33.5 (SCH), 62.3 (C-6), 71.7 (C-2), 73.2 (C-4), 76.0 (C-5), 79.5 (C-3), 83.8 (C-1), 108.5 (C-10); R_f = 0.62 (PE/EtOAc 60:40); IR (atr-film): $\tilde{\nu}$ [cm^{-1}] = 3407, 2954, 2929, 2857, 1472, 1385, 1358, 1223, 1241, 1141, 1110, 1075, 1025, 962, 876, 836, 772, 714, 582, 532, 477; HRMS (ESI): m/z calculated for $C_{18}H_{37}O_5SSi^+$ $[M+H]^+$: 393.2125; found: 393.2121; m.p.: 45.3 °C; $[\alpha]_D^{20}$ = –15.5 (c = 1.0, $CHCl_3$)

S3.12 Synthesis of Isopropyl 2-*O*-[4-nitrophenyloxy(carbonyl)]-3,4-*O*-(1-methylethylidene)-6-*O*-(*tert*-butyldimethylsilyl)-1-thio-β-D-galactopyranoside (12)

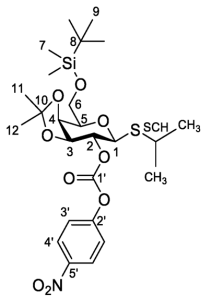

Carbohydrate **9** (1.00 g, 2.55 mmol) was dissolved in dry pyridine (20.0 mL) under nitrogen atmosphere. 4-nitrophenyl chloroformate (2.26 g, 11.2 mmol) was added portion wise and the reaction mixture was stirred for 20 h. The reaction mixture was diluted with CH_2Cl_2 and washed with water. The organic phase was dried with anhydrous $MgSO_4$ and concentrated under reduced pressure. The residue was purified by flash-column chromatography on SiO_2 (petroleum ether/ethyl acetate 85:15) to yield a white solid (1.23 g, 2.21 mmol, 87%). ^{1}H-NMR (600 MHz, $CDCl_3$): δ [ppm] = 0.08 (s, 6 H, 7-H), 0.89 (s, 9 H, 9-H), 1.33 (d, $^3J_{CH3,SCH}$ = 6.8 Hz, 3 H, CH_3), 1.33 (d, $^3J_{CH3,SCH}$ = 6.8 Hz, 3 H, CH_3), 1.36 (s, 3 H, 11-H or 12-H), 1.56 (s, 3 H, 11-H or 12-H), 3.21 (septet, $^3J_{SCH,CH3}$ = 6.8 Hz, 1 H, SCH), 3.81–3.93 (m, 3 H, 5-H, 6-H), 4.27 (dd, $^3J_{3,2}$ = 7.3 Hz, $^3J_{3,4}$ = 5.2 Hz, 1 H, 3-H), 4.32 (dd, $^3J_{4,3}$ = 5.2 Hz, $^3J_{4,5}$ = 1.4 Hz, 1 H, 4-H), 4.53 (d, $^3J_{1,2}$ = 10.4 Hz, 1 H, 1-H), 4.85 (dd, $^3J_{2,1}$ = 10.4 Hz, $^3J_{2,3}$ = 7.3 Hz, 1 H, 2-H), 7.37–7.45 (m, 2 H, 2′-H), 8.21–8.31 (m, 2 H, 3′-H); ^{13}C-NMR (151 MHz, $CDCl_3$): δ [ppm] = –5.4 (C-7), –5.2 (C-7), 18.4 (C-8), 24.1 (CH_3), 24.2 (CH_3), 25.9 (C-9), 26.5, 28.0 (C-11, C-12), 35.8 (SCH), 62.1 (C-6), 73.6 (C-4), 76.8 (C-3), 77.3 (C-5), 77.8 (C-2), 82.4 (C-1), 110.8 (C-10), 122.0 (C-2′), 125.4 (C-3′), 145.6 (C-4′), 152.1 (C-2′), 155.7 (C-1′); R_f = 0.73 (PE/EtOAc 70:30); IR (atr-film): $\tilde{\nu}$ [cm^{-1}] = 2954, 2929, 2853, 1768, 1617, 1594, 1519, 1492, 1464, 1374, 1345, 1307, 1247, 1215, 1164, 1117, 1072, 989, 957, 878, 836, 774, 751, 707, 674, 641, 573, 536, 499; HRMS (ESI): m/z calculated for $C_{25}H_{40}NO_9SSi^+$ $[M+H]^+$: 558.2188; found: 558.2186; m.p.: 135.0 °C; $[\alpha]_D^{20}$ = 48.8 (c = 1.0, $CHCl_3$)

S3.13 Synthesis of Isopropyl 6-*O*-(trityl)-1-thio-β-D-galactopyranoside (S7)

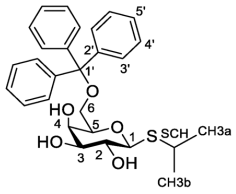

Carbohydrate **S7** was synthesized using a modified procedure of Du *et al.*[18] Isopropyl β-D-1-thiogalactopyranoside (**1a**) (5.00 g, 21.0 mmol) was dissolved in dry pyridine (5 mL) under nitrogen atmosphere. Trityl chloride (TrCl) (11.7 g, 42.0 mmol) and 4-dimethylaminopyridine (DMAP) (256 mg, 2.10 mmol) were added and the reaction mixture was stirred for 18 h at room temperature. The reaction mixture was diluted with ethyl acetate and subsequently washed with water (3×), saturated $NaHCO_3$ solution (1×) and saturated NaCl solution (1×). The organic phase was dried with anhydrous $MgSO_4$ and concentrated under reduced pressure. The residue was purified by flash-column chromatography on SiO_2 (petroleum ether/ethyl acetate 50:50) to yield a white solid (7.68 g, 16.0 mmol, 76%). ^{1}H-NMR (600 MHz, DMSO-d_6): δ [ppm] = 1.28 (d, $^3J_{CH3,SCH}$ = 6.8 Hz, 3 H, CH_3), 1.31 (d, $^3J_{CH3,SCH}$ = 6.8 Hz, 3 H, CH_3), 2.93 (dd, $^2J_{6a,6b}$ = 9.7 Hz, $^3J_{6a,5}$ = 3.7 Hz, 1 H, 6-H_a), 3.20–3.28 (m, 2 H, SCH, 6-H_b), 3.28–3.32 (m, 2 H, 2-H, 3-H), 3.56 (brs, 1 H, 4-H), 3.61 (dd, ^3J = 7.7 Hz, $^3J_{5,6a}$ = 3.7 Hz, 1 H, 5-H), 4.36–4.39 (m_c, 1 H, 1-H), 4.42 (d, $^3J_{4\text{-OH},4}$ = 4.5 Hz, 1 H, 4-OH), 4.82 (d, $^3J_{3\text{-OH},3}$ = 4.6 Hz, 1 H, 3-OH), 4.92 (d, $^3J_{2\text{-OH},2}$ = 5.2 Hz, 1 H, 2-OH), 7.25 (t, $^3J_{5',4'}$ = 7.2 Hz, 3 H, 5′-H), 7.32 (t, $^3J_{4',5'}$ = 7.6 Hz, 6 H, 4′-H), 7.41 (d, $^3J_{3',4'}$ = 7.4 Hz, 6 H, 3′-H); ^{13}C-NMR (151 MHz, DMSO-d_6): δ [ppm] = 23.7 (CH_3), 23.8 (CH_3), 33.6 (SCH), 64.0 (C-6), 69.3 (C-4), 69.8 (C-2), 74.5 (C-3), 77.6 (C-5), 84.8 (C-1), 85.7 (C-1′), 126.9 (C-5′), 127.8 (C-4′), 128.3 (C-3′), 143.9 (C-2′); R_f = 0.11 (PE/EtOAc 50:50); IR (atr-film): $\tilde{\nu}$ [cm^{-1}] = 3400, 3062, 2925, 2870, 1736, 1594, 1490, 1448, 1368, 1240, 1152, 1060, 1030, 899, 872, 833, 766, 746, 701, 650, 632, 584; HRMS (ESI): m/z calculated for $C_{28}H_{36}NO_5S^+$ $[M+NH_4]^+$: 498.2309; found: 498.2311; m.p.: 68.8 °C; $[\alpha]_D^{20}$ = –23.5 (c = 1.0, $CHCl_3$)

S3.14 Synthesis of Isopropyl 2,3,4-tri-*O*-(4-methoxybenzyl)-6-*O*-trityl-1-thio-β-D-galactopyranoside (S8)

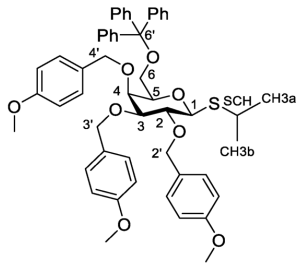

Carbohydrate **S8** was synthesized using modified procedures of Ruda *et al.*[19] Carbohydrate **S7** (100 mg, 208 µmol) and 4-methoxybenzyl chloride (PMB-Cl) (126 µL, 936 mmol) was dissolved in dry DMF (2.00 mL) under nitrogen atmosphere. The mixture was added dropwise over 30 min via a syringe pump to NaH (60%, 37.5 mg, 936 µmol) in dry DMF (2.00 mL) and was stirred for 18 h at room temperature. After completion, the reaction mixture was cooled to 0 °C and quenched by the addition of MeOH. Ethyl acetate was added, and the mixture was washed with water (3×) and saturated NaCl solution. The organic phase was dried with anhydrous $MgSO_4$ and concentrated under reduced pressure. The residue was purified by flash-column chromatography on SiO_2 (petroleum ether/ethyl acetate 90:10 to ethyl acetate/methanol 90:10) to yield a white solid (129 mg, 153 µmol, 74%). ^{1}H-NMR (600 MHz, DMSO-d_6): δ [ppm] = 1.27 (d, $^3J_{CH3,SCH}$ = 6.8 Hz, 3 H, CH_3), 1.30 (d, $^3J_{CH3,SCH}$ = 6.8 Hz, 3 H, CH_3), 2.82 (dd, $^2J_{6a,6b}$ = 9.5 Hz, $^3J_{6a,5}$ = 4.5 Hz, 1 H, 6-H_a), 3.17–3.28 (m, 2 H, 6-H_b, SCH), 3.40 (t, $^3J_{2,3}$ = 9.4 Hz, 1 H, 2-H), 3.63 (dd, $^3J_{3,2}$ = 9.4 Hz, $^3J_{3,4}$ = 2.9 Hz, 1 H, 3-H), 3.70–3.74 (m, 1 H, 5-H), 3.72 (s, 3 H, OCH_3), 3.73 (s, 3 H, OCH_3), 3.74 (s, 3 H, OCH_3), 3.88 (d, $^3J_{4,3}$ = 2.9 Hz, 1 H, 4-H), 4.23 (d, $^2J_{4'a,4'b}$ = 11.0 Hz, 1 H, 4-H_a), 4.53–4.62 (m, 5 H, 1-H, 2′-H, 3′-H_a, 4′-H_b), 4.67 (d, $^2J_{3'b,3'a}$ = 11.4 Hz, 1 H, 3′-H_b), 6.72–6.79 (m, 2 H, arom. H), 6.85–6.92 (m, 6 H, arom. H), 7.20–7.25 (m, 2 H, arom. H), 7.25–7.41 (m, 17 H, arom. H); ^{13}C-NMR (151 MHz, DMSO-d_6): δ [ppm] = 23.7 (CH_3), 23.7 (CH_3), 34.3 (SCH), 55.0 (OCH_3), 63.6 (C-6), 71.2 (C-3′), 73.3 (C-4′), 73.9 (C-4), 74.1 (C-2′), 76.7 (C-5), 77.8 (C-2), 82.8 (C-3), 83.3 (C-1), 85.9 (C-1′), 113.4 (arom. C), 113.6 (arom. C), 127.0 (arom. C), 127.9 (arom. C), 128.2 (arom. C), 129.3 (arom. C), 129.3 (arom. C), 129.4 (arom. C), 130.4 (arom. C), 130.5 (arom. C), 130.6 (arom. C), 143.7 (arom. C), 158.6 (arom. C), 158.7 (arom. C), 158.7 (arom. C); R_f = 0.05 (PE/EtOAc 90:10); IR (atr-film): $\tilde{\nu}$ [cm^{-1}] = 3038, 2931, 2835, 1612, 1586, 1512, 1449, 1360, 1302, 1245, 1173, 1152, 1078, 1031, 899, 820, 747, 705, 650, 632, 600, 515; HRMS (ESI): m/z calculated for $C_{52}H_{60}NO_8S^+$ $[M+NH_4]^+$: 858.4034; found: 858.4031; m.p.: 53.4 °C; $[\alpha]_D^{20}$ = 6.4 (c = 1.0, $CHCl_3$)

S3.15 Synthesis of Isopropyl 2,3,4-tri-*O*-(4-methoxybenzyl)-1-thio-β-D-galactopyranoside (10)

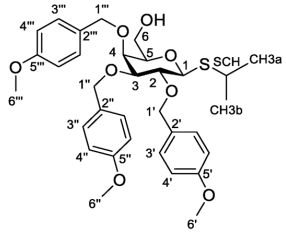

Carbohydrate **10** was synthesized using modified procedures of Ruda *et al*.[19] Carbohydrate **S8** (1.28 g, 1.52 mmol) was dissolved in dry CH_2Cl_2 (63 mL) under nitrogen atmosphere and cooled to 0 °C. Camphorsulfonic acid (CSA) (37.6 mg, 167 µmol) in methanol (6.3 mL) was added and the reaction mixture was allowed to warm to room temperature. The reaction mixture was stirred for 48 h. After completion, the solvent was evaporated under reduced pressure. The residue was purified by flash-column chromatography on SiO_2 (petroleum ether/ethyl acetate 70:30 to petroleum ether/ethyl acetate 30:70) to yield a white solid (662 mg, 1.11 mmol, 73%). The spectroscopic data are consistent with previously reported literature values.[20] ^{1}H-NMR (600 MHz, $CDCl_3$): δ [ppm] = 1.32 (d, $^3J_{CH3,SCH}$ = 6.8 Hz, 3 H, CH_3), 1.33 (d, $^3J_{CH3,SCH}$ = 6.8 Hz, 3 H, CH_3), 3.21 (septet, $^3J_{SCH,CH3}$ = 6.8 Hz, 1 H, SCH), 3.34–3.38 (m, 1 H, 5-H), 3.40 (ddd, $^2J_{6a,6b}$ = 11.1 Hz, $^3J_{6a,5}$ = 8.2 Hz, $^3J_{6a,6\text{-}OH}$ = 5.1 Hz, 1 H, 6-H_a), 3.53 (dd, $^3J_{3,2}$ = 9.3 Hz, $^3J_{3,4}$ = 2.8 Hz, 1 H, 3-H), 3.70–3.79 (m, 3 H, 2-H, 4-H, 6-H_b), 3.80 (s, 6 H, OCH_3), 3.82 (s, 3 H, OCH_3), 4.46 (d, $^3J_{1,2}$ = 9.7 Hz, 1 H, 1-H), 4.59 (d, $^2J_{1'''a,1'''b}$ = 11.7 Hz, 1 H, 1‴-H_a), 4.68 (d, $^2J_{1''a,1''b}$ = 11.4 Hz, 1 H, 1″-H_a), 4.71 (d, $^2J_{1'a,1'b}$ = 9.8 Hz, 1 H, 1′-H_a), 4.72 (d, $^2J_{1''b,1''a}$ = 11.4 Hz, 1 H, 1″-H_b), 4.82 (d, $^2J_{1'b,1'a}$ = 9.8 Hz, 1 H, 1′-H_b), 4.87 (d, $^2J_{1'''b,1'''a}$ = 11.7 Hz, 1 H, 1‴-H_b), 6.86 (d, $^3J_{4',3'}$ = 8.5 Hz, 2 H, 4′-H), 6.86 (d, $^3J_{4''',3'''}$ = 8.5 Hz, 2 H, 4‴-H), 6.89 (d, $^3J_{4'',3''}$ = 8.5 Hz, 2 H, 4″-H), 7.25 (d, $^3J_{3''',4'''}$ = 8.5 Hz, 2 H, 3‴-H), 7.31 (d, $^3J_{3'',4''}$ = 8.5 Hz, 2 H, 3″-H), 7.33 (d, $^3J_{3',4'}$ = 8.5 Hz, 2 H, 3′-H); ^{13}C-NMR (151 MHz, $CDCl_3$): δ [ppm] = 24.1 (CH_3), 35.4 (CH_3), 55.4 (SCH), 55.4, 55.4 (C-6′, C-6″, C-6‴), 62.4 (C-6), 72.6 (C-4), 73.0 (C-1″), 73.6 (C-1‴), 75.6 (C-1′), 78.6 (C-2), 78.7 (C-5), 84.1 (C-3), 85.2 (C-1), 113.8, 113.9, 114.0 (C-4′, C-4″, C-4‴), 129.4 (C-3″), 130.1 (C-3‴), 130.2 (C-3′), 130.5, 130.6, 130.7 (C-2′, C-2″, C-2‴), 159.4, 159.4, 159.5 (C-5′, C-5″, C-5‴).; R_f = 0.09 (PE/EtOAc 70:30); IR (atr-film): $\tilde{\nu}$ [cm^{-1}] = 3355, 2948, 2910, 2864, 2841, 1614, 1585, 1513, 1462, 1360, 1302, 1249, 1169, 1136, 1097, 1081, 1050, 1028, 996, 875, 819, 776, 700, 636, 603, 568, 515; HRMS (ESI): m/z calculated for $C_{33}H_{46}NO_8S^+$ $[M+NH_4]^+$: 616.2939; found: 616.2945; m.p.: 137.2 °C; $[\alpha]_D^{20}$ = –12.7 (c = 1.0, $CHCl_3$).

S3.16 Synthesis of {[7-(Diethylamino)-2-oxo-2*H*-chromen-4-yl]methyl}-(2,3,4-Tri-*O*-acetyl)-α-L-arabinopyranose (13)

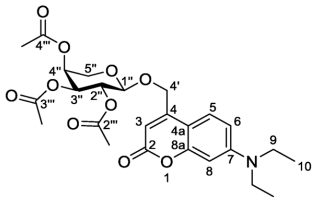

Coumarin **13** was synthesized using a modified procedure of Binder *et al.*[16] A Schlenk tube was charged with 500 mg molecular sieve (5 Å) and carbohydrate **8** (200 mg, 0.59 mmol) dissolved in dry CH_2Cl_2 (10 mL) under nitrogen atmosphere. A second Schlenk tube was charged with 500 mg molecular sieve (5 Å) and coumarin **3** (438 mg, 1.77 mmol) dissolved in dry CH_2Cl_2 (10 mL) under nitrogen atmosphere. After stirring for 1 h the dissolved carbohydrate **8** was added to the coumarin solution. Silver triflate (182 mg, 708 µmol) was added and the reaction was stirred for 21 h at room temperature in the dark. The reaction mixture was filtered over celite to remove the molecular sieve. The solvent was removed under reduced pressure and the residue was purified by flash-column chromatography on aluminium oxide (neutral) (petroleum ether/ethyl acetate 50:50) to yield a yellow solid (176 mg, 348 µmol, 59%). ^{1}H-NMR (600 MHz, $CDCl_3$): δ [ppm] = 1.18 (t, $^3J_{10,9}$ = 7.1 Hz, 6 H, 10-H), 2.00 (s, 3 H, CH_3), 2.04 (s, 3 H, CH_3), 2.13 (s, 3 H, CH_3), 3.39 (q, $^3J_{9,10}$ = 7.1 Hz, 4 H, 9-H), 3.65 (dd, $^2J_{5''a,5''b}$ = 12.8 Hz, $^3J_{5''a,4''}$ = 2.1 Hz, 1 H, 5″-H$_a$), 4.04 (dd, $^2J_{5''b,5''a}$ = 12.8 Hz, $^3J_{5''b,4''}$ = 4.0 Hz, 1 H, 5″-H$_b$), 4.58 (d, $^3J_{1'',2''}$ = 6.4 Hz, 1 H, 1″-H), 4.67 (dd, $^2J_{4'a,4'b}$ = 14.7 Hz, $^4J_{4'a,3}$ = 1.3 Hz, 1 H, 4′-H$_a$), 4.93 (dd, $^2J_{4'b,4'a}$ = 14.7 Hz, $^4J_{4'b,3}$ = 1.3 Hz, 1 H, 4′-H$_b$), 5.07 (dd, $^3J_{3'',2''}$ = 8.8 Hz, $^3J_{3'',4''}$ = 3.5 Hz, 1 H, 3″-H), 5.24 (dd, $^3J_{2'',3''}$ = 8.8 Hz, $^3J_{2'',1''}$ = 6.4 Hz, 1 H, 2″-H), 5.27 (ddd, $^3J_{4'',5''b}$ = 4.0 Hz, $^3J_{4'',3''}$ = 3.5 Hz, $^3J_{4'',5''a}$ = 2.1 Hz, 1 H, 4″-H), 6.17 (t, $^4J_{3,4'}$ = 1.3 Hz, 1 H, 3-H), 6.51 (d, $^4J_{8,6}$ = 2.6 Hz, 1 H, 8-H), 6.56 (dd, $^3J_{6,5}$ = 8.9 Hz, $^4J_{6,8}$ = 2.6 Hz, 1 H, 6-H), 7.27 (d, $^3J_{5,6}$ = 8.9 Hz, 1 H, 5-H); ^{13}C-NMR (151 MHz, $CDCl_3$): δ [ppm] = 12.5 (C-10), 20.8, 20.8, 21.0 (CH_3), 45.0 (C-9), 62.8 (C-5″), 65.9 (C-4′), 67.3 (C-4″), 69.1 (C-2″), 69.8 (C-3″), 98.1 (C-8), 99.6 (C-1″), 106.5 (C-4a), 107.1 (C-3), 108.8 (C-6), 124.8 (C-5), 150.5 (C-4), 150.6 (C-7), 156.4 (C-8a), 162.0 (C-2), 169.5 (C-2‴), 170.2 (C-3‴), 170.4 (C-4‴); R_f = 0.51 (PE/EtOAc 50:50); IR (atr-film): $\tilde{\nu}$ [cm^{-1}] = 2972, 1744, 1710, 1602, 1527, 1419, 1358, 1217, 1138, 1062, 1022, 601, 530; HRMS (ESI): m/z calculated for $C_{25}H_{32}NO_{10}^+$ $[M+NH_4]^+$: 506.2021; found: 506.2028; m.p.: 113.6 °C; $[\alpha]_D^{20}$ = 36.4 (c = 0.25, $CHCl_3$); UV-Vis (MeOH): λ_{max} (ε) = 246 nm (11206 dm^3 mol^{-1} cm^{-1}), 379 (16536).

S3.17 Synthesis of {[7-(Diethylamino)-2-oxo-2*H*-chromen-4-yl]methyl}-α-L-arabinopyranose (2b)

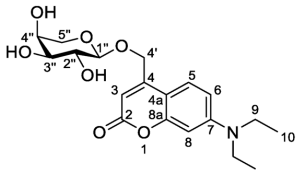

Photocaged arabinose **2b** was synthesized using modified procedures of Bier *et al*.[21] Coumarin **13** (135 mg, 267 µmol) was dissolved in MeOH (0.60 mL) and stirred at room temperature in the dark. Ammonia in MeOH (7 M, 230 µL, 1.61 mmol) was added and the reaction mixture was stirred until complete conversion. The solvent was evaporated under reduced pressure to yield a yellow solid (100 mg, 264 µmol, quant.). ^{1}H-NMR (600 MHz, Aceton-d_6): δ [ppm] = 1.20 (t, $^{3}J_{10,9}$ = 7.1 Hz, 6 H, 10-H), 3.50 (q, $^{3}J_{9,10}$ = 7.1 Hz, 4 H, 9-H), 3.59 (dd, $^{2}J_{5''a,5''b}$ = 12.4 Hz, $^{3}J_{5''a,4''}$ = 1.9 Hz, 1 H, 5″-H$_a$), 3.59–3.64 (m, 1 H, 3″-H), 3.68 (d, $^{3}J_{4''\text{-OH},4''}$ = 4.3 Hz, 1 H, 4″-OH), 3.71 (ddd, $^{3}J_{2'',3''}$ = 8.4 Hz, $^{3}J_{2'',1''}$ = 6.7 Hz, $^{3}J_{2'',2''\text{-OH}}$ = 4.1 Hz, 1 H, 2″-H), 3.82–3.86 (m, 1 H, 4″-H), 3.91 (dd, $^{2}J_{5''b,5''a}$ = 12.4 Hz, $^{3}J_{5''b,4''}$ = 3.3 Hz, 1 H, 5″-H$_b$), 3.98 (d, $^{3}J_{3''\text{-OH},3''}$ = 5.5 Hz, 1 H, 3″-OH), 4.41 (d, $^{3}J_{1'',2''}$ = 6.7 Hz, 1 H, 1″-H), 4.47 (d, $^{3}J_{2''\text{-OH},2''}$ = 4.1 Hz, 1 H, 2″-OH), 4.76 (dd, $^{2}J_{4'a,4'b}$ = 15.2 Hz, $^{4}J_{4'a,3}$ = 1.4 Hz, 1 H, 4′-H$_a$), 4.98 (dd, $^{2}J_{4'b,4'a}$ = 15.2 Hz, $^{4}J_{4'b,3}$ = 1.4 Hz, 1 H, 4′-H$_b$), 6.26 (t, $^{4}J_{3,4'}$ = 1.4 Hz, 1 H, 3-H), 6.49 (d, $^{4}J_{8,6}$ = 2.6 Hz, 1 H, 8-H), 6.69 (dd, $^{3}J_{6,5}$ = 9.0 Hz, $^{4}J_{6,8}$ = 2.6 Hz, 1 H, 6-H), 7.47 (d, $^{3}J_{5,6}$ = 9.0 Hz, 1 H, 5-H); ^{13}C-NMR (151 MHz, Aceton-d_6): δ [ppm] = 12.7 (C-10), 45.1 (C-9), 66.3 (C-5″), 66.4 (C-4′), 68.9 (C-4″), 72.3 (C-2″), 73.9 (C-3″), 98.0 (C-8), 104.1 (C-1″), 106.9 (C-3), 107.1 (C-4a), 109.4 (C-6), 126.0 (C-5), 151.5 (C-7), 152.9 (C-4), 157.2 (C-8a), 161.8 (C-2); R_f = 0.33 (PE/EtOAc 50:50); IR (atr-film): $\tilde{\nu}$ [cm^{-1}] = 3443, 2954, 2921, 2847, 1706, 1623, 1527, 1441, 1360, 1328, 1138, 1088, 1011, 855, 824, 794, 763, 610, 511; HRMS (ESI): m/z calculated for $C_{19}H_{26}NO_7^+$ [M+H]$^+$: 380.1704; found: 380.1697; m.p.: 129–130 °C; $[\alpha]_D^{20}$ = –18.6 (c = 0.5, MeOH); UV-Vis (MeOH): λ_{max} (ε) = 272 nm (60914 dm^3 mol^{-1} cm^{-1}), 388 (17236).

reversed-phase HPLC: t_R = 4.5 min; column: *HyperClone* 5 µ ODS (C18) 120 (*Phenomenex*); detection (UV): 388 nm; eluent: H_2O/MeOH 40:60; flowrate: 0.5 mL/min; column temperature: 25 °C; sample solvent: H_2O.

S3.18 Synthesis of [7-(Diethylamino)-2-oxo-2*H*-chromen-4-yl]methyl acetate (S9)

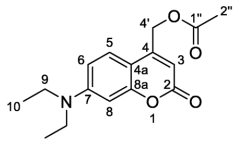

Coumarin **S9** was synthesized using a modified procedure of Gandioso *et al.*[22] Coumarin **3** (500 mg, 2.02 mmol) was dissolved in dry CH_2Cl_2 (35 mL) under nitrogen atmosphere. 4-Dimethylaminopyridine (DMAP) (299 mg, 2.43 mmol) and acetic acid (139 µL, 2.43 mmol) were added, and the reaction mixture was cooled to 0 °C. *N*,*N*′-Dicyclohexylcarbodiimide (DCC) (501 mg, 2.43 mmol) was added at 0 °C and the reaction mixture was stirred for 20 h in the dark. After filtration, the organic filtrate was washed with 1 M HCl and saturated $NaHCO_3$ solution. The organic phase was dried with anhydrous $MgSO_4$ and concentrated under reduced pressure. The residue was purified by flash-column chromatography on SiO_2 (CH_2Cl_2) to yield a red solid (518 mg, 1.79 mmol, 89%). The spectroscopic data are consistent with previously reported literature values.[22] ^{1}H-NMR (600 MHz, $CDCl_3$): δ [ppm] = 1.19 (t, $^3J_{10,9}$ = 7.1 Hz, 6 H, 10-H), 2.18 (s, 3 H, 2″-H), 3.40 (q, $^3J_{9,10}$ = 7.1 Hz, 4 H, 9-H), 5.20 (d, $^4J_{4',3}$ = 1.3 Hz, 2 H, 4′-H) 6.11 (t, $^4J_{3,4'}$ = 1.3 Hz, 1 H, 3-H), 6.50 (d, $^4J_{8,6}$ = 2.6 Hz, 1 H, 8-H), 6.56 (dd, $^3J_{6,5}$ = 9.0 Hz, $^4J_{6,8}$ = 2.6 Hz, 1 H, 6-H), 7.27 (d, $^3J_{5,6}$ = 9.0 Hz, 1 H, 5-H); ^{13}C-NMR (151 MHz, $CDCl_3$): δ [ppm] = 12.5 (C-10), 20.9 (C-2″), 44.9 (C-9), 61.4 (C-4′), 97.9 (C-8), 106.1 (C-4a), 106.5 (C-3), 108.8 (C-6), 124.5 (C-5), 149.5 (C-4), 150.8 (C-7), 156.4 (C-8a), 162.0 (C-2), 170.3 (C-1″); R_f = 0.57 (PE/EtOAc 50:50); IR (atr-film): $\tilde{\nu}$ [cm^{-1}] = 2974, 1748, 1706, 1597, 1527, 1440, 1415, 1376, 1337, 1272, 1240, 1196, 1140, 1074, 1013, 933, 841, 823, 811, 666, 598, 560; HRMS (ESI): m/z calculated for $C_{16}H_{20}NO_4^+$ $[M+H]^+$: 290.1387; found: 290.1389; m.p.: 108.3 °C.

S3.19 Synthesis of [7-(Diethylamino)-2-thioxo-2*H*-chromen-4-yl]methyl acetate (S10)

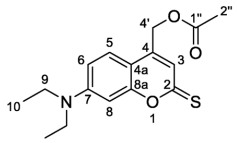

Coumarin **S10** was synthesized using a modified procedure of Gandioso *et al.*[22] Coumarin **S9** (2.00 g, 6.91 mmol) was dissolved in dry toluene (237 mL) under nitrogen atmosphere. Lawesson's reagent (1.82 g, 4.49 mmol) was added, and the reaction mixture was heated to reflux for 12 h in the dark. The solution was concentrated under reduced pressure. The residue was purified by flash-column chromatography on SiO_2 (CH_2Cl_2) to yield an orange solid (1.78 g, 5.83 mmol, 84%). The spectroscopic data are consistent with previously reported literature values.[22] ^{1}H-NMR (600 MHz, $CDCl_3$): δ [ppm] = 1.22 (t, $^3J_{10,9}$ = 7.1 Hz, 6 H, 10-H), 2.19 (s, 3 H, 2″-H), 3.43 (q, $^3J_{9,10}$ = 7.1 Hz, 4 H, 9-H), 5.18 (d, $^4J_{4',3}$ = 1.3 Hz, 2 H, 4′-H), 6.66 (dd, $^3J_{6,5}$ = 9.0 Hz, $^4J_{6,8}$ = 2.6 Hz, 1 H, 6-H), 6.68 (d, $^3J_{8,6}$ = 2.6 Hz, 1 H, 8-H), 7.06 (t, $^4J_{3,4'}$ = 1.3 Hz, 1 H, 3-H), 7.34 (d, $^3J_{5,6}$ = 9.0 Hz, 1 H, 5-H); ^{13}C-NMR (151 MHz, $CDCl_3$): δ [ppm] = 12.5 (C-10), 20.9 (C-2″) 45.1 (C-9), 61.1 (C-4′), 97.6 (C-8), 108.3 (C-4a), 110.4 (C-6), 120.7 (C-3), 124.6 (C-5), 142.0 (C-4), 151.2 (C-7), 159.1 (C-8a), 170.4 (C-1″), 197.3 (C-2); R_f = 0.60 (CH_2Cl_2); IR (atr-film): $\tilde{\nu}$ [cm^{-1}] = 2971, 1743, 1625, 1574, 1516, 1432, 1399, 1376, 1354, 1290, 1250, 1217, 1197, 1180, 1147, 1071, 1029, 967, 855, 822, 795, 652; HRMS (ESI): m/z calculated for $C_{16}H_{20}NO_3S^+$ $[M+H]^+$: 306.1158; found: 306.1160; m.p.: 137.9 °C

S3.20 Synthesis of [2-(Dicyanomethylene)-7-(diethylamino)-2*H*-chromen-4-yl]methyl acetate (S11)

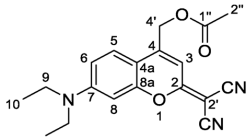

Coumarin **S11** was synthesized using a procedure of Gandioso *et al.*[22] Coumarin **S10** (1.00 g, 3.27 mmol) was dissolved in dry MeCN (100 mL) under nitrogen atmosphere. After addition of malononitrile (1.09 g, 16.5 mmol) and triethylamine (NEt_3) (9.13 mL, 65.5 mmol), the reaction mixture was stirred for 20 min at room temperature in the dark. The reaction mixture became intensely red. Silver nitrate (1.12 g, 6.58 mmol) was added and the reaction mixture was stirred for additional 4 h at room temperature in the dark. The reaction mixture was filtered and concentrated under reduced pressure. The residue was purified by flash-column chromatography on SiO_2 (CH_2Cl_2) to yield an orange-red solid (616 mg, 1.83 mmol, 56%). The spectroscopic data are consistent with previously reported literature values.[22] ^{1}H-NMR (600 MHz, $CDCl_3$): δ [ppm] = 1.24 (t, $^3J_{10,9}$ = 7.1 Hz, 6 H, 10-H), 2.21 (s, 3 H, 2″-H), 3.45 (q, $^3J_{9,10}$ = 7.1 Hz, 4 H, 9-H), 5.24 (d, $^4J_{4',3}$ = 1.2 Hz, 2 H, 4′-H), 6.62 (d, $^3J_{8,6}$ = 2.6 Hz, 1 H, 8-H), 6.70 (dd, $^3J_{6,5}$ = 9.0 Hz, $^4J_{6,8}$ = 2.6 Hz, 1 H, 6-H), 6.75 (t, $^4J_{3,4'}$ = 1.2 Hz, 1 H, 3-H), 7.34 (d, $^3J_{5,6}$ = 9.0 Hz, 1 H, 5-H); ^{13}C-NMR (151 MHz, $CDCl_3$): δ [ppm] = 12.5 (C-10), 20.9 (C-2″), 45.3 (C-9), 55.9 (C-2′), 61.2 (C-4′), 97.9 (C-8), 106.2 (C-3), 107.4 (C-4a), 111.1 (C-6), 113.9 (CN), 114.6 (CN), 125.0 (C-5), 146.1 (C-4), 151.6 (C-7), 155.1 (C-8a), 170.3 (C-1″), 171.9 (C-2); R_f = 0.48 (PE/EtOAc 70:30); IR (atr-film): $\tilde{\nu}$ [cm^{-1}] = 2969, 2924, 2215, 1750, 1638, 1586, 1524, 1430, 1358, 1320, 1259, 1224, 1148, 1079, 816, 687; HRMS (ESI): m/z calculated for $C_{19}H_{20}N_3O_3^+$ $[M+H]^+$: 338.1499; found: 338.1495; m.p.: 202–203 °C.

S3.21 Synthesis of 2-(Dicyanomethylene)-7-(diethylamino)-4-(hydroxymethyl)-2*H*-chromen (4)

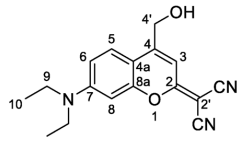

Coumarin **4** was synthesized using a procedure of Fournier *et al.*[23] Coumarin **S11** (500 mg, 1.48 mmol) was dissolved in dry EtOH (316 mL) under nitrogen atmosphere. After addition of HCl in EtOH (1.25 M, 2.96 mL, 3.71 mmol), the reaction mixture was heated to reflux for 15 h in the dark. Then, the reaction mixture was concentrated under reduced pressure. The residue was purified by flash-column chromatography on SiO_2 (dichloromethane/acetone 95:5) to yield an orange-red solid (403 mg, 1.36 mmol, 92%). The spectroscopic data are consistent with previously reported literature values.[23] ^{1}H-NMR (600 MHz, $CDCl_3$): δ [ppm] = 1.24 (t, $^3J_{10,9}$ = 7.1 Hz, 6 H, 10-H), 3.45 (q, $^3J_{9,10}$ = 7.1 Hz, 4 H, 9-H), 4.89 (s, 2 H, 4′-H), 6.63 (d, $^3J_{8,6}$ = 2.6 Hz, 1 H, 8-H), 6.71 (dd, $^3J_{6,5}$ = 9.0 Hz, $^4J_{6,8}$ = 2.6 Hz, 1 H, 6-H), 6.98 (s, 1 H, 3-H), 7.36 (d, $^3J_{5,6}$ = 9.0 Hz, 1 H, 5-H); ^{13}C-NMR (151 MHz, $CDCl_3$): δ [ppm] = 12.6 (C-10), 45.4 (C-9), 54.9 (C-2′), 60.8 (C-4′), 97.8 (C-8), 105.4 (C-3), 107.7 (C-4a), 111.2 (C-6), 114.2 (CN), 115.0 (CN), 125.0 (C-5), 151.4 (C-4), 151.6 (C-7), 154.9 (C-8a), 172.3 (C-2); R_f = 0.44 (CH_2Cl_2/acetone 95:5); IR (atr-film): $\tilde{\nu}$ [cm^{-1}] = 3431, 2972, 2918, 2199, 1741, 1634, 1575, 1504, 1418, 1355, 1319, 1254, 1189, 1144, 1085, 821, 686, 508; MS (ESI, positive ion): m/z (%) = 296.3 (100) $[M+H]^+$; m.p.: 179–180 °C

S3.22 Synthesis of [2-(Dicyanomethylene)-7-(diethylamino)-2*H*-chromen-4-yl]methyl (4-nitrophenyl) carbonate (6)

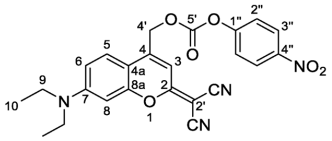

Coumarin **6** was synthesized using modified procedures of Gao *et al.*[9] and Fomina *et al.*[10] Coumarin **4** (250 mg, 846 µmol) was dissolved in dry CH_2Cl_2 (15.0 mL) under nitrogen atmosphere. *N*,*N*-Diisopropylethylamine (DIPEA) (295 µL, 1.69 mmol) was added and the reaction mixture was stirred for 15 min before 4-nitrophenyl chloroformate (341 mg, 1.69 mmol) was added portion wise. The reaction mixture was stirred for 22 h and diluted with CH_2Cl_2. It was washed with 1 M HCl (1×) and saturated $NaHCO_3$ solution (3×). The organic phase was dried with anhydrous $MgSO_4$ and concentrated under reduced pressure. The residue was purified by flash-column chromatography on SiO_2 (petroleum ether/ethyl acetate 70:30) to yield a red solid (179 mg, 389 µmol, 46%). ^{1}H-NMR (600 MHz, $CDCl_3$): δ [ppm] = 1.25 (t, $^3J_{10,9}$ = 7.1 Hz, 6 H, 10-H), 3.46 (q, $^3J_{9,10}$ = 7.1 Hz, 4 H, 9-H), 5.42 (s, 2 H, 4′-H), 6.61 (d, $^3J_{8,6}$ = 2.5 Hz, 1 H, 8-H), 6.69 (dd, $^3J_{6,5}$ = 9.0 Hz, $^4J_{6,8}$ = 2.5 Hz, 1 H, 6-H), 6.80 (s, 1 H, 3-H), 7.35 (d, $^3J_{5,6}$ = 9.0 Hz, 1 H, 5-H), 7.43 (m_c, 2 H, 2″-H), 8.31 (m_c, 2 H, 3″-H); ^{13}C-NMR (151 MHz, $CDCl_3$): δ [ppm] = 12.6 (C-10), 45.2 (C-9), 56.5 (C-2′), 65.5 (C-4′), 97.6 (C-8), 106.3 (C-3), 106.7 (C-4a), 110.9 (C-6), 113.7 (CN), 114.5 (CN), 121.9 (C-2″), 124.9 (C-5), 125.6 (C-3″), 144.2 (C-4), 145.9 (C-4″), 152.0 (C-7), 152.2 (C-5′), 155.2, 155.2 (C-8a, C-1″), 171.7 (C-2); R_f = 0.28 (PE/EtOAc 60:40); IR (atr-film): $\tilde{\nu}$ [cm^{-1}] = 2215, 1774, 1638, 1584, 1548, 1523, 1489, 1432, 1350, 1321, 1259, 1216, 1148, 1083, 860; HRMS (ESI): m/z calculated for $C_{24}H_{21}N_4O_6^+$ $[M+H]^+$: 461.1456; found: 461.1457; m.p.: 209–211 °C

S3.23 Synthesis of Isopropyl 2-*O*-{[(dicyanomethylene)-7-(diethylamino)-2*H*-chromen-4-yl]methyloxy(carbonyl)}-3,4-*O*-(1-methylethylidene)-6-*O*-(*tert*-butyldimethylsilyl)-1-thio-β-D-galactopyranoside (13)

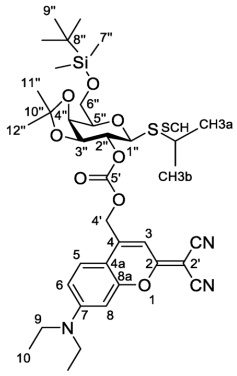

Coumarin **13** was synthesized using modified procedures of Suzuki *et al.*[24] Coumarin **6** (0.12 g, 0.25 mmol) was dissolved in dry CH_2Cl_2 (4.0 mL) under nitrogen atmosphere. After the addition of 4-dimethylaminopyridine (DMAP) (31 mg, 0.26 mmol) and carbohydrate **9** (90 mg, 0.23 mmol) the reaction mixture was stirred for 20 h at room temperature in the dark. Then, it was diluted with CH_2Cl_2, washed with saturated $NaHCO_3$ and saturated NaCl solution. The organic phase was dried with anhydrous $MgSO_4$ and concentrated under reduced pressure. The residue was purified by flash-column chromatography on SiO_2 (petroleum ether/ethyl acetate 80:20) to yield a red solid (0.15 g, 0.22 mmol, 96%). ^{1}H-NMR (600 MHz, $CDCl_3$): δ [ppm] = 0.07 (s, 3 H, 7″-H), 0.07 (s, 3 H, 7″-H), 0.89 (s, 9 H, 9″-H), 1.23 (t, $^3J_{10,9}$ = 7.1 Hz, 6 H, 10-H), 1.29 (d, $^3J_{CH3,SCH}$ = 6.8 Hz, 3 H, CH_3), 1.30 (d, $^3J_{CH3,SCH}$ = 6.8 Hz, 3 H, CH_3), 1.35 (s, 3 H, 11″-H or 12″-H), 1.55 (s, 3 H, 11″-H or 12″-H), 3.19 (septet, $^3J_{SCH,CH3}$ = 6.8 Hz, 1 H, SCH), 3.44 (q, $^3J_{9,10}$ = 7.1 Hz, 4 H, 9-H), 3.80–3.89 (m, $^3J_{5'',4''}$ = 5.6 Hz, 3 H, 5″-H, 6″-H), 4.23 (dd, $^3J_{3'',2''}$ = 7.3 Hz, $^3J_{3'',4''}$ = 5.3 Hz, 1 H, 3″-H), 4.29 (dd, $^3J_{4'',3''}$ = 5.3 Hz, $^3J_{4'',5''}$ = 1.9 Hz, 1 H, 4″-H), 4.49 (d, $^3J_{1'',2''}$ = 10.4 Hz, 1 H, 1″-H), 4.79 (dd, $^3J_{2'',1''}$ = 10.4 Hz, $^3J_{2'',3''}$ = 7.3 Hz, 1 H, 2″-H), 5.25 (dd, $^3J_{4'a,\,4'b}$ = 15.5 Hz, $^4J_{4'a,3}$ = 1.2 Hz, 1 H, 4′-H_a), 5.39 (dd, $^3J_{4'b,\,4'a}$ = 15.5 Hz, $^4J_{4'b,3}$ = 1.2 Hz, 1 H, 4′-H_b), 6.58 (d, $^4J_{8,6}$ = 2.6 Hz, 1 H, 8-H), 6.64 (dd, $^3J_{6,5}$ = 9.1 Hz, $^4J_{6,8}$ = 2.6 Hz, 1 H, 6-H), 6.81 (m_c, 1 H, 3-H), 7.29 (d, $^3J_{5,6}$ = 9.1 Hz, 1 H, 5-H); ^{13}C-NMR (151 MHz, $CDCl_3$): δ [ppm] = –5.4 (C-7″), –5.3 (C-7″), 12.6 (C-10), 18.3 (C-8″), 24.0 (CH_3), 24.1 (CH_3), 25.9 (C-9″), 26.5, 28.0 (C-11″, C-12″), 35.8 (SCH), 45.1 (C-9), 55.9 (C-2′), 62.1 (C-6″), 64.7 (C-4′), 73.6 (C-4″), 77.0 (C-3″), 77.2 (C-5″), 77.3 (C-2″), 82.4 (C-1″), 97.5 (C-8), 106.0 (C-3), 106.8 (C-4a), 110.6 (C-10″), 110.8 (C-6), 114.0 (CN), 114.5 (CN), 124.9 (C-5), 145.4 (C-4), 151.8 (C-7), 154.2 (C-5′), 155.0 (C-8a), 171.9 (C-2); R_f = 0.24 (PE/EtOAc 80:20); IR (atr-film): $\tilde{\nu}$ [cm^{-1}] = 2955, 2929, 2859, 2216, 1756, 1639, 1586, 1548, 1525, 1432, 1383, 1356, 1319, 1257, 1223, 1196, 1148, 1111, 1078, 1047, 983, 871, 839, 760; HRMS (ESI): m/z calculated for $C_{36}H_{52}N_3O_8SSi^+$ $[M+H]^+$: 714.3239; found: 714.3237; m.p.: 79–81 °C; $[\alpha]_D^{20}$ = –18.0 (c = 0.1, $CHCl_3$).

S3.24 Synthesis of Isopropyl 2-*O*-{[(dicyanomethylene)-7-(diethylamino)-2*H*-chromen-4-yl]methyloxy(carbonyl)}-1-thio-β-D-galactopyranoside (1c)

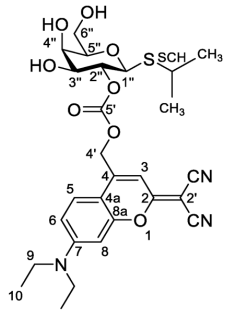

Photocaged IPTG **1c** was synthesized using modified procedures of Suzuki *et al.*[24] Coumarin **13** (0.10 g, 0.14 mmol) was dissolved in CH_2Cl_2 (1.0 mL) and cooled to 0 °C. After the addition of trifluoroacetic acid (TFA) (1.0 mL, 13 mmol) and water (40 µL, 2.2 mmol), the reaction mixture was stirred for 10 min at 0 °C in the dark. Then the reaction mixture was concentrated under reduced pressure. The residue was purified by flash-column chromatography on SiO_2 (ethyl acetate) to yield a red solid (72 mg, 0.13 mmol, 92%). ^{1}H-NMR (600 MHz, Aceton-d_6): δ [ppm] = 1.18–1.28 (m, 12 H, 10-H, CH_3), 3.20 (septet, $^3J_{SCH,CH3}$ = 6.8 Hz, 1 H, SCH), 3.59 (q, $^3J_{9,10}$ = 7.1 Hz, 4 H, 9-H), 3.67 (t, $^3J_{5'',4''}$ = 5.6 Hz, 1 H, 5″-H), 3.77 (m, 2 H, 6″-H), 3.86 (dd, $^3J_{3'',2''}$ = 9.3 Hz, $^3J_{3'',4''}$ = 3.4 Hz, 1 H, 3″-H), 4.10 (d, $^3J_{4'',3''}$ = 3.4 Hz, 1 H, 4″-H), 4.65 (d, $^3J_{1'',2''}$ = 10.1 Hz, 1 H, 1″-H), 4.88 (dd, $^3J_{2'',1''}$ = 10.1 Hz, $^3J_{2'',3''}$ = 9.3 Hz, 1 H, 2″-H), 5.43 (d, $^3J_{4'a,\,4'b}$ = 15.5 Hz, 1 H, 4′-H_a), 5.53 (d, $^3J_{4'b,\,4'a}$ = 15.5 Hz, 1 H, 4′-H_b), 6.74–6.79 (m, 2 H, 3-H, 8-H), 6.91 (dd, $^3J_{6,5}$ = 9.1 Hz, $^4J_{6,8}$ = 2.6 Hz, 1 H, 6-H), 7.63 (d, $^3J_{5,6}$ = 9.1 Hz, 1 H, 5-H); ^{13}C-NMR (151 MHz, Aceton-d_6): δ [ppm] = 12.7 (C-10), 24.2 (CH_3), 24.6 (CH_3), 35.5 (SCH), 45.5 (C-9), 55.1 (C-2′), 62.3 (C-6″), 65.4 (C-4′), 70.4 (C-4″), 73.4 (C-3″), 77.3 (C-2″), 79.8 (C-5″), 83.5 (C-1″), 97.6 (C-8), 106.0 (C-3), 107.7 (C-4a), 111.9 (C-6), 114.3 (CN), 115.2 (CN), 126.8 (C-5), 147.9 (C-4), 153.0 (C-7), 155.1 (C-5′), 155.9 (C-8a), 172.6 (C-2); R_f = 0.23 (EtOAc); IR (atr-film): $\tilde{\nu}$ [cm^{-1}] = 3359, 2954, 2924, 2855, 2216, 1748, 1672, 1638, 1584, 1522, 1433, 1381, 1320, 1258, 1193, 1139, 1076, 1053, 984, 800, 725; HRMS (ESI): m/z calculated for $C_{27}H_{34}N_3O_8S^+$ $[M+NH_4]^+$: 560.2061; found: 560.2055; m.p.: 153.8 °C; $[\alpha]_D^{20}$ = 74 (c = 0.1, $CHCl_3$); UV-Vis [Tris buffer (20 mM, pH 7.5)/MeCN 1:1]: λ_{max} (ε) = 252 nm (18618 dm^3 mol^{-1} cm^{-1}), 276 (14338), 488 (18938).

reversed-phase HPLC: t_R = 14.6 min; column: *HyperClone* 5 µ ODS (C18) 120 (*Phenomenex*); detection (UV): 488 nm; eluent: H_2O/MeOH 40:60; flowrate: 0.5 mL/min; column temperature: 25 °C; sample solvent: Tris buffer (20 mM, pH 7.5)/MeCN 1:1.

S3.25 Synthesis of Isopropyl 2-*O*-{[7-(diethylamino)-2-oxo-2*H*-chromen-4-yl]methyloxy(carbonyl)}-3,4-*O*-(1-methylethylidene)-6-*O*-(*tert*-butyldimethylsilyl)-1-thio-β-D-galactopyranoside (14)

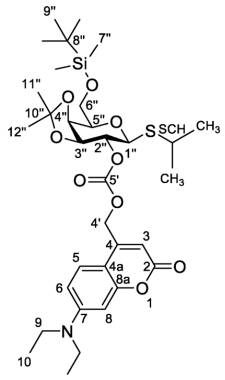

Coumarin **14** was synthesized using modified procedures of Suzuki *et al.*[24] Coumarin **5** (98 mg, 0.24 mmol) was dissolved in dry CH_2Cl_2 (2 mL) under nitrogen atmosphere. After the addition of 4-dimethylaminopyridine (DMAP) (30 mg, 0.24 mmol) and carbohydrate **9** (85 mg, 0.22 mmol) the reaction mixture was stirred for 20 h at room temperature in the dark. Then, it was diluted with CH_2Cl_2, washed with saturated $NaHCO_3$ and saturated NaCl solution. The organic phase was dried with anhydrous $MgSO_4$ and concentrated under reduced pressure. The residue was purified by flash-column chromatography on SiO_2 (petroleum ether/ethyl acetate 80:20) to yield a yellow solid (0.11 g, 0.17 mmol, 77%). ^{1}H-NMR (600 MHz, $CDCl_3$): δ [ppm] = 0.06 (s, 3 H, 7″-H), 0.07 (s, 3 H, 7″-H), 0.89 (s, 9 H, 9″-H), 1.19 (t, $^3J_{10,9}$ = 7.1 Hz, 6 H, 10-H), 1.29 (d, $^3J_{CH3,SCH}$ = 6.8 Hz, 3 H, CH_3), 1.30 (d, $^3J_{CH3,SCH}$ = 6.8 Hz, 3 H, CH_3), 1.35 (s, 3 H, 11″-H or 12″-H), 1.56 (s, 3 H, 11″-H or 12″-H), 3.17 (septet, $^3J_{SCH,CH3}$ = 6.8 Hz, 1 H, SCH), 3.40 (q, $^3J_{9,10}$ = 7.1 Hz, 4 H, 9-H), 3.79–3.91 (m, 3 H, 5″-H, 6″-H), 4.22 (dd, $^3J_{3'',2''}$ = 7.3 Hz, $^3J_{3'',4''}$ = 5.3 Hz, 1 H, 3″-H), 4.29 (d, $^3J_{4'',3''}$ = 5.2 Hz, $^3J_{4'',5''}$ = 1.9 Hz, 1 H, 4″-H), 4.48 (d, $^3J_{1'',2''}$ = 10.4 Hz, 1 H, 1″-H), 4.80 (dd, $^3J_{2'',1''}$ = 10.4 Hz, $^3J_{2'',3''}$ = 7.3 Hz, 1 H, 2″-H), 5.23 (d, $^3J_{4'a,\,4'b}$ = 14.9 Hz, 1 H, 4′-H_a), 5.38 (d, $^3J_{4'b,\,4'a}$ = 14.9 Hz, 1 H, 4′-H_b), 6.21 (s, 1 H, 3-H), 6.50 (d, $^4J_{8,6}$ = 2.6 Hz, 1 H, 8-H), 6.56 (dd, $^3J_{6,5}$ = 9.0 Hz, $^4J_{6,8}$ = 2.6 Hz, 1 H, 6-H), 7.25 (d, $^3J_{5,6}$ = 9.0 Hz, 1 H, 5-H); ^{13}C-NMR (151 MHz, $CDCl_3$): δ [ppm] = –5.4 (C-7″), –5.3 (C-7″), 12.5 (C-10), 18.3 (C-8″), 24.0 (CH_3), 24.1 (CH_3), 25.9 (C-9″), 26.5, 28.0 (C-11″, C-12″), 35.7 (SCH), 44.9 (C-9), 62.1 (C-6″), 65.0 (C-4′), 73.5 (C-4″), 76.9 (C-3″), 77.1 (C-5″), 77.1 (C-2″), 82.5 (C-1″), 98.0 (C-8), 106.0 (C-4a), 106.7 (C-3), 108.8 (C-6), 110.6 (C-10″), 124.4 (C-5), 148.7 (C-4), 150.7 (C-7), 154.3 (C-5′), 156.4 (C-8a), 162.0 (C-2); R_f = 0.24 (PE/EtOAc 80:20); IR (atr-film): $\tilde{\nu}$ [cm^{-1}] = 2969, 2931, 2870, 1745, 1713, 1603, 1527, 1420, 1356, 1336, 1217, 1139, 1094, 1064, 1023, 841, 751, 667, 601, 510; HRMS (ESI): m/z calculated for $C_{33}H_{52}NO_9SSi^+$ $[M+H]^+$: 666.3127; found: 666.3124; m.p.: 69 °C; $[\alpha]_D^{20}$ = 16 (c = 0.1, $CHCl_3$).

S3.26 Synthesis of Isopropyl 2-*O*-{[7-(diethylamino)-2-oxo-2*H*-chromen-4-yl]methyloxy(carbonyl)}-1-thio-β-D-galactopyranoside (1b)

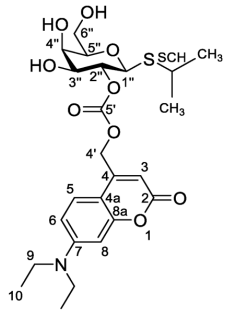

Photocaged IPTG **1b** was synthesized using modified procedures of Suzuki *et al.*[24] Coumarin **14** (159 mg, 238 µmol) was dissolved in CH_2Cl_2 (1 mL) and cooled to 0 °C. After the addition of trifluoroacetic acid (TFA) (1.70 mL, 22.2 mmol) and water (68.8 µL, 3.82 mmol), the reaction mixture was stirred for 10 min at 0 °C in the dark. Then the reaction mixture was concentrated under reduced pressure. The residue was purified by flash-column chromatography on SiO_2 (ethyl acetate) to yield a yellow solid (117 mg, 229 µmol, 96%). ^{1}H-NMR (600 MHz, Aceton-d_6): δ [ppm] = 1.21 (t, $^3J_{10,9}$ = 7.1 Hz, 6 H, 10-H), 1.25 (d, $^3J_{CH3,SCH}$ = 6.7 Hz, 3 H, CH_3), 1.29 (d, $^3J_{CH3,SCH}$ = 6.7 Hz, 3 H, CH_3), 3.21 (septet, $^3J_{SCH,CH3}$ = 6.7 Hz, 1 H, SCH), 3.51 (q, $^3J_{9,10}$ = 7.1 Hz, 4 H, 9-H), 3.67 (t, $^3J_{5'',4''}$ = 5.6 Hz, 1 H, 5″-H), 3.77 (m, 2 H, 6″-H), 3.84 (dd, $^3J_{3'',2''}$ = 9.3 Hz, $^3J_{3'',4''}$ = 3.4 Hz, 1 H, 3″-H), 4.08 (d, $^3J_{4'',3''}$ = 3.4 Hz, 1 H, 4″-H), 4.65 (d, $^3J_{1'',2''}$ = 10.1 Hz, 1 H, 1″-H), 4.87 (dd, $^3J_{2'',1''}$ = 10.1 Hz, $^3J_{2'',3''}$ = 9.3 Hz, 1 H, 2″-H), 5.33 (d, $^3J_{4'a,4'b}$ = 15.2 Hz, 1 H, 4′-H_a), 5.45 (d, $^3J_{4'b,4'a}$ = 15.2 Hz, 1 H, 4′-H_b), 6.09 (s, 1 H, 3-H), 6.52 (d, $^4J_{8,6}$ = 2.6 Hz, 1 H, 8-H), 6.72 (dd, $^3J_{6,5}$ = 9.0 Hz, $^4J_{6,8}$ = 2.6 Hz, 1 H, 6-H), 7.48 (d, $^3J_{5,6}$ = 9.0 Hz, 1 H, 5-H); ^{13}C-NMR (151 MHz, Aceton-d_6): δ [ppm] = 12.7 (C-10), 24.2 (CH_3), 24.6 (CH_3), 35.6 (SCH), 45.2 (C-9), 62.3 (C-6″), 65.4 (C-4′), 70.4 (C-4″), 73.5 (C-3″), 77.0 (C-2″), 79.9 (C-5″), 83.8 (C-1″), 98.1 (C-8), 106.5 (C-4a), 106.7 (C-3), 109.5 (C-6), 125.9 (C-5), 150.5 (C-4), 151.8 (C-7), 155.4 (C-5′), 157.3 (C-8a), 161.4 (C-2); R_f = 0.24 (EtOAc); IR (atr-film): $\tilde{\nu}$ [cm^{-1}] = 3405, 2962, 2925, 2862, 1755, 1679, 1603, 1528, 1424, 1357, 1255, 1200, 1139, 1054, 984, 800, 725; HRMS (ESI): m/z calculated for $C_{24}H_{34}NO_9S^+$ [M+H]$^+$: 512.1949; found: 512.1952; m.p.: 96.0 °C; $[\alpha]_D^{20}$ = 28 (c = 0.1, $CHCl_3$); UV-Vis [Tris buffer (20 mM, pH 7.5)/MeCN 1:1]: λ_{max} (ε) = 246 nm (21496 dm^3 mol^{-1} cm^{-1}), 386 (24984).

reversed-phase HPLC: t_R = 9.8 min; column: *HyperClone* 5 µ ODS (C18) 120 (*Phenomenex*); detection (UV): 392 nm; eluent: H_2O/MeOH 40:60; flowrate: 0.5 mL/min; column temperature: 25 °C; sample solvent: Tris buffer (20 mM, pH 7.5)/MeCN 1:1.

S3.27 Synthesis of Isopropyl 2,3,4-tri-*O*-(4-methoxybenzyl) 6-*O*-{[7-(diethylamino)-2-oxo-2*H*-chromen-4-yl]methyloxy(carbonyl)}-1-thio-β-D-galactopyranoside (16)

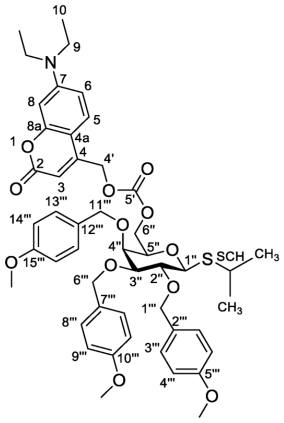

Coumarin **16** was synthesized using modified procedures of Suzuki *et al.*[24] Coumarin **5** (60 mg, 0.15 mmol) was dissolved in dry CH_2Cl_2 (2.0 mL) under nitrogen atmosphere. After the addition of 4-dimethylaminopyridine (DMAP) (20 mg, 0.16 mmol) and carbohydrate **10** (96 mg, 0.16 mmol) the reaction mixture was stirred for 20 h at room temperature in the dark. Then, it was diluted with CH_2Cl_2, washed with saturated $NaHCO_3$ and saturated NaCl solution. The organic phase was dried with anhydrous $MgSO_4$ and concentrated under reduced pressure. The residue was purified by flash-column chromatography on SiO_2 (petroleum ether/ethyl acetate 60:40) to yield a yellow solid (84 mg, 0.10 mmol, 66%). ^{1}H-NMR (600 MHz, $CDCl_3$): δ [ppm] = 1.20 (t, $^3J_{10,9}$ = 7.1 Hz, 6 H, 10-H), 1.31 (d, $^3J_{CH3,SCH}$ = 6.8 Hz, 6 H, CH_3), 3.20 (septet, $^3J_{SCH,CH3}$ = 6.8 Hz, 1 H, SCH), 3.41 (q, $^3J_{9,10}$ = 7.1 Hz, 4 H, 9-H), 3.52–3.58 (m, 2 H, 3″-H, 5″-H), 3.74–3.84 (m, 11 H, 2″-H, 4″-H, OCH_3), 4.03 (dd, $^2J_{6''a,6''b}$ = 10.9 Hz, $^3J_{6''a,5''}$ = 5.9 Hz, 1 H, 6″-H_a), 4.29 (dd, $^2J_{6''b,6''a}$ = 10.9 Hz, $^3J_{6''b,5''}$ = 6.6 Hz, 1 H, 6″-H_b), 4.47 (d, $^3J_{1,2}$ = 9.7 Hz, 1 H, 1-H), 4.58 (d, $^2J_{11'''a,11'''b}$ = 11.5 Hz, 1 H, 11‴-H_a), 4.67–4.74 (m, 3 H, 1‴-H_a, 6‴-H), 4.81 (d, $^2J_{1'''b,1'''a}$ = 9.8 Hz, 1 H, 1‴-H_b), 4.90 (d, $^2J_{11'''b,11'''a}$ = 11.5 Hz, 1 H, 11‴-H_b), 5.21 (m_c, 2 H, 4′-H), 6.12 (t, $^4J_{3,4'}$ = 1.3 Hz, 1 H, 3-H), 6.51 (d, $^4J_{8,6}$ = 2.6 Hz, 1 H, 8-H), 6.57 (dd, $^3J_{6,5}$ = 9.0 Hz, $^4J_{6,8}$ = 2.6 Hz, 1 H, 6-H), 6.84 (d, $^3J_{14''',13'''}$ = 8.5 Hz, 2 H, 14‴-H), 6.86 (d, $^3J_{4''',3'''}$ = 8.5 Hz, 2 H, 4‴-H), 6.89 (d, $^3J_{9''',8'''}$ = 8.5 Hz, 2 H, 9‴-H), 7.24 (d, $^3J_{13''',14'''}$ = 8.5 Hz, 2 H, 13‴-H), 7.26 (d, $^3J_{5,6}$ = 9.0 Hz, 1 H, 5-H), 7.31 (d, $^3J_{8''',9'''}$ = 8.5 Hz, 2 H, 8‴-H), 7.32 (d, $^3J_{3''',4'''}$ = 8.5 Hz, 2 H, 3‴-H); ^{13}C-NMR (151 MHz, $CDCl_3$): δ [ppm] = 12.6 (C-10), 24.0 (CH_3), 35.6 (SCH), 44.9 (C-9), 55.4, 55.4, 55.4 (OCH_3), 64.8 (C-4′), 67.2 (C-6″), 72.3 (C-4″), 73.0 (C-6‴), 73.8 (C-11‴), 75.6 (C-1‴), 75.6 (C-5″), 78.3 (C-2″), 83.9 (C-3″), 85.2 (C-1″), 98.0 (C-8), 105.9 (C-4a), 106.7 (C-3), 108.8 (C-6), 113.8, 113.9, 114.0 (C-4‴, C-9‴, C-14‴), 124.4 (C-5), 129.4 (C-8‴), 130.1 (C-3‴), 130.2 (C-13‴), 130.4, 130.5, 130.7 (C-2‴, C-7‴, C-12‴), 148.7 (C-4), 150.9 (C-7), 154.3 (C-5′), 156.4 (C-8a), 159.4, 159.4, 159.4 (C-5‴, C-10‴, C-15‴), 161.8 (C-2); R_f = 0.31 (PE/EtOAc 60:40); IR (atr-film): $\tilde{\nu}$ [cm^{-1}] = 2966, 2930, 2906, 2864, 2835, 1753, 1715, 1604, 1513,

1422, 1357, 1244, 1173, 1078, 1032, 822, 570, 519; HRMS (ESI): m/z calculated for $C_{48}H_{61}N_2O_{12}S^+$ $[M+NH_4]^+$: 889.3940; found: 889.3929; m.p.: 93.6 °C; $[\alpha]_D^{20} = -18.8$ (c = 1.0, $CHCl_3$).

S3.28 Synthesis of Isopropyl 6-*O*-{[7-(diethylamino)-2-oxo-2*H*-chromen-4-yl]methyloxy(carbonyl)}-1-thio-β-D-galactopyranoside (1d)

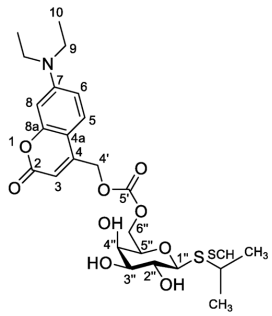

Photocaged IPTG **1d** was synthesized using modified procedures of Suzuki *et al.*[24] Coumarin **16** (40 mg, 46 µmol) was dissolved in CH_2Cl_2 (1.0 mL) and cooled to 0 °C. After the addition of trifluoroacetic acid (TFA) (0.33 mL, 4.3 mmol) and water (13 µL, 0.73 mmol), the reaction mixture was stirred in the dark for 10 min at 0 °C and 1 h at room temperature. Then the reaction mixture was concentrated under reduced pressure. The residue was purified by flash-column chromatography on SiO_2 (petroleum ether/ethyl acetate 50:50 to 10:90) to yield a yellow solid (20 mg, 39 µmol, 78%). ^{1}H-NMR (600 MHz, $CDCl_3$): δ [ppm] = 1.19 (t, $^3J_{10,9}$ = 7.1 Hz, 6 H, 10-H), 1.31 (d, $^3J_{CH3,SCH}$ = 6.7 Hz, 3 H, CH_3), 1.32 (d, $^3J_{CH3,SCH}$ = 6.7 Hz, 3 H, CH_3), 3.15–3.25 (m, 2 H, SCH, 2″-OH), 3.31 (s, 1 H, 4″-OH), 3.40 (q, $^3J_{9,10}$ = 7.1 Hz, 4 H, 9-H), 3.62–3.71 (m, 2 H, 2″-H, 3″-H), 3.74 (s, 1 H, 3″-OH), 3.80 (m_c, 1 H, 5″-H), 4.04 (brs, 1 H, 4″-H), 4.40 (dd, $^3J_{6a'',6b''}$ = 11.4 Hz, $^3J_{6a'',5''}$ = 5.0 Hz, 1 H, 6″-H_a), 4.42 (m_c, 1 H, 1″-H), 4.48 (dd, $^3J_{6b'',6a''}$ = 11.4 Hz, $^3J_{6b'',5''}$ = 7.2 Hz, 1 H, 6″-H_b), 5.23 (dd, $^3J_{4'a,4'b}$ = 15.2 Hz, $^4J_{4'a,3}$ = 1.3 Hz, 1 H, 4′-H_a), 5.27 (dd, $^3J_{4'b,4'a}$ = 15.2 Hz, $^4J_{4'b,3}$ = 1.3 Hz, 1 H, 4′-H_b), 6.12 (dd, $^4J_{3,4'a}$ = 1.3 Hz, $^4J_{3,4'b}$ = 1.3 Hz, 1 H, 3-H), 6.49 (d, $^4J_{8,6}$ = 2.6 Hz, 1 H, 8-H), 6.56 (dd, $^3J_{6,5}$ = 9.0 Hz, $^4J_{6,8}$ = 2.6 Hz, 1 H, 6-H), 7.26 (d, $^3J_{5,6}$ = 9.0 Hz, 1 H, 5-H); ^{13}C-NMR (151 MHz, $CDCl_3$): δ [ppm] = 12.6 (C-10), 24.1 (CH_3), 24.3 (CH_3), 36.1 (SCH), 44.9 (C-9), 64.9 (C-4′), 67.4 (C-6″), 68.8 (C-4″), 70.4 (C-2″), 74.6 (C-3″), 75.9 (C-5″), 86.1 (C-1″), 97.9 (C-8), 105.9 (C-4a), 106.5 (C-3), 108.9 (C-6), 124.5 (C-5), 148.9 (C-4), 150.9 (C-7), 154.7 (C-5′), 156.4 (C-8a), 162.0 (C-2); R_f = 0.35 (EtOAc); IR (atr-film): $\tilde{\nu}$ [cm^{-1}] = 3424, 2971, 2923, 2870, 1751, 1720, 1605, 1528, 1423, 1356, 1266, 1196, 1143, 1100, 1080, 1052, 1031, 967, 871, 828, 791, 743; HRMS (ESI): m/z calculated for $C_{24}H_{34}NO_9S^+$ $[M+H]^+$: 512.1949; found: 512.1953; m.p.: 85–87 °C; $[\alpha]_D^{20}$ = 22.0 (c = 0.1, $CHCl_3$); UV-Vis [Tris buffer (20 mM, pH 7.5)/MeCN 1:1]: λ_{max} (ε) = 273 nm (28210 dm^3 mol^{-1} cm^{-1}), 386 (12004).

reversed-phase HPLC: t_R = 8.0 min; column: *HyperClone* 5 µ ODS (C18) 120 (*Phenomenex*); detection (UV): 386 nm; eluent: H_2O/MeOH 40:60; flowrate: 0.5 mL/min; column temperature: 25 °C; sample solvent: Tris buffer (20 mM, pH 7.5)/MeCN 1:1.

S3.29 Synthesis of [Isopropyl 3,4-*O*-(1-methylethylidene)-6-*O*-(tert-butyldimethylsilyl)-1-thio-β-D-galactopyranoside] {[7-(diethylamino)-2-oxo-2*H*-chromen-4-yl]methyl} ethane-1,2-diylbis(methylcarbamate) (18)

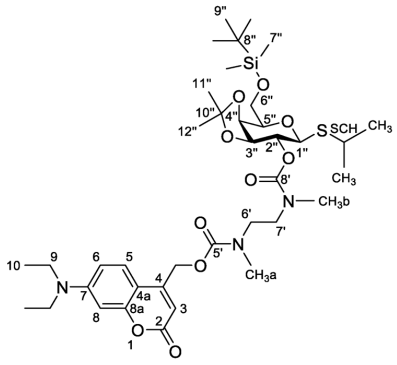

Coumarin **18** was synthesized using modified procedures of Wang *et al.*[25] Coumarin **7** (227 mg, 628 µmol) was dissolved in dry CH_2Cl_2 (11 mL) under nitrogen atmosphere. After the addition of 4-dimethylaminopyridine (DMAP) (6 mg, 0.06 mmol), carbohydrate **12** (200 mg, 359 µmol) and *N*,*N*-diisopropylethylamine (DIPEA) (1.10 mL, 6.29 mmol) the reaction mixture was stirred for 24 h at room temperature in the dark. Then, it was diluted with CH_2Cl_2, washed with saturated $NaHCO_3$ and saturated NaCl solution. The organic phase was dried with anhydrous $MgSO_4$ and concentrated under reduced pressure. The residue was purified by flash-column chromatography on SiO_2 (petroleum ether/ethyl acetate 50:50) to yield a slightly yellow foam (270 mg, 346 µmol, 97%). ^{1}H-NMR (600 MHz, $CDCl_3$): δ [ppm] = 0.06 (s, 6 H, 7″-H), 0.88 (s, 9 H, 9″-H), 1.20 (t, $^3J_{10,9}$ = 7.1 Hz, 6 H, 10-H), 1.23–1.33 (m, 9 H, CH_3, 11-H or 12-H), 1.55 (s, 3 H, 11-H or 12-H), 2.86–3.07 (m, 6 H, CH_3a, CH_3b), 3.17 (septet, $^3J_{SCH,CH3}$ = 6.8 Hz, 1 H, SCH), 3.28–3.62 (m, 4 H, 6′-H, 7′-H), 3.41 (q, $^3J_{9,10}$ = 7.1 Hz, 4 H, 9-H), 3.75–3.90 (m, 3 H, 5″-H, 6″-H), 4.13–4.22 (m, 1 H, 3″-H), 4.22–4.28 (m, 1 H, 4″-H), 4.44–4.55 (m, 1 H, 1″-H), 4.79–4.91 (m, 1 H, 2″-H), 5.20–5.30 (m, 2 H, 4′-H), 6.03–6.13 (m, 1 H, 3-H), 6.50 (d, $^3J_{8,6}$ = 2.6 Hz, 1 H, 8-H), 6.57 (d, $^3J_{6,5}$ = 9.0 Hz, 1 H, 6-H), 7.27–7.36 (m, 1 H, 5-H); ^{13}C-NMR (151 MHz, $CDCl_3$): δ [ppm] = –5.4 (C-7″), –5.3 (C-7″), 12.6 (C-10), 18.4 (C-8″), 23.9 (CH_3), 24.0 (CH_3), 25.9 (C-9″), 26.5, 28.0 (C-11″, C-12″), 34.9 (SCH), 35.0 (CH_3a/b), 35.3 (CH_3a/b), 35.6 (CH_3a/b), 35.9 (CH_3a/b), 36.0 (CH_3a/b), 36.1 (CH_3a/b), 44.9 (C-9), 46.7, 46.8, 47.2, 47.3, 47.5, 48.0, 48.1 (C-6′, C-7′), 62.2 (C-4′), 62.5 (C-6″), 62.7 (C-6″), 73.6, 73.6, 73.7 (C-2″, C-4″), 77.1 (C-5″), 77.5 (C-3″), 77.6 (C-3″), 77.6 (C-3″), 82.6 (C-1″), 82.7 (C-1″), 82.8 (C-1″), 82.9 (C-1″), 97.9 (C-8), 105.9, 106.1, 106.4 (C-3, C-4a), 108.8 (C-6),

110.4 (C-10″), 124.4 (C-5), 124.5 (C-5), 124.6 (C-5), 124.7 (C-5), 150.5, 150.6, 150.8 (C-4, C-7), 155.1, 155.3, 155.5, 155.6 (C-5′, C-8′), 156.3 (C-8a), 156.4 (C-8a), 162.1 (C-2); R_f = 0.31 (PE/EtOAc 50:50); IR (atr-film): $\tilde{\nu}$ [cm^{-1}] = 2960, 2930, 2859, 1710, 1606, 1529, 1466, 1422, 1358, 1219, 1125, 1081, 874, 839, 779; HRMS (ESI): m/z calculated for $C_{38}H_{62}N_3O_{10}SSi^+$ $[M+H]^+$: 780.3920; found: 780.3935; m.p.: 68.0 °C; $[\alpha]_D^{20}$ = 0.4 (c = 1.0, $CHCl_3$).

S3.30 Synthesis of (Isopropyl 1-thio-β-D-galactopyranoside) {[7-(diethylamino)-2-oxo-2*H*-chromen-4-yl]methyl} ethane-1,2-diylbis(methylcarbamate) (1e)

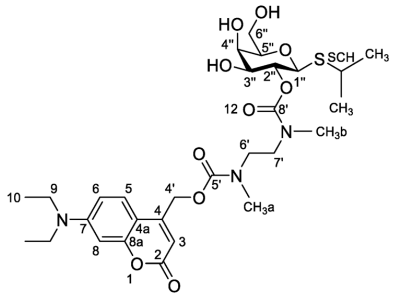

Photocaged IPTG **1e** was synthesized using modified procedures of Suzuki *et al.*[24] Coumarin **18** (0.11 mg, 0.14 mmol) was dissolved in trifluoroacetic acid (TFA) (1.0 mL) and cooled to 0 °C. After the addition of water (41 µL, 2.3 mmol) the reaction mixture was stirred for 10 min at 0 °C in the dark. Then the reaction mixture was concentrated under reduced pressure. The residue was purified by flash-column chromatography on SiO_2 (ethyl acetate/methanol 95:5) to yield a yellow solid (89 mg, 0.14 mmol, quant.). The product was a mixture of cis and trans isomers on carbamate bonds. ^{1}H-NMR (600 MHz, DMSO-d_6, 60 °C): δ [ppm] = 1.15 (t, $^3J_{10,9}$ = 7.0 Hz, 6 H, 10-H), 1.19 (d, $^3J_{CH3,SCH}$ = 6.8 Hz, 3 H, CH_3), 1.22 (d, $^3J_{CH3,SCH}$ = 6.8 Hz, 3 H, CH_3), 2.85 (s, 3 H, CH_3a or CH_3b), 2.95 (brs, 3 H, CH_3a or CH_3b), 3.07–3.12 (m, 1 H, SCH), 3.34–3.47 (m, 9 H, 9-H, 6′-H, 7′-H, 5″-H), 3.50 (dd, $^2J_{6''a,6''b}$ = 10.9 Hz, $^3J_{6''a,5''}$ = 6.0 Hz, 1 H, 6″-H$_a$), 3.54 (dd, $^2J_{6''b,6''a}$ = 10.9 Hz, $^3J_{6''b,5''}$ = 6.0 Hz, 1 H, 6″-H$_b$), 3.56 (brs, 1 H, 3″-H), 3.78 (d, $^3J_{4'',3''}$ = 3.3 Hz, 1 H, 4″-H), 4.48 (brs, 1 H, 1″-H), 4.72 (dd, $^3J_{2'',1''}$ = 10.1 Hz, $^3J_{2'',3''}$ = 9.3 Hz, 1 H, 2″-H), 5.25 (s, 2 H, 4′-H), 5.95 (s, 1 H, 3-H), 6.53 (d, $^4J_{8,6}$ = 2.6 Hz, 1 H, 8-H), 6.71 (dd, $^3J_{6,5}$ = 9.0 Hz, $^4J_{6,8}$ = 2.6 Hz, 1 H, 6-H), 7.48 (d, $^3J_{5,6}$ = 9.0 Hz, 1 H, 5-H); ^{13}C-NMR (151 MHz, DMSO-d_6, 60 °C): δ [ppm] = 12.0 (C-10), 23.4 (CH_3), 23.8 (CH_3), 33.7 (SCH), 34.7, 34.9 (CH_3a/b), 43.7 (C-9), 45.9, 46.1 (C-6′, C-7′), 60.3 (C-6″), 61.9 (C-4′), 68.4 (C-4″), 72.1 (C-2″), 72.6 (C-3″), 78.9 (C-5″), 82.7 (C-1″), 96.8 (C-8), 104.6 (C-3), 105.3 (C-4a), 108.7 (C-6), 125.0 (C-5), 150.4 (C-7), 151.0 (C-4), 154.5 (C-5′), 155.1 (C-8′), 155.6 (C-8a), 160.3 (C-2); R_f = 0.15 (EtOAc/MeOH 95:5); IR (atr-film): $\tilde{\nu}$ [cm^{-1}] = 3406, 2966, 2928, 2870, 1697, 1603, 1526, 1484, 1423, 1357, 1274, 1200, 1133, 1078, 862, 825, 803, 759; HRMS (ESI): m/z calculated for $C_{29}H_{44}N_3O_{10}S^+$ $[M+H]^+$: 626.2742; found:

626.2753; m.p.: 95.5 °C; $[\alpha]_D^{20}$ = –22.6 (c = 1.0, $CHCl_3$); UV-Vis [Tris buffer (20 mM, pH 7.5)/MeCN 1:1]: λ_{max} (ε) = 272 nm (17662 dm^3 mol^{-1} cm^{-1}), 305 (4142), 386 (17184).

reversed-phase HPLC: t_R = 8.2 min; column: *HyperClone* 5 µ ODS (C18) 120 (*Phenomenex*); detection (UV): 386 nm; eluent: H_2O/MeOH 40:60; flowrate: 0.5 mL/min; column temperature: 25 °C; sample solvent: Tris buffer (20 mM, pH 7.5)/MeCN 1:1.

S3.31 Synthesis of [(2,3,4-Tri-*O*-acetyl)-α-L-arabinopyranosyl] {[7-(diethylamino)-2-oxo-2*H*-chromen-4-yl]methyl} ethane-1,2-diylbis(methylcarbamate) (17)

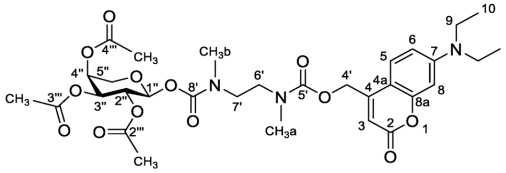

Coumarin **17** was synthesized using modified procedures of Wang *et al.*[25] Coumarin **7** (57 mg, 0.16 mmol) was dissolved in dry CH_2Cl_2 (2.9 mL) under nitrogen atmosphere. After the addition of 4-dimethylaminopyridine (DMAP) (2.0 mg, 16 µmol), carbohydrate **11** (40 mg, 91 µmol) and *N*,*N*-diisopropylethylamine (DIPEA) (0.28 mL, 1.6 mmol) the reaction mixture was stirred for 24 h at room temperature in the dark. Then, it was diluted with CH_2Cl_2, washed with saturated $NaHCO_3$ and saturated NaCl solution. The organic phase was dried with anhydrous $MgSO_4$ and concentrated under reduced pressure. The residue was purified by flash-column chromatography on SiO_2 (petroleum ether/ethyl acetate 30:70) to yield a slightly yellow foam (51 mg, 77 µmol, 85%). The product was a mixture of cis and trans isomers on carbamate bonds. ^{1}H-NMR (600 MHz, $CDCl_3$): δ [ppm] = 1.19 (t, $^3J_{10,9}$ = 7.1 Hz, 6 H, 10-H), 1.99–2.07 (m, 6 H, CH_3), 2.09–2.16 (m, 3 H, CH_3), 2.88–2.98 (m, 3 H, CH_3b), 2.98–3.07 (m, 3 H, CH_3a), 3.18–3.68 (m, 4 H, 6′-H, 7′-H), 3.40 (q, $^3J_{9,10}$ = 7.1 Hz, 4 H, 9-H), 3.77 (m_c, 1 H, 5″-H_a), 3.98 (dd, $^2J_{5b,5a}$ = 12.9 Hz, $^3J_{5b,4}$ = 3.7 Hz, 1 H, 5″-H_b), 5.06–5.33 (m, 5 H, 2″-H, 3″-H, 4″-H, 4′-H), 5.52–5.61 (m, 1 H, 1″-H), 6.01–6.13 (m, 1 H, 3-H), 6.50 (s, 1 H, 8-H), 6.57 (d, $^3J_{6,5}$ = 9.0 Hz, 1 H, 6-H), 7.26–7.34 (m, 1 H, 5-H); ^{13}C-NMR (151 MHz, $CDCl_3$): δ [ppm] = 12.5 (C-10), 20.7 (CH_3), 20.7 (CH_3), 20.8 (CH_3), 20.9 (CH_3), 21.0 (CH_3), 34.7, 34.7, 34.8, 35.2, 35.5, 35.5, 35.6, 35.8 (CH_3a, CH_3b), 44.9 (C-9), 46.3, 46.4, 46.9, 46.9, 47.1, 47.3, 47.6 (C-6′, C-7′), 62.4 (C-4′), 62.5 (C-4′), 62.7 (C-4′), 63.5 (C-5″), 63.6 (C-5″), 64.4 (C-5″), 64.5 (C-5″), 67.2, 67.6, 67.7, 68.2, 68.3 (C-2″, C-4″), 69.7 (C-3″), 69.8 (C-3″), 70.3 (C-3″), 70.4 (C-3″), 93.5 (C-1″), 93.6 (C-1″), 93.9 (C-1″), 94.1 (C-1″), 98.0 (C-8), 105.8, 105.9, 106.2, 106.4 (C-3, C-4a), 108.8 (C-6), 124.4 (C-5), 124.5 (C-5), 124.6 (C-5), 150.3, 150.4, 150.5, 150.7 (C-4, C-7), 153.9 (C-8′), 154.1 (C-8′), 154.4 (C-8′), 155.2 (C-5′), 155.3 (C-5′), 155.6 (C-5′), 155.7 (C-5′), 156.3 (C-8a), 162.0 (C-2), 162.1 (C-2), 169.5, 169.7, 169.8, 169.9, 169.9, 169.9, 170.0, 170.2, 170.3,

170.3 (C-2‴, C-3‴, C-4‴); R_f = 0.25 (PE/EtOAc 30:70); IR (atr-film): $\tilde{\nu}$ [cm^{-1}] = 2972, 2930, 1746, 1713, 1605, 1528, 1422, 1371, 1221, 1137, 1088, 1055, 760; m.p.: 82.7 °C; $[\alpha]_D^{20}$ = 10.6 (c = 1.0, $CHCl_3$)

S3.32 Synthesis of (α-L-Arabinopyranosyl) {[7-(diethylamino)-2-oxo-2*H*-chromen-4-yl]methyl} ethane-1,2-diylbis(methylcarbamate) (2c)

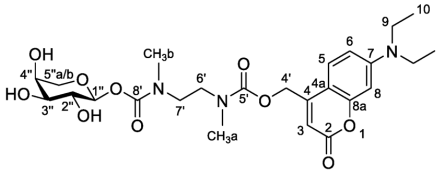

Photocaged arabinose **2c** was synthesized using modified procedures of Binder *et al.*[16] Coumarin **17** (40 mg, 60 µmol) was dissolved in MeOH (0.20 mL) and stirred at room temperature in the dark. Ammonia in MeOH (7 M, 54 µL, 0.38 mmol) was added and the reaction mixture was stirred until complete conversion. The solvent was evaporated under reduced pressure to yield a yellow solid (28 mg, 52 µmol, 86%). The product was a mixture of cis and trans isomers on carbamate bonds. ^{1}H-NMR (600 MHz, $CDCl_3$): δ [ppm] = 1.20 (t, $^3J_{10,9}$ = 7.1 Hz, 6 H, 10-H), 2.92–2.98 (m, 3 H, CH_3b), 2.99–3.05 (m, 3 H, CH_3a), 3.05–3.99 (m, 4 H, 6′-H, 7′-H), 3.41 (q, $^3J_{9,10}$ = 7.1 Hz, 4 H, 9-H), 3.63–3.70 (m, 1 H, 5″-H_a), 3.70–3.78 (m, 1 H, 3″-H), 3.78–3.92 (m, 1 H, 2″-H), 3.92–3.99 (m, 1 H, 4″-H), 3.99–4.09 (m, 1 H, 5″-H_b), 5.14–5.32 (m, 2 H, 4′-H), 5.32–5.46 (m, 1 H, 1″-H), 6.03–6.17 (m, 1 H, 3-H), 6.52 (s, 1 H, 8-H), 6.57–6.68 (m, 1 H, 6-H), 7.27–7.36 (m, 1 H, 5-H); ^{13}C-NMR (151 MHz, $CDCl_3$): δ [ppm] = 12.5 (C-10), 34.5, 34.6, 34.9, 35.4, 35.8, 36.2 (CH_3a, CH_3b), 45.0 (C-9), 46.5, 46.7, 47.1, 47.4, 47.5, 47.5 (C-6′, C-7′), 62.4 (C-4′), 62.5 (C-4′), 62.9 (C-4′), 63.1 (C-4′), 66.6 (C-5″), 66.8 (C-5″), 66.8 (C-5″), 68.2 (C-4″), 70.6 (C-2″), 70.8 (C-2″), 71.0 (C-2″), 73.3 (C-3″), 73.4 (C-3″), 73.6 (C-3″), 96.4 (C-1″), 96.5 (C-1″), 96.6 (C-1″), 98.0 (C-8), 105.9, 106.0 (C-3, C-4a), 109.1 (C-6), 124.5 (C-5), 124.6 (C-5), 150.4, 150.5, 151.4 (C-4, C-7), 154.6 (C-8′), 154.7 (C-8′), 156.0, 156.0, 156.2, 156.3, 156.6 (C-5′, C-8a), 162.6 (C-2), 162.7 (C-2); R_f = 0.08 (EtOAc/MeOH 95:5); IR (atr-film): $\tilde{\nu}$ [cm^{-1}] = 3423, 2966, 2927, 1703, 1603, 1528, 1490, 1423, 1357, 1275, 1216, 1131, 1080, 827, 761; HRMS (ESI): m/z calculated for $C_{25}H_{36}N_3O_{10}^+$ $[M+H]^+$: 538.2395; found: 538.2397; m.p.: 67–73 °C; $[\alpha]_D^{20}$ = 5.0 (c = 1.0, $CHCl_3$); UV-Vis [Tris buffer (20 mM, pH 7.5)/MeCN 1:1]: λ_{max} (ε) = 273 nm (28656 dm^3 mol^{-1} cm^{-1}), 385 (14070).

reversed-phase HPLC: t_R = 18.3 min; column: *HyperClone* 5 µ ODS (C18) 120 (*Phenomenex*); detection (UV): 385 nm; eluent: H_2O/MeOH 55:45; flowrate: 0.5 mL/min; column temperature: 25 °C; sample solvent: Tris buffer (20 mM, pH 7.5)/MeCN 1:1.

S3.33 4,5-Bis(ethoxycarbonylmethoxy)-2-nitrobenzylalcohol (22)

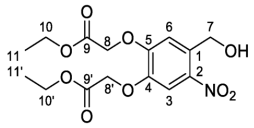

Alcohol **22** was synthesized using a procedure of Ni *et al*.[26] 4,5-Bis(ethoxycarbonylmethoxy)-2-nitrobenzaldehyde (**20**) (881 mg, 2.48 mmol) was dissolved in a mixture of CH_2Cl_2, EtOH and acetic acid (35:5:1, 10.0 mL). After the solution was cooled to 0 °C $NaBH_4$ (188 mg, 4.96 mmol, 2.00 Äq.) was added and the reaction mixture was stirred for 3 h at 0 °C. The reaction was quenched by addition of 1 M HCl (2 mL), diluted with ethyl acetate and washed with saturated NaCl solution. The organic phase was dried with anhydrous $MgSO_4$ and concentrated under reduced pressure. The residue was purified by flash-column chromatography on SiO_2 (toluene/ethyl acetate 80:20) to yield a yellow solid (649 mg, 1.82 mmol, 73%). The spectroscopic data are consistent with previously reported literature values.[26] ^{1}H-NMR (600 MHz, $CDCl_3$): δ [ppm] = 1.30 (t, $^3J_{11,10 \text{ or } 11',10'}$ = 7.2 Hz, 3 H, 11-H or 11′-H), 1.31 (t, $^3J_{11,10 \text{ or } 11',10'}$ = 7.2 Hz, 3 H, 11-H or 11′-H), 2.13 (br, 1 H, OH), 4.28 (q, $^3J_{10,11 \text{ or } 10',11'}$ = 7.2 Hz, 2 H, 10-H or 10′-H), 4.28 (q, $^3J_{10,11 \text{ or } 10',11'}$ = 7.2 Hz, 2 H, 10-H or 10′-H), 4.77 (s, 2 H, 8-H or 8′-H), 4.83 (s, 2 H, 8-H or 8′-H), 4.94 (s, 2 H, 7-H), 7.17 (s, 1 H, 3-H or 6-H), 7.70 (s, 1 H, 3-H or 6-H); ^{13}C-NMR (151 MHz, $CDCl_3$): δ [ppm] = 14.3, 14.3 (C-11, C-11′), 61.8, 61.9 (C-10, C-10′), 62.5 (C-7), 66.2 (C-8′), 66.6 (C-8), 112.0, 113.5 (C-3, C-6), 133.6, 140.4 (C-1, C-2), 146.5 (C-5), 152.7 (C-4), 167.8 (C-9′), 168.1 (C-9); R_f = 0.32 (Toluol/EtOAc 80:20); IR (atr-film): $\tilde{\nu}$ [cm^{-1}] = 2992, 1742, 1580, 1507, 1282, 1193, 1072, 1019, 792; MS (ESI, positive ion): m/z (%) = 380.2 (100) $[M+Na]^+$, 737.3 (5) $[2M+Na]^+$; m.p.: 76 °C.

S3.34 4,5-Bis(ethoxycarbonylmethoxy)-2-nitrobenzyl bromide (23)

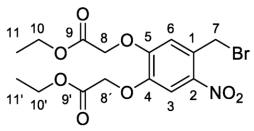

Bromide **23** was synthesized using a procedure of Tietze *et al*.[27] A Schlenk tube was charged with Alcohol **22** (1.00 g, 2.80 mmol) and tetrabromomethane (CBr_4) (1.16 g, 3.50 mmol) dissolved in dry CH_2Cl_2 (14.0 mL) under nitrogen atmosphere in the dark. A second Schlenk tube was charged with triphenylphosphane (PPh_3) (918 mg, 3.50 mmol) dissolved in dry CH_2Cl_2 under nitrogen atmosphere. Both solutions were cooled to 0 °C and the cooled PPh_3 solution was added dropwise to the dissolved alcohol **22**. The reaction mixture was stirred for 10 min at 0 °C and 6 h at room temperature. SiO_2 was added to the reaction mixture and the solvent was removed under reduced pressure. The residue was purified by flash-column chromatography on SiO_2 (petroleum ether/ethyl acetate 65:35) to yield a white solid (1.13 g, 2.69 mmol, 96%). ^{1}H-NMR (600 MHz, $CDCl_3$): δ [ppm] = 1.31 (t, $^3J_{11,10}$ = 7.1 Hz, 3 H, 11-H), 1.31 (t, $^3J_{11',10'}$ = 7.1 Hz, 3 H, 11′-H), 4.29 (q,$^3J_{10,11;10',11'}$ = 7.1 Hz, 4 H, 10-H, 10′-H), 4.78 (2, 2 H, 8′-H), 4.81 (s, 2 H, 7-H), 4.83 (s, 2 H, 8-H), 6.94 (s, 1 H, 6-H), 7.65 (s, 1 H, 3-H); ^{13}C-NMR (151 MHz, $CDCl_3$): δ [ppm] = 14.3 (C-11), 14.3 (C-11′), 29.7 (C-7), 61.9 (C-10), 62.0 (C-10′), 66.5 (C-8), 66.5 (C-8′), 112.1 (C-3), 117.2 (C-6), 128.5 (C-2), 141.2 (C-1), 147.6 (C-5), 151.9 (C-4), 167.7 (C-9), 167.8 (C-9′); R_f = 0.62 (PE/EtOAc 60:40); IR (atr-film): $\tilde{\nu}$ [cm^{-1}] = 2992, 1739, 1616, 1581, 1522, 1479, 1449, 1409, 1380, 1356, 1339, 1289, 1264, 1202, 1184, 1120, 1080, 1043, 1025, 930, 881, 798, 758, 732, 672; HRMS (ESI): m/z calculated for $C_{15}H_{18}O_8NBrNa^+$ $[M+Na]^+$: 442.0108; found: 442.0108; m.p.: 118°C.

S3.35 Ethyl-2-*O*-[4,5-bis(ethoxycarbonylmethoxy)-2-nitrobenzyl]salicylate (24)

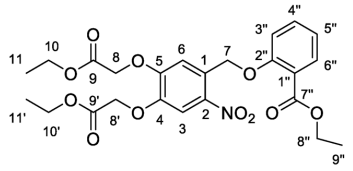

Ethyl salicylate (0.11 mL, 0.71 mmol) was dissolved in dry acetone (1.0 mL) and dry K_2CO_3 (56 mg, 0.40 mmol) was added. After stirring for 10 min bromide **23** (0.10 g, 0.24 mmol) was added and the reaction mixture was stirred for 2 d at room temperature in the dark. After completion, the solvent was removed under reduced pressure. The residue was dissolved in ethyl acetate and subsequently washed with water and saturated $NaHCO_3$ solution. The organic phase was dried with anhydrous $MgSO_4$ and concentrated under reduced pressure. The residue was purified by flash-column chromatography on SiO_2 (petroleum ether/ethyl acetate 80:20) to yield a white solid (0.11 g, 0.22 mmol, 92%). ^{1}H-NMR (600 MHz, $CDCl_3$): δ [ppm] = 1.25 (t, $^3J_{11,10}$ = 7.1 Hz, 3 H, 11-H), 1.31 (t, $^3J_{11',10'}$ = 7.1 Hz, 3 H, 11′-H), 1.40 (t, $^3J_{9'',8''}$ = 7.1 Hz, 3 H, 9″-H), 4.23 (q, $^3J_{10,11}$ = 7.1 Hz, 2 H, 10-H), 4.29 (q, $^3J_{10',11'}$ = 7.1 Hz, 2 H, 10′-H), 4.38 (q, $^3J_{8'',9''}$ = 7.1 Hz, 2 H, 8″-H), 4.81 (s, 2 H, 8′-H), 5.05 (s, 2 H, 8-H), 5.52 (s, 2 H, 7-H), 7.03 (dd, $^3J_{5'',4''}$ = 7.5 Hz, $^3J_{5'',6''}$ = 7.5 Hz, 1 H, 5″-H), 7.14 (d, $^3J_{3'',4''}$ = 8.4 Hz, 1 H, 3″-H), 7.53 (dd, $^3J_{4'',3''}$ = 8.4 Hz, $^3J_{4'',5''}$ = 7.5 Hz, 1 H, 4″-H), 7.82 (s, 1 H, 3-H), 7.93 (d, $^3J_{6'',5''}$ = 7.5 Hz, 1 H, 6″-H), 8.23 (s, 1 H, 6-H); ^{13}C-NMR (151 MHz, $CDCl_3$): δ [ppm] = 14.2 (C-11), 14.3 (C-11′), 14.5 (C-9″), 60.7 (C-8″), 61.6 (C-10), 61.7 (C-10′), 65.8 (C-8), 66.8 (C-8′), 67.3 (C-7), 111.9 (C-3), 112.8 (C-6), 113.2 (C-3″), 119.8 (C-1″), 120.8 (C-5″), 130.8 (C-1), 132.1 (C-6″), 134.2 (C-4″), 138.9 (C-2), 146.1 (C-4), 153.4 (C-5), 158.0 (C-2″), 165.2 (C-7″), 168.0 (C-9), 168.3 (C-9′); R_f = 0.23 (PE/EtOAc 70:30); IR (atr-film): $\tilde{\nu}$ [cm^{-1}] = 3104, 2992, 1771, 1743, 1713, 1582, 1524, 1488, 1449, 1425, 1377, 1329, 1291, 1242, 1195, 1112, 1080, 1020, 895, 859, 826, 803, 753, 700, 683, 661; HRMS (ESI): m/z calculated for $C_{24}H_{27}O_{11}NNa^+$ [M+Na]$^+$: 528.1476; found: 528.1476; m.p.: 133 °C

S3.36 2-*O*-[4,5-Bis(carboxymethoxy)-2-nitrobenzyl]salicylic acid (BC-cSal) (21)

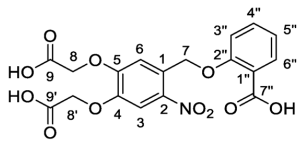

To a solution of salicylate **24** (200 mg, 396 µmol) in MeOH (11.9 mL) a 0.2 M solution of KOH (11.9 mL, 2.37 mmol) was added. The reaction mixture was heated to 60 °C and stirred until complete conversion (4 h). After the reaction was completed as indicated by TLC, 1 M HCl was added and the precipitate was filtered off and washed. The precipitate was dried to yield a white solid (153 mg, 363 µmol, 92%). ^{1}H-NMR (600 MHz, DMSO-d_6): δ [ppm] = 4.89 (s, 2 H, 8′-H), 4.91 (s, 2 H, 8-H), 5.49 (s, 2 H, 7-H), 7.06 (dd, $^{3}J_{5'',6''}$ = 7.0 Hz, $^{3}J_{5'',4''}$ = 6.9 Hz 1 H, 5″-H), 7.22 (d, $^{3}J_{3'',4''}$ = 7.9 Hz, 1 H, 3″-H), 7.56 (dd, $^{3}J_{4'',3''}$ = 7.9 Hz, $^{3}J_{4'',5''}$ = 6.9 Hz, 1 H, 4″-H), 7.72 (s, 1 H, 3-H), 7.79 (d, $^{3}J_{6'',5''}$ = 7.0 Hz, 1 H, 6″-H), 7.80 (s, 1 H, 6-H); ^{13}C-NMR (151 MHz, DMSO-d_6): δ [ppm] = 65.0 (C-8), 65.5 (C-8′), 66.7 (C-7), 110.4 (C-3), 112.2 (C-6), 113.7 (C-3″), 120.7 (C-1″), 120.7 (C-5″), 128.7 (C-1), 131.6 (C-6″), 133.7 (C-4″), 139.0 (C-2), 145.9 (C-4), 152.2 (C-5), 157.1 (C-2″), 166.9 (C-7″), 169.1 (C-9), 169.8 (C-9′); IR (atr-film): $\tilde{\nu}$ [cm^{-1}] = 2923, 1708, 1801, 1585, 1525, 1490, 1428, 1380, 1331, 1285, 1245, 1214, 1079, 1027, 900, 849, 821, 750, 698, 671; HRMS (ESI): m/z calculated for $C_{18}H_{15}O_{11}NK^{+}$ [M+K]$^{+}$: 460.0276; found: 460.0276; m.p.: 264 °C (decay); UV-Vis [sodium phosphate buffer (100 mM, pH 7.4)]: λ_{max} (ε) = 290 nm (5027 dm^3 mol^{-1} cm^{-1}), 346 (5852).

reversed-phase HPLC: t_R = 9.6 min; column: *HyperClone* 5 µ ODS (C18) 120 (*Phenomenex*); detection (UV): 346 nm; eluent: sodium phosphate buffer (100 mM, pH 7.4)/MeOH 15:85; flowrate: 0.5 mL/min; column temperature: 25 °C; sample solvent: sodium phosphate buffer (100 mM, pH 7.4).

S3.37 Sodium 2-*O*-[4,5-bis(carboxymethoxy)-2-nitrobenzyl]salicylate (25)

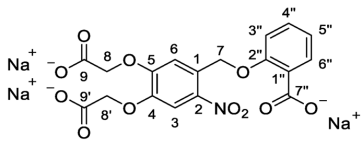

To a solution of salicylic acid **21** (60 mg, 0.14 mmol) in MeOH (2.5 mL) a 0.2 M solution of NaOH (2.1 mL, 0.43 mmol) was added. The reaction mixture was stirred for 5 min before it was lyophilised overnight to yield a solid (69 mg, 0.14 mmol, quant.). ^{1}H-NMR (600 MHz, D_2O): δ [ppm] = 4.56 (s, 2 H, 8′-H), 4.62 (s, 2 H, 8-H), 5.43 (s, 2 H, 7-H), 7.03 (d, $^{3}J_{3'',4''}$ = 8.2 Hz, 1 H, 3″-H), 7.06 (ddd, $^{3}J_{5'',6''}$ = 7.5 Hz, $^{3}J_{5'',4''}$ = 7.4 Hz, $^{4}J_{5'',3''}$ = 1.0 Hz, 1 H, 5″-H), 7.36 (ddd, $^{3}J_{4'',3''}$ = 8.2 Hz, $^{3}J_{4'',5''}$ = 7.4 Hz, $^{4}J_{4'',6''}$ = 1.8 Hz, 1 H, 4″-H), 7.41 (s, 1 H, 3-H), 7.46 (dd, $^{3}J_{6'',5''}$ = 7.5 Hz, $^{3}J_{6'',4''}$ = 1.8 Hz, 1 H, 6″-H), 7.74 (s, 1 H, 6-H); ^{13}C-NMR (151 MHz, D_2O): δ [ppm] = 67.3, 67.3 (C-8, C-8′), 67.6 (C-7), 109.4 (C-3), 111.4 (C-6), 113.8 (C-3″), 121.4 (C-5″), 128.3 (C-6″), 129.5 (C-1), 129.7 (C-4″), 130.2 (C-1″), 139.0 (C-2), 145.7 (C-4), 152.1 (C-5), 154.1 (C-2″), 174.9 (C-9), 175.4 (C-9′), 176.0 (C-7″); IR (atr-film): $\tilde{\nu}$ [cm^{-1}] = 3216, 1603, 1553, 1521, 1425, 1382, 1329, 1273, 1214, 1100, 1070, 1020, 855, 818, 753, 695, 663; m.p.: 245 °C (decay).

S4 Supporting data

S4.1 UV-Vis spectra of compounds

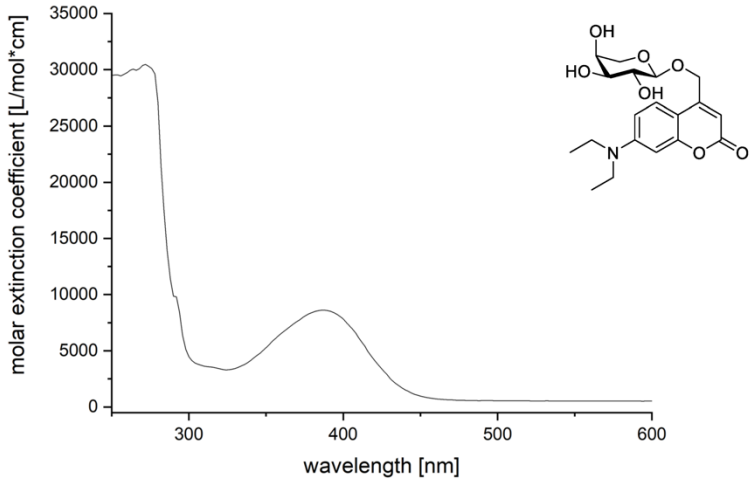

Figure S1: UV-Vis spectrum of compound **2b** (0.10 mM in MeOH, 25 °C).

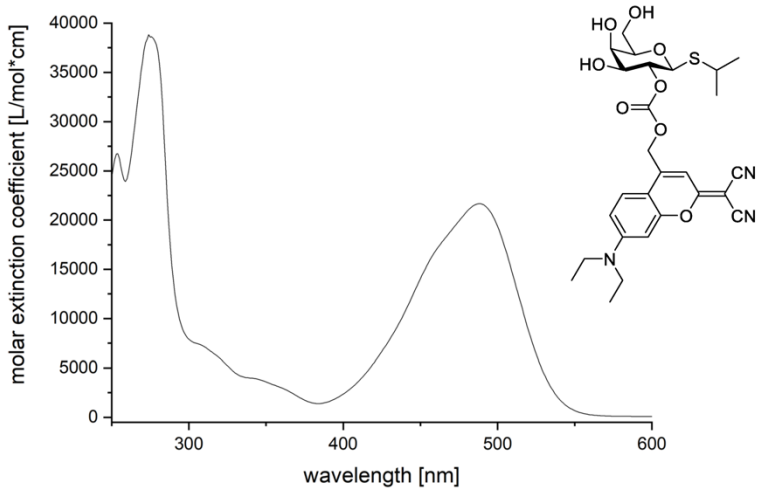

Figure S2: UV-Vis spectrum of compound **1c** [0.05 mM in Tris buffer (20 mM, pH 7.5)/MeCN 50:50, 25 °C].

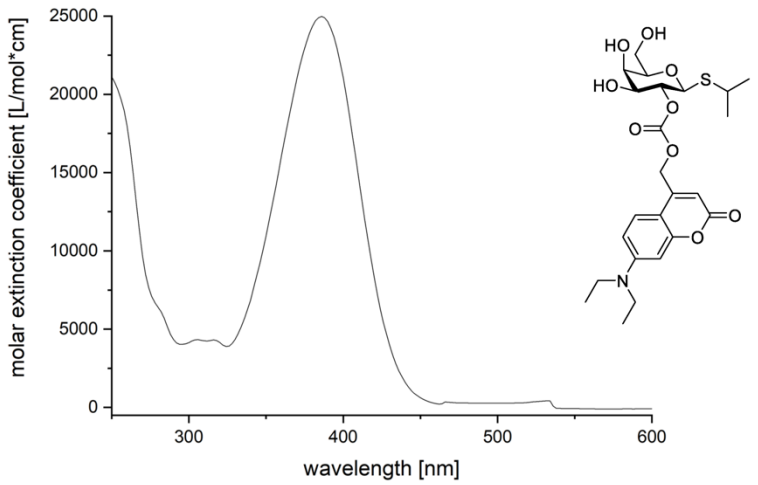

Figure S3: UV-Vis spectrum of compound **1b** [25.0 μM in Tris buffer (20 mM, pH 7.5)/MeCN 50:50, 25 °C].

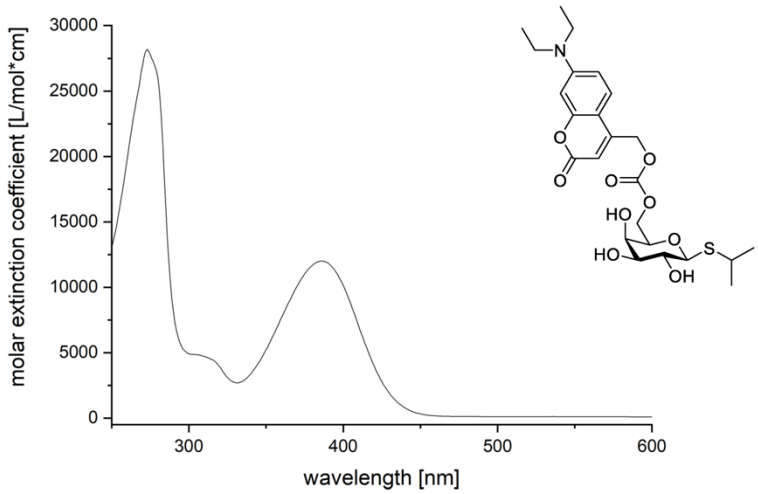

Figure S4: UV-Vis spectrum of compound **1d** [0.05 mM in Tris buffer (20 mM, pH 7.5)/MeCN 50:50, 25 °C].

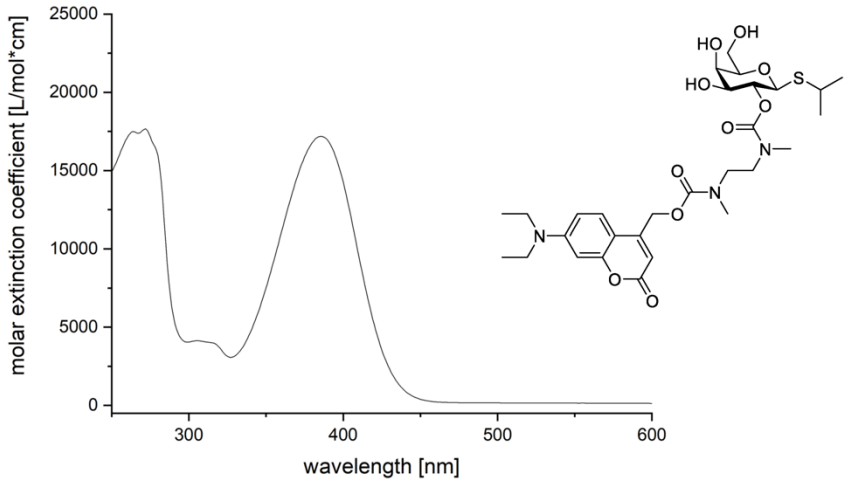

Figure S5: UV-Vis spectrum of compound **1e** [0.05 mM in Tris buffer (20 mM, pH 7.5)/MeCN 50:50, 25 °C].

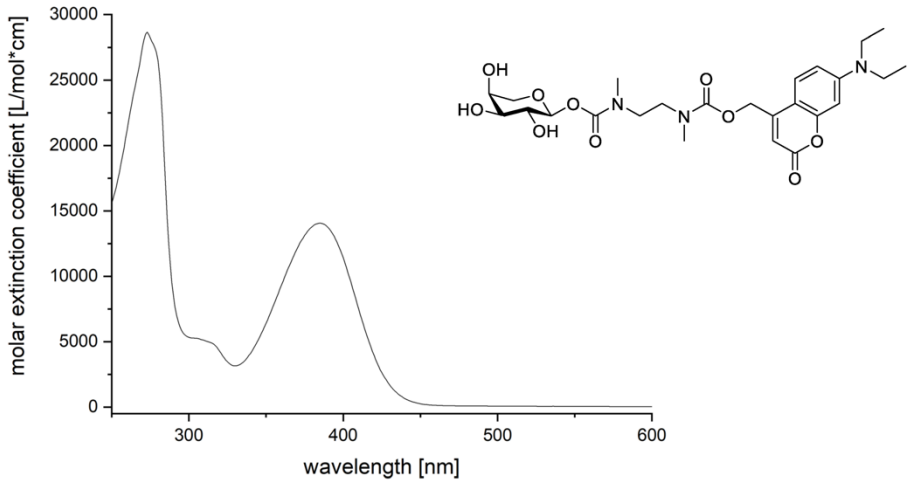

Figure S6: UV-Vis spectrum of compound **2c** [0.05 mM in Tris buffer (20 mM, pH 7.5)/MeCN 50:50, 25 °C].

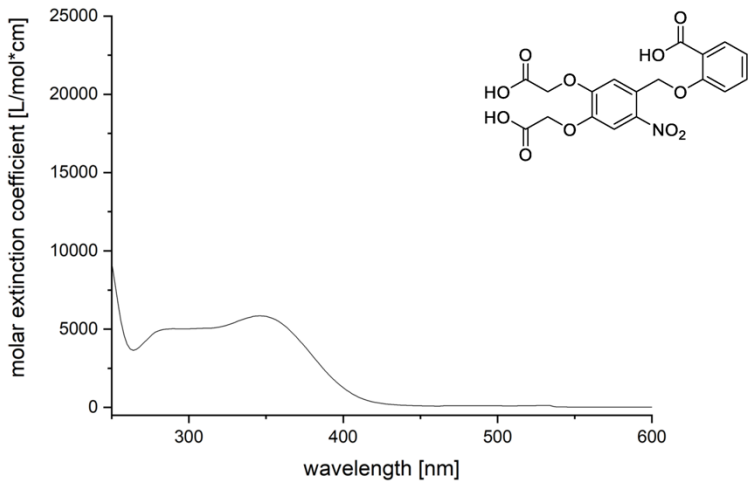

Figure S7: UV-Vis spectrum of compound **21** [125 μM in sodium phosphate buffer (100 mM, pH 7.4), 25 °C].

S4.2 Photon flux densities of light sources

Table S3: Determined photon flux densities ($q_{n,p}$)

wavelength	$q_{n,p}$ (mol s^{-1})
365 nm	6.49×10^{-8}
405 nm	1.91×10^{-7}
430 nm	1.22×10^{-7}

S4.3 Determination of uncaging half-life times

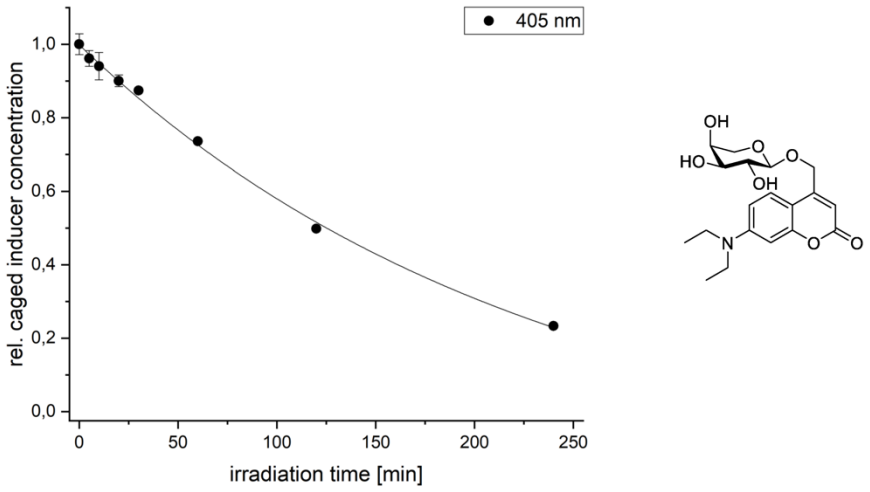

Figure S8: *In vitro* decay of **2b** (1 mM in H_2O/DMSO 99:1) via reversed-phase HPLC after irradiation with 405 nm (44.6 mW cm^{-2}, room temperature).

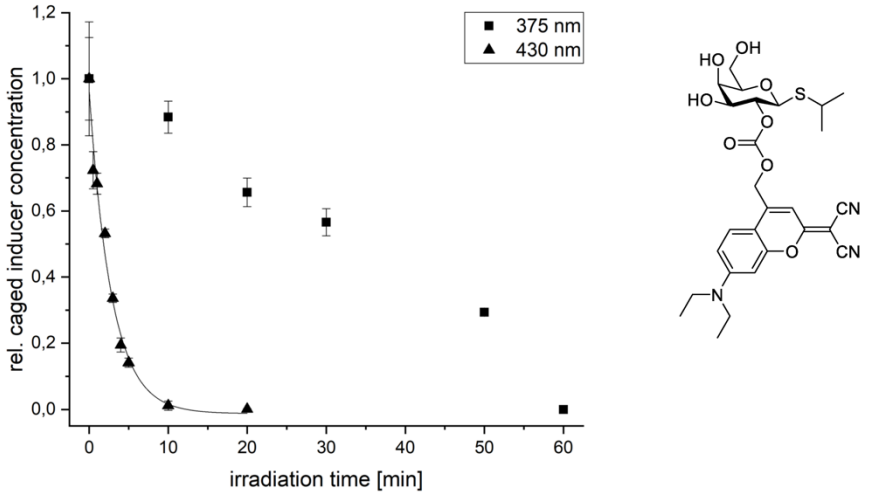

Figure S9: *In vitro* decay of **1c** [0.5 mM in Tris buffer (20 mM, pH 7.5)/MeCN 1:1] via reversed-phase HPLC after irradiation with 375 nm (6.4 mW cm^{-2}, room temperature) and 430 nm (45.6 mW cm^{-2}, room temperature).

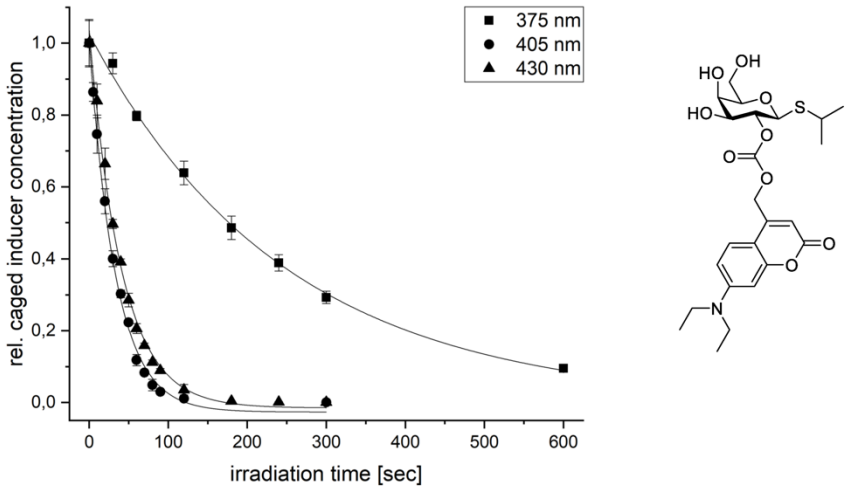

Figure S10: *In vitro* decay of **1b** [0.5 mM in Tris buffer (20 mM, pH 7.5)/MeCN 1:1] via reversed-phase HPLC after irradiation with 375 nm (6.4 mW cm^{-2}, room temperature), 405 nm (44.6 mW cm^{-2}, room temperature) and 430 nm (45.6 mW cm^{-2}, room temperature).

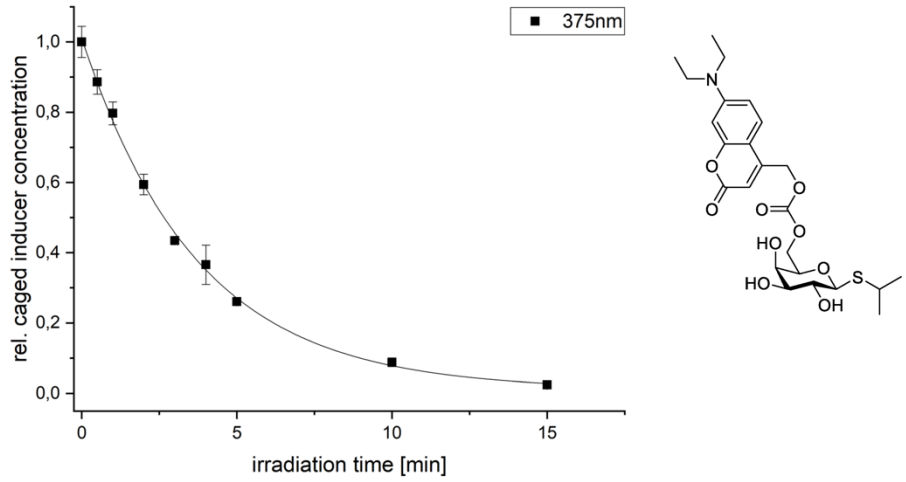

Figure S11: *In vitro* decay of **1d** [0.5 mM in Tris buffer (20 mM, pH 7.5)/MeCN 1:1] via reversed-phase HPLC after irradiation with 375 nm (6.4 mW cm^{-2}, room temperature).

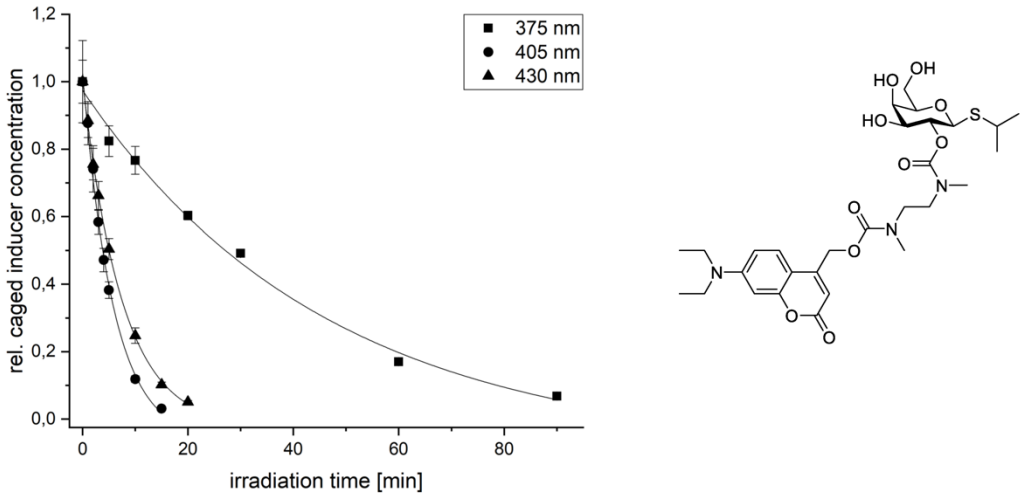

Figure S12: *In vitro* decay of **1e** [0.5 mM in Tris buffer (20 mM, pH 7.5)/MeCN 1:1] via reversed-phase HPLC after irradiation with 375 nm (6.4 mW cm^{-2}, room temperature), 405 nm (44.6 mW cm^{-2}, room temperature) and 430 nm (45.6 mW cm^{-2}, room temperature).

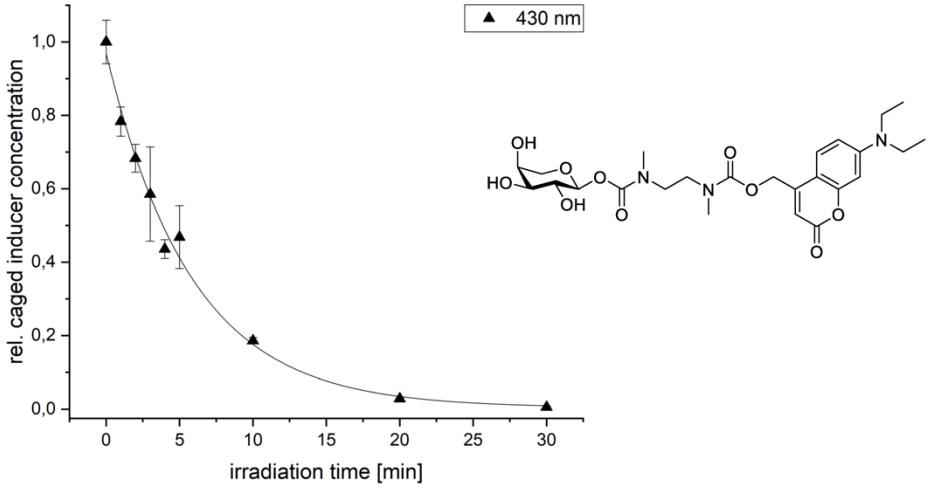

Figure S13: *In vitro* decay of **2c** [0.5 mM in Tris buffer (20 mM, pH 7.5)/MeCN 1:1] via reversed-phase HPLC after irradiation with 430 nm (45.6 mW cm^{-2}, room temperature).

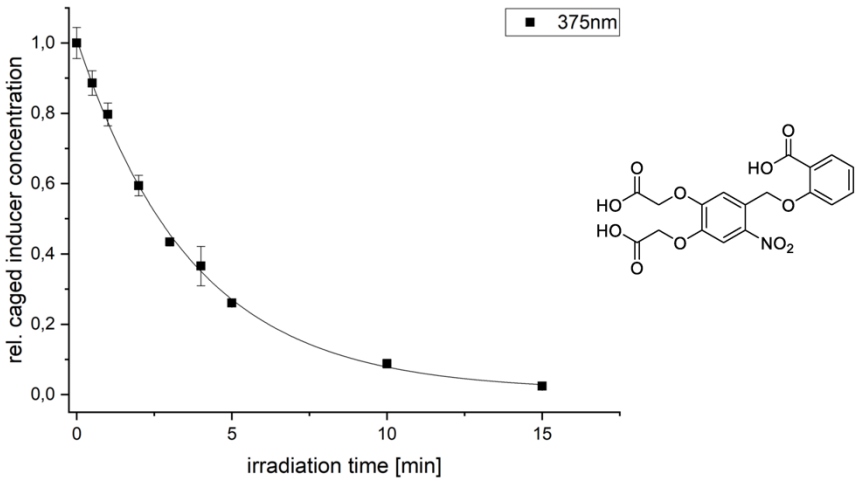

Figure S14: *In vitro* decay of **21** [0.5 mM in sodium phosphate buffer (100 mM, pH 7.4)] via reversed-phase HPLC after irradiation with 375 nm (6.4 mW cm^{-2}, room temperature).

Table S3: Fitting parameters and uncaging half-life times $t_{0.5}$ for **1b–e**, **2b–c** and **21** at different wavelength.

photocaged inducer	λ [nm]	y_0	A_1	t_1	k	$t_{0.5}$ [min]
2b	375	-0,19104	1,18966	230,51535	0,00434	159,78106
1c	430	-0,01254	0,97483	2,83993	0,35212	1,96849
1b	375	0,0004873	1,02624	246,92187	0,00405	171,1532
1b	405	-0,02632	1,03705	33,42057	0,02992	23,16538
1b	430	-0,01504	1,05356	40,75615	0,02454	28,25001
1d	375	0,01084	1,00002	3,7118	0,26941	2,57283
1e	375	-0,09535	1,06979	46,27316	0,02161	32,07411
1e	405	-0,06395	1,09129	5,79684	0,17251	4,01806
1e	430	-0,02656	1,03055	7,48242	0,13365	5,18642
2c	430	0,00417	0,96575	5,79819	0,17247	4,019
21	375	-0,00435	0,9935	3,52342	0,28382	2,44225

S4.4 HPLC-Traces

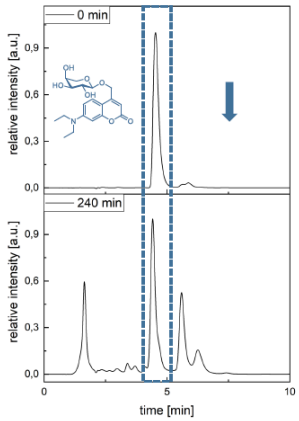

Figure S15: UV traces at 388 nm of the reversed-phase HPLC analysis of **2b** (1 mM in H_2O/DMSO 99:1) before irradiation and after 240 min of irradiation at 405 nm (44.6 mW cm^{-2}, room temperature).

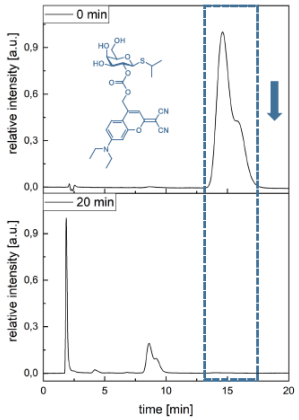

Figure S16: UV traces at 488 nm of the reversed-phase HPLC analysis of **1c** [0.5 mM in Tris buffer (20 mM, pH 7.5)/MeCN 50:50] before irradiation and after 20 min of irradiation at 430 nm (45.6 mW cm^{-2}, room temperature).

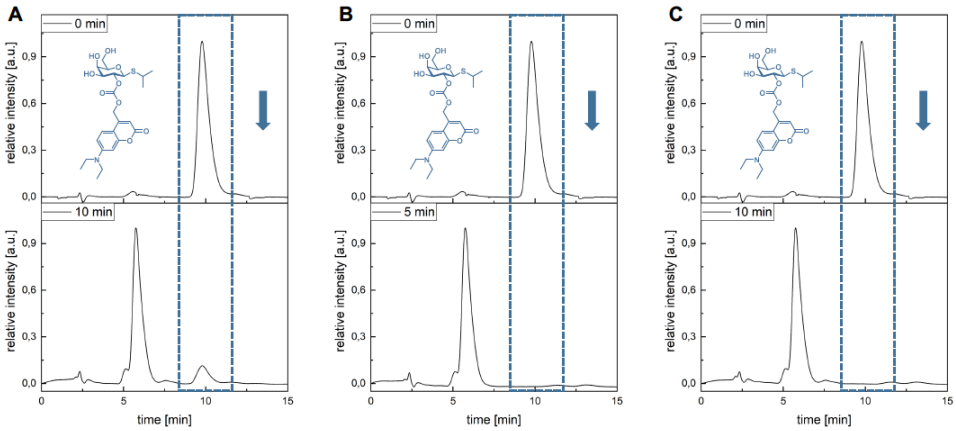

Figure S17: **A**) UV traces at 392 nm of the reversed-phase HPLC analysis of **1b** [0.5 mM in Tris buffer (20 mM, pH 7.5)/MeCN 50:50] before irradiation and after 10 min of irradiation at 375 nm (6.4 mW cm^{-2}, room temperature); **B**) UV traces at 392 nm of the reversed-phase HPLC analysis of **1b** [0.5 mM in Tris buffer (20 mM, pH 7.5)/MeCN 50:50] before irradiation and after 5 min of irradiation at 405 nm (44.6 mW cm^{-2}, room temperature); **C**) UV traces at 392 nm of the reversed-phase HPLC analysis of **1b** [0.5 mM in Tris buffer (20 mM, pH 7.5)/MeCN 50:50] before irradiation and after 10 min of irradiation at 430 nm (45.6 mW cm^{-2}, room temperature).

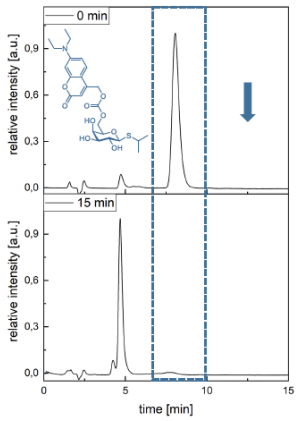

Figure S18: UV traces at 386 nm of the reversed-phase HPLC analysis of **1d** [0.5 mM in Tris buffer (20 mM, pH 7.5)/MeCN 50:50] before irradiation and after 15 min of irradiation at 375 nm (6.4 mW cm^{-2}, room temperature).

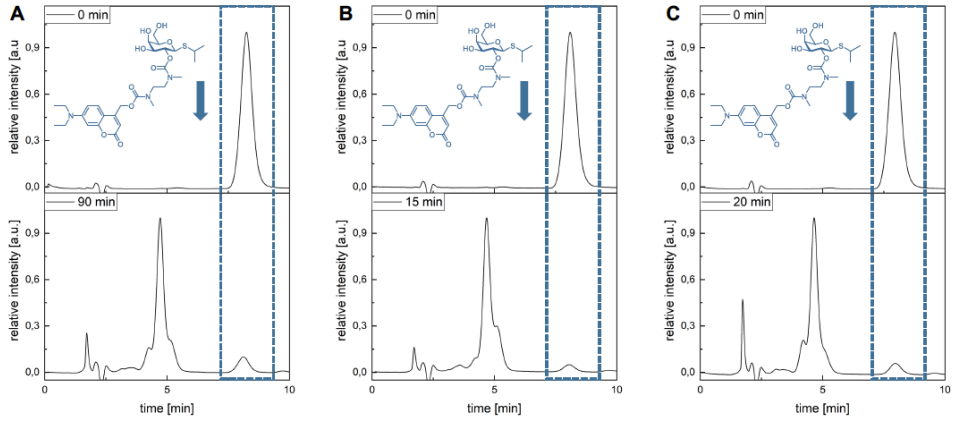

Figure S19: **A**) UV traces at 386 nm of the reversed-phase HPLC analysis of **1e** [0.5 mM in Tris buffer (20 mM, pH 7.5)/MeCN 50:50] before irradiation and after 10 min of irradiation at 375 nm (6.4 mW cm^{-2}, room temperature); **B**) UV traces at 386 nm of the reversed-phase HPLC analysis of **1e** [0.5 mM in Tris buffer (20 mM, pH 7.5)/MeCN 50:50] before irradiation and after 5 min of irradiation at 405 nm (44.6 mW cm^{-2}, room temperature); **C**) UV traces at 386 nm of the reversed-phase HPLC analysis of **1e** [0.5 mM in Tris buffer (20 mM, pH 7.5)/MeCN 50:50] before irradiation and after 10 min of irradiation at 430 nm (45.6 mW cm^{-2}, room temperature).

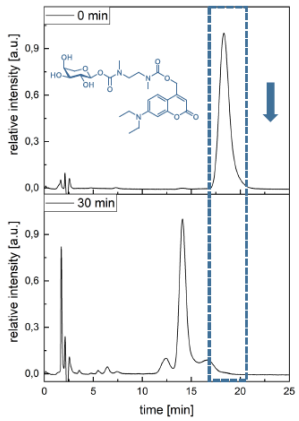

Figure S20: UV traces at 385 nm of the reversed-phase HPLC analysis of **2c** [0.5 mM in Tris buffer (20 mM, pH 7.5)/MeCN 50:50] before irradiation and after 10 min of irradiation at 430 nm (45.6 mW cm^{-2}, room temperature).

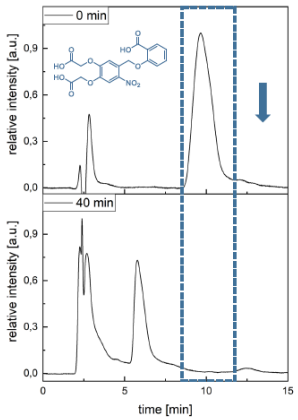

Figure S21: UV traces at 346 nm of the reversed-phase HPLC analysis of **21** [0.5 mM in sodium phosphate buffer (100 mM, pH 7.4)] before irradiation and after 15 min of irradiation at 375 nm (6.4 mW cm^{-2}, room temperature).

S4.5 Stability measurements

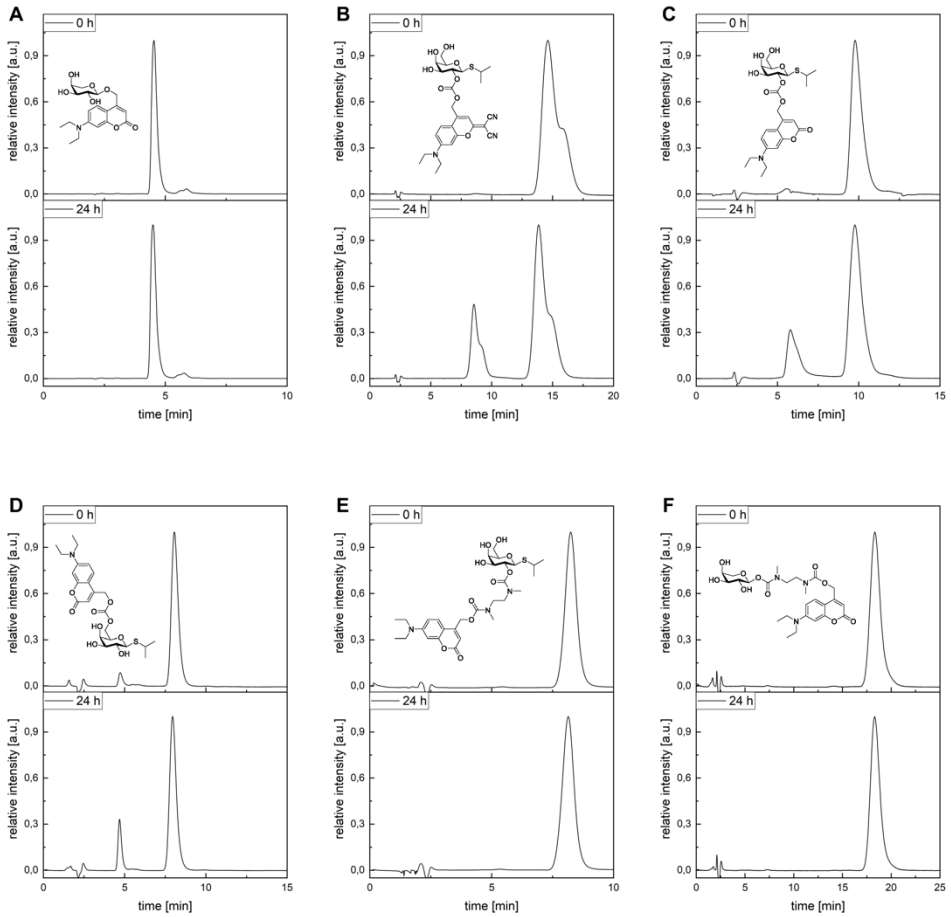

Figure S22: UV traces at absorption maxima of the reversed-phase HPLC analysis of **2b** (**A**), **1c** (**B**), **1b** (**C**), **1d** (**D**), **1e** (**E**) and **2c** (**F**) for determination of stability. The reported values in Table **1** are means of triplicate measurements.

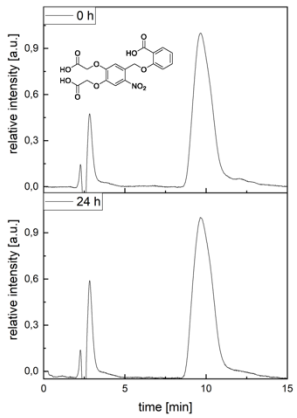

Figure S23: UV traces at absorption maxima of the reversed-phase HPLC analysis of **21** for determination of stability. The reported value is the mean of triplicate measurements.

S4.6 ESI measurements

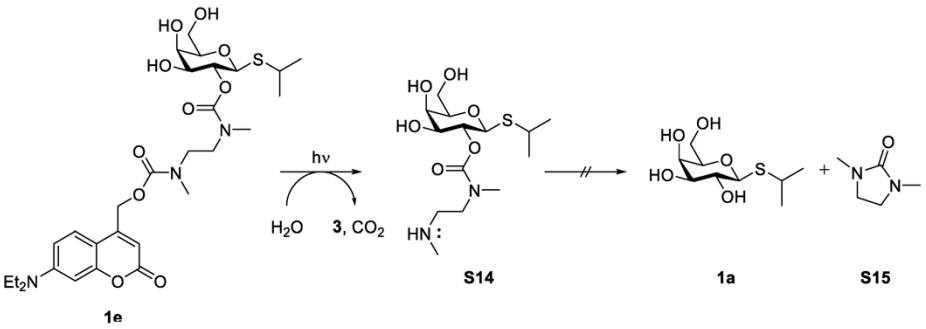

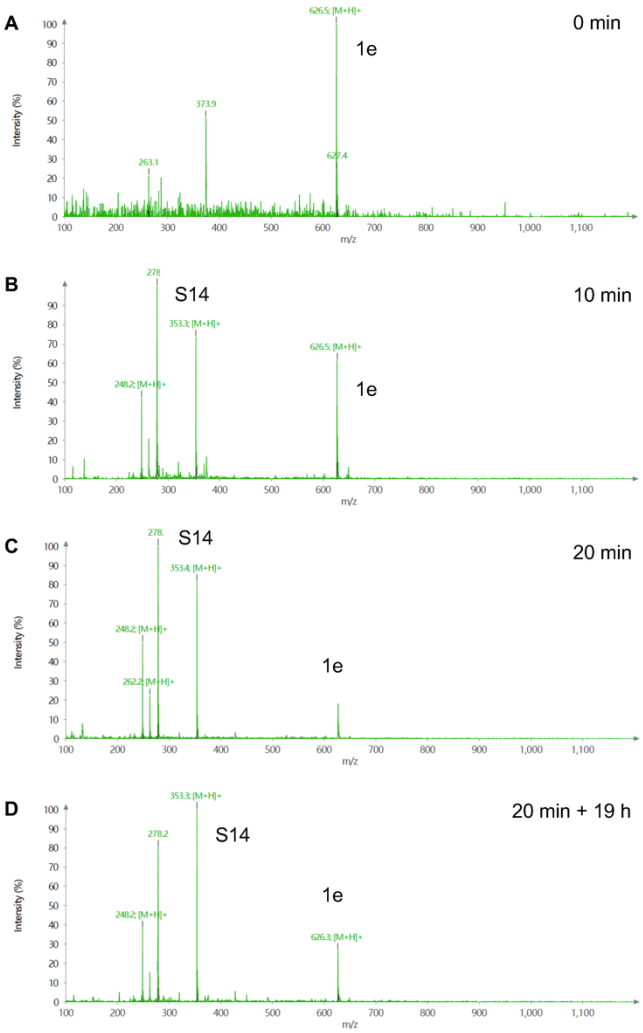

Figure S24: ESI-MS measurements of **1e** (1 mM in MeOH/H_2O 1:1) for detection of the intermediate **S14** after irradiation with 430 nm (45.6 mW cm^{-2}, room temperature) for **A**) 0 min; **B**) 10 min; **C**) 20 min; **D**) 20 min plus allowing it to stand for 19 h at room temperature.

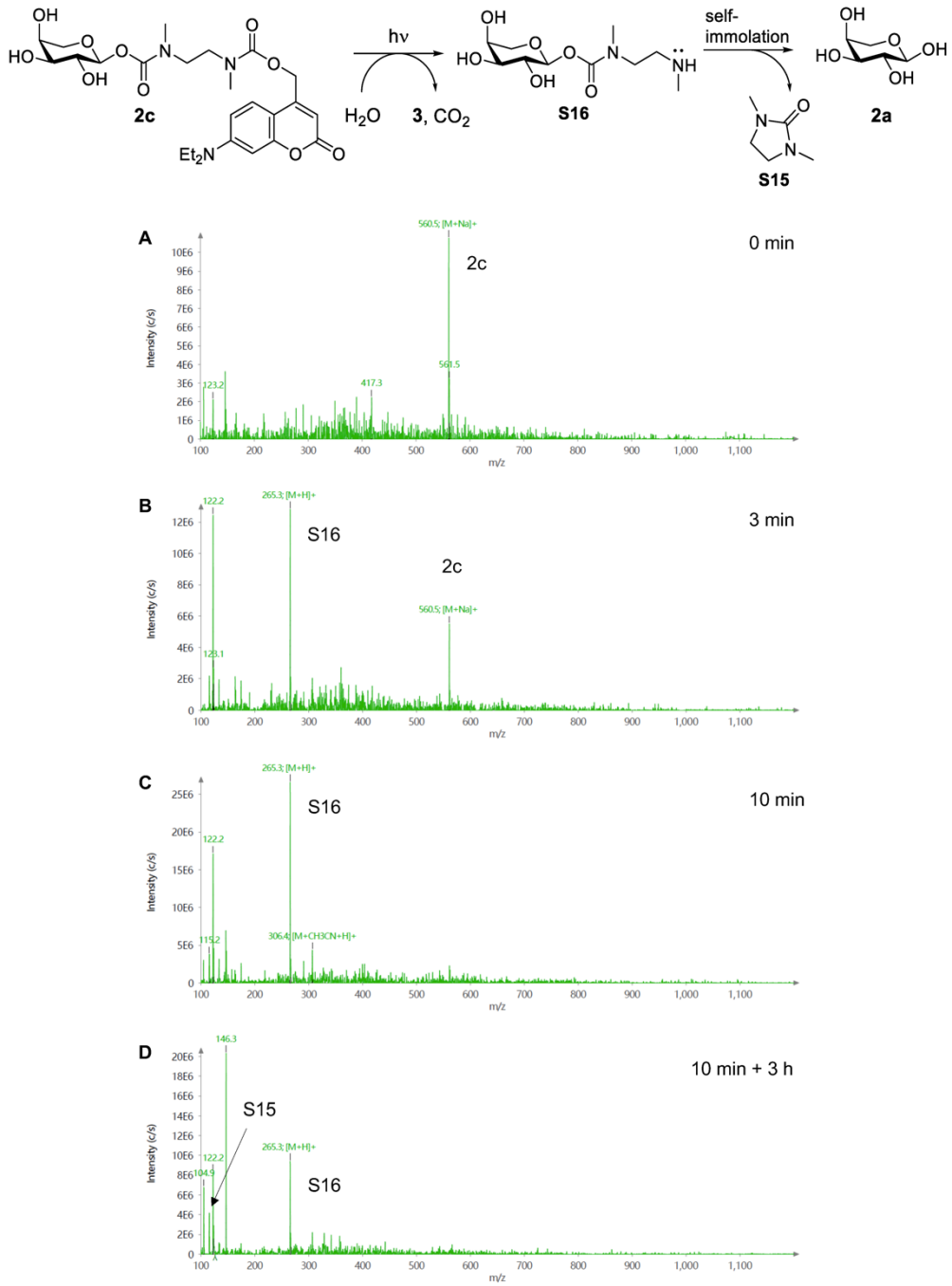

Figure S25: ESI-MS measurements of **2c** (1 mM in MeOH/H_2O 1:1) for monitoring of the intermediate **S16** after irradiation with 430 nm (45.6 mW cm^{-2}, room temperature) for **A**) 0 min; **B**) 3 min; **C**) 10 min; **D**) 10 min plus allowing it to stand for 3 h at room temperature.

S4.7 Toxicity of both the novel photocaged inducer variants and the light exposure

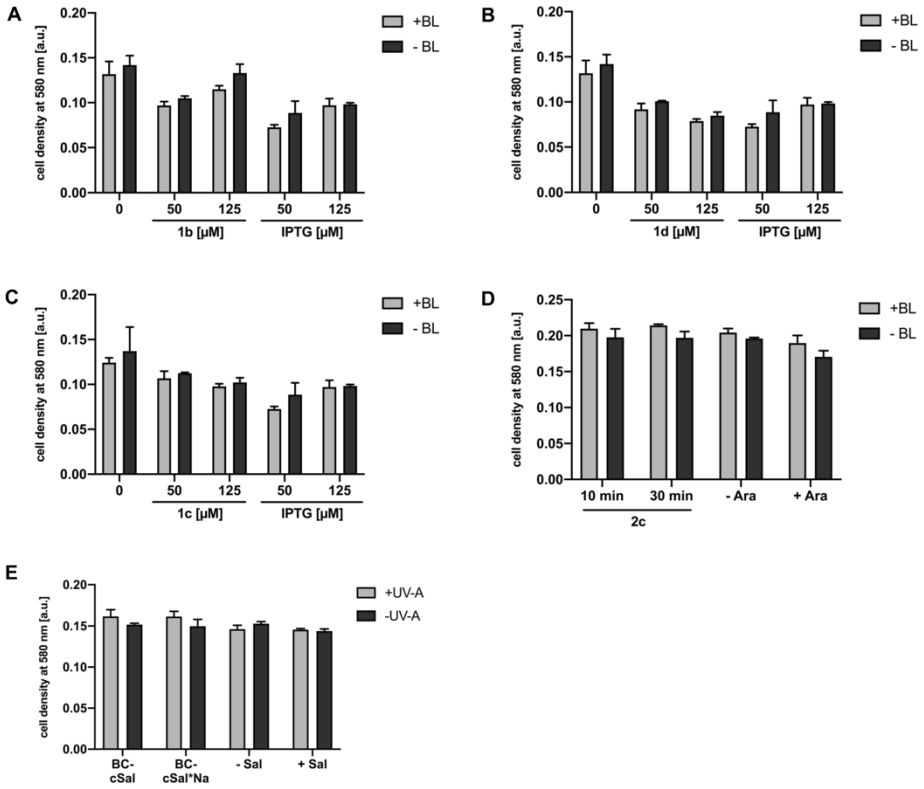

Figure S26: A–C: Growth of *E. coli* Tuner (DE3)/pRhotHi-2-lacI-eYFP expression cultures in the presence of the novel photocaged IPTG variants **1b** (**A**), **1d** (**B**) or **1c** (**C**) compared to uninduced (0 µM) and induced (50 or 125 µM IPTG) cultures. Cells were grown in LB medium at 30 °C and 1200 rpm over 20 h using a ThermoMixer C (Eppendorf, Germany). Cell growth was analysed by determining the optical density at 580 nm. After 2.5 h, formation of photoproducts was induced in cultures *via* blue light exposure at 447 nm for 10 min (BL; ~10 mW cm^{-2}) and conventional IPTG (**1a**) was added manually. **D**: Growth of *E. coli* LMG194/pBTBX-2-mCherry expression cultures in the presence of the novel photocaged arabinose variant **2c** (50 µM) compared to uninduced (-Ara; 0 µM) and induced (+Ara; 50 µM) cultures. Cells were grown in LB medium at 37 °C and 1200 rpm over 20 h using a ThermoMixer C (Eppendorf, Germany). Cell growth was analysed by determining the optical density at 580 nm. After 2.5 h, formation of photoproducts was induced in cultures *via* blue light exposure at 447 nm for 10 min or 30 min (BL; ~10 mW cm^{-2}) and conventional arabinose (**2a**) was added manually. **E**: Growth of *E. coli* Tuner(DE3)/pBNTmcs-mCherry expression cultures in the presence of the novel photocaged salicylic acid (Sal) variants BC-cSal (**21**) and BC-cSal*Na (**25**) compared to uninduced (-Sal; 0 µM) and induced (+ Sal; 1000 µM Sal) cultures. Cells were grown in LB medium at 30 °C and 1200 rpm over 20 h using a ThermoMixer C (Eppendorf, Germany). Cell growth was analysed by determining the optical density at 580 nm. After 2.5 h formation of photoproducts was induced in cultures *via* light exposure at 365 nm for 30 min (~1 mW cm^{-2}) and conventional Sal was added manually. Values are means of biological triplicate measurements and error bars indicate the respective standard deviation.

S4.8 *In vivo* results of photocaged IPTG 1e

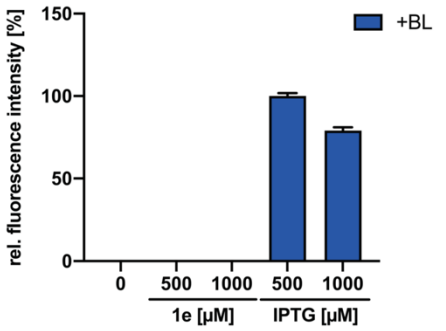

Figure S27: Normalized *in vivo* eYFP fluorescence intensity of *E. coli* Tuner (DE3)/pRhotHi-2-lacI-eYFP expression cultures supplemented with 500 µM or 1000 µM of the photocaged compound **1e**. All cultures were incubated in the dark for 20 h in LB medium at 30 °C and light-mediated induction of reporter gene expression was performed after 2.5 h by blue light exposure at 447 nm (BL; ~90 mW cm^2) for 10 min or the addition of respective amounts of conventional IPTG (**1a**). *In vivo* fluorescence intensities were determined by using a BioLector system (λ_{ex} = 508 nm, λ_{em} = 532 nm), normalized to cell densities and are shown in relation to the respective fluorescence intensities of a culture induced with conventional IPTG (**1a**). Values are means of triplicate measurements. Error bars indicate the respective standard deviations.

S4.9 NMR spectra of compounds

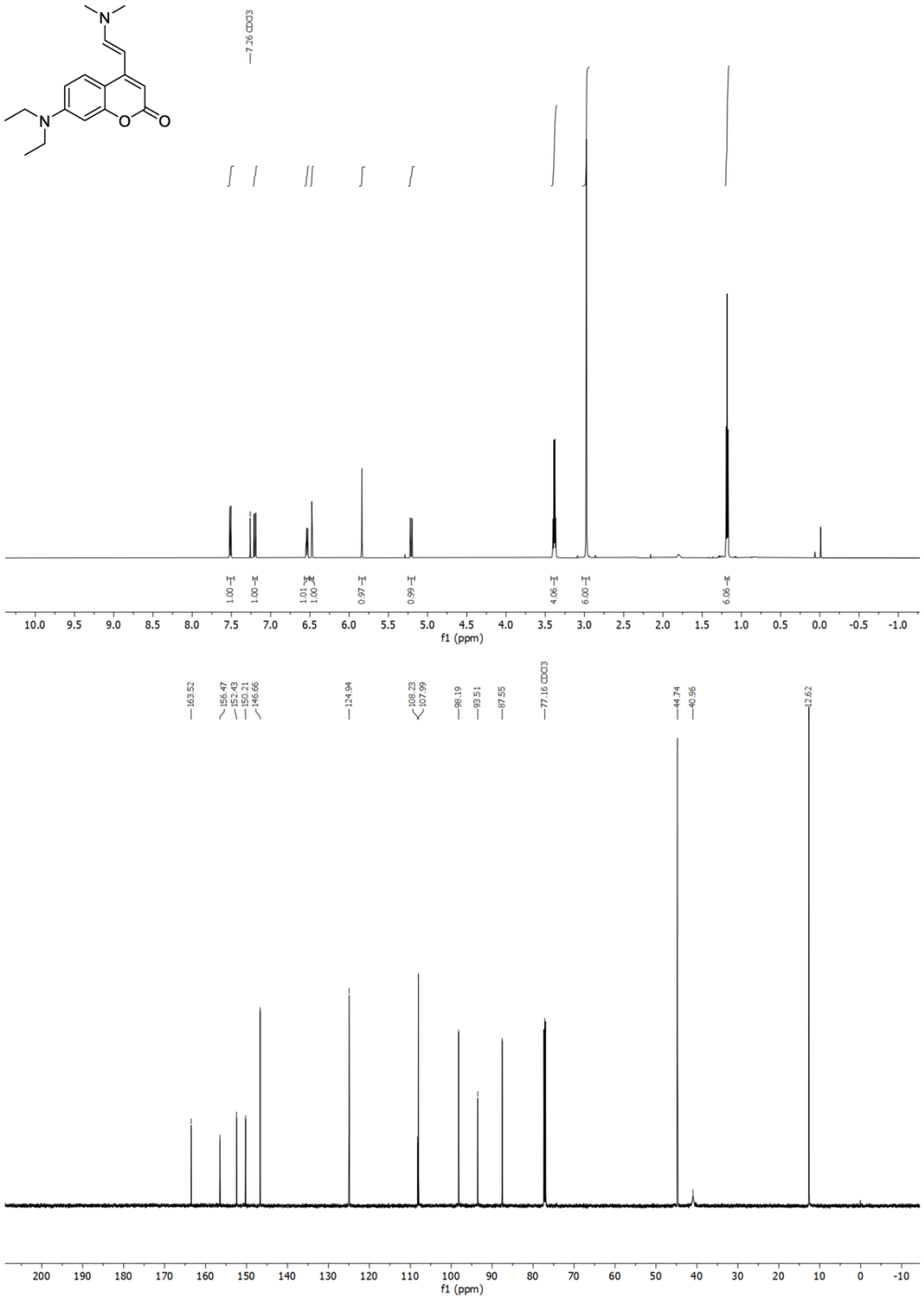

Figure S29: ^{1}H- and ^{13}C-NMR spectra of **S2** in $CDCl_3$ (600 MHz/151 MHz).

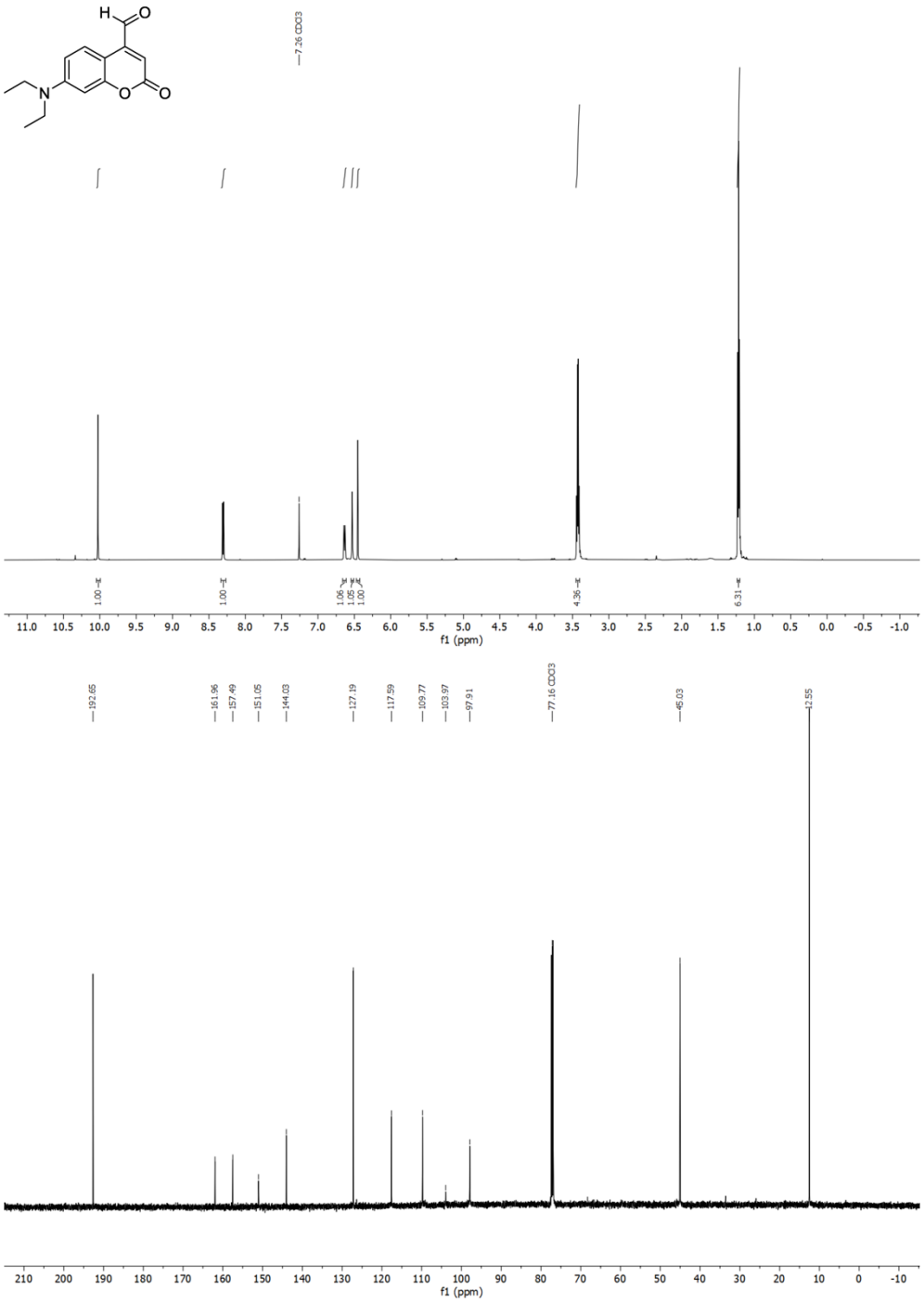

Figure S30: ^{1}H- and ^{13}C-NMR spectra of **S3** in $CDCl_3$ (600 MHz/151 MHz).

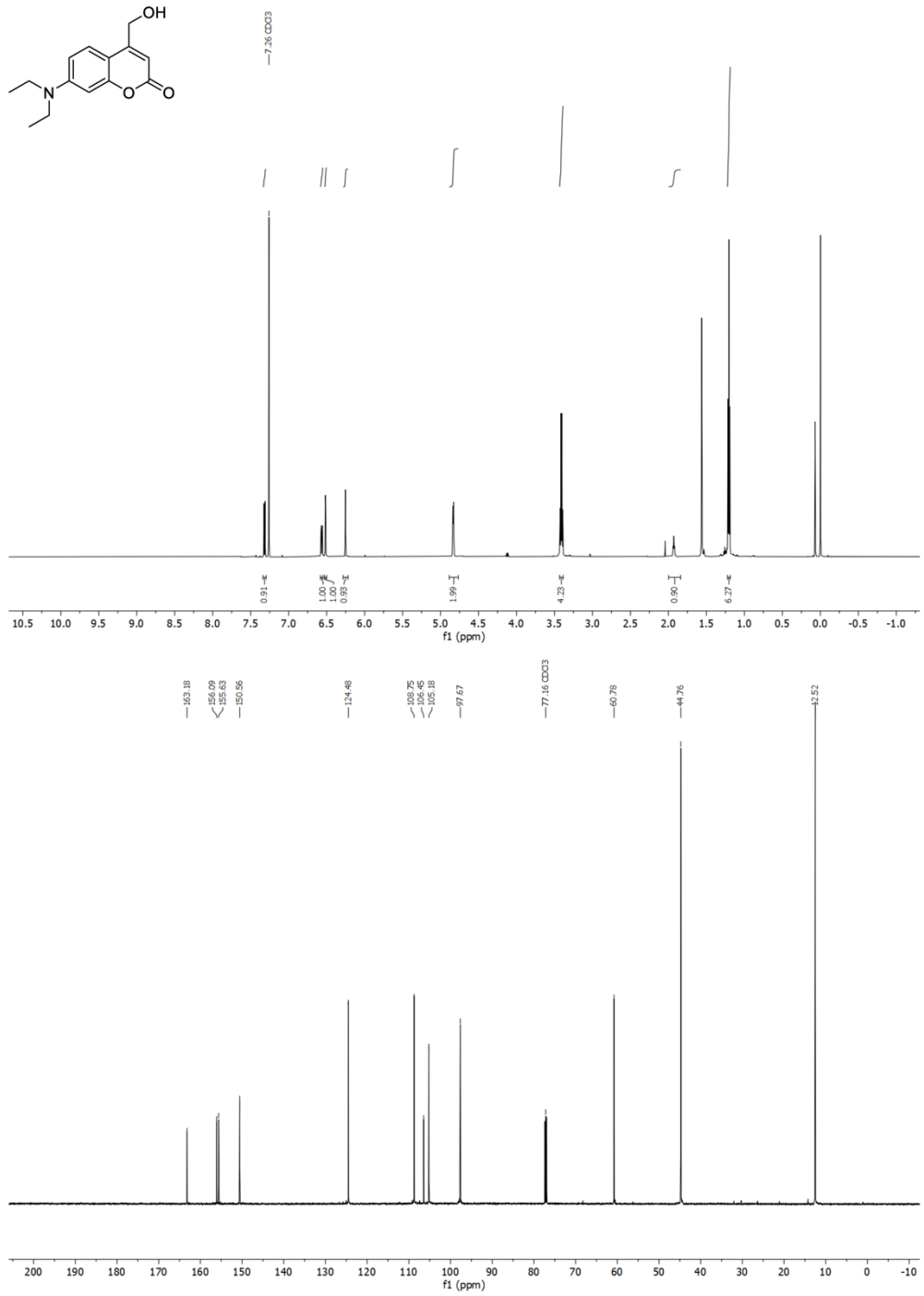

Figure S31: ^{1}H- and ^{13}C-NMR spectra of **3** in $CDCl_3$ (600 MHz/151 MHz).

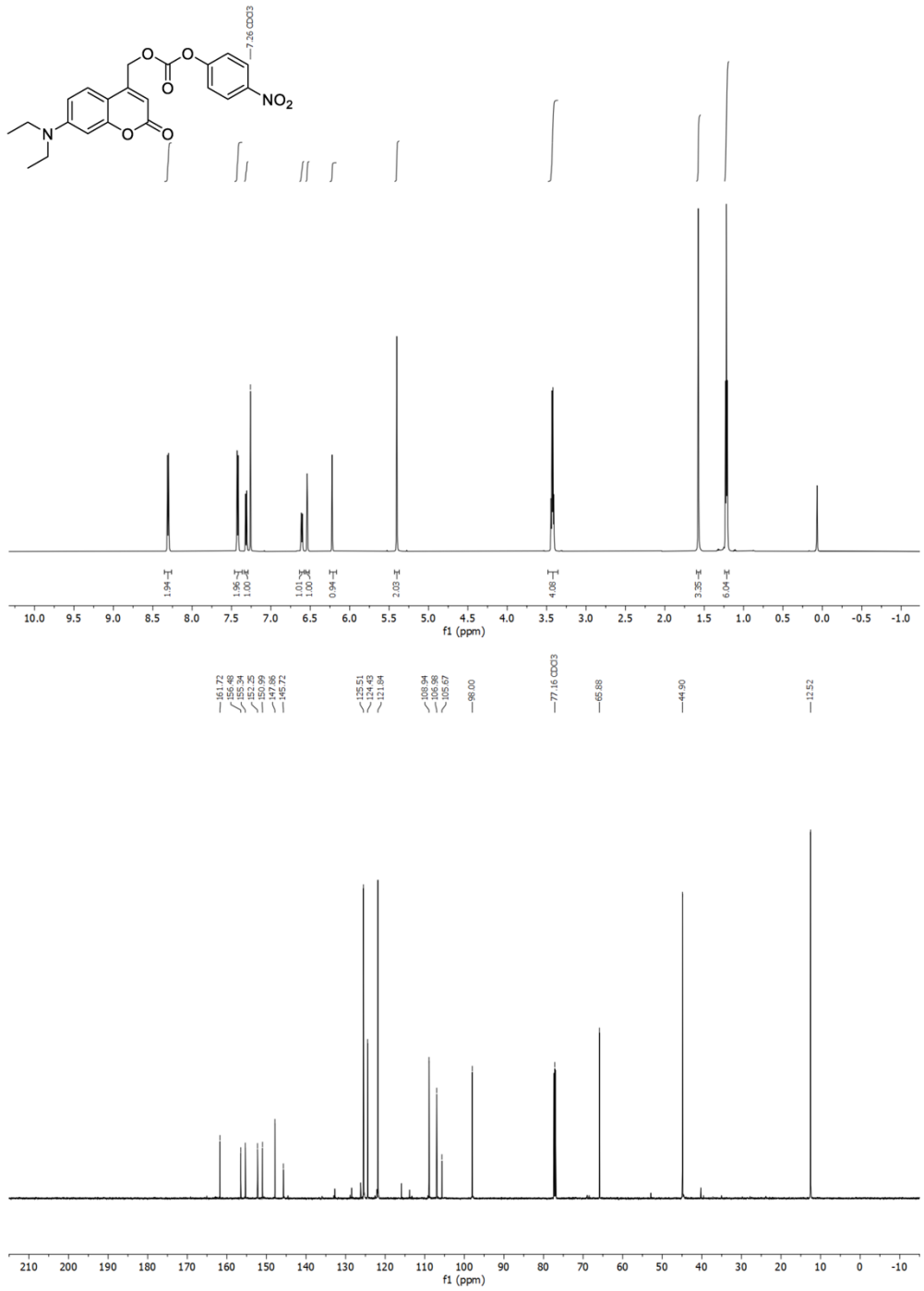

Figure S32: ^{1}H- and ^{13}C-NMR spectra of **5** in $CDCl_3$ (600 MHz/151 MHz).

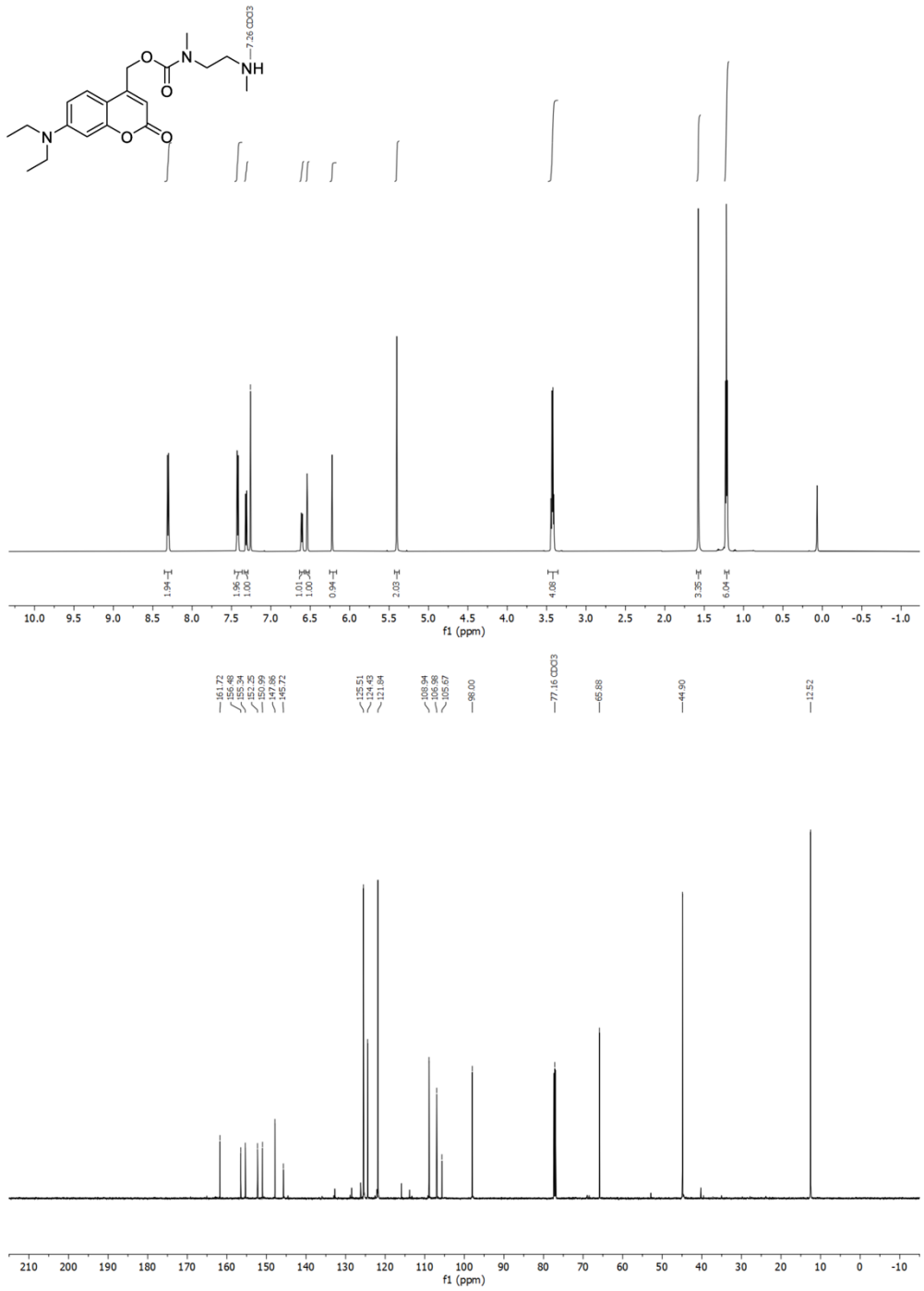

Figure S33: ^{1}H- and ^{13}C-NMR spectra of **7** in $CDCl_3$ (600 MHz/151 MHz).

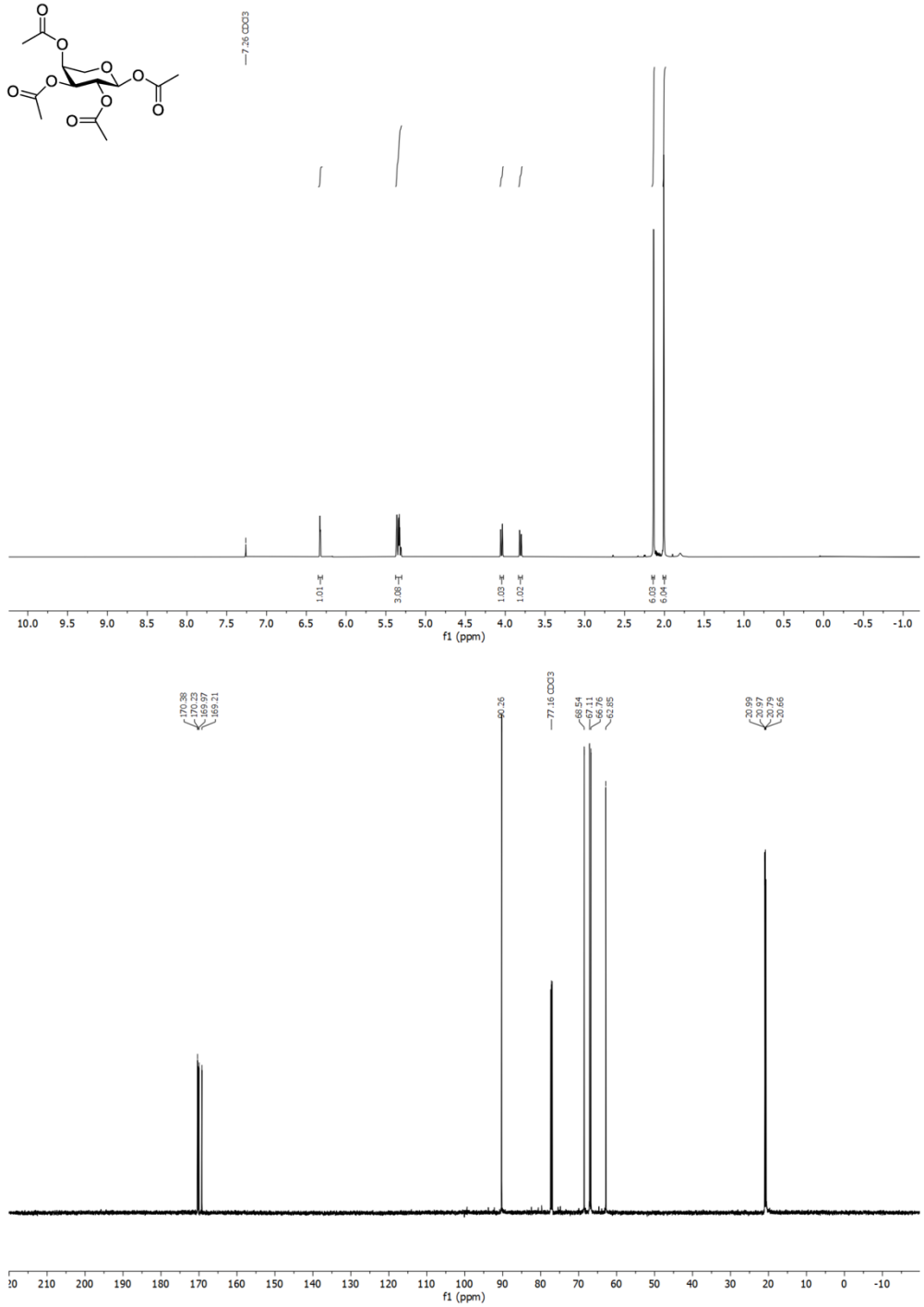

Figure S34: ^{1}H- and ^{13}C-NMR spectra of **S4** in $CDCl_3$ (600 MHz/151 MHz).

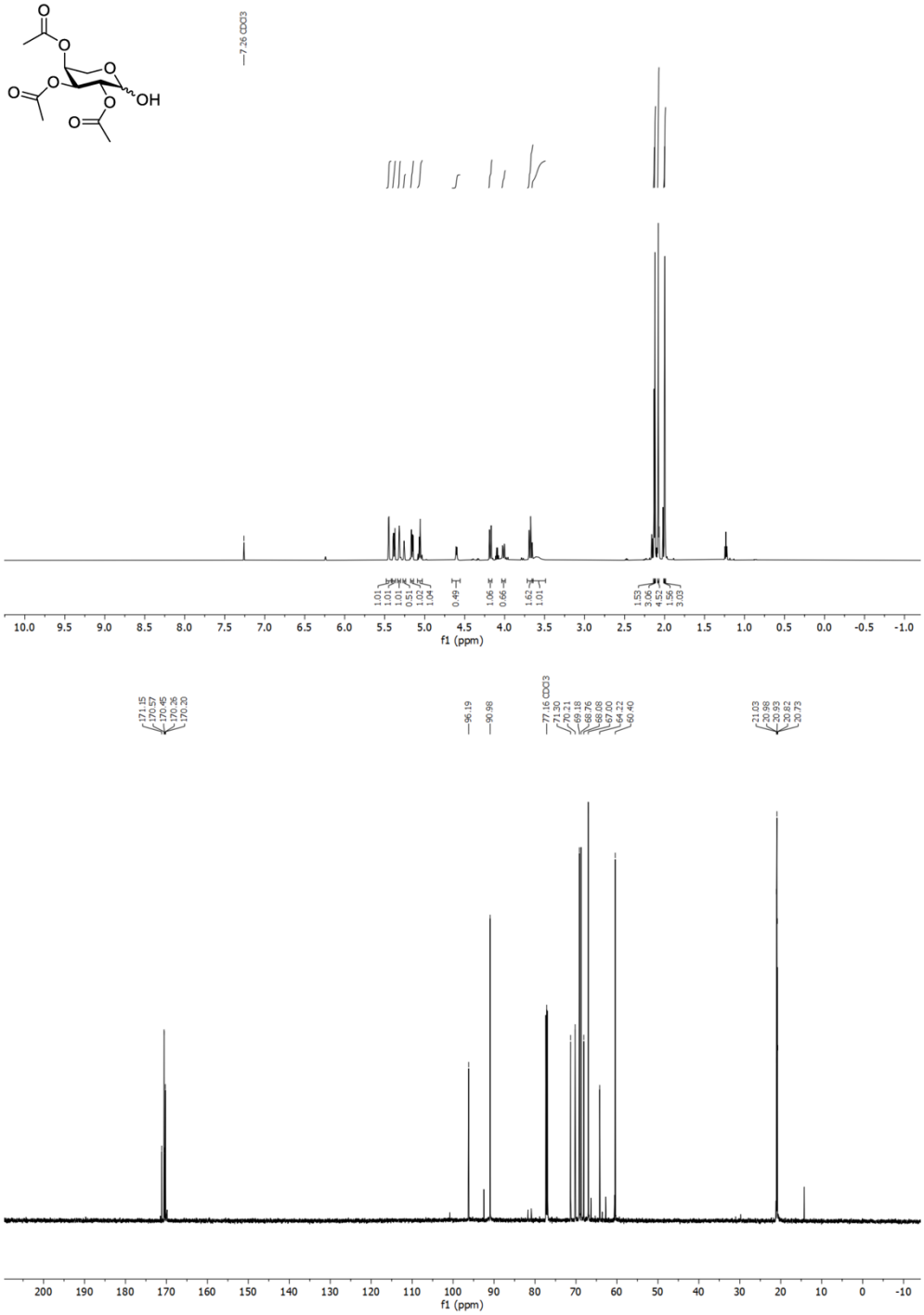

Figure S35: ^{1}H- and ^{13}C-NMR spectra of **S5** in $CDCl_3$ (600 MHz/151 MHz).

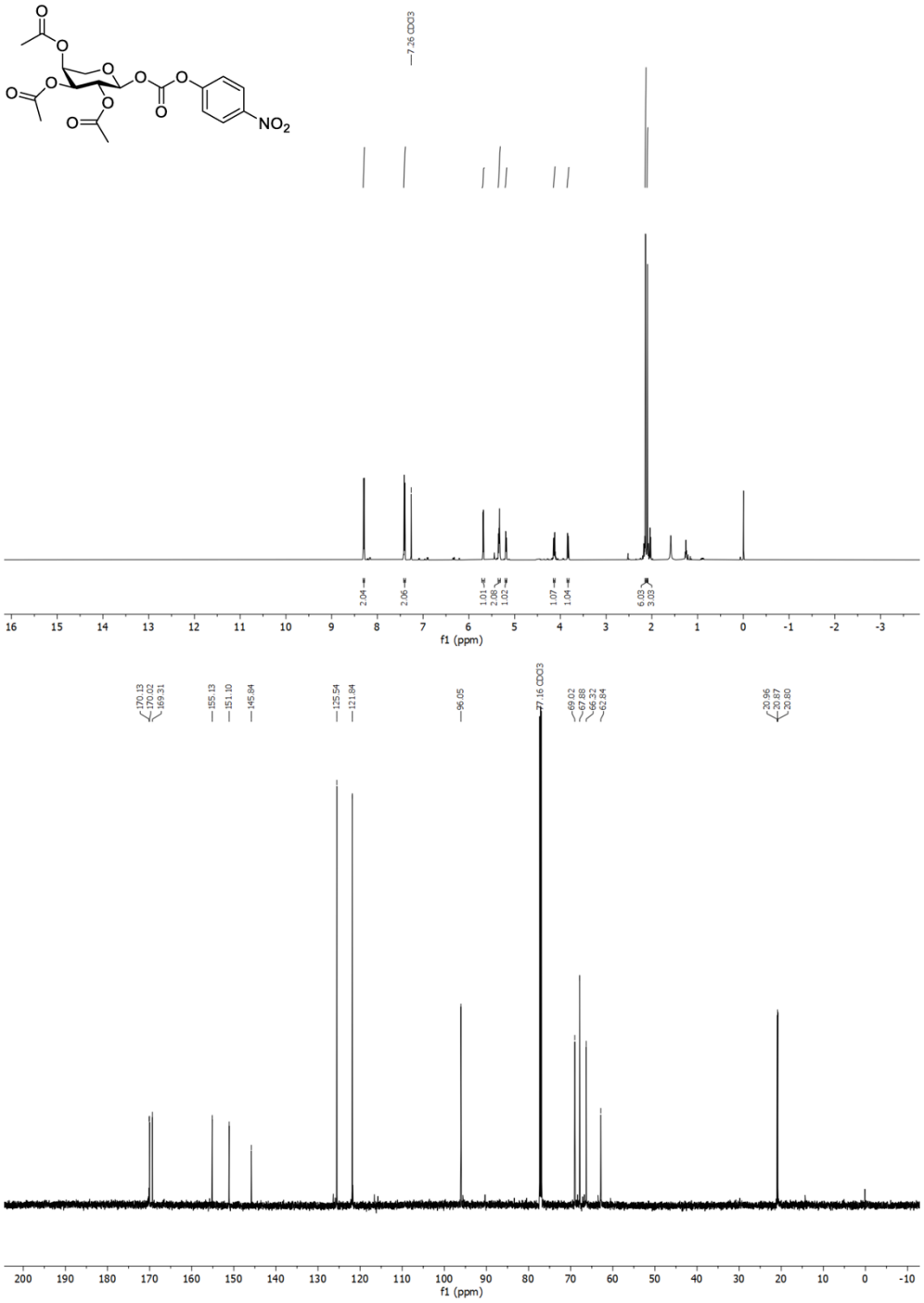

Figure S36: ^{1}H- and ^{13}C-NMR spectra of **11** in $CDCl_3$ (600 MHz/151 MHz).

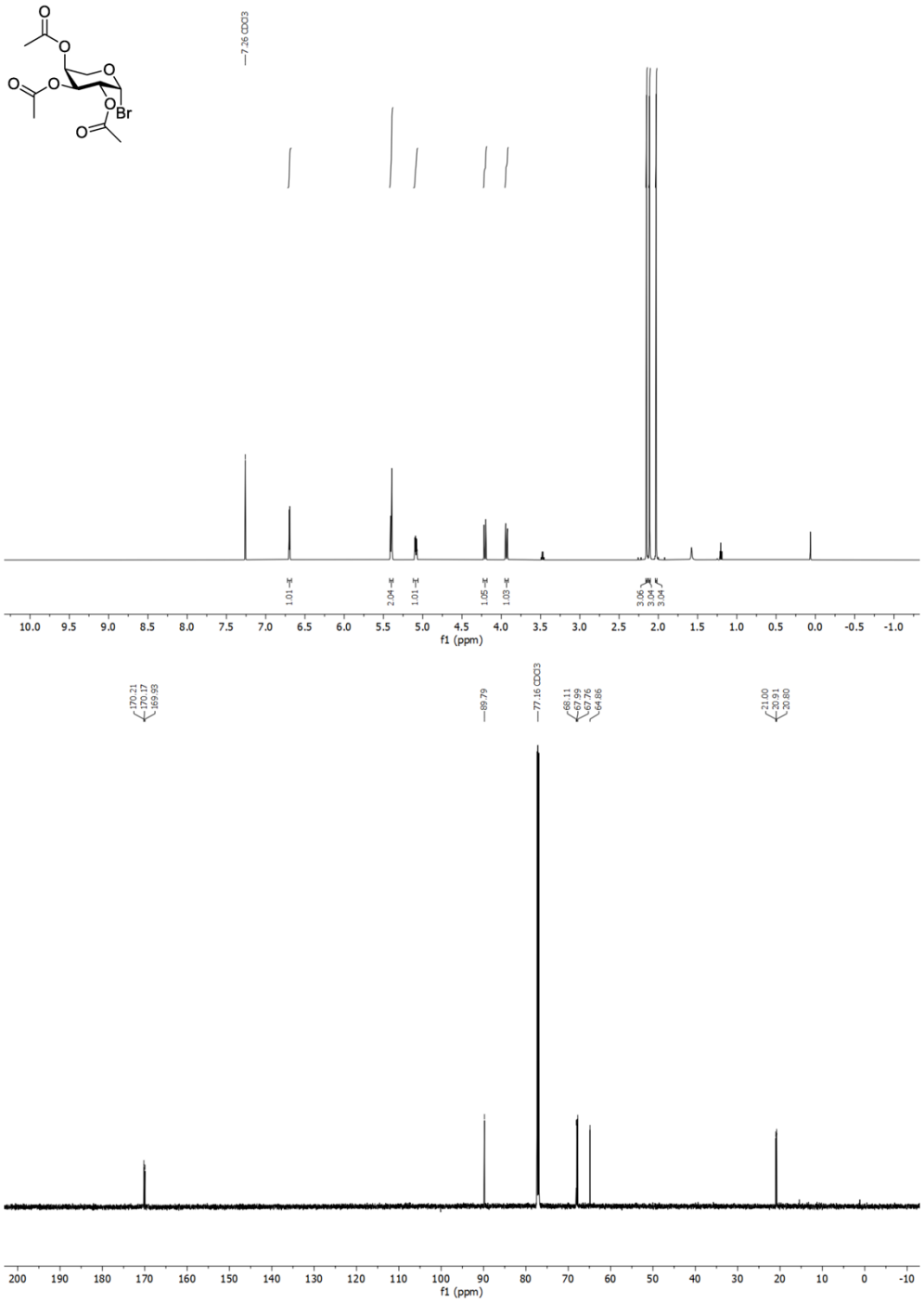

Figure S37: ^{1}H- and ^{13}C-NMR spectra of **8** in $CDCl_3$ (600 MHz/151 MHz).

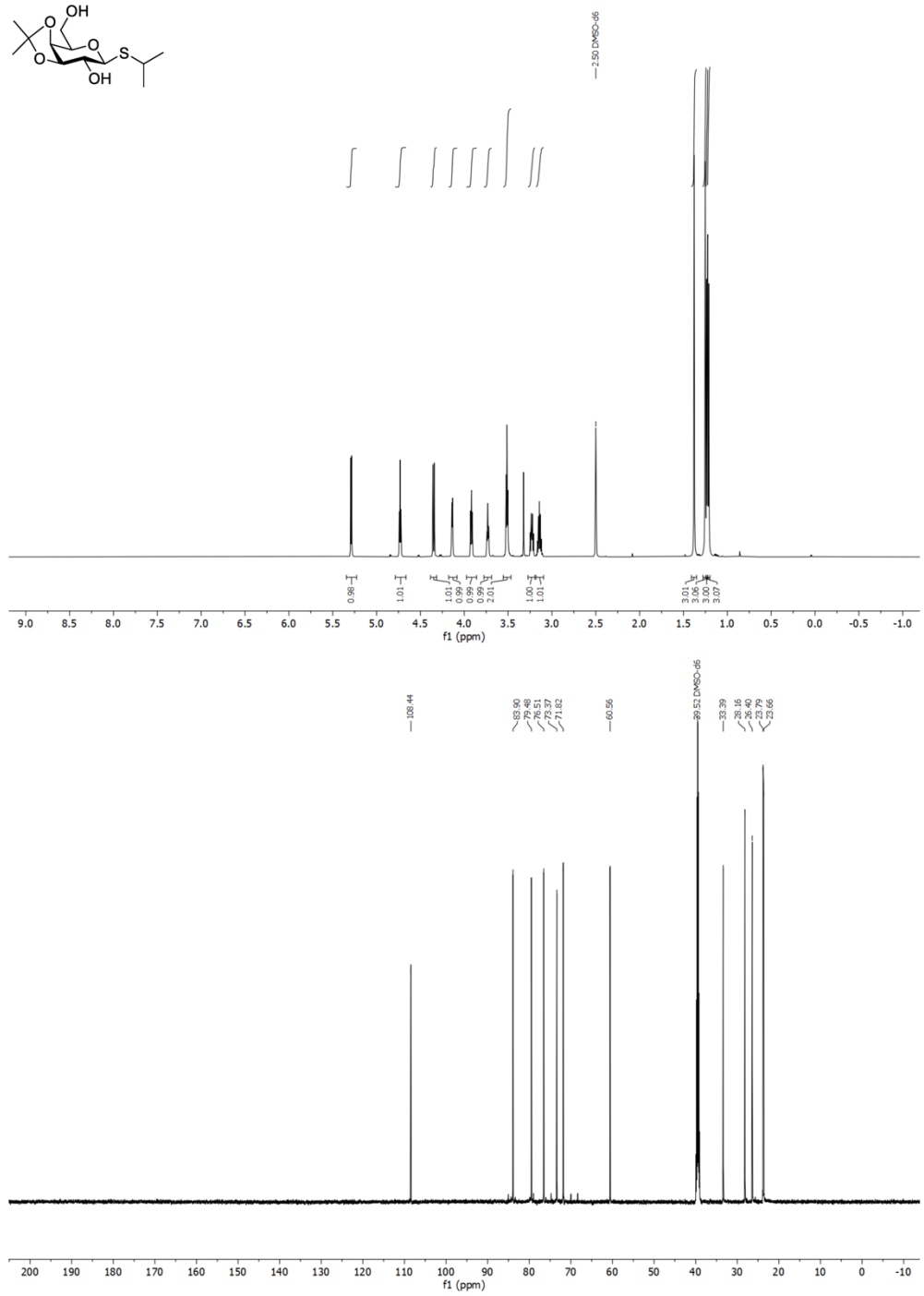

Figure S38: ^{1}H- and ^{13}C-NMR spectra of **S6** in DMSO-d_6 (600 MHz/151 MHz).

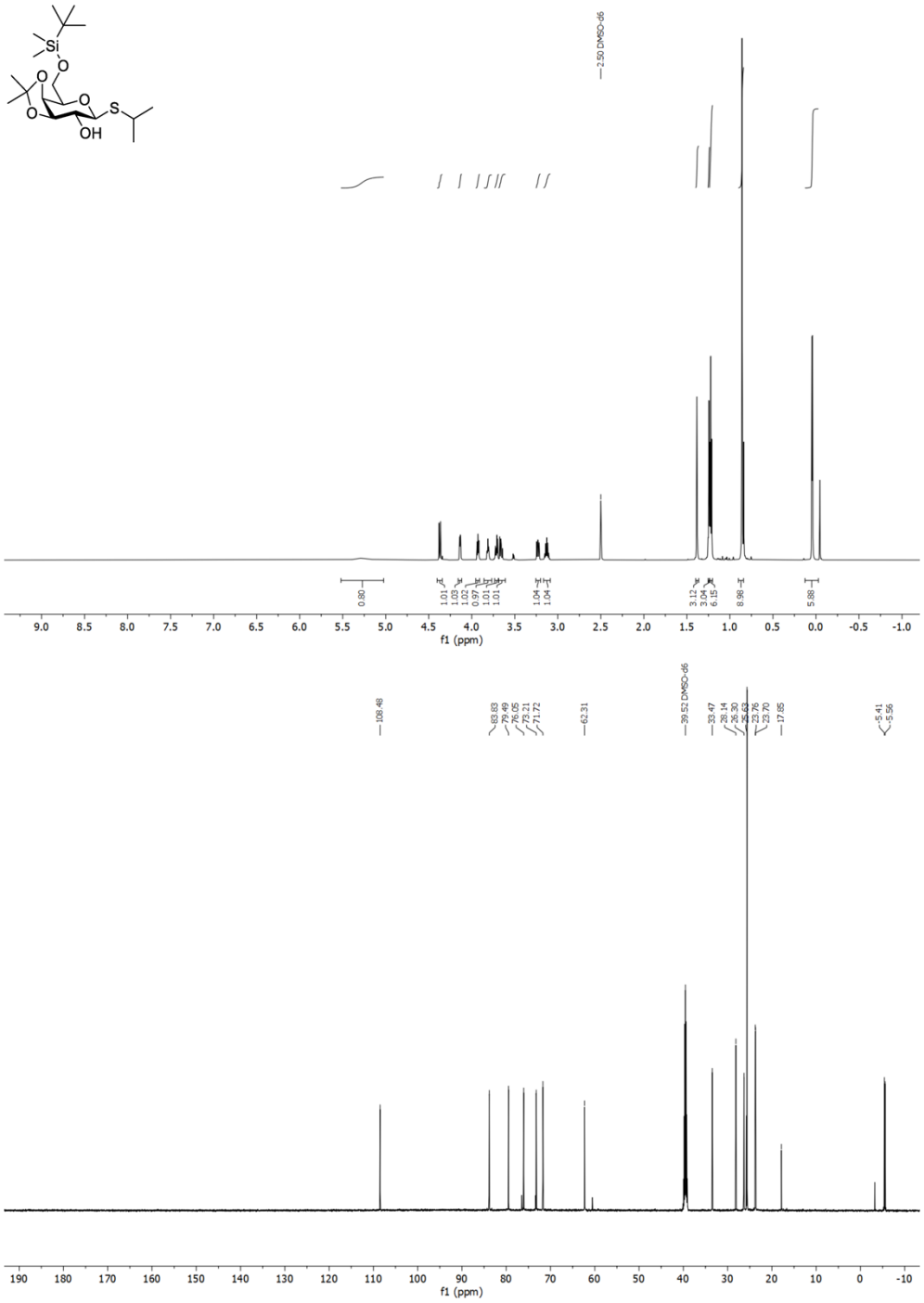

Figure S39: ^{1}H- and ^{13}C-NMR spectra of **9** in DMSO-d_6 (600 MHz/151 MHz).

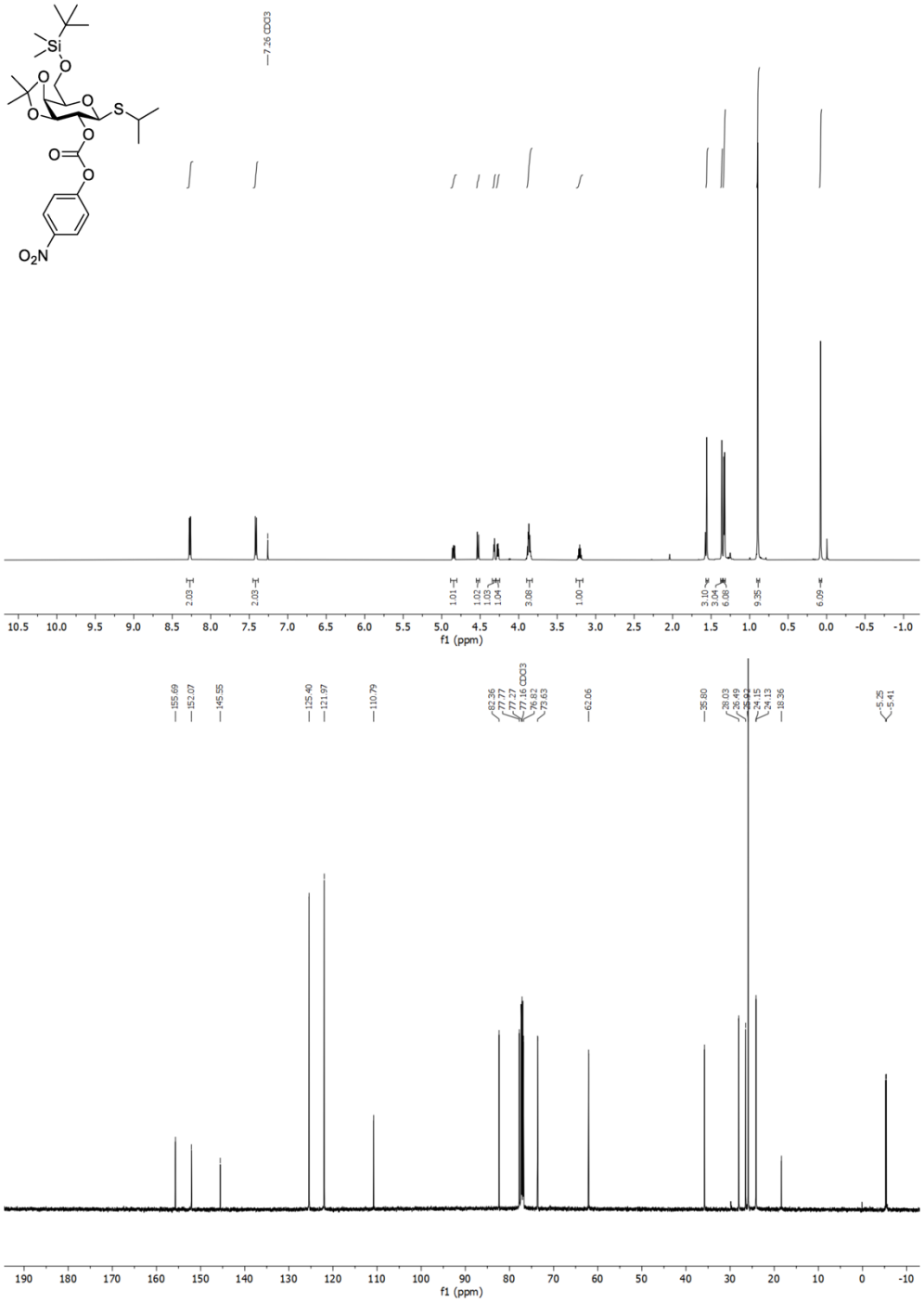

Figure S40: ^{1}H- and ^{13}C-NMR spectra of **12** in $CDCl_3$ (600 MHz/151 MHz).

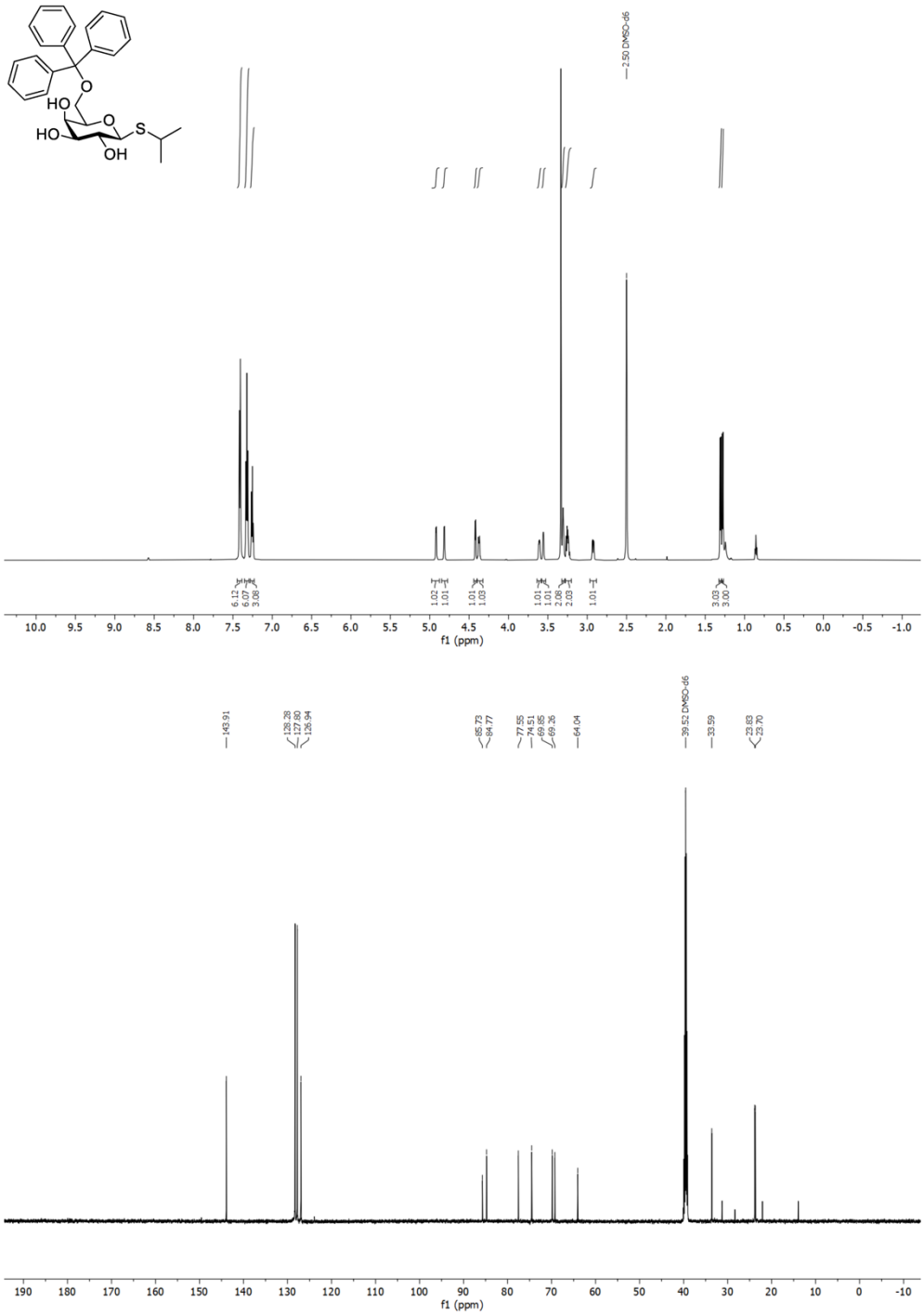

Figure S41: ^{1}H- and ^{13}C-NMR spectra of **S7** in DMSO-d_6 (600 MHz/151 MHz).

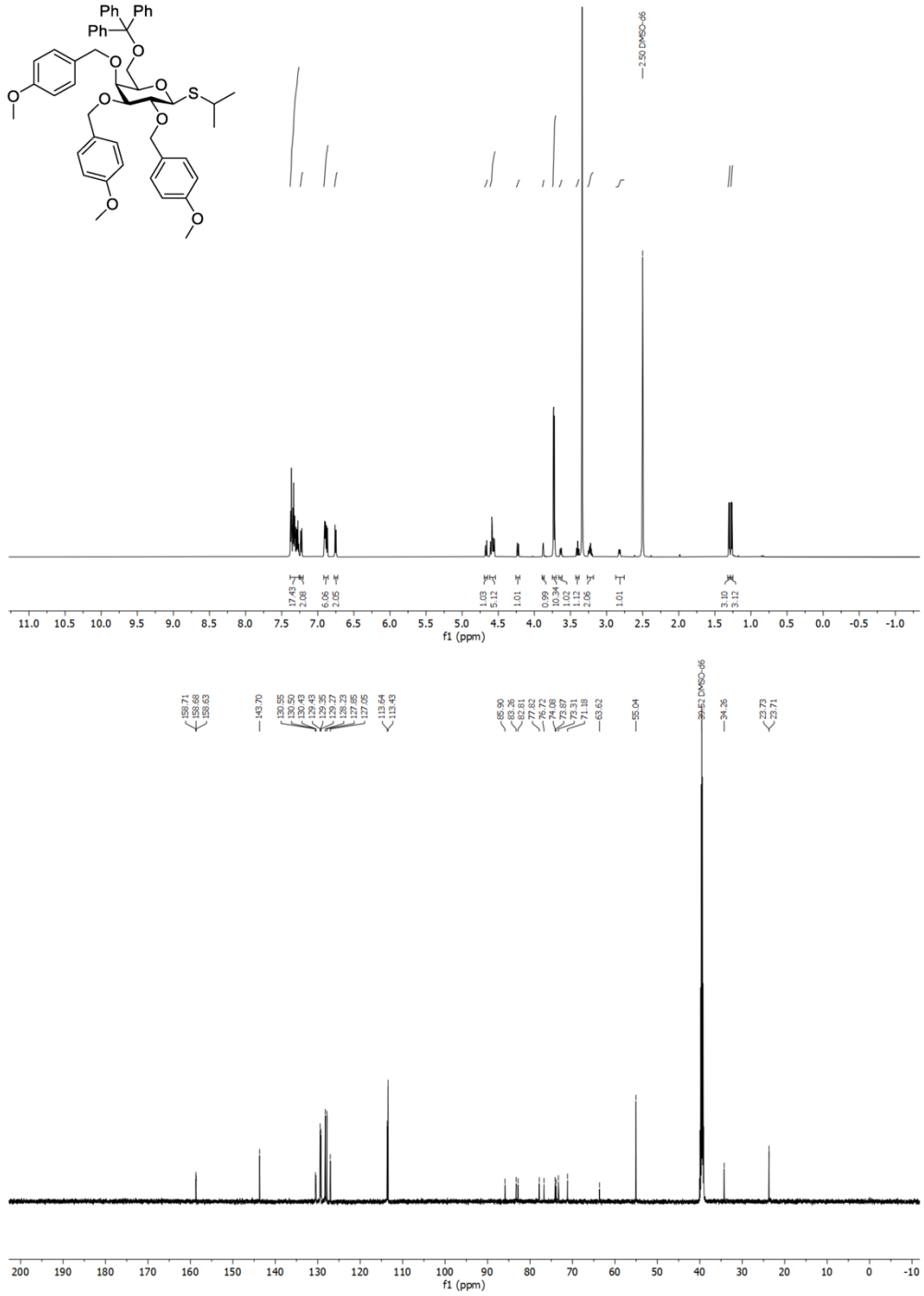

Figure S42: ^{1}H- and ^{13}C-NMR spectra of **S8** in DMSO-d_6 (600 MHz/151 MHz).

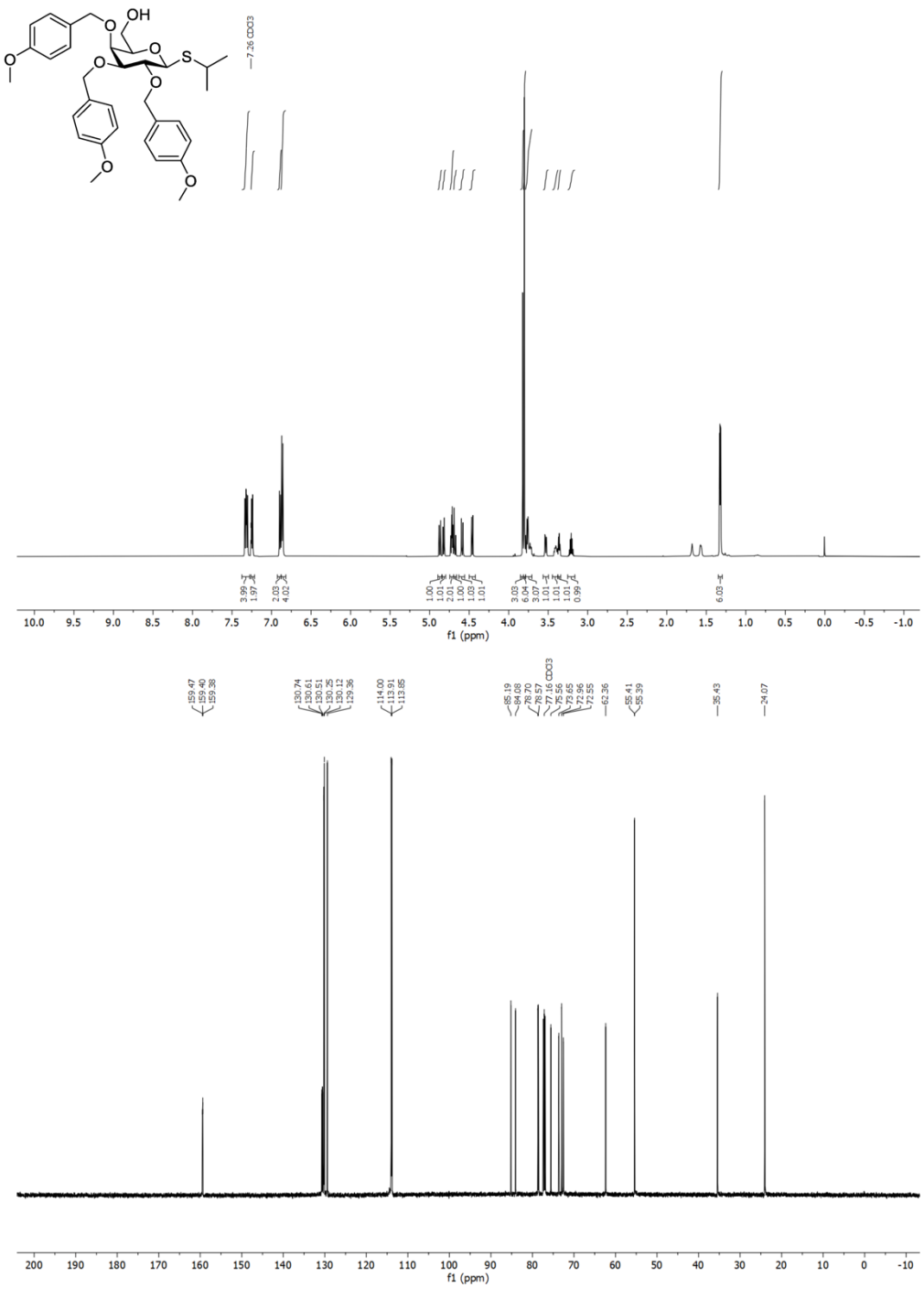

Figure S43: ^{1}H- and ^{13}C-NMR spectra of **10** in $CDCl_3$ (600 MHz/151 MHz).

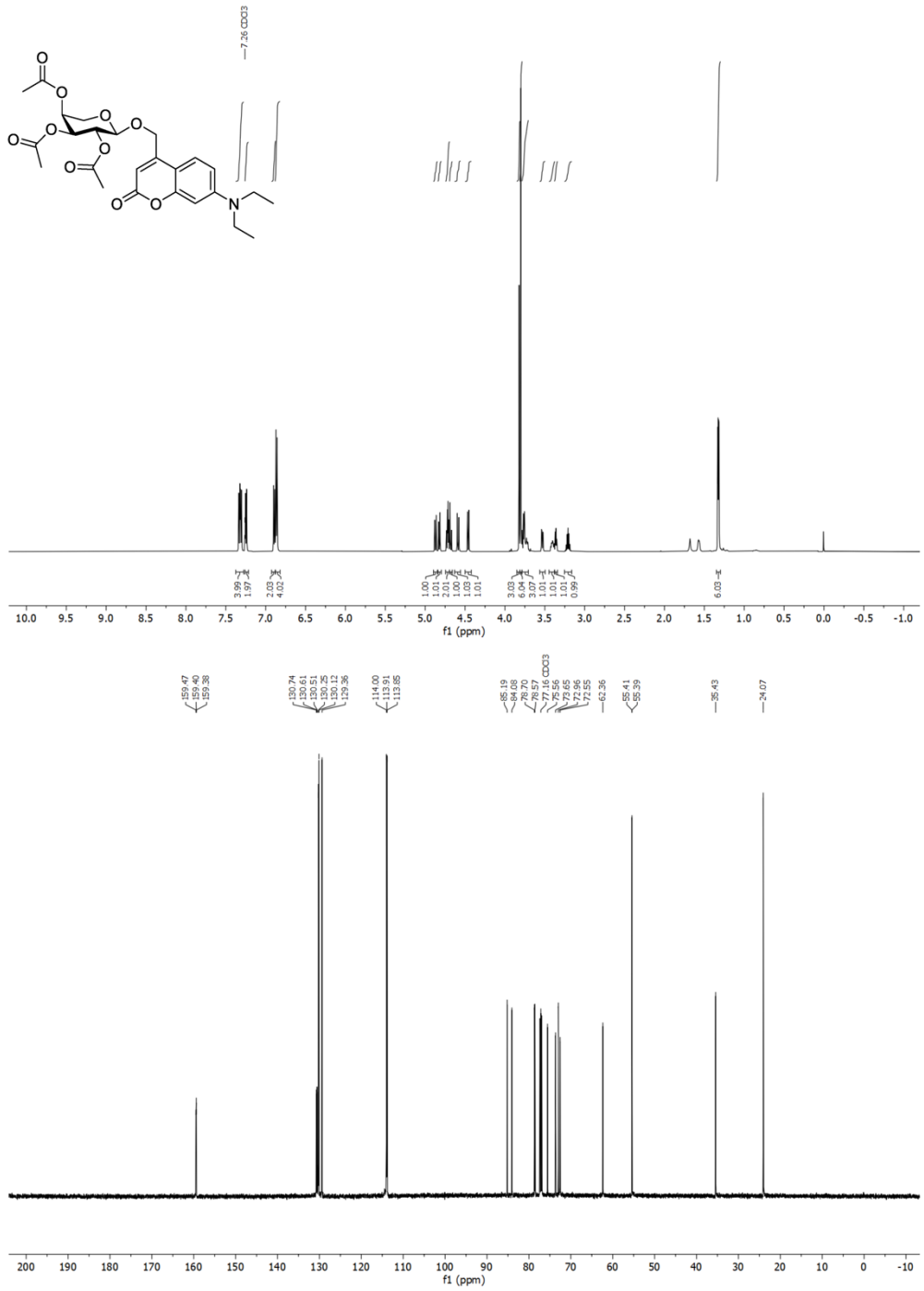

Figure S44: ^{1}H- and ^{13}C-NMR spectra of **13** in $CDCl_3$ (600 MHz/151 MHz).

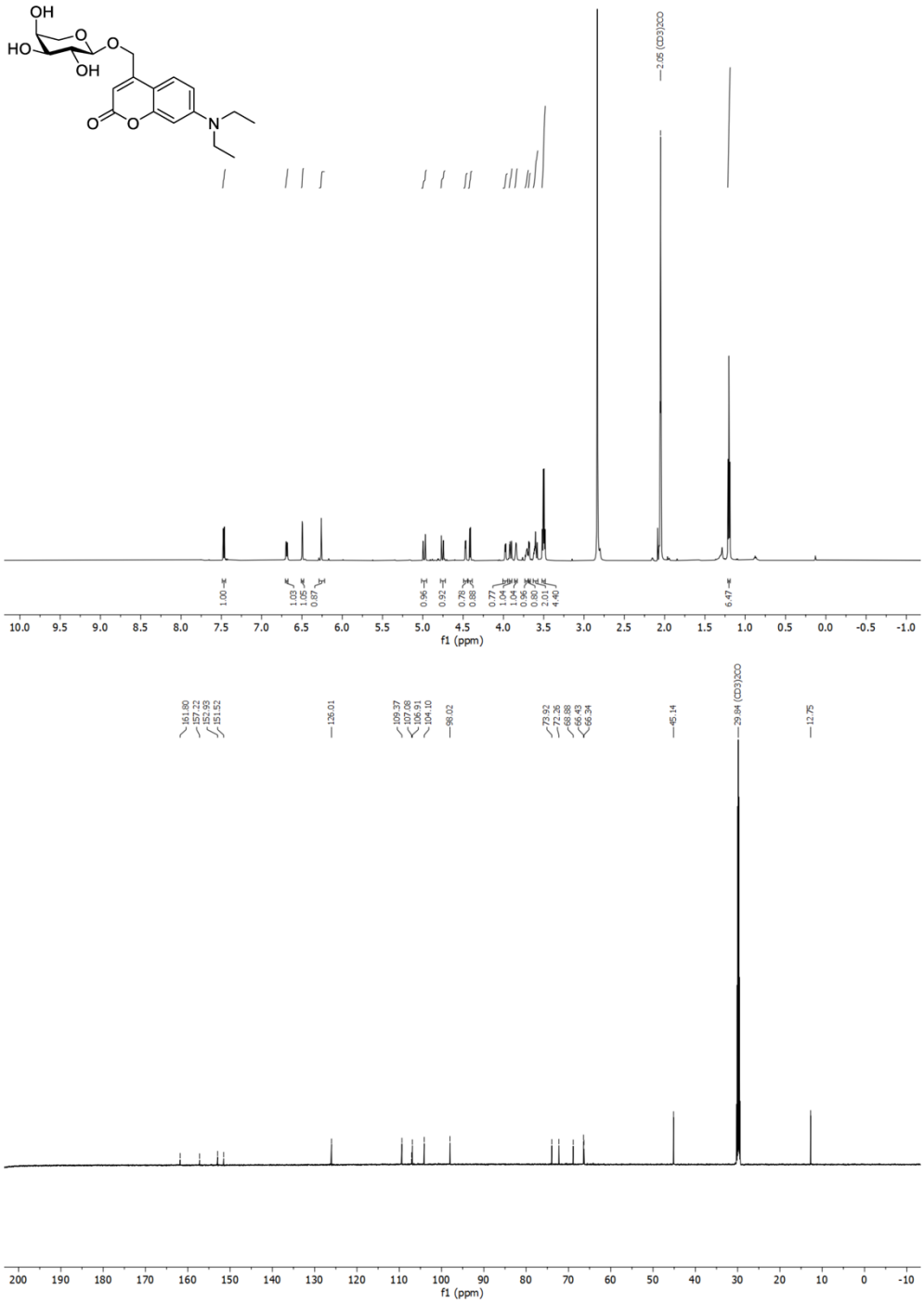

Figure S45: ^{1}H- and ^{13}C-NMR spectra of **2b** in acetone-d_6 (600 MHz/151 MHz).

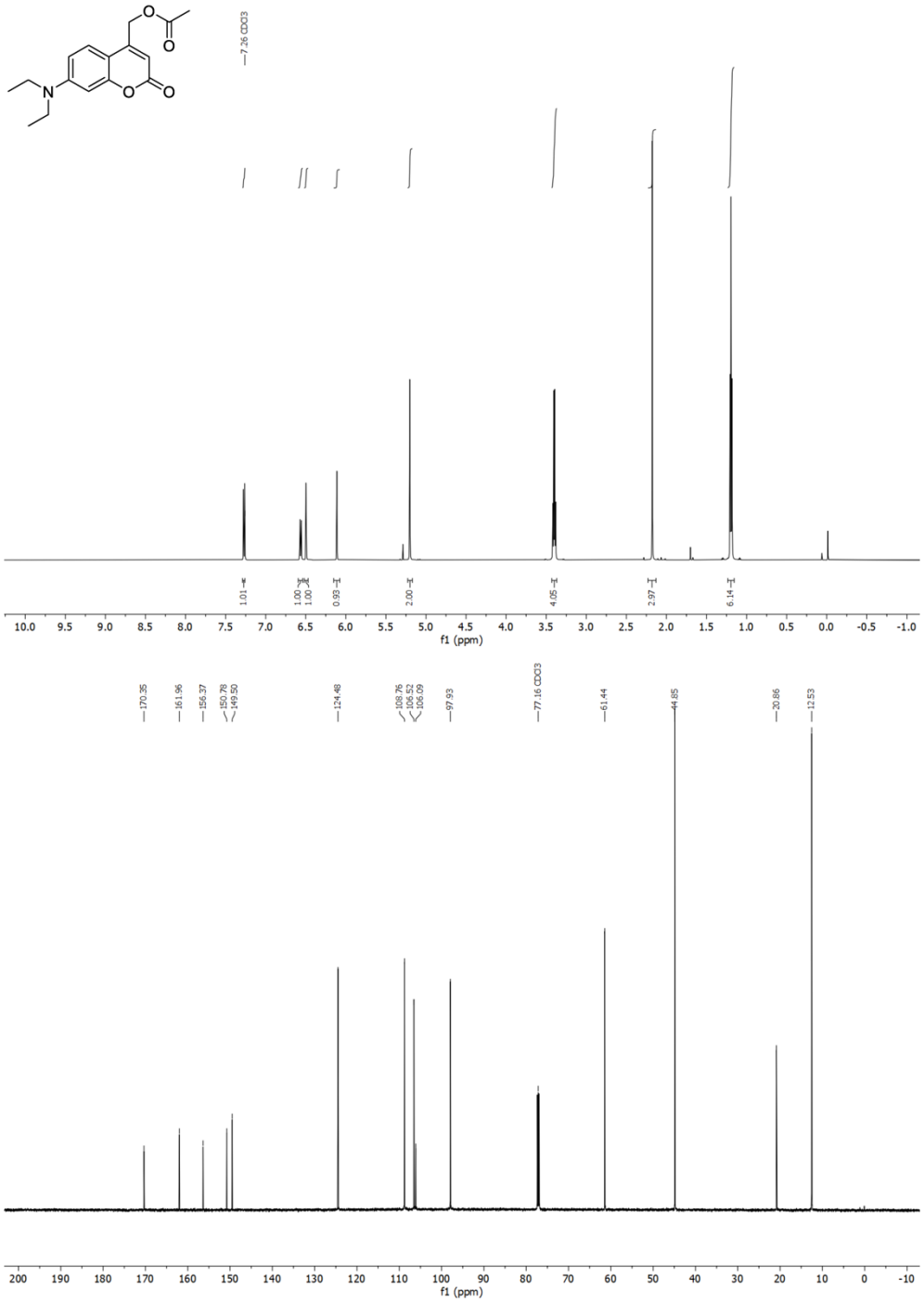

Figure S46: ^{1}H- and ^{13}C-NMR spectra of **S9** in $CDCl_3$ (600 MHz/151 MHz).

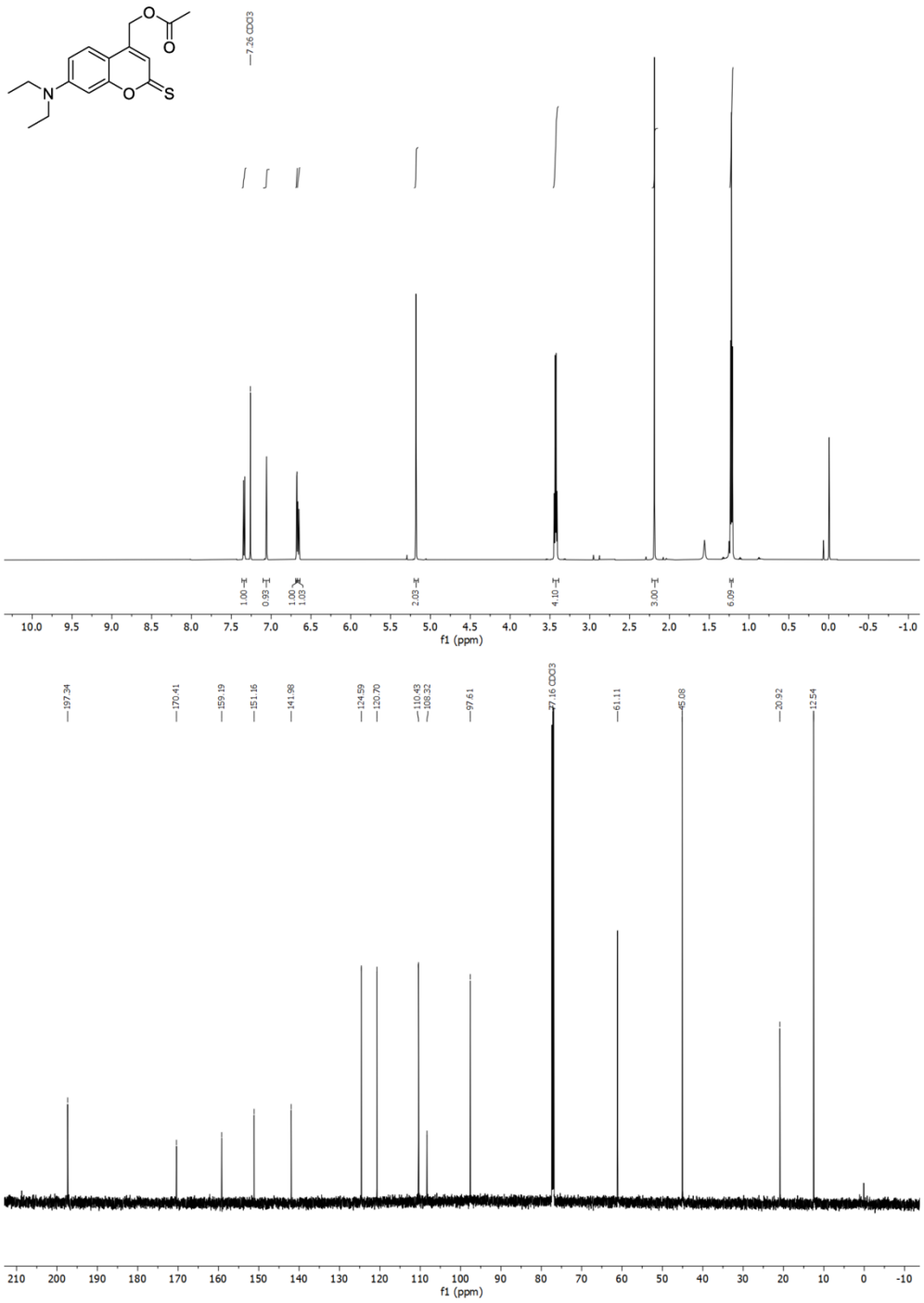

Figure S47: ^{1}H- and ^{13}C-NMR spectra of **S10** in $CDCl_3$ (600 MHz/151 MHz).

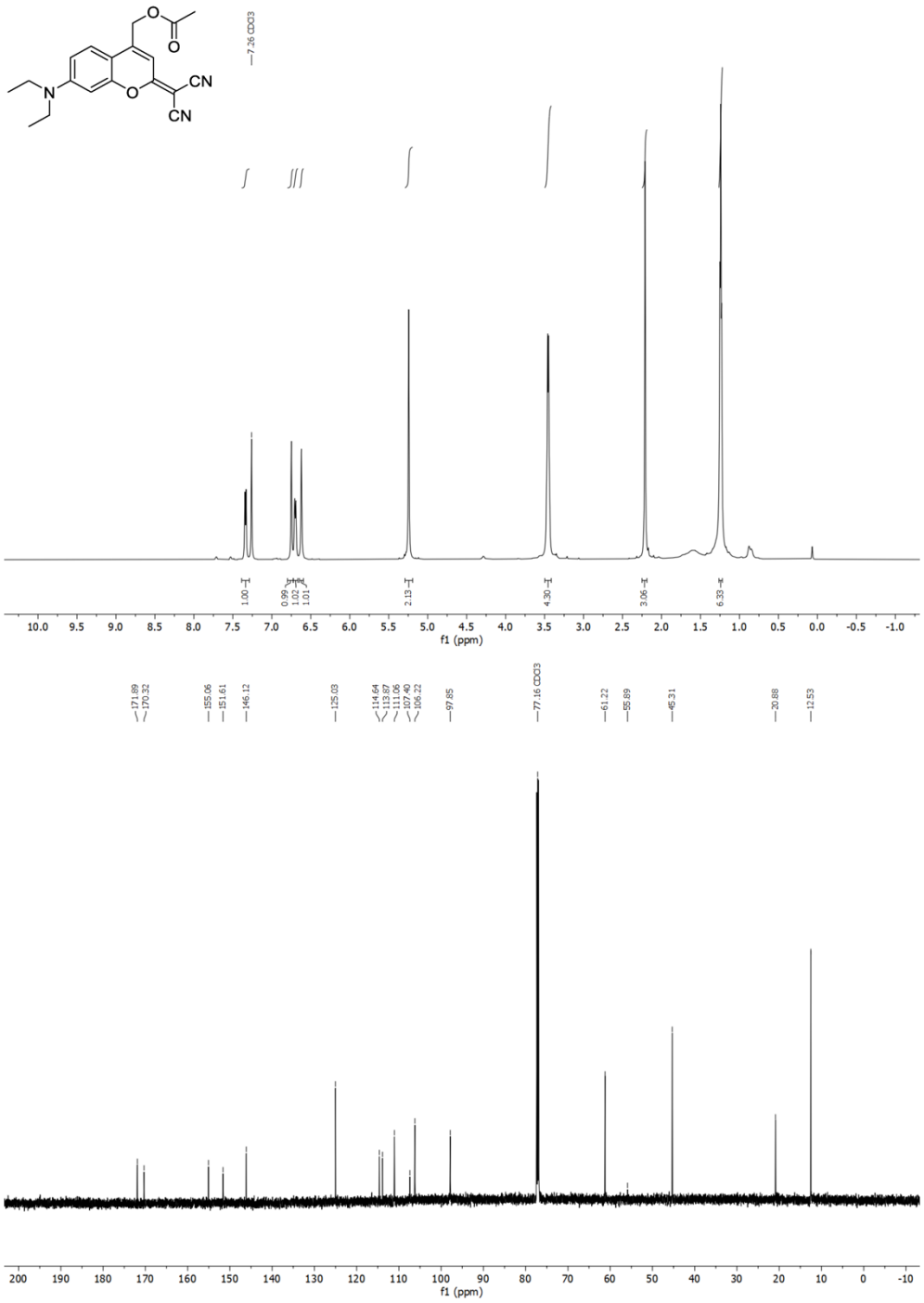

Figure S48: ^{1}H- and ^{13}C-NMR spectra of **S11** in $CDCl_3$ (600 MHz/151 MHz).

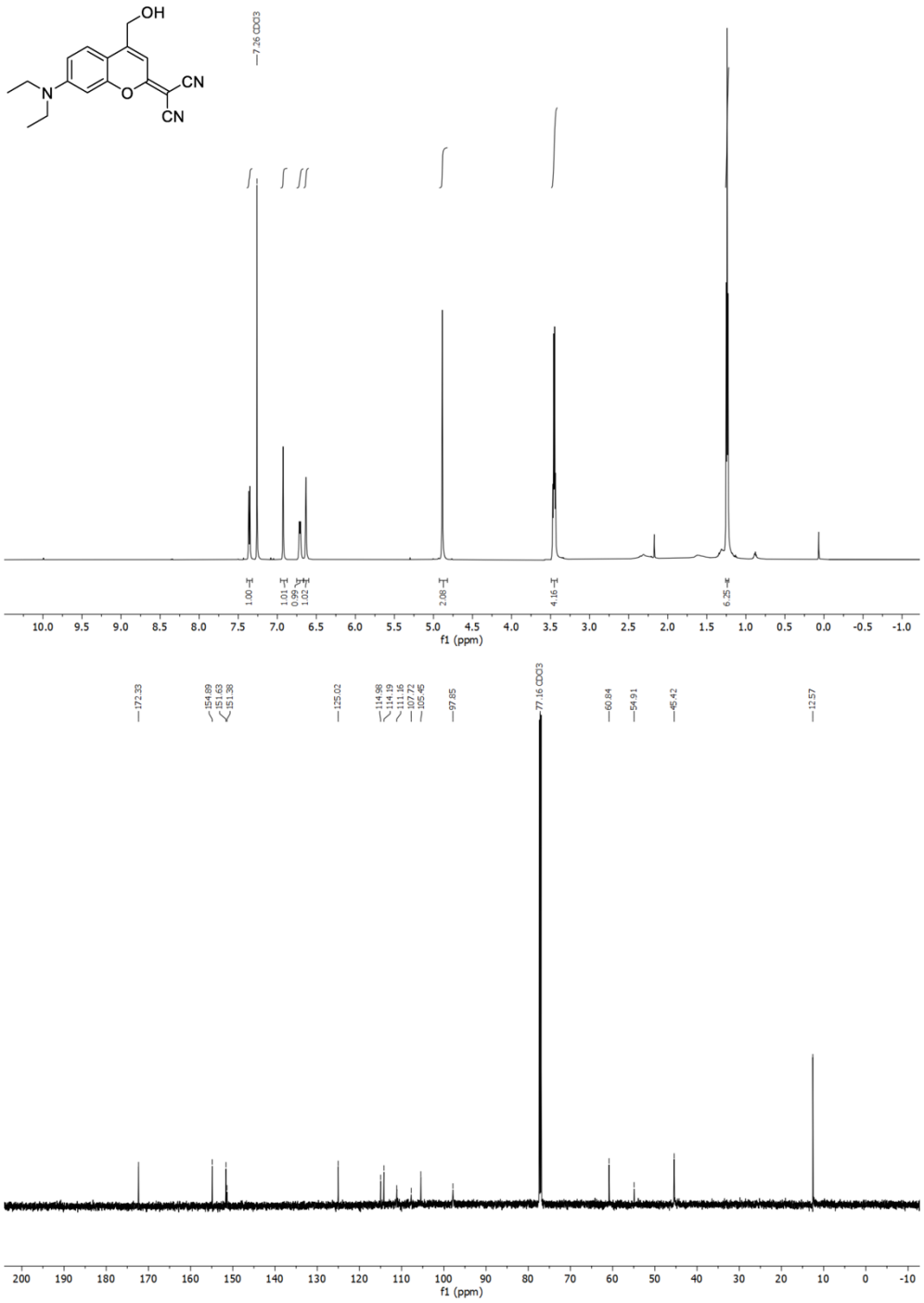

Figure S49: ^{1}H- and ^{13}C-NMR spectra of **4** in $CDCl_3$ (600 MHz/151 MHz).

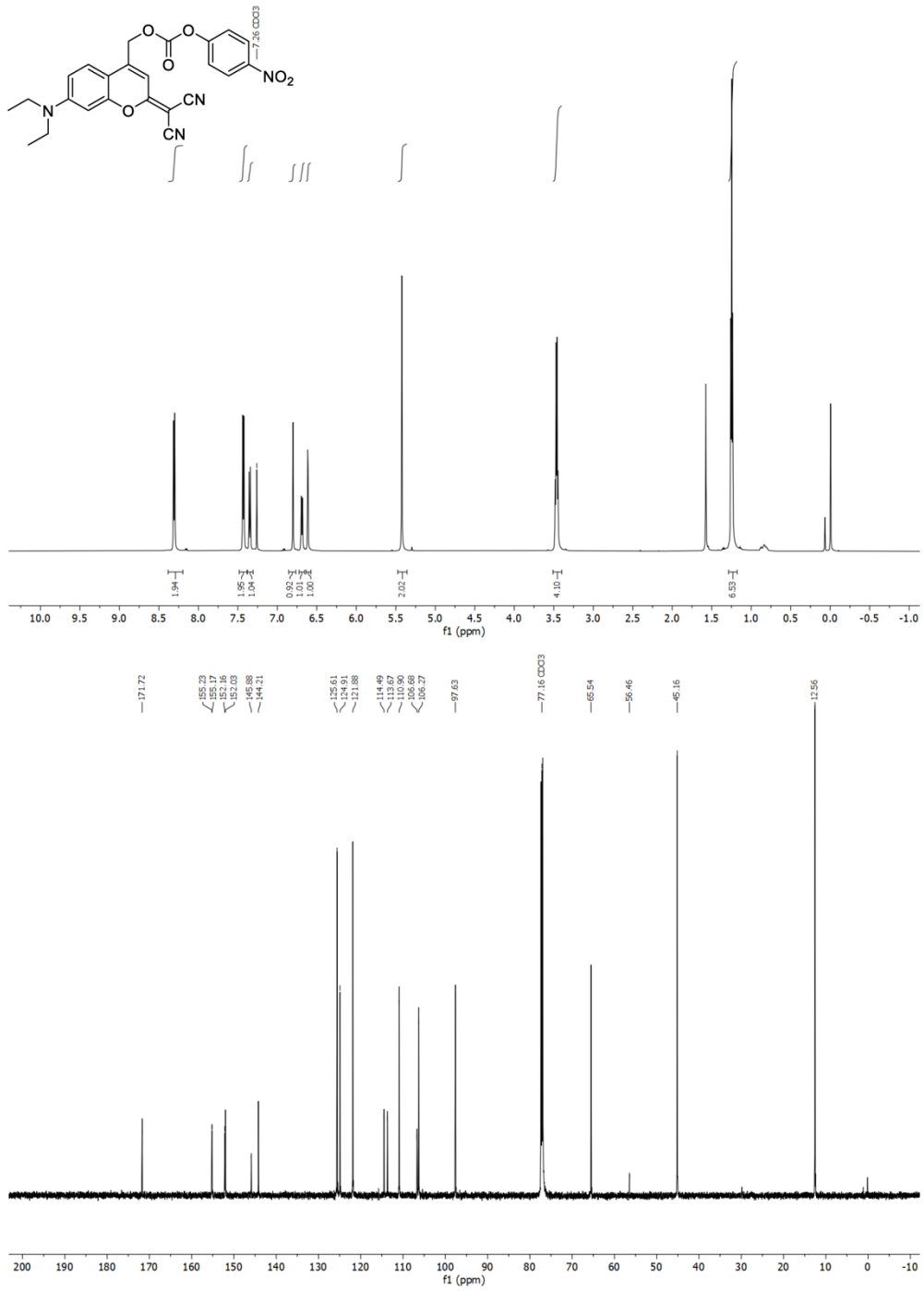

Figure S50: ^{1}H- and ^{13}C-NMR spectra of **6** in $CDCl_3$ (600 MHz/151 MHz).

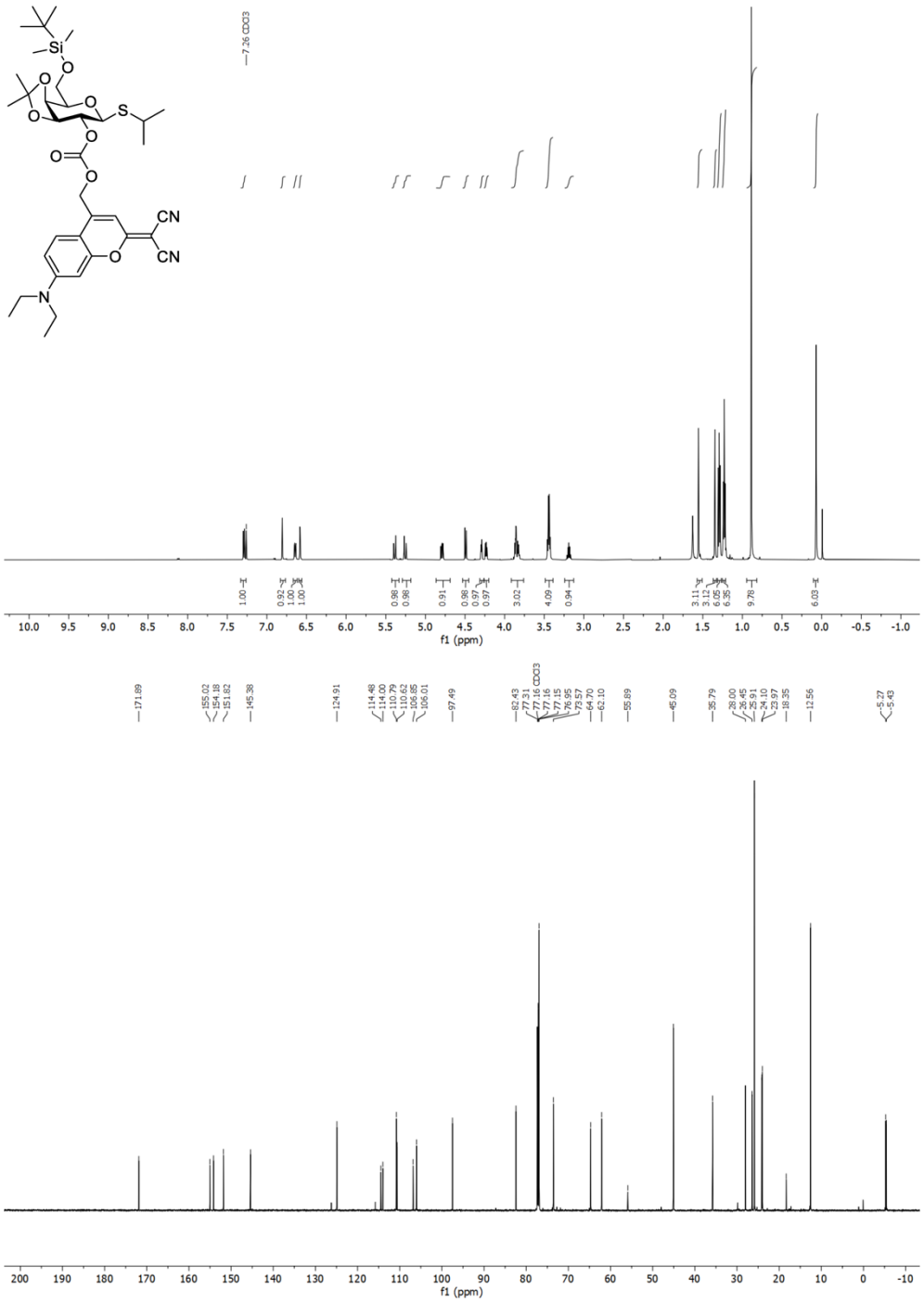

Figure S51: ^{1}H- and ^{13}C-NMR spectra of **13** in $CDCl_3$ (600 MHz/151 MHz).

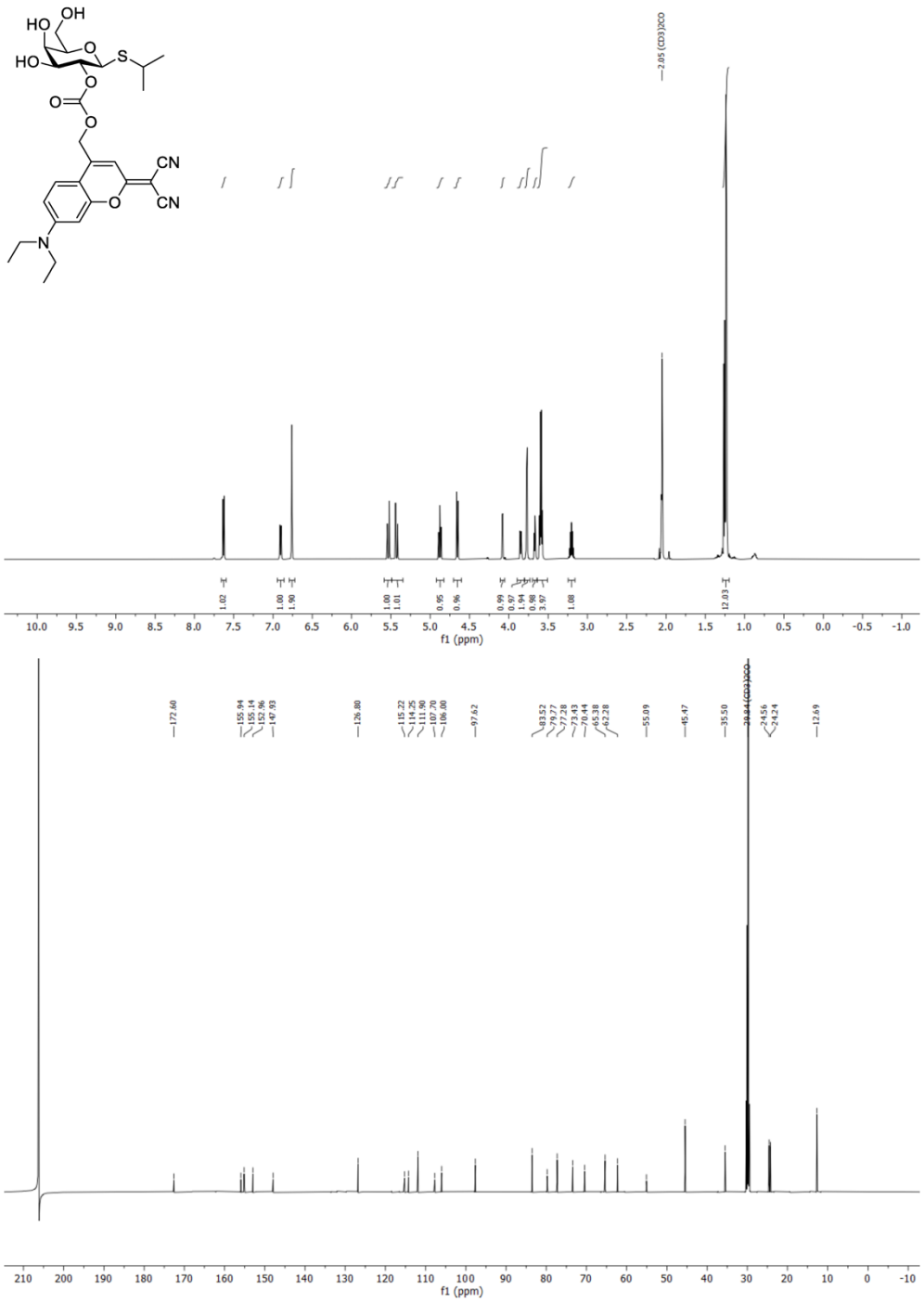

Figure S52: ^{1}H- and ^{13}C-NMR spectra of **1c** in acetone-d_6 (600 MHz/151 MHz).

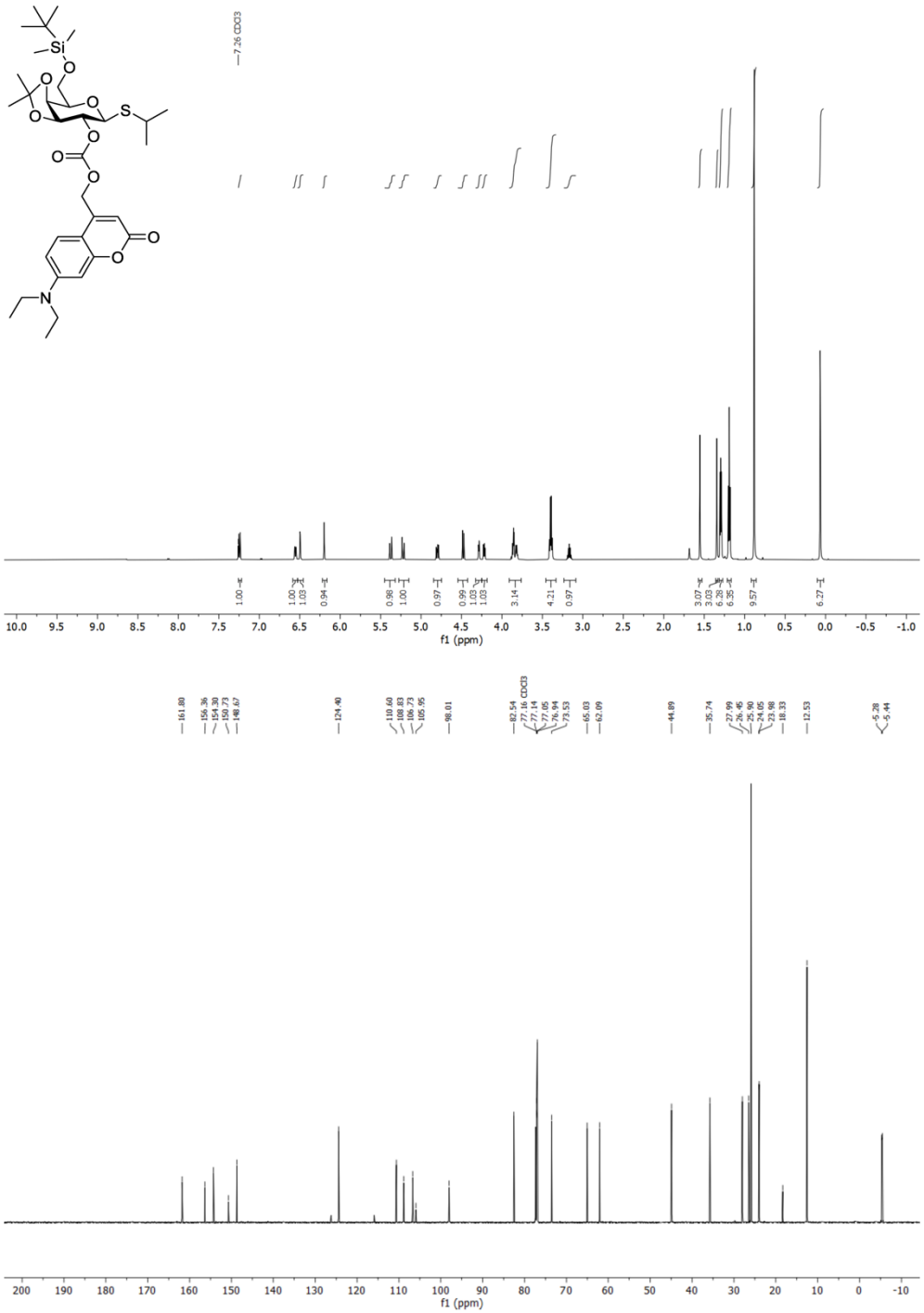

Figure S53: ^{1}H- and ^{13}C-NMR spectra of **14** in $CDCl_3$ (600 MHz/151 MHz).

S88

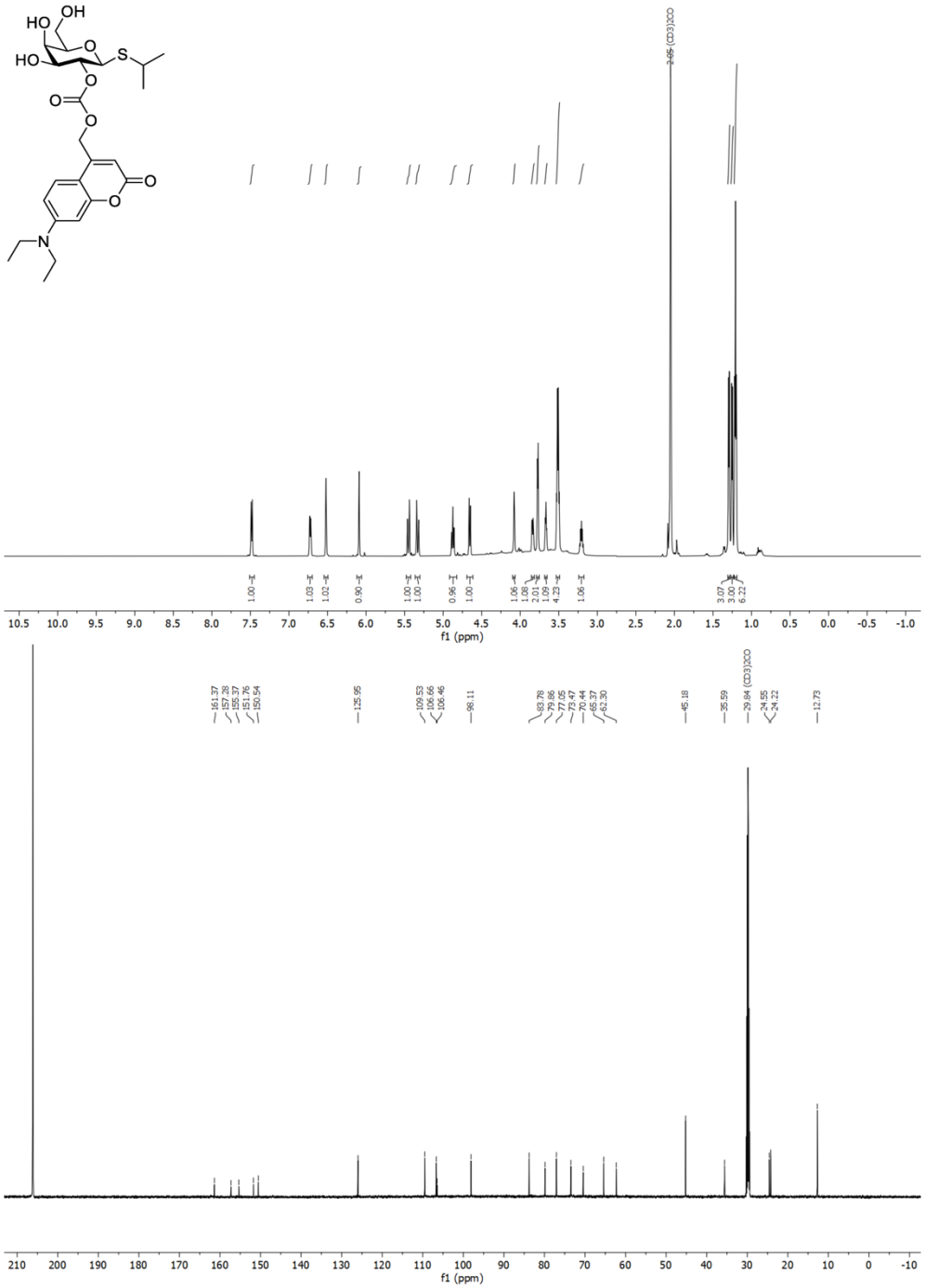

Figure S54: ^{1}H- and ^{13}C-NMR spectra of **1b** in acetone-d_6 (600 MHz/151 MHz).

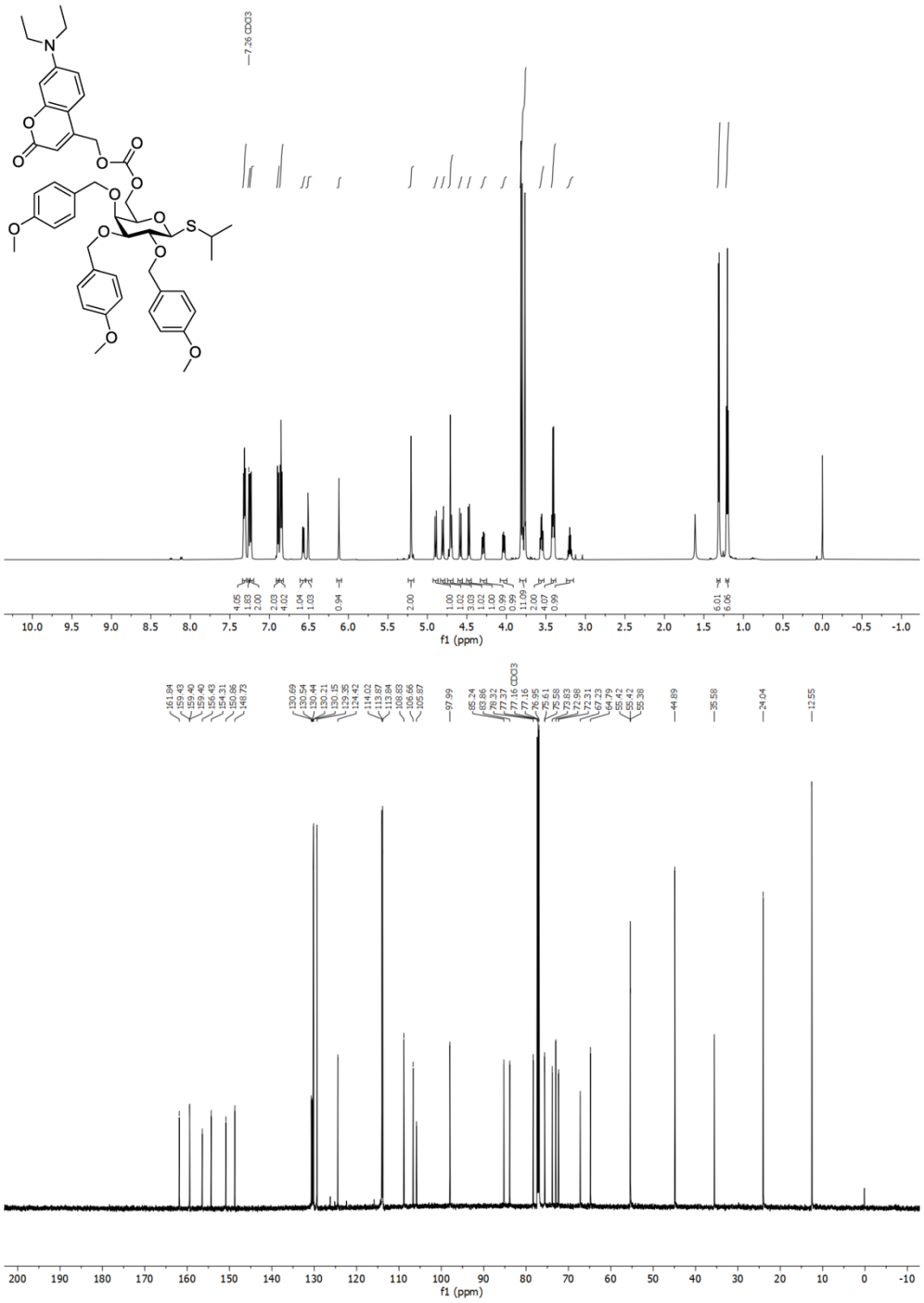

Figure S55: ^{1}H- and ^{13}C-NMR spectra of **16** in $CDCl_3$ (600 MHz/151 MHz).

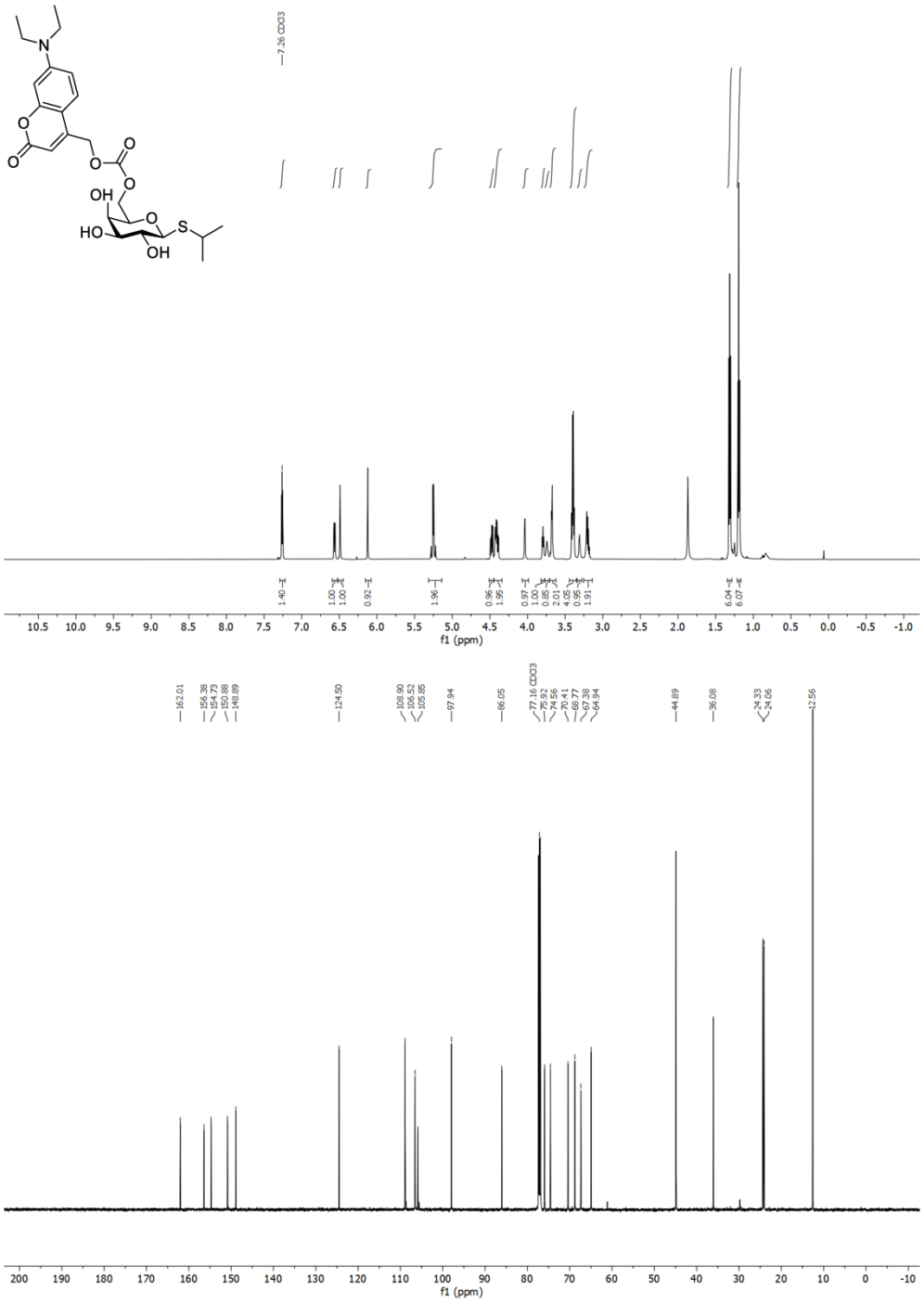

Figure S56: ^{1}H- and ^{13}C-NMR spectra of **1d** in $CDCl_3$ (600 MHz/151 MHz).

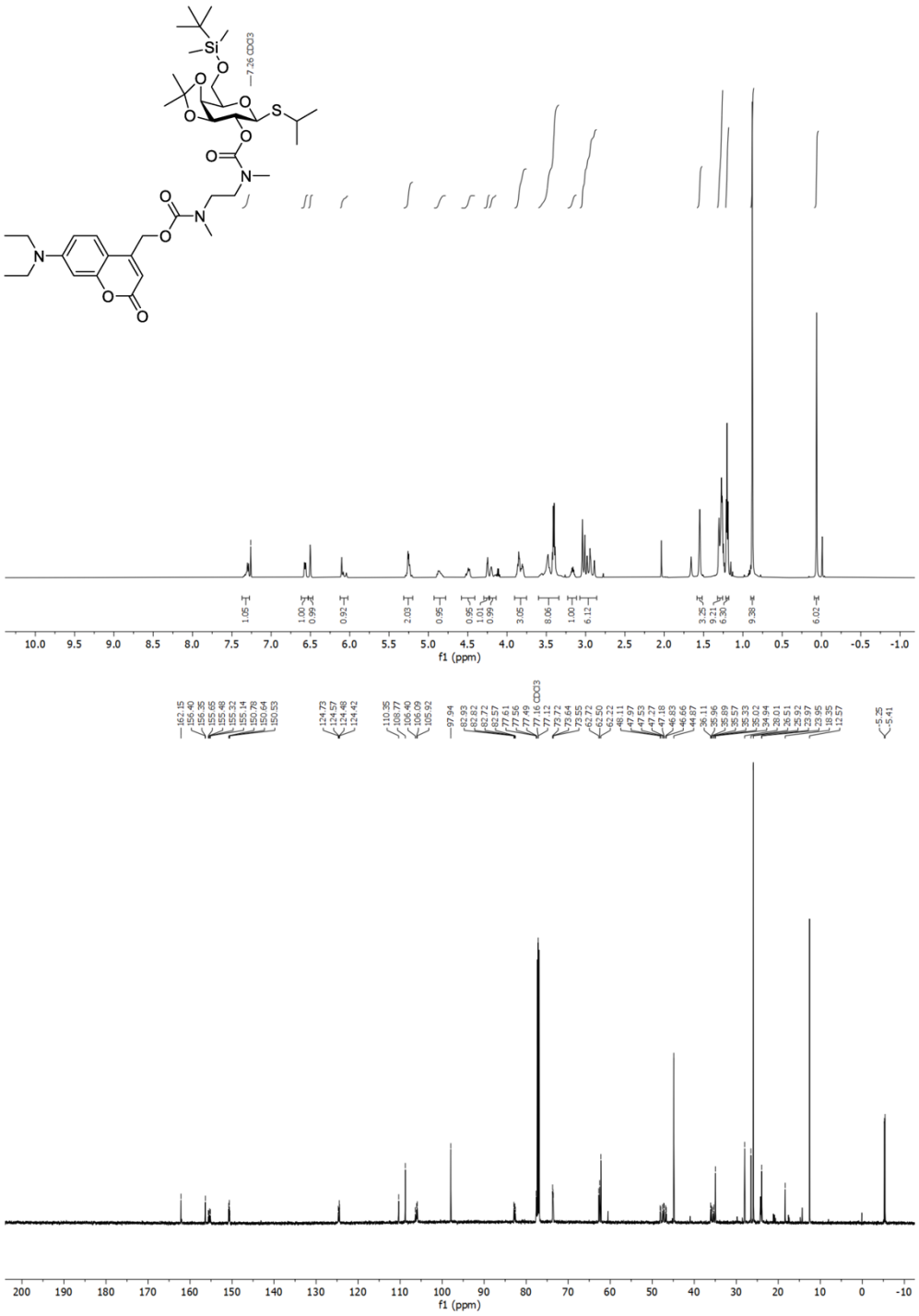

Figure S57: ^{1}H- and ^{13}C-NMR spectra of **18** in $CDCl_3$ (600 MHz/151 MHz).

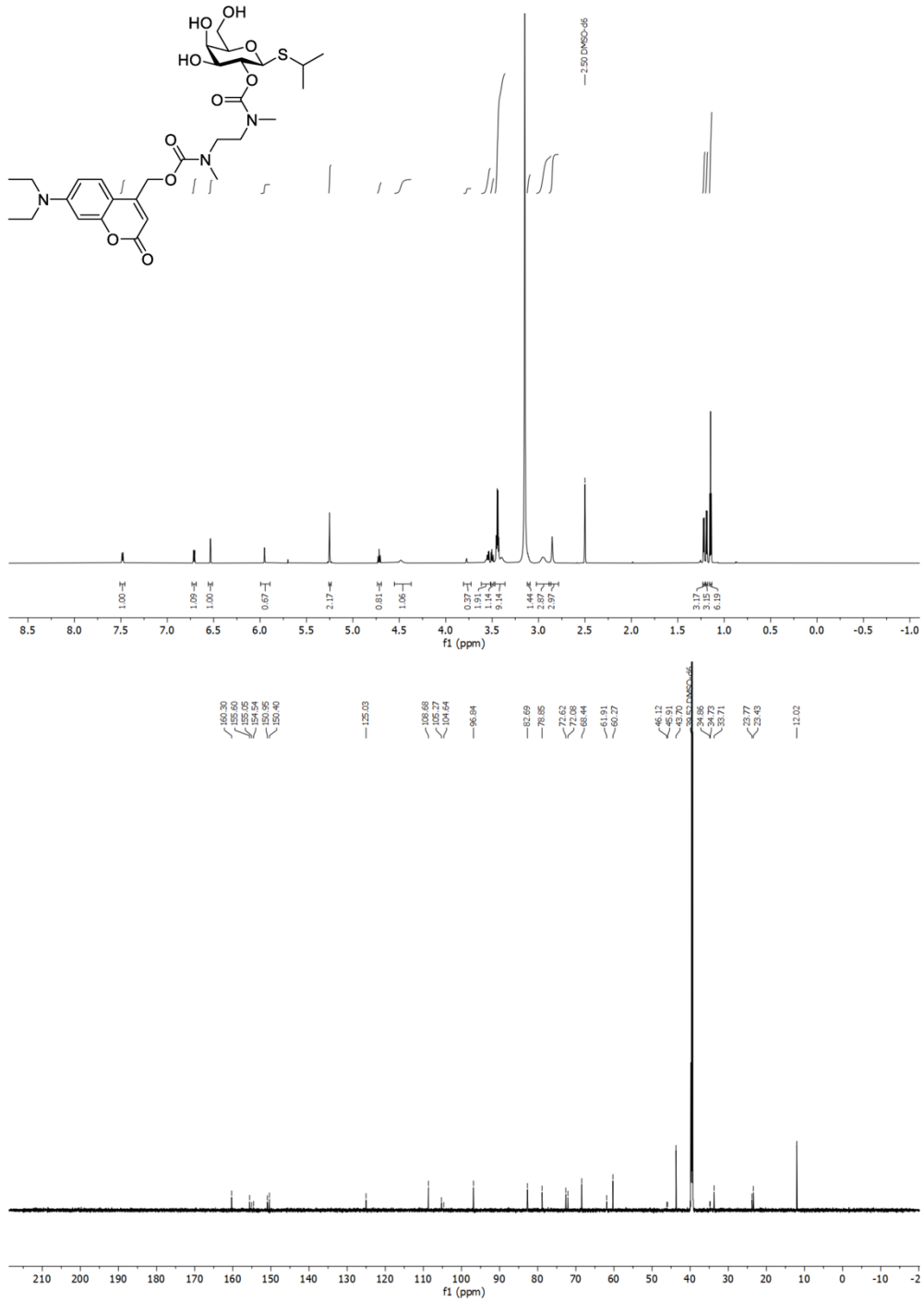

Figure S58: ^{1}H- and ^{13}C-NMR spectra of **1e** in DMSO-d_6 (600 MHz/151 MHz) at 60 °C.

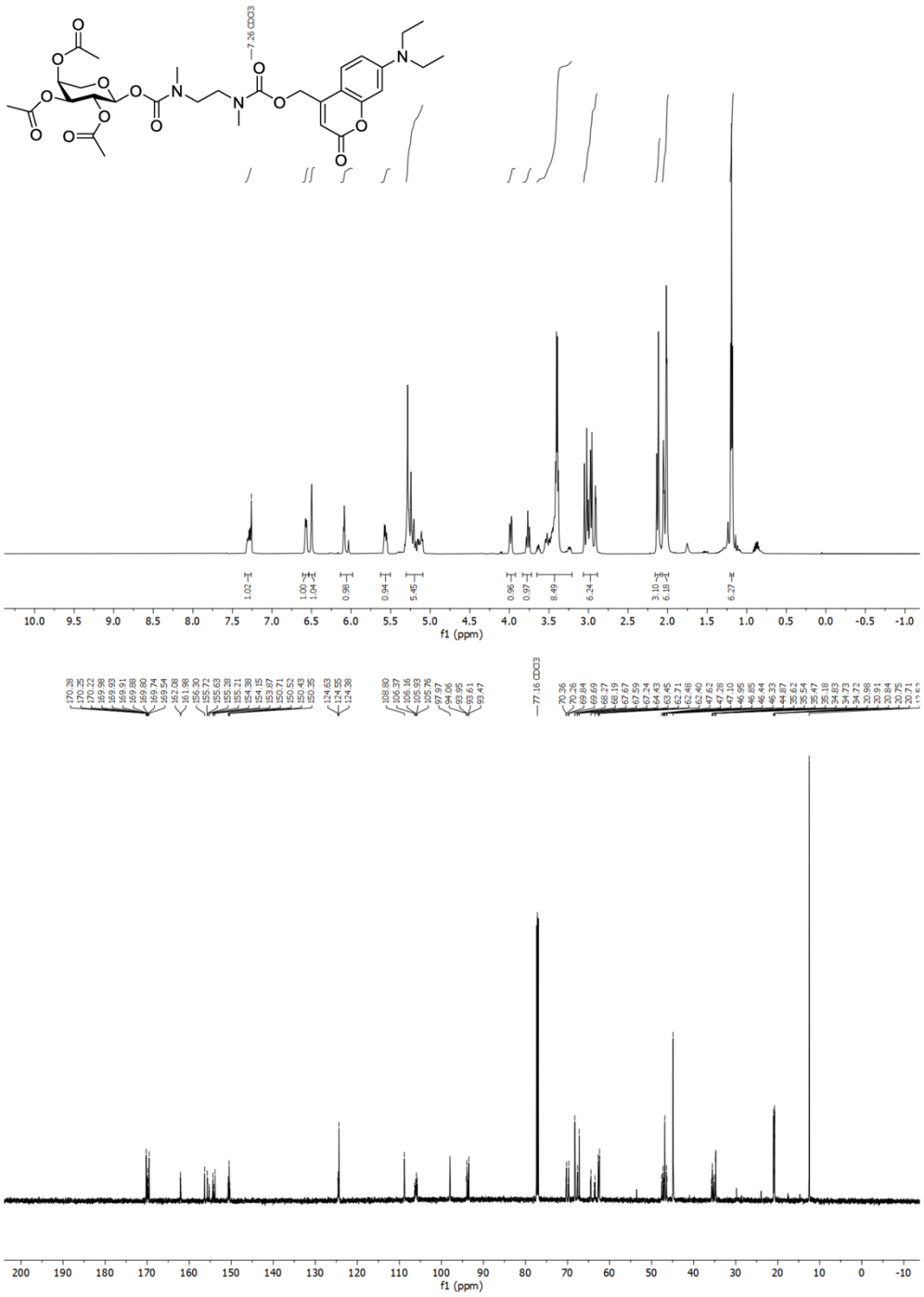

Figure S59: ^{1}H- and ^{13}C-NMR spectra of **17** in $CDCl_3$ (600 MHz/151 MHz).

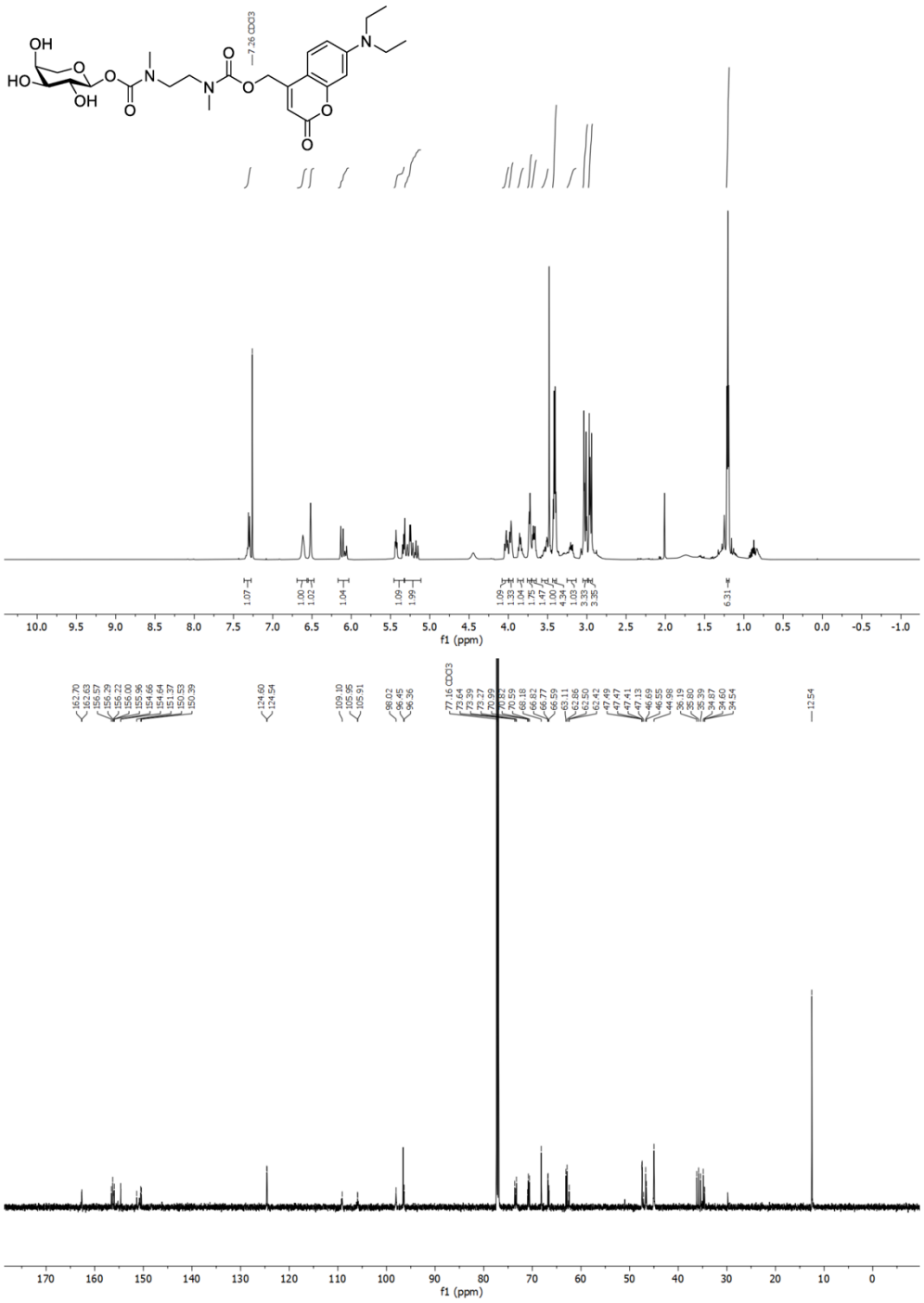

Figure S60: ^{1}H- and ^{13}C-NMR spectra of **2c** in $CDCl_3$ (600 MHz/151 MHz).

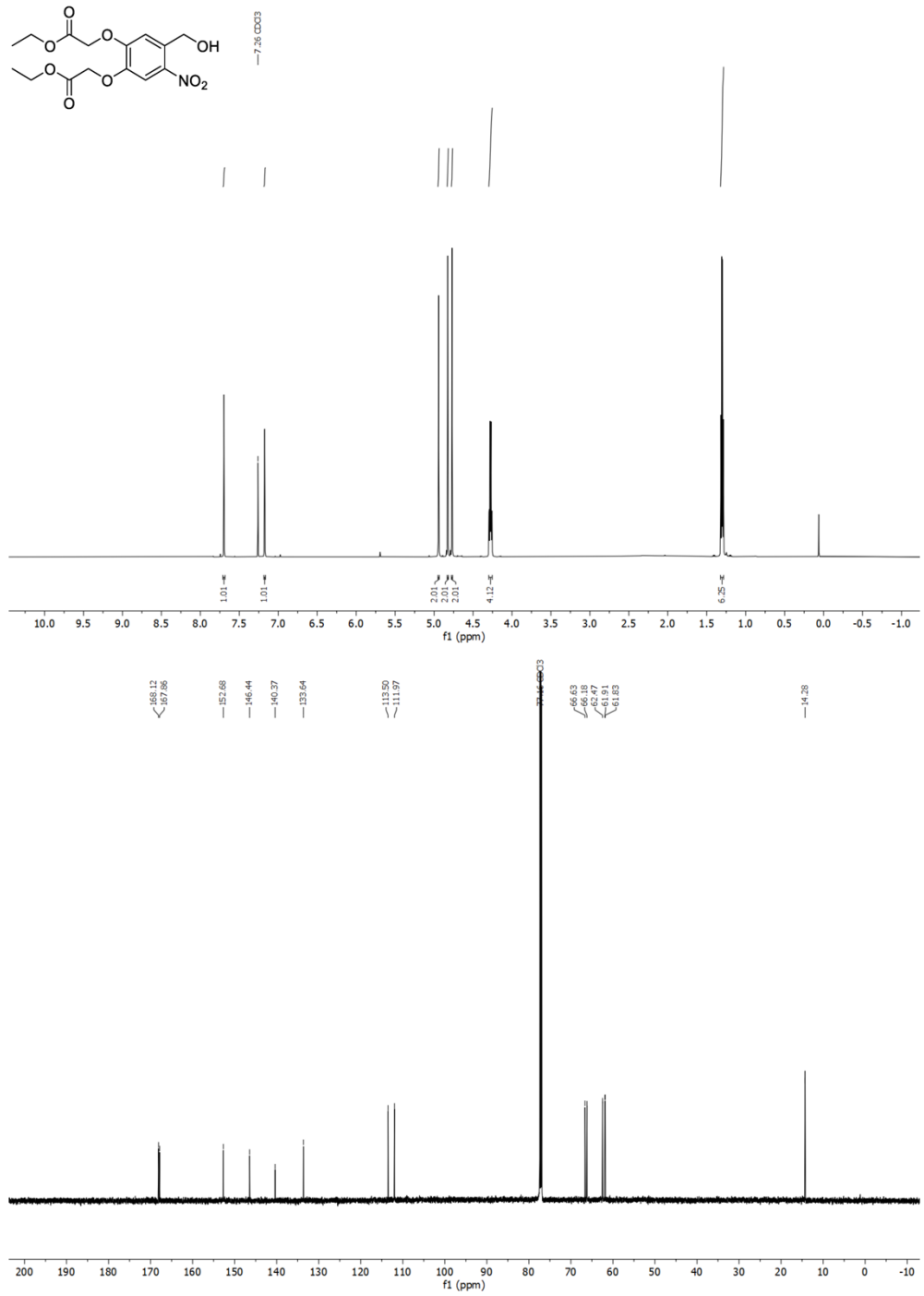

Figure S61: ^{1}H- and ^{13}C-NMR spectra of **22** in $CDCl_3$ (600 MHz/151 MHz).

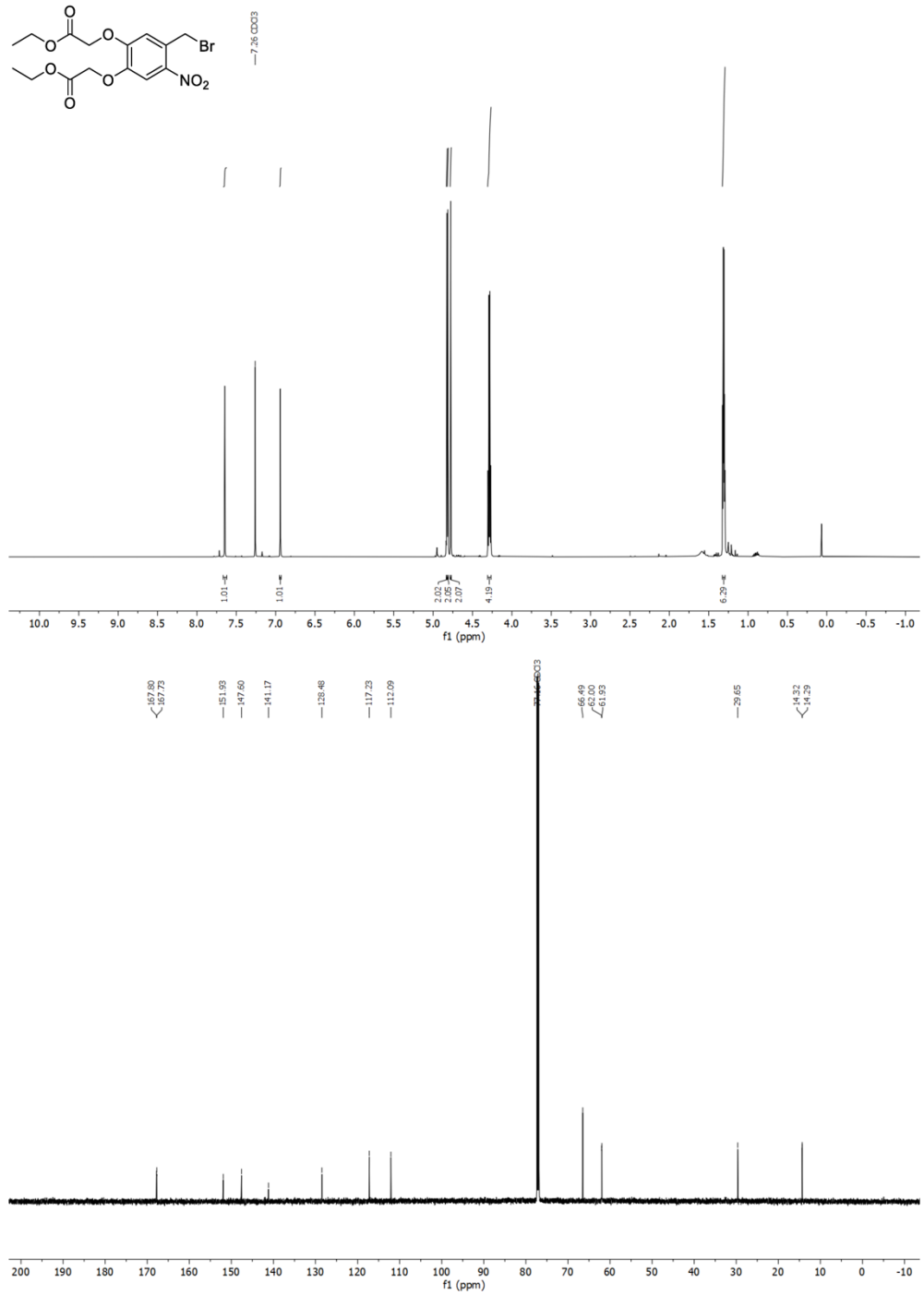

Figure 62: ^{1}H- and ^{13}C-NMR spectra of **23** in $CDCl_3$ (600 MHz/151 MHz).

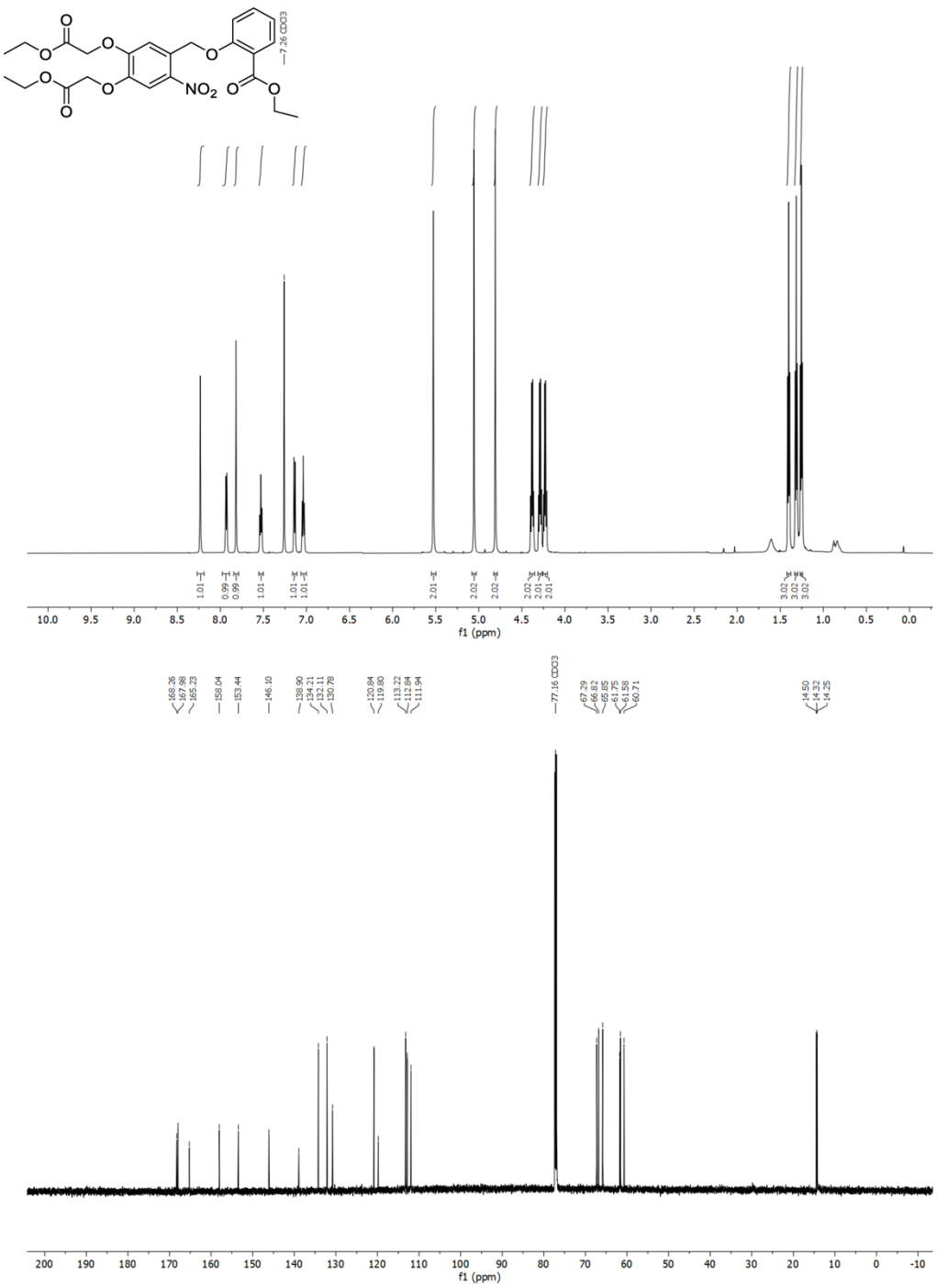

Figure S63: ^{1}H- and ^{13}C-NMR spectra of **24** in $CDCl_3$ (600 MHz/151 MHz).

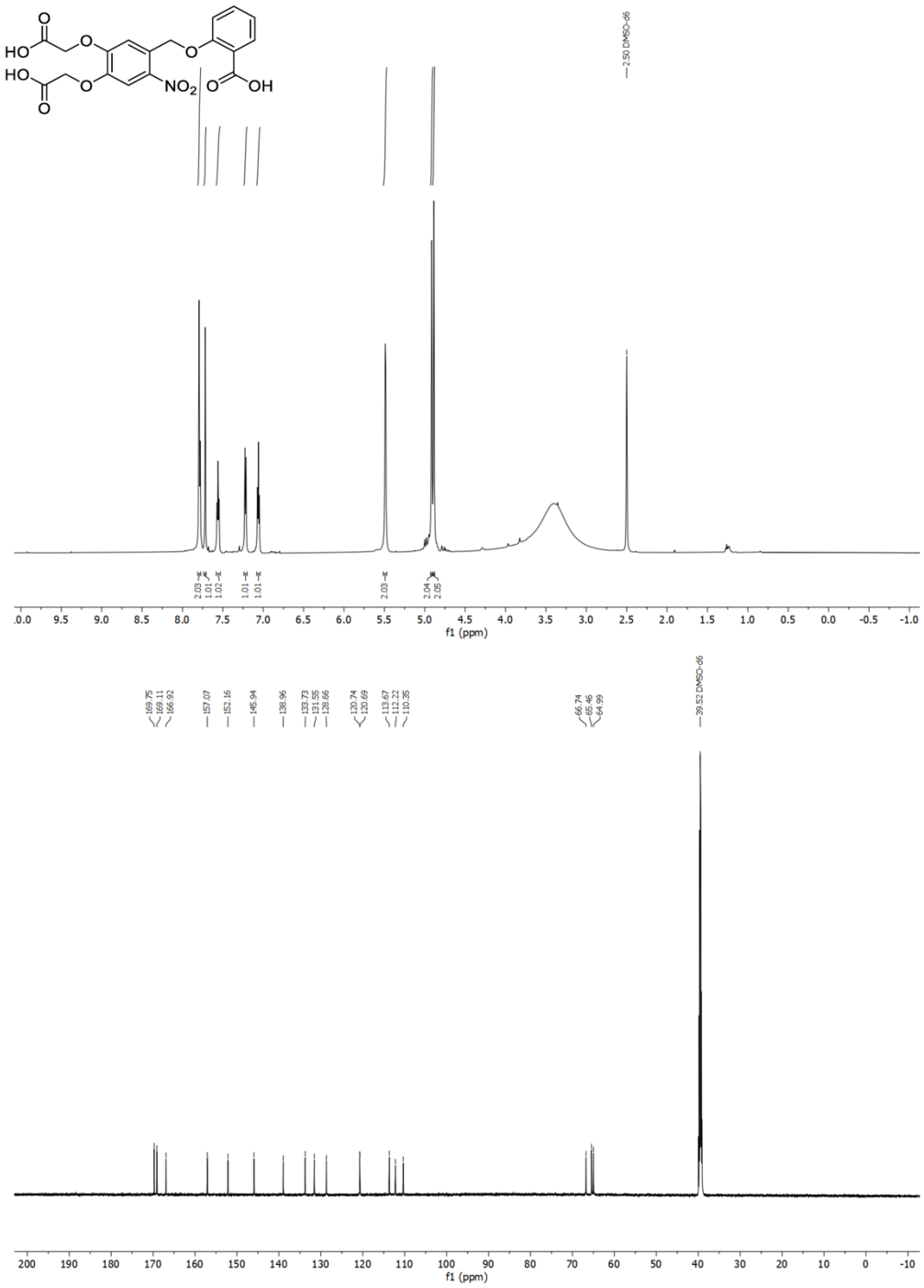

Figure S64: ^{1}H- and ^{13}C-NMR spectra of **21** in DMSO-d_6 (600 MHz/151 MHz).

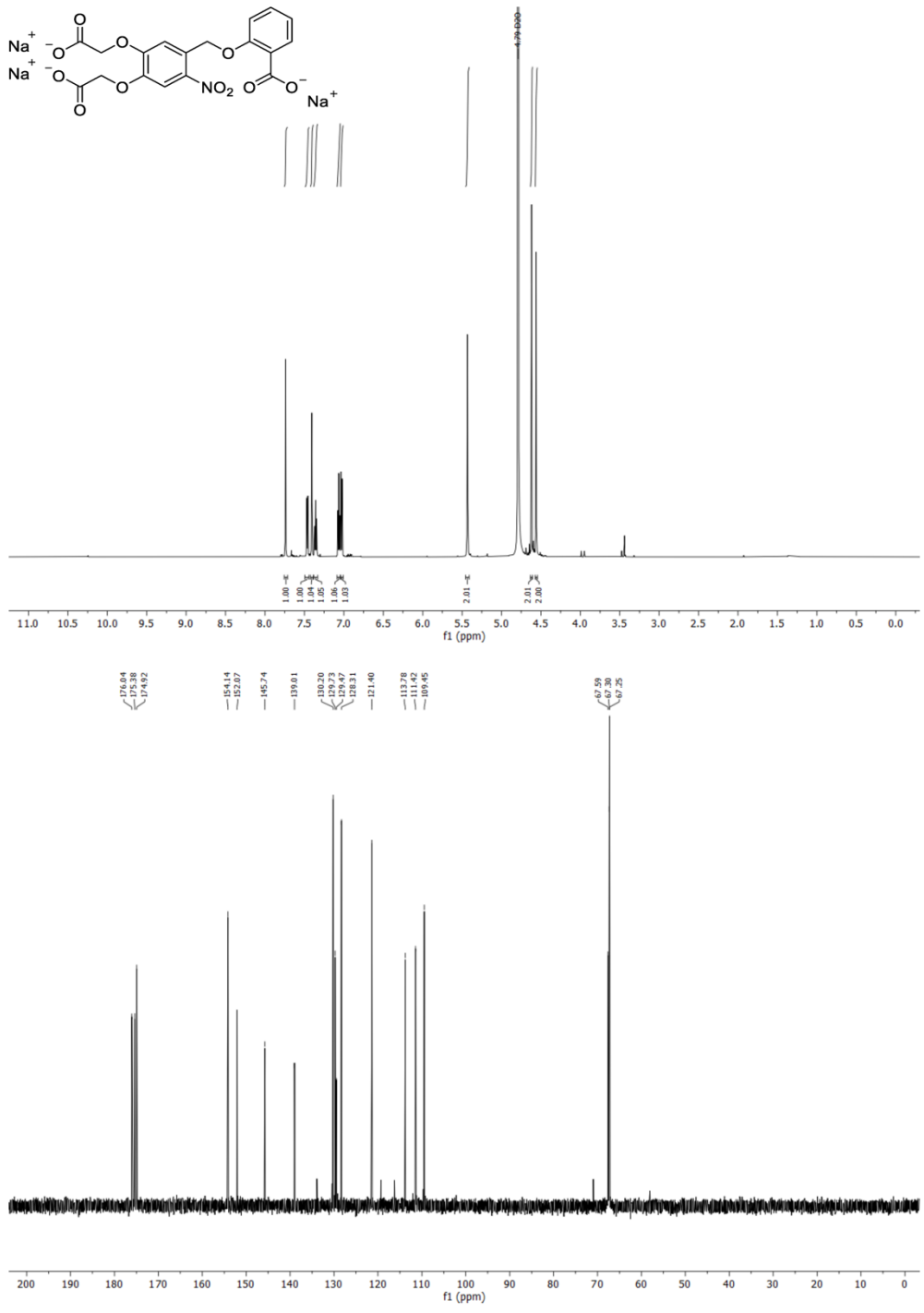

Figure S65: ^{1}H- and ^{13}C-NMR spectra of **25** in D_2O (600 MHz/151 MHz).

[1] D. Hanahan, *J. Mol. Biol.* **1983**, *166*, 557-580.

[2] L. M. Guzman, D. Belin, M. J. Carson, J. Beckwith, *J. Bacteriol.* **1995**, *177*, 4121.

[3] D. Binder, A. Grünberger, A. Loeschcke, C. Probst, C. Bier, J. Pietruszka, W. Wiechert, D. Kohlheyer, K.-E. Jaeger, T. Drepper, *Integr. Biol.* **2014**, *6*, 755-765.

[4] D. Binder, C. Probst, A. Grünberger, F. Hilgers, A. Loeschcke, K.-E. Jaeger, D. Kohlheyer, T. Drepper, *PLoS One* **2016**, *11*, e0160711.

[5] S. Balzer, V. Kucharova, J. Megerle, R. Lale, T. Brautaset, S. Valla, *Microb. Cell Fact.* **2013**, *12*, 26.

[6] S. Verhoef, H. Ballerstedt, R. J. M. Volkers, J. H. de Winde, H. J. Ruijssenaars, *Appl. Microbiol. Biotechnol.* **2010**, *87*, 679-690.

[7] a) J. E. Prior, M. D. Lynch, R. T. Gill, *Biotechnol. Bioeng.* **2010**, *106*, 326-332; b) N. Oberleitner, A. K. Ressmann, K. Bica, P. Gärtner, M. W. Fraaije, U. T. Bornscheuer, F. Rudroff, M. D. Mihovilovic, *Green Chem.* **2017**, *19*, 367-371.

[8] T. Weinrich, M. Gränz, C. Grünewald, T. Prisner, M. Göbel, *Eur. J. Org. Chem.* **2017**, *2017*, 491-496.

[9] Z. Gao, P. Yuan, D. Wang, Z. Xu, Z. Li, X. Shao, *Bioorg. Med. Chem. Lett.* **2017**, *27*, 2528-2535.

[10] N. Fomina, C. L. McFearin, M. Sermsakdi, J. M. Morachis, A. Almutairi, *Macromolecules* **2011**, *44*, 8590-8597.

[11] D. Wahler, O. Boujard, F. Lefèvre, J.-L. Reymond, *Tetrahedron* **2004**, *60*, 703-710.

[12] V. Duléry, O. Renaudet, C. Philouze, P. Dumy, *Carbohydr. Res.* **2007**, *342*, 894-900.

[13] Annaleise R. Grummitt, Margaret M. Harding, Pia I. Anderberg, A. Rodger, *Eur. J. Org. Chem.* **2003**, *2003*, 63-71.

[14] S. André, D. Specker, N. V. Bovin, M. Lensch, H. Kaltner, H.-J. Gabius, V. Wittmann, *Bioconjugate Chem.* **2009**, *20*, 1716-1728.

[15] K. P. R. Kartha, H. J. Jennings, *J. Carbohydr. Chem.* **1990**, *9*, 777-781.

[16] D. Binder, C. Bier, A. Grünberger, D. Drobietz, J. Hage-Hülsmann, G. Wandrey, J. Büchs, D. Kohlheyer, A. Loeschcke, W. Wiechert, K.-E. Jaeger, J. Pietruszka, T. Drepper, *ChemBioChem* **2016**, *17*, 296-299.

[17] Y. Du, G. Gu, G. Wei, Y. Hua, R. J. Linhardt, *Org. Lett.* **2003**, *5*, 3627-3630.

[18] Y. Du, M. Zhang, F. Yang, G. Gu, *J. Chem. Soc., Perkin Trans. 1* **2001**, 3122-3127.

[19] K. Ruda, J. Lindberg, P. J. Garegg, S. Oscarson, P. Konradsson, *J. Am. Chem. Soc.* **2000**, *122*, 11067-11072.

[20] H. Wang, W.-G. Li, K. Zeng, Y.-J. Wu, Y. Zhang, T.-L. Xu, Y. Chen, *Angew. Chem. Int. Ed.* **2019**, *58*, 561-565.

[21] C. Bier, D. Binder, D. Drobietz, A. Loeschcke, T. Drepper, K.-E. Jaeger, J. Pietruszka, *Synthesis* **2017**, *49*, 42-52.

[22] A. Gandioso, M. Palau, A. Nin-Hill, I. Melnyk, C. Rovira, S. Nonell, D. Velasco, J. García-Amorós, V. Marchán, *ChemistryOpen* **2017**, *6*, 375-384.

[23] L. Fournier, I. Aujard, T. Le Saux, S. Maurin, S. Beaupierre, J. B. Baudin, L. Jullien, *Chem. - Eur. J.* **2013**, *19*, 17494-17507.

[24] A. Z. Suzuki, T. Watanabe, M. Kawamoto, K. Nishiyama, H. Yamashita, M. Ishii, M. Iwamura, T. Furuta, *Org. Lett.* **2003**, *5*, 4867-4870.

[25] R. Wang, K. Cai, H. Wang, C. Yin, J. Cheng, *Chem. Commun.* **2018**, *54*, 4878-4881.

[26] J. Ni, D. A. Auston, D. A. Freilich, S. Muralidharan, E. A. Sobie, J. P. Y. Kao, *J. Am. Chem. Soc.* **2007**, *129*, 5316-5317.

[27] L. Tietze, M. Müller, S.-C. Duefert, K. Schmuck, I. Schuberth, *Chem. - Eur. J.* **2013**, *19*, 1726-1731.

V.4. SUPPORTING INFORMATION FOR CHAPTER II.1.4 – WAVELENGTH-SELECTIVE CONTROL OF GENE EXPRESSION IN *PSEUDOMONAS PUTIDA*

Supporting Information

Wavelength-selective control of mono- and di-rhamnolipid synthesis in *Pseudomonas putida* using photocaged compounds

Fabienne Hilgers[+][a], Fabian Hogenkamp[+][b], Nora Lisa Bitzenhofer[a], Stephan Thies[a], Karl-Erich Jaeger[a, c], Jörg Pietruszka*[b, c] and Thomas Drepper*[a]

[a] F. Hilgers, N.L. Bitzenhofer, Dr. S. Thies, Prof. Dr. K.-E. Jaeger, Dr. T. Drepper
Institute of Molecular Enzyme Technology Heinrich Heine University Düsseldorf at Forschungszentrum Jülich
Stetternicher Forst, 52426 Jülich (Germany)

[b] F. Hogenkamp, Prof. Dr. J. Pietruszka
Institute of Bioorganic Chemistry, Heinrich Heine University Düsseldorf at Forschungszentrum Jülich
Stetternicher Forst, 52426 Jülich (Germany)

[c] Prof. Dr. K.-E. Jaeger, Prof. Dr. J. Pietruszka
Institute of Bio- and Geosciences (IBG-1: Biotechnology), Forschungszentrum Jülich
Stetternicher Forst, 52426 Jülich (Germany)

[+] These authors contributed equally to this work.
* Corresponding authors.

Table of Contents

S1 Supporting methods

S1.1 Bacterial strains and plasmids

All bacterial strains, plasmids and oligonucleotides used in this study are listed in Table S1.

Table S1: Bacterial strains, plasmids and oligonucleotides used in this study.

Strains, plasmids, oligonucleotides	Relevant features, description or sequences [a]	References
	Strains	
***E. coli* DH5α**	*F⁻ Φ80lacZΔM15 Δ(lacZYA-argF) U169 recA1 endA1 hsdR17 phoA supE44 thi-1 gyrA96 relA1 deoR*	[1]
***P. putida* KT2440**	Wild type	
***P. putida* KT2440 SK40**	*rhlAB, eYFP*, attTn7 integrated, P_{nagAa}*/nagR, Gm*^{R}*, tnsABCD*	[2]
P. putida* KT2440 SK40/ *rhlC	*rhlAB, eYFP*, attTn7 integrated, P_{nagAa}*/nagR, Gm*^{R}*, tnsABCD,* pVLT33-rhlC	This work
	Plasmids	
pVLT33-GFPmut3	R6K, RSF1010 *lacI*^{q}, Kan^R, P_{tac} with *EcoR*I *Xba*I inserted *gfpmut3*	[3]
pJT'Tmcs-mCherry	Amp^R, Gm^R, vector for *Ptac* and *tac* RBS controlled expression with *Xho*I/*Xba*I inserted *mCherry*	[4]
pBNTmcs(t)-Km	Km^R, vector for *PnagAa* and *tac* RBS controlled expression	[5]
pBNTmcs-mCherry-Km	pBNTmcs(t)-Km derivative with *EcoR*I/*Xba*I inserted *mCherry*	[6]
pBNTmcs-mCherry-Gm	Gm^R, vector for *PnagAa* and *tac* RBS controlled expression with *EcoR*I /*Xba*I inserted *mCherry*	This work
pVLT33-rhlC	R6K, RSF1010 *lacI*^{q}, Kan^R, P_{tac} with inserted *rhlC*	[7]
	Oligonucleotides	
1) FH_IF_pBNT_fw	Binds at the 3' end of the kanamycin resistance gene on pBNTmcs-mCherry-Km plasmid 5'- TCAGAATTGGTTAATTGGTTGTAAC -3'	This work
2) FH_IF_pBNT_rev	Binds at the 5' end of the kanamycin resistance gene on pBNTmcs-mCherry-Km plasmid 5'- CGTCCTTGCGCCGCTTCTC -3'	This work
3) FH_IF_Gm_fw	Binds at the 5' end of the gentamicin resistance gene, inserts overhangs for Infusion cloning 5'- AGCGGCGCAAGGACGGACTGTTTTTTTGT ACAGTCTATGC -3'	This work
4) FH_IF_Gm_rev	Binds at the 3' end of gentamicin resistance gene, inserts overhangs for Infusion cloning 5'- ATTAACCAATTCTGATTAGGTGGCGGTAC TTGGG -3'	This work

S1.2 General methods for chemical synthesis procedures

All chemicals for synthesis were obtained from commercial suppliers and used without further purification unless stated otherwise. Solvents were reagent grade and were dried as well as purified by common methods. Thin-layer chromatography (TLC) was performed using pre-coated silica gel plates (Polygram® SIL G/UV, Macherey-Nagel) and components were visualized via oxidative staining or UV-light. Flash chromatography was performed on silica gel (Merck silica gel 60 (0.063−0.200 µm) and solvents for flash chromatography (petroleum ether/ethyl acetate/dichloromethane/*n*-pentane) were distilled prior to use. Optical rotation was determined at 20 °C on a Perkin Elmer Polarimeter 241 MC against sodium D-line and melting points were recorded using a Büchi melting point B-545 apparatus. The NMR spectra (^{1}H and ^{13}C) were measured at 20 °C on a Bruker Avance/DRX 600 spectrometer in deuterated solvents ($CDCl_3$). The chemical shifts are given in ppm relative to the solvent (^{1}H: $CDCl_3$ = 7.26 ppm/ ^{13}C: $CDCl_3$ = 77.16 ppm). Signals were assigned by means of H-COSY-, HSQC- and HMBC-experiments and splitting patterns are reported as singlet (s), doublet (d), triplet (t), multiplet (m), and broad singlet (brs). The IR spectra were recorded with a Perkin Elmer SpectrumOne IR-spectrometer ATR (Waltham, USA). HRMS (ESI) spectra were recorded by the centrum of analytics of the Heinrich Heine University. UV-Vis absorption spectra were recorded on a Genesys 10S UV/VIS Spectrophotometer (Thermo Scientific) and uncaging experiments were performed in a quartz cuvette with the LUMOS 43® from Atlas Photonics at 375 nm or 430 nm. Light intensity was quantified using a Thermal Power Sensor (S302C, Thorlabs Inc, USA) and the decay was detected by a Jasco HPLC system [column: Hyperclone 5 µ ODS (C18) 120 (Phenomenex)] combined with an UV/Vis-detector.

S1.3 Experimental procedures for the preparation of compounds

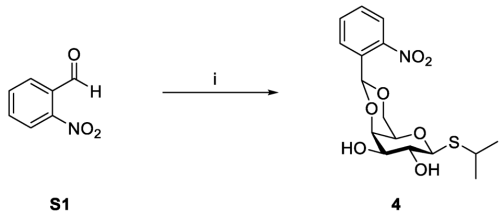

S1 **4**

Scheme S1: Synthetic scheme for preparation of NB-cIPTG (**4**). Reagents and conditions: i) IPTG, sulfuric acid, 0 °C → rt, 22 h.

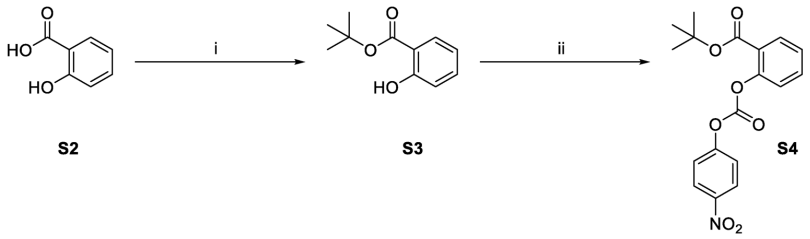

S2 **S3** **S4**

Scheme S2: Synthetic scheme for preparation of compound **S4**. Reagents and conditions: i) DMAP, DCC, *tert*-butyl alcohol, THF, rt, 18 h; ii) 4-nitrophenyl chloroformate, DIPEA, CH_2Cl_2, rt, 22 h.

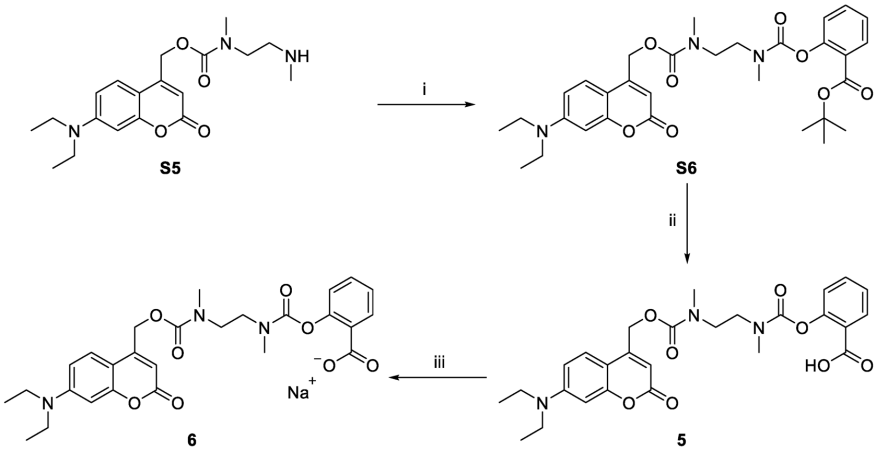

S5 **S6** **6** **5**

Scheme S3: Synthetic scheme for preparation of DC-cSal (**5**) and the corresponding sodium salt **6**. The synthesis of coumarin **S5** was reported previously [6]. Reagents and conditions: i) **S4**, DIPEA, DMAP, CH_2Cl_2, rt, 22 h; ii) TFA, CH_2Cl_2, 0 °C → rt, 1 h; iii) NaOH (0.2 M), MeOH, rt, 5 min.

Synthesis of NB-cIPTG (4)

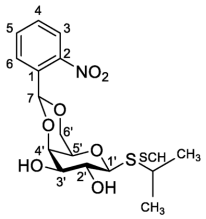

A solution of IPTG (300 mg, 1.26 mmol) and 2-nitrobenzaldehyde (**S1**)(571 mg, 3.78 mmol) in DMSO (3 mL) sulfuric acid (450 µL, 8.40 mmol) was carefully added dropwise under nitrogen atmosphere. To avoid heating, the reaction mixture was cooled with an ice-water bath during the addition. The reaction mixture was allowed to warm up to room temperature. After 22 h the reaction mixture was quenched with water and extracted with ethyl acetate. The organic phase was dried with anhydrous $MgSO_4$ and concentrated under reduced pressure. The residue was purified by flash-column chromatography on SiO_2 (*n*-pentane/ethyl acetate 40:60) to yield a white solid (152 mg, 0.41 mmol, 32%). ^{1}H-NMR (600 MHz, $CDCl_3$): δ [ppm] = 1.33 (d, $^3J_{CH3,SCH}$ = 6.8 Hz, 3 H, CH_3), 1.35 (d, $^3J_{CH3,SCH}$ = 6.8 Hz, 3 H, CH_3), 2.51 (brs, 1 H, 3′-OH), 2.58 (brs, 1 H, 2′-OH), 3.25 (septet, $^3J_{SCH,CH3}$ = 6.8 Hz, 1 H, SCH), 3.53 (s, 1 H, 5′-H), 3.67–3.74 (m, 2 H, 2′-H, 3′-H), 4.08 (dd, $^2J_{6'a,6'b}$ = 12.5 Hz, $^3J_{6'a,5'}$ = 1.9 Hz, 1 H, 6′-H_a), 4.28–4.34 (m, 2 H, 4′-H, 6′-H_b), 4.41 (d, $^3J_{1',2'}$ = 9.2 Hz, 1′-H), 6.17 (s, 1 H, 7-H), 7.51 (ddd, $^3J_{4,3}$ = 8.1 Hz, $^3J_{4,5}$ = 7.8 Hz, $^4J_{4,6}$ = 1.3 Hz, 1 H, 4-H), 7.63 (ddd, $^3J_{5,6}$ = 7.8 Hz, $^3J_{5,4}$ = 7.8 Hz, $^4J_{5,3}$ = 1.3 Hz, 1 H, 5-H), 7.86 (dd, $^3J_{3,4}$ = 8.1 Hz, $^4J_{3,5}$ = 1.3 Hz, 1 H, 3-H), 7.92 (dd, $^3J_{6,5}$ = 7.8 Hz, $^4J_{6,4}$ = 1.3 Hz, 1 H, 6-H); ^{13}C-NMR (151 MHz, $CDCl_3$): δ [ppm] = 24.1 (CH_3), 24.3 (CH_3), 35.5 (SCH), 69.8 (C-6′), 70.1 (C-5′), 70.3 (C-2′), 74.0 (C-3′), 76.2 (C-4′), 85.7 (C-1′), 96.9 (C-7), 124.1 (C-3), 128.3 (C-6), 130.0 (C-4), 131.6 (C-1), 133.1 (C-5), 148.3 (C-2); R_f = 0.17 (*n*-pentane/EtOAc 40:60); IR (atr-film): $\tilde{\nu}$ [cm^{-1}] = 3387, 2910, 1738, 1524, 1445, 1360, 1340, 1237, 1202, 1165, 1104, 1037, 991, 971, 944, 909, 876, 851, 815, 789, 736, 703, 685, 597, 541; HRMS (ESI): m/z calculated for $C_{16}H_{25}N_2O_7S^+$ $[M+NH_4]^+$: 389.1377; found: 389.1379; m.p.: 130.2 °C; $[\alpha]_D^{20}$ = –45 (c = 0.12, $CHCl_3$); UV-Vis (MeOH/H_2O 3:7): λ_{max} (ε) = 260 nm (3415 ε/dm^3 mol^{-1} cm^{-1}).

reversed-phase HPLC: t_R = 9.7 min; column: *HyperClone* 5 µ ODS (C18) 120 (*Phenomenex*); detection (UV): 260 nm; eluent: MeOH/H_2O 30:70; flowrate: 1.0 mL/min; column temperature: 25 °C; sample solvent: MeOH/H_2O 3:7.

Synthesis of tert-butyl 2-hydroxybenzoate (S3)

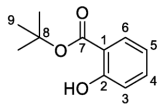

Tert-butyl 2-hydroxybenzoate (**S3**) was synthesized using a procedure of Kluger *et al.* [8]. Salicylic acid (3.00 g, 21.7 mmol) and DMAP (107 mg, 876 µmol) were suspended in dry *tert*-butyl alcohol (75.0 mL). DCC (4.84 g, 23.5 mmol) dissolved in dry THF (30.0 mL) was added dropwise over 30 min to the reaction mixture and it was stirred for 18 h. The reaction mixture was concentrated under reduced pressure and the residue was resolved in diethylether. Oxalic acid (3.17 g, 35.3 mmol) was added in portions and the precipitate was filtered and washed with an aqueous solution of saturated $NaHCO_3$ solution. The organic phase was concentrated under reduced pressure. The residue was purified by flash-column chromatography on SiO_2 (*n*-pentane/CH_2Cl_2 60:40) to yield a colorless oil (2.22 g, 11.4 mmol, 53%). The spectroscopic data are consistent with previously reported literature values [8]. ^{1}H-NMR (600 MHz, $CDCl_3$): δ [ppm] = 1.61 (s, 9 H, 9-H), 6.85 (ddd, $^3J_{5,6}$ = 8.0 Hz, $^3J_{5,4}$ = 7.2 Hz, $^4J_{5,3}$ = 1.2 Hz, 1 H, 5-H), 6.95 (dd, $^3J_{3,4}$ = 8.4 Hz, $^4J_{3,5}$ = 1.2 Hz, 1 H, 3-H), 7.42 (ddd, $^3J_{4,3}$ = 8.4 Hz, $^3J_{4,5}$ = 7.2 Hz, $^4J_{4,6}$ = 1.7 Hz, 1 H, 4-H), 7.78 (dd, $^3J_{6,5}$ = 8.0 Hz, $^4J_{6,4}$ = 1.7 Hz, 1 H, 6-H), 11.04 (s, 1 H, 2-OH); ^{13}C-NMR (151 MHz, $CDCl_3$): δ [ppm] = 28.4 (C-9), 82.9 (C-8), 114.0 (C-1), 117.6 (C-3), 119.0 (C-5), 130.3 (C-6), 135.3 (C-4), 161.9 (C-2), 170.0 (C-7); R_f = 0.70 (*n*-pentane/CH_2Cl_2 60:40); IR (atr-film): $\tilde{\nu}$ [cm^{-1}] = 3151, 2980, 1667, 1613, 1586, 1477, 1370, 1331, 1307, 1247, 1217, 1170, 1149, 1136, 1090, 1033, 879, 845, 821, 802, 754, 700, 667, 564, 531, 516; HRMS (ESI): m/z calculated for $C_{11}H_{14}NaO_3^+$ $[M+Na]^+$: 217.0835; found: 217.0835.

Synthesis of tert-butyl 2-(((4-nitrophenoxy)carbonyl)oxy)benzoate (S4)

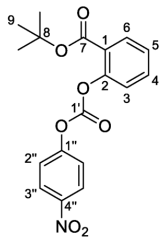

Tert-butyl 2-hydroxybenzoate (**S3**) (300 mg, 1.54 mmol) was dissolved in dry CH_2Cl_2 (3.80 mL) under nitrogen atmosphere. *N*,*N*-Diisopropylethylamine (DIPEA) (0.67 mL, 3.85 mmol) was added and the reaction mixture was stirred for 15 min before 4-nitrophenyl chloroformate (776 mg, 3.85 mmol) was added in portions. The reaction mixture was stirred for 22 h and diluted with CH_2Cl_2 (5 mL). It was washed with 1 M HCl (20 mL) and saturated $NaHCO_3$ (3×20 mL) solution. The organic phase was dried with anhydrous $MgSO_4$ and concentrated under reduced pressure. The residue was purified by flash-column chromatography on SiO_2 twice (1. petroleum ether/ethyl acetate 90:10; 2. *n*-pentane/CH_2Cl_2 50:50) to yield a white solid (226 mg, 0.63 mmol, 41%). ^{1}H-NMR (600 MHz, $CDCl_3$): δ [ppm] = 1.59 (s, 9 H, 9-H), 7.25 (dd, $^3J_{3,4}$ = 8.1 Hz, $^4J_{3,5}$ = 1.2 Hz, 1 H, 3-H), 7.37 (ddd, $^3J_{5,6}$ = 7.8 Hz, $^3J_{5,4}$ = 7.8 Hz, $^4J_{5,3}$ = 1.2 Hz, 1 H, 5-H), 7.54 (m_c, 2 H, 3″-H), 7.58 (ddd, $^3J_{4,3}$ = 8.1 Hz, $^3J_{4,5}$ = 7.8 Hz, $^4J_{4,6}$ = 1.7 Hz, 1 H, 4-H), 8.01 (dd, $^3J_{6,5}$ = 7.8 Hz, $^4J_{6,4}$ = 1.7 Hz, 1 H, 6-H), 8.31 (m_c, 2 H, 2″-H); ^{13}C-NMR (151 MHz, $CDCl_3$): δ [ppm] = 28.3 (C-9), 82.4 (C-8), 122.0 (C-3″), 123.0 (C-3), 124.6 (C-1), 125.5 (C-2″), 126.9 (C-5), 132.2 (C-6), 133.8 (C-4), 145.7 (C-4″), 150.4 (C-2), 150.9 (C-1′), 155.8 (C-1″), 163.6 (C-7); R_f = 0.13 (*n*-pentane/CH_2Cl_2 50:50); IR (atr-film): $\tilde{\nu}$ [cm^{-1}] = 2972, 1716, 1613, 1594, 1520, 1493, 1474, 1412, 1369, 1341, 1304, 1279, 1224, 1204, 1160, 1117, 1011, 941, 886, 858, 816, 749, 686, 660, 527, 493; HRMS (ESI): m/z calculated for $C_{18}H_{21}N_2O_7^+$ $[M+NH_4]^+$: 377.1343; found: 377.1341; m.p.: 110.3 °C.

Synthesis of (*tert*-butyl 2-hydroxybenzoate) {[7-(diethylamino)-2-oxo-2*H*-chromen-4-yl]methyl} ethane-1,2-diylbis(methylcarbamate) (S6)

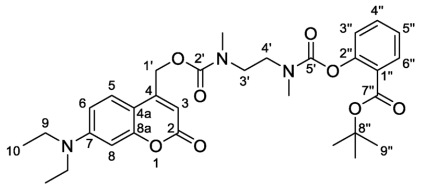

Coumarin **S6** was synthesized using a modified procedure of Fomina *et al.* [9]. To a solution of Coumarin **S5** [6] (176 mg, 0.49 mmol) in dry CH_2Cl_2 (8.8 mL) under nitrogen atmosphere compound **S4** (100 mg, 0.28 mmol), *N*,*N*-diisopropylethylamine (DIPEA) (0.85 mL, 4.88 mmol) and 4-dimethylaminopyridine (DMAP) (6.12 mg, 0.05 mmol) were added. The reaction mixture was stirred at room temperature for 22 h. It was diluted with CH_2Cl_2 and subsequently washed with saturated $NaHCO_3$ solution (3×7.5 mL) and saturated NaCl solution (1×7.5 mL). The organic phase was dried with anhydrous $MgSO_4$ and concentrated under reduced pressure. The residue was purified by flash-column chromatography on SiO_2 (petroleum ether/ethyl acetate 50:50) to yield a yellow solid (129 mg, 0.22 mmol, 79%). The product was obtained as a mixture of cis- and trans- isomers on carbamate bonds. ^{1}H-NMR (600 MHz, $CDCl_3$): δ [ppm] = 1.19 (t, $^3J_{10,9}$ = 7.0 Hz, 6 H, 10-H), 1.54 (s, 9 H, 9″-H), 2.95–3.20 (m, 6 H, CH_3), 3.39 (q, $^3J_{9,10}$ = 7.0 Hz, 4 H, 9-H), 3.47–3.70 (m, 4 H, 3′-H, 4′-H), 5.19–5.30 (m, 2 H, 1′-H), 6.04–6.14 (m, 1 H, 3-H), 6.45–6.52 (m, 1 H, 8-H), 6.52–6.58 (m, 1 H, 6-H), 7.04–7.12 (m, 1 H, 3″-H), 7.19–7.25 (m, 1 H, 5″-H), 7.26–7.34 (m, 1 H, 5-H) 7.41–7.49 (m, 1 H, 4″-H), 7.81–7.87 (m, 1 H, 6″-H); ^{13}C-NMR (151 MHz, $CDCl_3$): δ [ppm] = 12.5 (C-10), 28.2 (C-9″), 28.2 (C-9″), 35.0 (CH_3), 35.2 (CH_3), 35.5 (CH_3), 35.6 (CH_3), 35.6 (CH_3), 35.7 (CH_3), 35.7 (CH_3), 35.8 (CH_3), 44.8 (C-9), 46.5, 47.0, 47.1, 47.1, 47.2, 47.6, 47.7, 47.9 (C-3′, C-4′), 62.5 (C-1′), 62.7 (C-1′), 62.8 (C-1′), 81.4 (C-8″), 81.5 (C-8″), 97.8 (C-8), 97.9 (C-8), 105.9, 106.1, 106.1, 106.3, 106.3 (C-3, C-4a), 108.7 (C-6), 108.8 (C-6), 108.8 (C-6), 123.8 (C-3″), 123.9 (C-3″), 123.9 (C-3″), 123.9 (C-3″), 124.4 (C-5), 124.5 (C-5), 124.6 (C-5), 125.4 (C-5″), 125.4 (C-5″), 125.5 (C-5″), 125.9 (C-1″), 126.0 (C-1″), 126.1 (C-1″), 131.3 (C-6″), 131.3 (C-6″), 131.3 (C-6″), 132.8 (C-4″), 132.9 (C-4″), 133.0 (C-4″), 150.4, 150.4, 150.5, 150.6, 150.7, 150.7, 150.8 (C-2″, C-4, C-7), 154.3, 154.7, 154.8, 155.3, 155.4, 155.6, 155.7, 156.3 (C-2′, C-5′, C-8a), 162.0 (C-2), 162.1 (C-2), 162.1 (C-2), 164.2 (C-7″), 164.3 (C-7″), 164.3 (C-7″); R_f = 0.24 (PE/EtOAc 50:50); IR (atr-film): $\tilde{\nu}$ [cm^{-1}] = 2975, 2932, 1715, 1602, 1528, 1420, 1395, 1358, 1306, 1277, 1201, 1158, 1126, 1081, 844, 824, 749, 702, 530, 466; HRMS (ESI): m/z calculated for $C_{31}H_{40}N_3O_8^+$ $[M+H]^+$: 582.2810; found: 582.2817; m.p.: 63–64 °C

Synthesis of DC-cSal (5)

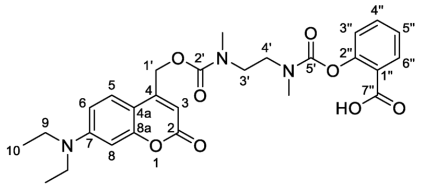

To a stirred solution of coumarin **S6** (166 mg, 0.29 mmol) in CH_2Cl_2 (4 mL) cold trifluoroacetic acid (TFA) (2 mL, 26.5 mmol) and H_2O (82.0 µL, 4.57 mmol) were added at 0 °C. The reaction mixture was allowed to warm to room temperature. After it was stirred for 1 h the solvent was removed under reduced pressure. The residue was purified by flash-column chromatography on SiO_2 (petroleum ether/ethyl acetate 30:70 → ethyl acetate/methanol 95:5) to yield a yellow solid (151 mg, 0.29 mmol, 99%). The product was obtained as a mixture of cis- and trans- isomers on carbamate bonds. ^{1}H-NMR (600 MHz, $CDCl_3$): δ [ppm] = 1.19 (t, $^3J_{10,9}$ = 7.0 Hz, 6 H, 10-H), 2.95–3.18 (m, 6 H, CH_3), 3.39 (q, $^3J_{9,10}$ = 7.0 Hz, 4 H, 9-H), 3.50–3.77 (m, 4 H, 3′-H, 4′-H), 5.18–5.36 (m, 2 H, 1′-H), 6.24–6.49 (m, 1 H, 3-H), 6.49–6.53 (m, 1 H, 8-H), 6.53–6.61 (m, 1 H, 6-H), 7.08–7.17 (m, 1 H, 3″-H), 7.22–7.36 (m, 2 H, 5-H, 5″-H), 7.48–7.56 (m, 1 H, 4″-H), 7.96–8.06 (m, 1 H, 6″-H); ^{13}C-NMR (151 MHz, $CDCl_3$): δ [ppm] = 12.5 (C-10), 34.0 (CH_3), 34.4 (CH_3), 34.8 (CH_3), 34.9 (CH_3), 35.0 (CH_3), 35.3 (CH_3), 44.9 (C-9), 45.9, 46.3, 46.4, 46.5, 47.0, 47.1 (C-3′, C-4′), 62.4 (C-1′), 62.5 (C-1′), 63.0 (C-1′), 97.9 (C-8), 105.5, 105.7, 105.7, 106.0, 106.2 (C-3, C-4a), 109.1 (C-6), 109.1 (C-6), 109.2 (C-6), 123.3, 123.8, 124.0, 124.2, 124.3, 124.4, 124.4, 124.5, 124.6, 125.7, 125.7, 125.8, 126.1 (C-5, C-1″, C-3″, C-5″), 131.9 (C-6″), 132.1 (C-6″), 132.2 (C-6″), 133.9 (C-4″), 133.9 (C-4″), 134.0 (C-4″), 134.2 (C-4″), 150.8, 150.8, 151.0, 151.1, 151.3, 151.4, 151.6 (C-2″, C-4, C-7), 154.5, 155.1, 155.2, 155.7, 155.9, 156.1, 156.1, 156.2, 156.2 (C-2′, C-5′, C-8a), 163.1 (C-2), 163.2 (C-2), 163.3 (C-2), 163.4 (C-2), 167.4 (C-7″), 167.6 (C-7″); R_f = 0.19 (PE/EtOAc 30:70); IR (atr-film): $\tilde{\nu}$ [cm^{-1}] = 2971, 2934, 1709, 1603, 1527, 1425, 1404, 1356, 1276, 1206, 1138, 1084, 828, 802, 753, 722; HRMS (ESI): m/z calculated for $C_{27}H_{32}N_3O_8^+$ $[M+H]^+$: 526.2184; found: 526.2185; m.p.: 106–107 °C; UV-Vis [sodium phosphate buffer (20 mM, pH 7.4)/MeOH 9:1]: λ_{max} (ε) = 248 nm (12098 ε/dm^3 mol^{-1} cm^{-1}), 307 (2096), 318 (2158), 395 (14438).

reversed-phase HPLC: t_R = 14.0 min; column: *HyperClone* 5 µ ODS (C18) 120 (*Phenomenex*); detection (UV): 395 nm; eluent: MeOH/sodium phosphate buffer (20 mM, pH 7.4) 40:60; flowrate: 0.5 mL/min; column temperature: 25 °C; sample solvent: sodium phosphate buffer (20 mM, pH 7.4)/MeOH 9:1.

Synthesis of DC-cSal*Na (6)

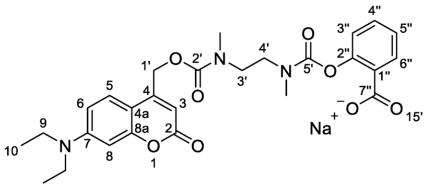

To a solution of DC-cSal (**5**) (29 mg, 55 µmol) in MeOH (1.0 mL) a 0.2 M solution of NaOH (0.28 mL, 55 µmol) was added. The reaction mixture was stirred for 5 min before it was lyophilised overnight to yield a solid (30 mg, 55 µmol, quant.).

^{1}H-NMR (600 MHz, $CDCl_3$): δ [ppm] = *measurement in process*; ^{13}C-NMR (151 MHz, $CDCl_3$): δ [ppm] = *measurement in process*

IR (ATR, Film): $\tilde{\nu}$ [cm^{-1}] = 3448, 2970, 2927, 1702, 1603, 1571, 1528, 1469, 1422, 1356, 1276, 1207, 1174, 1126, 1088, 836, 799, 756; m.p.: 155–156 °C.

S2 Supporting data

S2.1 Induction response of P_{nagAa}/P_{tac}-based system in *P. putida*/ combi

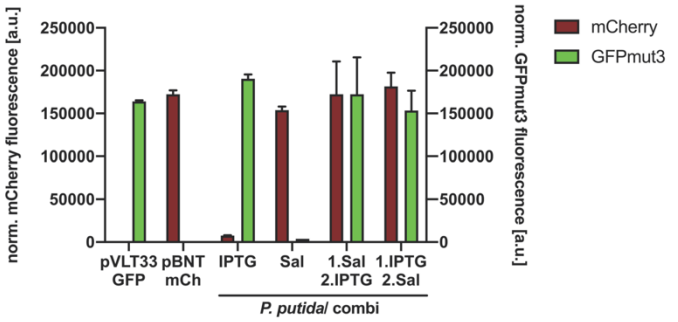

Figure S1: Normalized fluorescence intensity of *P. putida*/ combi expression cultures supplemented with either 50 µM salicylic acid (Sal) or 500 µM IPTG or both inducers in reverse orders. All cultures were incubated in the dark for 20 h in LB medium at 30 °C and 1200 rpm. Induction was performed after 3 h and additionally, for cultures supplemented with both inducers, after 5 h of cultivation. The induction response of the strain *P. putida*/ combi was compared to cultures of the strains *P. putida*/ pVLT33-GFP or *P. putida*/ pBNT-mCherry as positive controls. *In vivo* fluorescence intensities were determined by using a Tecan Infinite M1000 Pro microplate reader (mCherry: λ_{ex}= 575 nm, λ_{em}= 610 nm; GFPmut3: λ_{ex}= 488 nm, λ_{em}= 527 nm) and normalized to cell densities. Values are means of triplicate measurements. Error bars indicate the respective standard deviations.

S2.2 Stability and toxicity of novel photocaged salicylic acid variants

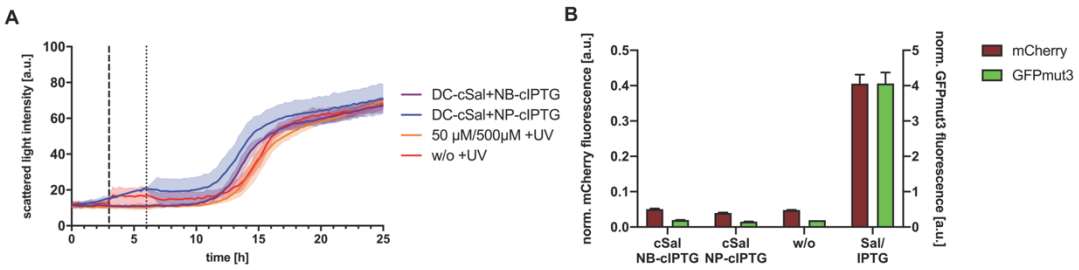

Figure S2: A) Growth curves of *P. putida* KT2440/combi expression cultures in the presence of DC-cSal and NB-cIPTG or NP-cIPTG compared to uninduced (0 µM, w/o) and induced (50 µM Sal and 500 µM IPTG) cultures. Cells were grown over 20 h using a BioLector system (LB medium, 30 °C, 1200 rpm). Cell growth was analyzed by determining the scattered light intensity. After 3 h, formation of DC-cSal photoproducts was induced in cultures *via* light exposure at 447nm (~10 mW cm^{-2}, 10 min; indicated by dashed lines) and after another 3 h formation of NB-cIPTG photoproducts *via* light exposure at 365 nm (~1 mW cm^{-2}, 30 min; indicated by dotted lines) or by the addition of conventional inducers. Values are means of triplicate measurements. Error bars indicate the respective standard deviations. **B)** Normalized fluorescence intensity of *P. putida* KT2440/combi expression cultures supplemented with 50 µM Sal or DEACM-NN-cSal (DC-cSal) and 500 µM IPTG or NB-cIPTG. All cultures were incubated in the dark for 20 h in LB medium at 30 °C and 1200 rpm. *In vivo* stability DC-cSal and NB-cIPTG is reflected by the low induction of reporter gene expression and was compared to cultures with and without both inducers. *In vivo* fluorescence intensities were determined by using a BioLector system (mCherry: λ_{ex}= 580 nm, λ_{em}= 610 nm; GFPmut3: λ_{ex}= 508 nm, λ_{em}= 532 nm) and normalized to cell densities. Values are means of triplicate measurements. Error bars indicate the respective standard deviations.

S2.3 Effect of light illumination on growth and fluorescence of *P. putida* expression cultures

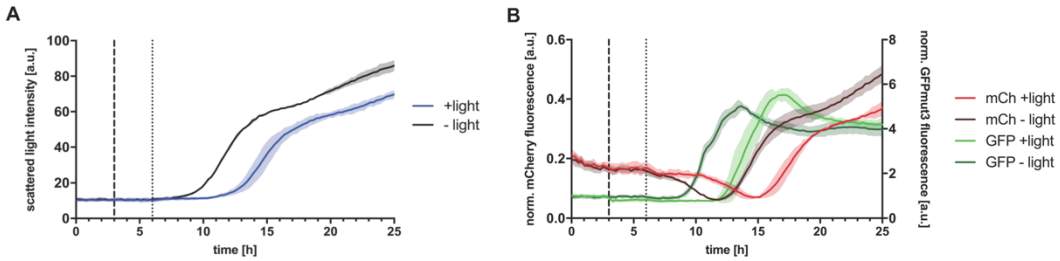

Figure S3: A) Growth curves of *P. putida* KT2440/ combi expression cultures in the presence (blue line) and in the absence (black line) of light exposure. Cells were grown over 20 h in LB medium at 30 °C and 1200 rpm using a BioLector system. Cell growth was analyzed by determining the scattered light intensity. After 3 h and 6 h (dashed and dotted lines), cultures were exposed to blue light (10 min, 447 nm, ~10 mW cm^{-2}) and UV-A light (30 min, 365 nm, ~1 mW cm^{-2}), respectively. Values are means of triplicate measurements. Error bars indicate the respective standard deviations. **B)** Increase of fluorescent reporter-mediated signals during cultivation of *P. putida* KT2440/ combi expression cultures in the presence (light red and green lines) and in the absence (dark red and green lines) of light exposure. Cells were grown over 20 h in LB medium at 30 °C and 1200 rpm. *In vivo* fluorescence intensities were determined by using a BioLector system (mCherry: λ_{ex}= 580 nm, λ_{em}= 610 nm, GFPmut3: λ_{ex}= 508 nm, λ_{em}= 532 nm) and normalized to cell densities. After 3 h and 6 h, cultures were induced by addition of 50 µM Sal and 500 µM IPTG and exposed to blue light (10 min, 447 nm, ~10 mW cm^{-2}) and UV-A light (30 min, 365 nm, ~1 mW cm^{-2}), respectively. Values are means of triplicate measurements. Error bars indicate the respective standard deviations.

S2.4 UV-Vis spectra of compounds

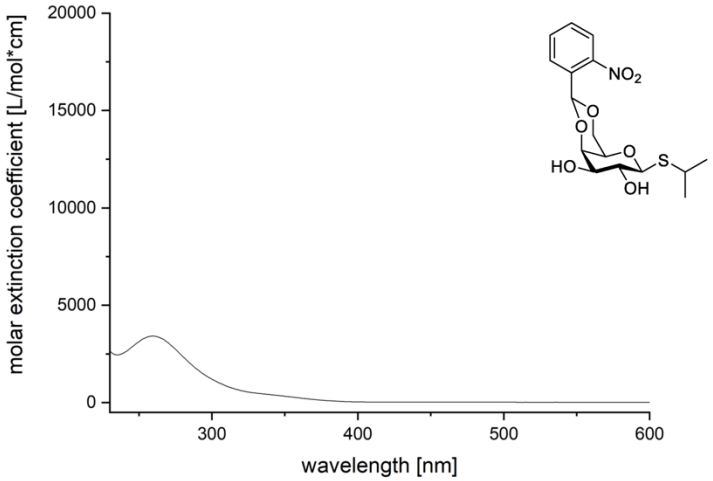

Figure S4: UV-Vis spectrum of compound NB-cIPTG (**4**) [0.25 mM in MeOH/H_2O 30:70, 25 °C].

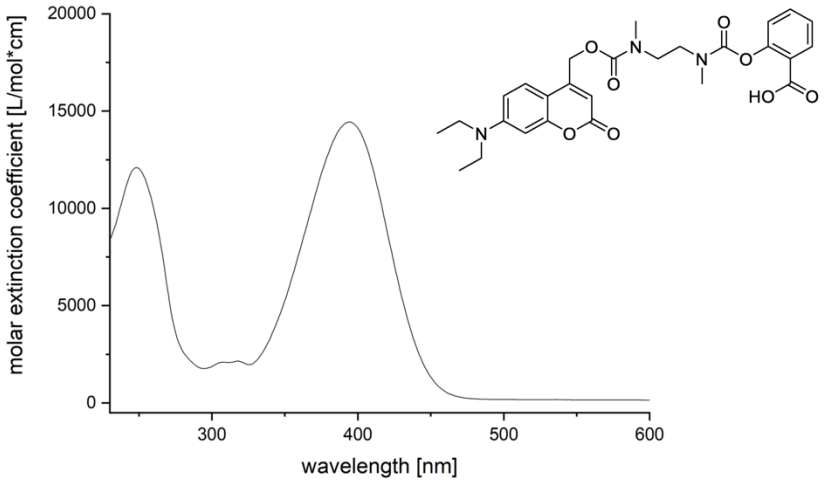

Figure S5: UV-Vis spectrum of compound DC-cSal (**5**) [0.05 mM in sodium phosphate buffer (20 mM, pH 7.4)/MeOH 90:10, 25 °C].

S2.5 Determination of uncaging half-life times

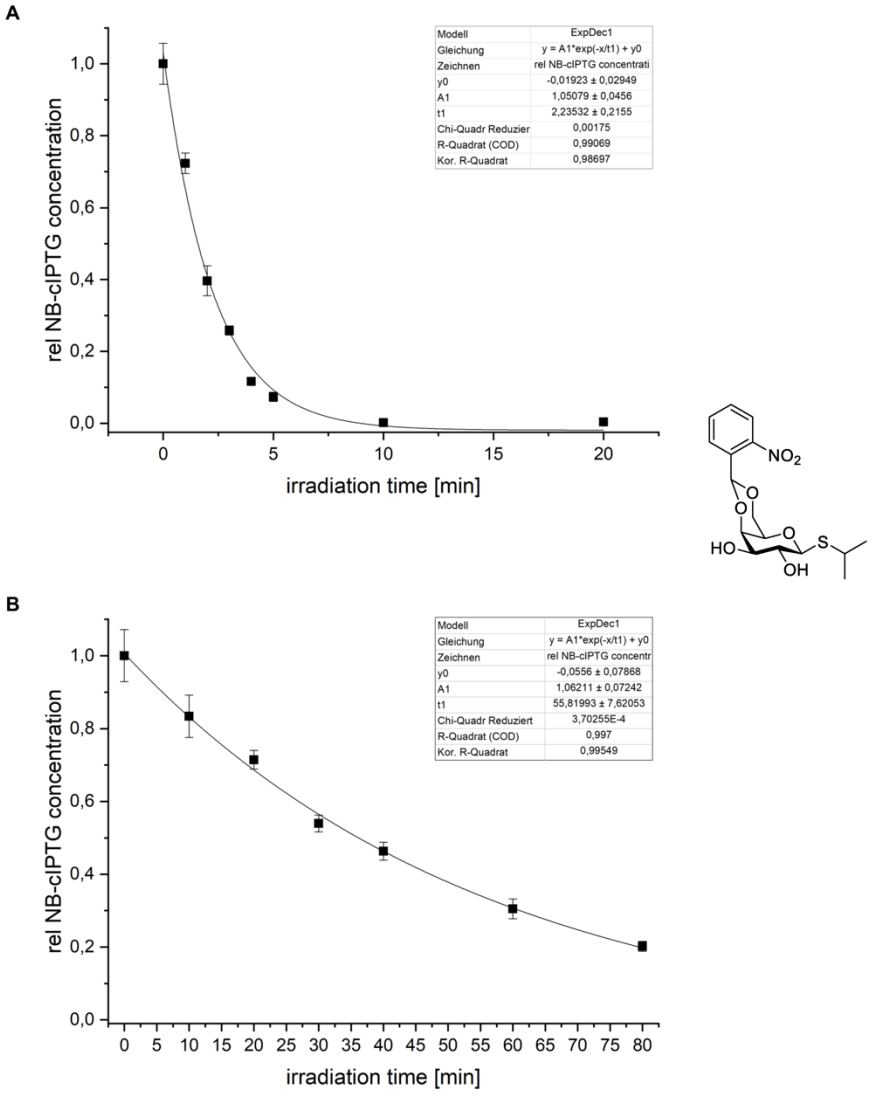

Figure S6: *In vitro* decay of NB-cIPTG (**4**) after irradiation with different wavelength controlled *via* reversed-phase HPLC (1 mM in MeOH/H_2O 30:70); **A**) 375 nm, 6.4 mW cm^{-2}, room temperature, **B**) 430 nm, 45.6 mW cm^{-2}, room temperature.

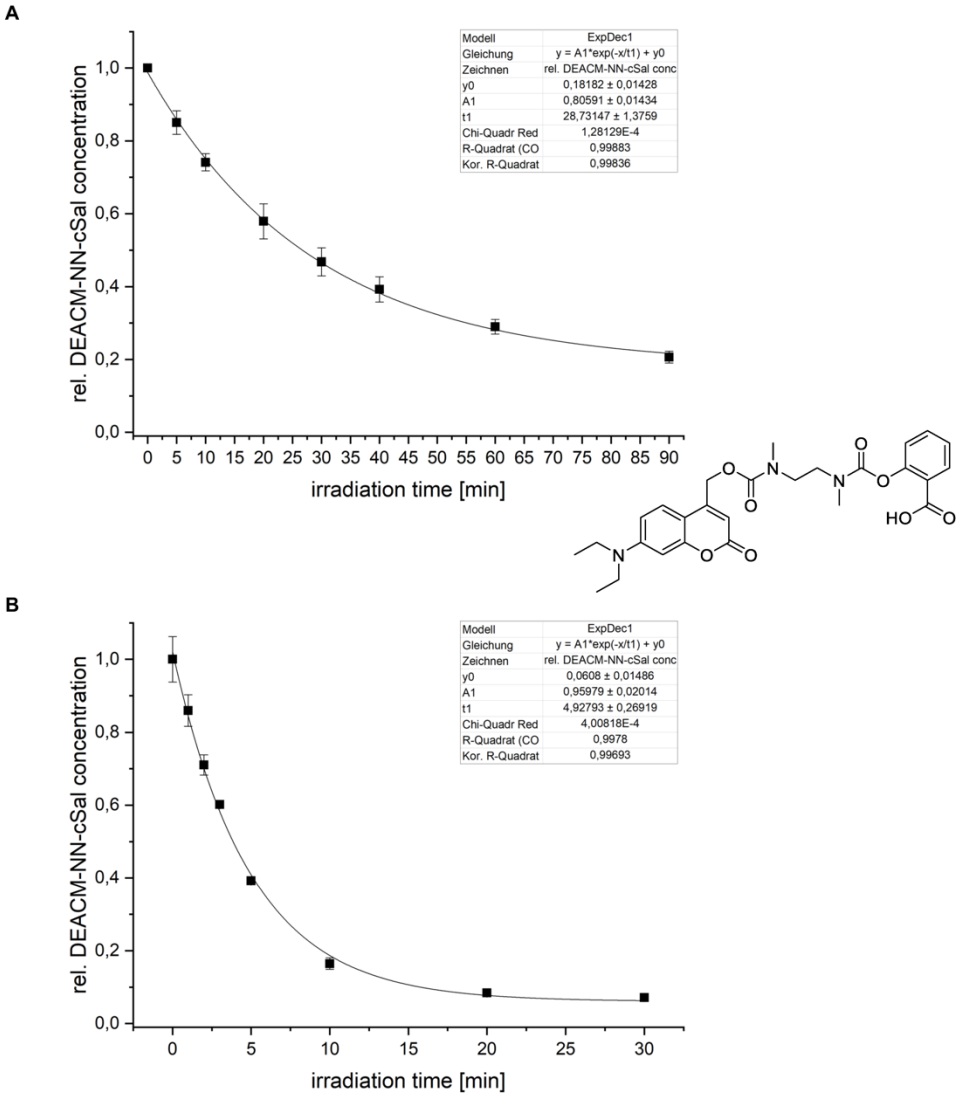

Figure S7: *In vitro* decay of DEACM-NN-cSal (**5**) after irradiation with different wavelength controlled *via* reversed-phase HPLC [1 mM in sodium phosphate buffer (20 mM, pH 7.4)/MeOH 90:10]; **A**) 375 nm, 6.4 mW cm^{-2}, room temperature, **B**) 430 nm, 45.6 mW cm^{-2}, room temperature.

Table S2: Fitting parameters and uncaging half-life times $t_{0.5}$ for NB-cIPTG (**4**) and DC-cSal (**5**) at different wavelength.

Photocaged inducer	**λ [nm]**	**y_0**	**A_1**	**t_1**	**k**	**$t_{0.5}$ [min]**
NB-cIPTG (**4**)	375	-0.01923	1.05079	2.23532	0.44736	1.5494
NB-cIPTG (**4**)	430	-0.0556	1.06211	55.81993	0.01791	38.69142
DC-cSal (**5**)	375	0.18182	0.80591	28.73147	0.03481	19.91514
DC-cSal (**5**)	430	0.0608	0.95979	4.92793	0.20293	3.41578

S2.6 HPLC-Traces

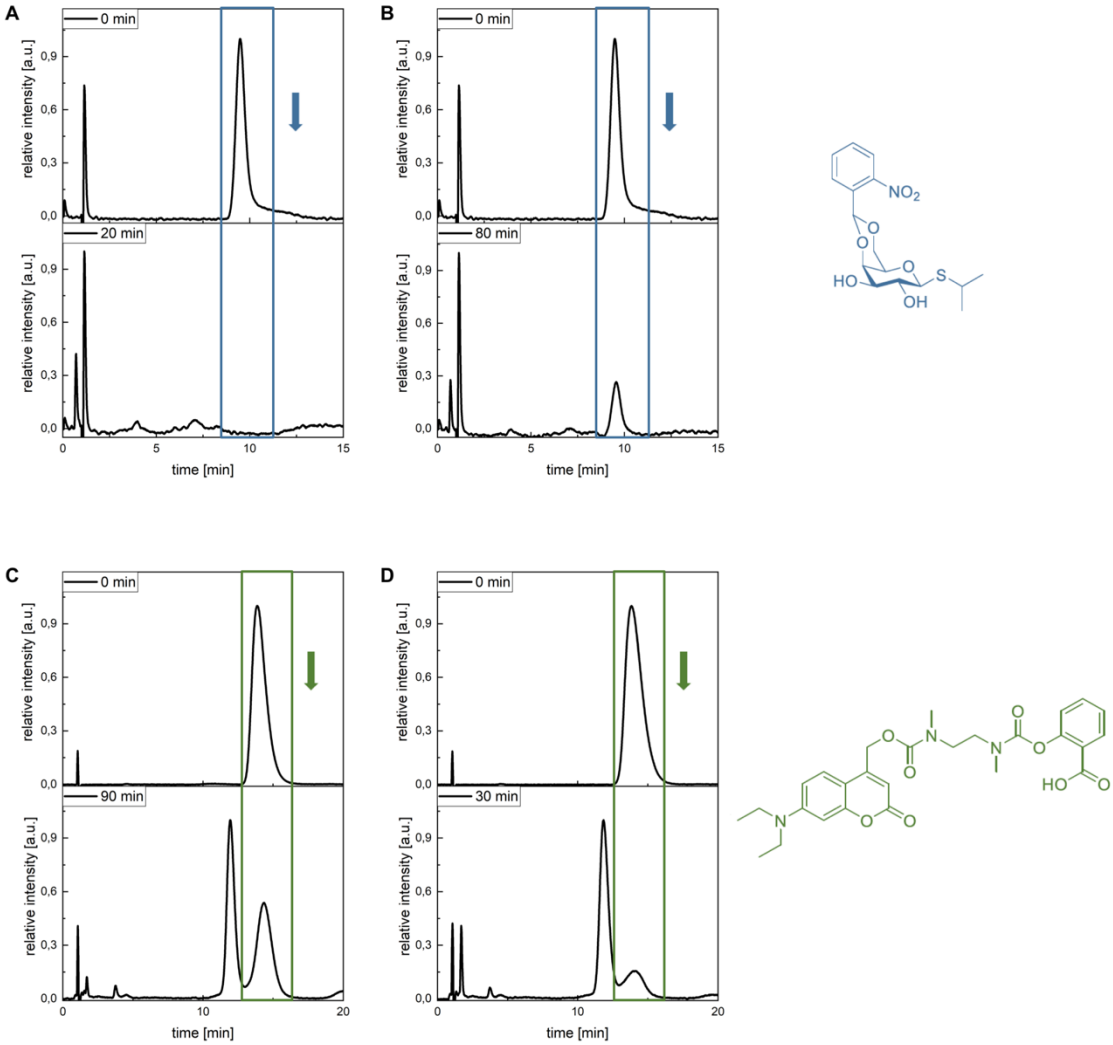

Figure S8: A) UV trace at 260 nm of the reversed-phase HPLC analysis of NB-cIPTG (**4**) (1 mM in MeOH/H_2O 30:70) before irradiation and after 20 min of irradiation at 375 nm (6.4 mW cm^{-2}, room temperature). **B**) UV trace at 260 nm of the reversed-phase HPLC analysis of NB-cIPTG (**4**) (1 mM in MeOH/H_2O 30:70) before irradiation and after 80 min of irradiation at 430 nm (45.6 mW cm^{-2}, room temperature). **C**) UV trace at 395 nm of the reversed-phase HPLC analysis of DC-cSal (**5**) [1 mM in sodium phosphate buffer (20 mM, pH 7.4)/MeOH 90:10] before irradiation and after 20 min of irradiation at 375 nm (6.4 mW cm^{-2}, room temperature). **D**) UV trace at 395 nm of the reversed-phase HPLC analysis of DC-cSal (**5**) [1 mM in sodium phosphate buffer (20 mM, pH 7.4)/MeOH 90:10] before irradiation and after 80 min of irradiation at 430 nm (45.6 mW cm^{-2}, room temperature).

S2.1 NMR spectra of compounds

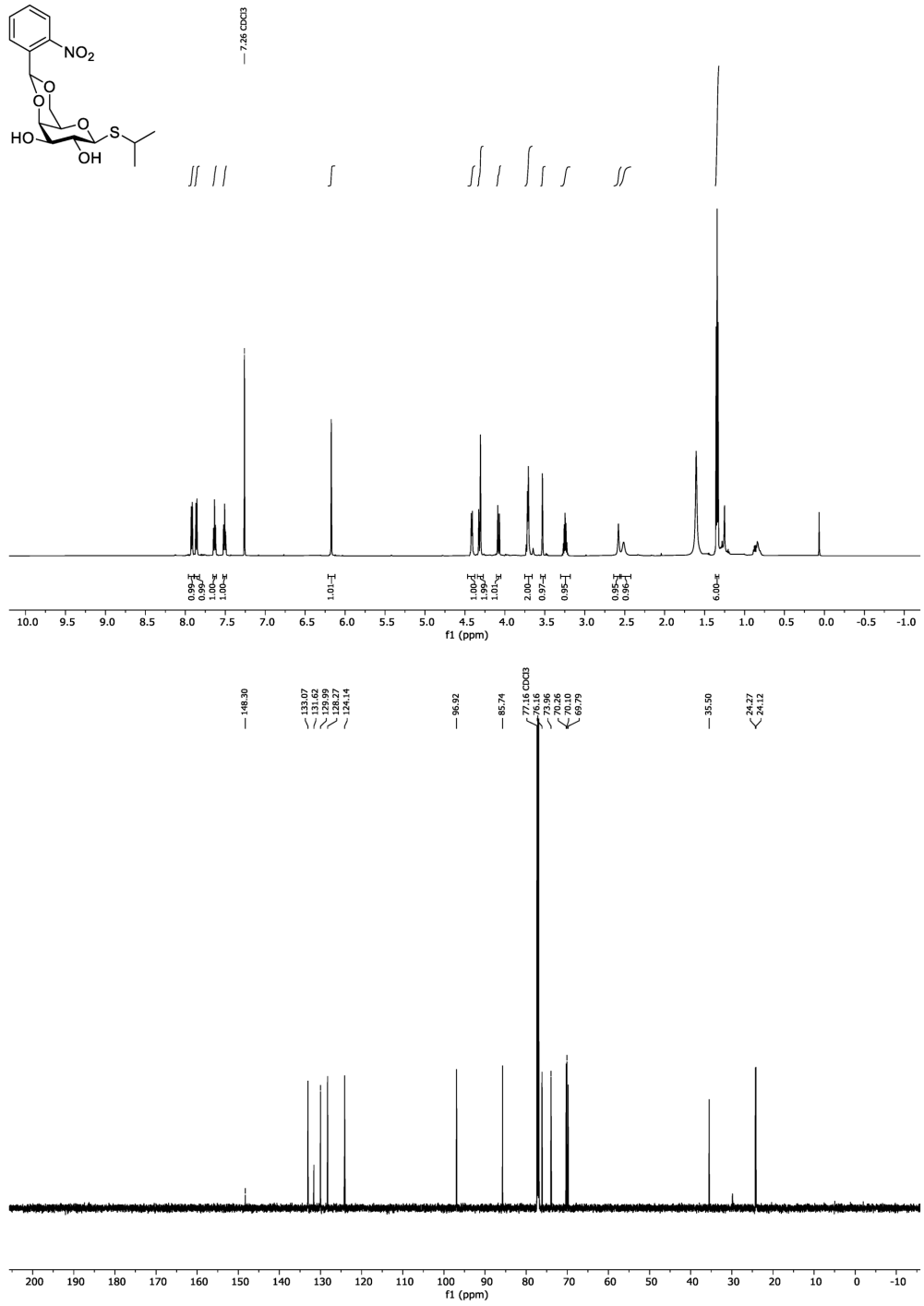

Figure S9: ^{1}H- and ^{13}C-NMR spectra of NB-cIPTG (**4**) in $CDCl_3$ (600 MHz/151 MHz).

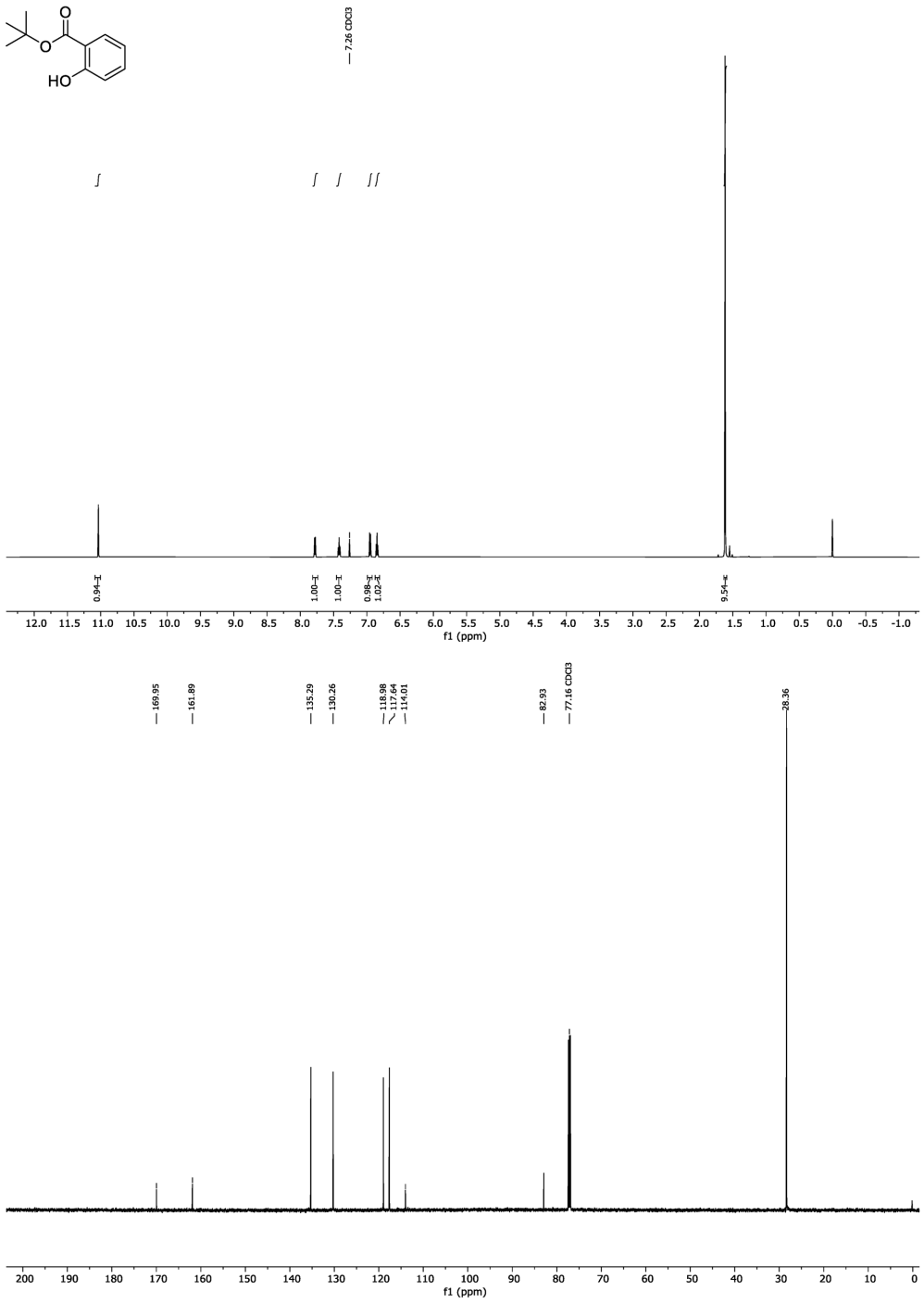

Figure S10: ^{1}H- and ^{13}C-NMR spectra of **S3** in $CDCl_3$ (600 MHz/151 MHz).

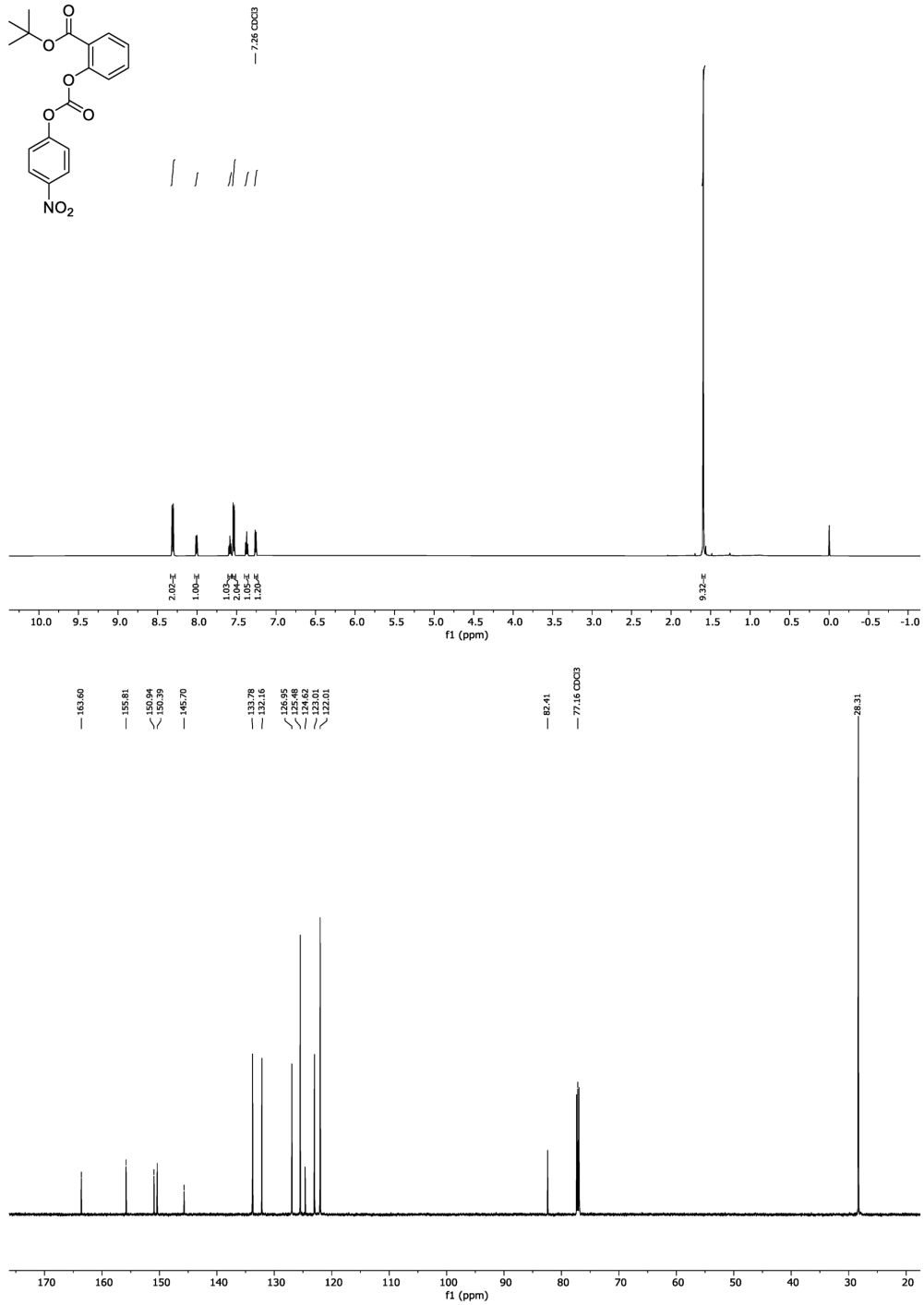

Figure S11: ^{1}H- and ^{13}C-NMR spectra of **S4** in $CDCl_3$ (600 MHz/151 MHz).

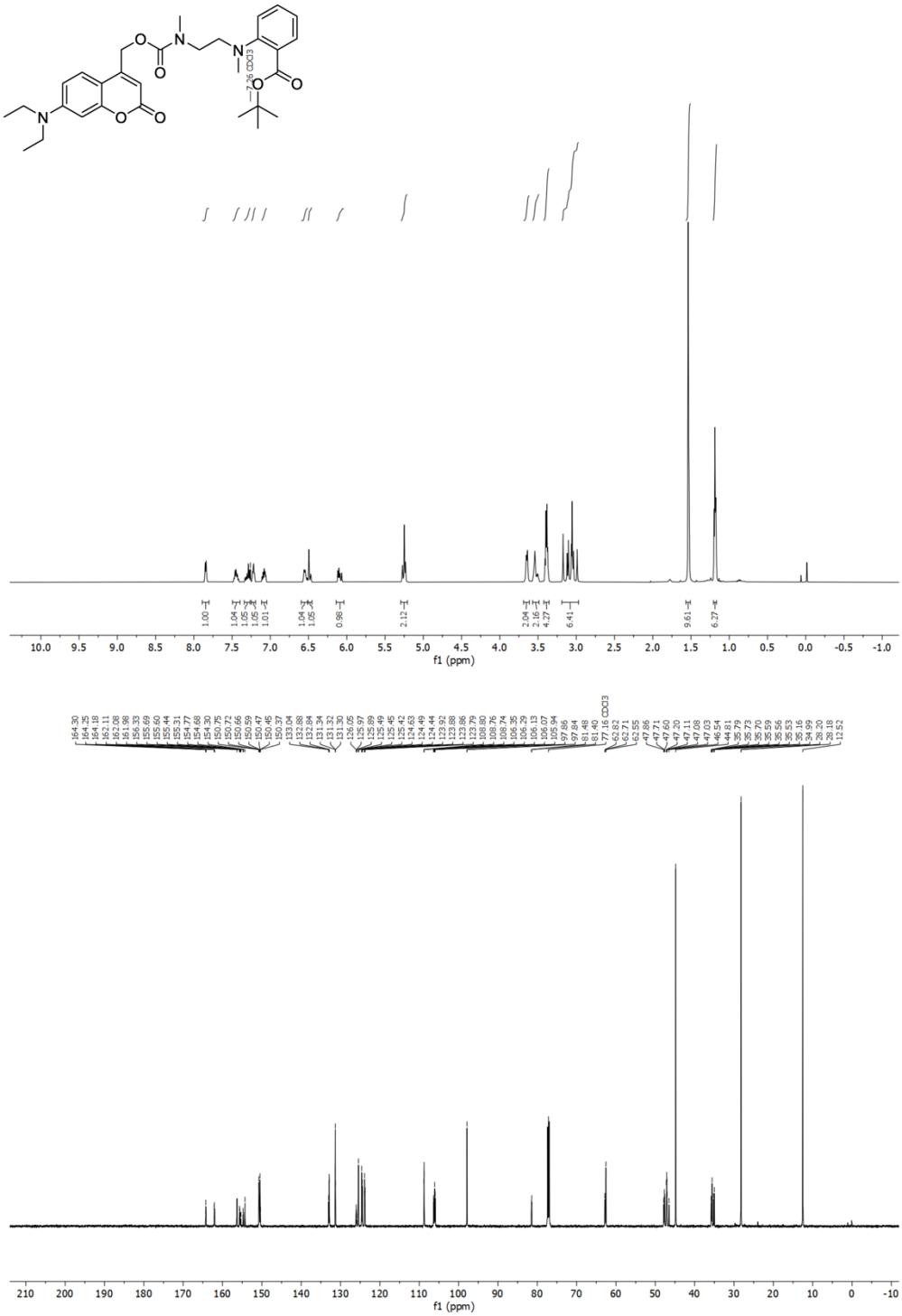

Figure S12: ^{1}H- and ^{13}C-NMR spectra of **S6** in $CDCl_3$ (600 MHz/151 MHz).

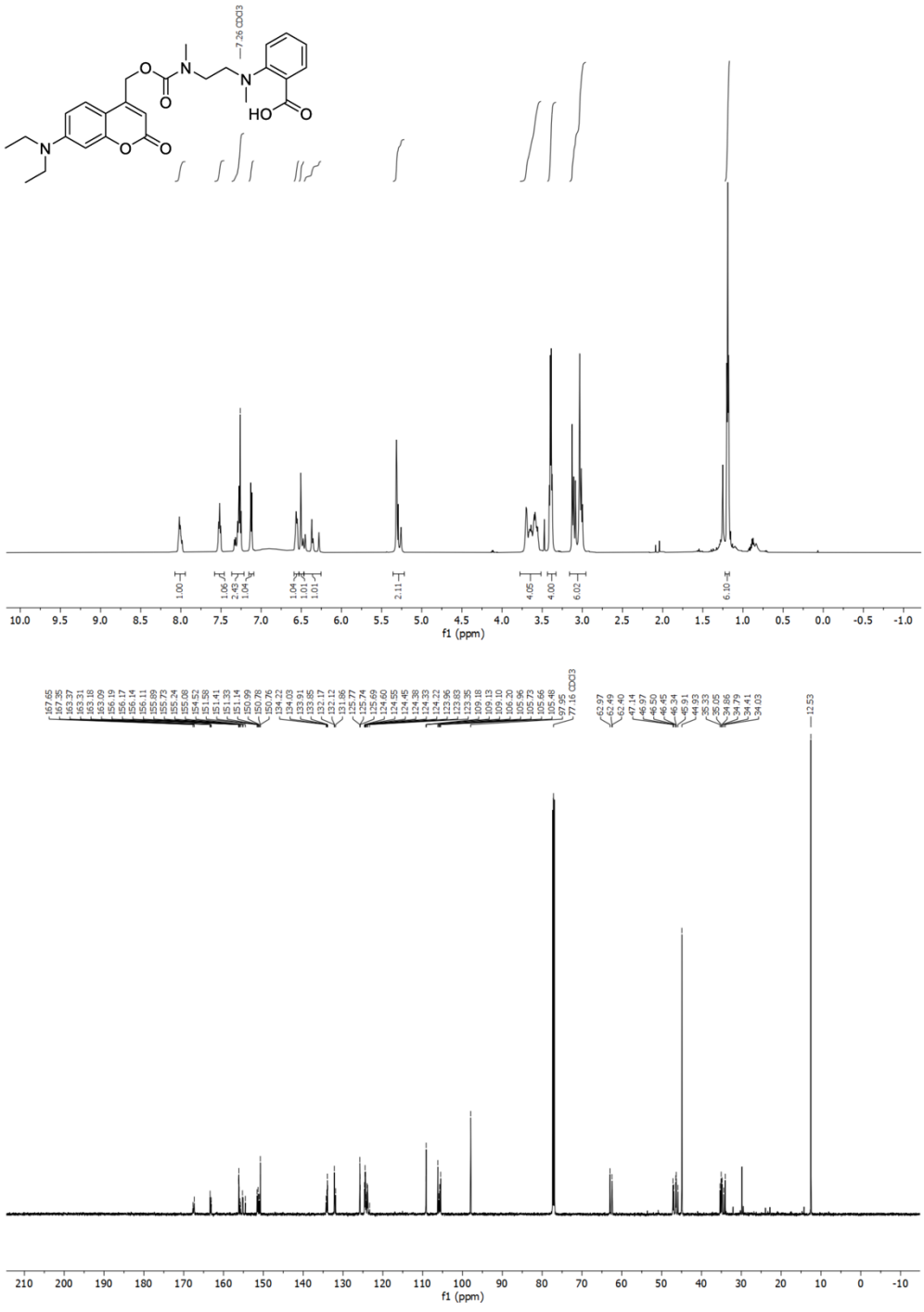

Figure S13: ^{1}H- and ^{13}C-NMR spectra of DC-cSal (**5**) in $CDCl_3$ (600 MHz/151 MHz).

References

1. Hanahan, D. Studies on transformation of *Escherichia coli* with plasmids. *J. Mol. Biol.* **1983**, *166*, 557–580.
2. Tiso, T.; Ihling, N.; Kubicki, S.; Biselli, A.; Schonhoff, A.; Bator, I.; Thies, S.; Karmainski, T.; Kruth, S.; Willenbrink, A.-L.; et al. Integration of genetic and process engineering for optimized rhamnolipid production using *Pseudomonas putida*. *Front. Bioeng. Biotechnol.* **2020**, *8*, 1–24.
3. Hogenkamp, F.; Hilgers, F.; Knapp, A.; Klaus, O.; Bier, C.; Binder, D.; Jaeger, K.-E.; Drepper, T.; Pietruszka, J. Effect of photocaged isopropyl β-D-1-thiogalactopyranoside solubility on light-responsiveness of LacI-controlled expression systems in different bacteria. *ChemBioChem* **2021**, *22,* 539–547.
4. Burmeister, A.; Hilgers, F.; Langner, A.; Westerwalbesloh, C.; Kerkhoff, Y.; Tenhaef, N.; Drepper, T.; Kohlheyer, D.; von Lieres, E.; Noack, S.; et al. A microfluidic co-cultivation platform to investigate microbial interactions at defined microenvironments. *Lab Chip* **2019**, *19*, 98–110.
5. Verhoef, S.; Ballerstedt, H.; Volkers, R.J.M.; de Winde, J.H.; Ruijssenaars, H.J. Comparative transcriptomics and proteomics of p-hydroxybenzoate producing *Pseudomonas putida* S12: novel responses and implications for strain improvement. *Appl. Microbiol. Biotechnol.* **2010**, *87*, 679–690.
6. Hogenkamp, F.; Hilgers, F.; Bitzenhofer, N.L.; Ophoven, V.; Haase, M.; Bier, C.; et al. Photocaged compounds for controlling bacterial gene expression – challenges, solutions, and surprising observations. *ChemBioChem.* **2021**, submitted.
7. Wittgens, A.; Kovacic, F.; Müller, M.M.; Gerlitzki, M.; Santiago-Schübel, B.; Hofmann, D.; Tiso, T.; Blank, L.M.; Henkel, M.; Hausmann, R.; et al. Novel insights into biosynthesis and uptake of rhamnolipids and their precursors. *Appl. Microbiol. Biotechnol.* **2017**, *101*, 2865–2878.
8. Kluger, R.; De Stefano, V.. Mechanism of site-directed protein cross-linking. Protein-directed selectivity in reactions of hemoglobin with aryl trimesates. *J Org Chem*. **2000**, 65, 214–219.
9. Fomina, N.; McFearin, C.L.; Sermsakdi, M.; Morachis, J.M.; Almutairi, A.; Low power, biologically benign NIR light triggers polymer disassembly. *Macromolecules*. **2011**;44, 8590–8597.

V.5. SUPPORTING INFORMATION FOR CHAPTER II.2.1 – FLUORESCENT PROTEINS AS GENETICALLY ENCODED PHOTOSENSITIZERS

Supplemental material

An optogenetic toolbox of LOV-based photosensitizers for light-driven killing of bacteria

Authors

Stephan Endres[1,2,§], Marcus Wingen[1,§], Joaquim Torra[3,§], Rubén Ruiz-González[3], Tino Polen[4], Gabriela Bosio[5,6], Nora Lisa Bitzenhofer[1], Fabienne Hilgers[1], Thomas Gensch[6], Santi Nonell[3,*], Karl-Erich Jaeger[1,4], Thomas Drepper[1,*]

Affiliations

[1] Institute of Molecular Enzyme Technology, Heinrich-Heine-University Düsseldorf, Forschungszentrum Jülich GmbH, Jülich, Germany

[2] m2p-labs GmbH, Baesweiler, Germany

[3]Institut Químic de Sarrià, Universitat Ramon Llull, Barcelona, Spain

[4] Institute of Bio- and Geosciences, IBG-1: Biotechnology, Forschungszentrum Jülich GmbH, Jülich, Germany

[5] Instituto de Investigaciones Teóricas y Aplicadas, Universidad Nacional de La Plata, Argentina.

[6] Institute of Complex Systems, ICS-4: Cellular Biophysics, Forschungszentrum Jülich GmbH, Jülich, Germany

[§] contributed equally to this work
* Corresponding authors
E-Mail: t.drepper@fz-juelich.de
santi.nonell@iqs.url.edu

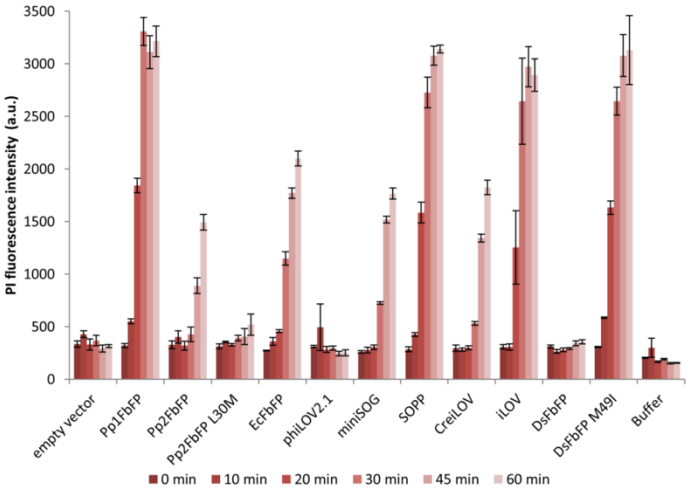

Supplemental figure S1. Raw data of the analysis of LOV-FP phototoxicity using propidium iodide as quantitative marker for dead *E. coli* cells. The bars show the raw PI fluorescence intensity (λ_{ex} = 535 nm, λ_{em} = 617 nm) over 60 minutes. Data represents the mean values of three independent experiments and the error bars the calculated standard deviations.

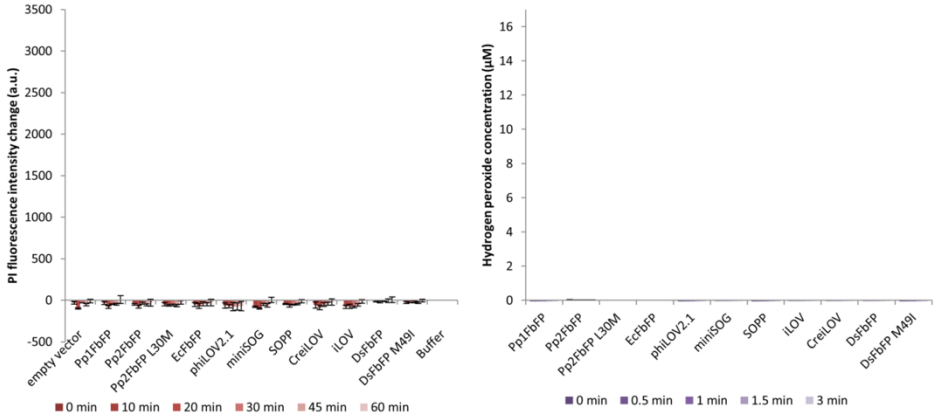

Supplemental figure S2. Control experiments of the PI assay and Amplex Red assay in the dark. A: PI toxicity assay in the dark. The data show the change in PI fluorescence intensity compared to that at t = 0. No significant changes could be observed. B: Amplex Red assay in the dark. The bars show the change in hydrogen peroxide concentration at different exposure times in the dark for all tested photosensitizes. No detectable H_2O_2 production was observed. The data represent the mean values of three independent experiments and the error bars the calculated standard deviations.

Supplemental figure S3. Analysis of heterogeneity of LOV-FP-mediated cell death at the single cell level.

The experiments devoted to study LOV-FP induced phototoxic effects in single *E. coli* cells via PI fluorescence detection were performed on a spinning disk confocal fluorescence microscope as previously described (Oreopoulos and Browne, 2014) First, *E. coli* BL21 (DE3) cells were transformed with the respective LOV-FP expression vector or empty vector. The transformed cells were cultivated overnight in TB media at 37 °C and subsequently induced in the stationary growth phase with 0.4 mM IPTG. The cells were harvested 3 h after induction, resuspended in PBS buffer (pH 7.4) and then immobilized on glass bottom 35 mm Petri dishes (ibidi, Martinsried, Germany), previously treated with Poly-L-Lysine (PLL) (0.1 mg.mL−1) (1 mL for 5 min). Samples were then placed directly inside a stage top incubator (Okolab S.R.L., Pozzuoli, Italy; environmental parameters set to 37 °C and 85% humidity in air atmosphere) on the stage of an inverted microscope (Ti-E, Nikon Europe BV, Düsseldorf, Germany). The inverted microscope was used as a spinning disk confocal microscope as described by Oreopoulos and Browne (2014) (ACALBFI, Groeben, Germany) with a spinning disk unit (CSU-W1; Yokogawa Electric Corporation, Tokyo, Japan) as the central part (more details in Rivas Aiello *et al.* 2018). Bright field images, as well as spinning disk confocal fluorescence images with excitation at 488 nm and 561 nm were taken with a 100X magnification oil immersion objective (plan apo chromat, NA=1.40, Nikon). Appropriate dichroic beam splitter and bandpass filters in the Optosplit unit allowed the detection of LOV-FP fluorescence (λ_{exc} = 488 nm (laser); λ_{obs} = 500 - 530 nm) or PI fluorescence (λ_{exc} = 561 nm (laser); λ_{obs} = 575 - 630 nm), respectively. First, *E. coli* cells were exposed to a buffer containing 1.5 μM PI for 5 to10 minutes and transmission (bright field; Supplemental Fig. S3A I, S3B I, S3C I), LOV-FP fluorescence (Supplemental Fig. S3A II, S3B II, S3C II) and PI fluorescence images (Supplemental Fig. S3A III, 3B III, 3C III) were acquired. Irradiation for photodynamic action was performed with fluorescence excitation lamp of the microscope (465-495 nm; 32 μW in an illuminated spot with 200 μm diameter (i.e., 102 mW cm^{-2})) and PI fluorescence images were recorded at several time points and a total illumination time of 10 minutes.

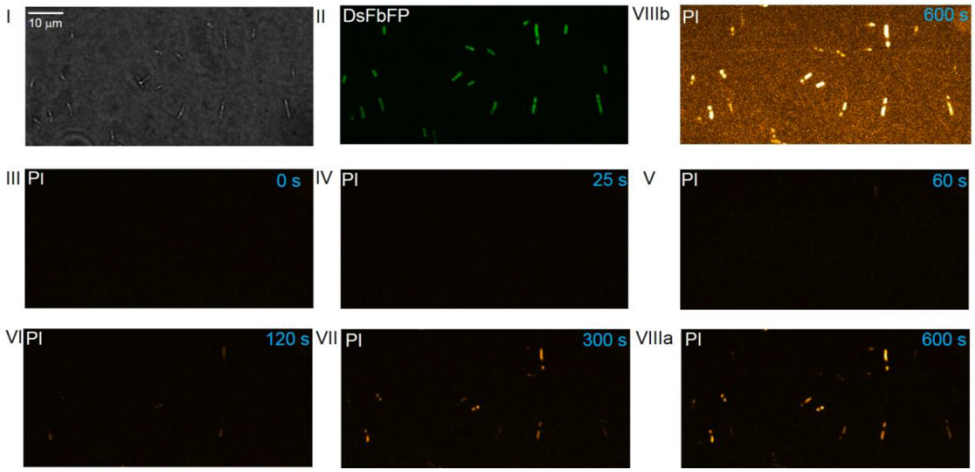

Supplemental figure S3A. Phototoxicity of DsFbFP. Images of DsFbFP expressing *E. coli* cells before blue light irradiation (I, bright field; II, DsFbFP fluorescence emission; III PI fluorescence emission) and PI emission images after different blue light exposures (460-490 nm; P=102 mW cm^{-2}) (IV – VIII). Fluorescence intensity scale for image II is 135-4135 and for III-VIIIa amounts to 135 – 10135 (II: λ_{exc}=488 nm, P=95 mW/cm^2, t=100 ms; III-VIIIb: λ_{exc}=561 nm, P=140 mW cm^{-2}, t=50 ms). VIIIb is the same image as VIIIa but with a ten-fold smaller scale (135-1135) for better visualization of phototoxic effect in all DsFbFP-expressing *E. coli* cells.

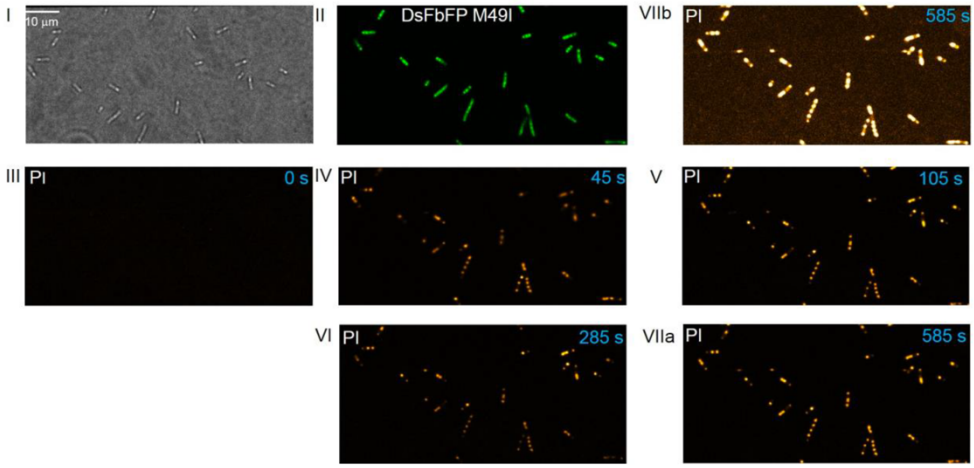

Supplemental figure S3B. Phototoxicity of DsFbFP M49I. Images of DsFbFP M49I expressing *E. coli* cells before blue light irradiation (I, bright field; II, DsFbFP fluorescence emission; III PI fluorescence emission) and PI emission images after different blue light exposures (460-490 nm; P=102 mW cm^{-2}) (IV – VIII). Fluorescence intensity scale for II is 135-4135 and for III-VIIa amounts to 135 – 28135 (II: λ_{exc}=488 nm, P=95 mW/cm^2, t=100 ms; III-VIIb: λ_{exc}=561 nm, P=140 mW cm^{-2}, t=50 ms). VIIb is the same image as VIIa but with a tenfold smaller scale (135-2935) for better visualization of phototoxic effect in all DsFbFP M49I-expressing *E. coli* cells. Please note that the bright field image (I) was shifted by accident (~5 µm to the bottom and 2 µm to the left), compared to the fluorescence images (II - VII).

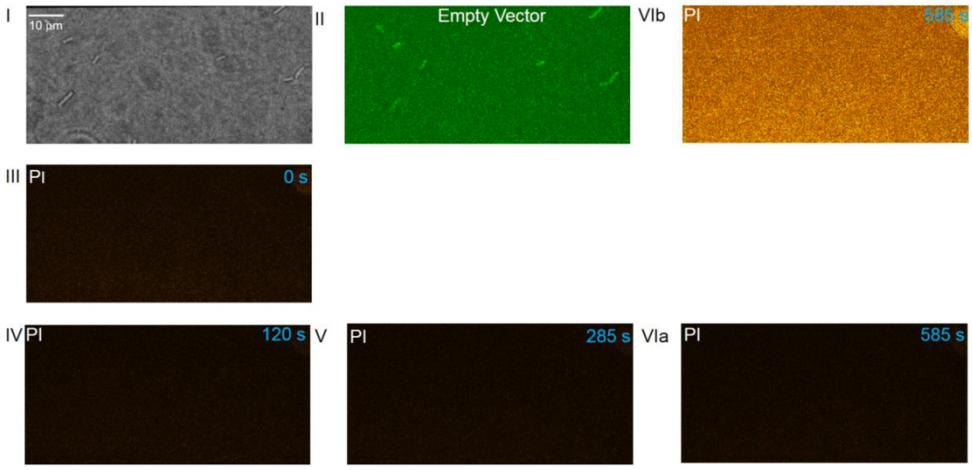

Supplemental figure S3C. Phototoxicity control experiment with *E. coli* cells carrying the empty expression vector. Images of *E. coli* cells before blue light irradiation (I, bright field; II, autofluorescence of endogenous flavins; III PI fluorescence emission) and PI emission images after different blue light exposures (460-490 nm; P=102 mW cm^{-2}) (IV – VI). Fluorescence intensity scale for II is 135-535 and for III-VIIa amounts to 135 – 4135 (II: λ_{exc}=488 nm, P=95 mW/cm^2, t=100 ms; III-VIIb: λ_{exc}=561 nm, P=140 mW cm^{-2}, t=50 ms). VIIb is the same image as VIIa but with a tenfold smaller scale (135-535) for better visualization of the absence of phototoxic effect in all *E. coli* cells transfected with empty vector.

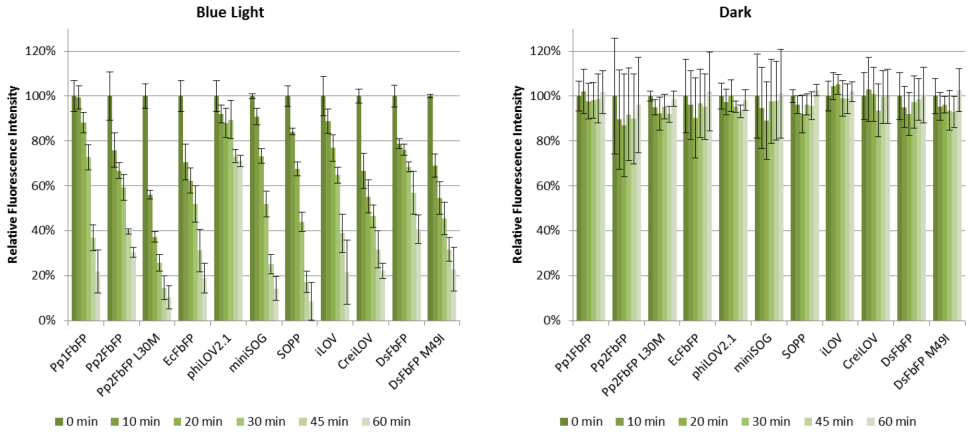

Supplemental figure S4. *In vivo* photobleaching of LOV-FP fluorescence intensities in dependence to blue light irradiation. The bars indicate the normalized LOV-PS fluorescence intensity (λ_{ex} = 450 nm, λ_{em} = 495 nm) for the light- (left) and control experiment (right). For this study, the same samples have been used as for the *in vivo* PI assay that is shown in Fig. 3. Prolonged irradiation with blue light (λ_{max} = 447 nm, ~ 10 mW cm^{-2}) led to a decreasing activity of all tested variants, whereas explicit differences were found. Some variants, like phiLOV2.1 showed only weak photobleaching whereas Pp2FbFP L30M appeared notably sensitive. As expected, no significant changes within the LOV-PS fluorescence activity was observed in the control experiment. The given data represents the mean values of three independent experiments and the error bars the calculated standard deviations.

References

Rivas Aiello, M., Castrogiovanni, D., Parisi, J., Azcárate, J., García Einschlag, F., Gensch, T., Bosio, G., Martire, D. Photodynamic Therapy in HeLa Cells Incubated with Riboflavin and Pectin-coated Silver Nanoparticles. *Photochem Photobiol* accepted (2018)

Oreopoulos, J., Berman, R., Browne, M. Spinning-disk confocal microscopy: present technology and future trends. *Meth Cell Biol* **123**, 153-175 (2014).

V.6. SUPPORTING INFORMATION FOR CHAPTER II.2.2 – PHOTOSENSITIZERS FOR ANTIMICROBIAL PHOTODYNAMIC INACTIVATION

Supplementary Figures

Genetically Encoded Photosensitizers as Light-Triggered Antimicrobial Agents

Fabienne Hilgers [1,†], Nora Lisa Bitzenhofer [1,†], Yannic Ackermann [1], Alina Burmeister [2,3], Alexander Grünberger [2,3], Karl-Erich Jaeger [1,3] and Thomas Drepper [1,*]

[1] Institute of Molecular Enzyme Technology, Heinrich-Heine-University Düsseldorf, Forschungszentrum Jülich GmbH, D-52428 Jülich, Germany
[2] Multiscale Bioengineering, Bielefeld University, D-33501 Bielefeld, Germany
[3] Institute of Bio- and Geosciences, IBG-1: Biotechnology, Forschungszentrum Jülich GmbH, D-52428 Jülich, Germany
† These authors contributed equally to this work.
* Correspondence: t.drepper@fz-juelich.de

The online version may be found at:
https://www.mdpi.com/1422-0067/20/18/4608/s1

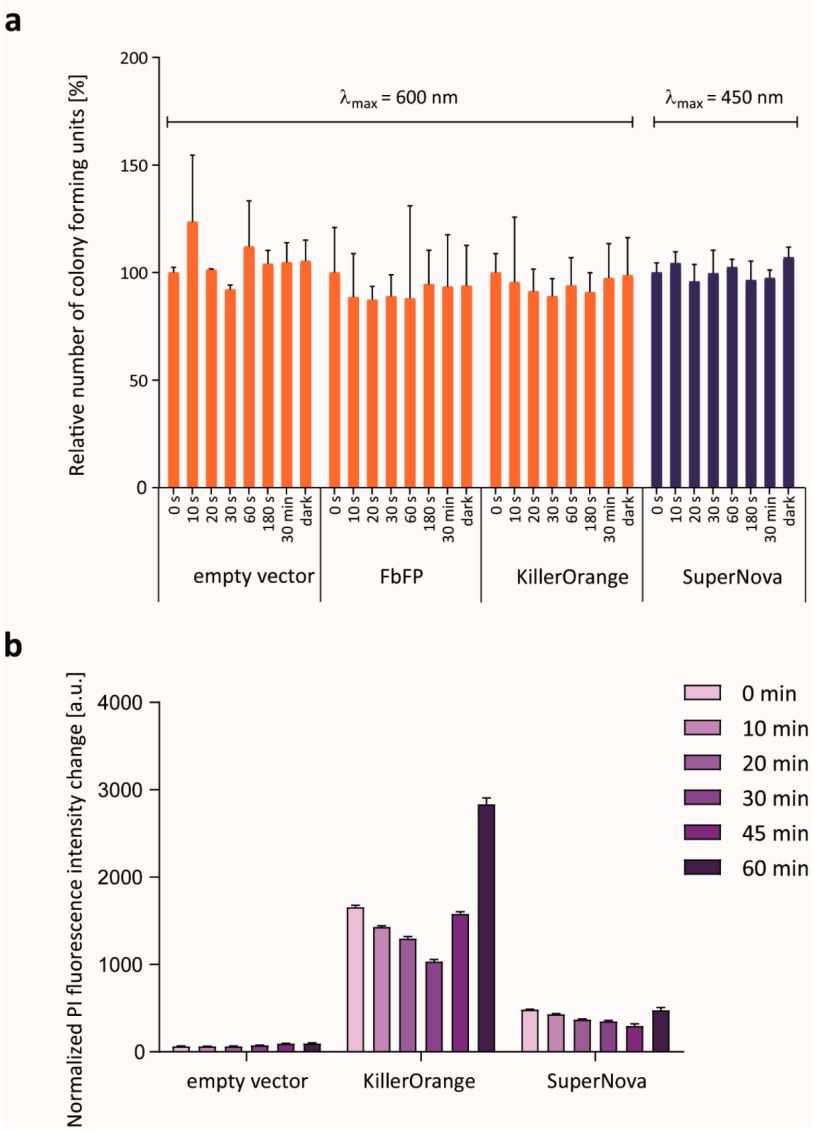

Figure S1: Control experiment for the evaluation of the wavelength- and light intensity-dependent phototoxicity of the individual PSs. (**a**) Evaluation of the wavelength-dependent photoactivation of the individual PSs using colony forming units (CFU). Control experiment for the evaluation of the wavelength-dependent photoactivation of the individual PSs using colony forming units (CFU). To exclude an influence on orange light (λ_{max} = 600 nm) on the LOV-based PSs, KillerOrange and the empty vector control as well as an influence of blue light (λ_{max} = 448 nm) on SuperNova, *E. coli* BL21 (DE3) harboring the respective expression vectors was used. After cultivation of expression cultures, cells were diluted to a finale $OD_{580\ nm}$ of 0.1 in PBS buffer (pH 7.4) and subsequently illuminated with the according light source (~130 mW cm^{-2}) for different illumination times. Aliquots of the irradiated samples have been transferred to LB agar plates and incubated over night at 37 °C in the dark. Data represent the mean values of the CFUs from three independent measurements. The corresponding standard deviations are indicated by error bars. (**b**) Quantitative in vivo phototoxicity studies of KillerOrange and SuperNova at high light intensities using the propidium iodide (PI) cell death assay. For the PI-based cell death assay, *E. coli* cells producing the PS KillerOrange and SuperNova were

adjusted to an $OD_{580\,nm}$ of 0.5 in PI assay buffer (pH 7.4) and illuminated with high light intensities of blue (130 mW cm^{-2}, λ_{max} = 447 nm) or orange light (138 mW cm^{-2}, λ_{max} = 600 nm). The bars indicate the change in PI fluorescence intensity (λ_{ex} = 535 nm; λ_{em} = 617 nm) in dependence on the exposure time. The data were normalized to the amount of functional protein per cell, to exclude an influence of different protein accumulation levels. The data represent the mean values of three independent experiments and the error bars indicate the calculated standard deviations.

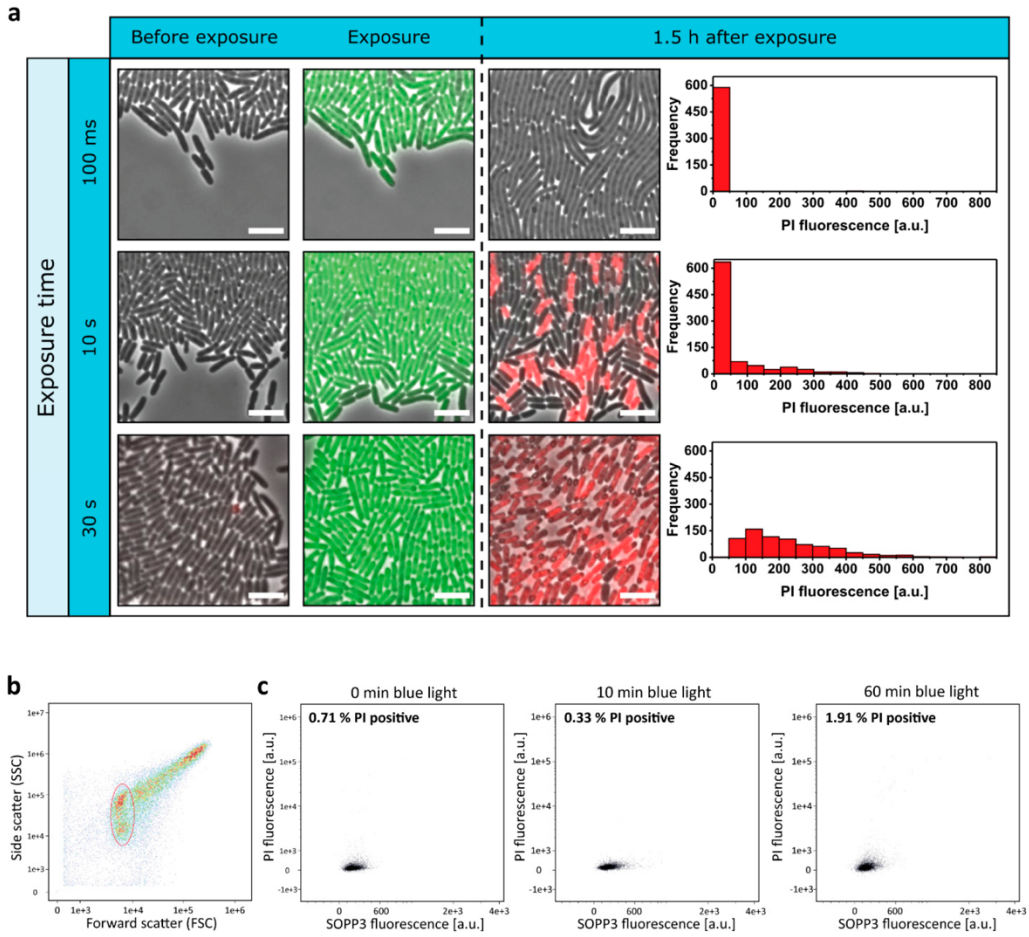

Figure S2: In vivo phototoxicity studies using the propidium iodide (PI) cell death assay as a quantitative marker for dead cells. (**a**) Images from microfluidic experiments with intracellular SOPP3 expression and different blue light exposure times. Images are shown for selected exposure times (100 ms, 10 s, 30 s) and time points during cultivation (before blue light exposure, at blue light exposure, 1.5 h after exposure). Both, the homogeneous distribution of SOPP3 expressed in individual cells of the microcolony at the time of exposure (indicated by the green fluorescence) and the PI fluorescence distributions 1.5 h after exposure for the corresponding exposure times are shown. Dead cells were stained red. The respective graphs represent the frequency of different PI fluorescence intensities within one microfluidic cell 1.5 h after exposure. While an exposure of 100 ms did not lead to PI positive cells at all and 10 s of blue light only addressed a few cells, the exposure of 30 s showed a nearly homogeneous PI fluorescence signal within the whole chamber. Scale bar = 5 µm. (**b**) Scatter plot of side versus forward scatter of *E. coli* cells harboring the expression vector pET28a-SOPP3, to identify cells of interest. A density plot was used to display the scattering. Regions with many events are displayed in red, regions with moderate events in green and regions with few events in blue. The gated population is circled in red. Doublets and cell accumulations were excluded with the help of the event gallery. This is a device-specific camera-enabled feature of the CellStream acquisition software, which displays a live flow of the sample in the channels to allow population verification and discrimination of duplicates. (**c**) *E. coli* BL21(DE3) cells harboring an empty vector were analyzed for fluorescence analysis and gated based on FSC and SSC to exclude cell debris and accumulation of cells. The fluorescence intensity of propidium iodide was measured using a 561 nm-laser (and a 611/31 nm (red) bandpass filter) and plotted using a log scale. Additionally, the intrinsic fluorescence was

analyzed with a 488 nm-laser and detected by a 528/46 nm bandpass filter. Dead *E. coli* cells (presented as red populations) are shifted to higher log values of the axis of abscissas and the percentage of dead cells is displayed in the upper left corner. Living cells are represented as black populations.

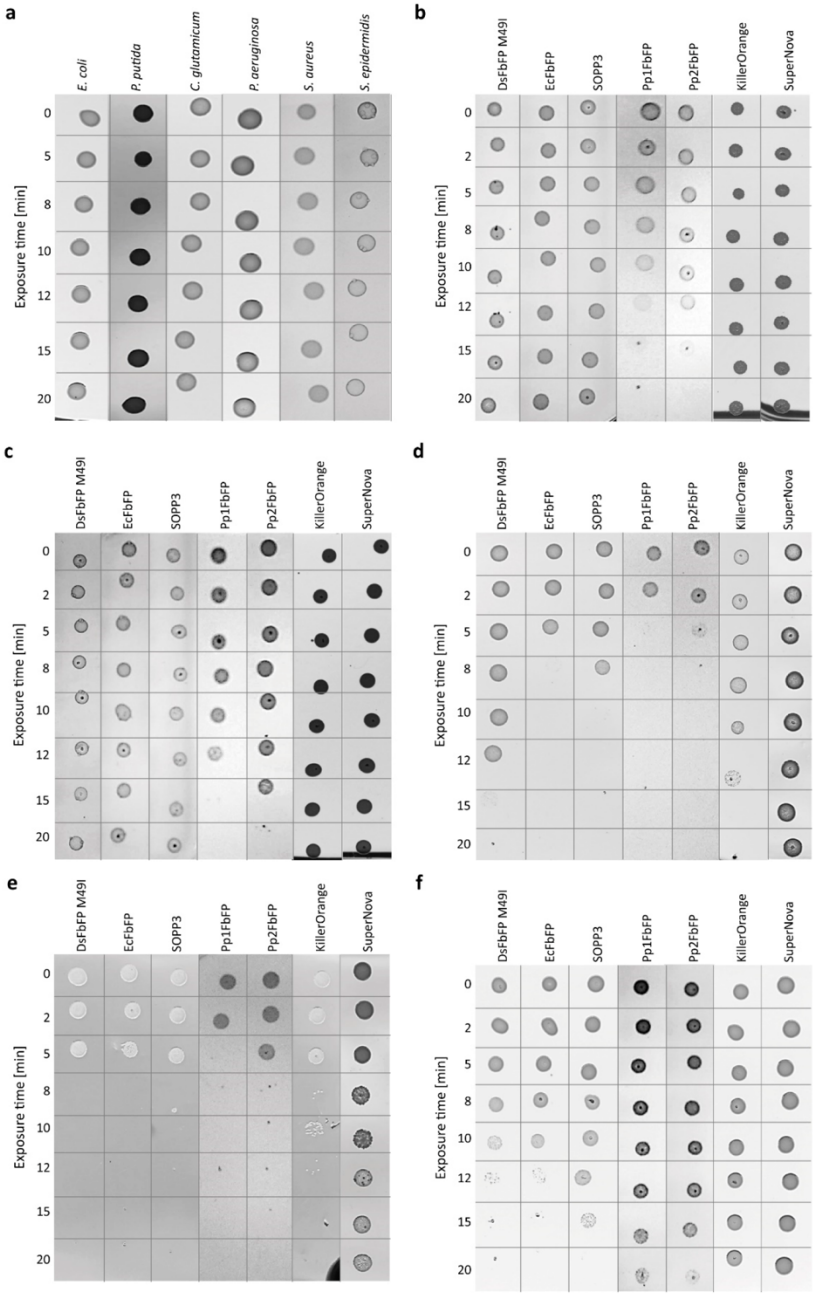

Figure S3: Extracellular antimicrobial activity of genetically-encoded PSs on bacteria. To investigate the effect of extracellularly added PSs, purified proteins have been analyzed by a plate spot assay. For this, bacterial cells ((**b**) *S. epidermidis* 12228; (**c**) *S. aureus* 25923; (**d**) *C. glutamicum* 13032; (**e**) *P. putida* KT2440; (**f**) *P. aeruginosa* PAO1) have been supplemented with the respective PS variant and then illuminated for different time periods with intense blue (λ_{max} = 448 nm, 130 mW cm^{-2}) or orange light (λ_{max} = 600 nm, 130 mW cm^{-2}). Subsequently, 3 µL of the irradiated cells were dropped on agar plates and incubated overnight. To exclude blue light toxicity, a plate spot assay without the addition of a photosensitizer has been performed as a control experiment (**a**).

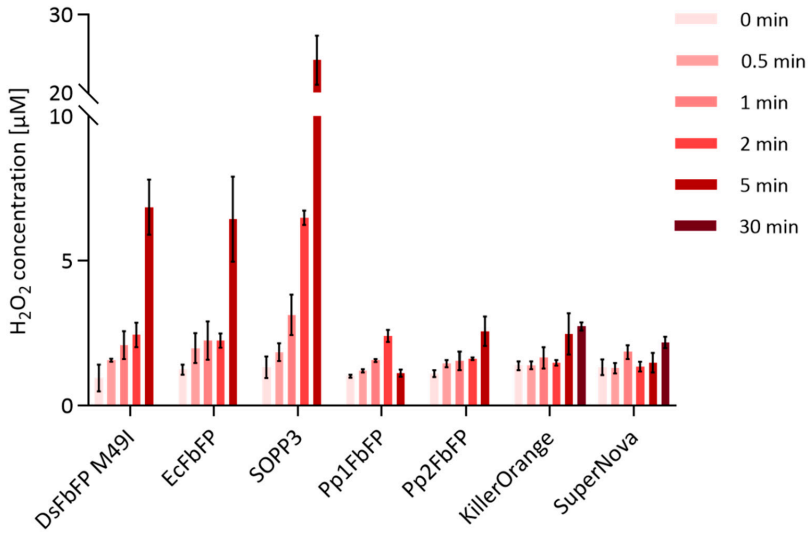

Figure S4: Quantification of PS-catalyzed hydrogen peroxide formation. Determination of H_2O_2, generated by DsFbFP M49I, EcFbFP, SOPP3, Pp1FbFP, Pp2FbFP, KillerOrange and SuperNova, was performed with the Amplex®Red Hydrogen Peroxide/Peroxidase Assay Kit (Molecular Probes, Invitrogen, part of Thermo Fisher Scientific, Eugene, USA) using purified photosensitizers adjusted to an $OD_{450\ nm}$ (LOV-based PSs and KillerOrange) or $OD_{580\ nm}$ (SuperNova) of 0.05. The measurements were performed according to the manufacturer's manual and as described by Endres *et al.* (2018) [1]. To accurately determine differences in ROS formation, the PSs have been illuminated with low light intensities (~10 mW cm^{-2}) with blue (λ_{max} = 447 nm) or orange (λ_{max} = 600 nm) light before adding the Amplex®Red reagent. Resorufin production (the product of the Amplex®Red reaction) was photometrically measured at 560 nm. To determine the final H_2O_2 concentration, a calibration curve was prepared (0 µM to 50 µM). The data represent the values of three independent experiments and the calculated standard deviations are indicated by error bars.

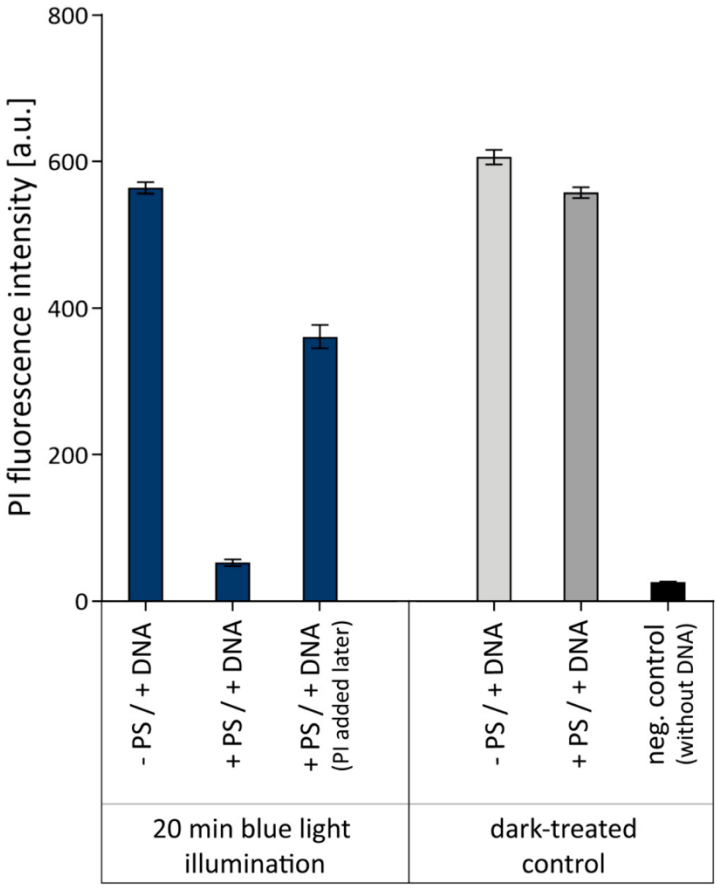

Figure S5: In vitro analysis to determine the influence of ROS on propidium iodide (PI). An in vitro experiment was performed to investigate the effect of PS-formed ROS on PI. The photosensitizer EcFbFP was mixed with salmon sperm DNA in PI assay buffer with or without PI and exposed to blue light (λ_{max} = 448 nm; 130 mW cm^{-2}) for 20 min. The PI fluorescence was then measured at λ_{ex} = 535 nm and λ_{em} = 617 nm. Samples without PI addition were supplemented with PI after illumination and prior to fluorescence detection. Unexposed samples as well as a negative control without the addition of DNA were carried as controls. The data represent the mean values of three independent experiments and the error bars indicated the calculated standard deviations.

Codon optimized DNA sequences of photosensitizing proteins for expression in *E. coli*, *P. putida* and *R. capsulatus* [a].

(a) SOPP3 (codon optimized) from *Arabidopsis thaliana* [2]

GGATCCATGGCATATGGAAAAAAGCTTTGTGATTACCGATCCGCGCCTGCCGGATAACCCGATTATTTTT
GCGAGCGATGGCTTTCTGGAACTGACCGAATATAGCCGCGAAGAAATTCTGGGCCGCAACGGCCGCTTT
CTGCAGGGCCCGGAAACCGATCAGGCGACCGTGCAGAAAATTCGCGATGCGATTCGCGATCAGCGCGA
AATTACCGTGCAGCTGATTAACTATACCAAAAGCGGCAAAAAATTTCTGAACCTGCTGAACCTGCAGCC
GATTCGCGATCAGAAAGGCGAACTGCAGGCGTTTATTGGCGTGGTGCTGGATGGCTAAGAATTCCTCGAG

(b) SuperNova (codon optimized) from *Anthomedusae sp* [3]

GGATCCATGGCATATGGGCAGCGAAGTGGGCCCGGCGCTGTTCCAGAGCGATATGACCTTCAAAATCTT
CATCGATGGCGAAGTGAACGGCCAGAAATTCACCATCGTGGCGGATGGCAGCAGCAAATTCCCGCATGG
CGATTTCAACGTGCATGCGGTGTGCGAAACCGGCAAACTGCCGATGAGCTGGAAACCGATCTGCCATCT
GATCCAGTATGGCGAACCGTTCTTCGCGCGCTATCCGGATGGCATCAGCCATTTCGCGCAGGAATGCTTC
CCGGAAGGCCTGAGCATCGATCGCACCGTGCGCTTCGAAAACGATGGCACCATGACCAGCCATCATACC
TATGAACTGGATGATACCTGCGTGGTGAGCCGCATCACCGTGAACTGCGATGGCTTCCAGCCGGATGGCC
CGATCATGCGCGATCAGCTGGTGGATATCCTGCCGAGCGAAACCCACATGTTCCCGCATGGCCCGAACG
CGGTGCGCCAGACCGCGACCATCGGCTTCACCACCGCGGATGGCGGCAAAATGATGGGCCATTTCGATA
GCAAAATGACCTTCAACGGCAGCCGCGCGATCGAAATCCCGGGCCCGCATTTCGTGACCATCATCACCA
AACAGACCCGCGATACCAGCGATAAACGCGATCATGTGTGCCAGCGCGAAGTGGCGTATGCGCATAGC
GTGCCGCGCATCACCAGCGCGATCGGCAGCGATGAAGATTGAGAATTCCTCGAG

(c) KillerOrange (codon optimized) from *Anthomedusae sp* [4]

GGATCCATGGCATATGGAATGCGGCCCGGCGCTGTTCCAGAGCGATATGACCTTCAAAATCTTCATCGAT
GGCGAAGTGAACGGCCAGAAATTCACCATCGTGGCGGATGGCAGCAGCAAATTCCCGCATGGCGATTTC
AACGTGCATGCGGTGTGCGAAACCGGCAAACTGCCGATGAGCTGGAAACCGATCTGCCATCTGATCCAG
TGGGGCGAACCGTTCTTCGCGCGCTATCCGGATGGCATCAGCCATTTCGCGCAGGAATGCTTCCCGGAAG
GCCTGAGCATCGATCGCACCGTGCGCTTCGAAAACGATGGCACCATGACCAGCCATCATACCTATGAAC
TGAGCGATACCTGCGTGGTGAGCCGCATCACCGTGAACTGCGATGGCTTCCAGCCGGATGGCCCGATCAT
GCGCGATCAGCTGGTGGATATCCTGCCGAGCGAAACCCACATGTTCCCGCATGGCCCGAACGCGGTGCG
CCAGCTGGCGTTCATCGGCTTCACCACCGCGGATGGCGGCCTGATGATGGGCCATCTGGATAGCAAAAT
GACCTTCAACGGCAGCCGCGCGATCGAAATCCCGGGCCCGCATTTCGTGACCATCATCACCAAACAGAT
GCGCGATACCAGCGATAAACGCGATCATGTGTGCCAGCGCGAAGTGGCGCATGCGCATAGCGTGCCGCG
CATCACCAGCGCGATCGGCAGCGATCAGGATTGAGAATTCCTCGAG

[a] Underlined sequences indicate inserted restriction sites.

Figure S6: Gene sequences of novel genetically-encoded photosensitizers. The sequences of the *sopp3* (**a**), the *killerorange* (**b**) and the *supernova* gene (**c**) are shown, which were used for the construction of the corresponding expression vectors. The gene sequences were codon optimized for expression in *E. coli* and corresponding genes were synthetically produced.

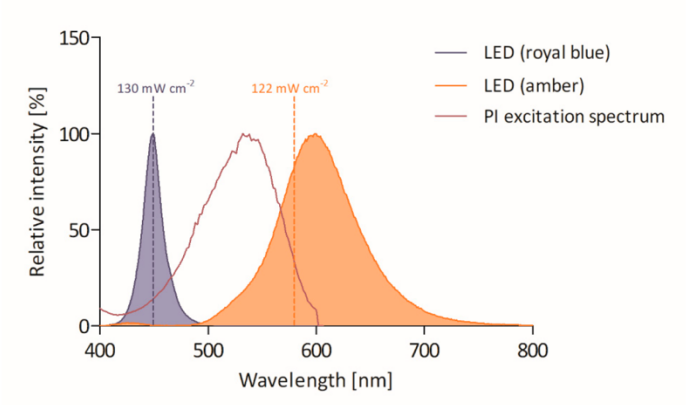

Figure S7: Emission spectra of blue and orange light-emitting high-power LEDs. The emission spectrum of a blue light-emitting LED (royal blue) shows a maximum at 448 nm. The orange light-emitting high-power LED (amber) has an emission maximum at 600 nm. The spectra were measured using a fluorescence spectrometer (Varian Cary Eclipse, Agilent Technologies, Ratingen, Germany). The dashed lines indicate the determined light intensities at the absorption maxima of the used PSs. To estimate the effect of PI-mediated absorption on the LED-mediated excitation of the PSs, the PI excitation spectrum is additionally shown (red line). The spectrum of PI (0.1 mg mL^{-1} salmon sperm in PBS buffer supplemented with 5 µM propidium iodide) was measured at an emission wavelength of 617 nm using a fluorescence spectrometer (Varian Cary Eclipse, Agilent Technologies, Ratingen, Germany. At the blue (450nm) and orange (600nm) emission maximum of the used LEDs, the absorption of PI is rather low and has almost equal and thus negligible effects on the excitation of the tested PSs.

Bacterial strains and plasmids

All bacterial strains, plasmids and oligonucleotides used in this study are listed in Table S1.

Table S1: Bacterial strains, plasmids and oligonucleotides used in this study.

[a] Underlined sequences indicate inserted restriction, mutation or homologous sites.

Strains, plasmids, oligonucleotides	Relevant features, description or sequences[a]	References
Strains		
C. glutamicum	Wild-type	[5]
E. coli DH5α	*F⁻Φ80lacZΔM15 Δ(lacZYA-argF) U169 recA1 endA1 hsdR17 phoA supE44 thi-1 gyrA96 relA1 deoR*	[6]
E. coli BL21(DE3)	*F⁻ ompT gal dcm lon hsdSB(rB⁻ mB⁻)λ(DE3 [lacI lacUV5-T7 gene 1 ind1 sam7 nin5])*	[7]
E. coli Tuner(DE3)	*F⁻ ompT gal dcm lon hsdSB (rB⁻ mB⁻) lacY1(DE3)*	Novagen
P. putida KT2440	Wild-type, recipient for conjugational plasmid transfer	[8]
P. aeruginosa PAO1	Wild-type	[9]
S. aureus	Wild-type	[10]
S. epidermidis	Wild-type	[11]
Plasmids		
pET28a(+)	P_{T7}, His6-Tag, MCS, *lacI*, *bla*, Km^R, pBR322 ori, f1 ori	Novagen
pET28a-RBS	P_{T7}, *aphII*, *lacI*, T7 Primer, Km^R	unpublished (Wingen)
pET28a-EcFbFP	*ecfbfp* controlled by the inducible P_{T7}; includes sequence for N-terminal His6-tag; Km^R	[12]
pET28a-Pp1FbFP	*pp1fbfp* controlled by the inducible P_{T7}; includes sequence for N-terminal His6-tag; Km^R	[12]
pET28a-Pp2FbFP	*pp2fbfp* controlled by the inducible P_{T7}; includes sequence for N-terminal His6-tag; Km^R	[12]
pET28a-DsFbFP M49I	*dsfbfp M49I* controlled by the inducible P_{T7}; includes sequence for N-terminal His6-tag; Km^R	[1]
pET28a-SOPP3	*sopp3* controlled by the inducible P_{T7}; includes sequence for N-terminal His6-tag; Km^R	This work
pET28a-KillerOrange	*killerorange* controlled by the inducible P_{T7}; includes sequence for N-terminal His6-tag; Km^R	This work
pET28a-SuperNova	*supernova* controlled by the inducible P_{T7}; includes sequence for N-terminal His6-tag; Km^R	This work
pURE-DsFbFP M49I-LecB	*dsfbfp M49I – lecB* fusion, includes sequence for expression by the inducible P_{T7}; N-terminal His6-tag; Amp^R	This work
Oligonucleotides		
1 IF_DsFbFPM49I_fow	Binds at the 5′ end of the *dsfbfp M49I* gene, contains homologous ends for InFusion® Cloning. 5′-AGGAGATATACCATGCGCAGACA TTATCGCGACCTGATAC-3′	This work

2 IF_DsFbFPM49I_rev	Binds at the 3′ end of the *dsfbfp m49i* gene, contains homologous ends for InFusion® Cloning and deletes stop codon of *dsfbfp m49i*. 5′-CGTCGTCGTCCTCGAAGACCGGGTT CTGGGCGC-3′	This work
3 IF_pURE_His_DsFbFP M49I_fo	Binds at the 5′ end of *dsfbfp m49i* gene on pURE DsFbFP M49I plasmid, contains His_6-Tag. 5′-ACCACCACCACCACCACATGCGC AGACATTATCGC-3′	This work
4 IF_pURE_His_DsFbFP M49I_re	Binds at the 5′ end of *dsfbfp m49i* gene on pURE DsFbFP M49I plasmid, contains His_6-Tag. 5′-GGTGGTGGTGGTGGTGCATGGTATA TCTCCTTCTTAAAG-3′	This work

References

1. Endres, S.; Wingen, M.; Torra, J.; Ruiz-González, R.; Polen, T.; Bosio, G.; Bitzenhofer, N.L.; Hilgers, F.; Gensch, T.; Nonell, S.; *et al*. An optogenetic toolbox of LOV-based photosensitizers for light-driven killing of bacteria. *Sci. Rep.* **2018**, *8*, 15021.
2. Westberg, M.; Bregnhøj, M.; Etzerodt, M.; Ogilby, P.R. No Photon Wasted: An Efficient and Selective Singlet Oxygen Photosensitizing Protein. *J. Phys. Chem. B* **2017**, *121*, 9366–9371.
3. Takemoto, K.; Matsuda, T.; Sakai, N.; Fu, D.; Noda, M.; Uchiyama, S.; Kotera, I.; Arai, Y.; Horiuchi, M.; Fukui, K.; et al. SuperNova, a monomeric photosensitizing fluorescent protein for chromophore-assisted light inactivation. *Sci. Rep.* **2013**, *3*, 2629.
4. Sarkisyan, K.S.; Zlobovskaya, O.A.; Gorbachev, D.A.; Bozhanova, N.G.; Sharonov, G. V.; Staroverov, D.B.; Egorov, E.S.; Ryabova, A. V.; Solntsev, K.M.; Mishin, A.S.; *et al*. KillerOrange, a Genetically Encoded Photosensitizer Activated by Blue and Green Light. *PLoS One* **2015**, *10*, e0145287.
5. Abe, S.; Takayama, K.-I.; Kinoshita, S. Taxonomical Studies on Glutamic acid-producing Bacteria. *J. Gen. Appl. Microbiol.* **1967**, *13*, 279–301.
6. Hanahan, D. Studies on transformation of *Escherichia coli* with plasmids. *J. Mol. Biol.* **1983**, *166*, 557–580.
7. Studier, F.W.; Moffatt, B.A. Use of bacteriophage T7 RNA polymerase to direct selective high-level expression of cloned genes. *J. Mol. Biol.* **1986**, *189*, 113–130.
8. Bagdasarian, M.; Lurz, R.; Rückert, B.; Franklin, F.C.; Bagdasarian, M.M.; Frey, J.; Timmis, K.N. Specific-purpose plasmid cloning vectors. II. Broad host range, high copy number, RSF1010-derived vectors, and a host-vector system for gene cloning in *Pseudomonas*. *Gene* **1981**, *16*, 237–247.
9. Holloway, B.W.; Krishnapillai, V.; Morgan, a F. Chromosomal genetics of *Pseudomonas*. *Microbiol. Rev.* **1979**, *43*, 73–102.
10. Treangen, T.J.; Maybank, R.A.; Enke, S.; Friss, M.B.; Diviak, L.F.; Karaolis, D.K.R.; Koren, S.; Ondov, B.; Phillippy, A.M.; Bergman, N.H.; *et al*. Complete Genome Sequence of the Quality Control Strain *Staphylococcus aureus* subsp. *aureus* ATCC 25923. *Genome Announc.* **2014**, *2*, 25923.
11. MacLea, K.S.; Trachtenberg, A.M. Complete Genome Sequence of *Staphylococcus epidermidis* ATCC 12228 Chromosome and Plasmids, Generated by Long-Read Sequencing. *Genome Announc.* **2017**, *5*, 4–5.
12. Wingen, M.; Potzkei, J.; Endres, S.; Casini, G.; Rupprecht, C.; Fahlke, C.; Krauss, U.; Jaeger, K.-E.; Drepper, T.; Gensch, T. The photophysics of LOV-based fluorescent proteins – new tools for cell biology. *Photochem. Photobiol. Sci.* **2014**, *13*, 875–883.

V.7. SUPPORTING INFORMATION FOR CHAPTER II.3.1 – HETEROLOGOUS SYNTHESIS OF PLANT TERPENES IN *R. CAPSULATUS*

Supplementary Material

Engineered *Rhodobacter capsulatus* as a phototrophic platform organism for the synthesis of plant sesquiterpenoids

Katrin Troost[1], Anita Loeschcke[1,*], Fabienne Hilgers[1], Armagan Yakup Özgür[1], Tim Moritz Weber[1], Beatrix Santiago-Schübel[2], Vera Svensson[1], Jennifer Hage-Hülsmann[1], Samer S. Habash[3], Florian M. W. Grundler[3], A. Sylvia S. Schleker[3], Karl-Erich Jaeger[1,4], Thomas Drepper[1,*]

[1]Institute of Molecular Enzyme Technology, Heinrich Heine University Düsseldorf, Düsseldorf, Germany

[2]Central Institute for Engineering, Electronics and Analytics ZEA-3: Analytics, Forschungszentrum Jülich GmbH, Jülich, Germany

[3]INRES-Molecular Phytomedicine, Rheinische Friedrich-Wilhelms-University Bonn, Bonn, Germany

[4]Institute of Bio- and Geosciences IBG-1: Biotechnology, Forschungszentrum Jülich GmbH, Jülich, Germany

The online version may be found at:
https://www.frontiersin.org/articles/10.3389/fmicb.2019.01998/full#supplementary-material

Supplementary Material

1 Supplementary Figures.

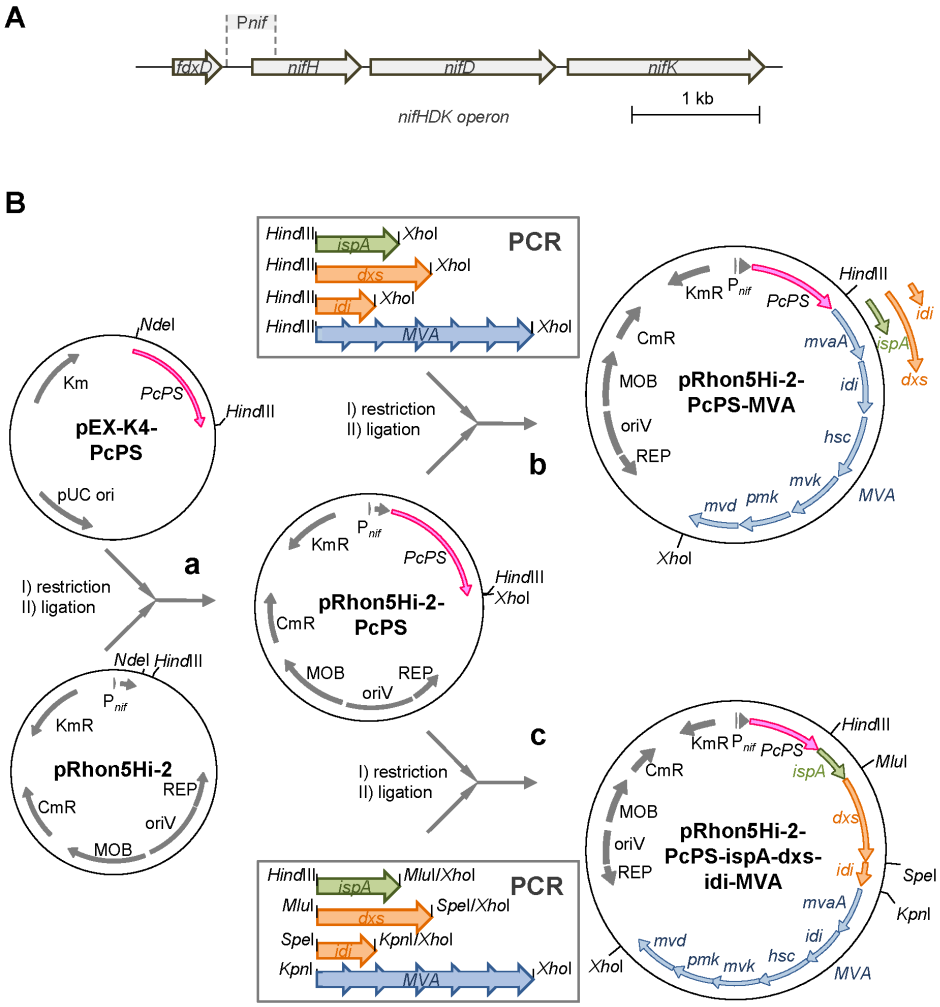

Supplementary Figure 1. Construction scheme of pRhon5Hi-2-based expression vectors for sesquiterpenoid production in *R. capsulatus*. (A) The *nifHDK* operon of *R. capsulatus* encodes the molybdenum dependent nitrogenase complex and comprises the structural genes *nifH* (dinitrogenase reductase), *nifD* and *nifK* (subunits of dinitrogenase). To exploit the phototrophic physiology of *R. capsulatus* for sesquiterpene production, we constructed the new expression plasmid pRhon5Hi-2 that carries the *nifHDK*-promoter region (P_{nif}): Dashed lines illustrate the genomic region which was

inserted as an *Nhe*I/*Xba*I fragment (NCBI Genbank Accession MG208548) into the respective sites of vector pRhotHi-2 (Katzke *et al*., 2010; doi:10.1016/j.pep.2009.08.008). As previously described, the broad-host range expression vector harbors two antibiotic resistance genes (chloramphenicol and kanamycin), an origin of replication (REP) and an origin of transfer (MOB). Target genes can be integrated into the multiple cloning site and are thereby placed under control of the P*nif* promoter. *fdxD*: Fe_2S_2 ferredoxin. **(B)** The scheme illustrates cloning steps for the example of patchoulol synthase PcPS from *Pogostemon cablin*. The synthase encoding gene was obtained as synthetic DNA fragment, flanked by recognition sequences for *Nde*I/*Hin*dIII, on a vector from Eurofins Genomics (pEX-K4-PcPS). The *PcPS* gene was isolated from the vector by use of *Nde*I/*Hin*dIII and ligated into likewise hydrolyzed expression vector pRhon5Hi-2 to yield pRhon5Hi-2-PcPS (**a**). Vectors pRhon5Hi-2-PcPS-ispA, pRhon5Hi-2-PcPS-dxs, pRhon5Hi-2-PcPS-idi and pRhon5Hi-2-PcPS-MVA were constructed by PCR-amplification of the respective genes with added recognition sequences for *Hin*dIII and *Xho*I in the primers, hydrolysis with these enzymes, and ligation of the fragments into likewise hydrolyzed pRhon5Hi-2-PcPS (**b**). The variant carrying the MVA gene cluster is depicted, while the other three alternative variants are conceptually indicated. For construction of vectors with incremental operons pRhon5Hi-2-PcPS-ispA, pRhon5Hi-2-PcPS-ispA-dxs, pRhon5Hi-2-PcPS-ispA-dxs-idi and pRhon5Hi-2-PcPS-ispA-dxs-idi-MVA, the genes were amplified with recognition sequences for different restriction endonucleases as depicted, added via the primers. Serial cloning of *ispA* as *Hin*dIII/*Xho*I fragment in the likewise hydrolyzed vector pRhon5Hi-2-PcPS, of *dxs* as *Mlu*I/*Xho*I fragment in the constructed pRhon5Hi-2-PcPS-ispA, of *idi* as *Spe*I/*Xho*I fragment in the constructed pRhon5Hi-2-PcPS-ispA-dxs and of the MVA gene cluster as *Kpn*I/*Xho*I fragment in the constructed vector pRhon5Hi-2-PcPS-ispA-dxs-idi yielded all constructs (**c**). Depicted is only the vector pRhon5Hi-2-PcPS-ispA-dxs-idi-MVA. KmR, *aphII* kanamycin resistence gene; CmR: chloramphenicol resistence gene; *ispA*, farnesyl pyrophosphate synthase gene from *R. capsulatus*; *dxs*, 1-deoxy-D-xylulose 5-phosphate synthase gene from *R. sphaeroides*; *idi*, isopentenyl pyrophosphate isomerase gene from *R. sphaeroides*; *MVA*, genes of the mevalonate biosynthesis pathway from *P. zeaxanthinifaciens*.

3

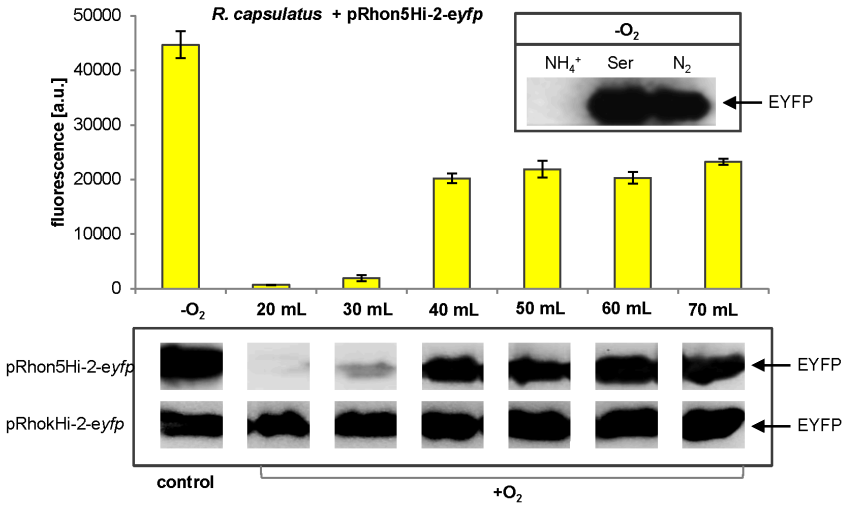

Supplementary Figure S2. Oxygen-dependent control of P_{nif}-mediated gene expression in *R. capsulatus*. Expression of the *eyfp* reporter gene was used as a measure to analyze the oxygen-sensitive P_{nif} promoter activity in *R. capsulatus* under different growth conditions. To this end, the reporter gene was cloned as an *Nde*I/*Hin*dIII fragment in the expression vector pRhon5Hi-2 under control of P_{nif}. Control cultures were cultivated under standard photoheterotrophic anaerobic conditions. **Upper panel:** *R. capsulatus* wildtype SB1003 carrying pRhon5Hi-2-*eyfp* was pre-cultivated in RCV medium with 0.1% ammonium, before test cultures were inoculated with an OD_{660nm} of 0.05 under aerobic conditions in 100 mL unbaffeled shake flasks ($+O_2$) with different filling volumes of RCV medium. Instead of ammonium, 0.1% serine was used as sole nitrogen source in order to exclusively control P_{nif} promotor activity via O_2 availability. After 48 h, cells equivalent to OD_{660nm} = 1 were harvested, re-suspended in SP-buffer (40 mM K_2HPO_4, 22 mM KH_2PO_4, 150 mM NaCl, 1 tablet of pH 8 Roche protease inhibitor per 250 mL; pH 7.2) and subjected to cell disruption using glass beads. Insoluble components of the extracts were pelleted and the supernatant containing soluble cellular proteins was incubated for 2 h before fluorescence analysis (excitation at 488 nm, emission 527 nm). Under phototrophic conditions ($-O_2$), cells exhibited the highest fluorescence signals, while samples from (micro)aerobic cultivation showed minor signals at 20 and 30 mL, and about 50% of the maximal values at 40 to 70 mL. Data represent mean values and respective standard deviations from three independent cultivations. **Lower panel:** To verify that fluorescence signals corresponded to protein expression, cell samples equivalent to OD_{660nm} = 1 were additionally subjected to SDS-PAGE and immunoblotting using antibodies *Anti-GFP* (Roche) and *Goat Anti-Mouse IgG (H+L)-HRP Conjugate* (BIO-RAD). A good correlation of protein bands with fluorescence signals was corroborated. To examine if results were indeed dependent on the promoter (and not otherwise physiology-related), protein expression was further evaluated in comparison to samples from likewise cultivated cells carrying an analogously cloned vector pRhokHi-2-*eyfp* (Katzke *et al*., 2010; doi:10.1016/j.pep.2009.08.008), where the reporter gene is under control of the constitutive P_{aphII} promoter. To further demonstrate the regulation of the P_{nif} promoter in dependence on the available nitrogen source, the EYFP-encoding reporter gene was expressed in *R. capsulatus* cells, where the respective test cultures were cultivated anaerobically

either with ammonium (NH_4^+; P_{nif} repressing conditions), or serine, or dinitrogen (Ser, N_2; P_{nif} derepressing conditions), as sole nitrogen sources in the medium (inset in upper panel).

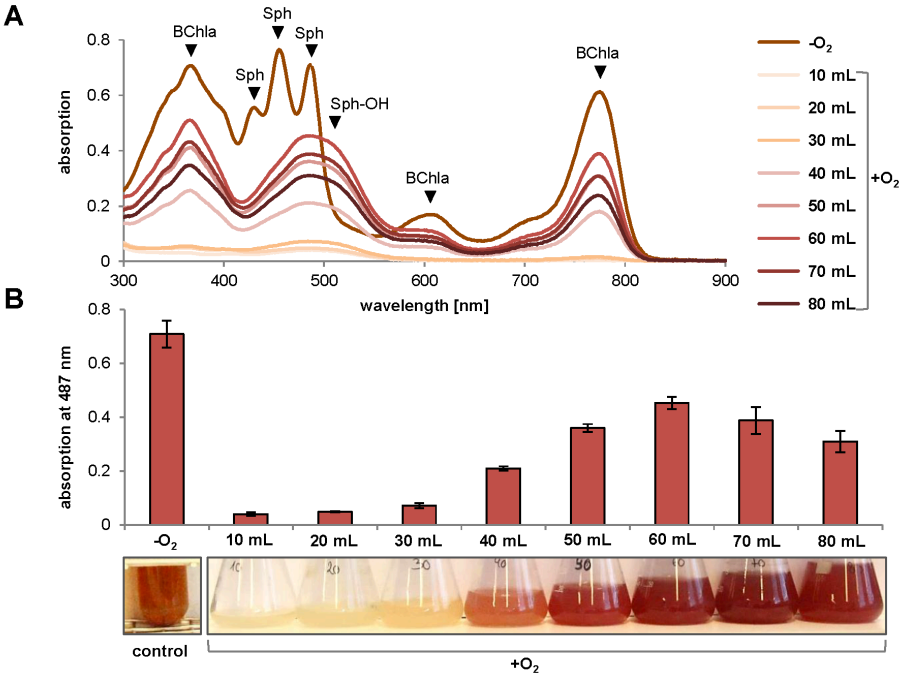

Supplementary Figure S3. Oxygen-dependent control of intrinsic terpene formation in *R. capsulatus*. Carotenoid formation was used as a measure to inspect the oxygen-sensitive intrinsic isoprenoid metabolism of *R. capsulatus* under different growth conditions. Control cultures were cultivated under standard photoheterotrophic anaerobic conditions. **(A)** *R. capsulatus* wildtype SB1003 was pre-cultivated in RCV medium with 0.1% ammonium, before test cultures were started with an OD_{660nm} of 0.05 under aerobic conditions in 100 mL unbaffeled shake flasks ($+O_2$) with different filling volumes of RCV medium supplemented with 0.1% serine. After 48 h, cells equivalent to OD_{660nm} = 1 were harvested and extracted with ethanol. Cell debris was pelleted and the supernatant containing cellular pigments was used for recording absorbance spectra from 300 to 900 nm in 1 nm intervals. Samples of phototrophically cultivated cells ($-O_2$) exhibited typical absorption maxima of bacteriochlorophyll *a* (BChla; 368, 600, and 770 nm), as well as characteristic maxima of the carotenoid spheroidene (Sph; 430, 456, and 487 nm). Under (micro)aerobic conditions, the same bacteriochlorophyll *a*-related absorption was detected (at lower levels), and the carotenoid-specific absorption of spheroidenone (Sph-OH; max. ~480 nm) was found, as expected. **(B)** Plotting the absorption at the wavelength of 478 nm in all samples showed that the pigment formation increased in $+O_2$ cultures with higher filling volumes up to 60 mL. Under this condition, about 65% of carotenoid-dependent absorption was reached compared to the photoheterotrophic anaerobic control. Data represent mean values and respective standard deviations from three independent cultivations.

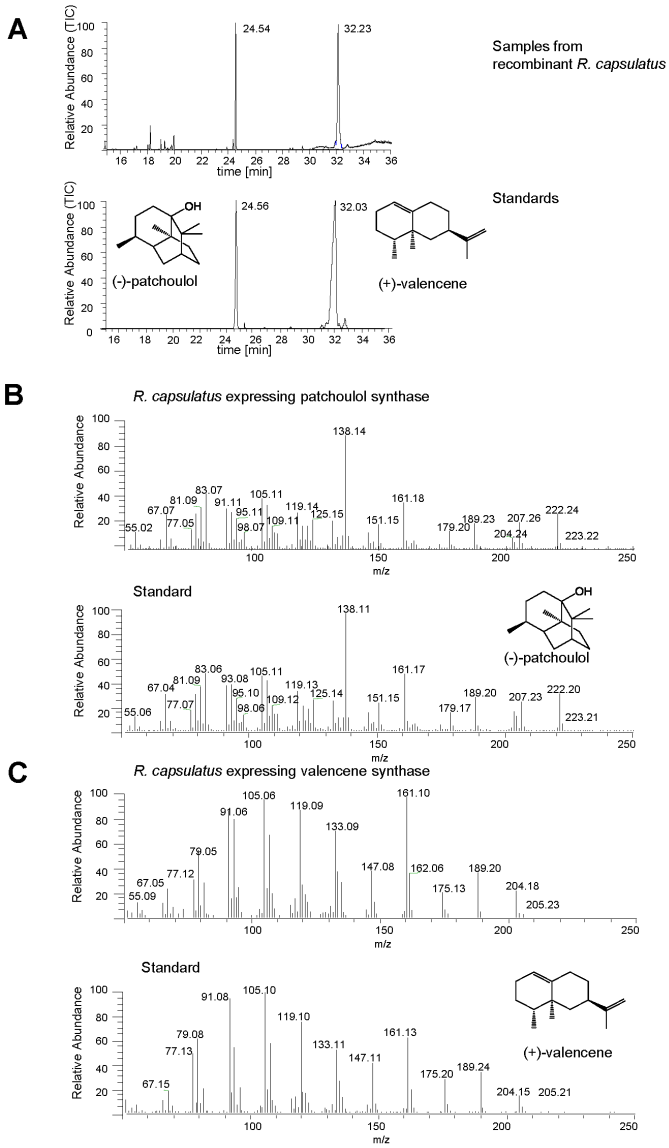

Supplementary Figure S4. GC-MS analysis of (-)-patchoulol and (+)-valencene from samples of recombinant *R. capsulatus*. (A) GC-MS chromatograms of (-)-patchoulol and (+)-valencene from recombinant *R. capsulatus* and the corresponding standards showing the same retention times. **(B)** EI-MS spectra of (-)-patchoulol from recombinant *R. capsulatus* and the corresponding standard at 24.5 min. **(C)** EI-MS spectra of (+)-valencene from recombinant *R. capsulatus* and the corresponding standard at 32.2 min. For GC-MS analysis, 1 µL of the samples was injected directly

into a Trace GC Ultra gas chromatograph coupled to ITQ 900 mass spectrometer (Thermo Scientific). Separation was achieved in a 30 m × 0.25 mm diameter capillary, with a 0.25 µm film of FS-5 supreme (CS Chromatographie Service). Split mode with a split ratio of 10 was used for the injector with the inlet temperature set to 250 °C. The oven was programmed to start at 100 °C and a 1 min hold, after which temperature increased to 300 °C at a rate of 5 °C/min. Helium was used as carrier gas and was adjusted to a flow rate of 1 mL/min. MS data were collected from 50 to 300 m/z during the temperature ramp.

7

2 Supplementary Methods.

Analysis of *n*-dodecane-mediated sesquiterpenoid extraction from phototrophically grown *R. capsulatus*.

Usually, sesquiterpenoids are extracted from microbial cell cultures via an *n*-dodecane layer (1/30 of the culture volume) which is added prior to cultivation and acts as an organic solvent phase (Rodriguez *et al*., 2014; doi:10.1038/nprot.2014.132). In the here presented work, we used the photosynthetic bacterium *R. capsulatus* as alternative sesquiterpenoid production host. After phototrophic cultivation, the sealed Hungate tubes were shaken horizontally at 30 °C and 130 rpm overnight in the dark in a Multitron Standard incubation shaker (Infors HT) to facilitate sesquiterpenoid extraction into the organic phase. Subsequently, 100 µL *n*-dodecane samples were subjected to gas chromatographic (GC) analysis as described in the Materials and Methods section.
To quantify the final product titers, calibration curves with authentic references (-)-patchoulol and (+)-valencene were used. However, the mere correlation of signals from *n*-dodecane extracted samples with the reference signals does not take into account extraction efficiencies of individual sesquiterpenoids when using *n*-dodecane as organic solvent. It can be assumed that, in dependence of their specific properties, different sesquiterpenoids only diffuse to a certain extent into the *n*-dodecane layer. In addition, terpenes that are produced in the cytoplasm of *R. capsulatus* can additionally be retained by the intracytoplasmic membrane system thereby further affecting the transfer into the organic phase. Therefore, we first determined the transfer efficiency of valencene and patchoulol from cultivation medium into *n*-dodecane in the presence of intact and disrupted *Rhodobacter* cells. For this purpose, the respective reference compounds were first mixed with 14 mL of phototrophically grown *R. capsulatus* SB1003 cells (cultivation parameters: anaerobic growth, 30 °C, approx. up to OD_{660nm} = 2.5) in appropriate amounts (giving signal intensities comparable to samples from *R. capsulatus* production cultures; patchoulol: 15 mg/L; valencene: 5.71 mg/L). For this purpose, 130.4 µL valencene, which is an oil, was added as a 10-fold dilution in diethyl ether, while the solid patchoulol had to be solved in diethyl ether prior to use gaining a 2 mg/mL stock solution of which 110.5 µL was added. After addition, the cultures were sealed and vortexed for 1 min. Subsequently, reference substances were extracted using *n*-dodecane as described above. The transfer efficiency was determined via GC analysis by comparing peak areas of the specific signals from appropriately diluted solutions to samples that had undergone extraction (**Supplementary Figure S5**).

Supplementary Figure S5: Transfer efficiency of the patchoulol (black bar) and valencene (grey bar) reference compounds from cultivation medium into the *n*-dodecane phase in the presence of intact *R. capsulatus* cells. For extraction, 15 mg/L patchoulol or 5.71 mg/L valencene were added to 14 mL cell cultures (OD_{660nm} = 2.5). For details, see text above. Data represent means and standard deviations of three independent measurements (n = 3).

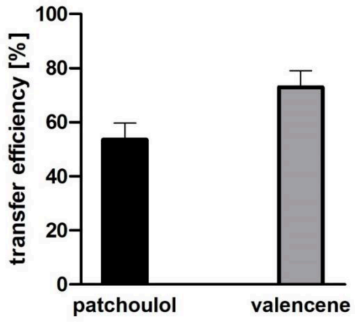

By using intact *R. capsulatus* cells, a transfer efficiency of 54% (patchoulol) and 73% (valencene) could be determined. Thus, it could be shown that there are some methodological losses, which have to be considered for product quantification.

To moreover analyze if putative interaction of intracellularly produced sesquiterpenoids with the *Rhodobacter* ICM can decrease product transfer, the experiment was repeated using disrupted cells. For this, equally cultivated *R. capsulatus* wildtype cells (OD_{660nm} = 2.5) were disrupted using a ball mill (3 x 10 min, 30 Hz, Mixer Mill MM 400, Retsch GmbH, Germany) and subsequently mixed with the same amount of reference compound as described previously. Extraction and quantification was performed as described for intact cell samples and signals were subsequently compared to those of the non-extracted reference compounds (**Supplementary Figure S6**).

Supplementary Figure S6: Transfer efficiency of the patchoulol (black bar) and valencene (grey bar) reference compounds from cultivation medium into the *n*-dodecane phase in the presence of disrupted *R. capsulatus* cells. For extraction, 15 mg/L patchoulol or 5.71 mg/L valencene were added to 14 mL cell lysate (OD_{660nm} = 2.5). For further details, see text above. Data represent means and standard deviations of three independent measurements (n = 3).

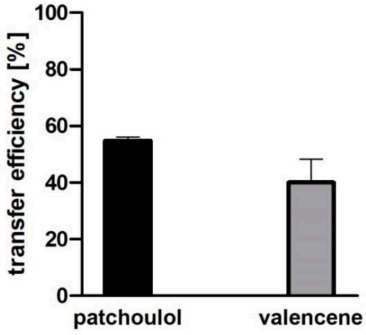

For patchoulol, no significant decrease of the transfer efficiency could be observed for lysed cells (55%) in comparison to the previous measurement using intact cells (54%). In contrast, a strong decrease of transfer efficiency could be detected for valencene (only 40%, in comparison to 73% when intact cells were used), suggesting that this more hydrophobic terpenoid (logP = 5.86 in

comparison to patchoulol with a logP of 4.19; values were calculated using the ALOGPS2.1 online tool described by Tetko *et al.* 2005; doi:10.1007/s10822-005-8694-y) can be retained more efficiently by the intracytoplasmic membrane system. Hence, for calculating the final production titers, individual transfer efficiencies for disrupted cell cultures (here termed c_t 'transfer efficiency coefficient'; patchoulol: 1.4521; valencene: 1.6) were taken into account.

Besides the above described negative effect of cellular components on the extraction efficiency, we further analyzed, if repeated *n*-dodecane-dependent sesquiterpenoid extraction should be considered for an optimal estimation of the overall production titers. Thus, an experiment with repeated sesquiterpenoid extractions from disrupted wildtype cultures that were mixed with reference compounds as described above was performed over four days (**Supplementary Figure S7**). For quantitative analysis of sesquiterpenoids, calibration curves with the authentic references of (-)-patchoulol and (+)-valencene ranging from 0.25 to 2 mg/500 µL *n*-dodecane, were used (slope: 380.37 and 475.37, respectively; see also depicted below in **Supplementary Figure S9**).

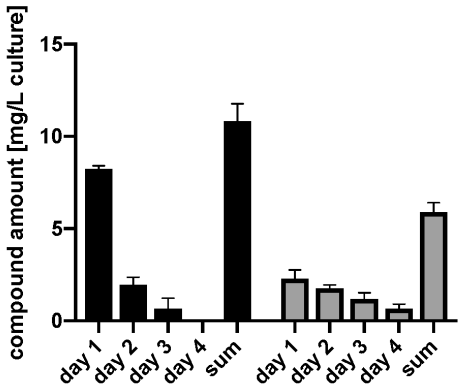

Supplementary Figure S7: Extraction efficiency of the patchoulol (black bars) and valencene (grey bars) reference compounds from cultivation medium in the presence of disrupted *R. capsulatus* cells by repeatedly using *n*-dodecane as organic solvent over four days. See text above for details. For repeated extraction, 15 mg/L patchoulol or 5.71 mg/L valencene were added to 14 mL cell lysate (OD_{660nm} = 2.5). Subsequently, 500 µL *n*-dodecane was used for 24 h over a time period of four days. Single extraction procedures were repeated four times and the sesquiterpenoid concentration of each fraction was analyzed via GC. Data represent means and standard deviations of three independent measurements (n = 3).

For patchoulol, the overall extraction efficiency was increased up to 32% by repeated extraction in comparison to the amount determined after the first extraction. For valencene, extraction efficiency increased even more (up to 157%). Therefore, we also took into account these factors by which the quantification on day 1 underestimates product titers (here termed c_{ex} 'coefficient for repeated extraction'; patchoulol: 1.3165; valencene: 2.5732 in order to calculate the final product titers.

Finally, we analyzed if the presence of an *n*-dodecane layer can positively or negatively affect sesquiterpene formation in *R. capsulatus* cells during cultivation. Therefore, an experiment with repeated sesquiterpene extraction out of production cultures that had been cultivated (5 days) with and without an *n*-dodecane layer before extraction was performed over four days (**Supplementary Figure S8**). For the analysis of sesquiterpene producing *R. capsulatus* cultures grown without a

solvent layer, equal amounts of *n*-dodecane were added after cultivation and prior to the extraction procedure.

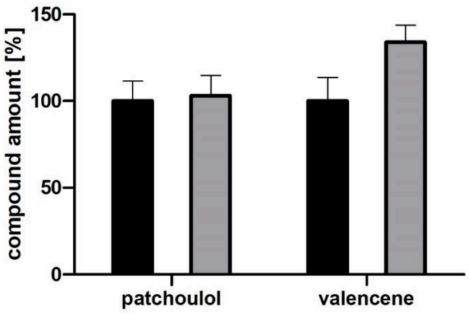

Supplementary Figure S8: Comparison of relative patchoulol and valencene formation in *R. capsulatus* production strains cultivated with (black bars) and without an *n*-dodecane layer (grey bars). Data was normalized to the amount of sesquiterpene extracted from cultures with *n*-dodecane. See text above for details. For *R. capsulatus* cultures containing the *n*-dodecane layer, 500 µL of the solvent was added before cultivation. In contrast, the same amount of solvent was added to cultures without *n*-dodecane after the cultivation. Compounds were extracted and analyzed as described above. Data represent means and standard deviations of three independent measurements (n = 3).

Almost no changes of sesquiterpene formation could be observed in the absence of the *n*-dodecane layer. Remarkably, production titers for valencene even increased slightly without using the organic solvent. Hence, the *n*-dodecane layer can alternatively be added after cultivation of the *Rhodobacter* production strains prior to the extraction procedure without any product losses.

In summary, product titers of *R. capsulatus* sesquiterpenoid production cultures were determined by analysis of *n*-dodecane extraction samples from disrupted cells. To this end, *R. capsulatus* strains were cultivated without the solvent, disrupted and then extracted one time with *n*-dodecane. Using the calibration curves obtained with reference compounds (**Supplementary Figure S9**) and taking into account above described results on losses of this procedure (**Supplementary Figure S6** and **S7**), we used the following equation for calculating the final patchoulol and valencene titers:

$$compound\ amount\left[\frac{mg}{L\ culture}\right] = \frac{pa}{s*v} * 1000\ mL * c_t * c_{ex}$$

$$pa = \ peak\ area\ [pA * s]$$

$$s = slope\ of\ calibration\ curve$$

$$v = culture\ volume\ [mL]$$

$$c_t = \ transfer\ efficiency\ coefficient$$

$$c_{ex} = \ coefficient\ for\ repeated\ extraction$$

Supplementary Figure S9: Quantification of extracted sesquiterpenes via calibration curves of patchoulol and valencene reference signals in GC-FID analyses. The signal intensities of the authentic reference compounds patchoulol **(A)** and valencene **(B)**, which were measured as peak areas [pA*s], were correlated to compound quantities [mg] in 500 µL-solutions with different concentrations. Mean values of detected signals of *n*-dodecane extraction samples from disrupted cells of the best *R. capsulatus* production strains (patchoulol: SB1003-MVA with pRhon5Hi-2-PcPS-ispA-dxs-idi, **(A)**; valencene: SB1003-MVA with pRhon5Hi-2-CnVS-ispA, **(B)**) are indicated (black lines from Y-axis to calibration line). Since extracts from *R. capsulatus* cultures were prepared with the same volume (500 µL) as were used for the dilutions of the reference compounds, the extracted amount of biosynthetic products [mg] could be deduced from the linear equations (indicated by dotted lines from calibration line to X-axis). These data were used for calculation of product levels in cultures, taking the used culture volume, and factors c_t and c_{ex} into account, as described above.

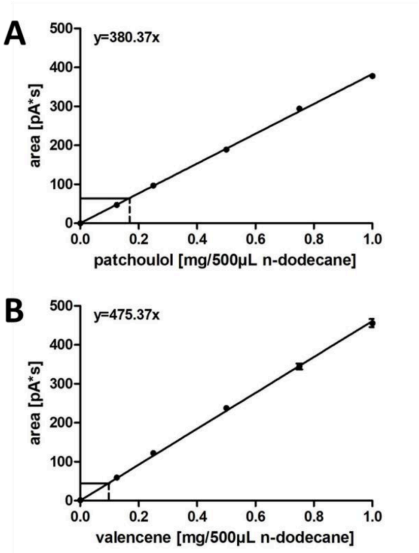

3 Supplementary Tables.

Supplementary Table S1. Codon optimized DNA sequences of plant genes for expression in *R. capsulatus*.

Patchoulol synthase PcPS from *Pogostemon cablin*

ATGGAACTGTATGCGCAGTCGGTGGGCGTGGGCGCCGCGTCGCGGCCGCTGGCGAACTTCCACCCCTGCGTGTGGGGCGATAAATTCATCGTCTATAACCCCCAGTCGTGCCAGGCCGGGGAG
CGGGAAGAGGCGGAAGAGCTGAAGGTCGAGCTCAAGCGGGAGCTGAAGGAAGCGAGCGATAACTATATGCGGCAGCTGAAAATGGTGGACGCCATCCAGCGCCTGGGGATCGATTATCTGT
TCGTCGAGGACGTCGATGAAGCCCTGAAGAACCTGTTCGAGATGTTCGATGCCTTCTGCAAAAACAACCATGACATGCATGCCACCGCCCTTTCCTTCCGGCTGCTGCGCCAGCATGGCTACCGC
GTCAGCTGCGAGGTCTTTGAGAAGTTCAAGGATGGGAAGGACGGCTTCAAGGTCCCGAACGAGGACGGCGCGGTCGCGGTGCTGGAATTTTTCGAAGCCACCCATCTGCGGGTCCACGGCGA
AGACGTGCTGGACAACGCCTTCGACTTCACGCGCAATTACCTTGAGTCCGTGTACGCCACCCTGAATGACCCGACCGCCAAACAGGTCCATAACGCGCTGAACGAGTTCTCGTTCCGCCGGGGC
CTGCCGCGCGTGGAAGCGCGCAAGTATATCTCCATCTATGAGCAATACGCGTCCCATCACAAGGGCCTTCTGAAGCTGGCGAAGCTGGACTTCAATCTGGTGCAAGCCCTGCATCGCCGCGAGC
TTTCCGAGGACTCGCGGTGGTGGAAAACCCTGCAAGTGCCCACGAAACTTTCGTTCGTGCGCGATCGGCTGGTCGAGTCGTACTTCTGGGCGTCCGGCTCGTACTTCGAGCCGAACTATAGCGT
CGCGCGCATGATCCTTGCGAAGGGGCTTGCCGTCCTGAGCCTGATGGATGATGTGTATGACGCGTATGGCACGTTTGAAGAGCTGCAGATGTTCACCGATGCGATCGAGCGCTGGGATGCGTC
CTGCCTGGACAAGCTGCCCGACTATATGAAAATCGTGTACAAAGCCCTTCTGGATGTCTTCGAAGAGGTCGACGAAGAACTGATCAAGCTGGGCGCGCCGTATCGCGCCTATTATGGGAAAGA
GGCGATGAAGTACGCGGCGCGGGCCTATATGGAGGAGGCCCAGTGGCGGGAGCAAAAACATAAGCCGACGACCAAAGAGTACATGAAGCTGGCCACCAAGACGTGCGGCTATATCACGCTG
ATCATCCTGTCGTGCCTGGGCGTGGAAGAAGGGATCGTCACGAAGGAAGCGTTCGATTGGGTGTTTTCCCGGCCGCCCTTTATCGAGGCGACCCTGATCATCGCCCGGCTGGTCAACGATATCA
CCGGCCATGAGTTCGAGAAGAAGCGCGAACATGTGCGCACCGCCGTGGAATGCTATATGGAGGAACATAAAGTCGGCAAGCAGGAGGTCGTGTCGGAGTTCTATAACCAGATGGAAAGCGCG
TGGAAGGATATCAATGAGGGCTTTCTGCGCCCCGTGGAATTCCCGATCCGCTGCTGTACCTGATCCTTAACTCCGTGCGGACCCTGGAGGTGATCTATAAGGAAGGCGACTCGTATACCCATGT
GGGCCCCGCGATGCAAAACATCATCAAGCAGCTGTACCTTCACCCGGTGCCCTATTGA

Valencene synthase CsVS from *Citrus sinensis*

ATGTCCTCGGGCGAGACCTTCCGGCCCACCGCGGATTTCCATCCCTCCCTGTGGCGGAATCATTTCCTTAAAGGCGCCTCCGATTTCAAGACCGTGGATCACACCGCCACGCAAGAGCGGCACGA
AGCGCTGAAAGAGGAGGTCCGGCGGATGATCACGGATGCCGAAGACAAGCCGGTCCAAAAGCTGCGCCTGATCGACGAGGTCCAGCGCCTGGGCGTGGCGTACCACTTCGAGAAGGAAATC
GGCGACGCGATCCAAAAACTGTGCCCCATCTACATCGACTCCAACCGCGCCGACCTGCATACGGTGTCCCTGCACTTCCGCCTGCTGCGGCAGCAGGGCATCAAGATCTCGTGCGATGTCTTCGA
AAAGTTCAAAGACGACGAGGGGCGGTTCAAATCGTCGCTTATCAACGATGTGCAAGGGATGCTGAGCCTGTACGAAGCGGCGTATATGGCCGTCCGCGGCGAGCACATCCTGGATGAGGCGA
TCGCCTTTACGACCACCCATCTTAAATCGCTGGTCGCGCAAGACCATGTGACGCCCAAGCTGGCCGAACAGATCAACCACGCGCTGTACCGCCCGCTGCGGAAGACCCTTCCCCGCCTGGAGGC
GCGCTATTTTATGTCGATGATCAACAGCACGTCGGACCACCTGTGCAACAAGACCCTGCTGAATTTCGCGAAACTGGATTTTAATATCCTTCTGGAGCTGCATAAGGAAGAGCTGAACGAGCTGA
CCAAATGGTGGAAGGACCTGGATTTCACCACGAAGCTGCCGTATGCCCGGGATCGCCTGGTGGAACTTTACTTCTGGGATCTGGGCACCTACTTCGAACCGCAGTACGCCTTCGGGCGCAAAAT
CATGACGCAGCTGAACTACATCCTGTCGATCATCGACGACACGTACGATGCGTATGGCACCCTGGAAGAACTGAGCCTGTTTACCGAGGCGGTGCAGCGCTGGAATATCGAGGCGGTGGACAT
GCTGCCGGAGTACATGAAGCTGATCTACCGGACCCTGCTGGATGCCTTCAATGAAATCGAGGAGGATATGGCCAAGCAGGGGCGCTCGCACTGCGTGCGCTACGCCAAGGAAGAAAACCAGA
AAGTGATCGGCGCGTATTCGGTCCAAGCCAAGTGGTTCAGCGAGGGCTATGTCCCGACCATCGAAGAATACATGCCGATCGCGCTGACCAGCTGCGCGTATACCTTTGTCATCACCAATTCCTTC
CTGGGCATGGGCGATTTCGCGACCAAGGAGGTGTTCGAGTGGATCTCGAACAACCCGAAGGTGGTGAAGGCCGCCTCGGTCATCTGCCGGCTTATGGACGATATGCAGGGCCACGAGTTTGA
GCAGAAGCGCGGCCACGTGGCGAGCGCGATCGAATGCTATACCAAGCAACATGGCGTGTCGAAGGAGGAAGCCATCAAGATGTTCGAGGAGGAAGTGGCCAATGCCTGGAAGGACATCAAC
GAAGAACTGATGATGAAGCCGACCGTGGTGGCGCGCCCGCTGCTGGGCACCATCCTGAACCTGGCGCGGGCGATCGACTTCATCTACAAGGAAGATGATGGCTACACCCATAGCTATCTGATC
AAAGACCAAATCGCGTCCGTGCTGGGCGATCATGTGCCGTTCTGA

Valencene synthase CnVS from *Callitropsis nootkatensis*

ATGGCGGAAATGTTCAACGGCAACAGCAGCAACGATGGCAGCAGCTGCATGCCGGTGAAAGATGCGCTGCGCCGCACCGGCAACCATCATCCGAACCTGTGGACCGATGATTTCATCCAGAGC
CTGAACAGCCCGTATAGCGATAGCAGCTATCATAAACATCGCGAAATCCTGATCGATGAAATCCGCGATATGTTCAGCAACGGCGAAGGCGATGAATTCGGCGTGCTGGAAAACATCTGGTTCG
TGGATGTGGTGCAGCGCCTGGGCATCGATCGCCATTTCCAGGAAGAAATCAAAACCGCGCTGGATTATATCTATAAATTCTGGAACCATGATAGCATCTTCGGCGATCTGAACATGGTGGCGCT
GGGCTTCCGCATCCTGCGCCTGAACCGCTATGTGGCGAGCAGCGATGTGTTCAAAAAATTCAAAGGCGAAGAAGGCCAGTTCAGCGGCTTCGAAAGCAGCGATCAGGATGCGAAACTGGAAAT
GATGCTGAACCTGTATAAAGCGAGCGAACTGGATTTCCCGGATGAAGATATCCTGAAAGAAGCGCGCGCGTTCGCGAGCATGTATCTGAAACATGTGATCAAAGAATATGGCGATATCCAGGA
AAGCAAAAACCCGCTGCTGATGGAAATCGAATATACCTTCAAATATCCGTGGCGCTGCCGCCTGCCGCGCCTGGAAGCGTGGAACTTCATCCATATCATGCGCCAGCAGGATTGCAACATCAGC
CTGGCGAACAACCTGTATAAAATCCCGAAAATCTATATGAAAAAAATCCTGGAACTGGCGATCCTGGATTTCAACATCCTGCAAAGCCAGCATCAGCATGAAATGAAACTGATCAGCACCTGGT
GGAAAAACAGCAGCGCGATCCAGCTGGATTTCTTCCGCCATCGCCATATCGAAAGCTATTTCTGGTGGGCGAGCCCGCTGTTCGAACCGGAATTCAGCACCTGCCGCATCAACTGCACCAAACT
GAGCACCAAAATGTTCCTGCTGGATGATATCTATGATACCTATGGCACCGTGGAAGAACTGAAACCGTTCACCACCACCCTGACCCGCTGGGATGTGAGCACCGTGGATAACCATCCGGATTATA
TGAAAATCGCGTTCAACTTCAGCTATGAAATCTATAAAGAAATCGCGAGCGAAGCGGAACGCAAACATGGCCCGTTCGTGTATAAATATCTGCAAAGCTGCTGGAAAAGCTATATCGAAGCGTA
TATGCAGGAAGCGGAATGGATCGCGAGCAACCATATTCCGGGCTTCGATGAATATCTGATGAACGGCGTGAAAAGCAGCGGCATGCGCATCCTGATGATCCATGCGCTGATCCTGATGGATAC
CCCGCTGAGCGATGAAATCCTGGAACAGCTGGATATCCCGAGCAGCAAAAGCCAGGCGCTGCTGAGCCTGATCACCCGCCTGGTGGATGATGTGAAAGATTTCGAAGATGAACAGGCGCATGG
CGAAATGGCGAGCAGCATCGAATGCTATATGAAAGATAACCATGGCAGCACCCGCGAAGATGCGCTGAACTATCTGAAAATCCGCATCGAAAGCTGCGTGCAGGAACTGAACAAAGAACTGCT
GGAACCGAGCAACATGCATGGCAGCTTCCGCAACCTGTATCTGAACGTGGGCATGCGCGTGATCTTCTTCATGCTGAACGATGGCGATCTGTTCACCCATAGCAACCGCAAAGAAATCCAGGAT
GCGATCACCAAATTCTTCGTGGAACCGATCATCCCGTAA

Supplementary Table S2. Oligonucleotides used in this study.

Name	Application	Nucleotide sequence (5'→3')
MVA gene cluster interposon vector		
Nif up for NdeI	PCR of *nifHDK* upstream region	ATATACATATGGGATCAGCCGGTTGATCAGC
Nif up rev KpnI-XbaI	PCR of *nifHDK* upstream region	ATATAGGTACCATCGATCCATCTAGACGGCCAGGTGCAGC ACGGTG
Nif dwn for XbaI-KpnI	PCR of *nifHDK* downstream region	TATATTCTAGATGGATCGATGGTACCCAAGGCGACGCTCT CGATGC
Nif dwn rev EcoRI-XhoI	PCR of *nifHDK* downstream region	TATATGAATTCCTCGAGGTCTGCGCGAGTTCCATGGG
MVA for XbaI	PCR of MVA gene cluster	ATATATCTAGAAATAATTTTGTTTAACTTTAAGAAGGAGATA TACATATGATGCAGAACGAAGAAGC
MVA rev KpnI NheI	PCR of MVA gene cluster	ATATAGGTACCATATAGCTAGCTCAACGCCCCTCGAACGG CG
GmR for NheI SpeI	PCR of aacC1 gene	ATATAGCTAGCACTAGTGACGCACACCGTGGAAACG
GmR rev KpnI	PCR of aacC1 gene	ATATAGGTACCGTTAGGTGGCGGTACTTGGG
mobTc for XhoI	PCR of oriT-Tet	TATATCTCGAGAAGCGAGCCAGCCGGTGG
mobTc rev XhoI	PCR of oriT-Tet	TATATCTCGAGCGAGGTGCCGCCGGCTTC
Construction of expression vector pRhonHi-2		
Pnif-fw	PCR of *nifHDK* promoter region	AATCGCTAGCTCCCGACAGAGGG
Pnif-rv	PCR of *nifHDK* promoter region	CGATTCTAGACGGCCAGGTGCA
Individual co-expression of precursor biosynthetic genes		
HindIII*ST_ispA fw	PCR of *ispA* gene	ATTAAGCTTTGAAAGAAGGAGATATAATGTTTTCCGAACGT TTG
XhoI_ispA rv	PCR of *ispA* gene	AATACTCGAGCTTGTCGCGTTCGATCACATAG
HindIII*ST_dxs fw	PCR of *dxs* gene	ATTAAGCTTTGAAAGAAGGAGATATAATGACCGACAGACC CTGC
XhoI_dxs rv	PCR of *dxs* gene	AATACTCGAGTCAGGCGCGGCGGGCGAG
HindIII*ST_idi fw	PCR of *idi* gene	ATTAAGCTTTGAAAGAAGGAGATATAATGACGGAAATGGT TCCCGC
XhoI_idi rv	PCR of *idi* gene	AATACTCGAGTTACTGCACGACGCGCAGC
HindIII*ST_MVA fw	PCR of MVA gene cluster	ATTAAGCTTTGAAAGAAGGAGATATAATGATGCAGAACGA AGAAGC
MVA rev XhoI	PCR of MVA gene cluster	ATATACTCGAGTCAACGCCCCTCGAACG
Co-expression of incremental operons of precursor biosynthetic genes		
HindIII*ST_ispA fw	PCR of *ispA* gene	ATTAAGCTTTGAAAGAAGGAGATATAATGTTTTCCGAACGT TTG
ispA rev XhoI MluI	PCR of *ispA* gene	ATATACTCGAGATATAACGCGTTCACTTGTCGCGTTCGAT CAC
dxs for MluI	PCR of *dxs* gene	ATATAACGCGTATAAGGAGATATACACATGACCGACAGAC CCTGC
dxs rev XhoI SpeI	PCR of *dxs* gene	ATATACTCGAGATATAACTAGTTCAGGCGCGGCGGGCGA G
idi for SpeI	PCR of *idi* gene	ATATAACTAGTGCCTTTGACAAGGAATTGAATGACGGAAAT GGTTCCCGC
idi rev XhoI KpnI	PCR of *idi* gene	ATATACTCGAGATATACCATGGTTACTGCACGACGCGCAG C
MVA for KpnI	PCR of MVA gene cluster	ATATACCATGGTCTAGAAATAATTTTGTTTAAC
MVA rev XhoI	PCR of MVA gene cluster	ATATACTCGAGTCAACGCCCCTCGAACG

Supplementary Table S3. Production of patchoulol and valencene in *R. capsulatus* SB1003.

Compound	Patchoulol	Valencene
***Rhodobacter capsulatus* strain**	**SB1003-MVA +PcPS-ispA-dxs-idi**	**SB1003-MVA +CnVS-ispA**
Titer at below defined time point (mg/L culture)	24±2 mg/L	18±3 mg/L
Time point of highest titer (h)	120 h	48 h
OD at the time point of highest titer (660 nm)	3.02±0.10	2.79±0.06
Cell mass at the time point of highest titer (gDCW/L culture)	1.81±0.06 gDCW/L	1.67±0.03 gDCW/L
Volumetric productivity (mg/L/h)[1]	0.20±0.02 mg/L/h	0.38±0.06 mg/L/h
Specific yield at above defined time point (mg/gDCW)	13.2±0.8 mg/gDCW	10.8±1.6 mg/gDCW
Specific productivity (mg/gDCW/h)[1]	0.11±0.01 mg/gDCW/h	0.22±0.03 mg/gDCW/h

[1]Productivities per hour were calculated based on product levels that were present at the time points when highest titers were reached, and are thus not necessarily maximal productivities.

V.8. SUPPORTING INFORMATION FOR CHAPTER II.3.2 – *R. CAPSULATUS* AS HETEROLOGOUS HOST FOR THE PRODUCTION OF BIOACTIVE TERPENES

Supplementary Materials

Heterologous Production of β-Caryophyllene and Evaluation of its Activity against Plant Pathogenic Fungi

Table of contents

The online version may be found at:
https://www.mdpi.com/2076-2607/9/1/168/s1

1. Supplementary methods

Bacterial strains and plasmids

All bacterial strains, plasmids and oligonucleotides used in this study are listed in Table S1.

Table S1. Bacterial strains and plasmids used in this study.

Strains, plasmids	Relevant features or description	References
	Strains	
***E. coli* DH5α**	*F⁻Φ80lacZΔM15 Δ(lacZYA-argF) U169 recA1 endA1 hsdR17 phoA supE44 thi-1 gyrA96 relA1 deoR*	[81]
***E. coli* S17-1**	Ec294::[RP4-2 (Tc^R::Mu)(Km^R::Tn7)] *recA, thi, pro, hsdR⁻ hsdM⁺* Tp^R Sm^R	[82]
***R. capsulatus* SB1003**	Wild-type, Rif^R	[83]
***R. capsulatus* SB1003-MVA**	SB1003-derivative, carrying the chromosomally intergrated MVA cluster from *Paracoccus zeaxanthinifaciens*, Rif^R, Gm^R	[39]
	Plasmids	
pRhon5Hi-2	pBBR1mcs (basic vector, rep mob Cm^R), pET22b (MCS, pelB), pBSL15 (aphII), P_{nif}	[39]
pRhon5Hi-2-QHS1	pRhon5Hi-2 with P_{nif} *QHS1*	This study
pRhon5Hi-2-QHS1-ispA	pRhon5Hi-2 with P_{nif} *QHS1-ispA*	This study

Analysis of *n*-dodecane-mediated β-caryophyllene extraction from phototrophically grown *R. capsulatus*.

The extraction of sesquiterpenoids from microbial cell cultures is mostly performed *via* a two-phase cultivation using an *n*-dodecane layer ($^1/_{30}$ of the culture volume) as solvent phase which is added prior to cultivation [88]. In analogy to our prior work [39], we performed the extraction and quantification of β-caryophyllene as described in the Materials and Methods section.

To quantify the final product titers, a calibration curve was generated using a pure β-caryophyllene reference from Sigma Aldrich. However, the correlation of signals from *n*-dodecane extracted samples with the reference signals does not take into account extraction efficiencies of β-caryophyllene when using *n*-dodecane as organic solvent. It can be assumed that, in dependence of its specific properties, it only diffuses to a certain extent into the *n*-dodecane layer. In addition, terpenes that are produced in the cytoplasm of *R. capsulatus* can additionally be retained by the intracytoplasmic membrane system thereby further affecting the transfer into the organic phase. Therefore, the transfer efficiency of β-caryophyllene from cultivation medium into *n*-dodecane in the presence of intact and disrupted *R. capsulatus* cells was first determined for both hungate and screw neck vials. For this purpose, the reference compound was first mixed with 14 mL or 4.5 mL of phototrophically grown *R. capsulatus* SB1003 cells (cultivation parameters: anaerobic growth, 30 °C, approx. up to OD_{660nm} = 2.5) in appropriate amounts (β-caryophyllene: 71.4 mg L^{-1} and 881.4 mg L^{-1}, respectively). For this purpose, 11.48 µL or 51.7 µL β-caryophyllene, which is an oil, was added as a 10-fold dilution in diethyl ether. After addition, the cultures were sealed and vortexed for 1 min. Subsequently, the reference substance was extracted using *n*-dodecane as described. The transfer efficiency was determined via GC analysis by comparing peak areas of the specific signals from appropriately diluted solutions to samples that had undergone extraction (**Figure S1**).

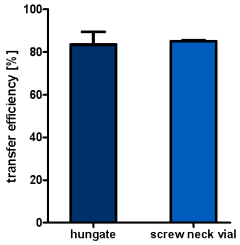

Figure S1. Transfer efficiency of the β-caryophyllene reference compound from cultivation medium into the *n*-dodecane phase in the presence of intact *R. capsulatus* cells in hungate (dark blue) and screw neck vials (light blue). For extraction, 71.4 mg L^{-1} or 881.4 mg L^{-1} β-caryophyllene were added to 14 mL or 4.5 mL cell culture (OD_{660nm} = 2.5), respectively. For details, see text above. Values are means of triplicate measurements. Error bars indicate the respective standard deviations.

By using intact *R. capsulatus* cells, a transfer efficiency of around 85% could be determined for both the hungate and the screw neck vial. Thus, it could be shown that there are some methodological losses, which have to be considered for product quantification. To moreover analyze if putative interaction of intracellularly produced sesquiterpenoids with the *Rhodobacter* ICM can further decrease product transfer, the experiment was repeated using disrupted cells. However, as the transfer efficiencies were nearly equal for the hungate and the screw neck vial, all further experiments were only performed for the hungate cultivation. First, equally cultivated *R. capsulatus* wildtype cells (OD_{660nm} = 2.5) were disrupted using a ball mill (3 × 10 min, 30 Hz, Mixer Mill MM 400, Retsch GmbH, Germany) and subsequently mixed with the same amount of reference compound as described previously. Extraction

and quantification were performed as described for intact cell samples and signals were subsequently compared to those of the non-extracted reference compounds (**Figure S2**).

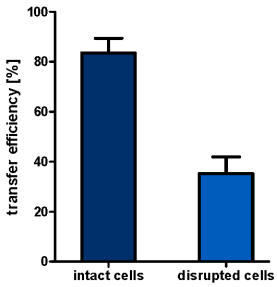

Figure S2. Transfer efficiency of the β-caryophyllene reference compound from cultivation medium into the *n*-dodecane phase in the presence of intact (dark blue) and disrupted (light blue) *R. capsulatus* cells. For extraction, 71.4 mg L^{-1} β-caryophyllene were added to 14 mL cell lysate (OD660nm = 2.5). For further details, see text above. Values are means of triplicate measurements. Error bars indicate the respective standard deviations.

It could be seen, that disrupted cells lead to a strong decrease of the extraction efficiency (35%) in comparison to the previous measurement using intact cells (85%), suggesting that this hydrophobic terpenoid (log*P* = 5.35; values were calculated using the ALOGPS2.1 online tool described by Tetko *et al.* 2005; doi:10.1007/s10822-005-8694-y) is strongly attached to the intracytoplasmic membrane system. Hence, for calculating the final production titers, the individual transfer efficiency for disrupted cell cultures (here termed c_t *or* 'transfer efficiency coefficient', factor: 1.6474) was taken into account.

Besides the above described negative effect of cellular components on the extraction efficiency, we further analyzed, if repeated *n*-dodecane-dependent sesquiterpenoid extraction should be considered for an optimal estimation of the overall production titers. Thus, an experiment with repeated sesquiterpenoid extractions from disrupted wildtype cultures that were mixed with the reference compound as described above was performed over four days (**Figure S3**). For quantitative analysis of β-caryophyllene, a calibration curve with the authentic reference compound ranging from 0.5 to 4 mg mL^{-1} *n*-dodecane, were used (slope: 382.16; see also depicted below in **Figure S5**).

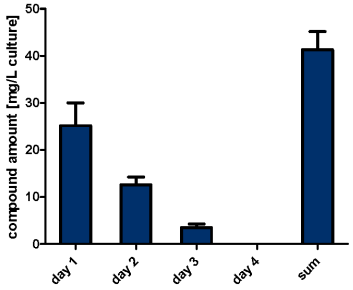

Figure S3. Extraction efficiency of the β-caryophyllene reference compound from cultivation medium in the presence of disrupted (dark blue) and intact (light blue) *R. capsulatus* cells by repeatedly using *n*-dodecane as organic solvent over four days. See text above for details. For repeated extraction, 71.4 mg L^{-1} β-caryophyllene were added to 14 mL cell lysate (OD660nm = 2.5). Subsequently, 500 µL *n*-dodecane was used for a 24 h extraction period over a total duration of four days. Single extraction procedures were repeated four times and the sesquiterpenoid concentration of each fraction was analyzed via GC. Values are means of triplicate measurements. Error bars indicate the respective standard deviations.

The overall extraction efficiency was increased by repeated extraction to 39% for disrupted cells in comparison to the amount determined after the first extraction. Therefore, it has also to be taken into account by which factor the quantification on day 1 underestimates product titers (here termed c_{ex} *or* 'coefficient for repeated extraction'; factor: 1.3897) in order to calculate the final product titers.

Finally, we analyzed if the presence of an *n*-dodecane layer positively or negatively affects the β-caryophyllene formation in *R. capsulatus* cells during cultivation. Therefore, an experiment with repeated sesquiterpene extraction out of production cultures that had been cultivated (3 days) with and without an *n*-dodecane layer before extraction was performed over four days (**Figure S4**). For the analysis of the β-caryophyllene producing *R. capsulatus* cultures grown without a solvent layer, equal amounts of *n*-dodecane were added after cultivation and prior to the extraction procedure.

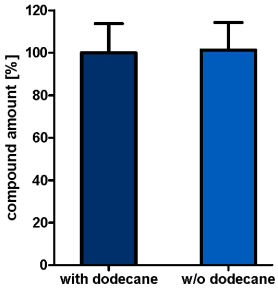

Figure S4. Comparison of relative β-caryophyllene formation in *R. capsulatus* production strains cultivated with (dark blue) and without an *n*-dodecane layer (light blue). Data was normalized to the amount of sesquiterpene extracted from cultures with *n*-dodecane. See text above for details. For *R. capsulatus* cultures containing the *n*-dodecane layer, 500 µL of the solvent was added before cultivation. In contrast, the same amount of solvent was added to cultures without *n*-dodecane after the cultivation. Compounds were extracted and analyzed as described above. Values are means of triplicate measurements. Error bars indicate the respective standard deviations.

Almost no changes of β-caryophyllene formation could be observed in the absence of the *n*-dodecane layer. Hence, the *n*-dodecane layer can alternatively be added after cultivation of the *Rhodobacter* production strains prior to the extraction procedure without any product losses. However, it must be considered that an addition of the organic solvent after cultivation is only reasonable for non-volatile terpenoids, as otherwise the product loss could be excessively high.

In summary, product titers of *R. capsulatus* β-caryophyllene production cultures were determined by analysis of *n*-dodecane extraction samples from disrupted cells. To this end, *R. capsulatus* strains were cultivated without the solvent, disrupted and then extracted one time with *n*-dodecane. Using the calibration curves obtained with reference compounds (**Figure S5**) and taking into account the cultivation parameters v and r_D, as well as the above described results on losses of this procedure (**Figure S2** and **S3**), equation 1 was used for calculating the final β-caryophyllene titers. The dodecane volume ratio r_D represents the ratio of the dodecane volume which was used for the calibration curve (1 mL) to the dodecane volume which was used as a solvent layer during extraction of the production cultures.

$$\text{compound amount}\left[\frac{mg}{L\ culture}\right] = \frac{pa}{s*v*r_D} * 1000\ mL * c_t * c_{ex} \quad (1)$$

$\boldsymbol{pa = \ peak\ area\ [pA * s]}$
$\boldsymbol{s = slope\ of\ calibration\ curve}$
$v = culture\ volume\ [mL]$
$r_D = dodecane\ volume\ ratio$
$c_t = \ transfer\ efficiency\ coefficient$
$c_{ex} = \ coefficient\ for\ repeated\ extraction$

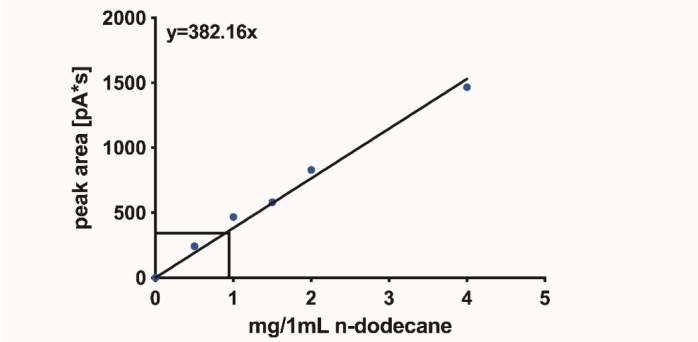

Figure S5. Quantification of extracted β-caryophyllene *via* a calibration curve of β-caryophyllene reference signals in GC-FID analyses. The signal intensities of the authentic reference compound, which were measured as peak areas [pA*s], were correlated to compound quantities [mg] in 1 mL solvent in different concentrations. Mean values of detected signals of *n*-dodecane extraction samples from disrupted cells of the best *R. capsulatus* production strain (SB1003-MVA with pRhon5Hi-2-QHS1-ispA) are indicated (black lines from Y-axis to calibration line). As the extracts from *R. capsulatus* cultures were prepared with *n*-dodecane volumes of 500 µL for hungate cultures and 150 µL for screw neck vials, the extracted amount of biosynthetic product [mg] could be calculated from the linear equations in consideration of the respective solvent amount. These data were used for calculation of product levels in cultures, taking the used culture volume, and factors r_D, c_t and c_{ex} into account, as described above.

2. Supplementary data

Emission range of used light sources and *in vivo* absorption spectrum of phototrophically grown *R. capsulatus* culture

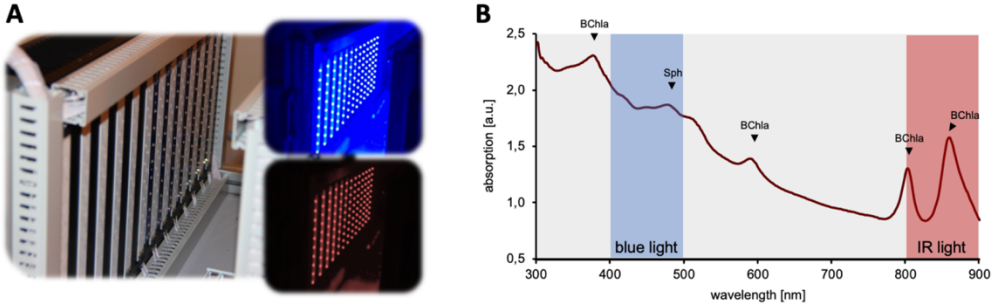

Figure S6. Emission range of different light sources and the absorption spectrum of phototrophically cultivated *R. capsulatus* cells. To illuminate phototrophic cell cultures of *R. capsulatus* more specifically, a custom-made LED panel (**A**) was developed by Vossloh-Schwabe Lighting Solutions GmbH & Co. KG (Kamp-Lintfort, Germany). Each LED array, carries 130 IR (λ_{max}= 850 nm, max. 5.6 mW cm^{-2}) and 130 blue-light LEDs (λ_{max} = 455 nm, 4.0 mW cm^{-2}) on a joint area of 1950 cm^2 (697 x 280 mm), suitable for specific excitation of photopigments spheroidene (indicated as Sph) and bacteriochlorophyll *a* (BChl *a*). In addition, the array offers 63 UV-A LEDs (λ_{max}= 364 nm, max. 7.6 mW cm^{-2}) in a separate area of 900 cm^2 (361 × 250 mm), suitable for applying photocaged inducers (see for example [128]) for future optogenetic approaches with *R. capsulatus*. Light intensity quantifications were conducted using a Thermal Power Sensor (S302C, Thorlabs Inc, USA). The emission maxima for the following light sources are shown in (**B**): (i) Blue LEDs emit blue light at around 450 nm (blue area) and (ii) IR LEDs emit light at around 850 nm (light red area). Additionally, a whole-cell absorption spectrum of a *R. capsulatus* culture is shown (dark red line). The three peaks at around 480 nm represent the carotenoid spheroidene, while the peaks at 380 nm, 600 nm, 800 nm and 860 nm represent BChl *a*.

Specifications of cultivation vessels for anaerobic growth of *R. capsulatus* cultures.

Table S2. Cultivation vessel specifications.

Cultivation vessel	Hungate	Screw neck vial
Vessel Specification	Hungate tube (Bellco Glass)	Screw neck vial N13, clear (MN)
Total volume	16.5 mL	4.5 mL
Working volume	15 mL	4.2 mL
Glass type	Type 1 class B borosilicate glass, transmission > 90% at 850 nm	Type 1 borosilicate glass (FIOLAX®), transmission > 90% at 850 nm
Wall thickness	1.05 mm	0.95 mm
Lateral surface area	~ 60.3 cm^2	~ 18.5 cm^2
Surface-to-volume-ratio	4.02 cm^{-1}	4.40 cm^{-1}

Productivities of β-caryophyllene in *R. capsulatus* SB1003 cultures.

Table S3. Production titers of β-caryophyllene in *R. capsulatus* SB1003 cultures.

Compound	**β-caryophyllene**	
Rhodobacter capsulatus strain	SB1003-MVA/pRhon5Hi-2-QHS1-ispA	
Cultivation vessel	Hungate tube	Screw neck vial
Titer at below defined time point (mg L^{-1} culture)	90.39 ± 18.61 mg L^{-1}	139.29 ± 31.35 mg L^{-1}
Time point of highest titer (h)	72 h	72 h
OD at the time point of highest titer (660 nm)	2.79 ± 0.09	2.50 ± 0.06
Cell mass at the time point of highest product titer (gDCW L^{-1} culture)	1.67 ± 0.05 gDCW L^{-1}	1.50 ± 0.04 gDCW L^{-1}
Volumetric productivity (mg L^{-1} h^{-1})[1]	1.26 ± 0.26 mg L^{-1} h^{-1}	1.93 ±0.44 mg L^{-1} h^{-1}
Specific yield at above defined time point (mg $gDCW^{-1}$)	54.01 ± 9.64 mg $gDCW^{-1}$	93.41 ±23.40 mg $gDCW^{-1}$
Specific productivity (mg $gDCW^{-1}$ h^{-1})[1]	0.75 ± 0.13 mg $gDCW^{-1}$ h^{-1}	1.30 ±0.32 mg $gDCW^{-1}$ h^{-1}

[1] Productivities per hour were calculated based on product levels that were present at the time points when highest titers were reached and are thus not necessarily maximal productivities.

Codon optimized DNA sequence of β-caryophyllene synthase QHS1 from *A. annua* for expression in *R. capsulatus*.

The shown sequence encompasses the QHS1 gene referring to the mRNA sequence published in GenBank: AF472361.1, encoding the QHS1 protein (UniProtKB - Q8SA63). At the 5'-end, the synthetic DNA fragment carries a short sequence derived from pET22b (between the *Xba*I and *Nde*I sites) harboring the corresponding ribosome binding site (RBS).

*Xba*I **RBS** Nde*I*/**Start**

TCTAGAAATAATTTTGTTTAACTTTAAG**AAGGAG**ATATACAT**ATG**AGCGTGAAAGAAGAAAAAGTGATC
CGCCCGATCGTGCATTTCCCGCCGAGCGTGTGGGCGGATCAGTTCCTGATCTTCGATGATAAACAGGCGG
AACAGGCGAACGTGGAACAGGTGGTGAACGAACTGCGCGAAGATGTGCGCAAAGATCTGGTGAGCAGC
CTGGATGTGCAGACCGAACATACCAACCTGCTGAAACTGATCGATGCGATCCAGCGCCTGGGCATCGCG
TATCATTTCGAAGAAGAAATCGAACAGGCGCTGCAGCATATCTATGATACCTATGGCGATGATTGGAAA
GGCCGCAGCCCGAGCCTGTGGTTCCGCATCCTGCGCCAGCAGGGCTTCTATGTGAGCTGCGATATCTTCA
AAAACTATAAAAAAGAAGATGGCAGCTTCAAAGAAAGCCTGACCAACGATGTGGAAGGCCTGCTGGAA
CTGTATGAAGCGACCTATCTGCGCGTGCAGGGCGAAGGCGTGCTGGATGATGCGCTGGTGTTCACCCGCA
CCTGCCTGGAAAAAATCGCGAAAGATCTGGTGCATACCAACCCGACCCTGAGCACCTATATCCAGGAAG
CGCTGAAACAGCCGCTGCATAAACGCCTGACCCGCCTGGAAGCGCTGCGCTATATCCCGATGTATGAAC
AGCAGGCGAGCCATAACGAAAGCCTGCTGAAACTGGCGAAACTGGGCTTCAACCTGCTGCAGAGCCTGC
ATCGCAAAGAACTGAGCGAAGTGAGCCGCTGGTGGAAAGGCCTGGATGTGCCGAACAACCTGCCGTAT
GCGCGCGATCGCATGGTGGAATGCTATTTCTGGGCGCTGGGCGTGTATTTCGAACCGAAATATAGCCAGG
CGCGCATCTTCCTGGCGAAAGTGATCAGCCTGGCGACCGTGCTGGATGATACCTATGATGCGTATGGCAC
CTATGAAGAACTGAAAATCTTCACCGAAGCGATCCAGCGCTGGAGCATCACCTGCATCGATATGCTGCC
GGAATATCTGAAACTGCTGTATCAGGGCGTGCTGGATATCTATATCGAAATGGAAGAAATCATGGGCAA
AGAAGGCAAAGCGCATCATCTGAGCTATGCGAAAGAAAGCATGAAAGAGTTCATCCGCAGCTATATGAT
GGAAGCGAAATGGGCGAACGAAGGCTATGTGCCGACCGCGGAAGAACACATGAGCGTGGCGTTCGTGA
GCAGCGGCTATAGCATGCTGGCGACCACCTGCTTCGTGGGCATGGGCGATATCGTGACCGATGAAGCGTT
CAAATGGGCGCTGACCAAACCGCCGATCATCAAAGCGAGCTGCGCGATCGCGCGCCTGATGGATGATAT
CCATAGCCAGAAAGAAGAAAAAGAACGCATCCATGTGGCGAGCAGCGTGGAAAGCTATATGAAACAGT
ATGATGTGACCGAAGAACATGTGCTGAAAGTGTTCAACAAAAAAATCGAAGATGCGTGGAAAGATATC
ACCCGCGAAAGCCTGGTGCGCAAAGATATCCCGATGCCGCTGATGATGCGCGTGATCAACCTGGCGCAG
GTGATGGATGTGCTGTATAAACATAAAGATGGCTTCACCAACGTGGGCGAAGAACTGAAAGATCATATC
AAAAGCCTGCTGGTGCATCCGATCCCGATC**TGA**AAGCTT

Stop *Hind*III

Bioactivities of β-caryophyllene and β-caryophyllene oxide against phytopathogenic fungi

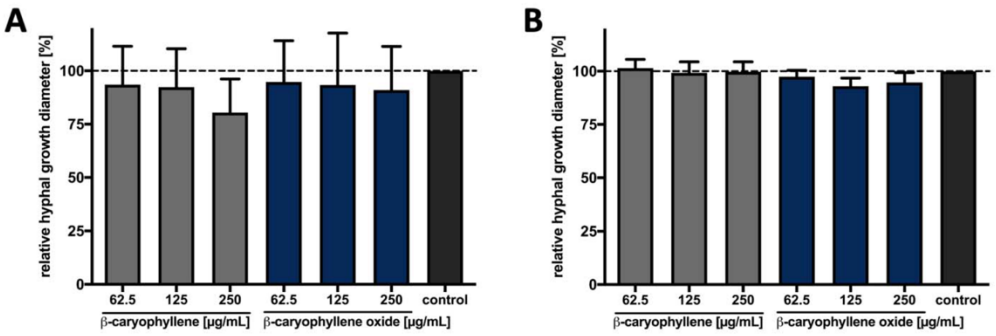

Figure S7. Effect of β-caryophyllene and β-caryophyllene oxide on the hyphal growth of plant pathogenic fungi. Effect of β-caryophyllene and β-caryophyllene oxide against A) *P. lingam* and B) *R. solani*. Final concentration of 62.5 µg mL^{-1}, 125 µg mL^{-1} and µg mL^{-1} of β-caryophyllene (gray bars) and β-caryophyllene oxide (blue bars) in PDA growth medium were used. Medium mixed with the solvents DMSO and Tween 20 (final concentrations, 0.5% and 1% *v/v*, respectively) was used as control. Fungal mycelium was placed in the center of each plate and incubated for 7 days at 24 °C. Subsequently, the diameter of the fungal colony was measured, and the relative growth percentage was calculated. Each bar represents the mean ± standard deviation of 3 independent biological replicates ($n = 9$). No significant differences based on ANOVA test ($P < 0.05$).

References

39. Troost, K.; Loeschcke, A.; Hilgers, F.; Özgür, A.Y.; Weber, T.M.; Santiago-Schübel, B.; Svensson, V.; Hage-Hülsmann, J.; Habash, S.S.; Grundler, F.M.W.; et al. Engineered *Rhodobacter capsulatus* as a Phototrophic Platform Organism for the Synthesis of Plant Sesquiterpenoids. *Front. Microbiol.* **2019**, *10*, 1998.
81. Hanahan, D. Studies on transformation of *Escherichia coli* with plasmids. *J. Mol. Biol.* **1983**, *166*, 557–580.
82. Simon, R.; Priefer, U.; Pühler, A. A Broad Host Range Mobilization System for *In Vivo* Genetic Engineering: Transposon Mutagenesis in Gram Negative Bacteria. *Bio/Technology* **1983**, *1*, 784–791.
83. Strnad, H.; Lapidus, A.; Paces, J.; Ulbrich, P.; Vlcek, C.; Paces, V.; Haselkorn, R. Complete genome sequence of the photosynthetic purple nonsulfur bacterium *Rhodobacter capsulatus* SB1003. *J. Bacteriol.* **2010**, *192*, 3545–3546.
88. Rodriguez, S.; Kirby, J.; Denby, C.M.; Keasling, J.D. Production and quantification of sesquiterpenes in *Saccharomyces cerevisiae*, including extraction, detection and quantification of terpene products and key related metabolites. *Nat. Protoc.* **2014**, *9*, 1980–1996.
128 Hogenkamp, F.; Hilgers, F.; Knapp, A.; Klaus, O.; Bier, C.; Binder, D.; Jaeger, K.-E.; Drepper, T.; Pietruszka, J. Effect of Photocaged Isopropyl β-D-1-Thiogalactopyranoside Solubility on Light-Responsiveness of LacI-controlled Expression Systems in Different Bacteria. *ChemBioChem* **2020**, doi:10.1002/cbic.202000377.

V.9. SUPPORTING INFORMATION FOR CHAPTER III.3.3 – HETEROLOGOUS PRODUCTION OF VERSATILE TERPENES IN *R. CAPSULATUS*

Production of C20, C30 and C40 terpenes in the engineered phototrophic bacterium *Rhodobacter capsulatus*

Jennifer Hage-Hülsmann[a,d,*], Oliver Klaus[a,*], Karl Linke[a], Katrin Troost[a], Lukas Gora[a], Fabienne Hilgers[a,e], Astrid Wirtz[b], Beatrix Santiago-Schübel[c], Anita Loeschcke[a,e,†], Karl-Erich Jaeger[a,b,d,e], Thomas Drepper[a,d,e,†]

[a] Institute of Molecular Enzyme Technology, Heinrich Heine University Düsseldorf, Forschungszentrum Jülich, Jülich, Germany

[b] Institute of Bio- and Geosciences IBG-1, Forschungszentrum Jülich, Jülich, Germany

[c] Central Division of Analytical Chemistry ZEA-3: Analytik/Biospec, Forschungszentrum Jülich, Jülich, Germany

[d] Cluster of Excellence on Plant Sciences (CEPLAS)

[e] Bioeconomy Science Center (BioSC), Forschungszentrum Jülich, Jülich, Germany

*equally contributed
† corresponding authors

Content **page**

Table S1. Sequences of terpene biosynthetic genes. Protein sequences that were used to design codon usage adapted genes are indicated with Genbank ID. Full length sequences were used unless truncations are specified. The start and stop codon of every gene is marked in bold.

Rc*CS from *Ricinus communis **[NCBI Protein XP_002513340.1]** **ATG**GCCCTGCCCTCGGCCGCGATGCAAAGCAACCCGGAAAAGCTGAACCTGTTCCACCGC CTGTCCAGCCTGCCCACCACCTCGCTTGAGTATGGGAATAATCGCTTCCCGTTCTTTTCG TCGTCGGCCAAATCGCACTTCAAGAAGCCGACGCAGGCGTGCCTTTCGTCGACGACCCAT CAGGAAGTGCGCCCGCTGGCCTATTTCCCCCCCACCGTCTGGGGGAACCGGTTCGCGTCG CTTACCTTCAACCCGTCGGAGTTCGAAAGCTATGACGAACGGGTGATCGTGCTGAAGAAG AAGGTCAAGGATATCCTGATCTCCTCGACCTCGGATTCGGTGGAGACCGTCATCCTGATC GACCTTCTTTGCCGCCTGGGCGTCAGCTATCATTTCGAAAACGATATCGAGGAACTGCTG TCGAAGATCTTCAACTCCCAGCCGGACCTTGTGGACGAAAAAGAGTGCGACCTGTACACC GCGGCGATCGTCTTCCGCGTCTTCCGCCAACATGGCTTCAAGATGTCGTCGGACGTCTTT TCGAAATTCAAAGATTCCGACGGCAAGTTCAAAGAGTCGCTGCGCGGCGACGCGAAGGGC ATGCTGTCCCTGTTTGAAGCGTCGCATCTGAGCGTGCATGGCGAAGACATCCTTGAGGAA GCGTTCGCCTTCACCAAAGATTATCTGCAATCGTCGGCGGTCGAGCTGTTCCCCAACCTG AAGCGGCATATCACCAACGCGCTGGAGCAGCCGTTCCATTCGGGGCGTCCCCCGCCTGGAG GCGCGCAAGTTCATCGACCTGTACGAAGCCGATATCGAGTGCCGGAACGAGACCCTGCTG GAATTTGCCAAGCTGGATTATAACCGCGTGCAGCTGCTGCATCAGCAAGAGCTGTGCCAG TTCTCGAAGTGGTGGAAGGATCTGAACCTGGCCTCGGACATCCCGTACGCCCGGGATCGG ATGGCGGAGATCTTCTTCTGGGCGGTCGCGATGTACTTCGAGCCCGATTATGCGCACACC CGCATGATCATCGCCAAAGTGGTGCTGCTTATCAGCCTGATCGACGACACCATCGACGCC TATGCCACCATGGAGGAAACCCATATCCTGGCGGAAGCGGTCGCCCGCTGGGACATGTCG TGCCTGGAGAAGCTGCCGGACTATATGAAAGTGATCTACAAGCTGCTGCTGAACACGTTC TCGGAGTTCGAGAAGGAGCTTACCGCCGAAGGGAAATCCTACTCGGTCAAGTATGGGCGG GAGGCGTTCCAGGAGCTGGTGCGCGGCTACTATCTTGAAGCCGTCTGGCGGGACGAGGGC AAGATCCCCTCGTTCGATGACTACCTGTACAACGGCTCGATGACCACCGGGCTGCCGCTG GTGAGCACCGCCTCGTTCATGGGCGTGCAGGAAATCACCGGCCTGAACGAATTCCAGTGG CTGGAAACCAATCCCAAACTGTCGTACGCCTCGGGGGCGTTCATCCGGCTGGTCAACGAC CTGACGTCCCATGTGACGGAACAGCAGCGCGGGCACGTGGCGTCCTGCATCGATTGCTAC ATGAACCAGCACGGGGTCTCGAAAGACGAAGCGGTGAAAATCCTGCAGAAGATGGCCACC GATTGCTGGAAGGAAATCAACGAGGAGTGCATGCGGCAGTCGCAGGTGTCGGTGGGGCAC CTGATGCGGATCGTGAACCTGGCGCGCCTTACCGACGTCTCGTACAAGTATGGCGATGGC TACACGGATTCGCAGCAGCTGAAACAGTTCGTGAAGGGCCTGTTCGTGGATCCGATCAGC ATCAAGCTT**TGA**
CrtY and CrtI from *Pantoea ananatis* **[NCBI Protein P21687.1 and P21685.1]** The intergenic sequence between *crtY* and *crtI* is the original sequence of the *crt* gene cluster from *Pantoea ananatis* (shown in blue) **ATG**CAACCCCATTACGACCTGATCCTTGTGGGGGCCGGGCTTGCGAACGGCCTTATCGCG CTGCGGCTCCAGCAGCAGCAACCCGATATGCGGATCCTCCTTATCGACGCCGCCCCGCAG GCGGGCGGGAACCATACGTGGTCCTTCCACCACGATGACCTCACGGAATCGCAACACCGG TGGATTGCCCCCCTGGTCGTCCATCATTGGCCGGATTATCAGGTCCGCTTCCCGACGCGC CGGCGCAAGCTGAACTCCGGCTATTTCTGCATCACGTCCCAGCGGTTTGCCGAAGTGCTC CAGCGGCAGTTCGGGCCGCACCTTTGGATGGACACGGCGGTCGCCGAGGTGAACGCGGAG TCCGTCCGGCTCAAGAAGGGCCAGGTGATCGGCGCGCGGGCCGTCATCGATGGGCGGGGC TACGCGGCGAACAGCGCCCTGTCGGTGGGCTTTCAGGCCTTCATCGGCCAGGAATGGCGG CTTTCGCACCCCCATGGGCTCTCCTCCCCCATCATCATGGATGCGACCGTCGATCAGCAA AACGGGTATCGCTTTGTGTACAGCCTGCCGCTTTCCCCGACCCGGCTCCTCATCGAGGAT ACCCACTACATCGATAACGCGACGCTCGACCCGGAATGCGCGCGGCAAAACATCTGCGAT TATGCGGCCCAACAGGGGTGGCAGCTTCAGACGCTGCTGCGGGAAGAGCAAGGCGCCCTC CCGATCACGCTGTCCGGGAACGCGGACGCCTTTTGGCAGCAGCGCCCCCTGGCCTGTTCG GGGCTCCGGGCGGGGCTGTTCCATCCCACCACCGGCTATTCCCTGCCCCTGGCGGTCGCC GTGGCGGATCGCCTCTCCGCGCTCGACGTCTTTACCTCCGCGAGCATCCATCATGCGATC ACCCATTTTGCGCGCGAGCGCTGGCAGCAGCAGGGCTTTTTCCGCATGCTGAACCGCATG CTGTTTCTCGCGGGGCCCGCGGACTCCCGCTGGCGGGTCATGCAGCGGTTTTACGGCCTC CCCGAGGACCTCATCGCGCGCTTTTATGCGGGGAAGCTCACCCTGACCGACCGGCTCCGG ATCCTGTCCGGCAAGCCGCCCGTGCCCGTCCTCGCGGCGCTCCAAGCGATCATGACCACG CATCGG**TGA**AGAGCGACTAC**ATG**AAGCCTACTACCGTCATCGGGGCCGGCTTTGGCGGCC TGGCCCTGGCCATCCGGTTGCAAGCCGCGGGTATCCCGGTGCTTCTGCTTGAGCAACGCG ACAAGCCGGGCGGCCGGGCCTACGTCTATGAAGACCAGGGGTTCACCTTCGATGCGGGCC CCACCGTCATCACCGACCCCAGCGCGATCGAGGAGCTGTTCGCCCTGGCCGGCAAGCAGC TTAAAGAGTACGTCGAGCTGCTGCCGGTCACCCCCTTCTATCGGCTGTGCTGGGAGTCGG GTAAAGTGTTCAACTACGACAATGACCAGACCCGGCTTGAGGCGCAGATCCAGCAGTTCA ACCCCCGCGACGTCGAGGGGTATCGGCAGTTCCTGGATTACTCCCGCGCCGTGTTCAAGG AGGGCTACCTCAAGCTCGGGACGGTGCCGTTCCTCAGCTTTCGTGATATGCTCCGGGCCG CCCCCCAGCTTGCCAAACTTCAGGCCTGGCGTTCCGTGTACAGCAAGGTCGCCAGCTACA TCGAAGATGAGCATCTGCGCCAGGCCTTTTCCTTTCACAGCCTGCTTGTCGGGGGGAACC CCTTCGCCACCAGCTCCATCTATACGCTGATTCACGCCCTGGAACGGGAATGGGGCGTGT GGTTTCCCCGCGGGGGCACCGGCGCCCTCGTCCAGGGTATGATTAAGCTGTTCCAGGACC TGGGGGGCGAGGTCGTGCTCAATGCGCGTGTCTCGCACATGGAGACCACGGGTAACAAGA

TCGAGGCGGTGCATCTCGAAGATGGGCGCCGTTTTCTGACCCAAGCGGTGGCGTCCAACG
CCGACGTGGTGCATACCTATCGCGACCTGCTCTCGCAGCACCCCGCGGCGGTGAAGCAGT
CCAATAAGCTGCAGACGAAGCGCATGAGCAATTCCCTGTTCGTGCTCTACTTCGGGCTCA
ACCATCATCATGACCAGCTTGCGCATCATACCGTGTGCTTTGGCCCGCGGTATCGCGAAC
TGATCGATGAGATCTTCAACCATGACGGCCTTGCCGAAGATTTTTCCCTCTACCTGCATG
CGCCGTGCGTGACCGACTCCAGCCTGGCGCCCGAGGGGTGCGGCAGCTATTACGTGCTCG
CGCCGGTGCCGCATCTTGGCACCGCGAACCTTGACTGGACCGTGGAAGGGCCTAAGTTGC
GCGACCGCATCTTCGCGTATCTTGAACAGCATTATATGCCCGGCCTTCGGAGCCAGCTGG
TCACCCATCGGATGTTCACCCCGTTCGACTTCCGCGACCAGCTTAACGCCTACCATGGCT
CCGCGTTCTCCGTGGAACCCGTGCTTACCCAGTCGGCGTGGTTCCGGCCGCATAATCGCG
ACAAGACCATCACGAACCTTTATCTGGTGGGCGCCGGCACCCACCCGGGCGCCGGCATCC
CCGGCGTGATCGGCTCCGCGAAGGCGACGGCCGGGCTTATGCTTGAAGACCTGATT**TGA**

SQS1 from *Arabidopsis thaliana*
[NCBI Protein NP_195190.1]

ATGGGCAGCCTGGGCACCATGCTGCGCTATCCGGATGATATCTATCCGCTGCTGAAAATG
AAACGCGCGATCGAAAAAGCGGAAAAACAGATCCCGCCGGAACCGCATTGGGGCTTCTGC
TATAGCATGCTGCATAAAGTGAGCCGCAGCTTCAGCCTGGTGATCCAGCAGCTGAACACC
GAACTGCGCAACGCGGTGTGCGTGTTCTATCTGGTGCTGCGCGCGCTGGATACCGTGGAA
GATGATACCAGCATCCCGACCGATGAAAAAGTGCCGATCCTGATCGCGTTCCATCGCCAT
ATCTATGATACCGATTGGCATTATAGCTGCGGCACCAAAGAATATAAAATCCTGATGGAT
CAGTTCCATCATGTGAGCGCGGCGTTCCTGGAACTGGAAAAAGGCTATCAGGAAGCGATC
GAAGAAATCACCCGCCGCATGGGCGCGGGCATGGCGAAATTCATCTGCCAGGAAGTGGAA
ACCGTGGATGATTATGATGAATATTGCCATTATGTGGCGGGCCTGGTGGGCCTGGGCCTG
AGCAAACTGTTCCTGGCGGCGGGCAGCGAAGTGCTGACCCCGGATTGGGAAGCGATCAGC
AACAGCATGGGCCTGTTCCTGCAGAAAACCAACATCATCCGCGATTATCTGGAAGATATC
AACGAAATCCCGAAAAGCCGCATGTTCTGGCCGCGCGAAATCTGGGGCAAATATGCGGAT
AAACTGGAAGATCTGAAATATGAAGAAAACACCAACAAAAGCGTGCAGTGCCTGAACGAA
ATGGTGACCAACGCGCTGATGCATATCGAAGATTGCCTGAAATATATGGTGAGCCTGCGC
GATCCGAGCATCTTCCGCTTCTGCGCGATCCCGCAGATCATGGCGATCGGCACCCTGGCG
CTGTGCTATAACAACGAACAGGTGTTCCGCGGCGTGGTGAAACTGCGCCGCGGCCTGACC
GCGAAAGTGATCGATCGCACCAAAACCATGGCGGATGTGTATGGCGCGTTCTATGATTTC
AGCTGCATGCTGAAAACCAAAGTGGATAAAAACGATCCGAACGCGAGCAAAACCCTGAAC
CGCCTGGAAGCGGTGCAGAAACTGTGCCGCGATGCGGGCGTGCTGCAGAACCGCAAAAGC
TATGTGAACGATAAAGGCCAGCCGAACAGCGTGTTCATCATCATGGTGGTGATCCTGCTG
GCGATCGTGTTCGCGTATCTGCGCGCGAAC**TAA**

Te*SQS from *Thermosynechococcus elongatus
[NCBI Protein NP_681887.1]

ATGCGCGTGGGCGTGAACCCGCCGATGATCCAGATGGTGCTGGAAAACCCGGTGAGCGTG
AAAGATGCGGAATGCTTCTGCCAGGAAATCCTGCCGCAGGTGAGCCGCACCTTCGCGCTG
AGCATCCGCTTCCTGCCGGGCAACCTGGGCCGCGCGGTGCTGGTGGCGTATCTGATCTGC
CGCATCGCGGATACCGTGGAAGATGATCCGGTGGCGAGCATCGCGGCGAAAACCGCGCTG
CTGGATCATCTGCTGCAGTGCTTCGATAGCCCGGCGCTGGCGAACAGCTATGGCGAAACC
GCGCGCGGCGTGCAGGGCGAACCGGCGCATGTGCAGCTGGTGAAACATACCGGCATCGTG
TTCACCCTGTATCGCAGCCTGCCGCGCACCAGCCAGCAGCATGTGCAGCGCTGGGTGAGC
GAAATGGTGCATGGCATGAAAAAATTCATCAACCTGTATCCGAACGGCATCCGCATCCAG
ACCCTGGCGGAATATAAAGAATATTGCTATTATGTGGCGGGCACCGTGGGCTATCTGCTG
ACCGATCTGTGGCATGAACATAGCCCGAGCATCGGCGCGGATGAATATCAGGTGCTGCTG
AAACGCTGCGCGGCGTTCGGCGAAGCGCTGCAGACCGTGAACATCCTGAAAGATATCGCG
TGGGATGCGGAACATGAAAACAGCATCTATATCCCGAACGAAAGCCTGATCCTGCAGGGC
AGCAGCCATCAGACCCTGCTGAGCGCGGAACATCTGCAGCAGAACCATGCGGCGATCAAA
GAACTGATCGCGCTGGCGTGGCATGATCTGGATGAAGCGCAGGCGTATCTGCTGAGCGTG
CCGAAAGCGGCGATCCCGATCCGCCTGTTCTGCGTGCTGCCGCTGCTGTTCGCGTATGCG
ACCCTGCGCGAACTGACCCATAGCACCGCGATGCTGCAGCCGGGCGGCGGCGTGAAAATC
AGCCGCGCGGAAGTGAAAAGCCTGATGGTGATGGGCCCGCTGAGCATCCTGAGCAACCAT
GGCCTGCGCTGGCTGATCGGCCAGGTGCGCCAGAAACCGTTCATCCTGGGCGGCCTG**TAA**

Bb*SQS from *Botryococcus braunii
[NCBI Protein AAF20201.1 with 26 amino acid truncation at the C-terminus]

ATGGGCATGCTGCGCTGGGGCGTGGAAAGCCTGCAGAACCCGGATGAACTGATCCCGGTG
CTGCGCATGATCTATGCGGATAAATTCGGCAAAATCAAACCGAAAGATGAAGATCGCGGC
TTCTGCTATGAAATCCTGAACCTGGTGAGCCGCAGCTTCGCGATCGTGATCCAGCAGCTG
CCGGCGCAGCTGCGCGATCCGGTGTGCATCTTCTATCTGGTGCTGCGCGCGCTGGATACC
GTGGAAGATGATATGAAAATCGCGGCGACCACCAAAATCCCGCTGCTGCGCGATTTCTAT
GAAAAAATCAGCGATCGCAGCTTCCGCATGACCGCGGGCGATCAGAAAGATTATATCCGC
CTGCTGGATCAGTATCCGAAAGTGACCAGCGTGTTCCTGAAACTGACCCCGCGCGAACAG
GAAATCATCGCGGATATCACCAAACGCATGGGCAACGGCATGGCGGATTTCGTGCATAAA
GGCGTGCCGGATACCGTGGGCGATTATGATCTGTATTGCCATTATGTGGCGGGCGTGGTG
GGCCTGGGCCTGAGCCAGCTGTTCGTGGCGAGCGGCCTGCAGAGCCCGAGCCTGACCCGC
AGCGAAGATCTGAGCAACCATATGGGCCTGTTCCTGCAGAAAACCAACATCATCCGCGAT
TATTTCGAAGATATCAACGAACTGCCGGCGCGCCGCGCATGTTCTGGCCGCGCGAAATCTGG
GGCAAATATGCGAACAACCTGGCGGAATTCAAAGATCCGGCGAACAAAGCGGCGGCGATG
TGCTGCCTGAACGAAATGGTGACCGATGCGCTGCGCCATGCGGTGTATTGCCTGCAGTAT
ATGAGCATGATCGAAGATCCGCAGATCTTCAACTTCTGCGCGATCCCGCAGACCATGGCG
TTCGGCACCCTGAGCCTGTGCTATAACAACTATACCATCTTCACCGGCCCGAAAGCGGCG

GTGAAACTGCGCCGCGGCACCACCGCGAAACTGATGTATACCAGCAACAACATGTTCGCG
ATGTATCGCCATTTCCTGAACTTCGCGGAAAAACTGGAAGTGCGCTGCAACACCGAAACC
AGCGAAGATCCGAGCGTGACCACCACCCTGGAACATCTGCATAAAATCAAAGCGGCGTGC
AAAGCGGGCCTGGCGCGCACCAAAGATGATACCTTCGATGAACTGCGCAGCCGCCTGCTG
GCGCTGACCGGCGGCAGCTTCTATCTGGCGTGGACCTATAACTTCCTGGATCTGCGCGGC
CCGGGCGATCTGCCGACCTTCCTGAGCGTGACCCAGCATTGGTGG**TGA**

Hs*SQS from *Homo sapiens
[NCBI Protein AAH09251.1 with 30 amino acid truncation at the N-terminus and 47 amino acid truncation at the C-terminus]

ATGGATCAGGATAGCCTGAGCAGCAGCCTGAAAACCTGCTATCGCTATCTGAACCAGACC
AGCCGCAGCTTCGCGGCGGTGATCCAGGCGCTGGATGGCGAAATGCGCAACGCGGTGTGC
ATCTTCTATCTGGTGCTGCGCGCGCTGGATACCCTGGAAGATGATATGACCATCAGCGTG
GAAAAAAAAGTGCCGCTGCTGCATAACTTCCATAGCTTCCTGTATCAGCCGGATTGGCGC
TTCATGGAAAGCAAAGAAAAAGATCGCCAGGTGCTGGAAGATTTCCCGACCATCAGCCTG
GAATTCCGCAACCTGGCGGAAAAATATCAGACCGTGATCGCGGATATCTGCCGCCGCATG
GGCATCGGCATGGCGGAATTCCTGGATAAACATGTGACCAGCGAACAGGAATGGGATAAA
TATTGCCATTATGTGGCGGGCCTGGTGGGCATCGGCCTGAGCCGCCTGTTCAGCGCGAGC
GAATTCGAAGATCCGCTGGTGGGCGAAGATACCGAACGCGCGAACAGCATGGGCCTGTTC
CTGCAGAAAACCAACATCATCCGCGATTATCTGGAAGATCAGCAGGGCGGCCGCGAATTC
TGGCCGCAGGAAGTGTGGAGCCGCTATGTGAAAAAACTGGGCGATTTCGCGAAACCGGAA
AACATCGATCTGGCGGTGCAGTGCCTGAACGAACTGATCACCAACGCGCTGCATCATATC
CCGGATGTGATCACCTATCTGAGCCGCCTGCGCAACCAGAGCGTGTTCAACTTCTGCGCG
ATCCCGCAGGTGATGGCGATCGCGACCCTGGCGGCGTGCTATAACAACCAGCAGGTGTTC
AAAGGCGCGGTGAAAATCCGCAAAGGCCAGGCGGTGACCCTGATGATGGATGCGACCAAC
ATGCCGGCGGTGAAAGCGATCATCTATCAGTATATGGAAGAAATCTATCATCGCATCCCG
GATAGCGATCCGAGCAGCAGCAAAACCCGCCAGATCATCAGCACCATCCGCACCCAGAAC
TGA

Mc*SQS from *Methylococcus capsulatus
[NCBI Protein CAA71097.1]

ATGAGCGGCACCCCGCCGAGCCAGCCGGCGCGCCATGAACATCTGAGCGATGATGAATTC
CAGGCGCATTTCCTGGATGGCGTGAGCCGCACCTTCGCGCTGACCATCCCGCGCCTGCCG
GAAGGCCTGGCGCGCCCGGTGAGCAACGGCTATCTGCTGTGCCGCATCGTGGATACCATC
GAAGATGAAGTGGCGCTGACCAGCACCCAGAAACGCCGCTATTGCGAACATTTCGCGCGC
GTGGTGGCGGGCACCGCGCCGGCGGCGCCGCTGGCGGATGAACTGTTCCCGCTGCTGAGC
GATCAGACCCTGGCGGCGGAACGCGAACTGATCGCGGCGATCCCGCGCGTGATCAGCATC
ACCCATGGCTTCGCGGCGCCGCAGCAGGAAGCGCTGGCGGAATGCGTGGCGACCATGAGC
CGCGGCATGGCGGAATTCCAGGATAAAGATCTGCGCCATGGCCTGGAAGATCTGCGCCAG
ATGGGCGATTATTGCTATTATGTGGCGGGCGTGGTGGGCGAAATGCTGACCCGCCTGTTC
TGCCATTATAGCCCGGAAATCGCGGCGCATCGCAGCCGCCTGATGGAACTGGCGTGCCCG
TTCGGCCAGGGCCTGCAGATGACCAACATCCTGAAAGATCTGTGGGATGATCATGCGCGC
GGCGTGTGCTGGCTGCCGCAGGAAGTGTTCACCGAATGCGGCTTCAGCCTGACCGAACTG
CGCCCGCATCATGCGAACCCGGATTTCGTGCGCGGCTTCGAACGCCTGATCGGCGTGGCG
CATGCGCATCTGCGCAACGCGCTGGAATATACCCTGCTGATCCCGCGCCATGAAACCGGC
ATCCGCGAATTCTGCCTGTGGGCGCTGGGCATGGCGGTGCTGACCCTGCGCAAAATCCAT
CGCCATCCGTATTTCAGCGATAGCGCGCAGGTGAAAATCACCCGCCAGGCGGTGAAAGCG
ACCATCGTGACCAGCCGCCTGACCCGCGGCAGCGATACCCTGCTGAAAGCGACCTTCCGC
CTGGCGGGCCTGGGCCTGCCGGCGGCGGTGCCGGCGGCGGTGCTGCAGCCGCGCCCGATC
GATATC**TGA**

Table S2. Oligonucleotides, plasmids and strains used in this study. Endonuclease restriction sites are underlined.

Oligonucleotides		
Name	**Application**	**Nucleotide sequence (5'→3')**
Cloning of *crtY-crtI* into pRhon5Hi-2 for β-carotene biosynthesis		
NdeI_crtI/Y Fw	PCR of *crtY-crtI*	ATATCATATGCAACCCCATTACGACCTGA
HindIII_crtI/Y rv	PCR of *crtY-crtI*	GATCAAGCTTTCAAATCAGGTCTTCAAGCATAAGC
Cloning of *SQS1* into pRhon5Hi-2 for squalene biosynthesis		
At-SQS-fw	PCR of *SQS1* (*A. thaliana*)	GCACCTGGCCGTCTAGAAATAATTTTGTTTAAC
At-SQS-rev	PCR of *SQS1* (*A. thaliana*)	TTTAAAAGCTTTACGTATCTTAAGTTAGTTCGCGCGCAG
Cloning of *ispA* into pRhon5Hi-2-RcCS and pRhon5Hi-2-crtY-crtI		
HindIII_ispA R.c. fw	PCR of *ispA* (*R. capsulatus*)	ATTAAGCTTTGAAAGAAGGAGATATAATGTTTTCCGAACGTTTG
XhoI_ispA R.c. rv	PCR of *ispA* (*R. capsulatus*)	ATATACTCGAGATATAACGCGTTCACTTGTCGCGTTCGATCAC
Plasmids		
Name		**Characteristics / Reference**
Plasmids used for cloning		
pRhon5Hi-2		pBBR22b backbone (pBBR1 ori & mob, pET22b MCS), Km^R,(pBSL15 *aphII*), P_{nif} (from *R. capsulatus*) (Troost et al., 2019)
pRhon5Hi-2-CnVS-ispA		pRhon5Hi-2, CnVS (*C. nootkatensis*), *ispA* (*R. capsulatus*) (Troost et al., 2019)
pRhon5Hi-2-CnVS-ispA-dxs-idi		pRhon5Hi-2-CnVS-ispA, *dxs*, *idi* (*R. sphaeroides*) (Troost et al., 2019)
Plasmids for casbene biosynthesis		
pRhon5Hi-2-RcCS		pRhon5Hi-2, RcCS (*R. communis*)
pRhon5Hi-2-RcCS -ispA		pRhon5Hi-2-RcCS, *ispA* (*R. capsulatus*)
pRhon5Hi-2-RcCS -ispA-dxs-idi		pRhon5Hi-2-RcCS-ispA, *dxs*, *idi* (*R. sphaeroides*)
Plasmids for β-carotene biosynthesis		
pRhon5Hi-2-crtY-crtI		pRhon5Hi-2, crtY-crtI (*P. ananatis*)
pRhon5Hi-2-crtY-crtI-ispA		pRhon5Hi-2-crtY-crtI, *ispA* (*R. capsulatus*)
pRhon5Hi-2-crtY-crtI-ispA-dxs-idi		pRhon5Hi-2-crtY-crtI-ispA, *dxs*, *idi* (*R. sphaeroides*)
Plasmids for squalene biosynthesis		
pRhon5Hi-2-SQS1		pRhon5Hi-2 carrying SQS1 (*A. thaliana*) (Loeschcke et al., 2017)
pRhon5Hi-2-SQS1-ispA		pRhon5Hi-2-SQS1, *ispA* (*R. capsulatus*)
pRhon5Hi-2-SQS1-ispA-dxs-idi		pRhon5Hi-2-SQS1-ispA, *dxs*, *idi* (*R. sphaeroides*)
Strains		
Name		**Characteristics or application / Reference**
Escherichia coli		
E. coli DH5α		Used for plasmid amplification / cloning (Hanahan, 1983)
E. coli S17-1		Used for conjugational plasmid transfer (Simon et al., 1983)
Rhodobacter capsulatus		
R. capsulatus SB1003		Wildtype strain, Rif^R (Strnad et al., 2010)
R. capsulatus SB1003-MVA		Strain SB1003 carrying the MVA gene cluster from *P. zeaxanthinifaciens* under control of P_{nif}, Rif^R/Gm^R (Troost et al., 2019)

Table S3. Specific β-carotene and squalene yields in *R. capsulatus*. Specific yields of β-carotene (upon expression of CrtY and CrtI of *P. ananatis*), and squalene (upon expression of SQS of different organisms: *At*, *A. thaliana*; *Bb*, *B. braunii*; *Te*, *T. elongatus*; *Hs*, *H. sapiens*; *Mc*, *M. capsulatus*) were calculated based on reached cell densities at the time point of cell harvesting for product analysis and a correlation of OD_{660nm} = 1 with 0.6 mgDCW (dry cell weight). Coloration indicates higher (darker) and lower (lighter) values for β-carotene (orange) and squalene (green). Co-expression of isoprenoid precursor biosynthetic genes *ispA* (of *R. capsulatus*), *dxs* and *idi* (of *R. sphaeroides*) and the MVA gene cluster (of *P. zeaxanthinifaciens*) is specified.

***Rhodobacter capsulatus* strain**	**specific yield [mg/gDCW]**					
	β-carotene (*crtY-crtI*)	**squalene** (SQS)				
		At	*Bb*	*Te*	*Hs*	*Mc*
SB1003	3.11 ± 0.92	46.44 ± 5.45	14.44 ± 1.23	10.00 ± 0.82	25.11 ± 2.20	39.33 ± 1.09
SB1003 *+ispA*	2.83 ± 1.01	41.11 ± 2.45	12.67 ± 0.72	5.56 ± 0.31	34.44 ± 0.83	57.78 ± 4.43
SB1003 *+ispA-dxs-idi*	15.06 ± 4.39	9.33 ± 0.47	3.22 ± 0.16	4.67 ± 0.47	19.56 ± 1.81	17.56 ± 2.20
SB1003-MVA	5.67 ± 3.73	28.33 ± 0.54	9.22 ± 0.57	13.33 ± 0.94	22.67 ± 0.47	40.89 ± 4.76
SB1003-MVA *+ispA*	7.39 ± 1.78	24.11 ± 0.16	11.67 ± 0.98	9.78 ± 0.63	35 ± 0.94	32,56 ± 6.53
SB1003-MVA *+ispA-dxs-idi*	7.22 ± 1.93	7.33 ± 1.52	11.44 ± 0.68	9.22 ± 1.66	27.00 ± 4.77	11.78 ± 1.37

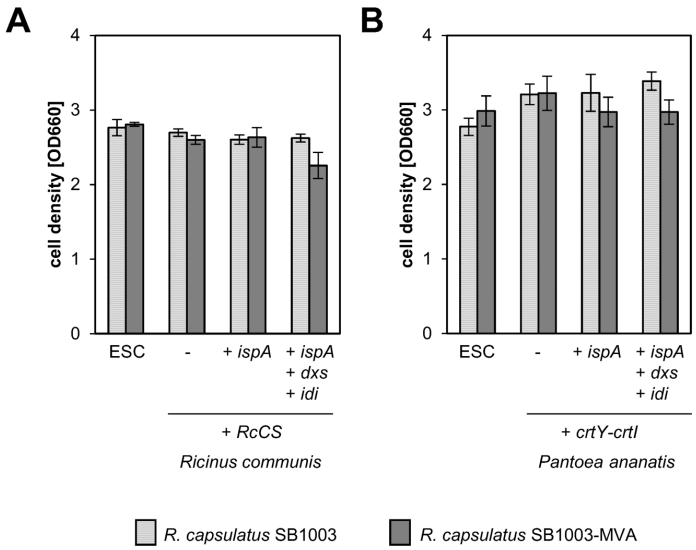

Fig. S1. Final cell densities of *R. capsulatus* casbene and β-carotene production cultures. Cell densities of *R. capsulatus* strains SB1003 (light gray) or SB1003-MVA (dark gray) with pRhon5Hi-2-based expression vectors carrying *RcCS* (from *R. communis*) or *crtY-crtI* (from *P. ananatis*) alone or in combination with *ispA* or *ispA-dxs-idi*, were analyzed, using empty strain controls (ESC) as a reference. To this end, the absorption of 1 mL diluted cell samples was measured at 660 nm at the time points of sampling for analysis of product accumulation, i.e. after 48 h of cultivation at 30 °C under anaerobic conditions in the light in RCV medium with serine. Data represent mean values of three independent cultivations with the respective standard deviations.

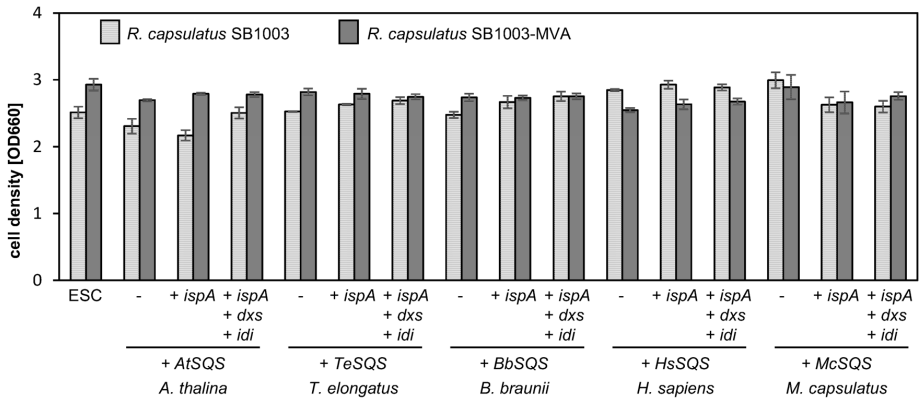

Fig. S2. Final cell densities of *R. capsulatus* squalene production cultures. Cell densities of *R. capsulatus* strains SB1003 (light gray) or SB1003-MVA (dark gray) with pRhon5Hi-2-based expression vectors carrying squalene synthases (SQS) from *A. thaliana* (*At*), *T. elongatus* (*Te*), *B. braunii* (*Bb*), *H. sapiens* (*Hs*) or *M. capsulatus* (*Mc*) alone or in combination with *ispA* or *ispA-dxs-idi*, were analyzed, using empty strain controls (ESC) as a reference. To this end, the absorption of 1 mL diluted cell samples was measured at 660 nm at the time points of sampling for analysis of product accumulation, i.e. after 48 h of cultivation at 30 °C under anaerobic conditions in the light in RCV medium with serine. Data represent mean values of three independent cultivations with the respective standard deviations.

EPILOGUE AND ACKNOWLEDGEMENTS

First of all, I like to thank Prof. Karl-Erich Jaeger for giving me the opportunity to work on this interesting and versatile topic, his continuous confidence in my work and his helpful advice on manuscripts, scientific presentations and much more.

Likewise, I like to thank Prof. Jörg Pietruszka, who kindly accepted to co-examine my thesis and who made it possible to successfully work on this topic at the intersection of biology and chemistry.

For his excellent supervision, my deepest thanks go to Dr. Thomas Drepper. Tom, thank you so much for working with me over the last few years. Your motivating nature, your confidence in my work, and your incomparable ability to show one how exciting the new (though sometimes negative) results are, have always helped me not to bury my head in the sand and to keep working.

Since the here presented thesis was conducted within the BioSC FocusLab CombiCom, I further like to thank all the project members for interesting FocusLab meetings, fruitful discussions, and successful cooperation projects. Further, I like to acknowledge our project coordinator Dr. Anita Loeschcke. Anita, thank you for your excellent and well-organized management of our FocusLab, your kind support on so many occasions and your cheerful and motivating way, which made every project meeting a little bit more exciting. Finally, I like to thank all my CombiCom companions, especially Robin, Steffi, Carl, Jungho, Peter and Jan for the cheering atmosphere during each meeting, PhD retreat and of course each little city trip.

In addition, I like to thank all IMET members, and particularly all Dreppers for welcoming me in Jülich and making me stay over the last eight years. The fact that the IMET became a second home, I owe first and foremost to you guys! So, thank you very much for your help in so many cases, the relaxed and funny working atmosphere, and for all of your kind support.

In particular, my sincere thanks belong to all IMET doctoral students and especially to my colleagues who became friends: Robin, Nora, Oli, Luzie, Patrick. Your mutual helpfulness, continuous support, as well as the legendary coffee breaks and the many leisure activities have made the years fly by. Additionally, I like to thank Dr. Achim Heck for his helpful advises in so many cases, the annual, extremely enjoyable microbiology practical course ☺, and for sure, the organizational work in the background, which made the daily work a lot easier. Further, I like to thank Dr. Stephan Thies and Vera Svensson for their unreserved kindness and constant support in so many scientific matters.

For his cooperation in photocaged compound synthesis and so many fruitful discussions, I like to sincerely thank Fabian Hogenkamp. Thank you, Fabi, for your continuous motivation, your expertise teaching me a lot about organic chemistry and your effort to successfully complete many projects.

The working group “Microscale bioengineering” of Prof. Alexander Grünberger, I like to thank for several amazing cooperation projects in the field of microfluidic single-cell analysis. Thank you, Alina and Alex, for teaching me a lot about this highly interesting topic and giving me insights into the very small world of microbes.

Additionally, I like to acknowledge all the bachelor and master students, I could (co)supervise in the lab. Thank you, Caro, Julian, Nora, Luzie, Yannic, Mona, Dani and Pauline, for your motivation and diligence, which encouraged me to continue and successfully complete projects. It was a pleasure to guide you on a small part of your way into science.

Schließlich möchte ich meinen Eltern, meiner Familie und meinen Freunden und ganz besonders Andreas für die stetige Unterstützung während der letzten Jahre danken. Ohne eure Geduld und euren Zuspruch wäre ich jetzt nicht da, wo ich bin – vielen, lieben Dank!

Heinrich Heine
Universität Düsseldorf

Eidesstattliche Versicherung

Ich, Frau Fabienne Hilgers, versichere an Eides statt, dass die vorliegende Dissertation von mir selbstständig und ohne unzulässige fremde Hilfe unter Beachtung der „Grundsätze zur Sicherung guter wissenschaftlicher Praxis an der Heinrich-Heine-Universität Düsseldorf“ erstellt worden ist.

Die Dissertation wurde in der vorgelegten oder in ähnlicher Form noch bei keiner anderen Institution eingereicht. Ich habe bisher keine erfolglosen Promotionsversuche unternommen.

Langenfeld, den _____ _____

Fabienne Hilgers